NUREG/CR–5395
EPRI/NP–6480
BAW–2080
Vol. 2

Multiloop Integral System Test (MIST): Final Report

Test Group 30, Mapping Tests

Prepared by G. O. Geissler/B&W

Prepared for
U.S. Nuclear Regulatory Commission
and
Electric Power Research Institute
and
Babcock & Wilcox Owners Group

AVAILABILITY NOTICE

Availability of Reference Materials Cited in NRC Publications

Most documents cited in NRC publications will be available from one of the following sources:

1. The NRC Public Document Room, 2120 L Street, NW, Lower Level, Washington, DC 20555

2. The Superintendent of Documents, U.S. Government Printing Office, P.O. Box 37082, Washington, DC 20013-7082

3. The National Technical Information Service, Springfield, VA 22161

Although the listing that follows represents the majority of documents cited in NRC publications, it is not intended to be exhaustive.

Referenced documents available for inspection and copying for a fee from the NRC Public Document Room include NRC correspondence and internal NRC memoranda; NRC Office of Inspection and Enforcement bulletins, circulars, information notices, inspection and investigation notices; Licensee Event Reports; vendor reports and correspondence; Commission papers; and applicant and licensee documents and correspondence.

The following documents in the NUREG series are available for purchase from the GPO Sales Program: formal NRC staff and contractor reports, NRC-sponsored conference proceedings, and NRC booklets and brochures. Also available are Regulatory Guides, NRC regulations in the *Code of Federal Regulations*, and *Nuclear Regulatory Commission Issuances*.

Documents available from the National Technical Information Service include NUREG series reports and technical reports prepared by other federal agencies and reports prepared by the Atomic Energy Commission, forerunner agency to the Nuclear Regulatory Commission.

Documents available from public and special technical libraries include all open literature items, such as books, journal and periodical articles, and transactions. *Federal Register* notices, federal and state legislation, and congressional reports can usually be obtained from these libraries.

Documents such as theses, dissertations, foreign reports and translations, and non-NRC conference proceedings are available for purchase from the organization sponsoring the publication cited.

Single copies of NRC draft reports are available free, to the extent of supply, upon written request to the Office of Information Resources Management, Distribution Section, U.S. Nuclear Regulatory Commission, Washington, DC 20555.

Copies of industry codes and standards used in a substantive manner in the NRC regulatory process are maintained at the NRC Library, 7920 Norfolk Avenue, Bethesda, Maryland, and are available there for reference use by the public. Codes and standards are usually copyrighted and may be purchased from the originating organization or, if they are American National Standards, from the American National Standards Institute, 1430 Broadway, New York, NY 10018.

DISCLAIMER NOTICE

For sale by the Superintendent of Documents, U.S. Government Printing Office
Washington, D.C. 20402

NUREG/CR-5395
EPRI/NP-6480
BAW-2080
Vol. 2

Multiloop Integral System Test (MIST): Final Report

Test Group 30, Mapping Tests

Date Published: December 1989

Principal Author
G. O. Geissler

Major Contributors

ARC		NPD
D. P. Birmingham	T. F. Habib	J. R. Gloudemans
J. E. Blake	F. Karimi-Azad	K. W. Turner
H. R. Carter	C. G. Koksal	
M. T. Childerson	T. E. Moskal	
R. P. Ferron	G. C. Rush	

Prepared by

Babcock & Wilcox
Nuclear Power Division
3315 Old Forest Road
Lynchburg, VA 24506-0935

Babcock & Wilcox
Research and Development Division
Alliance Research Center
1562 Beeson Street
Alliance, OH 44601

Prepared for

Division of Systems Research
Office of Nuclear Regulatory Research
U. S. Nuclear Regulatory Commission
Washington, DC 20555
NRC FINs B8909, D1734

Electric Power Research Institute
P. O. Box 10412
Palo Alto, CA 94303

Babcock & Wilcox Owners Group
P. O. Box 10935
Lynchburg, VA 24506-0935

ABSTRACT

The multiloop integral system test (MIST) is part of a multiphase program started in 1983 to address small-break loss-of-coolant accidents (SBLOCAs) specific to Babcock & Wilcox-designed plants. MIST is sponsored by the U.S. Nuclear Regulatory Commission, the Babcock & Wilcox Owners Group, the Electric Power Research Institute, and Babcock & Wilcox. The unique features of the Babcock & Wilcox design, specifically the hot leg U-bends and steam generators, prevented the use of existing integral system data or existing integral system facilities to address the thermal-hydraulic SBLOCA questions. MIST and two other supporting facilities were specifically designed and constructed for this program, and an existing facility -- the once-through integral system (OTIS) -- was also used. Data from MIST and the other facilities will be used to benchmark the adequacy of system codes, such as RELAP-5 and TRAC, for predicting abnormal plant transients. The MIST Mapping Tests were performed to traverse the early post-SBLOCA events slowly. The tests investigated the effect of test-to-test variations in boundary system controls, and only the primary fluid mass varied during a specific test in Test Group 30. The specifications, conduct, observations, and results of these tests are described in this report.

CONTENTS

Contents (Cont'd)

List of Tables

List of Figures

Figures (Cont'd)

Figures (Cont'd)

Figures (Cont'd)

Figures (Cont'd)

Figures (Cont'd)

Figures (Cont'd)

Figures (Cont'd)

Figures (Cont'd)

Figures (Cont'd)

Figures (Cont'd)

Figures (Cont'd)

EXECUTIVE SUMMARY

Introduction

The multiloop integral system test (MIST) was a scaled 2-by-4 (2 hot legs and 4 cold legs) physical model of a Babcock & Wilcox (B&W), lowered-loop, nuclear steam supply system (NSSS). MIST was designed to operate at typical plant pressures and temperatures. Experimental data obtained from this facility during post-small-break loss-of-coolant accident (SBLOCA) testing are used for computer code benchmarking.

MIST consisted of two 19-tube, once-through steam generators, a reactor, a pressurizer, 2 hot legs, and 4 cold legs with scaled reactor coolant pumps. Other loop components included a closed secondary system, 4 simulated reactor vessel vent valves (RVVVs), a pressurizer power-operated relief valve (PORV), hot leg and reactor vessel upper head vents, high-pressure injection (HPI), core flood system, and critical flow orifices for scaled leak simulation. Guard heaters, used in conjunction with passive insulation to reduce model heat loss, were used on all primary system components as well as the steam generator secondaries. The MIST facility is illustrated in Figure 1.

Boundary Systems

The MIST boundary systems were sized to power-scale the plant boundary conditions. HPI and auxiliary feedwater (AFW) characteristics were based on composite plant characteristics. Scaled model vents were included in both hot legs and in the reactor vessel upper head. Leaks were located in the cold leg suction and discharge piping, the upper and lower elevations of steam generator B (for tube rupture simulation), and in the downcomer-to-reactor vessel crossover pipe (to provide symmetric effects on the two loops for the Mapping Tests). The desired vent and leak flows were obtained using power-scaled restrictors.

Heat Losses and Guard Heaters

MIST was designed to minimize heat losses from the reactor coolant system. Fin effects (instrument penetrations through the insulation) were minimized by using 1/4-inch penetrations for most of the instrumentation. Heat losses due to conduction through component supports were minimized by designing the supports to reduce the cross-sectional area and placing insulating blocks between load-bearing surfaces. The reactor coolant system piping and vessels were covered with passive insulation, active insulation (or guard heaters), and an outer-sealed jacket (to prevent chimney effects). The guard heaters were divided into 42 zones, each controlled by a zonal temperature difference and pipe metal temperature.

Instrumentation

MIST had approximately 850 instruments. These instruments were interfaced to a computer-controlled, high-speed data acquisition system. MIST instrumentation consisted of measurements of temperature, pressure, and differential pressure. Fluid level and phase indications were provided by optical viewports, conductivity probes, differential pressures, and gamma densitometers. Mass flow rates at the system boundaries were measured using Corioles flowmeters and weigh scales. Loop mass flow rates were measured using venturis or turbine meters.

Transient Test Program

The MIST transient tests were defined to generate integral system data for code benchmarking. The transient test series was divided into the following seven groups:

- Mapping
- Boundary systems
- Leak and HPI configuration
- Leak-HPI cooling (feed and bleed)
- Steam generator tube rupture
- Noncondensible gas (NCG) and venting
- Reactor coolant pump (RCP) operation

The Mapping Tests were intended to examine the initial post-SBLOCA transient interactions. In these tests, the primary system inventory was carefully controlled and slowly varied to allow the examination of the normally rapid and overlapping post-SBLOCA events.

The boundary system controls were varied singly in Test Group 30. Each of these tests was based on the nominal boundary system characteristics of Test Group 30. These nominal characteristics included a scaled 5-cm^2 downcomer-to-reactor vessel crossover pipe leak, automatic and independent RVVV actuation on differential pressure, automatic guard heater control, constant steam generator pressure and level control, and constant core power control.

One off-nominal leak size was tested in Group 30, a scaled 10-cm^2 leak. One test varied the leak location, cold leg B1 discharge. The pressurizer was isolated in one test. HPI was not actuated (performed with reduced core power and leak size) in one test. Two tests varied the steam generator secondary control level. The RVVVs were maintained closed for one test. The reactor coolant pumps were operated throughout one test.

The Mapping Tests, with the exception of the reactor coolant pumps on test, were initialized in natural circulation with the HPI flow rate equal to the leak flow rate. The tests were initiated by establishing an imbalance between the leak and HPI flow rates that resulted in primary system inventory depletion. Each of the natural circulation Mapping Tests depressurized to saturated conditions, gradually increased in pressure, and then remained at a relatively constant pressure as the flow interruption phenomena occurred. Backflow from the downcomer into the cold leg discharge pipes was observed to be a major contributor to the flow interruption phenomena, the establishment of intra-cold leg flow, and the voiding of the cold legs. Each natural circulation test, with the exception of the closed RVVVs, exhibited a sequential occurrence for the cold leg flow interruptions, i.e., flow interruption did not occur simultaneously in all four cold legs. The closed RVVVs test exhibited an atypical flow interruption response as alternating loop pulsating flow was established followed by flow interruption in one loop while the other loop continued in a pulsating flow manner.

Subsequent to flow interruption, each natural circulation test repressurized. The closed RVVV test also repressurized as pulsating loop flow was established. The increased leak size test and the closed RVVV test repressurized the least amount. The cold leg discharge leak test and the two tests that varied the steam generator secondary level control attained the greatest pressures and resulted in PORV actuations.

Either AFW and/or pool BCM was attained in each natural circulation test with the exception of the cold leg discharge leak (this test was terminated prior to achieving BCM due to an inoperable automatic PORV control). For the tests that attained BCM, the BCM was not sustaining. This action resulted in a primary system pressure response that decreased as BCM was established and increased as BCM terminated. Those tests that achieved pool BCM depressurized to a primary system pressure that approached the steam generator secondary pressure as the test termination criteria were met. Two tests terminated prior to attaining pool BCM. These were the tests for reduced steam generator secondary level in both steam generators (terminated as a result of exceeding a test facility design limit, high core heater rod temperature, as core uncovery occurred) and the previously discussed cold leg discharge leak.

The pumps-on Mapping Test was also initialized with the HPI flow rate equal to the leak flow rate. This test also involved the gradual reduction of primary system inventory by imbalancing the leak and HPI flow rate. However, all four model pumps were kept in operation at rated speed throughout the test. Five distinct types of pump operation were observed and pump characterization information was obtained. The pump characteristics were compared to SEMISCALE/RELAP predictions.

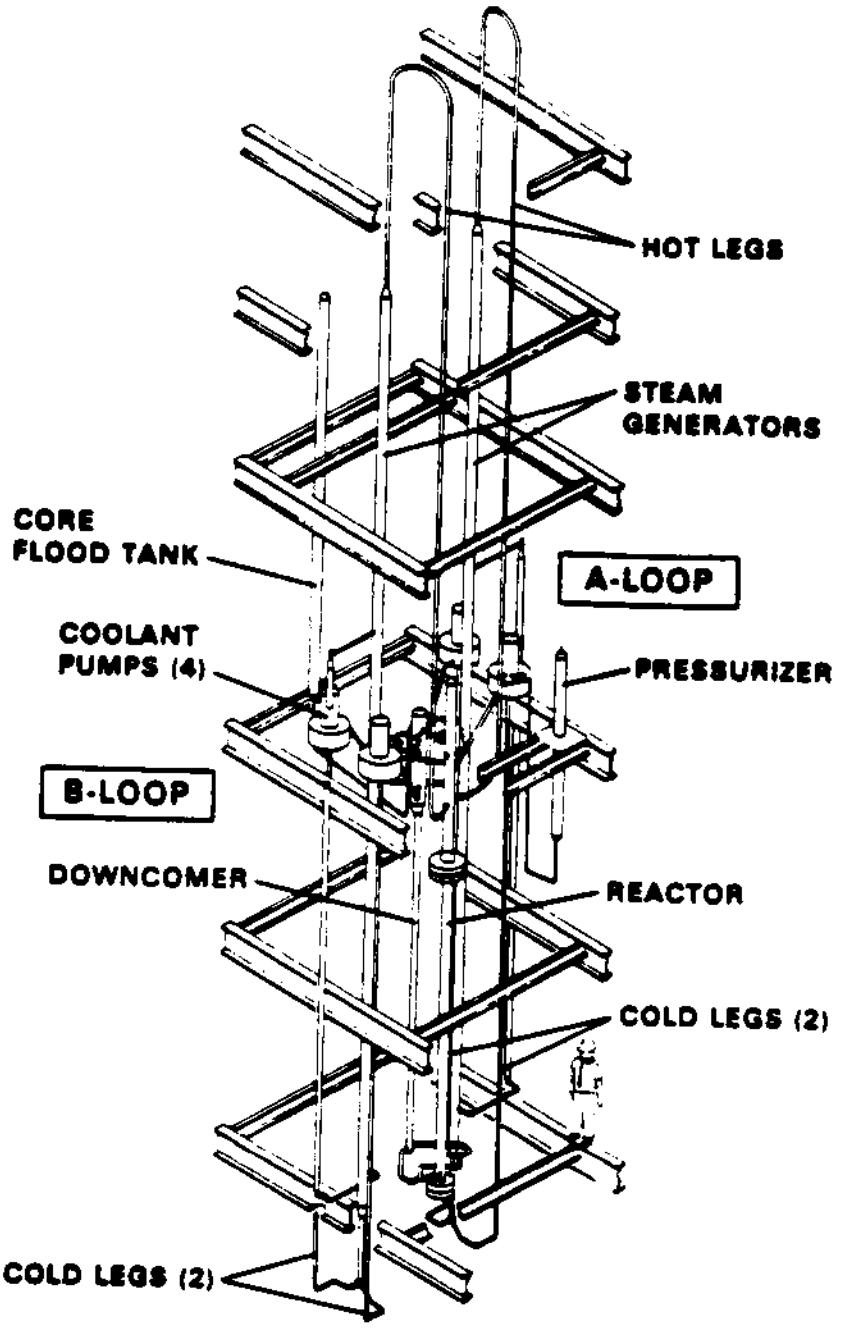

Figure 1. Reactor Coolant System -- Multiloop Integral System Test (MIST)

1. INTRODUCTION

The multiloop integral system test (MIST) was a 2-by-4, full pressure and temperature simulation of the lowered-loop plants designed by Babcock & Wilcox (B&W). MIST was sponsored by the U.S. Nuclear Regulatory Commission, the B&W Owners Group, the Electric Power Research Institute, and B&W. The MIST testing program included debug, characterization, mapping, and transient tests. The natural circulation mapping tests and the reactor coolant pumps-on mapping test of Group 30 are reported herein.

The MIST design, features, and instruments are outlined in section 2. The Group 30 test specifications are provided in section 3, the control of these tests and the instrument performance are described in section 4, section 5 provides the major observations and key data plots of each test, and section 6 is a summary of the Group 30 test results. Appendix A contains microfiche of key plots that encompass the entire testing time period for each test.

The MIST Mapping Tests were performed to traverse the early post-small-break loss-of-coolant accident (SBLOCA) events slowly and with each of the boundary system controls held constant. Only the primary fluid mass was varied during each test. This was accomplished by imbalancing the high-pressure injection (HPI) and leak flow rates. Each Mapping Test was performed in a similar manner. The boundary system controls were varied among the tests but were held constant throughout a test. The nominal leak site location was in the reactor vessel-to-downcomer crossover pipe. This location was chosen so that loop conditions would be affected in a symmetrical manner.

The MIST Mapping Tests were examined in Test Group 30. The tests performed (presented in the order discussed in section 5) and the varied boundary system control were as follows:

Test Number	Scaled Leak Size and Location	Varied Boundary System
3003AA	5-cm^2 Reactor Vessel-Downcomer Leak	Nominal Test
3001BB	5-cm^2 Reactor Vessel-Downcomer Leak	Pressurizer Isolated
3009AA	5-cm^2 Cold Leg Discharge Leak	Leak Location
300605	5-cm^2 Reactor Vessel-Downcomer Leak	Imbalanced Steam Generator Secondary Levels (A = 10 ft, B = 31.6 ft)
3007CC	5-cm^2 Reactor Vessel-Downcomer Leak	10-ft Steam Generator Secondary Levels
300504	5-cm^2 Reactor Vessel-Downcomer Leak	Reactor Vessel Vent Valves Manually Closed
3004CC	1-cm^2 Reactor Vessel-Downcomer Leak	No HPI and Reduced Power
300001	10-cm^2 Reactor Vessel-Downcomer Leak	Leak Size
300806	5-cm^2 Reactor Vessel-Downcomer Leak	Reactor Coolant Pumps Operating

The Mapping Tests were planned to be performed using a nominal 10-cm^2 scaled leak size. However, the inability of the steam generators to attain and maintain the desired secondary pressure when the 10-cm^2 leak was used necessitated the use of a smaller leak.

The results obtained from these tests, even though a smaller nominal leak size was used, met the proposed objective of this test group and provided additional insight into the post-SBLOCA phenomena.

2. FACILITY DESCRIPTION

2.1. Introduction

MIST was a scaled, 2-by-4 (2 hot legs and 4 cold legs) model of a B&W, lowered-loop, nuclear steam supply system (NSSS). MIST was designed to operate at typical plant pressures and temperatures. Experimental data obtained from this facility during post-SBLOCA testing are used for computer code benchmarking.

The reactor coolant system of MIST was scaled according to the following criteria, listed in order of descending priority: elevation, post-SBLOCA flow phenomena, component volume, and irrecoverable pressure drop. MIST consisted of two 19-tube, once-through steam generators; reactor; pressurizer; 2 hot legs; and 4 cold legs each with a scaled reactor coolant pump.

Other loop components in MIST included a closed secondary system; 4 simulated reactor vessel vent valves (RVVVs); a pressurizer power-operated relief valve (PORV); hot leg and reactor vessel upper-head vents; high-pressure injection; core flood system; and critical flow orifices for scaled leak simulation. Guard heaters, used in conjunction with passive insulation to reduce model heat loss, were included on the steam generator secondaries and on all primary coolant components. The system was also capable of noncondensible gas addition at selected loop sites.

The approximately 850 MIST instruments were interfaced to a computer-controlled, high-speed data acquisition system. MIST instrumentation consisted of measurements of temperature, pressure, and differential pressure. Fluid level and phase indications were provided by optical viewports, gamma densitometers, conductivity probes, and differential pressures. Mass flow rates in the circulation loop were measured using venturis and a cooled thermocouple and at the system boundaries using Corioles flowmeters and weigh scales.

2.2. MIST Design

MIST was a scaled, full-pressure, experimental facility arranged to represent the B&W lowered-loop plant design. Like the plant, MIST was a 2-by-4 arrangement with 2 hot legs and 4 cold legs, as shown in Figure 2.1. MIST was designed for prototypical fluid conditions, with emphasis on being leak-tight and minimizing heat loss.

Scaling of MIST followed the approach and priorities used for OTIS[1]; that is, elevation, post-SBLOCA phenomenon, component and piping volumes, and irrecoverable pressure losses. MIST was at full elevation throughout. The only elevations compromised were the top of the pressurizer, the top plenum of the reactor vessel, the inlet and outlet of the steam generator plenums, and several incidental, stagnant fluid zones. Key interfaces were maintained -- these included the hot-leg, U-bend spillover; upper and lower tubesheets of the steam generator (secondary faces); cold-leg low point; pump discharge; cold- and hot-leg nozzles; core (throughout); and points of emergency core cooling system (ECCS) injection.

Two-phase behavior during voiding of the hot-leg U-bend and flow interruption was sufficiently prototypical; that is, both the plant and the model were expected to encounter phase separation early in the post-SBLOCA transient. Hot leg pipes in MIST were large enough to admit bubbly flow.

Fluid volume was 40% larger than power-to-volume scaling would dictate; the hot legs, cold legs, and upper downcomer were oversized. This atypicality was imposed by the previously described two-phase characteristics and by considering component irrecoverable pressure losses. The excess volume of the hot leg slowed the rate of level decrease for power-scaled draining and similarly retarded the rate of level increase for power-scaled injection. Although the excess volume of loop fluid delayed system heatup and cooldown, this effect was minor compared to the long-term impact on system energy of leak versus high-pressure injection (HPI) cooling. The concentration of excess volume in the piping runs decreased fluid velocities in the hot legs and cold legs and therefore lengthened the transit time of loop fluid. Irrecoverable pressure drops were well preserved.

The MIST core and steam generators were full-length subsections of their plant counterparts. As shown on Figure 2.2, the core consisted of a 7-by-7 array of 45 full-length, 0.430-inch-diameter heater rods and four simulated incore guide tubes. Plant-typical fuel pin pitch and grid geometry were used. The simulated rods were capable of full-scale power output but were limited to approximately 10% of scaled power for the planned MIST testing. (The ratio of plant power to MIST power was 817.) A fixed, axial heat flux profile (peak-to-average flux ratio = 1.25) and a flat, radial heat flux profile were used.

The steam generators, shown in Figure 2.3, each contained 19 full-length tubes. The tubing diameter (5/8-inch OD), material, and tube bundle's triangular pitch (7/8 inch, tube centerline to centerline) were prototypical. The geometry of the tube support plant (TSP) was similar to the plant and provided equivalent characteristics of irrecoverable pressure loss.

The hot legs used 2.5-inch, schedule-80 piping (2.32 inch ID). This diameter admitted bubbly flow and approximated the irrecoverable pressure loss of a plant hot leg. With the schedule-80 piping, the metal-to-fluid volume ratio in MIST was only 20% greater than that of the plant. The horizontal runs in the hot leg, as noted in Figure 2.1, were approximately 1 foot long to accommodate the gamma densitometers. The hot-leg U-bend maintained pipe diameter; a 1.61-foot bend radius was used to conform to the model system layout. The elevation of the hot U-bend spillover was prototypical. Phase separation at the U-bend was predicted to occur at approximately 18% of full power versus 8% in the plant. Beyond the U-bend, the hot leg piping in the model extended 12 feet (versus 1.5 feet in the plant) to span the height of the plant steam generator's inlet plenum.

The four cold legs preserved elevation throughout. Two-inch, schedule-80 piping (1.939-inch ID) was used primarily to match irrecoverable pressure drop. This piping size also preserved cold-leg Froude number, which influences the mixing of HPI and RVVV fluid streams. The cold leg horizontal piping runs were shortened, but the slope of the plant cold leg discharge piping was approximately maintained. HPI was injected into the sloping pipes at the appropriate elevation; the diameter of the model HPI nozzle was

selected to preserve the ratio of fluid momentum between the cold leg and HPI.

A model reactor coolant pump was mounted in each cold leg. Suction and discharge orientations were prototypical. The pumps delivered single-phase scaled flows at plant-typical heads, allowed for simulated pump bumps by matching the plant pump spinup and coastdown times, and permitted operation under single- and two-phase conditions. However, the pumps preserved neither specific speed nor the two-phase degradation characteristics of the plant pumps.

The MIST reactor vessel employed an external annular downcomer, as shown in Figure 2.1. Cold-leg coupling was restricted by using fins in the downcomer annulus to form quadrants, as noted in Figure 2.4. The annular gap was 1.4 inches; the gap at each fin was 0.4 inches. Each downcomer quadrant was connected to a separate RVVV simulation and cold leg. The two nozzles on the core flood tank were connected at the interface between two downcomer quadrants.

The geometry of the model downcomer was annular down to the elevation of the top of the core. Just above the top of the core, the downcomer was gradually reconfigured to form a single pipe for the remaining elevation. The lower downcomer region obtained roughly power-scaled fluid volume over the elevation of the core. Four model RVVVs were used to simulate eight plant valves.[2] The MIST RVVVs could be controlled individually or in unison. Individual controllers provided automatic actuation of the valves on the upper plenum to downcomer-quadrant pressure differences. The MIST RVVVs thus provided the head-flow response of the plant valves. But partially open operation was not possible in MIST; therefore, detailed valve dynamics of the plant flapper valves were absent.

The MIST pressurizer was power-to-volume scaled and contained heaters and spray. The lower pressurizer elevations were prototypical, as were those of the surge line. The model pressurizer height was reduced from that of the plant to increase the diameter, thus lessening atypical fluid stratification and the likelihood of spray impinging the vessel wall.

One core flood tank was used in MIST. This tank was power-to-volume scaled to represent the two plant tanks. The model tank was installed vertically, with the bottom of the tank at a prototypical elevation. The injection line from the tank to the nozzle on the downcomer was sized to preserve plant-typical irrecoverable losses, and the nozzle was sized to maintain the plant ratio of (core-flood) injected fluid momentum to the downcomer fluid momentum.

2.3. Boundary Systems

The MIST boundary systems were sized to power-scale the plant boundary conditions. HPI and auxiliary feedwater (AFW) head-flow characteristics were based on composite plant characteristics. Scaled model vents were included in each hot leg and in the reactor vessel upper head. Controlled leaks were located in the cold leg suction and discharge piping and at the upper and lower elevations of steam generator B (for tube rupture simulation). The desired vent and leak flow rates were obtained using critical flow orifices of power-scaled areas.

2.4. Heat Losses and Guard Heaters

MIST was designed to minimize heat losses from the reactor coolant system. Fin effects (instrument penetrations through the insulation) were minimized by using 1/4-inch penetrations for most of the instrumentation. Heat losses due to conduction through component supports were minimized by designing the supports to reduce the cross-sectioned area and by placing ceramic blocks between load-bearing surfaces. The reactor coolant system piping and vessel were covered with passive insulation, guard heaters, and a sealed outer jacket (to prevent chimney effects). The insulation arrangement is illustrated in Figure 2.5. The guard heaters were divided into 42 zones, each controlled by a zonal temperature difference and a pipe metal temperature. This system provided a differential temperature control as a function of temperature. Detailed finite-difference analysis of the insulation system indicated that heat loss was strongly dependent on metal temperature and weakly related to fluid state. The control temperature difference required to minimize heat losses was determined experimentally at several loop temperatures.

However, the guard heaters did not compensate for all the loop heat losses. For example, large local losses at the gamma densitometers and viewports were not compensated. Had these local losses been compensated, the requisite increased metal temperature would have generated atypically large metal stored energy. The total MIST primary system heat loss at 650F was approximately 18 kW or 0.55% of scaled full power. This heat loss was attributable to the previously discussed uncompensated heat losses.

2.5. Instrumentation

The MIST instrumentation was selected and distributed based on the input from experimenters and code analysts. This instrument selection process considered the needs of code benchmarking, indication of thermal-hydraulic phenomena, and system closure.

The approximately 850 MIST instruments were interfaced to a computer-controlled, high-speed, data acquisition system. MIST instrumentation consisted of measurements of temperature, pressure, and differential pressure. Fluid level and phase indications were provided by optical viewports, conductivity probes, differential pressures, and gamma densitometers. Mass flow measurements at the system boundaries were made using Corioles flowmeters and weigh scales. Mass flow rate measurements in the loop were performed with venturis or turbines. Tables 2.5.1 and 2.5.2 provide a summary of the MIST instrumentation by component and instrument type.

The largest grouping of instrumentation was in the two steam generators. About 250, or 30%, of the instruments were located in these two components. The steam generator instrumentation provided for the measurement of fluid temperature, metal and differential temperature, total guard heater power, differential pressure, gauge pressure, and conductivity (for void determination). The allocation of instruments to the steam generators resulted from the judgement that observations of AFW wetting effects and steam generator heat transfer were of major importance. Several other micro- and multidimensional phenomena were also of considerable interest: noncondensible gas blanketing of primary tubes, intermittent radial advancement of condensation fronts in the region of the AFW nozzle, and boiler-condenser heat transfer in the region of the secondary pool.

The core and RVVV instrumentation measured fluid temperature, metal and differential temperature, total guard heater and core power, conductivity (for void determination), and gauge and differential pressures. The core instrument distribution concentrated on the axially varying parameters. A flat, radial heat flux profile was used in the core, and radial maldistribution of inlet flow was expected to result in only minor variations of enthalpy. Therefore, the majority of the incore temperature instrumentation was located in a single, interior flow channel. Radial temperature variations at the core outlet were recorded, but with a limited number of instruments. The core instrument allocation provided core heat input, inlet and exit fluid properties, and fluid gradients within the reactor vessel. In addition, collapsed levels and regional void fractions were available. Single-phase vent valve mass flow rates were also available.

Downcomer instruments measured fluid temperature, metal and differential temperature, total guard heater power, and differential pressures. Forty fluid thermocouples were concentrated in the upper downcomer, detailing mixing information for the RVVV, core flood, and cold leg streams. Six additional fluid thermocouples were spaced uniformly in the lower downcomer to indicate the extent of mixing as the fluid left the upper downcomer. Downcomer flow rate was measured using a venturi and a cooled thermocouple probe.

Table 2.5.1 MIST Instrumentation by Component

Component	Number of Instruments
Cold legs	164
Core flood	7
Hot legs	121
Pressurizer	25
Primary boundary systems	72
Reactor vessel and core	169
Steam generators	249
Steam generator feedwater and steam circuit	44
TOTAL	851

Table 2.5.2 MIST Instrumentation by Measurement Type

Measurement Type	Number of Instruments
Conductivity probes	36
Cooled thermocouple	12
Differential pressure	133
Differential temperature	42
Fluid temperature	381
Gamma densitometer	12
Limit switches	79
Mass flow	9
Metal temperature	69
Miscellaneous	17
Power	48
Pressure	9
Volumetric flow	4
TOTAL	851

Cold leg instrumentation provided fluid and metal temperatures, differential temperatures, total guard heater power, and differential pressures. Gamma densitometers were also used. Cold leg flow rates were measured using venturis located in the suction piping of each cold leg. For tests requiring full forced flow, turbines were used in place of the venturis. In addition, the reactor coolant pump power, speed, and head rise were measured.

Special instrument groupings, thermocouple rakes, and gamma densitometers, were installed in the cold legs upstream and downstream of the HPI injection points to indicate thermal stratification, density, and void fraction near the junction of the cold legs and downcomer.

Hot leg instrumentation measured fluid and metal temperatures, differential temperatures, total guard heater power, and differential pressures. Void measurements using gamma densitometers and conductivity probes were also made. In addition, viewports provided visual data to assess the local flow regime. The density of the hot leg instruments provided detailed fluid temperature gradients, local void fractions, and overall collapsed level. A

conductivity probe, combined with local differential pressures in the U-bend region, provided additional information regarding loop refill and spillover. Gamma densitometers in the hot leg horizontals downstream of the reactor vessel's outlet nozzle and viewports in the 29-foot elevation and at the U-bend high points provided information regarding fluid state and flow conditions. A fifth and sixth viewport in the hot leg horizontals near the densitometers probed the developing flow regimes upstream of the vertical hot leg piping.

The boundary systems, which included HPI, leaks, vents, and gas addition, were provided with fluid thermocouples, absolute and differential pressure transmitters, mass flowmeters, and weigh scales. These instruments provided mass and energy closure for the facility. Additional information regarding the design and instrumentation of MIST may be found in the Facility Specification[3] and in the Instrument Report.[4]

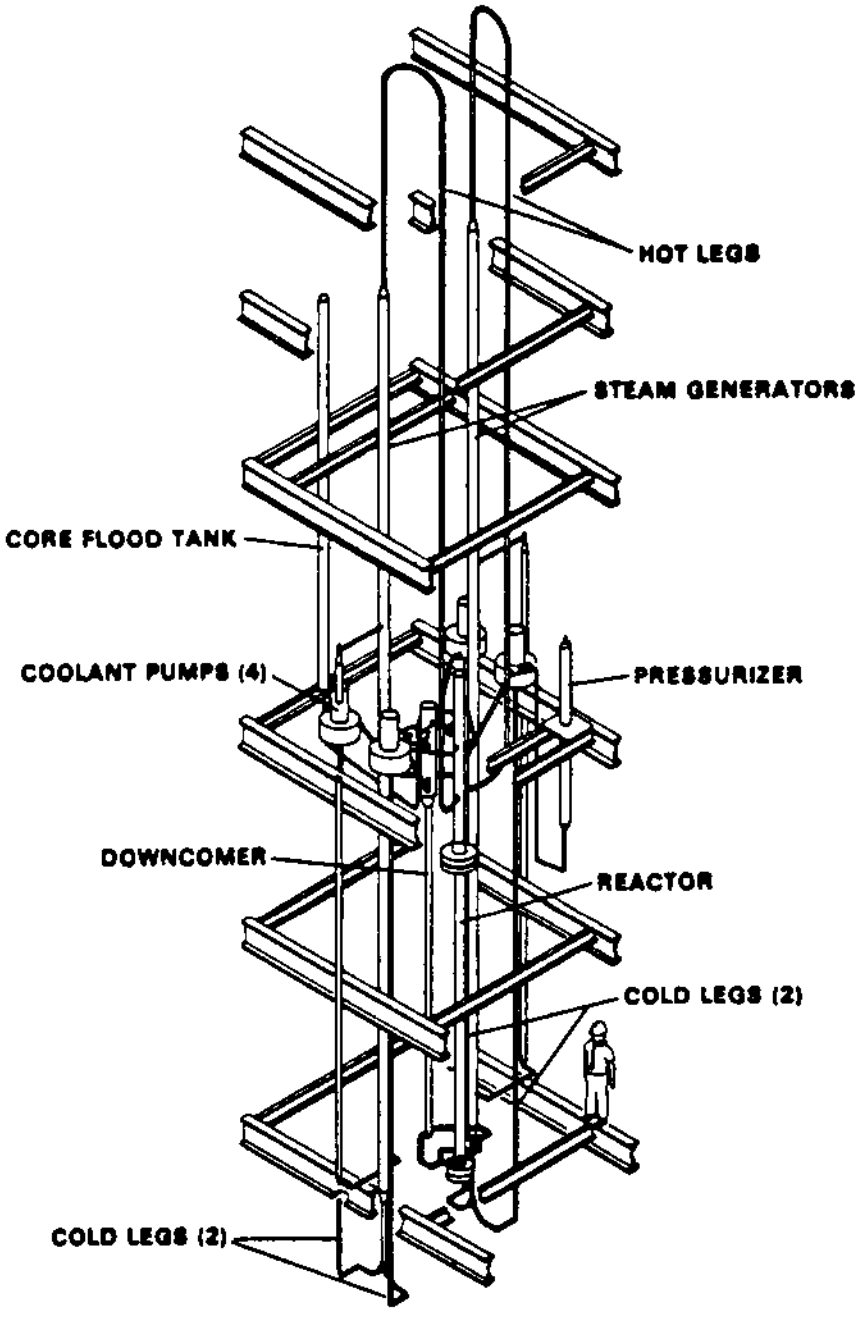

Figure 2.1. Reactor Coolant System -- MIST

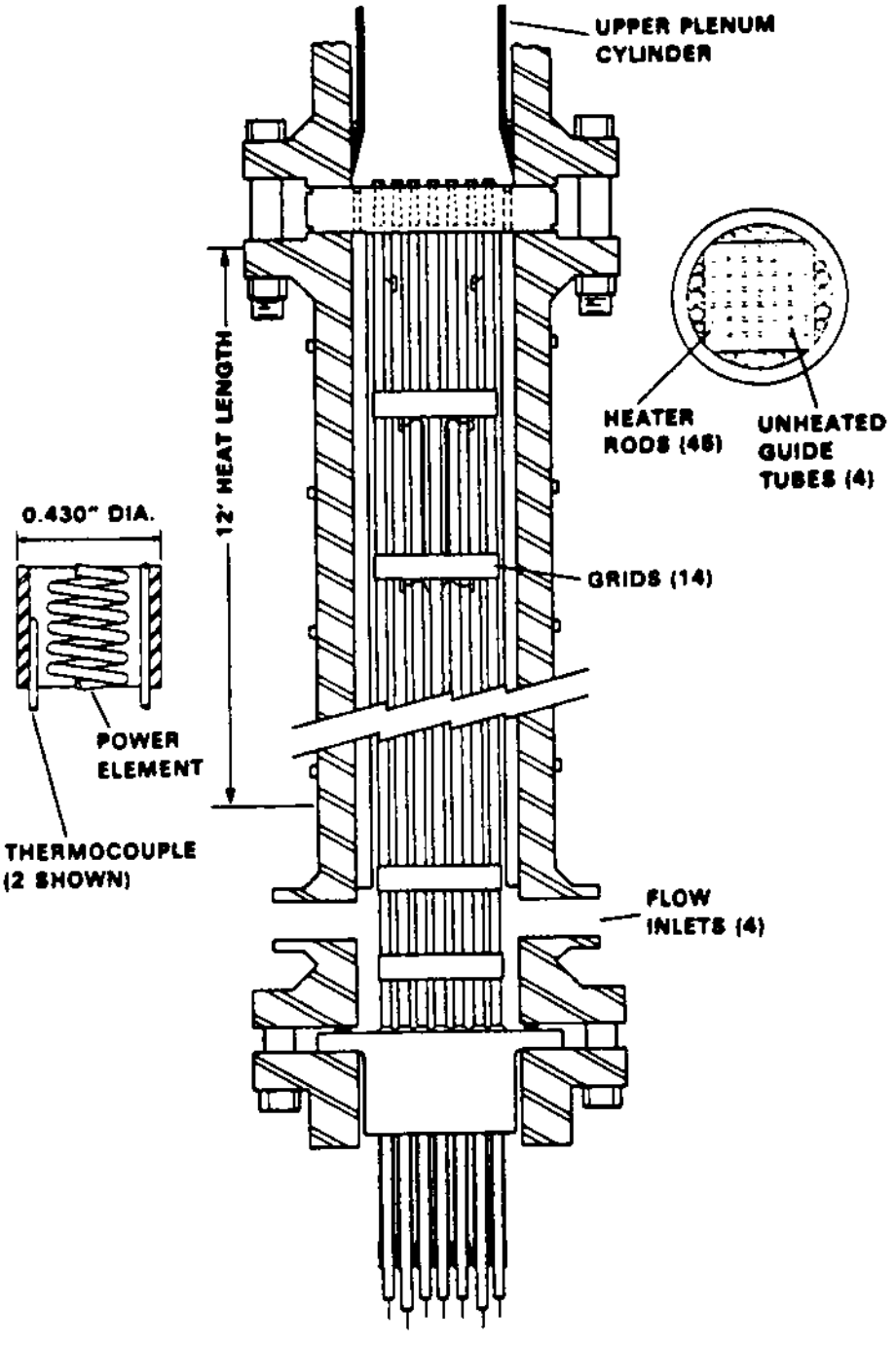

Figure 2.2. MIST Core Arrangement

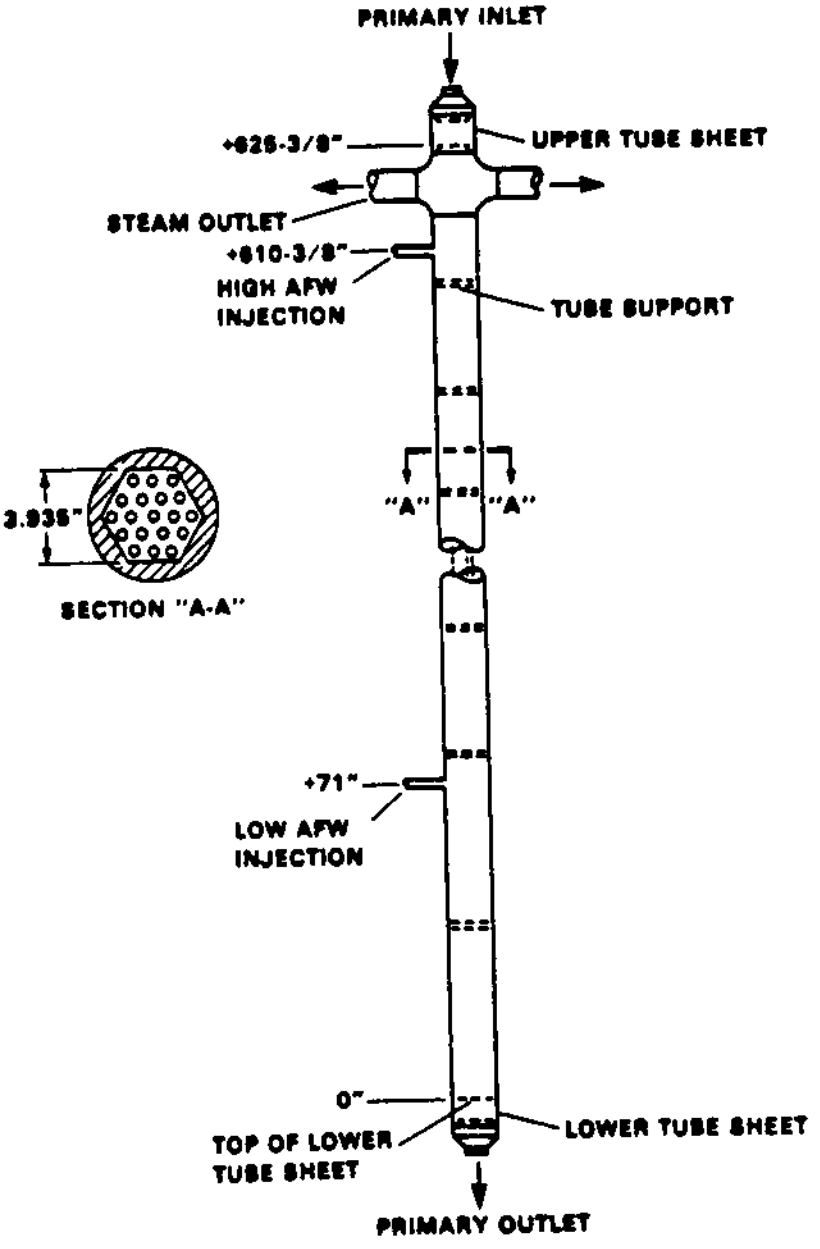

Figure 2.3. Nineteen-Tube, Once-Through Steam Generator

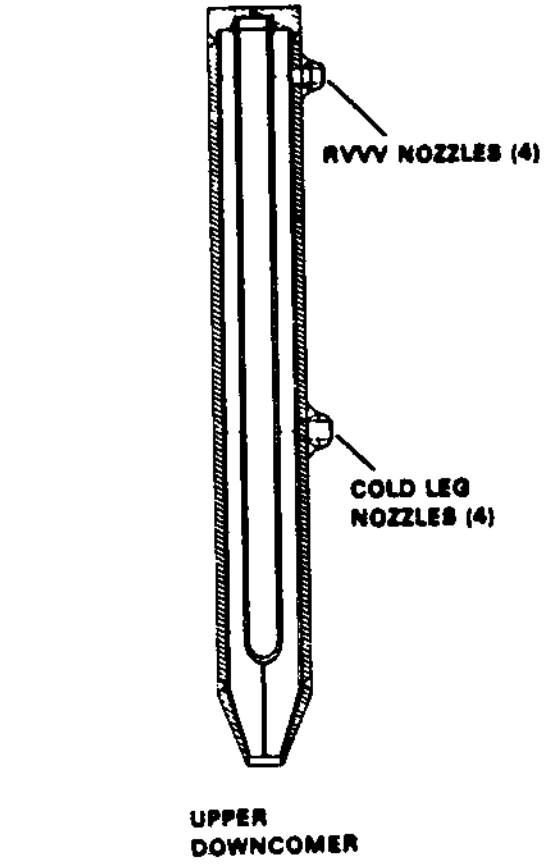

Figure 2.4. Upper Downcomer Arrangement

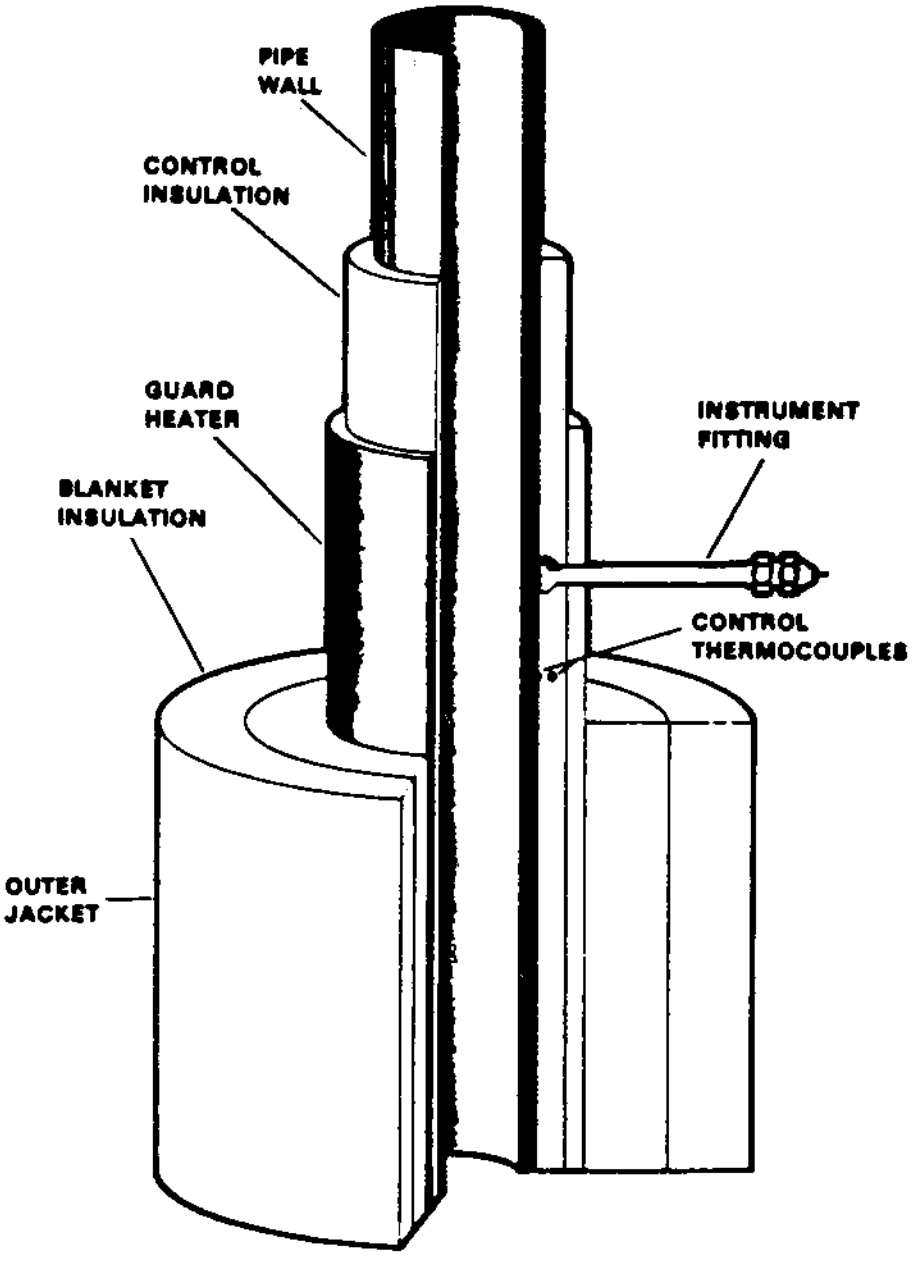

Figure 2.5. MIST Insulation Arrangement

3. TEST SPECIFICATIONS

The specifications for Group 30 of the Mapping Tests have been extracted from the MIST Test Specifications.[5]

3.1. Purpose

The system conditions at the transitions among the early post-SBLOCA events are to be accurately determined in the Mapping Tests. These events include saturated and two-phase natural circulation, intermittent circulation, flow interruption, and the BCM.

The early events are difficult to examine both during testing and in code predictions. The events occur in quick succession and while both the boundary and system conditions are varying rapidly. These initial events are important to the subsequent transient. For example, sustained primary circulation supports heat transfer and primary depressurization, while prolonged flow interruption causes primary repressurization.

The Mapping Tests will be performed to traverse the early events slowly and with each of the boundary system controls held constant. Only the primary fluid mass is to be varied during a test. Primary fluid mass is to be slowly decreased by imbalancing the HPI and leak flow rates. The transient system interactions are to be observed with these imposed nearly constant conditions. This technique will permit the relatively precise determination of the conditions governing each of the early events and the transitions among them. These determinations can be used directly to verify the ability of the system codes to predict the early interactions.

The observations from the Mapping Tests may also be used to correlate event occurrence to system conditions, i.e., to "map" performance versus conditions. The boundary system settings are selected to highlight the differences among the early transient sequences. Each of the Mapping Tests is to separately provide the primary conditions at which the early interactions

occur. The larger objective of these tests is then to compare the conditions among the Mapping Tests, both to gain insight into their correlation and to identify the conditions at which code benchmarking of the early interactions would best be performed. The correlated results may be integrated with those of the recent hot leg U-bend (HLUB) flow regime and separation tests at Science Applications Incorporated (SAI) and Argonne National Laboratory (ANL).

3.2. Background

The Mapping Tests examine the events that occur early in the post-SBLOCA transient. The discussion that follows outlines these initial system interactions. This discussion pinpoints system boundary conditions likely to affect the early events, and hence, the system conditions that should be varied within the test matrix.

3.2.1. Transient Events from Initiation to BCM

A small break (other than an upper-pressurizer break) quickly leads to pressurizer draining and loop depressurization to saturation. The continuing inventory depletion causes vapor to flow up the hot leg, with saturated fluid spilling over the HLUB; the magnitude of this vapor flow is governed by the amount of core steam production in excess of the rate of steam flow out the RVVVs and condensed by HPI, the rate of inventory depletion (which affects the rate of flashing of the hot leg fluid), and the rate of displacement of fluid from the reactor vessel (by upper head voiding). The flow of saturated fluid over the HLUB spillover is quickly interrupted as the system inventory depletes further and as the upper elevation two-phase mixture separates. Interruption of flow and of primary-to-secondary heat transfer may increase the rate of core steam production; increased voiding in the vessel may cause the fluid displacement from the vessel to exceed the rate of system inventory depletion, and hence, to momentarily refill the hot leg and to reactivate HLUB spillover flow. Should the reactor vessel level descend to the elevation of the hot leg nozzles, the hot leg vapor flow rate may increase sufficiently to also reactivate loop flow. Finally, the interruption is completed and primary-to-secondary transfer is precluded. The primary system will repressurize in response to the imbalance, if any, between current core power and HPI-leak cooling. Should the primary repressurize to the PORV

setpoint, relief valve actuation will accelerate the rate of inventory depletion (not only by the discharge of pressurizer steam through the valve, but also by diversion of loop liquid to the pressurizer). In the absence of PORV actuation, the primary level may decrease due to an imbalance between HPI and leak flow rates. The primary level will thus descend to the upper elevation of the steam generator and establish a condensing surface. The ensuing condensation of primary vapor within the steam generator (the "Boiler-Condenser Mode" or "BCM") will occur at the AFW injection elevation if the AFW system is active (this is the so-called "AFW-BCM"). If AFW is not being injected, the primary level within the steam generator will cross the secondary liquid-vapor interface and the pool BCM will result. The primary depressurizes readily with either type of BCM, thus completing the early transient events.

3.2.2. Governing Conditions (During the Initial Events)

The initial post-SBLOCA transient just discussed suggests several conditions governing flow interruption and BCM:

- Break size determines the rate of depressurization and (primary liquid) inventory depletion.
- Inventory depletion causes U-bend voiding and subsequent interruption.
- Core power, flow rate, and inlet subcooling determine the rate of core steam generation.
- RVVV actuation discharges core-generated steam and thus reduces the flow rate of vapor up the hot leg.
- The rate of HPI introduction with a saturated system largely determines the condensing capacity in the downcomer-cold leg regions (and hence the long-term RVVV vapor venting rate). HPI-leak cooling versus core power affects primary repressurization.
- The pre-transient hot leg and reactor vessel upper head (RVUH) fluid and metal temperatures, and their variation through the early part of the transient, affect the rate and amount of hot leg and RVUH flashing with system depressurization.
- The AFW status will affect the BCM. The steam generator secondary pool level and also the secondary pressure determine the effectiveness and duration of the BCM.

3.3. Test Conduct

Each of the Mapping Tests is to be performed in a similar manner, as outlined in section 3.3.1. Sections 3.3.2 and 3.3.3 describe the testing phases. Measurement requirements are given in section 3.3.4.

3.3.1. Outline

Each of the Mapping Tests is to be performed in a similar and straightforward fashion. Boundary system controls are varied among the tests as indicated in Table 3.1, but these control settings are to be held constant throughout a test. Each test consists of three phases. These phases are summarized in Table 3.2. A pretest phase, labelled "0," is a half-hour allowance for final stabilization at the test initial conditions. After the loop conditions have been determined to be stable in Phase 0, the test is begun by recording these steady-state conditions in Phase 1. The phases are structured so that each test can take no longer than 5 hours (and the entire Mapping Test effort can take no more than 50 hours). An allowance for equipment anomalies is obtained from those tests that do not require the entire 5 hours to complete. No allowance for repeat tests is appropriate because control during testing is limited to HPI flow rate adjustments according to a specified schedule. The time required for each test is the sum of the duration of the phases, as listed in Table 3.2. The maximum test duration is thus 5 hours. The drains alluded to in Table 3.2 (Phase 2) and in the detailed test specifications involve reducing the HPI flow rate by a specified amount. The exact amount of leak-HPI flow rate imbalance is not critical. The HPI flow rate deficit should simply be set as close as convenient to the specified value considering the equipment and instrument capabilities and the constancy of the loop interactions. Achieving and maintaining a drain rate that is within 10% of that specified, or whatever is practical, is preferable to continually adjusting the HPI flow rate to better match the specified drain rate. The same situation exists when balancing the HPI and leak flow rates (during the stabilization and steady-state phases). The HPI controls should be readjusted toward the desired value at approximately quarter-hour intervals. The HPI adjustments should be made gradually rather than abruptly.

3.3.2. Steady State (Phases 0 and 1)

In Phase 1, steady-state data are to be recorded for 10 minutes at the specified initial conditions. The preceding phase, Phase 0, provides 30 minutes in which to ascertain loop stabilization at the test initial conditions before beginning to record and store data. The initial conditions are listed in Table 3.3. The primary system is to be initialized in subcooled natural circulation at 1750 psia with a pressurizer level of 2.5 ft (2.5 ft of liquid within the pressurizer). The steam generator secondaries are to be held at 1010 psia. Core power, leak configuration, RVVV status, steam generator secondary level, and RCP status are inter-test variables and are listed in Table 3.1. Pressurizer status is also an inter-test variable; the pressurizer is to be isolated at the start of draining in Test 1.

For the Nominal Mapping Test 3 (300300), the core power is to be 3.5% of scaled full power plus 0.4% to compensate for losses to ambient (cf. Appendix D of Reference 5). The nominal steam generator secondary level control is constant at 31.6 ft. Also for the nominal conditions, the RVVVs are to be controlled in automatic/independent and the RCPs are not used.

MIST is to be initialized (through Phases 0 and 1) with the specified leak active and with the HPI mass flow rate adjusted to approximately equal the leak mass flow rate. The tolerance on HPI flow rate is discussed in section 3.3.1 and in the Acceptance Criteria, section 3.5. The nominal configuration uses a 5-cm^2 leak at the bottom of the reactor vessel downcomer. This leak location will affect loop conditions symmetrically. At 1750 psia, the 5-cm^2 critical flow area will discharge about 600 lbm/h, which is also the required initial HPI mass flow rate. Leak flow rate versus temperature and pressure is shown in Figure 3.1. The scaled HPI head-flow characteristics are also shown, but they are not to be applied during these Mapping Tests. Rather, HPI is to be adjusted to balance leak flow and then reduced during the drain phases to obtain the specified rate of primary inventory depletion.

3.3.3. Gradual Inventory Reductions (Phase 2)

The gradual inventory reduction is to be started after at least 10 minutes of steady-state data have been recorded at the specified initial conditions. Initiate (drain) Phase 2 by gradually reducing the HPI flow rate to obtain a

leak-HPI flow rate imbalance (i.e., a drain rate) of approximately 50 lbm/h. This action is accomplished by throttling the HPI flow rate to approximately 90% of its value at steady state. Allow the pressurizer heaters to trip on low level.

An imbalance of approximately 50 lbm/h is to be held for 2.8 hours to lower the total primary fluid inventory from 900 to 760 lbm. In the estimates of events versus inventories in Table 3.4, most of the early post-SBLOCA events are expected to occur during this initial, gradual draining phase. These expected events include pressurizer draining, loop depressurization to saturation, intermittent and then interrupted loop flow, and perhaps AFW-BCM. For those tests in which the core power exceeds the capacity of HPI-leak cooling, the primary system will repressurize upon flow interruption. This repressurization will precipitate a pressurizer insurge, further reduce the loop fluid inventory, and thus hasten the progression of the transient.

The drain rate (leak-HPI flow rate imbalance) is gradually increased as the test progresses. The drain rate is to be increased from approximately 50 to 100 lbm/h at 3 h, and from 100 to 150 lbm/h for the final half hour of testing. The drain rate schedule is given in Table 3.2. The drain rate is increased to ensure that the transient events of interest are observed while traversing them as slowly as practical. The final inventory is expected to obtain pool BCM (with a 31.6-ft secondary level), as indicated in Table 3.4. The diversion of loop fluid to the pressurizer, or PORV discharges, will augment the imposed loop fluid inventory reductions.

The HPI flow rate is to be readjusted periodically to reattain the desired imbalance. The interval between HPI adjustments should be approximately 15 minutes. When adjustments are required, and when the drain rate is being increased between draining phases (Table 3.2), the change is to be made gradually rather than abruptly to minimize the impact of the adjustment itself. An adjustment duration of about 1 to 2 minutes is appropriate.

3.3.4. Measurement Requirements

Measurements are to be recorded at intervals of 10 seconds (or less) throughout each test, from pre-test steady state through termination. The instrument requirements are specified in Appendix F of Reference 5.

3.4. Test Matrix

Table 3.1 lists the Mapping Tests and contains six variables: pressurizer status, core power, leak configuration, RVVV status, steam generator (secondary) level, and RCP status. The "Leak Configuration" column of Table 3.1 lists the leak size and location. The leak size sets the HPI-leak energy removal capacity, rather than the rates of inventory loss and initial depressurization. This arrangement is used because the HPI head-flow characteristics are not to be applied in the Mapping Tests. Rather, the HPI flow rate is set to the leak flow rate to obtain steady state, and subsequently reduced to effect a draining rate (Tables 3.2 and 3.5) equal to the difference between the leak and HPI flow rates. The significance and settings of each of these inter-test variables are described in the subsections that follow.

3.4.1. Nominal Mapping Test 3 (300300)

The Nominal Mapping Test is to be conducted at 3.5% core power (plus 0.4% to compensate for losses to ambient, as discussed in Appendix D of Reference 5). The nominal leak size of 5-cm^2 will discharge about 600 lbm/h initially and 450 lbm/h as the primary system depressurizes to saturation. The HPI flow rate will be adjusted to approximately equal to the leak flow rate during stabilization periods and reduced by about 10% to gradually reduce the total primary system fluid inventory (the drain rates and timing are specified in Table 3.2). The heatup of HPI from its injection temperature (~90F) toward saturation and its subsequent discharge out the leak will remove energy from the primary system at a rate that is equivalent to about 3% of scaled full power. Core power is thus expected to exceed HPI-leak cooling with these nominal settings. The excess vapor generated in the core must traverse the hot leg. Primary repressurizations are expected to occur during periods of interrupted flow. Such repressurizations will force loop liquid

into the pressurizer and will thus accentuate the effects being produced by the controlled and deliberate reduction of primary inventory.

The primary may repressurize to the PORV actuation point in this test or in subsequent tests. PORV control is to be left unaltered, the PORV will actuate at 2350 psia and reset at 2300 psia. Such an actuation will again augment the controlled reductions of primary inventory.

3.4.2. Isolated Pressurizer Test 1 (300101)

The pressurizer gains inventory during primary repressurization and vice versa. This pressurizer behavior tends to dampen primary pressure variations both directly, due to its surge-tank behavior, and indirectly by its impact on the loop events. For example, an interruption of loop flow may be offset by BCM heat transfer if the pressurizer insurge is sufficient to expose a steam generator condensing surface. A BCM depressurization may be weakened as the fluid drawn out of the pressurizer tends to recover the condensing surface. These pressurizer functions are of interest to the mapping effort, but equally important is the ability to be able to examine the integral-system interactions without the complicating effects of the pressurizer. Test 1 performes this function. The system is to be initialized as usual, with the pressurizer in service. As shown in the test phases listed in Table 3.2, the stabilization and steady-state phases are to be performed as usual. Following the 10 minutes of steady-state data, manually deenergize the pressurizer main heaters and isolate the pressurizer just after the start of the first drain. Caution: If the primary system repressurizes to 2350 psia, abort the test and take the appropriate measures to reduce primary pressure.

3.4.3. Increased Leak Size Test 0 (300001)

A 10-cm^2 leak is used in Test 0, rather than the 5-cm^2 leak used in the Nominal Test. The HPI-leak condensation capacity now exceeds core power and the vapor flow up the hot leg should be greatly reduced from that of the Nominal Test. Separation at the HLUB should occur more readily, the system (liquid) inventory at the first flow interruption should be increased, and the primary may not repressurize after flow interruption.

3.4.4. No HPI-Leak Cooling Test 4 (300423)

HPI is not activated and a leak is not opened (initially) in Test 4. The reduced core power, 1% plus losses to ambient, is almost equal to the excess of core power over HPI-leak condensing capacity in the Nominal Mapping Test (300300). The absence of HPI in this test (300423) will alter the system fluid temperatures and may promote lower-elevation voiding.

The drain schedule of Table 3.2 does not apply to Test 4. The HPI is to remain inactive in Test 4; the gradual reduction of the loop fluid inventory is to be accomplished by opening a scaled 1-cm^2 leak (in the lower downcomer-to-reactor vessel line) after 10 minutes of steady-state data have been acquired. Use the reactor vessel upper head vent if necessary. The rate of inventory loss will be about 60 lbm/h. Continue with this configuration until 3.5 h, then simultaneously close the 1-cm^2 leak and open the 2-cm^2 lower downcomer-reactor vessel leak. Continue testing until 4.5 h. The final inventory (due only to the imposed draining) will be the same as that in the other Mapping Tests with the RCPs turned off.

3.4.5. RVVV Closed Test 5 (300504)

The RVVVs are kept (manually) closed in Test 5. Vapor flow up the hot leg is maximized. Two-phase natural circulation will be sustained as will be the delay (in terms of system inventory depletion) of flow interruption. But the downcomer fluid will be unheated by steam vented from the RVVV so that a restart of loop flow will subcool the core region fluid. The primary may repressurize relatively rapidly during a sustained flow interruption, but loop flow may not interrupt.

3.4.6. Imbalanced Steam Generator Levels Test 6 (300605)

Unequal steam generator secondary levels are to be maintained throughout Test 6. Use a minimum level (~5 ft) in steam generator A and 31.6 ft in steam generator B, both with constant steam generator level control. This imposed secondary asymmetry will propagate to the primary system. In particular, pool BCM will occur in loop B while it is precluded by the low steam generator secondary level in loop A.

3.4.7. Minimum Steam Generator Level Test 7 (300705)

Mapping Test 7 uses a minimum steam generator secondary level of approximately 10 ft. AFW effects are highlighted by minimizing the pool height. Forward loop flow in single-phase circulation will be sustained only with (high elevation) AFW cooling (the elevation of the steam generator secondary pool is below that of the core mid-height). The BCM will be most affected by this change, but the characteristics of intermittent primary circulation may also be altered. Increase the primary system drain rate as required.

3.4.8. RCPs On Test 8 (300806)

Mapping Test 8 uses forced flow. Two-phase circulation will be greatly prolonged. The transport of primary vapor to the steam generators should obtain BCM heat transfer immediately upon the saturation of the loop fluid. The customary flow interruption events are delayed until the pump cavitates. An accelerated drain schedule is used for this pumps-on test to ensure that the requisite relatively large inventory reductions will be attained during the test. This schedule is given in Table 3.5.

This pumps-on Mapping Test would ideally be performed concurrently with the other Mapping Tests and at the full-scaled forced flow rate. The primary flow rates must be measured throughout this test. Thus, the test must be scheduled after the loop has been reconfigured for forced flow.

3.4.9. Cold Leg B1 Discharge Leak Test 9 (300903)

Test 9 uses the cold leg B1 discharge leak site that corresponds to the location used during most of the MIST Transient Tests. This test will introduce the effects of the asymmetric leak location on loop performance. The resulting dissimilarities between loops may render analysis more difficult, nevertheless, this test will be useful when applying the results of the symmetric-loop tests to the usual MIST transients.

3.5. Acceptance Criteria

- At least 10 minutes of steady-state data are recorded at the specified initial conditions.
- The specified boundary system control settings are maintained throughout each test.

- The drains (reductions of total primary fluid inventory by adjusting the HPI flow rate) are performed as scheduled and as specified. Actual and specified times agree to within 1 minute, and actual and specified drain rates agree within 50%.

  The precise amount of leak-HPI flow rate imbalance is not critical, as discussed in section 3.3.1. Establishing and maintaining a drain rate that is about ($\pm$50%) equal to that specified is preferable to continuously or repeatedly adjusting the HPI flow rate. The acceptance criterion of $\pm$50% was selected to provide operator flexibility while retaining the gradual draining concept of the tests.

- Data are recorded at intervals of 10 seconds or less throughout each test. The critical measurements specified in Appendix F of Reference 5 apply.

Table 3.1 Group 30 Mapping Test Matrix

		PZR Status* --	Core Power** (%)	Leak Configuration, Size (cm^2)/Location***	RVVV Status**** --	Steam Generator Level (ft)*****	RCP Status --
Settings	1	Unisolated	3.5	5/DC	Automatic	31.6	Off
	2	Isolated	1	10/DC	Closed	A=min, B=31.6	On
	3	--	--	0	--	Minimum	--
	4	--	--	5/B1-CLD	--	--	--
Setting Tolerance		NA	0.05	NA	NA	*	NA
Test Number							
3	300300	*	*	*	*	*	*
1	300101	**					
0	300001						
4	300423		**	***			
5	300504				**		
6	300605					**	
7	300705					***	
8	300806						**
9	300903			****			

*PZR status 2, isolated: Isolate the PZR after the steady state, at the beginning of the first drain.

**Augment core power by 0.4% to offset losses to ambient (cf. Appendix D).

***Leak configuration "DC" denotes the lower reactor vessel-downcomer leak site. As discussed in the text, the imposed leak size determines the HPI-leak heat removal capacity rather than the rate of inventory loss. The "0" setting uses scaled 1-cm^2 and 2-cm^2 leaks to effect the drain, as discussed in section 3.4.5.

****The "automatic" RVVV settings are 0.125 and 0.04 psi to open and close, with control in automatic/independent.

*****The 31.6-ft steam generator level corresponds to 95% on the Operate Range. "Minimum" denotes the lowest steam generator secondary level while retaining stable steam generator control. All use high-elevation AFW injection with AFW at 110 $\pm$ 20F. Setting "2" uses constant steam generator level control with steam generator A at the minimum level and steam generator B at 31.6 ft.

Table 3.2 Mapping Test Sequence With RCPs Off

The listed rates and drained amounts are approximate; a fluid density of 50 lbm/ft^3 has been used. "Draining" is accomplished by adjusting the HPI flow rate to obtain an imbalance between the leak and HPI flow rates. The "Amount Remaining" entries include only draining -- PZR refill or PORV actuation will obtain actual loop fluid inventories below those listed. See text for testing details. This table does not apply to Test 4 (0 leak) and Test 8 (RCPs in Operation).

	Test Phase	Time		Drain Rate			Amount Drained Per Phase		Amount Remaining After Drain	
		Start	End	Duration	lbm/h	ft^3/h	lbm	ft^3	lbm	ft^3
0	Pre-test stabilization	-30 min	"0"	30 min	0	0	0	0	900	18
1	Pre-test steady state	0	10 min	10 min	0	0	0	0	900	18
2	Drain									
	2a: 50 lbm/h	10 min	3 h	2.8 h	50	1	140	2.8	760	15.2
	2b: 100 lbm/h	3 h	4 h	1 h	100	2	100	2.0	660	13.2
	2c: 150 lbm/h	4 h	4.5 h	0.5 h	150	3	75	1.5	585	11.7

Table 3.3 Conditions, Mapping Tests (Group 30)

Quantity	Initial Conditions Specification	Maximum Deviation	Control During Testing
PRIMARY			
Core power, %	(cf. Table 3.1)	0.05	Constant at initial value.
Pressure, psia	1750	25	No control, allowed to vary. (Pressurizer main heaters deenergized.)
Pressurizer level, ft (within PZR)	2.5	0.2	No control, allowed to vary.*
SECONDARIES			
Pressure, psia	1010	10	Constant
Level, ft	(cf. Table 3.1)	1	Same as initial, constant level control.

NOTES

- Maintain the PORV in automatic overpressure control mode with setpoints 2350 and 2300 psia to open and reclose.
- Maintain the RVVV control mode status specified in Table 3.1.
- Use no primary vents or NCG injections.
- Maintain the RCPs as specified in Table 3.1.
- Maintain constant core power and steam generator controls (all as specified per test in Table 3.1).
- Maintain the specified leak configuration.
- The CFT will not be used.
- Maintain high-elevation AFW injection (minimum-wetting nozzle, AFW at 110 ± 20F).
- Maintain the guard heaters in operation with automatic control.

*The PZR heaters will trip on low level.

Table 3.4 Estimated Loop Fluid Volume Versus Condition

The volume difference between the "max" and "min" entries represents the contributions due to upper reactor vessel and downcomer voiding and the maximum fluid density difference between the hot legs and steam generators. The pressurizer has been assumed to remain empty; cold leg voiding has been ignored.

Condition	Volume	
	max	min
Initial, pressurizer level = 2.5 ± 0.2 ft	18.01	
Saturated loop (pressurizer drained)	17.53	
Interrupted flow, steam generator primary level @ UTS	17.5	14.6
Steam generator level at secondary (31.6 ft)	14.6	12.1

Table 3.5 Mapping Test Sequence With RCPs Operating (Test 8)

The listed rates and drained amounts are approximate; a fluid density of 50 lbm/ft^3 has been used. "Draining" is accomplished by adjusting the HPI flow rate to obtain an imbalance between the leak and HPI flow rates. The "Amount Remaining" entries include only draining -- PZR refill or PORV actuation will obtain actual loop fluid inventories below those listed. See text for testing details.

	Test Phase	Time		Drain Rate			Amount Drained Per Phase		Amount Remaining After Drain	
		Start	End	Duration	lbm/h	ft^3/h	lbm	ft^3	lbm	ft^3
0	Pre-test stabilization	-30 min	"0"	30 min	0	0	0	0	900	18
1	Pre-test steady	0	10 min	10 min	0	0	0	0	900	18
2	Drain									
	2a: 50 lbm/h	10 min	1 h	0.8 h	50	1	40	0.8	860	17.2
	2b: 100 lbm/h	1 h	2 h	1 h	100	2	100	2.0	760	15.2
	2c: 200 lbm/h	2 h	3 h	1 h	200	4	200	4.0	560	11.2
	2d: 300 lbm/h	3 h	4 h	1 h	300	6	300	6.0	260	5.2
	2e: 400 lbm/h	4 h	4.5 h	0.5 h	400	8	200	4.0	60	1.2

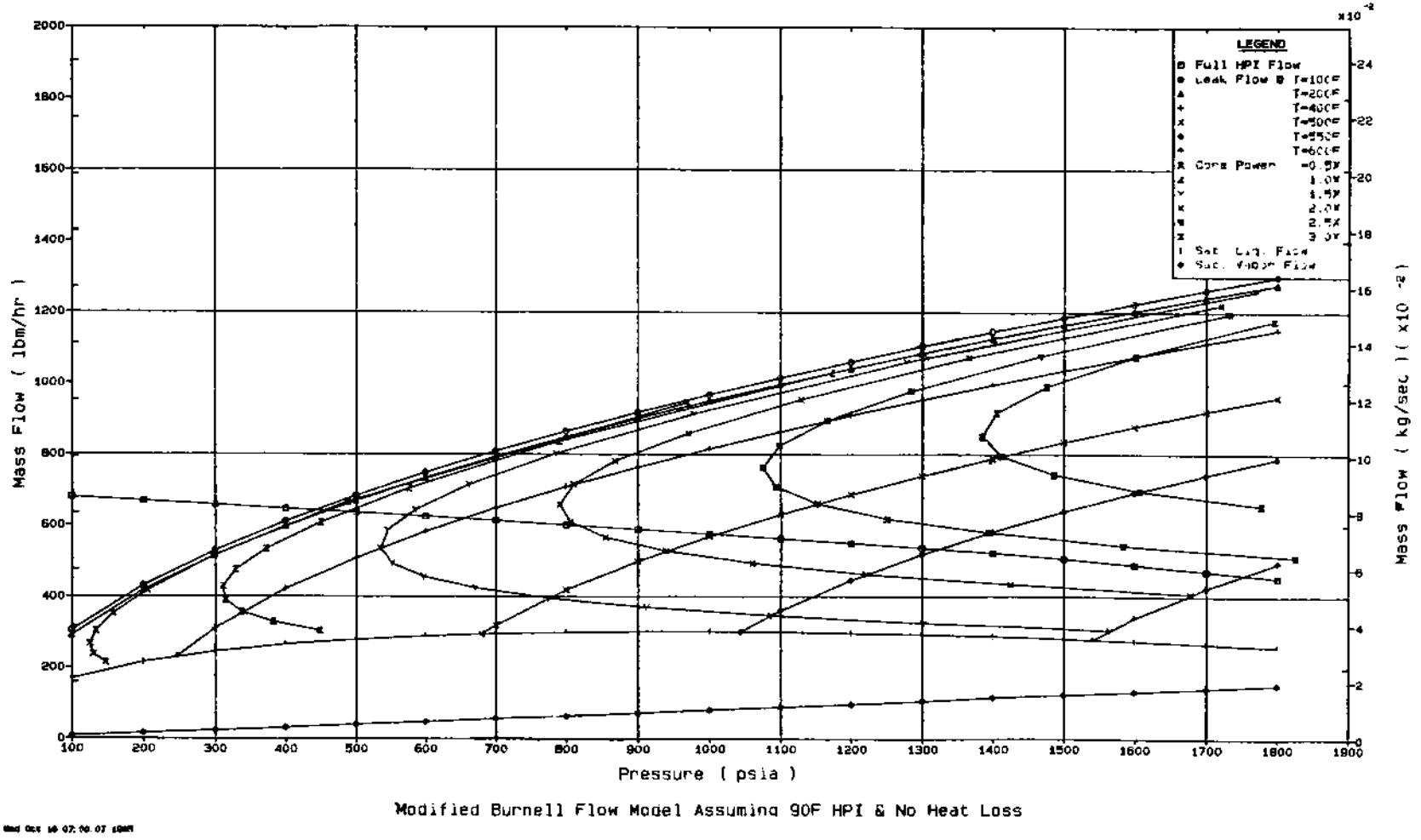

Figure 3.1. MIST Equilibrium Plot for a 10-cm^2 Leak

4. PERFORMANCE

The acceptability of each of Test 300001, 3001BB, 3003AA, 3004CC, 300504, 300605, 3007CC, 3009AA, and 300806 was determined by examining both the conduct of the test and the performance of the measurement systems. The acceptance criteria for each test were defined in the corresponding test procedure, which was based on MIST Test specifications.[5] Any condition, action, or measurement that did not meet the acceptance criteria was evaluated for its impact on test acceptability. The tests reported herein are only those that were determined to be acceptable. Any specific deviations of these tests from the acceptance criteria are described in this section.

The review of test conduct included the following checks for each test:

- o System conditions and stability just prior to test initiation
- o Sequence and timing of the test initiation actions
- o Performance of the manual and automatic control functions
- o Test termination criteria and the sequence of actions

The impact of out-of-specification conditions or actions was assessed. The deviations of those tests that were determined to be acceptable are described in Section 4.1.

The following pre-test and post-test data qualification checks were performed for each test:

- o The acquisition of the critical measurements
- o The operation of the measurement systems within their calibrated range of operation
- o The acquisition of instrument readings within their expected range of operation

- o Self-consistent measurements, considering both comparable measurements and derived quantities

The appropriate measurement uncertainty was used to assess the individual measurements. The impact of the individual out-of-specification conditions was assessed. The deviations of the critical measurements of those tests that were determined to be acceptable are noted in Section 4.2.

4.1 Conduct

All the tests specified were acceptable as performed. All initial conditions were acceptable except as specified in Section 4.1.1. Test initiations and terminations were acceptable. Operation of the control systems and manual interactions during the test transients were acceptable for all the tests except as noted below and discussed in Section 4.1.3.

In Tests 300001, 3001BB, 3004CC, 300504, 300605, 3007CC and 3009AA, during periods with the steam generator secondary decoupled from the primary, one or both steam generators depressurized below the control set point of 1010 psia. This was caused by leakage through the steam control valves. The event did not impact the acceptability of these tests.

During Tests 3001BB and 300605, the reactor vessel downcomer leak orifice plugged and interrupted the draindown schedule but did not impact test acceptability. In Test 300605, a backup leak was used for the remainder of the test.

Tests 3007CC and 3009AA were aborted prior to achieving pool boiler-condenser mode of heat transfer. Test 3007CC was aborted when the high fluid temperature in the core tripped core power at 130 minutes, and Test 3009AA was terminated at 236 minutes, as a result of manual actuation of the PORV due to excessive primary pressure.

In Test 300806, data from many critical differential pressure transmitters were not acquired during most or all of the test duration. These transmitters had to be valved out of service during the RCP forced circulation to prevent damage to the transmitters. Five guard heater control differential temperature measurements were failed, however, a control scheme modification for these zones accommodated the failures. The pressurizer surge line fluid

temperature measurement was failed, and the initial surge line temperature was set by applying a fixed guard heater power for that zone during the pre-test steady state period.

4.1.1 Initial Conditions

Initial conditions for the tests were defined by the governing test procedure, ARC-TP-713, and are repeated in Table 4.1.1 along with the actual values from each test. All initial conditions were met except for the steam generator secondary pressures, pressurizer surge line fluid temperature and the time rate of change of the A steam generator inlet primary fluid temperature (P1RT01) in Test 300001; pressurizer surge line fluid temperature in Tests 3001BB, 3003AA, and 300504; and pressurizer surge line fluid temperature and feedwater temperature in Test 3009AA.

In Test 300806, the reactor coolant pumps were running during the steady state period, which had contributed to the failure to meet three of the steady state criteria imposed on the initial conditions. The pressurizer level was oscillating by about 0.6 ft/h, but the maximum slope during the oscillations was about 0.9 ft/h. H2RT01 and P1RT02 were oscillating, and both had a maximum slope of 3.4 F/h, although the general trend of the data was within $\pm$ 3F/h. The pressurizer surge line fluid temperature initial condition was not met, since the surge line fluid temperature measurement (PZTC01) was failed.

The failing initial condition values for the group 30 tests are underlined in Table 4.1.1 to aid in their identification. These deviations did not impact test acceptability.

4.1.2 Test Initiation

The initiation actions in all the tests were acceptable as performed. At the start of all the tests, with the exception of 3004CC, HPI and leak flow rates were in equilibrium as required. Test initiation was triggered by reducing HPI flow to within 50 lbm/hr of leak flow. During test 3004CC, the HPI was not used. As a result, there were no leak/HPI actions required to initiate this test.

In all the tests, with the exception of Test 3001BB and 300806, the pressurizer heaters tripped shortly after test initiation on low level as

required. The pressurizer collapsed water level at time of heater trip was between 20.0 to 20.8 ft. Test 3001BB was performed with the pressurizer isolated as required. In Test 300806, the pressurizer main heaters tripped off on low pressurizer level of 19.4 ft.

4.1.3 Control During Testing

The performance of automatic control systems and manual interactions during the test transients is described in this section. The controls for high pressure injection, core flood tank, pressurizer main heaters, auxiliary feedwater to steam generators A and B, core power, pilot operated relief valve, steam pressure control, level control for steam generators A and B, reactor coolant pump, leak and vent system performed acceptably for all the tests in this group except as noted in the following text.

Steam Generator Secondary Level Control

Steam generator constant level control was used in all the tests. Constant level control was performed to maintain both steam generator levels at 31.6 $\pm$ 1 ft during Tests 300001, 3001BB, 3003AA, 3004CC, 300504, 3009AA, and 300806, generator A at 10 ft and generator B at 31.6 ft during Test 300605, and both generators at 10 ft during Test 3007CC.

Steam generator A and B constant level controls performed acceptably in all the tests. Steam generator levels were maintained within the desired control tolerance except for isolated deviations. These deviations occurred in all the tests during periods of loop transients that subjected the steam generators to rapid changes in heat transfer load. These deviations were relatively short in duration, and small in magnitude. The longest deviation occurred during Test 3001BB and lasted for about 10 minutes. The largest deviation occurred during Test 300605 where the level in generator B decreased 6.2 ft below the desired control tolerance.

Steam Pressure Control

Performance of steam pressure control was examined using the steam generator secondary pressures, S1GP01 and S2GP01. The steam pressure in both generators was to remain constant at 1010 $\pm$ 10 psia during the entire transient in all the tests.

The steam pressure control performed well during periods of primary-to-secondary heat transfer in the steam generators, and only isolated deviations occurred below and above the control tolerance during these periods. However, during periods when the steam generator secondary was decoupled from the primary due to the absence of heat transfer, leakage through the steam control valves resulted in depressurization of the steam generators below the control tolerance. This depressurization occurred for both steam generators in Tests 300001, 3001BB, 3004CC and 3007CC; in steam generator B in Tests 300504 and 3009AA; and in steam generator A in Test 300605. A maximum depressurization rate of 150 psi/hr occurred in generator B during Test 300504. In Test 300806, the secondary pressures were maintained between 1000 and 1020 psia for the entire test, as expected.

Steam Generator Auxiliary Feedwater

During all the tests in this group, the auxiliary feedwater responded to the secondary level control as required, and head/flow control did not apply. Feedwater control was acceptable in all the tests.

Pilot-Operated Relief Valve (PORV)

In Tests 300001, 3001BB, 3003AA, 3004CC, 300504, and 300806, primary pressure remained below the 2350 psia actuation pressure and the PORV remained closed, as required. During Tests 300605, 3007CC and 3009AA, however, the PORV opened. The PORV control was acceptable in Test 300605. The control anomalies in Tests 3007CC and 3009AA are described in the following paragraphs.

During Test 3007CC, the PORV opened three times. At 77 minutes, the PORV was manually actuated at a primary pressure of about 2310 psia. Following this action, the PORV was automatically opened at about 84 and 122 minutes at a primary pressure of about 2310 psia. This pressure was 40 psia below the desired pressure of 2350 psia. However, this difference did not impact test acceptability.

During Test 3009AA, the PORV did not automatically open when the primary loop pressure increased to the actuation pressure of 2350 psia. The PORV was manually opened when primary pressure reached 2384 psia. This action defined the time of test abortion. Although performance of the PORV control was not acceptable, a repetition was not warranted and this test was acceptable as

performed.

High Pressure Injection (HPI)

As required, HPI was used in all the tests except 3004CC. In Tests 300001, 3001BB, 3003AA, 300504, 300605, and 3009AA, the HPI was to be manually throttled to establish a leak/HPI flow rate imbalance of approximately 50 lbm/hr (± 50%) for 2.8 hours, 100 lbm/hr for 1 hour, and 150 lbm/hr for 0.5 hour. In Test 3007CC, leak/HPI imbalance was to be established initially at 300 lbm/hr until hot leg flows interrupted, then 100 lbm/hr for 2 hours, and then 200 lbm/hr until pool boiler condenser mode was established in either steam generator. In Test 300806, the leak/HPI imbalance was to be maintained at 50, 100, 200, 300, and 400 lbm/hr for 50, 60, 60, 60, and 30 ± 1 minutes, respectively.

Manual control of HPI was satisfactorily performed during all the tests. The leak/HPI imbalance was achieved on schedule for each rate desired by decreasing HPI flow. The imbalances were manually controlled to the best of the operator's ability, but this frequently resulted in the imbalance being no better than ± 50 to 100% of the desired.

From 203 to 229 minutes in Test 3001BB and 132 to 162 minutes in 300605, the control of leak/HPI imbalance was impaired by the partial plugging of the leak orifice. This event did not impact test acceptability.

During Test 3009AA, the 50 lbm/hr leak/HPI imbalance was interrupted at 168 minutes by two-phase flow out of the leak. This reduced the leak flow rate. To compensate, HPI was reduced. However, loop transients prevented the operator from regaining the desired imbalance until the test was aborted at 236 minutes. Imbalances of 100 and 150 lbm/hr were not performed in this test due to the early test abortion.

In Test 300806, The 400 lbm/hr imbalance was not achievable because the HPI had already been shut off to achieve the 300 lbm/h imbalance.

Core Flood Tank

The core flood tank was isolated and not used for all the tests in this group, as required.

Pressurizer Main Heaters

In all the tests with the exception of 3001BB, the pressurizer main heaters were tripped off on low pressurizer level at test initiation and the control for pressurizer main heater power (PZWM04) was manually set to zero power as required. For Test 3001BB, the pressurizer was isolated and no control action was required.

Core Power

For all tests except Test 3004CC, the core power was specified to be 128.7 $\pm$ 1.65 kW for the entire test, except 3004CC, in which core power was constant at 46.2 $\pm$ 1.65 kW.

The core power was acceptably controlled and remained within the control tolerance in all the tests in this group with the exception of 300605 and 3007CC. In Test 300605, the core power was manually shut off at about 149 minutes (lasting for 30 seconds) to regain facility pressure control. During Test 3007CC, the core power control remained constant until 130 minutes when it was automatically tripped due to high fluid temperature. This event defined the test abortion and beginning of test termination activity. Test acceptability was not impacted in either test.

Reactor Coolant Pump Operation

The reactor coolant pumps were only required for Test 300806. In this test, the pumps ran at 100% speed for the entire test, as intended.

Reactor Vessel Vent Valve Control

The reactor vessel vent valves (RVVVs) were set to automatic "independent" control mode for all tests except 300504 and 300806. For these two tests, the RVVVs were manually closed, as intended, for the entire test.

Leak and Vent System Control

For all tests in this group, all leaks and vents were actuated in accordance to the test procedure. The hot leg vents and the reactor vessel upper head vent were used to remove voids from the primary loop following test termination. Listed below are the measured throat diameter of the leaks used in MIST group 30 tests:

Test	Leak Site	Leak Size	Throat Diameter
3009AA	B2 Cold Leg Discharge	5-cm^2	0.0325 inch
3003AA	RV lower Downcomer	5-cm^2	0.0348 inch
3007CC	RV lower Downcomer	5-cm^2	0.0348 inch
3001BB	RV lower Downcomer	5-cm^2	0.0348 inch
300504	RV lower Downcomer	5-cm^2	0.0348 inch
300605	RV lower Downcomer	5-cm^2	0.0348 inch
300806	RV lower Downcomer	5-cm^2	0.0348 inch
300001	RV lower Downcomer	10-cm^2	0.0491 inch
3004CC	RV lower Downcomer	1-cm^2	0.0156 inch

4.1.4 Termination

Test termination activities for all the tests in this group were specified to be based on either an elapsed time of 4.5 hours after start of data save or the occurrence of pool boiler-condenser mode (BCM) heat transfer in either steam generator.

Test termination activities were acceptable for all the tests in this group. Tests 300001, 3001BB, 3003AA, 3004CC, 300605 and 300806 were terminated when pool BCM heat transfer was reached on either or both steam generators. Test 300504 was terminated based on a maximum elapsed time of 4.5 hours. Test 3007CC was terminated when the core power was tripped due to high fluid temperature. Test 3009AA was terminated due to high primary pressure (2384 psia) by manually opening the PORV. Termination of Tests 3007CC and 3009AA occurred prior to achieving pool BCM heat transfer. This did not impact test acceptability in either test. In all cases, the loop was refilled and the reactor vessel upper head void was removed prior to termination of saving data, except for Test 300806. In this test, the reactor vessel head vent was not completely vented before saving data was terminated.

4.2 Instruments

Each of the nine tests in the Group 30 series used a common set of instrumentation. The critical instruments in this set are defined in Table 4.2.1. The instrument measurements were performed by computer-automated data qualification activities and manual examination of the analysis plots. Data qualification activities for each test in Group 30 were performed at steady state pre-test initial conditions, during the test transient, and after test termination as summarized in the following.

Check	Purpose	Time of Performance		
		Before Test	During Test	After Test
NOREAD	Definition of instruments not acquiring data	x	x	x
ANDCHK	Calibration check of the Analogic data acquisition system	x		x
ZEROS	Zero check of instrument transmitters	x		x
RANGE	Validity of instrument measurement as compared to expected range	x	x	x
CONSIS	Instrument and derived quantity consistency check	x	x	x

As a result of these manual and automatic data qualification checks applied to the measurements and derived quantities in the test data base, the critical instruments identified in Table 4.2.2 were determined to be invalid during all or part of Tests 300001, 3001BB, 3003AA, 3004CC, 300504, 300605, 3007CC, 3009AA. In most instances, there was sufficient redundancy in the group of critical instruments so that the individual failure did not violate the requirements of the Critical Instrument List. In the other cases, the existence of the failed critical instrument did not warrant repeating the test. For the 18 conductivity probes identified by Note 1, the measurement system error was not identified until after the test series was completed. In this instance, the void fraction obtained from the neighboring differential pressure measurement provided sufficient backup except for the reactor vessel probes, RVCP01-04. The absence of these measurements did not warrant repeating the test.

The critical instruments that were not available during all or part of Test 300806 are listed in Table 4.2.3. Twenty-two (22) critical instruments were unavailable without sufficient backup instrumentation as defined in the test procedure. These instruments included 16 differential pressure transmitters that were not valved into service during the test, five guard heater control differential temperatures, and the pressurizer spray line fluid temperature. Most differential pressure transmitters in the primary loop were valved out

of service for much or all of Test 300806 to avoid overranging and damaging them during the RCP forced circulation. Approval to continue testing without the five differential temperatures was obtained through PMG transmittal 566, 606, and 716. The absence of the pressurizer surge line temperature was not as important in this test as for the natural circulation mapping tests, where it was crucial for the surge line fluid temperature control.

Prior to and after completion of the test, a "zero" reading was obtained for all differential pressure and pressure transmitters, mass flowmeters, weigh tank load cells, and reactor core voltage and current measurements. For those critical instruments that failed the zero check (defined in the Immediate Report for each test), the magnitude of the failure was small enough such that measurement performance was not degraded to a condition that warranted test repeat. The instrumentation performance during these tests was fully acceptable based upon this check.

Table 4.1.1
Test Initial Conditions

System	Parameter	VTAB	Units	Desired	Tolerance	Actual Values 300001	3001BB	3003AA	3004CC	300504	300605	3007CC	3009AA	300806
Primary														
	Pressure	RVGP01	psia	1750	±25	1732	1762	1747	1761	1757	1758	1733	1754	1759
	Core power	RVWM20 (test 3004CC at 46.2 KW)	KW	128.7	± 1.65	128.3	128.5	128.7	46.2	128.7	129.4	128.9	128.2	129.5
	Pressurizer level	PZLV20	ft	20.5 and varying less than ±0.6 ft/hr	±0.2	20.5 and steady	20.5 and steady	20.6 and steady	20.7 and steady	20.5 and steady	20.3 and steady	20.6 and steady	20.3 and steady	20.4 ****
	Pressurizer surge line fluid temperature	PZTC01	F	*	±5	PZRF20 -38.0	PZRF20 -35.9	HITC11 +6.6	PZRF20 -24.8	PZRF20 -29.8	HITC11 -4.5	HITC11 -0.3	HITC11 -5.1	was failed **** *****
	Fluid/metal temperatures	**	F	Varying less than 3 F/hr over a 30 min. interval	all acceptable	all except for P1RT02: + 4.5 F/hr	accept.	accept.	accept.	accept.	accept.	accept.	accept.	all acceptable except for H2RT02 and P1RT02 ******
Secondary														
	Pressure	S1GP01 S2GP01	psia	1010	±10	889 872	1014 1016	1012 1015	1016 1016	1015 1016	1013 1013	1013 1014	1014 1016	1009.3 1009.7
	Level	S1LV20 S2LV20	ft	***	±1.0	31.4 31.8	31.6 31.7	31.5 31.8	31.5 31.5	31.6 31.7	9.9 31.5	10.4 10.4	31.5 31.7	30.9 31.1

Table 4.1.1

Test Initial Conditions (cont'd.)

System	Parameter	VTAB	Units	Desired	Tolerance	Actual Values 300001	3001BB	3003AA	3004CC	300504	300605	3007CC	3009AA	300806
	Feedwater temperature	SFRT01	deg F	100	± 20	NA*******	104.2	114.0	100.2	102.5	114.1	109.4	119.3	127.5
		SFRT02		(110 for Test 300806)		NA*******	104.1	114.7	101.1	104.2	119.8	110.6	120.4	128.3

* For Tests 300001, 3001BB, 3004CC and 300504, surge fluid temperature was to be adjusted to obtain subcooling of 22 F (PZRF20 - PZTC01).
For Tests 3003AA, 300605, 3007CC and 3009AA, surge line fluid temperature, PZTC01, was to be adjusted to match hot leg fluid temperature, H1TC11.

** The following fluid and metal temperature measurements were used to define steady state (minimum time interval of 30 minutes without test operator manual control adjustments):

Fluid: H1RT01, H2RT01, P1RT02, P2RT02.
Metal: P1MT01, P2MT01, C1MT04, C2MT04, C3MT04, C4MT04, RVMT24, RVMT25.

*** All the tests were to be initiated with both steam generator levels at 31.6 ft except 300605 and 3007CC. Test 300605 was to be initiated with generator A at 10 ft and generator B at 31.6 ft. Test 3007CC was to be initiated with both generator levels at 10.5 ft.

**** Pressurizer level was oscillating since the reactor coolant pumps were running during the steady state period. The general trend during the 30-minute period before the test was about 0.9 ft/h.

***** PZTC01 was failed. Test 300806 was performed with the reactor coolant pumps running, therefore, the initial condition for the pressurizer surge line temperature is not as important as for the natural circulation tests.

****** H2RT01 and P1RT02 were oscillating and both had a maximum slope of 3.4 F/h, yet the general trend of the data was within ± 3F/h.

******* Not applicable as AFW flow was zero.

Table 4.2.1

Critical Instruments for the Group 30 Test Series

Component	Instrument Type	Critical Instruments	Tests 300806
Reactor Vessel	Ammeter	RVAM01	Same
	Conductivity Probe	RVCP01-04	"
	Differential Pressure Transmitter	RVDP01, RVDP03-09	"
	Differential Temperature	RVDT01-04,23	"
	Pressure Transmitter	RVGP01	"
	Limit Switch	RVLS01-04	"
	Metal Thermocouple	RVMT01-04,23	"
		RVMT05-22 (12 of 18)	"
	Fluid Thermocouple	RVTC01,02,RVTC16-20	"
		RVTC03-15 (9 of 13)	"
		RVTC21-23 (2 of 3)	"
	Voltmeter	RVVM01	
Hot Legs	Conductivity Probe	H1CP01-10 (5 of 10)	Same
		H2CP01-10 (5 of 10)	"
	Differential Pressure Transmitter	H1DP01,04,09-12,14	"
		H2DP01,04,09-12,14,16	"
	Differential Temperature	H1DT01-04	"
		H2DT01-04	"
	Limit Switch	H1LS01,H2LS01	"
	Metal Thermocouple	H1MT01-04	"
		H2MT01-04	"
	Resistance Temperature Detector	H1RT01 or H1TC01,	"
		H2RT01 or H2TC01,	"
	Fluid Thermocouple	H1TC02-09 (5 of 8)	"
		H2TC02-09 (5 of 8)	"
		H1TC10-12 (1 of 3)	"
		H2TC10-12 (1 of 3)	"
		H1TC13-19 (5 of 7)	"
		H2TC13-19 (5 of 7)	"

Table 4.2.1
Critical Instruments for the Group 30 Test Series (cont'd)

Component	Instrument Type	Critical Instruments	Tests 300806
Steam Generator A	Differential Pressure Transmitter	P1DP04,S1DP01,S1DP03	Same
	Differential Temperature	S1DT01-05	"
	Pressure Transmitter	P1GP01,S1GP01	"
	Metal Thermocouple	S1MT01-05	"
	Resistance Temperature Detector	P1RT01,02	"
	Fluid Thermocouple	P1TC01-03,13-16,23-26,	"
		33-36 (10 of 15)	"
		P1TC18,27,28,37,38	"
		(3 of 5)	"
		P1TC09-12,19-22,29-32	"
		(8 of 12)	"
		S1TC01,02,26 (2 of 3)	"
		S1TC03-12 (7 of 10)	"
		S1TC13-23,25 (8 of 12)	"
		S1TC24	
Steam Generator B	Conductivity Probe	S2CP01-12 (6 of 12)	Same
	Differential Pressure Transmitter	P2DP06,S2DP01,S2DP12	"
		S2DP02-11 (5 of 10)	"
	Differential Temperature	S2DT01-05	"
	Pressure Transmitter	P2GP01,S2GP01	
	Metal Themocouple	S2MT01-05	
	Resistance Temperature Detector	P2RT01,02	"
	Fluid Thermocouple	P2TC01-13 (9 of 13)	"
		P2TC14-28 (10 of 15)	"
		P2TC29-43 (10 of 15)	"
		P2TC44-53 (7 of 10)	"
		S2TC01-08,55 (6 of 9)	"
		S2TC09-19 (7 of 11)	"
		S2TC20-33,54 (10 of 15)	"
		S2TC34-53 (13 of 20)	"

Table 4.2.1
Critical Instruments for the Group 30 Test Series (Cont'd.)

Component	Instrument Type	Critical Instruments	Tests 300806
Cold Legs (n=1,2,3,4)	Differential Pressure Transmitter	C1DP01,C2DP01,C2DP09 CnDP02,03,04,06,07,08	CnDP01,02,07,08
	Differential Temperature	CnDT01-03	Same
	Metal Thermocouples	CnMT01-03	"
	Resistance Temperature Detector	CnRT01,02	"
	Fluid Thermocouple	CnTC02	"
		CnTC03-06 (3 of 4)	"
		CnTC07-10 (3 of 4)	"
		CnTC11-14 (3 of 4)	"
	Ammeter	None	CnAM01
	Tachometer	"	CnTA01,02
	Power	"	CnWM01
	Turbine Flowmeter	"	CnTM01
Reactor Vessel Downcomer	Differential Pressure transmitter	DCDP01,02,05-08	DCDP01-03,05-08
	Differential Temperature	DCDT01-03	Same
	Metal Thermocouple	DCMT01-03	
	Resistance Temperature Detector	DCRT01	"
	Fluid Thermocouple	DCTC01-04,	"
		DCTC05-12, (5 of 8)	"
		DCTC13-40 (19 of 28)	"
		DCTC41-46 (4 of 6)	"

Table 4.2.1
Critical Instruments for the Group 30 Test Series (Cont'd.)

Component	Instrument Type	Critical Instruments	Tests 300806
Pressurizer	Differential Pressure Transmitter	PZDP01,02	Same
	Differential Temperature	PZDT01,02	PZDT01-03
	Pressure Transmitter	PZGP01	Same
	Metal Thermocouple	PZMT01,02	"
	Resistance Temperature Detector	PZRT01 or PZTC09	"
	Fluid Thermocouple	PZTC01, 02	PZTC01,02,10
		PZTC04-08 (4 of 5)	Same
	Power Controller	PZWM04	"
	Limit Switches	None	PZLS01
HPI	Differential Pressure Transmitter	HPDP01	Same
	Flowmeter	HPMM01-05	"
	Fluid Thermocouple	HPTC01	"
Single-Phase Vent System	Load Cell	V1LC01,02	Same
	Limit Switch	V1LS01,02	"
		V1LS06 (3009AA only)	None
	Fluid Thermocouple	V1TC02 (3009AA only)	None
	Flowmeter	V1MM01	Same
Leak Enthalpy	Pressure Transmitter	LQGP01 (3009AA only)	None
	Flowmeter	LQMM01 (3009AA only)	None
	Fluid Thermocouple	LQTC01-04 (3009AA only)	None

Table 4.2.1
Critical Instruments for the Group 30 Test Series (Cont'd.)

Component	Instrument Type	Critical Instruments	Tests 300806
Two-Phase Vent System	Load Cell	V2LC01-04	Same
	Limit Switch	V2LS03-06	"
	Flowmeter	V2MM01-03	"
	Fluid thermocouple	V2TC01-04	"
Core Flood Tank	Limit Switch	CFLS01,02 (1 of 2)	Same
Gas Addition	Fluid Thermocouple	GATC02-04 (1 of 3	Same
Feedwater Circuit	Differential Pressure Transmitter	SFDP01-06	Same
	Resistance Temperature Detector	SFRT01,02	"
Steam Circuit	Differential Pressure Transmitter	SSDP01-06	Same
	Resistance Temperature Detector	SSRT01,02	"
	Fluid Temperature	SSTC01,03 (1 of 2) SSTC02,04 (1 of 2)	"
Miscel-laneous	Resistance Temperature Detector Shunt	MSSRF01	Same
	Reference Oven Temperature	MSTC01-07	Same

Table 4.2.2

Critical Instruments Not Available for the Group 30 Test Series

Instrument	Description	300001	3001BB	3003AA	3004CC	300504	300605	3007CC	3009AA	Backup Available
CFLS01	Loop A header isolation valve limit switch			x					x	Yes
C1TC04	Pump suction fluid temperature at 2.36 ft	x	x	x	x	x	x		x	Yes
H1CP01,02	Hot leg fluid conductivity probes	*	*	*	*	*	*	*	*	Yes
H1CP06	Hot leg fluid conductivity probe at 59.72 ft	x	x	x	x	x	x	x	x	Yes
H2CP09	Hot leg fluid conductivity probe at 66.78 ft	x	x	x	x	x	x	x	x	Yes
P1TC09	Generator A primary fluid temperature at 51.06 ft			x						Yes
P1TC30	Generator A primary fluid temperature at 50.58 ft	x	x	x	x	x	x	x	x	Yes
P1TC35	Generator A primary fluid temperature at 39.08 ft	x	x	x	x	x	x	x	x	Yes
P2TC12	Generator B primary fluid temperature at 49.50 ft	x	x	x	x	x	x	x	x	Yes
RVCP01-04	Reactor vessel fluid conductivity probes	*	*	*	*	*	*	*	*	No
RVTC07	Core fluid temperature (mid bundle) at 13.15 ft	x	x	x	x	x	x	x	x	Yes
S1TC04	Generator A secondary fluid temperature at 11.07 ft	x	x	x	x	x	x	x	x	Yes
S1TC16	Generator A secondary fluid temperature at 38.19 ft	x	x	x	x	x	x	x	x	Yes
S1TC19	Generator A secondary fluid temperature at 41.28 ft	x	x	x	x	x	x		x	Yes
S1TC22	Generator A secondary fluid temperature at 47.03 ft						x			Yes
S2TC12	Generator B secondary fluid temperature at 14.27 ft	x	x	x	x	x	x		x	Yes
S2TC13	Generator B secondary fluid temperature at 20.19 ft	x	x	x	x	x	x		x	Yes
S2TC16	Generator B secondary fluid temperature at 26.27 ft	x	x	x	x	x	x		x	Yes
S2TC24	Generator B secondary fluid temperature at 38.19 ft	x	x	x	x	x	x		x	Yes
S2CP01-12	Generator B secondary conductivity probes	*	*	*	*	*	*	*	*	No
V2LC01	Load cell on RVHV/HPV weight tank 1			**						No

Notes:

* Raw data obtained with these conductivity probes can not be processed due to a measurement problem observed after completing these tests.

** Unavailable from 379 to 383 minutes.

Table 4.2.3

Critical Instruments Not Available for Test 300806 Series

Instrument	Description	Periods (1)	Periods (2)	Periods (3)	Backup Available
C1DP01	OTSG-A outlet-PSLP (1) Loop A1 -3.15 to -7.85		x		No
C1DP02	PSLP to RCP inlet-loop A1 -7.85 to 23.46		x		No
C1DP08	RCP to DC nozzle (25.48 or 24.30) to 20.94			x	No
C1DT01	Guard heater zone 1 control-loop A1 2.60	x			No
C2DP01	OTSG-B outlet PSLP (1) Loop B1 -3.14 to -7.83		x		No
C2DP02	PSLP to RCP inlet-loop B1 -7.83 to 23.48		x		No
C2DP08	RCP to DC nozzle (25.49 or 24.30) to 20.94			x	No
C2TC04	Pump suction fluid temperature loop B1 2.39	x			Yes
C3DP02	PSLP to RCP inlet-loop A2 -7.86 to 23.47		x		No
C3DP08	RCP to DC nozzle (25.47 or 24.21) to 20.94			x	No
C3DT03	Guard heater zone 3 Control-loop A2 23.48	x			No
C4DP02	PSLP to RCP inlet-loop B2 -7.87 to 23.48		x		No
C4DP08	RCP to DC nozzle (25.49 or 24.32) to 20.94			x	No
C4DT01	Guard heater zone 1 control-loop B2 2.59	x			No
C4DT03	Guard heater zone 3 control-loop B2 23.47	x			No
C4TC10	Pump discharge rake-loop B2 24.93	x			Yes
DCDP01	Upper downcomer overall fluid DP 15.53 to 24.34		x		No
DCDP02	Lower downcomer overall fluid DP 1.54 to 15.53		x		No
DCDP03	Downcomer circumferential DP @ CL 20.94	x			No
DCDP05	Venturi DP-mid flow range 5.41 to 6.79	x			No
DCDP06	Venturi DP-low flow range 5.41 to 6.79	x			No
DCDP07	Venturi DP-reverse direction 4.04 to 5.41	x			No
DCDP08	Lower Downcomer lower-plenum DP 1.54 to -1.03	x			No
H1CP02	Hot leg fluid conductivity probe 28.54	x			Yes
H1DP01	Hot leg nozzle to U-bend DP 20.94 to 66.65			x	No
H1DP04	Hot leg nozzle range DP 27.92 to 30.20		x		No
H1DP09	Hot leg narrow range DP 62.59 to 64.83	x			No
H1DP10	Hot leg narrow range DP 64.83 to 66.65	x			No
H1DP11	Hot leg narrow range DP 64.83 to 66.65	x			No
H1DP12	Hot leg narrow range DP 62.57 to 64.83		x		No
H1DP14	OTSG-A inlet to U-bend DP 53.10 to 66.65		x		No
H2CP06	Hot leg fluid conductivity probe 59.69	x			Yes
H2CP08	Hot leg fluid conductivity probe 65.65	x			Yes
H2DP01	Hot leg nozzle to U-bend DP 20.92 to 66.61			x	No
H2DP04	Hot leg narrow range DP 27.89 to 30.14		x		No
H2DP09	Hot leg narrow range DP 62.56 to 64.81	x			No
H2DP10	Hot leg narrow range DP 64.81 to 66.61	x			No
H2DP11	Hot leg narrow range DP 64.81 to 66.61	x			No
H2DP12	Hot leg narrow range DP 62.56 to 64.81		x		No
H2DP14	OTSG-B inlet to U-bend DP 53.09 to 66.61		x		No
P1DP04	OTSG-A primary overall DP -3.15 to 53.1		x		No
P1TC30	OTSG-A primary fluid temperature 50.58	x			Yes
P2DP06	OTSG-B primary overall DP -3.11 to 53.09		x		No
P2TC01	OTSG-B primary fluid temperature 50.50	x			Yes
P2TC12	OTSG-B primary fluid temperature 49.50	x			Yes

Table 4.2.3

Critical Instruments Not Available for Test 300806 Series (cont'd)

Instrument		Periods (1)	Periods (2)	Periods (3)	Backup Available
P2TC30	OTSG-B primary fluid temperature 29.25	x			Yes
P2TC35	OTSG-B primary fluid temperature 20.17	x			Yes
P2TC40	OTSG-B primary fluid temperature 14.25	x			Yes
PZTC01	Surge line vertical fluid temperature 27.01	x			No
RVDT01	Core inlet guard heater control DT 1.88	x			No
RVDP01	Overall vessel fluid DP -1.03 to 29.00			x	No
RVDP03	Core top to hot leg nozzle DP 16.77 to 21.25			x	No
RVDP04	Hot leg to RVVV line fluid DP 21.25 to 24.15		x		No
RVDP05	RVVV to top of vessel fluid DP 24.15 to 29.00		x		No
RVDP06	DP control for RVVV 1	x			No
RVDP07	DP control for RVVV 2	x			No
RVDP08	DP control for RVVV 3	x			No
RVDP09	DP control for RVVV 4	x			No
S1TC04	OTSG-A secondary fluid temperature 8.07	x			Yes
S1TC16	OTSG-A secondary fluid temperature 38.19	x			Yes
S2CP04	OTSG-B secondary conductivity probe 30.04	x			Yes

Notes:

(1) These instruments were unavailable for the entire test. The differential pressure transmitters would have been overranged and possibly damaged by the high differential pressures during the RCP forced circulation, so they were valved out of service to prevent damage. Project Management Group approval for a modified guard heater control scheme that did not use C1DT01, C3DT03, C4DT01, C4DT03, and RVDT01 was obtained through PMG transmittals 566, 606, and 716. The pressurizer surge line fluid temperature was not as important as for the other natural circulation mapping tests.

(2) These 18 critical differential pressure transmitters were available, but often overranged, only from 2.1 to 207.6 minutes.

(3) These 16 critical differential pressure transmitters were available only from 178.2 to 207.6 minutes.

5. OBSERVATIONS

The objective of the Mapping Tests was to aid in the identification of the system conditions at the transitions among the early SBLOCA events. For the natural circulation test, these events included saturated and two-phase natural circulation, intermittent circulation, flow interruption, and the boiler-condenser mode (BCM).

The Mapping Tests were performed by traversing the early SBLOCA events slowly with each of the boundary system controls held constant. Only the primary fluid mass was varied during each test by imbalancing the HPI and leak flow rates.

The tests were performed by initializing the primary system in either forced circulation or subcooled natural circulation at 1750 psia with 2.5 ft of liquid in the pressurizer. The steam generator secondary side pressures were to be maintained at 1010 psia.

For the Nominal Test conditions, the core power was 3.5% of scaled full power (plus 0.4% to compensate for losses to ambient), the steam generator secondary level control was constant at 31.6 ft, the reactor vessel vent valves were controlled in the automatic/independent mode, and a scaled 5-cm^2 leak was located in the downcomer-to-reactor vessel crossover pipe (this leak location was chosen to affect the conditions in each loop in a symmetrical manner). The tests were performed by initially balancing the HPI and leak flow rates and then reducing the HPI flow rate to obtain a specified primary system inventory depletion rate.

The Mapping Test Group varied core power, leak configuration, reactor vessel vent valve status, steam generator secondary level, reactor coolant pump status and HPI status. Table 5.1 provides the specified and the actual initial conditions for each of the Mapping Tests performed under natural circulation conditions.

During the conduct of the natural circulation Mapping Tests, the changing primary system conditions that affected the leak flow rate impacted the loop operator's ability to maintain the specified imbalance between the leak and HPI flow rates. Rapid changes in the primary system pressure and the fluid conditions (temperature and phase) at the leak site significantly affected the leak flow rate and the head-flow relationship of the HPI pump. Thus, the loop operator was required to manually change the HPI flow rate to maintain the specified imbalance between the leak and HPI flow rates. Under many circumstances, this imbalance was very difficult to maintain. This difficulty did not appear to affect the overall response of the primary system, however, local phenomena may have been affected.

The Mapping Tests exhibited very similar responses. A brief summary of the key events that were observed to occur in these tests is provided below to aid in the identification of the system conditions at the transitions among the early SBLOCA events. This summary can be used as a guide to identify the key events presented in the more detailed discussions that appear in the Observation Sections for each individual test. The key events in the order of occurrence are as follows:

- Upon the establishment of the leak-HPI deficit, the primary system depressurized to saturated conditions.
- When the reactor vessel upper head began voiding, a slight primary system repressurization trend began.
- When steam was discharged through the reactor vessel vent valves into the downcomer, the reactor vessel vent valves began cycling (open-close) as a result of the pressure in the downcomer and reactor vessel equalizing.
- The primary loop flow responded to the cyclical steam flow through the reactor vessel vent valves (oscillated) and exhibited a decreasing trend.
- As the downcomer level descended toward the cold leg nozzle elevation, counter-current flow occurred at the cold leg nozzles.
- As the upper downcomer region voided down to the cold leg nozzle elevation, the steam flowed backwards into the cold leg discharge pipes and caused a momentary flow interruption followed by the establishment of intra-cold leg flow.

- The backflow of steam into the cold leg discharge pipes caused complete voiding of these pipes and flow interrupted. The cold leg flow interruptions occurred in a sequential manner (generally, the order of cold leg flow interruption was B1, A2, A2, and B2) and at essentially a constant pressure.

- The flow interruption resulted in a heatup of the core region fluid and the primary system repressurized. The repressurization resulted in subcooled fluid in the hot legs.

- The continued heatup of the core region fluid propagated into the hot legs and a hot leg heatup commenced.

- The hot leg and core region heatup resulted in the spillover of fluid at the U-bend and the eventual establishment of a sufficient amount of driving head that resulted in forward loop flow.

- As forward loop flow occurred, the voids in the cold legs collapsed. Colder fluid at a higher flow rate entered the core region and the primary loop driving head decreased, resulting in flow interruption. Thus, intermittent loop flow was established.

- Intermittent flow continued as the primary system pressure remained on an increasing trend.

- Continued loss of primary system inventory, as a result of the leak-HPI deficit, resulted in the establishment of BCM and the primary system depressurized.

- The rapid depressurization caused by the BCM resulted in flashing and superheating steam (caused by metal heat). Superheated steam backflowed into the cold legs, flow interrupted, BCM was terminated and the primary system repressurized.

- BCM was re-established and the primary system depressurized (approached the steam generator secondary side pressure).

The remainder of this section details the response and phenomena observed for the Group 30 tests. Key events and conditions for all the natural circulation Mapping Tests are summarized in Table 5.2.

An overview of the interactions, a description of the pump parameters, and pump performance by phases are provided for the pumps-on Mapping Test.

Table 5.1 Mapping Tests Group 30 Initial Conditions

		Symcified	300SAA Nominal Test	300188 Isolated Pressurizer	3009AA Cold Leg Discharge Leak	300605 Unbalanced Steam Generator Levels	3007CC 10 ft Steam Generator Levels	300504 Closed Reactor Vessel Vent Valves	3006CC Reduced Core Power No HPI	300001 Increased Leak Size
Scaled leak size, cm		5 1 and 2 10	5 --- ---	5 --- ---	5 --- ---	5 --- ---	5 --- ---	5 --- ---	--- 1 and 2 ---	--- --- 10
Leak location*		DC-RV B1 CLD	DC-RV ---	DC-RV ---	--- B1 CLD	DC-RV ---	DC-RV ---	DC-RV ---	DC-RV ---	DC-RV ---
Primary Conditions										
Core power, % full power (1% = 33 kW)		3.9 ± .05 1.4 ± .05	3.91 ---	3.88 ---	3.88 ---	3.96 ---	3.91 ---	3.91 ---	--- 1.39	3.91 ---
Pressure, psia		1750 ± 25	1747	1762	1754	1759	1733	1760	1761	1731
Hot leg inlet temperature, F**	Hot leg A Hot leg B	--- ---	573 573	575 575	574 575	577 577	577 577	572 573	564 564	533 534
Core exit subcooling, F***		---	43	43	42	41	38	46	53	83
Reactor vessel inlet temperature, F****		---	529	530	532	532	532	522	541	480
Cold leg flow rate, lbm/h	Cold leg A1 Cold leg A2 Cold leg B1 Cold leg B2	--- --- --- ---	1545 1528 1555 1535	1600 1574 1482 1454	1563 1538 1600 1559	1354 1344 1455 1629	1407 1391 1400 1381	1673 1644 1697 1666	1226 1204 1205 1203	1284 1262 1309 1307
Leak flow rate lbm/h		---	366	389	365	320	383	390	0	943

Table 5.1 Mapping Tests Group 30 Initial Conditions (Cont'd)

			3003AA	3001BB	3009AA	3006D5	3007CC	3005Q6	3004CE	3000D1
		Specified	Nominal Test	Isolated Pressurizer	Cold Leg Discharge Leak	Unbalanced Steam Generator Levels	10 ft Steam Generator Levels	Closed Reactor Vessel Vent Valves	Reduced Core Power No HPI	Increased Leak Size
HPI flow rate, lbm/h	Nozzle A1	---	99	99	95	87	97	101	0	231
	Nozzle A2	---	99	99	95	87	98	101	0	244
	Nozzle B1	---	98	97	92	83	94	98	0	238
	Nozzle B2	---	99	98	92	86	97	100	0	947
	Total		395	393	374	343	386	400	0	947
Pressurizer level elevation, ft		20.5 ± 0.2	20.5	20.5	20.3	20.3	20.5	20.7	20.6	20.6
Secondary Conditions										
Pressure, psia	Steam generator A	1010 ± 10	1012	1014	1015	1013	1013	1014	1017	882
	Steam generator B	1010 ± 10	1014	1016	1016	1013	1014	1016	1016	863
Level, ft	Steam generator A	31.6 ± 1.0	31.5	31.6	31.5	--	--	31.6	31.5	31.5
		10 ± 1.0	--	--	--	9.9	10.5	--	--	--
	Steam generator B	31.6 ± 1.0	31.8	31.7	31.7	31.6	--	31.7	31.5	31.8
		10 ± 1.0	--	--	--	--	10.4	--	--	--
AFW flow rate, lbm/h	Steam generator A	---	91	97	93	89	90	90	41	0
	Steam generator B	---	80	74	87	102	81	83	35	0
AFW temperature, F*****	Steam generator A	110 ± 20	114	104	119	114	110	103	101	--
	Steam generator B	110 ± 20	115	104	121	120	111	104	101	--
Steam flow rate, lbm/h	Steam generator A	---	83	91	87	78	87	83	36	0
	Steam generator B	---	83	76	88	99	80	81	32	0
Steam temperature, F******	Steam generator A		568	569	570	570	572	567	561	
	Steam generator B		568	569	569	571	571	568	561	

*In the DC-RV, the leak location is in the crossover pipe between the downcomer and the reactor vessel. In the B1 CLD, the leak is located in the sloping portion of the B1 cold leg discharge pipe.

**Values are from the hot leg inlet RTDs.

***Values used the core exit temperature from thermocouple RVTC11 and saturation temperature at the reactor vessel pressure.

****Values are from the downcomer RTD.

*****Values used the AFW RTDs.

******Values used the steam thermocouples.

Table 5.2 Mapping Test Group 30 Test Results Summary

		3003AA	3001BB	3009AA	300605	3007CC	300504	3004CC	300001
		Nominal Test	Isolated Pressurizer	Cold Leg Discharge Leak	Unbalanced Steam Generator Levels	10-ft Steam Generator Levels	Closed Reactor Vessel Vent Valves	Reduced Core Power No HPI	Increased Leak Size
Scaled leak size, cm		5	5	5	5	5	5	1 and 2	10
Leak location		DC-RV*	DC-RV*	B1 CLD**	DC-RV*	DC-RV*	DC-RV*	DC-RV*	DC-RV*
Core power, % full power		3.9	3.9	3.9	3.9	3.9	3.9	1.4	3.9
Steam generator secondary levels A/B, ft		31.6/31.6	31.6/31.6	31.6/31.6	10/31.6	10/10	31.6/31.6	31.6/31.6	31.6/31.6
Minimum pressure attained during the initial depressurization as the primary system saturated, psia		1300	1300	1300	1335	1420	1292	1180	1135
Cold leg flow interruption sequence and primary system pressure when flow interruption occurred, psia		B1/1450 A1/1460 A2/1460*** B2/1460***	B1/1450 A1/1460 A2/1470*** B2/1470***	B1/1440 B2/1520*** A1/1550*** A2/1600	B1/1480*** A1/1480*** A2/1500 B2/1500	B1/1480 A1/1520*** A2/1520*** B2/1575	A1/1400**** A2/1400**** B1/1400**** B2/1400****	B1/1230 A1/1230 B2/1250 A2/1270	B1/1200 A2/1200 B2/1190 A1/1220
Maximum primary pressure attained during the repressurization phase, psia		2225	2290	2380	2350	2310	1770	1940	1570
Number of PORV actuations that occurred		0	0	1	3	3	0	0	0
Primary loop that provided heat transfer via AFW-BCN subsequent to the repressurization phase		A	A	NA*****	B	A and B	A	Did not occur	Did not occur
Primary loop that initially attained pool BCN		B	B	NA*****	B	NA******	B	A	A
Minimum primary pressure attained following BCN (at test termination), psia		1110	1060	NA*****	1120	NA******	1050	1070	1070
Indicated primary system mass, lbm	Initial Final	990 610	965 520	990 800	940 505	973 610	950 597	948 542	1010 590
Test termination time, min		281	319	239	256	130	259	230	318

*Leak is located in the crossover pipe between the downcomer and the reactor vessel.

**Leak is located in the sloping portion of the cold leg B1 discharge pipe.

***Flow interruption occurred essentially simultaneously in these cold legs.

****Transition to pulsating alternate loop flow.

*****Manual PORV actuation occurred. Test terminated prior to the occurrence of this event.

******Core power tripped due to core uncovery which resulted in high core heater rod temperature. Test terminated prior to this event.

5.1. Nominal Mapping Test (3003AA)

The initial drain of the primary system was caused by establishing a leak-HPI flow deficit of ~50 lb/h, i.e., HPI flow was initially equal to the leak flow and was then reduced so that the leak flow exceeded the HPI flow. This drain depleted the pressurizer inventory (Figure 5.1.1, See 1) and primary system pressure decreased (Figure 5.1.2, See 1). The primary system pressure stabilized at ~1300 psia (corresponding to the saturation pressure at the core exit temperature) when the pressurizer inventory was completely depleted.

The primary system continued to lose inventory and the reactor vessel head began to void (Figure 5.1.1, See 2). The voiding of the reactor vessel head resulted in a gradual increase in the primary system pressure (Figure 5.1.2, See 2).

The reactor vessel level continued to decrease and, as it descended to the reactor vessel vent valve elevation, began discharging steam through the open reactor vessel vent valves into the downcomer. The discharge of steam rather than liquid into the downcomer initiated voiding in the downcomer (Figure 5.1.3, See 1). The discharge of steam through the reactor vessel vent valves also decreased the flow rate from the reactor vessel to the downcomer and resulted in a decreased upper downcomer flow rate. This decreased flow rate affected the core inlet conditions as observed by the decreased downcomer flow rate (Figure 5.1.4, See 1) and core inlet temperature (Figure 5.1.5, See 1). The decrease in the core flow rate more than offset the decrease in the core inlet temperature, and the core exit temperature increased (Figure 5.1.6, See 1). Thus, an increased primary system repressurization rate was observed (Figure 5.1.7, See 1).

As the upper downcomer fluid temperature increased (as a result of steam condensation) and the downcomer level descended below the reactor vessel vent valve elevation, the available condensing surface decreased. Therefore, steam flow through the reactor vessel vent valves decreased further and the pressure in the reactor vessel head and the downcomer began to equalize. This pressure equalization resulted in a decrease in the reactor vessel vent valve pressure drop to the close setpoint of 0.04 psi (Figure 5.1.8, See 1) and the reactor vessel vent valves closed (Figure 5.1.9, See 1).

The closed reactor vessel vent valves terminated the reactor vessel-to-downcomer flow and thus decreased the core inlet flow rate to the sum of the four cold leg flow rates. The decreased core flow rate resulted in the increased voiding of the reactor vessel head and primary pressure increased. A pressure imbalance was therefore reestablished between the reactor vessel head and the downcomer, which attained the reactor vessel vent valve open setpoint of 0.125 psi (Figure 5.1.8, See 2), and the reactor vessel vent valve(s) opened (Figure 5.1.9, See 2). The open reactor vessel vent valve(s) relieved steam into the downcomer, the downcomer level decreased, the pressure in the reactor vessel and downcomer equalized again, and the reactor vessel vent valve(s) closed. This phenomenon continued and was demonstrated by the characteristic cycling (Figure 5.1.9, See 3) of the reactor vessel vent valve(s) as the downcomer level decreased.

The cyclical operation of the reactor vessel vent valve(s) resulted in primary loop flow oscillations as flow was alternately discharged through the reactor vessel vent valve(s). The flow oscillations affected the primary fluid temperatures and system pressure, both of which also responded in an oscillatory manner (Figure 5.1.6, See 2 and Figure 5.1.7, See 2). The primary system loop flow was observed to exhibit a decreasing trend as the reactor vessel vent valve(s) continued cycling (Figure 5.1.10, See 1).

The reactor vessel and the downcomer levels continued their decreasing trends during the cyclical response of the reactor vessel vent valve(s). As the downcomer level approached the cold leg nozzle elevation, hot fluid (initially liquid and then steam) entered the cold leg discharge pipes at the top of the pipe. Thus, counter-current flow began occurring in the cold leg discharge pipes. (The occurrence of counter-current flow was determined by the response of the cold leg nozzle thermocouple rakes, Figure 5.1.11, See 1).

The steam that entered the cold leg discharge pipes was exposed to an increased condensation site and was condensed. The cold leg refilled, thus terminating the cold leg condensation site, the reactor vessel head and downcomer pressure again equalized, and the reactor vessel vent valve(s) closed. This phenomenon continued at an increased frequency (Figure 5.1.9,

See 4) as the downcomer level continued on a decreasing trend. The increased frequency of this phenomenon resulted in increased steam flow through the reactor vessel vent valve(s) and into the cold legs. The divergence of more fluid from the reactor vessel to the cold legs resulted in a decreased hot leg flow rate and an increased backflow of steam into the cold leg discharge pipes. Both of these effects impeded forward flow in the cold legs. The reduced hot leg flow (primary loop flow) resulted in a decreased flow rate of colder fluid from the steam generator exit (Figure 5.1.10, See 1). The reduced primary loop flow rate resulted in a decreased downcomer flow rate and an increased core inlet temperature (Figure 5.1.5, See 2) as less colder fluid became available to mix with the fluid discharged through the reactor vessel vent valve(s). These effects resulted in an increased core exit temperature, steam generation, and system pressure, thus discharging more steam from the reactor vessel into the downcomer.

The primary loop flow mixed with the HPI fluid in the cold leg discharge pipes and provided the condensation mechanism for the steam that entered these pipes from the downcomer. As the primary loop flow rate continued decreasing, the ability to condense the steam entering the cold leg discharge pipe from the downcomer also decreased. Eventually, the downcomer level descended to the cold leg nozzle elevation and exposed the entire cross-sectional area of the cold leg pipes to steam. When this event occurred, the reactor vessel vent valves opened and remained open. The condensation sites in the cold leg discharge pipes were insufficient to condense the resulting increased steam flow rate and backflow occurred in all four cold legs. The backflow of fluid in the cold leg discharge pipes was confirmed by the observed fluid temperature responses at the cold leg nozzle thermocouple rakes (Figure 5.1.11, See 2) and the reactor coolant pump discharge resistance temperature detector (RTD) and thermocouple rakes (Figure 5.1.12, See 1 and Figure 5.1.13, See 1). The cold leg nozzle temperatures responded to backflow by increasing in temperature towards saturation as more steam entered the cold leg discharge pipe. The fluid temperatures near the reactor coolant pump initially decreased rapidly (as colder fluid that resided in the pipe between the HPI nozzle and the reactor coolant pump discharge was forced backwards up the cold leg discharge pipe) and then rapidly increased to saturation as steam reached the reactor coolant pump elevation. The backflow

of steam into the cold legs momentarily interrupted forward loop flow in all four cold legs (Figure 5.1.10, See 2 and Figure 5.1.14, See 1). The backflow in cold legs A1 and B1 propagated into the cold leg suction pipe (as observed by the decrease then increase in fluid temperatures, Figure 5.1.15, See 1 and Figure 5.1.16, See 1). When this event occurred intra-cold leg flow was established, i.e., backflow in cold legs A1 and B1 and forward flow in cold legs A2 and B2 (Figure 5.1.10, See 3 and Figure 5.1.14, See 2). The influx of steam into cold legs A1 and B1 resulted in a partial voiding of these cold legs (Figure 5.1.17, See 1 and Figure 5.1.18, See 1).

During the period when cyclical reactor vessel vent valve operation occurred, the hot leg riser and steam generator stub levels also oscillated (Figure 5.1.19, See 1). The steam generator stub levels exhibited a decreasing trend that indicated void formation in the upper portion of the stubs. The hot leg riser levels, however, appeared to remain above the spillover elevation (although the level may be intermittently dropping below the spillover elevation) and steam generator heat transfer (although decreasing) continued through the momentary flow interruption (Figure 5.1.20, See 1 and Figure 5.1.21, See 1).

As the cold legs and the reactor vessel voided (the reactor vessel level dropped below the hot leg nozzle elevation), the hot leg riser levels rapidly increased (full), and the steam generator stub levels gradually increased (Figure 5.1.19, See 2). During this time, intra-cold leg flow was established and apparently, even though the hot leg risers were full, a minimal amount of fluid was flowing up the hot legs and through the steam generator as indicated by the minimal amount of steam generator heat transfer (Figure 5.1.20, See 2 and Figure 5.1.21, See 2). Thus, the major flow path was from the reactor vessel through the reactor vessel vent valves into the downcomer, flowed backwards through one cold leg of each loop, flowed forwards through the other cold leg of each loop, and discharged back into the downcomer and back to the reactor vessel inlet.

The fluid flowing up the hot leg risers spilled over the U-bend and resulted in the gradual increase in the steam generator stub levels. As these levels increased, the elevation driving head increased and primary loop flow, via the hot leg and through the steam generator, was established. The steam

generator stub level of loop B increased faster than that of loop A and primary flow in loop B was established prior to that in loop A (Figure 5.1.14, See 3 and Figure 5.1.10, See 4). Primary loop flow and the order of occurrence was confirmed by the establishment of increased steam generator heat transfer (Figure 5.1.20, See 3 and Figure 5.1.21, See 3), the decrease in the suction pipe temperatures of cold legs A1 and B1 (Figure 5.1.15, See 2 and Figure 5.1.16, See 2), and the collapse of the voids in cold legs A1 and B1 (Figure 5.1.17, See 2 and Figure 5.1.18, See 2).

The flow in cold leg B1 reversed again (Figure 5.1.14, See 4) prior to the complete voiding of the cold leg B1 discharge pipe (Figure 5.1.18, See 3). When the cold leg B1 discharge pipe voided completely (the cold leg B1 suction pipe partially voided), the cold leg B1 flow interrupted (Figure 5.1.14, See 5). During this time, the cold leg A1 flow interrupted for a brief period and then reestablished forward flow. Cold leg A1 continued to flow in the forward direction (as did cold legs A2 and B2) for an additional approximately 17 minutes during which time the cold leg B1 flow was interrupted. The cold leg A1 then was observed to experience backflow again and complete voiding of the discharge pipe, with partial voiding of the suction pipe followed by flow interruption (Figure 5.1.10, See 5). The hot leg riser levels appeared to be above the U-bend spillover elevation when flow interrupted in cold legs B1 and A1 (Figure 5.1.19, See 3 and 4). Primary loop flow was maintained in both loops during and subsequent to the occurrence of flow interruption in cold legs A1 and B1 by means of flow through cold legs A2 and B2. Although forward flow was observed in cold legs A2 and B2, counter-current flow (steam into and liquid out of these cold legs) existed at the cold leg nozzle rakes (Figure 5.1.22, See 1 and Figure 5.1.23, See 1).

The primary system pressure, after decreasing to a minimum value of approximately 1300 psia at loop saturation, gradually increased to approximately 1450 psia when the flow reversals occurred and stabilized at approximately 1460 psia as cold legs A1 and B1 interrupted. The primary system remained at approximately 1460 psia while forward loop flow was maintained in cold legs A2 and B2 (Figure 5.1.7, See 3).

Continued draining of the primary system resulted in increased voiding and decreasing levels in the reactor vessel, downcomer, and the suction pipes of

cold legs A1 and B1 (Figure 5.1.3, See 2, Figure 5.1.17, See 3, and Figure 5.1.18, See 4).

The downcomer fluid temperature near the reactor vessel inlet (DCRT01) increased and attained saturation (Figure 5.1.24, See 1). When the downcomer saturated, a decreased condensing capability resulted. More steam entered cold leg A1 and further voided its suction pipe (Figure 5.1.25, See 1). More steam also entered cold leg A2 as a momentary increase in fluid temperature was observed across the cold leg A2 nozzle thermocouple rake (Figure 5.1.26, See 1). The increased backflow into cold leg A2 impeded forward loop flow in this cold leg (Figure 5.1.27, See 1). The decreased flow rate and saturated core inlet temperature resulted in increased core steam production that was forced up the hot legs. Thus, after the flow decrease was observed in cold leg A2, it was immediately followed by an increase in primary loop flow (Figure 5.1.27, See 2).

The increased primary loop flow was reflected in cold legs A2 and B2, which had been maintaining forward flow, and in cold legs A1 and B1, which had been interrupted (Figure 5.1.27, See 2 and Figure 5.1.28, See 1). The increased cold leg flow rates resulted in the partial collapse of voids in the suction of cold legs A1 and B1, the downcomer, and the reactor vessel (Figure 5.1.25, See 2, Figure 5.1.29, See 1, and Figure 5.1.30, See 1). The collapse of these lower region voids caused the hot leg riser and stub levels to decrease as they rapidly drained toward the reactor vessel (Figure 5.1.30, See 2 and Figure 5.1.31, See 1). The drain of the hot leg risers impeded steam flow up the hot legs; thus, steam was immediately discharged through the reactor vessel vent valves into the cold legs (all four cold leg discharge pipes were completely voided -- Figure 5.1.25, See 3 and Figure 5.1.29, See 2) and primary loop flow was completely interrupted (Figure 5.1.27, See 3 and Figure 5.1.28, See 2).

Total primary loop flow interruption immediately resulted in increased core steam generation, thus voiding the lower regions (reactor vessel, downcomer, and cold legs) and increasing the primary system pressure (Figure 5.1.32, See 1). The rapid voiding of the cold leg A2 and B2 discharge pipes resulted in a rapid increase in the hot leg riser levels (Figure 5.1.33, See 1). The hot

leg riser and stub levels then increased at a lower rate (Figure 5.1.33, See 2) as the reactor vessel and downcomer regions voided (Figure 5.1.34, See 1).

As the primary system pressure increased, the fluid in the hot legs, which was at saturated conditions prior to the pressure increase, became subcooled. Steam that entered the hot legs was therefore condensed in the hot legs and a heatup (progressing from the hot leg inlet upwards) of the hot leg fluid commenced (Figure 5.1.35, See 1 and Figure 5.1.36, See 1). As the hot leg fluid temperatures increased, the liquid expanded and, therefore, the hot leg levels increased (Figure 5.1.33, See 2). The steam generator stub levels also increased during the hot leg heatup (Figure 5.1.33, See 2). The stub levels increased as a result of lower region voiding, which displaced colder fluid that resided in the steam generators upward into the stub region. This action was observed by the decreased fluid temperatures in both stubs (Figure 5.1.37, See 1 and Figure 5.1.38, See 1). As the hot leg heatup continued, the hot leg riser fluid began spilling over the U-bends. The hot leg A riser fluid temperatures increased at a faster rate than those in hot leg B. This faster heatup rate was caused by the presence of the pressurizer in loop A. As the lower regions voided, the primary system pressurized and the pressurizer began to fill (Figure 5.1.30, See 3). The fluid that entered the pressurizer traversed hot leg A from the reactor vessel outlet to the pressurizer surge line nozzle. Thus, a predominant flow path was established that resulted in an increased steam flow into hot leg A. This increased flow rate resulted in a faster heatup of the fluid in hot leg A and resulted in a spillover in loop A prior to one in loop B.

The displacement of subcooled liquid from the hot leg risers over the U-bends and into the hot leg stubs decreased the elevation head in the hot leg risers, thus enhancing the steam flow into the hot leg. The increased steam flow into the hot leg increased the heatup rate, the fluid expansion rate, and therefore the spillover flow rate. The fluid spilling over into the steam generator identified the onset of primary loop flow (small in magnitude) and began collapsing the voids in the cold leg A suction pipes (Figure 5.1.25, See 4). This action was also observed in the suction temperatures of cold legs A1 and A2 (Figure 5.1.39, See 1 and Figure 5.1.40, See 1). The B cold legs did not indicate void collapse or a fluid temperature reduction

during this period (Figures 5.1.29, 5.1.41, and 5.1.42), thus confirming the occurrence of spillover in loop A and none occurring in loop B. As the hot leg heatups continued (at an increasing rate), the primary loop driving head increased and forward primary loop flow occurred in both loops. This occurrence of primary loop flow was of a significant magnitude to collapse all the voids in the four cold legs (Figures 5.1.25, See 5 and 5.1.29, See 3) and caused a partial collapse of the reactor vessel and downcomer voids (Figure 5.1.34, See 2).

The collapse of the lower region voids resulted in the drain of the steam generator primary and a decreased collapsed liquid level in the hot legs (Figure 5.1.33, See 3). These events occurred apparently as a result of flashing liquid to steam in the hot leg risers, which was caused by the pressure reduction when the lower region voids collapsed.

The increased primary loop flow rate resulted in a decrease in the core inlet temperature (Figure 5.1.43, See 1) as primary fluid that was cooled by the heat transfer in the steam generators traversed the cold legs and the downcomer. The reduced core inlet temperature reduced the primary loop driving head sufficiently to cause primary loop flow interruption (Figure 5.1.27, See 4 and Figure 5.1.28, See 3).

Heat transfer was established in the steam generators (Figure 5.1.44, See 1 and Figure 5.1.45, See 1) as both steam generator primary levels decreased below the upper tubesheet (Figure 5.1.30, See 4 and Figure 5.1.31, See 2). The steam generator heat transfer reduced the primary system pressure (Figure 5.1.32, See 2) and some of the core region fluid flashed to steam (Figure 5.1.34, See 3). The loss of primary loop flow permitted steam that resided in the reactor vessel head to be discharged through the reactor vessel vent valves into the downcomer and eventually flashing resulted in backflow into the cold leg discharge pipes, again voiding all four cold legs (Figure 5.1.25, See 6 and Figure 5.1.29, See 4).

The flow interruption again resulted in the repressurization of the primary system (Figure 5.1.32, See 3). The steam generator A primary level had descended and remained well below the upper tubesheet elevation (Figure 5.1.33, See 4), thus a condensation surface was available for the establishment of AFW-BCM. However, AFW-BCM was not established because the repres-

surization, caused by the interruption of loop flow, again resulted in subcooled fluid in the hot leg risers (Figure 5.1.35, See 2 and Figure 5.1.36, See 2), which condensed core region steam in the hot legs.

The lower region voiding, hot leg heatup, level swell, spillover, forward loop flow, lower region void collapse, steam generator primary drain, hot leg flashing, and flow interruption phenomena continued (cyclical response) as the primary system lost inventory. Brief periods of AFW-BCM began to occur (Figures 5.1.44, See 2 and Figure 5.1.45, See 2) during the drain of the steam generator primary. However, the AFW-BCM was not sustaining because of the loss of the natural circulation driving head that interrupted loop flow. When the primary loop flow interrupted, the primary system began to repressurize (as the lower regions voided) which again resulted in subcooled fluid in the hot legs. The primary system was on an increasing pressure trend (oscillating as voids formed and collapsed) and reached a maximum pressure of approximately 2225 psia (Figure 5.1.32, See 4). During this repressurization phase, the pressurizer inventory also increased and attained a level of approximately 28 ft, or 1 ft below being completely full (Figure 5.1.31).

When the steam generator primary levels descended and approached the steam generator upper tubesheet, the previously discussed phenomena were slightly altered due to the existence of a condensing surface in the steam generators. The available condensing surface initiated the AFW-BCM in both steam generators (Figures 5.1.44, See 3 and 5.1.45, See 3). AFW-BCM altered the observed phenomena by the elimination of the spillover event, which was replaced by the release of steam from the hot leg riser subsequent to attaining saturated conditions in the hot legs. When the AFW-BCM occurred, the primary system pressure began a decreasing trend (Figure 5.1.32, See 5). However, the pressure remained oscillatory, as the loss of the natural circulation driving head continued to cause flow interruptions, and the lower region voiding and void collapse phenomena continued. Each of the flow pulses that occurred during this phase of the test indicated a period of forward flow in both cold legs of each loop followed by a period of intra-cold leg flow and then flow interruption (Figure 5.1.27, See 5 and Figure 5.1.28, See 4).

As the AFW-BCM continued in both steam generators, the maximum primary pressure decreased to approximately 2000 psia. At this time, asymmetric loop

responses occurred. AFW-BCM terminated in steam generator B (Figure 5.1.45, See 4) while steam generator A continued in AFW-BCM (Figure 5.1.44, See 4). The loss of heat transfer in steam generator B resulted in an increasing trend of the primary system pressure (Figure 5.1.32, See 6), again oscillating as flow interruption, lower region voiding and the void collapse phenomena continued.

The cause for the loss of heat transfer in steam generator B was not obvious. The combination of a number of condition variations between loops A and B could account for the loss of heat transfer in B rather than in A. However, a predominant flow path appeared to be established again in the loop A. The data indicated that the loop A cold legs voided more than the loop B cold legs (Figure 5.1.25, See 7 and Figure 5.1.29, See 5). As the voiding-void collapse phenomena continued, larger hot leg and steam generator primary level swings were observed in loop A (Figure 5.1.33, See 5), thus a larger condensing surface was exposed in steam generator A during each cycle. The availability of a greater condensing surface in steam generator A appeared to have established a predominant flow path through loop A, initiated AFW-BCM in steam generator A (Figure 5.1.44, See 4), and depressurized the primary system. The depressurization resulted in the flashing of the fluid in hot leg B, and some steam generator heat transfer was observed (Figure 5.1.45, See 5). The decreased steam flow from the reactor vessel to hot leg B therefore resulted in the eventual loss of AFW-BCM in steam generator B.

The increased voiding observed in the A cold legs appeared to be the cause for the establishment of the predominant loop A flow path. Numerous potential reasons for this occurrence exist (heat loss, guard heating in particular near the U-bend, physical geometry of the cold legs, individual HPI flow rates, steam generator secondary controls, etc.) and further investigation may be warranted.

Following the termination of AFW-BCM in loop B, the hot leg riser and the steam generator primary levels in loop B began a decreasing trend (Figure 5.1.33, See 6). The loop A hot leg riser and steam generator primary levels did not exhibit this decreasing trend. The B levels continued to exhibit the oscillatory response characteristic of the lower region voiding-void collapse phenomena. However, since AFW-BCM did not occur in loop B, high flow rates

in the B cold legs did not occur and voids in the loop B cold legs did not collapse (Figure 5.1.29, See 6). The loop A cold leg voids collapsed completely as a result of the continued occurrence of AFW-BCM (Figure 5.1.25, See 8).

The decreasing loop B hot leg and steam generator primary levels, while the levels in loop A remained higher, indicated that loop B inventory was transferred to loop A during the draindown. This event was confirmed by the fluid temperatures in the cold leg B suction pipes and the cold leg B discharge pipe (reactor coolant pump discharge rake), which indicated forward flow during the loop B draindown (See 1 on Figures 5.1.41, 5.1.42, 5.1.46, and 5.1.47).

When the steam generator B primary level descended to the secondary pool elevation (Figure 5.1.48, See 1), pool BCM was initiated in steam generator B. As the feedwater actuated in steam generator B, steam generator heat transfer was established and the primary system rapidly depressurized from approximately 1900 to 1290 psia (Figure 5.1.49, See 1). During this depressurization, inventory was transferred from loop A to loop B, as was evidenced by the decreasing hot leg riser and steam generator primary levels in loop A while loop B levels increased (Figure 5.1.50, See 1).

This depressurization resulted in a pressurizer drain into hot leg A (Figure 5.1.51, See 1), which apparently helped to maintain the AFW-BCM in loop A. The lower region voiding-void collapse phenomena continued in loop A (Figure 5.1.52, See 1), however, steam flow from the core into hot leg A decreased as loop B became active. The reduced flow in loop A eventually resulted in the complete voiding of the cold leg A discharge pipes, and void collapse in the cold leg discharge pipes no longer occurred (Figure 5.1.52, See 2).

As the depressurization continued, all four cold legs indicated superheated fluid conditions within the cold leg discharge pipe. Each cold leg indicated superheated fluid conditions at the top of the cold leg nozzle (e.g., See 1 on Figures 5.1.53 through 5.1.56) and cold legs A1 and B1 indicated superheated fluid conditions near the reactor coolant pump (e.g., See 1 on Figures 5.1.57 through 5.1.60). The superheated conditions at the cold leg nozzles were apparently caused by the metal heat in the upper downcomer as the primary system depressurized (Figure 5.1.61, See 1). As the primary loop

flow decreased and interrupted, superheated steam backflowed into the cold leg discharge pipes and intra-cold leg flow appears to have been established with cold legs A1 and B1 having backflow and cold legs A2 and B2 having forward flow (Figure 5.1.62, See 1 and Figure 5.1.63, See 1). The diversion of core-generated steam into cold legs A1 and B1 resulted in a reduced primary loop flow rate. Thus, a reduction in steam generator heat transfer occurred and the primary system repressurized from 1290 to 1590 psia (Figure 5.1.49, See 2).

During this repressurization, inventory was transferred from the hot leg risers and steam generator primary of both loops to the downcomer, reactor vessel, and the pressurizer (Figures 5.1.48, See 2 and 5.1.51, See 2). The repressurization also resulted in the de-superheating (attained saturated conditions) of the cold legs (See 2 on Figure 5.1.53 through 5.1.61). The increasing pressurizer level indicated that a predominant loop flow path for the core-generated steam was again established in loop A. The fluid conditions in both hot leg risers remained saturated during this repressurization (Figure 5.1.64, See 1 and Figure 5.1.65, See 1), indicating that a sufficient amount of steam flow entered both hot legs to maintain saturated conditions as the system repressurized. The steam flow into the hot legs apparently maintained either saturated liquid or two-phase conditions in the hot legs. With the flow into hot leg A being greater than that into hot leg B, a higher steam quality existed in hot leg A and more steam was released to a larger condensing surface in steam generator A (the steam generator primary level of A was lower than B). Therefore, steam generator A continued to steam (at a decreased rate) throughout the repressurization whereas the steam generator B steaming rate decreased and terminated (Figures 5.1.66, See 1 and 5.1.67, See 1). Although steam generator A continued to steam, AFW terminated (apparently due to overfeeding above the control setpoint) and did not actuate when the steam generator A primary level descended to the pool elevation (Figure 5.1.51, See 3).

As the steam generator A secondary inventory was boiled off, the level decreased, reached the control setpoint, and AFW actuated (Figure 5.1.66, See 2). This actuation established BCM in loop A and the primary system depressurized (Figure 5.1.49, See 3).

This depressurization caused the flashing of the fluid in hot leg B and increased the steaming of steam generator B (Figure 5.1.67, See 2). Actuation of the steam generator B AFW was also delayed as a result of the secondary level exceeding the control setpoint (Figure 5.1.48, See 3). The hot leg A and steam generator A primary levels increased as inventory was transferred from the reactor vessel, downcomer, pressurizer, and loop B (Figure 5.1.48, See 4 and Figure 5.1.51, See 4).

The decreasing steam generator B secondary level (as a result of secondary boiloff) eventually decreased to the level control setpoint, AFW was actuated (Figure 5.1.67, See 3), and BCM occurred in loop B. The steam flow from the reactor vessel into hot leg A was therefore reduced as loop B BCM occurred. This event resulted in a reduced heat transfer and a reduction in the steam and feedwater flow in steam generator A (Figure 5.1.66, See 3). An inventory transfer from loop A to loop B occurred as the loop A hot leg and steam generator primary levels were observed to decrease while those in loop B increased (Figure 5.1.50, See 2).

The previously described observation, wherein BCM occurred initially in one loop (A) with an increase in inventory of the loop that experienced BCM followed by the occurrence of BCM in the other (B) with a corresponding increase in inventory, has been termed "alternate loop BCM."

The alternate loop BCM resulted in a depressurization of the primary system from approximately 1590 to 1110 psia (Figure 5.1.49, See 4). The cold legs again attained superheated conditions during the depressurization (See 3 on Figures 5.1.53 through 5.1.61). The test was then terminated (281 minutes) as the establishment of pool BCM was a termination criteria for the Mapping Tests.

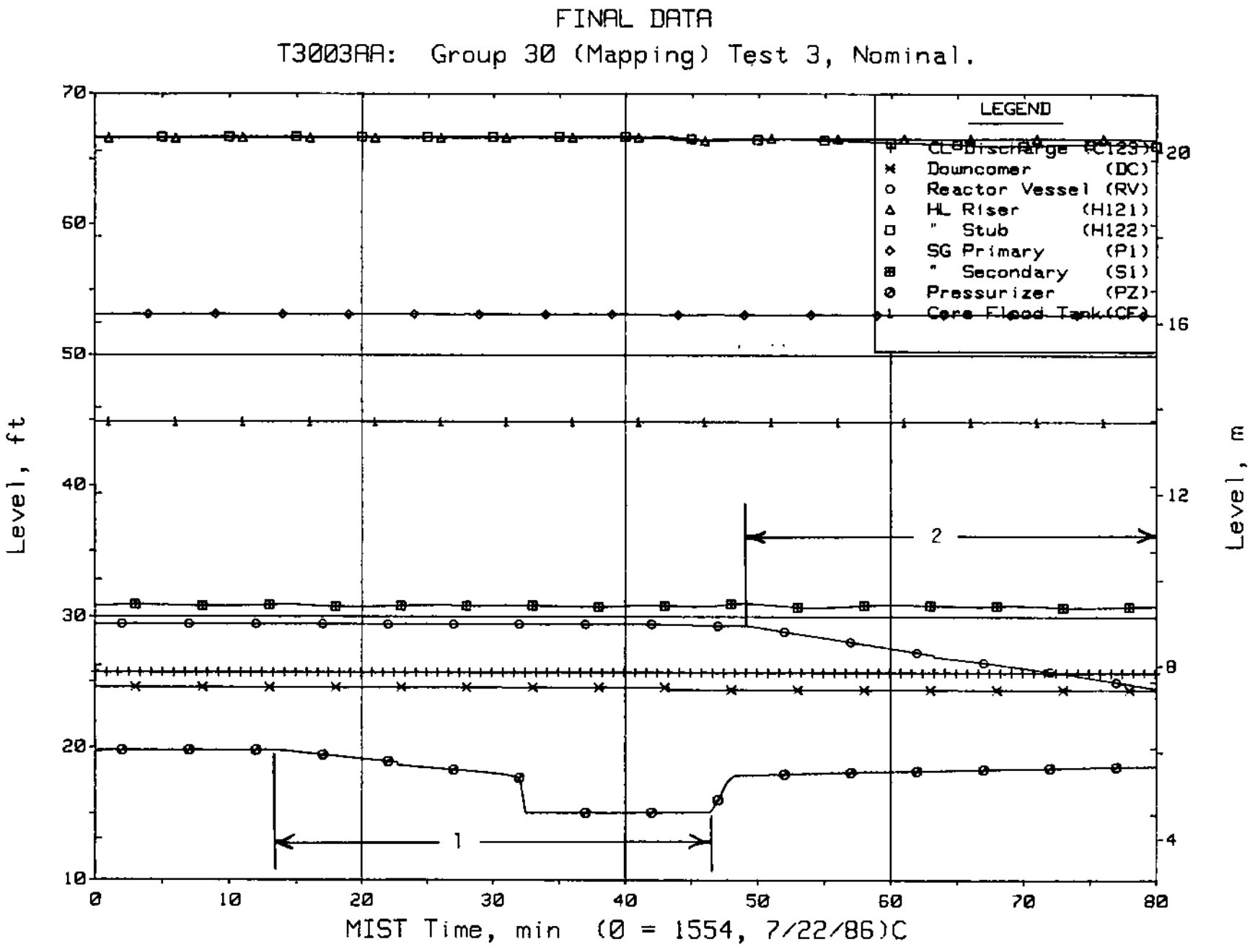

Figure 5.1.1. Loop A Collapsed Liquid Levels (LV20s)

Mon Feb 6 13:19:00 1989

PRLV1

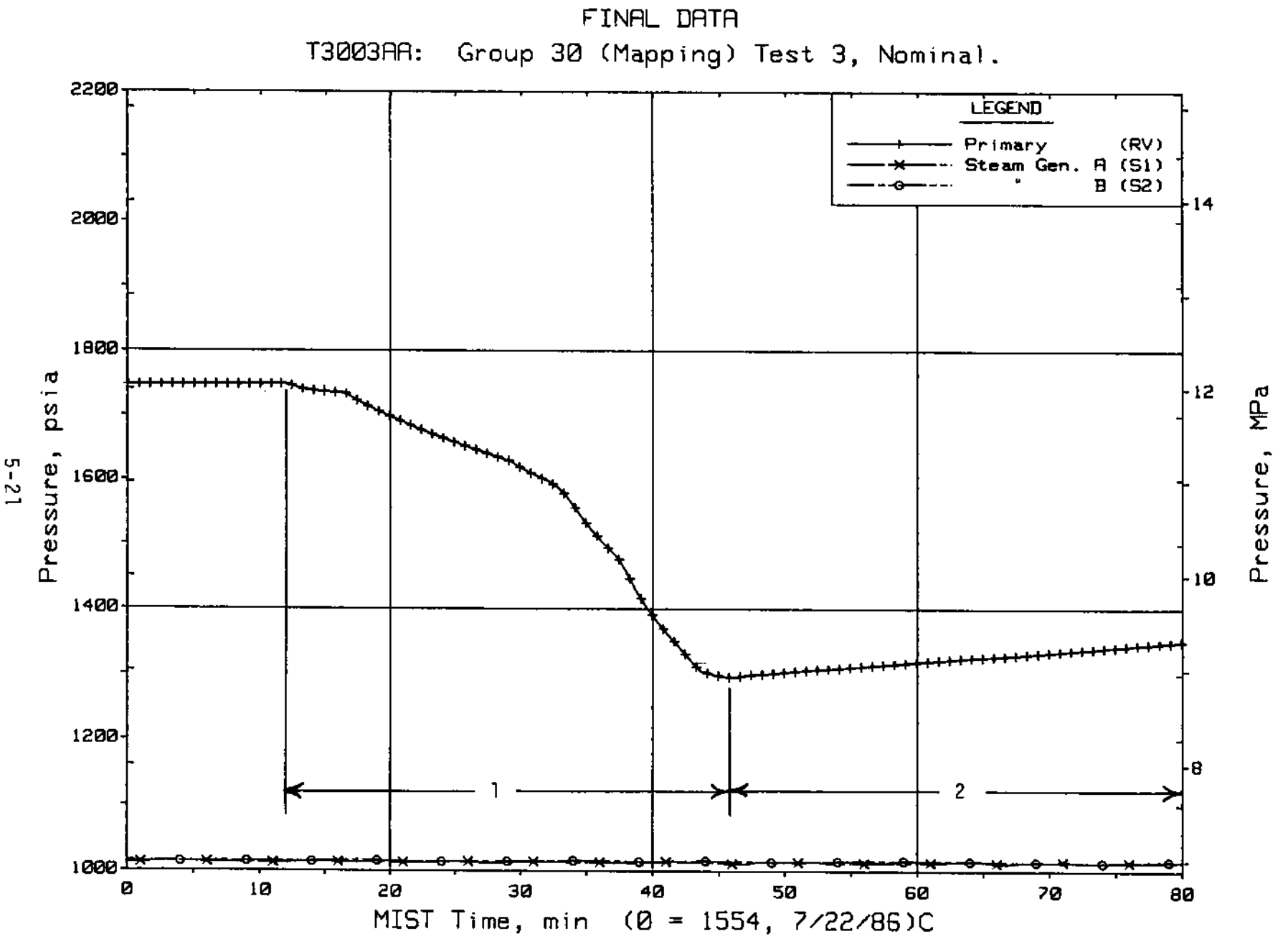

Figure 5.1.2. Primary and Secondary System Pressures (GP01s)

Mon Feb 6 13:21:58 1989

PSGP1

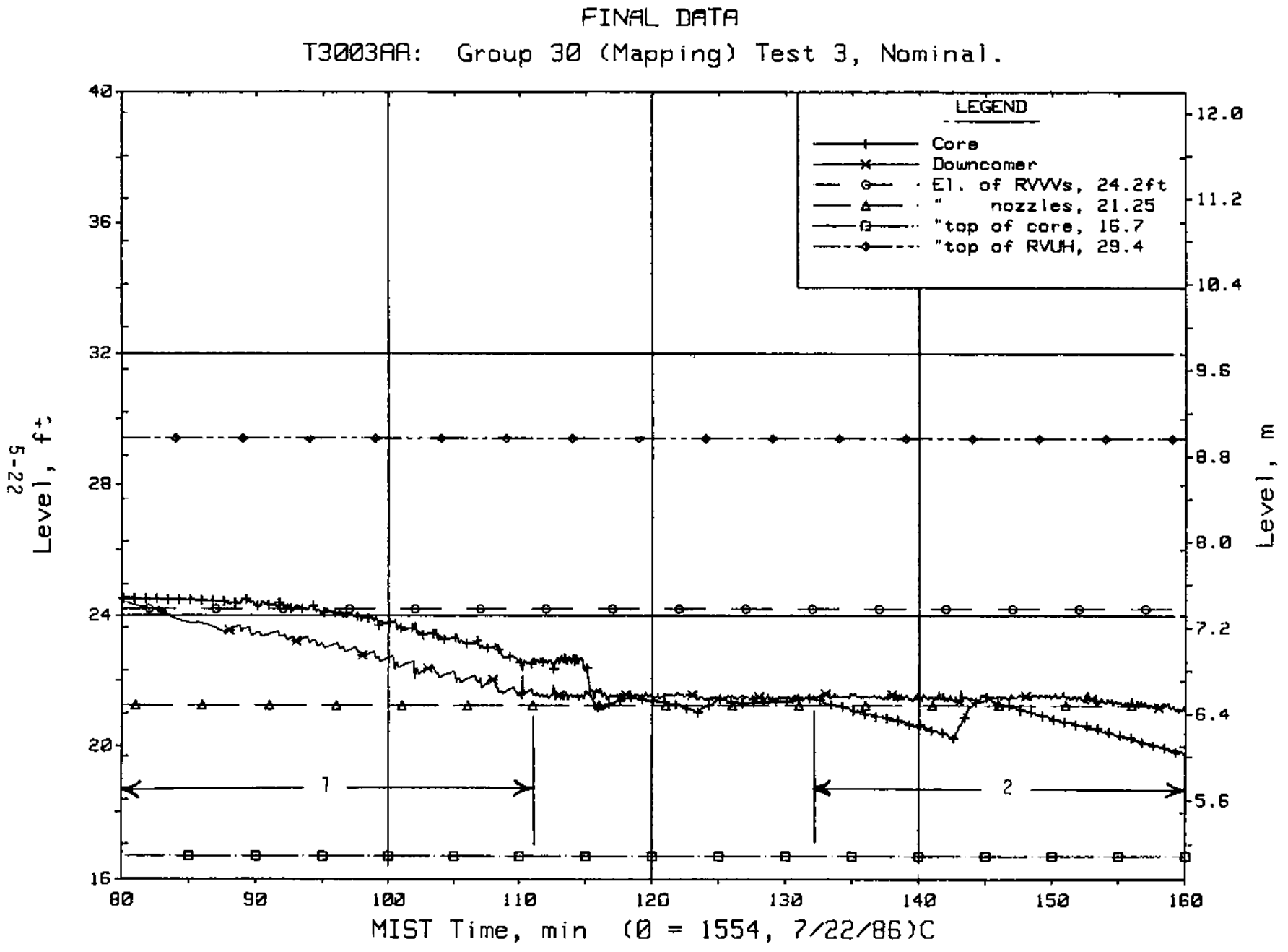

Figure 5.1.3. Core Region Collapsed Liquid Levels

Wed Feb 8 14:45:28 1989

COLV1

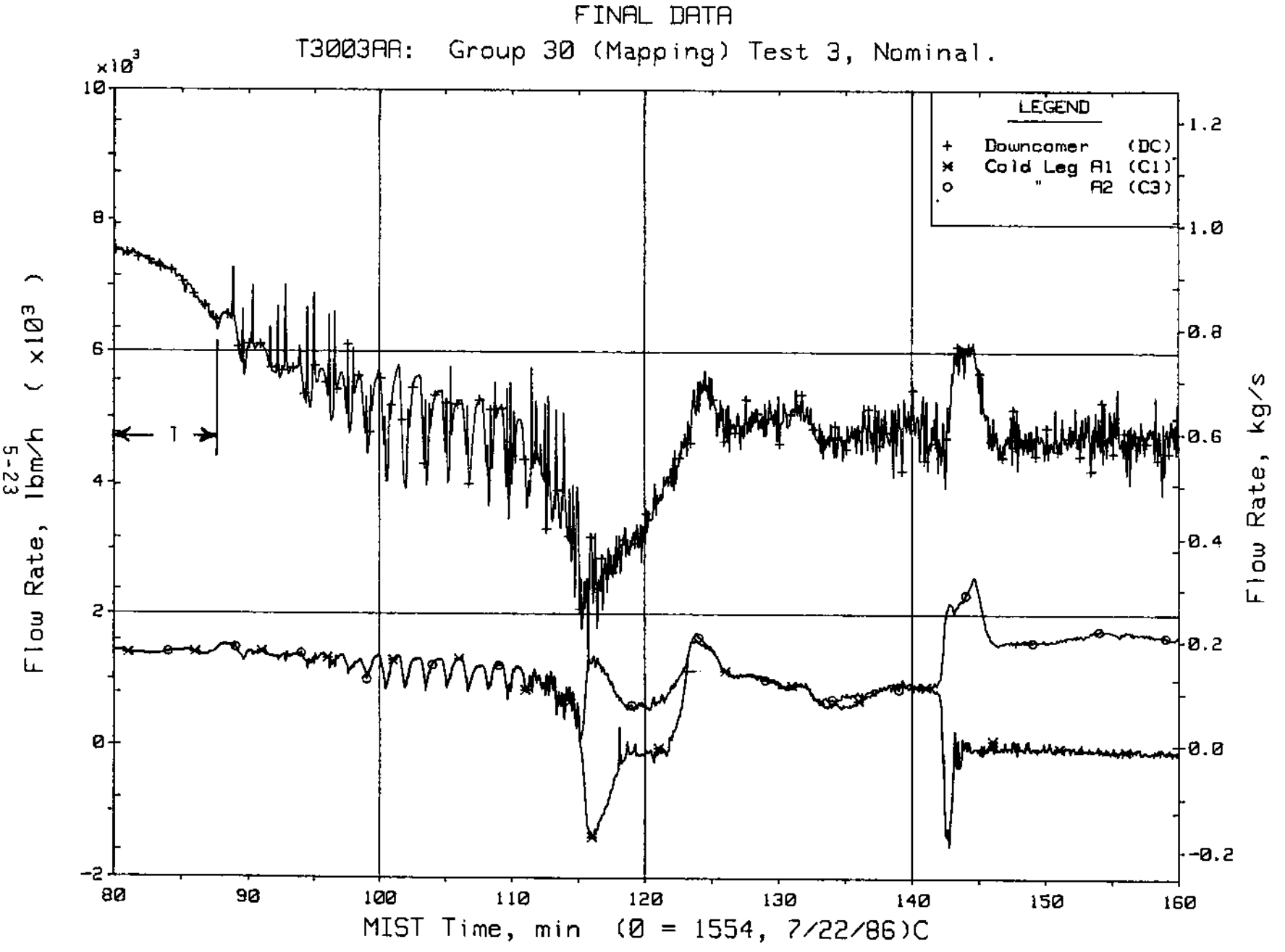

Figure 5.1.4. Primary System (Venturi) Flow Rates (VN20s)

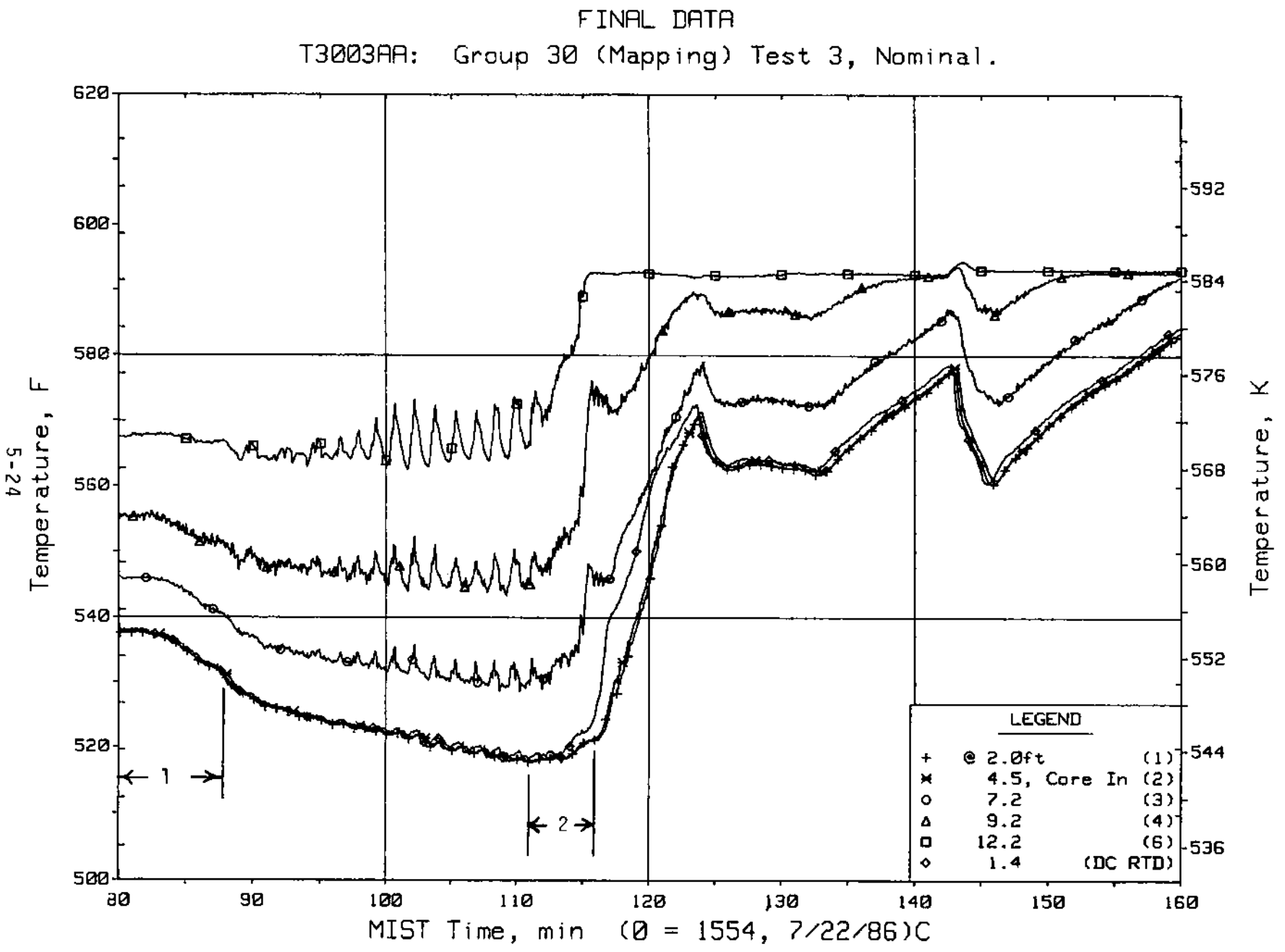

Figure 5.1.5. Reactor Vessel Lower-Elevation Fluid Temperatures (RVTCs)

Mon Feb 6 13:30:19 1989

RVTC1

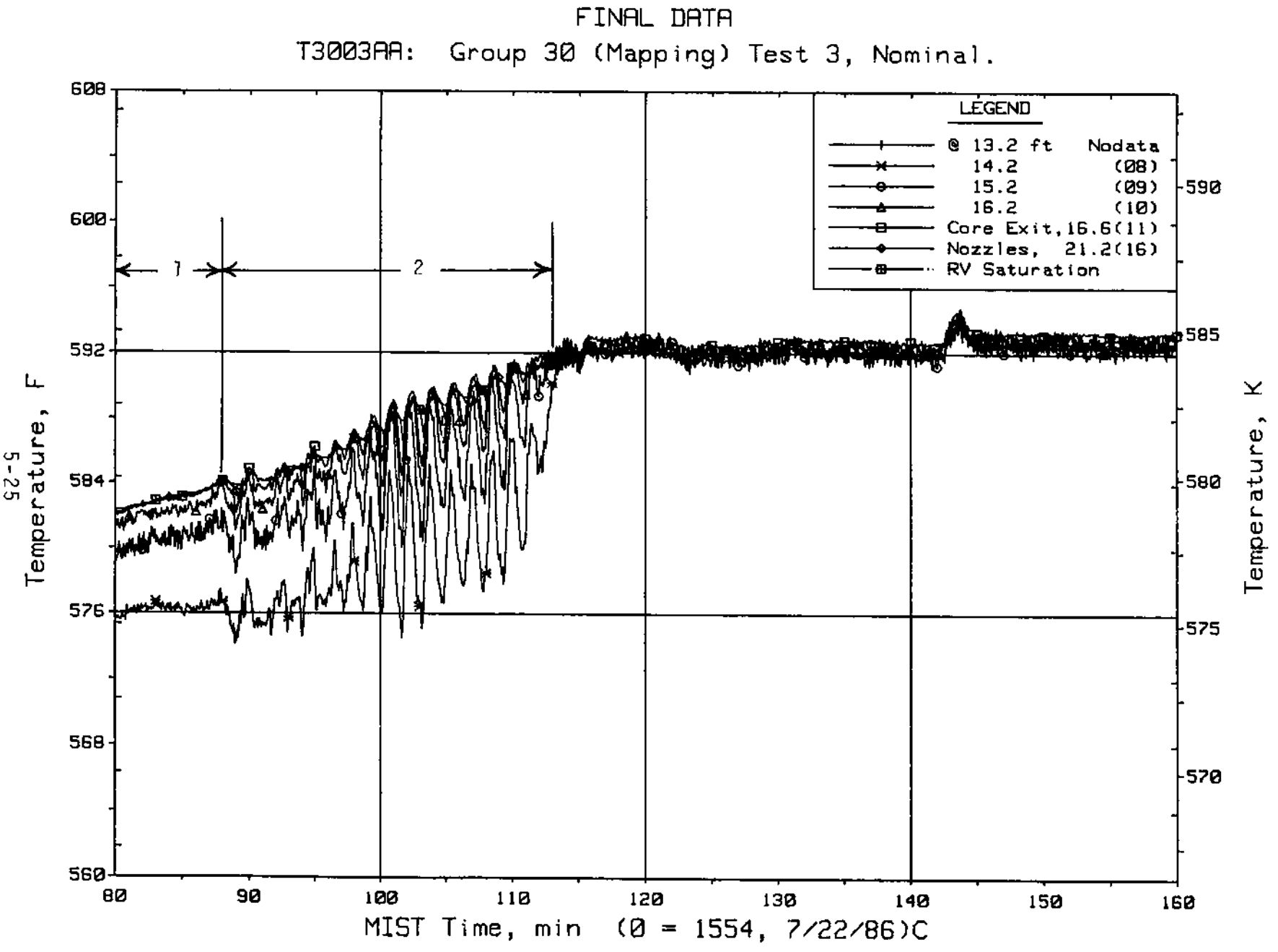

Figure 5.1.6. Reactor Vessel Mid-Elevation Fluid Temperatures (RVTCs)

Wed Feb 8 14:55:06 1989

RVTC2

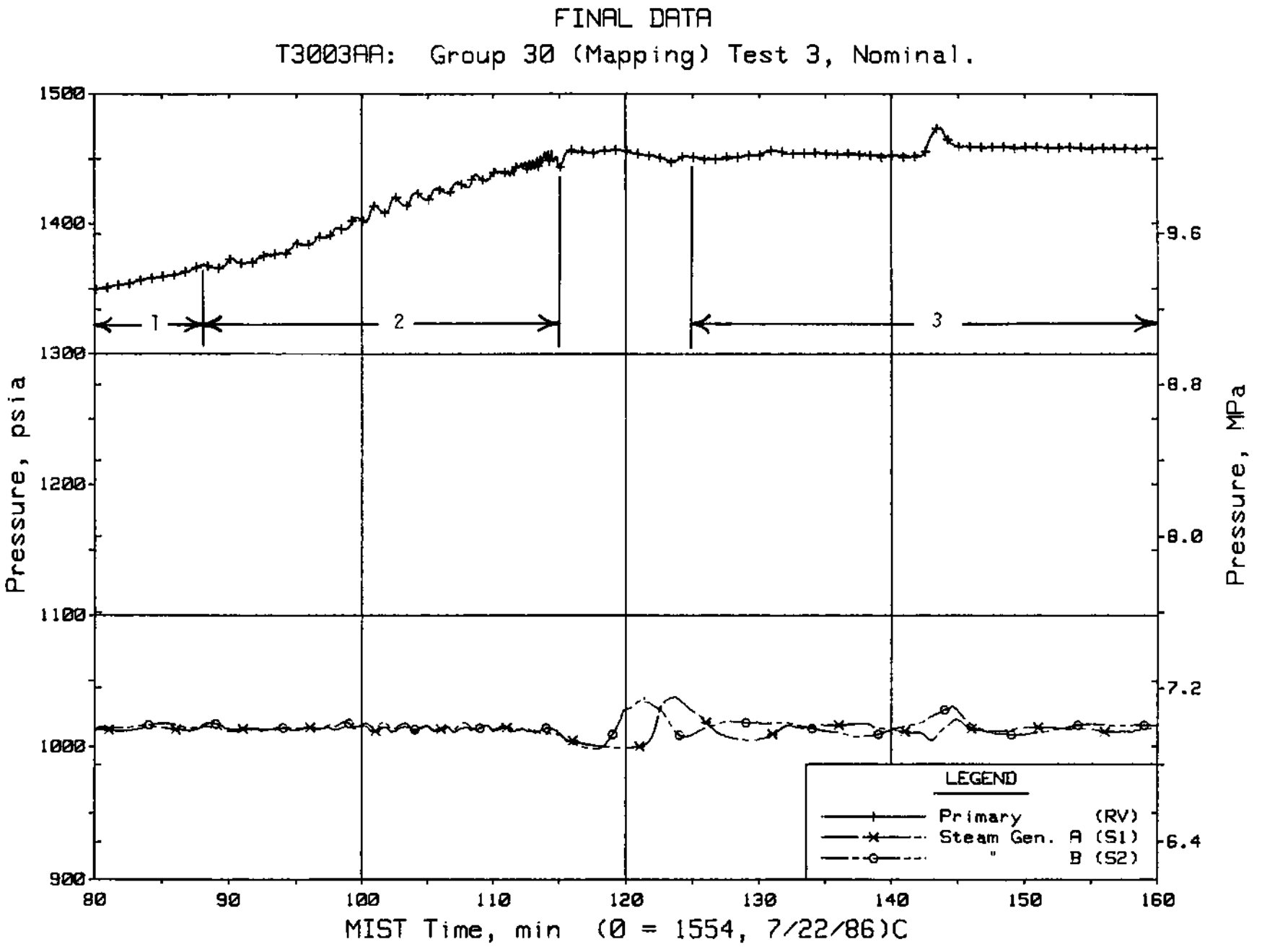

Figure 5.1.7. Primary and Secondary System Pressures (GP01s)

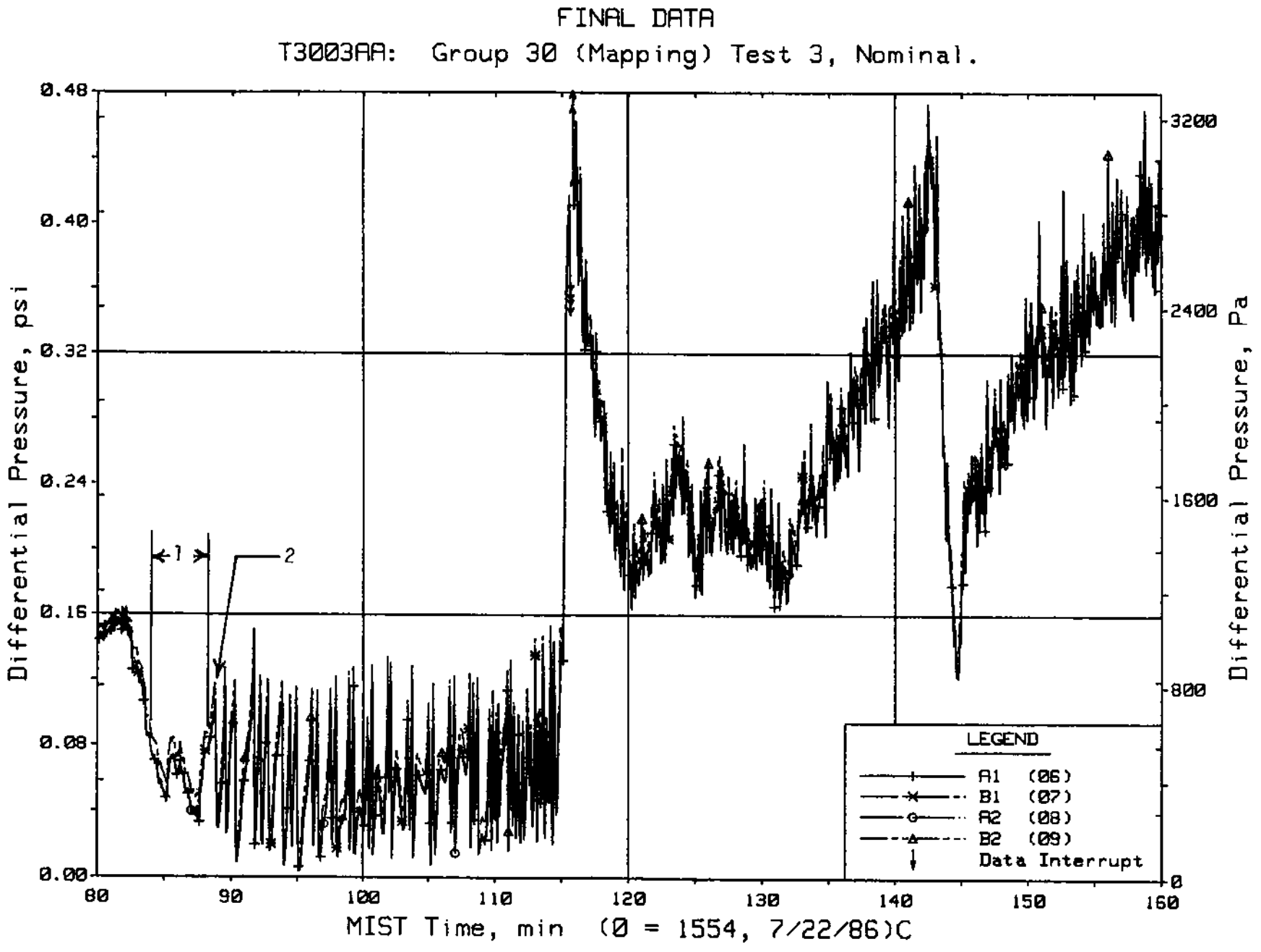

Figure 5.1.8. Reactor Vessel Vent Valve Differential Pressures (RVDPs)

Tue Feb 7 13:19:35 1989

VVDP1

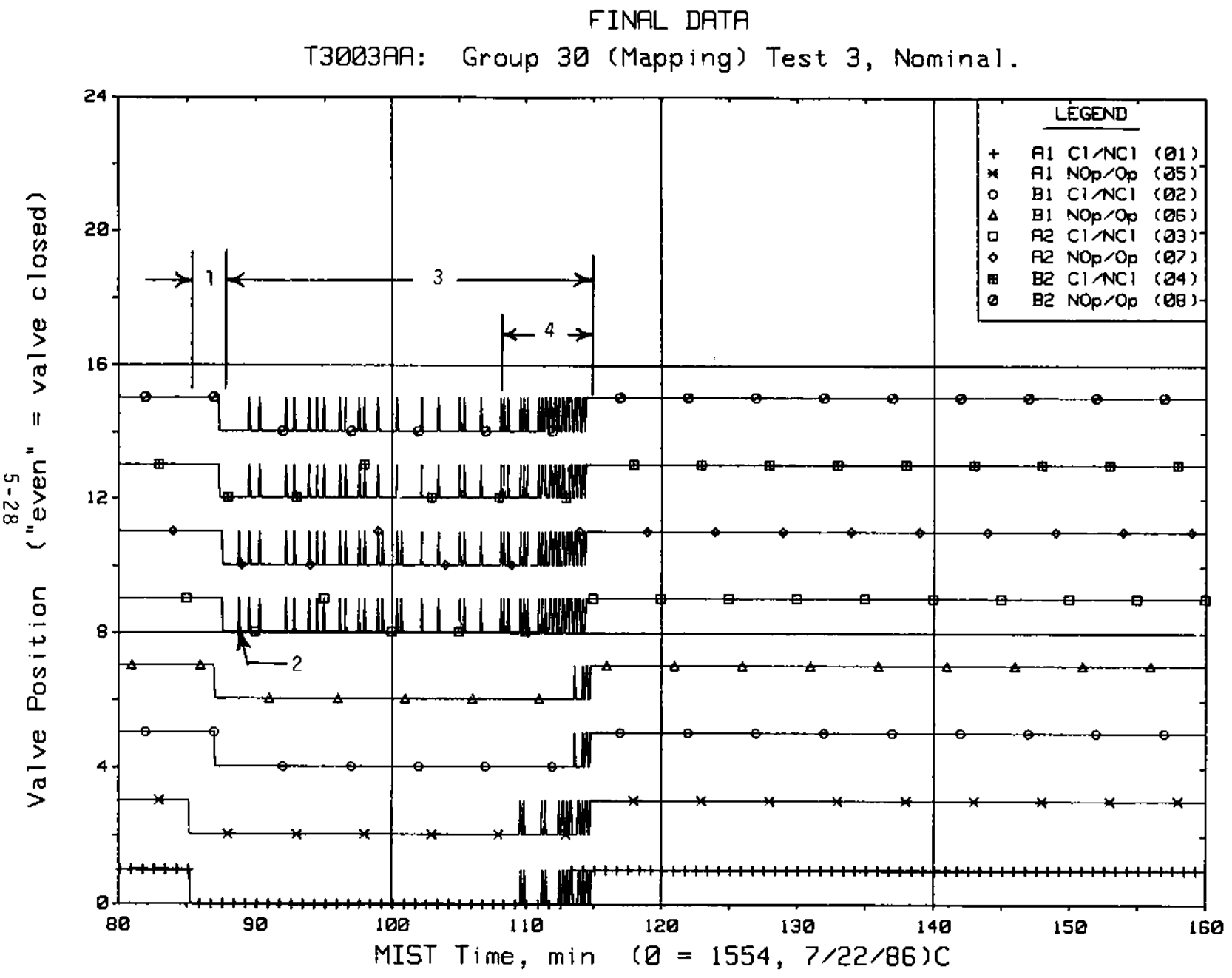

Figure 5.1.9. Reactor Vessel Vent Valve Limit Switch Indications (RVLSs)

Thu Feb 9 14:25:32 1989

VVLS2

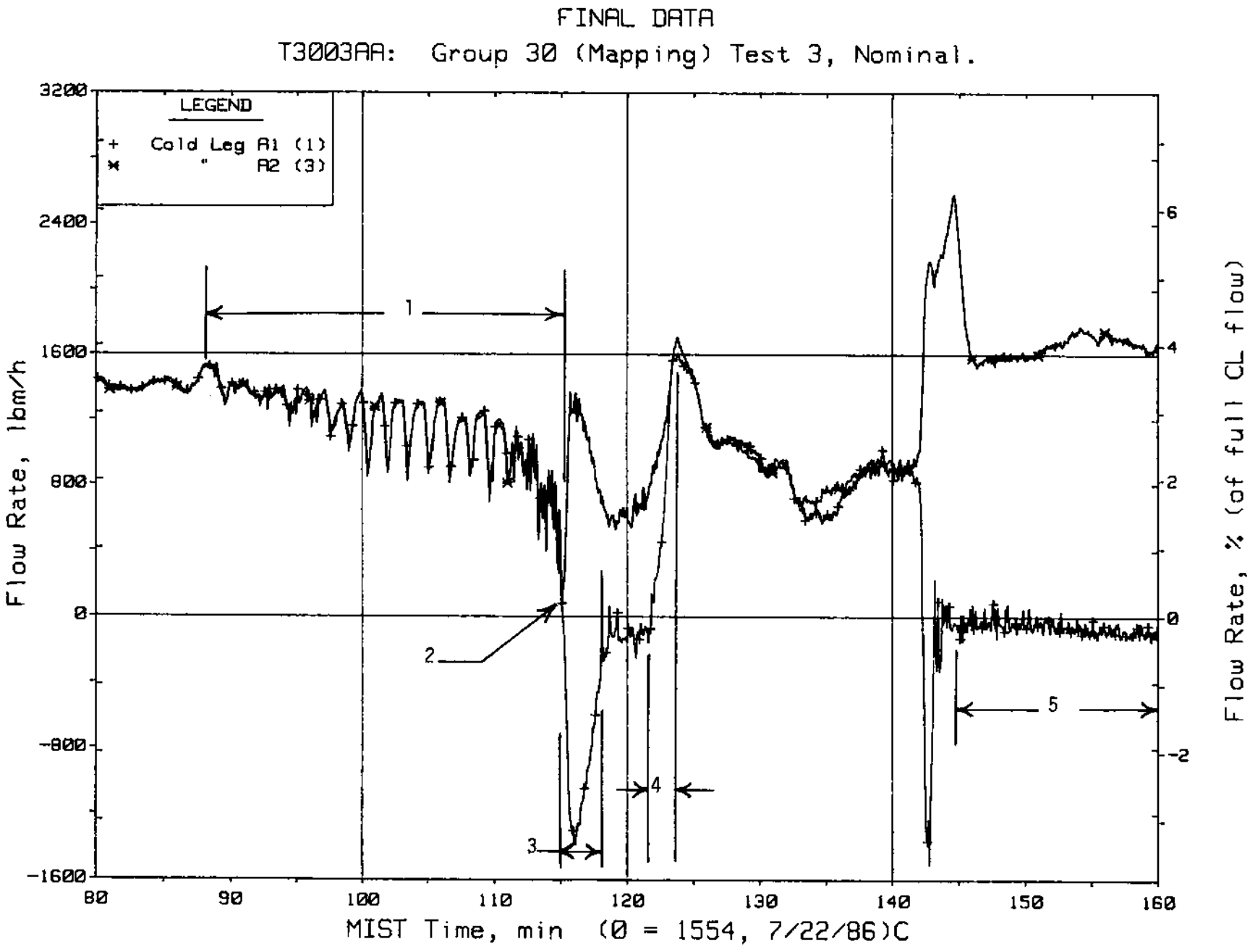

Figure 5.1.10. Loop A Cold Leg (Venturi) Flow Rates (VN20s)

Mon Feb 6 14:00:28 1989

PRFLS

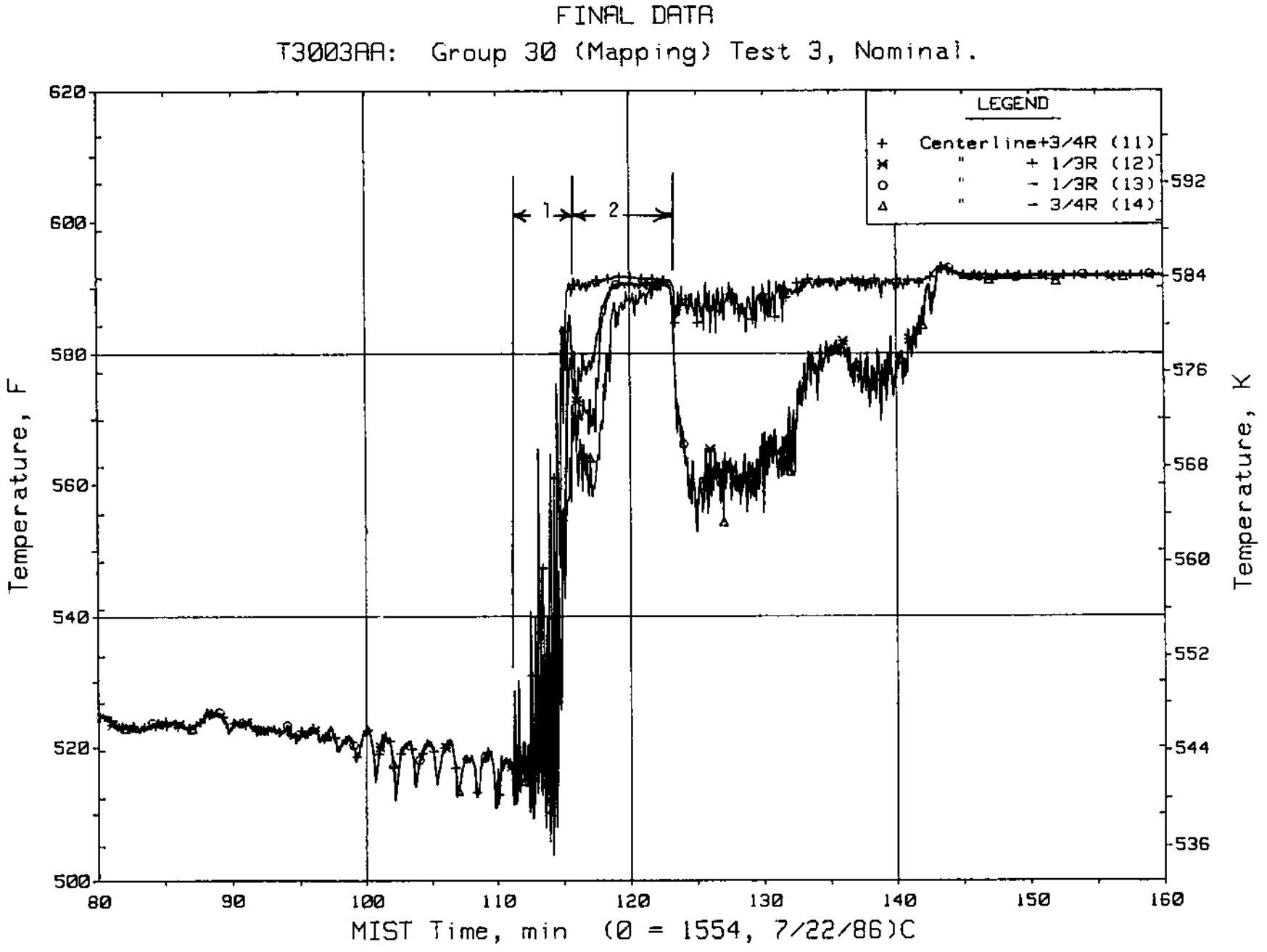

Figure 5.1.11. Cold Leg A1 Nozzle Rake Fluid Temperatures (21.2 ft, C1TCs)

Mon Feb 6 14:03:30 1989

C1TC4

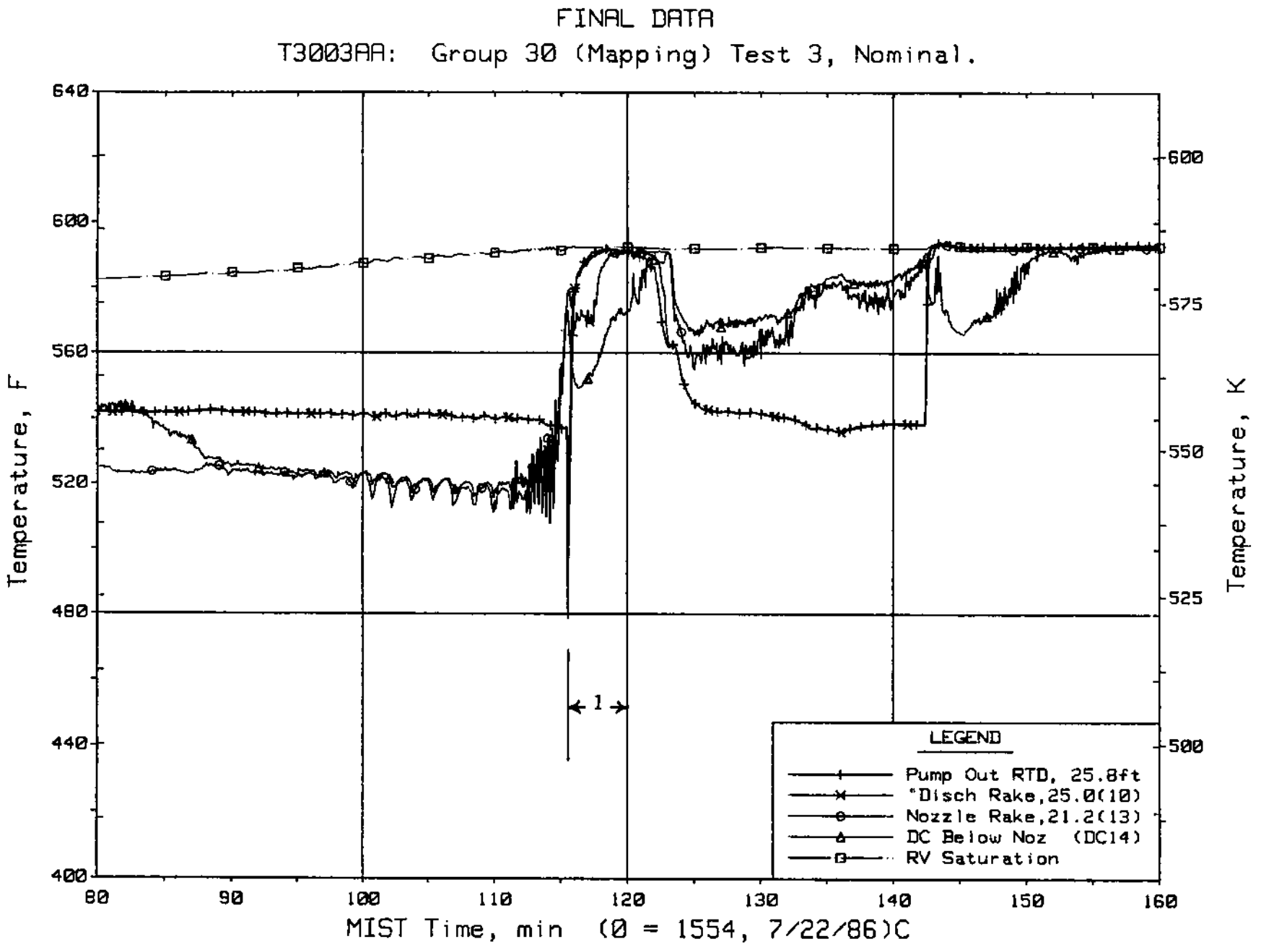

Figure 5.1.12. Cold Leg A1 Discharge Fluid Temperatures (C1TCs)

Tue Feb 7 14:45:47 1989

C1TC2

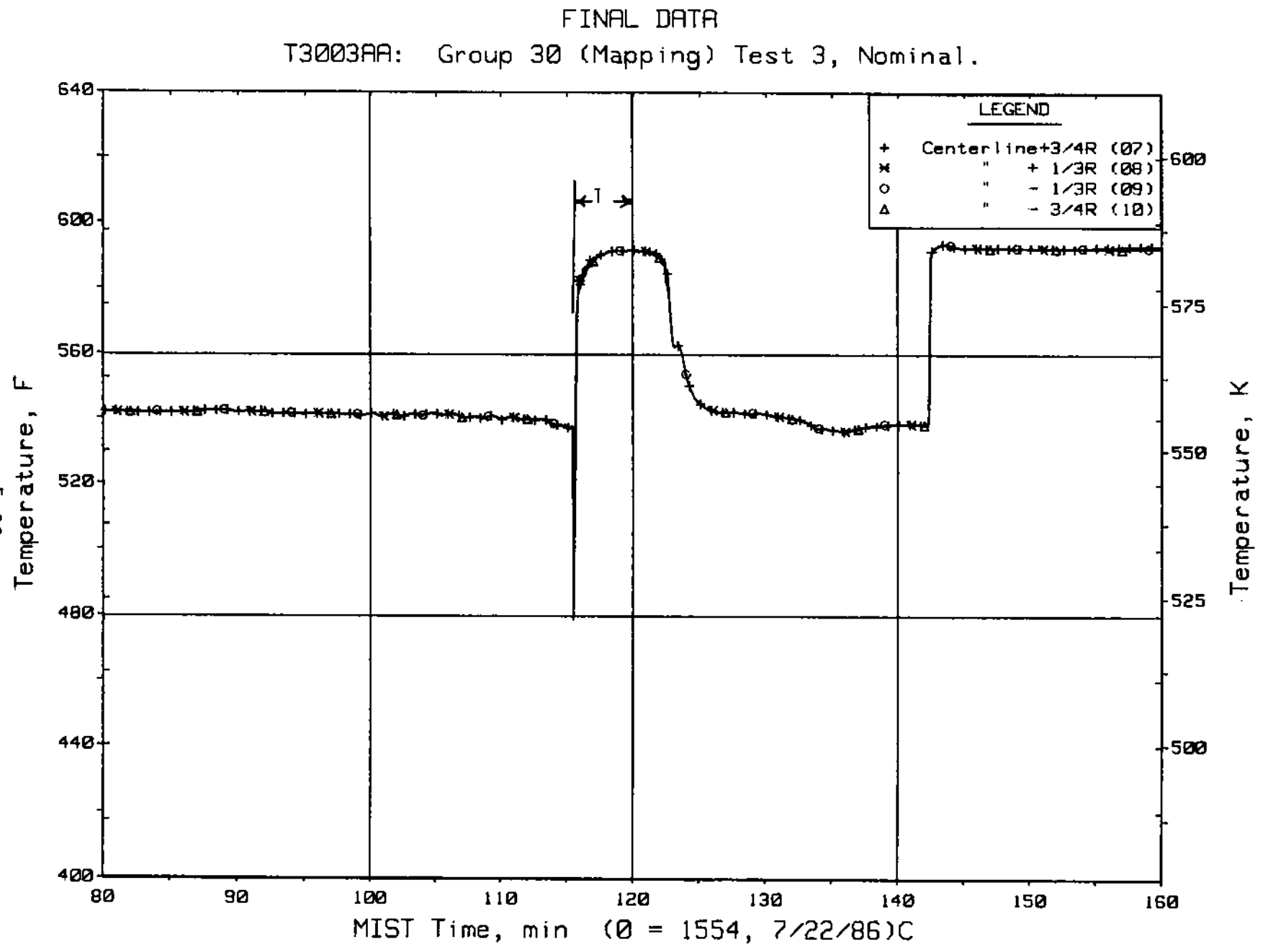

Figure 5.1.13. Cold Leg A1 Pump Discharge Rake Fluid Temperatures (25 ft, C1TCs)

Tue Feb 7 14:52:02 1989

C1TC3

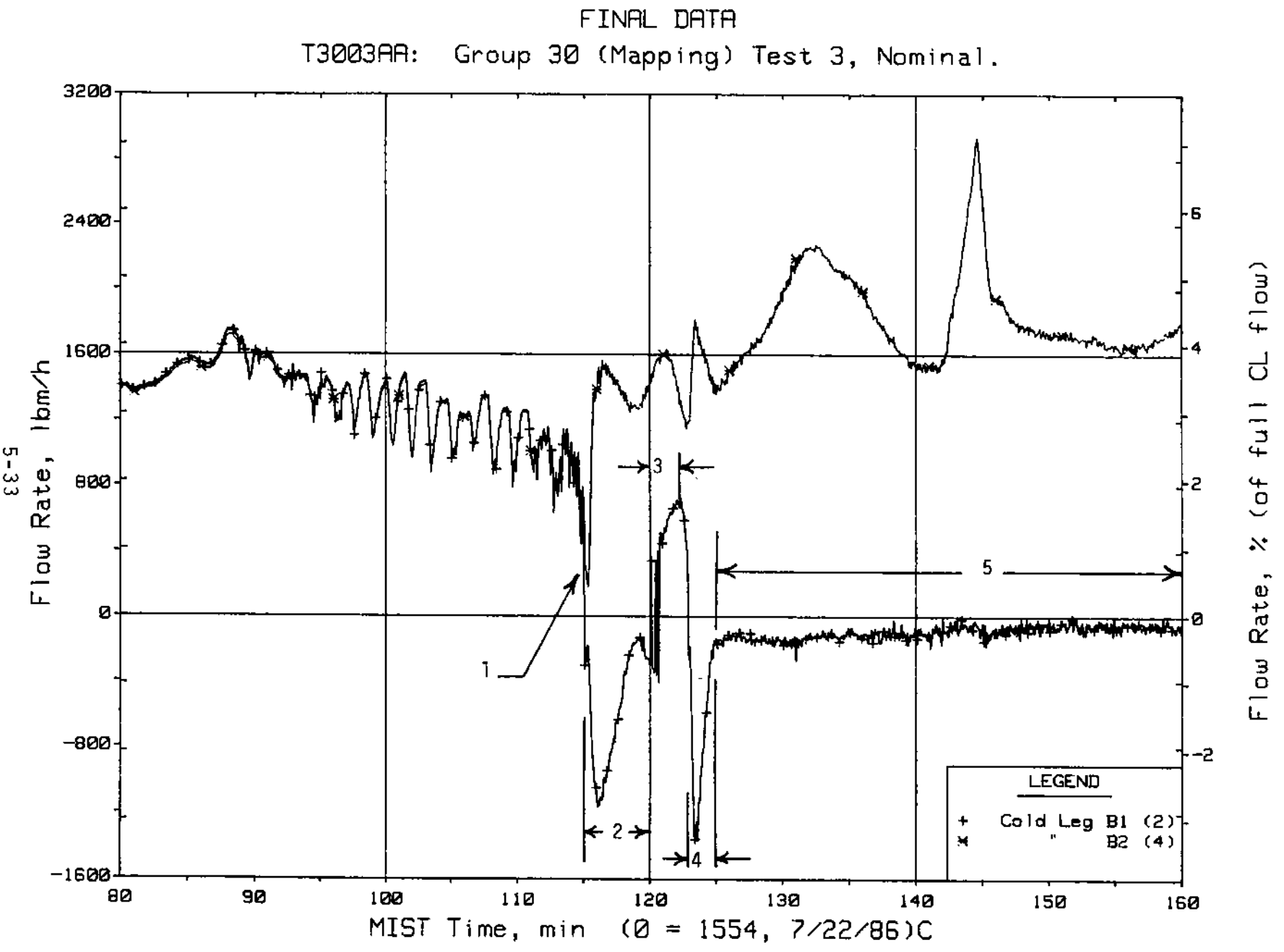

Figure 5.1.14. Loop B Cold Leg (Venturi) Flow Rates (CNVN20s)

Mon Feb 6 14:13:55 1989

PRFL6

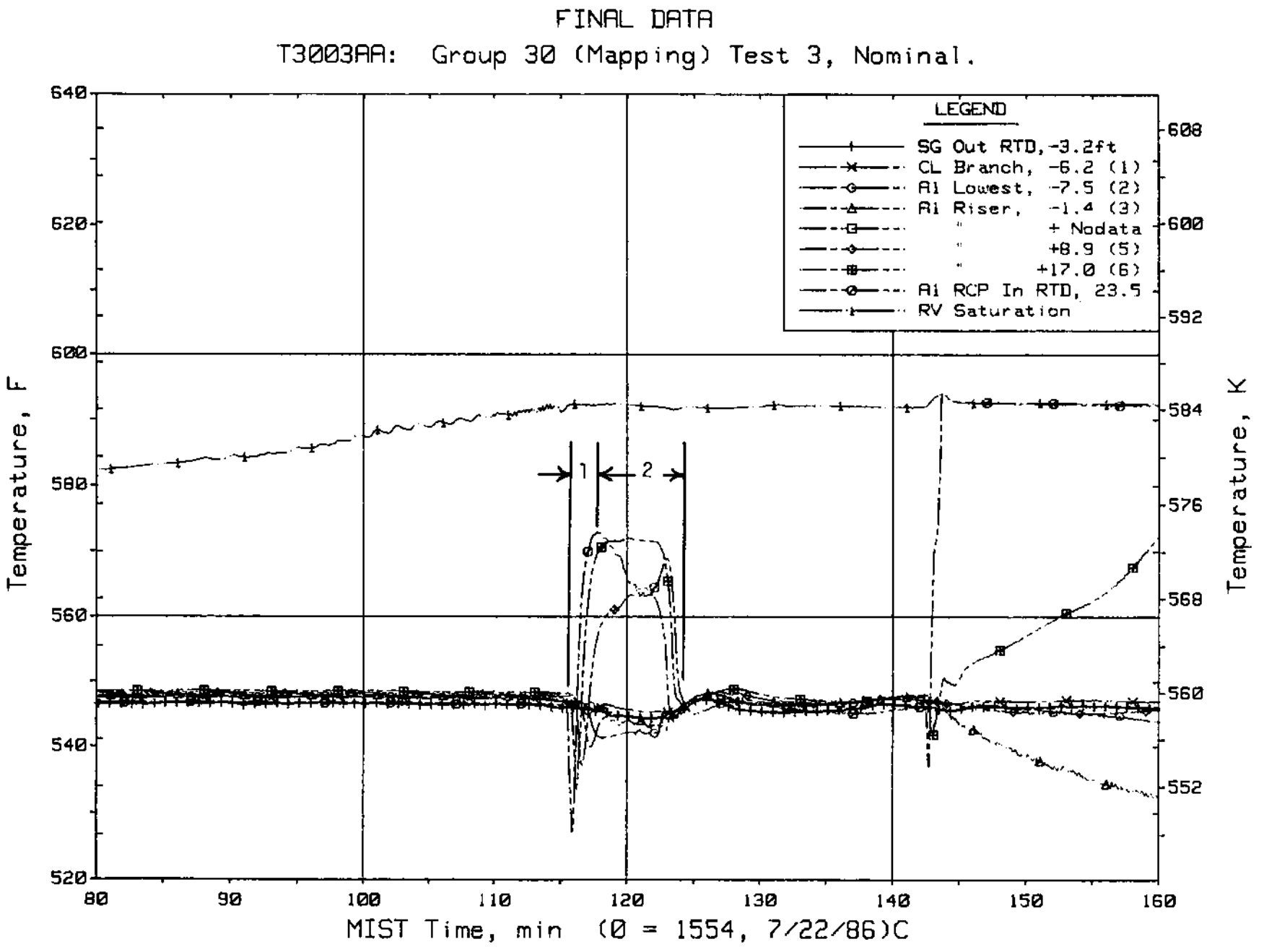

Figure 5.1.15. Cold Leg A1 Suction Fluid Temperatures (C1TCs)

Mon Feb 6 14:18:50 1989

C1TC1

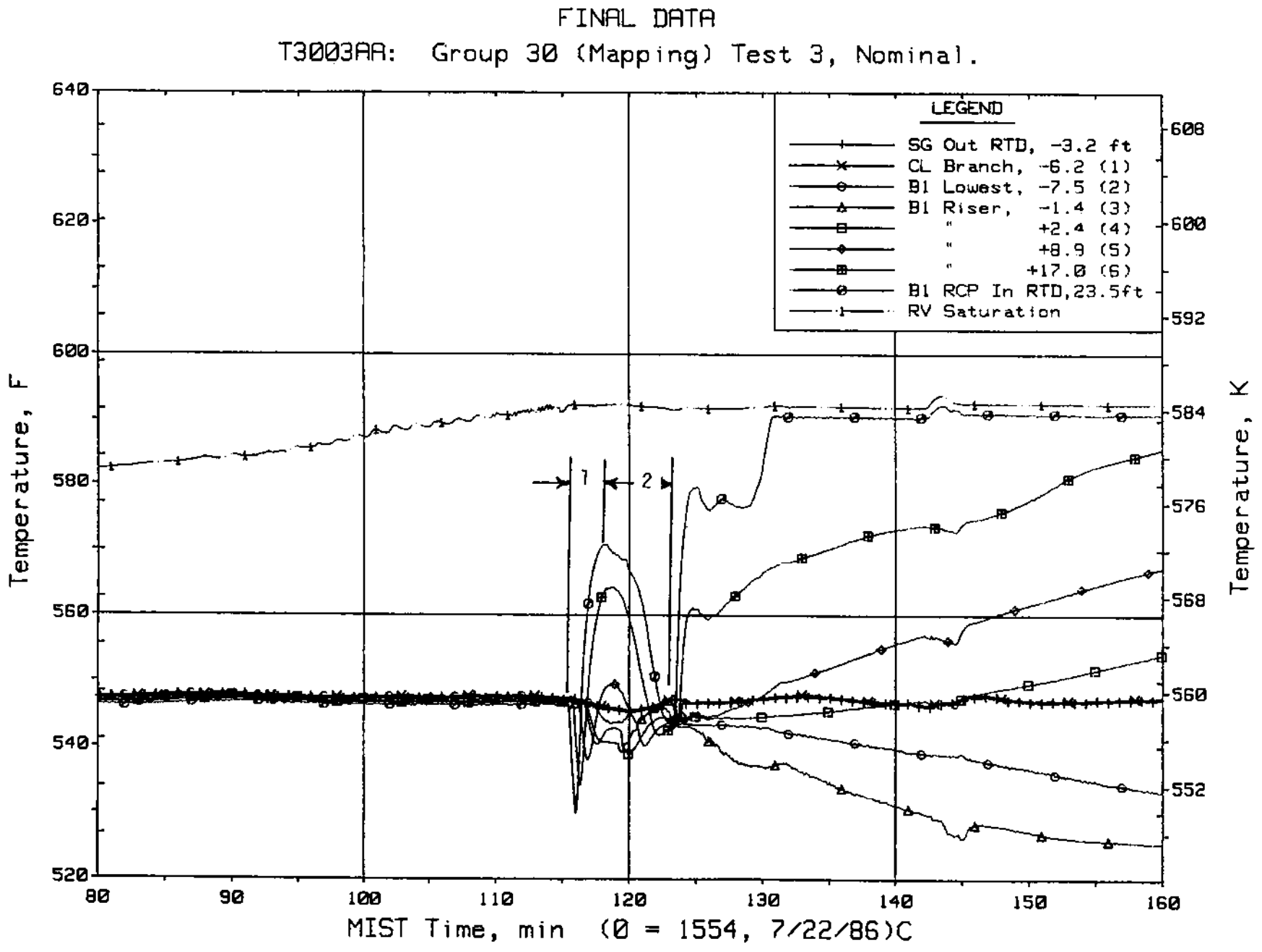

Figure 5.1.16. Cold Leg B1 Suction Fluid Temperatures (C2TCs)

Mon Feb 6 14:23:39 1989

C2TC1

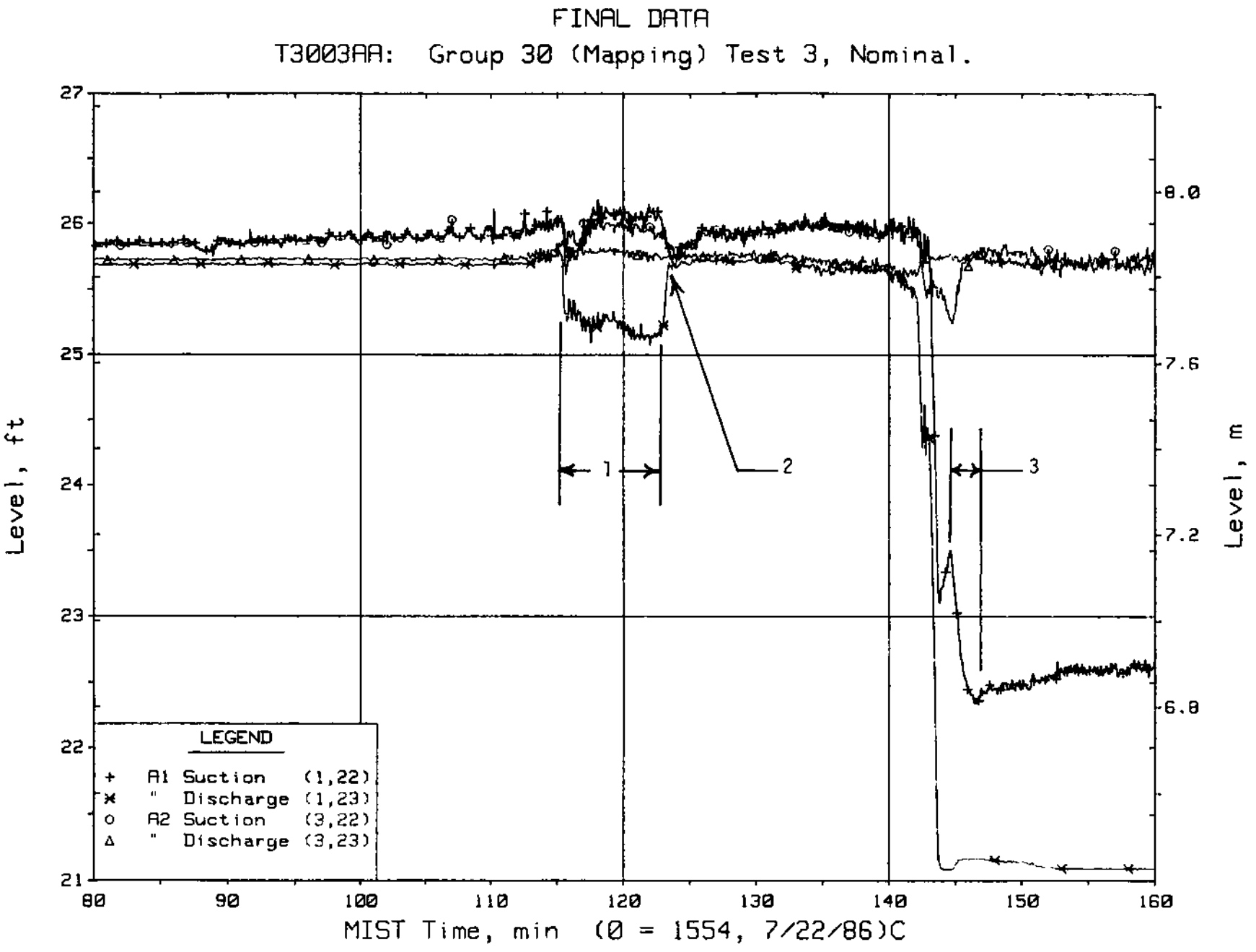

Figure 5.1.17. Loop A Cold Leg Collapsed Liquid Levels (LVs)

Mon Feb 6 14:27:01 1989

CLLV1

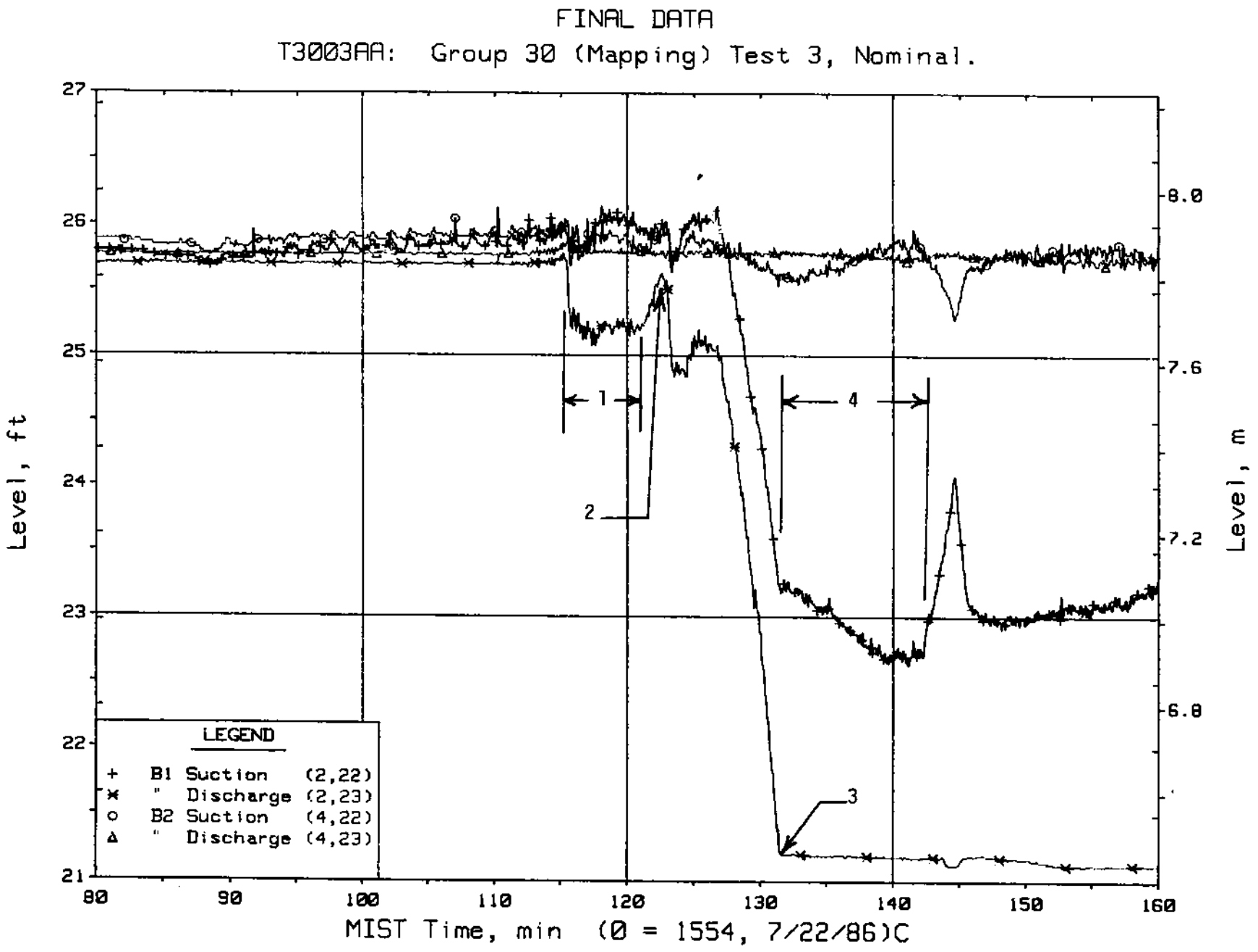

Figure 5.1.18. Loop B Cold Leg Collapsed Liquid Levels (LVs)

Mon Feb 6 14:29:58 1989

CLLV2

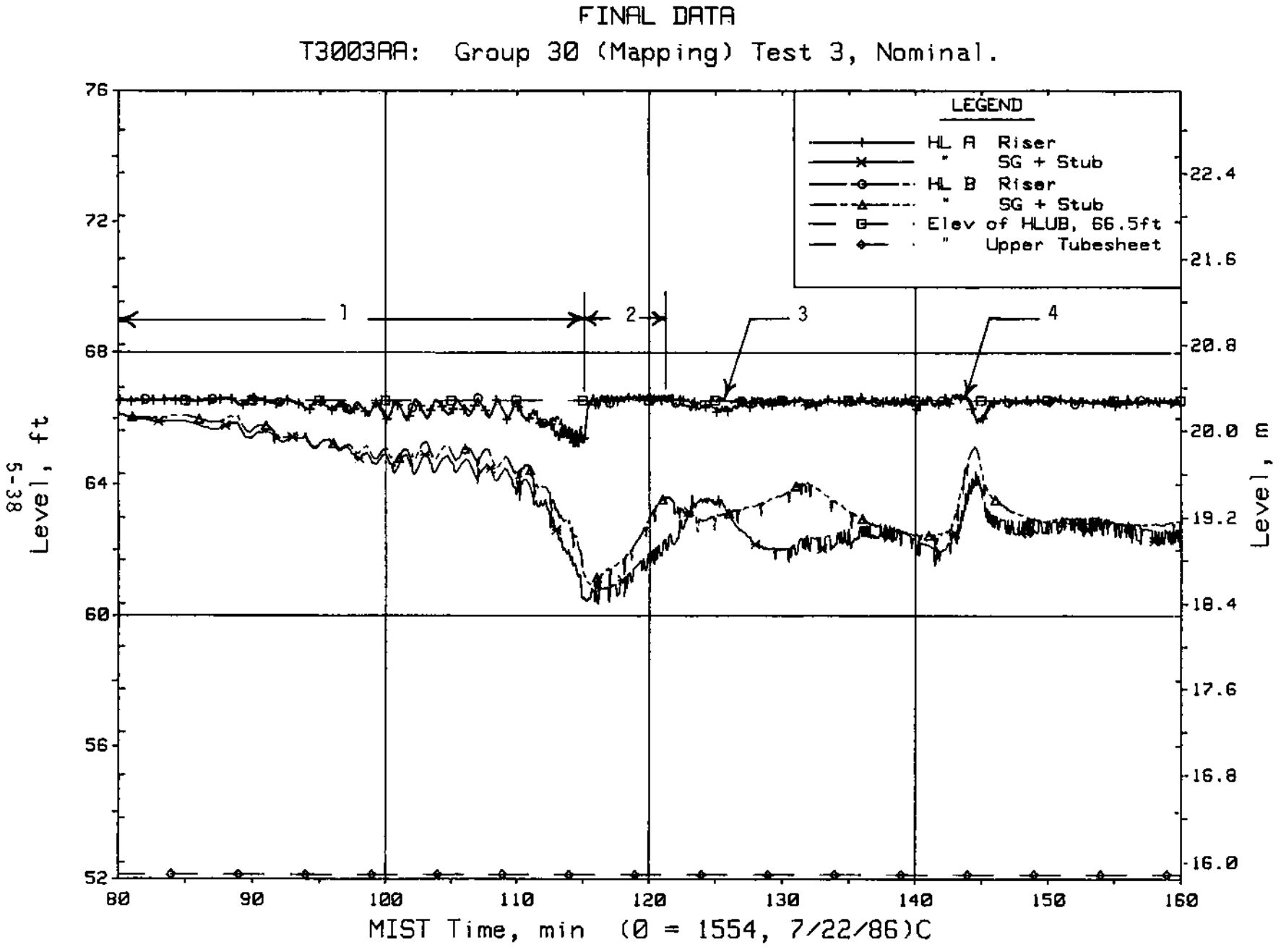

Figure 5.1.19. Hot Leg Riser and Stub Collapsed Liquid Levels

Thu Feb 9 14:18:49 1989

HLLV1

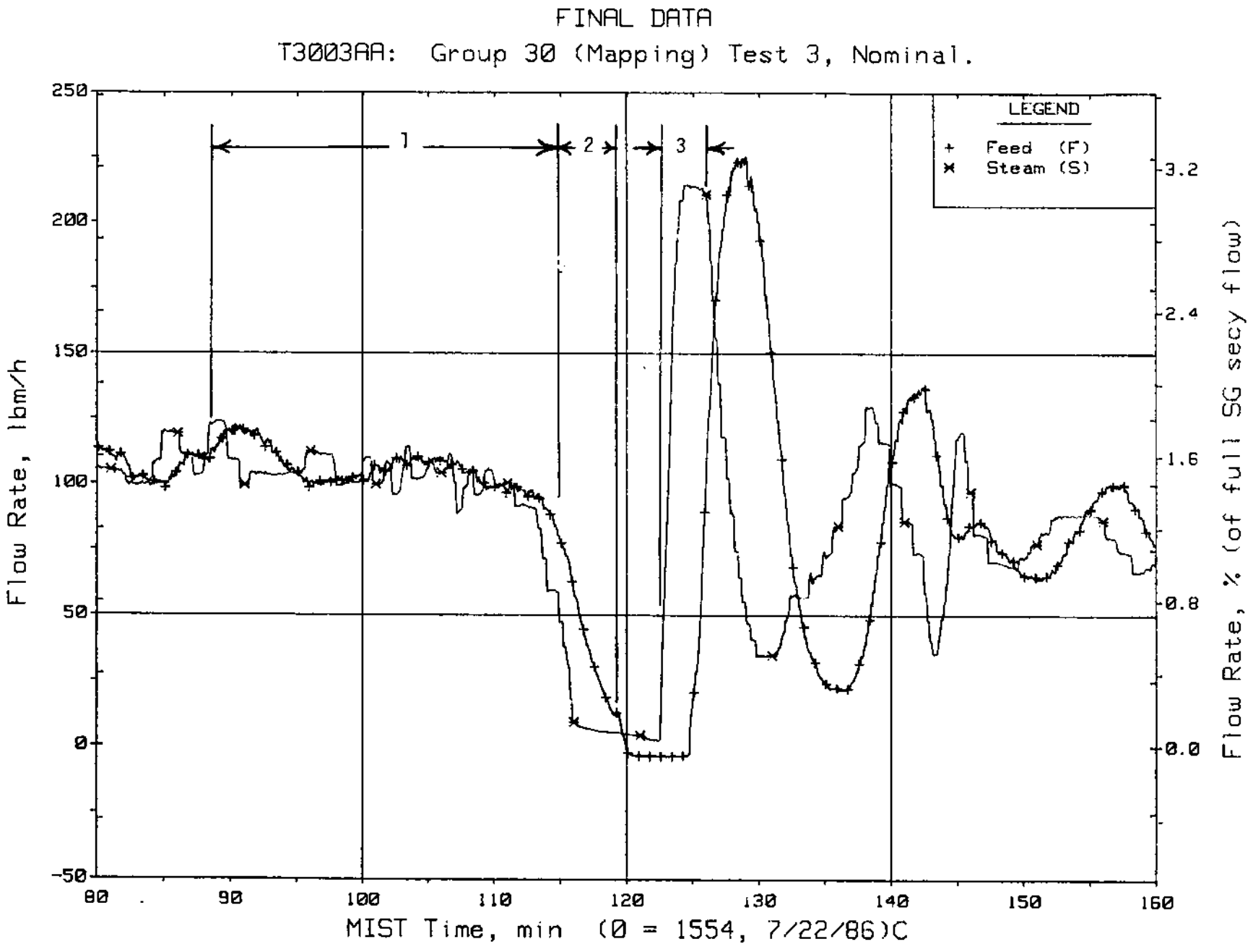

Figure 5.1.20. Steam Generator A Flow Rates (OR20s)

Mon Feb 6 14:39:08 1989

SCFL1

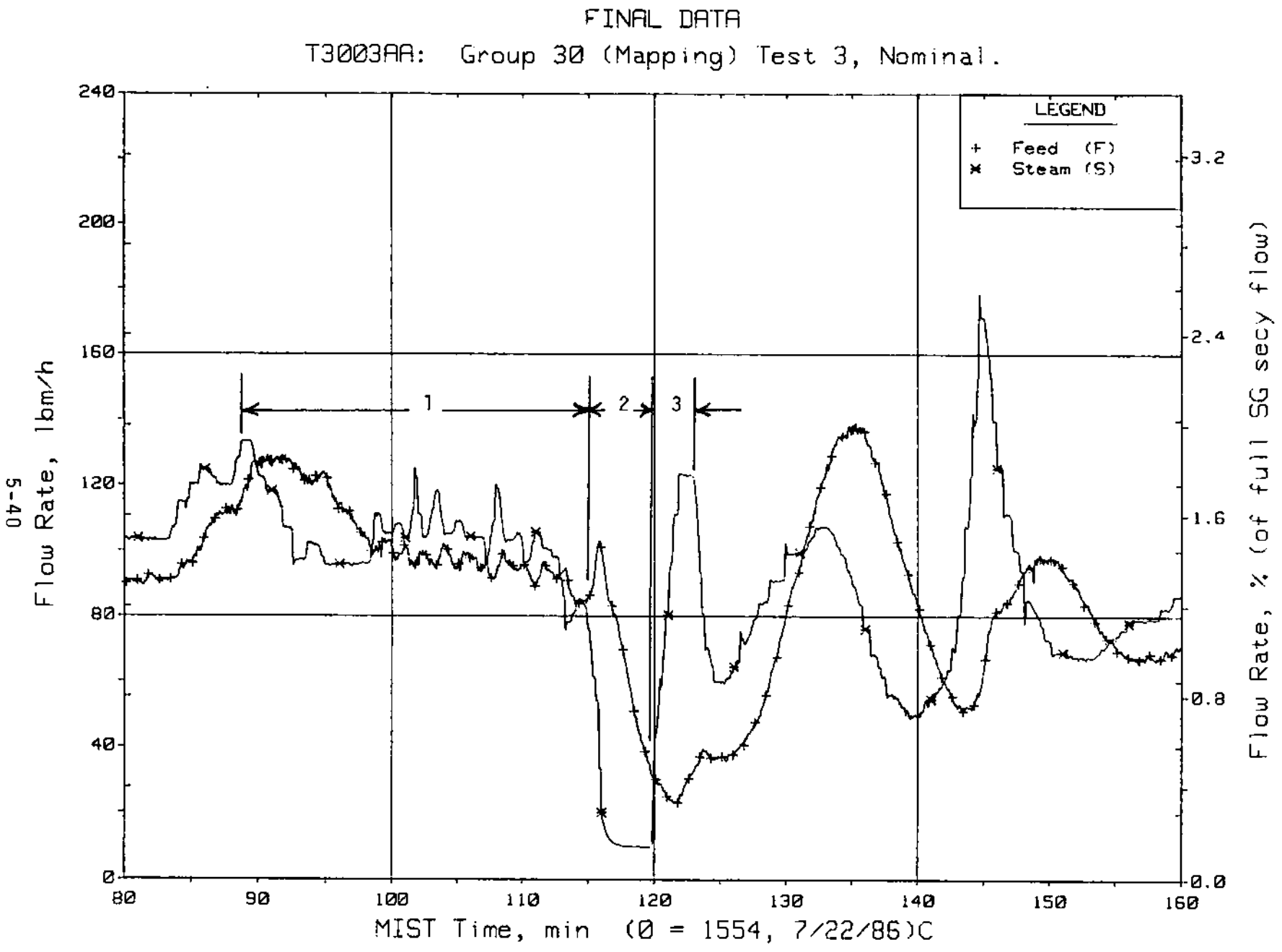

Figure 5.1.21. Steam Generator B Flow Rates (OR21s)

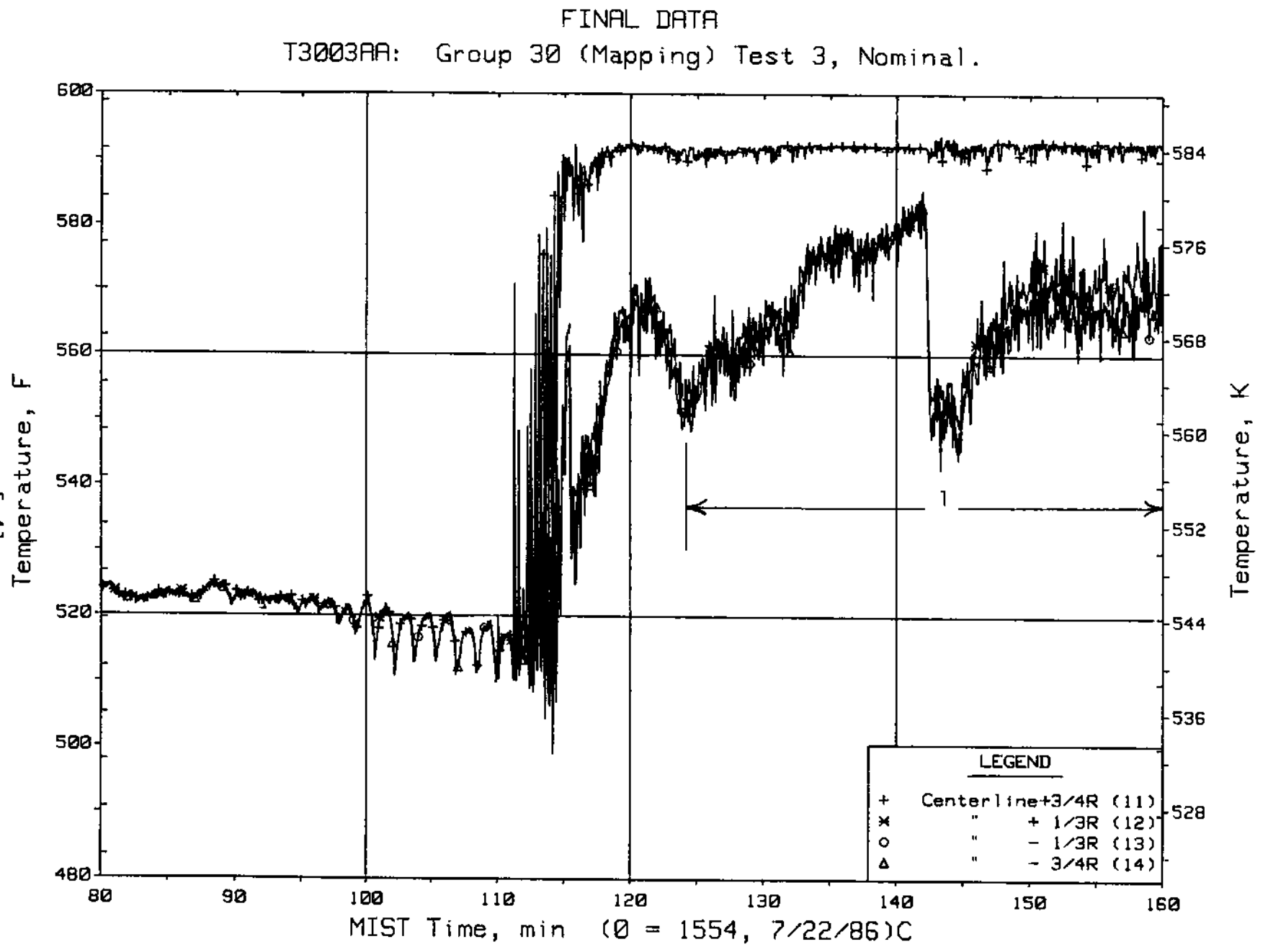

Figure 5.1.22. Cold Leg A2 Nozzle Rake Fluid Temperatures (21.2 ft, C3TCs)

Wed Feb 8 15:01:41 1989

C3TC4

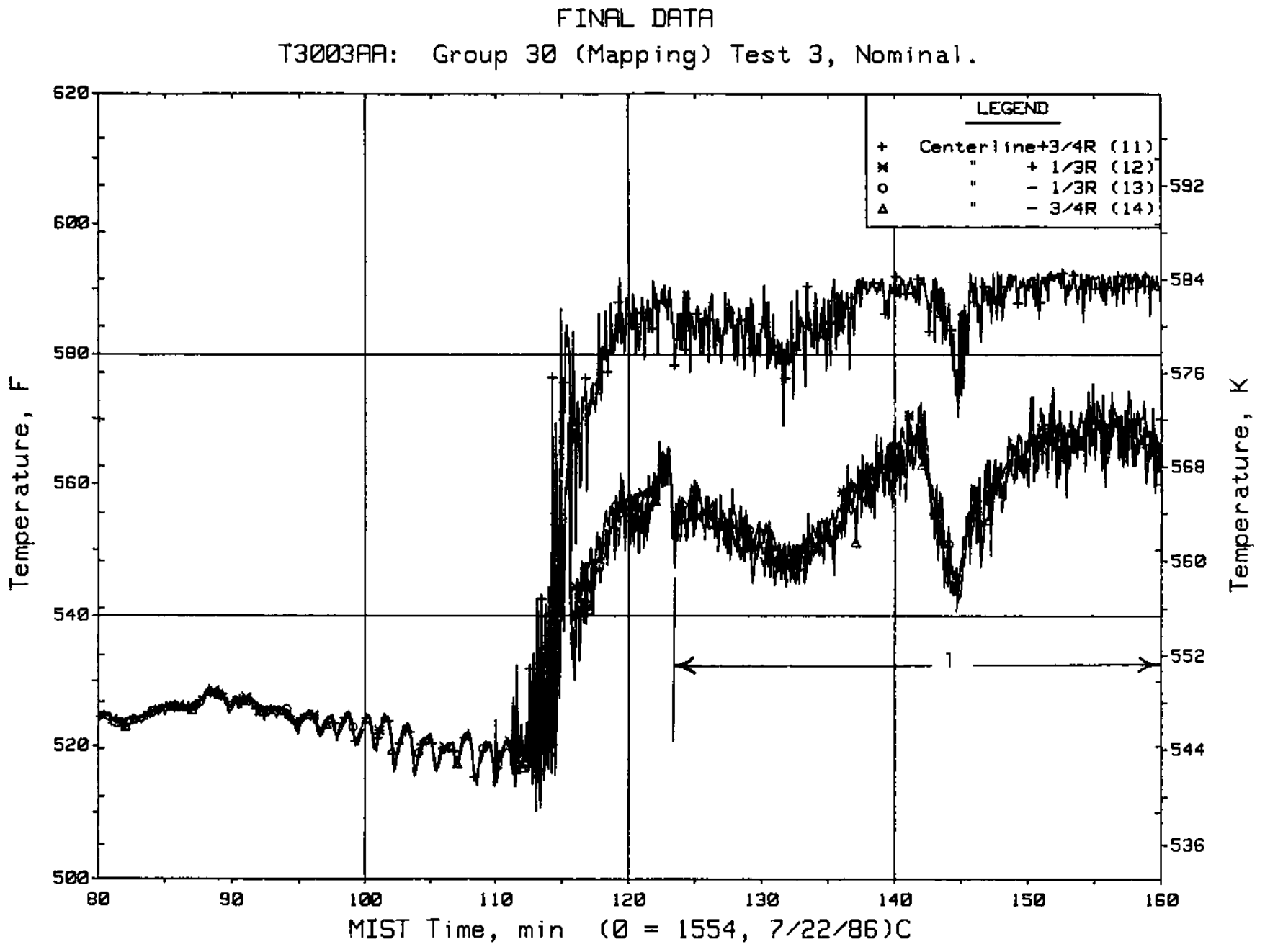

Figure 5.1.23. Cold Leg B2 Nozzle Rake Fluid Temperatures (21.2 ft, C4TCs)

Wed Feb 8 15:06:00 1989

C4TC4

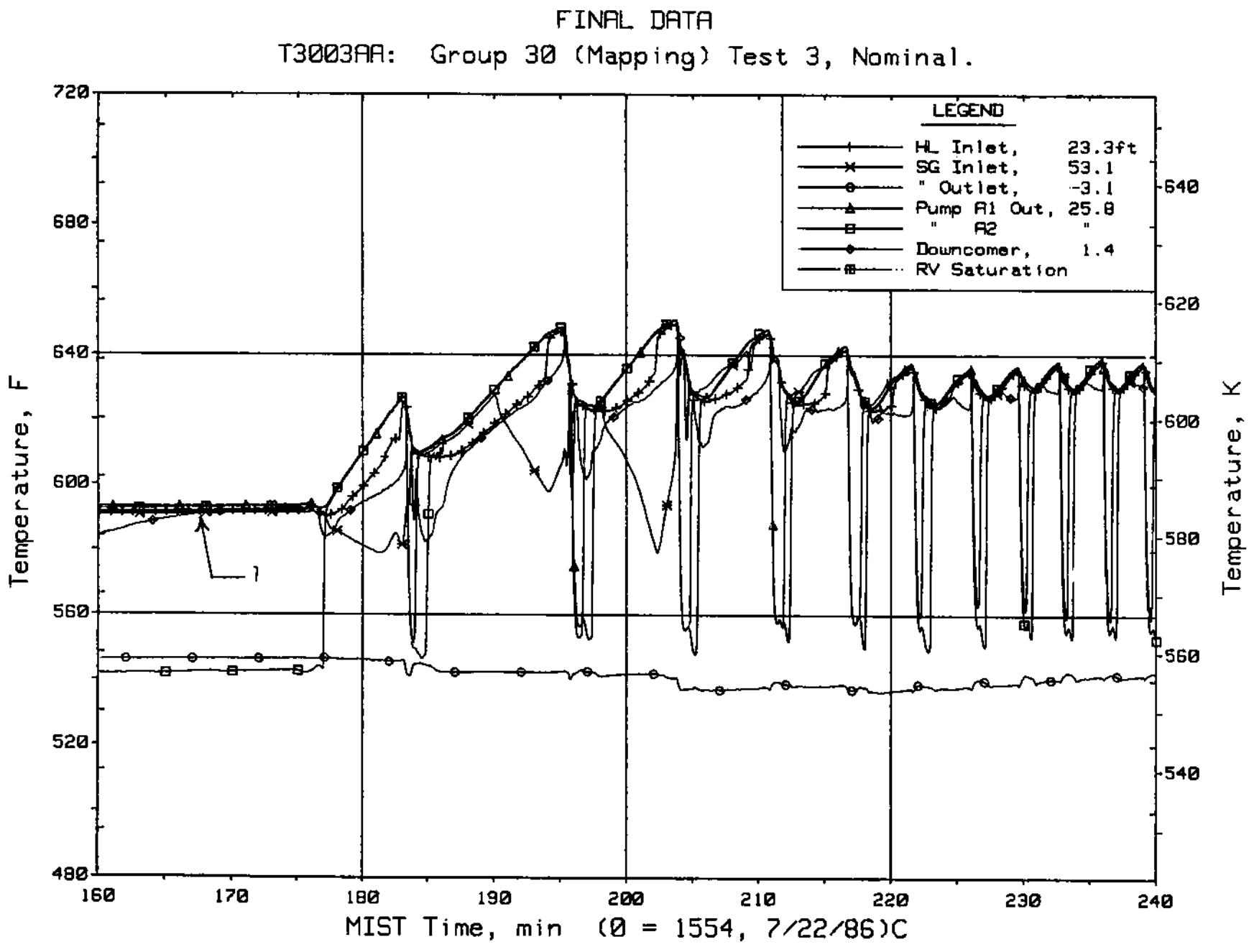

Figure 5.1.24. Loop A Primary Fluid Temperatures (RTDs)

Wed Feb 8 15:15:05 1989

PRRT1

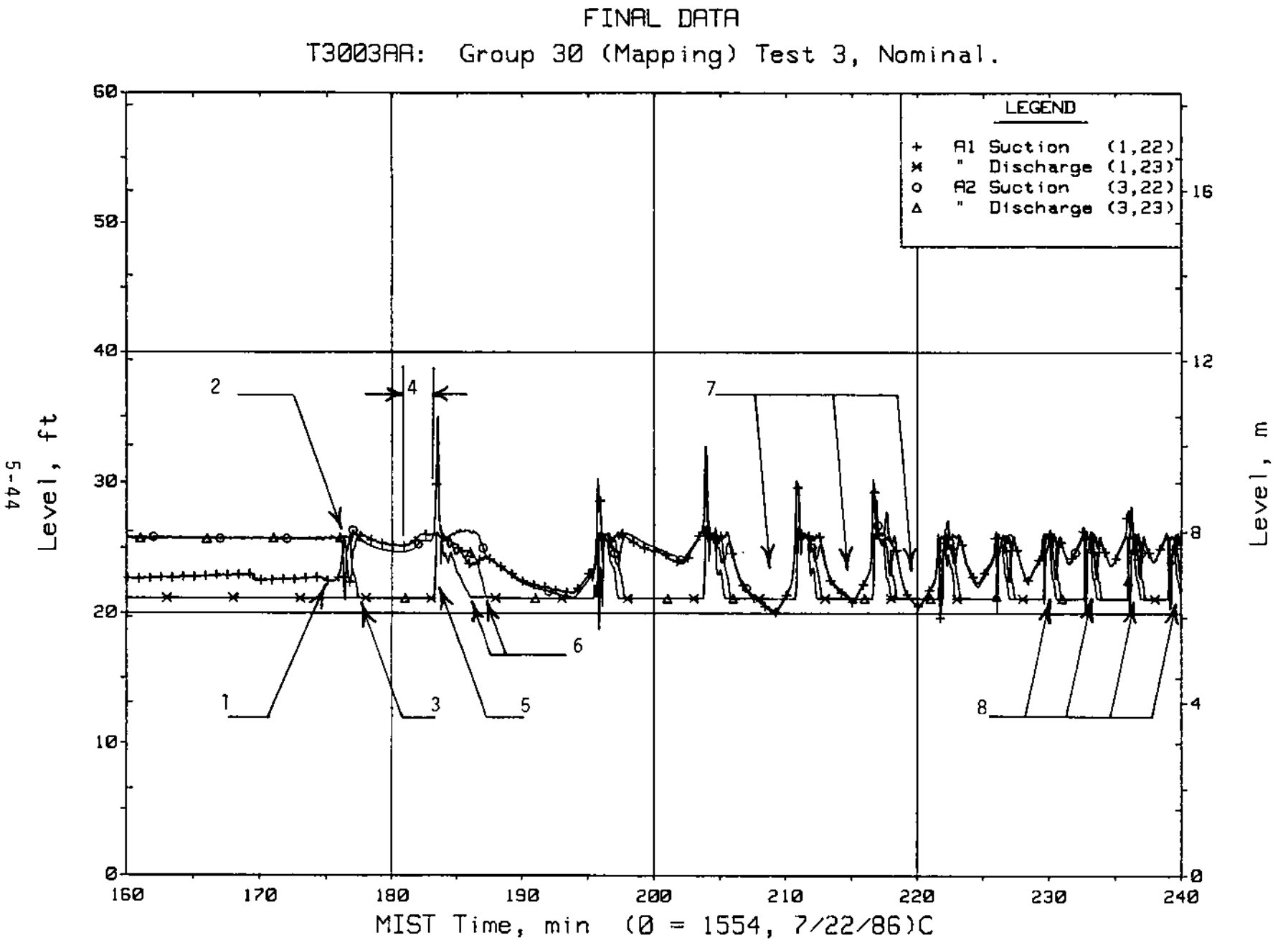

Figure 5.1.25. Loop A Cold Leg Collapsed Liquid Levels (LVs)

Wed Feb 8 15:20:11 1989

CLLV1

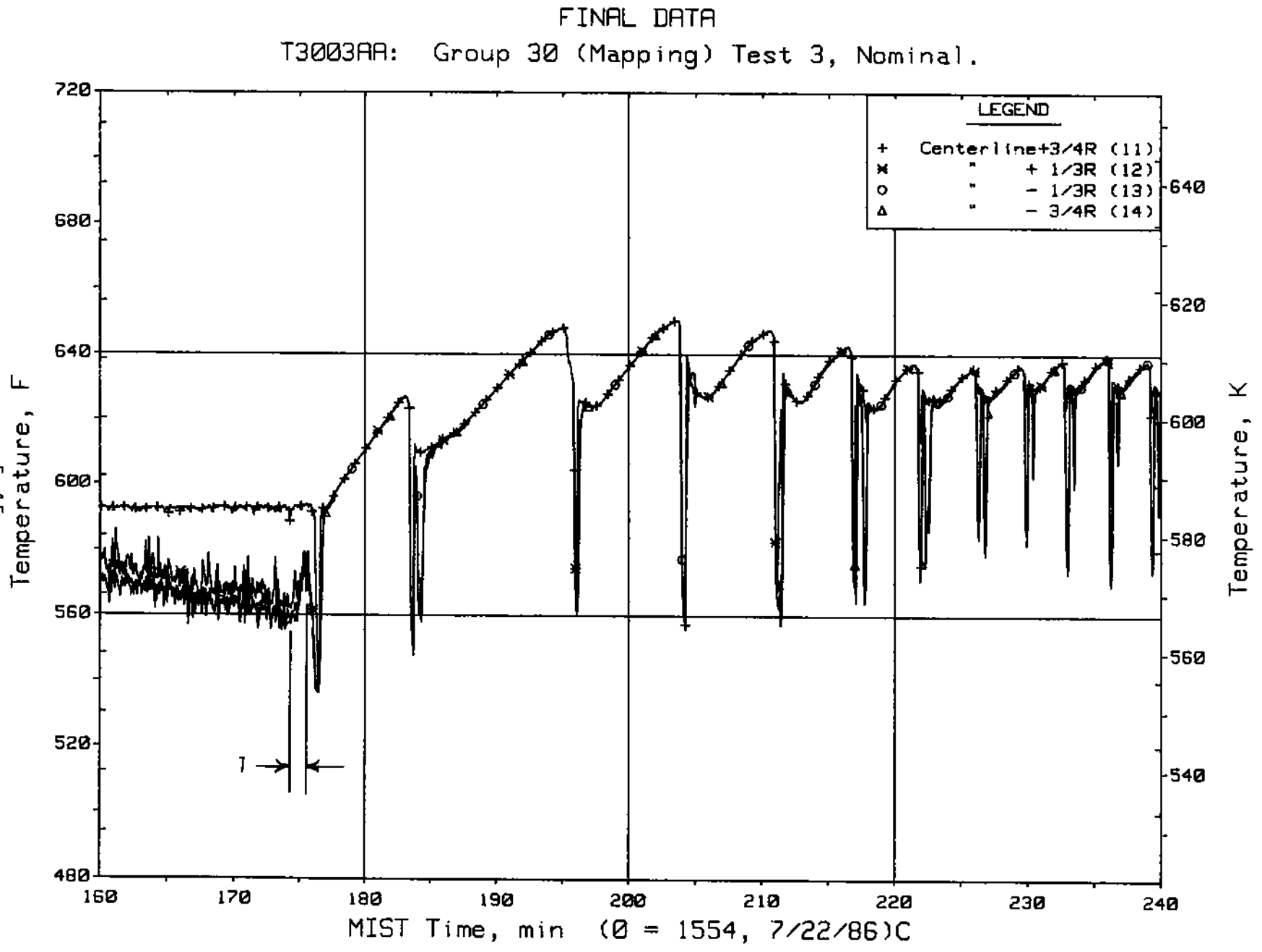

Figure 5.1.26. Cold Leg A2 Nozzle Rake Fluid Temperatures (21.2 ft, C3TCs)

Wed Feb 8 15:33:45 1989

C3TC4

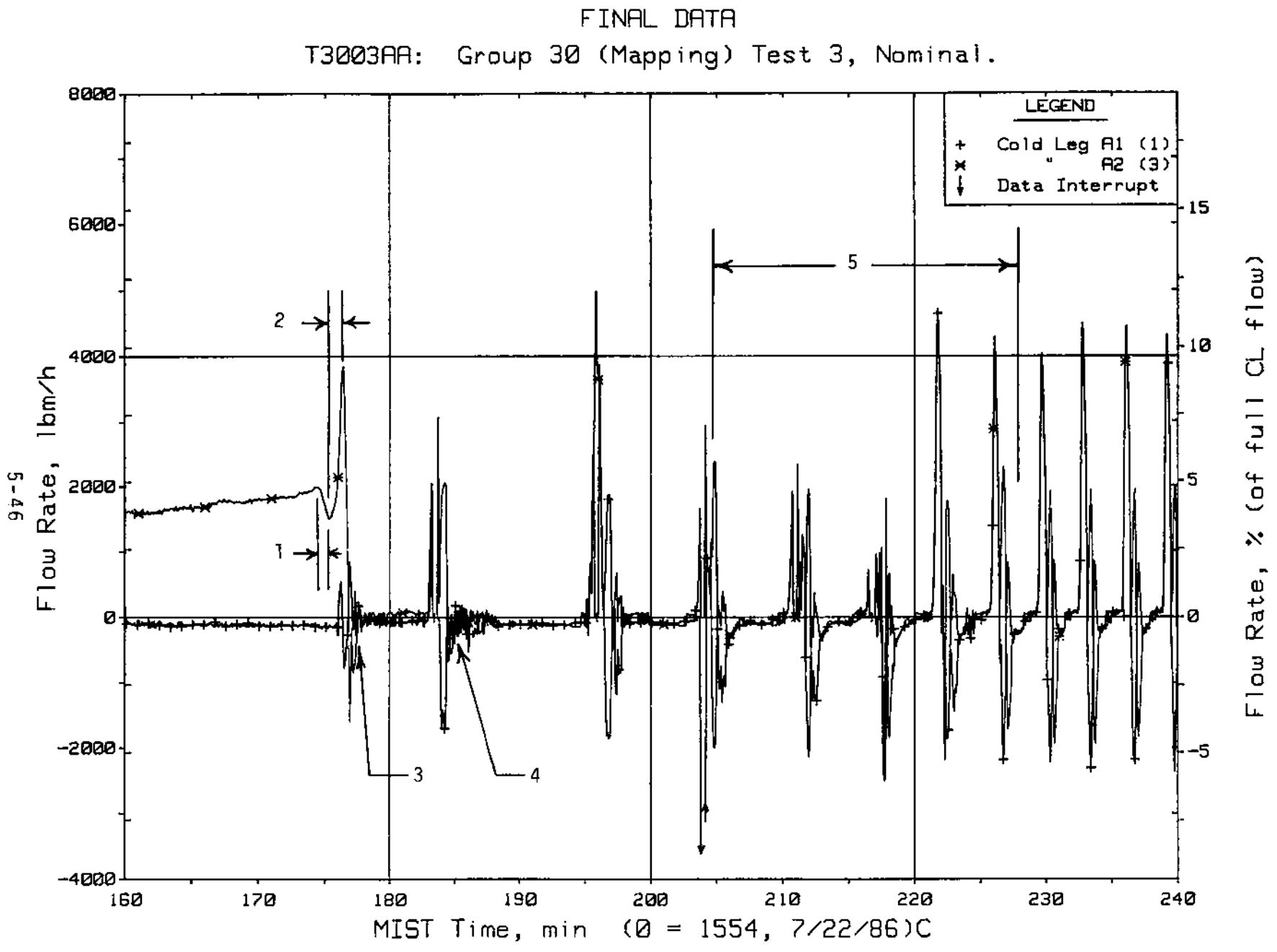

Figure 5.1.27. Loop A Cold Leg (Venturi) Flow Rates (VN20s)

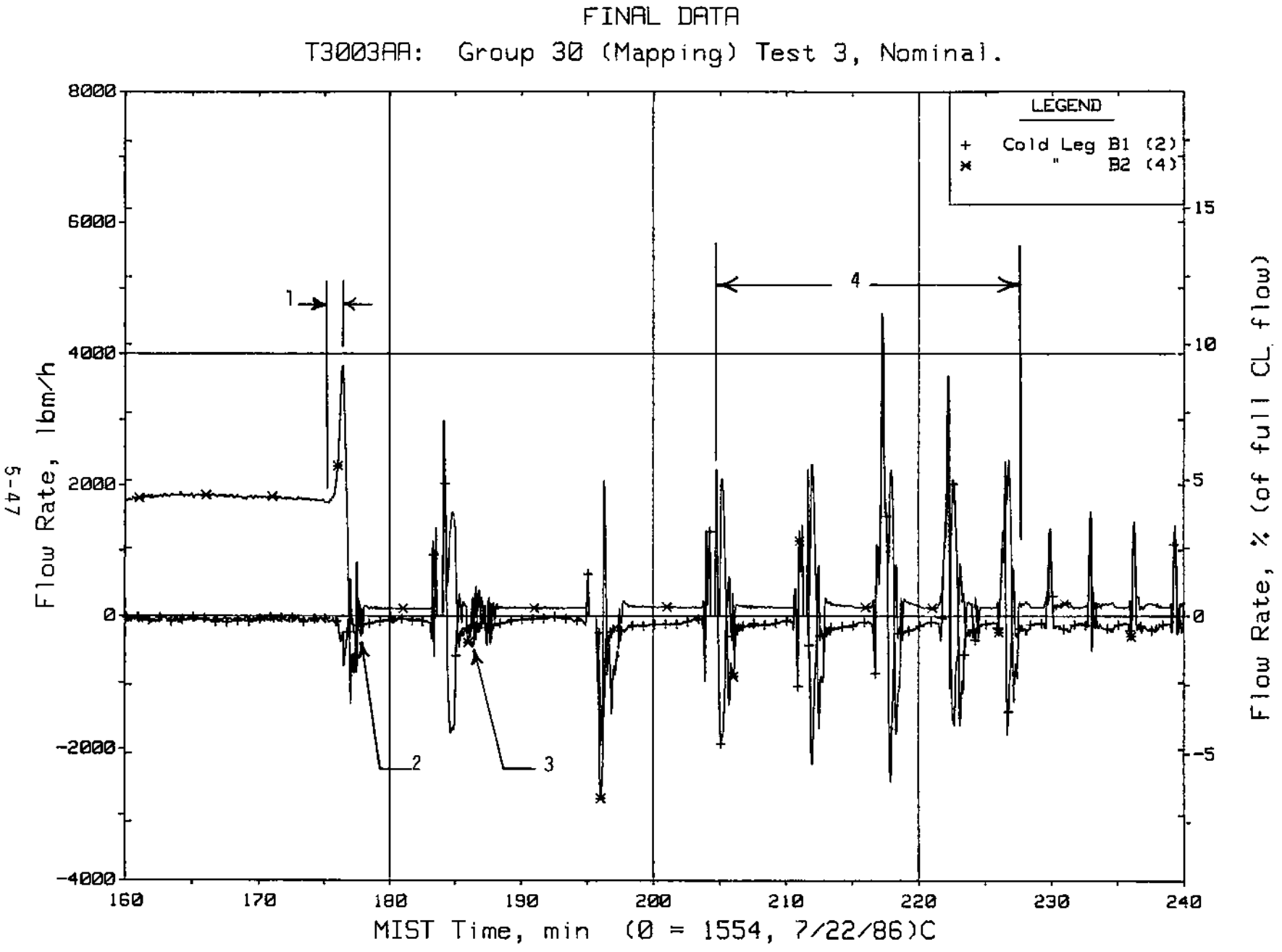

Figure 5.1.28. Loop B Cold Leg (Venturi) Flow Rates (VN20s)

Thu Mar 16 15:12:23 1989

PRFL6

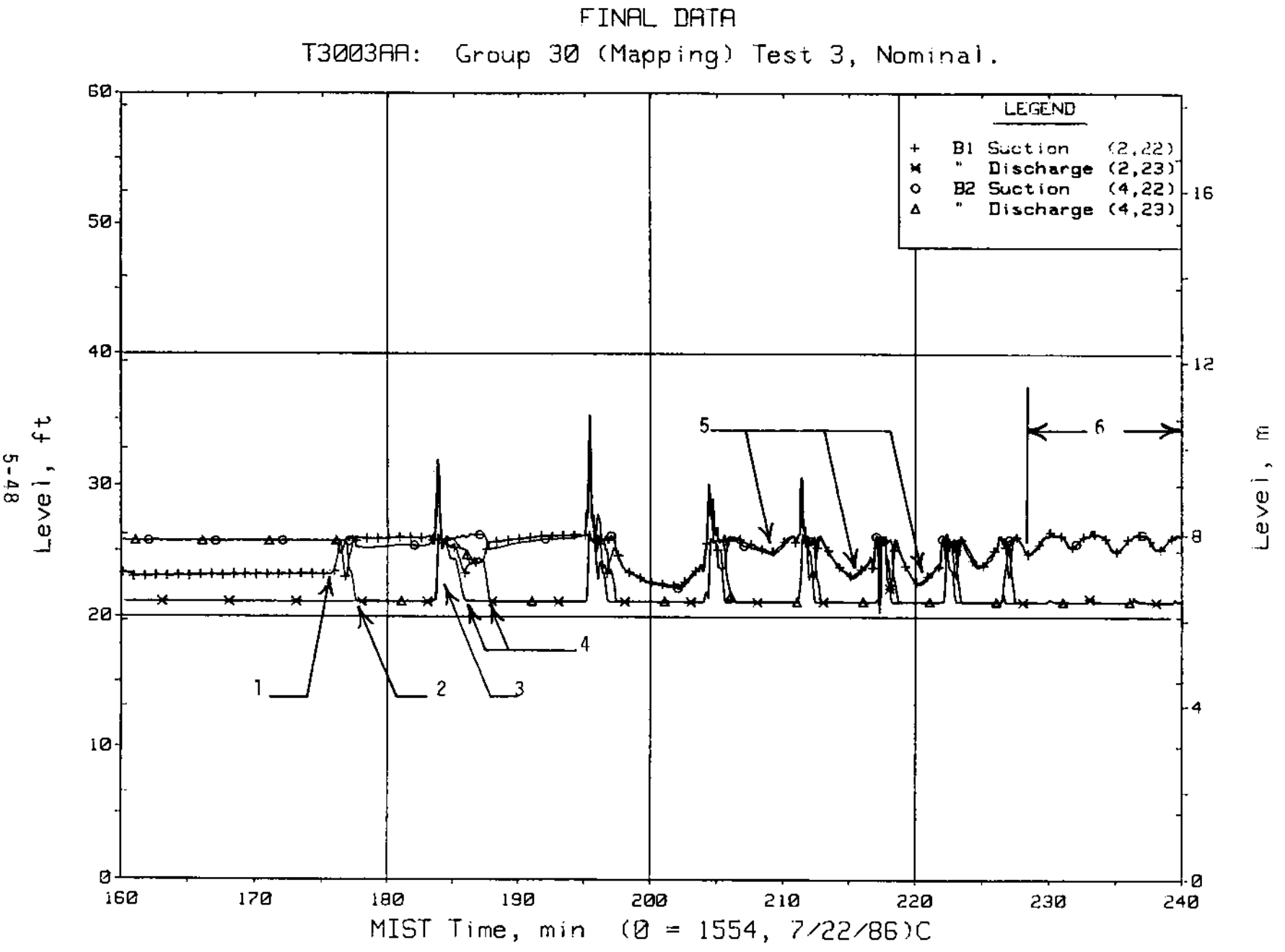

Figure 5.1.29. Loop B Cold Leg Collapsed Liquid Levels (LVs)

Thu Feb 9 09:57:46 1989

CLLV2

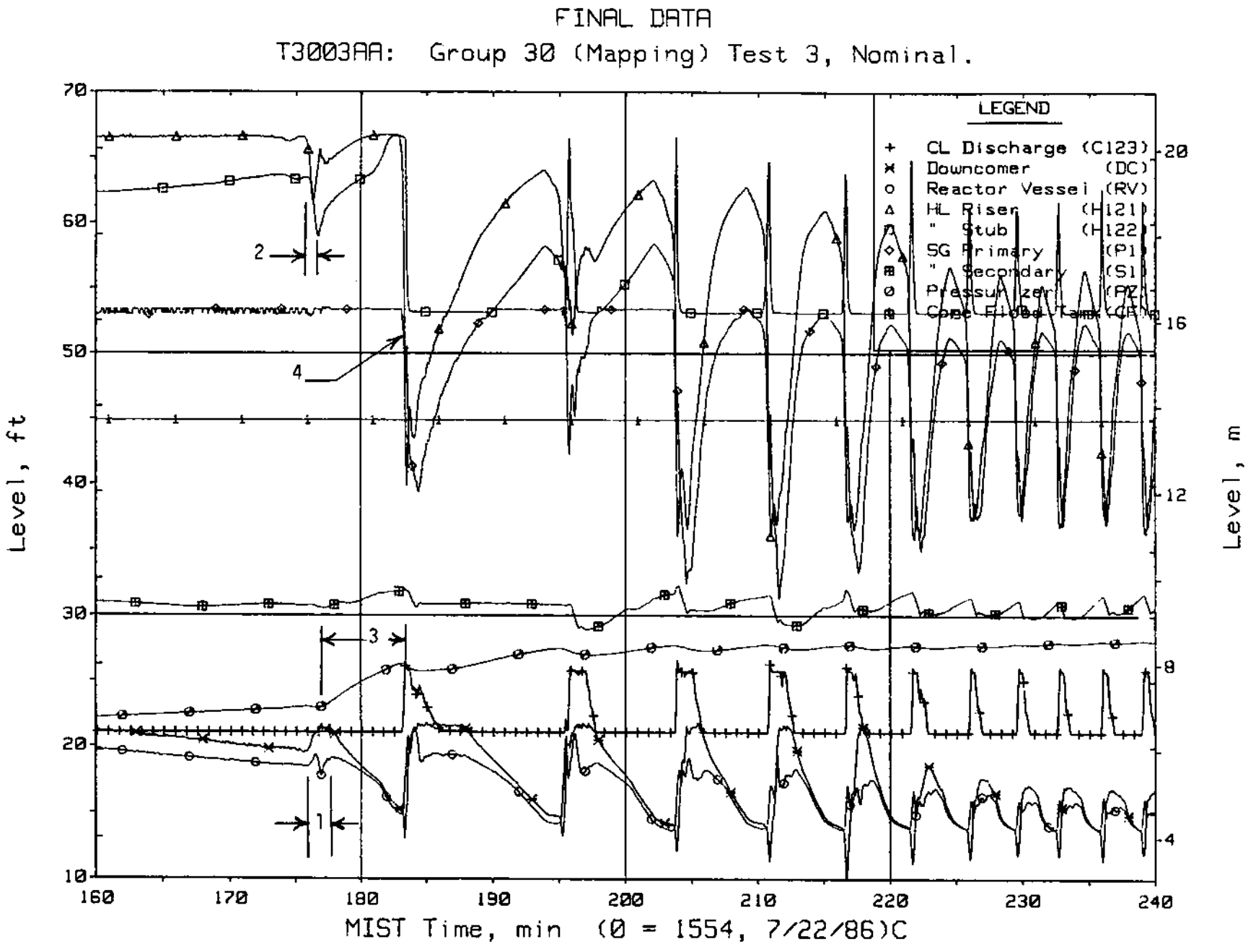

Figure 5.1.30. Loop A Collapsed Liquid Levels (LV20s)

Tue Feb 7 15:38:48 1989

PRLV1

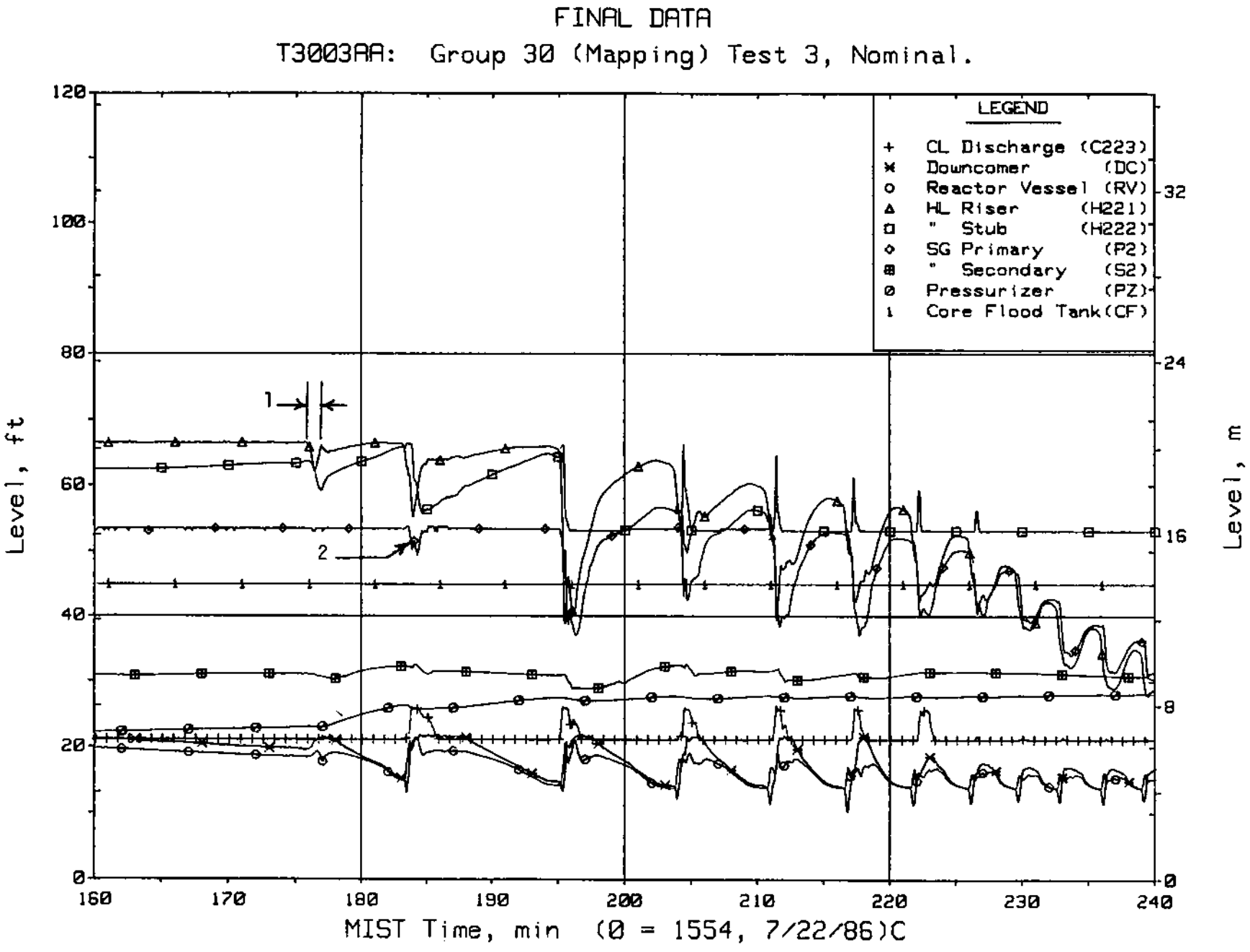

Figure 5.1.31. Loop B Collapsed Liquid Levels (LV20s)

Thu Feb 9 10:04:13 1989

PRLV2

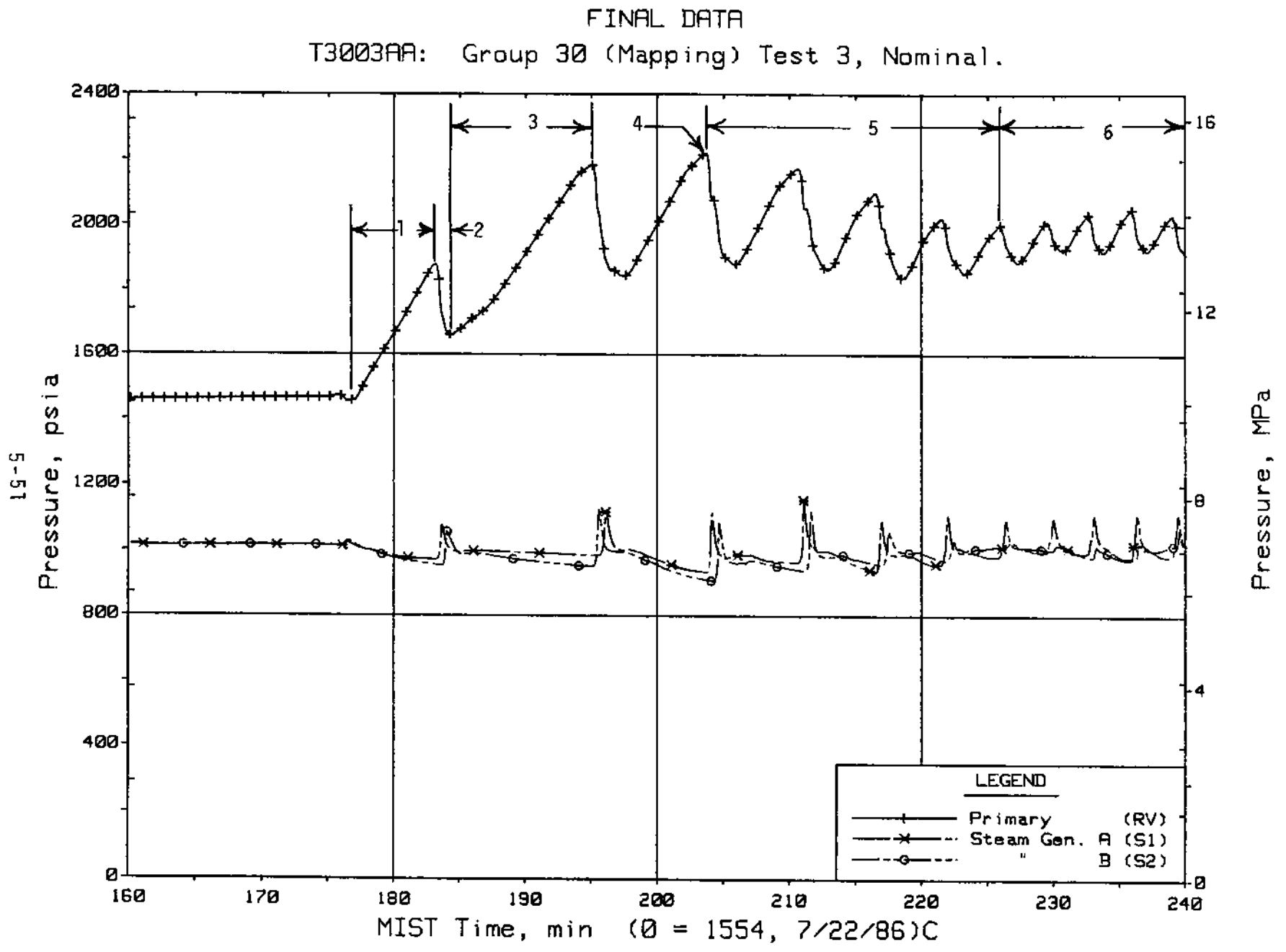

Figure 5.1.32. Primary and Secondary System Pressures (GPOIs)

Thu Feb 9 10:12:25 1989

PSGP1

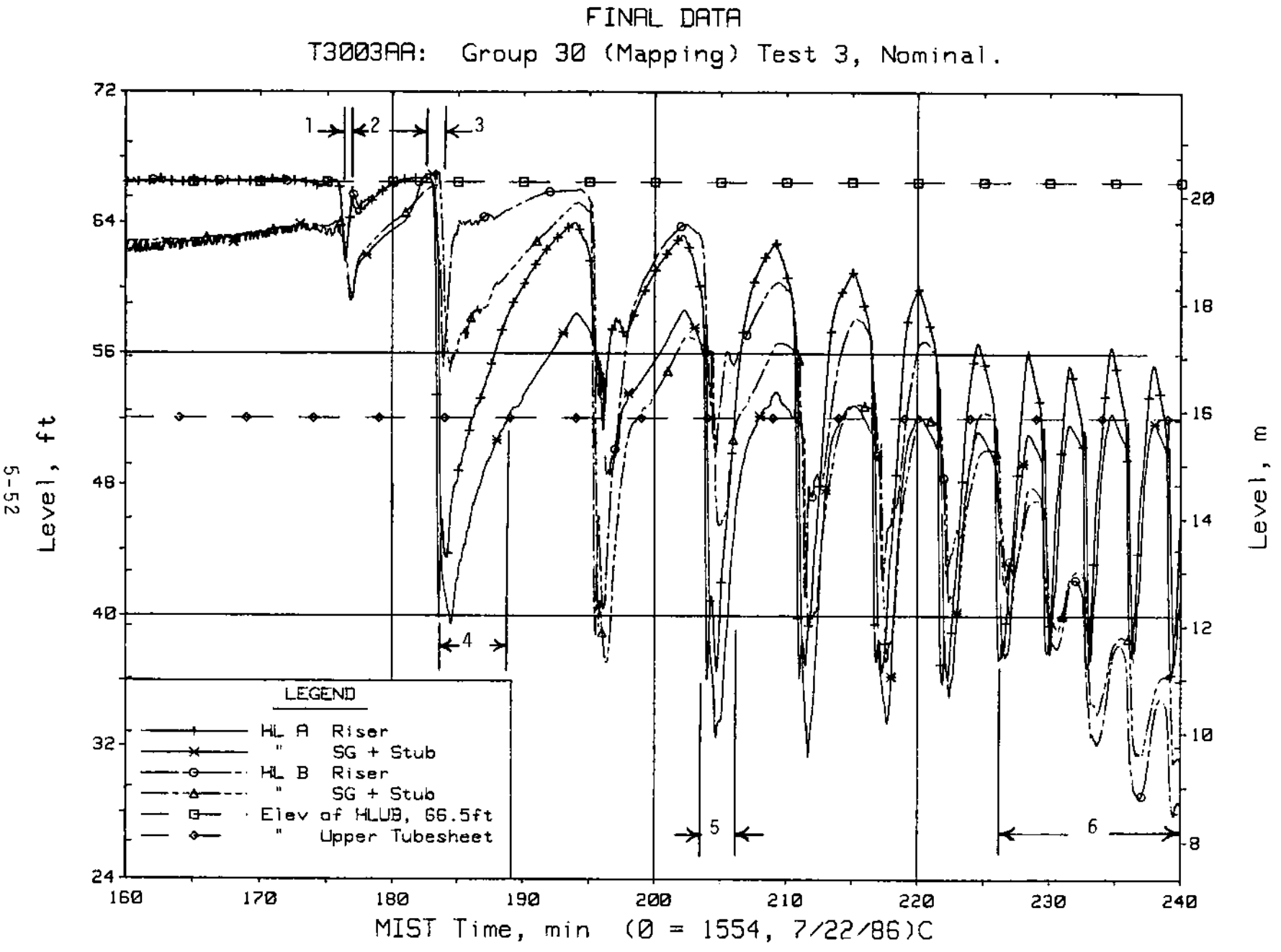

Figure 5.1.33. Hot Leg Riser and Stub Collapsed Liquid Levels

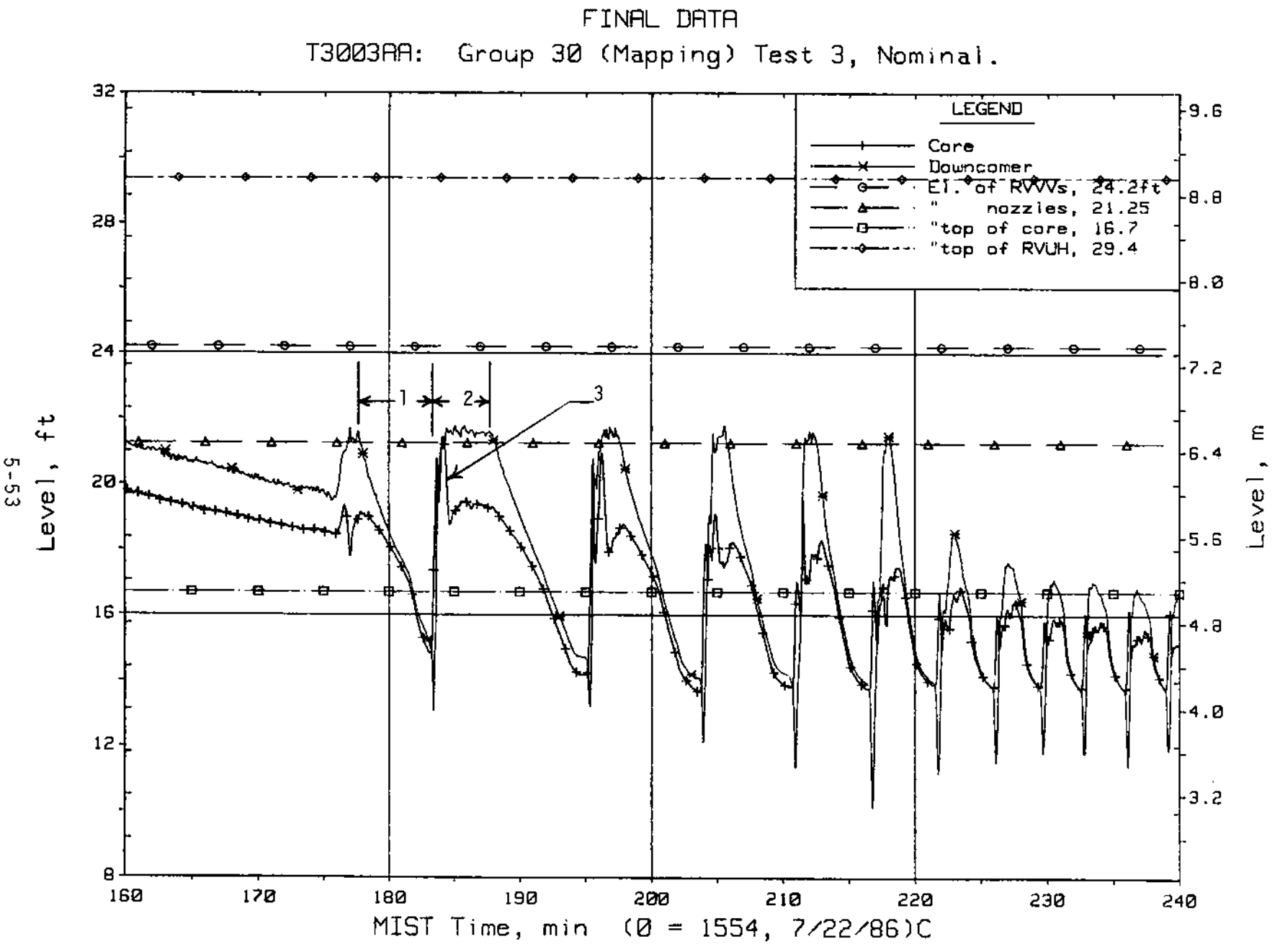

Figure 5.1.34. Core Region Collapsed Liquid Levels

Tue Feb 7 15:55:55 1989

COLV1

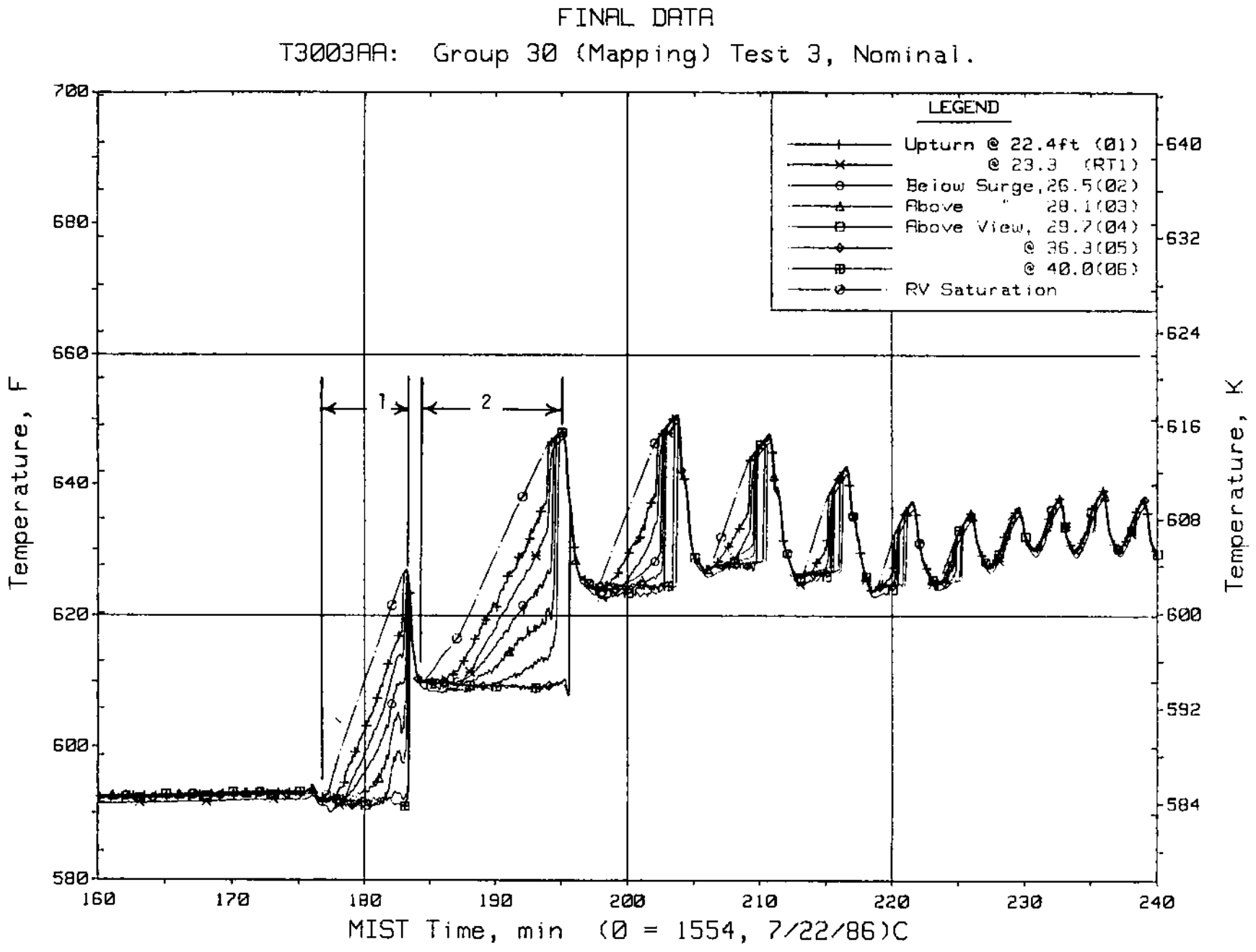

Figure 5.1.35. Hot Leg A Lower-Elevation Riser Fluid Temperatures (H1TCs)

Tue Feb 7 16:00:26 1989

H1TC1

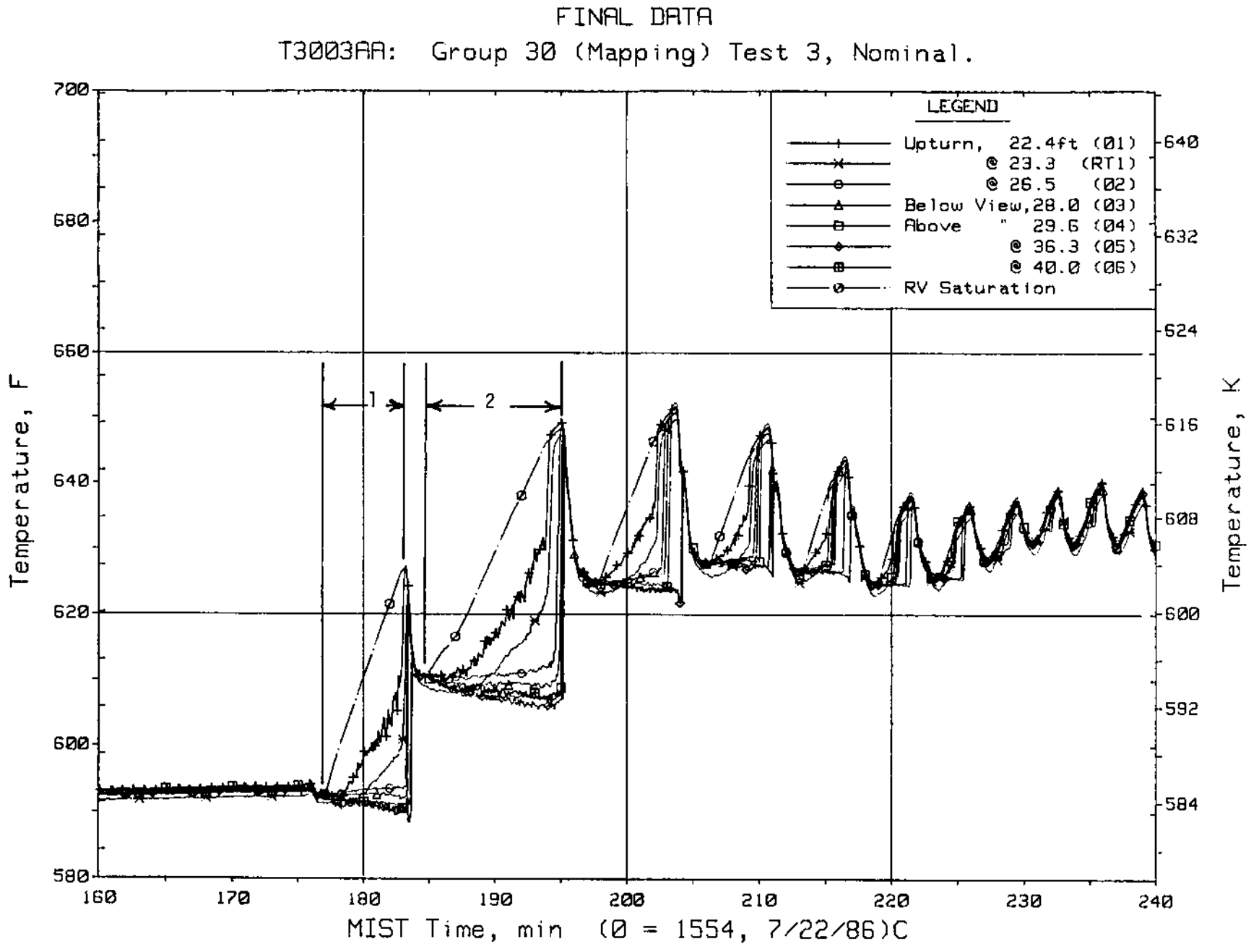

Figure 5.1.36. Hot Leg B Lower-Elevation Riser Fluid Temperatures (H2TCs)

Tue Feb 7 16:05:13 1989

H2TC1

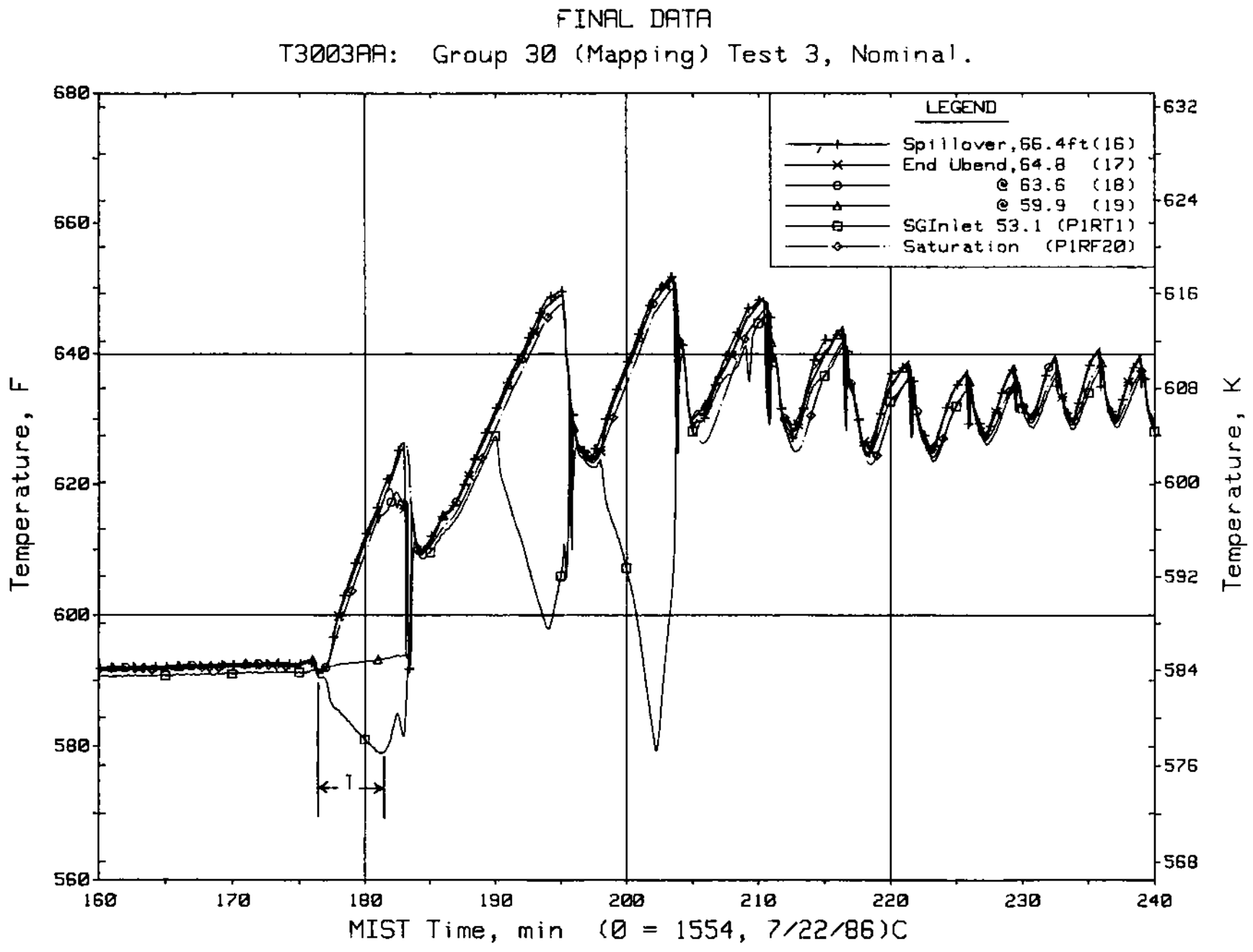

Figure 5.1.37. Hot Leg A Fluid Temperatures Beyond U-Bend (HITCs)

Tue Feb 7 16:10:13 1989

HITC3

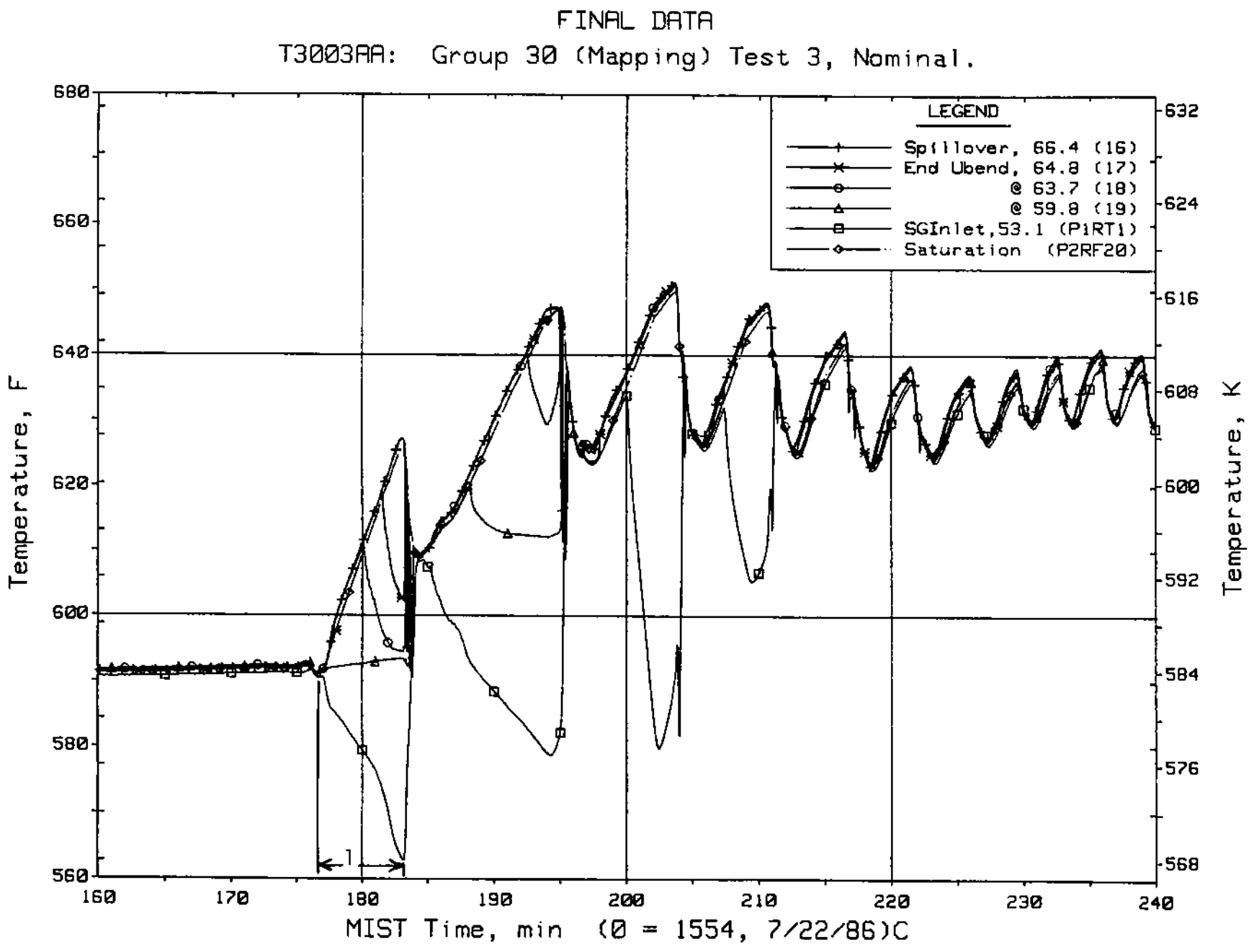

Figure 5.1.38. Hot Leg B Fluid Temperatures Beyond U-Bend (H2TCs)

Tue Feb 7 16:14:14 1989

H2TC3

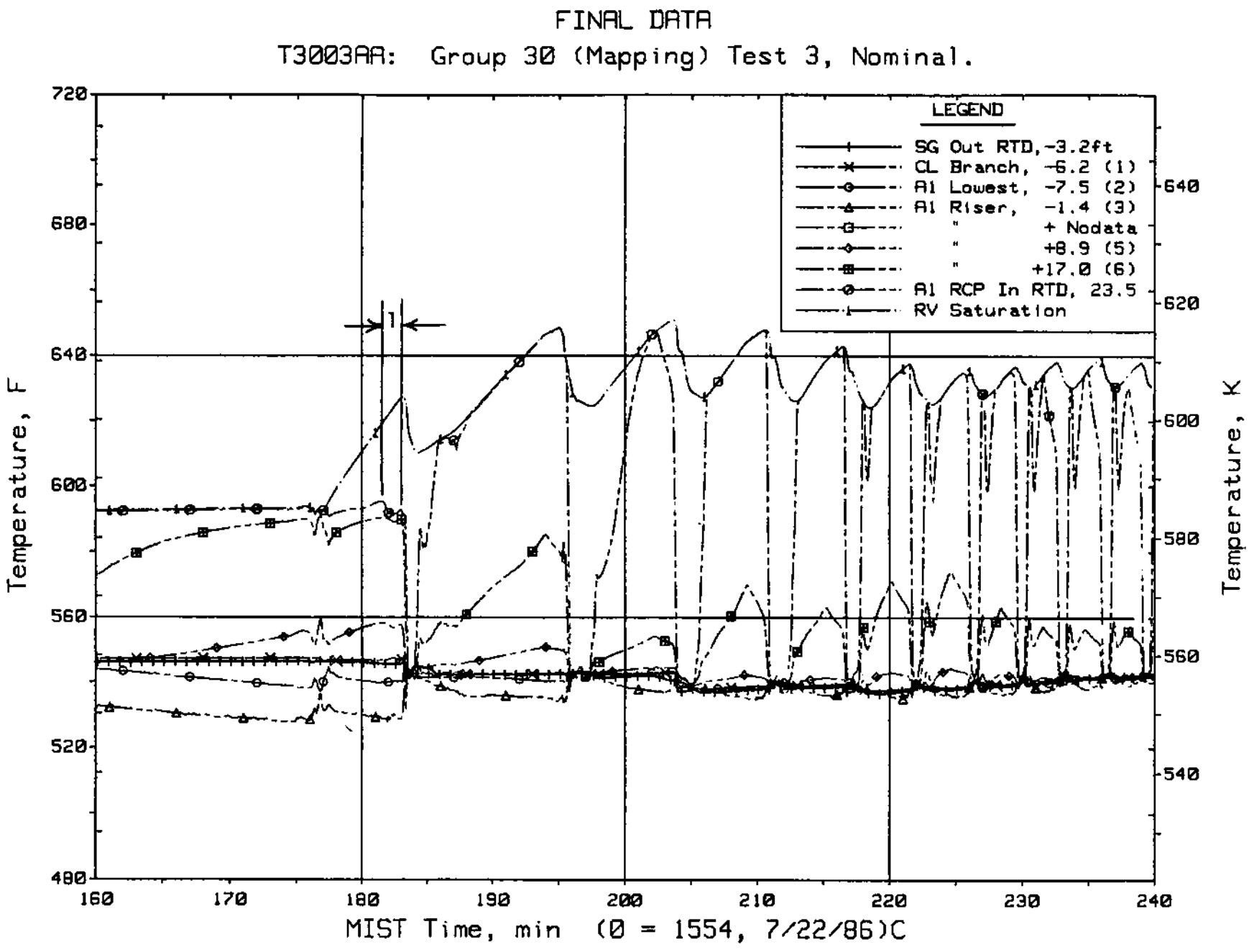

Figure 5.1.39. Cold Leg A1 Suction Fluid Temperatures (C1TCs)

Thu Feb 9 10:25:00 1989

C1TC1

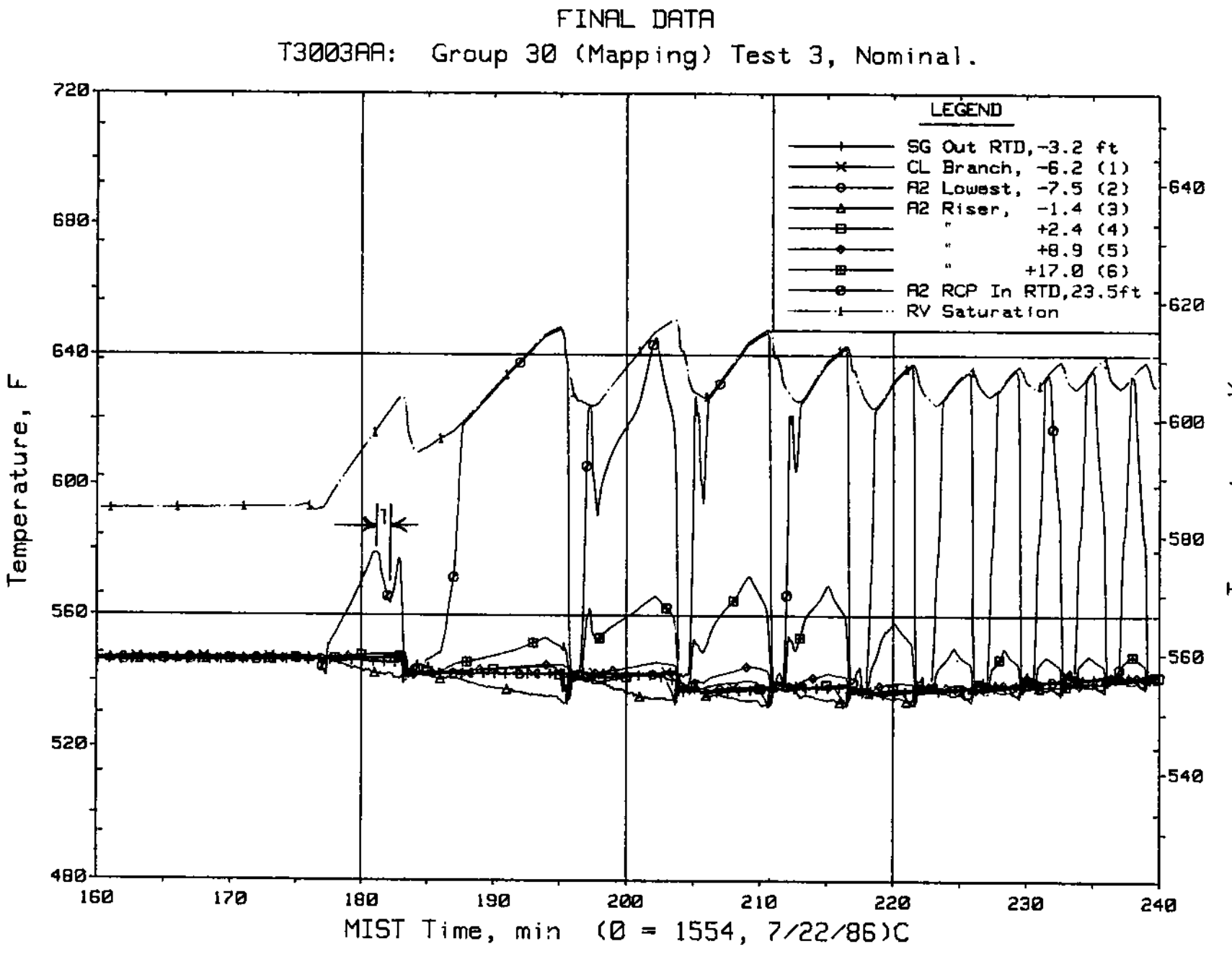

Figure 5.1.40. Cold Leg A2 Suction Fluid Temperatures (C3TCs)

Thu Feb 9 10:35:44 1989

C3TC1

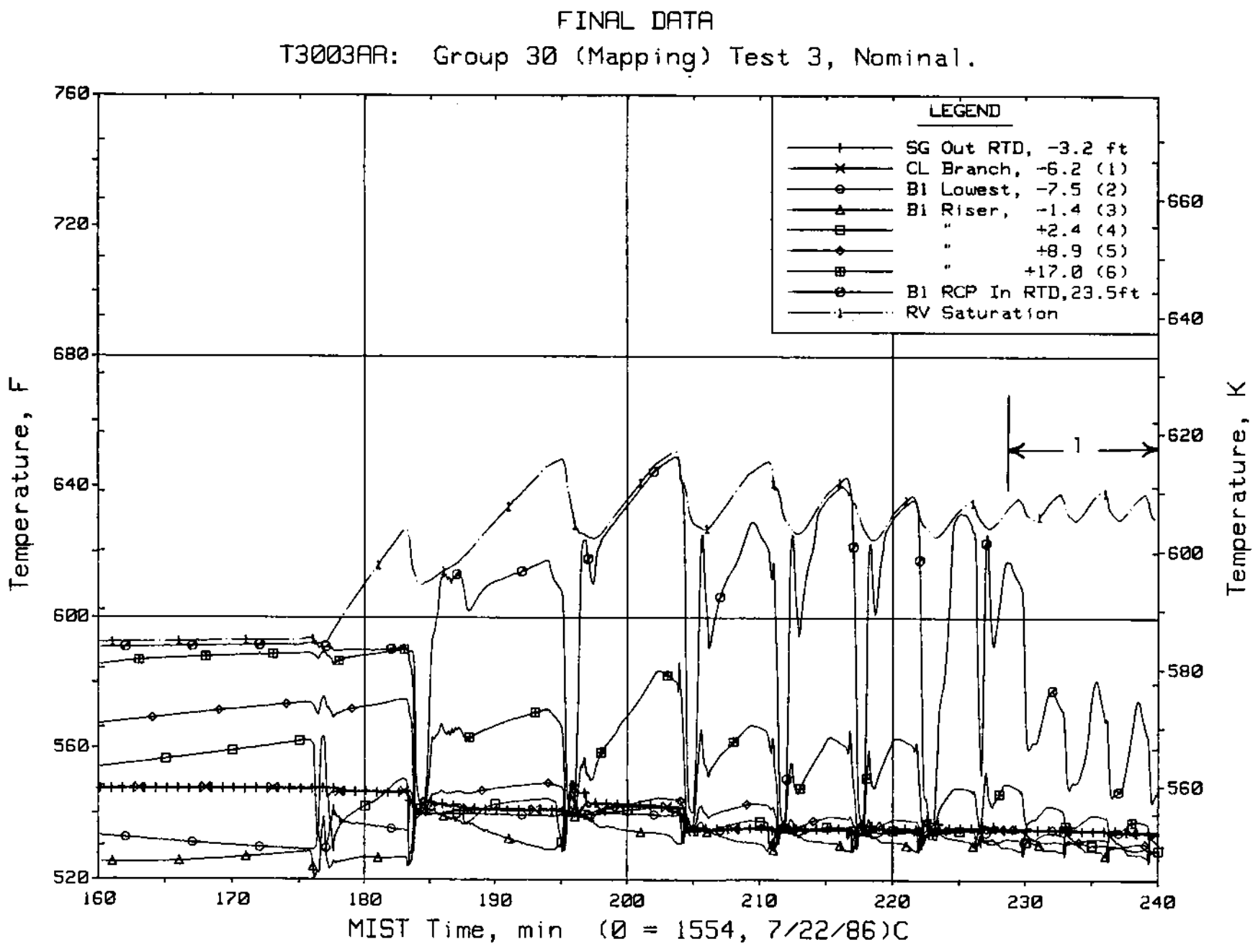

Figure 5.1.41. Cold Leg B1 Suction Fluid Temperatures (C2TCs)

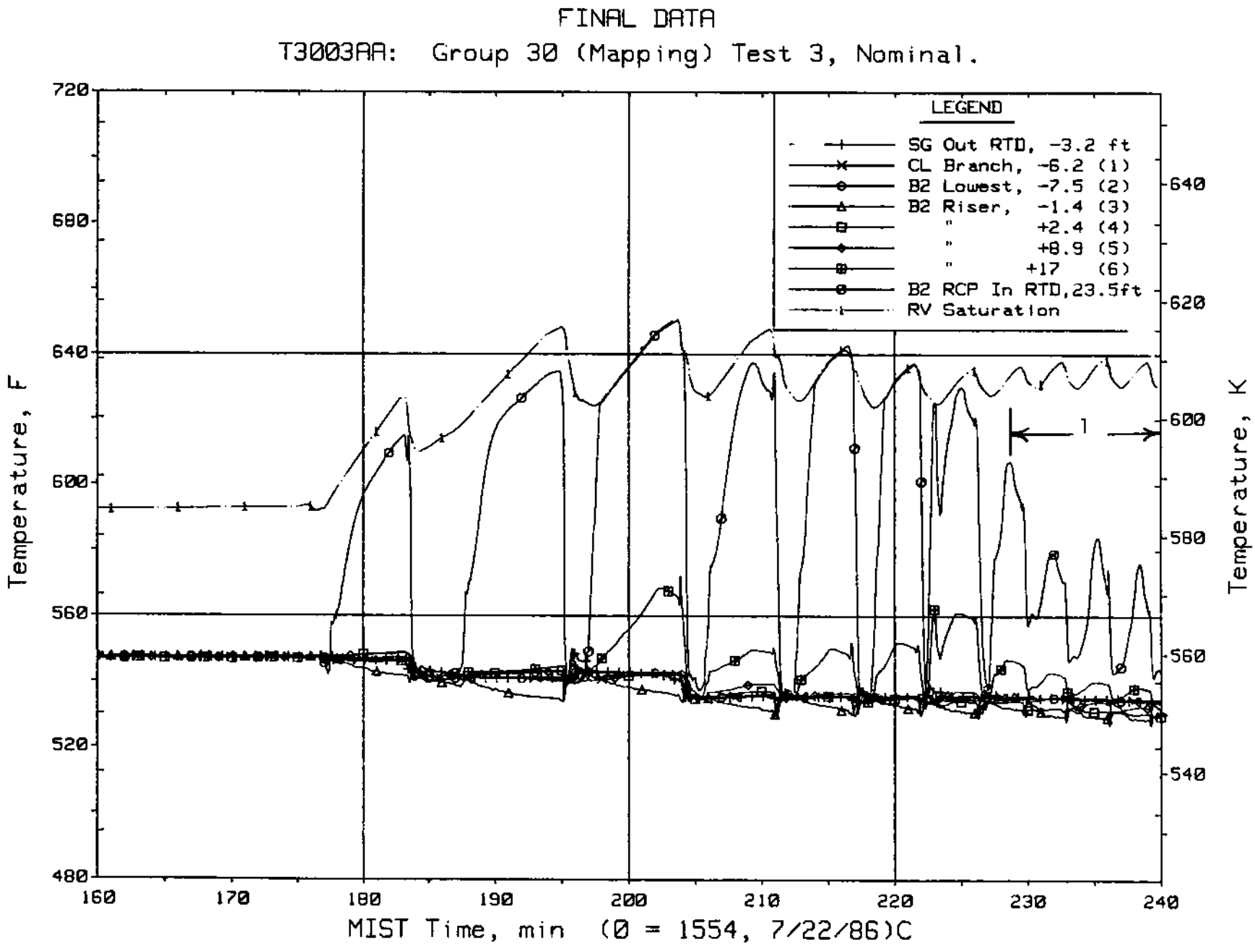

Figure 5.1.42. Cold Leg B2 Suction Fluid Temperatures (C4TCs)

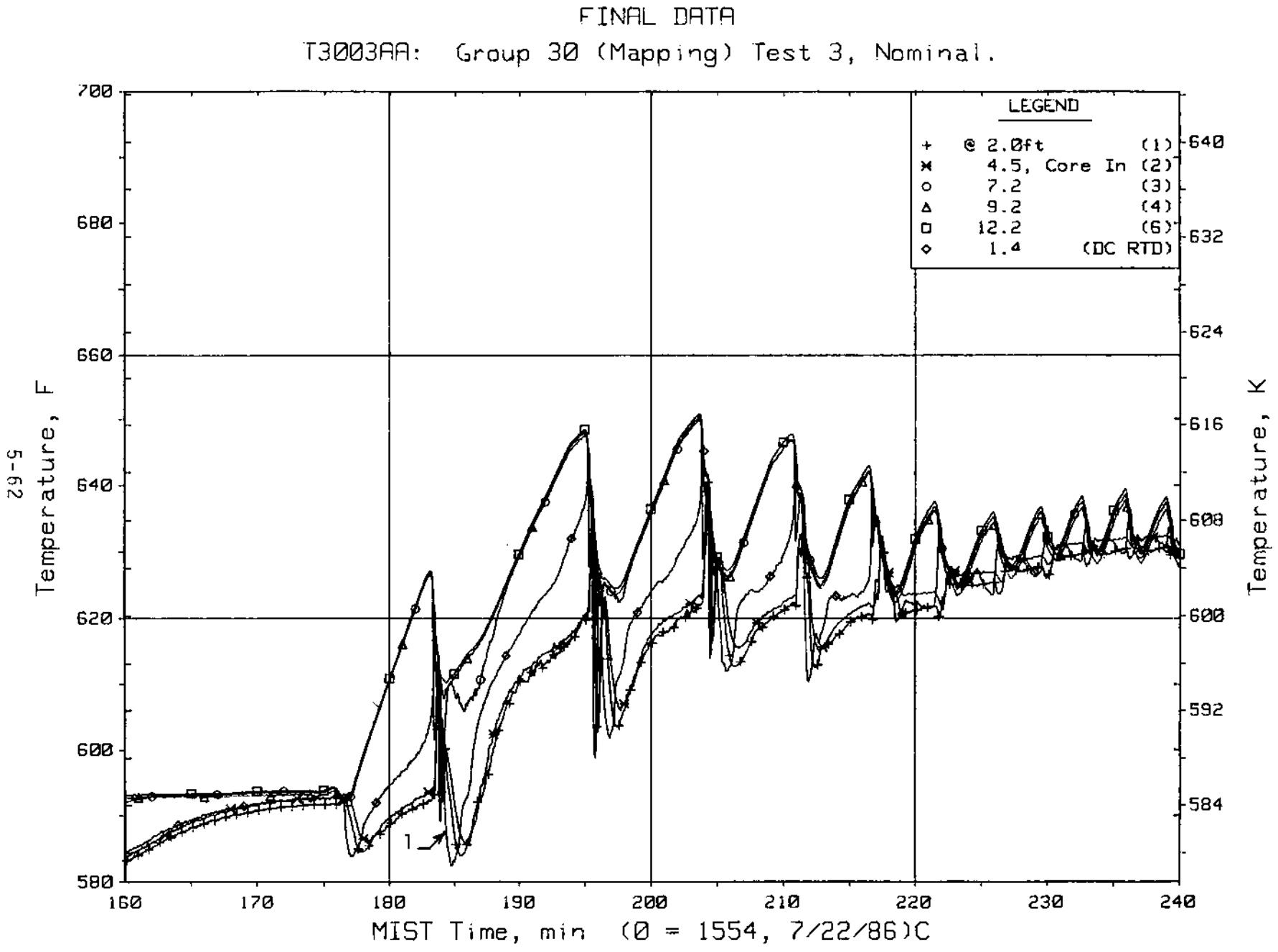

Figure 5.1.43. Reactor Vessel Lower-Elevation Fluid Temperatures (RVTCs)

Tue Jan 31 16:12:43 1989

RVTC1

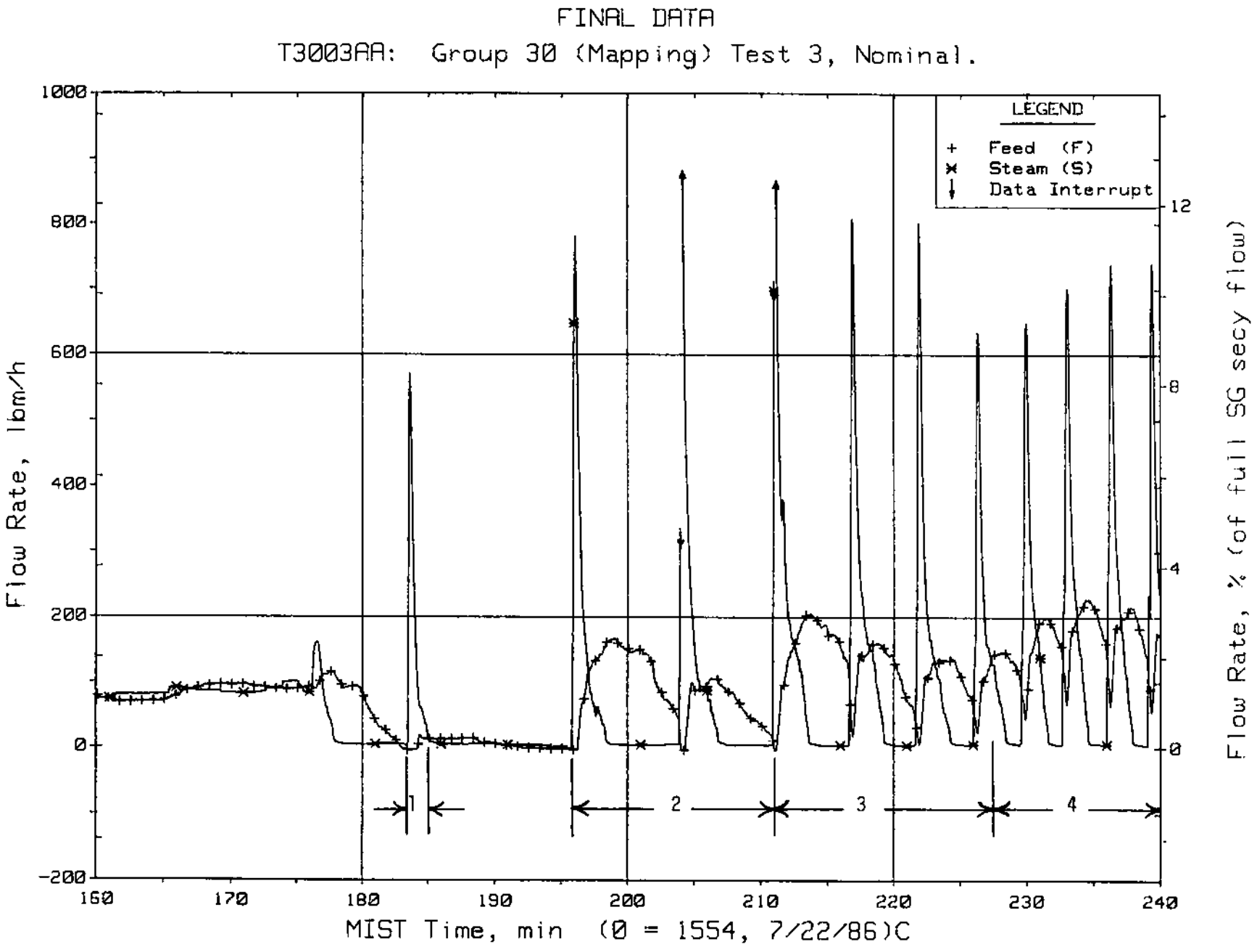

Figure 5.1.44. Steam Generator A Flow Rates (OR20s)

Tue Feb 7 16:38:20 1989

SCFL1

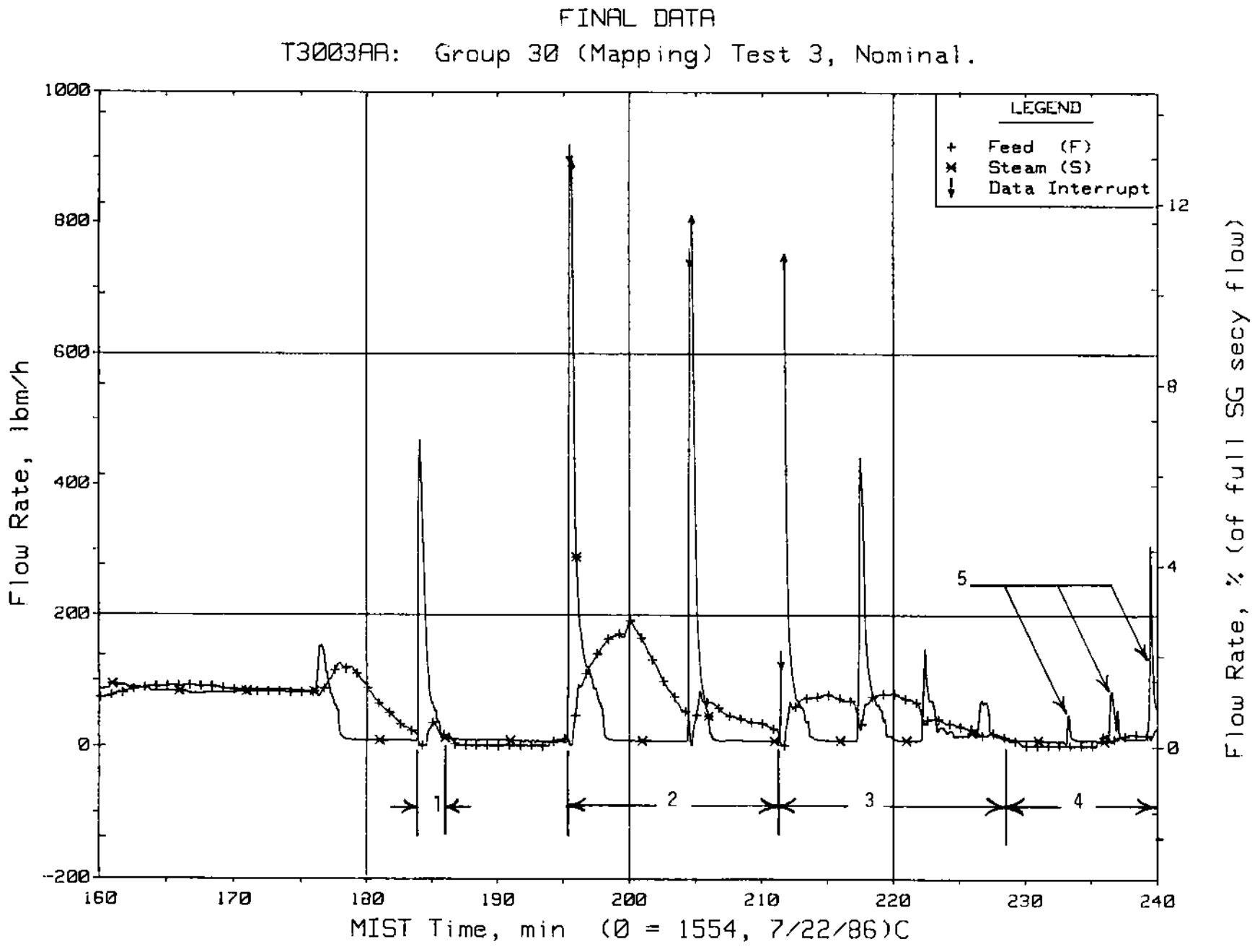

Figure 5.1.45. Steam Generator B Flow Rates (OR21s)

Tue Feb 7 16:40:50 1989

SCFL2

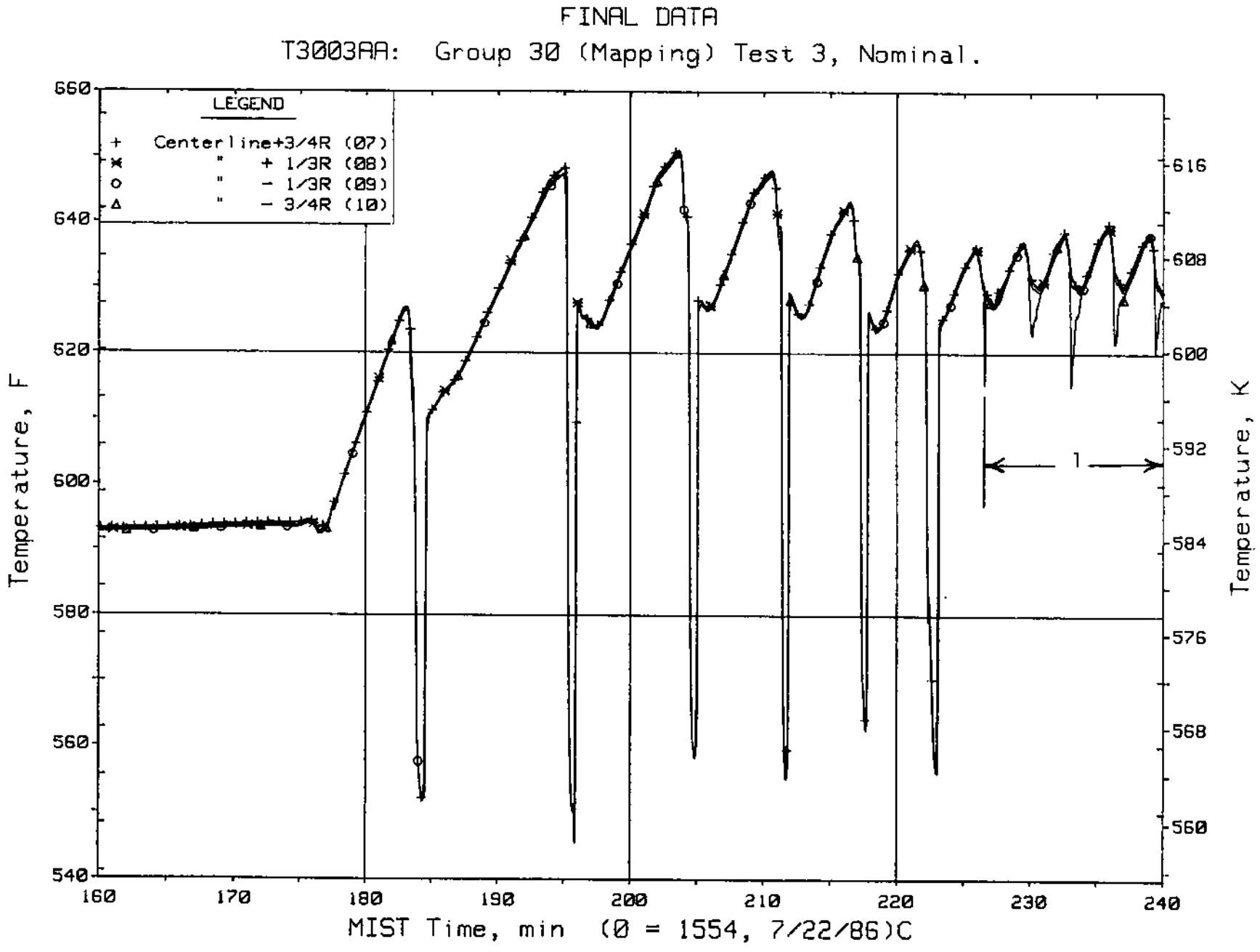

Figure 5.1.46. Cold Leg B1 Pump Discharge Rake Fluid Temperatures (25 ft, C2TCs)

Tue Feb 7 16:43:58 1989

C2TC3

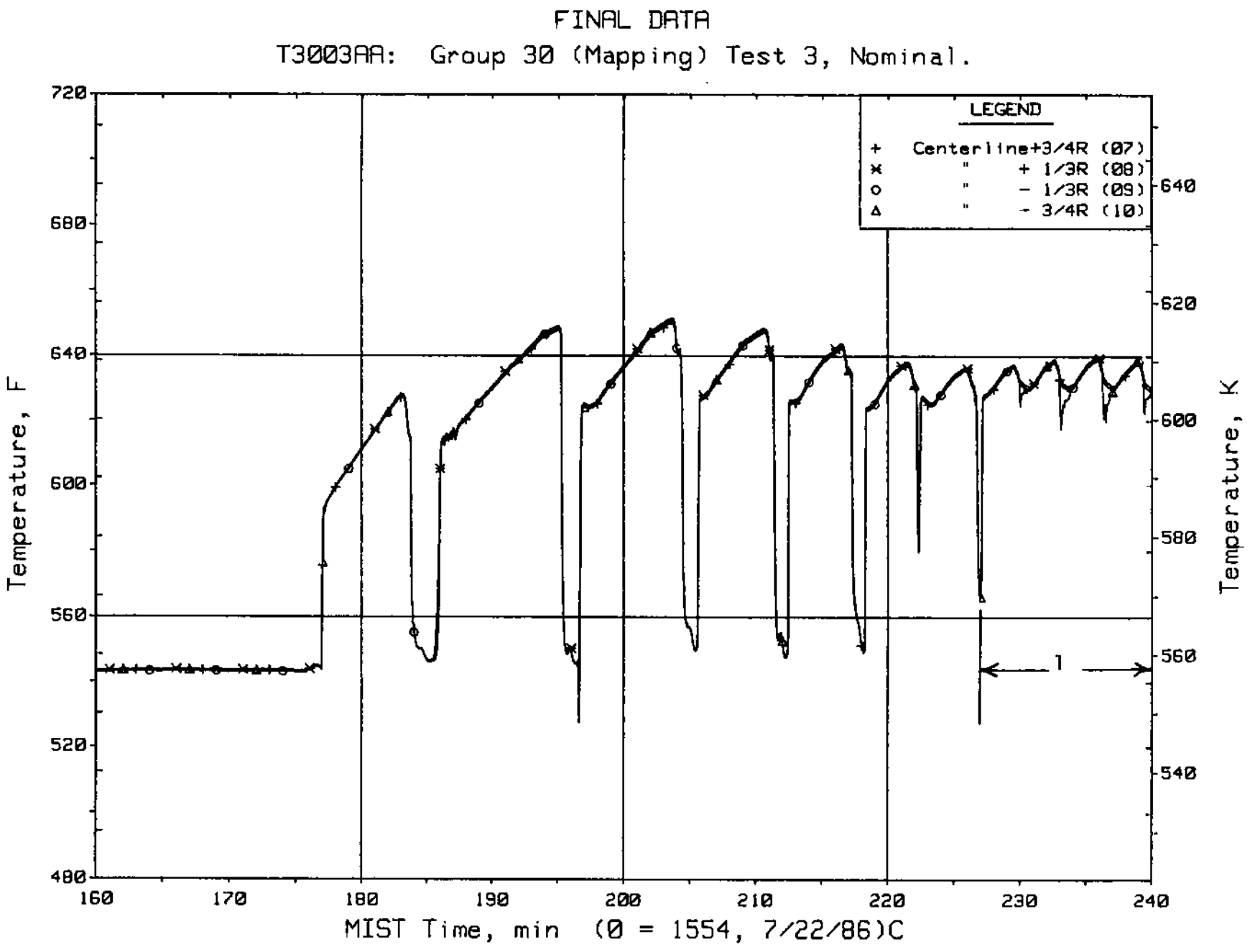

Figure 5.1.47. Cold Leg B2 Pump Discharge Rake Fluid Temperatures (25 ft, C4TCs)

Thu Feb 9 10:48:48 1989

C4TC3

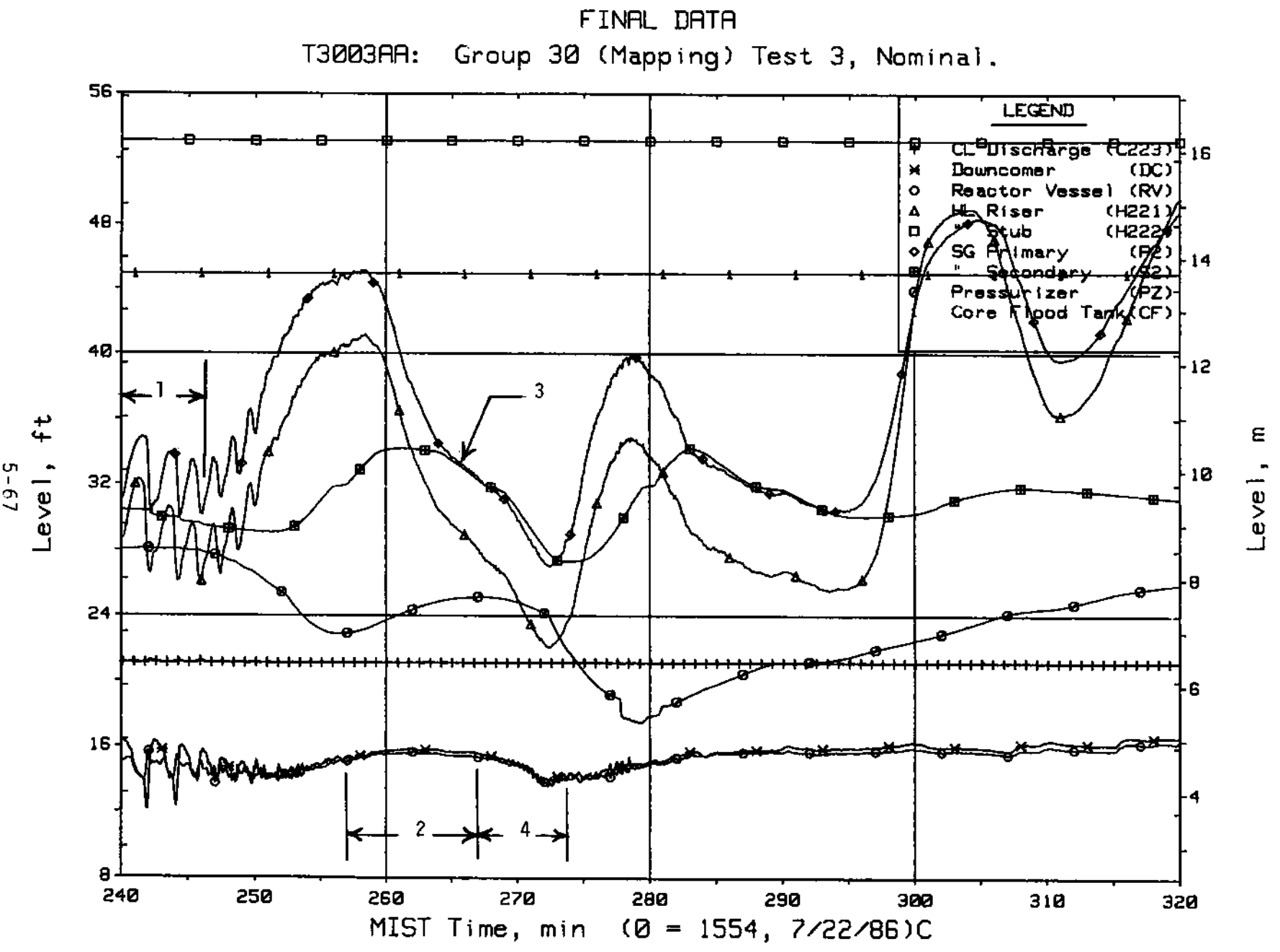

Figure 5.1.48. Loop B Collapsed Liquid Levels (LV20s)

Wed Feb 8 13:30:16 1989

PRLV2

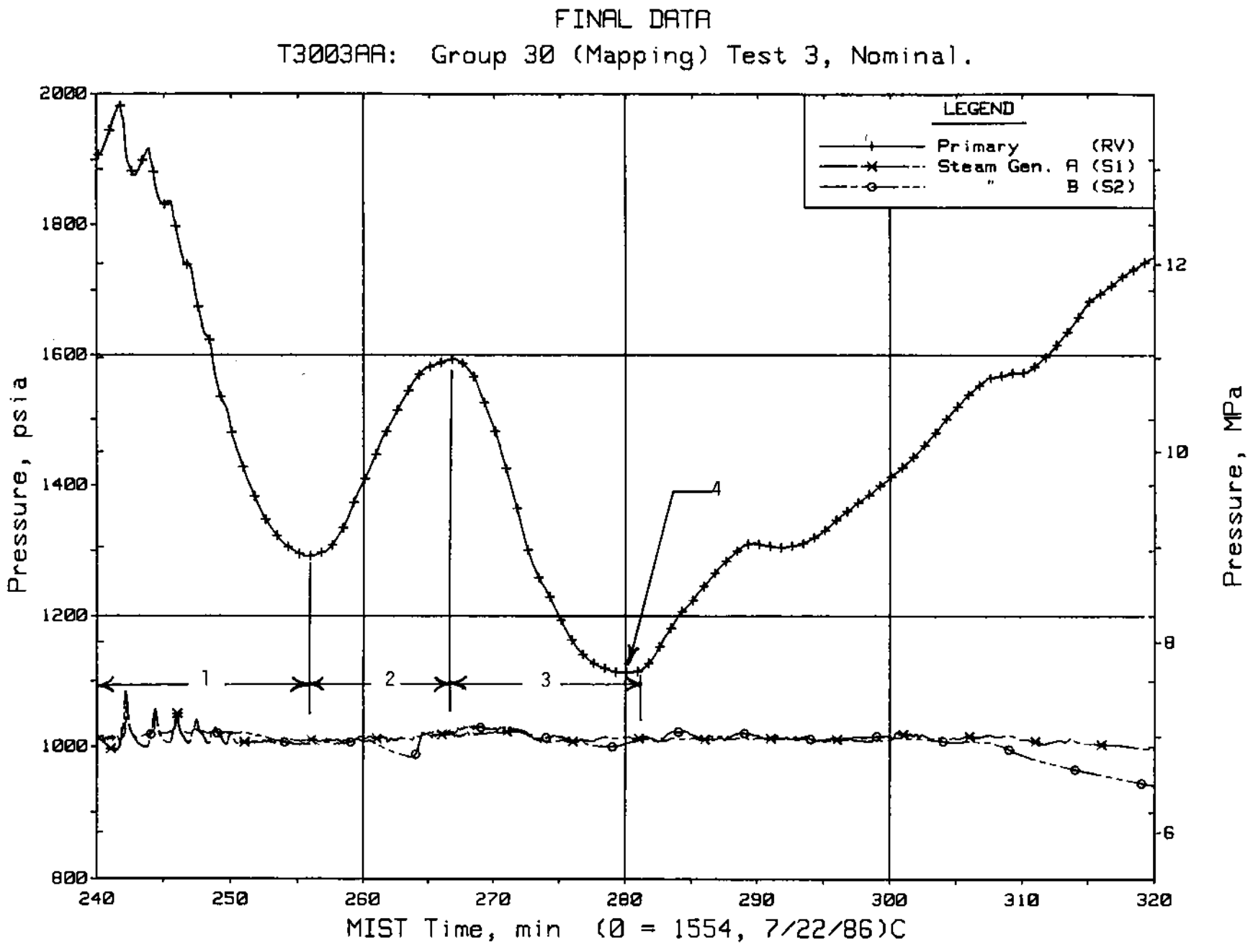

Figure 5.1.49. Primary and Secondary System Pressures (GPOIs)

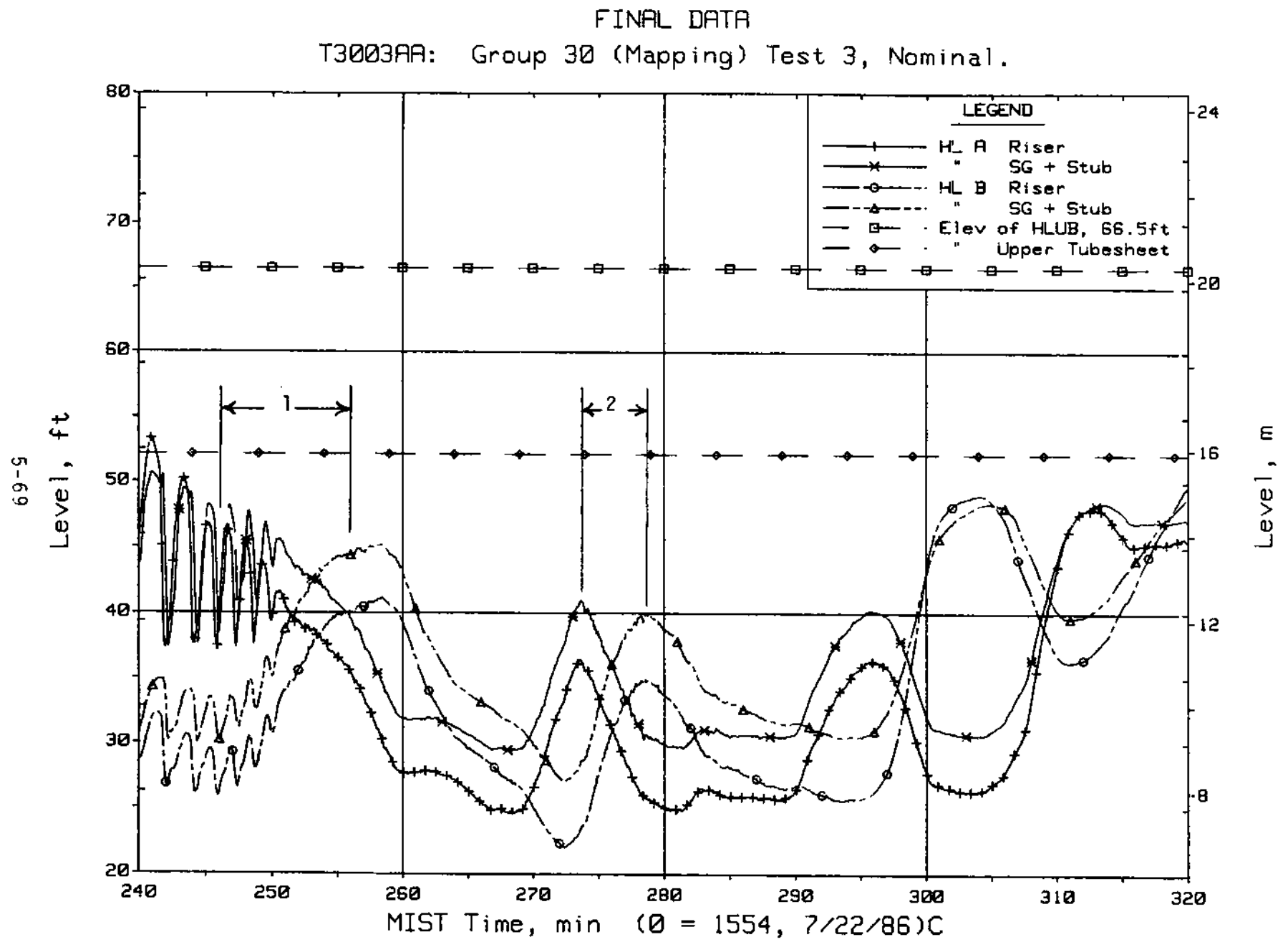

Figure 5.1.50. Hot Leg Riser and Stub Collapsed Liquid Levels

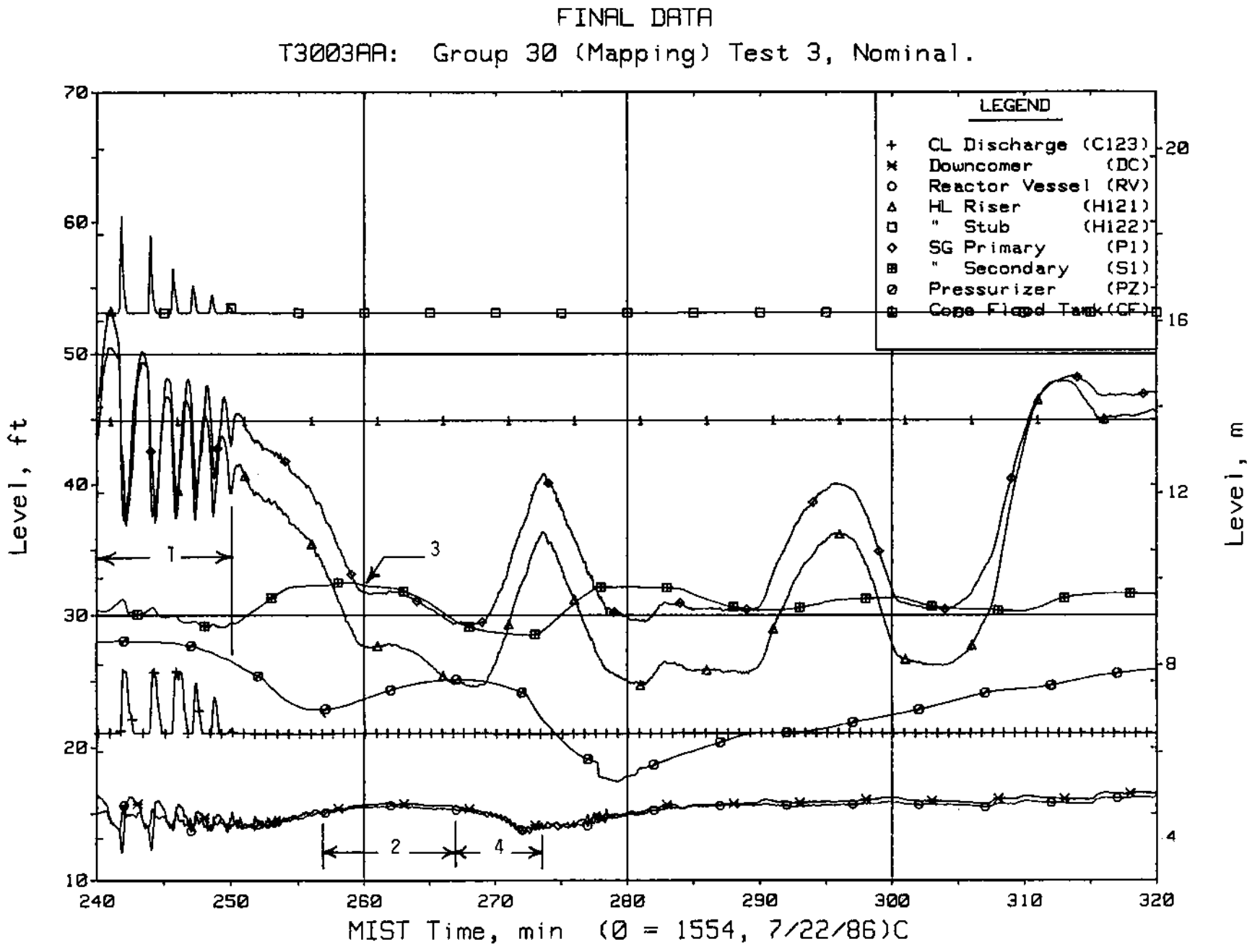

Figure 5.1.51. Loop A Collapsed Liquid Levels (LV20s)

Wed Feb 8 13:42:47 1989

PRLV1

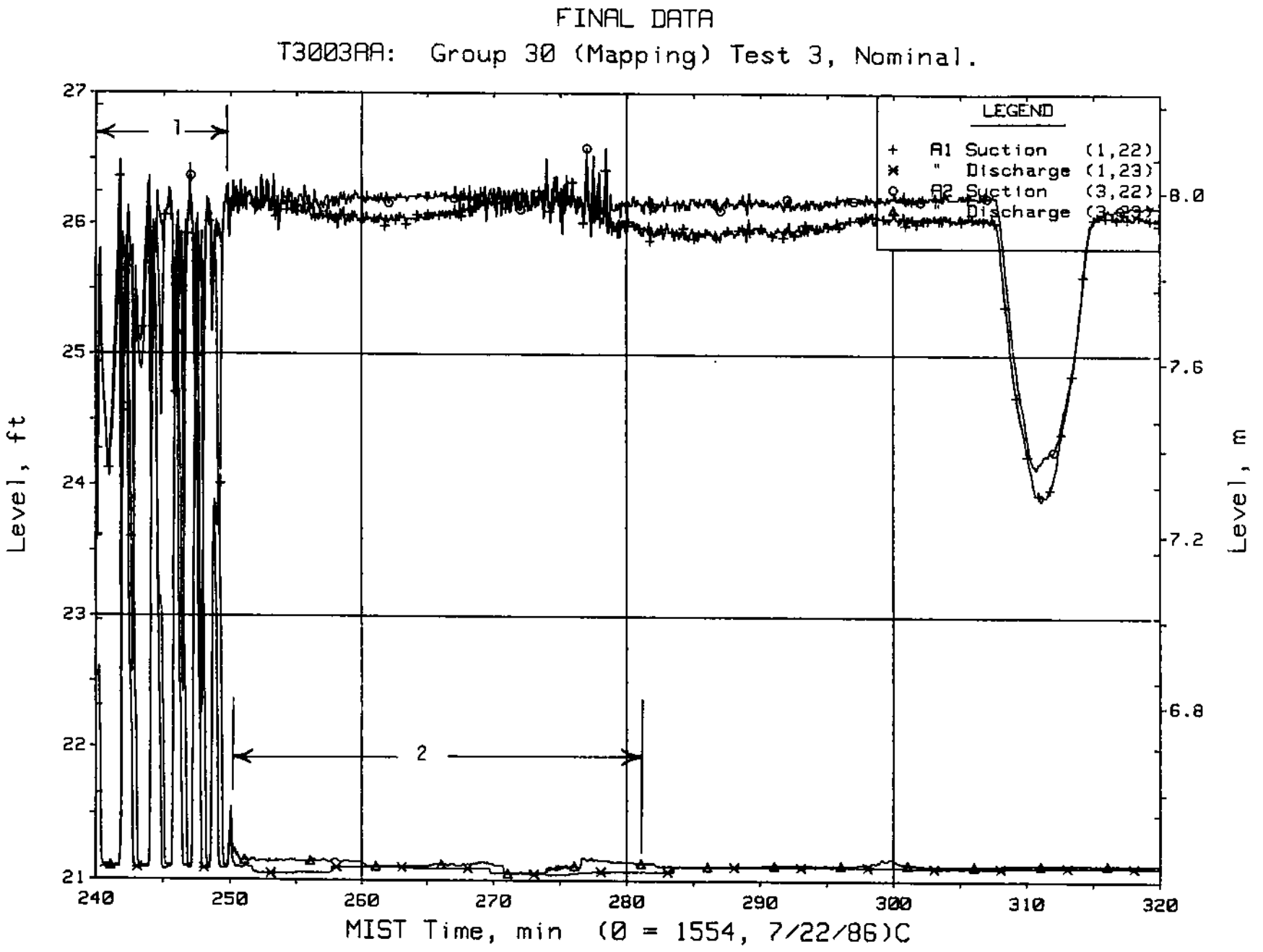

Figure 5.1.52. Loop A Cold Leg Collapsed Liquid Levels (LVs)

Wed Feb 8 13:57:30 1989

CLLV1

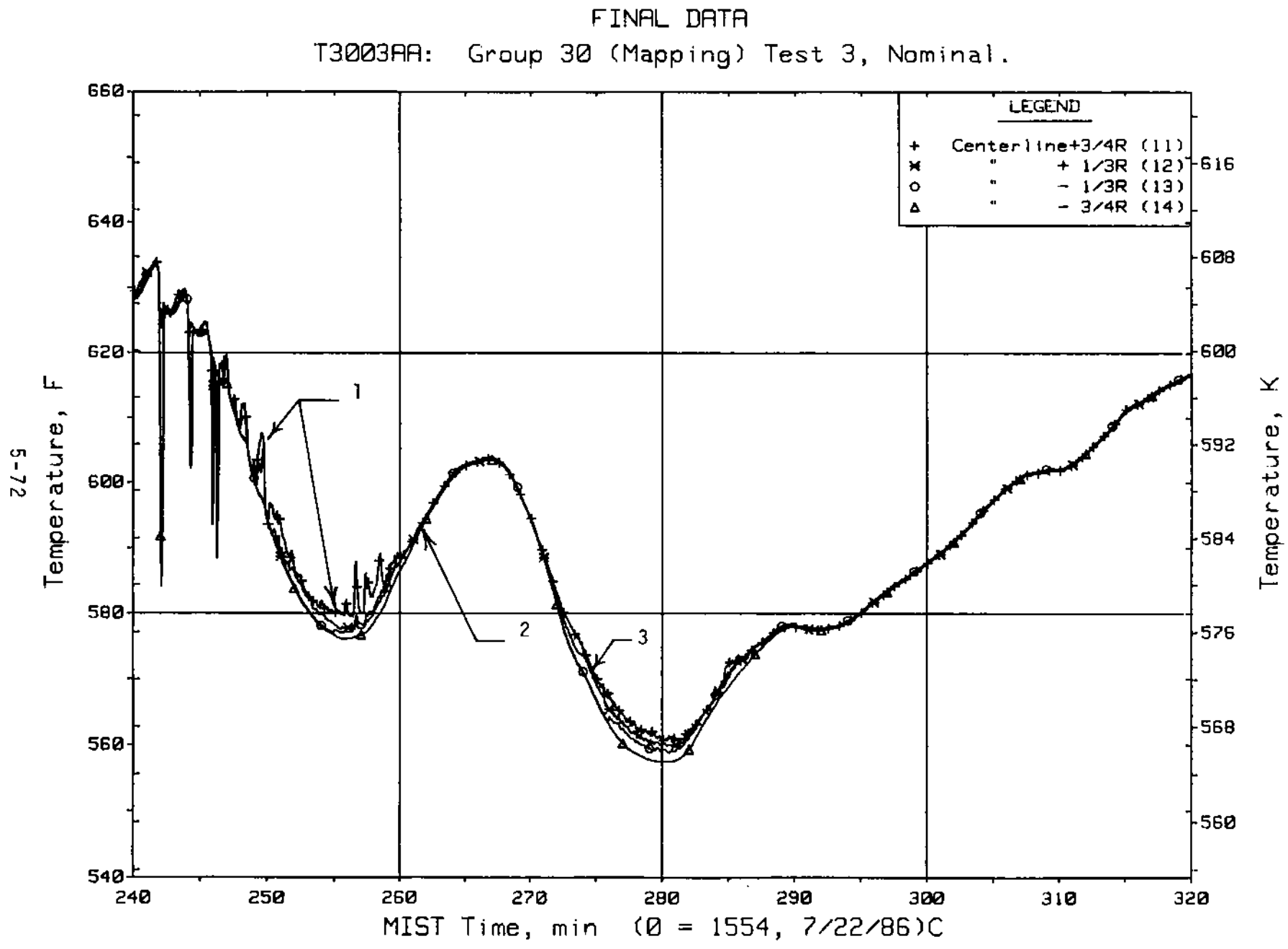

Figure 5.1.53. Cold Leg A1 Nozzle Rake Fluid Temperatures (21.2 ft, C1TCs)

Wed Feb 8 14:00:28 1989

C1TC4

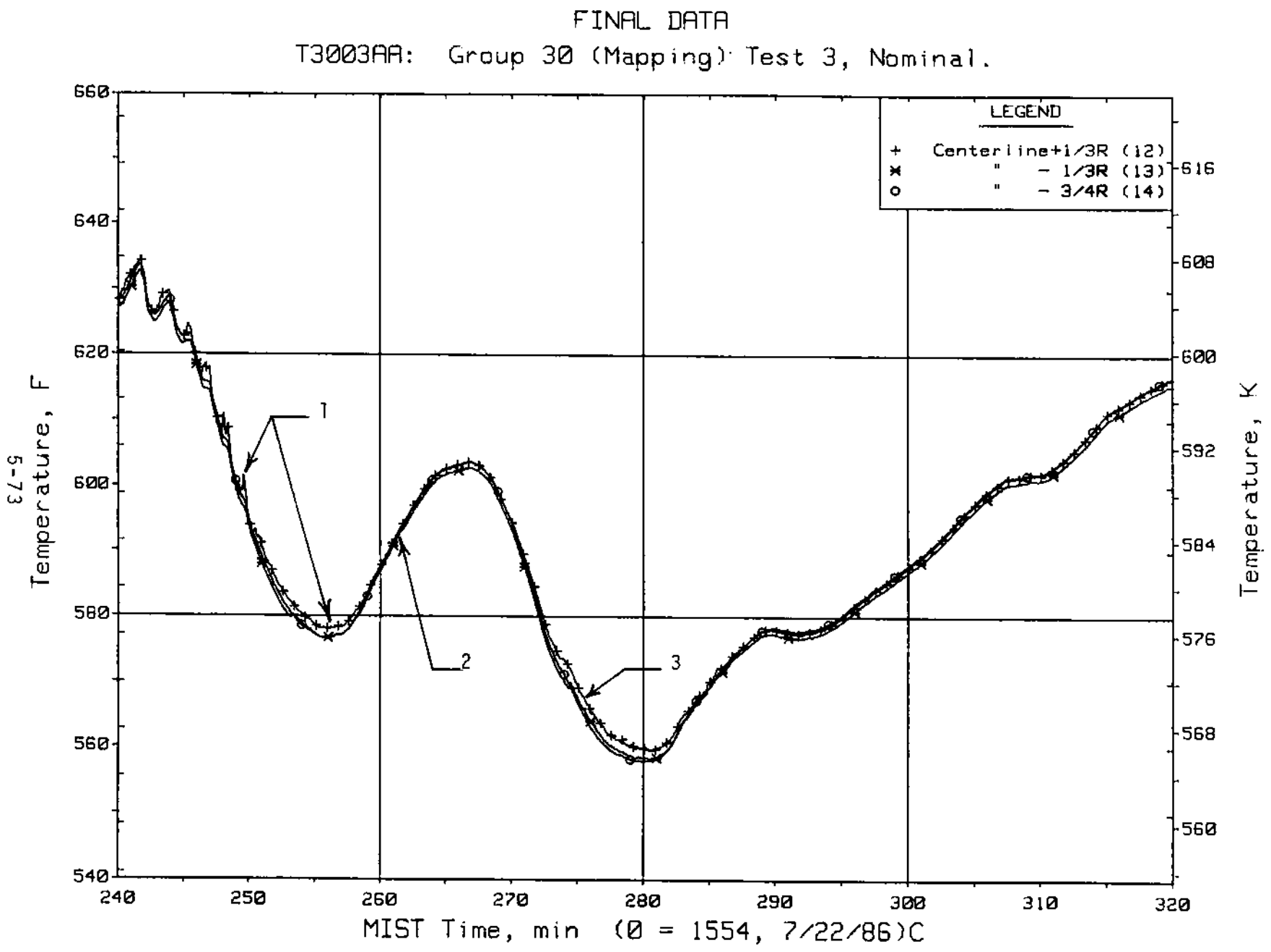

Figure 5.1.54. Cold Leg B1 Nozzle Rake Fluid Temperatures (21.2 ft, C2TCs)

Wed Feb 8 14:03:17 1989

C2TC4

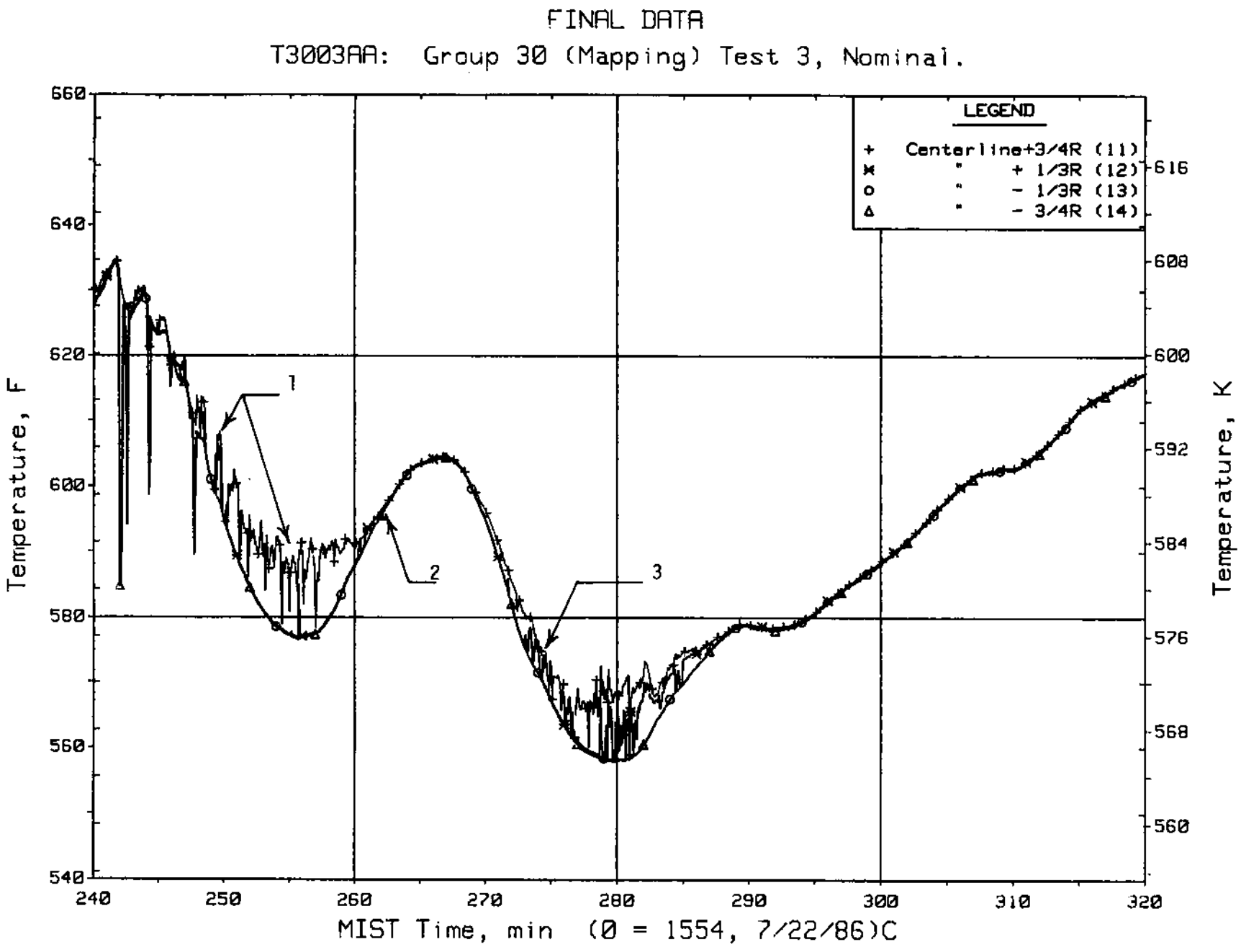

Figure 5.1.55. Cold Leg A2 Nozzle Rake Fluid Temperatures (21.2 ft, C3TCs)

Wed Feb 8 14:06:23 1989

C3TC4

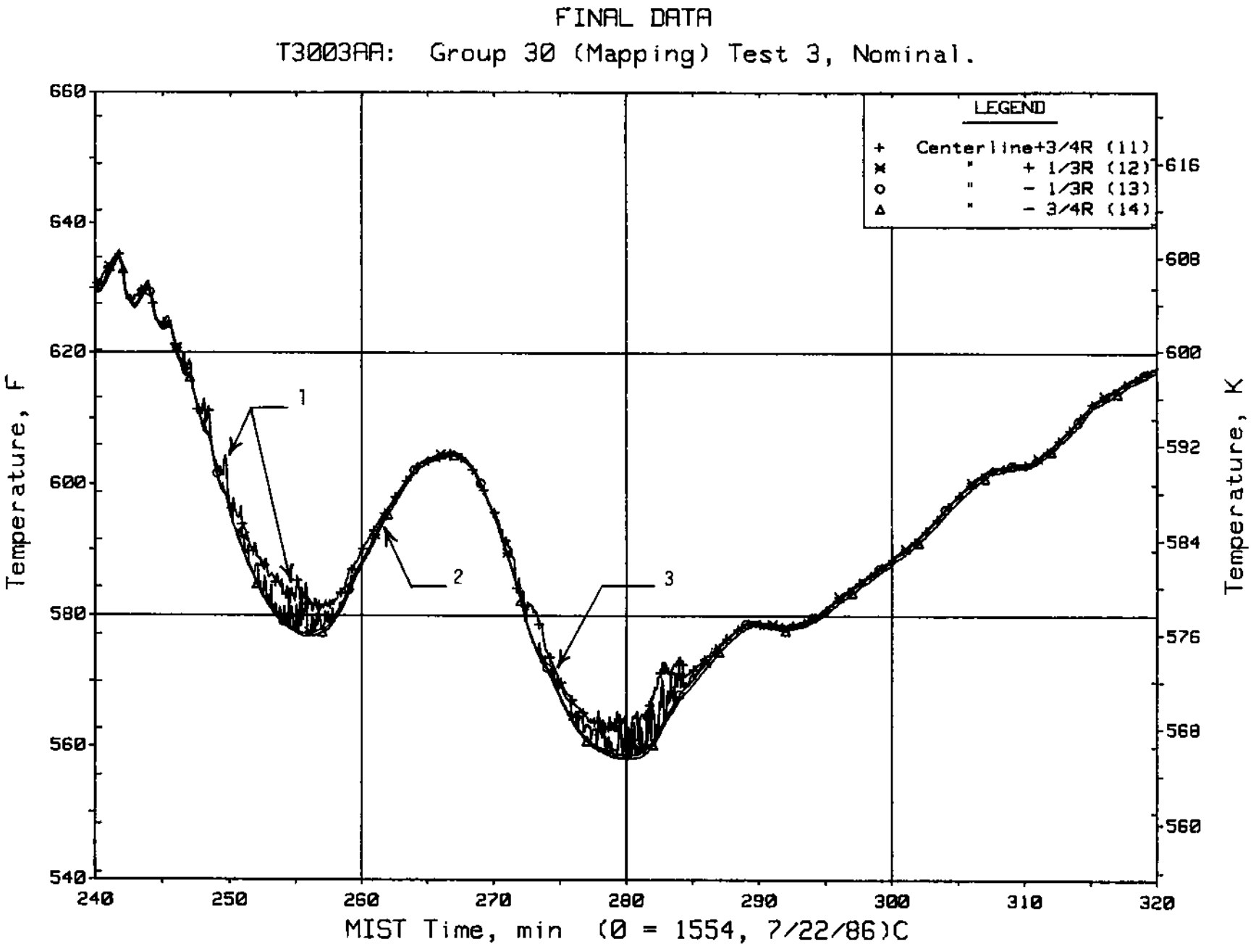

Figure 5.1.56. Cold Leg B2 Nozzle Rake Fluid Temperatures (21.2 ft, C4TCs)

Wed Feb 8 14:09:31 1989

C4TC4

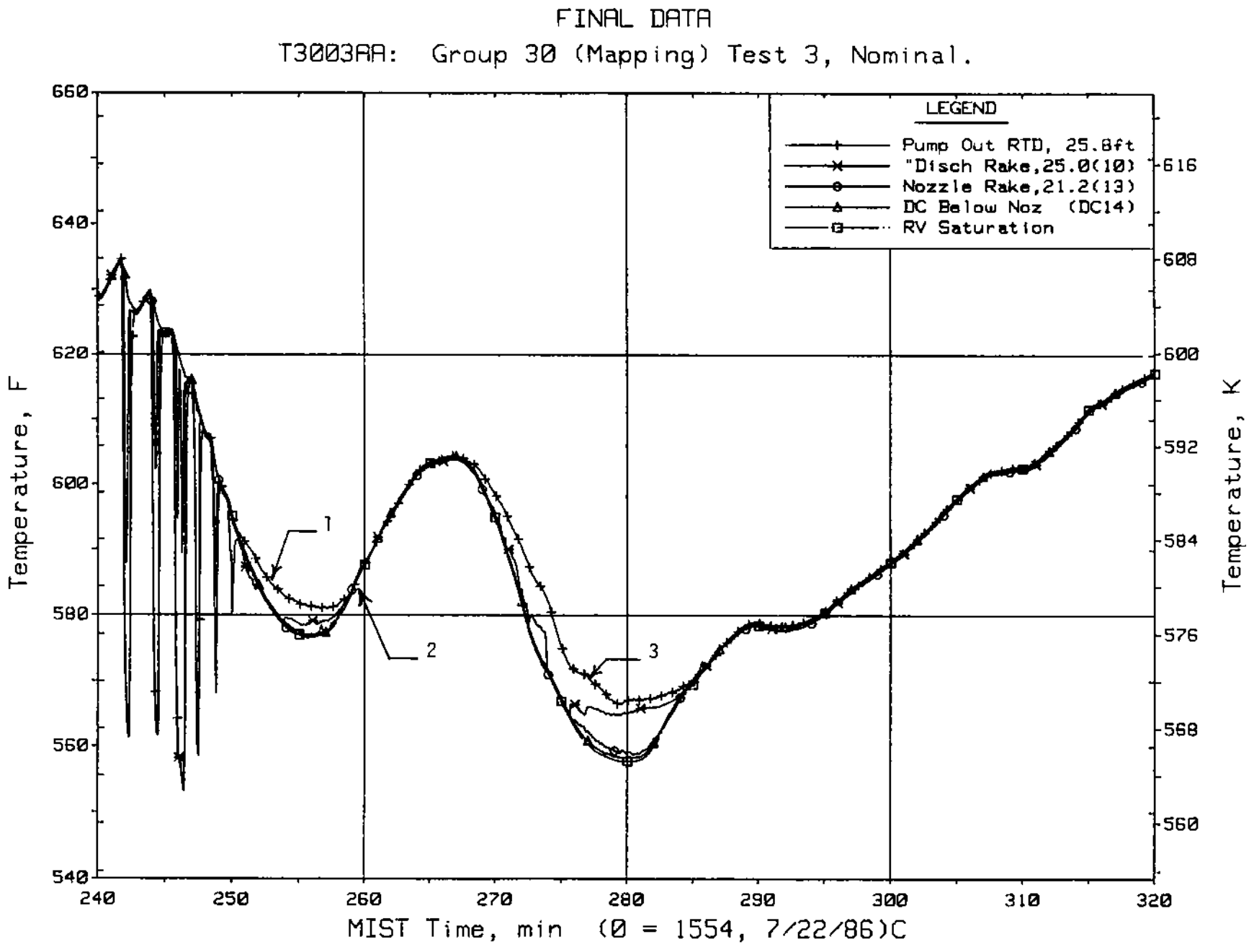

Figure 5.1.57. Cold Leg A1 Discharge Fluid Temperatures (C1TCs)

Wed Feb 8 14:13:01 1989

C1TC2

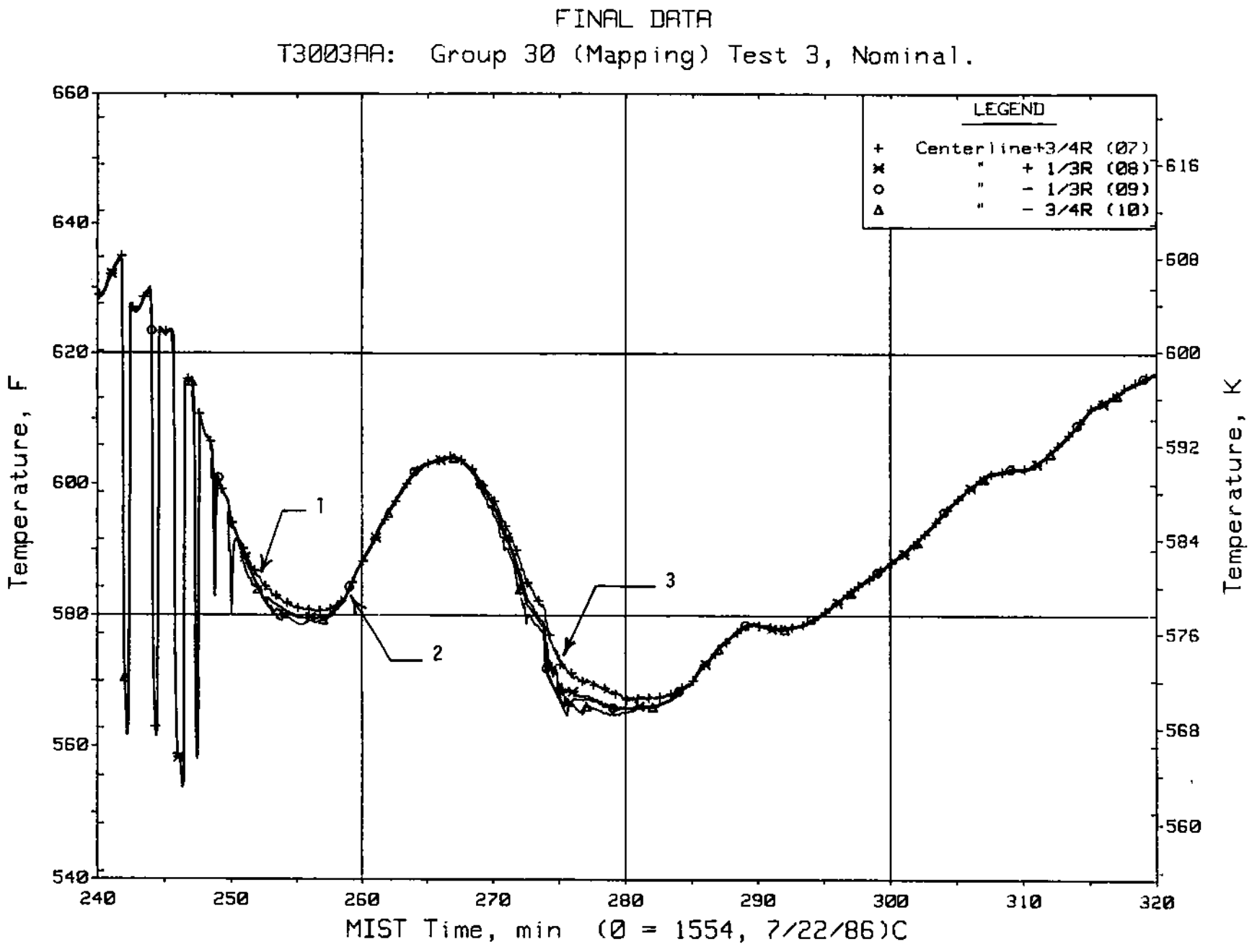

Figure 5.1.58. Cold Leg A1 Pump Discharge Rake Fluid Temperatures (25 ft, C1TCs)

Wed Feb 8 14:16:21 1989

C1TC3

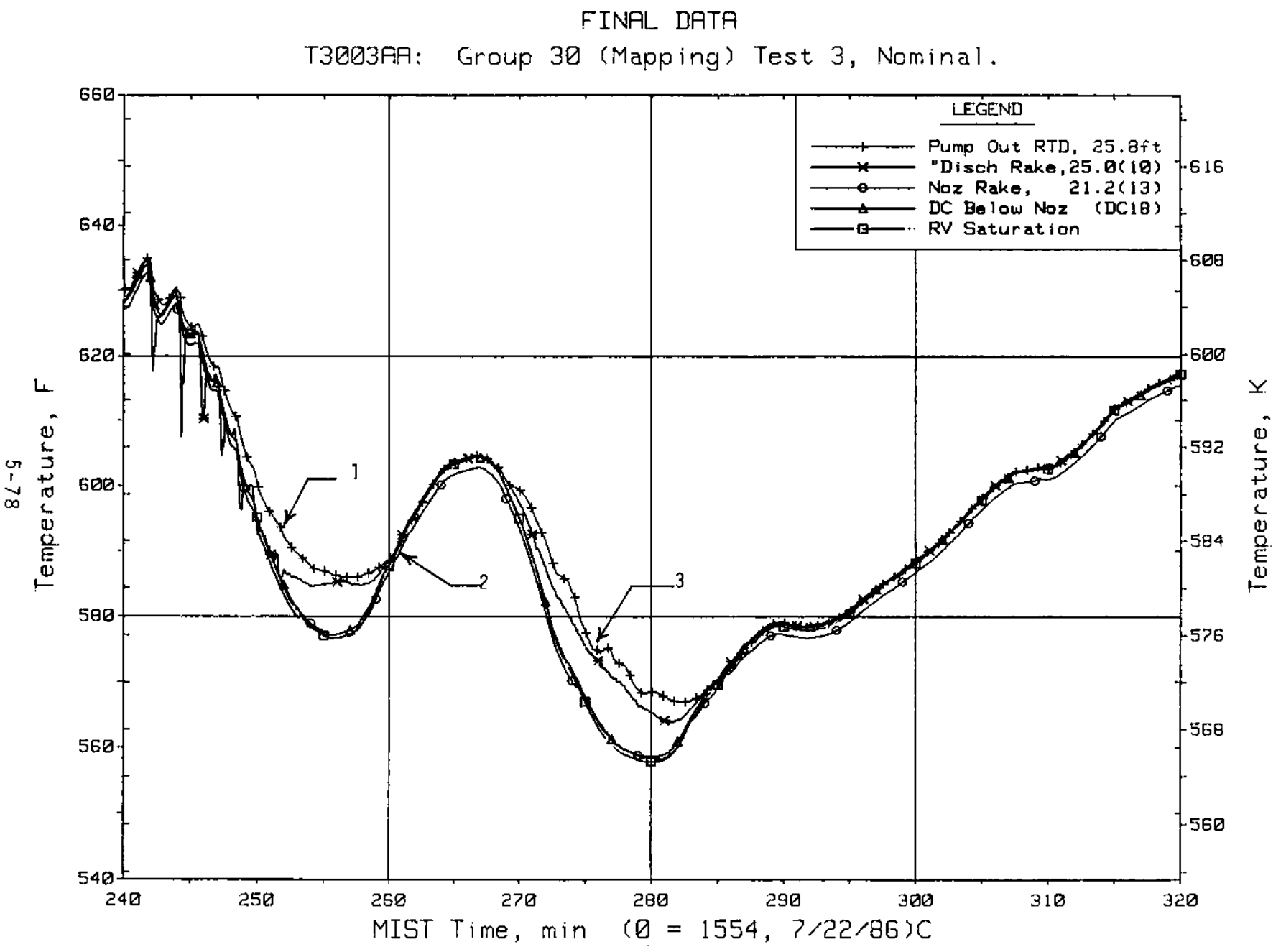

Figure 5.1.59. Cold Leg B1 Discharge Fluid Temperatures (C2TCs)

Wed Feb 8 14:19:48 1989

C2TC2

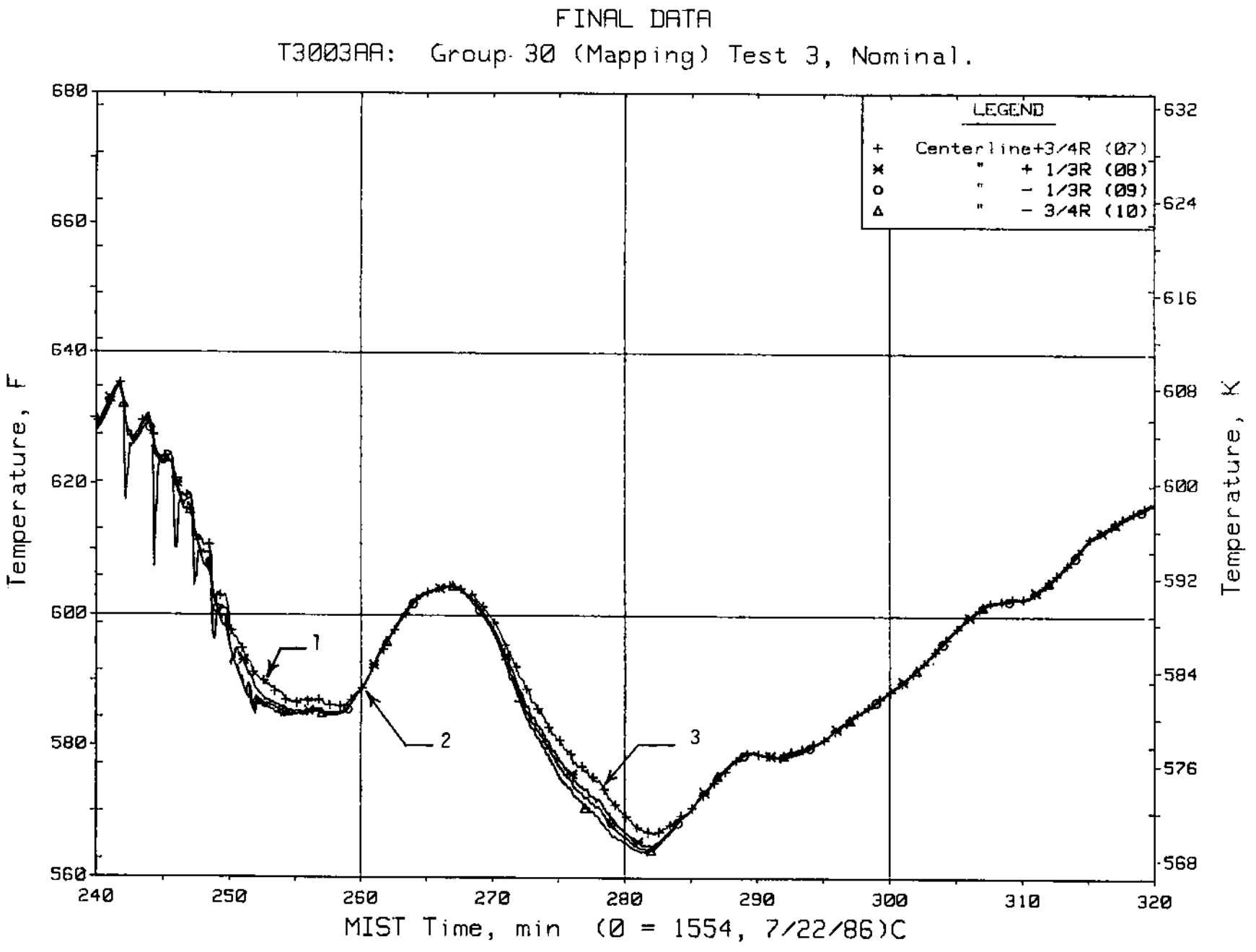

Figure 5.1.60. Cold Leg B1 Pump Discharge Rake Fluid Temperatures (25 ft, C2TCs)

Wed Feb 8 14:23:04 1989

C2TC3

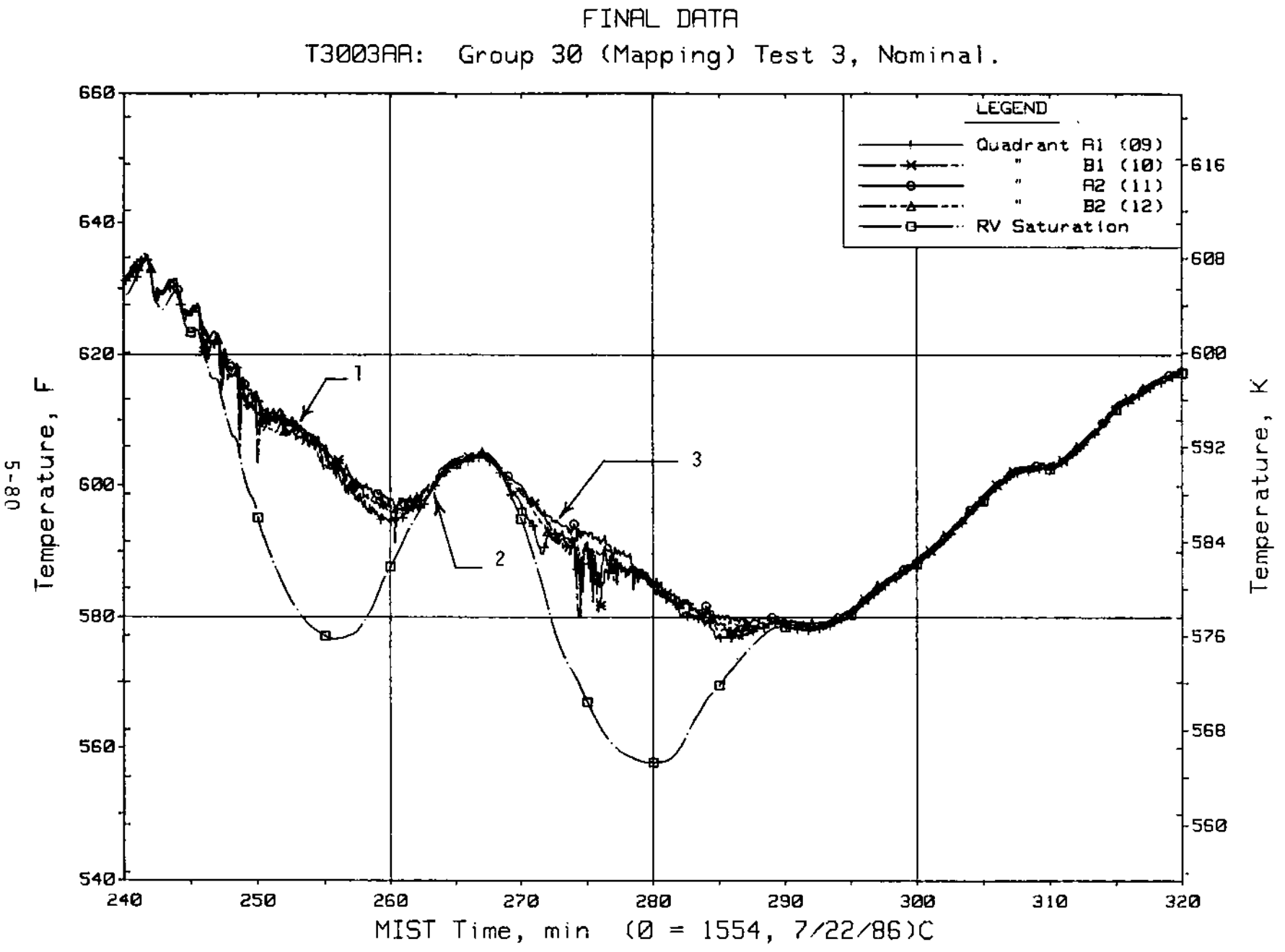

Figure 5.1.61. Downcomer Fluid Temperatures Above Nozzles, Elevation 21.9 ft (DCTCs)

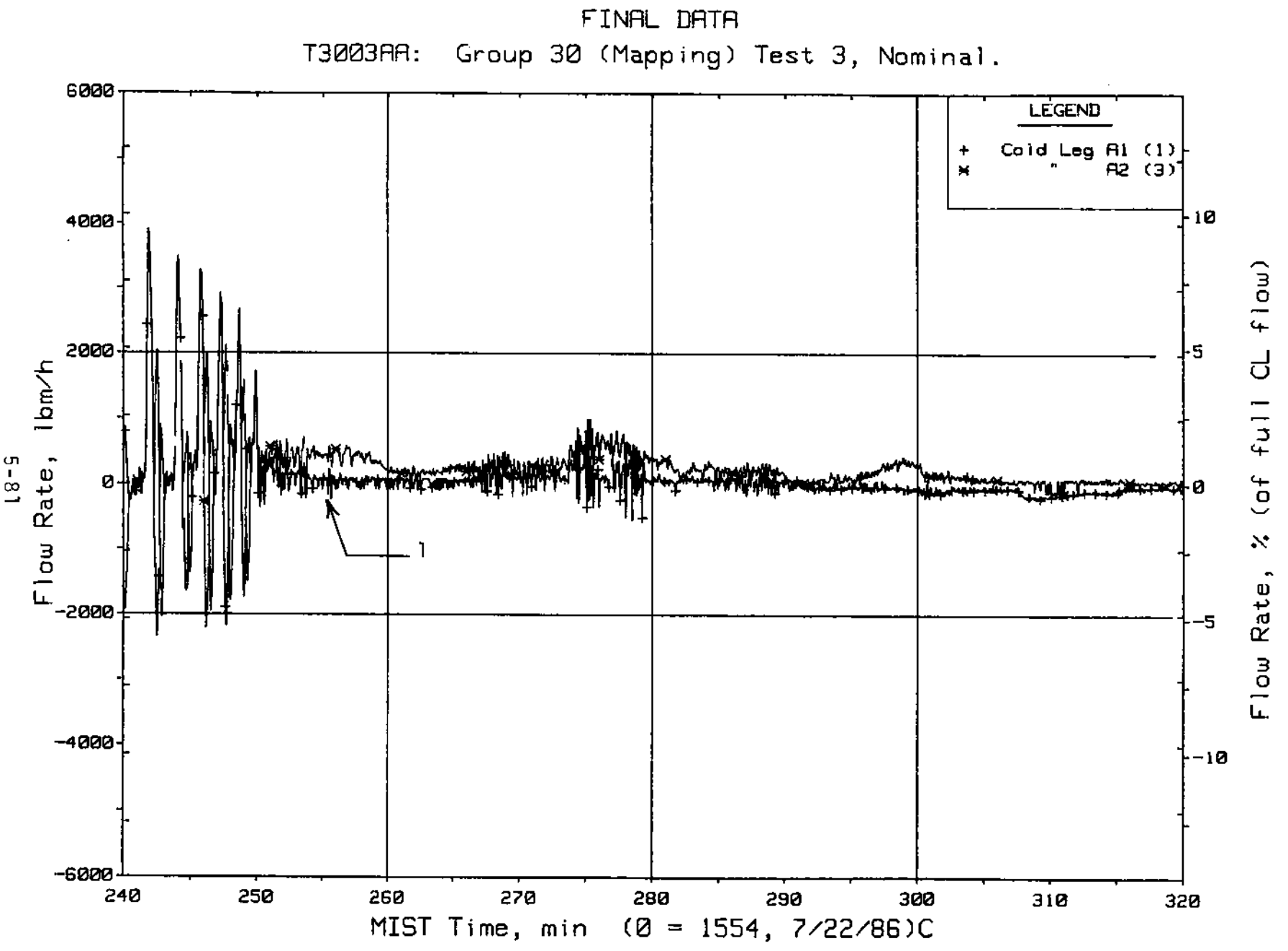

Figure 5.1.62. Loop A Cold Leg (Venturi) Flow Rates (VN20s)

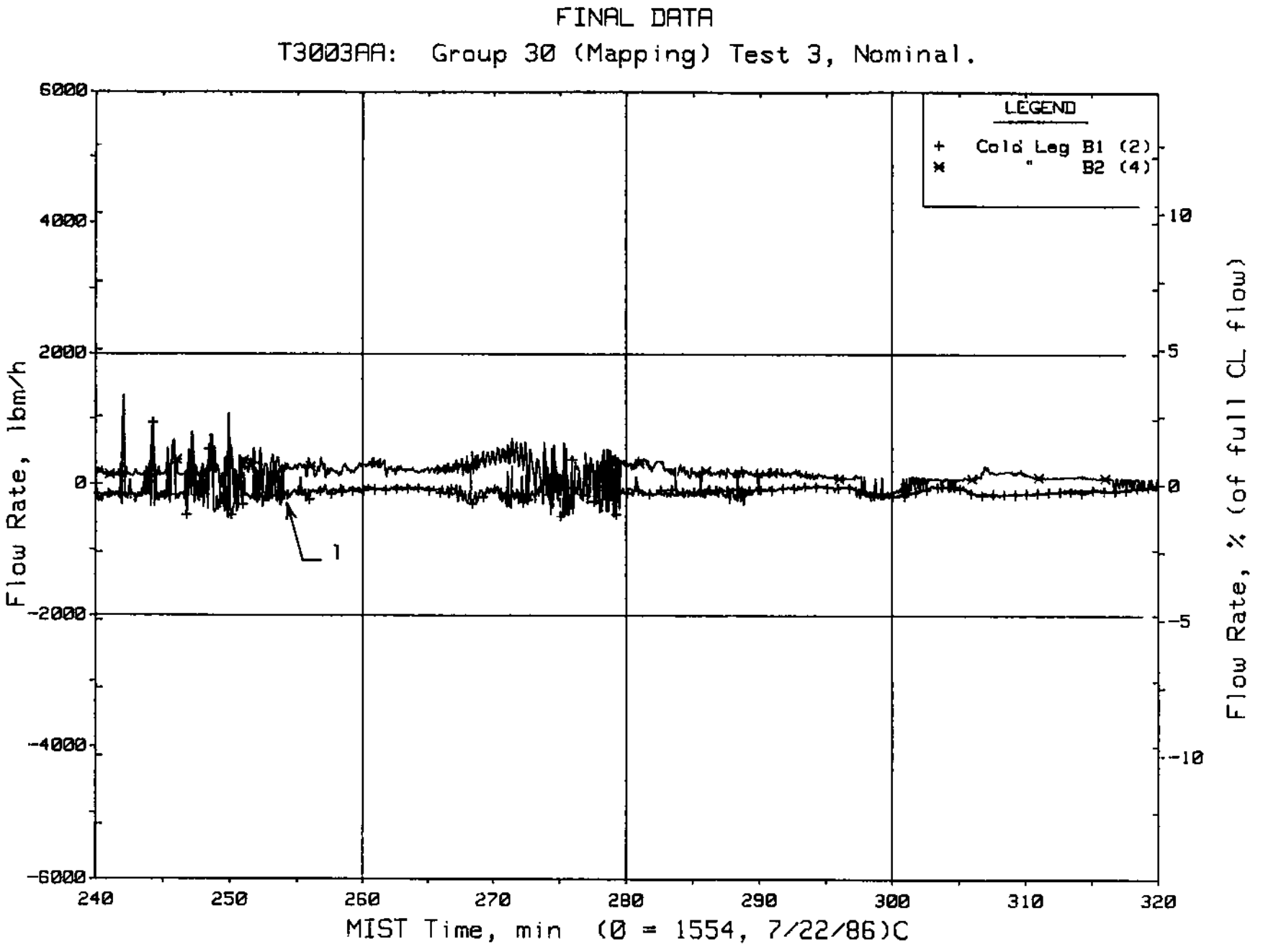

Figure 5.1.63. Loop B Cold Leg (Venturi) Flow Rates (VN20s)

Thu Feb 9 11:28:13 1989

PRFL6

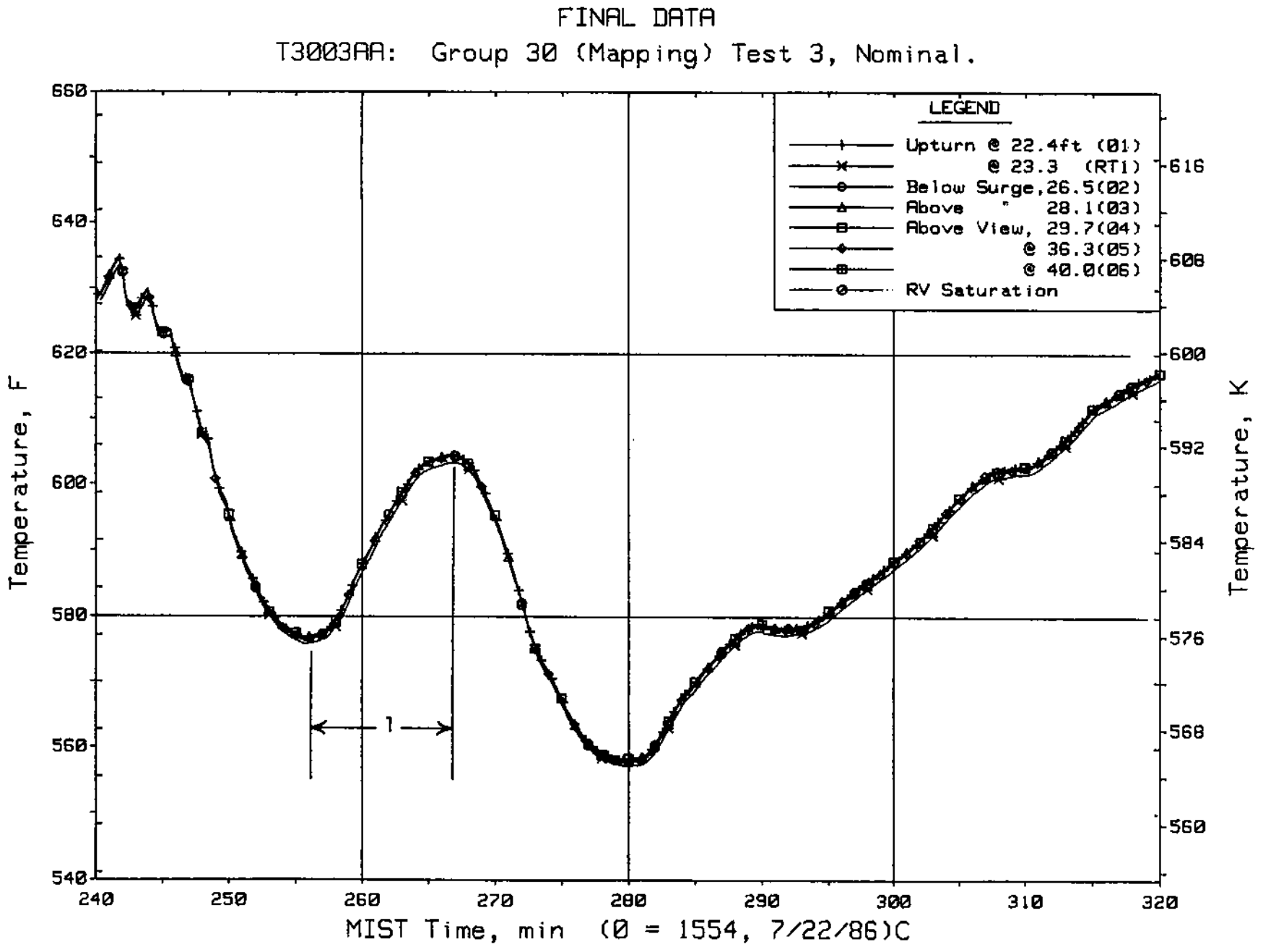

Figure 5.1.64. Hot Leg A Lower-Elevation Riser Fluid Temperatures (H1TCs)

Thu Feb 9 11:34:07 1989

H1TC1

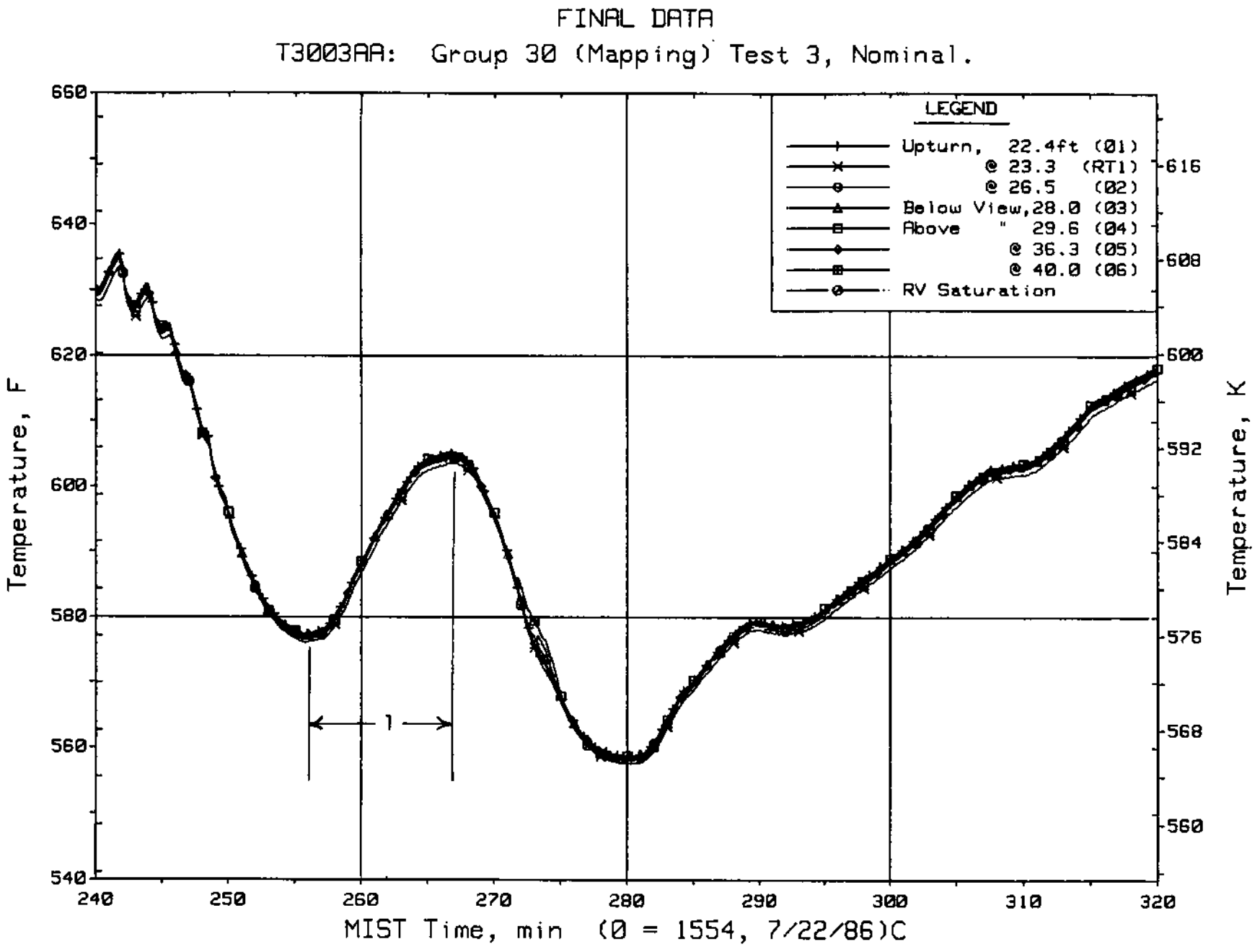

Figure 5.1.65. Hot Leg B Lower-Elevation Riser Fluid Temperatures (H2TCs)

Wed Feb 8 14:42:44 1989

H2TC1

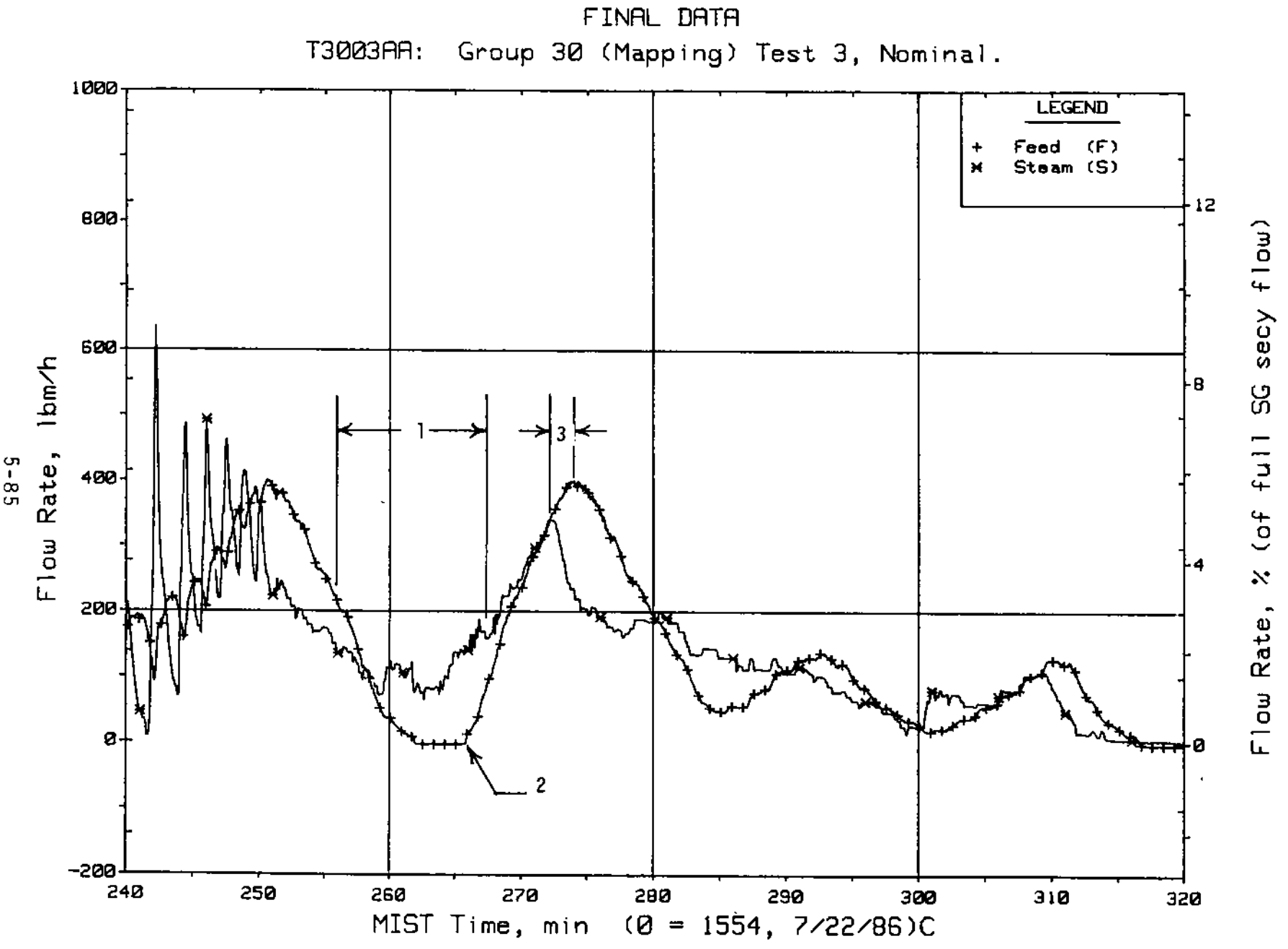

Figure 5.1.66. Steam Generator A Flow Rates (OR20s)

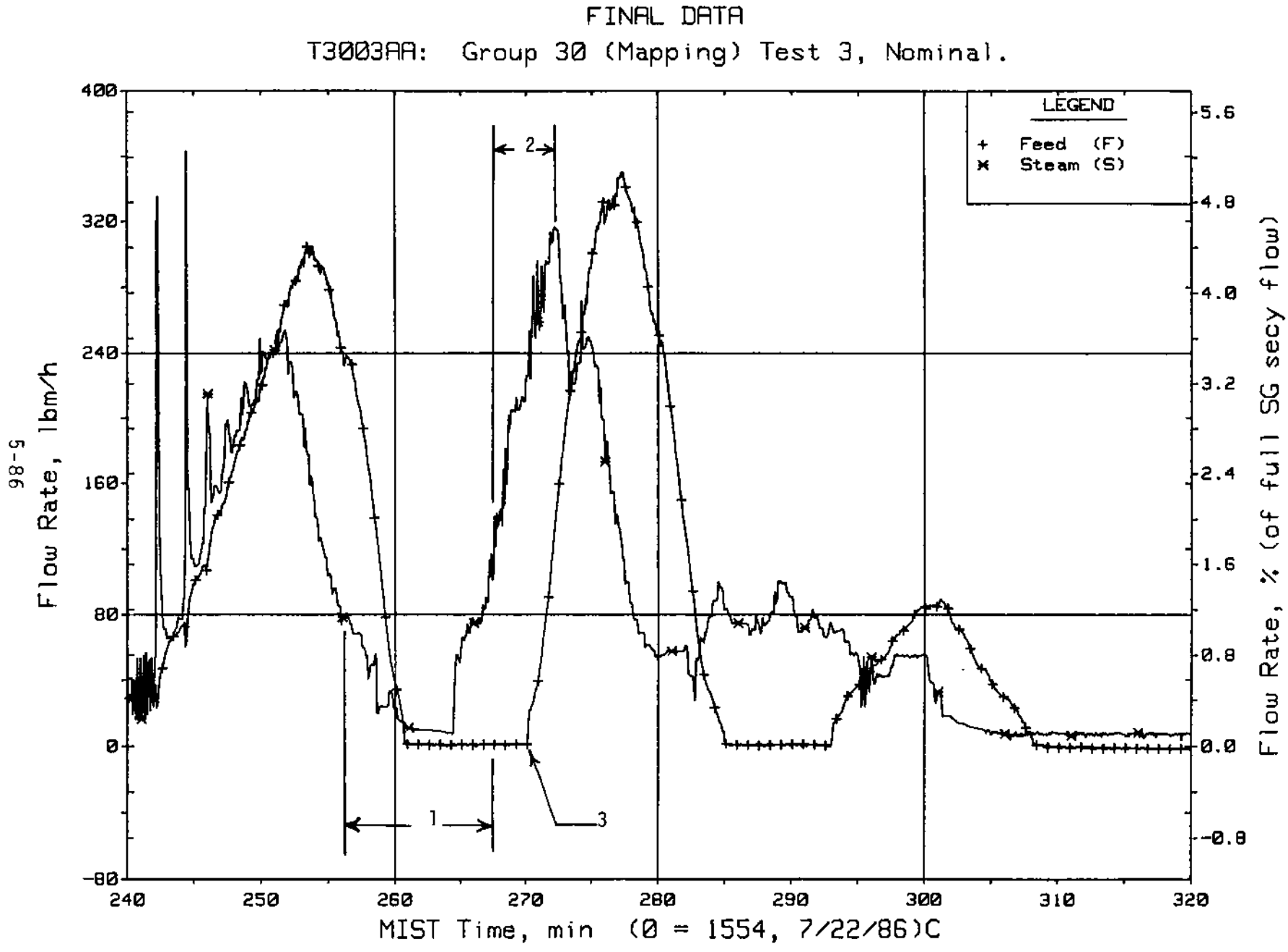

Figure 5.1.67. Steam Generator B Flow Rates (OR21s)

5.2. Isolated Pressurizer Test (3001BB)

The initial drain of the primary system resulted in a depressurization to ~1300 psia (Figure 5.2.1, See 1), which corresponded to the saturation pressure at the core exit temperature. The saturation pressure attained was identical to that of the Nominal Test (3003AA) and the only difference in the response between these tests was that loop saturation occurred sooner for the isolated pressurizer test. The difference occurred because the pressurizer inventory for the Nominal Test had to be depleted prior to attaining saturated conditions at the core exit.

The primary system response for this test then proceeded to essentially duplicate that observed in the Nominal Test (3003AA). The loss of primary system inventory resulted in the reactor vessel head voiding (Figure 5.2.2, See 1) and a gradual increase in primary system pressure (Figure 5.2.1, See 2).

The phenomena observed in Test 3001BB then replicated that observed in the Nominal Test (3003AA). The reactor vessel head voided and reached the reactor vessel vent valve elevation, the downcomer voided, reactor vessel vent valve cycling commenced, and backflow occurred in the cold legs. When the downcomer level descended to the cold leg nozzle elevation, the reactor vessel vent valves opened and remained open, therefore permitting a backflow of steam into the cold leg discharge pipes, and a momentary flow interruption occurred in each cold leg.

Subsequent to the momentary flow interruption, intra-cold leg flow was established only in loop A (cold leg A1 flowed backward and cold leg A2 flowed forward -- Figure 5.2.3, See 1). The flow continued in the forward direction in both B cold legs after the momentary flow interruption occurred (Figure 5.2.4, See 1). However, counter-current flow was observed at each cold leg nozzle (as indicated by the response of the cold leg nozzle thermocouple rakes) of each cold leg that indicated forward flow (See 1 on Figures 5.2.5 through 5.2.7).

The cold leg A1 discharge and suction pipes partially voided during the flow reversal (Figure 5.2.8, See 1). Forward flow, however, was reestablished in cold leg A1 (Figure 5.2.3, See 2), and the voids in cold leg A1 collapsed

(Figure 5.2.8, See 2). As forward flow was reestablished in cold leg A1, loop B flow decreased and resulted in a flow reversal followed shortly thereafter by the voiding of the discharge pipe (Figure 5.2.9, See 1). Intra-cold leg flow was observed in the B cold legs and then flow interruption occurred in cold leg B1 (Figure 5.2.4, See 2).

The phenomena observed above for the flow interruption are similar to that observed for the Nominal Test (3003AA). The only difference between the response of these two tests was that for the Nominal Test, backflow occurred in both cold legs A1 and B1 immediately after the momentary flow interruption occurred, whereas for Test 3001BB, only cold leg A1 exhibited this response. The other discussed responses were similar for both tests.

As the drain continued, Test 3001BB experienced the same flow interruption phenomena as the Nominal Test. The order in which the cold leg flows interrupted, i.e., B1, A1 followed by A2 and B2 simultaneously (Figure 5.2.4, See 2, Figure 5.2.10, See 1, Figure 5.2.11, See 1 and Figure 5.2.12, See 1), was identical to that observed in the Nominal Test. When flow interrupted in cold legs A2 and B2 (thus complete interruption of primary loop flow) the downcomer had attained saturated conditions over its entire length (Figure 5.2.13, See 1), which was also similar to the Nominal Test.

Subsequent to complete flow interruption the hot leg riser levels indicated that they were full (Figure 5.2.14, See 1), however, the loss of natural circulation driving head prevented the establishment of primary loop flow. Prior to the flow interruption, steam generator heat transfer had not been affected (See 1, Figures 5.2.15 and 5.2.16). These observations were also similar to those of the Nominal Test. The flow interruptions occurred at a constant primary system pressure, ~1450 psia (Figure 5.2.17, See 1), which was also identical to that of the Nominal Test.

Following the complete loop flow interruption, steam generator heat transfer was terminated (See 2 on Figure 5.2.15 and Figure 5.2.16), the reactor vessel and downcomer regions voided further (Figure 5.2.18, See 1), and the primary system pressure increased (Figure 5.2.17, See 2). These responses were also similar to those observed in the Nominal Test (3003AA).

The increasing primary system pressure resulted in the subcooling of the liquid in the hot leg risers (See 1 on Figure 5.2.19 and Figure 5.2.20). The hot leg riser heatup phenomena (as discussed in the Nominal Test) commenced as the primary system repressurized.

Differences between the isolated pressurizer test (3001BB) and the Nominal Test (3003AA) were observed during the hot leg heatup (repressurization phase) of the tests. Test 3001BB did not establish a predominant flow path in loop A apparently as a result of the pressurizer being isolated. Therefore, both hot leg risers exhibited a somewhat similar heatup response (See 2 on Figure 5.2.19 and Figure 5.2.20). The spillover occurred in the loop whose hot leg inlet temperature attained saturated conditions first. This action resulted in the first spillover occurring in loop B (Figure 5.2.20, See 3), the second spillover in loop A (Figure 5.2.19, See 3), and the third spillover in loop B (Figure 5.2.20, See 4).

The initial heatup of the hot leg risers was relatively uniform as the first spillover was approached. Although loop B experienced the initial spillover, loop A also spilled over the U-bend slightly later. This event was observed by the establishment of heat transfer in both steam generators (Figure 5.2.21, See 1). The spillovers resulted in forward flow in each cold leg (Figure 5.2.11, See 2 and Figure 5.2.12, See 2), which completely collapsed the cold leg voids (Figure 5.2.22, See 1 and Figure 5.2.23, See 1) and partially collapsed the reactor vessel and downcomer voids (Figure 5.2.18, See 2).

The second heatup resulted in a spillover in loop A only. This result was observed by the establishment of heat transfer in only steam generator A (Figure 5.2.21, See 2). Forward flow was established in the A cold legs (Figure 5.2.11, See 3), which collapsed the voids in the A cold legs (Figure 5.2.22, See 2) and partially collapsed the reactor vessel and downcomer voids (Figure 5.2.18, See 3). Forward flow was not observed in the B cold legs (Figure 5.2.12, See 3) and the voids in the B cold legs did not collapse (Figure 5.2.23, See 2). The third heatup resulted in a spillover in loop B only and can be observed on the previously discussed figures.

During the repressurization phase, the maximum primary pressure attained was 2290 psia, and it occurred after the third hot leg riser heatup (Figure

5.2.21, See 3). This pressure compares to a maximum primary pressure of 2225 psia after the third hot leg riser heatup for the Nominal Test.

A significantly different system response was observed (after the third hot leg riser heatup and spillover occurred) for the isolated pressurizer test (3001BB) that was not observed in the Nominal Test (3003AA). The isolated pressurizer test reestablished primary flow in loop B while loop A remained interrupted. This different response was apparently caused by the plugging of the leak orifice as the leak flow rate decreased markedly during the third hot leg riser heatup (Figure 5.2.24, See 1). The HPI flow rate was maintained during the period in which the leak orifice plugged. Therefore, the primary loop inventory increased (Figure 5.2.25, See 1) and primary system pressure eventually decreased (Figure 5.2.21, See 4) as HPI flow exceeded the leak flow.

The loop operators successfully reestablished the leak flow rate when a second leak orifice of the same size and at the same location was valved into the system (Figure 5.2.26, See 1). The primary system then appeared to repeat the previously observed flow interruption of the B cold legs. The flow interruption occurred first in cold leg B1 and the primary system pressure remained essentially constant and at approximately the same pressure (1475 psia to 1500 psia) as was observed during the previous flow interruption for this test, i.e., prior to the plugging of the leak orifice. The primary system then exhibited the lower region voiding, repressurization, hot leg riser heatup, spillover, forward loop flow, and lower region void collapse phenomena as observed previously. The maximum pressure attained during this repressurization phase was 2250 psia (Figure 5.2.27, See 1), which was similar to that observed during the previous complete flow interruption that occurred prior to the plugging of the leak orifice. Therefore, the plugged leak orifice had apparently no effect on the resultant response of the primary system.

The remainder of this test exhibited phenomena similar to the Nominal Test (3003AA), however, the response was not as similar as had been observed through the repressurization phase.

AFW-BCM was established in both steam generators and, as observed in the Nominal Test, loop A established the predominant flow path. The loop B heat

transfer decreased (Figure 5.2.28, See 1), while the loop A heat transfer increased (Figure 5.2.29, See 1). The primary system pressure decreased to approximately 1625 psia during the AFW-BCM (Figure 5.2.27, See 2). The pressure response was similar to that of the Nominal Test in that an oscillatory system behavior resulted from the lower region voiding-void collapse phenomena. However, the magnitude of the depressurization as a result of the AFW-BCM was considerably larger for the isolated pressurizer test, 625 psi versus 325 psi for the Nominal Test.

The hot leg and steam generator primary levels also responded similarly to those observed for the Nominal Test (3003AA) in that the loop A levels remained relatively high (Figure 5.2.30, See 1) while the loop B levels decreased and descended to the secondary pool elevation (Figure 5.2.31, See 1). When the steam generator B primary level descended to the secondary pool elevation, increased heat transfer occurred in loop B (Figure 5.2.28, See 2) and loop A heat transfer decreased and then terminated (Figure 5.2.29, See 2). Coincident with the loss of heat transfer, the leak flow decreased (apparently the leak orifice had plugged again) and the loop operator decreased the HPI flow rate to maintain the leak-HPI deficit (Figure 5.2.32, See 1). Leak and HPI flow were reestablished approximately 7 minutes later (Figure 5.2.32, See 2). Loop B heat transfer was not maintained and the primary system repressurized (Figure 5.2.27, See 3). During this phase of the test, the loop A hot leg and steam generator primary levels decreased (Figure 5.2.30, See 2), while the loop B hot leg and steam generator primary levels increased (Figure 5.2.31, See 2) and then decreased (Figure 5.2.33, See 1). The primary system pressure attained a maximum value of 2280 psia during this repressurization (Figure 5.2.34, See 1).

This response differed from that observed in the Nominal Test (3003AA). The Nominal Test, when pool BCM occurred in loop B, depressurized to approximately 1300 psia, however, AFW-BCM was maintained in loop A as a result of the discharge of the pressurizer inventory into hot leg A. When heat transfer terminated in the Nominal Test, the primary system repressurized to approximately 1590 psia.

As the steam generator primary level of both loops descended to the secondary pool elevation and when the secondary level attained the control setpoint

(Figure 5.2.35, See 1), AFW was actuated, steam generator heat transfer resulted, and the primary system depressurized to 1060 psia (Figure 5.2.34, See 2). This depressurization resulted in superheated conditions in the downcomer and the cold legs as was observed in the Nominal Test.

The isolated pressurizer test was terminated at the test time of 319 minutes based upon the establishment of the pool BCM termination criteria.

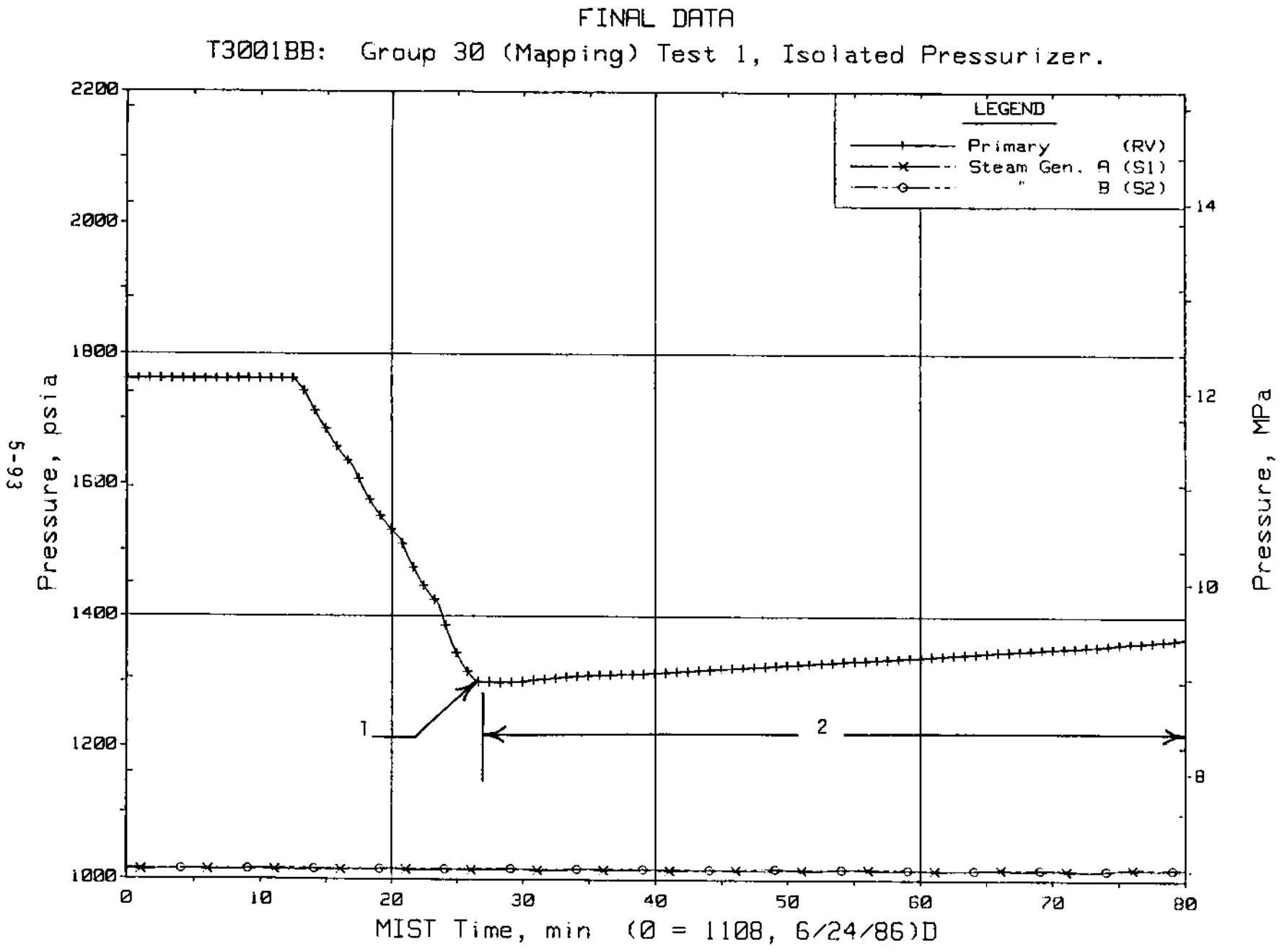

Figure 5.2.1. Primary and Secondary System Pressures (GP01s)

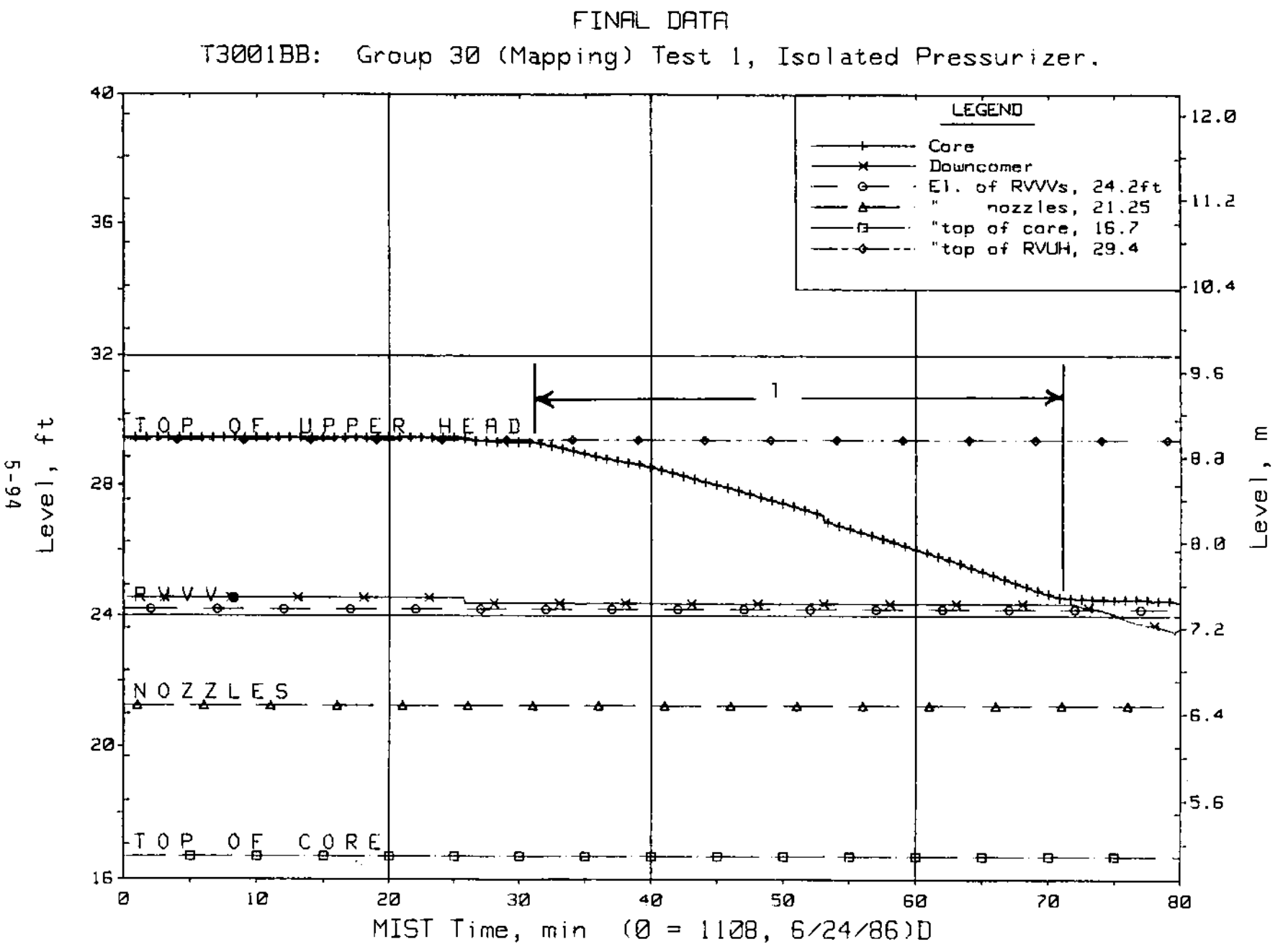

Figure 5.2.2. Core Region Collapsed Liquid Levels

Wed Feb 15 13:43:11 1989

COLV1

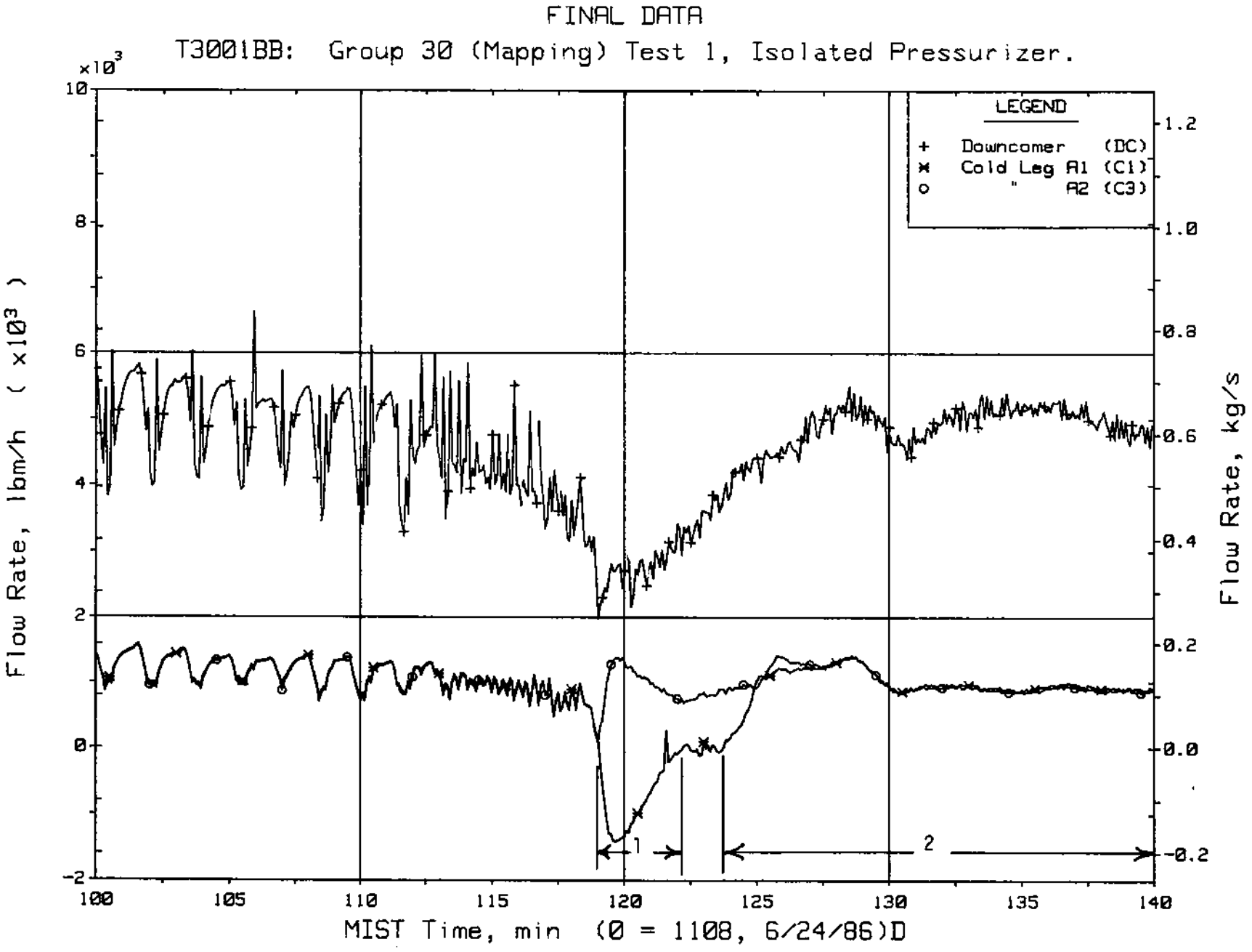

Figure 5.2.3. Primary System (Venturi) Flow Rates (VN20s)

Thu Feb 16 11:21:15 1989

PRFL1

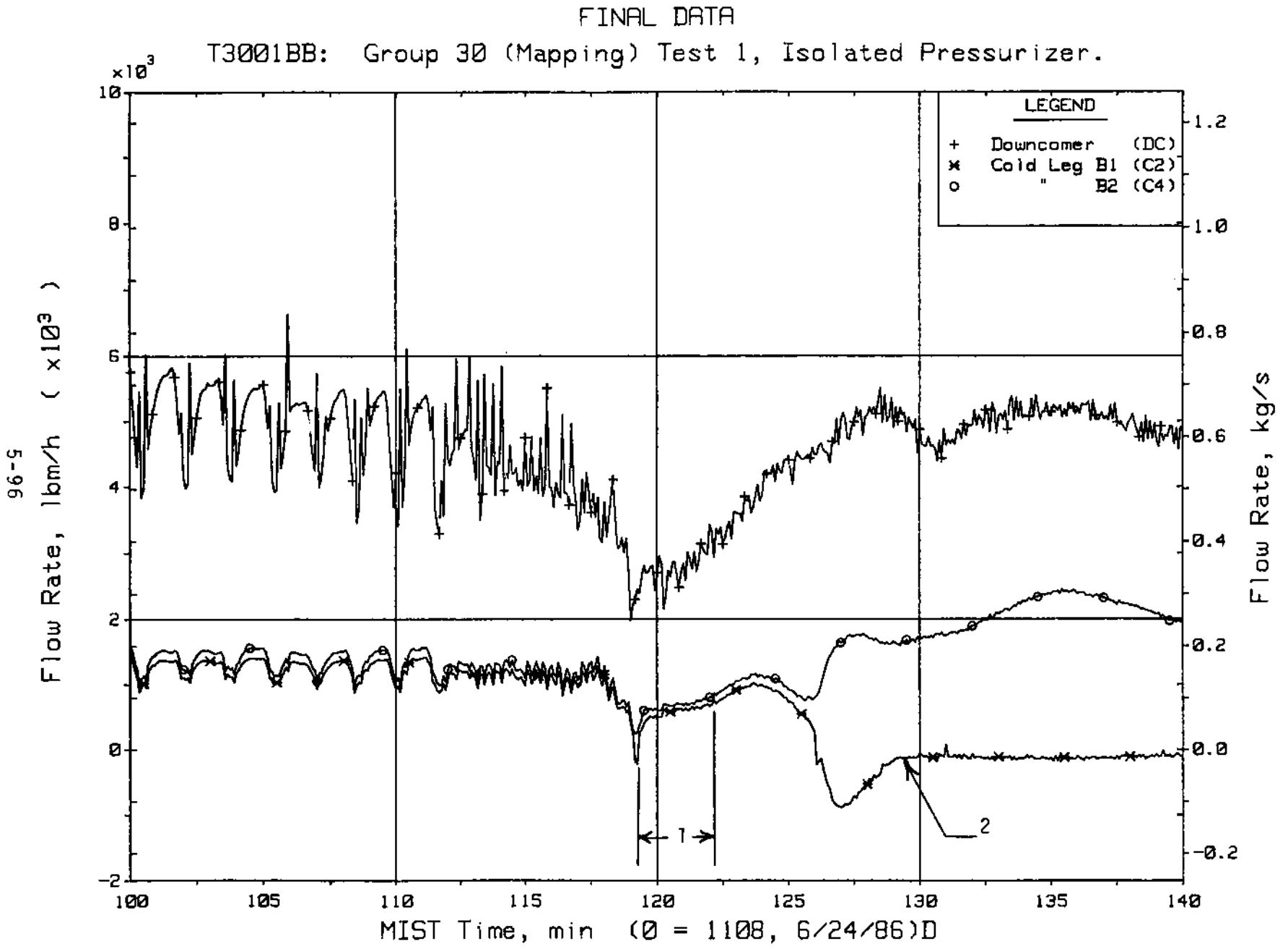

Figure 5.2.4. Primary System (Venturi) Flow Rates (VN20s)

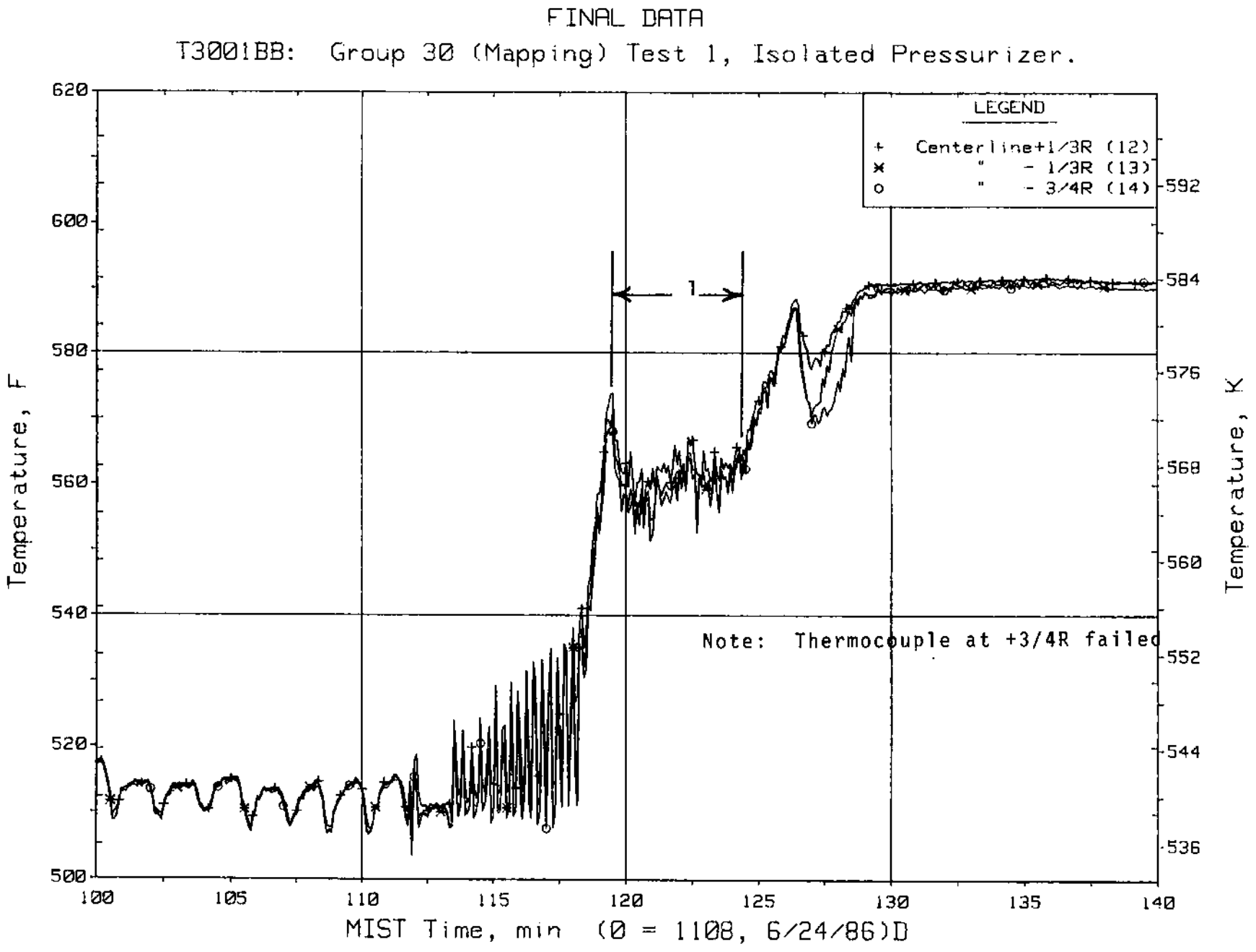

Figure 5.2.5. Cold Leg B1 Nozzle Rake Fluid Temperatures (21.2 ft, C2TCs)

Wed Feb 15 15:05:19 1989

C2TC4

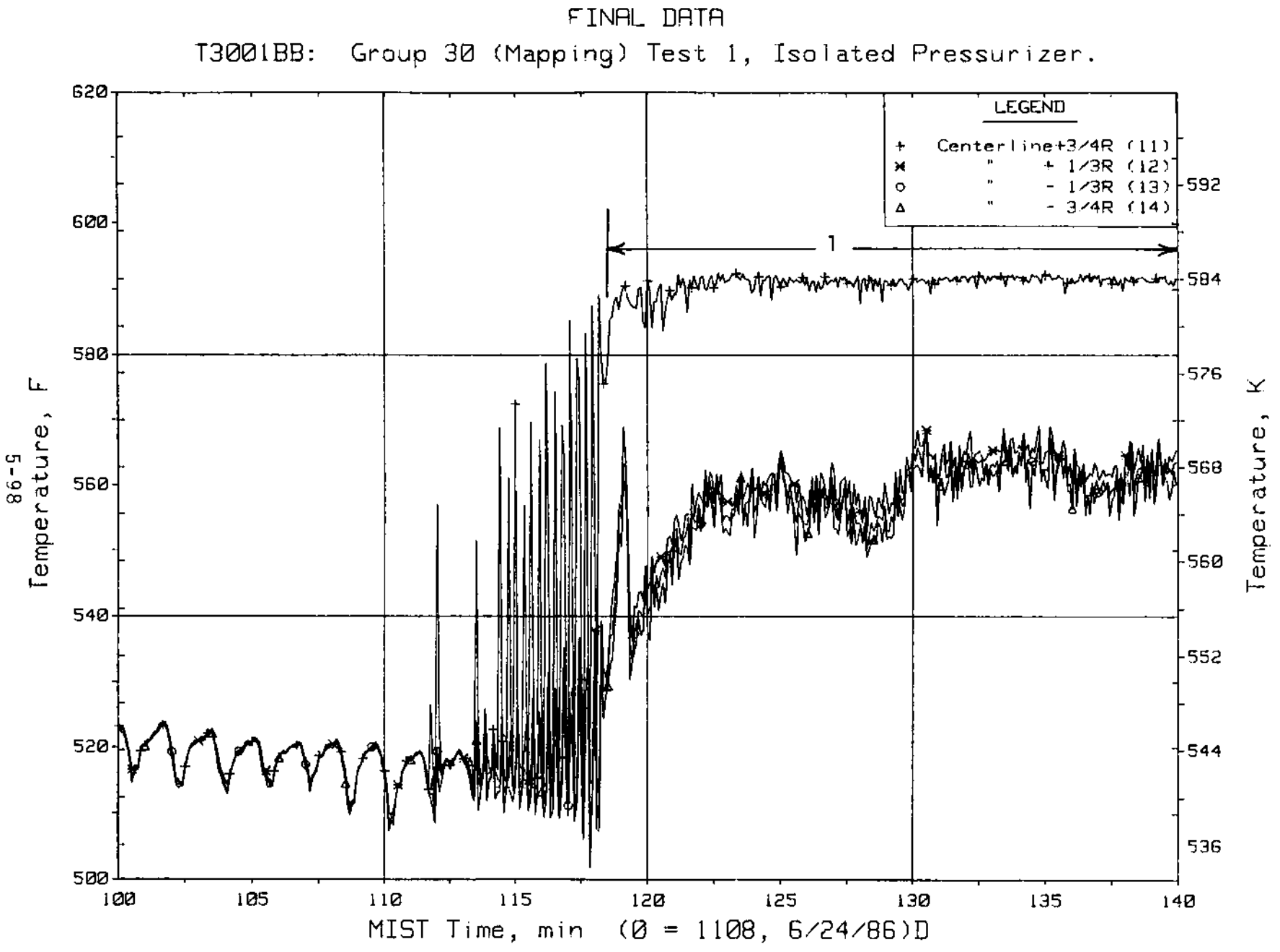

Figure 5.2.6. Cold Leg A2 Nozzle Rake Fluid Temperatures (21.2 ft, C3TCs)

Wed Feb 15 15:07:58 1989

C3TC4

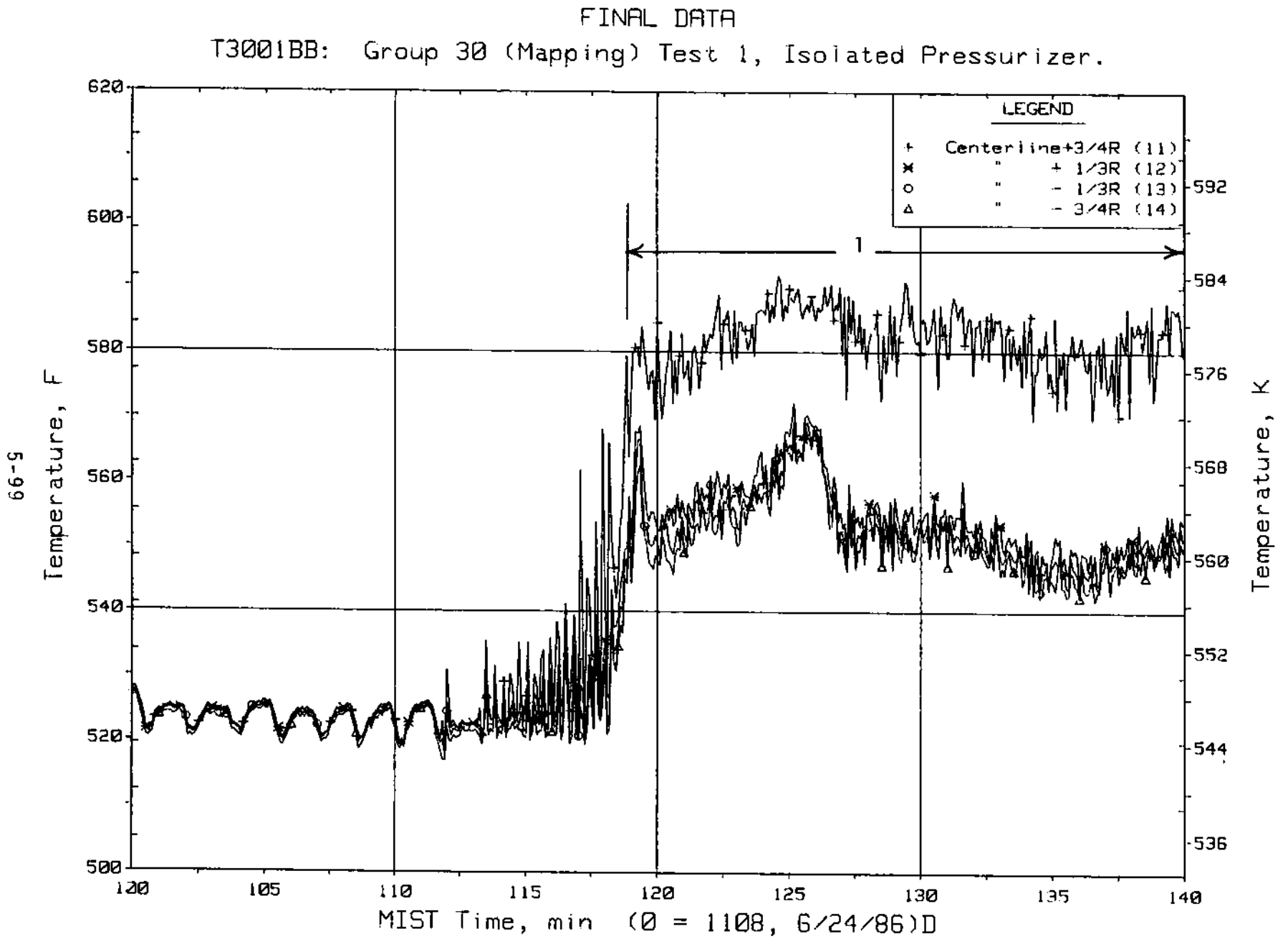

Figure 5.2.7. Cold Leg B2 Nozzle Rake Fluid Temperatures (21.2 ft, C4TCs)

Wed Feb 15 15:10:37 1989

C4TC4

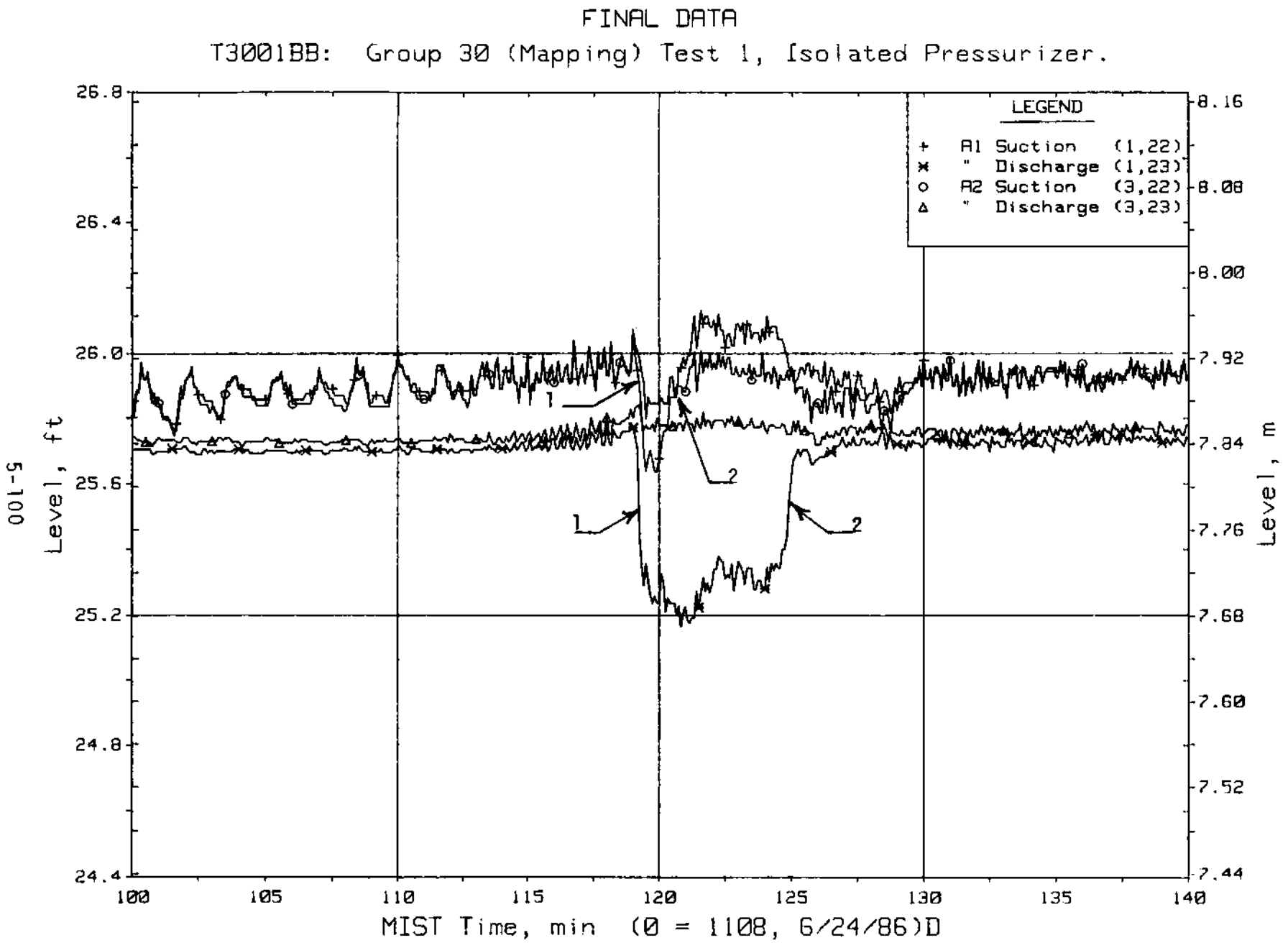

Figure 5.2.8. Loop A Cold Leg Collapsed Liquid Levels (LVs)

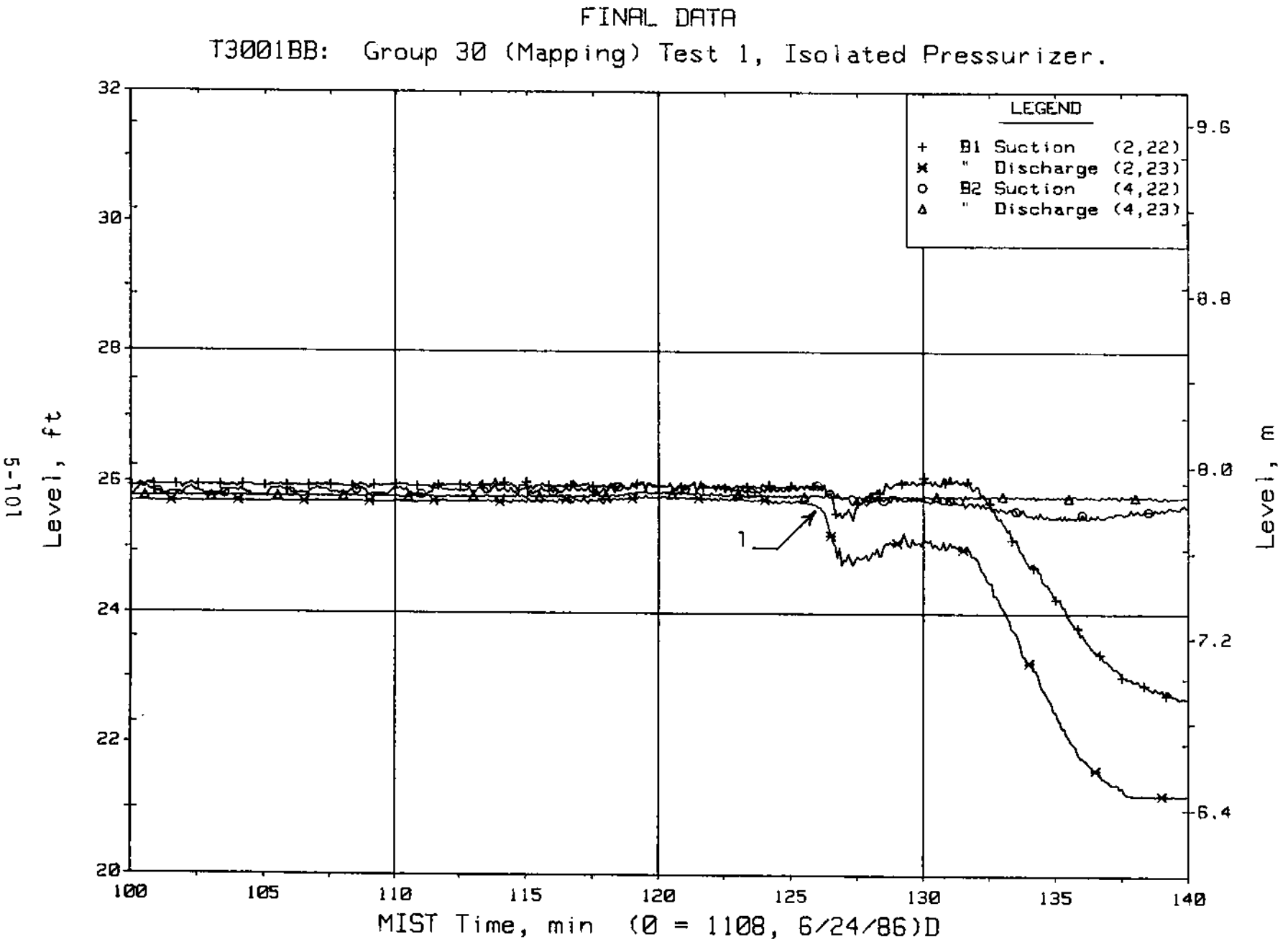

Figure 5.2.9. Loop B Cold Leg Collapsed Liquid Levels (LVs)

Wed Feb 15 15:30:22 1989

CLLV2

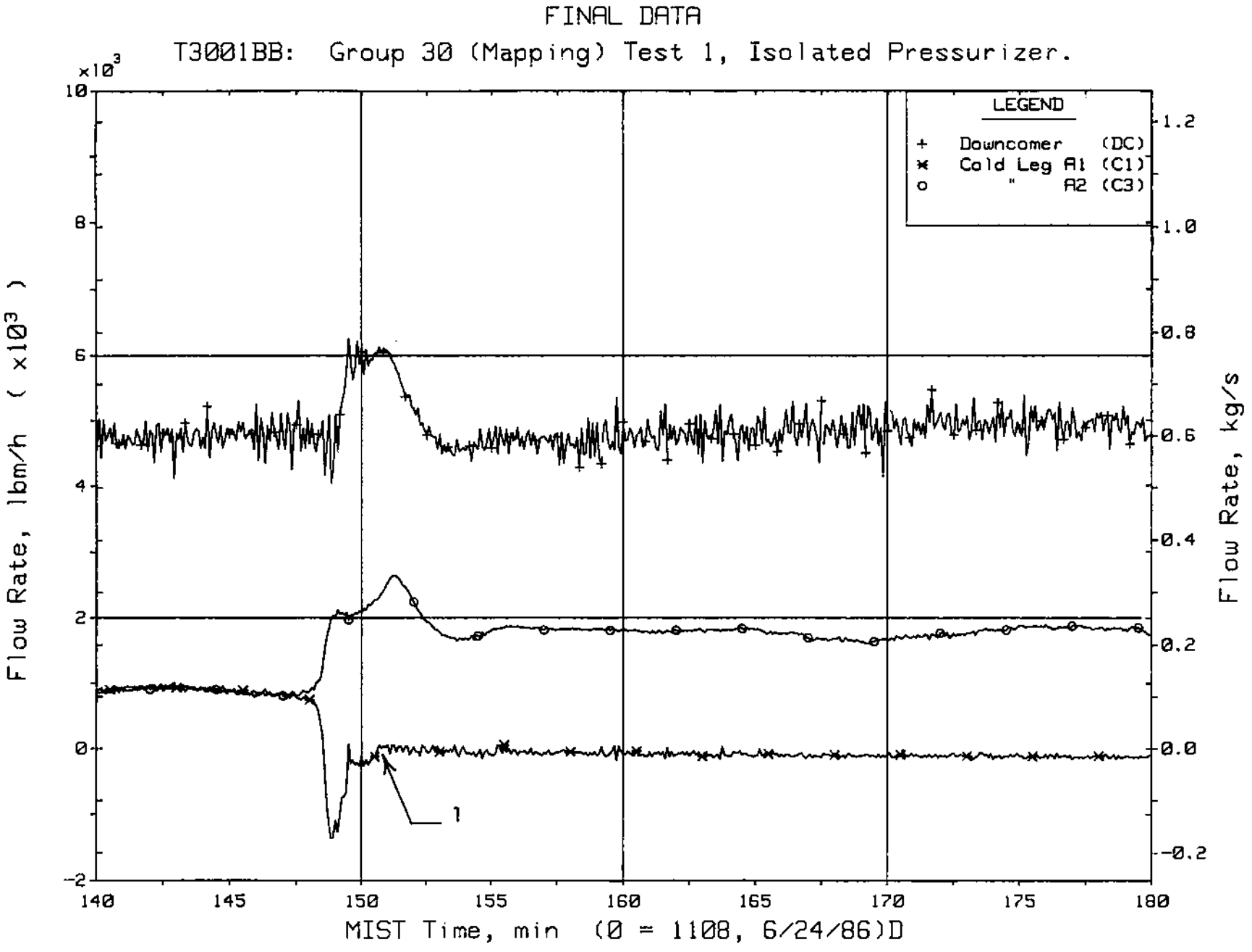

Figure 5.2.10. Primary System (Venturi) Flow Rates (VN20s)

Thu Feb 16 11:25:52 1989

PRFL1

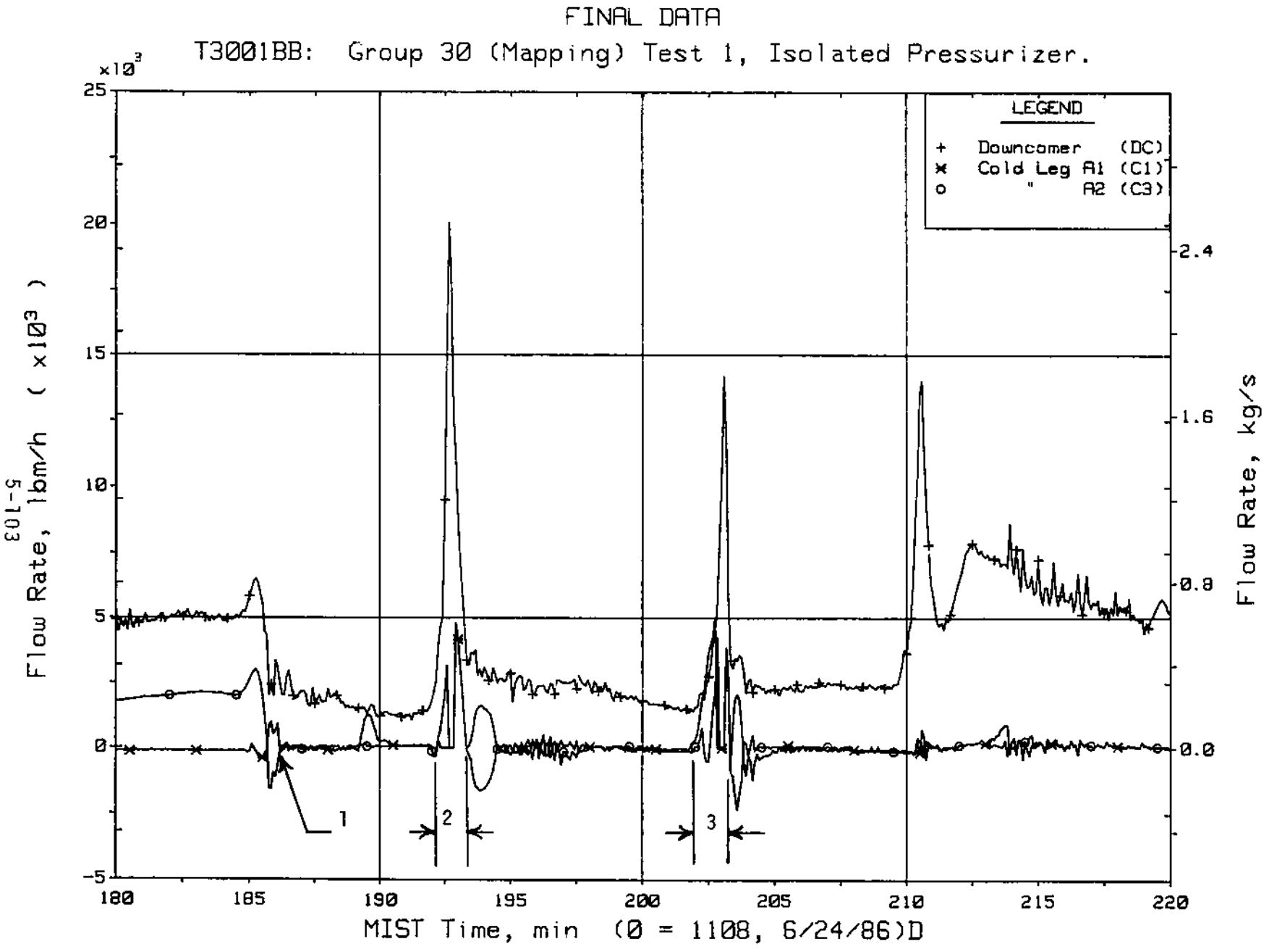

Figure 5.2.11. Primary System (Venturi) Flow Rates (VN20s)

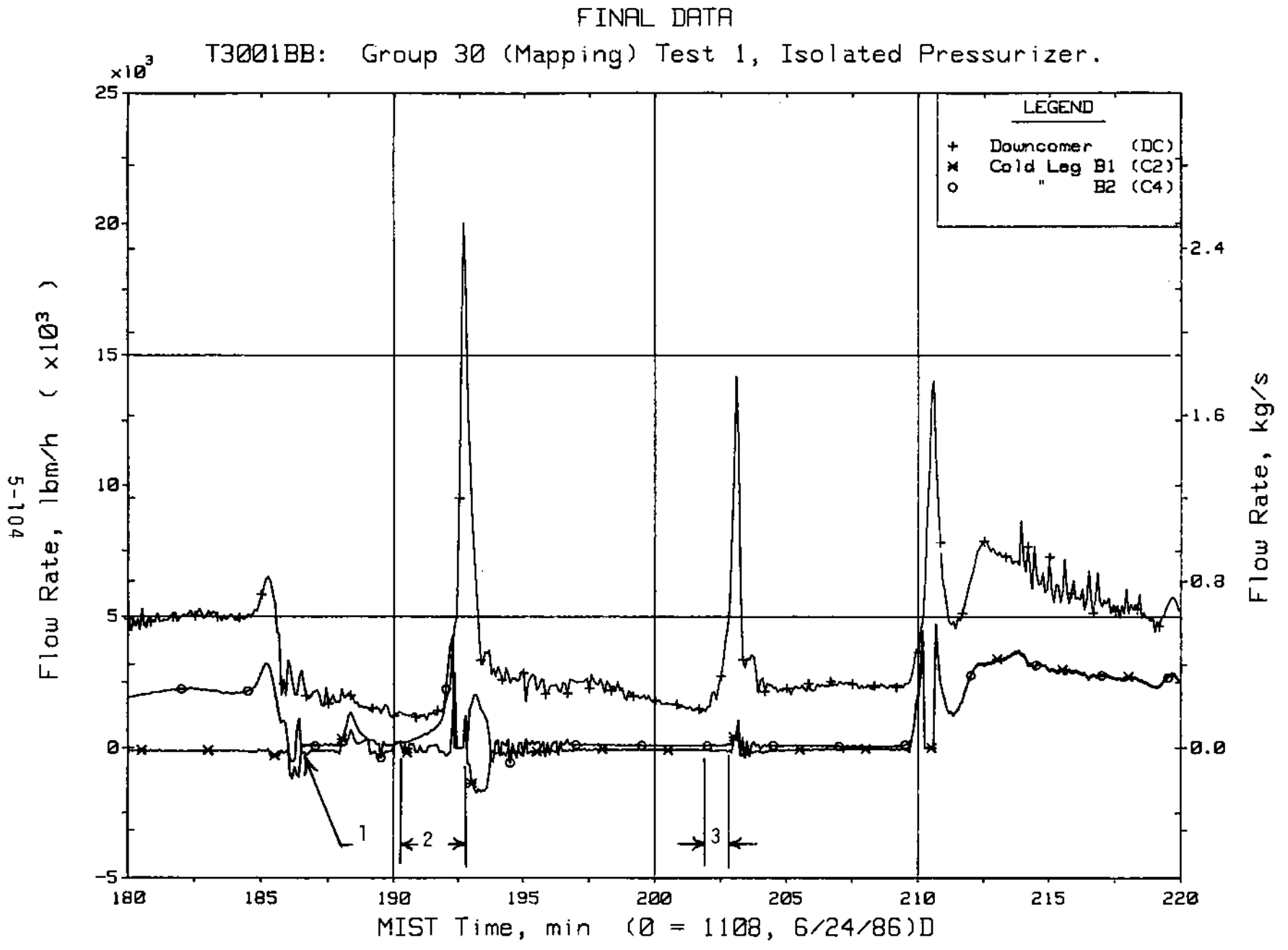

Figure 5.2.12. Primary System (Venturi) Flow Rates (VN20s)

Thu Feb 16 11:32:39 1989

PRFL2

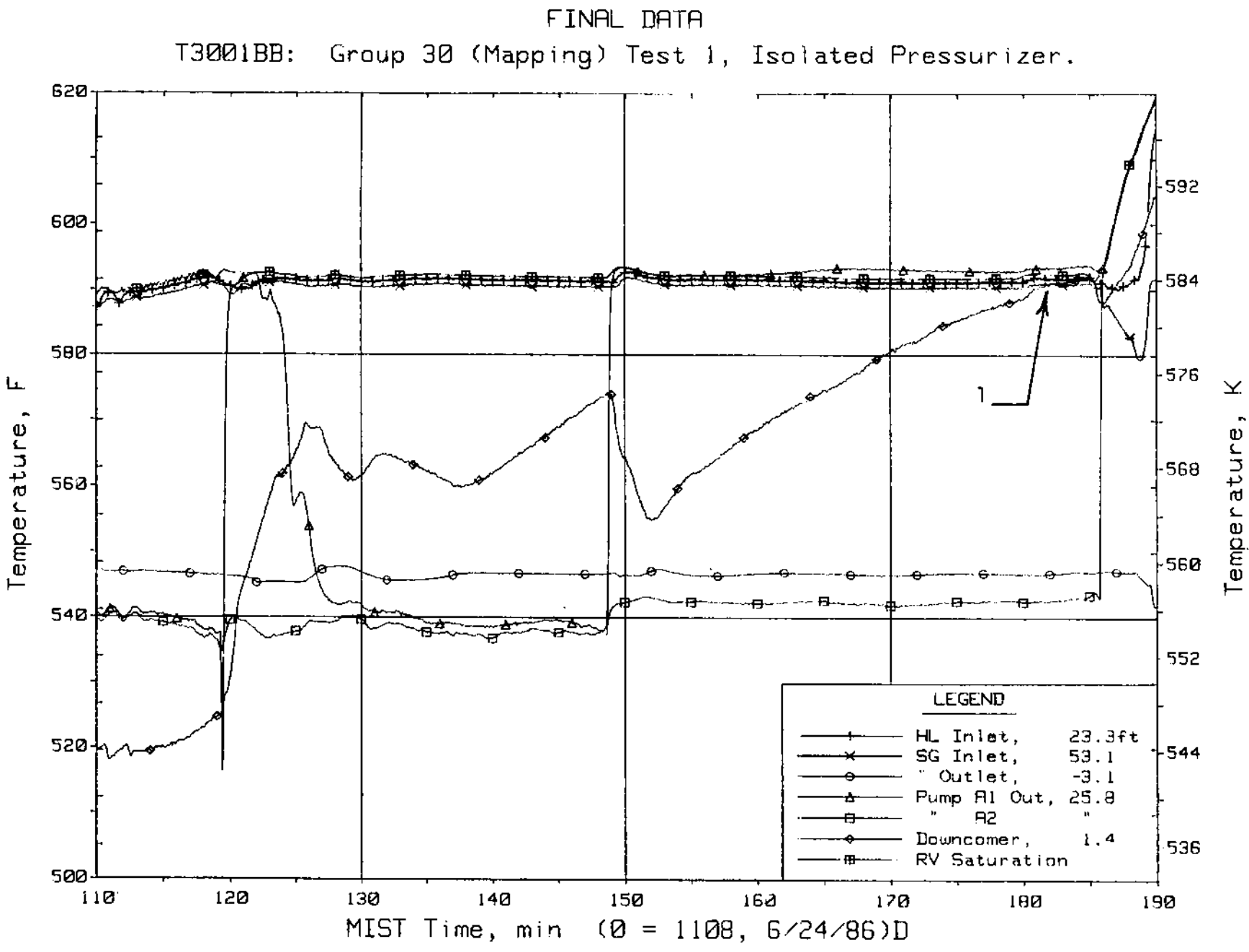

Figure 5.2.13. Loop A Primary Fluid Temperatures (RTDs)

Tue Feb 14 17:51:41 1989

PRRT1

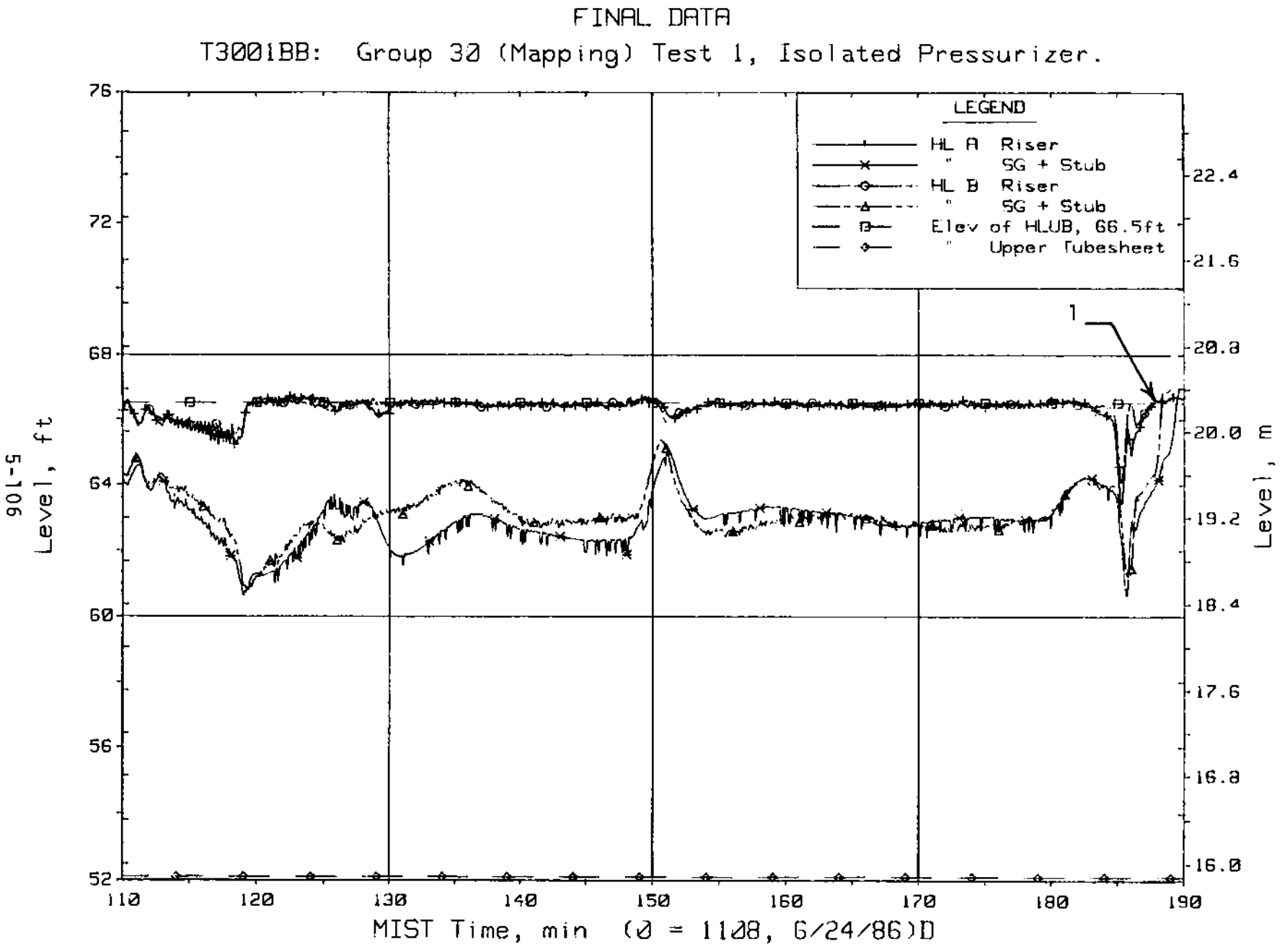

Figure 5.2.14. Hot Leg Riser and Stub Collapsed Liquid Levels

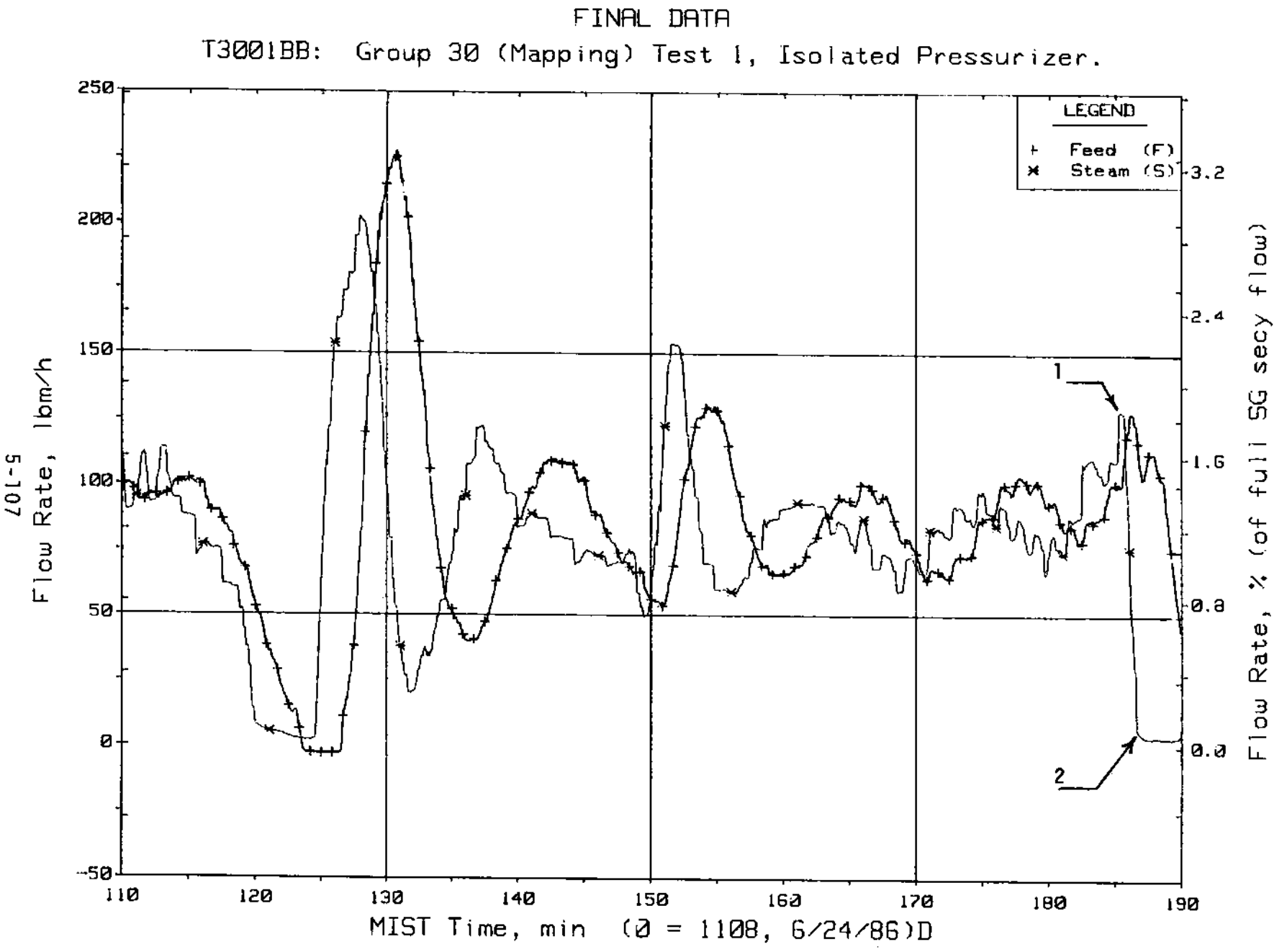

Figure 5.2.15. Steam Generator A Flow Rates (SaOR20s)

Tue Feb 14 17:43:24 1989

SCFL1

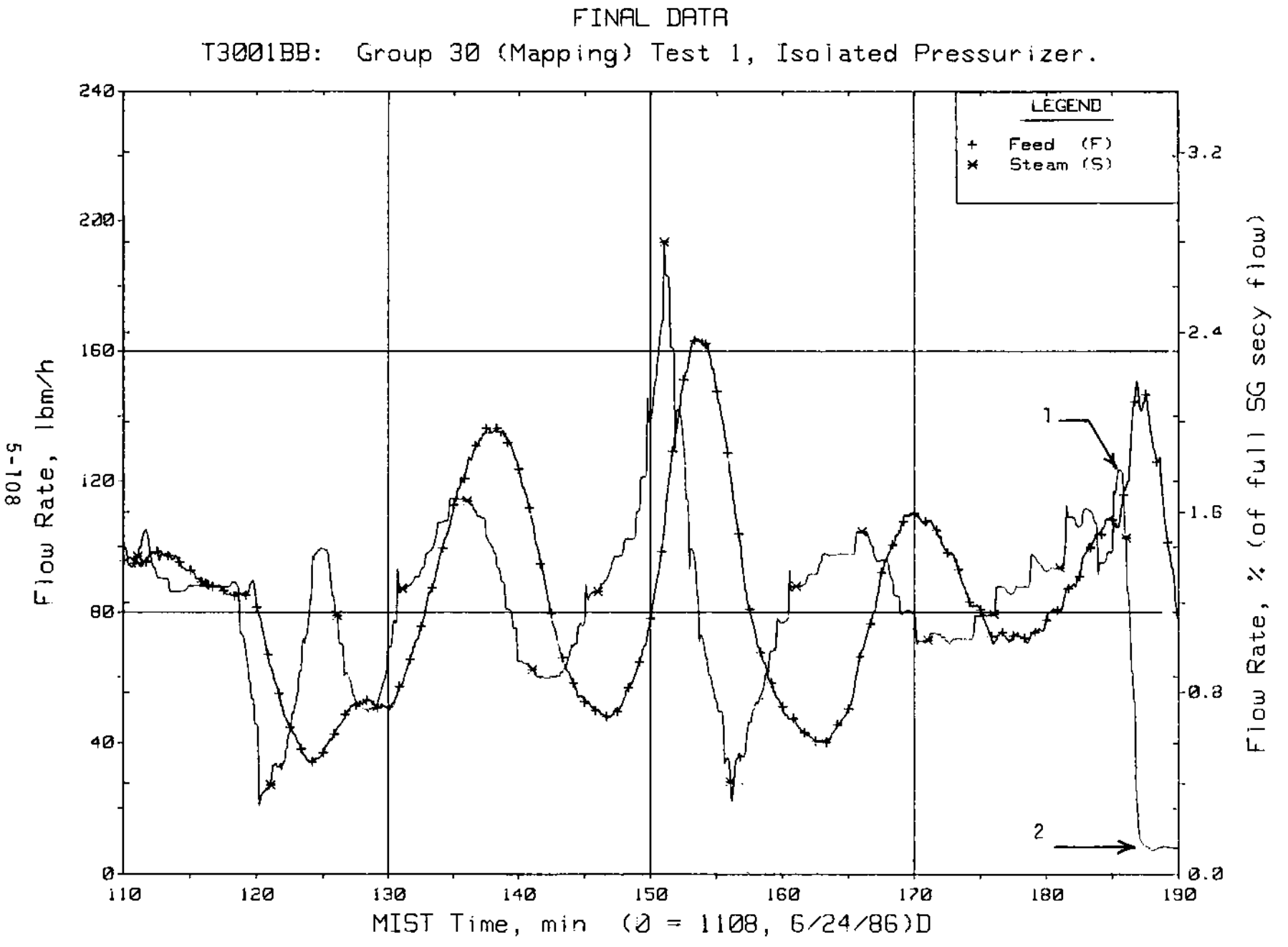

Figure 5.2.16. Steam Generator B Flow Rates (SaOR21s)

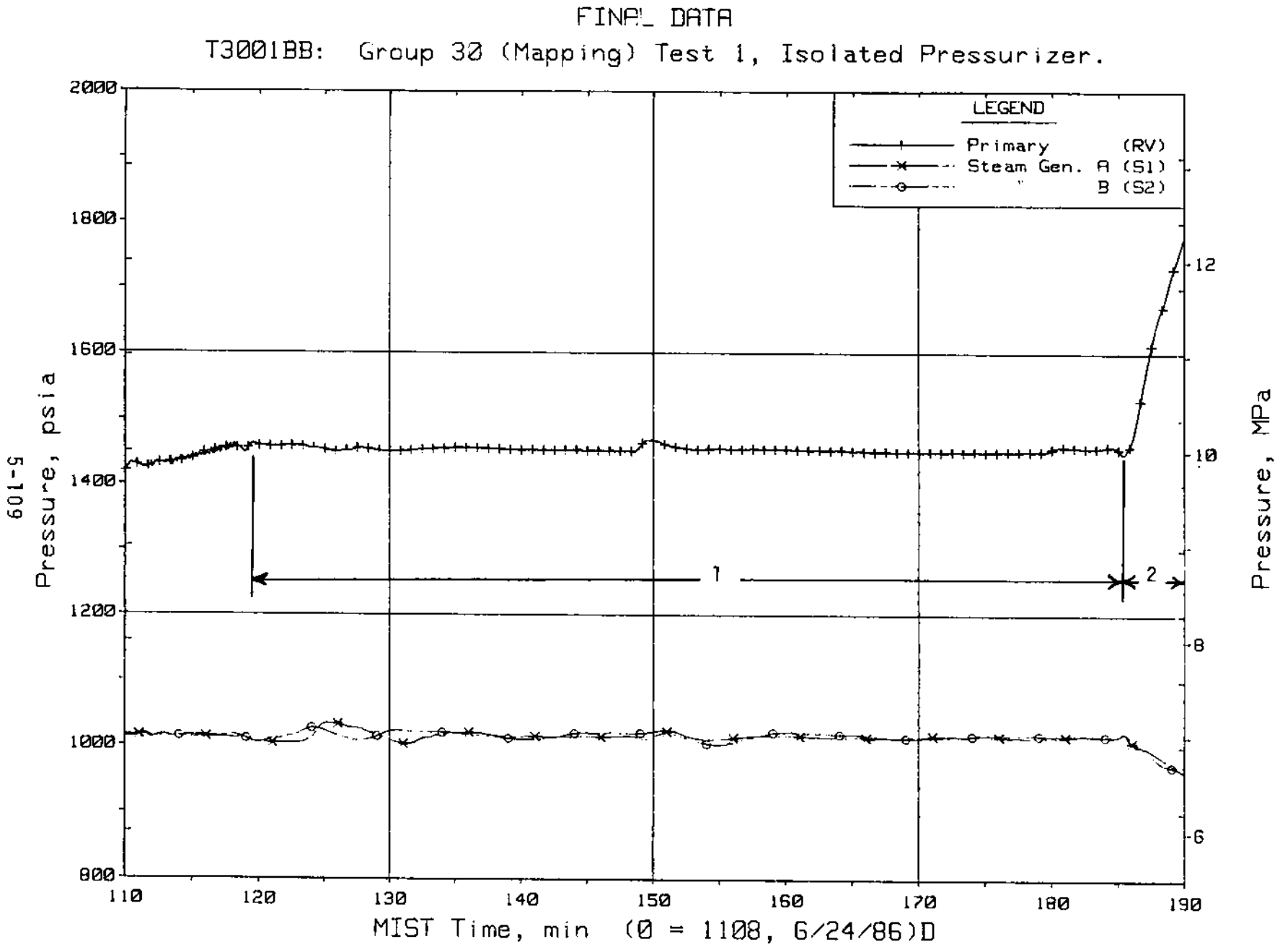

Figure 5.2.17. Primary and Secondary System Pressures (GP01s)

Tue Feb 14 17:38:30 1989

PSGP1

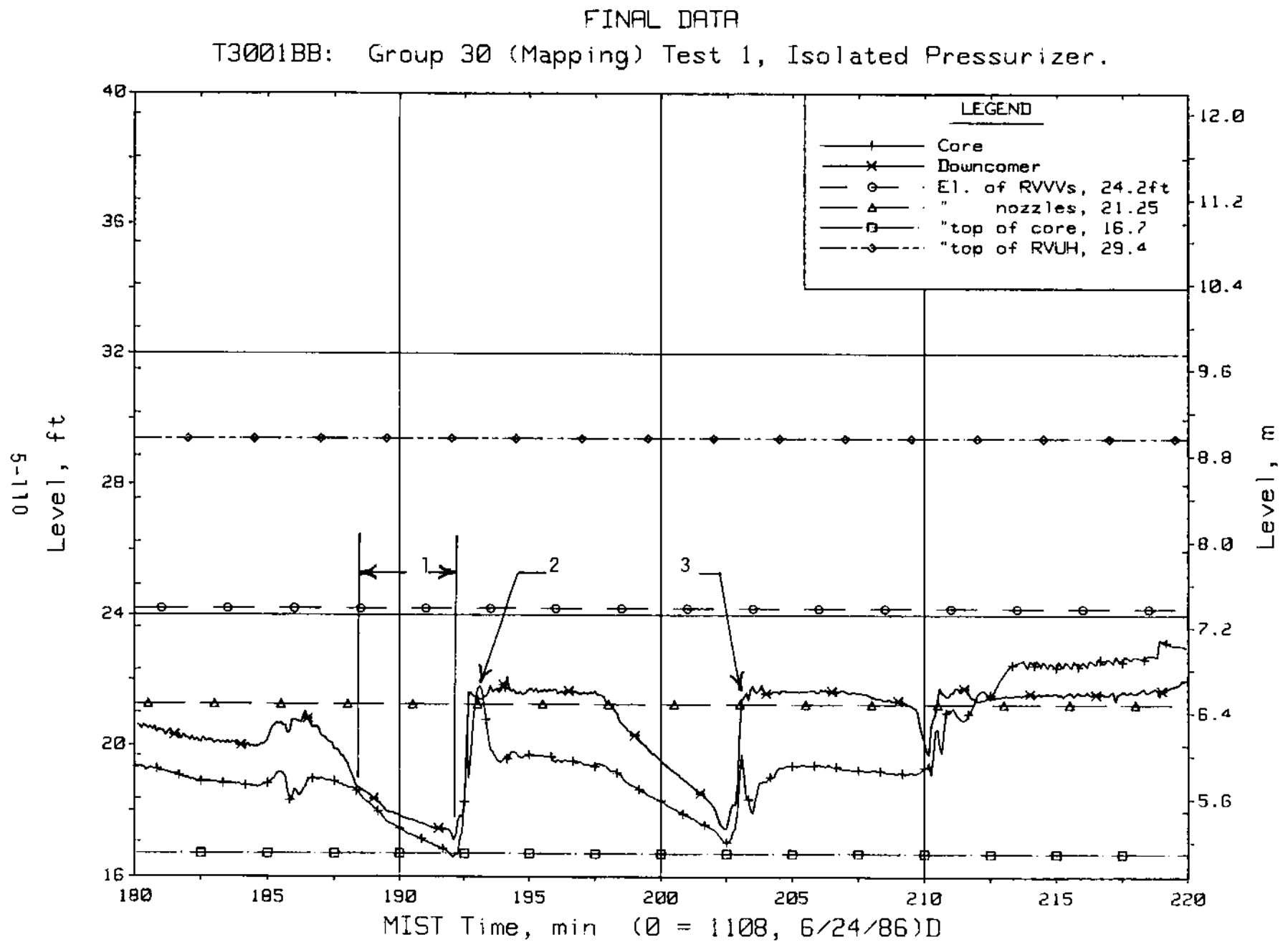

Figure 5.2.18. Core Region Collapsed Liquid Levels

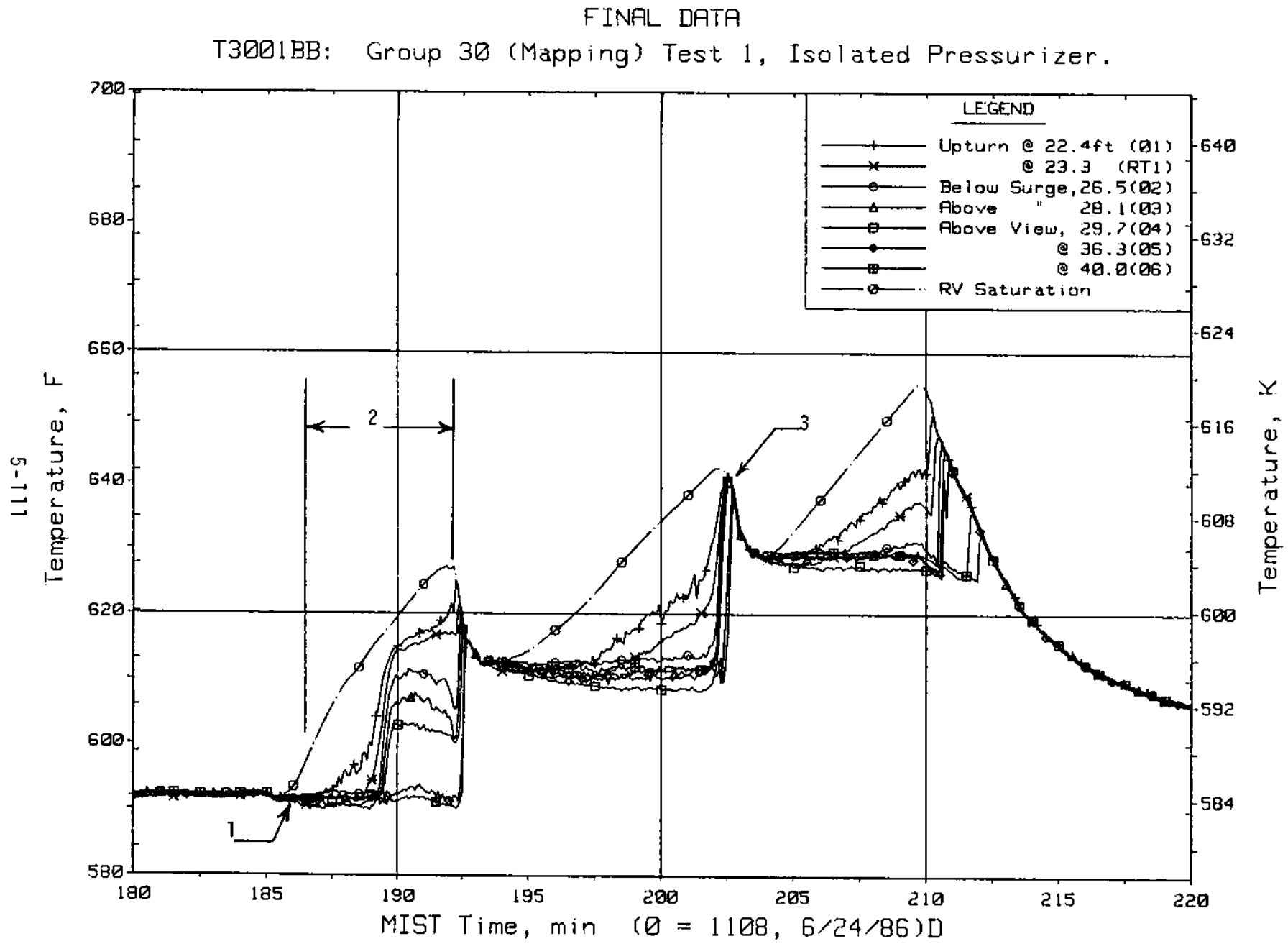

Figure 5.2.19. Hot Leg A Lower-Elevation Riser Fluid Temperatures (H1TCs)

Wed Feb 15 15:41:27 1989

H1TC1

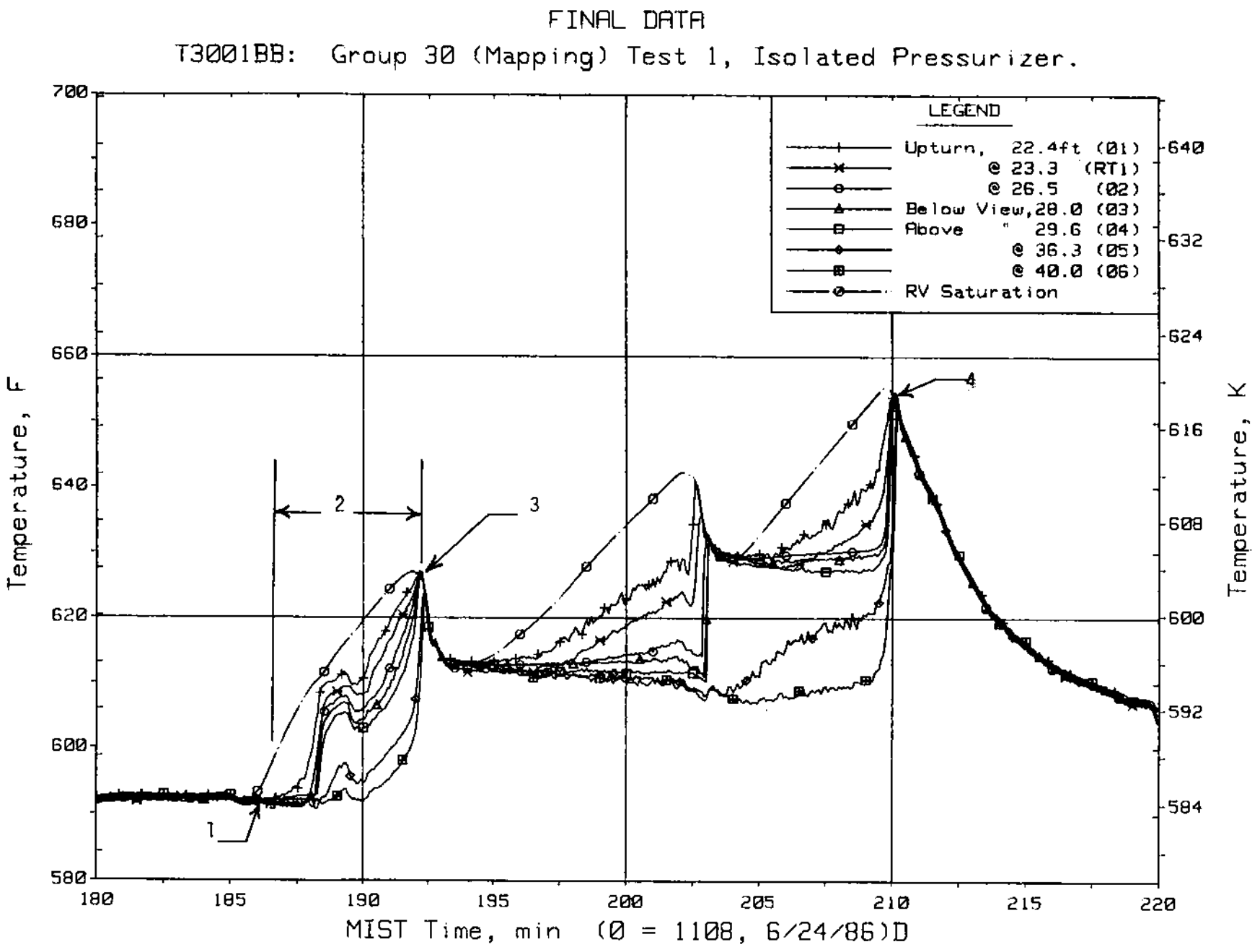

Figure 5.2.20. Hot Leg B Lower-Elevation Riser Fluid Temperatures (H2TCs)

Wed Feb 15 15:45:02 1989

H2TC1

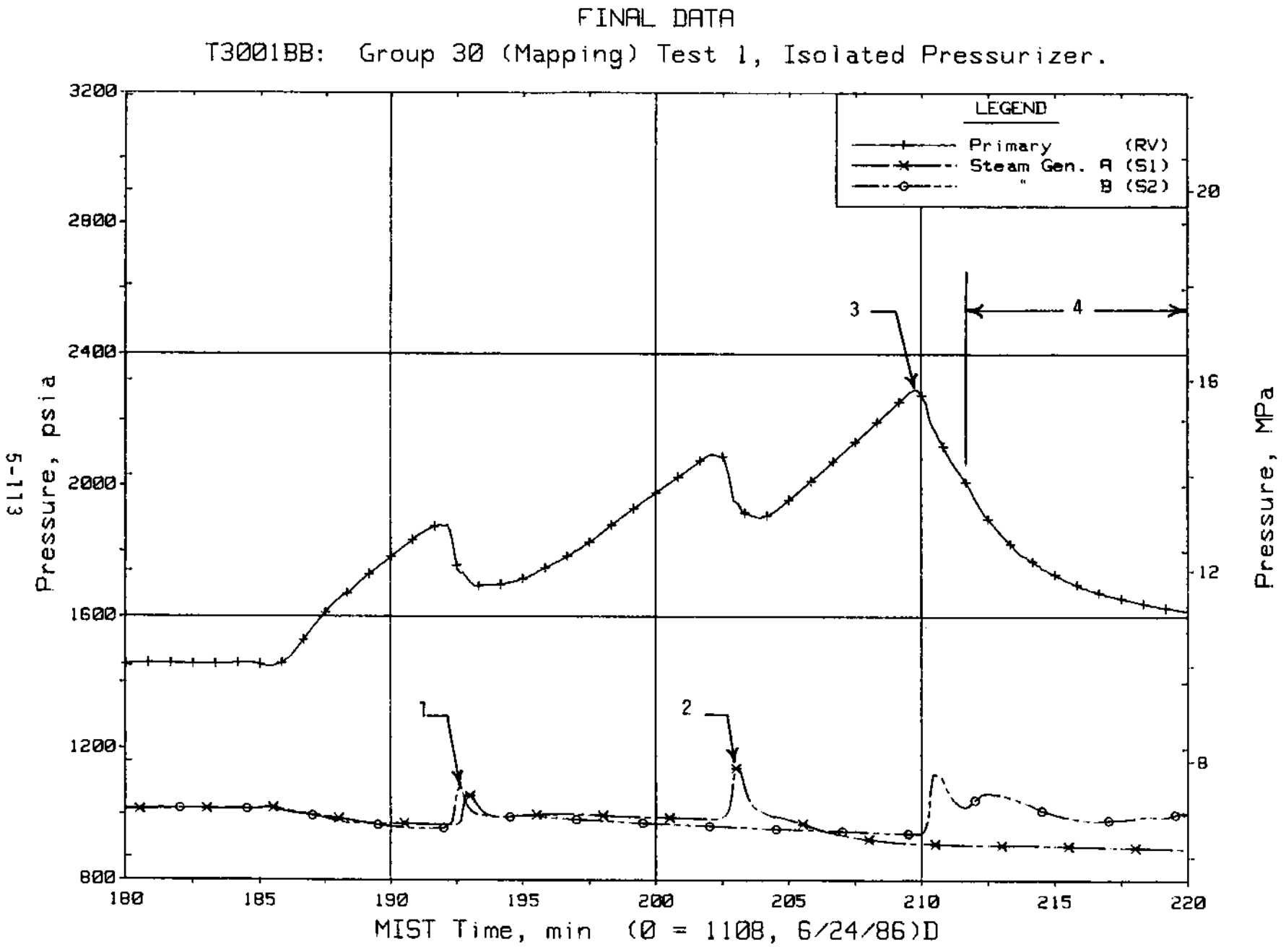

Figure 5.2.21. Primary and Secondary System Pressures (GP01s)

Wed Feb 15 15:47:45 1989

PSGP1

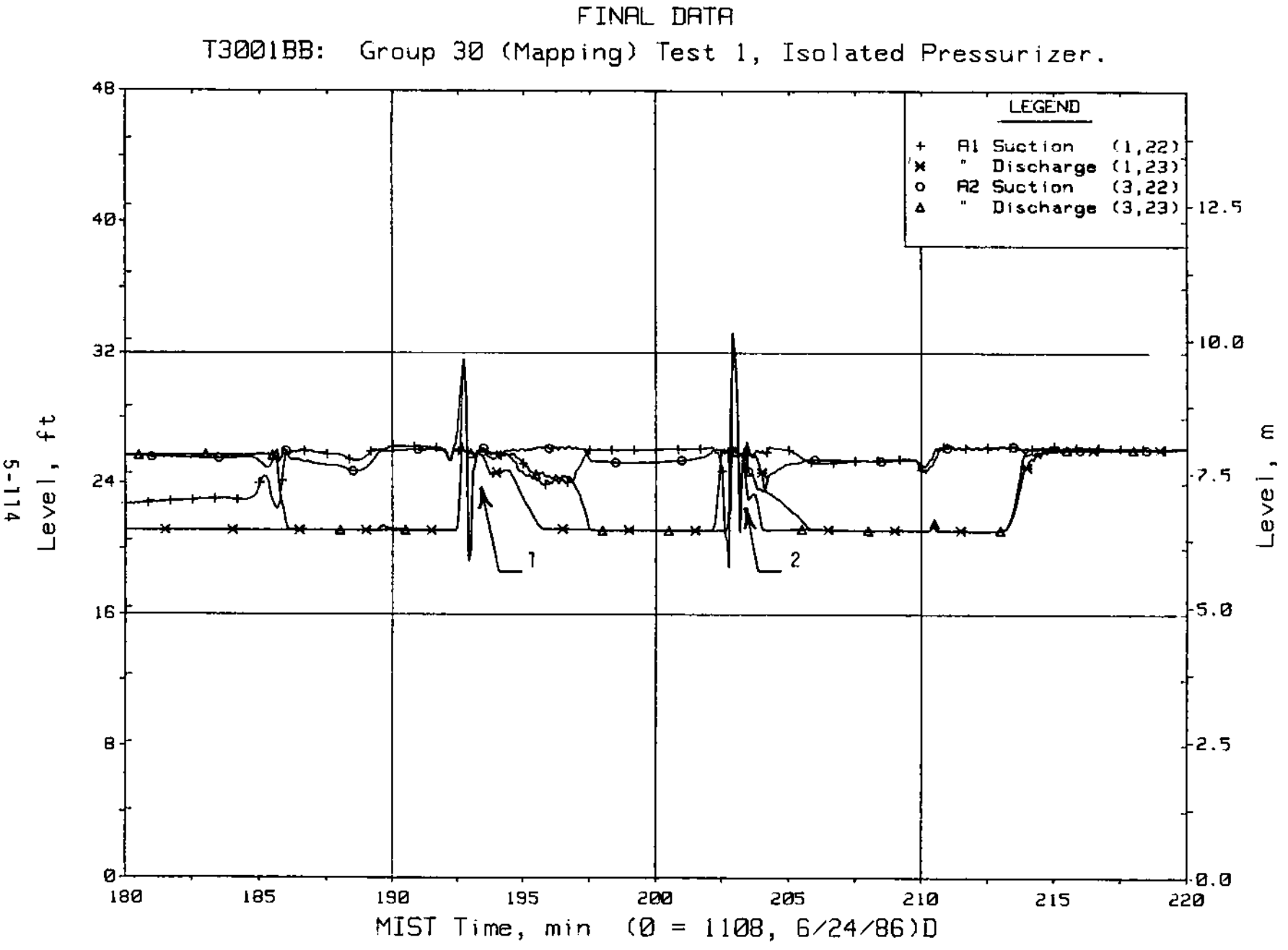

Figure 5.2.22. Loop A Cold Leg Collapsed Liquid Levels (LVs)

Thu Feb 16 10:12:16 1989

CLLV1

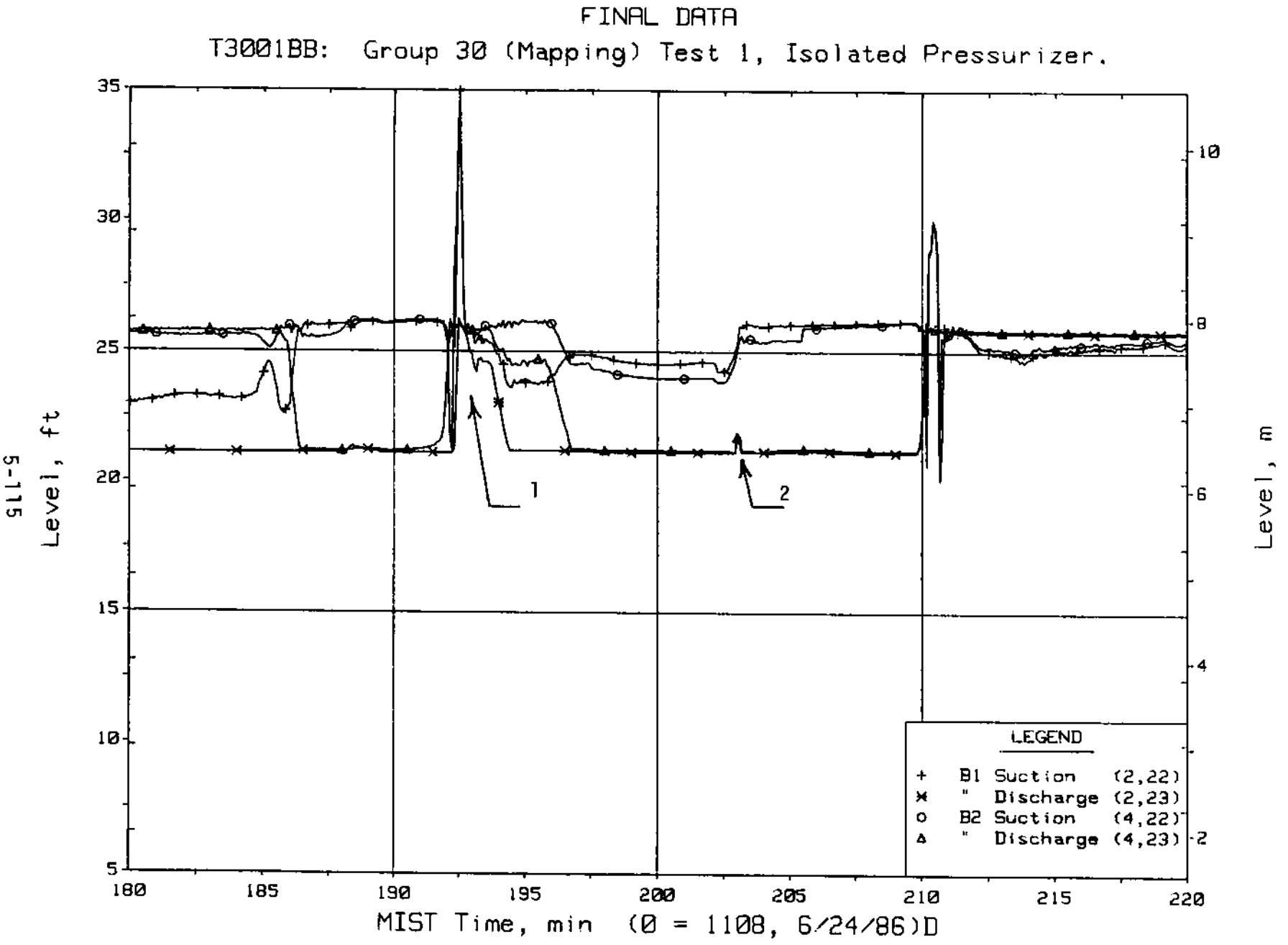

Figure 5.2.23. Loop B Cold Leg Collapsed Liquid Levels (LVs)

Thu Feb 16 10:16:10 1989

CLLV2

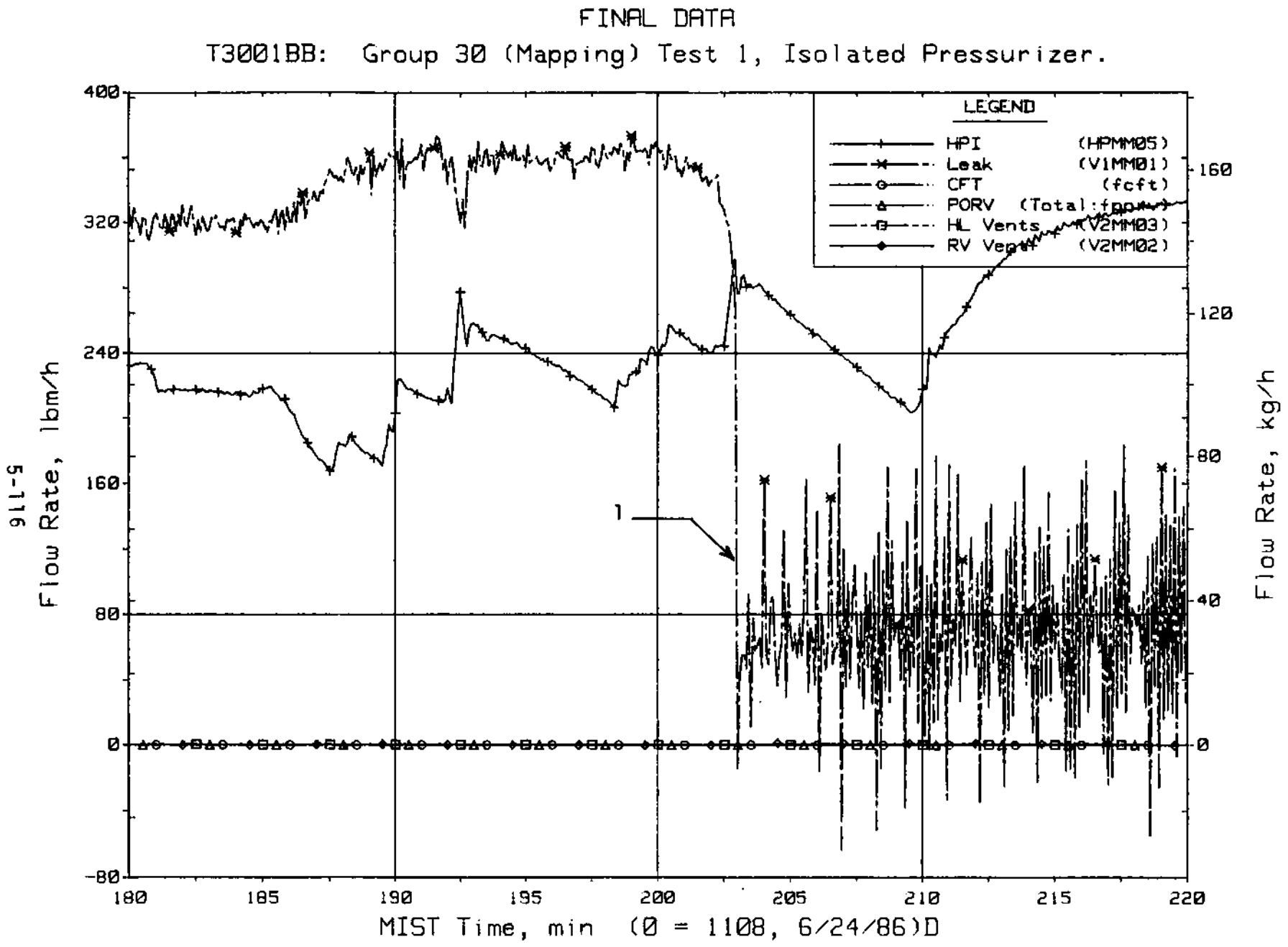

Figure 5.2.24. Primary System Boundary Flow Rates

Thu Feb 16 10:38:21 1989

PRFL3p

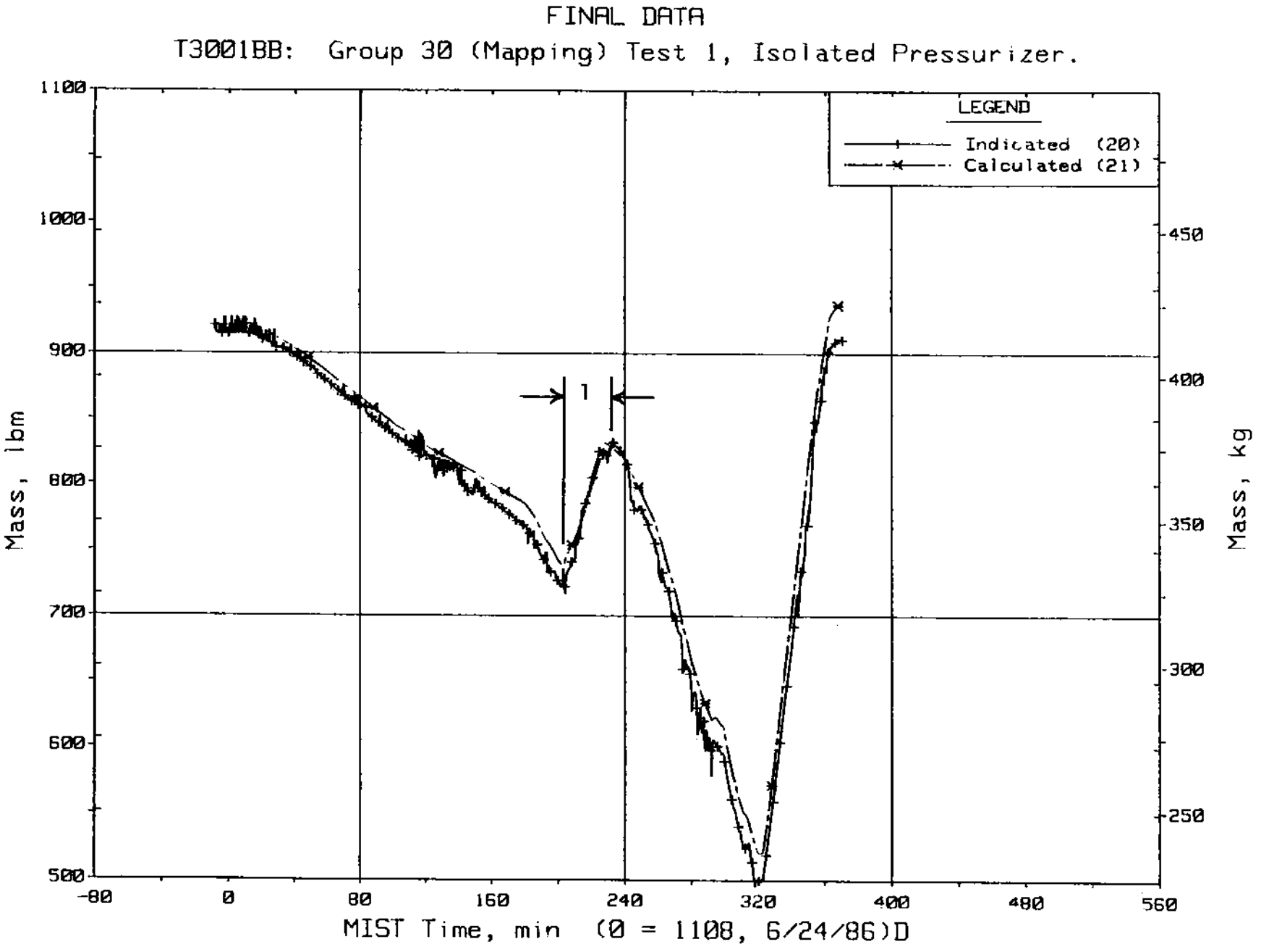

Figure 5.2.25. Primary System Total Fluid Mass (PLMLs)

Thu Feb 16 10:22:44 1989

PRML1

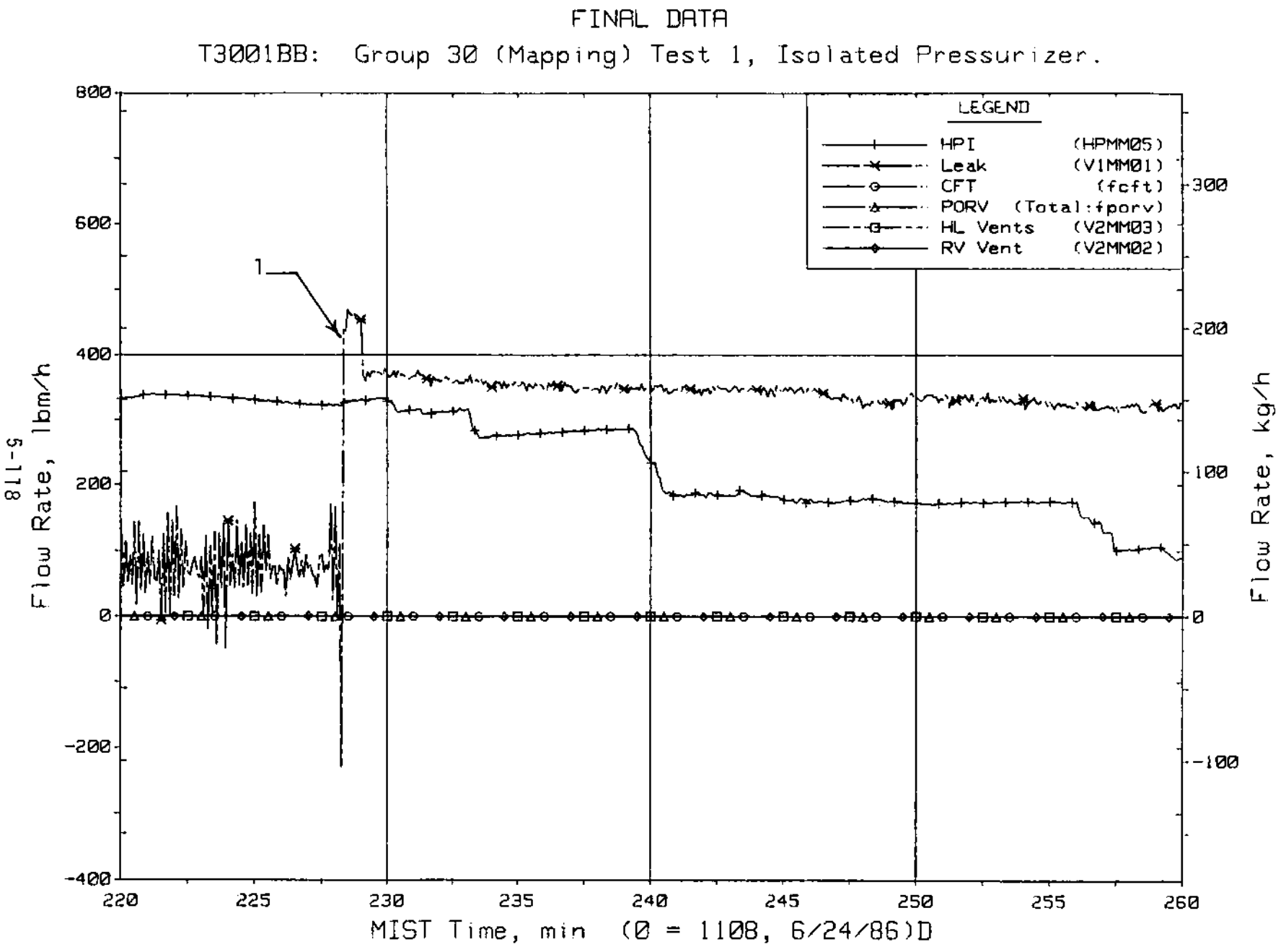

Figure 5.2.26. Primary System Boundary Flow Rates

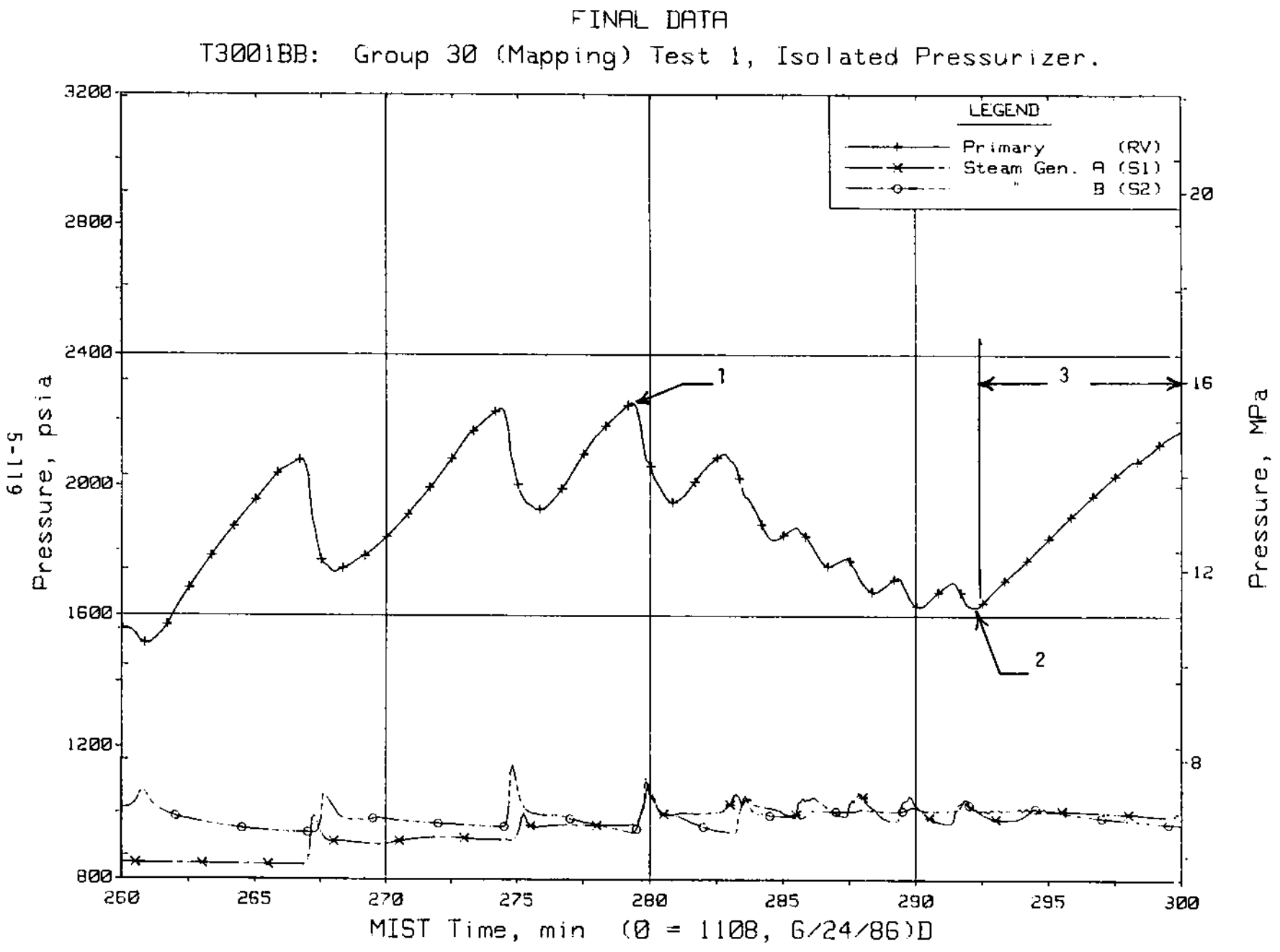

Figure 5.2.27. Primary and Secondary System Pressures (GPOIs)

Tue Feb 14 18:08:48 1989

PSGP1

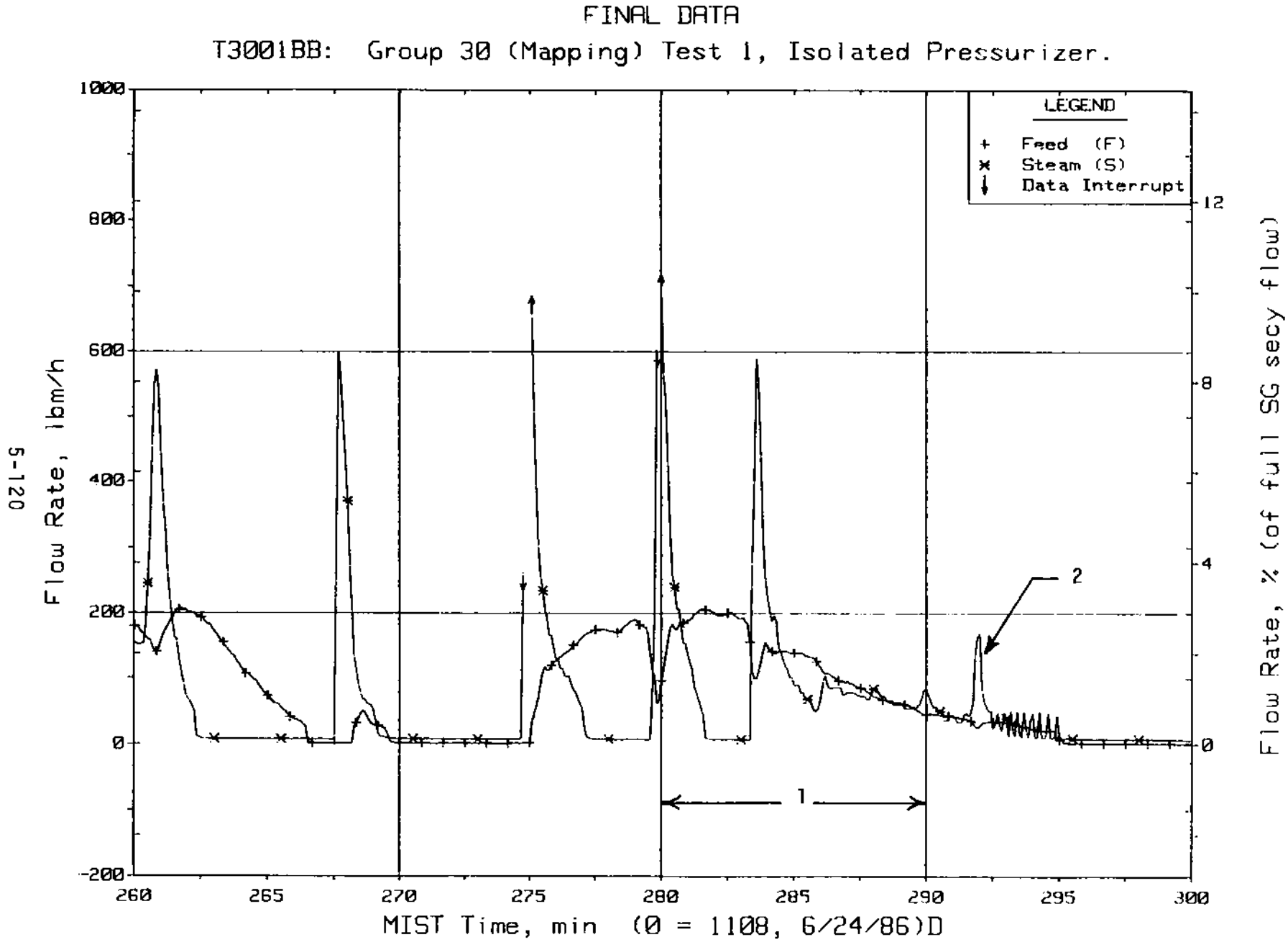

Figure 5.2.28. Steam Generator B Flow Rates (SaOR21s)

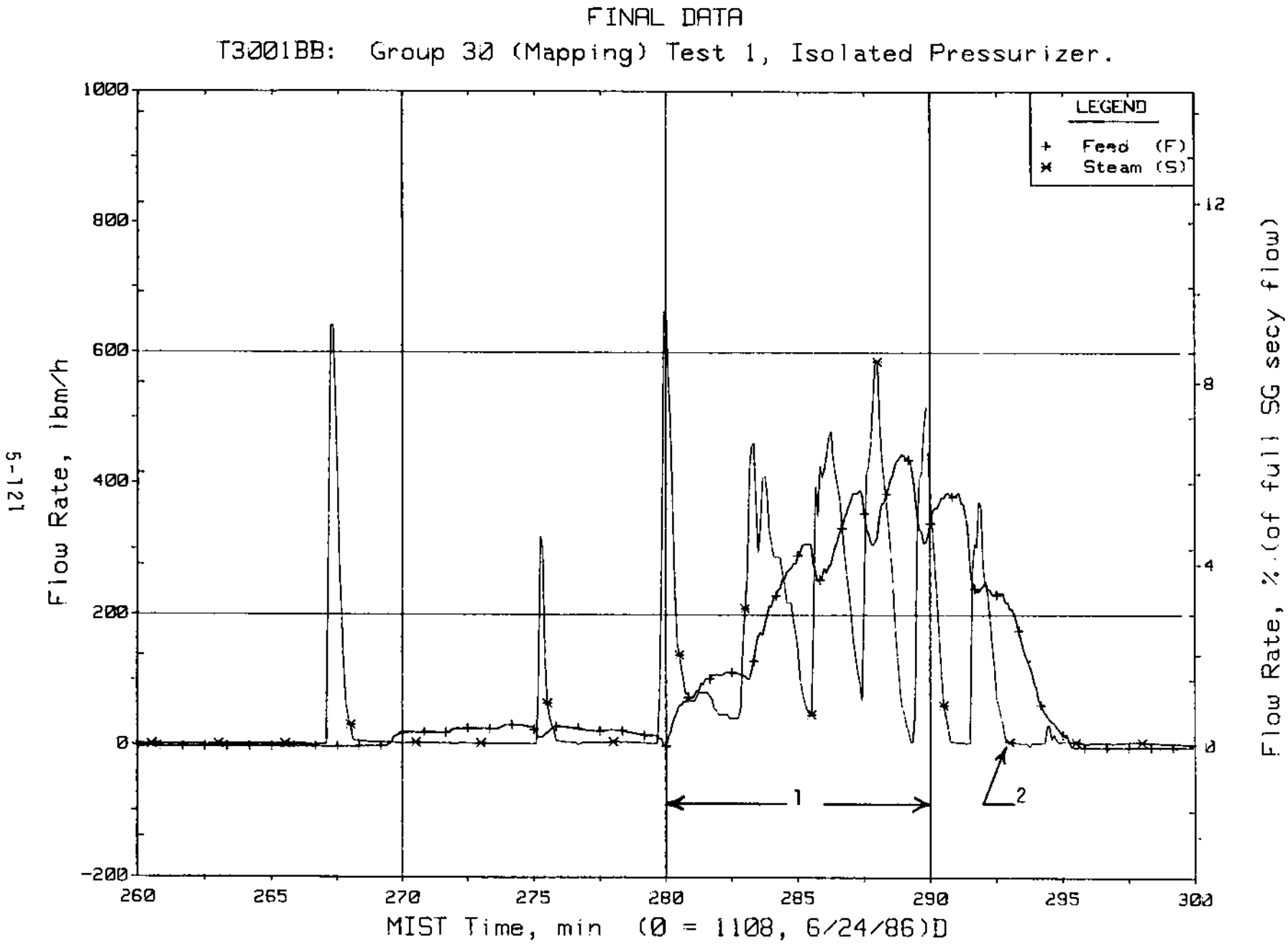

Figure 5.2.29. Steam Generator A Flow Rates (SaOR20s)

Tue Feb 14 18:04:22 1989

SCFL1

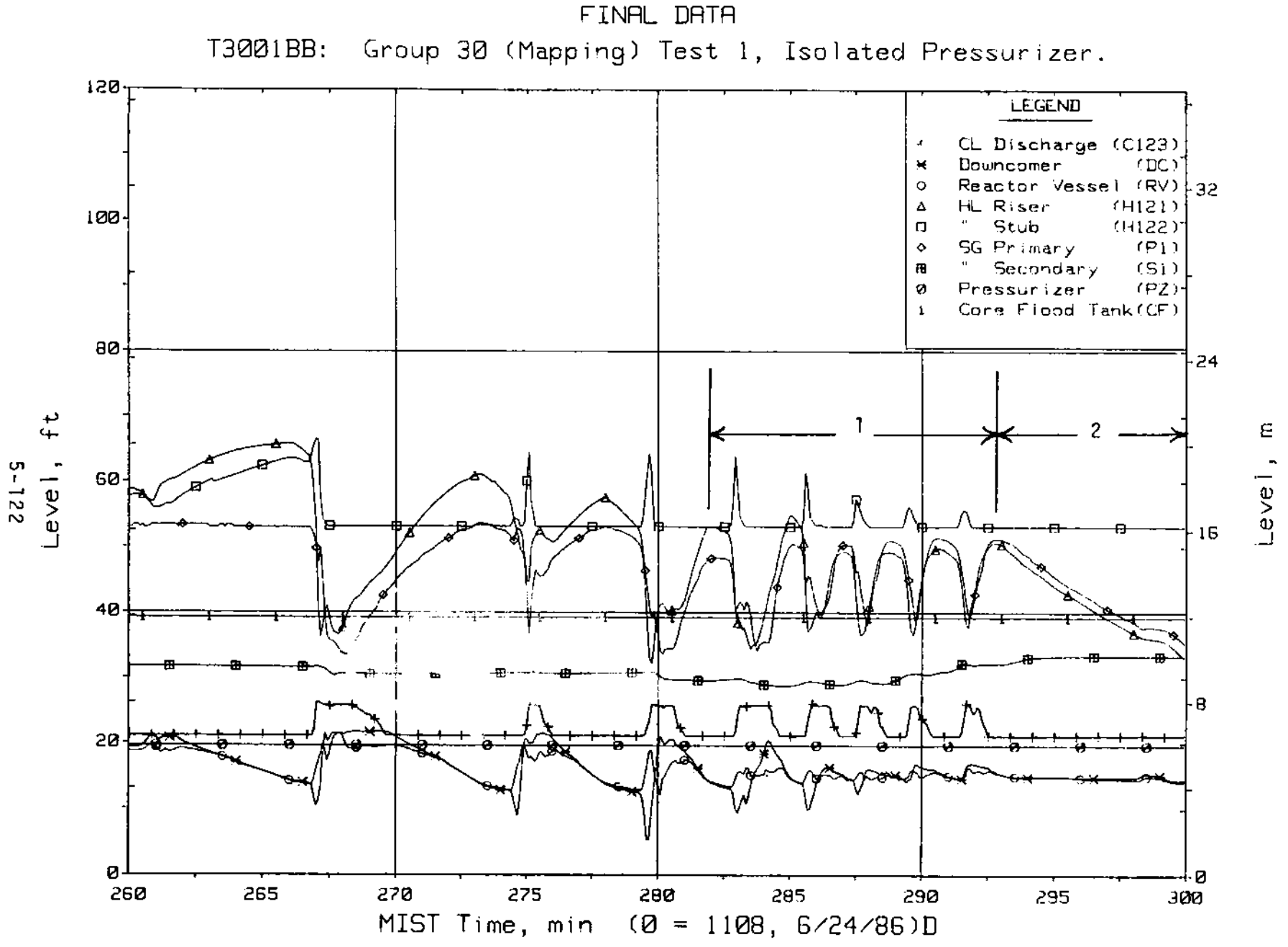

Figure 5.2.30. Loop A Collapsed Liquid Levels (LV20s)

Tue Feb 14 18:02:09 1989

PRLV1

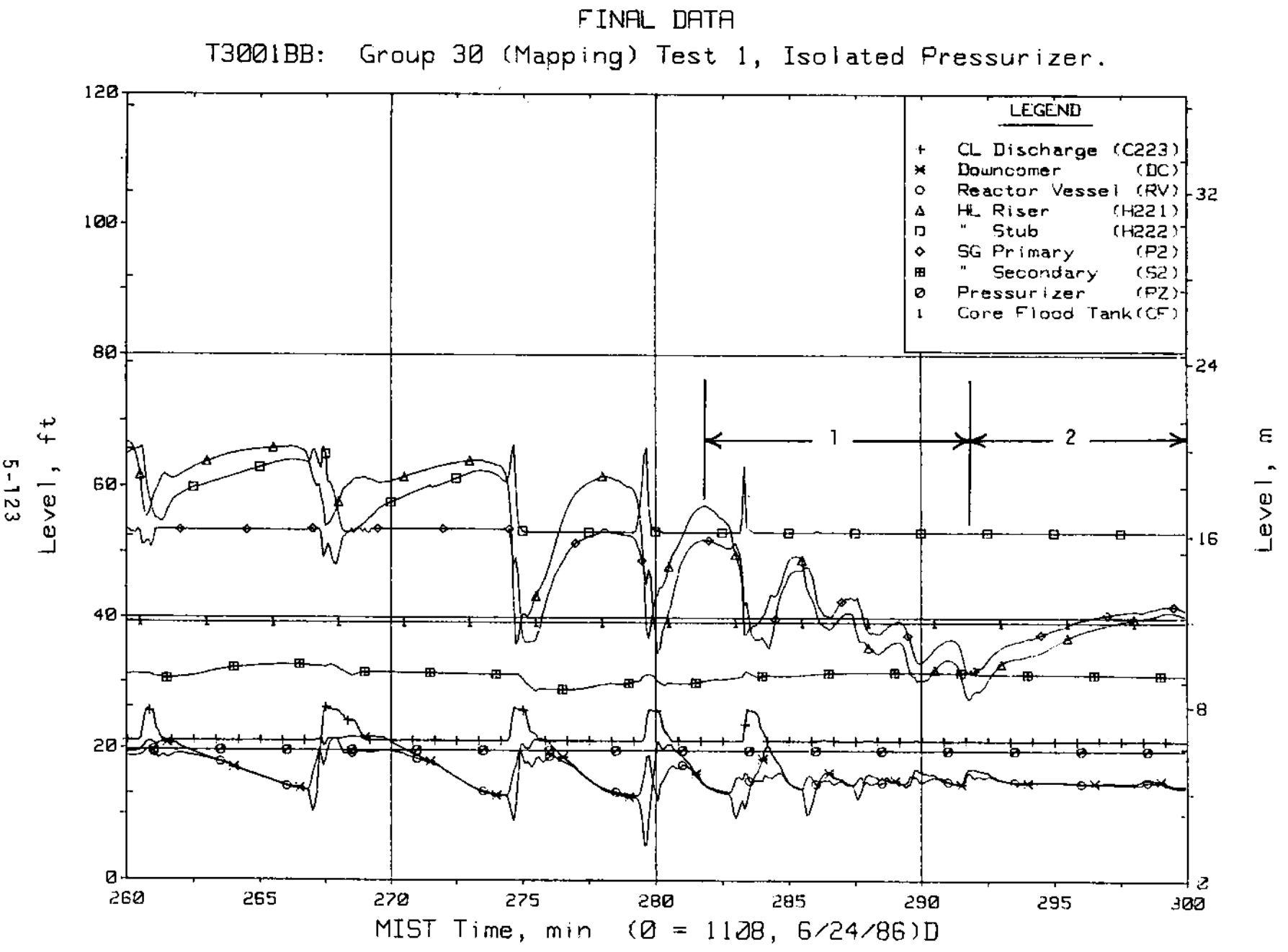

Figure 5.2.31. Loop B Collapsed Liquid Levels (LV20s)

Tue Feb 14 17:58:40 1989

PRLV2

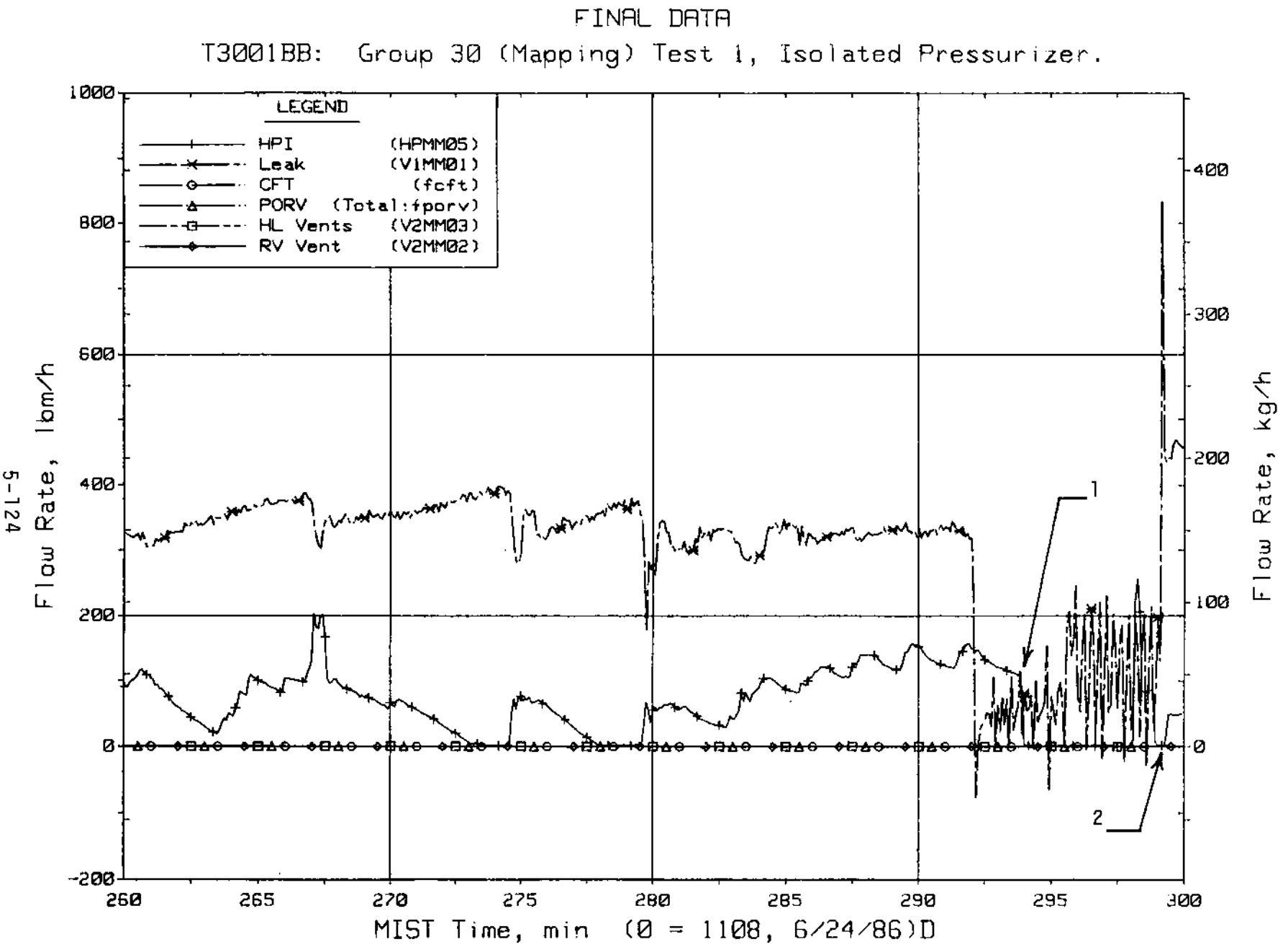

Figure 5.2.32. Primary System Boundary Flow Rates

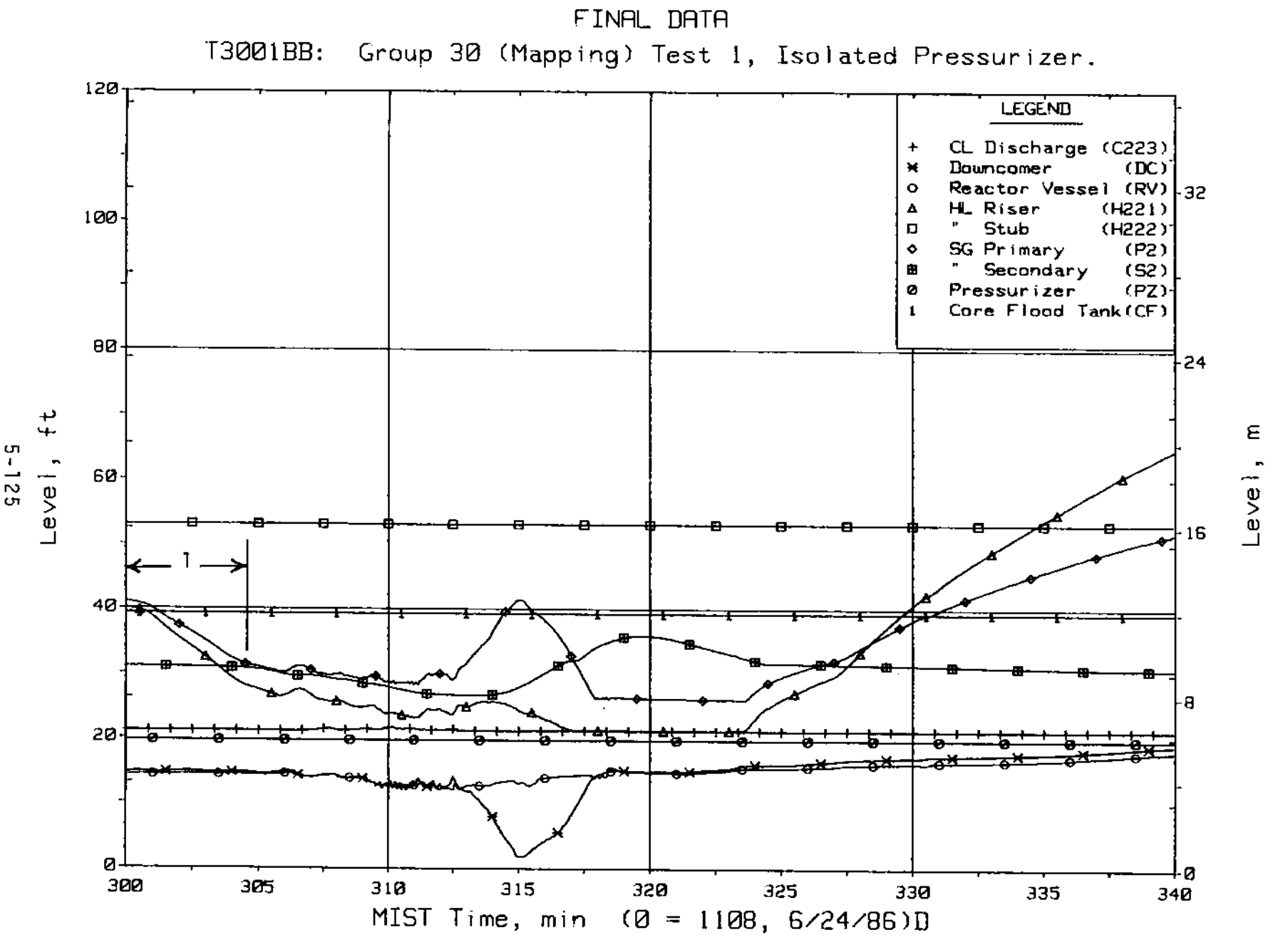

Figure 5.2.33. Loop B Collapsed Liquid Levels (LV20s)

Thu Feb 16 10:56:57 1989

PRLV2

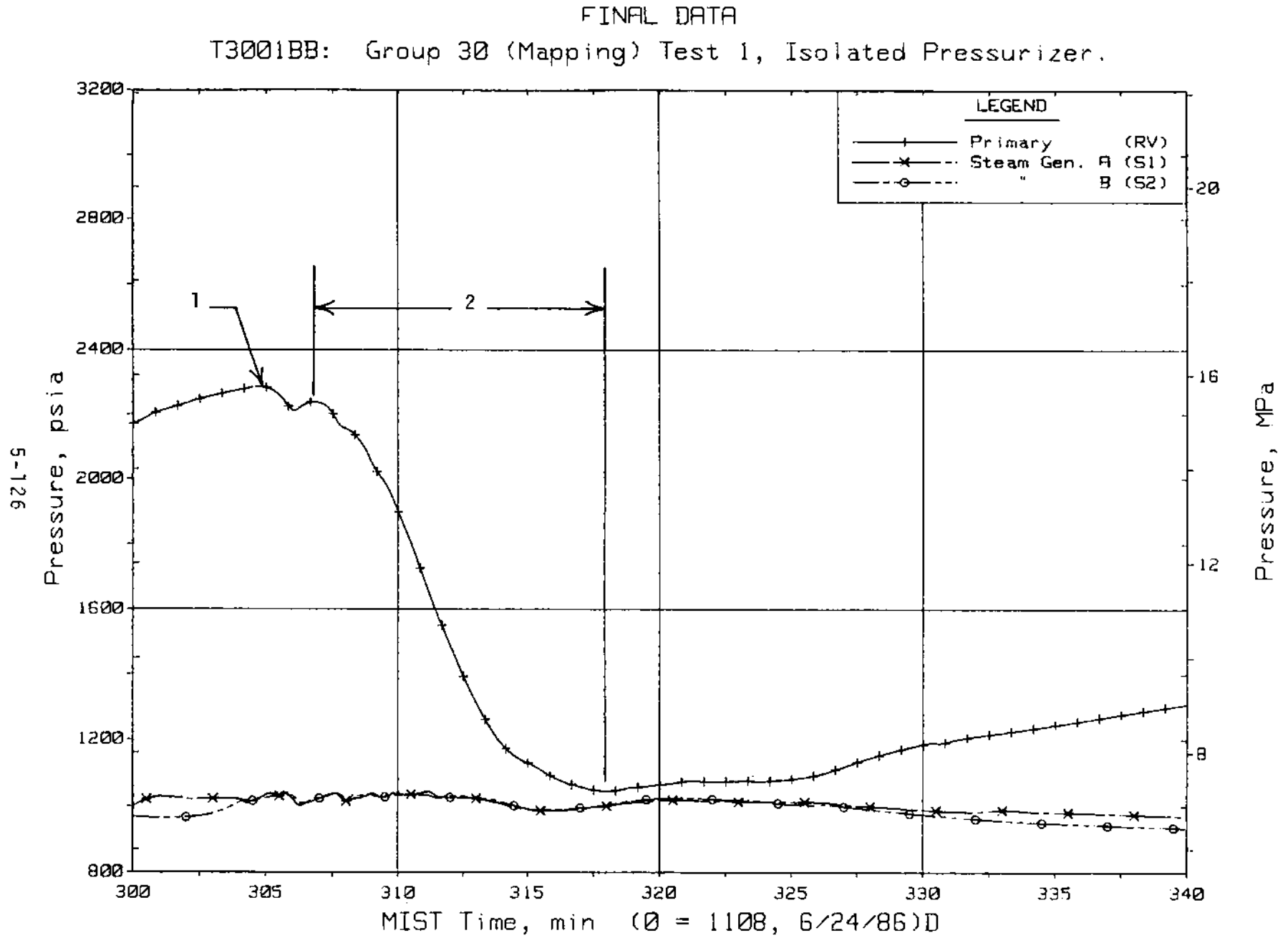

Figure 5.2.34. Primary and Secondary System Pressures (GP01s)

Thu Feb 16 10:53:36 1989

PSGP1

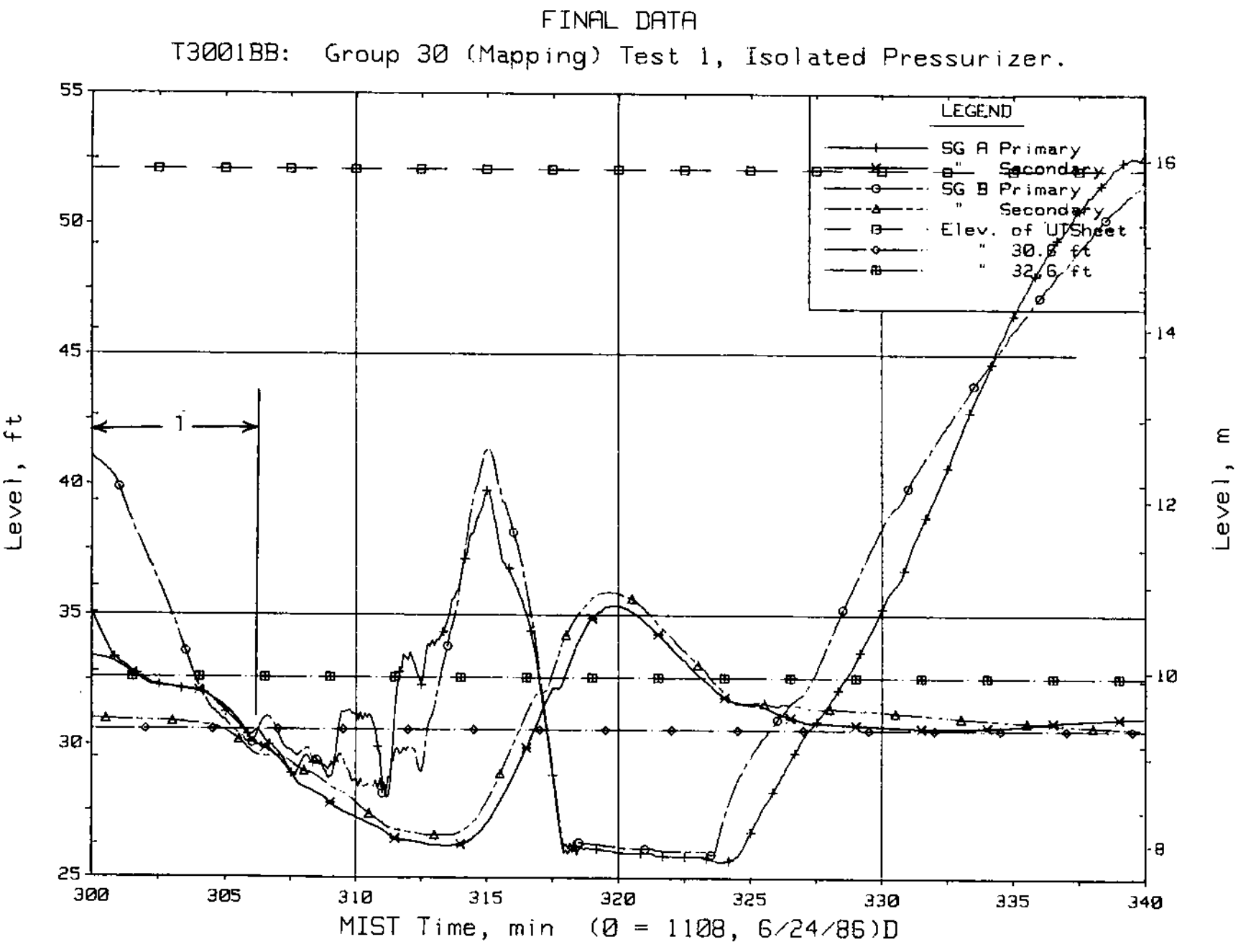

Figure 5.2.35. Steam Generator Collapsed Liquid Levels

Thu Feb 16 10:51:09 1989

SGLV2

5.3. Cold Leg Discharge Leak Test (3009AA)

The initial drain of the primary system resulted in a depressurization to ~1300 psia (Figure 5.3.1, See 1), which corresponded to the saturation pressure at the core exit temperature. The saturation pressure attained was identical to that of the Nominal Test (3003AA).

The primary system response for this test then proceeded to essentially duplicate that observed in the Nominal Test (3003AA). The loss of primary system inventory resulted in the reactor vessel head voiding (Figure 5.3.2, See 1) and a gradual increase in primary system pressure (Figure 5.3.1, See 2).

The phenomena observed in Test 3009AA then replicated that observed in the Nominal Test (3003AA). The reactor vessel head voided, the reactor vessel level reached the reactor vessel vent valve elevation, the downcomer voided, reactor vessel vent valve cycling commenced, and backflow occurred in the cold legs. When the downcomer level descended to the cold leg nozzle elevation, the reactor vessel vent valves opened and remained open, therefore permitting a backflow of steam into the cold leg discharge pipes. A momentary flow interruption occurred in each cold leg.

Subsequent to the momentary flow interruption, intra-cold leg flow was established in both loops [cold leg A1 flowed backward and cold leg A2 flowed forward (Figure 5.3.3, See 1), cold leg B1 flowed backward and cold leg B2 flowed forward (Figure 5.3.4, See 1)]. As in the Nominal Test, forward flow was reestablished in cold leg A1 (Figure 5.3.3, See 2), cold leg B1 flow interrupted (Figure 5.3.4, See 2), the cold leg B1 discharge pipe and the cold leg B1 suction pipe partially voided (Figure 5.3.5, See 1). The flow interruption of cold leg B1 also occurred at approximately the same pressure (1450 psia) as that of the Nominal Test.

Subsequent to the voiding of the cold leg B1 discharge pipe, the local phenomena that occurred in Test 3009AA differed from that observed in the Nominal Test (3003AA). Test 3009AA had the leak site located in the cold leg B1 discharge pipe, whereas the Nominal Test and all other Mapping Tests had the leak site located in the crossover pipe between the downcomer and the reactor vessel. As the cold leg B1 discharge pipe voided, the local conditions

at the leak site changed from single-phase liquid to a two-phase mixture to eventually single-phase steam. Thus, the leak flow rate decreased as the cold leg B1 discharge pipe voided (Figure 5.3.6, See 1).

The decreased leak flow rate resulted in a decrease in the steam flow from the reactor vessel to the cold legs by way of the reactor vessel vent valves (Figure 5.3.7, See 1). Therefore, more of the core-generated steam was directed into the hot legs (appears to have been directed primarily into loop B) and primary loop flow increased (Figure 5.3.3, See 3 and Figure 5.3.4, See 3). The decreased leak flow rate also affected the leak-HPI deficit and caused the loop operator to decrease the HPI flow rate in an effort to maintain the deficit (Figure 5.3.6, See 2). However, when the HPI flow was decreased, the leak flow also decreased (Figure 5.3.6, See 3). This action was apparently a result of the increased steam quality at the leak site, which was caused by decreasing the HPI flow. Therefore, a further reduction in the steam flow from the reactor vessel to the cold legs by way of the reactor vessel vent valves was observed (Figure 5.3.7, See 2). Again, more of the core-generated steam was directed into the hot legs (appears to have been directed primarily into loop A) and primary loop flow increased (Figure 5.3.3, See 4). As the leak flow continued to decrease, the reactor vessel vent valve flow also continued to decrease and the pressure differential across the reactor vessel vent valves began to equalize (Figure 5.3.8, See 1). This behavior led to the closure of the reactor vessel vent valves (Figure 5.3.9, See 1), which caused all the core-generated steam to enter the hot legs, thus resulting in a rapid increase in the flow rate of both primary loops. This increase in primary loop flow is observed in all four cold legs (Figure 5.3.3, See 5 and Figure 5.3.4, See 4). The forward flow in cold leg B1 resulted in the collapse of the voids in the cold leg B1 suction and discharge pipes (Figure 5.3.5, See 2), thus the leak flow rate increased (Figure 5.3.6, See 4) as single-phase liquid was discharge out the leak. The collapse of the voids in cold leg B1 and the loss of the natural circulation driving head (as a result of the increased core flow rate that decreased the fluid temperatures in the core region and the hot legs) resulted in a rapid increase in the pressure differential across the reactor vessel vent valves (Figure 5.3.8, See 2) and the reactor vessel vent valves opened (Figure 5.3.9, See 2).

Again, backflow occurred in cold legs A1 and B1 while forward flow was observed in cold legs A2 and B2 (Figure 5.3.3, See 6 and Figure 5.3.4, See 5). The loop operator observed the increased leak flow rate and increased the HPI flow in an attempt to maintain the leak-HPI deficit (Figure 5.3.6, See 5). The open reactor vessel vent valves, however, permitted core-generated steam to enter the cold legs and the cold leg A1, A2, and B1 discharge pipes began to void (Figure 5.3.5, See 3 and Figure 5.3.10, See 1). As the voiding of these cold legs progressed, the flow in cold legs A1, A2, and B1 interrupted (Figure 5.3.3, See 7 and Figure 5.3.4, See 6), however, flow in cold leg B2 increased (Figure 5.3.4, See 7). The flow interruption in loop A was confirmed by the lack of heat transfer in steam generator A (Figure 5.3.11, See 1), while loop B flow was confirmed by the initiation of heat transfer in steam generator B (Figure 5.3.12, See 1).

The conditions at this time in loops A and B appear to confirm that the primary loop flow interruption was caused by the discharge of steam through the reactor vessel vent valves, which voided both of the A cold leg discharge pipes. The conditions that led to this conclusion are as follows:

- The levels of hot legs A and B indicated collapsed liquid levels at the U-bend elevation (See 1 on Figure 5.3.13 and Figure 5.3.14).
- The stub levels of both A and B indicated collapsed liquid levels below the U-bend but above the steam generator upper tubesheet (See 2 on Figure 5.3.13 and Figure 5.3.14).
- Steam generator A did not steam while steam generator B began steaming (See 1 on Figure 5.3.11 and Figure 5.3.12).
- AFW was on in both steam generators A and B (See 2 on Figure 5.3.11 and Figure 5.3.12).
- The decrease in the hot leg level (See 3 on Figures 5.3.13 and 5.3.14) prior to the flow interruption occurred when the loop flows increased (Figure 5.3.3, See 5 and Figure 5.3.4, See 4). This action indicates that the hot legs were full but that steam had entered the hot legs; thus, the hot leg levels indicated a reduced collapsed liquid level.

Therefore, the potential for loop flow existed in both loops but occurred only in loop B. Cold leg B2 was the only cold leg that was not voided, thus providing a flow path via loop B.

When the cold leg B1 discharge pipe voided, the fluid conditions at the leak site again changed and the leak flow decreased. When the loop operator observed the decreased leak flow, he again reduced the HPI flow rate in an attempt to reestablish the leak-HPI deficit (Figure 5.3.6, See 6). The reduction in the HPI flow rate resulted in a reduced condensation capability in the cold legs, therefore further reducing the steam flow through the reactor vessel vent valves (Figure 5.3.7, See 3). When this event occurred, more of the core-generated steam was directed into the hot legs and cold leg A2 began to indicate forward flow (Figure 5.3.3, See 8). Again, as the reactor vessel vent valve flow decreased, the pressure differential across the valves began to equalize (Figure 5.3.8 See 3) and the valves closed (Figure 5.3.9, See 3). The core-generated steam was therefore forced into the hot legs and a rapid increase in primary loop flow occurred. The increase in the primary loop flow was observed in all four cold legs (Figure 5.3.3, See 9 and Figure 5.3.4, See 8). Again, the cold leg discharge voids collapsed (Figure 5.3.5, See 4 and Figure 5.3.10, See 2), the leak flow rate increased as single-phase liquid was discharged out the leak (Figure 5.3.6, See 7), the reactor vessel vent valves opened (Figure 5.3.9, See 4), and backflow occurred in cold legs A1 and B1 (Figure 5.3.3, See 10 and Figure 5.3.4, See 9). The open reactor vessel vent valves again permitted core-generated steam to enter the cold leg discharge pipes. Cold legs A1, B1, and B2 voided (Figure 5.3.5, See 5 and Figure 5.3.10, See 3) followed by flow interruption in these cold legs (Figure 5.3.3, See 11 and Figure 5.3.4, See 10), while cold leg A2 established forward loop flow (Figure 5.3.3, See 12).

The two previously discussed flow interruptions indicate that a predominant flow path for the core-generated steam that entered into the hot legs was established in loop B for the first occurrence and in loop A for the second occurrence. Each of these flow interruptions resulted in increased primary system pressure (Figure 5.3.15, See 1) and subcooled conditions in the hot leg (Figure 5.3.16, See 1 and Figure 5.3.17, See 1). After the first flow interruption, the establishment of a predominant flow path in loop B appears to be random. However, after the second flow interruption, the establishment of a predominant flow path in loop A appears to be caused by the location of the pressurizer in loop A, i.e., as the primary pressure increased, the pressurizer inventory increased, therefore more fluid from the reactor vessel

entered hot leg A. The primary system pressure increased from ~1450 to ~1600 psia during this phase of the test (Figure 5.3.15, See 2).

The fluid conditions at the leak site changed again as cold leg B1 voided (Figure 5.3.6, See 8). The loop operator decreased the HPI flow rate and eventually terminated HPI (Figure 5.3.6 See 9) in an effort to maintain the leak-HPI deficit. Cold leg A2 continued to indicate forward flow (Figure 5.3.3, See 13), however core-generated steam began entering hot leg B, thus initiating a heatup of the fluid in hot leg B (Figure 5.3.17, See 2). This heatup eventually resulted in the establishment of forward flow in loop B (Figure 5.3.4, See 11), the collapse of the voids in the cold legs followed by the revoiding of all the cold legs (Figure 5.3.5, See 6 and Figure 5.3.10, See 4), and the primary system repressurization (Figure 5.3.15, See 3).

The primary system response then replicated that of the Nominal Test (3003AA) as observed by the increasing oscillatory pressure response (Figure 5.3.15, See 4), which resulted from the hot leg heatup, forward loop flow, lower region void collapse, and revoiding of the lower regions. The primary system pressure increased to a value that exceeded the PORV opening setpoint (2350 psia), however the PORV did not open automatically. The loop operator noticed this omission and manually opened the PORV (Figure 5.3.6, See 10). The loop operator then closed the leak and terminated the test (~239 minutes) because facility design limits may have been exceeded had the test continued with the malfunctioning PORV.

The maximum primary system pressure attained during the repressurization phase of Test 3009AA was ~2380 psia (Figure 5.3.15, See 5) versus a maximum pressure of ~2225 psia for the Nominal Test (3003AA). This difference in the maximum primary system pressure appears to result from the observed differences in the primary system response prior to complete flow interruption. For the Nominal Test (3003AA), complete flow interruption occurred at a primary system pressure of ~1450 psia. For the cold leg discharge leak test (3009AA), complete flow interruption occurred at a primary system pressure of ~1600 psia. During the repressurization phase, the increase in primary system pressure was essentially equal for both tests (770 psi for the Nominal Test and 780 psi for Test 3009AA). Therefore, the maximum primary system

pressure attained appears to be dependent upon the initial primary system pressure when complete flow interruption occurred.

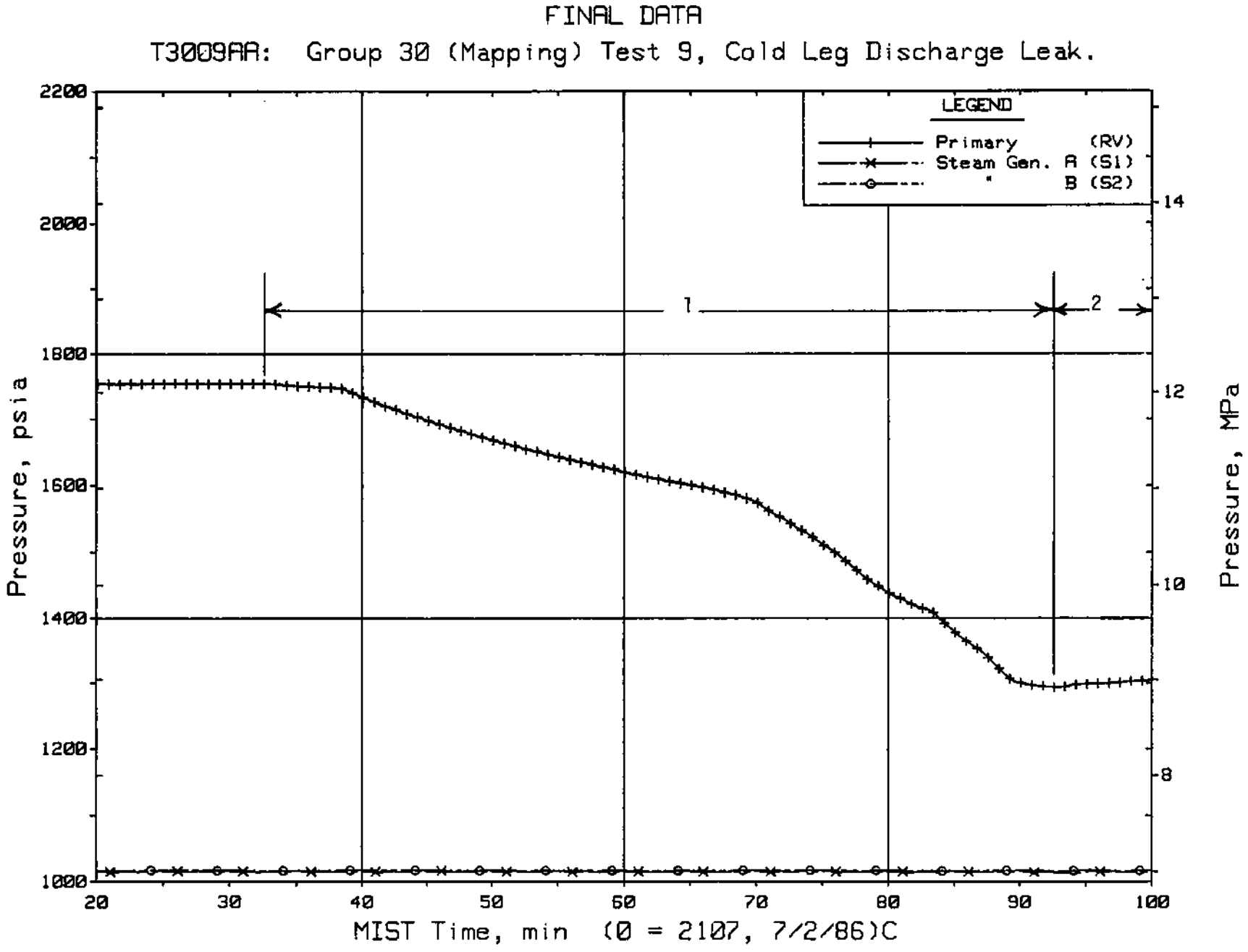

Figure 5.3.1. Primary and Secondary System Pressures (GP01s)

Tue Feb 14 10:38:59 1989

PSGP1

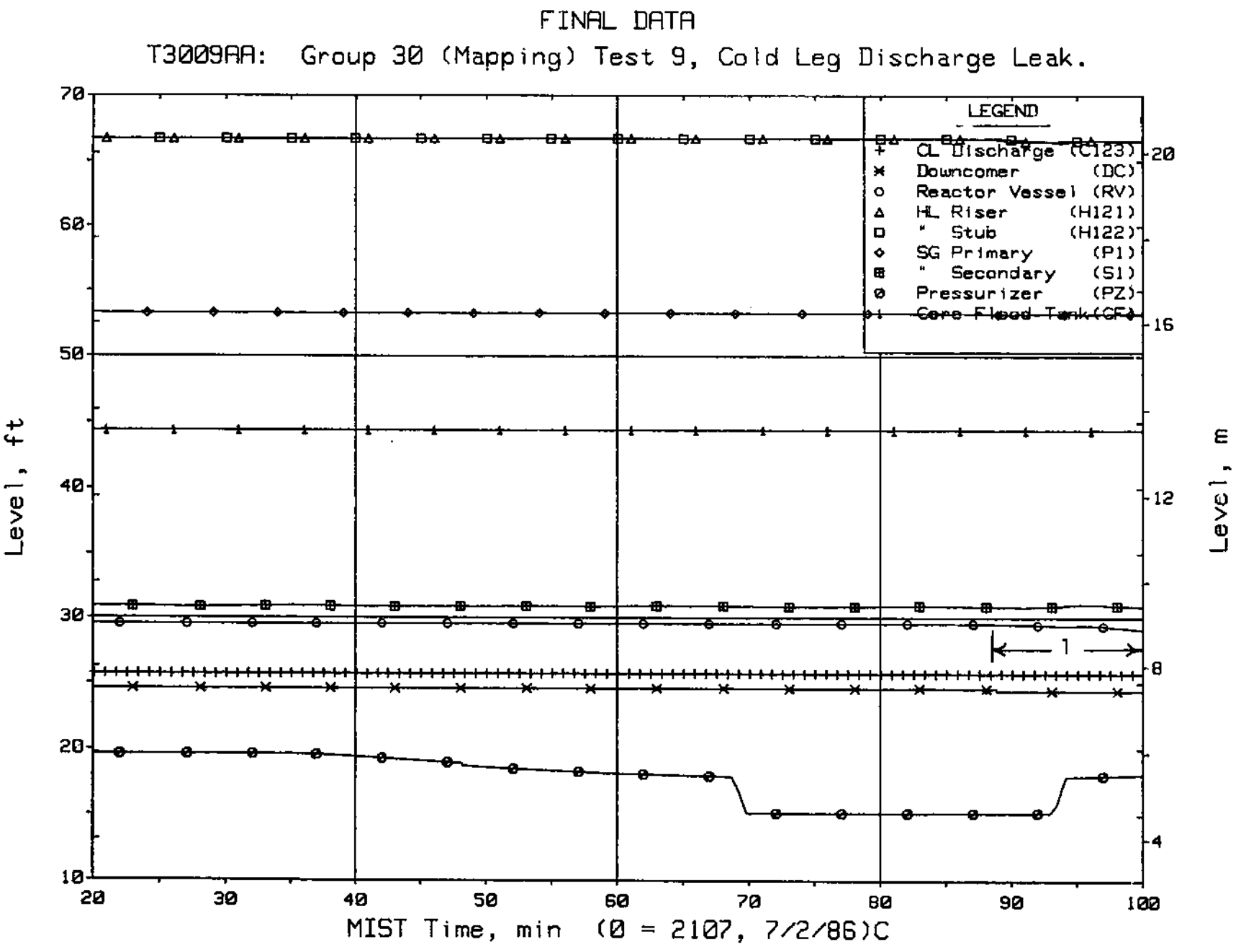

Figure 5.3.2. Loop A Collapsed Liquid Levels (LV20s)

Tue Feb 14 10:43:27 1989

PRLV1

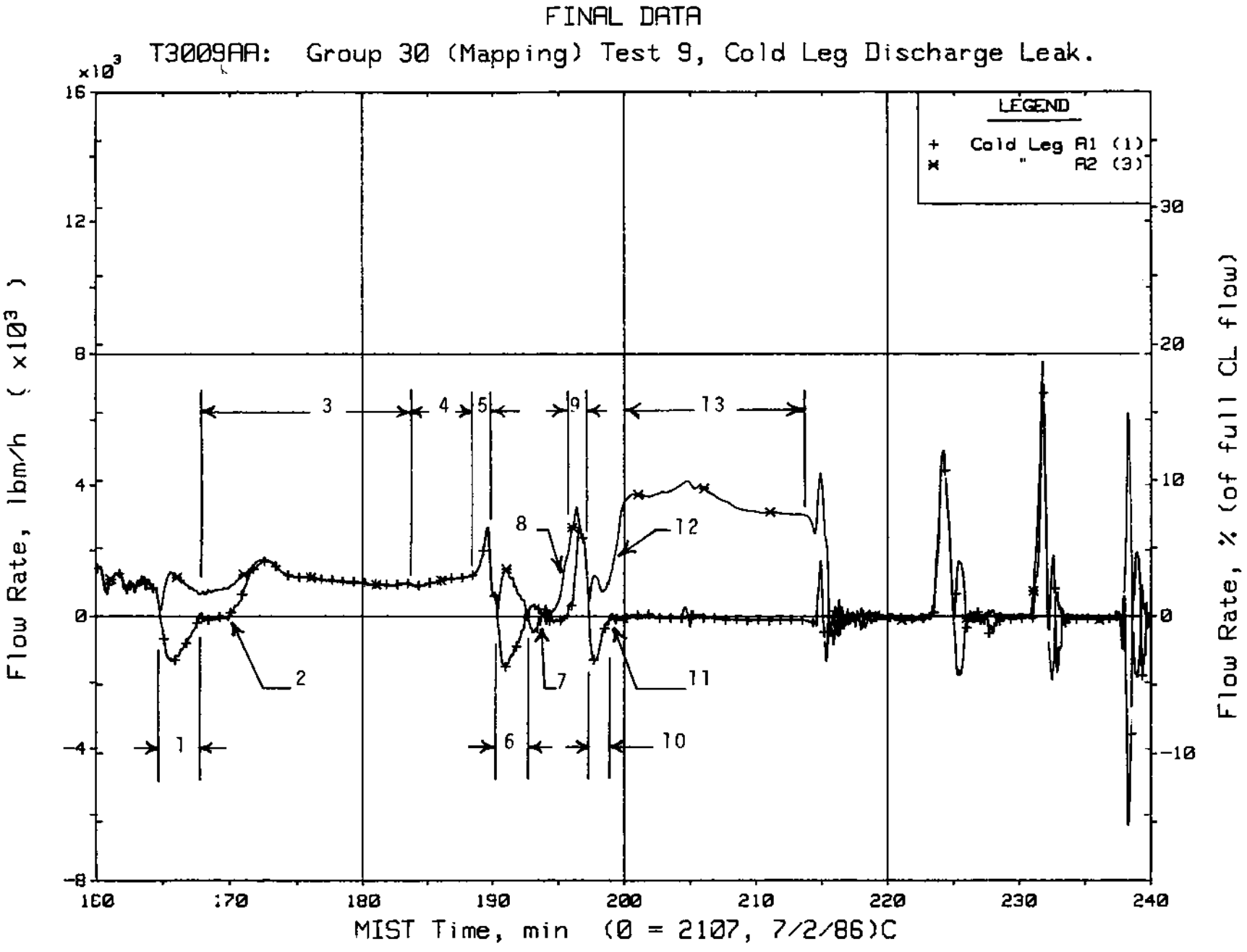

Figure 5.3.3. Loop A Cold Leg (Venturi) Flow Rates (CnVN20s)

Tue Feb 14 10:46:02 1989

PRFL5

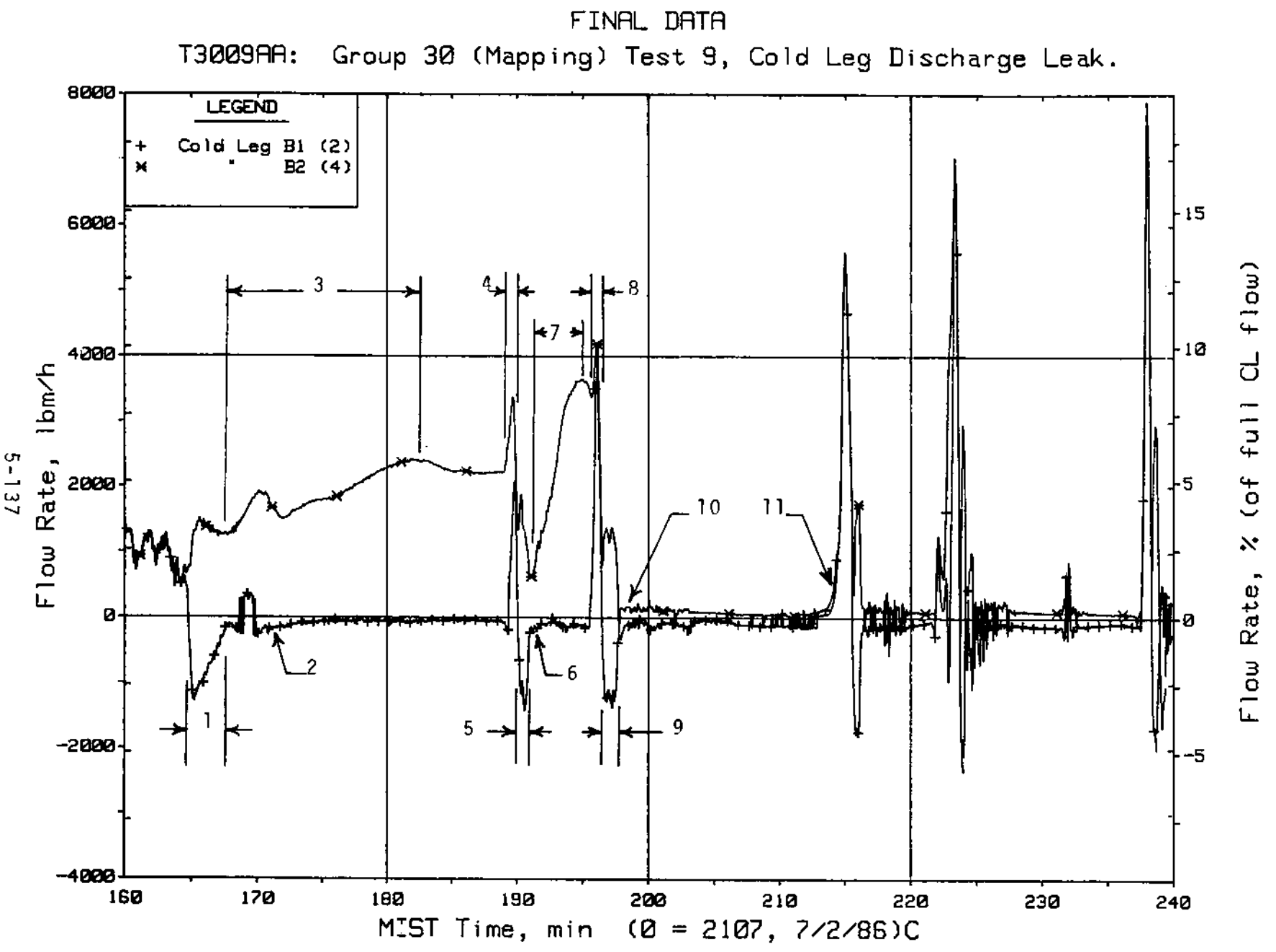

Figure 5.3.4. Loop B Cold Leg (Venturi) Flow Rates (CnVN20s)

Tue Feb 14 10:51:17 1989

PRFL6

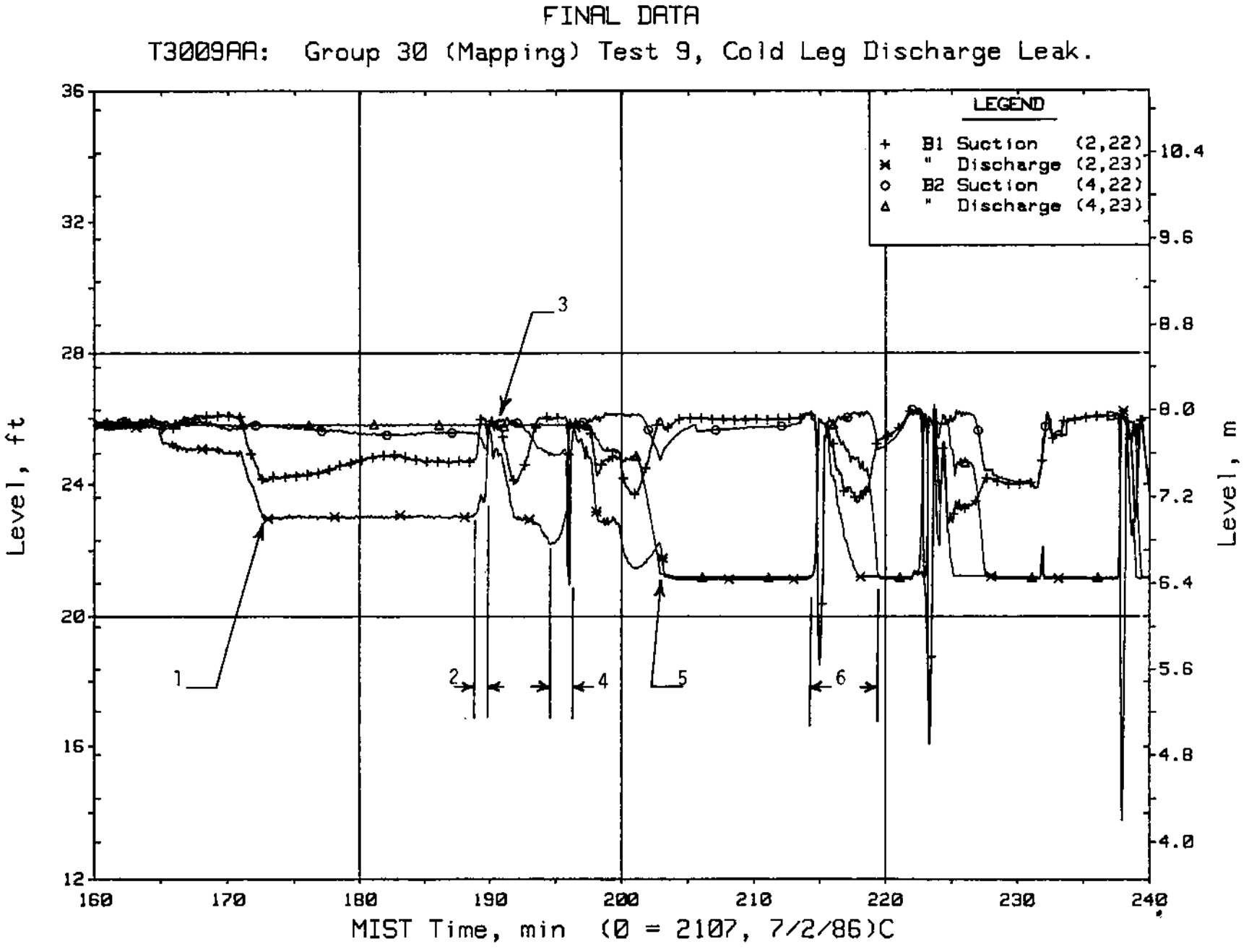

Figure 5.3.5. Loop B Cold Leg Collapsed Liquid Levels (LVs)

Tue Feb 14 13:26:03 1989

CLLV2

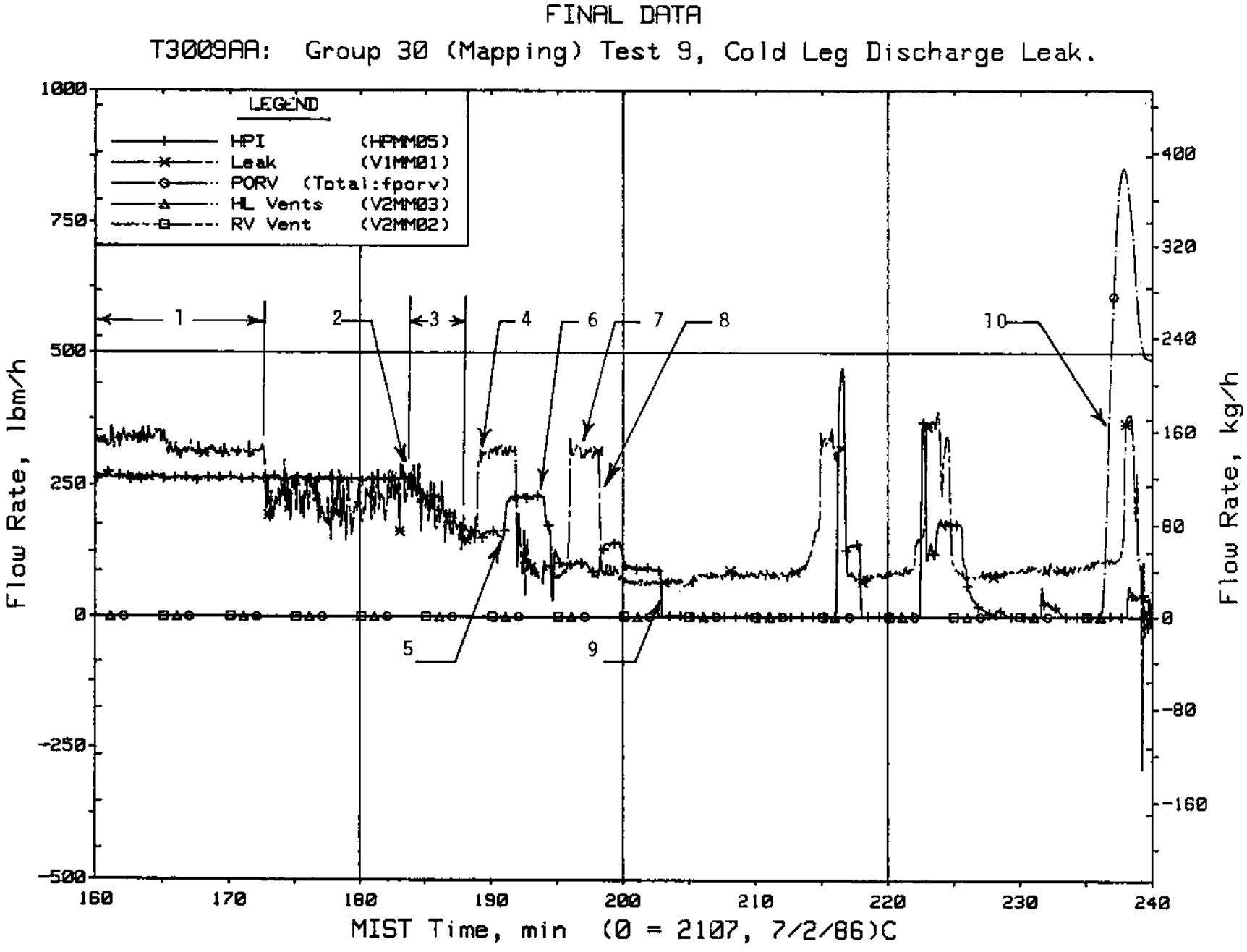

Figure 5.3.6. Primary System Boundary Flow Rates

Tue Feb 14 13:35:08 1989

PRFL3p

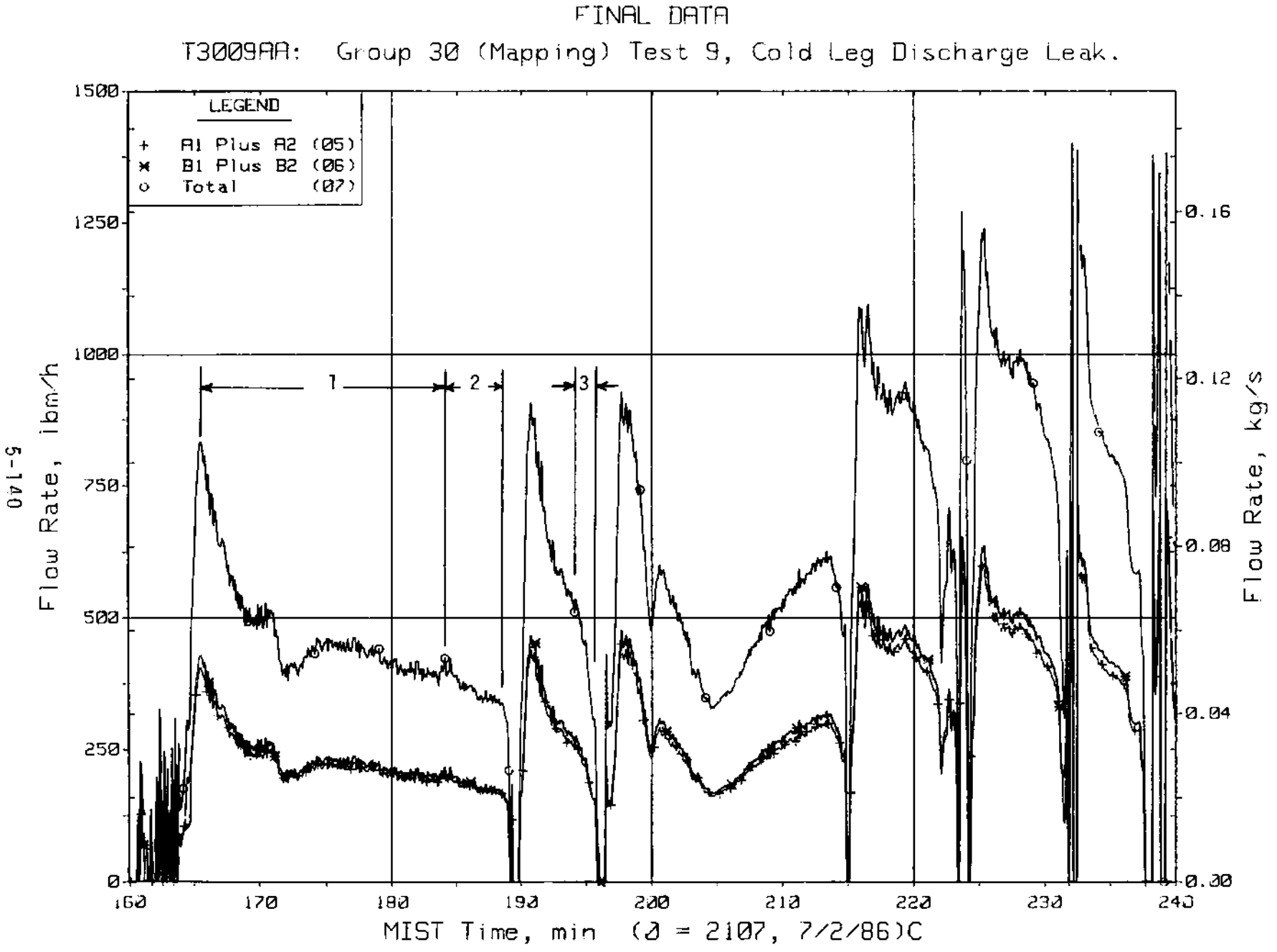

Figure 5.3.7. Composite Reactor Vessel Vent Valve Flow Rates (RVORs)

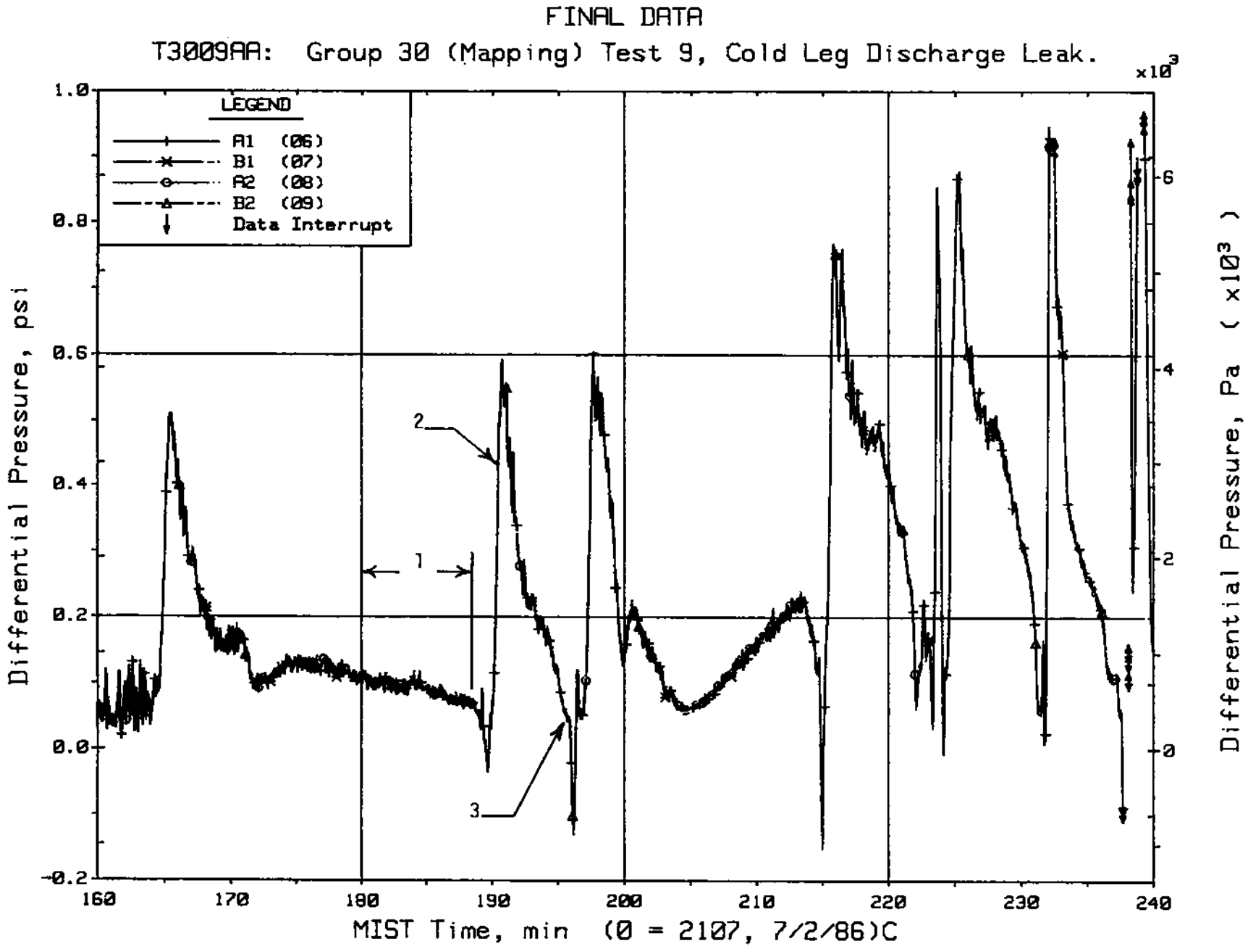

Figure 5.3.8. Reactor Vessel Vent Valve Differential Pressures (RVDPs)

Tue Feb 14 14:01:52 1989

VVDP1

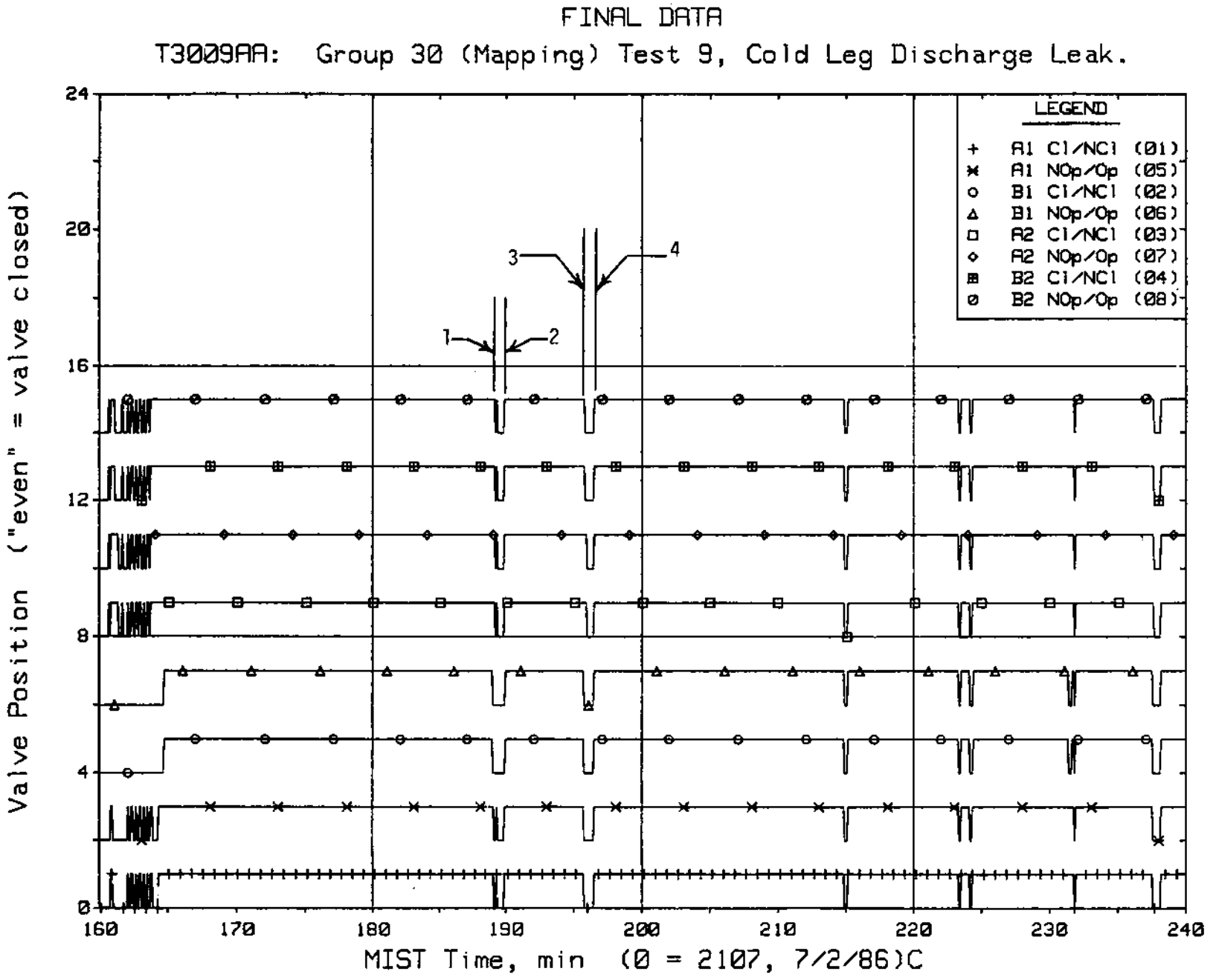

Figure 5.3.9. Reactor Vessel Vent Valve Limit Switch Indications (RVLSs)

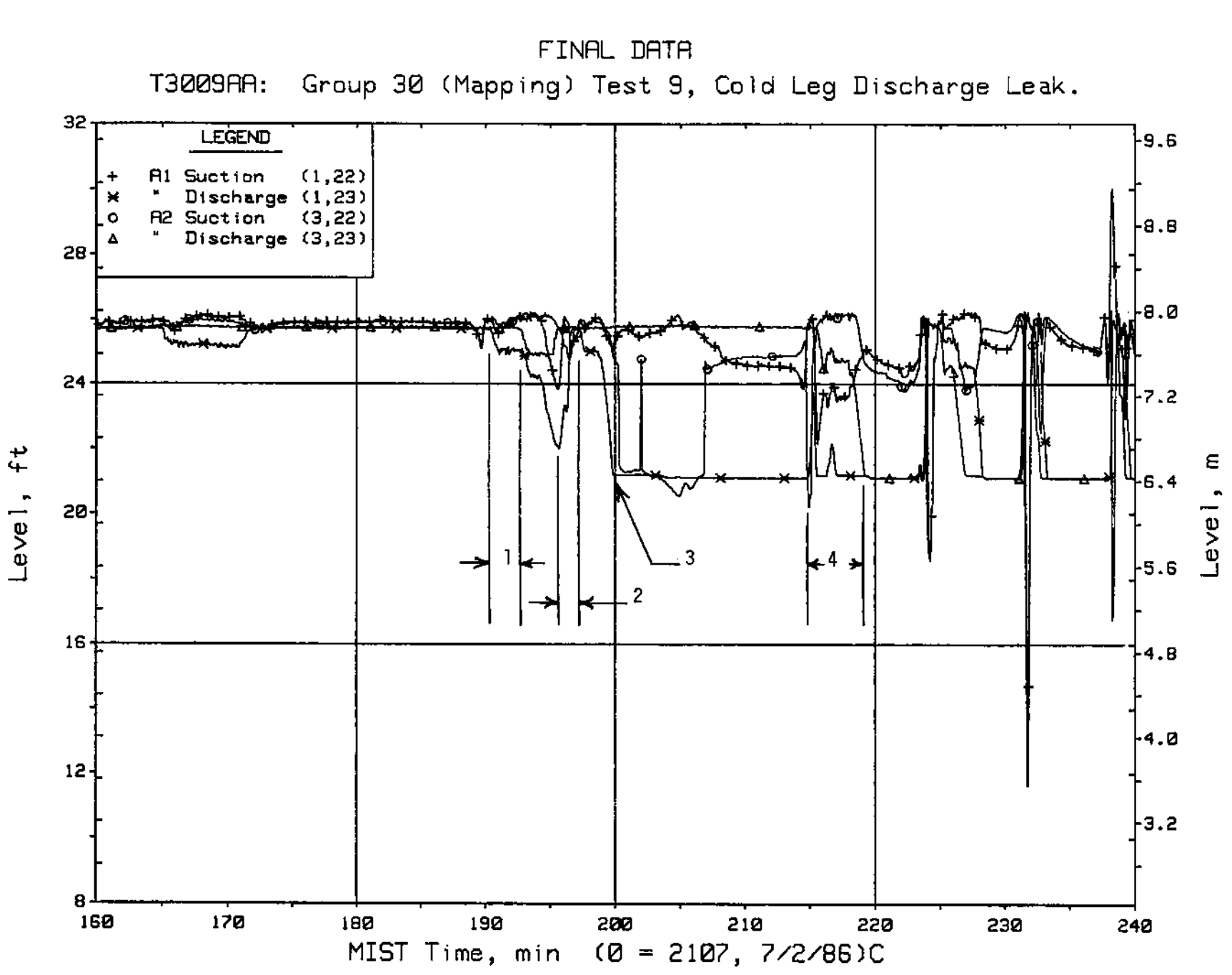

Figure 5.3.10. Loop A Cold Leg Collapsed Liquid Levels (LVs)

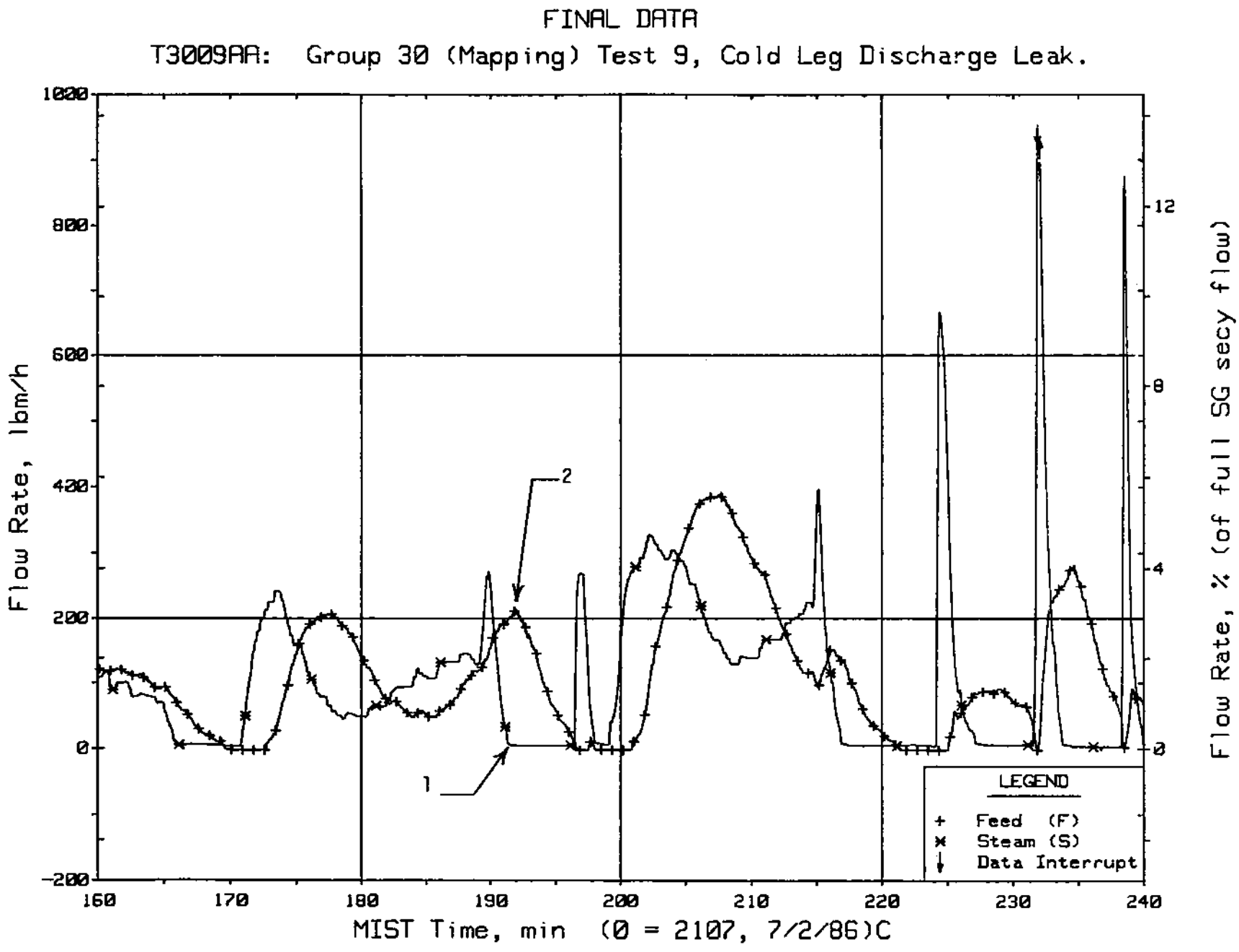

Figure 5.3.11. Steam Generator A Flow Rates (SaOR20s)

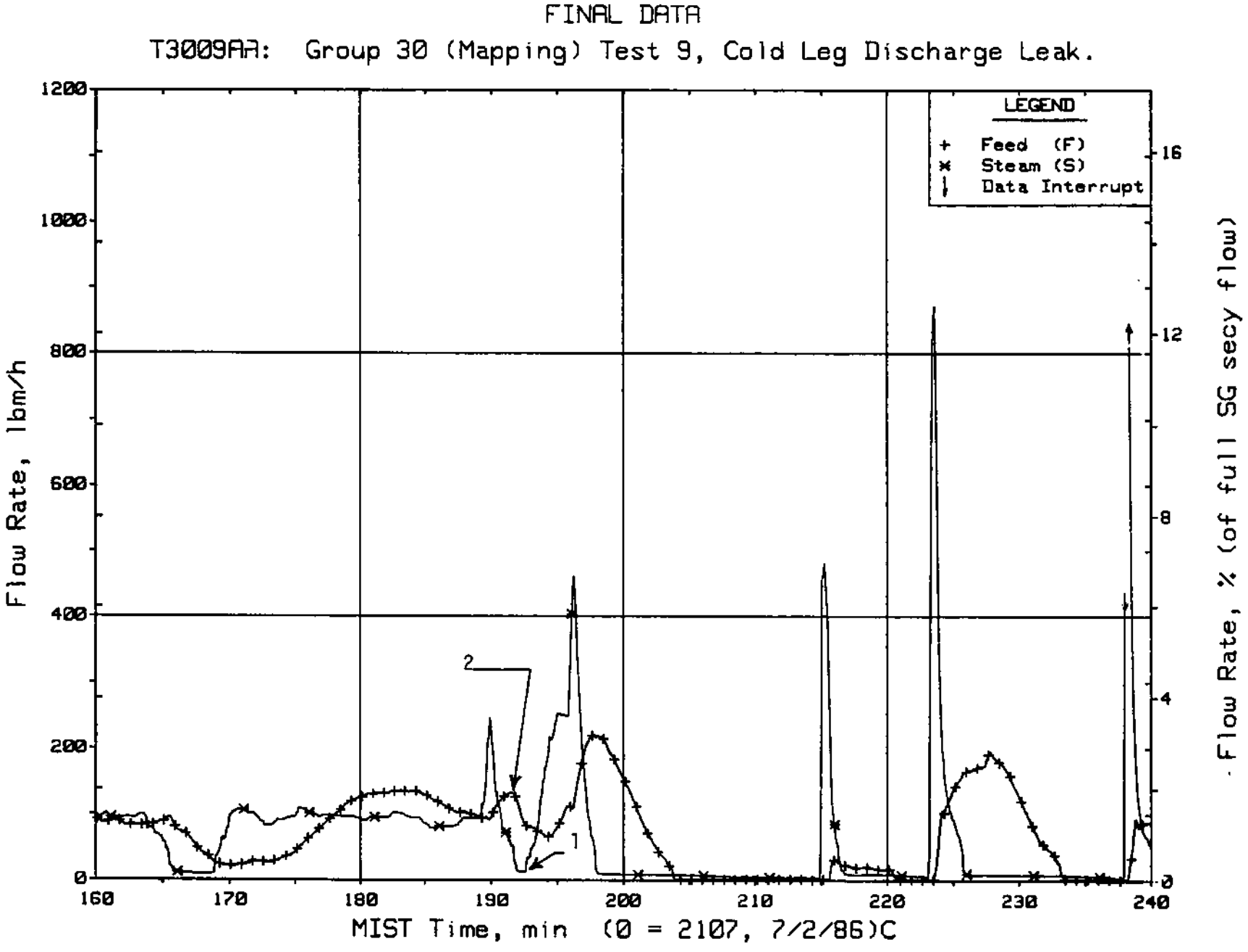

Figure 5.3.12. Steam Generator B Flow Rates (SaOR21s)

Tue Feb 14 11:27:41 1989

SCFL2

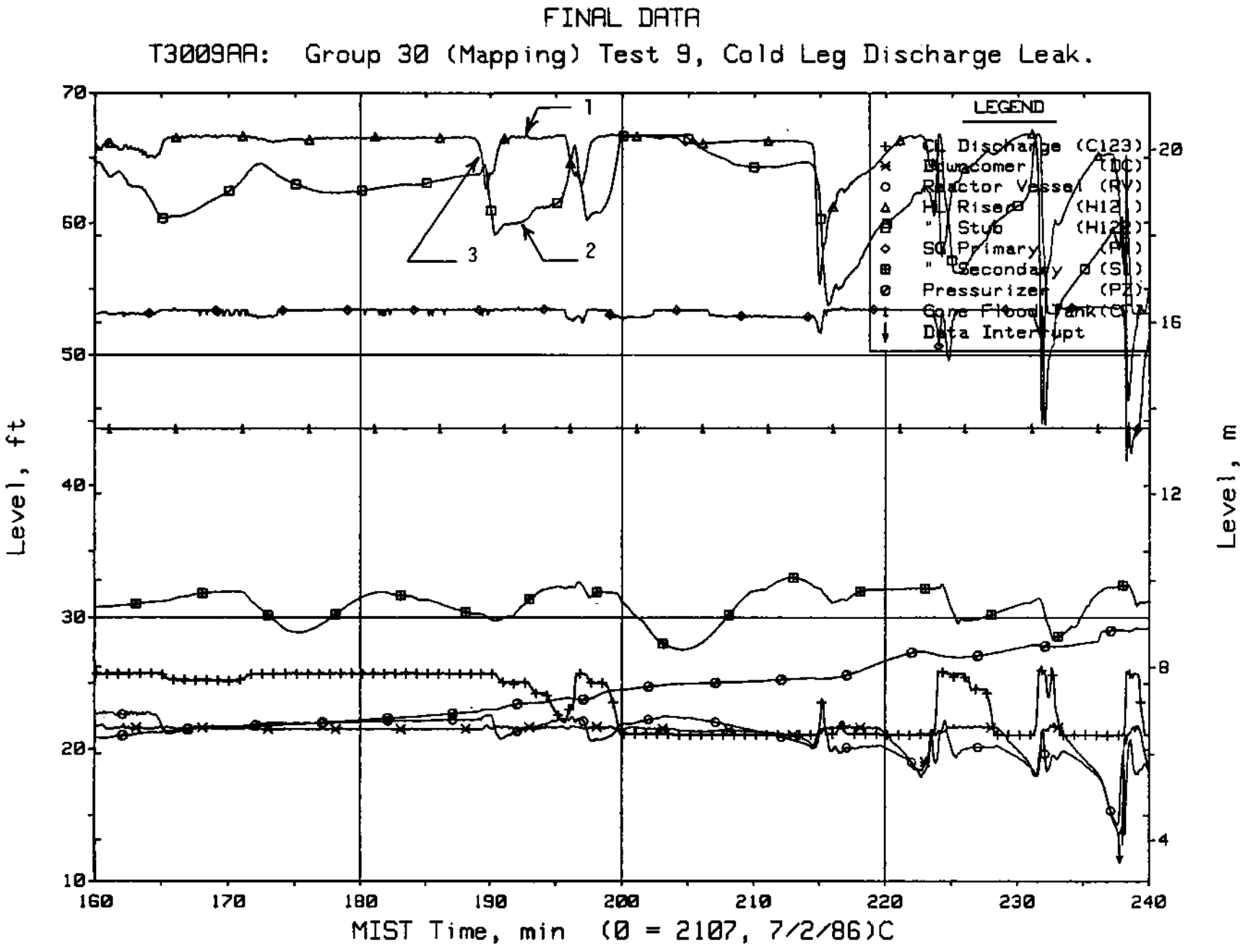

Figure 5.3.13. Loop A Collapsed Liquid Levels (LV20s)

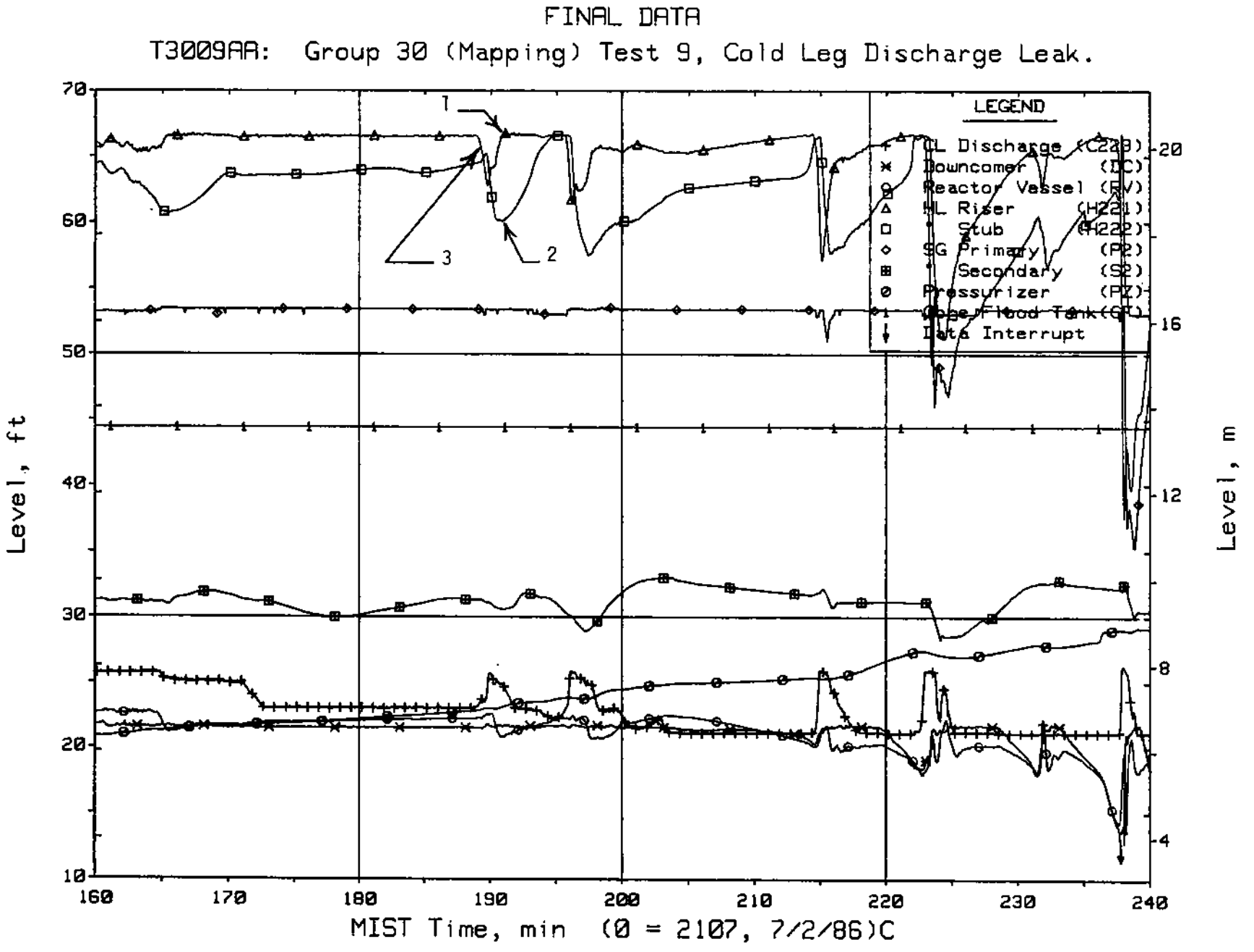

Figure 5.3.14. Loop B Collapsed Liquid Levels (LV20s)

Tue Feb 14 13:44:58 1989

PRLV2

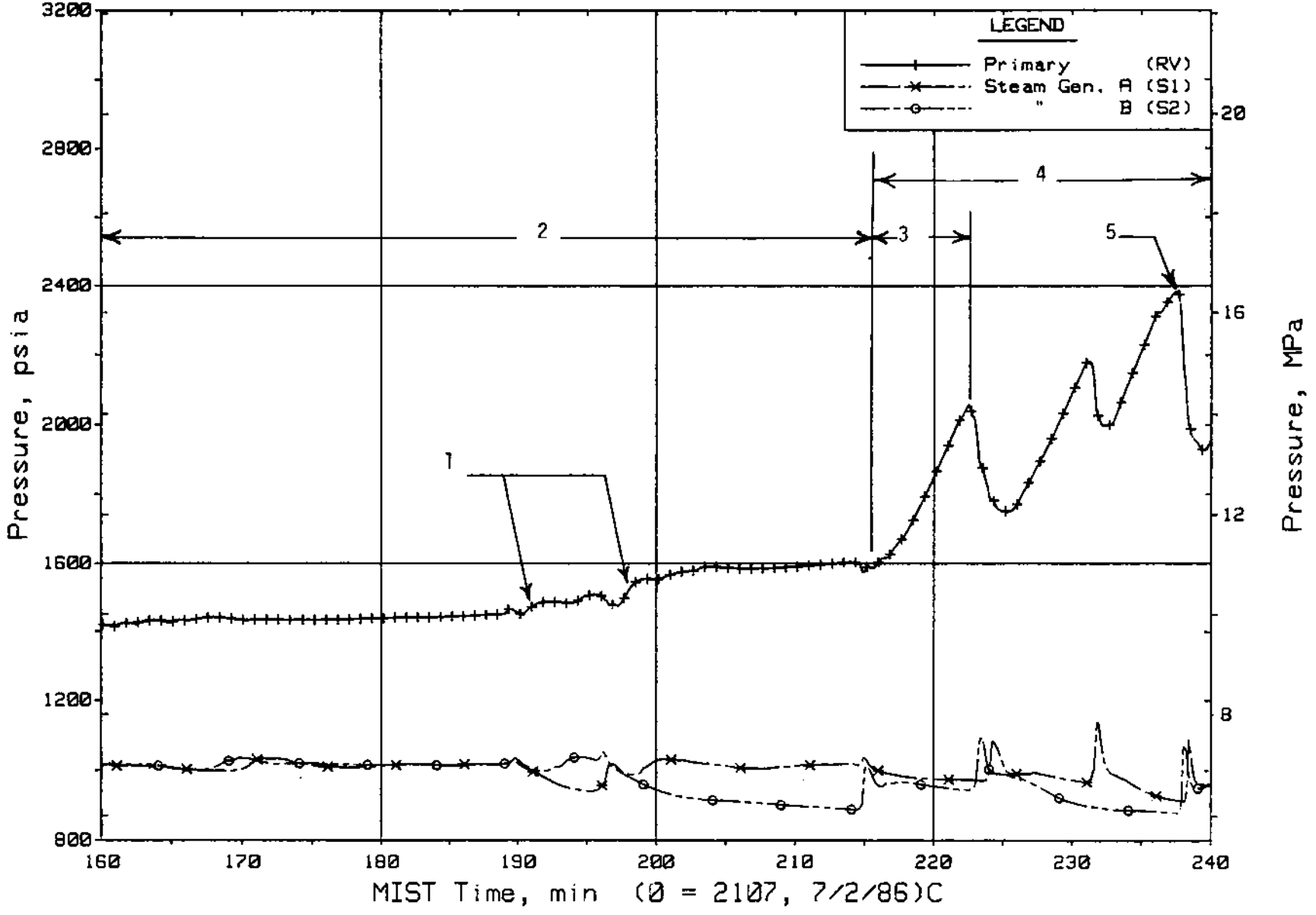

Figure 5.3.15. Primary and Secondary System Pressures (GPOIs)

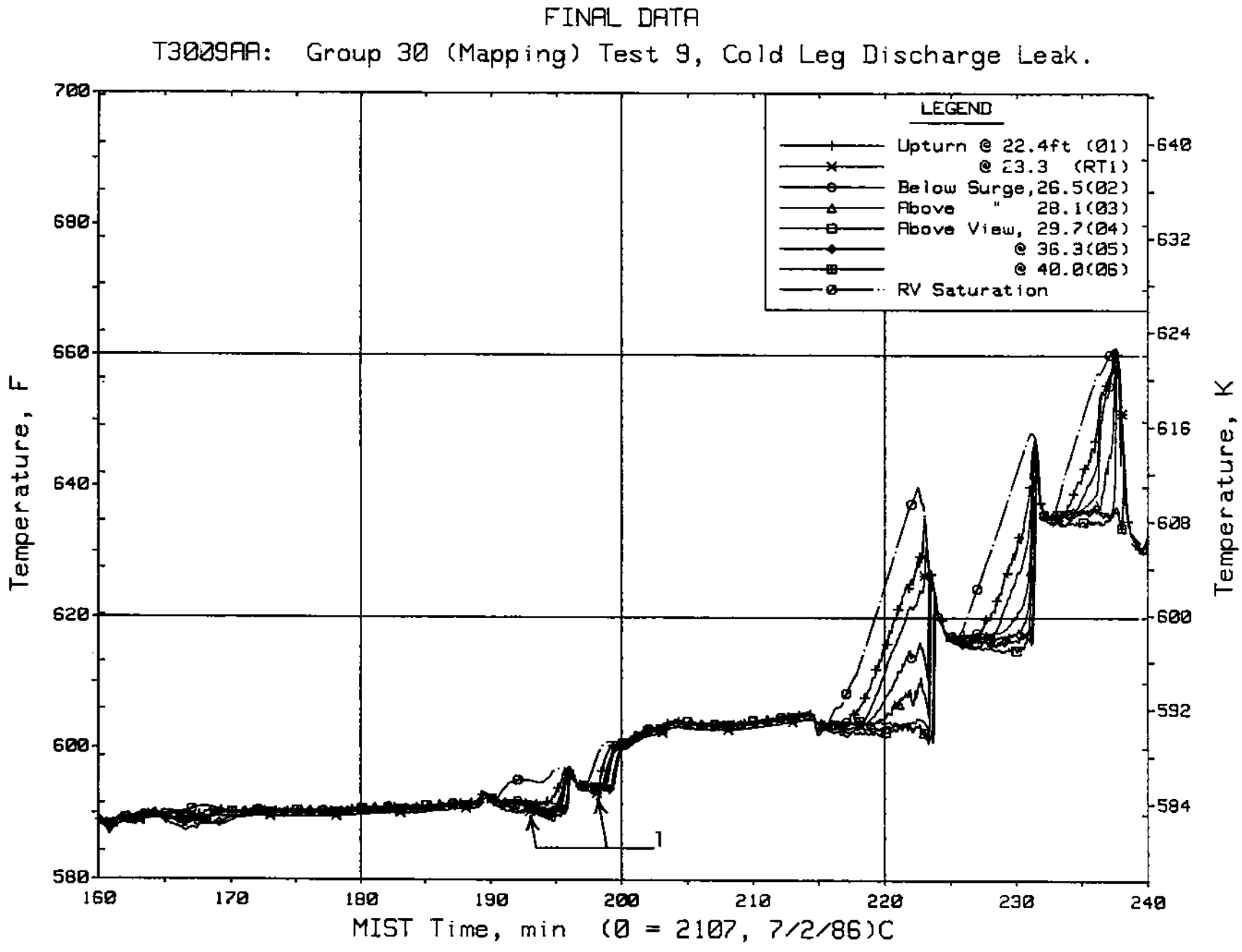

Figure 5.3.16. Hot Leg A Lower-Elevation Riser Fluid Temperatures (H1TCs)

Tue Feb 14 11:44:11 1989

H1TC1

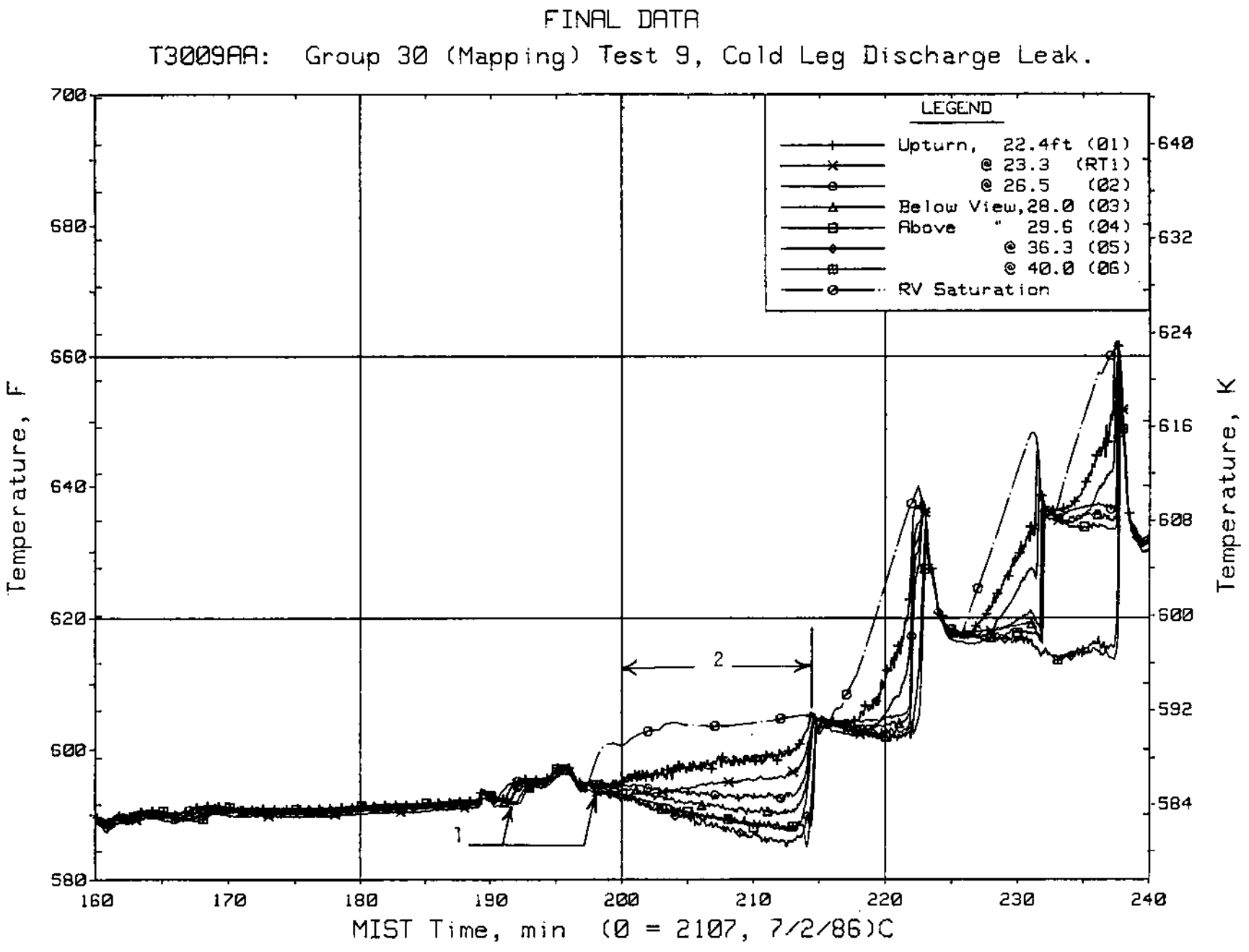

Figure 5.3.17. Hot Leg B Lower-Elevation Riser Fluid Temperatures (H2TCs)

Tue Feb 14 15:22:01 1989

H2TC1

5.4. Unbalanced Steam Generator Test (300605)

Test 300605 was performed with the control setpoint for the secondary level in steam generator A set at approximately 10 ft and that in steam generator B set at the nominal level (31.6 ft). This test was initially specified to maintain the steam generator A secondary level at 5 ft. However, level control difficulties were experienced and the level control setpoint was increased to 10 ft to obtain better level control. This change still maintained the elevation of the secondary pool below the core mid-height elevation so that AFW rather than pool effects would be highlighted during the BCM.

The following loop asymmetries were observed at the initialized conditions:

Loop B primary flow was greater than loop A primary flow (Figures 5.4.1 and 5.4.2).

Steam generator B secondary flow rates were greater than steam generator A flow rates (Figures 5.4.3 and 5.4.4).

Cold leg B nozzle fluid temperatures were greater than cold leg A nozzle fluid temperatures (Figures 5.4.5, 5.4.6, 5.4.7, and 5.4.8).

The observed primary and secondary flow differences result from the imposed steam generator secondary level asymmetry. The lower cold leg nozzle fluid temperatures in loop A resulted from the mixed-mean temperature after HPI fluid (equal amounts injected into each cold leg) was injected into a lower cold leg flow rate.

The initial drain of the primary system resulted in a depressurization to approximately 1335 psia (Figure 5.4.9, See 1), which corresponded to the saturation pressure at the core exit temperature. The saturation pressure attained was slightly higher (~30 psi) than that of the Nominal Test (3003AA) and resulted from a slightly higher core exit temperature for Test 300605.

The primary system response for this test then proceeded to essentially duplicate that observed in the Nominal Test (3003AA). The loss of primary system inventory resulted in the reactor vessel head voiding (Figure 5.4.10, See 1) and a gradual increase in primary system pressure (Figure 5.4.9, See 2). As the primary system pressure increased, the pressurizer level increased (Figure 5.4.10, See 2). This diversion of primary loop inventory resulted

in a decrease in the primary flow in loop B and eventually equalized the primary loop flow in both loops (Figure 5.4.11, See 1 and Figure 5.4.12, See 1).

The phenomena observed in Test 300605 then replicated that observed in the Nominal Test (3003AA). The reactor vessel head voided and reached the reactor vessel vent valve elevation, the downcomer voided, reactor vessel vent valve cycling commenced, and backflow occurred in the cold legs. When the downcomer level descended to the cold leg nozzle elevation, the reactor vessel vent valves opened and remained open, therefore permitting a backflow of steam into the cold leg discharge pipes. A momentary flow interruption occurred in each cold leg.

Subsequent to the momentary flow interruption, intra-cold leg flow was established in both loops (cold legs A1 and B1 flowed backward while cold legs A2 and B2 flowed forward, See 2 on Figures 5.4.11 and 5.4.12). After the flow reversal, a period of reduced forward flow was observed in cold legs A1 and B1 (See 3 on Figures 5.4.11 and 5.4.12). Counter-current flow was observed at the cold leg nozzle thermocouple rake of cold legs A2 and B2 during the period when forward flow existed in these cold legs (See 1 on Figures 5.4.13 and 5.4.14). The cold legs that experienced flow interruption (A1 and B1) indicated saturated conditions (steam) at the cold leg nozzle thermocouple rake (See 1 on Figures 5.4.15 and 5.4.16).

As the drain continued, Test 300605 experienced the same flow interruption phenomena as the Nominal Test. The order in which the cold leg (B1, A1, A2, then B2) flows interrupted (Figure 5.4.11, See 4, Figure 5.4.12, See 4, Figure 5.4.17, See 1, and Figure 5.4.18, See 1) was slightly different from that observed in the Nominal Test (3003AA, where the flow in cold leg A2 and B2 interrupted simultaneously).

This difference in the order of the cold leg flow interruption was apparently a result of asymmetrical steam generator performance. The initiation of voiding in cold leg A2, which led to flow interruption, appears to have resulted from the lower steam generator A secondary level and/or the delay in the actuation of AFW in steam generator A after secondary steam flow was established. Subsequent to the cold leg A1 flow interruption, the flow rate of A2 was observed to be lower than that of B2 (Figure 5.4.11, See 5 and

Figure 5.4.12, See 5). This difference in flow was caused by a difference in the steam generator primary axial fluid temperature distributions (See 1 on Figures 5.4.19 and 5.4.20). This difference apparently resulted from the asymmetric steam generator secondary levels and the status of AFW in each steam generator (both steam generators began steaming, however, steam generator B AFW actuated whereas generator A AFW did not actuate, Figure 5.4.21, See 1 and Figure 5.4.22, See 1). The axial fluid temperature distribution directly affected the axial density distribution, thus impacting the loop driving head for natural circulation. Since the steam generator A primary axial fluid temperatures were higher than those in steam generator B, a lower flow rate resulted in loop A. The lower flow rate in loop A therefore increased the potential for the backflow of steam from the downcomer into cold leg A2 and was observed from the indication of saturated conditions at the top of the cold leg A2 nozzle rake (Figure 5.4.13, See 2) while the cold leg B2 nozzle rake indicated subcooled conditions across the pipe (Figure 5.4.14, See 2).

The flow interruption of cold leg B2 also resulted in a system response different from that observed in the Nominal Test (3003AA). Cold leg B2 had continued flowing while the other three cold legs had interrupted. The reduced primary system flow rate resulted in an increasing core inlet temperature. The core inlet temperature eventually saturated (Figure 5.4.23, See 1), thus resulting in higher steam production in the core. When this event occurred, more steam was directed into the hot legs, forward flow was reestablished in all four cold legs, and the voids in the cold legs collapsed. Revoiding of the cold leg discharge pipes occurred, which interrupted flow in cold legs A1, B1, and B2 while cold leg A2 reestablished forward flow (Figure 5.4.17, See 2 and Figure 5.4.18, See 2). The restart of forward flow in loop A was apparently due to the heatup of the hot leg A fluid (caused by the location of the pressurizer, which established a predominant flow path) that occurred as the cold leg B2 flow interrupted. The forward flow in cold leg A2 subcooled the fluid entering the core and loop flow was sustained until the core inlet saturated (Figure 5.4.23, See 2). A response similar to that discussed above was observed when the core saturated; however, forward flow occurred only in cold legs A1 and A2 while the cold leg B flows remained

interrupted. This action was then followed by the complete flow interruption of the A cold legs (Figure 5.4.17, See 3).

The flow interruptions occurred at essentially a constant pressure of ~1490 to 1540 psia (Figure 5.4.24, See 1). This event was similar to that observed in the Nominal Test with the exception of the flow interruption of cold leg A2 after flow had restarted. The latter flow interruption occurred at ~1580 psia (Figure 5.4.24, See 2).

Similar phenomena as observed in the Nominal Test (3003AA) occurred as the primary system repressurized. The maximum pressure attained during the repressurization phase was ~2350 psia (Figure 5.4.25, See 1) and was greater than that observed for the Nominal Test (~2225 psia). However, the maximum pressure attained may have been limited by the PORV actuation. The difference in the maximum primary pressure appears to result from the difference in the primary system pressure when complete flow interruption occurred (also observed in Test 3009AA).

Three automatic PORV actuations occurred during this test (Figure 5.4.26, See 1). The pressurizer inventory had been increasing during the repressurization phase (Figure 5.4.27, See 1). The first PORV actuation resulted in a completely full pressurizer (Figure 5.4.27, See 2). Each PORV actuation resulted in a depletion of primary system inventory as observed by the decreasing trend in the loop A hot leg and steam generator primary levels, while the loop B levels remained relatively high (Figure 5.4.28, See 1).

Just prior to the first PORV actuation, the core power tripped automatically (Figure 5.4.29, See 1) due to a high metal temperature. The core power was quickly restored by the loop operator and the test continued. This momentary core power trip did not affect the overall primary system response, with the only observed impact being a slight, momentary decrease in primary system pressure (Figure 5.4.25, See 2).

Lower region voiding, hot leg heatup, spillover, forward flow, lower region void collapse, and revoiding of the lower regions occurred. However, the predominant flow path was in loop B. The pressurizer had filled completely, as discussed above, and therefore did not aid in the establishment of a predominant flow path via loop A. The steam generator level controls appear

to have affected the establishment of the predominant flow path. The secondary level in steam generator A was greater than the level control setpoint (~10 ft) during this phase of the test (Figure 5.4.30). Therefore, as steam generator A steamed, AFW did not actuate (Figure 5.4.31). The steam generator B secondary level did decrease to its control setpoint (~31.6 ft) and AFW actuated (Figure 5.4.32). The lag time for the steam generator B secondary level to increase to the control setpoint (and therefore terminate AFW) was of sufficient duration that a subsequent spillover in loop B occurred prior to the termination of AFW (Figure 5.4.32, See 1). Steam generator B AFW remained active and therefore established and maintained the predominant flow path via loop B.

The lower region void collapse/revoiding phenomena continued with only the voids in the B cold legs collapsing while the A cold legs remained voided. The primary system pressure then began an oscillatory decreasing trend (Figure 5.4.25, See 3). This depressurization trend was very gradual and apparently was a result of a single loop (B) cooldown. During this time the hot leg A riser level indicated intermittent periods of being completely voided (Figure 5.4.28, See 2).

As the primary system continued to depressurize (Figure 5.4.33, See 1), the pressurizer drained and the steam generator A primary level was maintained at an elevation above the steam generator A secondary pool elevation (Figure 5.4.34, See 1). Therefore, pool BCM in the inactive loop (as observed in the Nominal Test) did not occur. During this time, the hot leg A riser level indicated that it was essentially completely voided (Figure 5.4.34, See 1). The primary system pressure decreased to approximately 1600 psia (Figure 5.4.33, See 2) during this phase of the test.

The depressurization resulted in superheated conditions (caused by the metal heat in the upper downcomer, Figure 5.4.35, See 1) within all the cold leg discharge pipes (e.g., Figure 5.4.36, See 1). This occurrence was similar to that observed in the Nominal Test (3003AA). The backflow of superheated steam into the cold legs (propagated up to the reactor coolant pumps) interrupted the loop B primary flow. This interruption resulted in decreased (eventually terminated) steam generator heat transfer (Figure 5.4.37, See 1)

and the primary system repressurized from ~1600 to ~2100 psia (Figure 5.4.38, See 1).

As the primary system repressurized, the core collapsed liquid level decreased to an elevation below the top of the heated length, and it remained below through test termination (Figure 5.4.39). Superheated conditions, however, were not observed at the core exit (Figure 5.4.40). This action indicated that a froth height covered the upper core region.

As the primary system repressurized, the hot leg B and steam generator primary levels decreased (Figure 5.4.41, See 1) while the pressurizer and the steam generator A primary levels gradually increased (Figure 5.4.42, See 1). When the steam generator B primary level descended to the secondary pool elevation (Figure 5.4.41, See 2), steam generator B began steaming and was followed by a delayed AFW actuation (Figure 5.4.43, See 1). The establishment of heat transfer in steam generator B resulted in a depressurization of the primary system (Figure 5.4.38, See 2). The predominant primary system flow path was via loop B (as a result of the higher secondary level) and cold leg B1. The depressurization resulted in an inventory transfer from the pressurizer and loop A to loop B as observed by the decreasing pressurizer and steam generator A primary levels (Figure 5.4.42, See 2) and the increasing loop B levels (Figure 5.4.41, See 3).

The forward flow established in cold leg B1 was sufficient to collapse the voids in the cold leg discharge pipe (Figure 5.4.44, See 1). However, the flashing of liquid in the reactor vessel, caused by the depressurization, resulted in steam flow through the reactor vessel vent valves and backflow into the cold leg discharge pipe, thus voiding the cold leg discharge pipe and interrupting flow. As this void collapse/revoiding phenomena continued (Figure 5.4.44, See 2), the steam in the downcomer became superheated (Figure 5.4.45, See 1) as a result of the depressurization and the metal heat in the downcomer.

The superheated steam entering the cold leg discharge pipe from the downcomer was eventually sufficient to evaporate all the HPI flow and loop flow in cold leg B1. Thus, cold leg B1 voided completely and remained voided (Figure 5.4.44, See 3). Steam generator B heat transfer continued subsequent to the complete voiding of cold leg B1 (Figure 5.4.43, See 2). The hot leg B level

then decreased (due to flashing) and the steam generator B primary level decreased as it drained (Figure 5.4.46, See 1). Hot leg A remained completely voided during this depressurization (Figure 5.4.46, See 2). Superheated fluid temperatures, apparently as a result of the metal heat and the guard heaters, existed over the entire length of the hot leg A riser (Figure 5.4.47, See 1) while the core exit (Figure 5.4.40) and hot leg B riser (Figure 5.4.48) fluid temperatures remained saturated.

The entire pressurizer inventory was discharged during this depressurization (Figure 5.4.42, See 3). The fluid temperatures in the pressurizer surge line appear to have remained near saturation (Figure 5.4.49, See 1) during the discharge of the pressurizer inventory, however, when the pressurizer emptied superheated fluid temperatures were observed in the surge line near the connection to the hot leg A riser (Figure 5.4.49, See 2) and subsequently at the low point of the pressurizer surge line (Figure 5.4.49, See 3).

The loop operator terminated the test when the steam generator B primary level descended to the secondary pool elevation (~256 minutes). The minimum primary system attained for this test was ~1120 psia, which was essentially identical to that observed for the Nominal Test (3003AA, ~1110 psia).

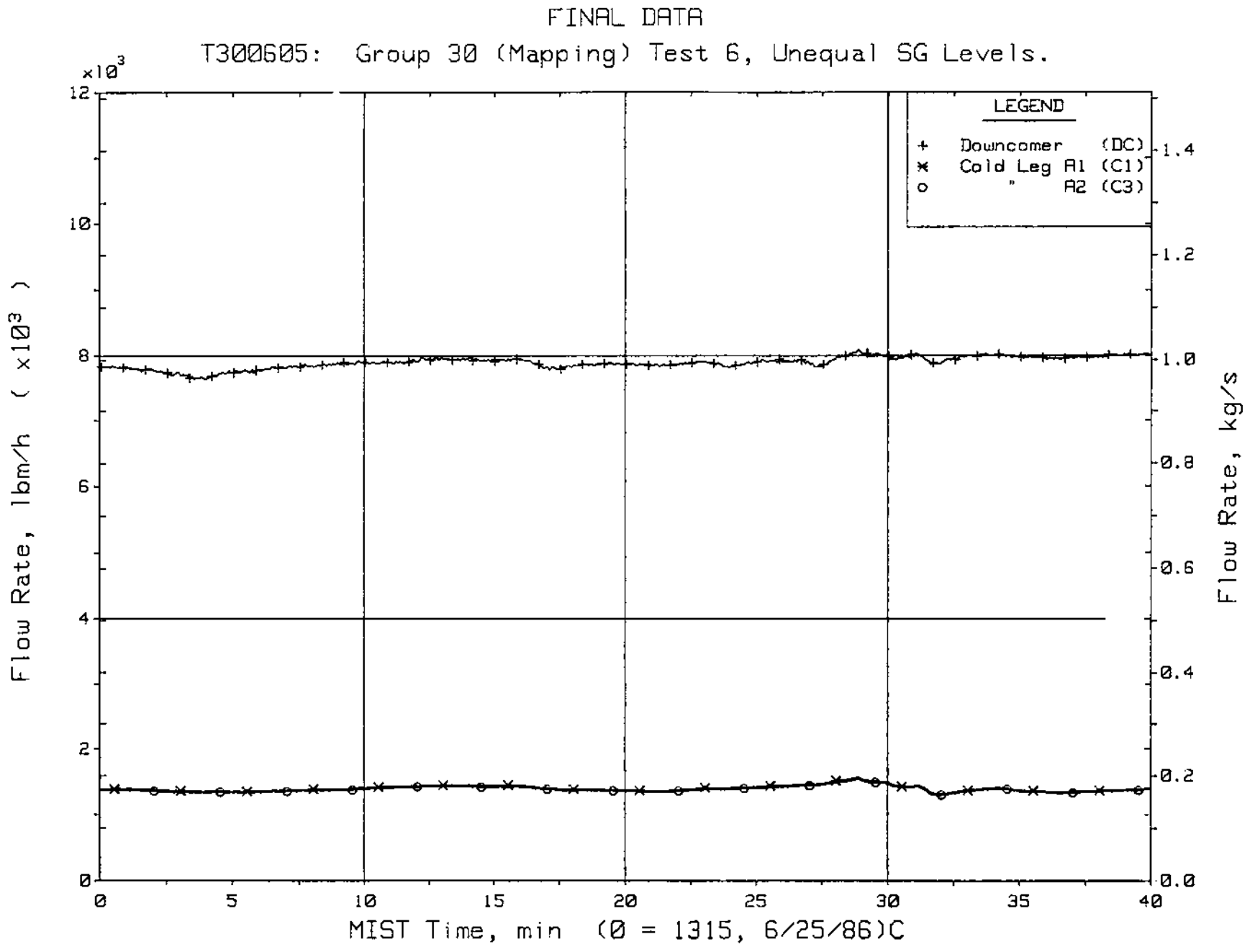

Figure 5.4.1. Primary System (Venturi) Flow Rates (VN20s)

Fri Feb 17 16:32:18 1989

PRFL1

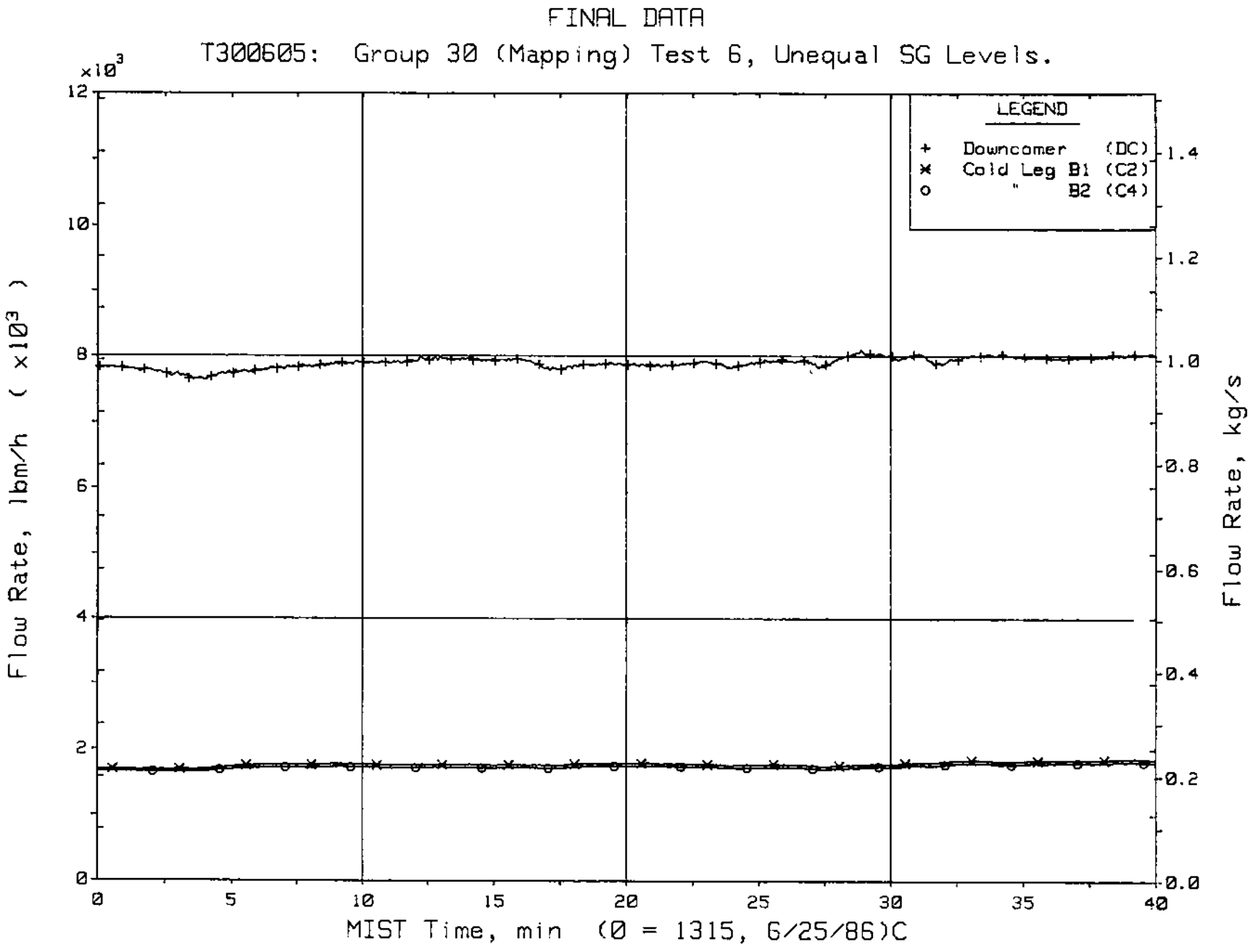

Figure 5.4.2. Primary System (Venturi) Flow Rates (VN20s)

Fri Feb 17 16:30:06 1989

PRFL2

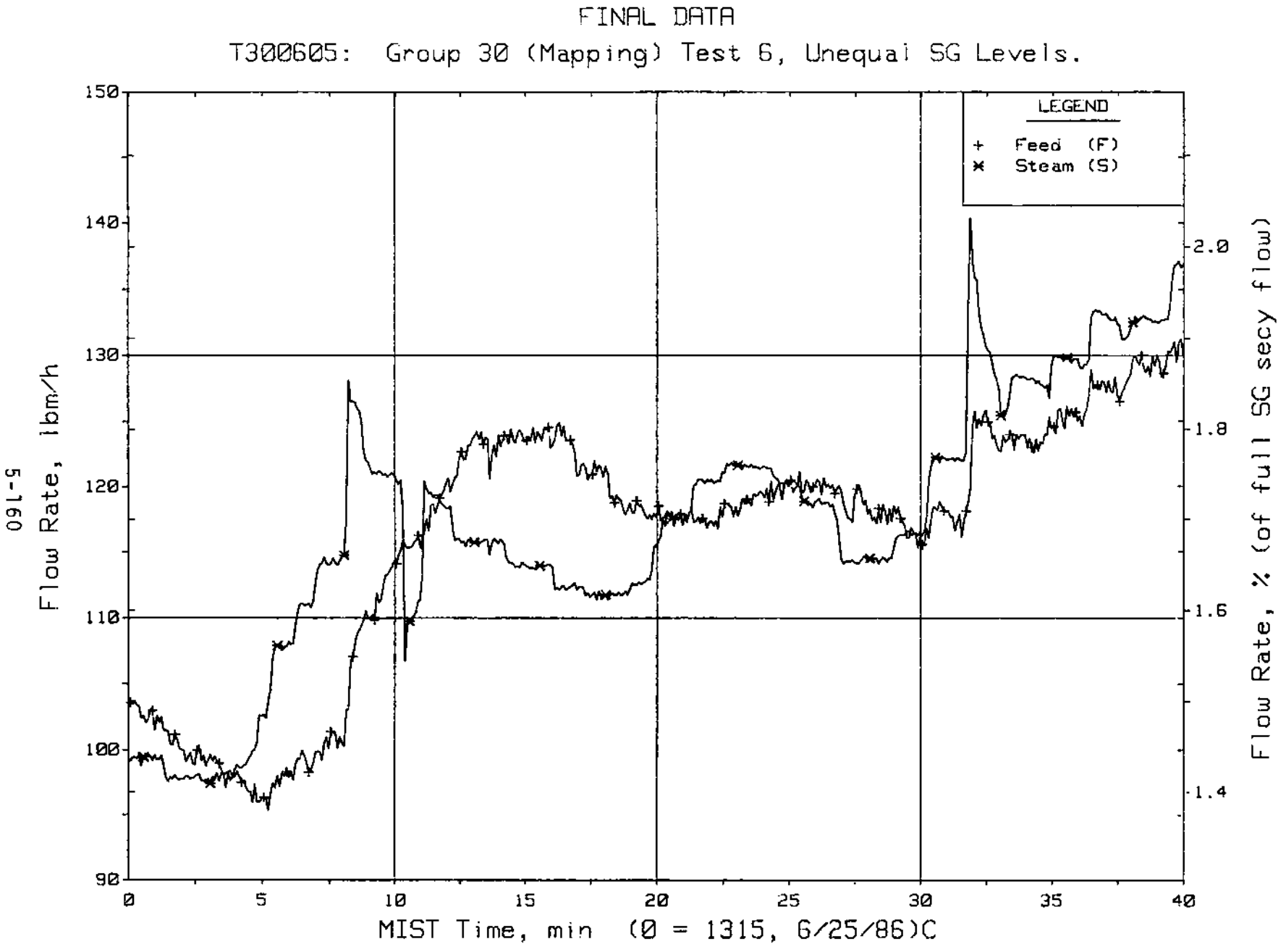

Figure 5.4.3. Steam Generator B Flow Rates (SaOR21s)

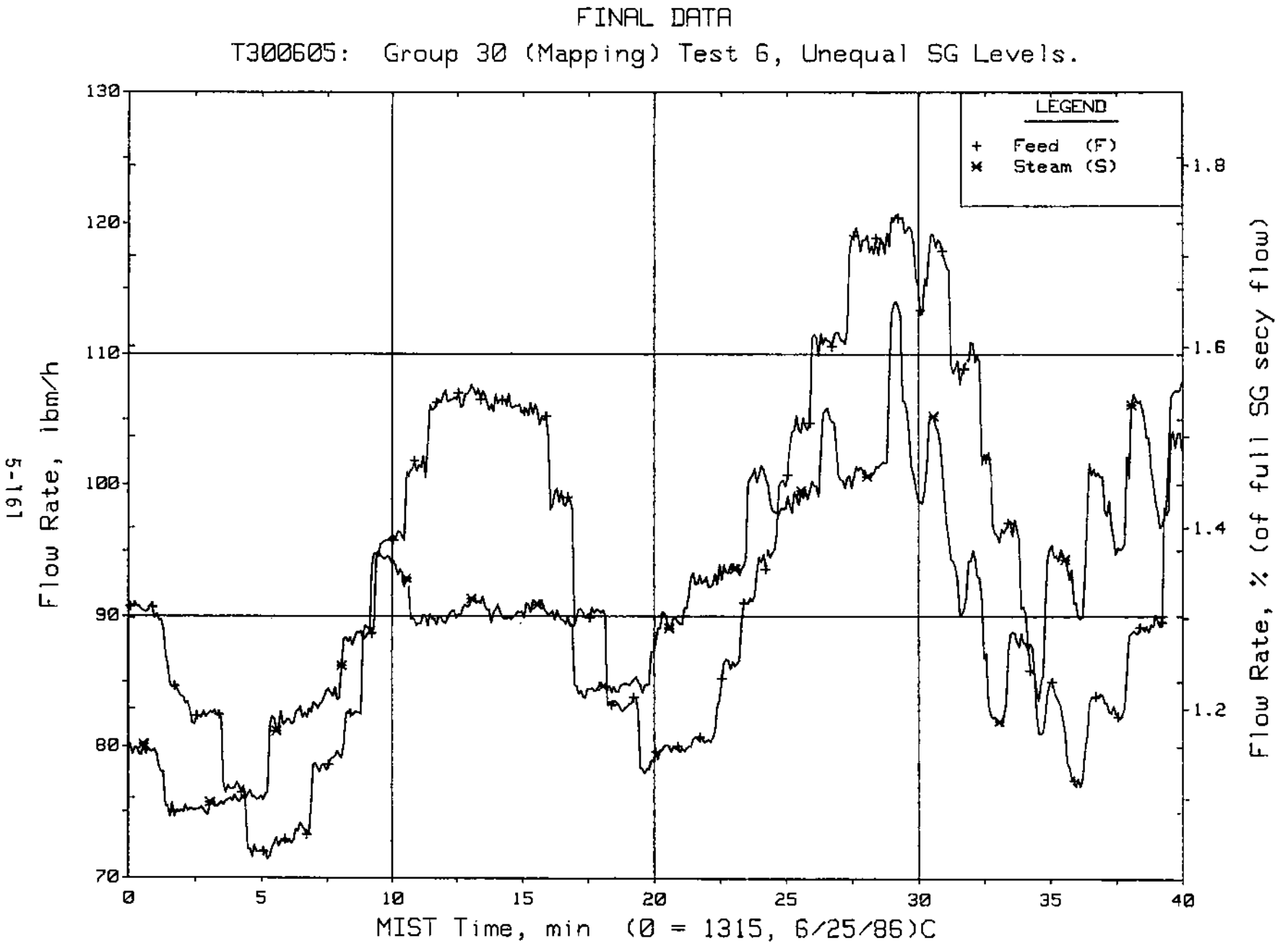

Figure 5.4.4. Steam Generator A Flow Rates (SaOR20s)

Fri Feb 17 16:26:01 1989

SCFL1

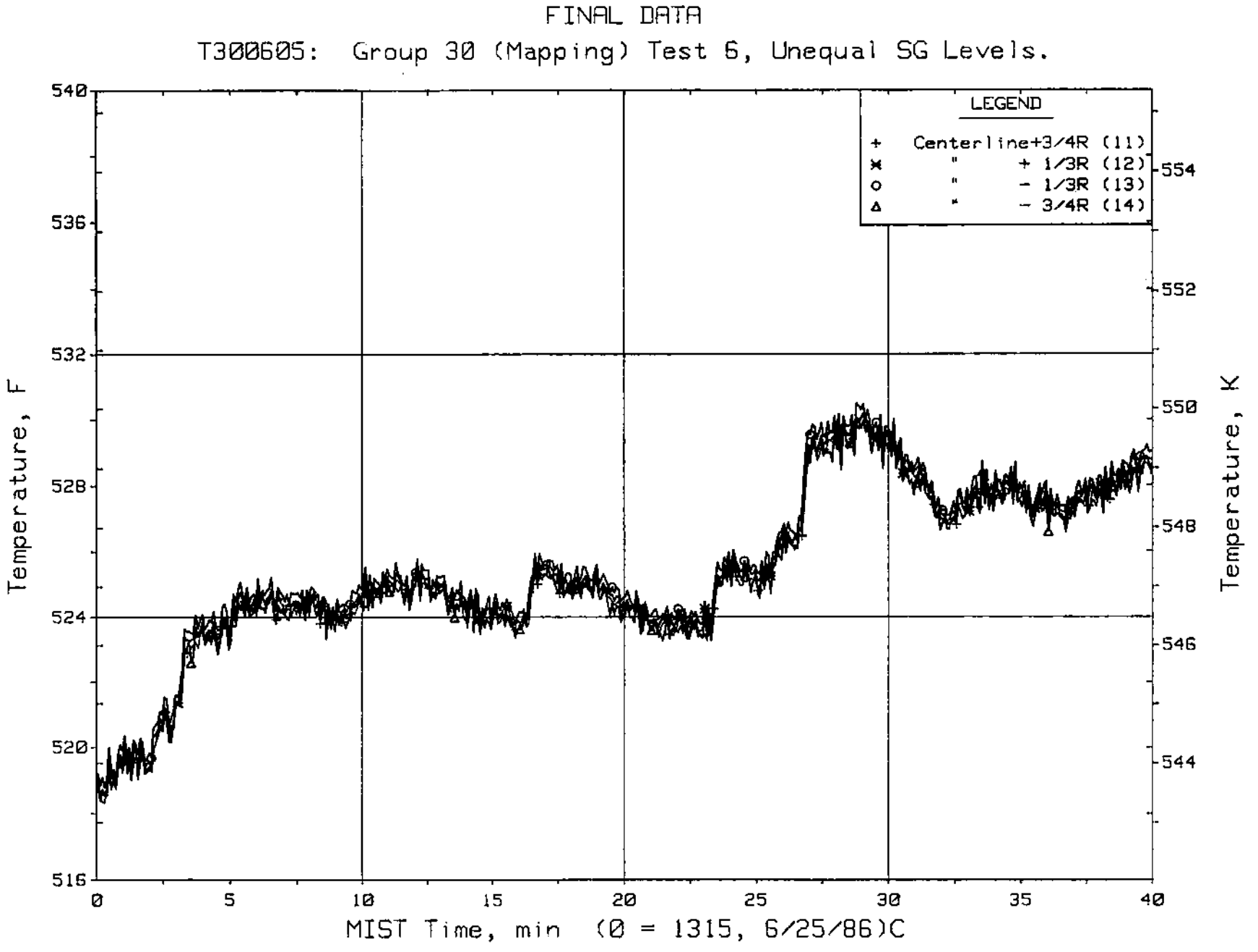

Figure 5.4.5. Cold Leg A1 Nozzle Rake Fluid Temperatures (21.2 ft, C1TCs)

Tue Feb 21 11:12:09 1989

C1TC4

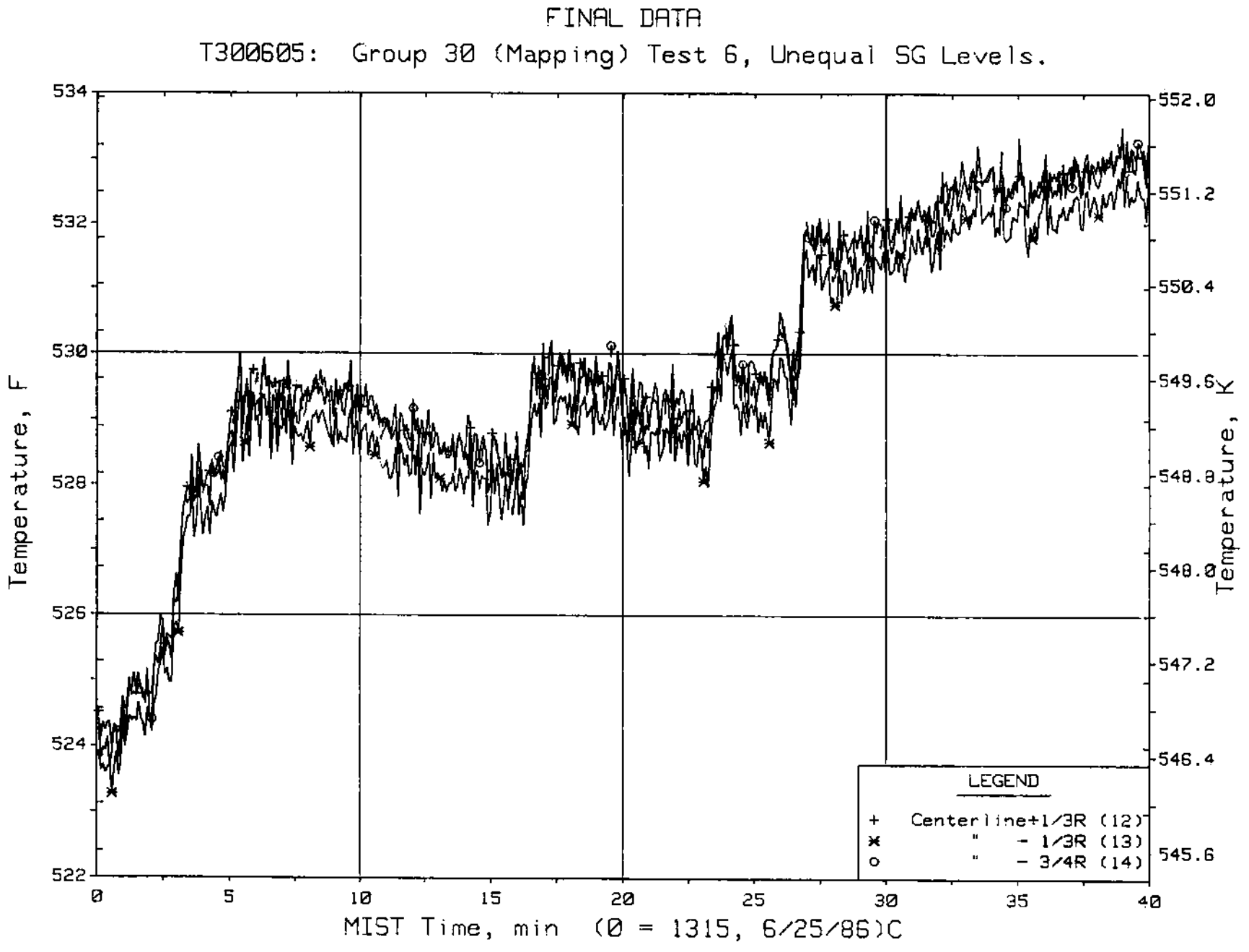

Figure 5.4.6. Cold Leg B1 Nozzle Rake Fluid Temperatures (21.2 ft, C2TCs)

Fri Feb 17 16:21:21 1989

C2TC4

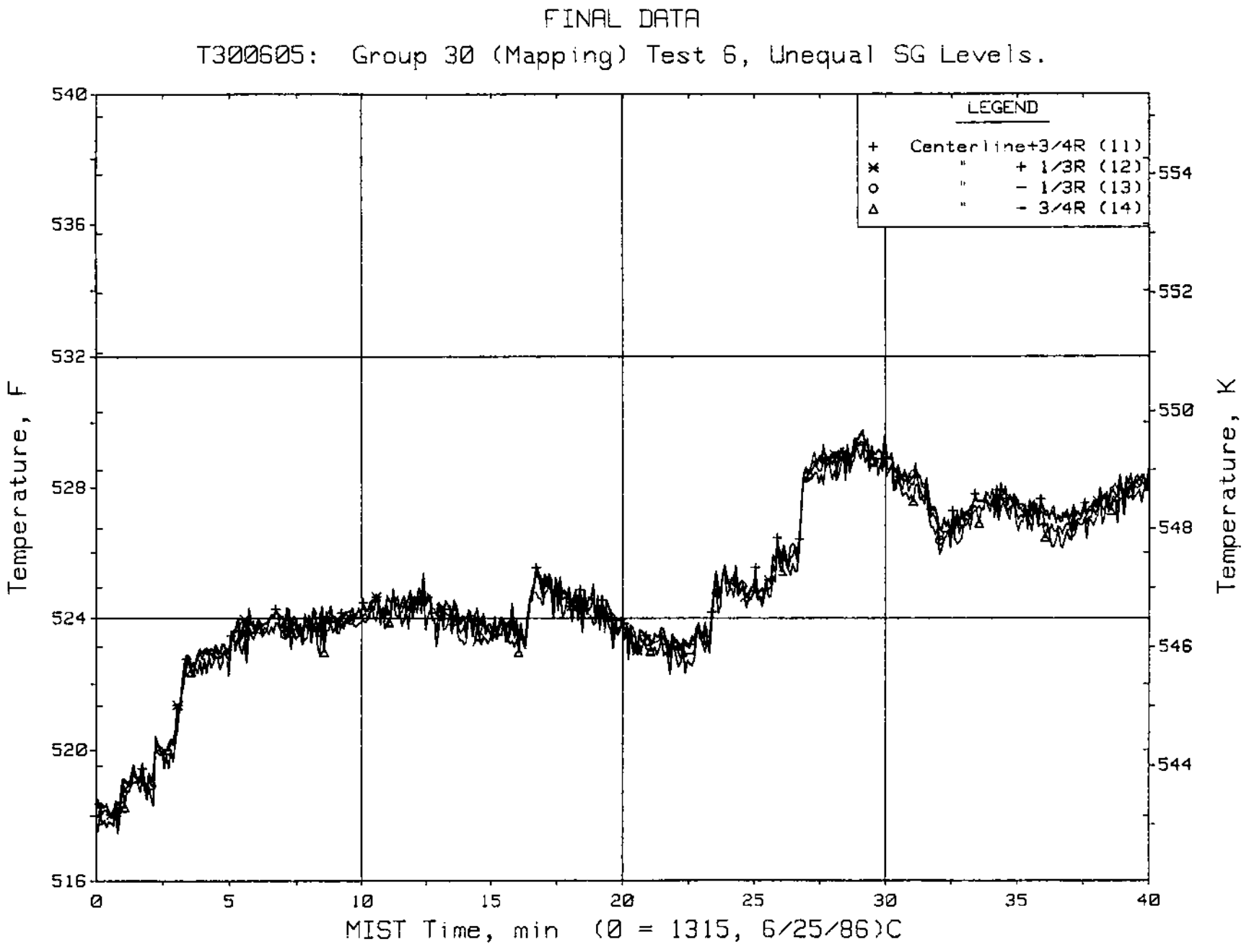

Figure 5.4.7. Cold Leg A2 Nozzle Rake Fluid Temperatures (21.2 ft, C3TCs)

Tue Feb 21 11:15:42 1989

C3TC4

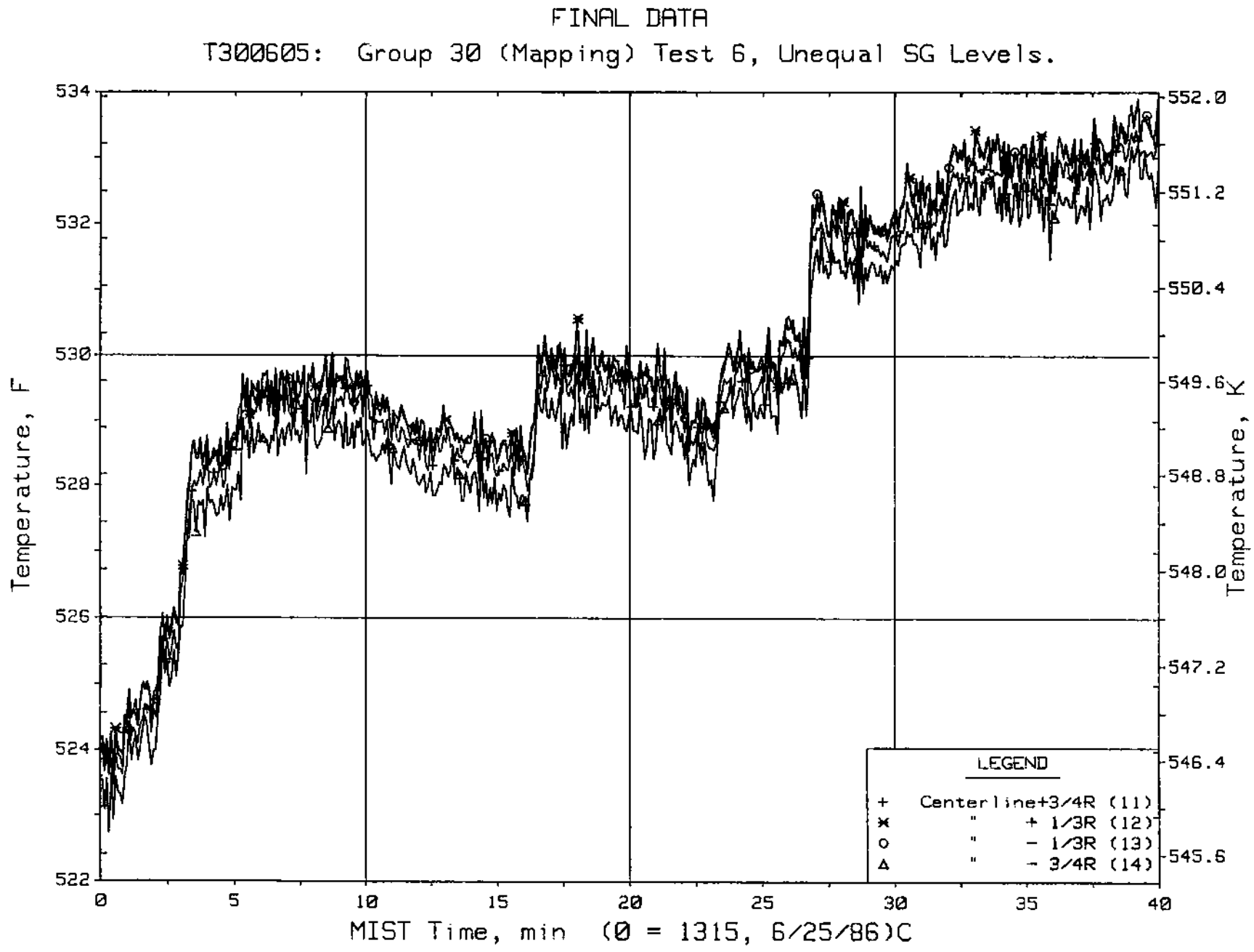

Figure 5.4.8. Cold Leg B2 Nozzle Rake Fluid Temperatures (21.2 ft, C4TCs)

Tue Feb 21 11:21:17 1989

C4TC4

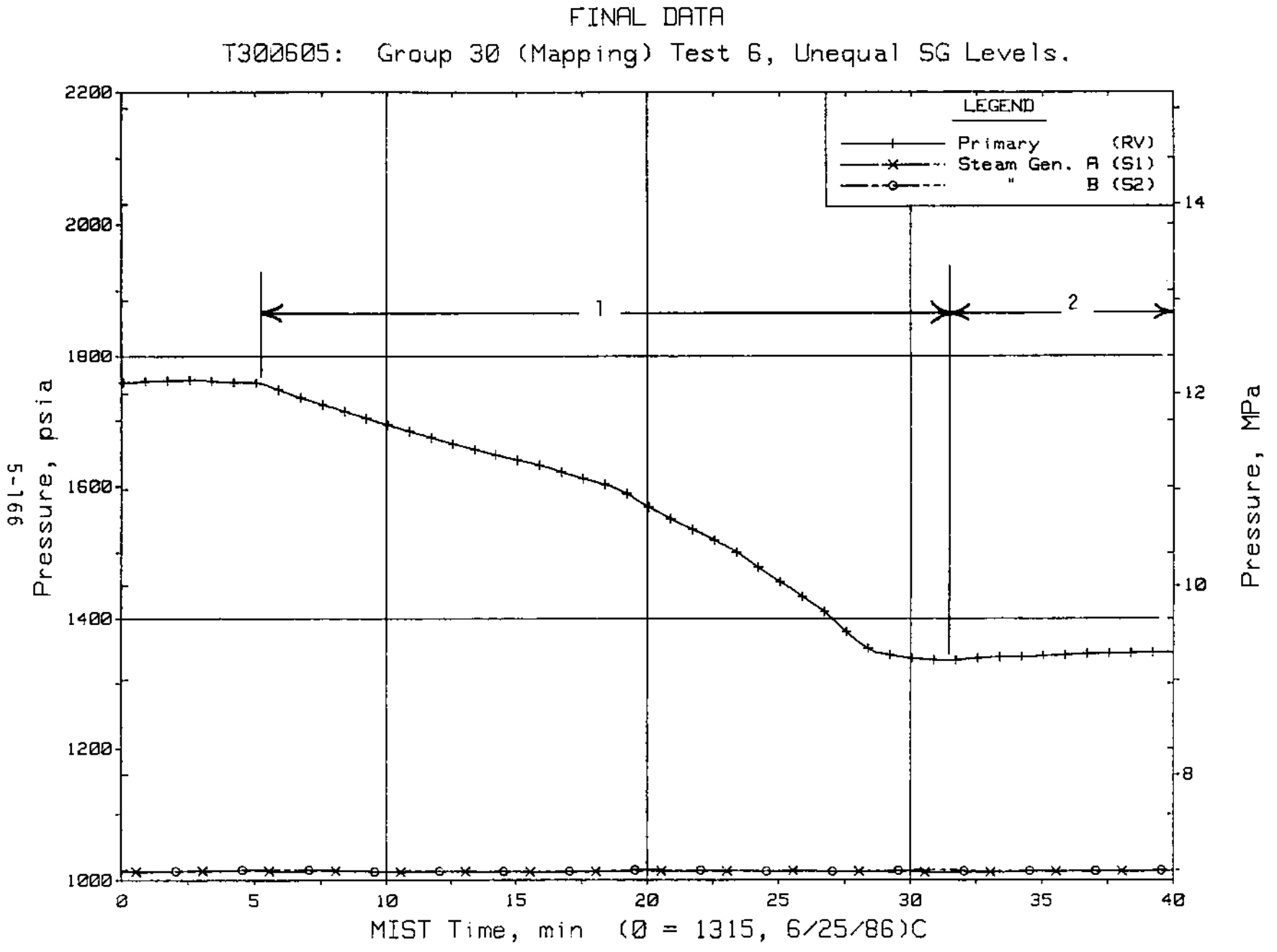

Figure 5.4.9. Primary and Secondary System Pressures (GPOls)

Fri Feb 17 16:13:57 1989

PSGP1

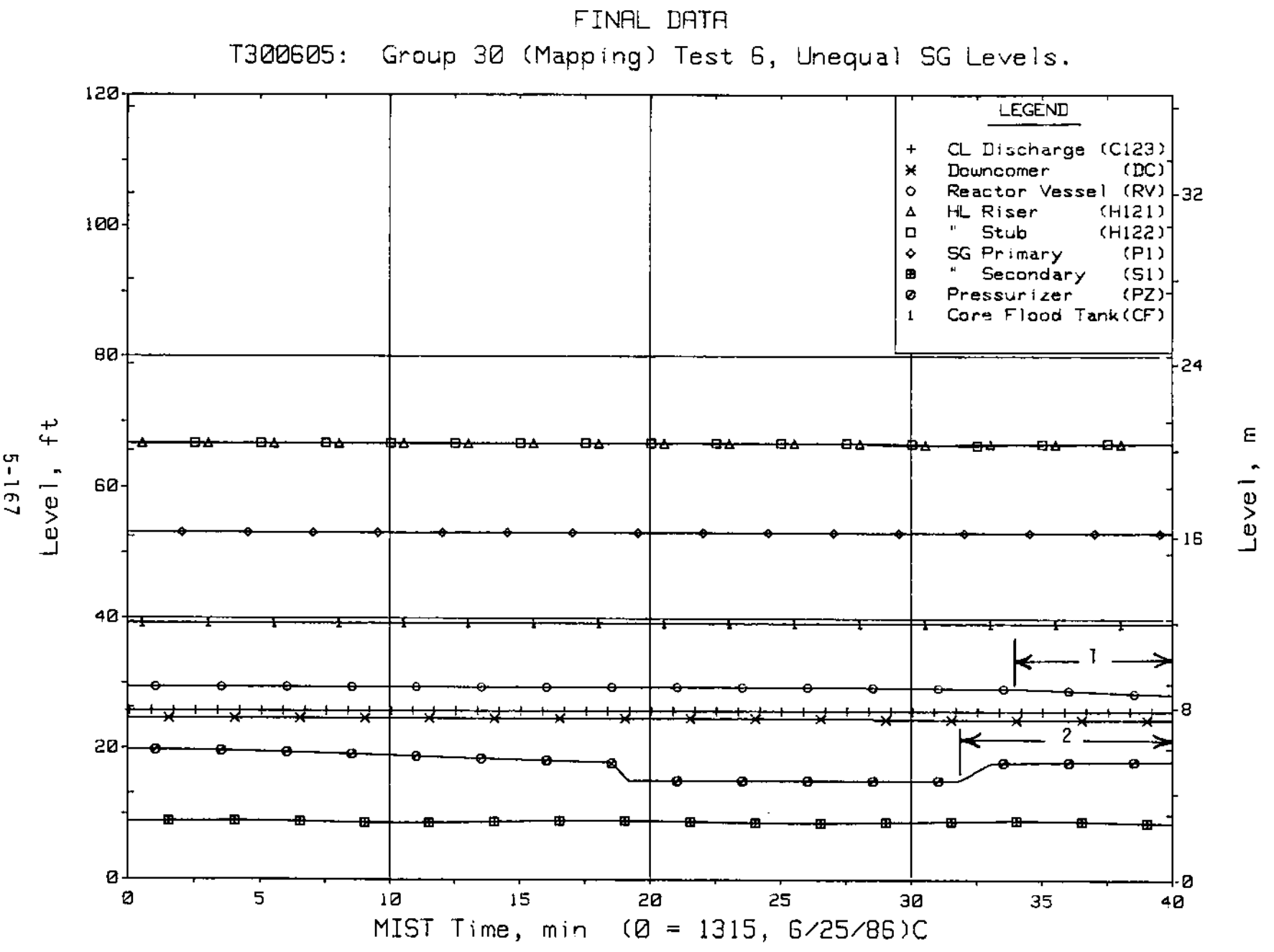

Figure 5.4.10. Loop A Collapsed Liquid Levels (LV20s)

Fri Feb 17 16:11:30 1989

PRLV1

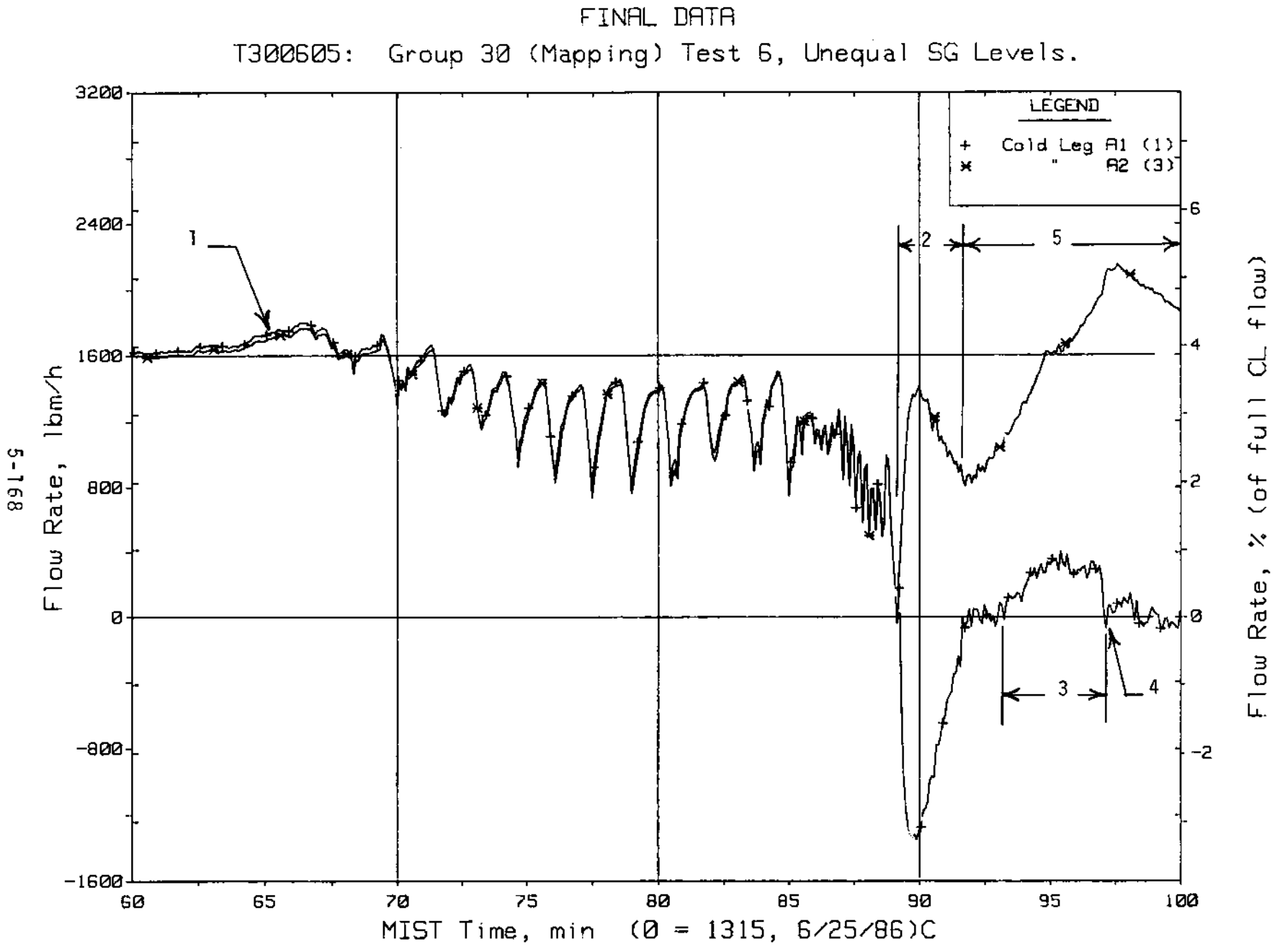

Figure 5.4.11. Loop A Cold Leg (Venturi) Flow Rates (CnVN20s)

Fri Feb 17 15:54:06 1989

PRFL5

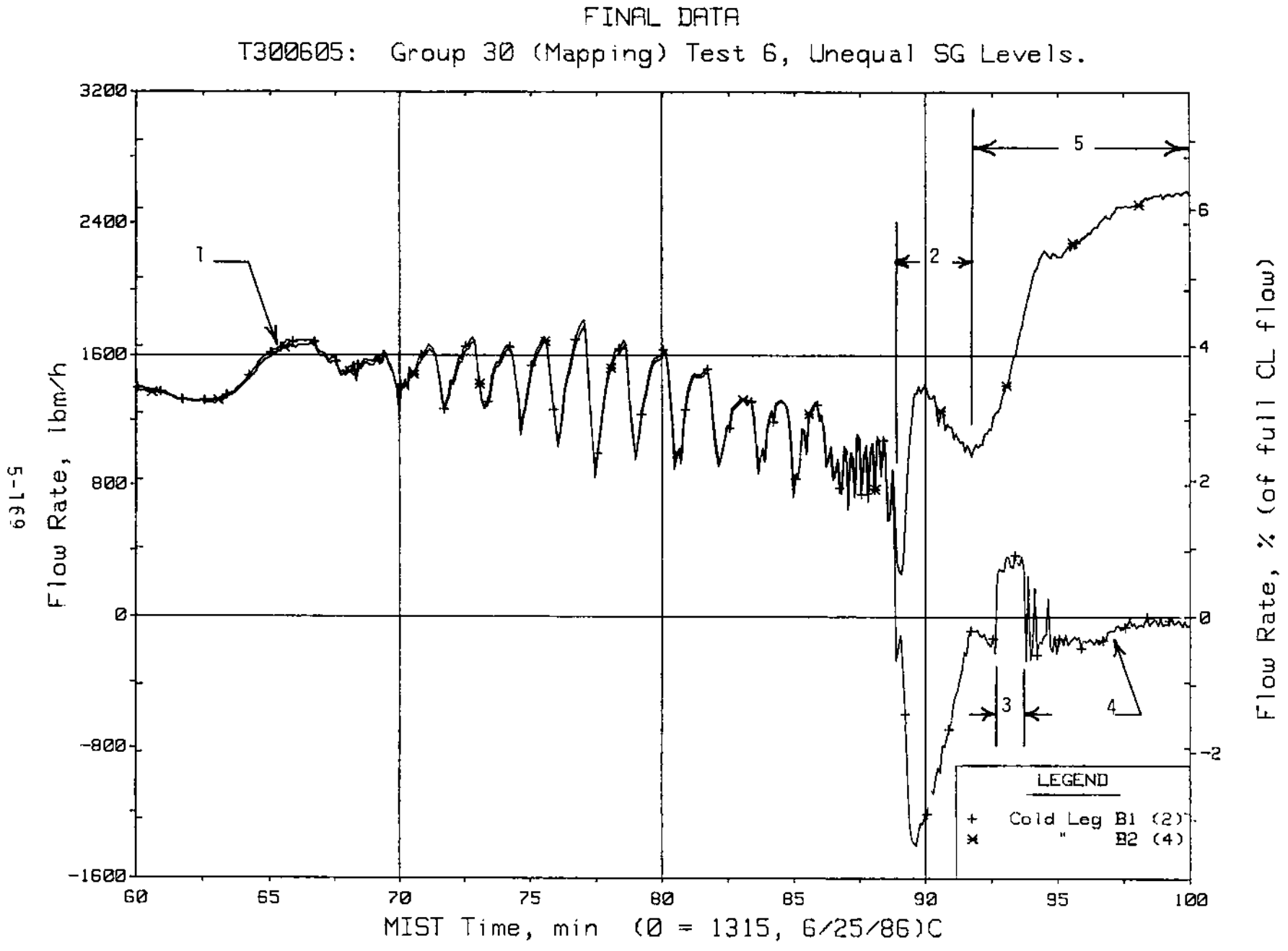

Figure 5.4.12. Loop B Cold Leg (Venturi) Flow Rates (CnVN20s)

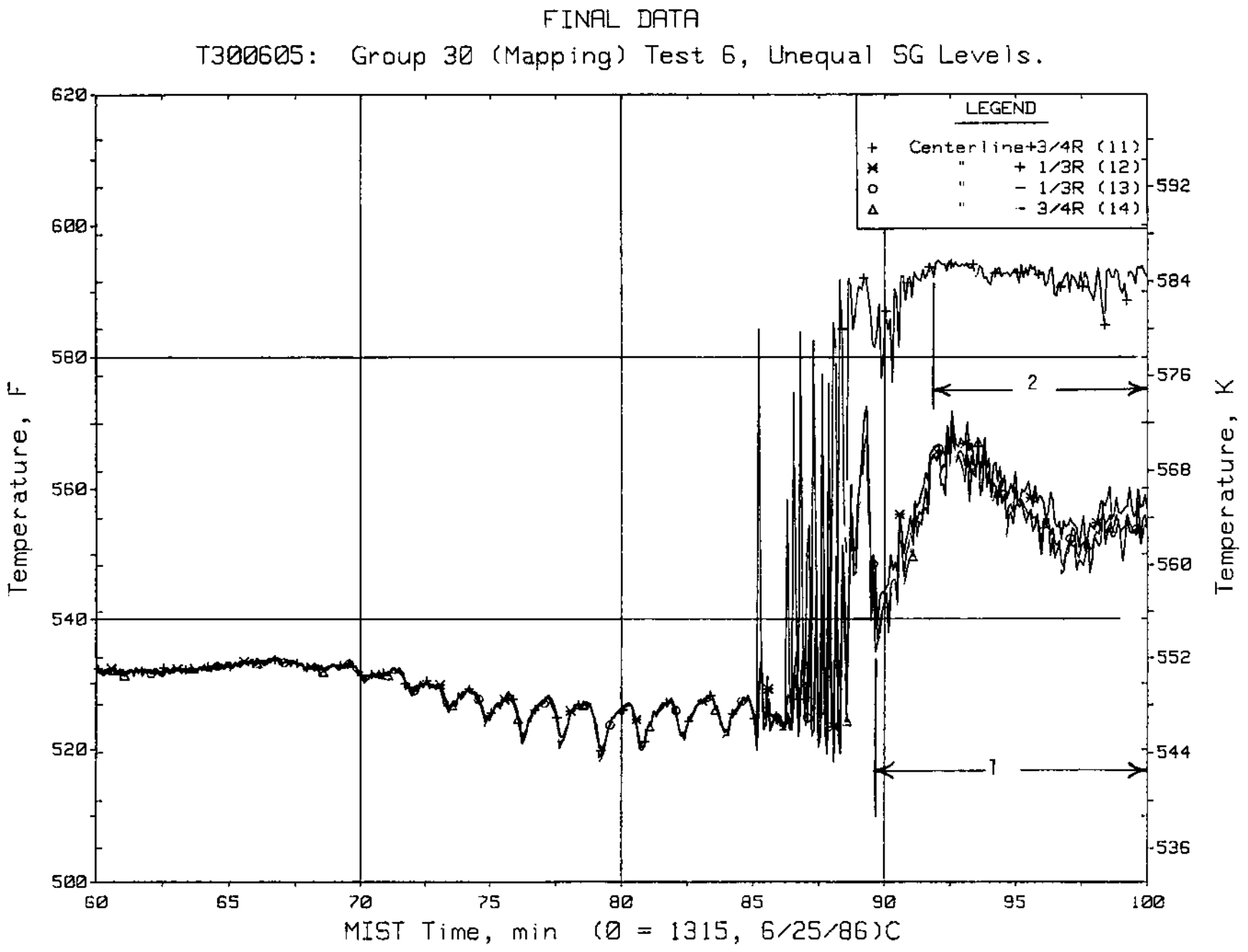

Figure 5.4.13. Cold Leg A2 Nozzle Rake Fluid Temperatures (21.2 ft, C3TCs)

Fri Feb 17 16:00:45 1989

C3TC4

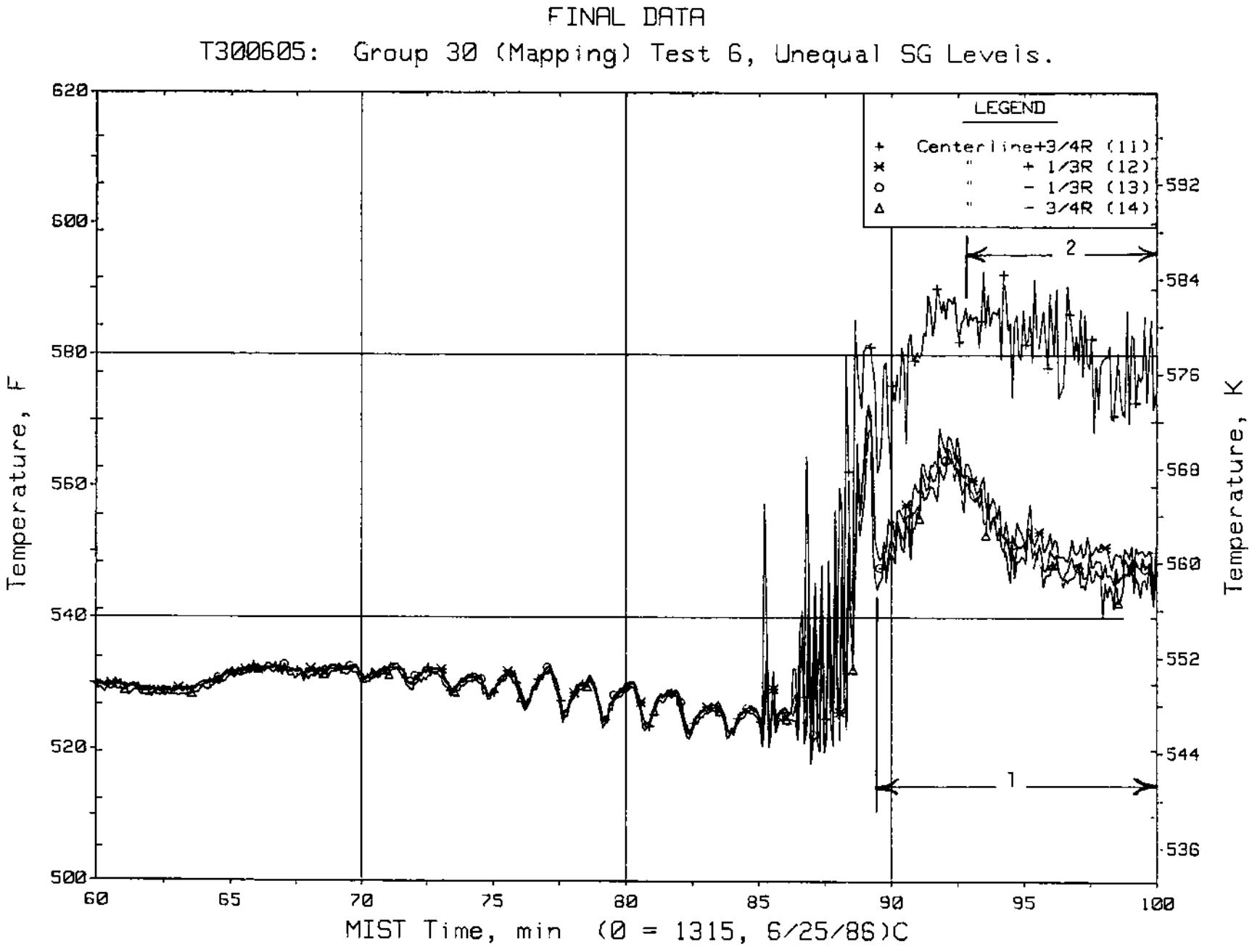

Figure 5.4.14. Cold Leg B2 Nozzle Rake Fluid Temperatures (21.2 ft, C4TCs)

Fri Feb 17 16:03:18 1989

C4TC4

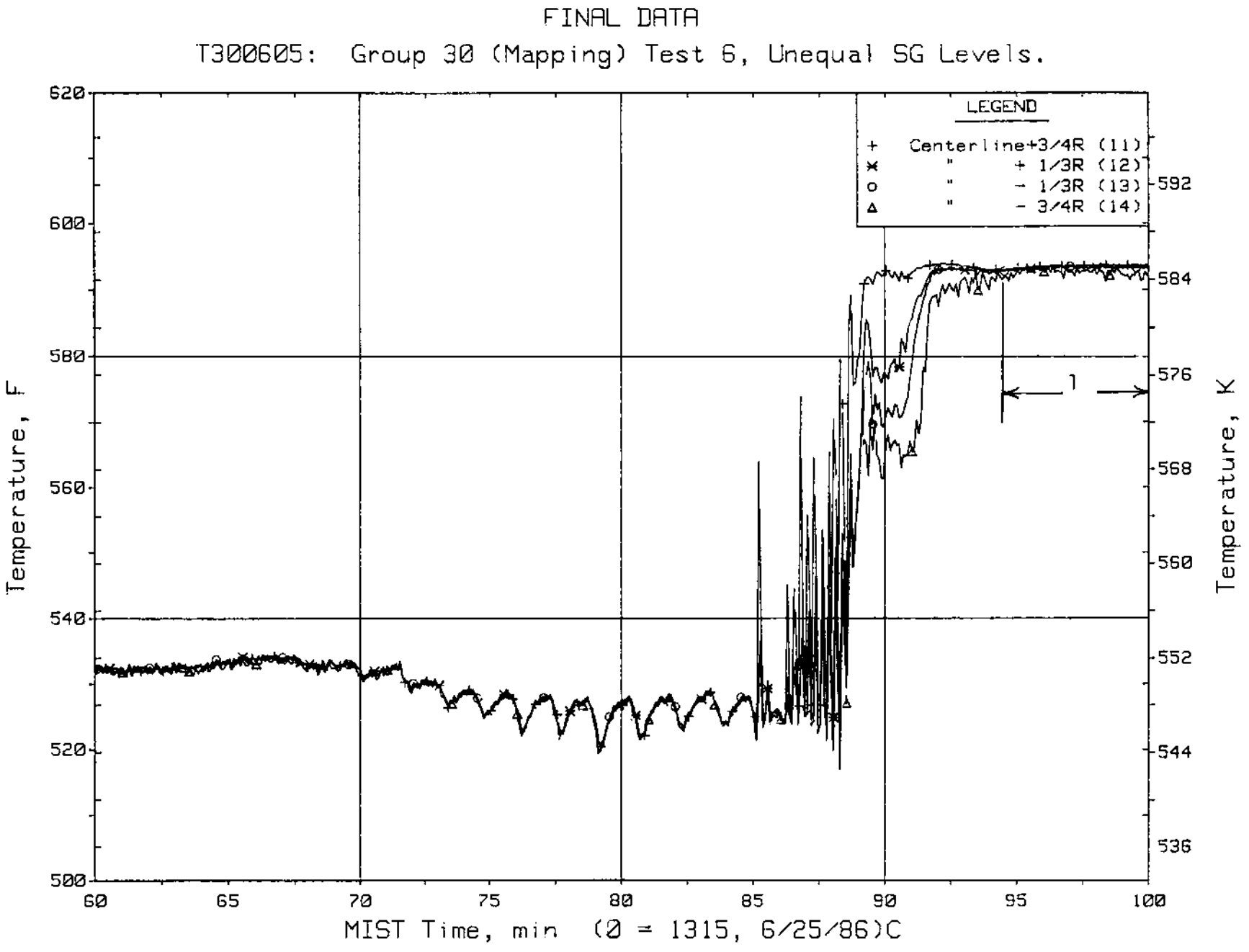

Figure 5.4.15. Cold Leg A1 Nozzle Rake Fluid Temperatures (21.2 ft, C1TCs)

Fri Feb 17 16:05:50 1989

C1TC4

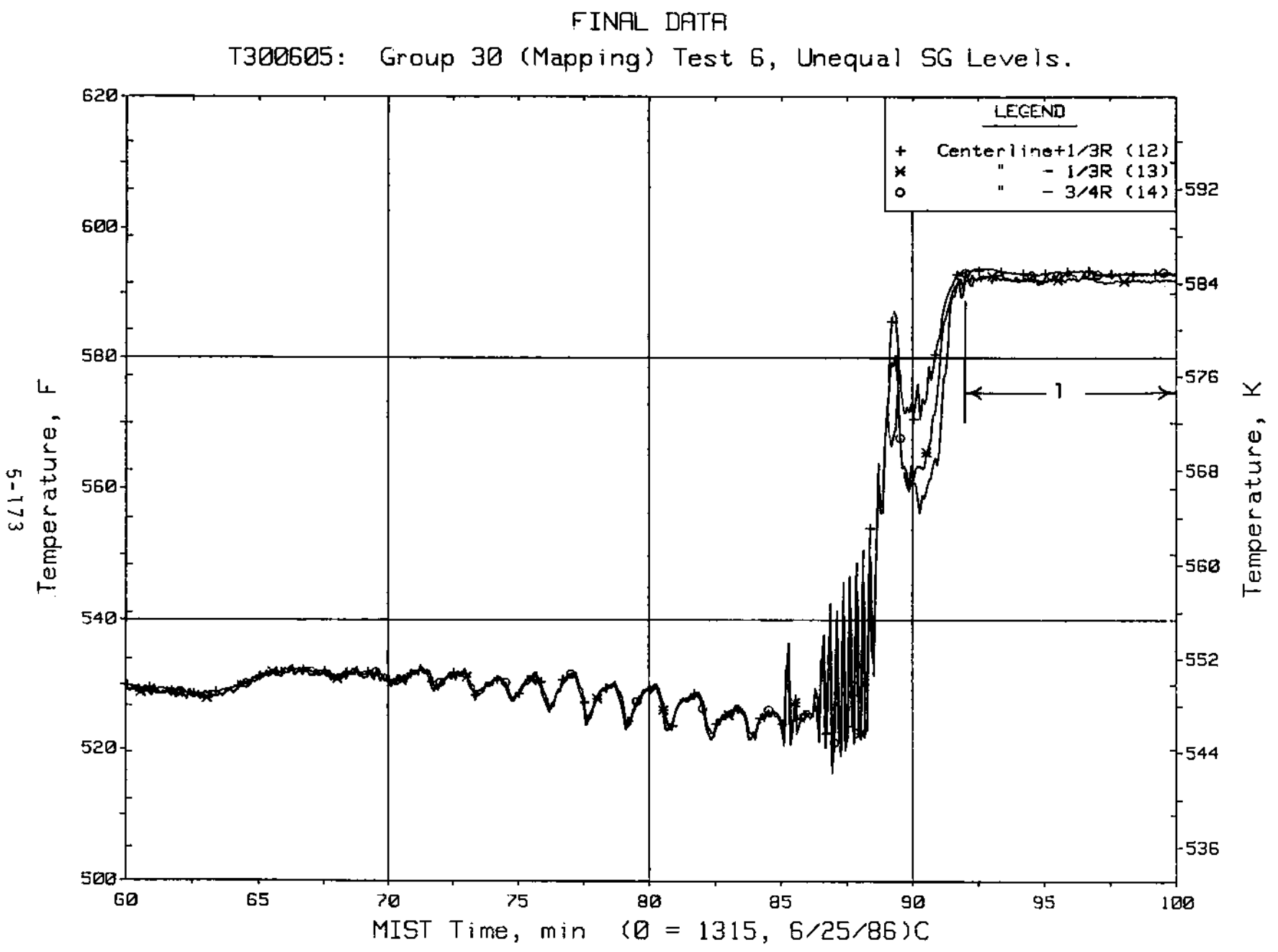

Figure 5.4.16. Cold Leg B1 Nozzle Rake Fluid Temperatures (21.2 ft, C2TCs)

Fri Feb 17 16:08:11 1989

C2TC4

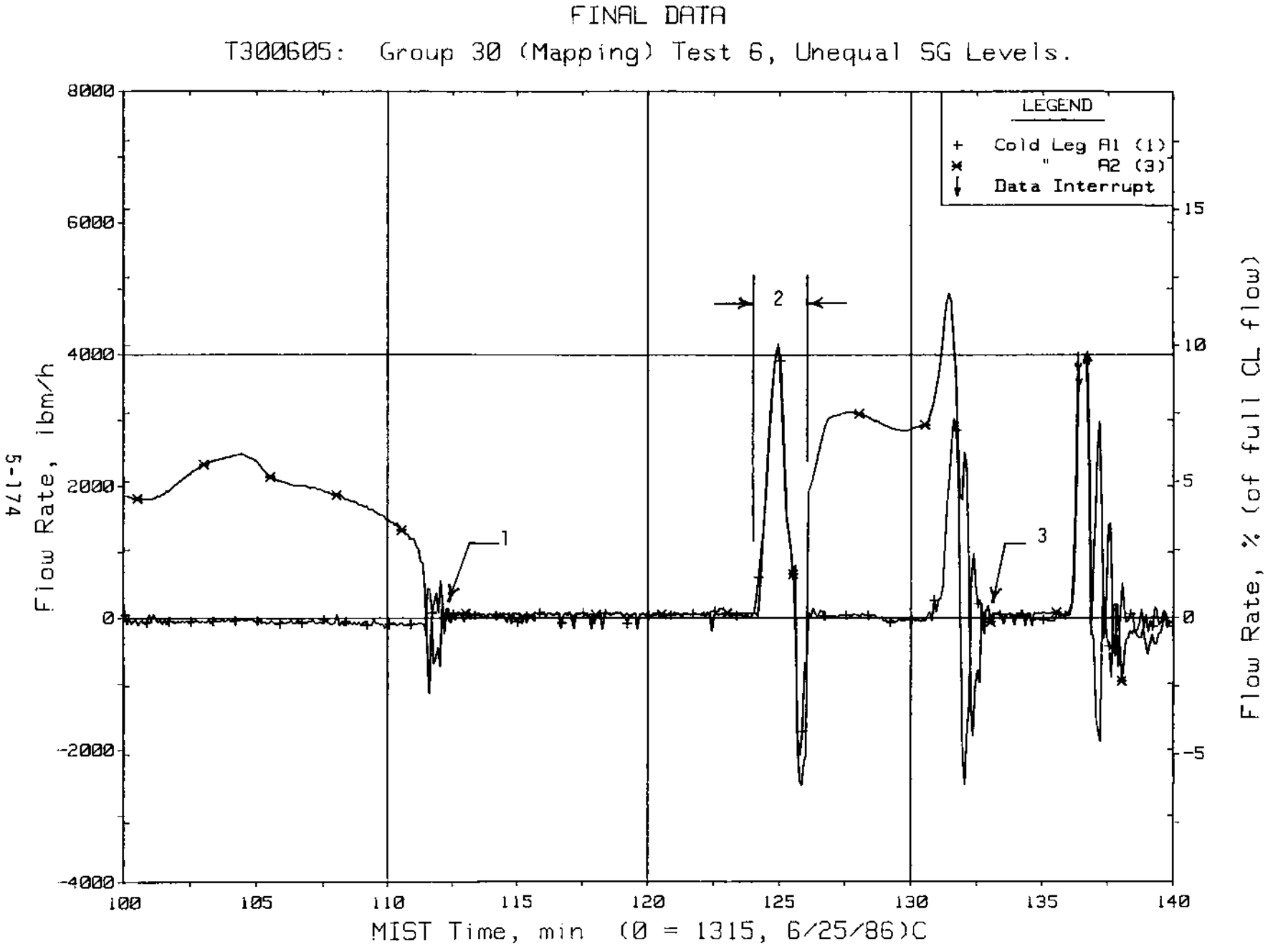

Figure 5.4.17. Loop A Cold Leg (Venturi) Flow Rates (CnVN2Os)

Tue Feb 28 15:12:44 1989

PRFL5

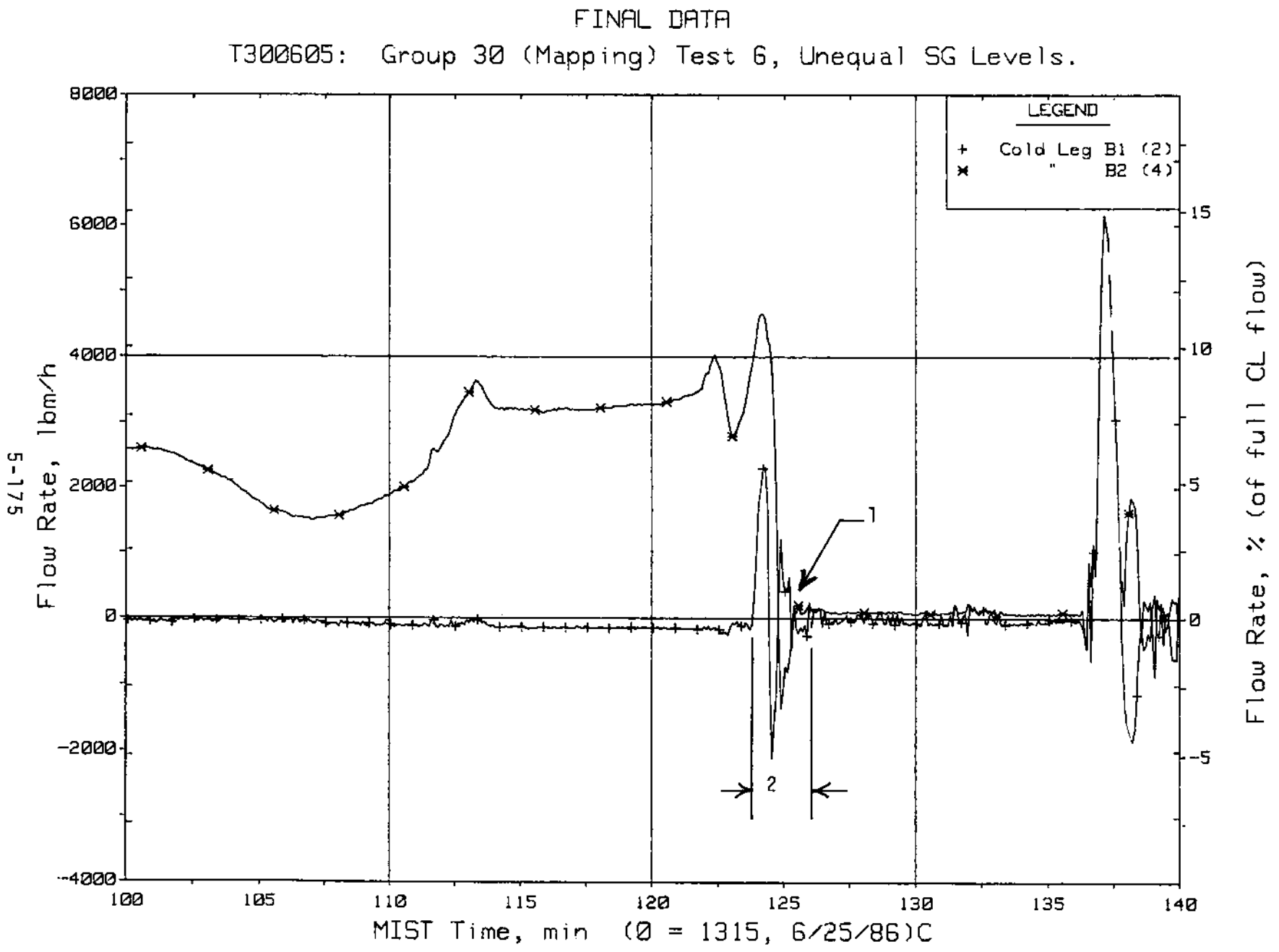

Figure 5.4.18. Loop B Cold Leg (Venturi) Flow Rates (CnVN20s)

Fri Feb 17 15:49:50 1989

PRFL6

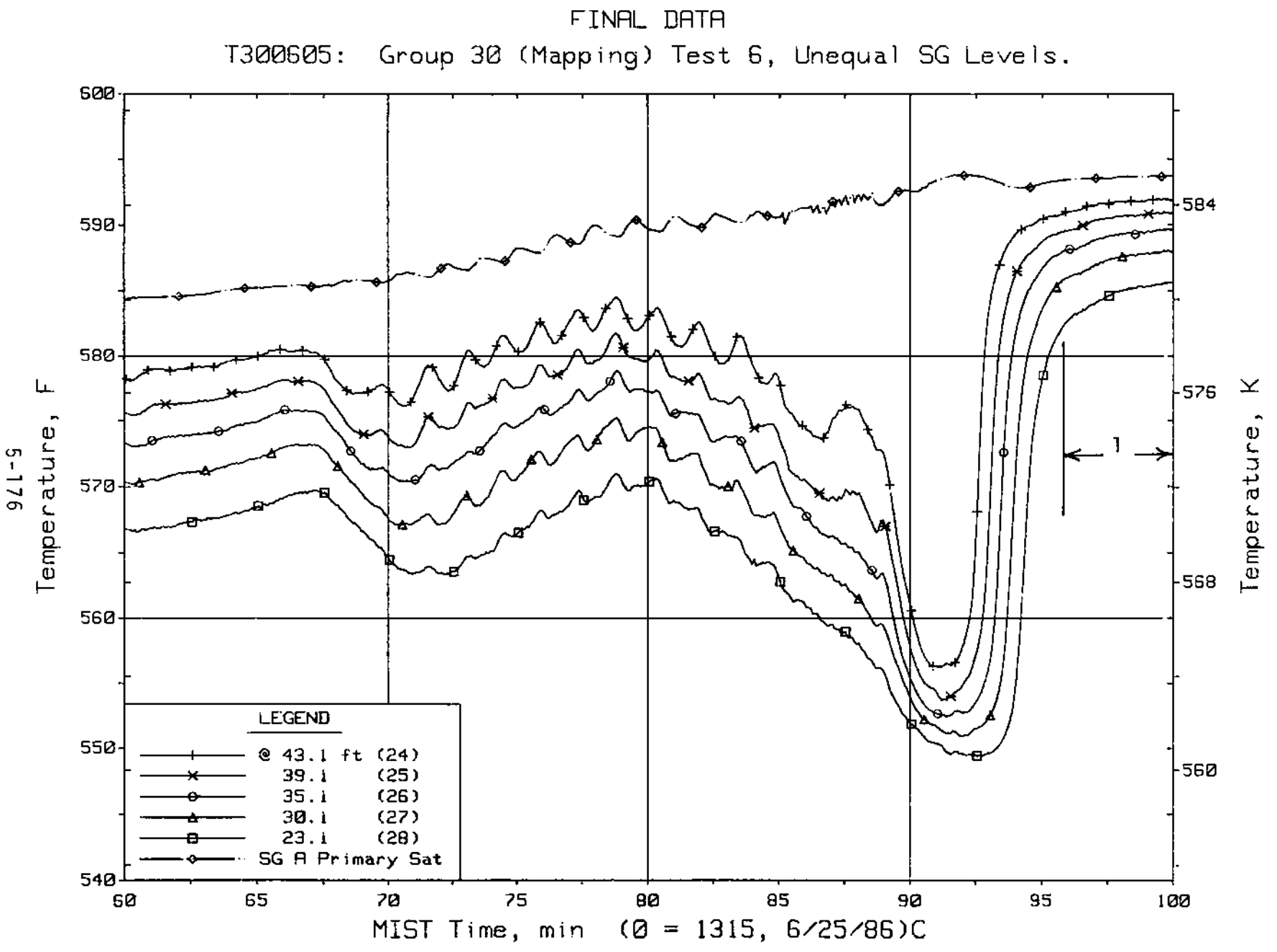

Figure 5.4.19. Steam Generator A Unwetted Tube (R) Lower-Elevation Primary Fluid Temperatures (P1TCs)

Fri Feb 17 15:34:23 1989

P1TC5

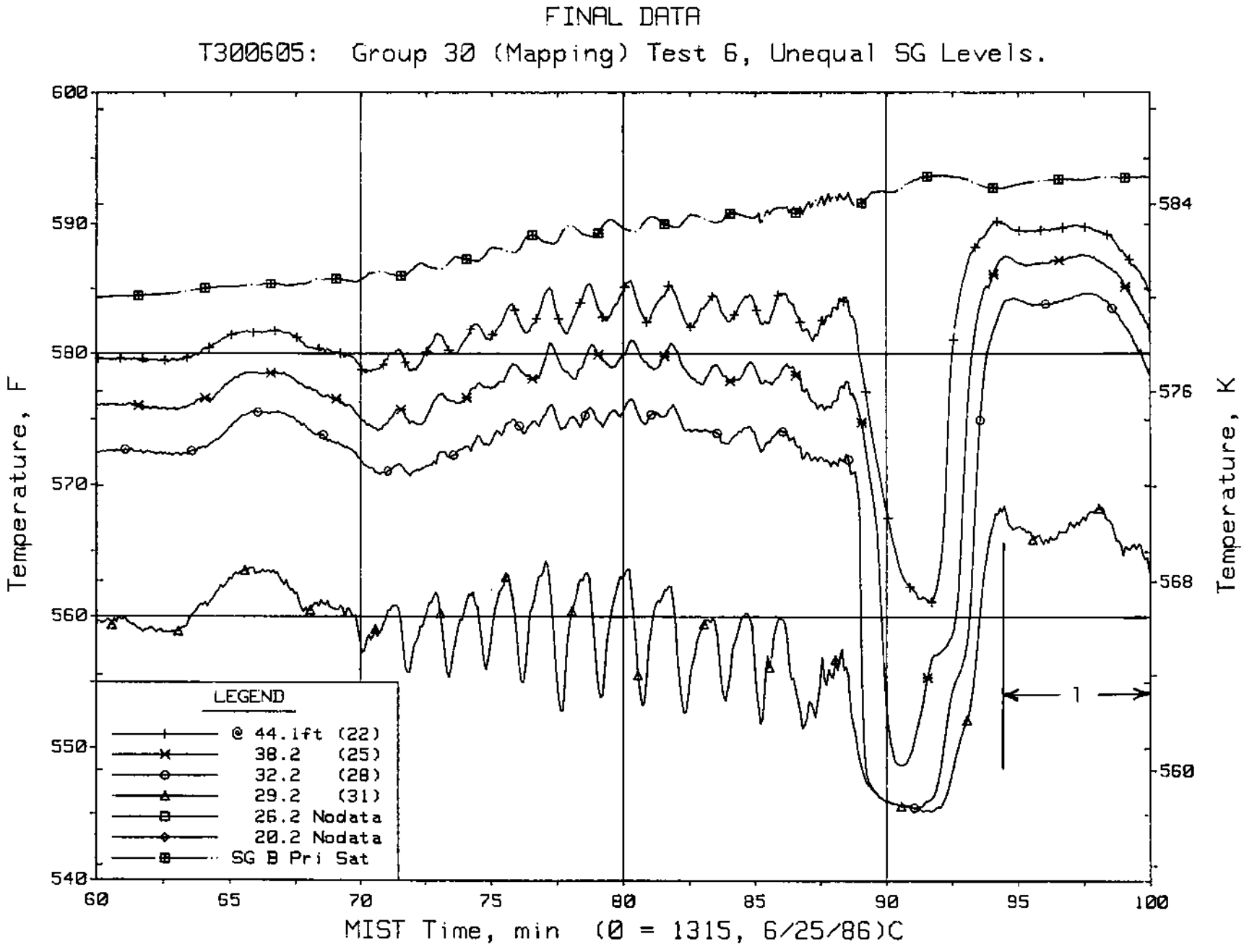

Figure 5.4.20. Steam Generator B Tube (R) Mid-Elevation Primary Fluid Temperatures (P2TCs)

Fri Feb 17 15:37:11 1989

P2TC8

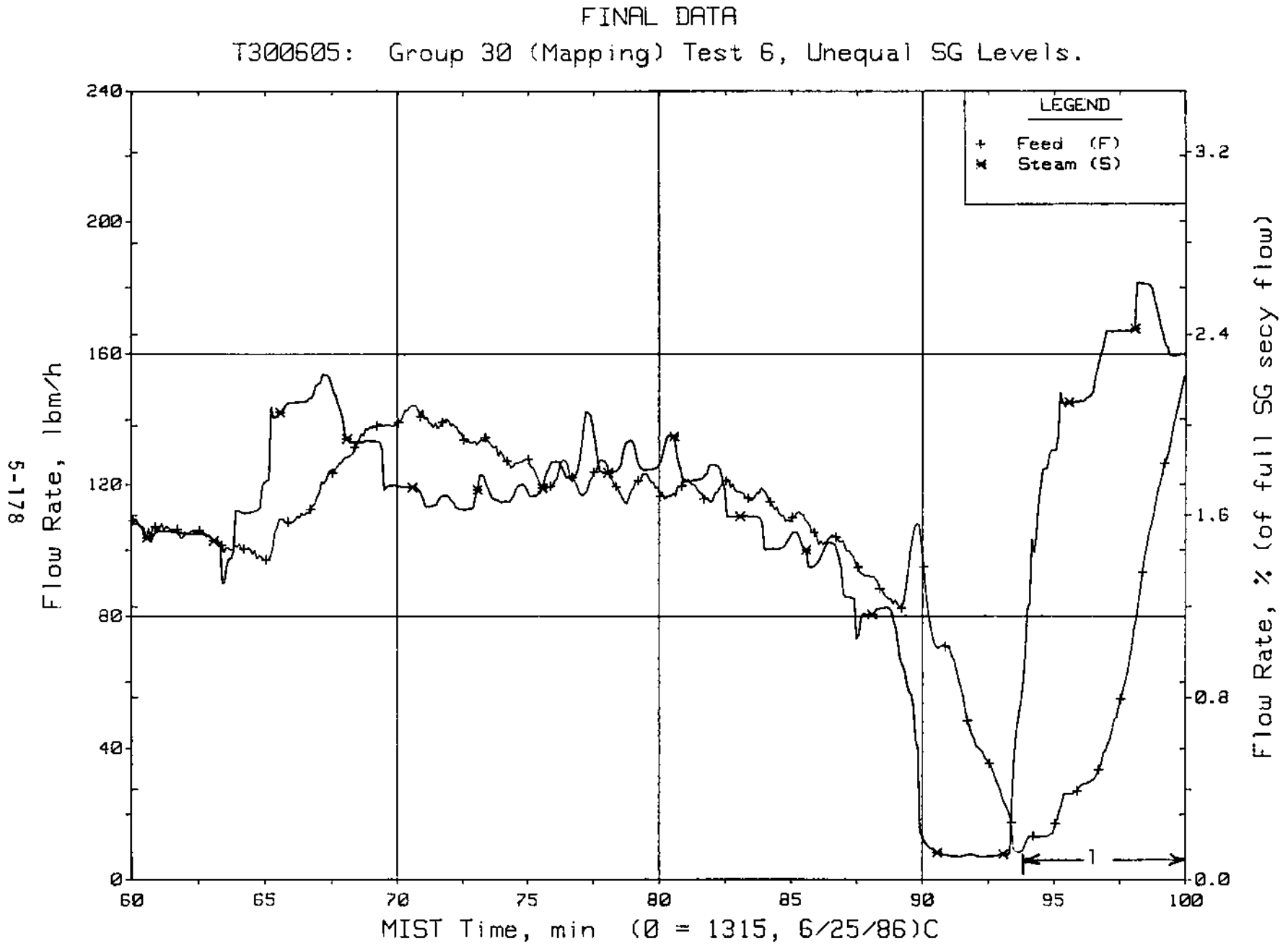

Figure 5.4.21. Steam Generator B Flow Rates (SaOR21s)

Tue Feb 21 13:41:33 1989

SCFL2

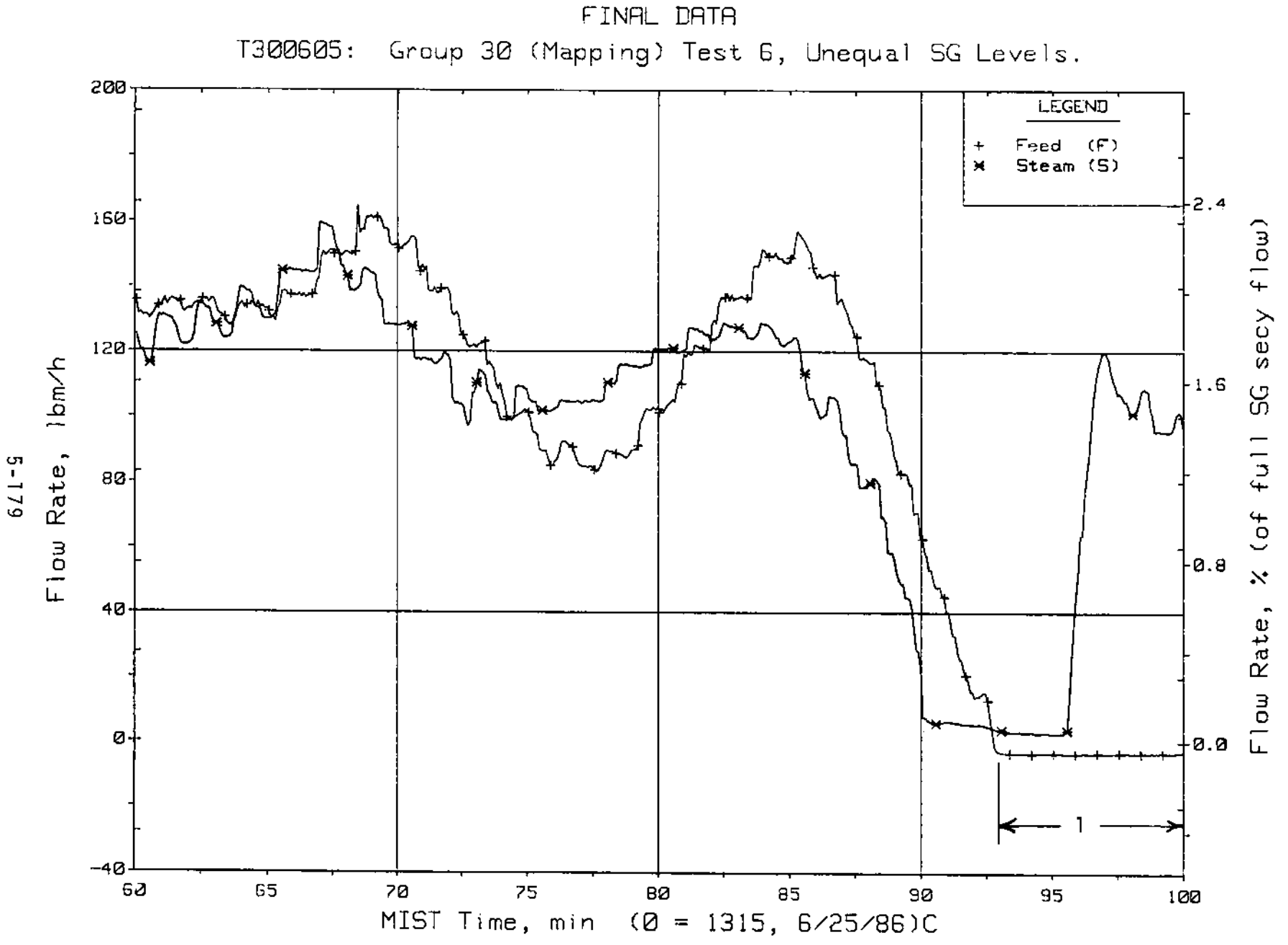

Figure 5.4.22. Steam Generator A Flow Rates (SaOR20s)

Tue Feb 21 13:44:39 1989

SCFL1

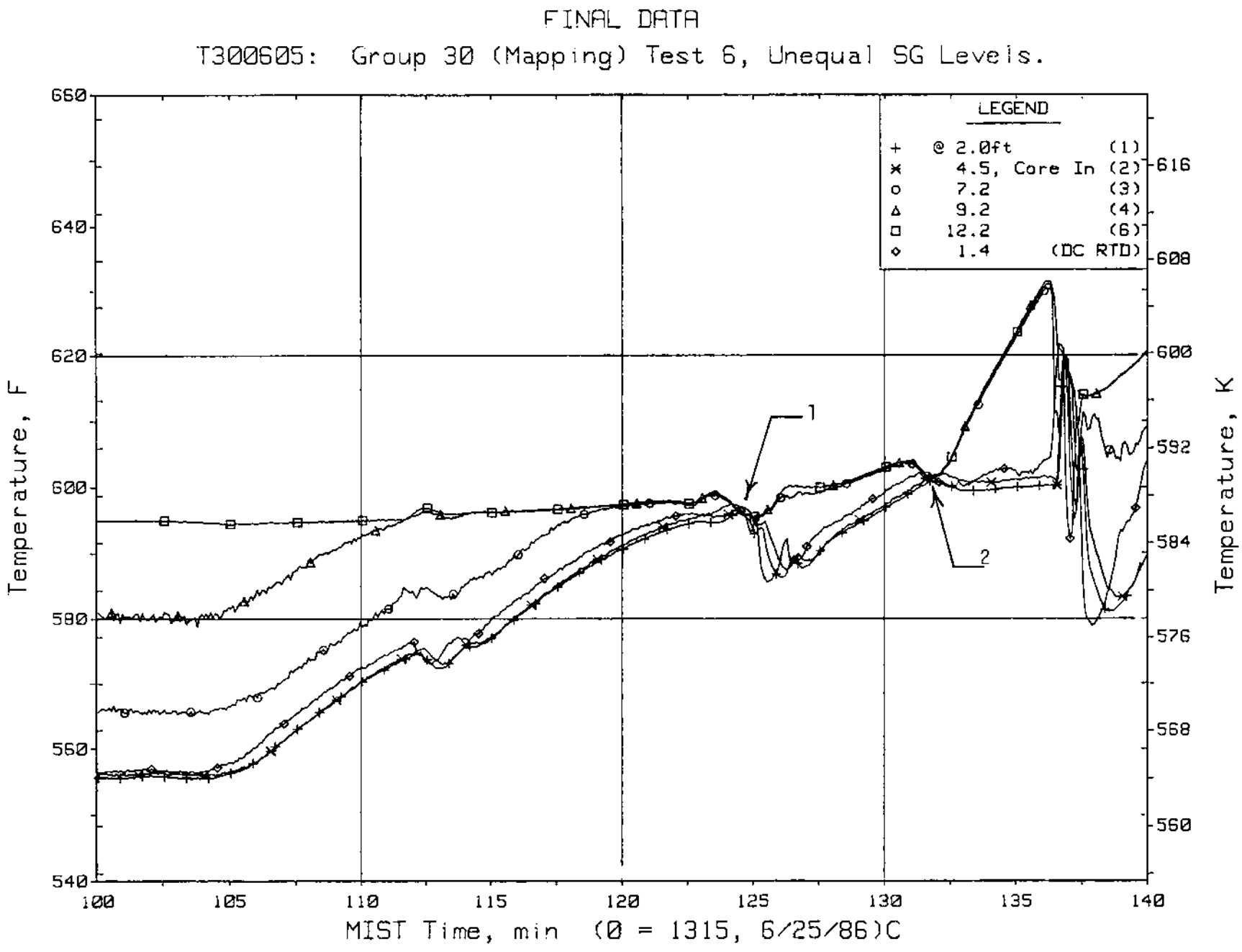

Figure 5.4.23. Reactor Vessel Lower-Elevation Fluid Temperatures (RVTCs)

Fri Feb 17 15:29:08 1989

RVTC1

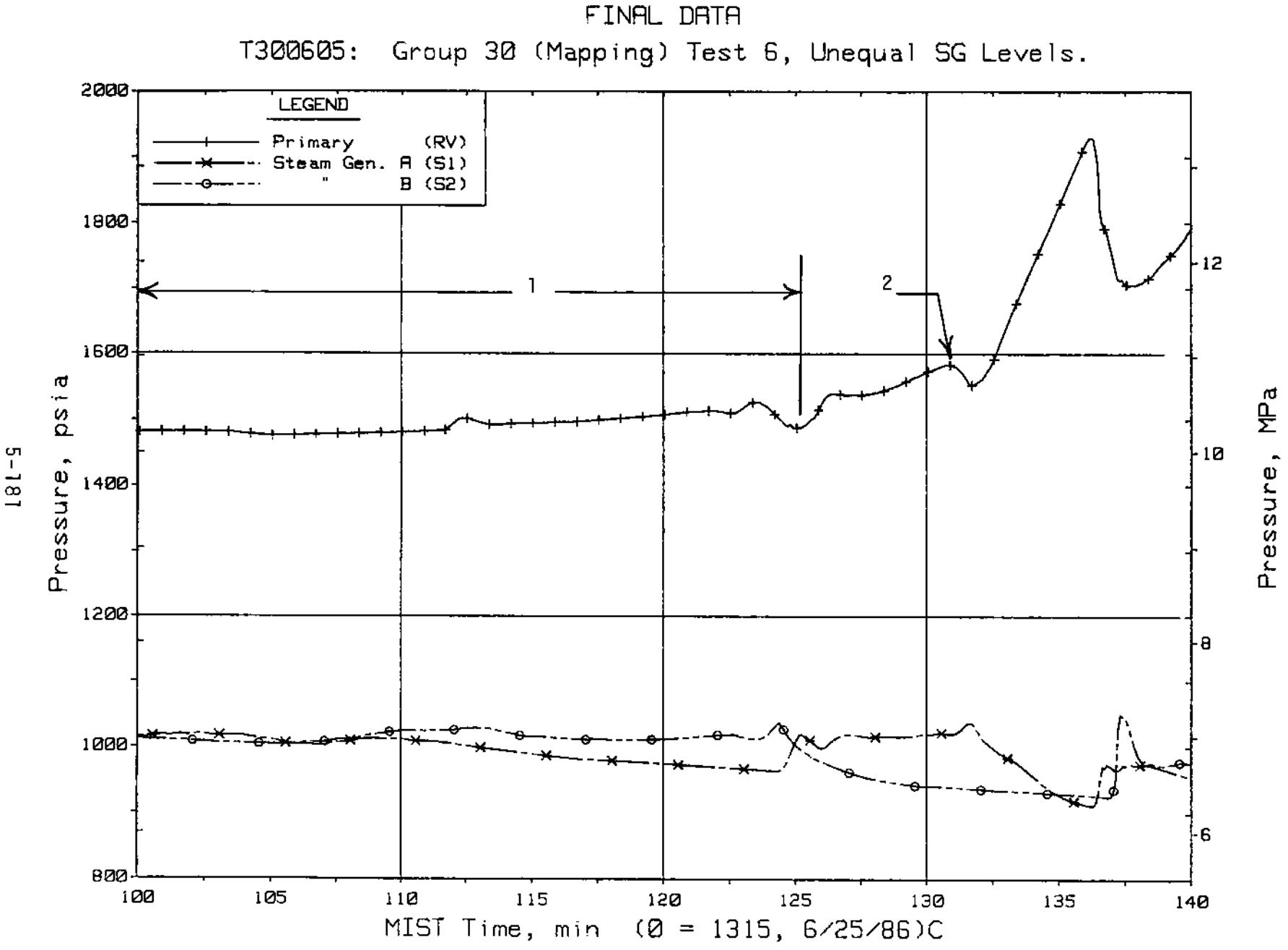

Figure 5.4.24. Primary and Secondary System Pressures (GP01s)

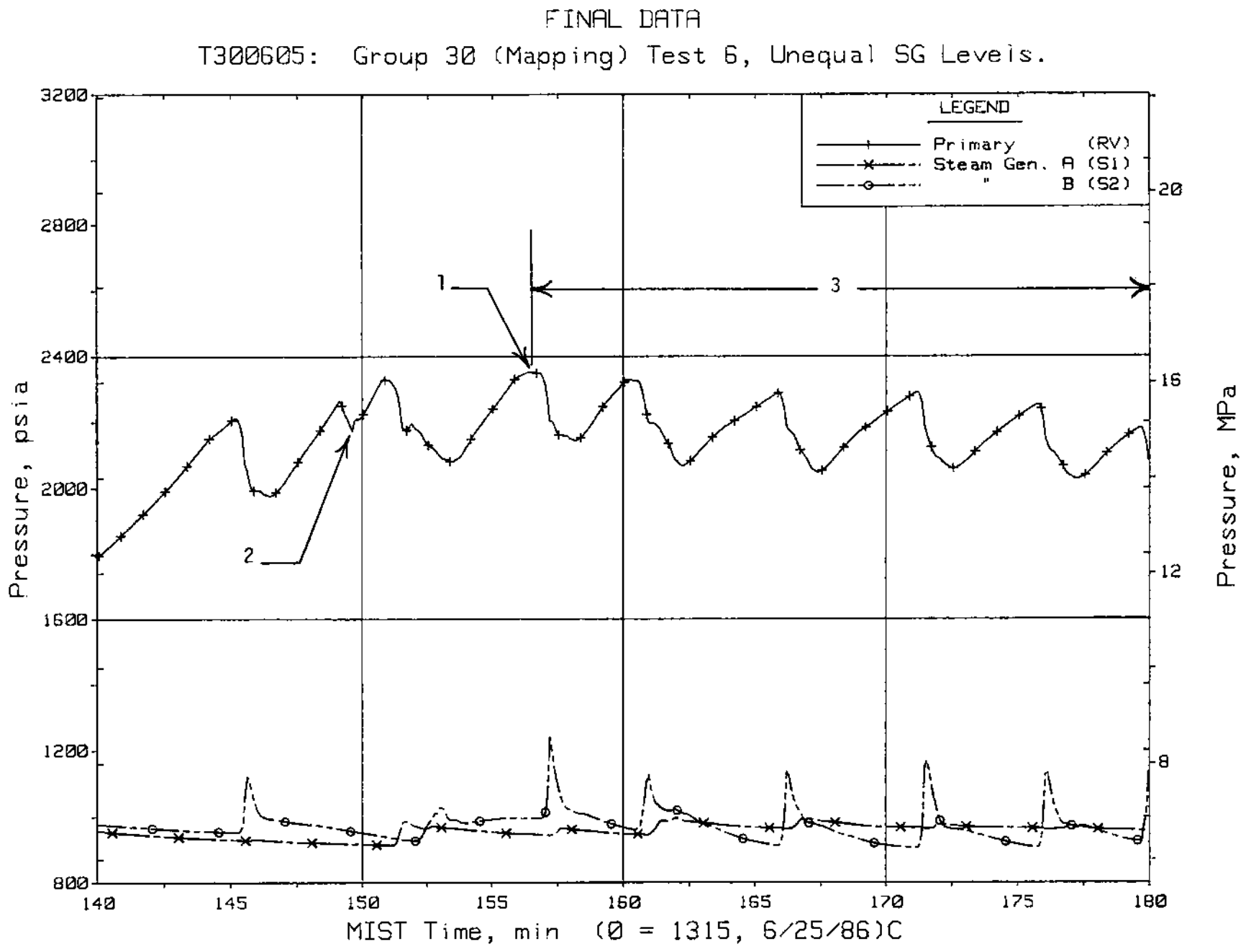

Figure 5.4.25. Primary and Secondary System Pressures (GP01s)

Tue Feb 21 13:48:30 1989

PSGP1

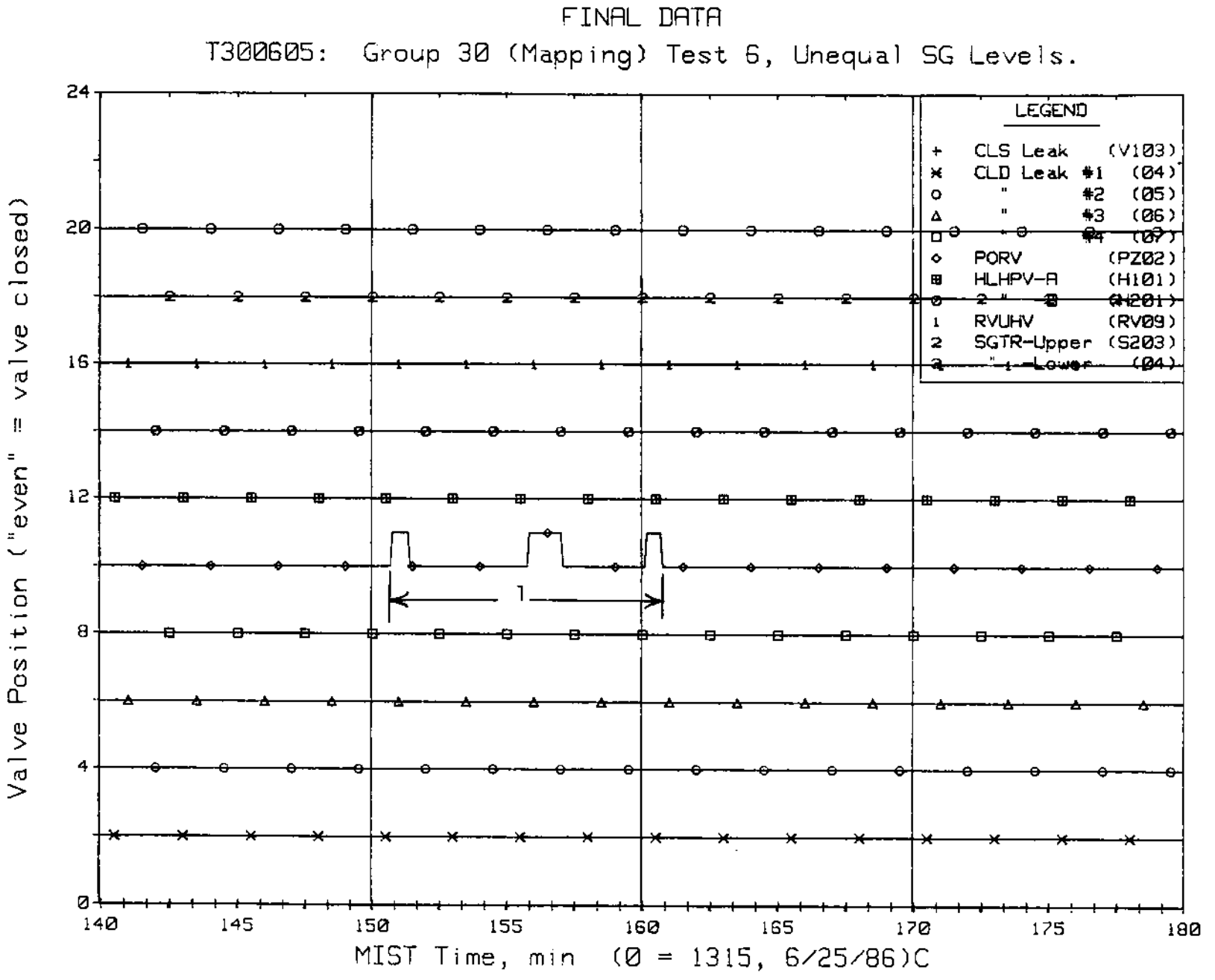

Figure 5.4.26. Primary System Discharge Limit Switch Indications (LSs)

Tue Feb 21 14:04:17 1989

PBLS1

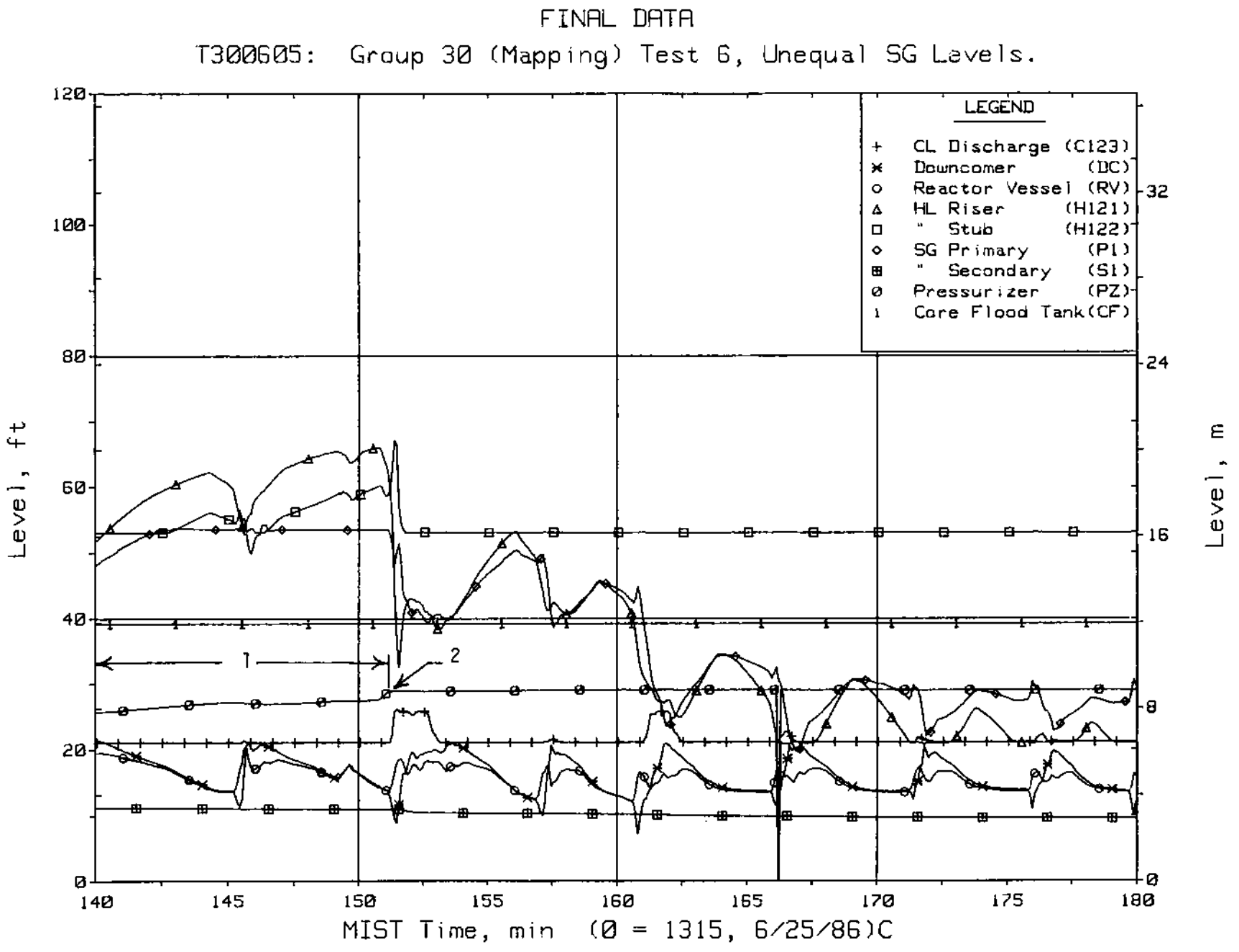

Figure 5.4.27. Loop A Collapsed Liquid Levels (LV20s)

Tue Feb 28 09:54:21 1989

PRLV1

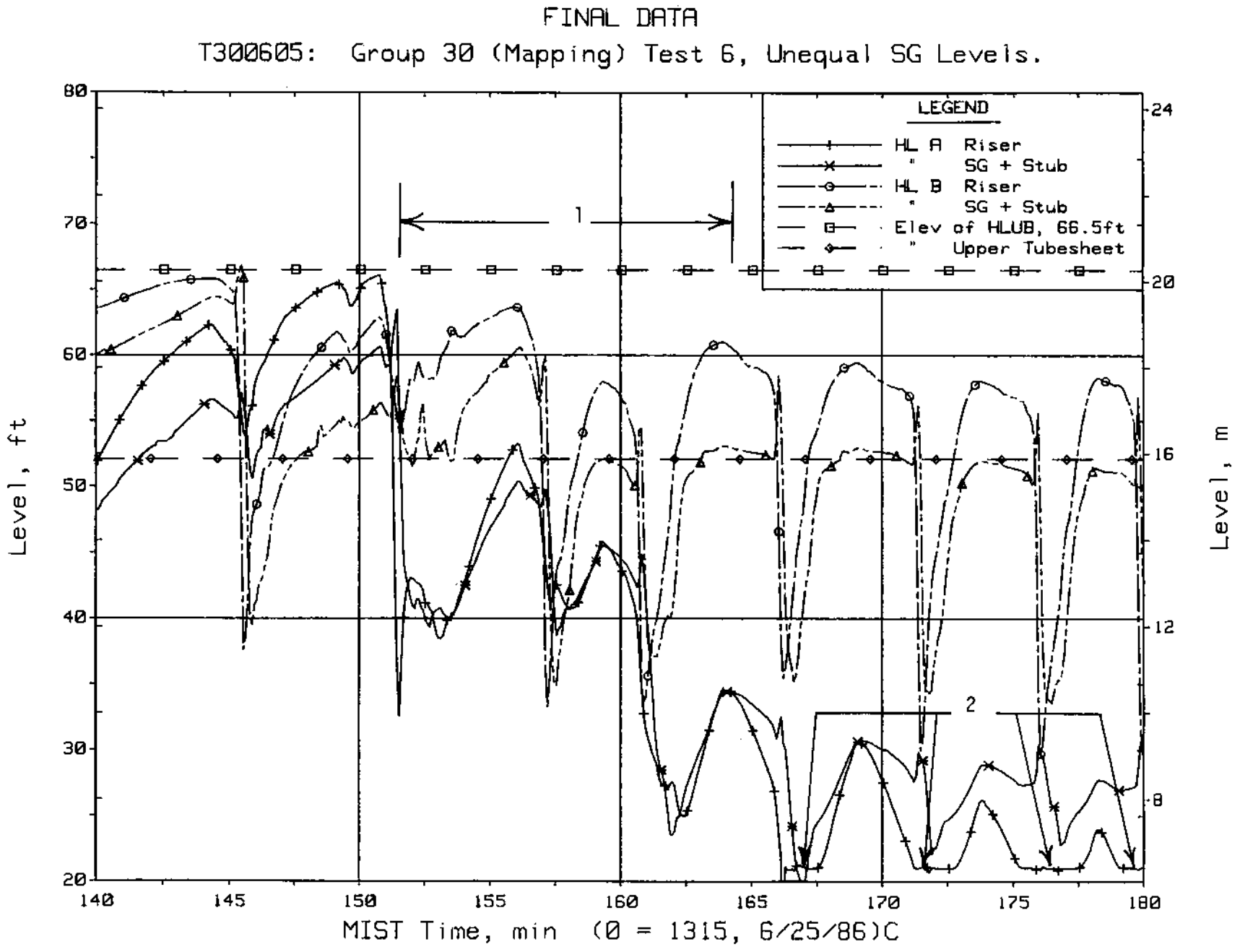

Figure 5.4.28. Hot Leg Riser and Stub Collapsed Liquid Levels

Tue Feb 28 09:59:56 1989

HLLV1

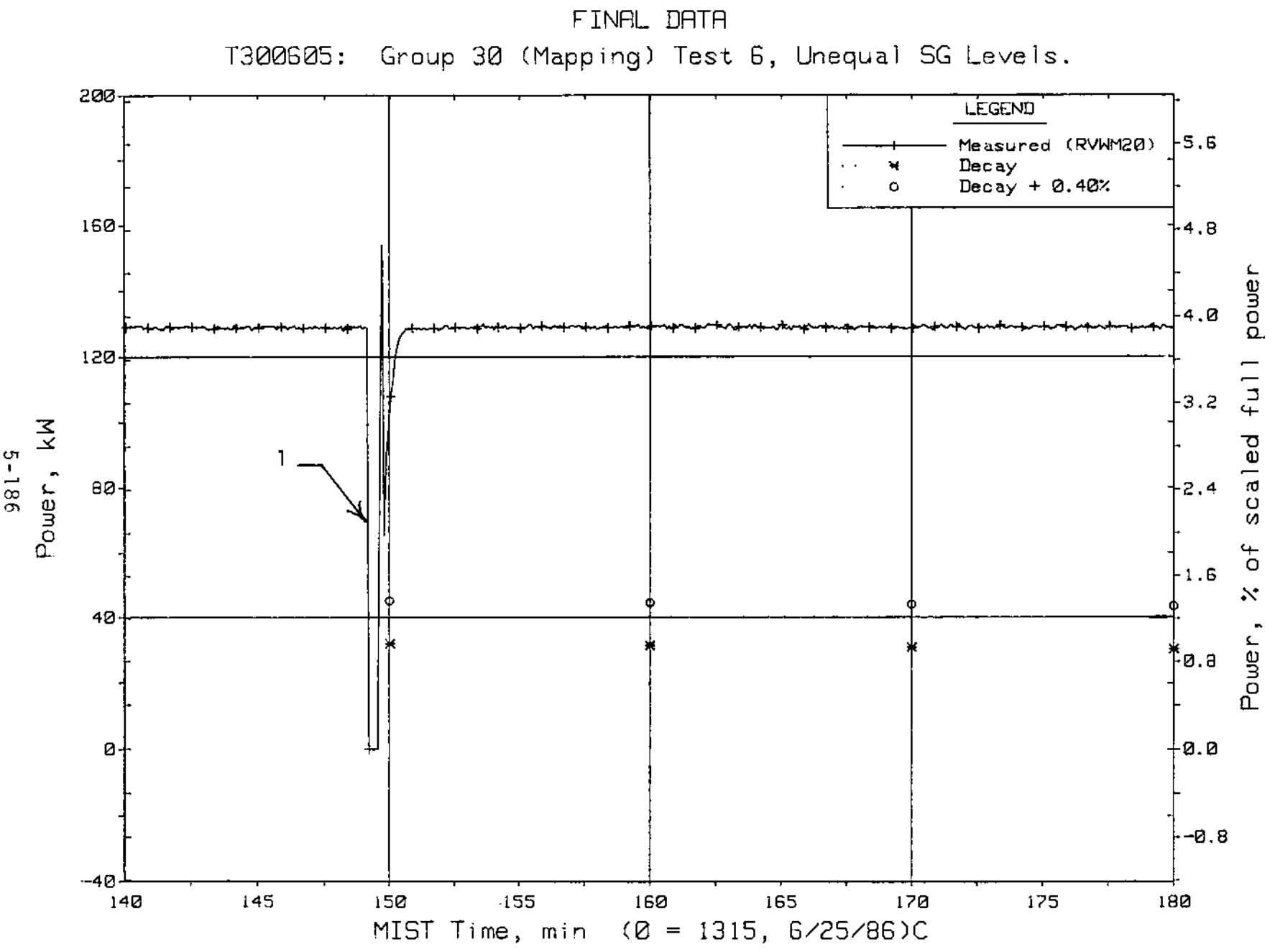

Figure 5.4.29. Core Power

Fri Feb 17 15:22:02 1989

RVKW1

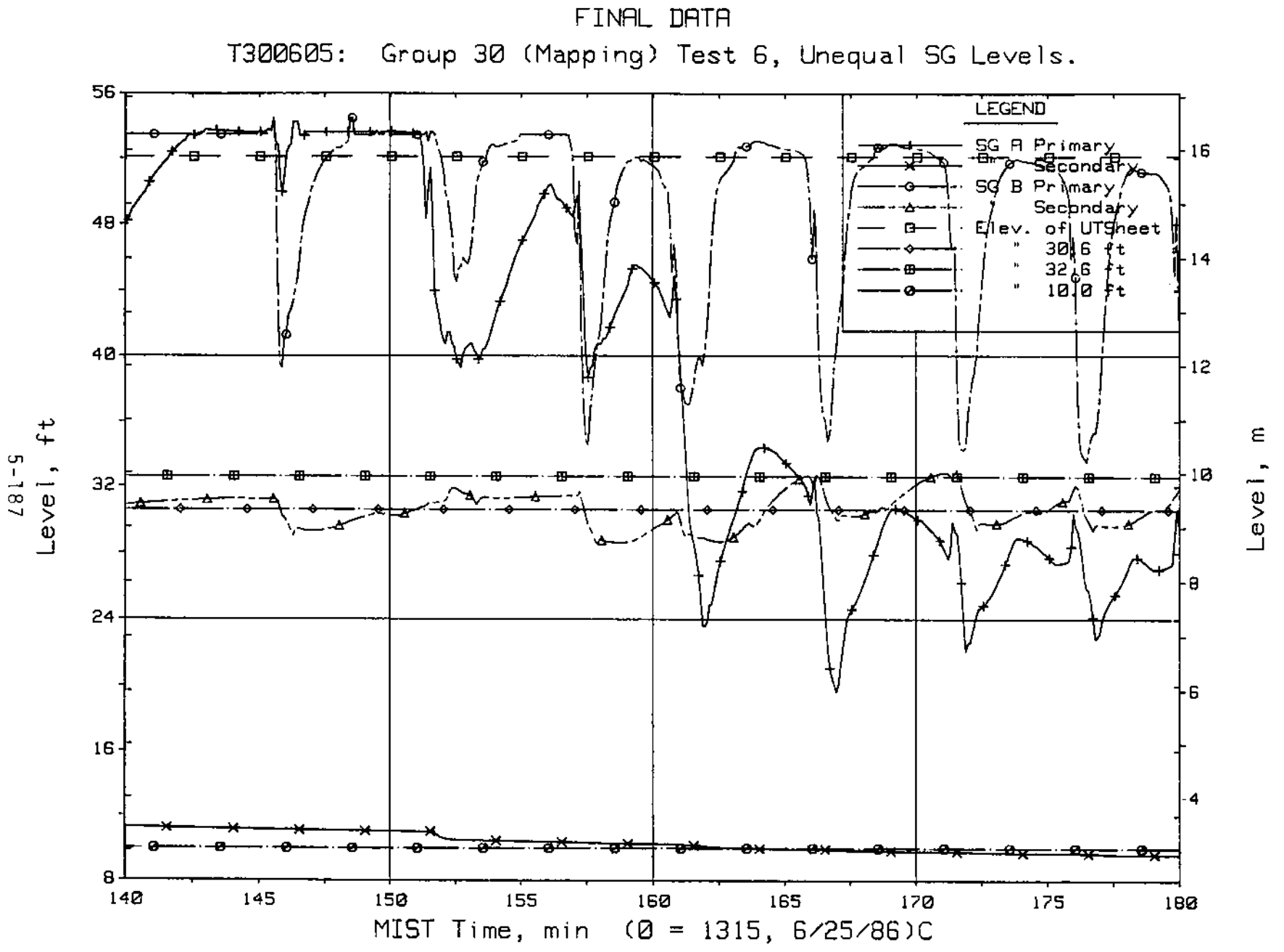

Figure 5.4.30. Steam Generator Collapsed Liquid Levels

Thu Mar 9 15:56:35 1989

SGLV2

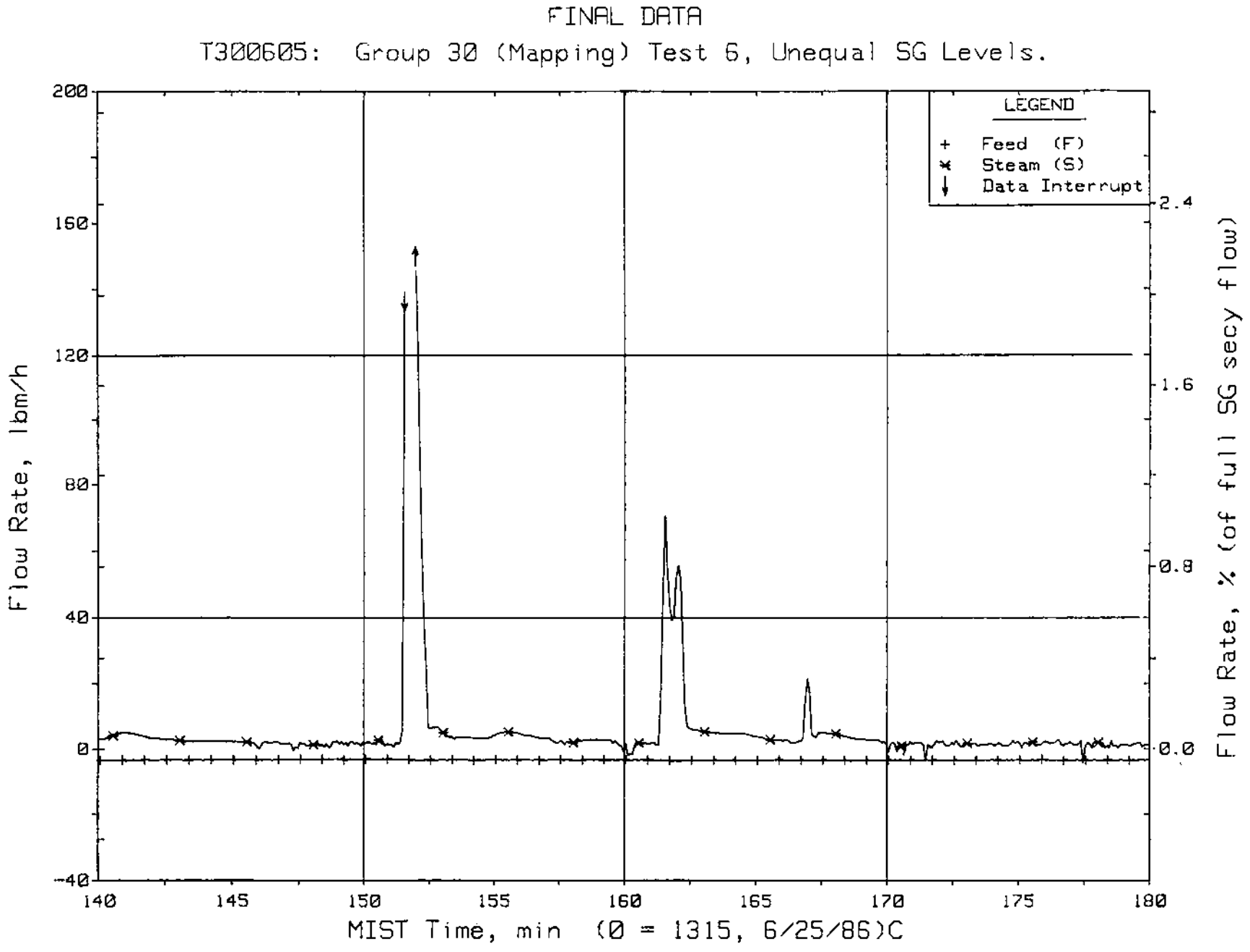

Figure 5.4.31. Steam Generator A Flow Rates (SaOR20s)

Fri Feb 17 15:24:07 1989

SCFL1

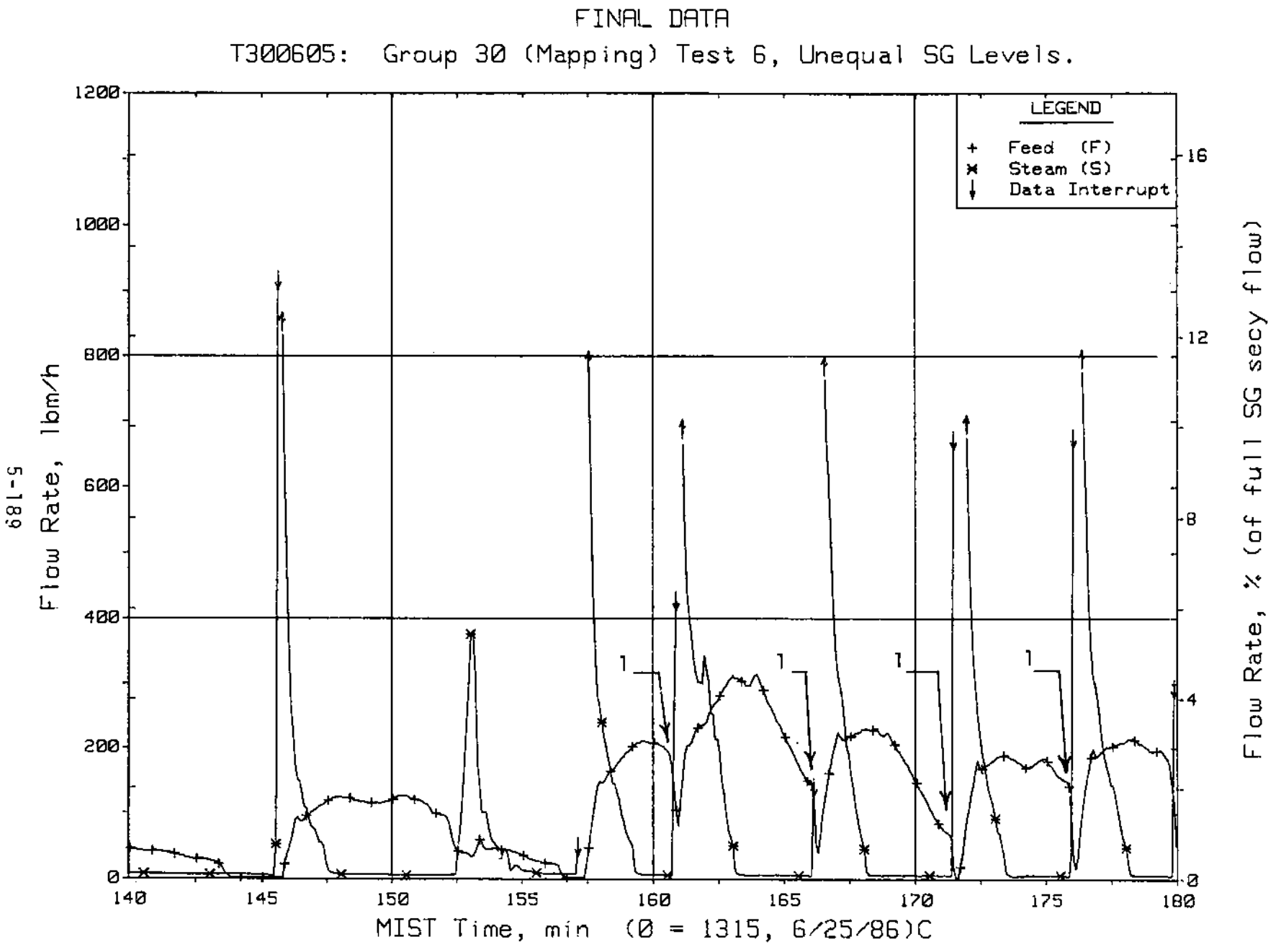

Figure 5.4.32. Steam Generator B Flow Rates (SaOR21s)

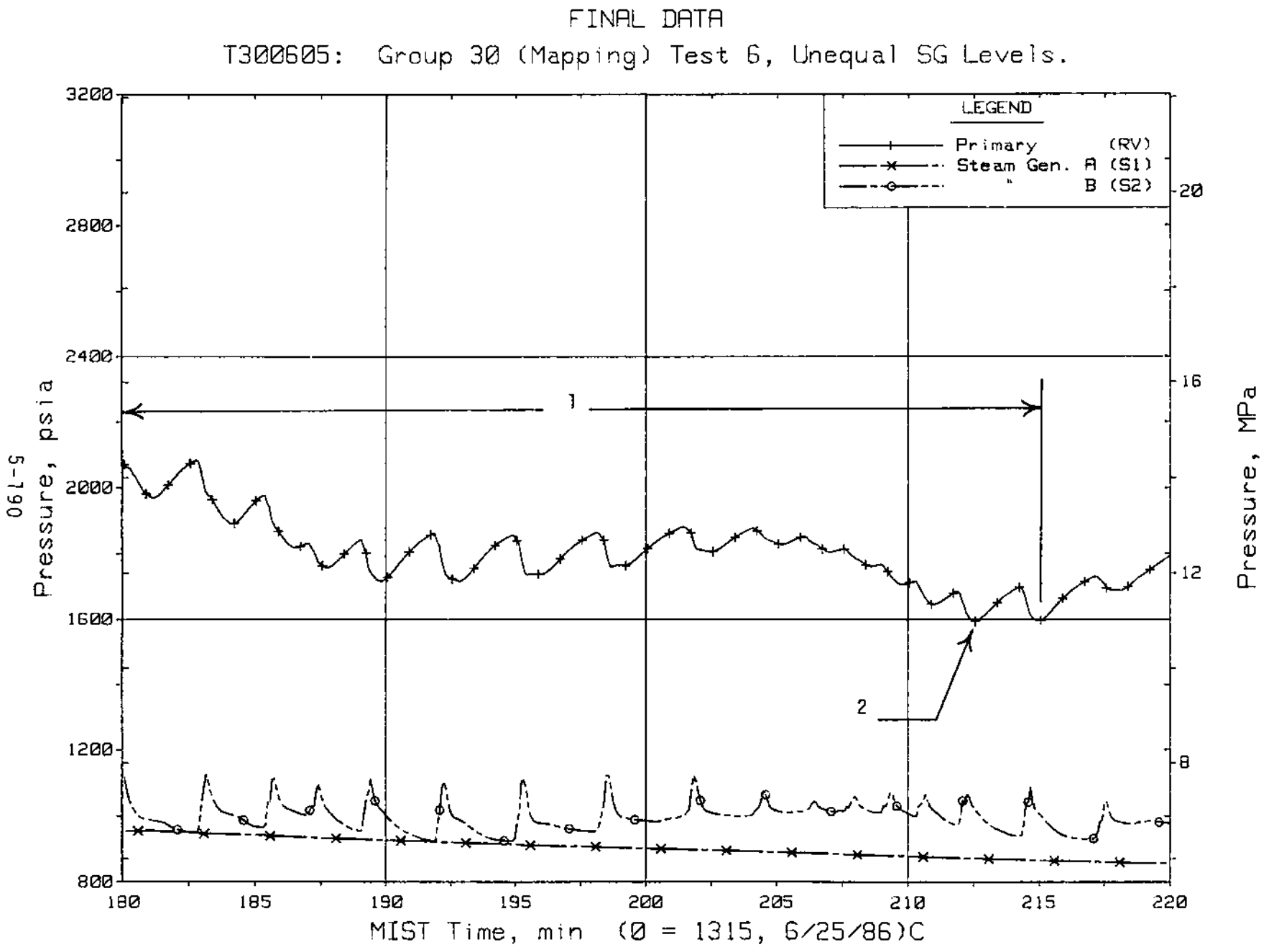

Figure 5.4.33. Primary and Secondary System Pressures (GP01s)

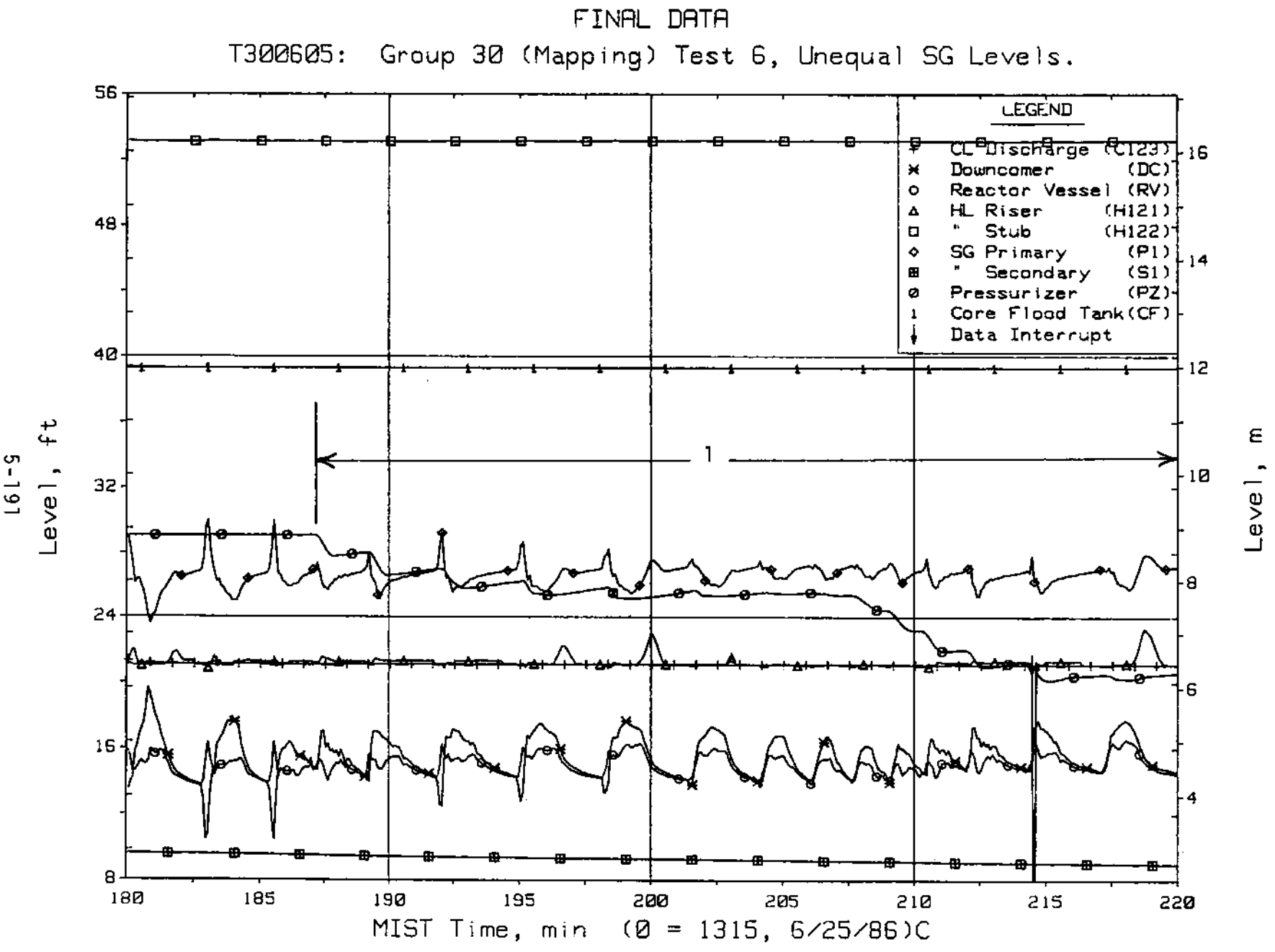

Figure 5.4.34. Loop A Collapsed Liquid Levels (LV20s)

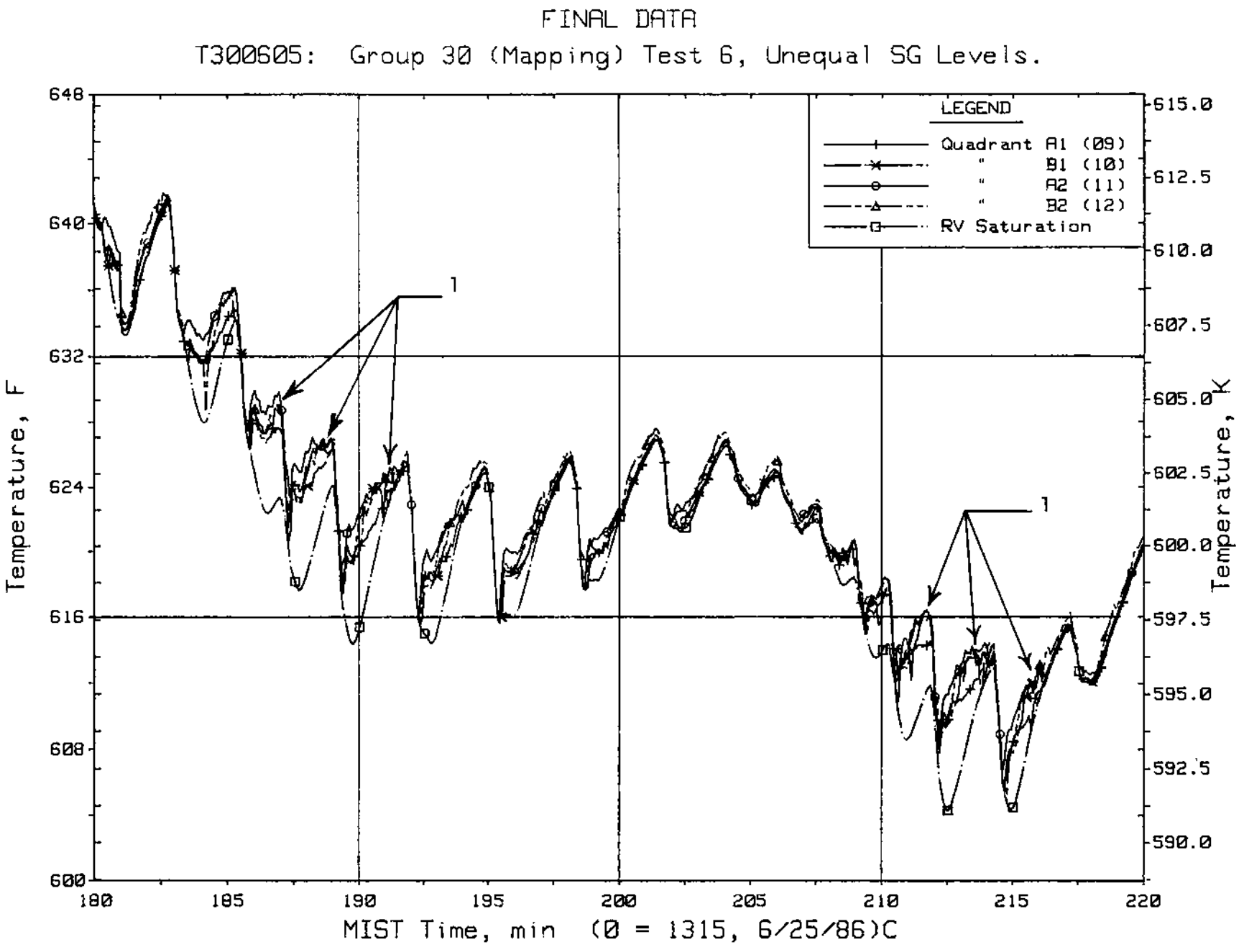

Figure 5.4.35. Downcomer Fluid Temperatures Above Nozzles, Elevation 21.9 ft (DCTCs)

Fri Feb 17 15:07:40 1989

DCTR6

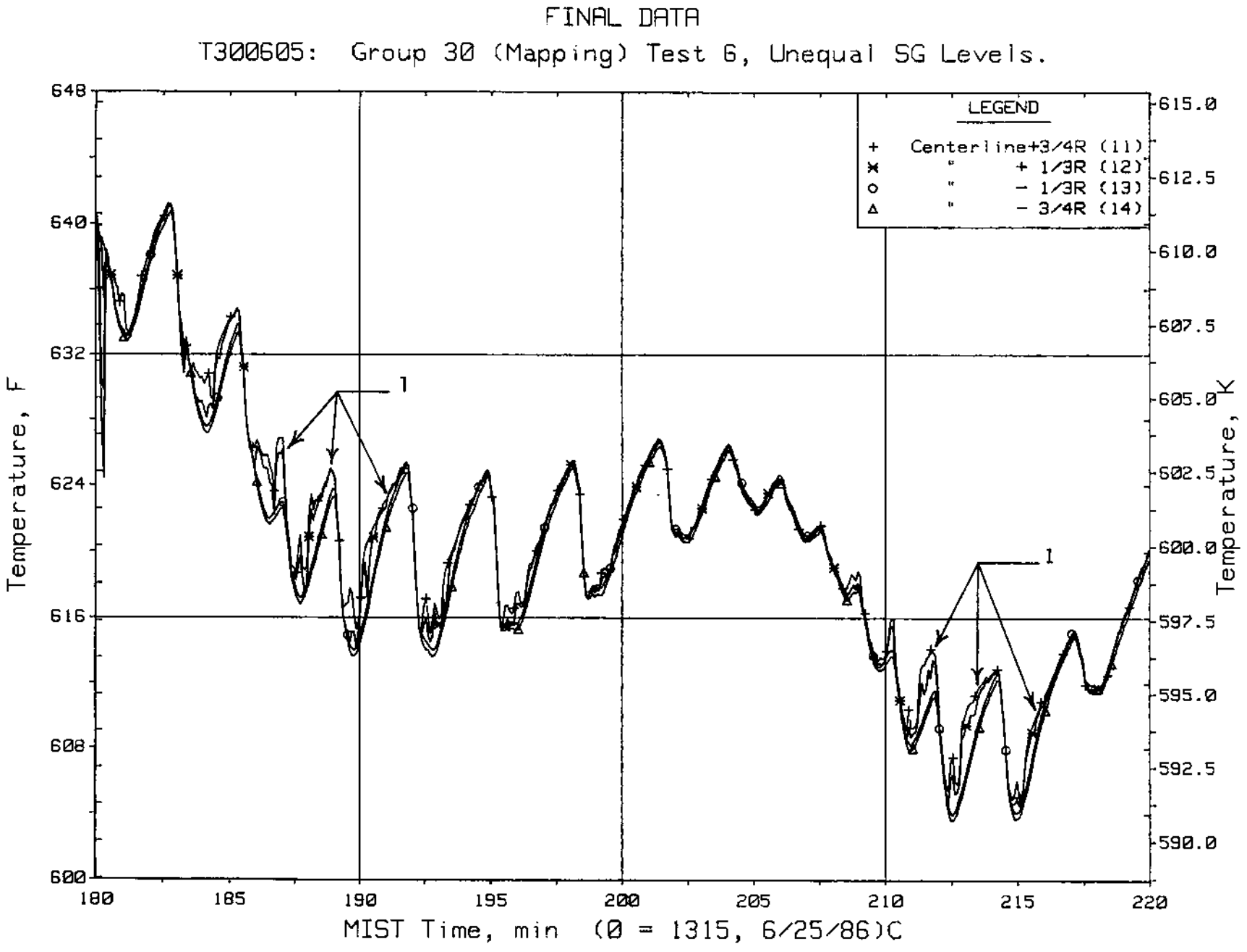

Figure 5.4.36. Cold Leg A1 Nozzle Rake Fluid Temperatures (21.2 ft, C1TCs)

Tue Feb 21 15:02:45 1989

C1TC4

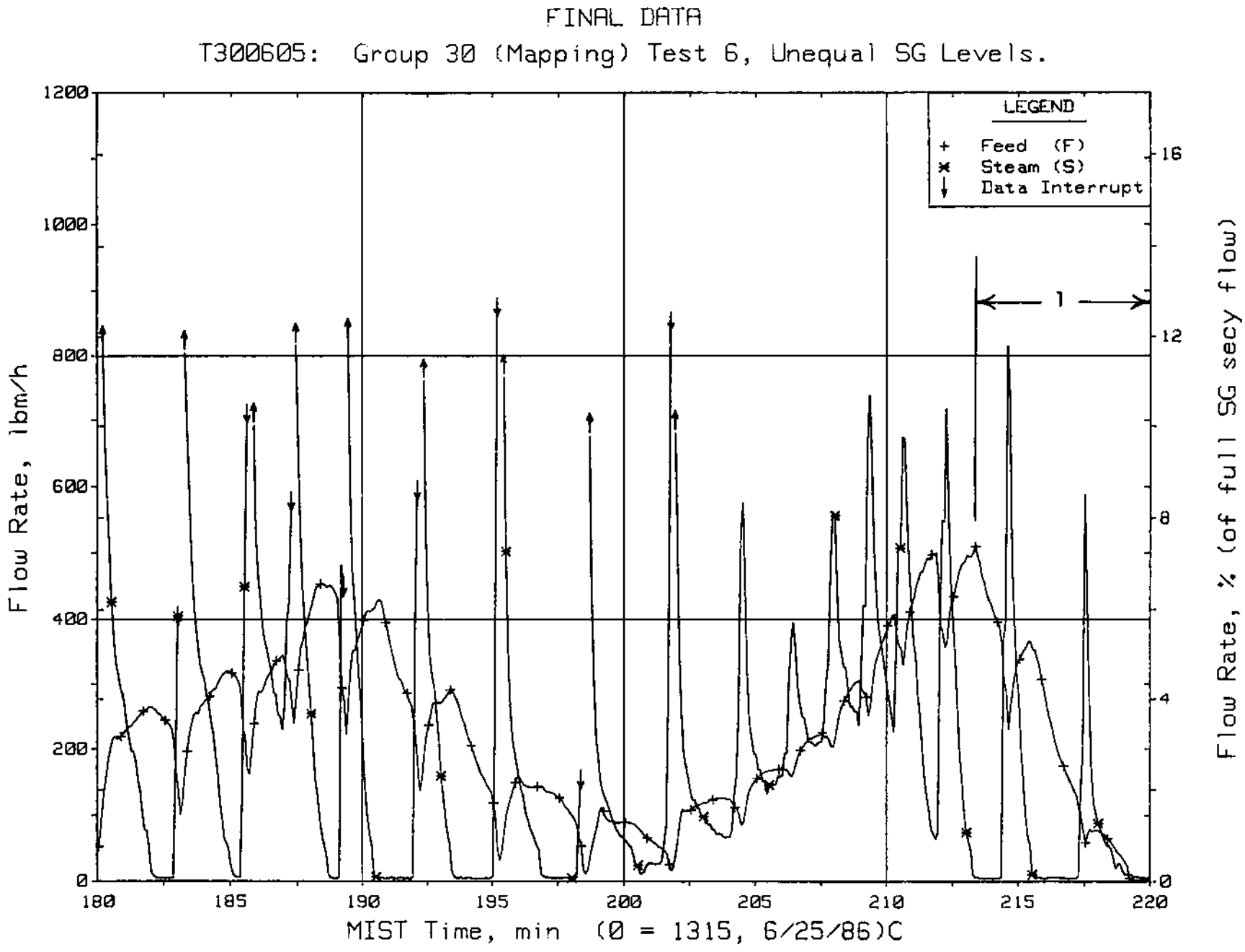

Figure 5.4.37. Steam Generator B Flow Rates (SaOR21s)

Tue Feb 21 15:12:34 1989

SCFL2

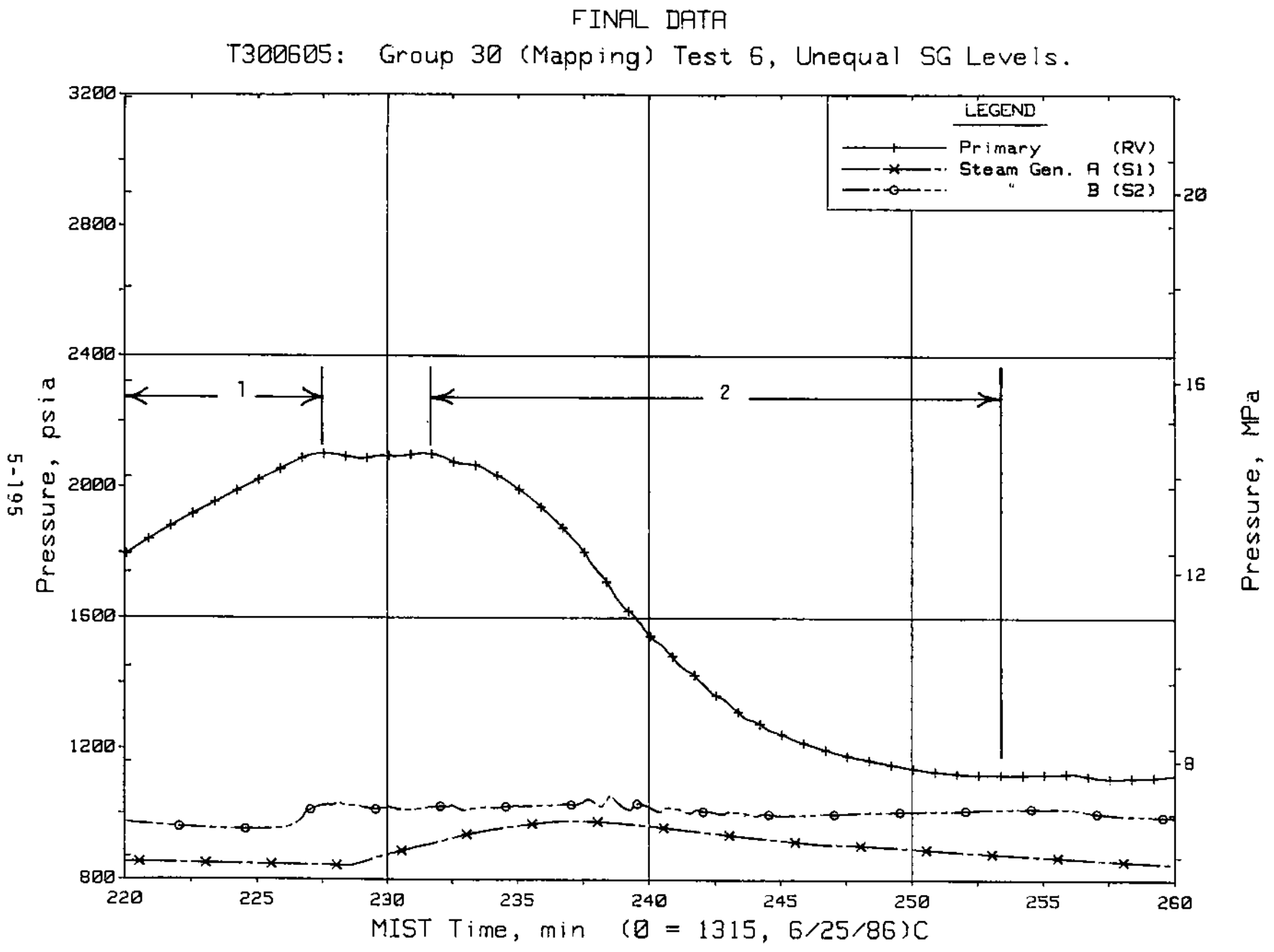

Figure 5.4.38. Primary and Secondary System Pressures (GP01s)

Tue Feb 21 15:16:20 1989

PSGP1

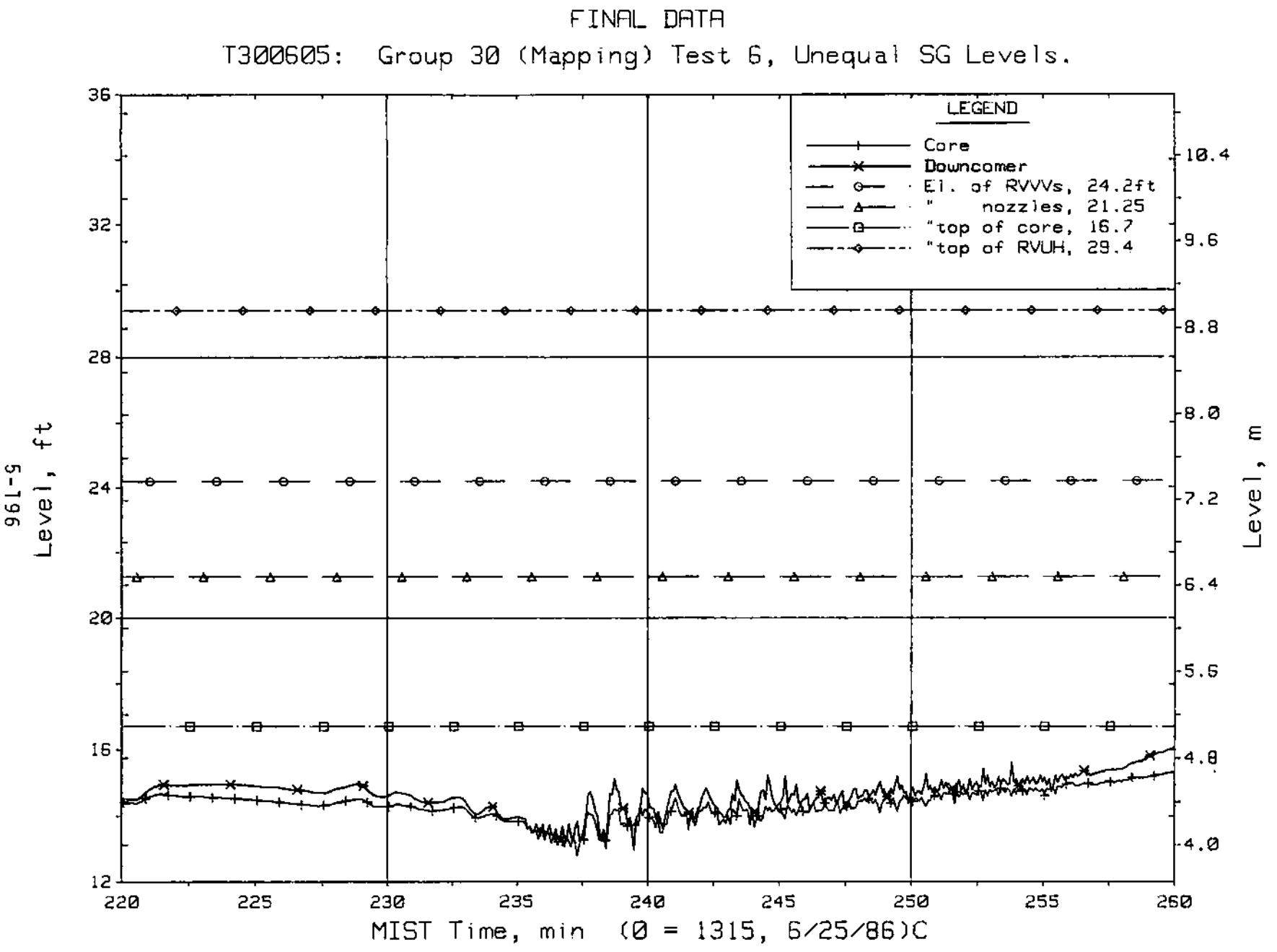

Figure 5.4.39. Core Region Collapsed Liquid Levels

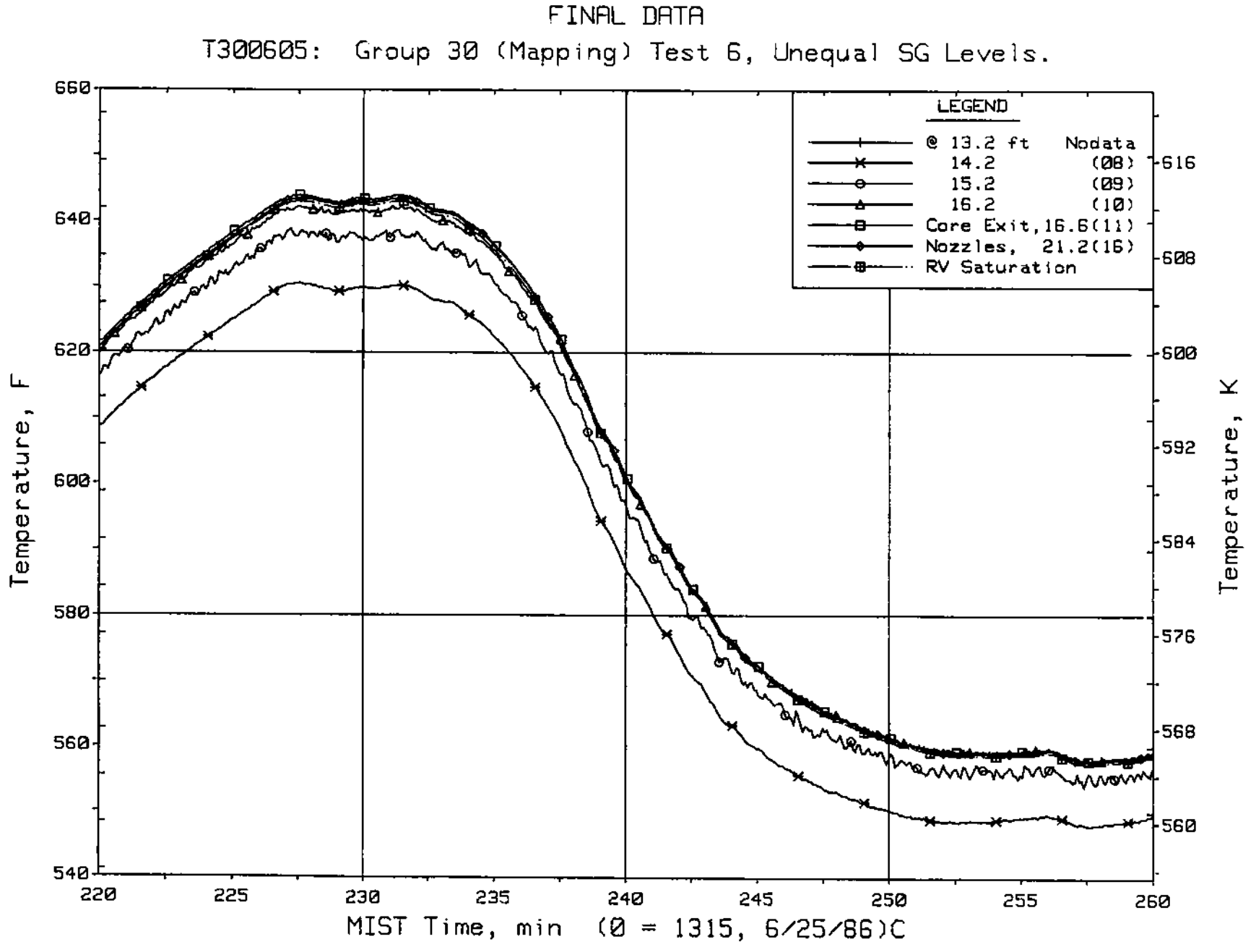

Figure 5.4.40. Reactor Vessel Mid-Elevation Fluid Temperatures (RVTCs)

Fri Feb 17 14:33:09 1989

RVTC2

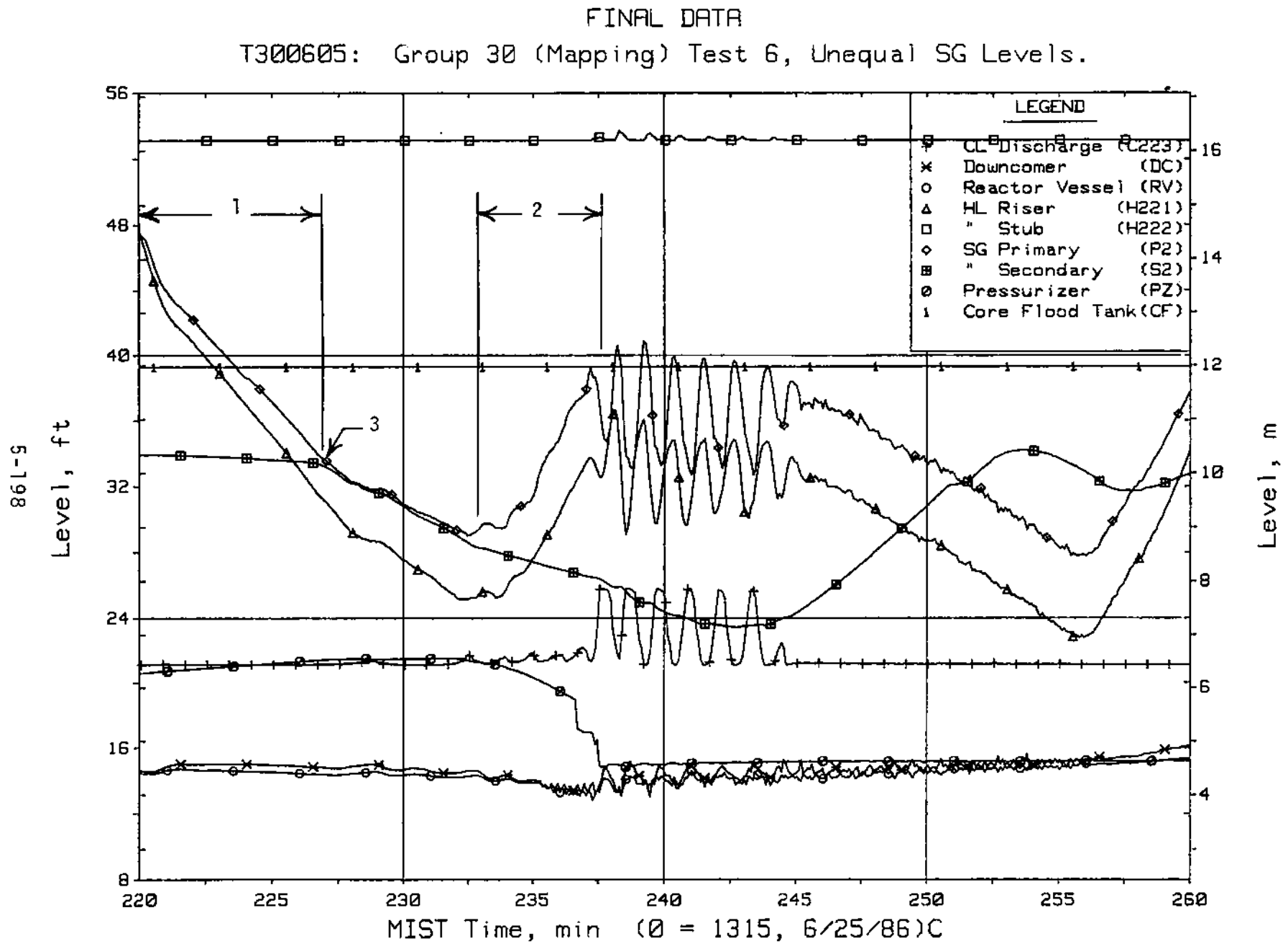

Figure 5.4.41. Loop B Collapsed Liquid Levels (LV20s)

Fri Feb 17 14:36:45 1989

PRLV2

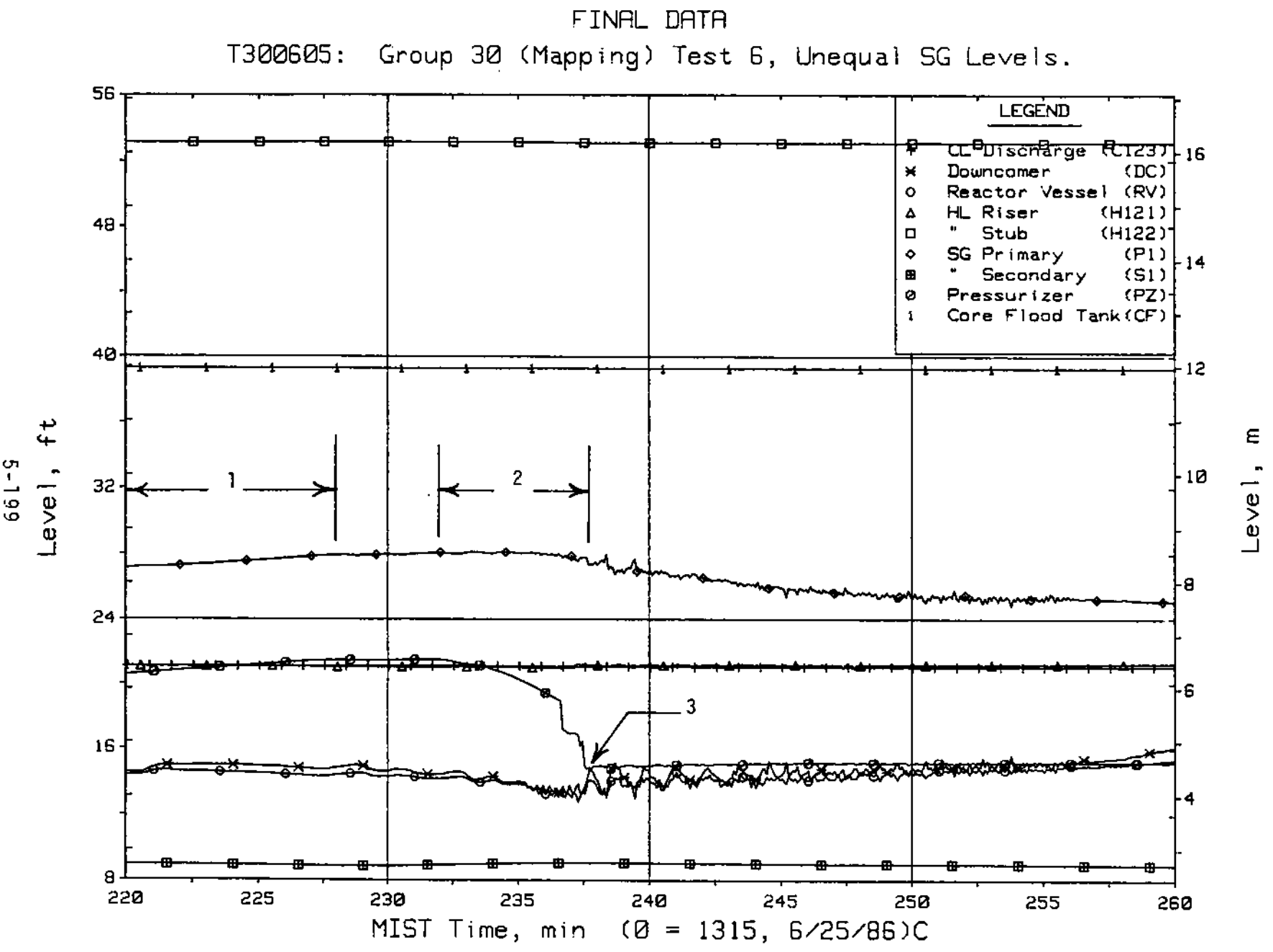

Figure 5.4.42. Loop A Collapsed Liquid Levels (LV20s)

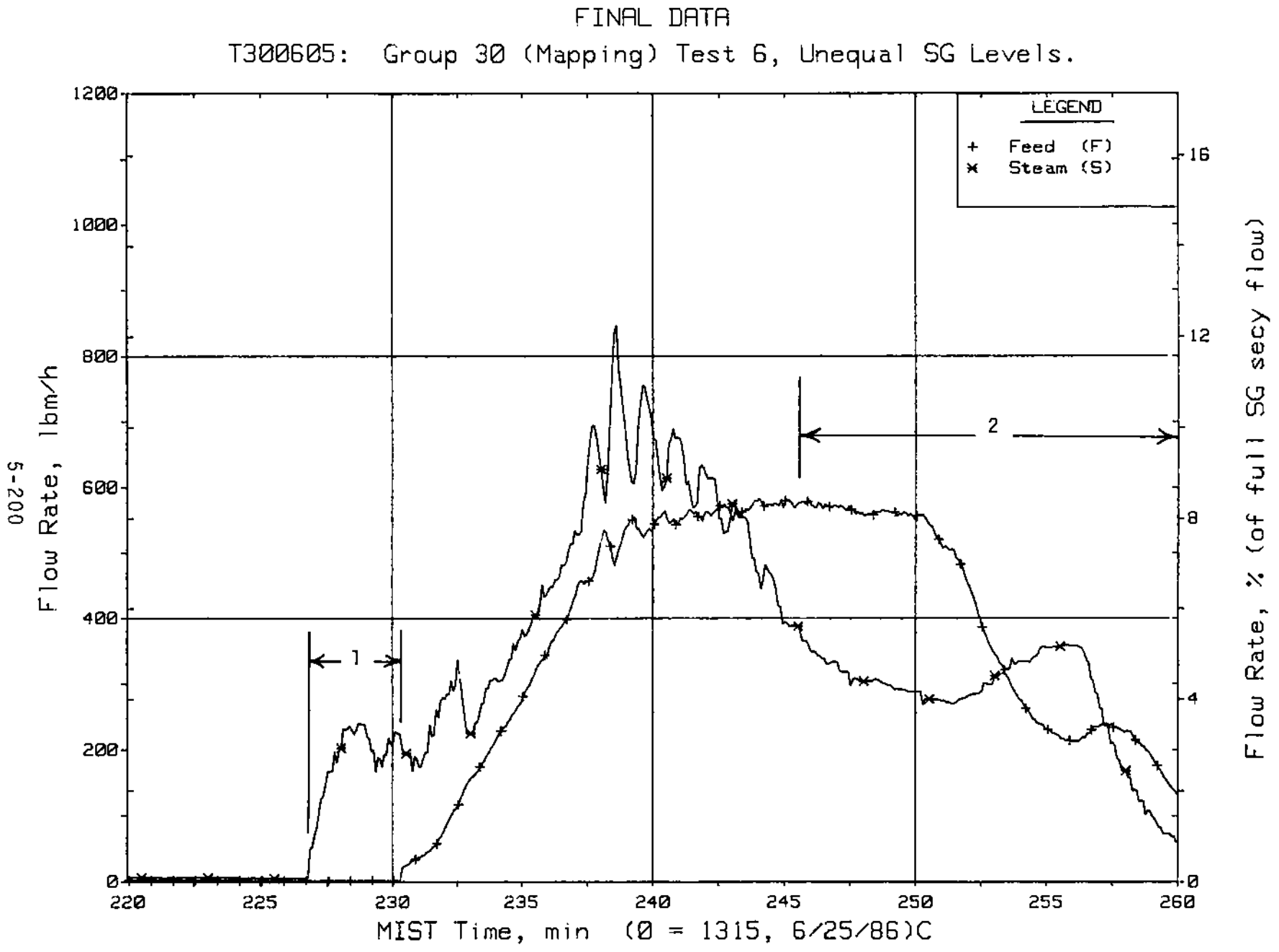

Figure 5.4.43. Steam Generator B Flow Rates (SaOR21s)

Fri Feb 17 14:42:25 1989

SCFL2

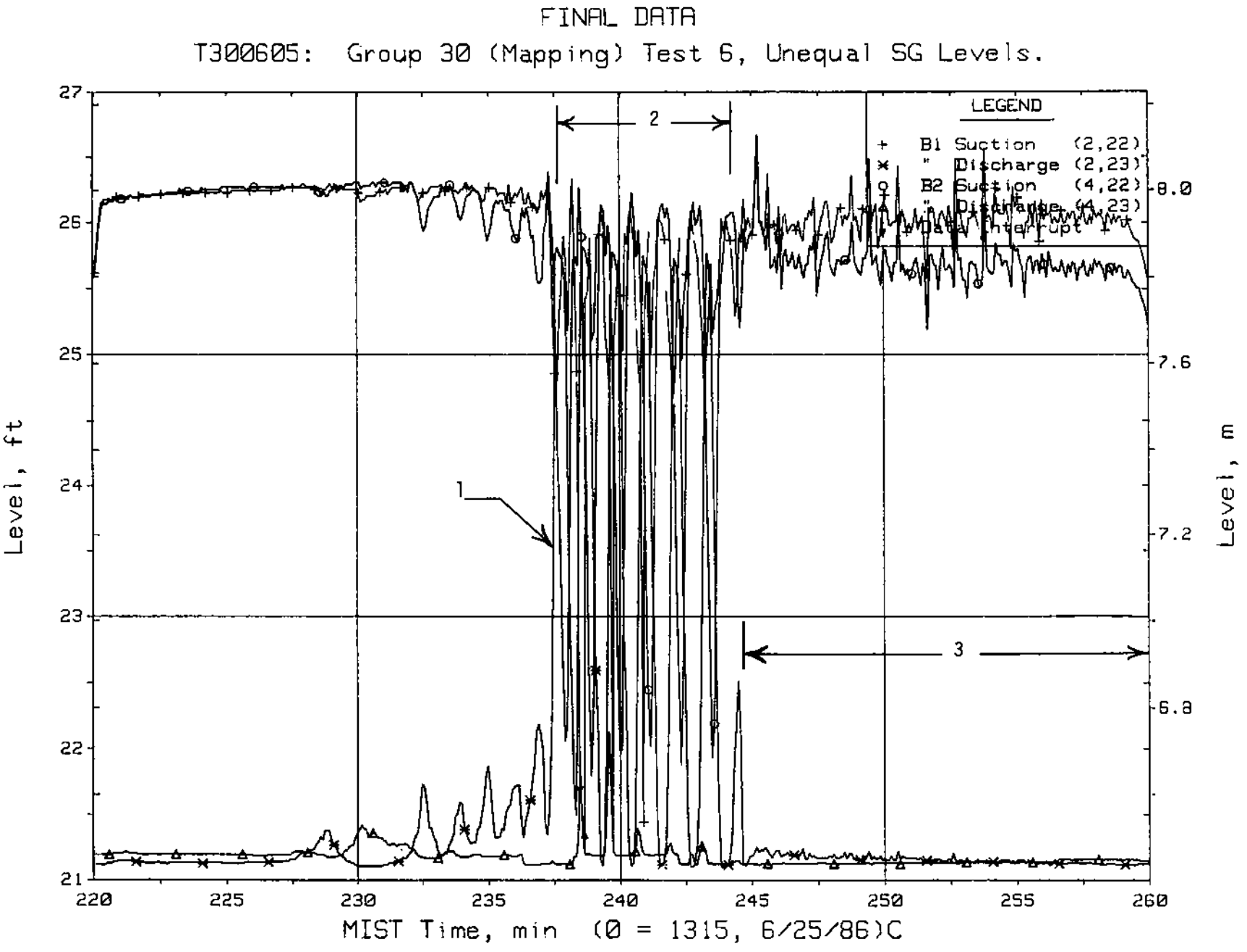

Figure 5.4.44. Loop B Cold Leg Collapsed Liquid Levels (LVs)

Tue Feb 21 15:26:52 1989

CLLV2

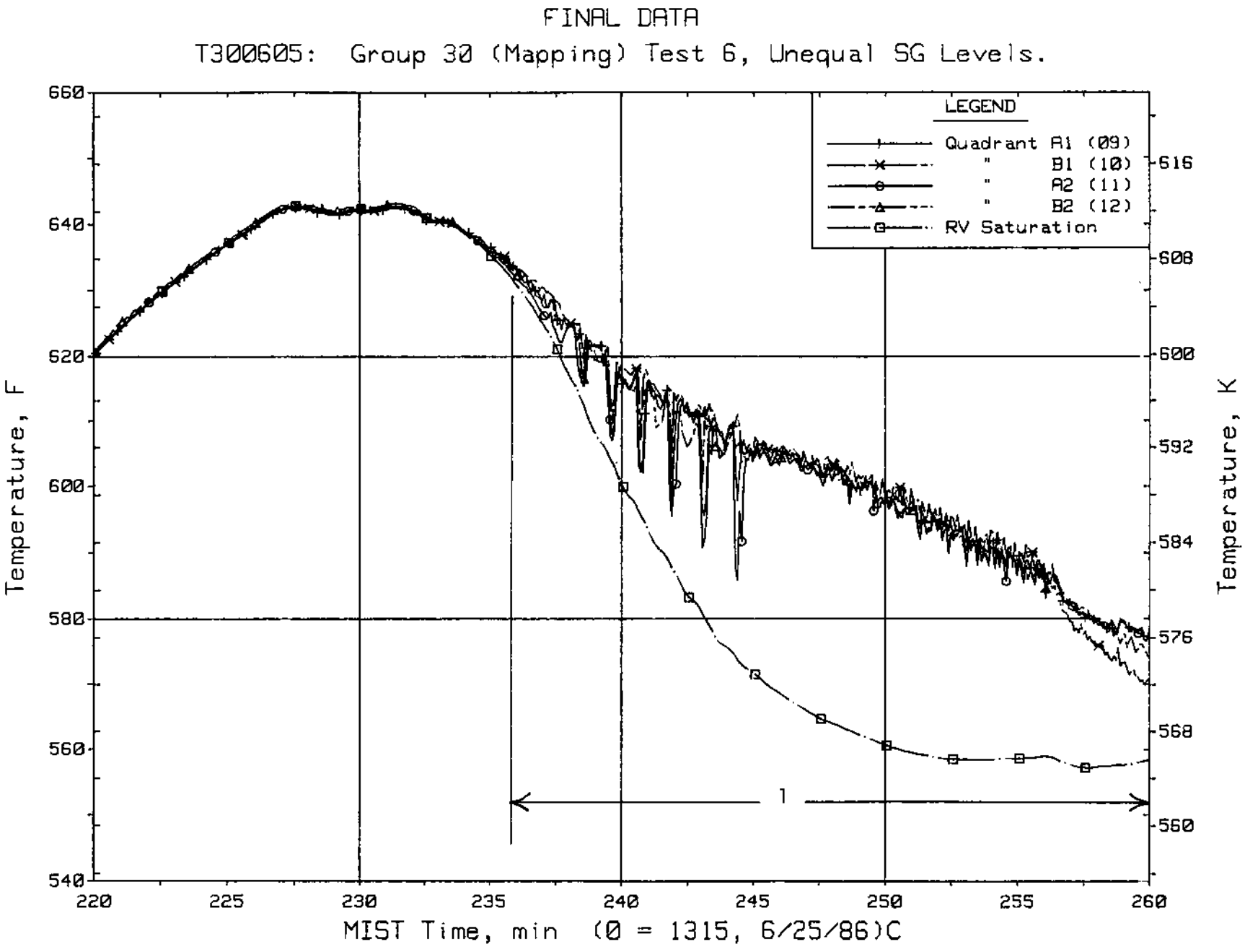

Figure 5.4.45. Downcomer Fluid Temperatures Above Nozzles, Elevation 21.9 ft (DCTCs)

Fri Feb 17 14:47:43 1989

DCTR6

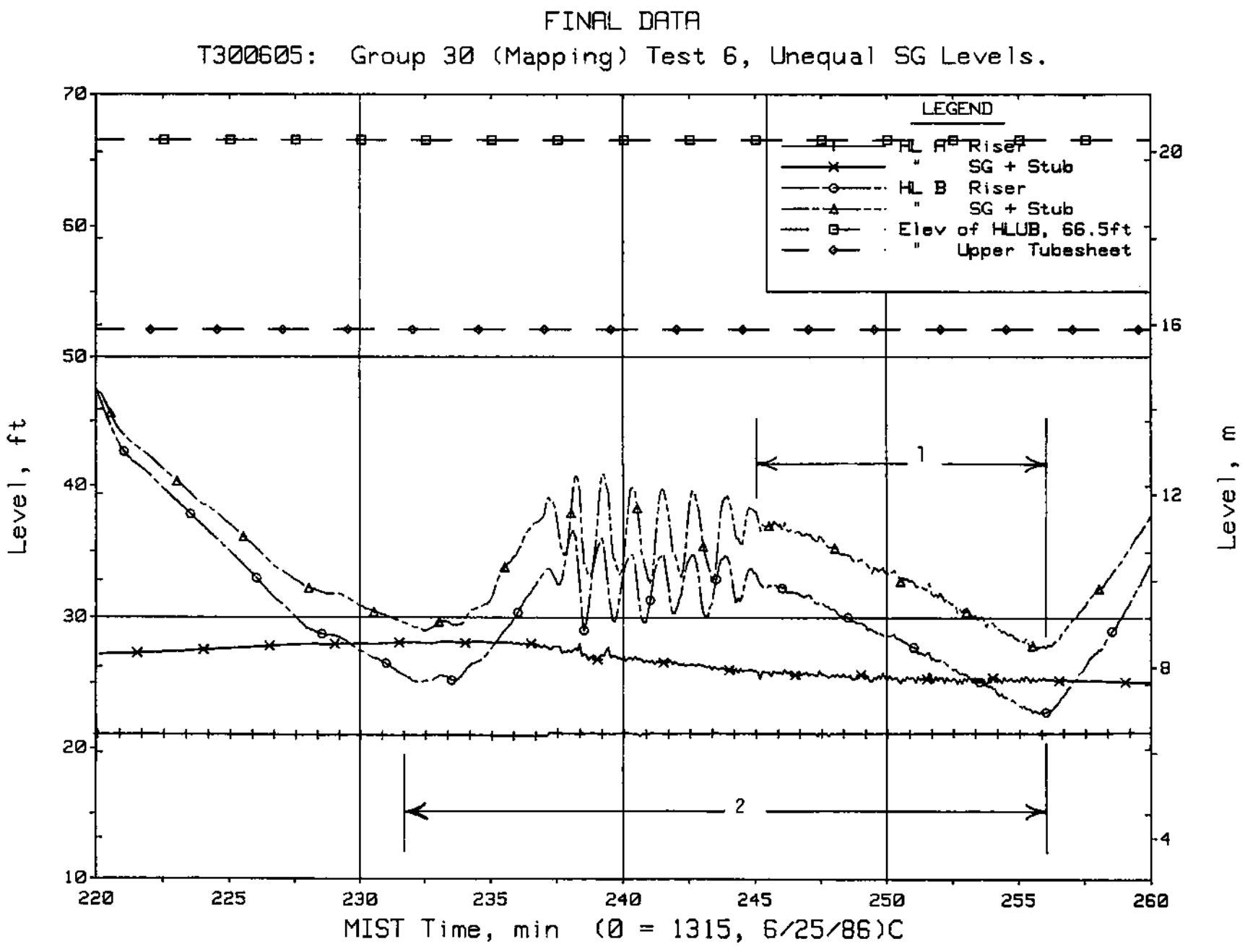

Figure 5.4.46. Hot Leg Riser and Stub Collapsed Liquid Levels

Thu Mar 9 15:42:27 1989

HLLV1

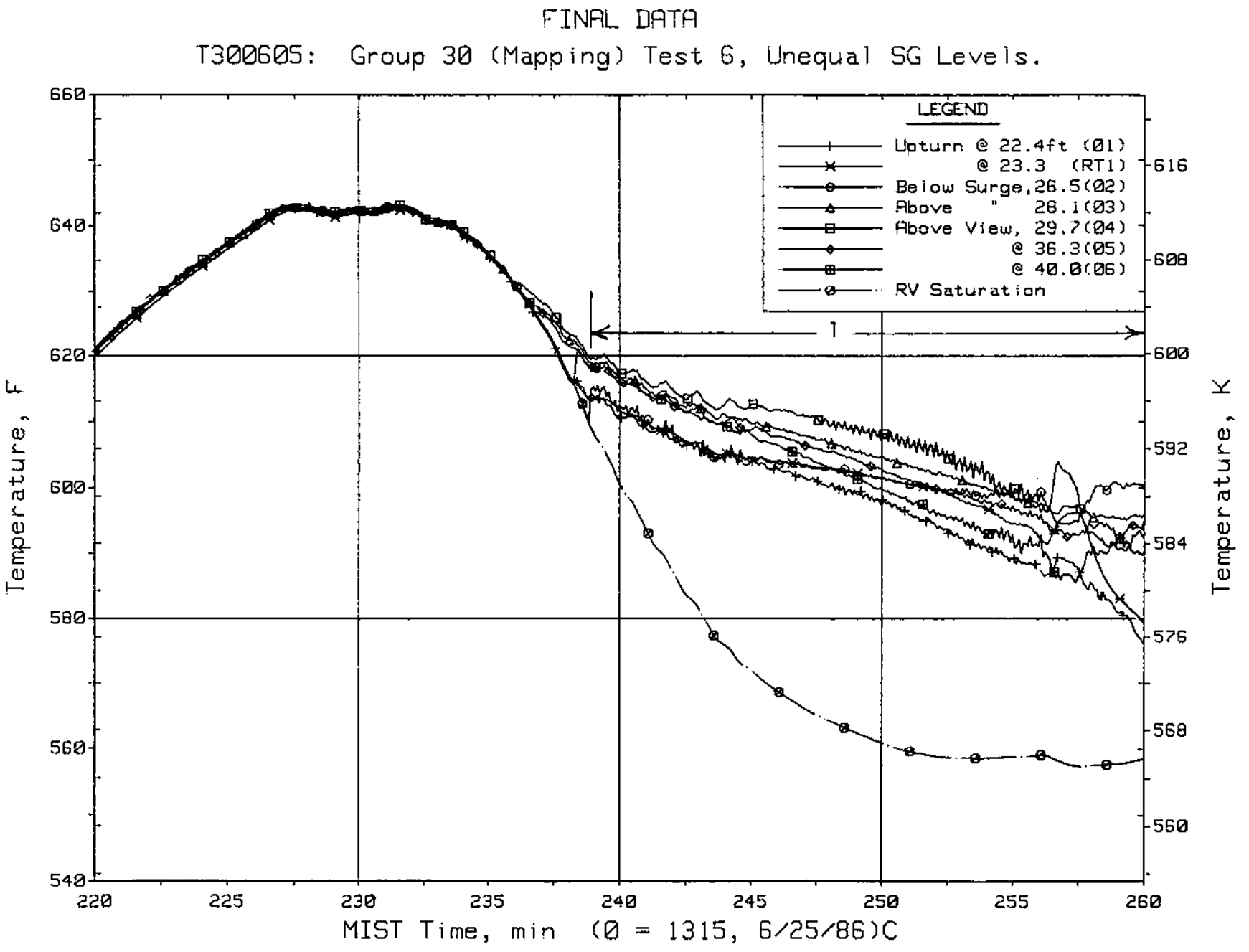

Figure 5.4.47. Hot Leg A Lower-Elevation Riser Fluid Temperatures (H1TCs)

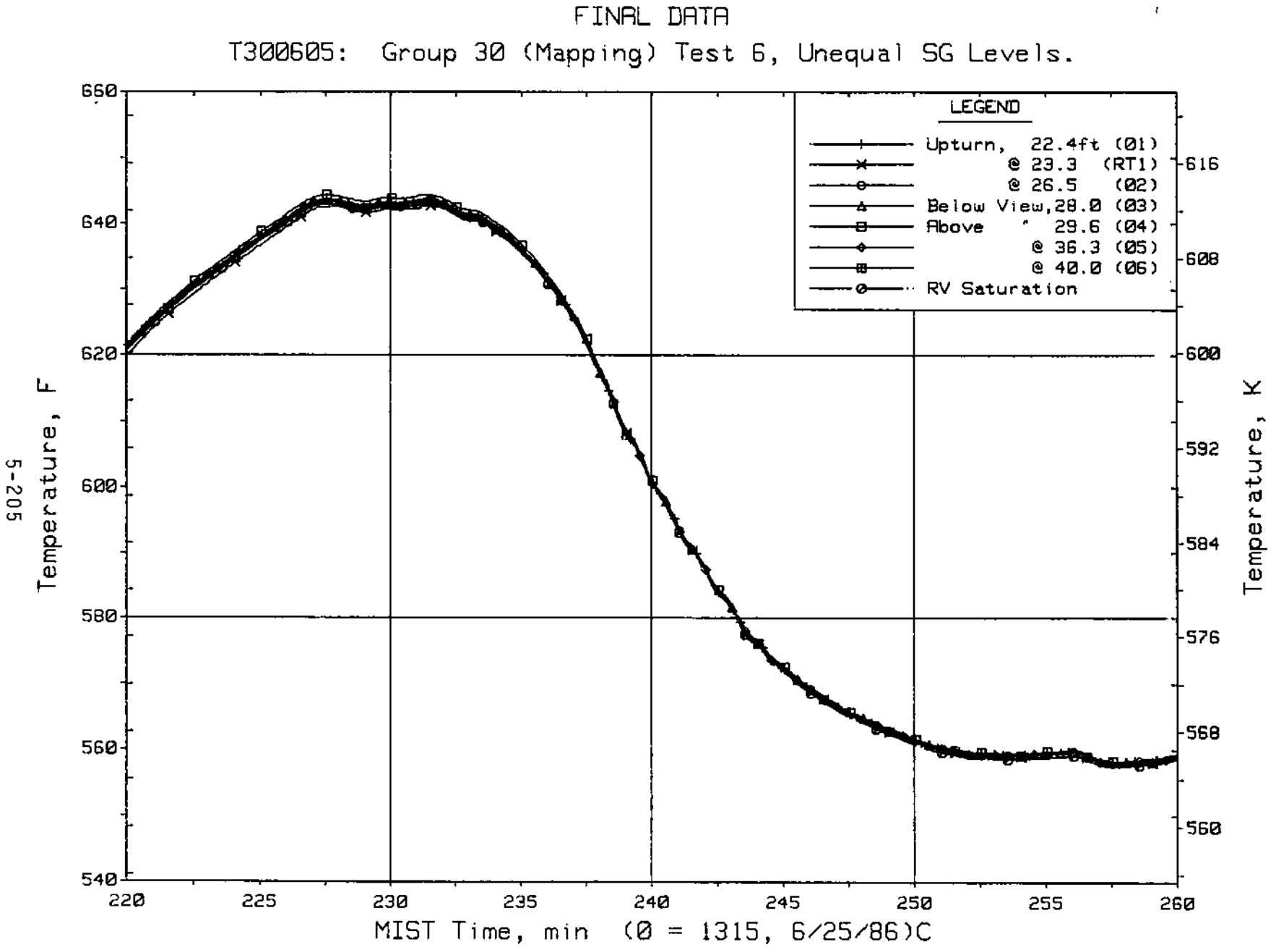

Figure 5.4.48. Hot Leg B Lower-Elevation Riser Fluid Temperatures (H2TCs)

Fri Feb 17 14:58:18 1989

H2TC1

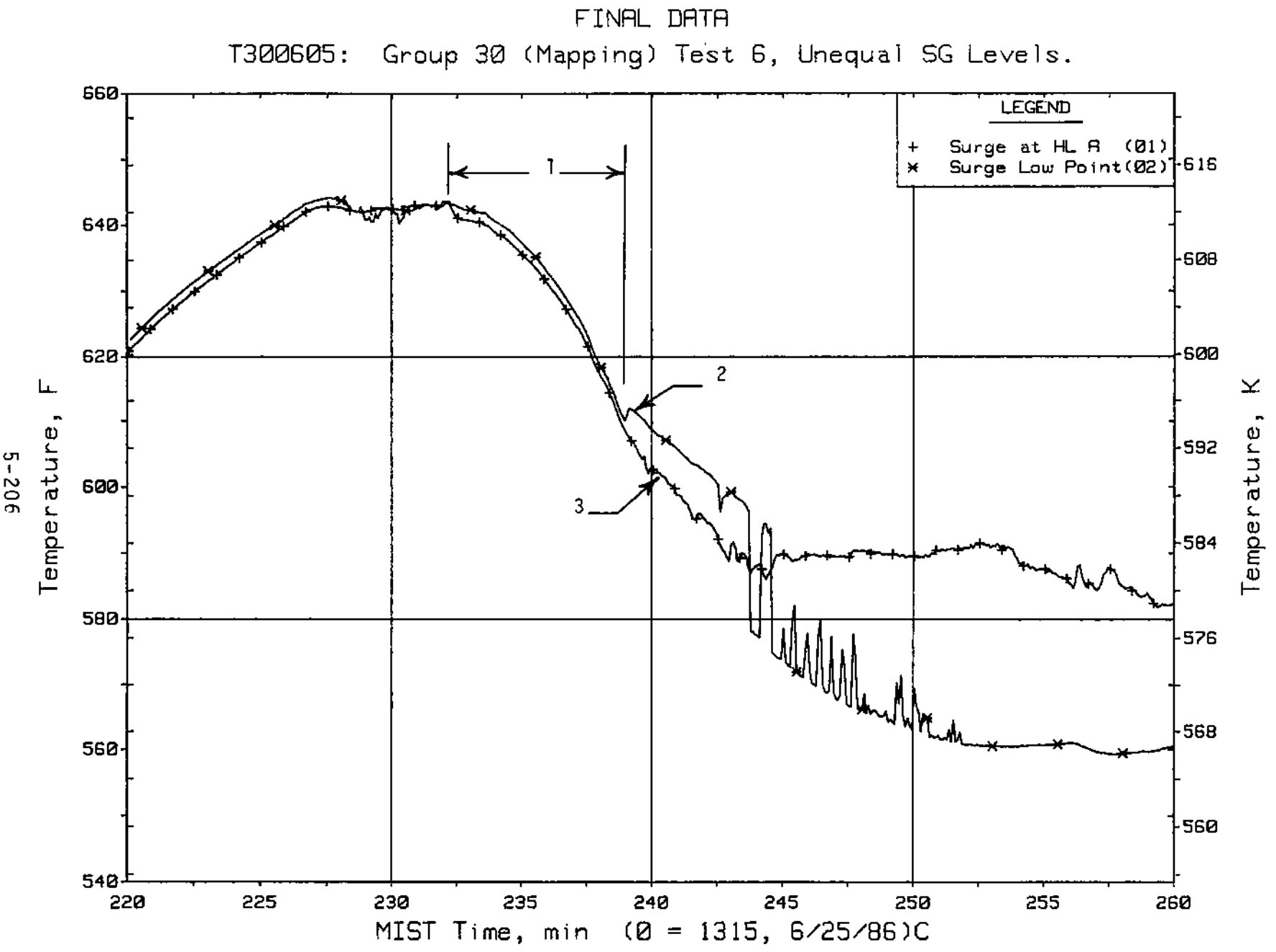

Figure 5.4.49. Pressurizer Surge and Spray Fluid Temperatures (PZTCs)

5.5. Steam Generator Secondary Levels at 10 ft Test (3007CC)

Test 3007CC was initially specified to maintain the steam generator secondary levels at 5 ft. However, level control difficulties were experienced at 5 ft. The level control setpoint was therefore increased to 10 ft to obtain better level control. This change still maintained the elevation of the secondary pool below the core mid-height elevation so that AFW rather than pool effects would be highlighted during the BCM.

This test repeated Test 300705, which had been terminated (due to plugged leak orifices) prior to attaining BCM. Test 3007CC was conducted in a manner that attempted to eliminate the duplication of the initial phases of Test 300705, thereby reduce testing time. This reduction was accomplished by initially establishing a high leak-HPI deficit and therefore rapidly depleting the primary system inventory.

Test 3007CC was initialized with the HPI flow equal to the leak flow rate. At test initiation, the HPI flow rate was decreased rapidly as the loop operator established a leak-HPI deficit of approximately 300 lb/h (Figure 5.5.1, See 1). This leak-HPI deficit was approximately 250 lb/h greater than that of the Nominal Test and resulted in a rapid primary system depressurization (Figure 5.5.2, See 1).

The reduction in HPI flow resulted in an increase in the mixed-mean temperature of the fluid in the cold leg discharge pipes (Figure 5.5.3, See 1). The mixing of this fluid with the fluid discharged through the reactor vessel vent valves therefore resulted in an increase in the downcomer fluid temperature (Figure 5.5.4, See 1). This increased fluid temperature propagated to the core inlet and outlet. The increased core exit temperature resulted in a higher primary system saturation pressure, ~1420 (Figure 5.5.2, See 2) versus ~1300 psia as observed in the Nominal Test when the pressurizer inventory had drained.

The phenomena observed in Test 3007CC then replicated that observed in the Nominal Test (3003AA). The reactor vessel head voided and reached the reactor vessel vent valve elevation, the downcomer voided, reactor vessel vent valve cycling commenced, and backflow occurred in the cold legs. When the downcomer level descended to the cold leg nozzle elevation, the reactor

vessel vent valves opened and remained open, thereby permitting a backflow of steam into the cold leg discharge pipes. A momentary flow interruption occurred in each cold leg.

Subsequent to the momentary flow interruption, intra-cold leg flow was established in both loops (cold legs A1 and B1 flowed backward while cold legs A2 and B2 flowed forward, See 1 on Figures 5.5.5 and 5.5.6). After the flow reversal, a brief period of reduced forward flow was observed in cold legs A1 and B1 (See 2 on Figures 5.5.5 and 5.5.6).

As the drain continued, Test 3007CC experienced the same flow interruption phenomena as the Nominal Test. The order in which the cold leg flows interrupted (B1, A1, B2, then A2) was similar to that observed for the Nominal Test. The increased leak-HPI deficit for Test 3007CC resulted in cold leg flow interruptions that occurred almost simultaneously in cold legs B1 and A1 (See 3 on Figures 5.5.5 and 5.5.6) followed by almost simultaneous flow interruptions in cold legs B2 and A2 (See 4 on Figures 5.5.5 and 5.5.6).

The flow interruptions occurred at a primary system pressure of approximately 1480 psia, which was also similar to that observed for the Nominal Test (3003AA). As a result of the complete flow interruption, the primary system pressure increased (Figure 5.5.2, See 3) and the fluid in the hot legs subcooled (See 1 on Figures 5.5.7 and 5.5.8).

Subsequent to the complete flow interruption, the loop operator increased HPI flow and established a leak-HPI deficit of approximately 100 lb/h (Figure 5.5.1, See 2). This leak-HPI deficit was chosen to be similar to that of the Nominal Test during the repressurization phase and the onset of BCM.

After the loop operator increased the HPI flow, forward flow was reestablished in cold leg B2 (Figure 5.5.6, See 5) and the primary system pressure stabilized at approximately 1530 psia (Figure 5.5.2, See 4). The reason for the reestablishment of forward flow by way of loop B and cold leg B2 is not understood. The predominant flow path was initially established in hot leg A as the pressurizer filled during the repressurization. This action is indicated by the increase in the hot leg inlet temperature occurring earlier in hot leg A than in hot leg B as the hot leg heatup began (Figure 5.5.7, See 2 and Figure 5.5.8, See 2). The hot leg A heatup then ceased and the hot leg

B heatup commenced and continued as the predominant flow path was established via loop B. The establishment of the predominant flow path via loop B may be caused by the slightly higher secondary level in steam generator B (Figure 5.5.9, See 1), thus a greater driving head existed in loop B.

The cold leg B2 flow interrupted again and complete flow interruption occurred again (Figure 5.5.10, See 1). The primary system response then replicated the phenomena observed in the Nominal Test (3003AA), i.e., lower region voiding, repressurization, hot leg heatup, establishment of forward flow, lower region void collapse, depressurization, and flow interruption. These phenomena continued and the primary system pressure increased from ~1540 to ~2310 psia (Figure 5.5.11, See 1). During this repressurization phase, the predominant flow path was established via loop A and appears to be caused by the location of the pressurizer in this loop (as described in the Nominal Test).

During the repressurization phase, two PORV actuations occurred (See 1 on Figures 5.5.12 and 5.5.13). The first PORV actuation was anticipated by the loop operator and was a manual actuation. The second PORV actuation was automatic. The pressurizer inventory had been increasing as the primary system repressurized (Figure 5.5.14, See 1). The pressurizer filled completely when the first PORV actuation occurred (Figure 5.5.14, See 2).

After the first PORV actuation, the hot leg and steam generator primary levels of both loops increased (Figure 5.5.15, See 1). The A levels then decreased and the B levels remained high and essentially constant (Figure 5.5.15, See 2). The indicated decreasing loop A levels appear to be caused by the heatup of hot leg A (leads the hot leg B heatup), the existence of steam and, therefore, voids in hot leg A. This event resulted in a decreasing indicated collapsed liquid level. The hot leg A fluid temperatures, however, indicated that the level increased during this time (Figure 5.5.16, See 1 and Figure 5.5.17, See 1) and appeared to result from the swell caused by the voids in the lower portion (and propagating upward) of hot leg A. The decreased density of the fluid in hot leg A resulted in a drain of the steam generator A primary fluid as the manometric balance of loop A was maintained.

Subsequent to the second PORV actuation, AFW-BCM was established. The lower region voiding-void collapse phenomena also occurred while BCM was in

progress, i.e., steam generator heat transfer was continuous (See 1 Figures 5.5.18 and 5.5.19) while the cold leg voids collapsed and revoided in response to the establishment of forward flow.

The phenomena observed in the cold legs at this time appears slightly different from that observed in the Nominal Test (3003AA). The voids in both cold leg B discharge pipes collapsed (e.g., Figure 5.5.20, See 1) coincident with a forward flow pulse. The voids in the cold leg A1 discharge pipe also collapsed (e.g., Figure 5.5.21, See 1), but to a lesser extent than observed in the cold legs of B, coincident with a forward flow pulse. The voids in the cold leg A2 discharge pipe, however, did not collapse (e.g., Figure 5.5.21, See 2). At this time in the transient, the reactor vessel and the downcomer levels were considerably below the cold leg nozzle elevation (Figure 5.5.22), thus exposing the cold leg discharge pipes to a steam environment.

The forward flow pulses were established simultaneously in each cold leg of B, however, the magnitude of the forward flow rate varied and the establishment of reverse flow initially alternated between cold legs B1 and B2 during the first four forward flow pulses (Figure 5.5.23, See 1). An alternating direction intra-cold leg flow pattern also developed in the B cold legs. An examination of the cold leg B venturi flow rates indicated that when loop flow was initiated both B cold legs experienced forward flow (Figure 5.5.23, See 2). The forward flow completely collapsed the void in the cold leg B2 discharge pipe (Figure 5.5.24, See 1), but only a partial collapse of the void in the cold leg B1 discharge pipe occurred (Figure 5.5.24, See 2). The cold leg B1 discharge pipe then voided completely (Figure 5.5.24, See 3) and the cold leg B1 suction pipe partially voided (Figure 5.5.24, See 4) as steam from the downcomer backflowed into the cold leg B1 discharge pipe (Figure 5.5.23, See 3). Thus, intra-cold leg flow was established with cold leg B1 indicating reverse flow (Figure 5.5.23, See 3) and cold leg B2 indicating forward flow (Figure 5.5.23, See 4). The backflow of steam into cold leg B1 resulted in the displacement of liquid from the B1 suction pipe into the B2 suction pipe, thus increasing the flow rate in the cold leg B2 (Figure 5.5.23, See 4). The loss of the primary loop driving head and the imbalanced driving head between the cold leg B1 and B2 suction pipes (as a result of

different fluid temperature distributions within the two suction pipes) resulted in another flow direction change that caused cold leg B1 to flow in the forward flow direction (Figure 5.5.23, See 5) and cold leg B2 to flow in the reverse flow direction (Figure 5.5.23, See 6). This indication of intra-cold leg flow did not result in the spillover of liquid from the suction pipe into the discharge pipe of cold leg B1, but was essentially balancing the elevation head (liquid levels) in both of the cold leg B suction pipes (Figure 5.5.24, See 5). At this time, the flow in both B cold legs interrupted (Figure 5.5.23, See 7), both B cold leg discharge pipes were completely voided (Figure 5.5.24, See 6) and both B cold leg suction pipe levels began decreasing (Figure 5.5.24, See 7). A difference in the levels in the suction pipes existed at this time and can be attributed to differences in the fluid temperatures. The fluid temperature differences in the cold leg suction pipes affected the driving head relationships and was responsible for the alternately established reverse flow (B1, B2, B1, B2) subsequent to each occurrence of primary loop flow for the first four flow pulses (Figure 5.5.23, See 8). The remaining three flow pulses resulted in a more symmetrical response in the B cold legs, however, a predominant reverse flow path still existed. The previous discussion was based on observations obtained from the cold leg flow meters and the cold leg level instrumentation. An examination of the cold leg fluid temperatures (Figures 5.5.25 through 5.5.30) can be used to verify the cold leg flow and level response.

The cold leg A flow response differed from that observed in the B cold legs at this time. Forward flow was observed to occur predominantly in cold leg A1 while cold leg A2 established reverse flow (Figure 5.5.31). The intra-cold leg flow as a result of balancing the levels in the suction pipes was also observed. The cold leg A2 discharge pipe remained essentially completely voided (Figure 5.5.32) during each of the flow pulses. The phenomena that occurred in the A cold legs appeared to be similar to those observed in the reactor vessel vent valves closed test (300504) where a flow pulse in one loop caused backflow in the other loop. During this time, with the exception of the last flow pulse, forward loop flow in the B cold legs occurred prior to any indication of flow in the A cold legs. Figures 5.5.33 through 5.5.38 are provided to investigate these phenomena further.

During the AFW-BCM, the primary system pressure decreased from approximately 2310 to approximately 1500 psia (Figure 5.5.39, See 1). The decreasing primary system pressure resulted in a drain of the pressurizer, which in turn resulted in an increase in the loop A hot leg and steam generator primary levels (Figure 5.5.40, See 1).

As the depressurization continued, superheated conditions occurred in the downcomer (Figure 5.5.41, See 1), propagated to the cold leg discharge pipes (Figure 5.5.42, See 1), and resulted in the complete voiding of the cold leg discharge pipes (Figure 5.5.20, See 2 and Figure 5.5.21, See 3), interrupting forward loop flow (See 1, Figure 5.5.43 and 5.5.44). The primary system repressurized (Figure 5.5.39, See 2). This response was similar to that observed in the Nominal Test (3003AA) as a result of a depressurization caused by BCM.

As the primary pressure increased, the pressurizer inventory increased as inventory was transferred first from loop A to the pressurizer (Figure 5.5.40, See 2). When the hot leg A level descended to the surge line elevation, inventory was then transferred from loop B to the pressurizer (Figure 5.5.45, See 1).

The primary system pressure increased to ~2310 psia (Figure 5.5.46, See 1) and the PORV opened (Figure 5.5.47, See 1). The PORV then remained open, the loop B levels continued to decrease and stabilized at approximately the same elevations as the loop A levels (Figure 5.5.48, See 1), the core and downcomer began voiding further (as indicated by the decreasing levels, Figure 5.5.49, See 1), and the primary system pressure remained essentially constant (Figure 5.5.46, See 2) even though the PORV was open.

The decreasing core level resulted in core uncovery (Figure 5.5.49, See 1) and superheated conditions occurred in the core (Figure 5.5.50, See 1). This event resulted in high core heater rod temperatures, the core power was tripped automatically (Figure 5.5.51, See 1), and the test was terminated (~130 minutes).

As the core region superheated, the hot legs also indicated superheat (See 1 on Figures 5.5.52 and 5.5.53), therefore at test termination the hot legs were completely voided. The pressurizer, however, contained a significant

amount of liquid inventory (Figure 5.5.54, See 1). Hot leg A indicated a greater degree of superheat to a higher elevation than did hot leg B. Thus, the influence of the pressurizer with the PORV open was observed to establish a predominant flow path by way of hot leg A.

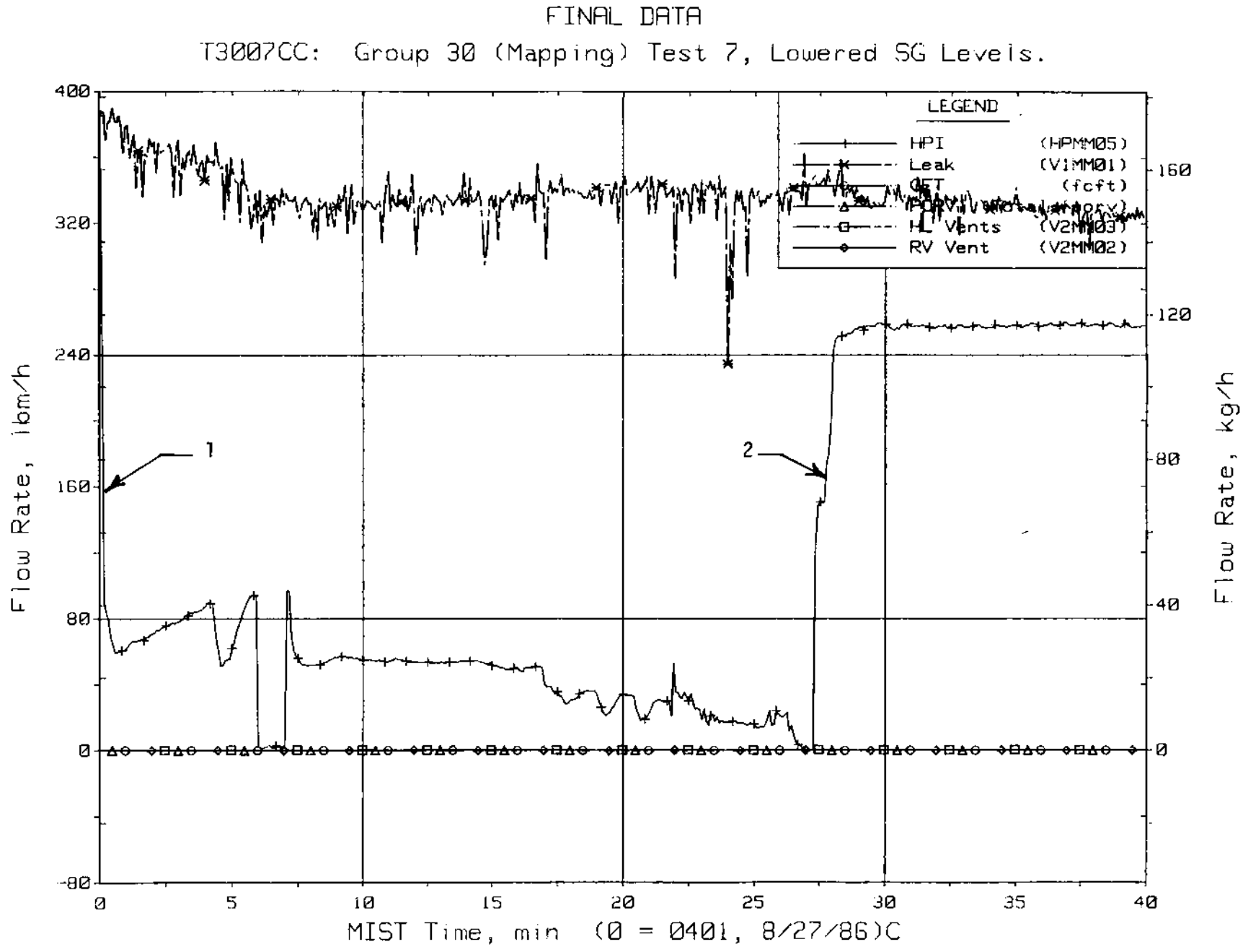

Figure 5.5.1. Primary System Boundary Flow Rates

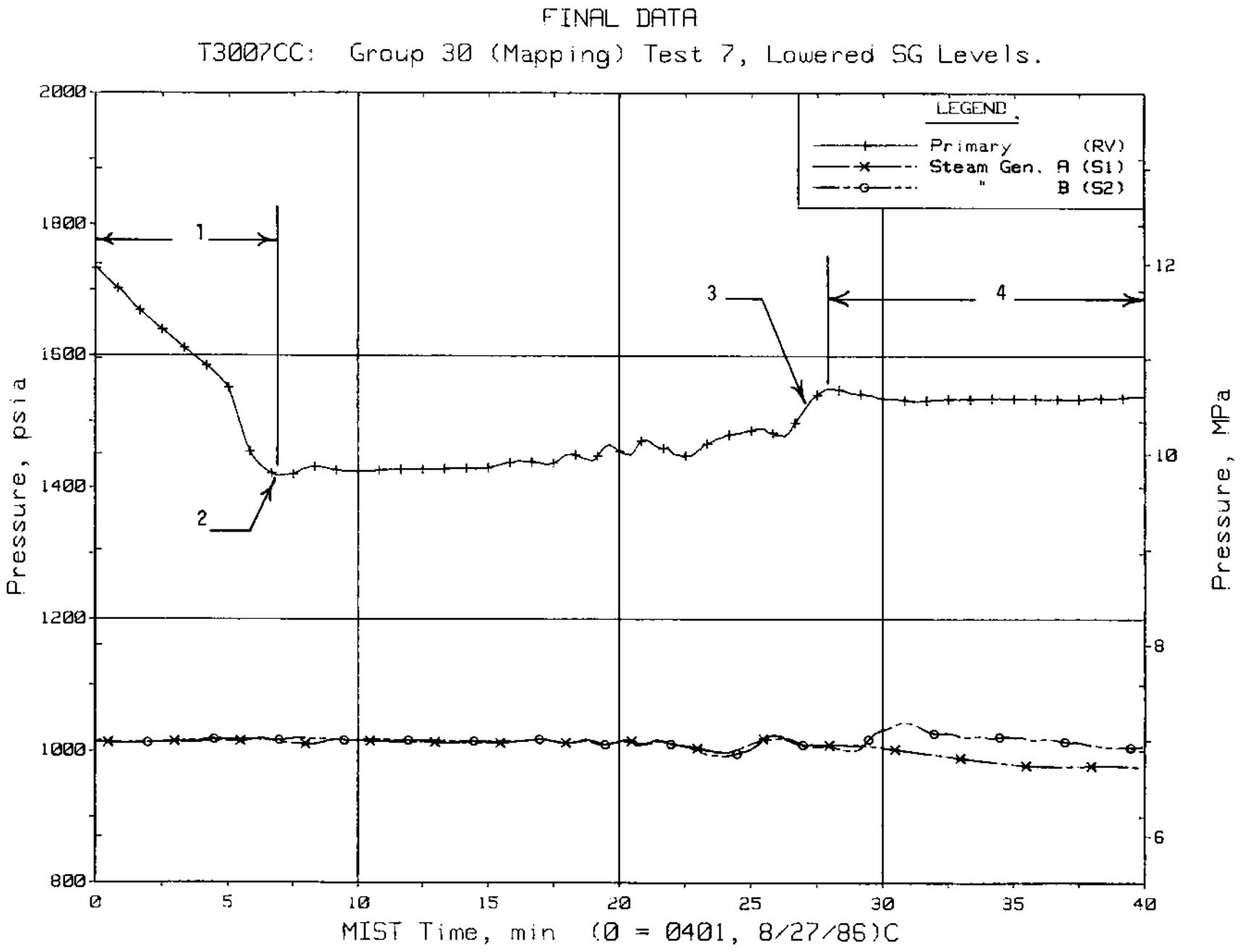

Figure 5.5.2. Primary and Secondary System Pressures (GP01s)

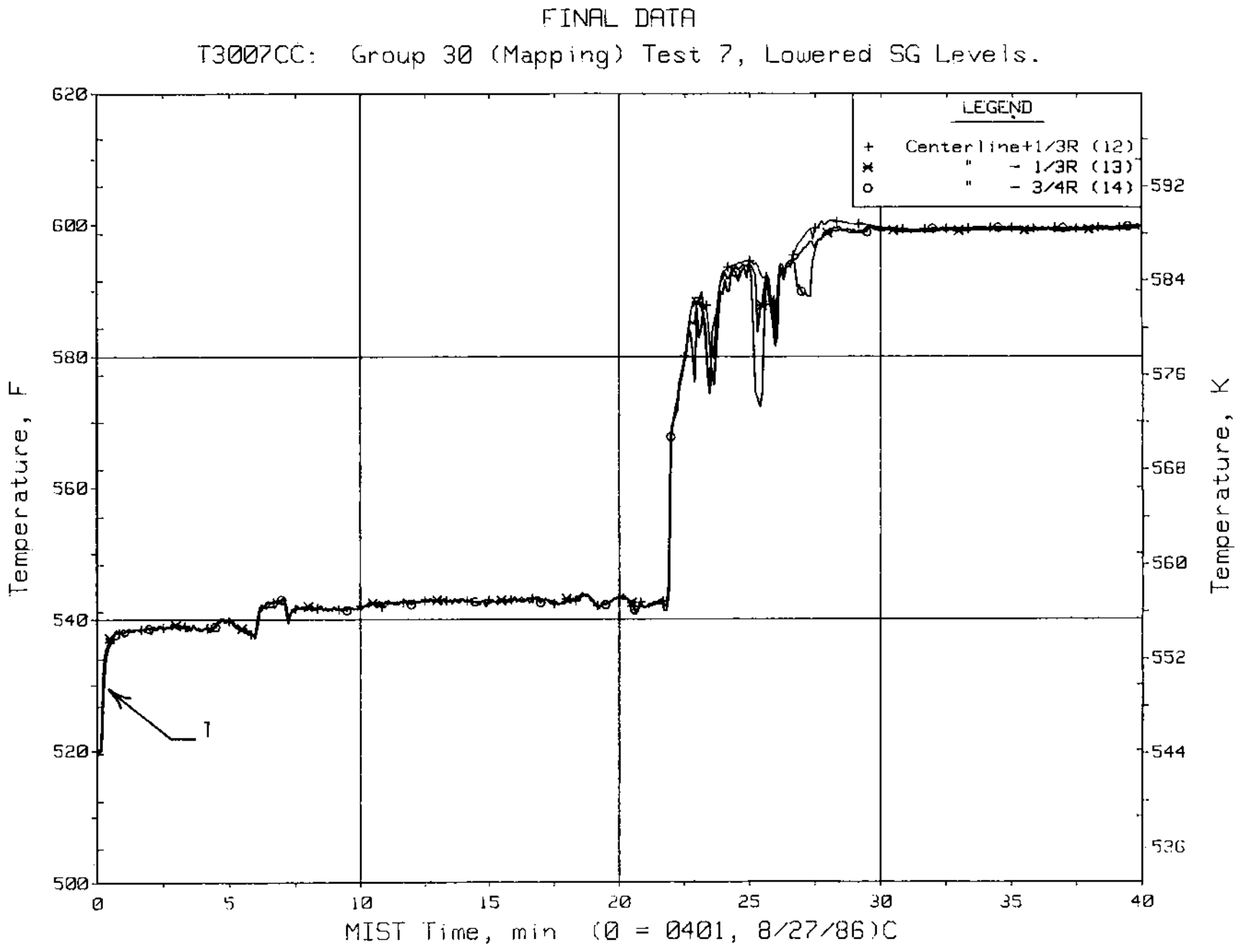

Figure 5.5.3. Cold Leg B1 Nozzle Rake Fluid Temperatures (21.2 ft, C2TCs)

Mon Feb 27 16:21:14 1989

C2TC4

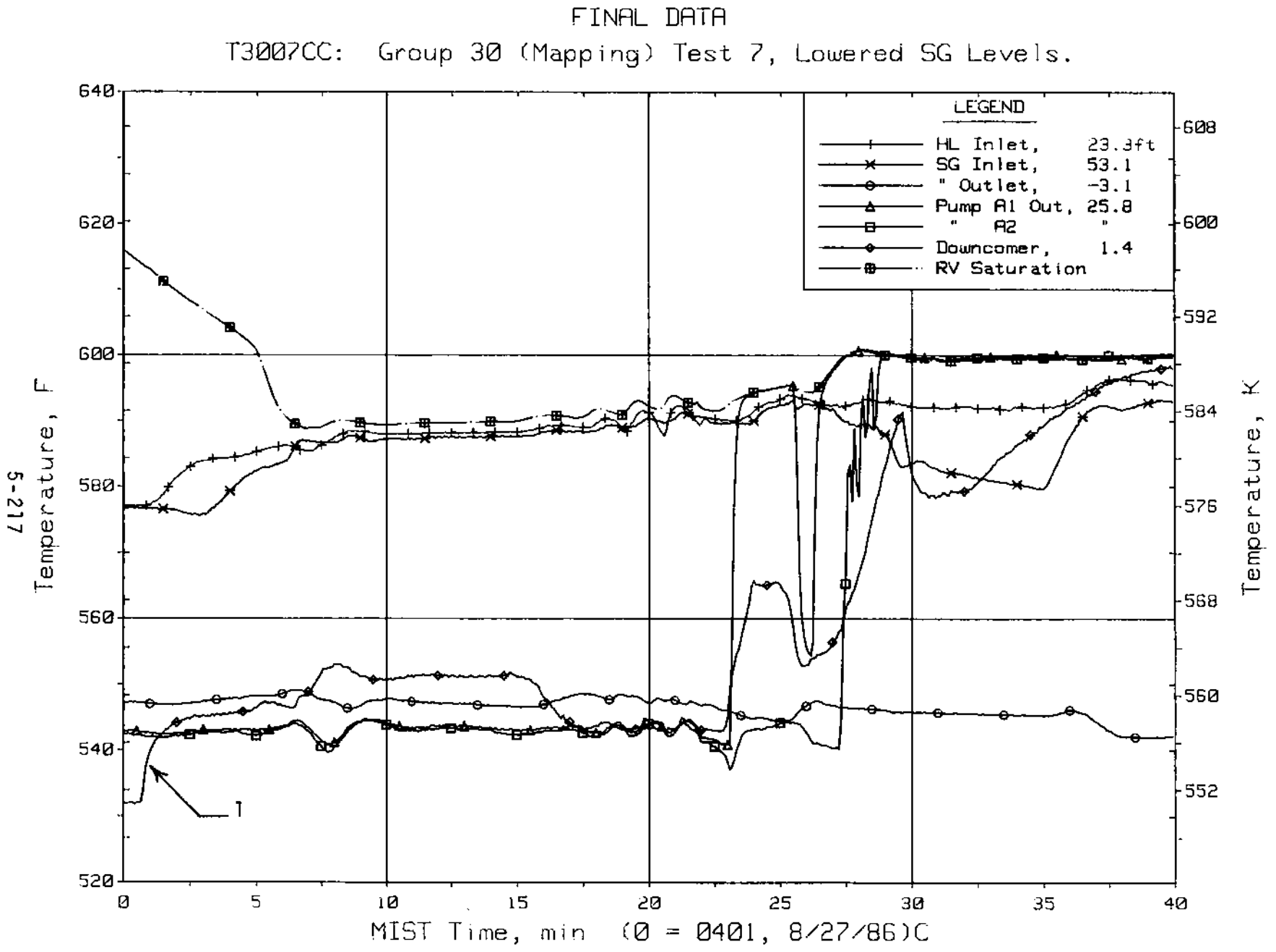

Figure 5.5.4. Loop A Primary Fluid Temperatures (RTDs)

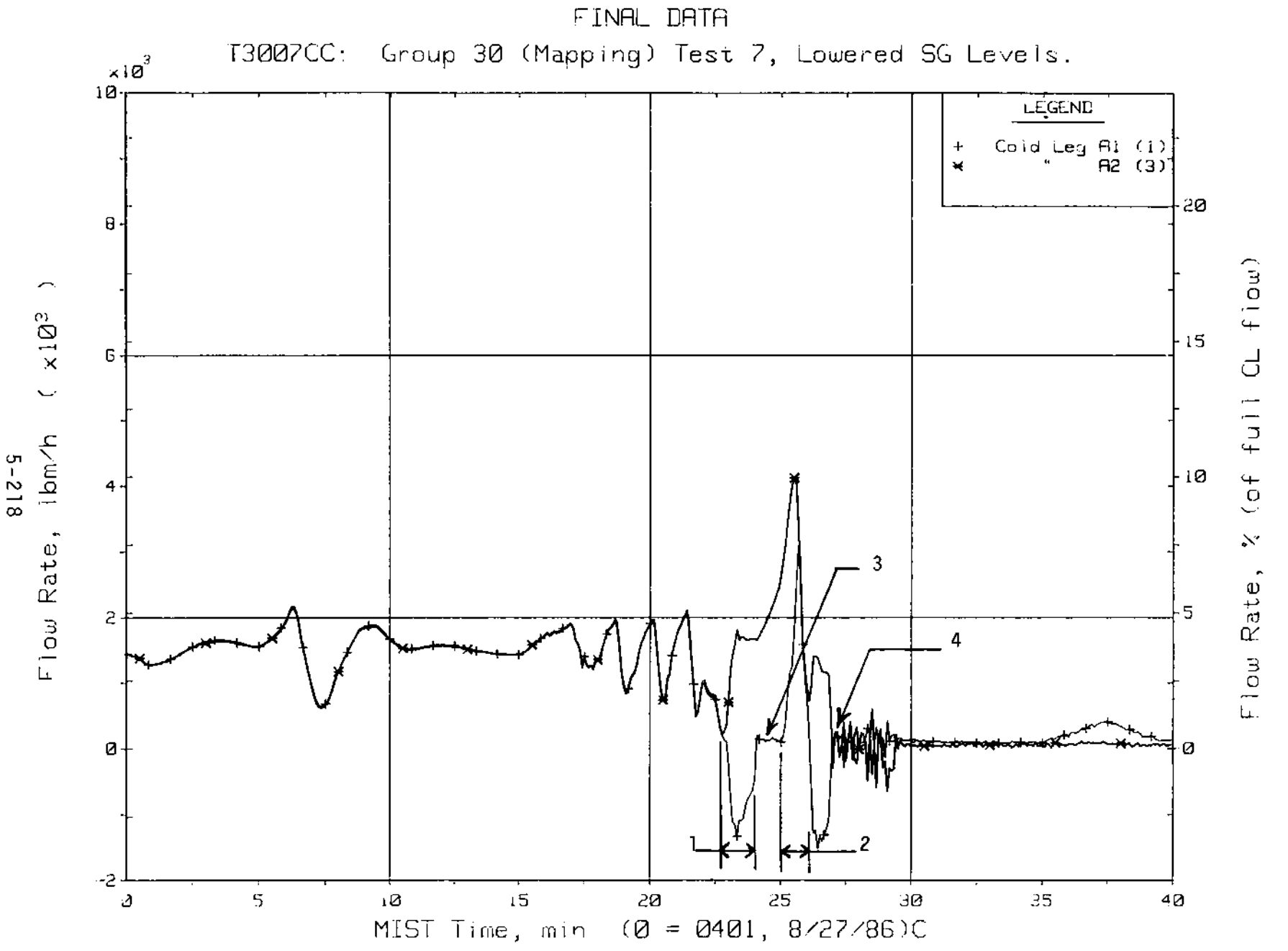

Figure 5.5.5. Loop A Cold Leg (Venturi) Flow Rates (CnVN20s)

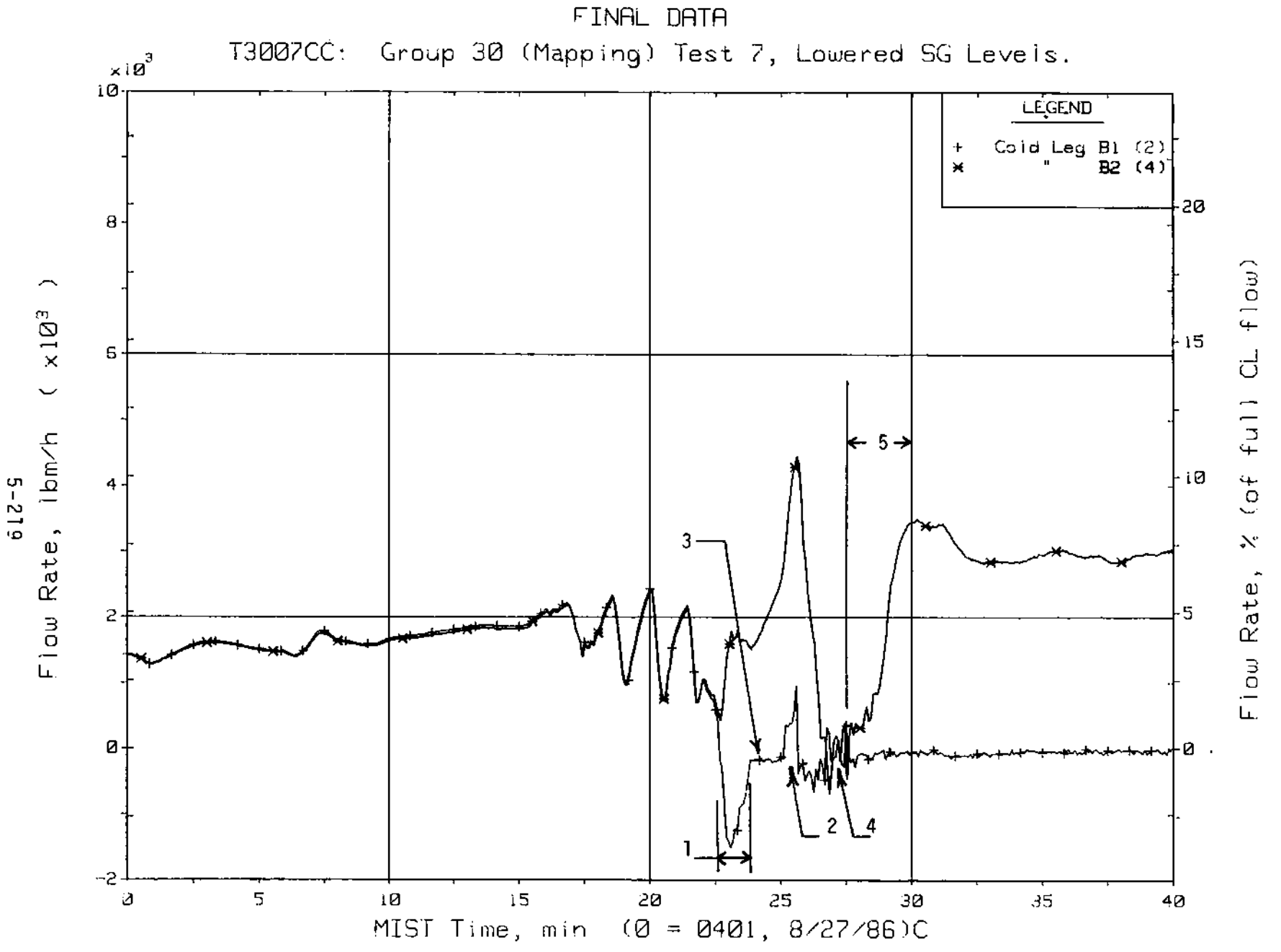

Figure 5.5.6. Loop B Cold Leg (Venturi) Flow Rates (CnVN20s)

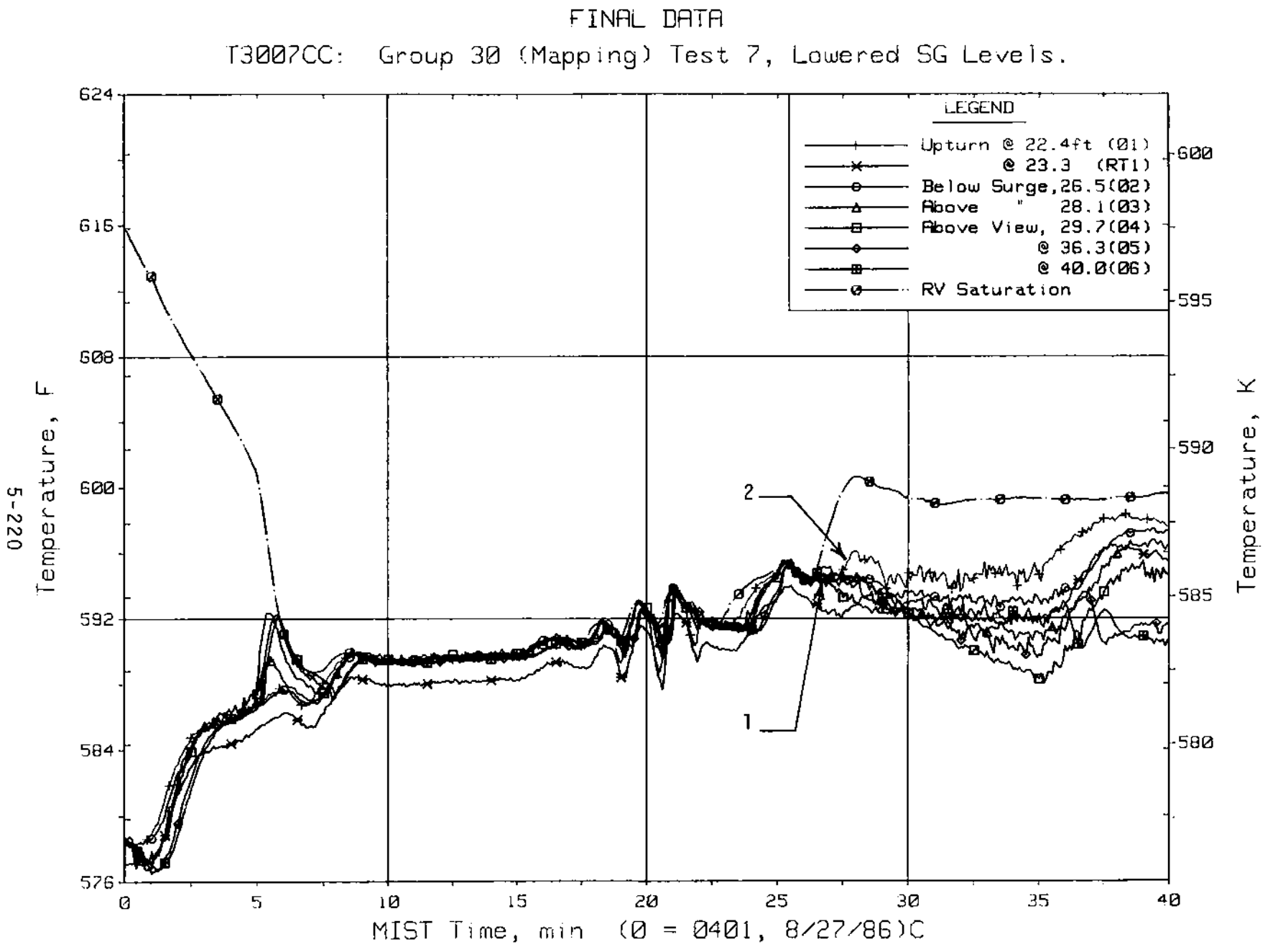

Figure 5.5.7. Hot Leg A Lower-Elevation Riser Fluid Temperatures (H1TCs)

Mon Feb 27 16:02:09 1989

H1TC1

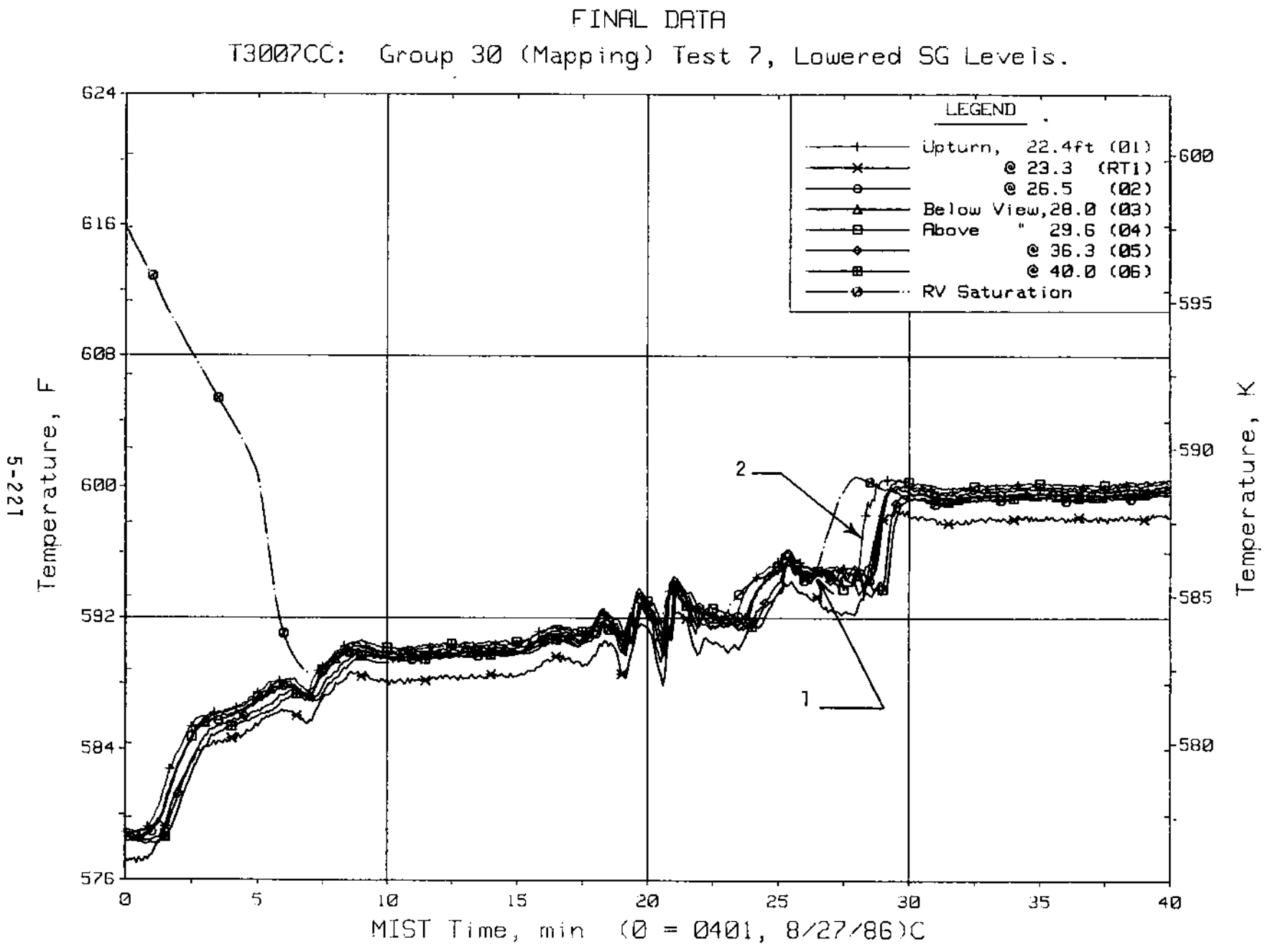

Figure 5.5.8. Hot Leg B Lower-Elevation Riser Fluid Temperatures (H2TCs)

Mon Feb 27 16:03:49 1989

H2TC1

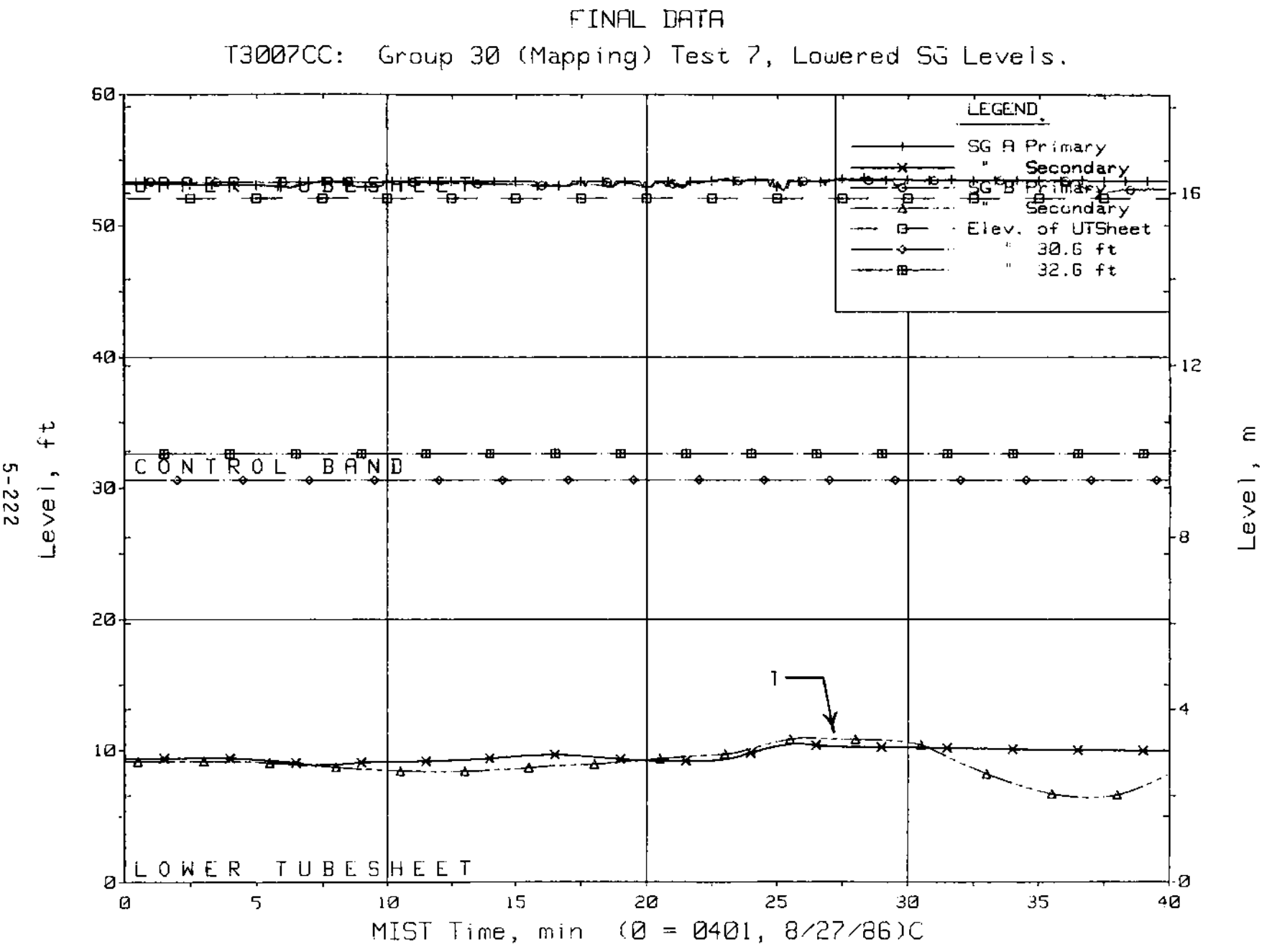

Figure 5.5.9. Steam Generator Collapsed Liquid Levels

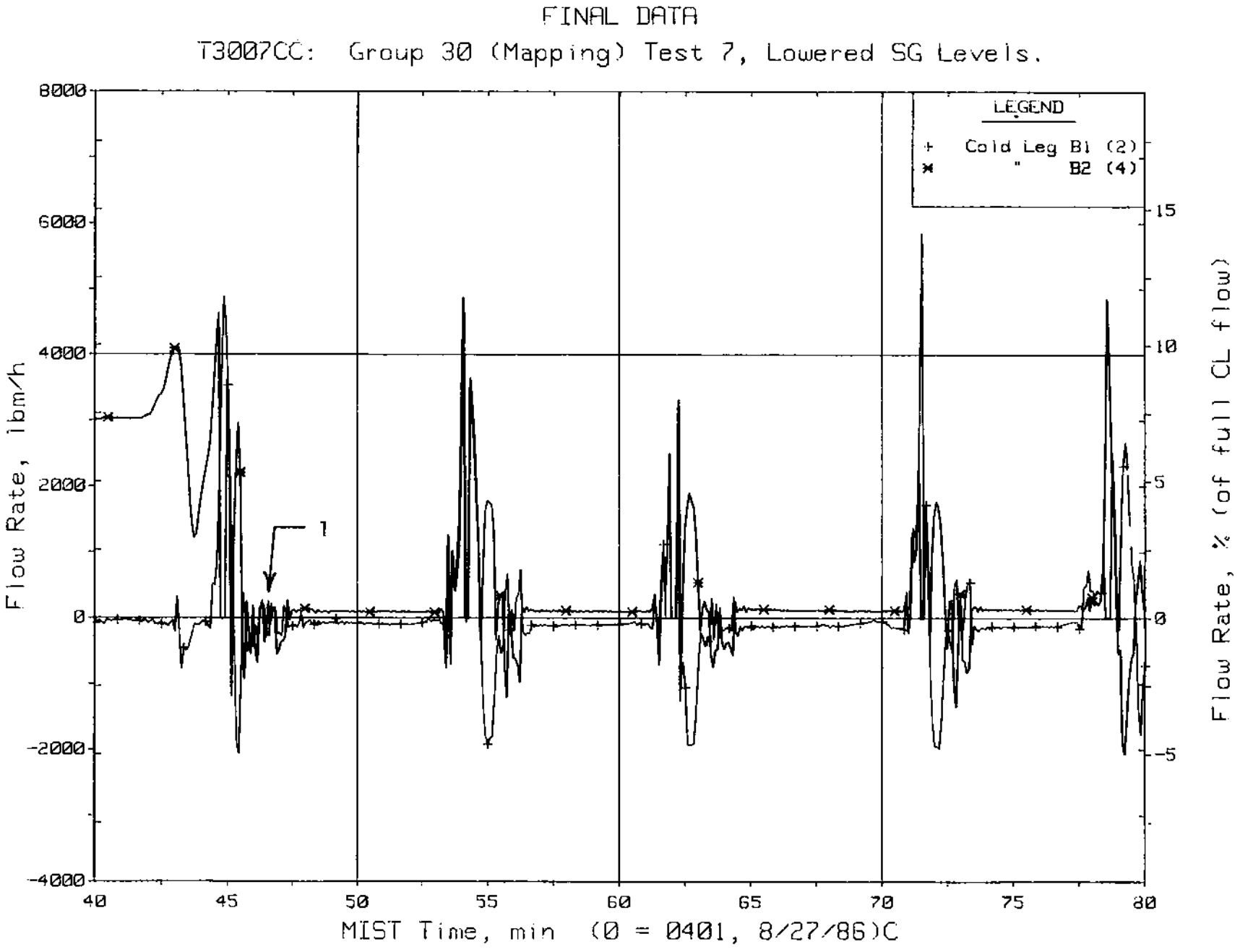

Figure 5.5.10. Loop B Cold Leg (Venturi) Flow Rates (CnVN2Os)

Mon Feb 27 15:54:13 1989

PRFLG

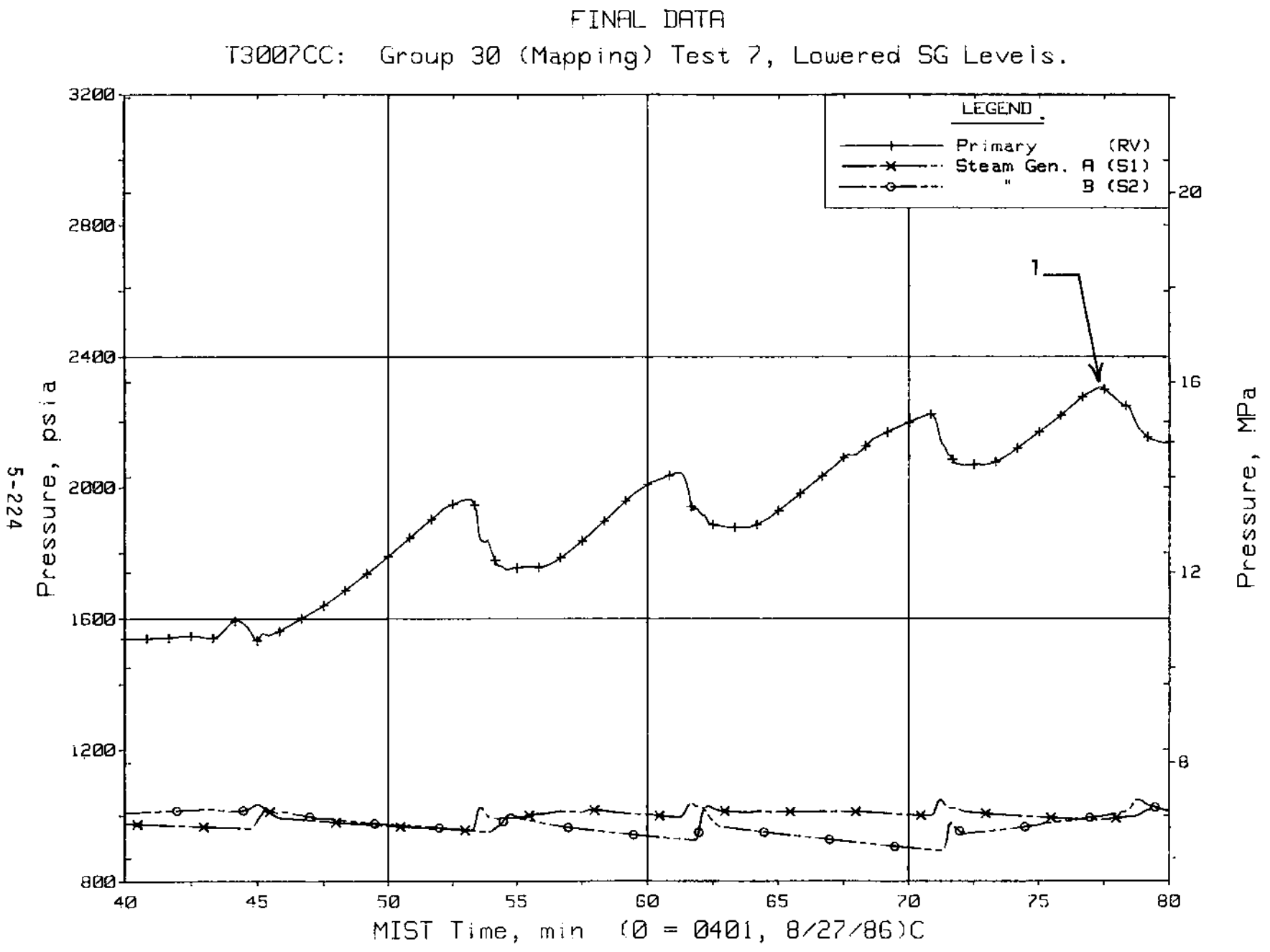

Figure 5.5.11. Primary and Secondary System Pressures (GP01s)

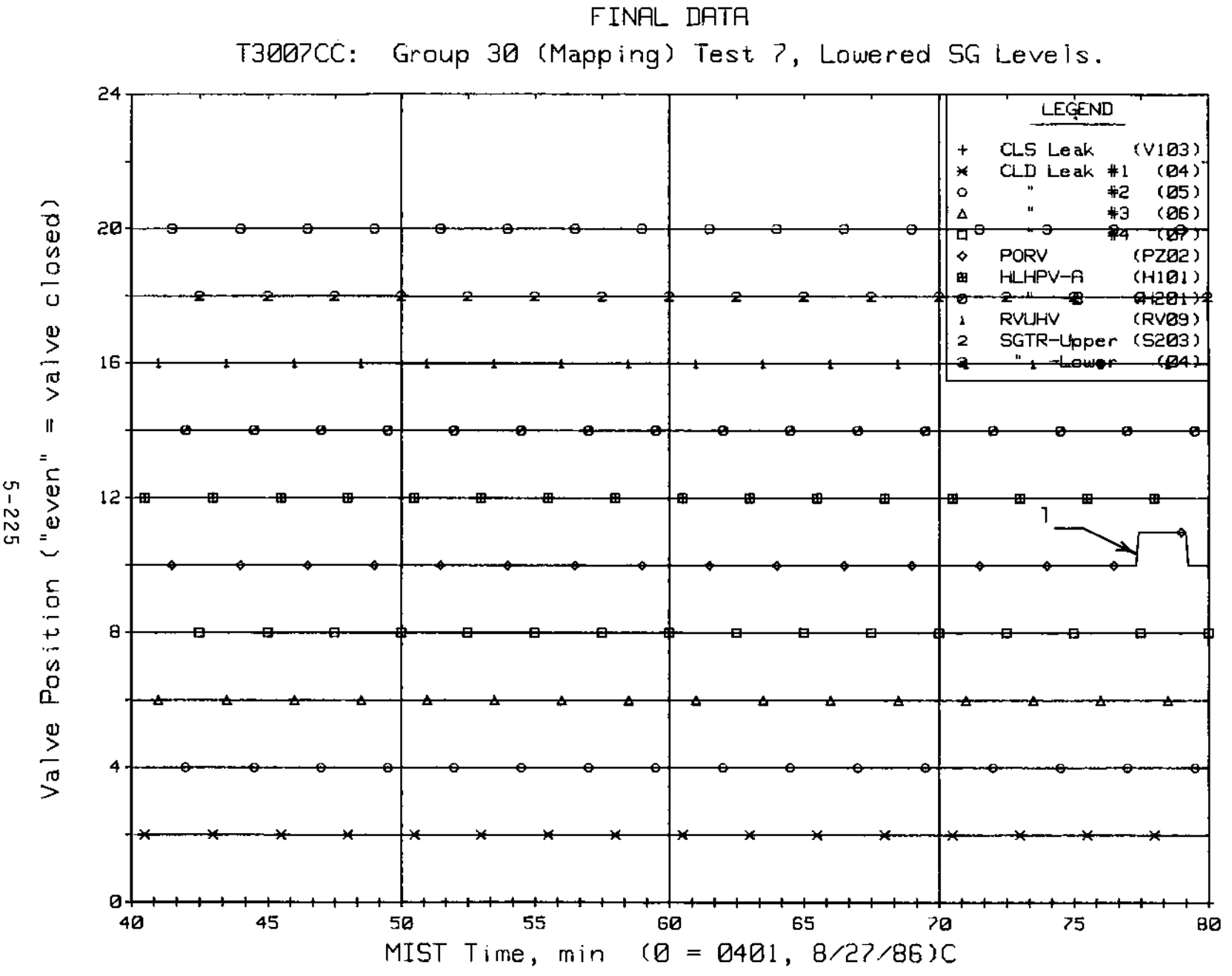

Figure 5.5.12. Primary System Discharge Limit Switch Indications (LSs)

Tue Feb 28 10:28:41 1989

PBLS1

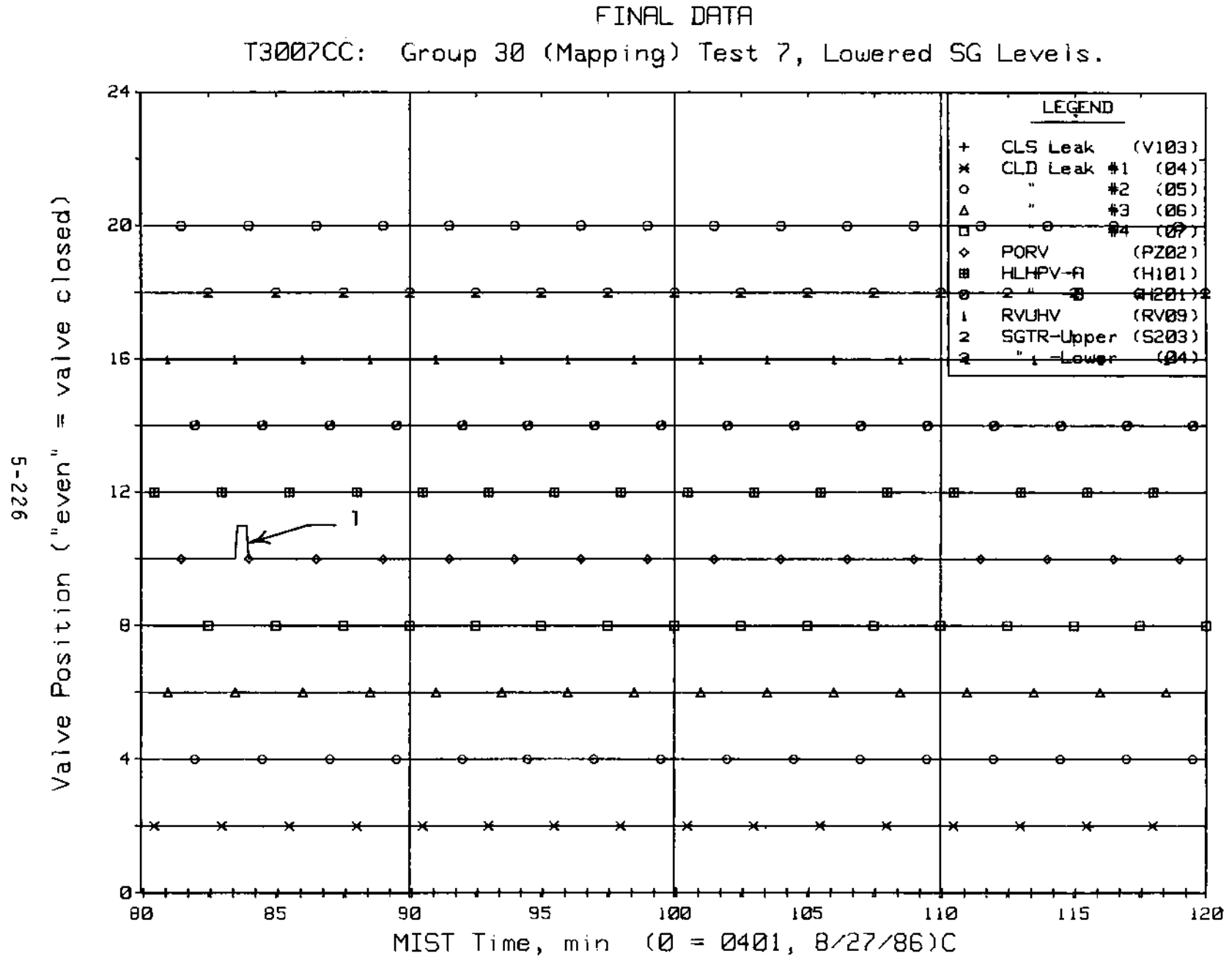

Figure 5.5.13. Primary System Discharge Limit Switch Indications (LSs)

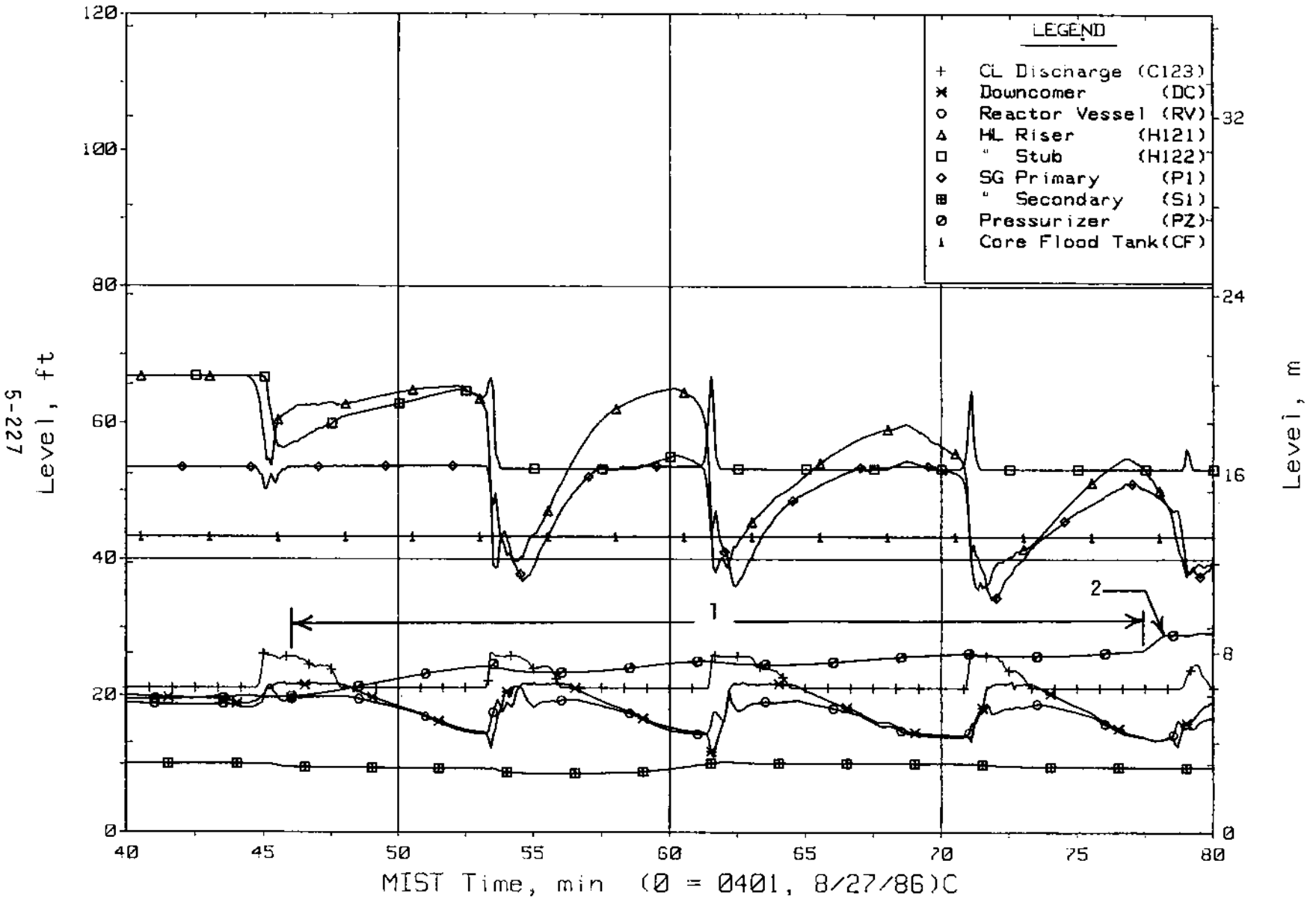

Figure 5.5.14. Loop A Collapsed Liquid Levels (LV20s)

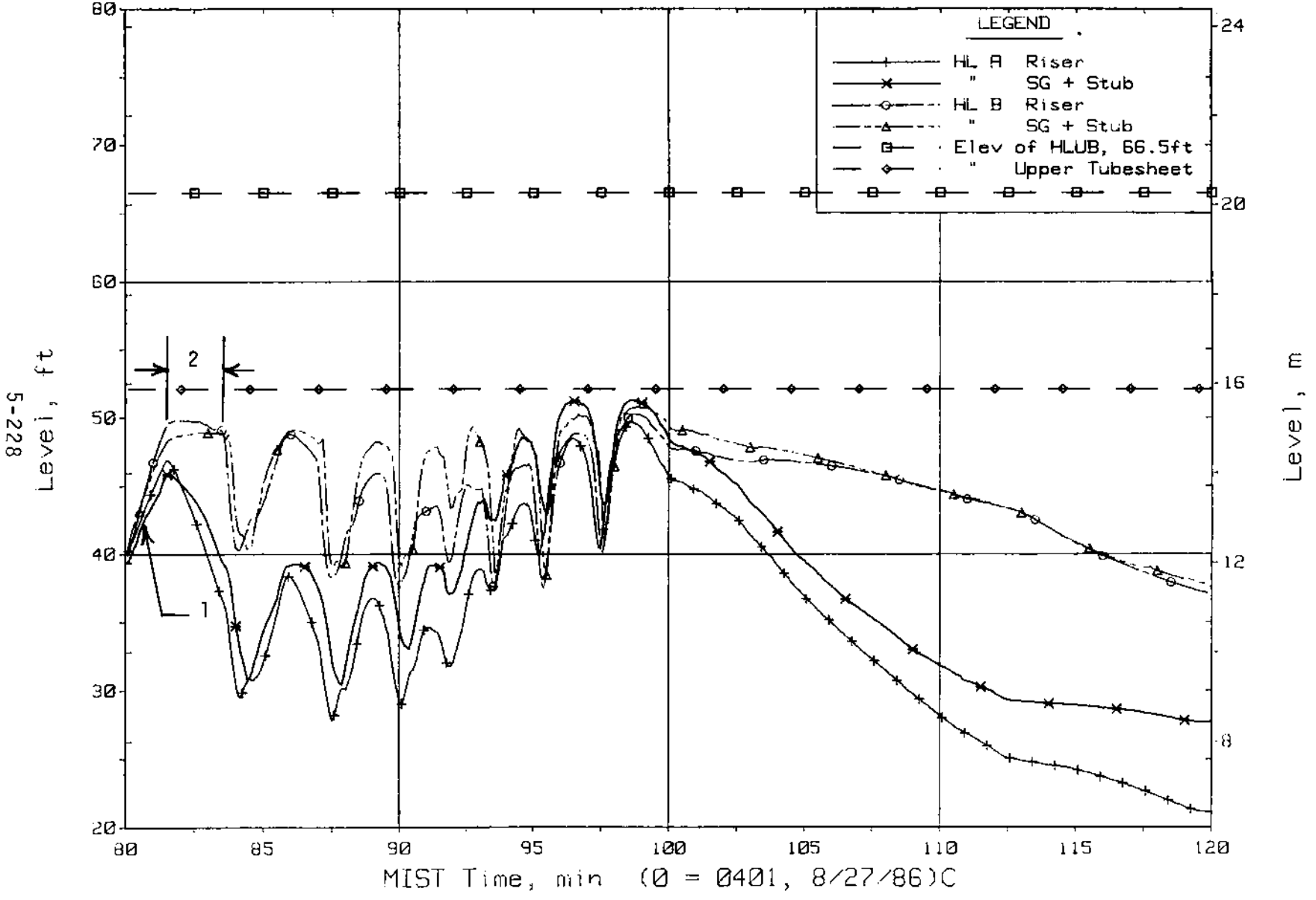

Figure 5.5.15. Hot Leg Riser and Stub Collapsed Liquid Levels

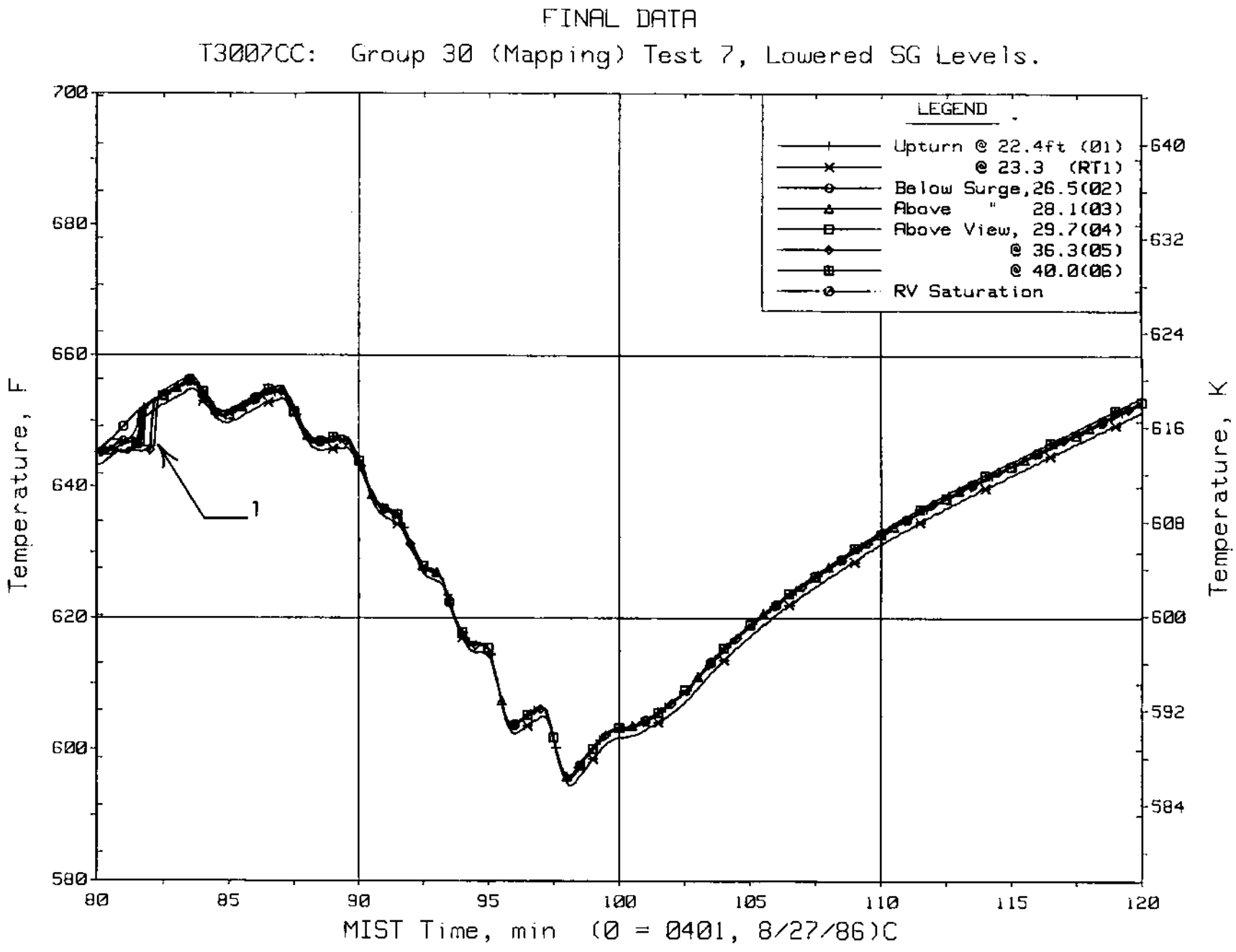

Figure 5.5.16. Hot Leg A Lower-Elevation Riser Fluid Temperatures (HITCs)

Mon Feb 27 15:27:53 1989

HITC1

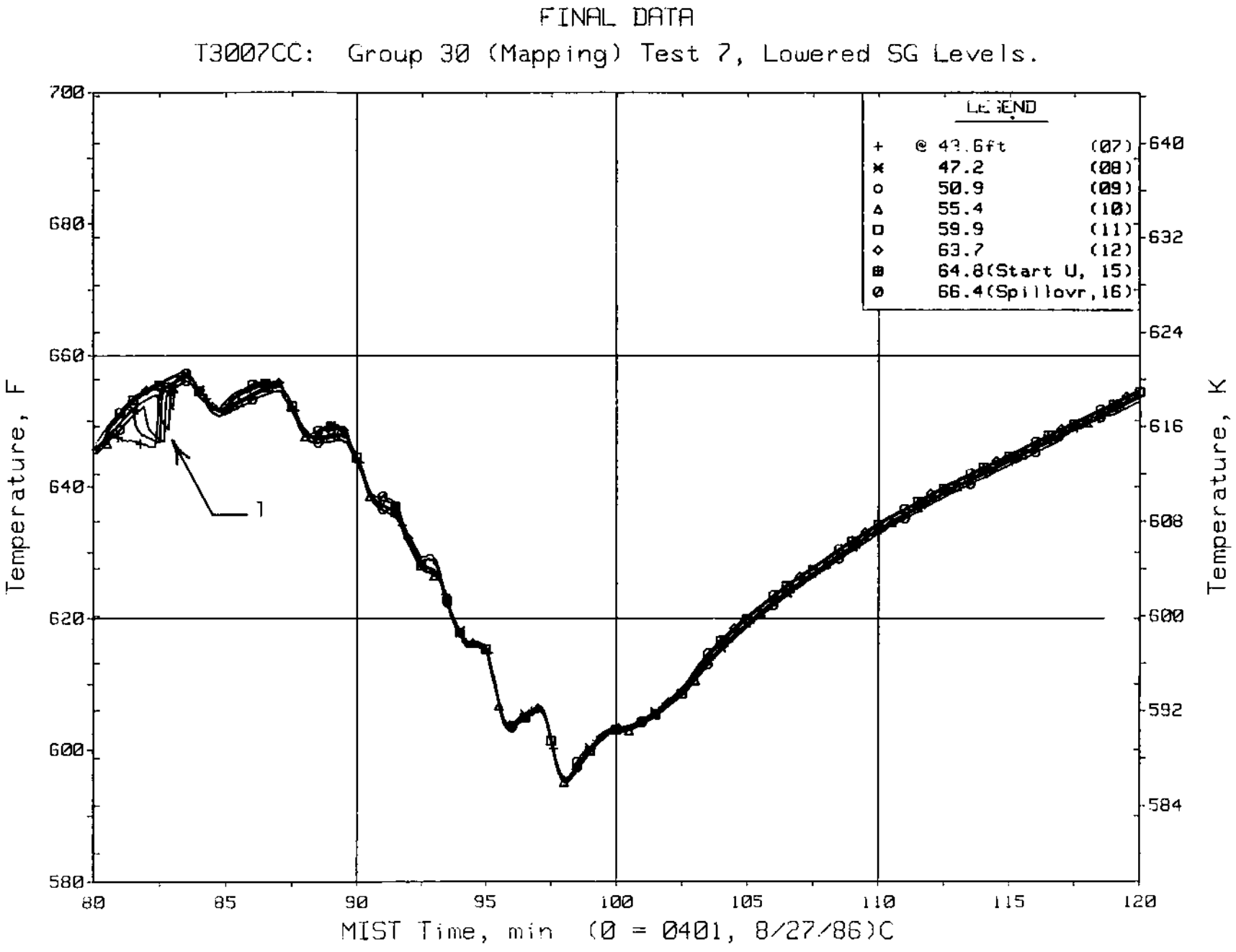

Figure 5.5.17. Hot Leg A Upper-Elevation Riser Fluid Temperatures (HITCs)

Mon Feb 27 15:23:09 1989

HITC2

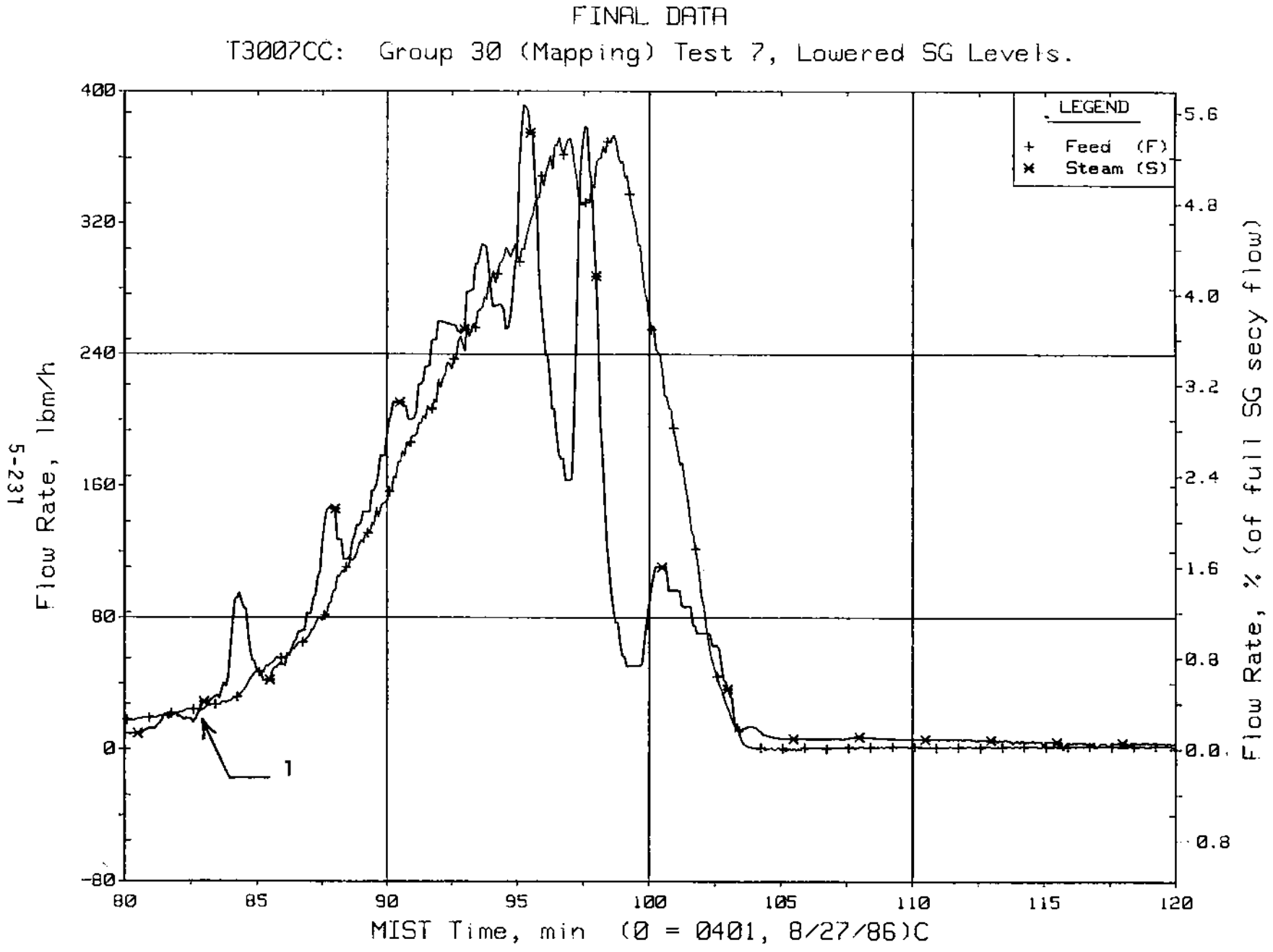

Figure 5.5.18. Steam Generator A Flow Rates (SaOR20s)

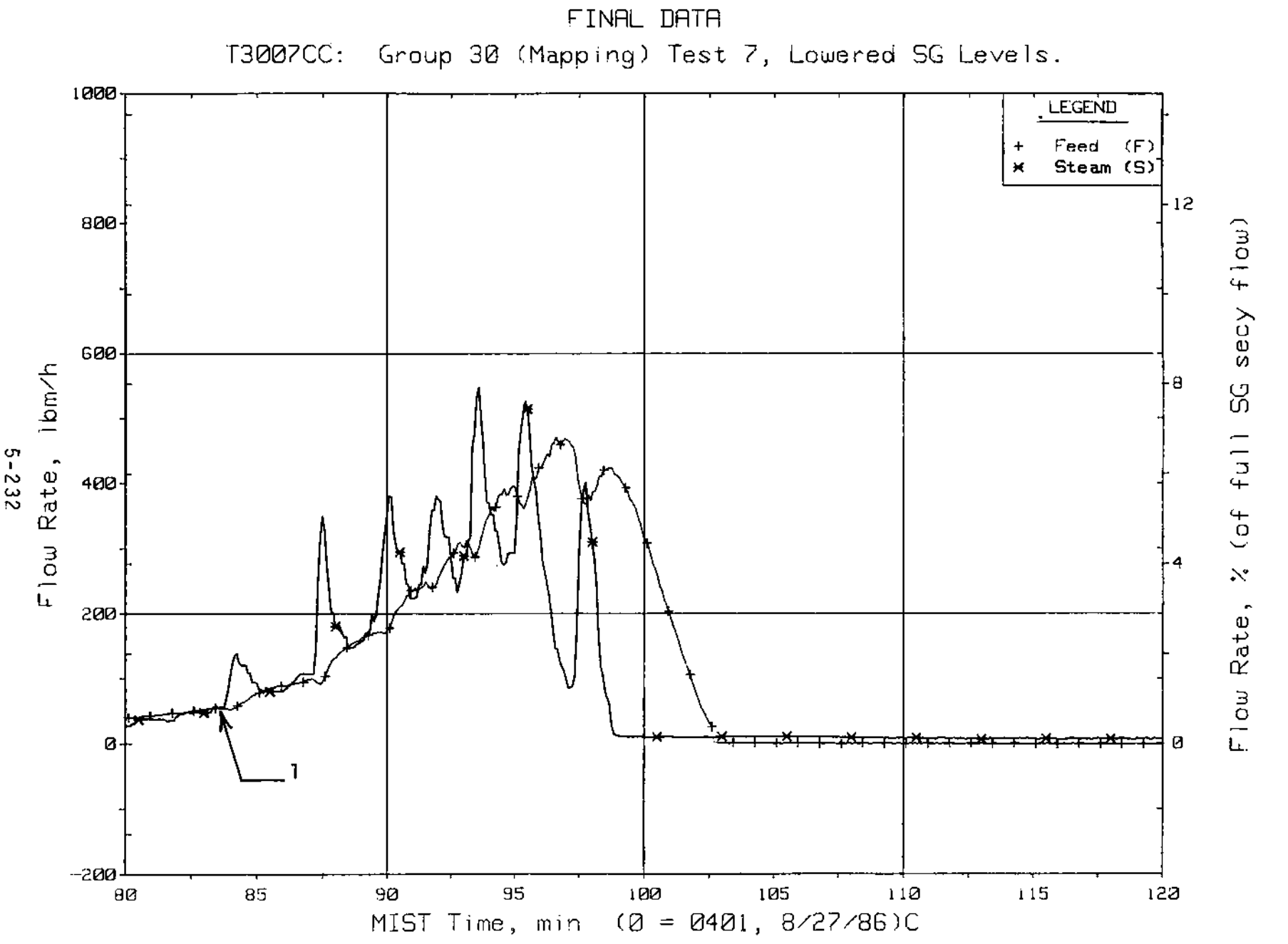

Figure 5.5.19. Steam Generator B Flow Rates (SaOR21s)

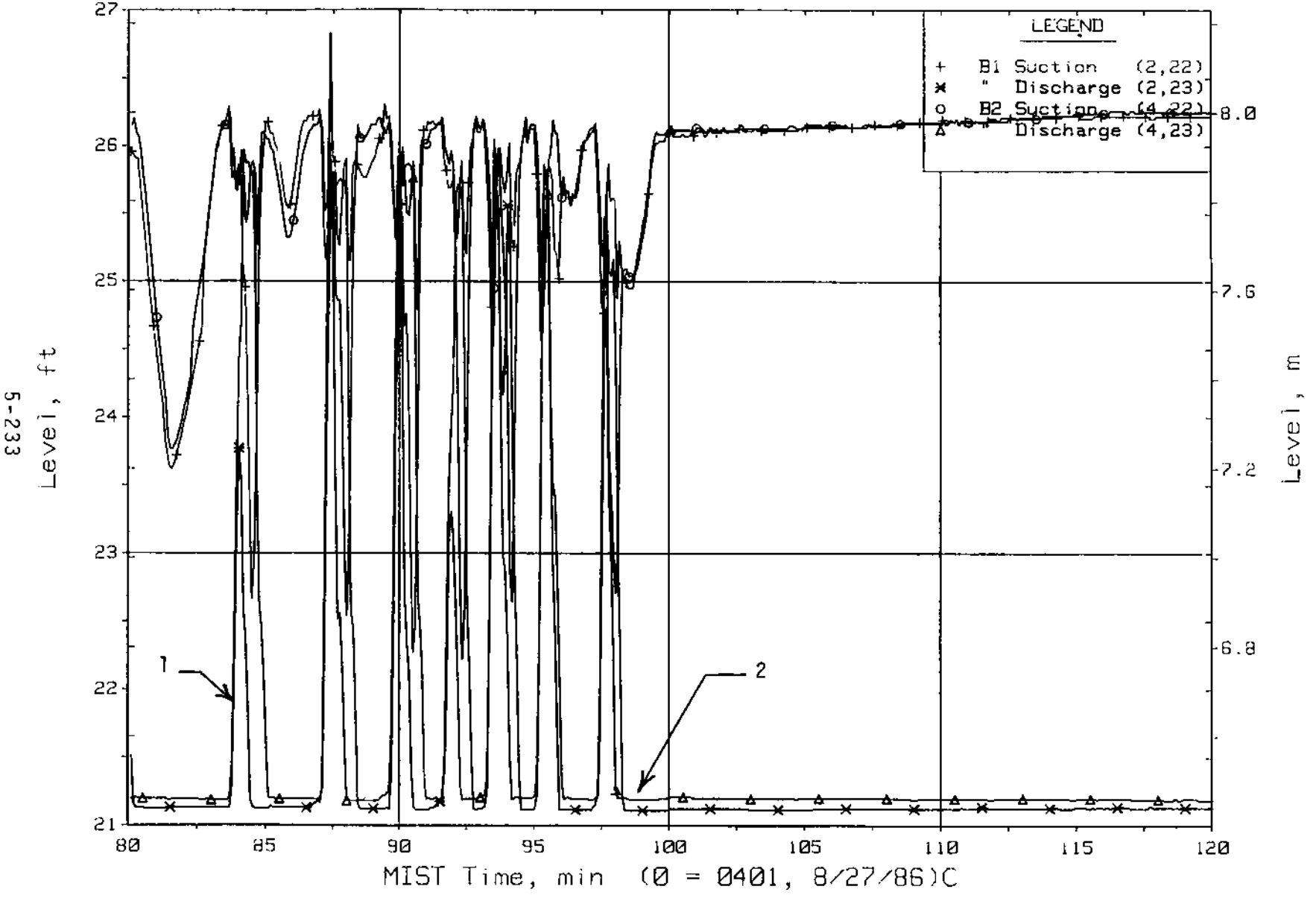

Figure 5.5.20. Loop B Cold Leg Collapsed Liquid Levels (LVs)

Mon Feb 02 15:01:24 1989

CLLV2

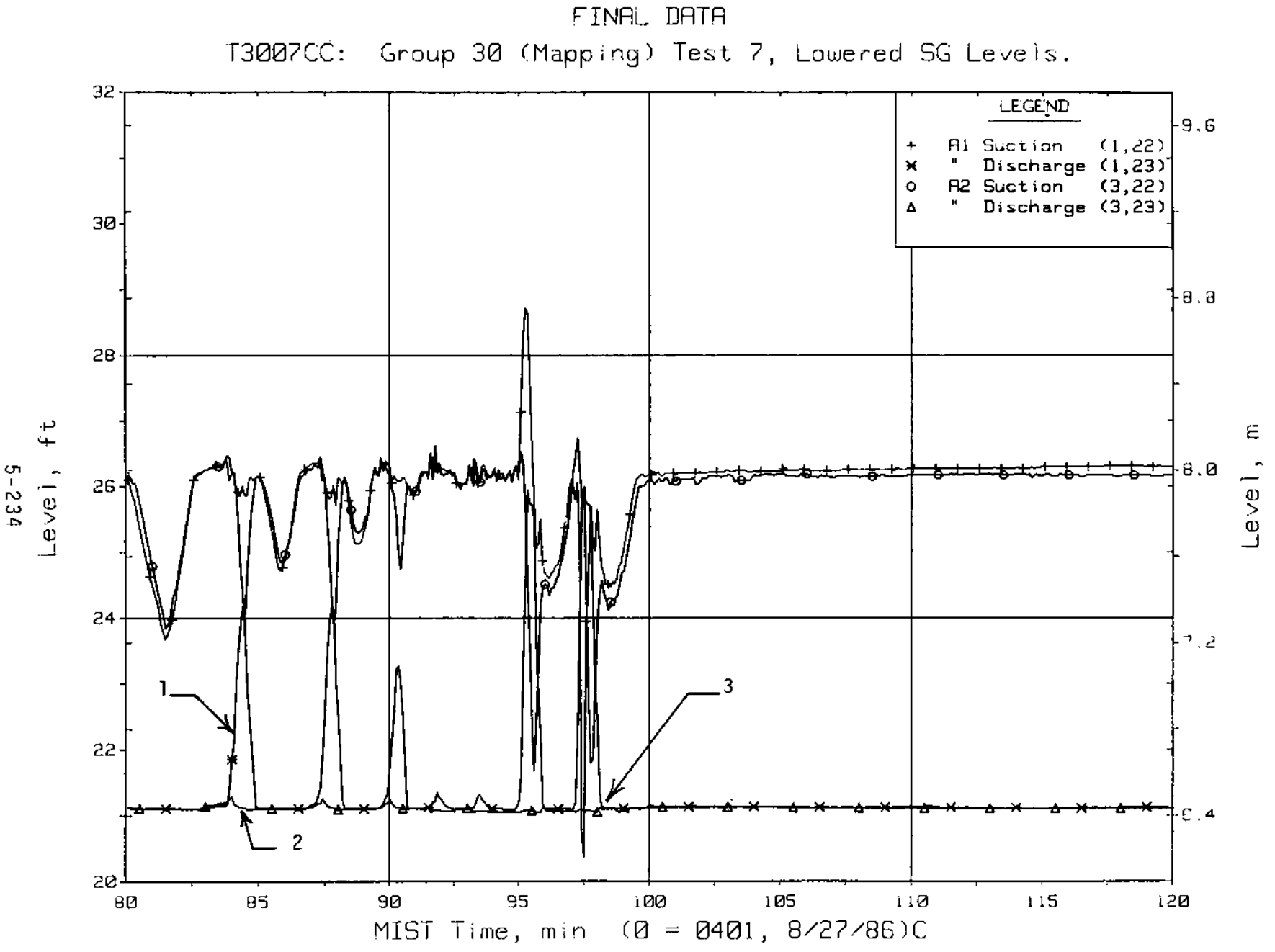

Figure 5.5.21. Loop A Cold Leg Collapsed Liquid Levels (LVs)

Mon Feb 27 15:09:59 1989

CLLV1

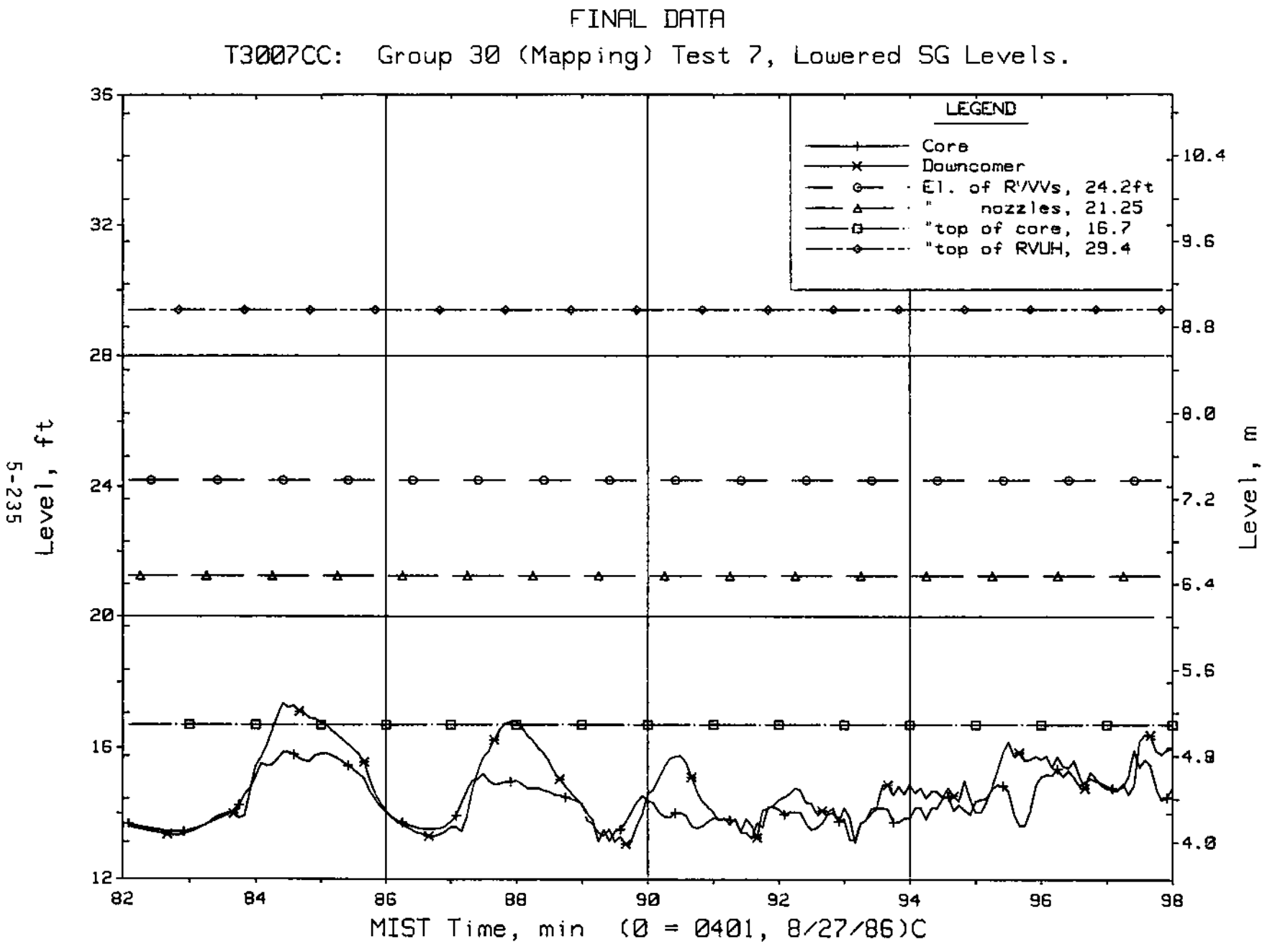

Figure 5.5.22. Core Region Collapsed Liquid Levels

Wed Mar 22 14:48:08 1989

COLV1

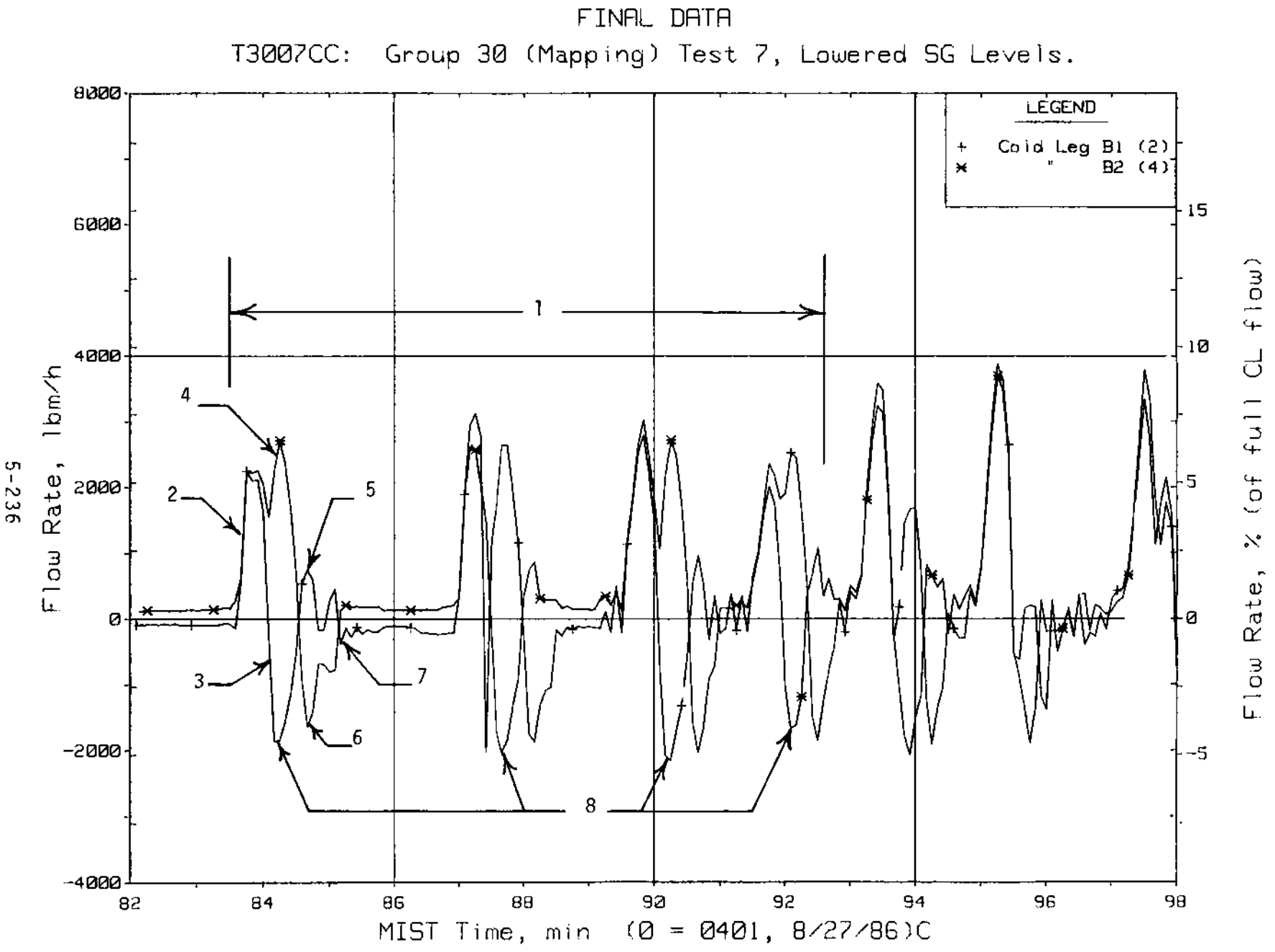

Figure 5.5.23. Loop B Cold Leg (Venturi) Flow Rates (CnVN20s)

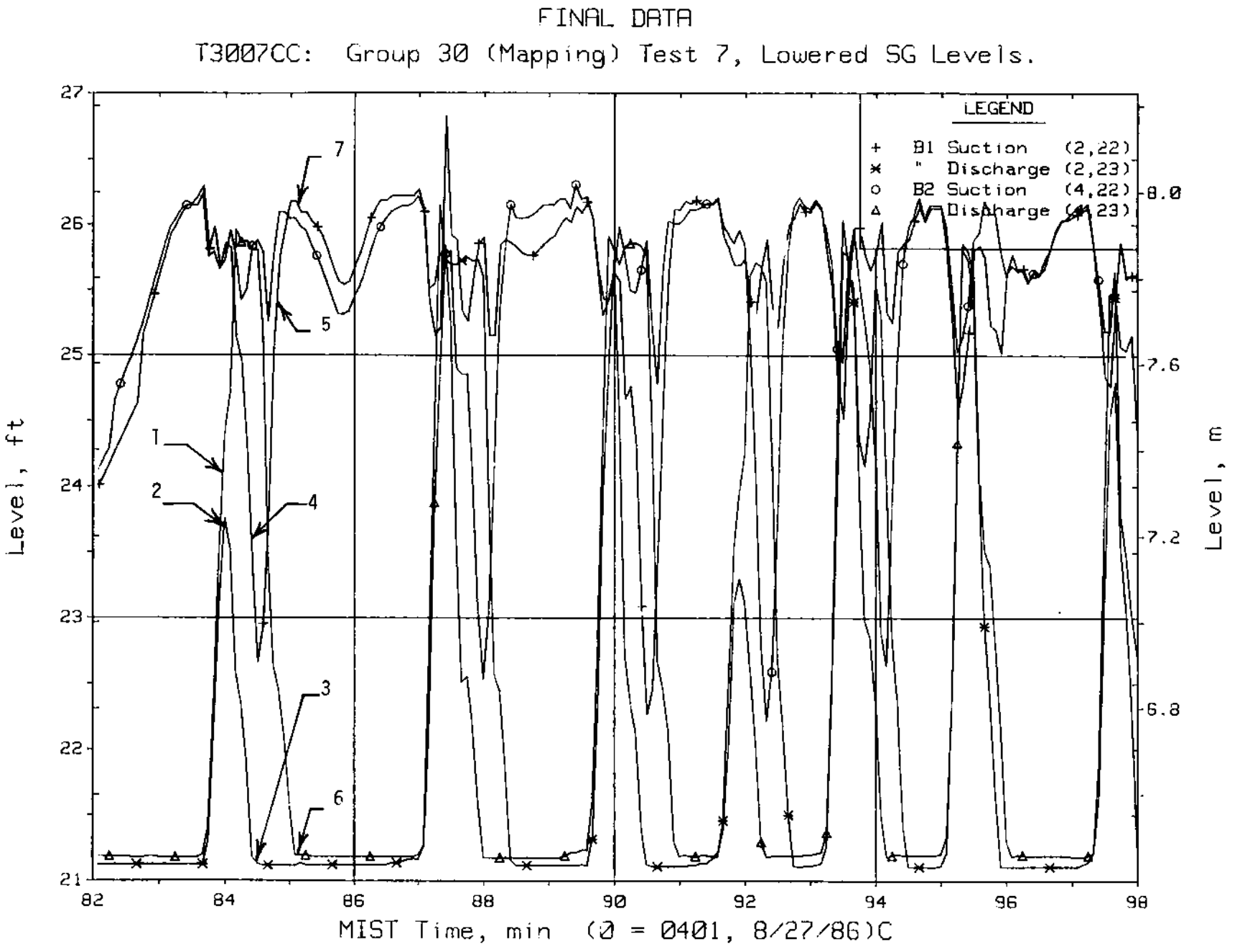

Figure 5.5.24. Loop B Cold Leg Collapsed Liquid Levels (LVs)

Thu Mar 23 10:30:48 1989

CLLV2

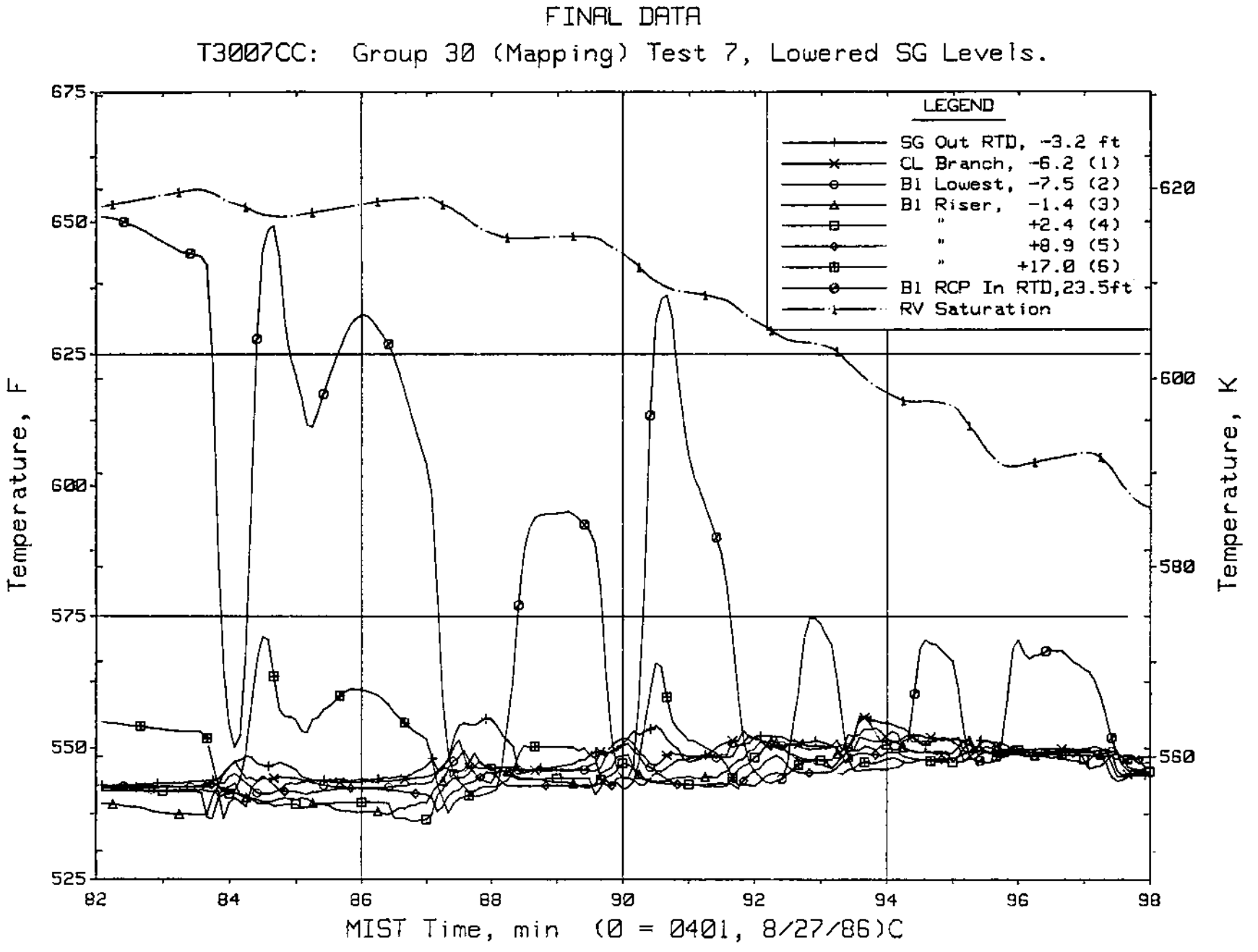

Figure 5.5.25. Cold Leg B1 Suction Fluid Temperatures (C2TCs)

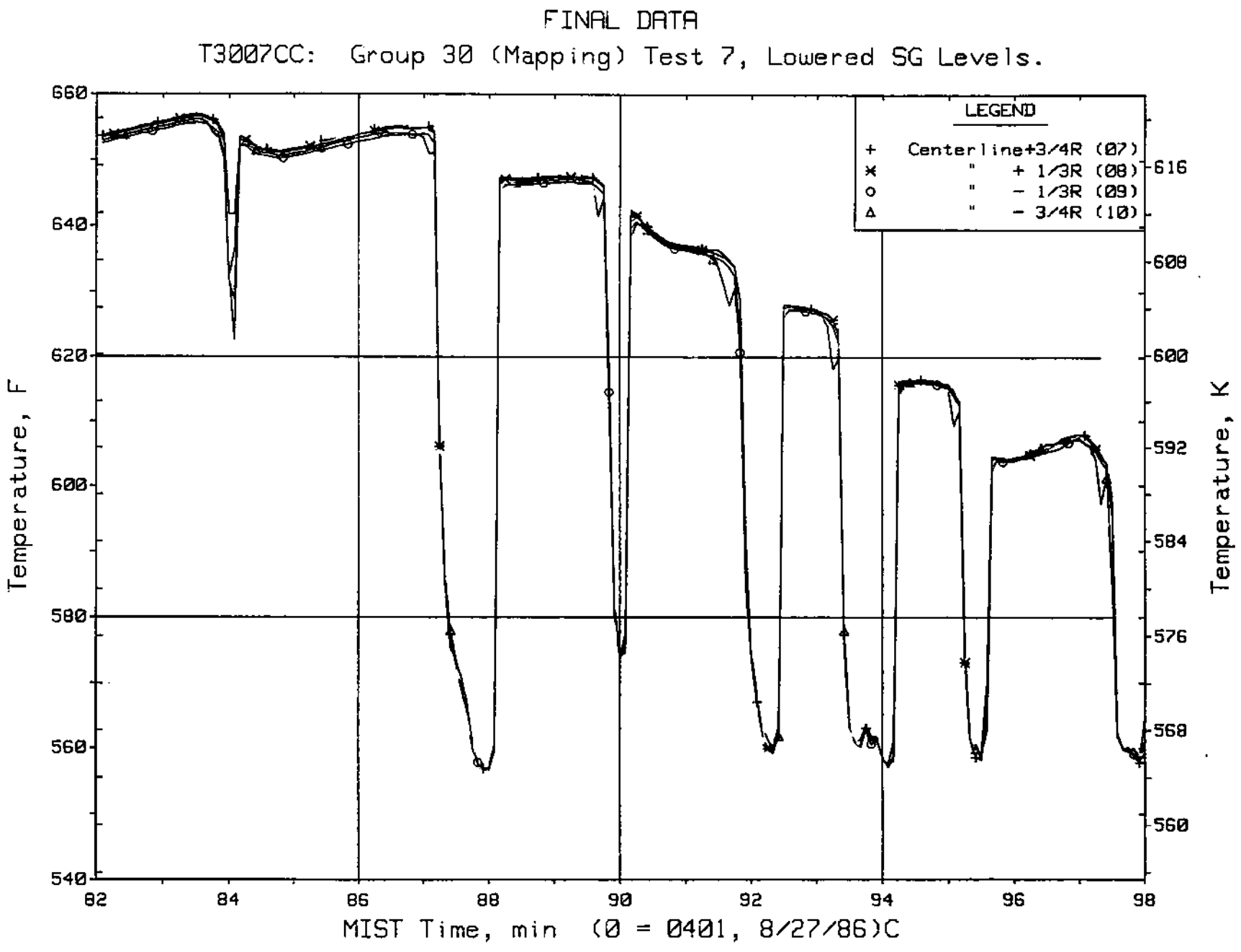

Figure 5.5.26. Cold Leg B1 Pump Discharge Rake Fluid Temperatures (25 ft, C2TCs)

Wed Mar 22 15:01:05 1989

C2TC3

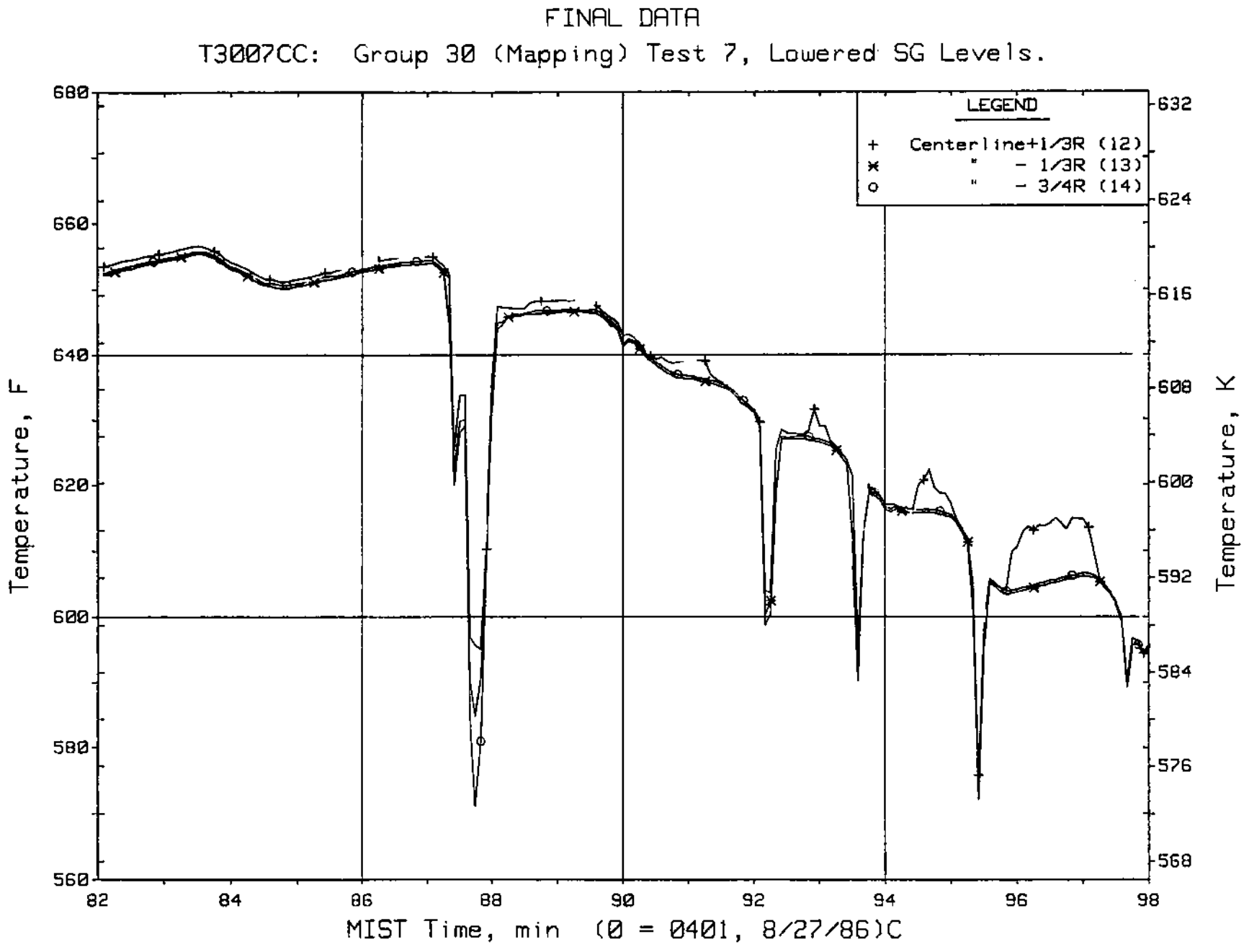

Figure 5.5.27. Cold Leg B1 Nozzle Rake Fluid Temperatures (21.2 ft, C2TCs)

Wed Mar 22 15:03:23 1989

C2TC4

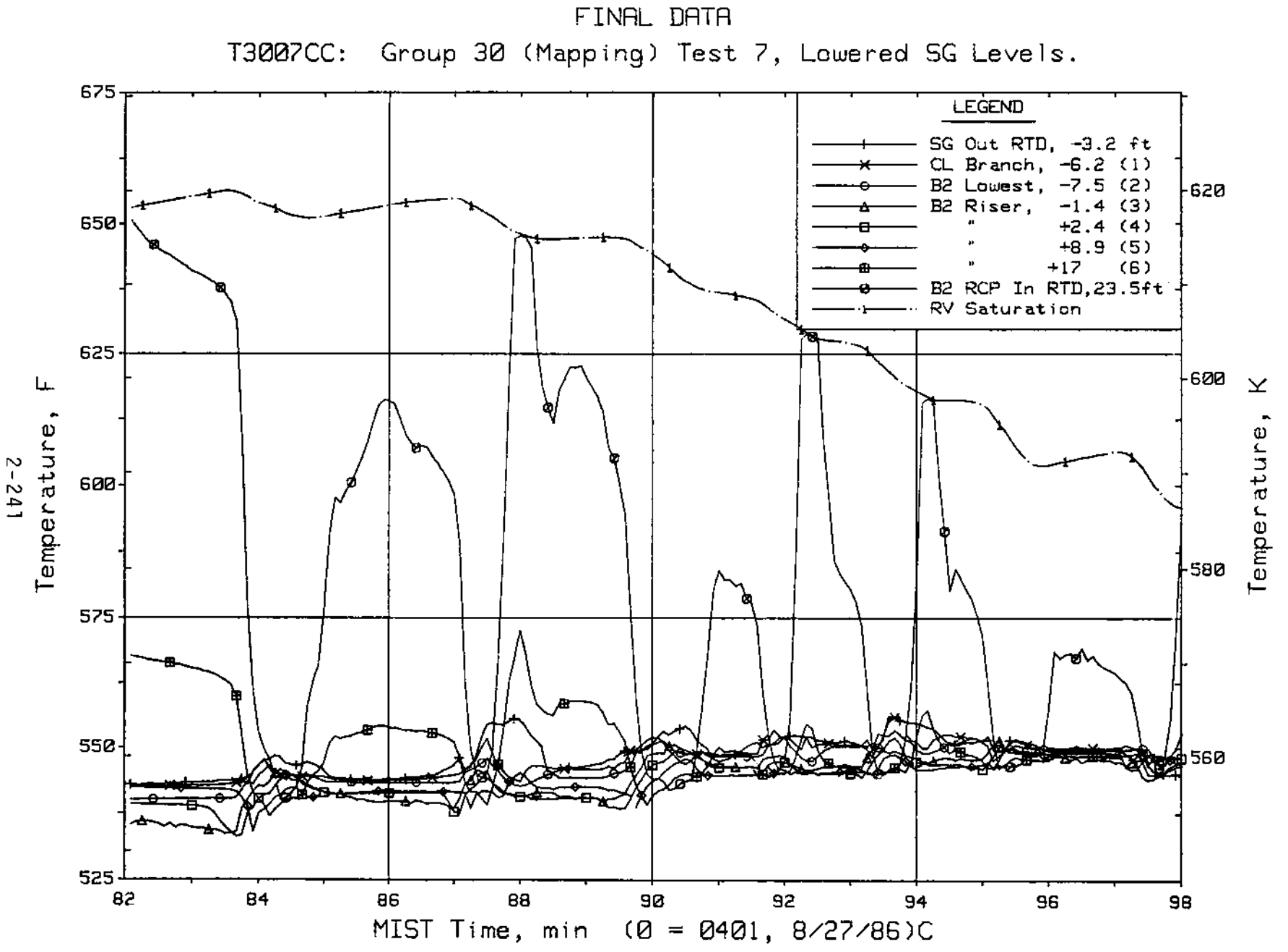

Figure 5.5.28. Cold Leg B2 Suction Fluid Temperatures (C4TCs)

Wed Mar 22 15:13:52 1989

C4TC1

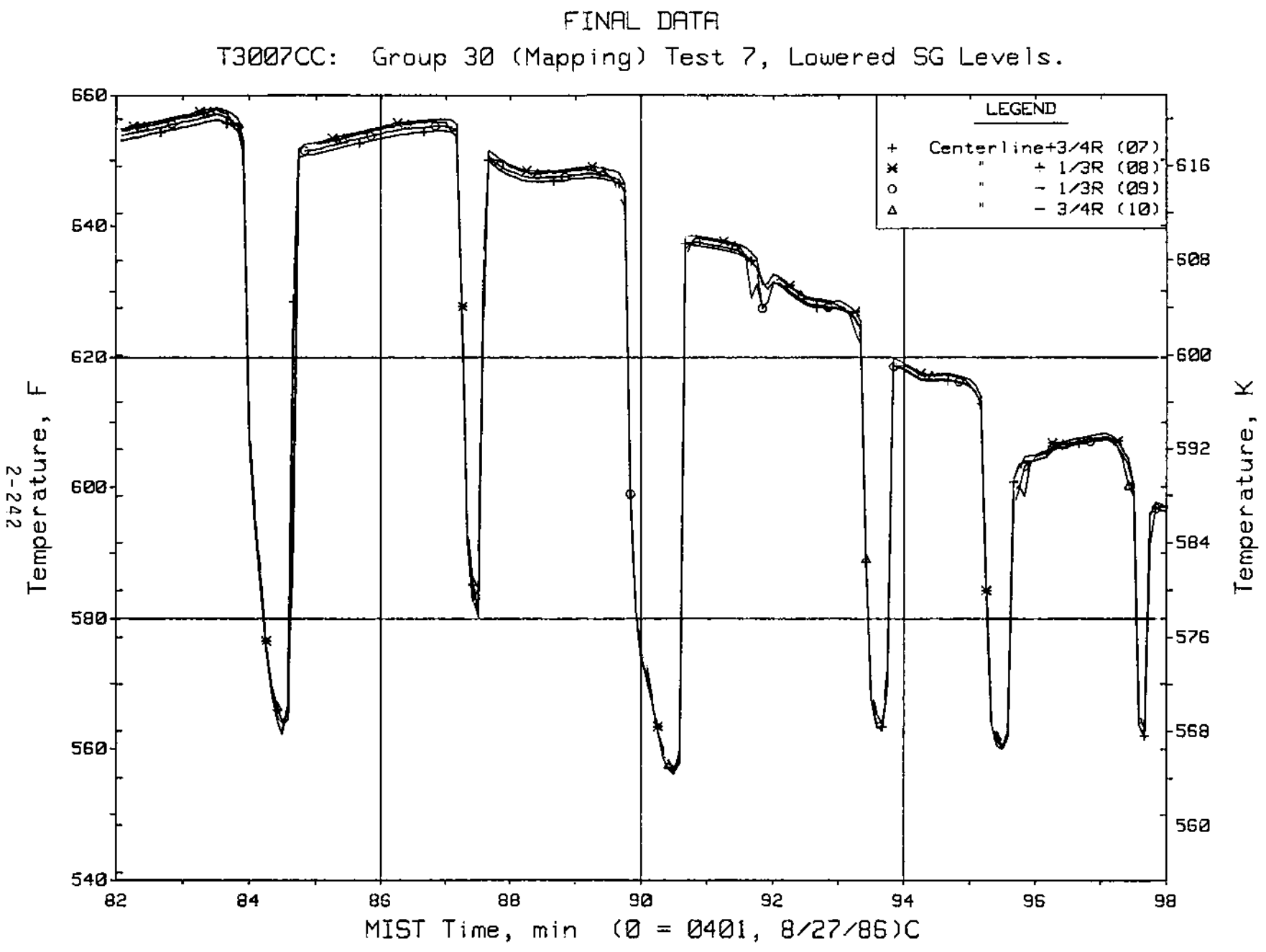

Figure 5.5.29. Cold Leg B2 Pump Discharge Rake Fluid Temperatures (25 ft, C4TCs)

Wed Mar 22 15:16:14 1989

C4TC3

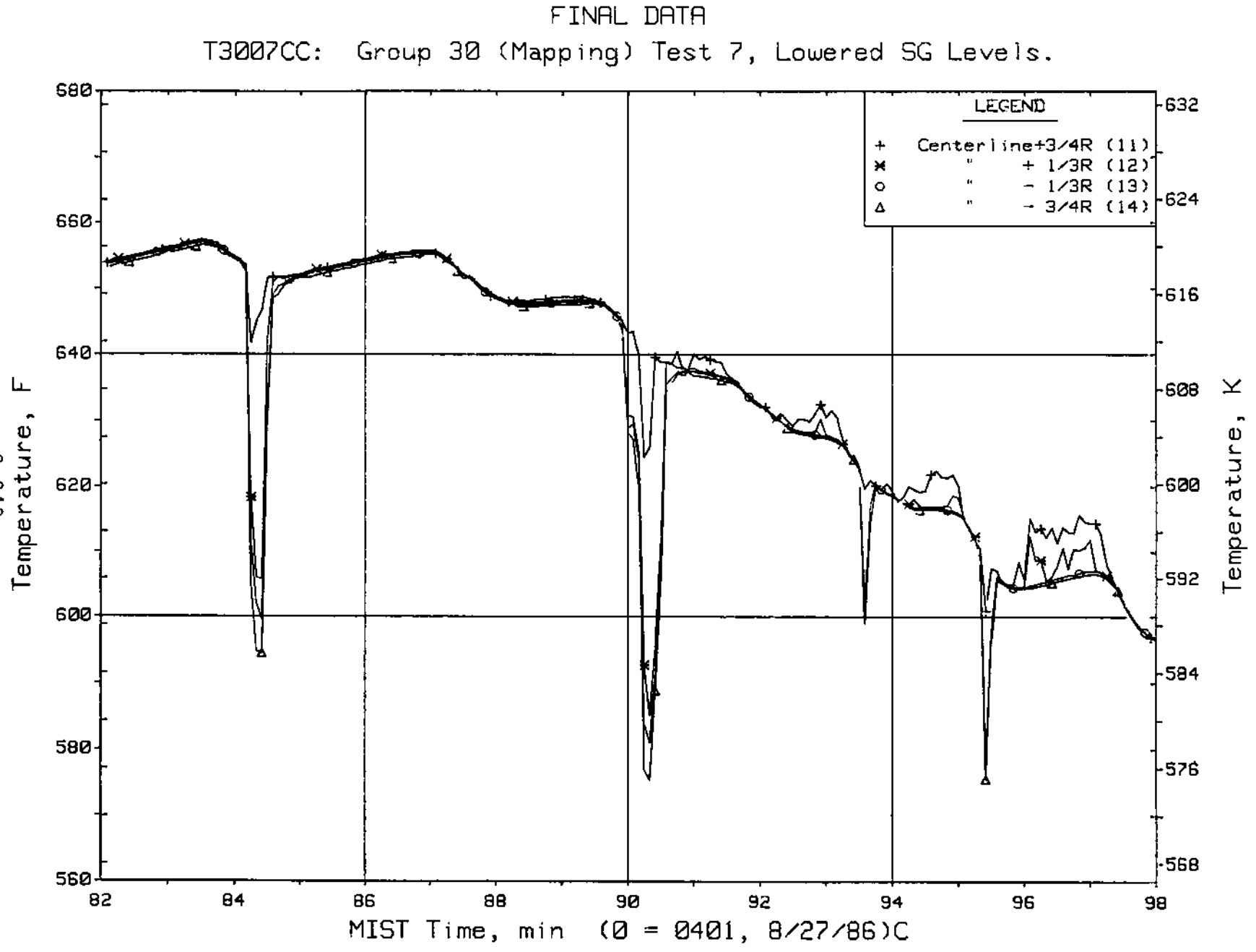

Figure 5.5.30. Cold Leg B2 Nozzle Rake Fluid Temperatures (21.2 ft, C4TCs)

Wed Mar 22 15:18:24 1989

C4TC4

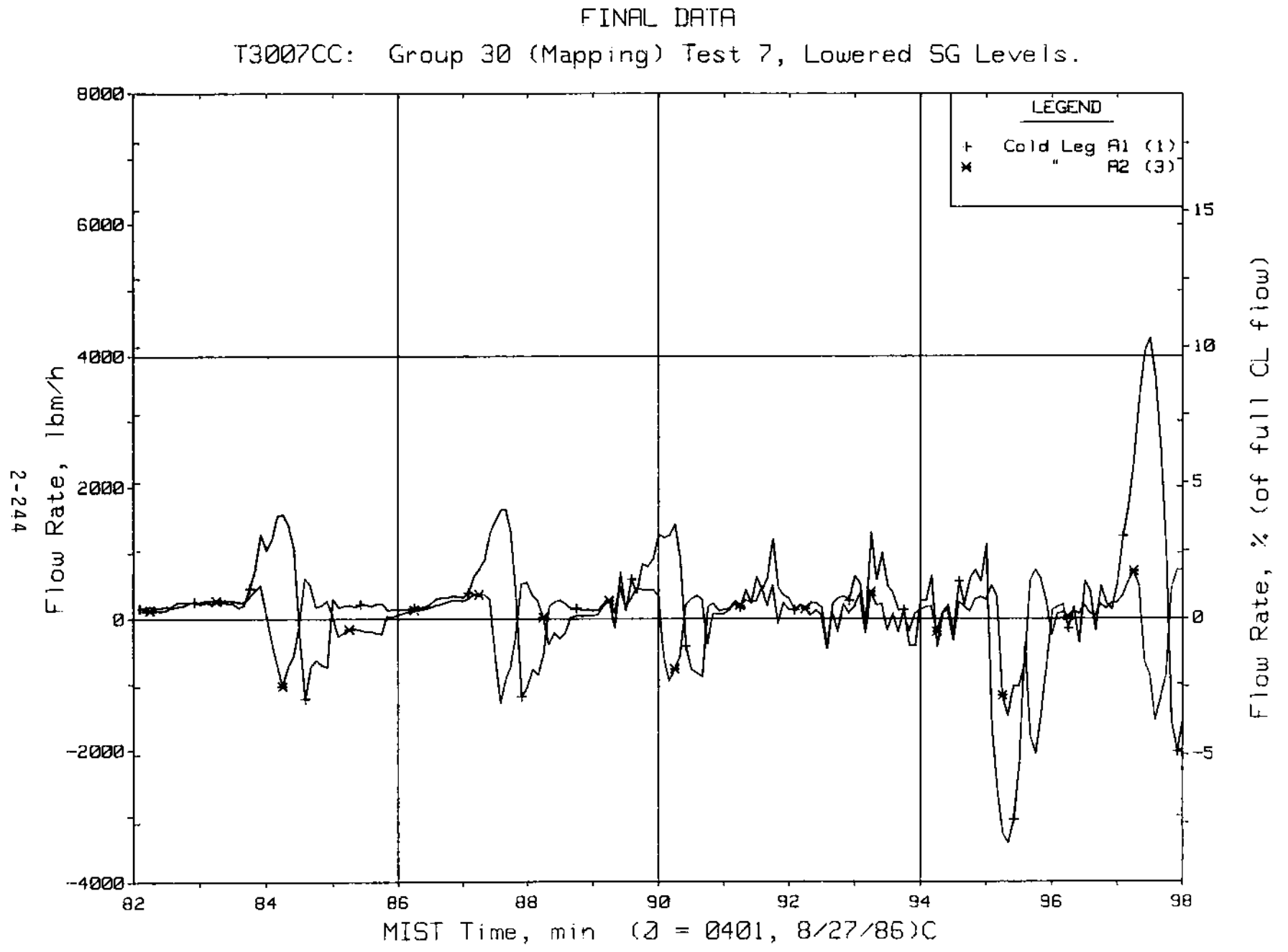

Figure 5.5.31. Loop A Cold Leg (Venturi) Flow Rates (CnVN20s)

Thu Mar 23 10:19:46 1989

PRFLS

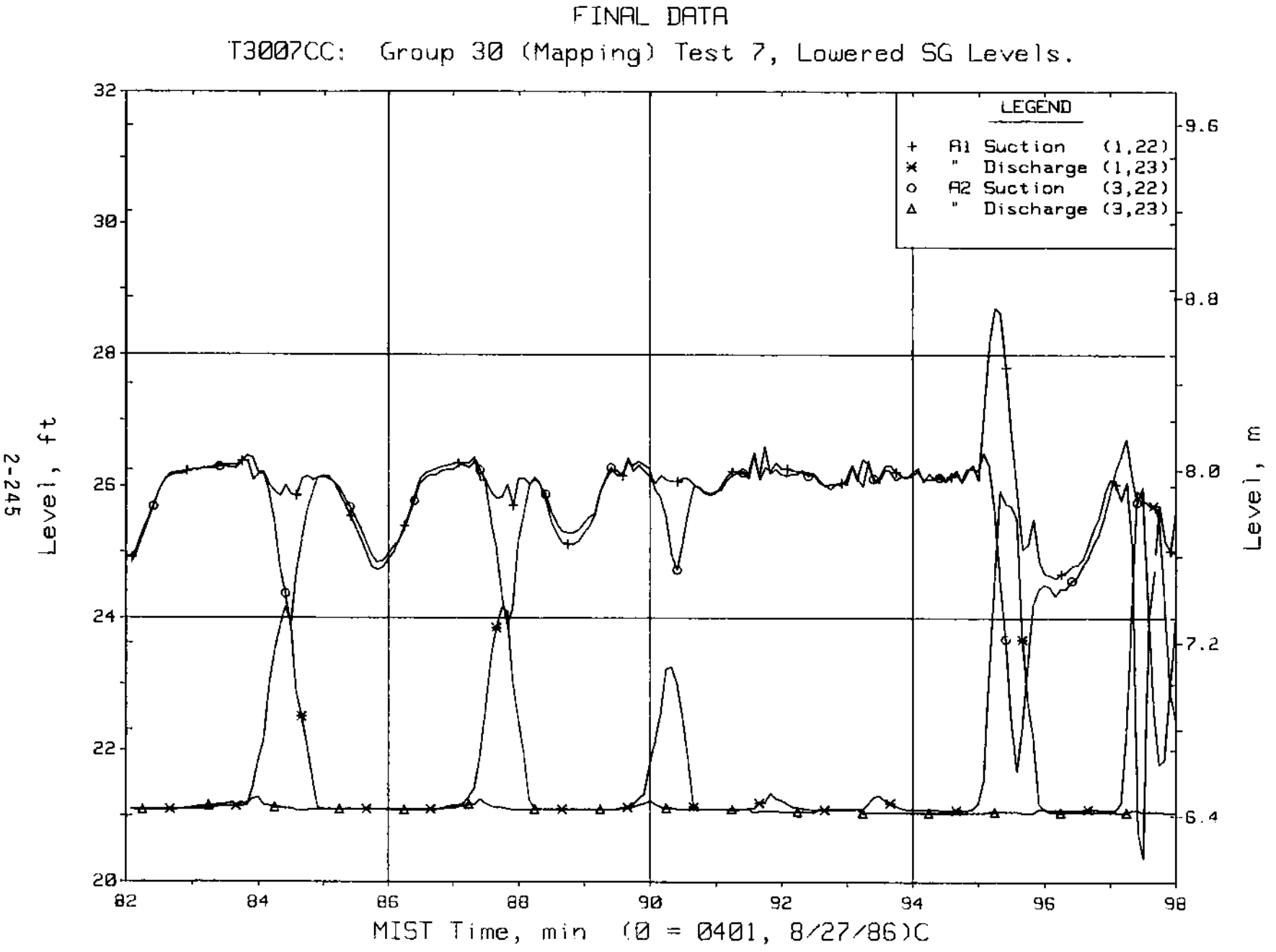

Figure 5.5.32. Loop A Cold Leg Collapsed Liquid Levels (LVs)

Thu Mar 23 10:28:43 1989

CLLV1

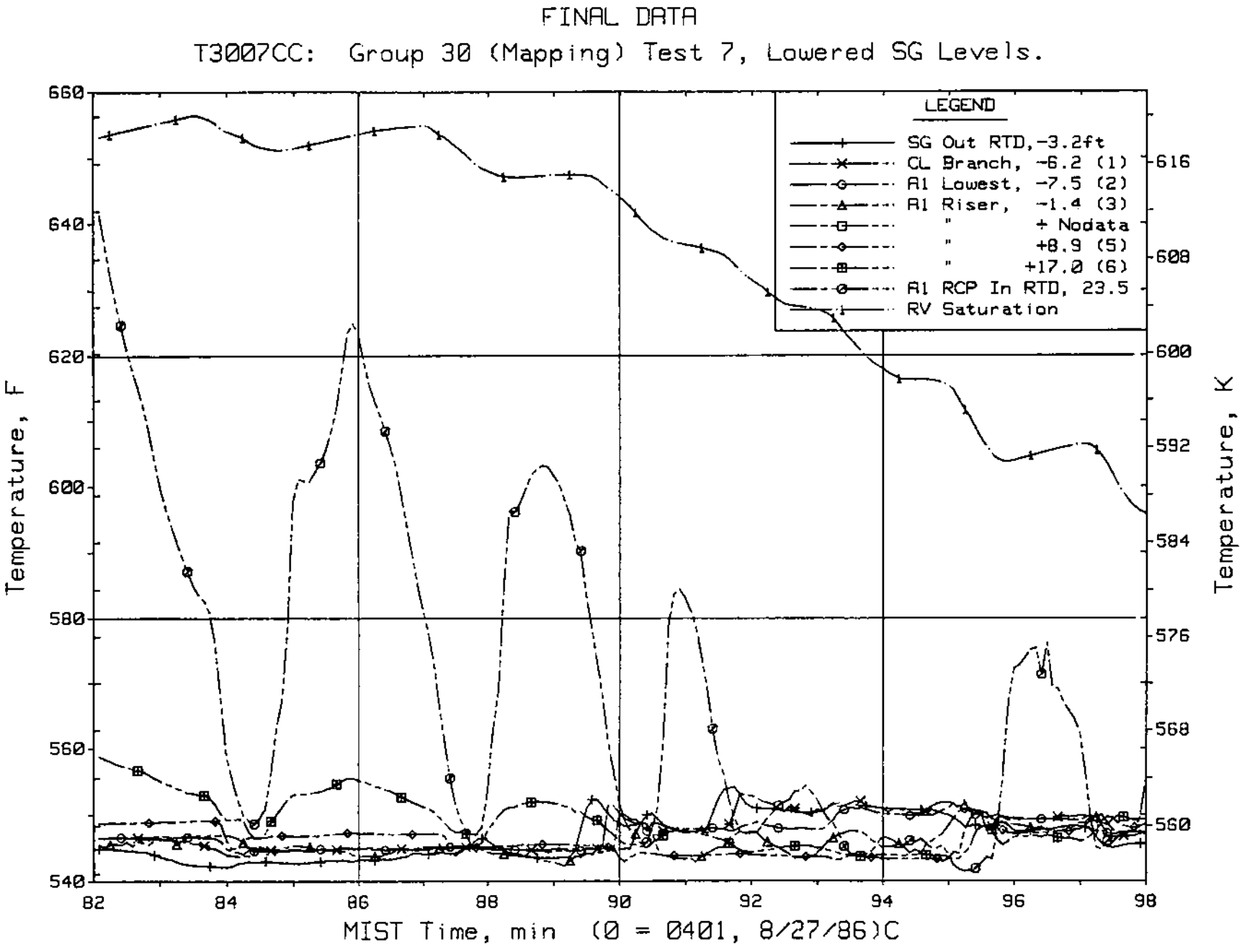

Figure 5.5.33. Cold Leg A1 Suction Fluid Temperatures (C1TCs)

Wed Mar 22 14:51:17 1989

C1TC1

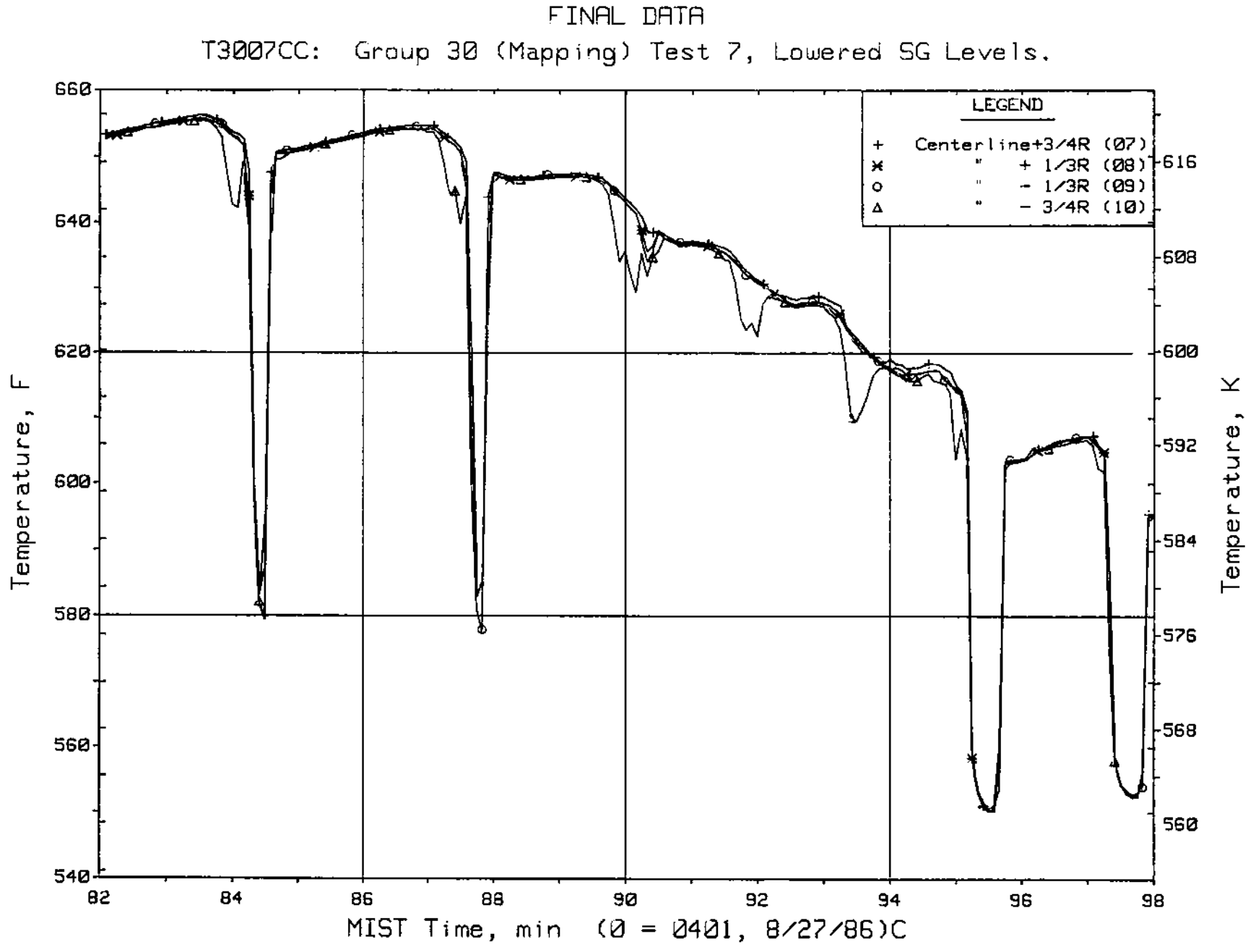

Figure 5.5.34. Cold Leg A1 Pump Discharge Rake Fluid Temperatures (25 ft, C1TCs)

Wed Mar 22 14:53:51 1989

C1TC3

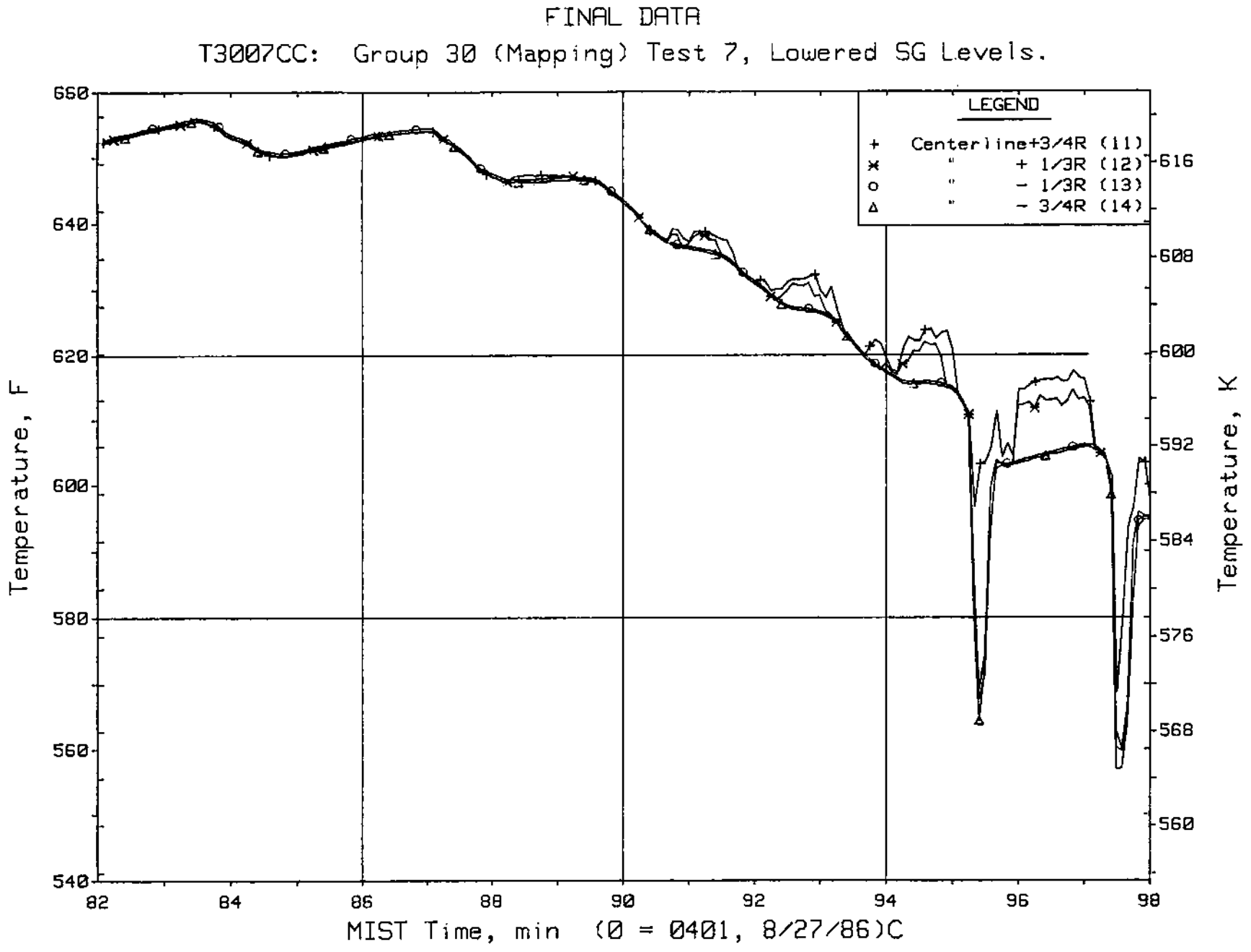

Figure 5.5.35. Cold Leg A1 Nozzle Rake Fluid Temperatures (21.2 ft, C1TCs)

Wed Mar 22 14:56:00 1989

C1TC4

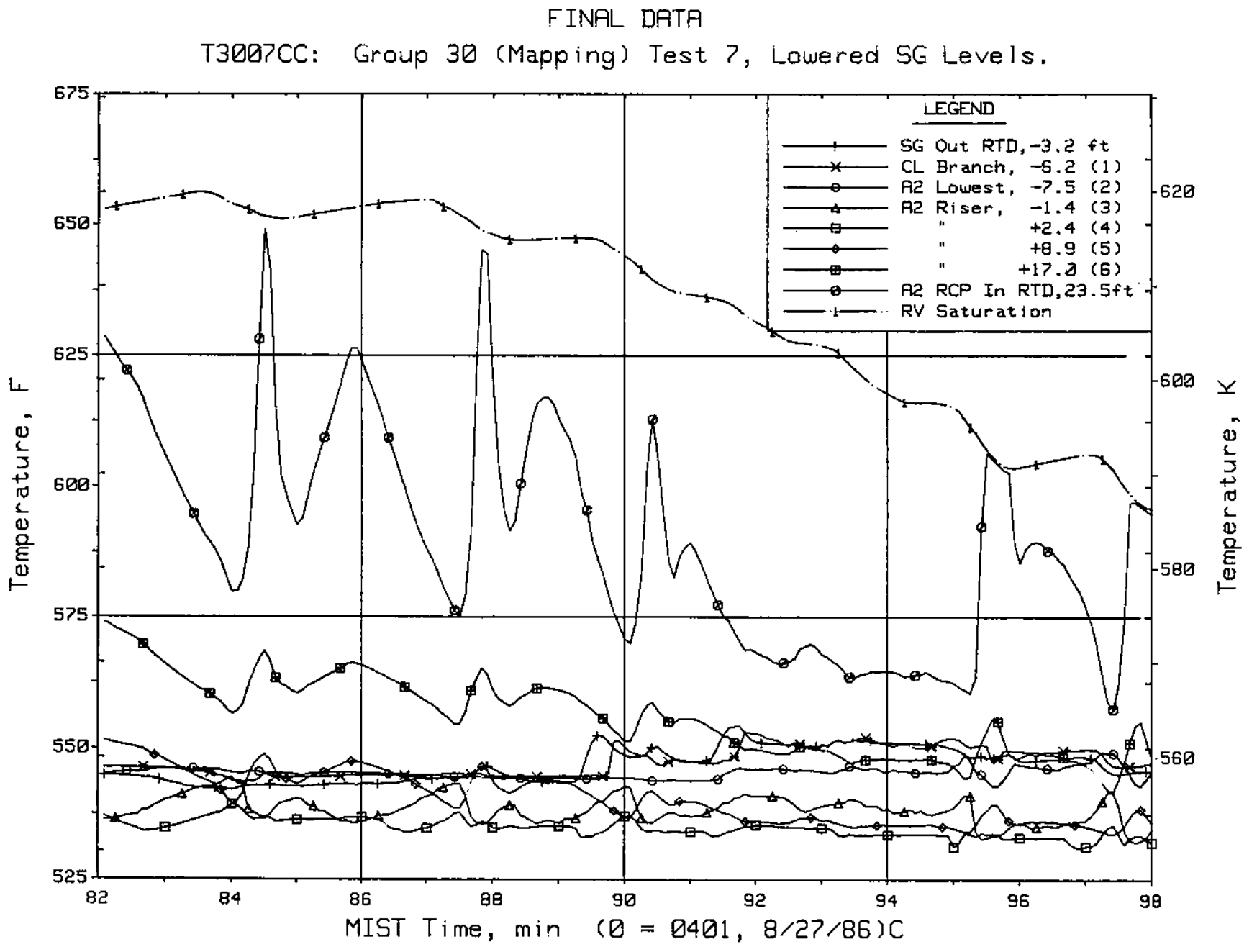

Figure 5.5.36. Cold Leg A2 Suction Fluid Temperatures (C3TCs)

Wed Mar 22 15:06:39 1989

C3TC1

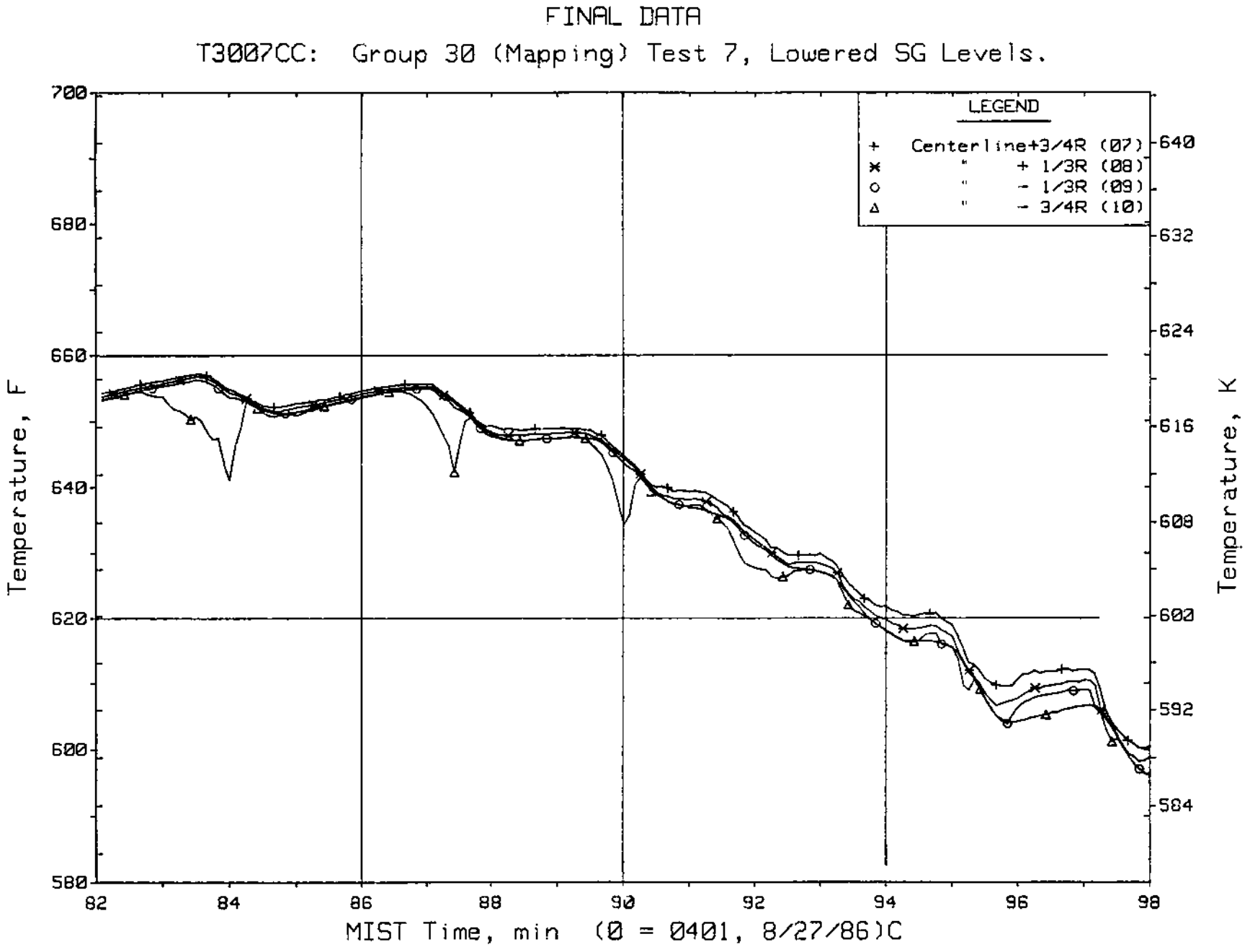

Figure 5.5.37. Cold Leg A2 Pump Discharge Rake Fluid Temperatures (25 ft, C3TCs)

Wed Mar 22 15:09:04 1989

C3TC3

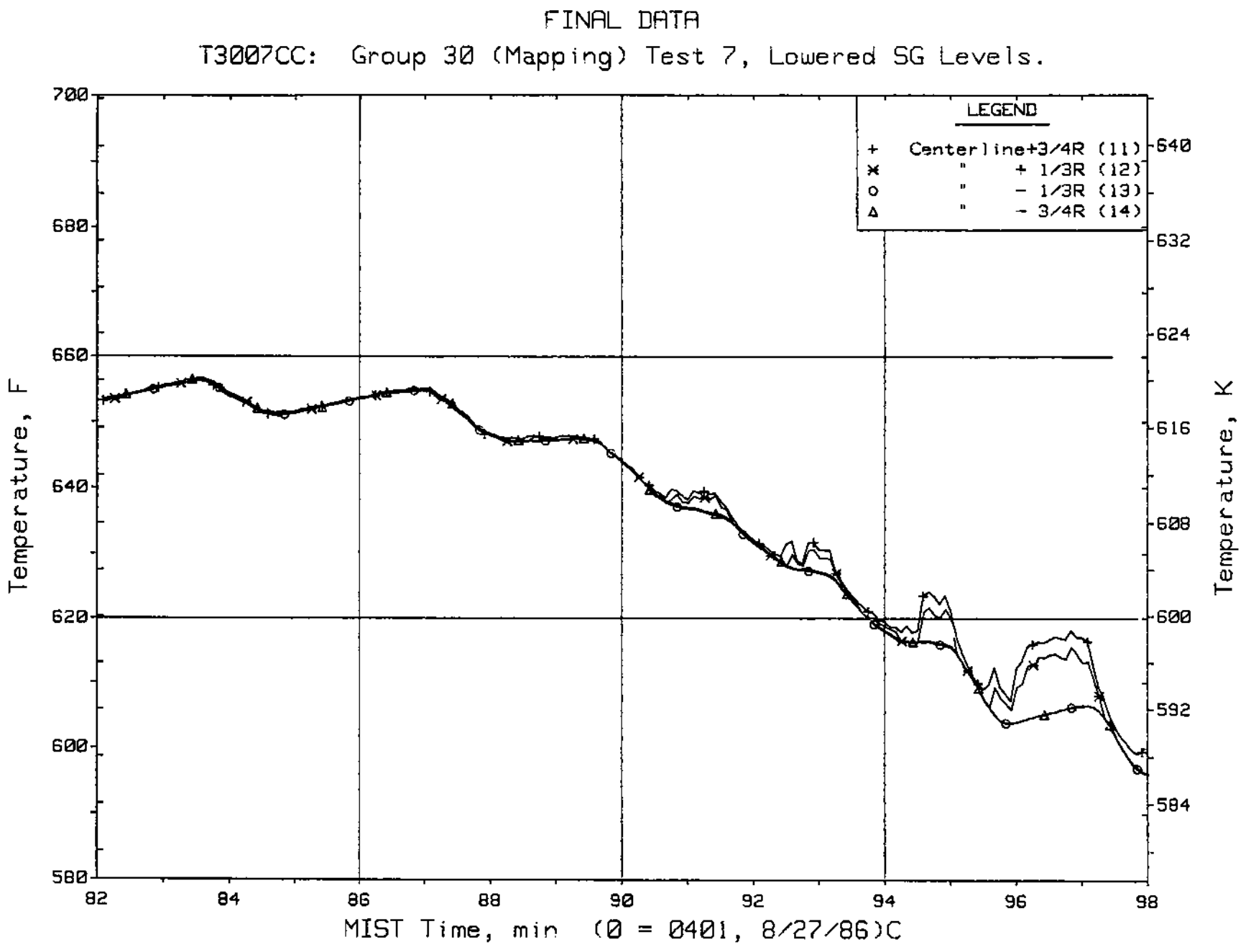

Figure 5.5.38. Cold Leg A2 Nozzle Rake Fluid Temperatures (21.2 ft, C3TCs)

Wed Mar 22 15:11:11 1989

C3TC4

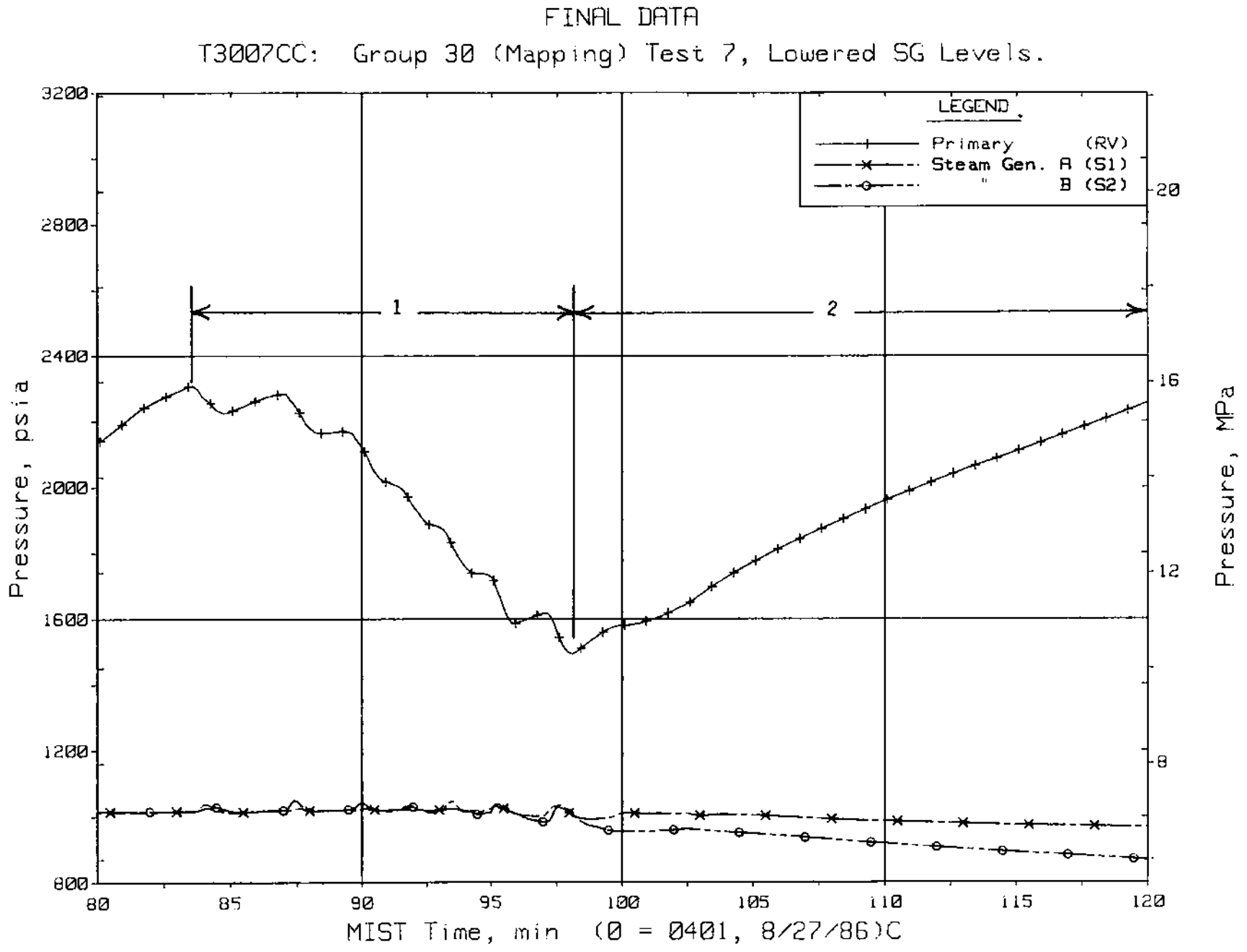

Figure 5.5.39. Primary and Secondary System Pressures (GP01s)

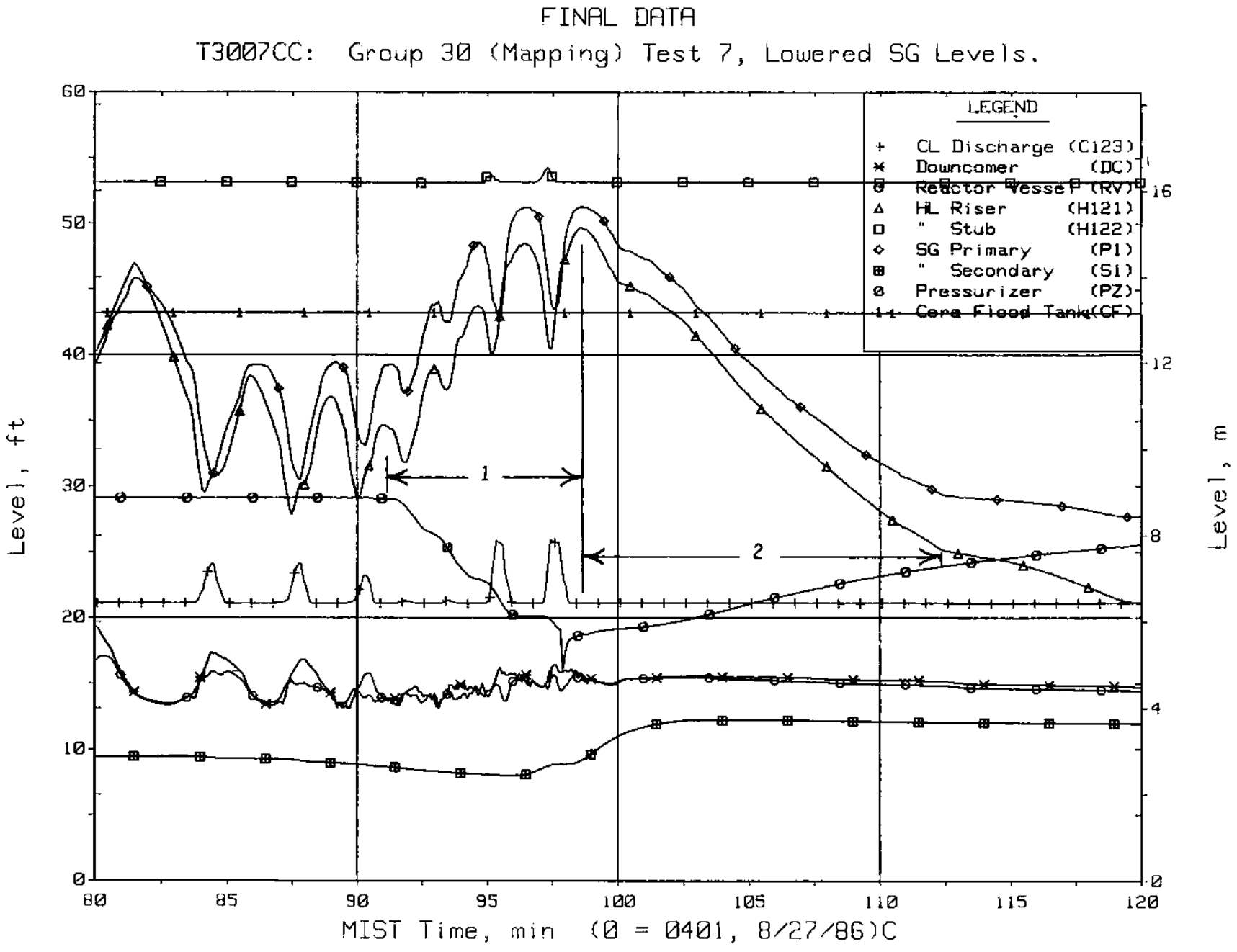

Figure 5.5.40. Loop A Collapsed Liquid Levels (LV20s)

Mon Feb 27 15:12:54 1989

PRLV1

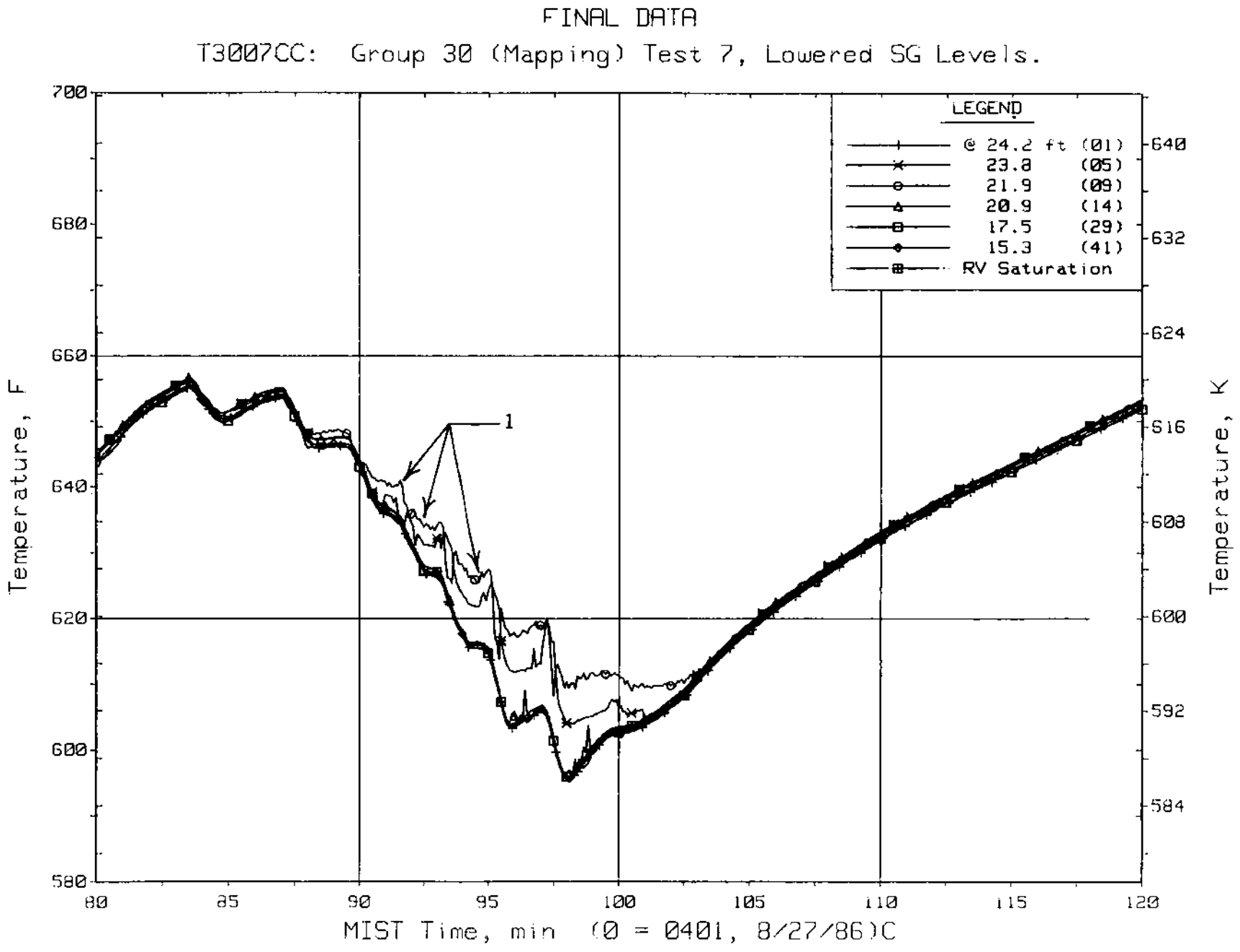

Figure 5.5.41. Downcomer Quadrant A1 Upper-Elevation Fluid Temperatures (DCTCs)

Mon Feb 27 15:09:23 1989

DCTC1

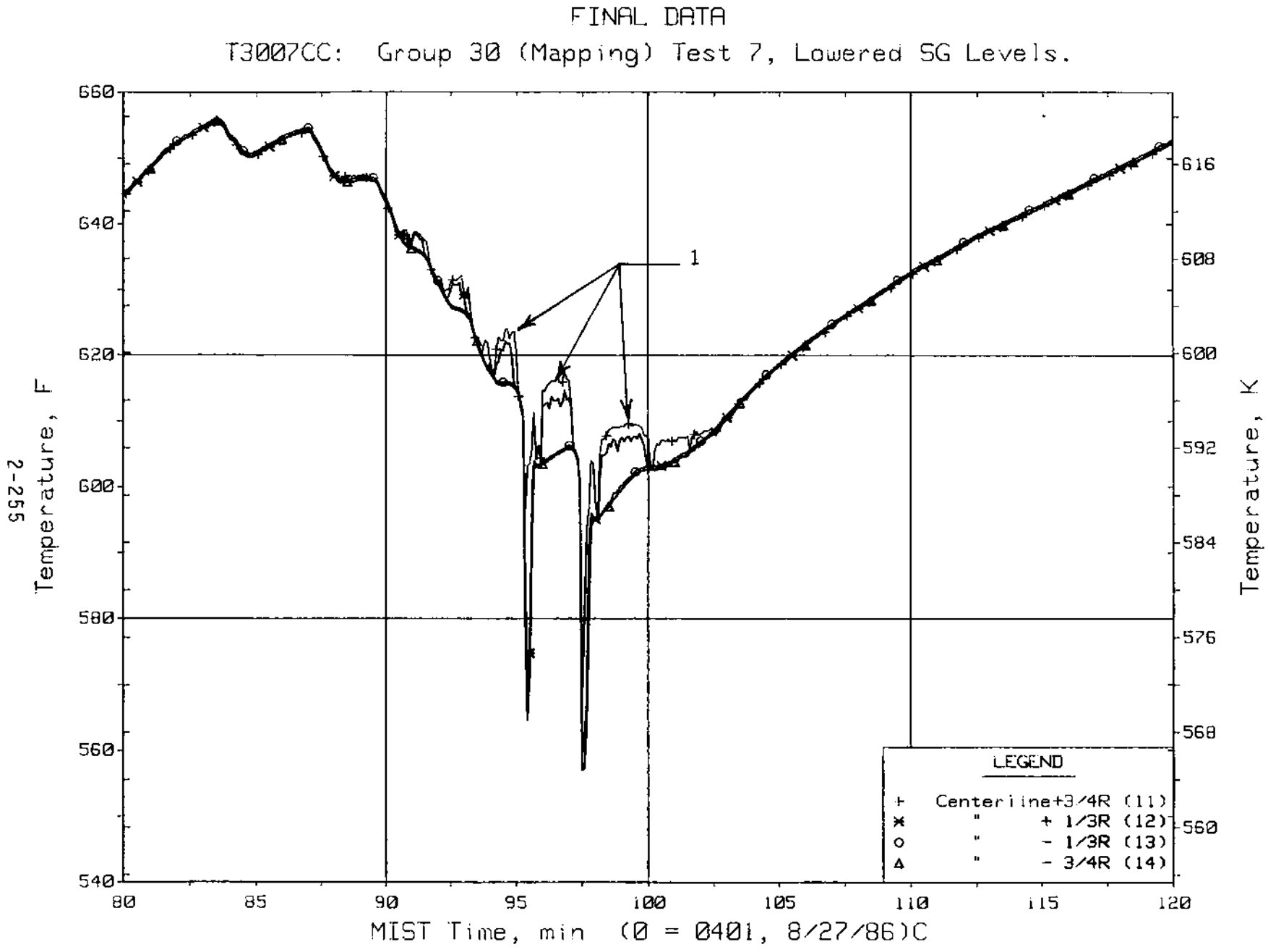

Figure 5.5.42. Cold Leg A1 Nozzle Rake Fluid Temperatures (21.2 ft, C1TCs)

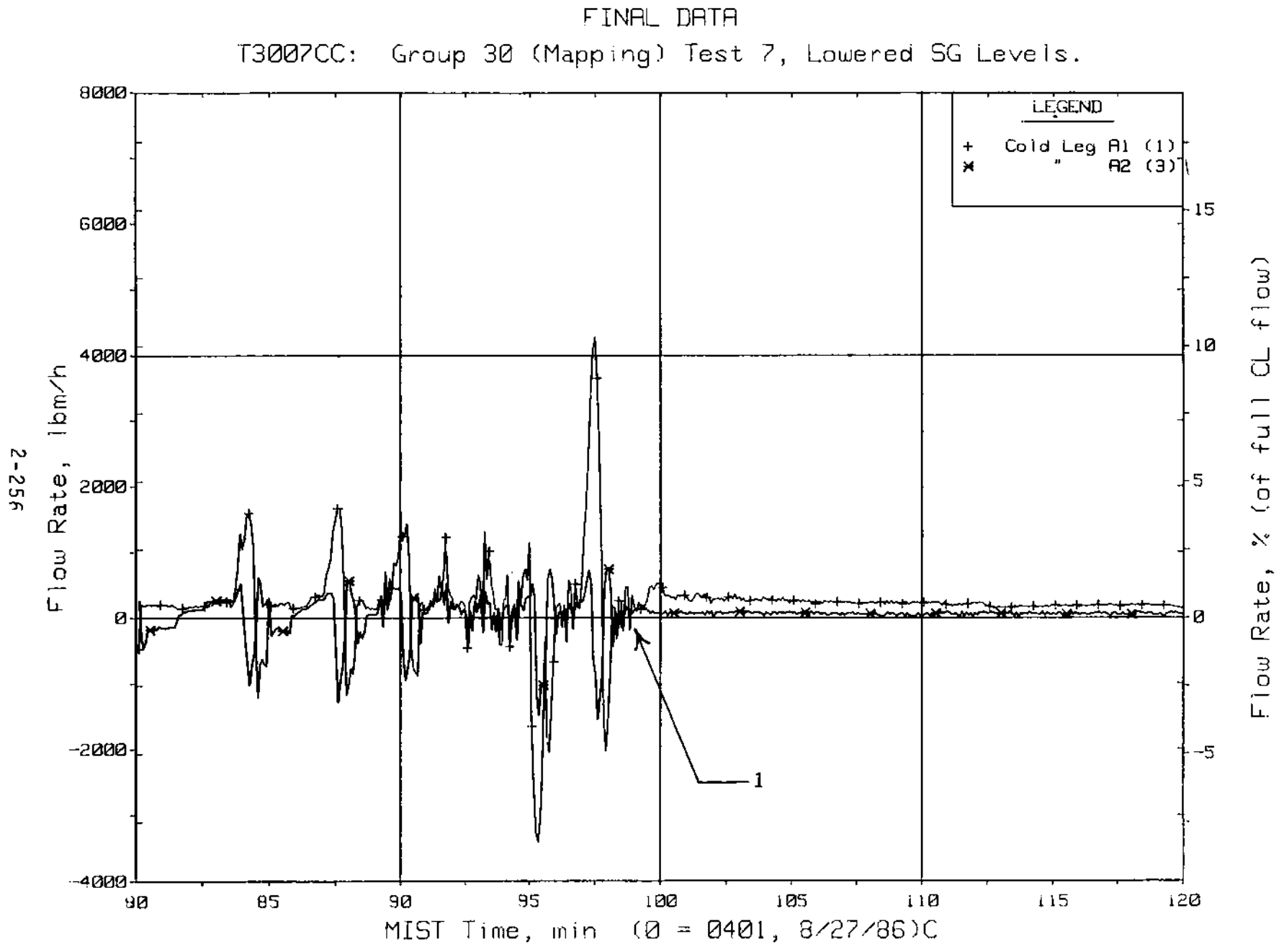

Figure 5.5.43. Loop A Cold Leg (Venturi) Flow Rates (CnVN20s)

Mon Feb 27 14:59:02 1989

PRFL5

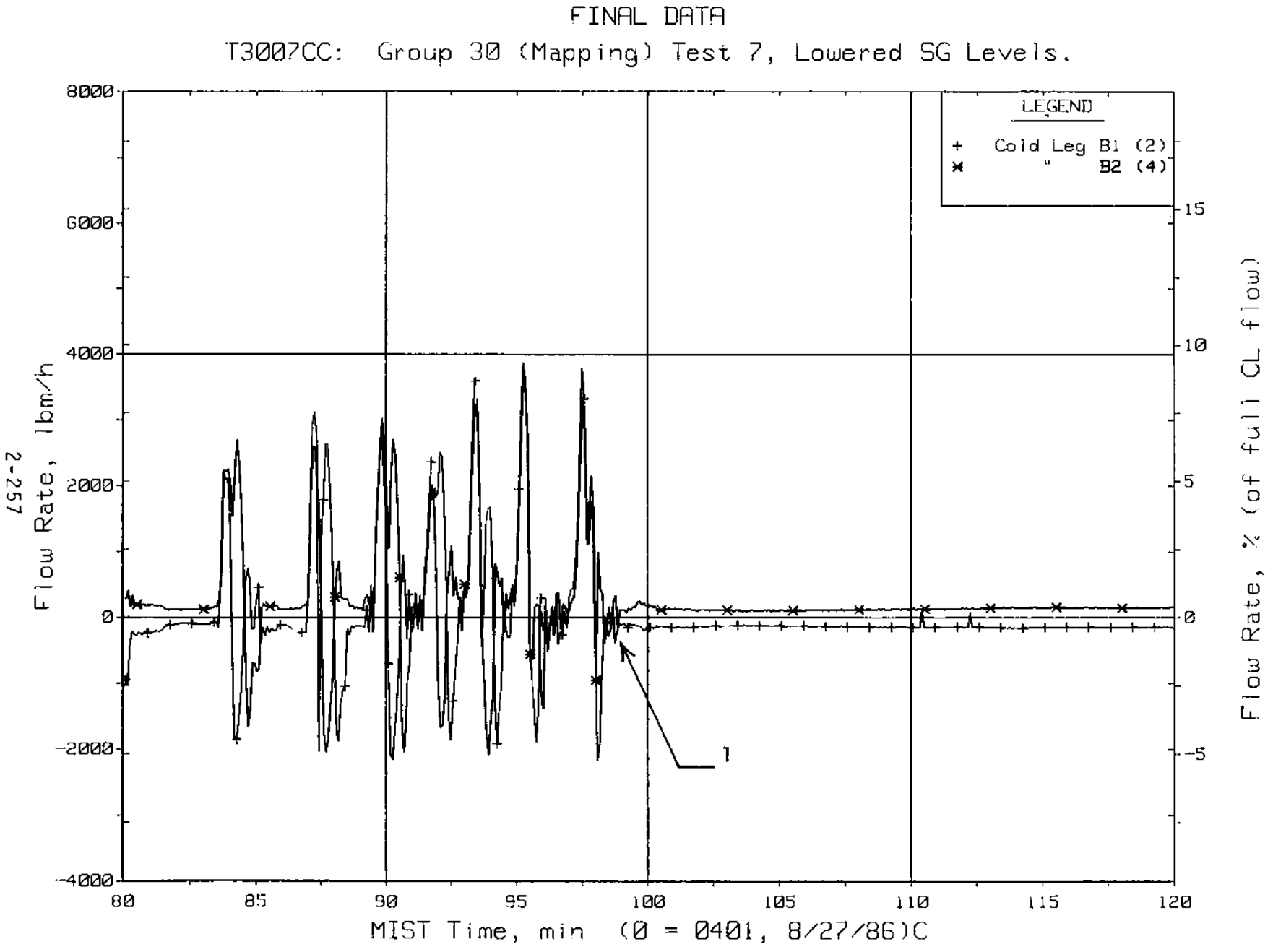

Figure 5.5.44. Loop B Cold Leg (Venturi) Flow Rates (CnVN20s)

Mon Feb 27 14:54:47 1989

PRFLG

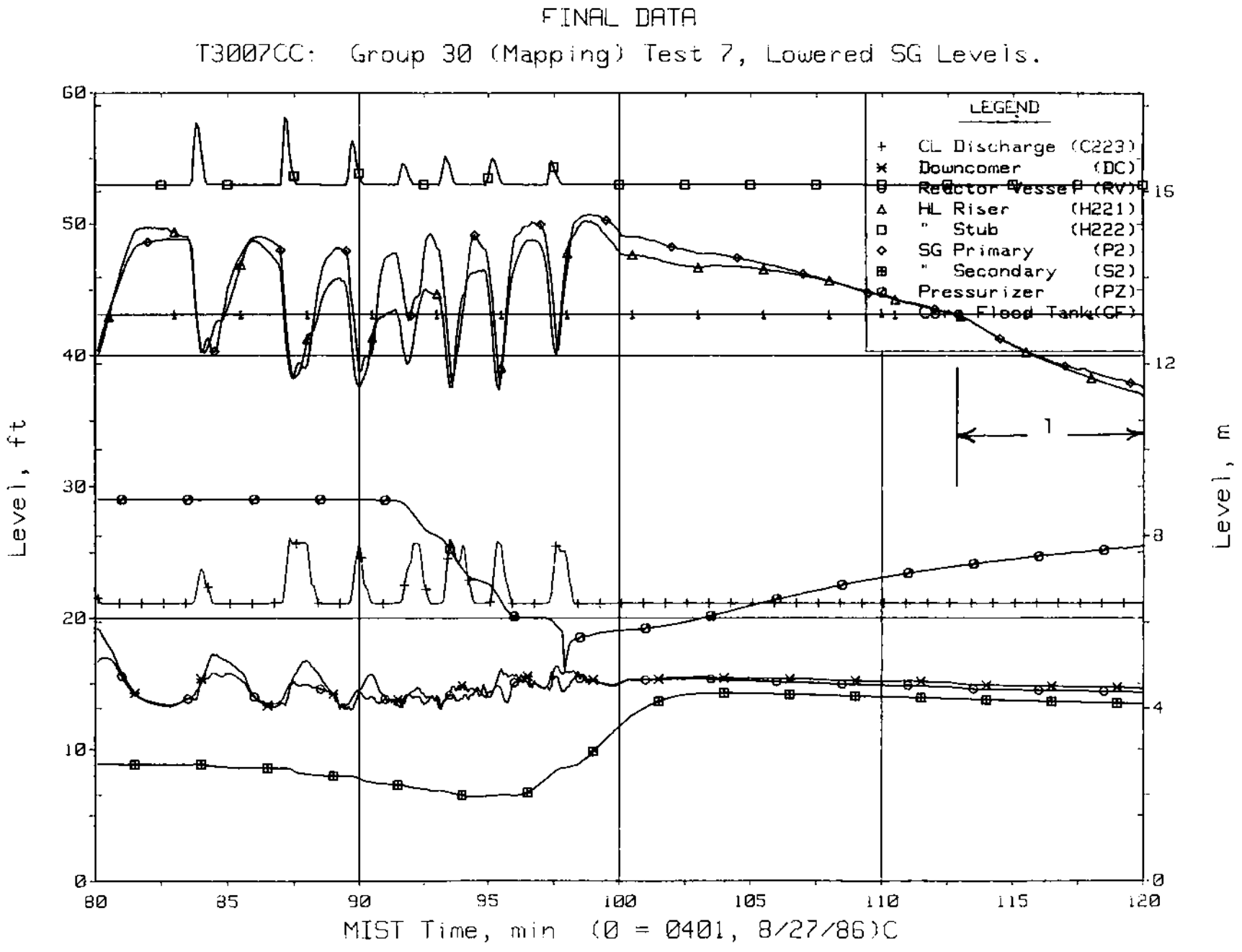

Figure 5.5.45. Loop B Collapsed Liquid Levels (LV20s)

Mon Feb 27 14:49:14 1989

PRLV2

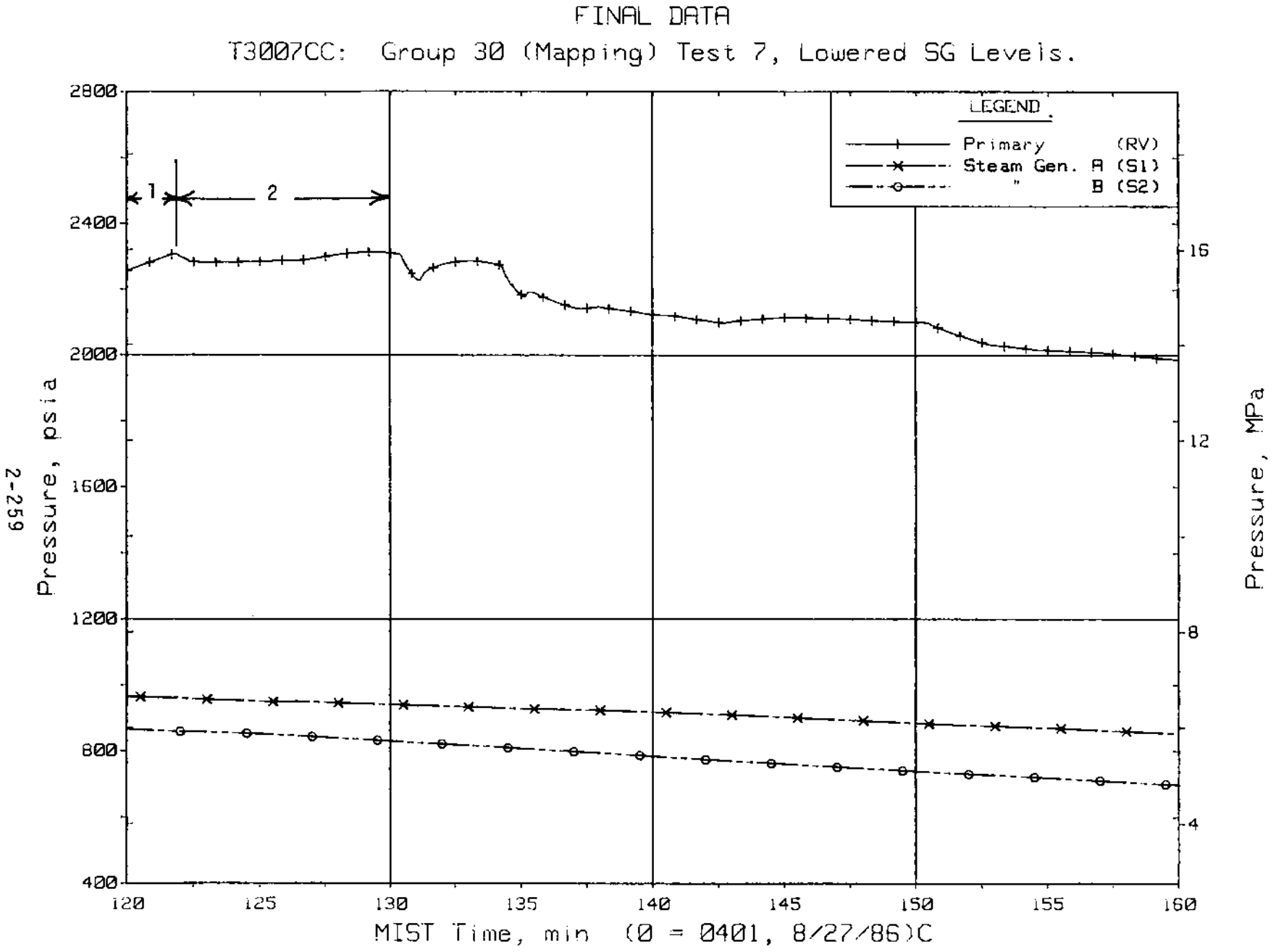

Figure 5.5.46. Primary and Secondary System Pressures (GP01s)

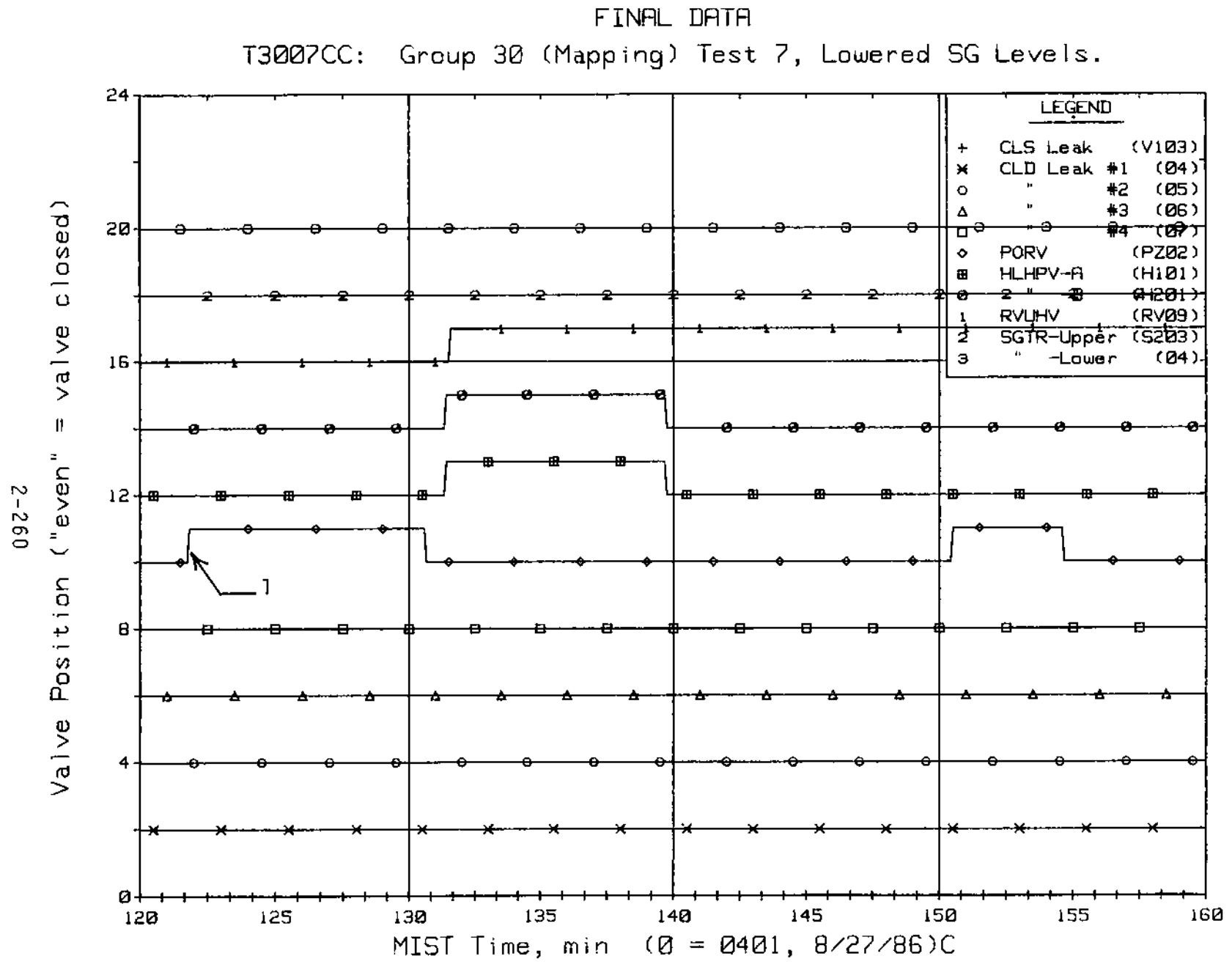

Figure 5.5.47. Primary System Discharge Limit Switch Indications (LSs)

Tue Feb 28 10:51:01 1989

PBLS1

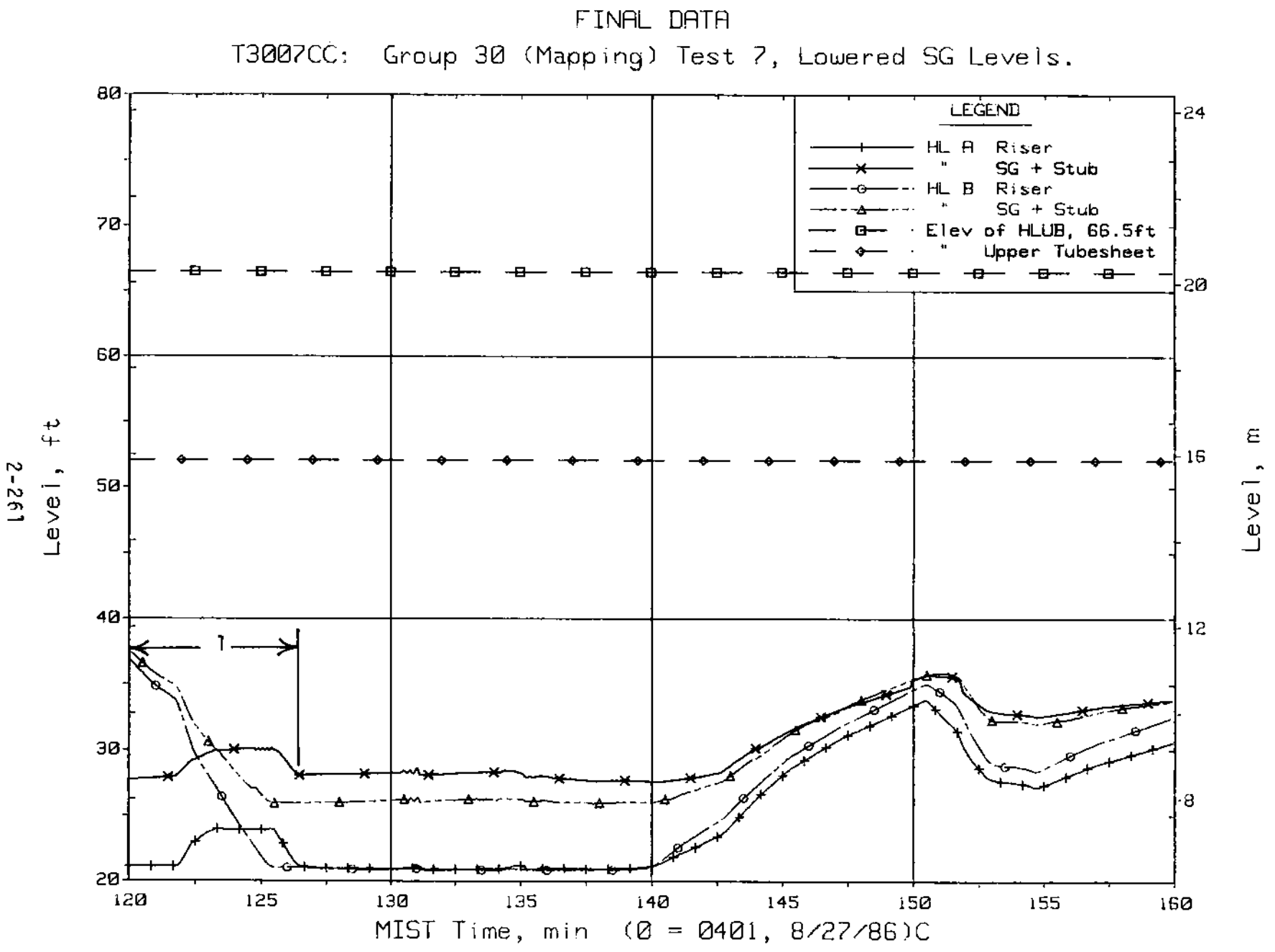

Figure 5.5.48. Hot Leg Riser and Stub Collapsed Liquid Levels

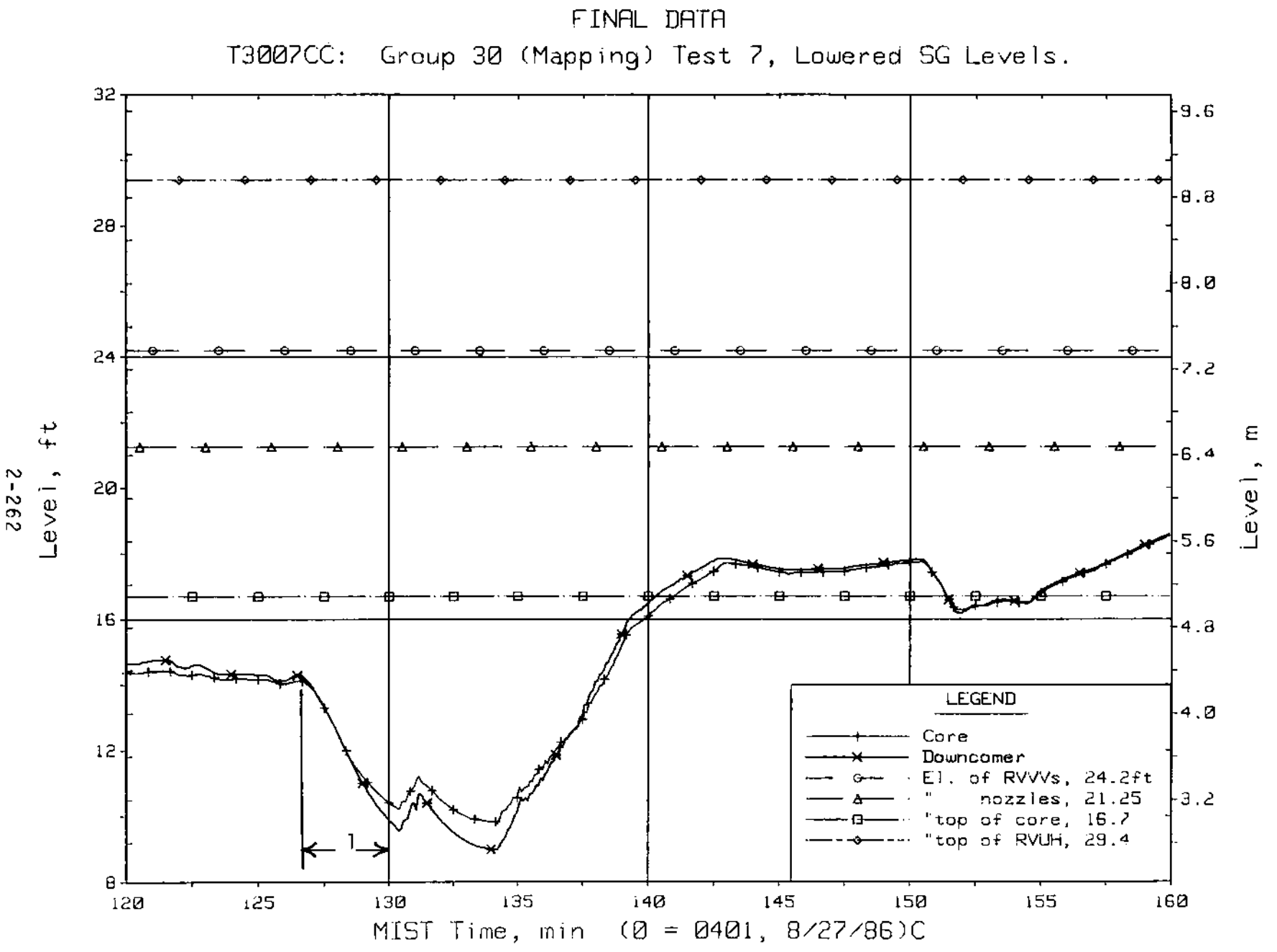

Figure 5.5.49. Core Region Collapsed Liquid Levels

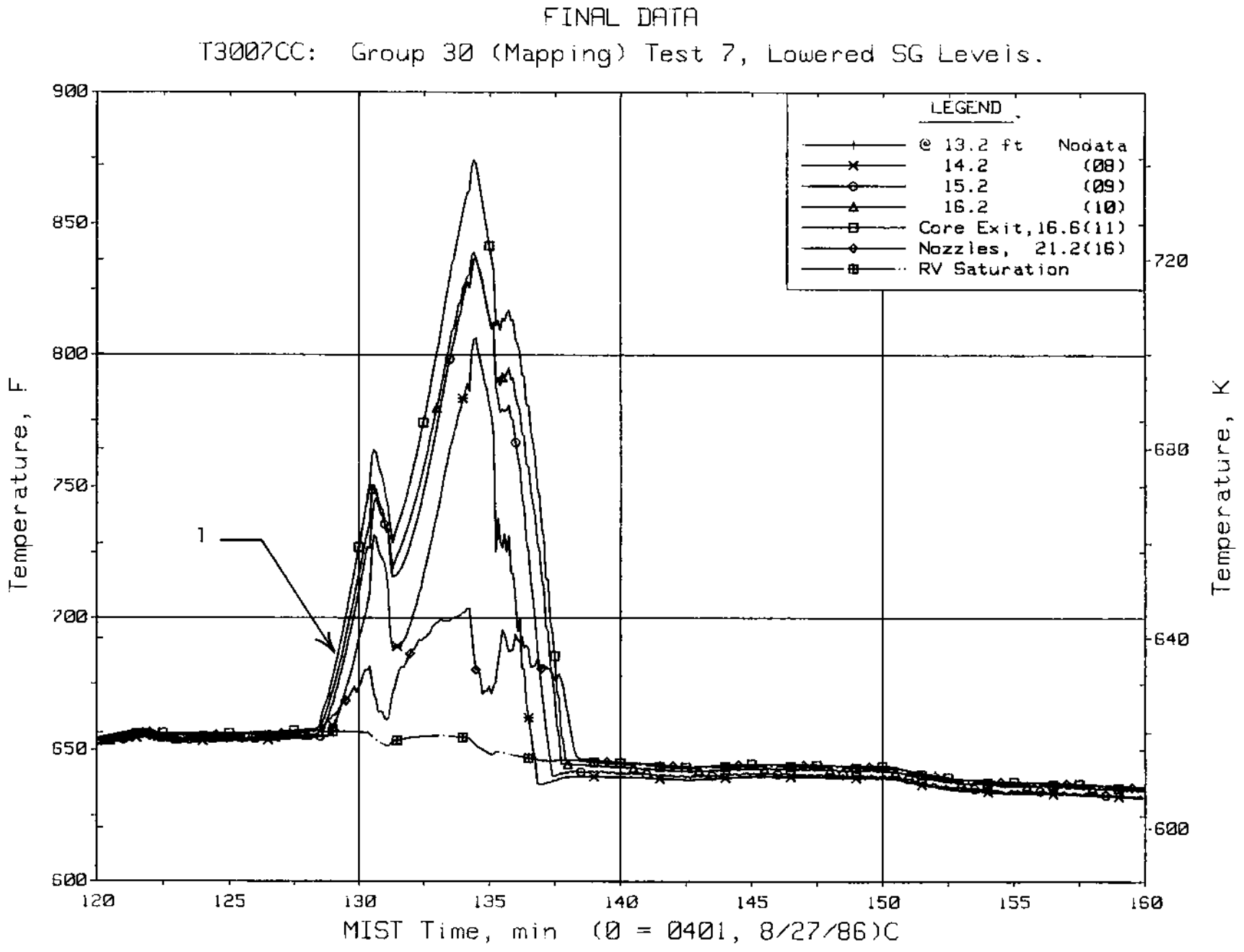

Figure 5.5.50. Reactor Vessel Mid-Elevation Fluid Temperatures (RVTCs)

Mon Feb 27 14:33:27 1989

RVTC2

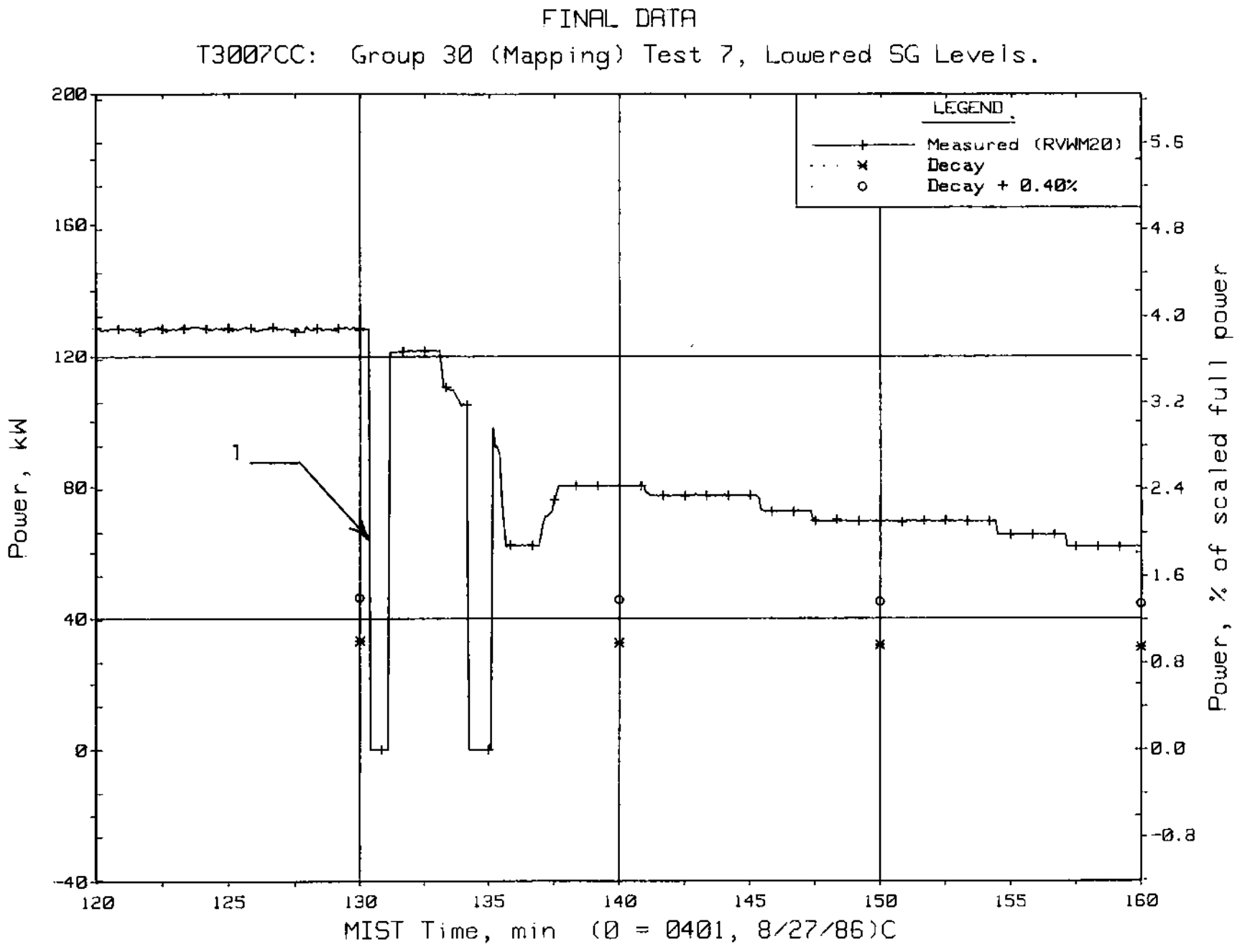

Figure 5.5.51. Core Power

Mon Feb 27 14:30:49 1989

RVKW1

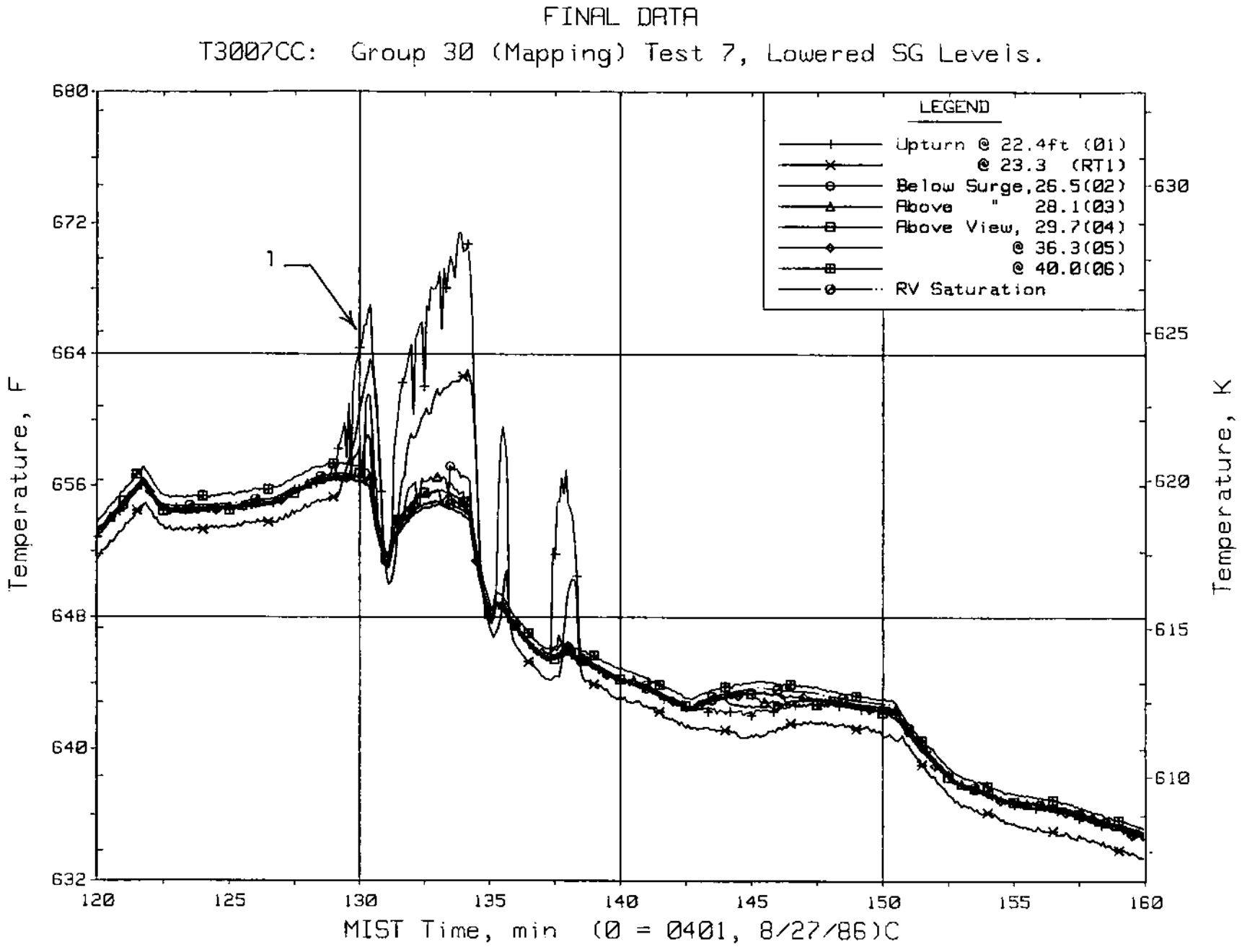

Figure 5.5.52. Hot Leg A Lower-Elevation Riser Fluid Temperatures (HITCs)

Mon Feb 27 14:28:41 1989

HITC1

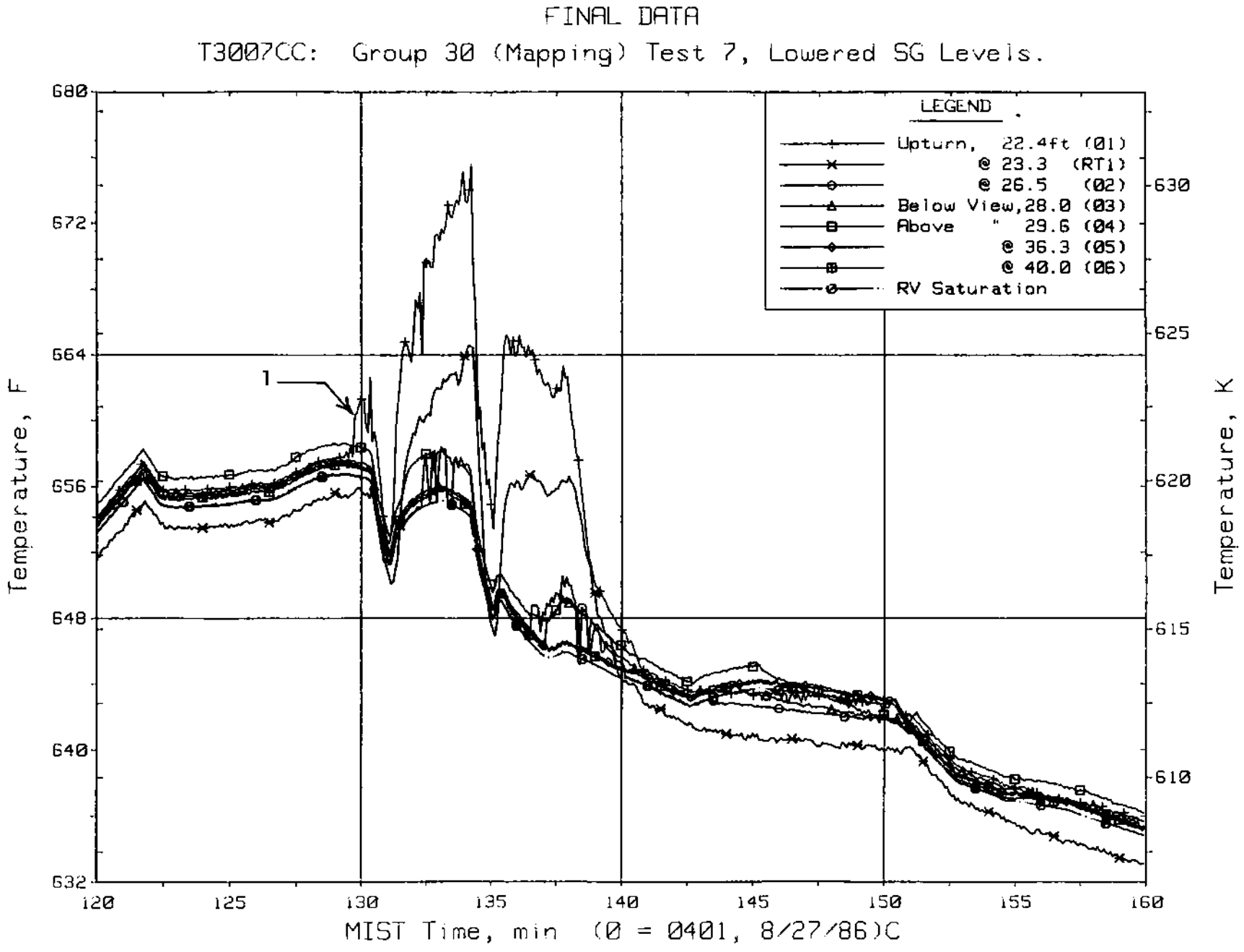

Figure 5.5.53. Hot Leg B Lower-Elevation Riser Fluid Temperatures (H2TCs)

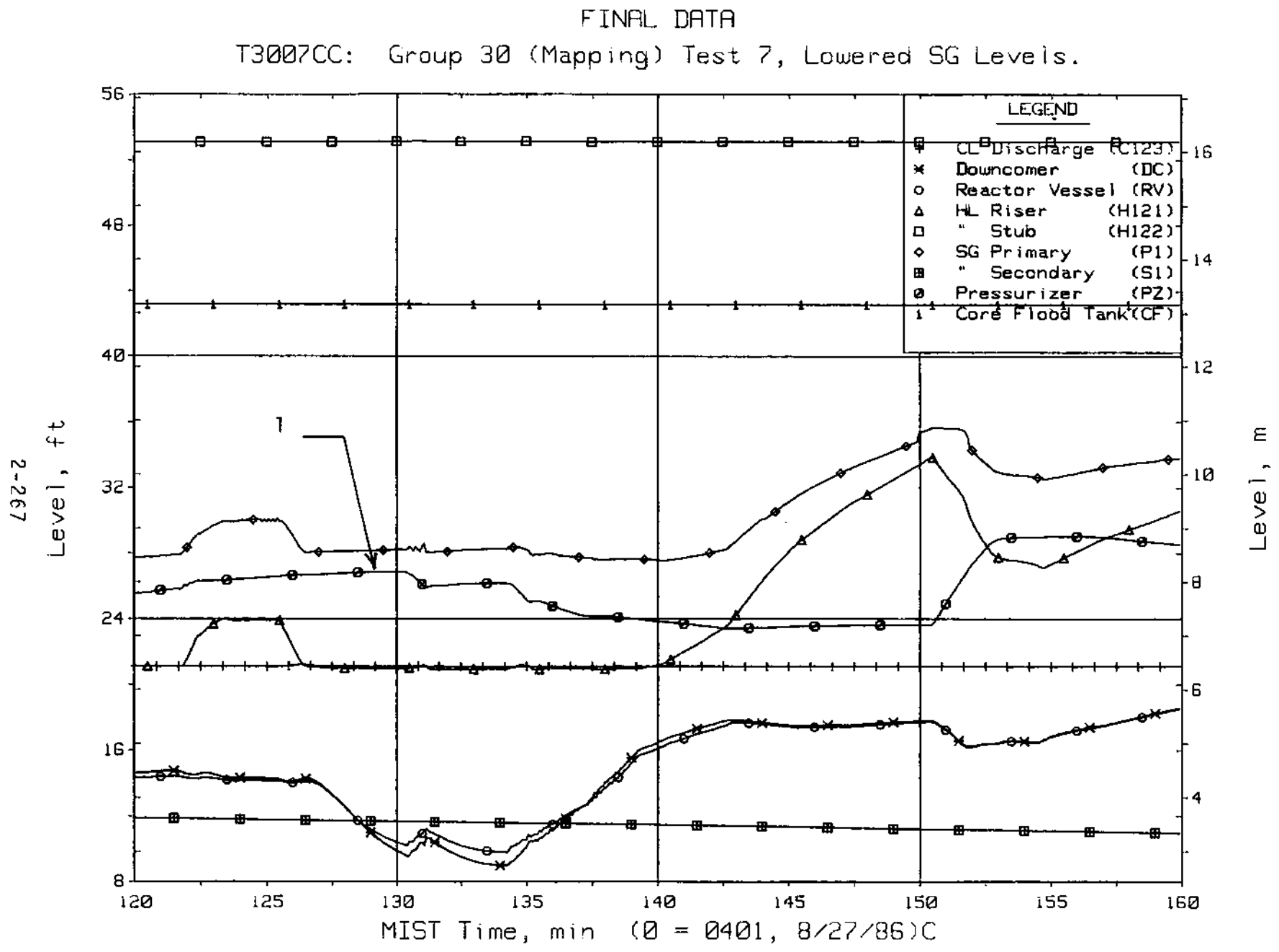

Figure 5.5.54. Loop A Collapsed Liquid Levels (LV20s)

Mon Feb 27 14:21:33 1989

PRLV1

5.6. Reactor Vessel Vent Valves Closed Test (300504)

Test 300504 was performed with the RVVVs manually closed and all other conditions similar to those of the Nominal Test (3003AA).

The leak-HPI deficit was established at test initiation and the primary system drain commenced. The primary system depressurized to ~1292 psia (Figure 5.6.1, See 1) as the core exit temperature saturated. The primary system pressure then gradually increased (Figure 5.6.1, See 2) as the reactor vessel began to void (Figure 5.6.2, See 1). The response of this test was similar to that of the Nominal Test (3003AA) until the reactor vessel level descended to the RVVV elevation. When this action occurred, the reactor vessel level continued decreasing and, as a result of the closed RVVVs, the downcomer remained full (Figure 5.6.3, See 1).

As the reactor vessel level continued to descend (Figure 5.6.4, See 1), the froth height was exposed to the hot leg nozzle and core-generated steam began entering the hot legs. As steam entered the hot legs, increased loop flow occurred (resulting from the change in the fluid density in the hot leg, thus increasing the natural circulation driving head). The increased loop flow resulted in a decrease in the core exit temperature (appears to subcool), which therefore decreased the flow into the hot leg. The core exit then saturated and steam again entered the hot legs, repeating the observed flow response. The phenomena continued and resulted in an oscillatory response in flow (See 1 on Figures 5.6.5 and 5.6.6), the reactor vessel level (Figure 5.6.3, See 2), and primary system pressure (Figure 5.6.7, See 1). The flow rates for both loops A and B responded symmetrically during this phase of the test, i.e., flow increased simultaneously and flow decreased simultaneously in both loops (See 1 on Figures 5.6.5 and 5.6.6).

As the primary system drain continued, the reactor vessel level continued on a decreasing trend and eventually descended to the hot leg nozzle elevation (Figure 5.6.3, See 3). When this event occurred, a direct flow path for the core-generated steam into the hot legs was established and an increase in flow was observed in both loops A and B (See 2 on Figures 5.6.5 and 5.6.6). The increased loop flow resulted in a decrease in the hot leg nozzle temperature (to below the saturation temperature; Figure 5.6.8, See 1) and increased the level in the reactor vessel (Figure 5.6.3, See 4). The effect of the

subcooled core exit temperature propagated into the hot legs as subcooled fluid flowed into the hot legs (See 1 on Figure 5.6.9 and Figure 5.6.10). The cooling of the core region and the hot legs decreased the natural circulation driving head, and a reduction in the loop flow rates was observed (See 1 on Figures 5.6.11 and 5.6.12).

An asymmetric loop flow response developed at this time. The flow rate of loop B exceeded that of loop A (See 2 on Figures 5.6.11 and 5.6.12) and as the core subcooled, more of the subcooled fluid entered hot leg B. This event resulted in a greater decrease in the loop B driving head as the subcooled fluid temperature propagated more rapidly up hot leg B. The effect of the discharge of subcooled fluid into the hot legs resulted in a flow reduction in both loops followed by a momentary flow interruption of loop B (Figure 5.6.12, See 3). The decreased loop flow rate then resulted in the heatup of the core region (Figure 5.6.13, See 1) and the loop driving head began increasing. Since hot leg B had subcooled to a greater extent than hot leg A, due to the higher flow rate in loop B, the driving head in loop A was greater than that of loop B. Thus, loop A flow increased (Figure 5.6.11, See 3) followed by loop B flow (Figure 5.6.12, See 4), with the loop A flow exceeding that of loop B. Again, the core subcooled and the subcooled fluid propagated up the hot legs as a result of the increased flow rate. The driving head thus decreased, the loop A flow interrupted momentarily (Figure 5.6.11, See 4), and a core heatup followed. Thus, an alternating loop flow pattern began to become established. An examination of the hot leg fluid temperatures provided insight to the previously discussed loop A flow interruption. As the loop A flow attained its peak value (Figure 5.6.11, See 5), the core fluid temperatures subcooled (Figure 5.6.13, See 2). The subcooled fluid entered hot leg A and rapidly propagated upwards (Figure 5.6.14, See 1), thus altering the loop A driving head and interrupting the loop A flow (Figure 5.6.11, See 4). The decreased loop A flow resulted in a heatup of the core region (Figure 5.6.13, See 3). As the core region heatup progressed, subcooled fluid that had resided in the reactor vessel entered and propagated up hot leg B (Figure 5.6.15, See 1). Thus, loop B flow began to increase (Figure 5.6.12, See 5). As the core heatup progressed, saturated conditions were attained and a heatup of hot leg B commenced (Figure 5.6.15,

See 2), thus further increasing the loop B driving head and, therefore, flow rate.

During the alternating loop flow phase of this test, backflow was observed in the cold legs of the loop that was inactive, i.e., when loop A established a forward flow pulse, some of the fluid that entered the downcomer flowed into the B cold legs and similarly when loop B established a forward flow pulse, backflow was observed in the A cold legs. This action can be observed by investigating the fluid temperature response in the cold legs and the hot leg stub. For example, at approximately 103.5 minutes, loop A established forward flow (Figure 5.6.16, See 1), while loop B flow was inactive (Figure 5.6.17, See 1). As loop A flow began increasing, the downcomer fluid temperature initially decreased (See 1 on Figures 5.6.18 and 5.6.19) as colder fluid, due to HPI that had resided in the A cold legs, flowed into the downcomer. As loop A flow increased, the nozzle temperature of cold legs B1 and B2 increased and approached the downcomer temperature (See 2 on Figures 5.6.18 and 5.6.19) as backflow began in the B cold legs. As loop A flow continued to increase, the downcomer temperature also increased as more fluid from the steam generator ("hot fluid") was mixed with the HPI (See 3 on Figures 5.6.18 and 5.6.19). This event was also reflected as backflow in cold legs B1 and B2 as an increase in their cold leg nozzle temperatures was observed (See 4 on Figures 5.6.18 and 5.6.19).

The backflow of fluid into the B cold legs resulted in the divergence of more HPI fluid backwards, i.e., flows up the cold leg discharge pipe towards the reactor coolant pump. This action was observed by the decrease in the reactor coolant pump discharge rake fluid temperature (See 5 on Figures 5.6.18 and 5.6.19). This colder fluid was also observed to spill over into the suction pipes of cold legs B1 and B2 (See 1 on Figures 5.6.20 and 5.6.21). As the spillover into the cold leg B suction pipes occurred, fluid was displaced into the steam generator primary and resulted in an increase in the hot leg B stub liquid level (Figure 5.6.22, See 1). This displacement of fluid upwards into the hot leg stub was confirmed by the fluid temperature response at the steam generator B inlet, i.e., colder fluid that resided in the steam generator primary was displaced upwards into the hot leg stub and the steam generator inlet temperature decreased (Figure 5.6.23, See 1).

The combined effects of the subcooling of the hot leg (in the loop that experienced the flow pulse) and the displacement of colder fluid to a higher elevation in the hot leg stub (in the loop that did not experience the flow pulse) resulted in the realignment of the loop natural circulation driving head and caused the observed alternating loop flow condition. That is, for this example, when the loop A flow pulse occurred, subcooled fluid entered hot leg A and resulted in a decrease in the loop A driving head, which eventually terminated loop A flow. Hot leg B, however, did not experience the subcooling effect since loop B did not flow. In addition, the forward flow of loop A resulted in backflow in loop B that raised the level of colder fluid in the hot leg stub. Thus, these combined effects reoriented the driving head so that the loop B driving head was larger and forward loop flow began to become established in loop B. Hot leg B began to heat up, fluid was displaced over the U-bend into the hot leg stub, the hot leg stub level increased, and a flow pulse occurred in loop B.

Each flow pulse was a result of the establishment of sufficient loop driving head that was developed by the heatup of the hot leg and the filling of the hot leg stub (as fluid spilled over the U-bend). These hot leg spillovers were similar to those observed in the Nominal Test (3003AA).

The alternating loop flow condition existed for approximately 15 minutes and each flow pulse occurred at a frequency of approximately 20 cycles per hour, i.e., loop flow occurred approximately every 3 minutes (Figure 5.6.5, See 3 and Figure 5.6.6, See 3).

Each flow pulse resulted in the partial collapse of the reactor vessel voids and the refill of the reactor vessel to an elevation above the hot leg nozzle elevation (Figure 5.6.3, See 5). The primary system pressure exhibited an increasing trend during the alternating loop flow phase of this test and attained a maximum pressure of 1770 psia (Figure 5.6.7, See 2). This maximum pressure was considerably lower than that observed during the repressurization phase in the Nominal Test (3003AA), which was 2225 psia.

The hot leg and steam generator primary levels of both loops responded in a similar manner during the alternating flow pulse phase of this test (Figure 5.6.24, See 1). Through approximately 108 minutes, the alternating flow pulse occurred in the loop that had the highest indicated hot leg stub or

steam generator primary level and hot leg level. The flow pulses occurred as the core and then the hot leg heated up, resulting in a spillover at the hot leg U-bend. At approximately 109.5 minutes, the indicated hot leg and steam generator primary levels of both loops were approximately equal and the flow pulse occurred in loop A (this was the final flow pulse of the alternating loop flow phase of this test).

Subsequent to this occurrence, forward loop flow appeared to be established simultaneously in both loops (See 1 on Figures 5.6.25 and 5.6.26). At this time, the hot leg A and steam generator A primary levels indicated lower elevations than those of loop B (See 1 on Figures 5.6.27 and 5.6.28). Spillover occurred only at the hot leg A U-bend (See 1 on Figures 5.6.29 and 5.6.30). The cold leg B suction pipes indicated lower fluid temperatures than those of loop A (See 1 on Figures 5.6.31 through 5.6.34). AFW was on in both steam generators, with the flow in A greater than the flow in B (See 1 on Figures 5.6.35 and 5.6.36). Steam generator A was still steaming as a result of the previous flow pulse, whereas steam generator B was not steaming (See 2 on 5.6.35 and 5.6.36).

The initiation of forward loop flow in both loops (See 1 on Figures 5.6.25 and 5.6.26) appeared to be caused by the nearly identical driving head in both loops. The heatup of hot leg A appeared to progress more rapidly than that of hot leg B and a spillover occurred in hot leg A (Figure 5.6.29, See 1). When the spillover occurred, loop A flow increased in magnitude to a value comparable to that observed during the previous flow pulses (Figure 5.6.25, See 2). Loop B flow, however, was considerably less than loop A flow (Figure 5.6.26, See 2).

Subsequent to this occurrence, only loop A experienced the flow pulse. However, the frequency at which the flow pulses occurred increased by a factor of two to approximately 40 cycles per hour (Figure 5.6.5, See 4). The establishment of the predominant pulsating flow path via loop A maintained primary-to-secondary heat transfer in steam generator A, whereas heat transfer in steam generator B terminated (Figure 5.6.7, See 3).

The establishment of the predominant flow path via loop A is not understood at this time. A number of potential reasons appear to exist (pressurizer location, loop hydraulic resistance, steam generator or control systems, heat

loss to ambient, downcomer circumferential resistance, elevation differences, spillover of cold (HPI) fluid into the cold leg suction pipe, etc.) and the cause may be a combination of a number of these reasons. Note that the loop operator had increased the HPI flow rate shortly before the interruption of flow in loop B in an attempt to maintain the leak-HPI deficit. Between approximately 106 and 107.5 minutes, the total HPI flow was increased approximately 150 lb/h (Figure 5.6.37, See 1). This increase was necessitated as a result of the HPI pump head-flow characteristics, i.e., response to the increasing primary system pressure. The backflow of colder (HPI) fluid and the spillover into the cold leg suction pipe appears to be the primary reason for the observed asymmetric response of the two loops. During the previously discussed alternating loop flow and predominant loop A flow phases of this test, HPI fluid was observed to flow in both directions in the cold leg discharge pipe during those periods when primary flow was interrupted. This response can be observed by examining the cold leg nozzle and the reactor coolant pump discharge fluid thermocouple response (for examples, See 1 on Figure 5.6.38 and Figure 5.6.39). As discussed previously, the HPI fluid that flows up the cold leg discharge pipe (backflow) was also observed to spill over into the cold leg suction pipe. The spillover occurred in the opposite loop from the loop that experienced the flow pulse, i.e., as forward loop flow occurred in loop A, fluid discharged from the A cold legs into the downcomer, backflowed into the B cold legs, and forced fluid over the B reactor coolant pump spillover elevation and into the B cold leg suction pipes; similarly, when the loop B flow pulse occurred, backflow and spillover into the cold leg A suction pipes was observed. The displacement of colder fluid into the cold leg suction pipe resulted in a decreased loop driving head. The cold leg B suction pipes appeared to attain lower temperatures during the alternating loop flow phase of this test. Loop B was also the loop that experienced backflow subsequent to the increased HPI flow (caused by the operator action). Thus, colder fluid resided in the cold leg discharge pipe prior to the occurrence of backflow. This event may explain the interruption of loop B flow since a larger driving head would be required to overcome the colder fluid in the cold leg suction pipe.

As loop A established the predominant flow path, the primary system pressure began to stabilize (although remaining oscillatory as flow pulsed) at

approximately 1700 psia (Figure 5.6.7, See 4). The loop A hot leg and steam generator primary levels stabilized, remaining at higher elevations than the loop B levels and the B levels exhibited a decreasing trend; however, all levels continued their oscillatory response (Figure 5.6.24, See 2). The loop A flow pulses continued to be characteristic of those observed previously, i.e., the core and hot leg heated up, subcooled fluid spilled over the hot leg U-bend (Figure 5.6.40, See 1), a forward flow pulse was established, the core was subcooled, flow was interrupted, and then the entire phenomena occurred again.

Coincident with the occurrence of each loop A flow pulse, backflow in the B cold legs was observed. The backflow resulted in the spillover of cold (HPI) fluid into the suction pipes of cold legs B1 and B2 (See 1 on Figures 5.6.41 and 5.6.42). However, the fluid spilling over into cold leg B1 suction reduced the cold leg suction temperature to a greater extent than that observed in the cold leg B2 suction. This reduced temperature may be caused by slightly higher HPI flow or colder fluid and or metal temperatures in cold leg B1.

As observed in the Nominal Test (3003AA) and the other Mapping Tests, cold leg B1 was more prone to establish reverse flow than cold leg B2. For Test 300504, this behavior was also true. The loop A flow pulse at approximately 130 minutes caused spillover to occur in both B cold legs. The cold leg B1 spillover, however, was of sufficient magnitude to establish reverse flow in cold leg B1 and forward flow in cold leg B2 (Figure 5.6.43, See 1). The establishment of intra-cold leg flow was confirmed by the fluid temperature response in the cold leg B suction pipes. The cold leg B1 suction fluid temperatures indicated that cold fluid spilled over into the suction pipe and traversed downward (Figure 5.6.44, See 1). As this colder fluid descended to the cold leg branch elevation, it entered the cold leg B2 suction pipe and decreased the fluid temperatures as the fluid traversed upward (Figure 5.6.45, See 1).

Subsequent to the establishment of intra-cold leg flow in loop B, AFW initiated (Figure 5.6.46, See 1) in steam generator B (since the pressure in steam generator B was below the control setpoint of 1010 psia, this AFW actuation was caused by the secondary level descending to the level control

setpoint). The injection and evaporation of the AFW apparently resulted in an increase in the steam generator B pressure to approximately 1010 psia (Figure 5.6.47, See 1).

Pulsating loop A flow, at a very regular frequency, and loop B intra-cold leg flow continued. During periods when the flow in A was interrupted, steam generator B drained and mixed small amounts of hotter fluid with the colder fluid that was flowing (intra-cold leg) around the cold leg B suction pipes. This action was observed by the response of the fluid temperature at the cold leg B branch (Figure 5.6.45, See 2), which increased in temperature (towards the steam generator outlet temperature) during each drain cycle. The magnitude of the drain flow rate was apparently small in relation to the intra-cold leg flow rate since the hotter fluid did not propagate up the cold leg suction pipe. Although the magnitude of this drain flow was small, some energy was removed from the draining fluid as it mixed with the colder fluid in the cold leg suction pipe. This action resulted in a gradual depressurization of the primary system (Figure 5.6.7, See 5).

The depressurization in turn resulted in an increased HPI flow rate (Figure 5.6.37, See 2) as the HPI pump responded to the change in the head-flow relationship. The flow in loop B was intra-cold leg (B1 reverse flow and B2 forward flow), thus the increased HPI flow resulted in decreased cold leg B1 suction temperatures (Figure 5.6.48, See 1), decreased cold leg B2 suction temperatures (Figure 5.6.49, See 1), and further decreased cold leg B2 nozzle temperatures (Figure 5.6.38, See 2) as HPI was injected into each cold leg discharge pipe.

The steam generator B primary level continued to drain and descended to an elevation near the secondary pool height (Figure 5.6.50, See 1). This action resulted in slightly increased steam generator B heat transfer as observed by the increased steam flow (Figure 5.6.51, See 1), and resulted in an increased primary system depressurization rate (Figure 5.6.7, See 6).

The increased depressurization rate resulted in a decreased leak flow and an increased HPI flow. The loop operator noticed these events and made adjustments to the HPI flow (decreased) in an attempt to maintain the leak-HPI deficit (Figure 5.6.52, See 1). The decreased HPI flow resulted in an increase in the cold leg B1 suction temperatures as less HPI fluid was mixed

with the reverse flow in cold leg B1 (Figure 5.6.53, See 1). This fluid temperature increase was also observed to propagate up the cold leg B2 suction pipe (Figure 5.6.54, See 1) as intra-cold leg flow continued. The increased fluid temperatures in the B cold legs resulted in an increased driving head in loop B, therefore more core-generated steam entered hot leg B, thus increasing the heat transfer in steam generator B (Figure 5.6.55, See 1). The primary pressure continued to decrease (Figure 5.6.56, See 1) and attained approximately 1340 psia.

Loop A continued to flow in a pulsating manner during this depressurization. However, the magnitude of the flow rate decreased (Figure 5.6.57, See 1) as some of the core-generated steam entered hot leg B. The hot leg A and steam generator A primary levels decreased while the hot leg B and steam generator B primary levels increased as the primary system depressurized (Figure 5.6.58, See 1). The core level oscillations also decreased in magnitude and the core level exhibited a decreasing trend that descended to an elevation below the hot leg nozzle (Figure 5.6.59, See 1). The core level response was caused by the decreased magnitude of the loop A flow which, in conjunction with the depressurization, resulted in a greater portion of the core region attaining saturated conditions (Figure 5.6.60, See 1). This continued depressurization resulted in an increasing HPI flow (caused by the head-flow characteristics of the pump) and, as discussed previously, resulted in a decrease in the loop B driving head, a decrease in steam generator heat transfer (Figure 5.6.55, See 2 and Figure 5.6.61, See 1), a repressurization of the primary system (Figure 5.6.56, See 2), and interruption of the flow in loop A (Figure 5.6.57, See 2) while intra-cold leg flow continued in loop B (Figure 5.6.62, See 1). The depressurization also caused superheated fluid temperatures in hot leg B (Figure 5.6.63, See 1).

As the primary system repressurized, the loop A and B hot leg and steam generator primary levels decreased (Figure 5.6.58, See 2). When the steam generator B primary level descended to the secondary pool elevation (Figure 5.6.64, See 1), an increase in the B steam and AFW flow rate occurred (Figure 5.6.55, See 3). This action is indicative of increased heat transfer, which should cause a primary system depressurization. However, for some unexplainable reason, the primary system pressure continued to increase and attained a

maximum pressure of 1690 psia (Figure 5.6.56, See 2). When the loop A steam generator primary level descended to the secondary pool elevation (Figure 5.6.65, See 1), an increase in the A steam and AFW flow rate occurred (Figure 5.6.61, See 2), heat transfer was established, and the primary system depressurized (Figure 5.6.56, See 3). However, another unexplainable response was observed at this time. Heat transfer was established in loop A; however, the cold leg A1 and A2 flowmeters indicated no flow at this time (Figure 5.6.57, See 3). The cold leg B1 and B2 flowmeters, however, did show an increase in the intra-cold leg flow rate (Figure 5.6.62, See 2) when heat transfer was established in steam generator B.

As the primary system pressure continued to decrease, the pressurizer inventory was discharged into hot leg A (Figure 5.6.65, See 2). When this action occurred, forward flow was established in both cold legs A1 and A2 (Figure 5.6.57, See 4). Simultaneously, the loop operator decreased the HPI flow rate (Figure 5.6.52, See 2) to reestablish the leak-HPI deficit. The flow from the A cold legs was discharged into the downcomer and was observed to immediately enter the cold leg B1 discharge pipe. This action was observed by the response of the fluid thermocouples in the cold legs. As loop A flow was established, the mixing of hotter fluid (discharged from the steam generator) with the HPI resulted in an increase of the cold leg A1 and A2 nozzle fluid temperatures (See 1 on Figures 5.6.66 and 5.6.67). This hotter fluid was discharged into the downcomer and entered the cold leg B1 discharge pipe (Figure 5.6.68, See 1). The backflow of this hotter fluid immediately propagated up the cold leg B1 discharge pipe, as observed by the increase in the B1 reactor coolant pump discharge rake fluid temperatures (Figure 5.6.69, See 1) and into the cold leg B1 suction pipe (Figure 5.6.53, See 2). Some of the fluid that had resided in the cold leg B1 suction pipe was also observed to enter the cold leg branch and flow upward into steam generator B as the fluid temperatures at the cold leg branch decreased (Figure 5.6.53, See 3).

Since intra-cold leg flow existed in loop B at this time (B1 flow was backward) and hotter fluid from the downcomer entered the cold leg B1 discharge pipe, the fluid density distribution relationship between cold legs B1 and B2 was altered. This alteration resulted in a decrease in the

established intra-cold leg driving head, and a decrease in the intra-cold leg flow rate occurred (Figure 5.6.62, See 3). The decrease in the B2 forward flow rate was apparently sufficient to permit the backflow of fluid from the downcomer into cold leg B2. This event was observed as a counter-current flow at the cold leg B2 nozzle thermocouple rake (Figure 5.6.70, See 1). The decreased intra-cold leg driving head, combined with the backflow of fluid into the cold leg B2 discharge pipe, resulted in a momentary flow interruption in the B cold legs (Figure 5.6.62, See 4).

The loop A flow during this depressurization was sufficient to cool the lower core region (Figure 5.6.71, See 1) and partially collapsed the core region voids (Figure 5.6.65, See 3). The resulting change in the fluid density altered the driving head and thus decreased and then interrupted loop A flow (Figure 5.6.57, See 5).

The primary system pressure had decreased to approximately 1100 psia (Figure 5.6.56, See 4) during this depressurization phase. As the loop flow interrupted, the primary system began to repressurize (Figure 5.6.56, See 5). Loop A flow remained interrupted and loop B reestablished intra-cold leg flow, B1 in reverse and B2 forward (Figure 5.6.62, See 5). The steam generator primary levels in both loops descended to the secondary pool elevation (Figure 5.6.64, See 2 and Figure 5.6.65, See 4) and both steam generators began steaming (Figure 5.6.55, See 4 and Figure 5.6.61, See 3). The primary system pressure, however, continued to increase, although at a reduced rate, and attained a maximum value of approximately 1450 psia (Figure 5.6.56, See 6). This increase was apparently caused by the delay in the actuation of AFW (Figure 5.6.55, See 5 and Figure 5.6.61, See 4) as a result of high steam generator secondary levels that were above the level control setpoint (Figure 5.6.64, See 2 and Figure 5.6.65, See 4). AFW then actuated and the primary system depressurized and resulted in a drain of the pressurizer. Flow was again established in loop A and similar responses were observed as occurred during the previous depressurization. The pressure decreased to approximately 1090 psia, and another repressurization to approximately 1210 psia occurred and was followed by another depressurization to approximately 1050 psia (Figure 5.5.56, See 7). The primary system

attained a stable BCM during this final depressurization and the test was terminated at approximately 259 minutes.

Although this test differed from the other Mapping Tests in that the RVVVs were closed, many similar phenomena and responses were observed. Throughout the entire test, the closed reactor vessel vent valves resulted in subcooled fluid conditions in all four cold legs.

The establishment of intra-cold leg flow appeared to be more difficult to develop under these subcooled fluid conditions. However, when intra-cold leg flow was established, it was more readily maintained.

The ability of fluid to be discharged from the cold legs of one loop into the downcomer and then backflow into the cold legs of the other loop highlighted the effect of the circumferential resistance of the downcomer.

This test appears to provide insight to the mechanism that caused the initiation of backflow in the Mapping Tests with operable reactor vessel vent valves. These other Mapping Tests also exhibited flow oscillations that resulted in reactor vessel vent valve closure. Therefore, when a sufficient amount of forward flow is established in one loop that causes the reactor vessel vent valves to close, the fluid being discharged out of this loop into the downcomer can initiate backflow in the other loop via the same mechanism, as was observed for the test with the vent valves closed.

The injection of HPI fluid into the subcooled fluid in the cold legs for this test had a greater effect on the mixed-mean temperature of the fluid in the cold legs than that observed in the other Mapping Tests where the cold legs were voided. The sensitivity of the primary system response to HPI flow adjustments, in an attempt to maintain the leak-HPI deficit, was therefore highlighted during this test.

The maximum primary system pressure attained during this test (with the RVVVs closed) was approximately 455 psi lower than that attained in the Nominal Test (3003AA) where the RVVVs were operable.

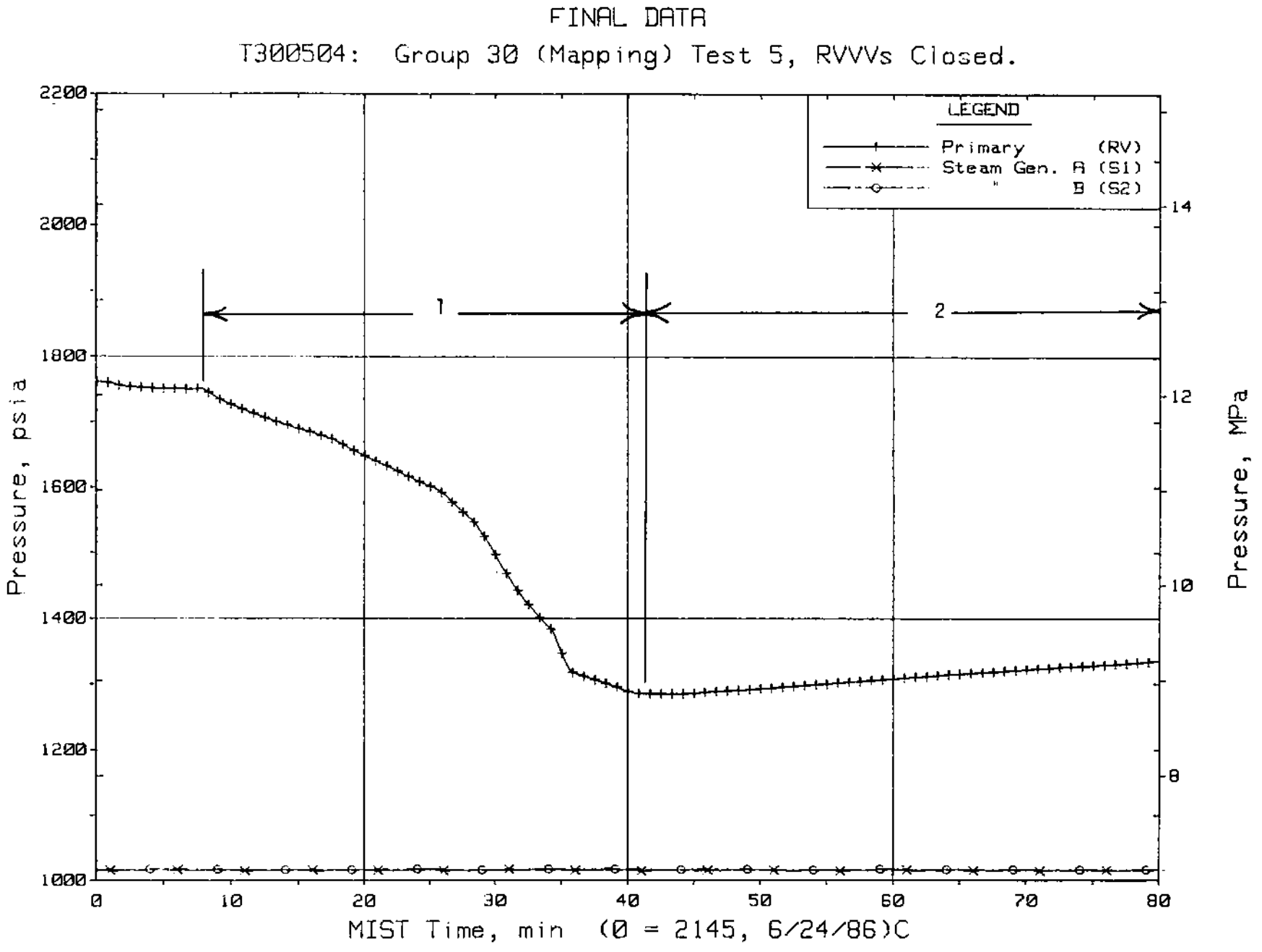

Figure 5.6.1. Primary and Secondary System Pressures (GPOls)

Wed Mar 1 16:28:33 1989

PSGP1

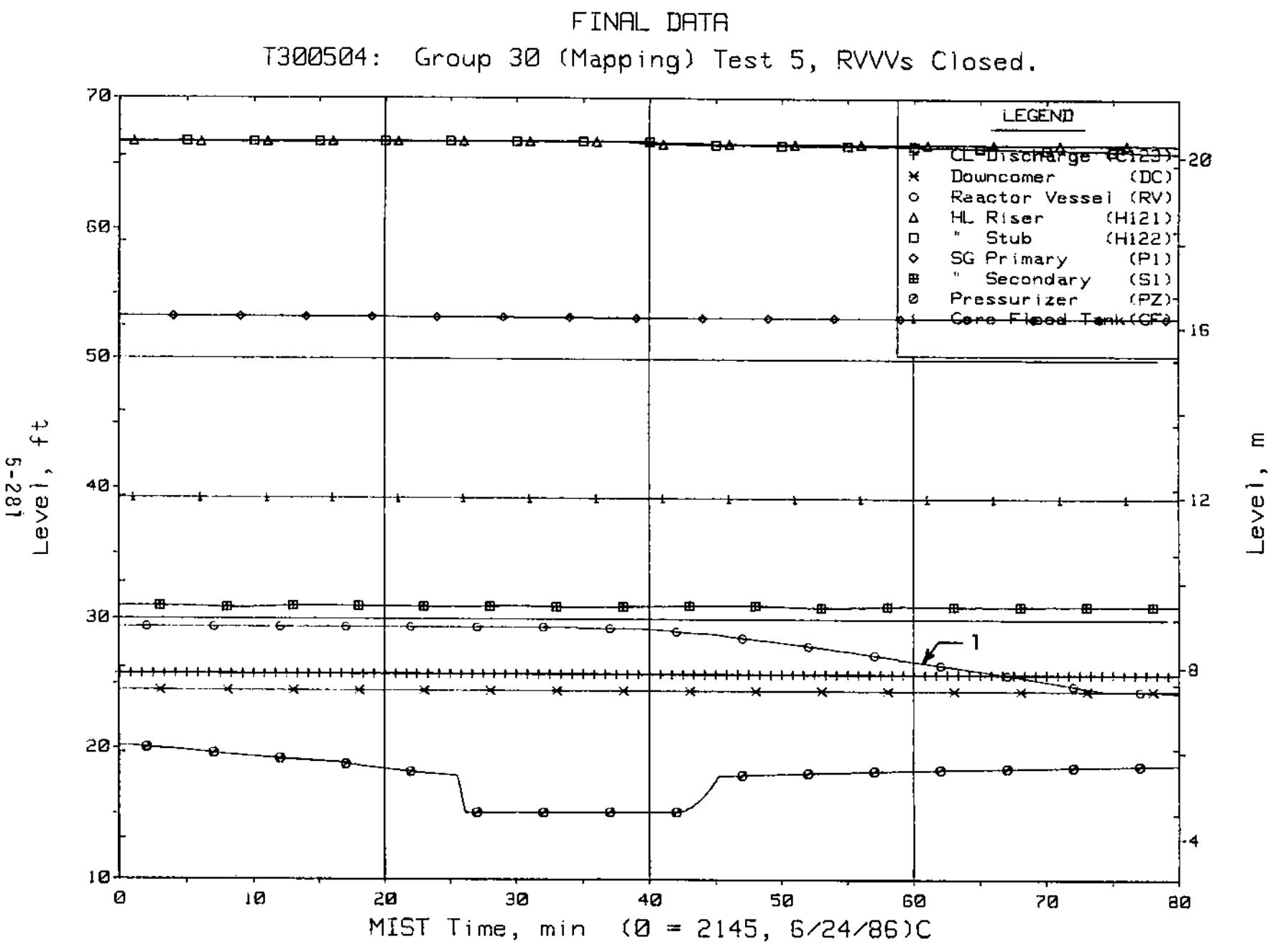

Figure 5.6.2. Loop A Collapsed Liquid Levels (LV20s)

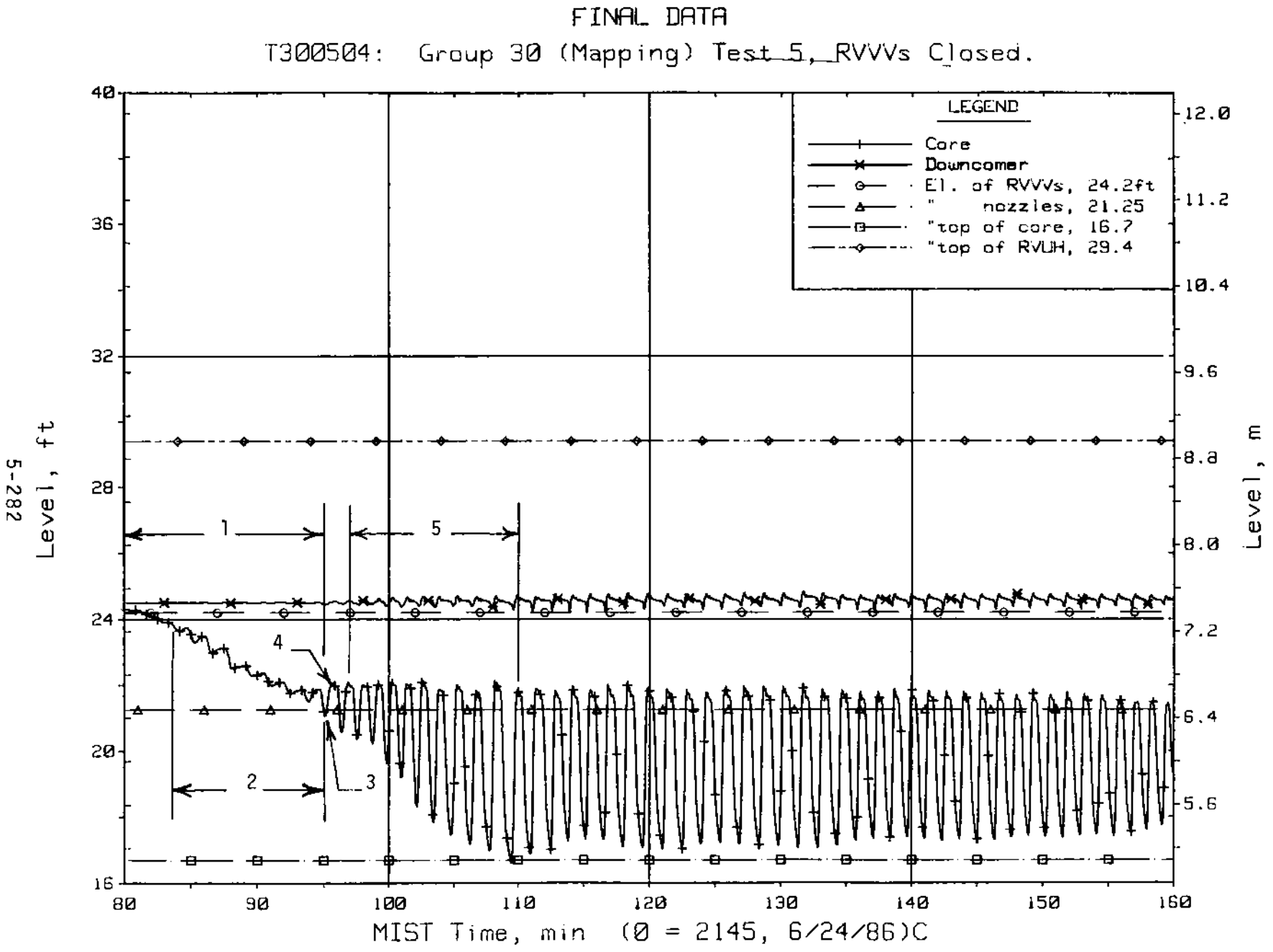

Figure 5.6.3. Core Region Collapsed Liquid Levels

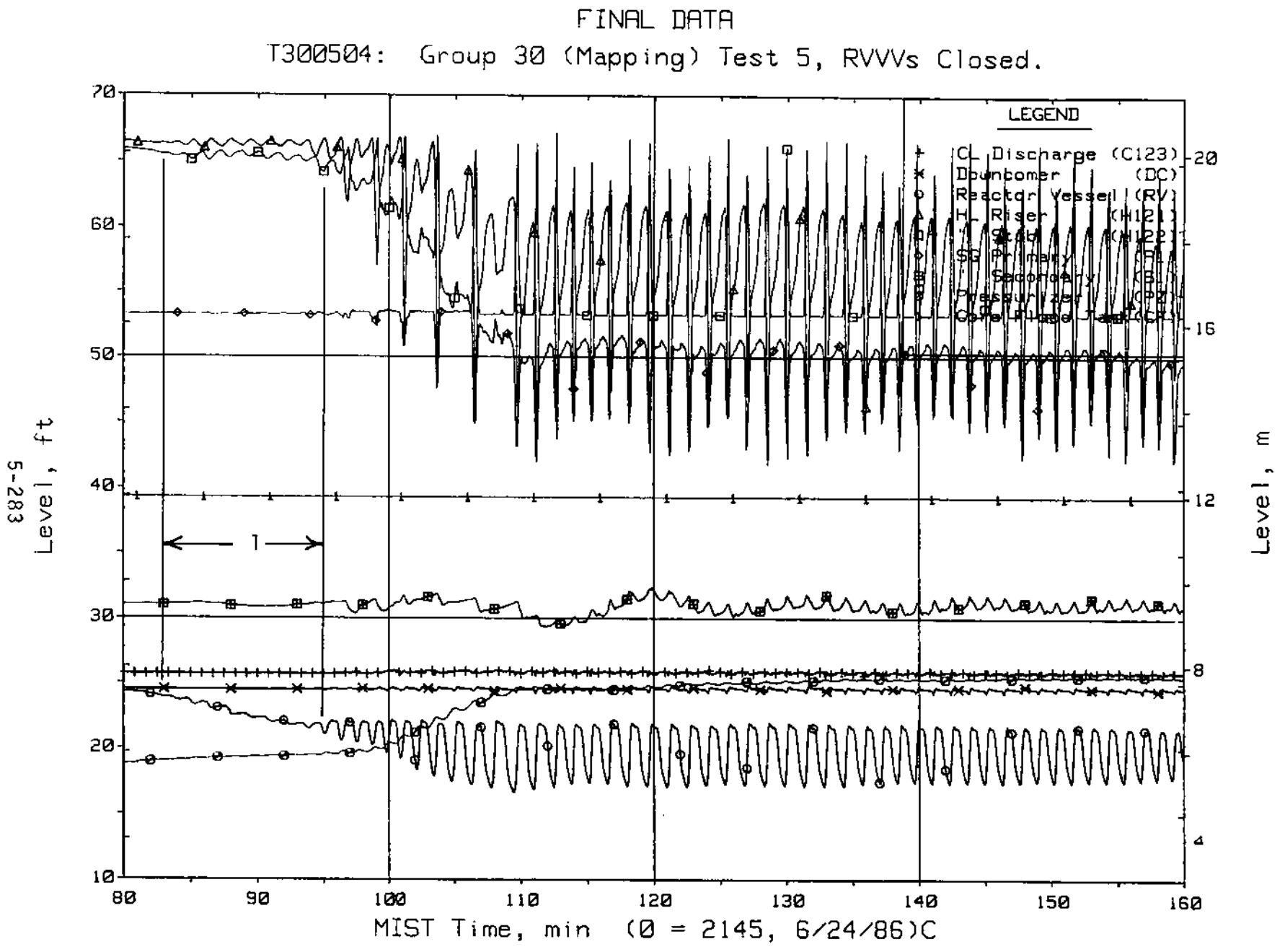

Figure 5.6.4. Loop A Collapsed Liquid Levels (LV20s)

Wed Mar 8 13:10:16 1989

PRLV1

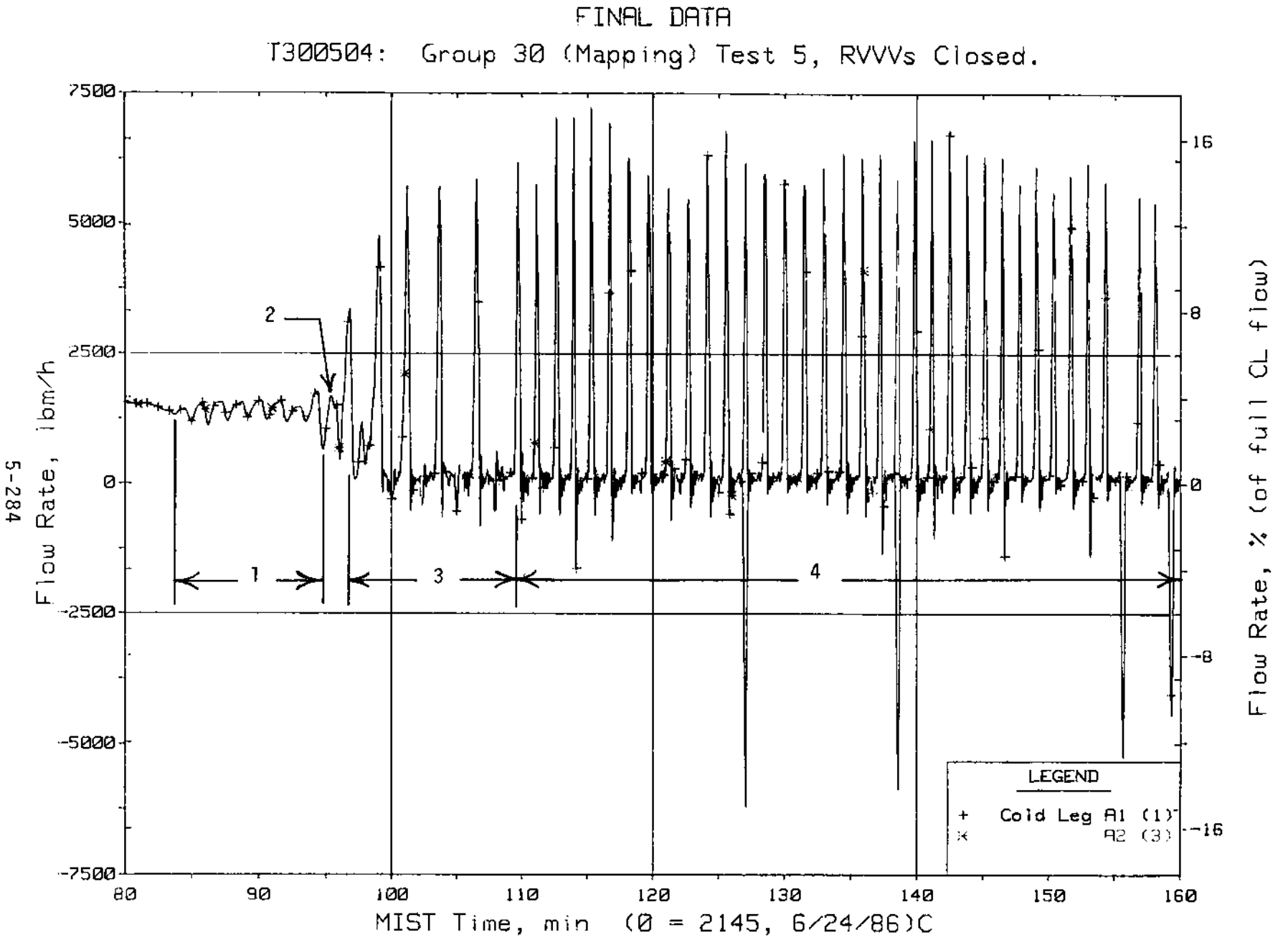

Figure 5.6.5. Loop A Cold Leg (Venturi) Flow Rates (CnVN20s)

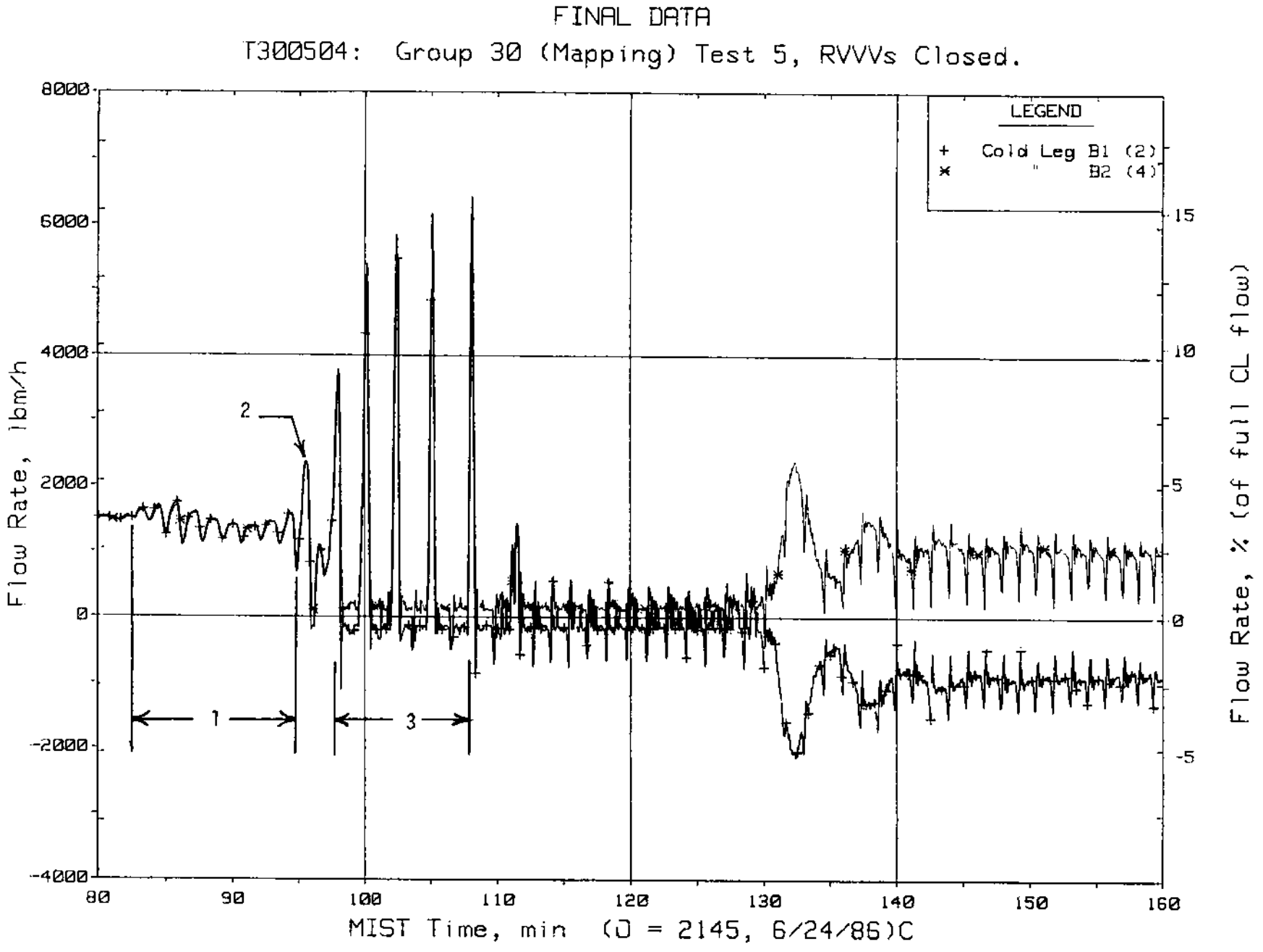

Figure 5.6.6. Loop B Cold Leg (Venturi) Flow Rates (CnVN20s)

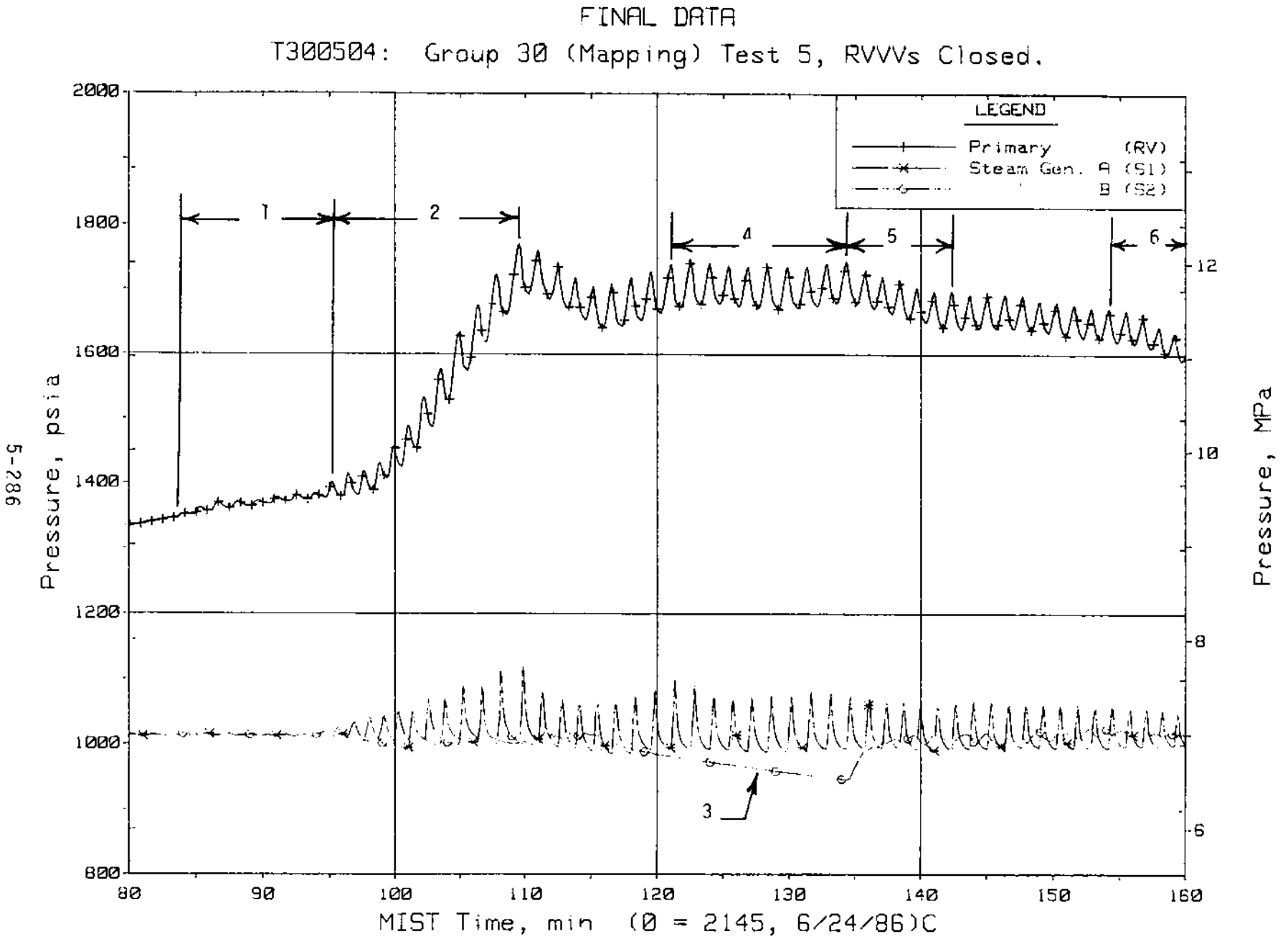

Figure 5.6.7. Primary and Secondary System Pressures (GPOIs)

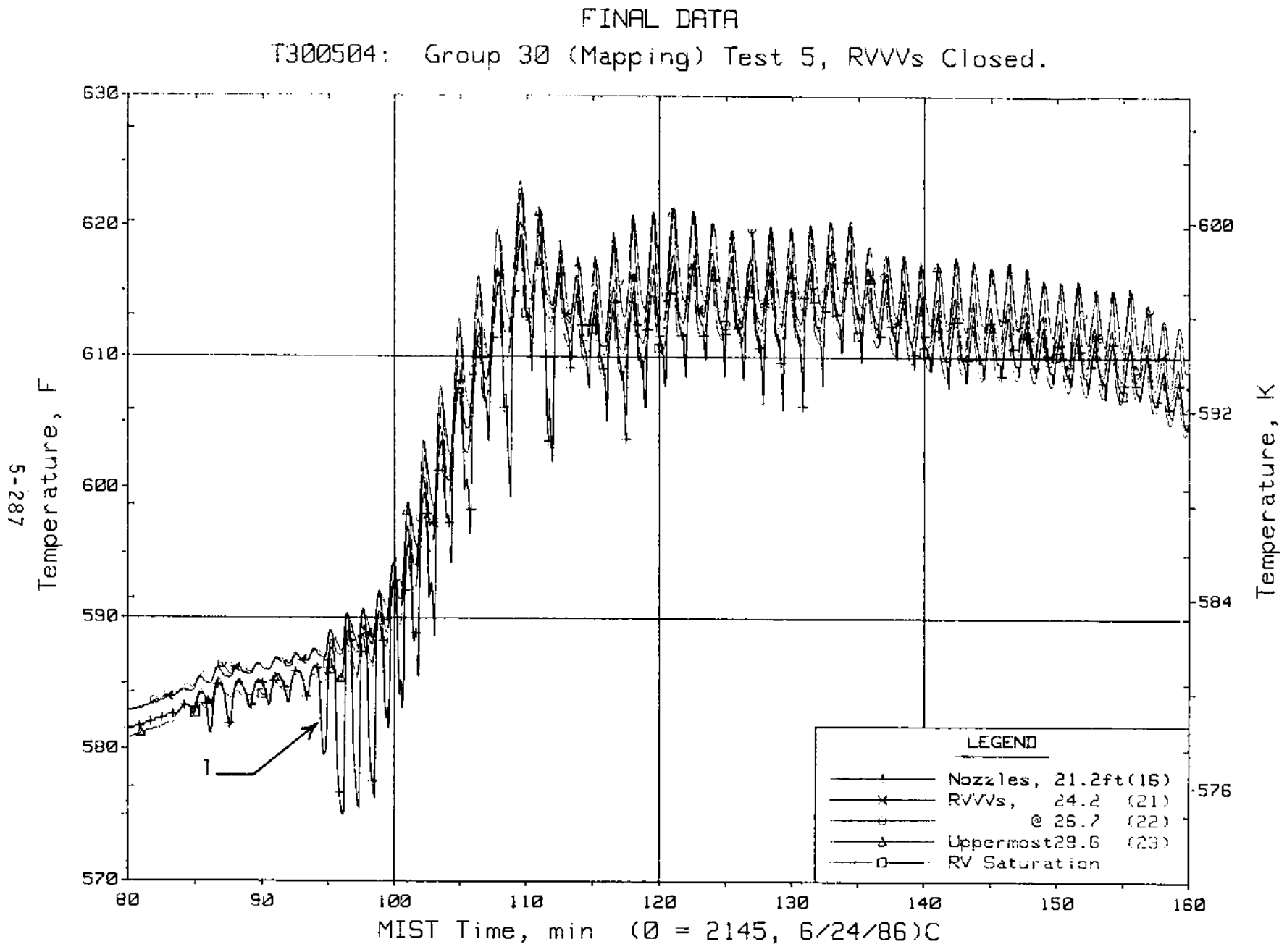

Figure 5.6.8. Reactor Vessel Upper-Elevation Fluid Temperatures (RVTCs)

Wed Mar 1 15:52:45 1989

RVTC3

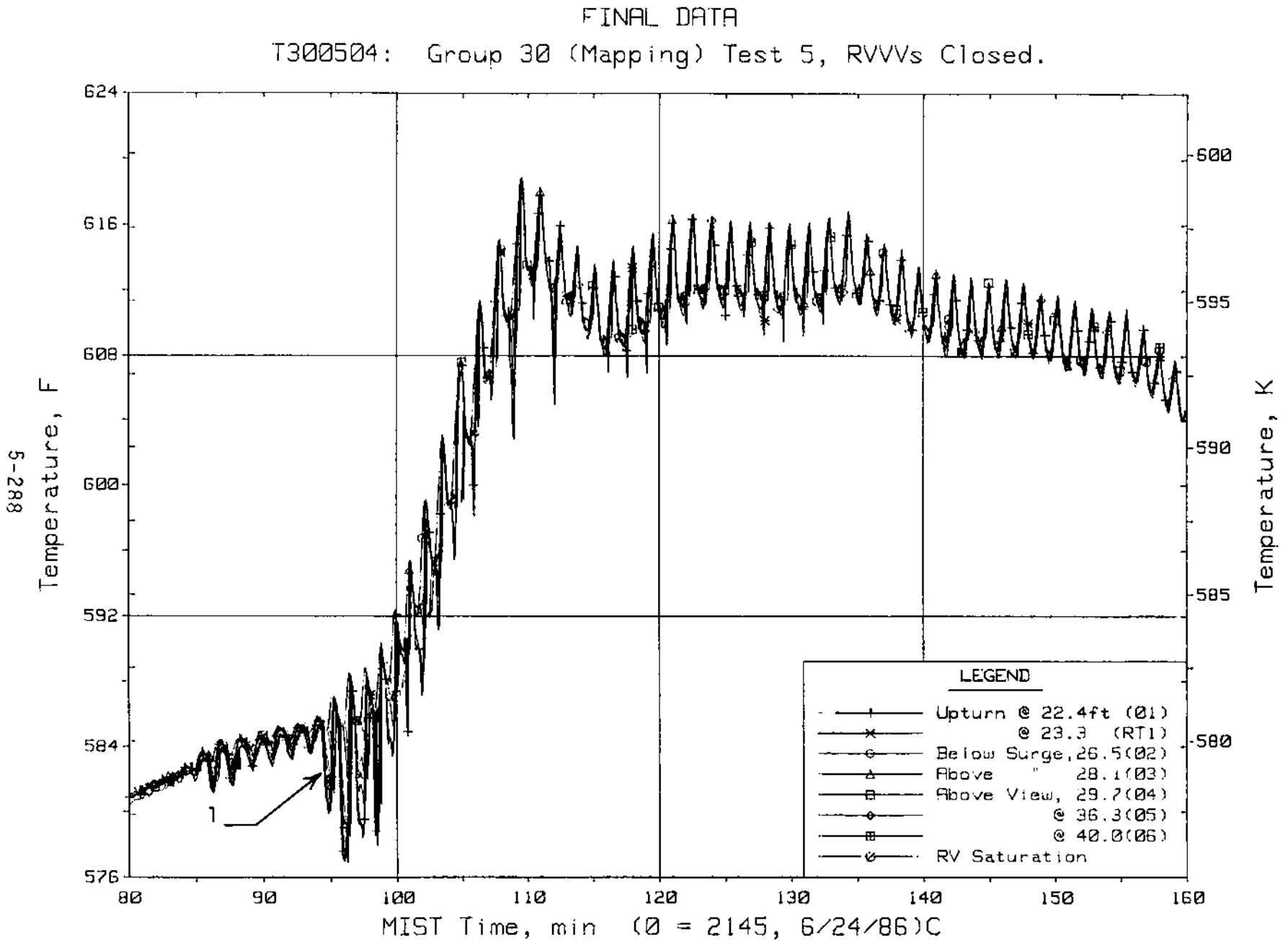

Figure 5.6.9. Hot Leg A Lower-Elevation Riser Fluid Temperatures (H1TCs)

Wed Mar 1 15:53:51 1989

H1TC1

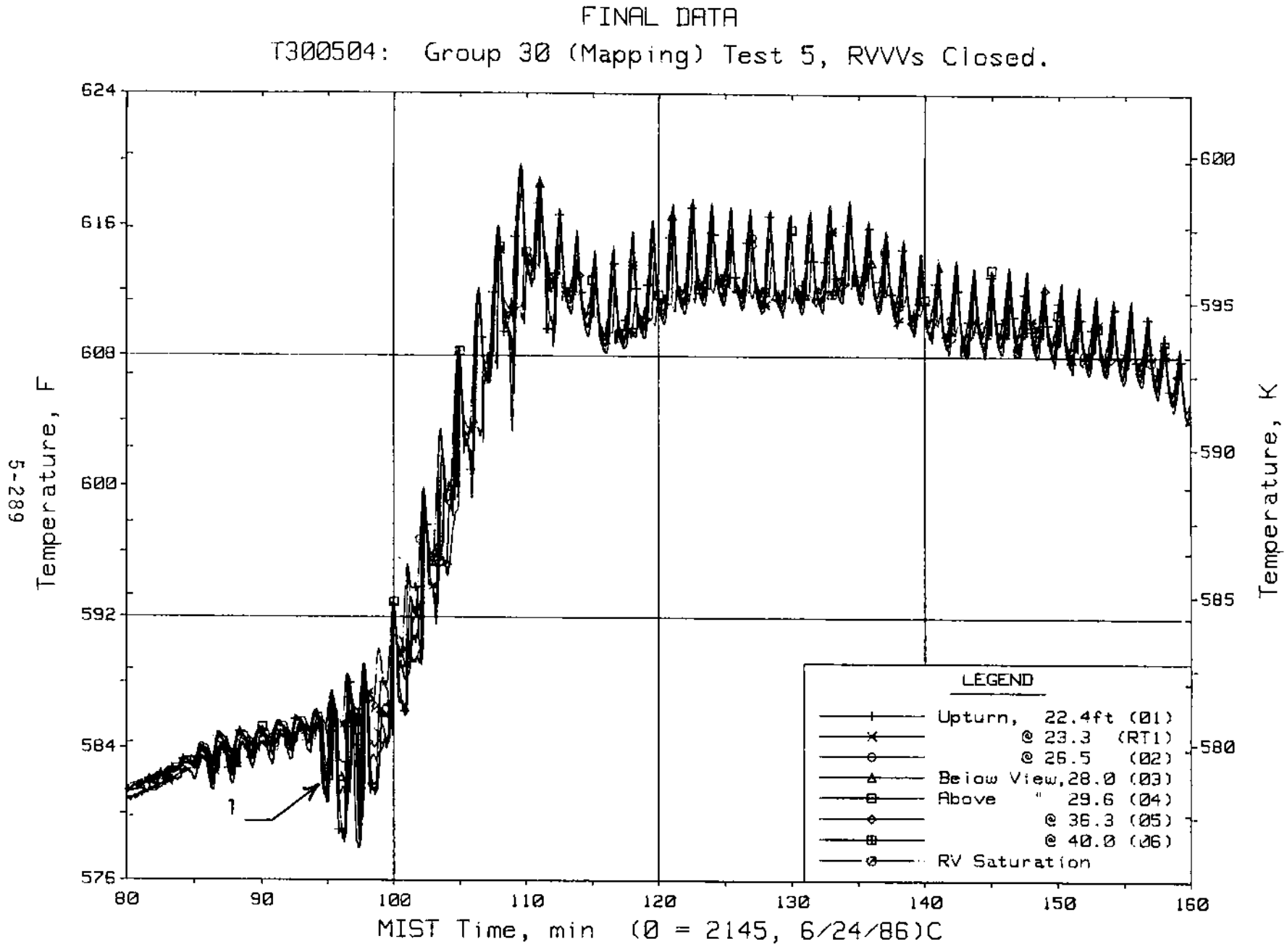

Figure 5.6.10. Hot Leg B Lower-Elevation Riser Fluid Temperatures (H2TCs)

Wed Mar 1 15:48:56 1989

H2TC1

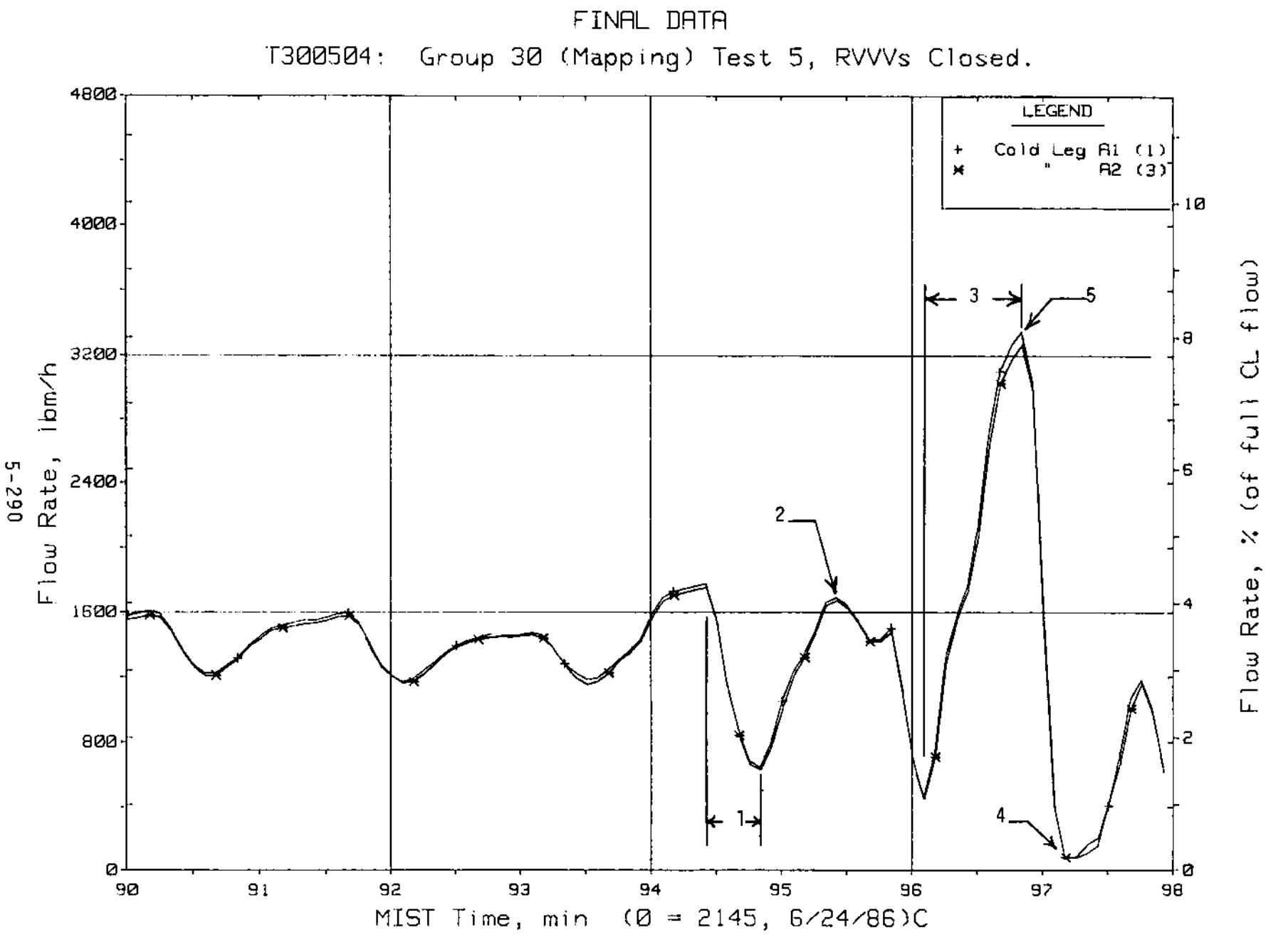

Figure 5.6.11. Loop A Cold Leg (Venturi) Flow Rates (CnVN20s)

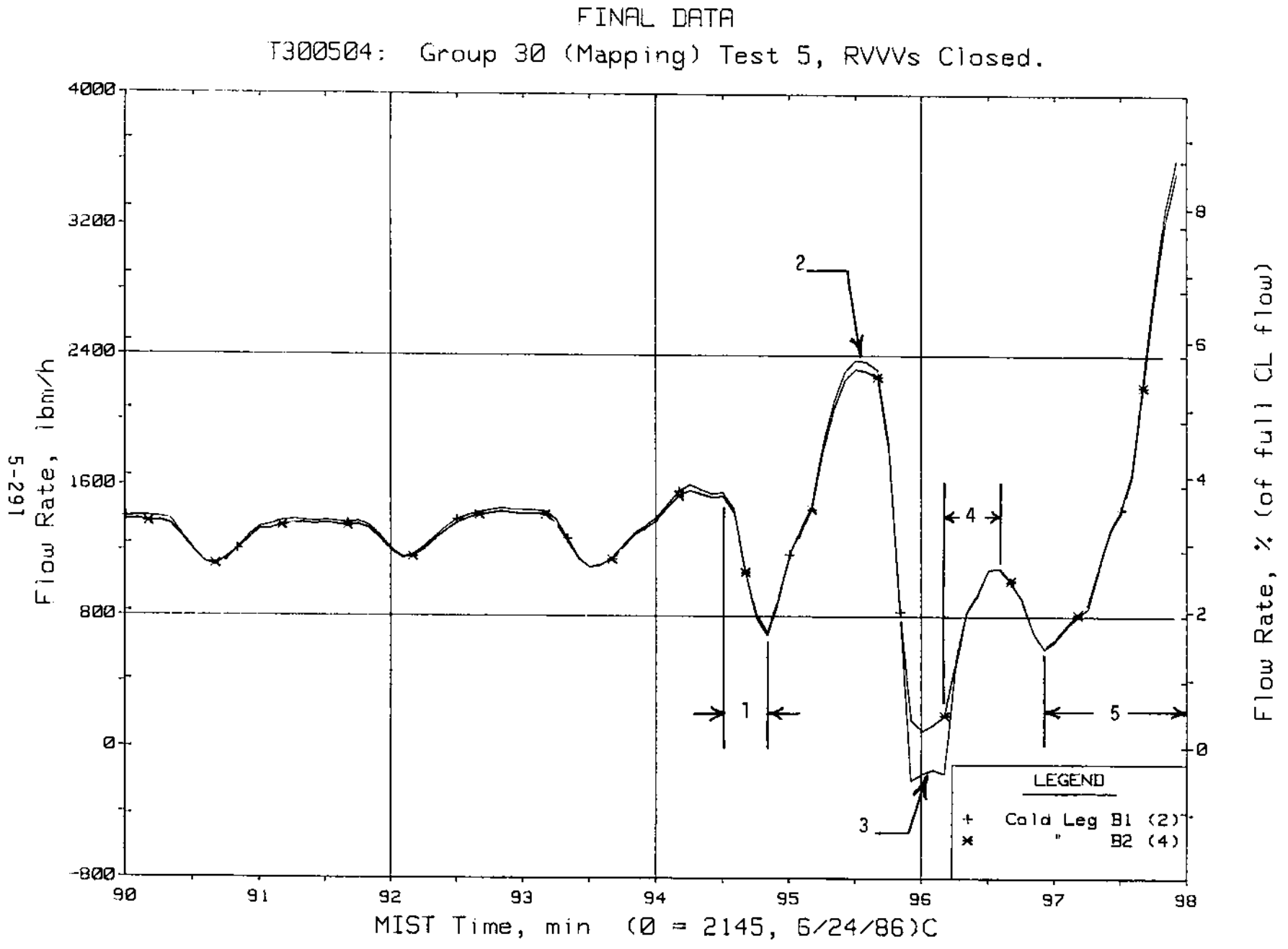

Figure 5.6.12. Loop B Cold Leg (Venturi) Flow Rates (CnVN2Os)

Wed Mar 1 15:48:55 1989

PRFLG

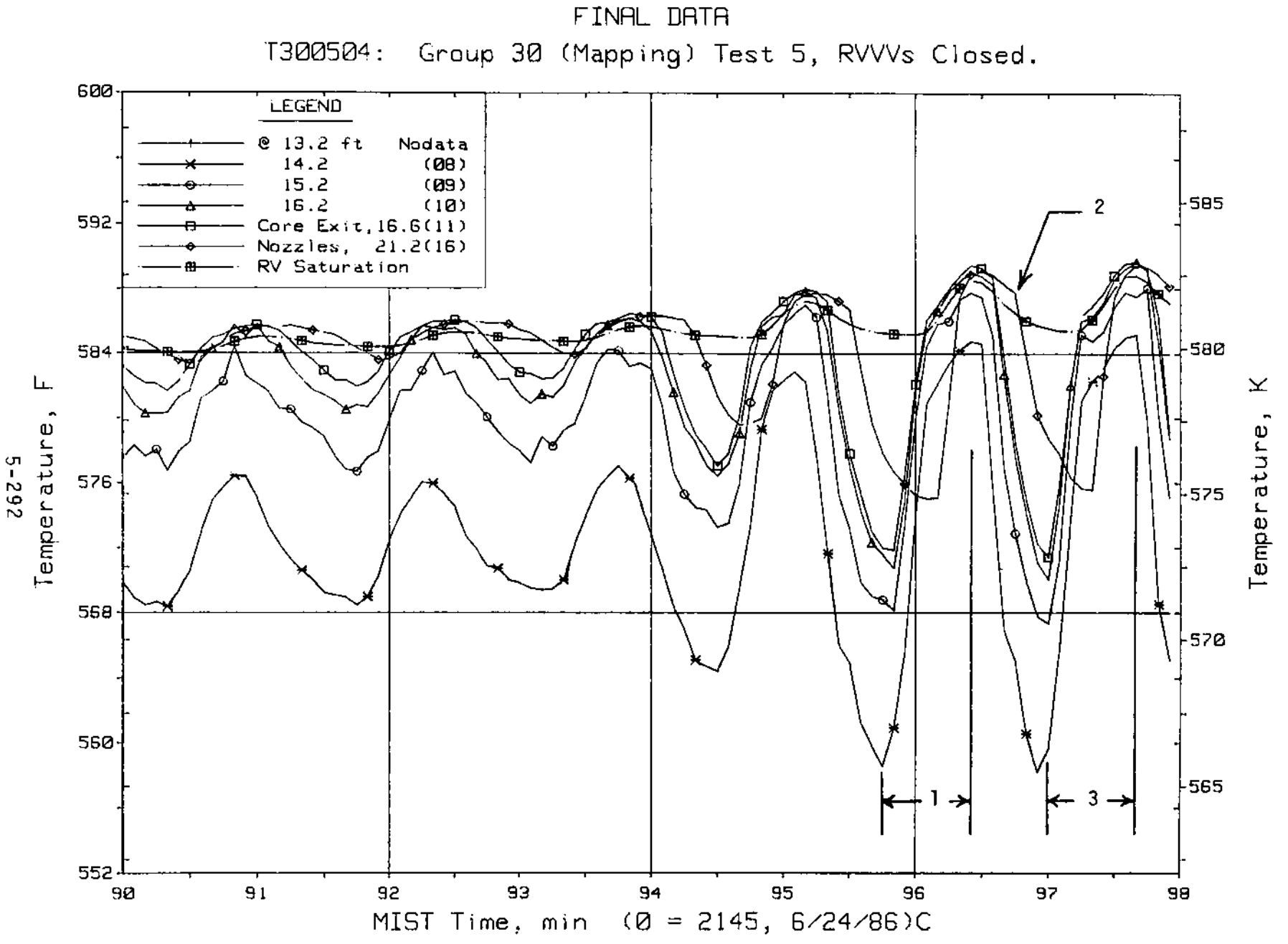

Figure 5.6.13. Reactor Vessel Mid-Elevation Fluid Temperatures (RVTCs)

Wed Mar 1 15:37:16 1989

RVTC2

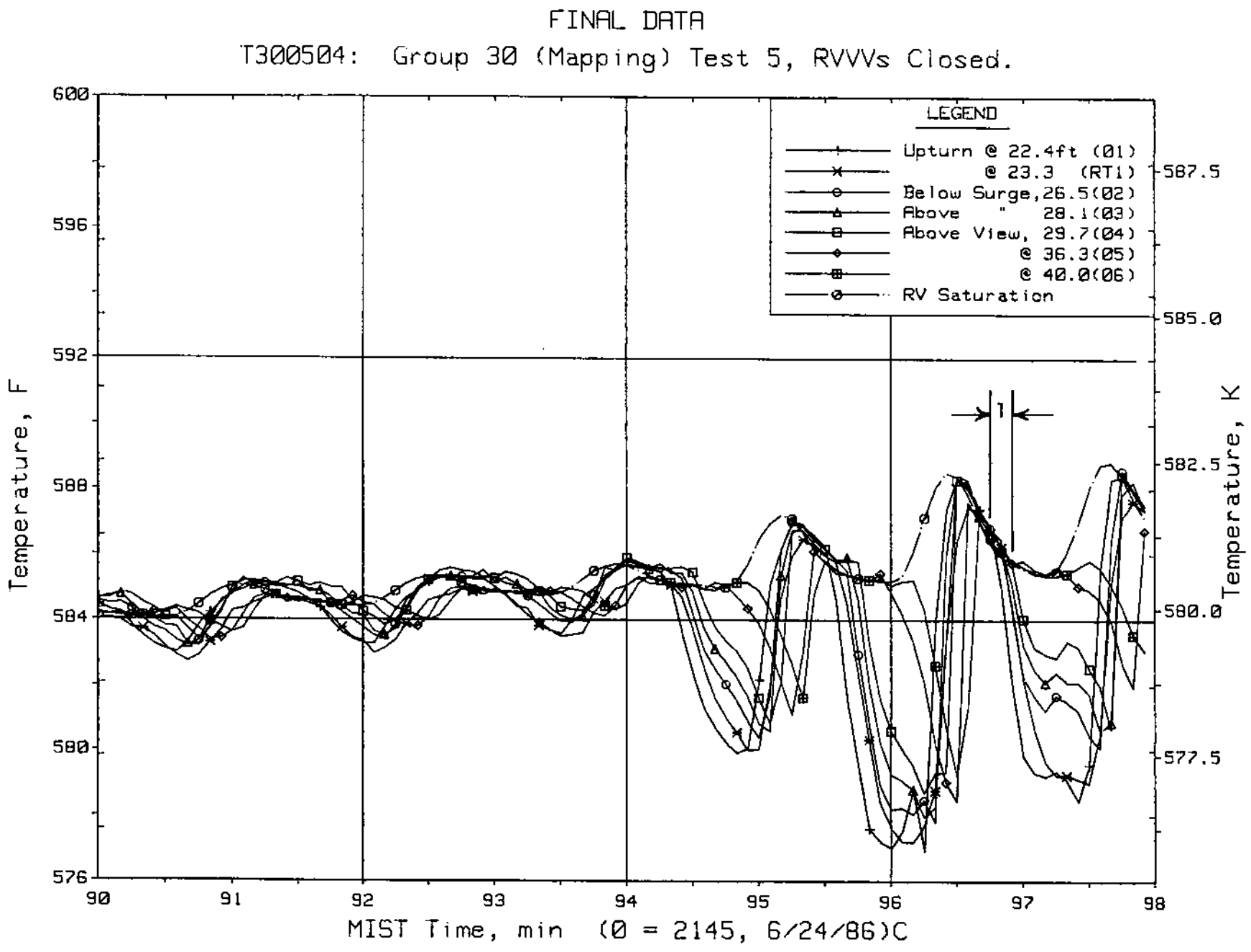

Figure 5.6.14. Hot Leg A Lower-Elevation Riser Fluid Temperatures (H1TCs)

Wed Mar 8 13:23:35 1989

H1TC1

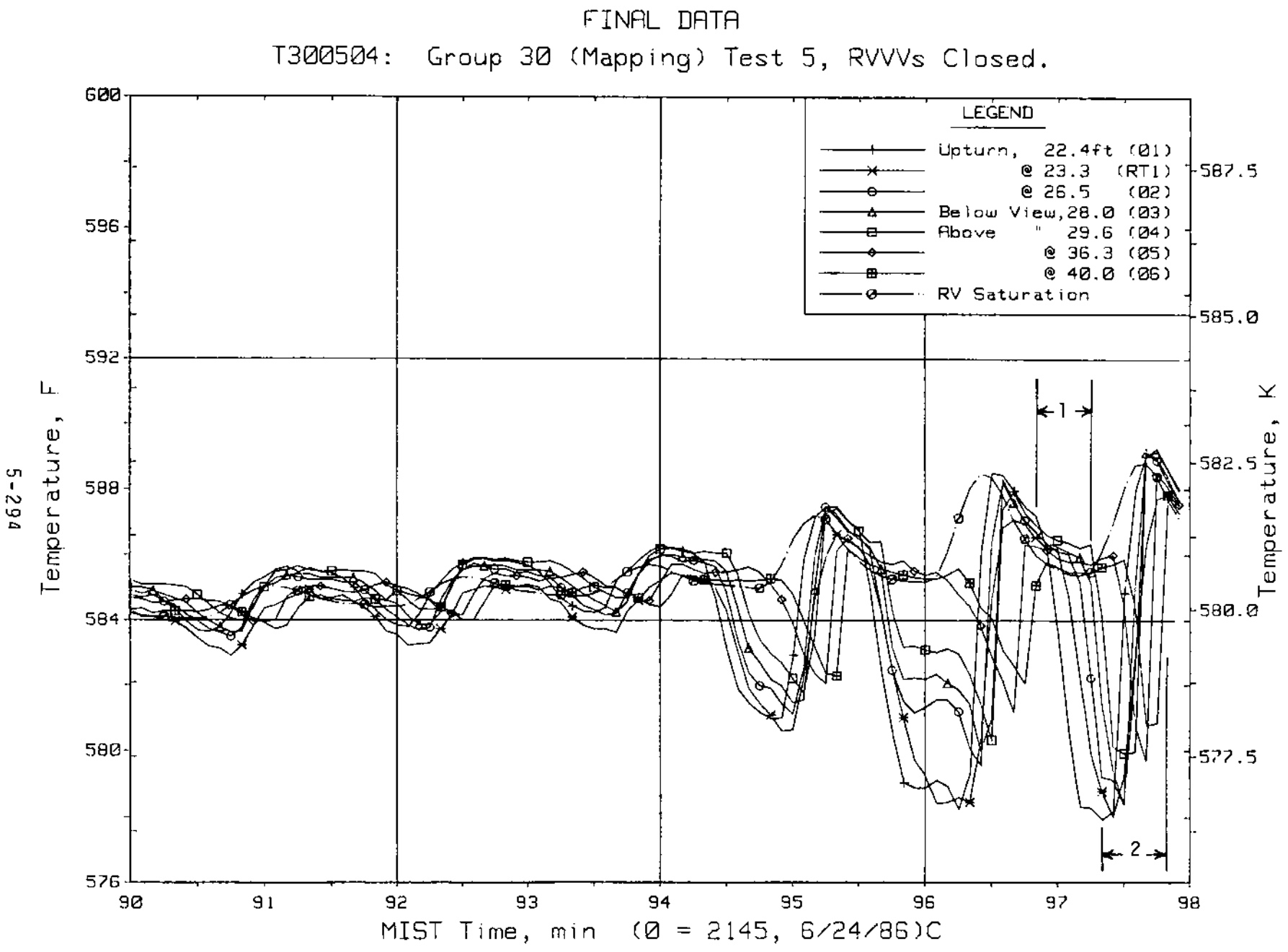

Figure 5.6.15. Hot Leg B Lower-Elevation Riser Fluid Temperatures (H2TCs)

Wed Mar 8 13:26:54 1989

H2TC1

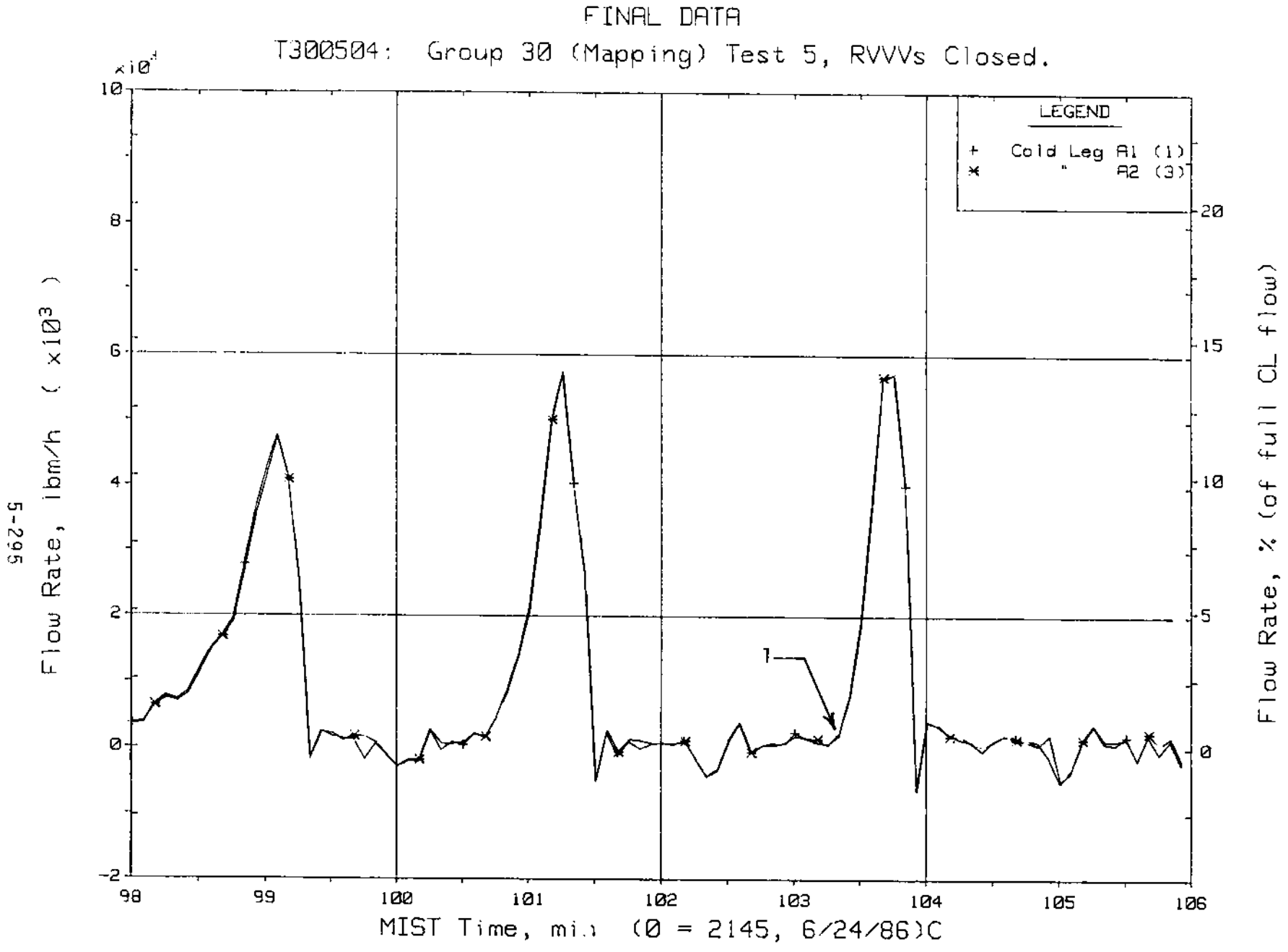

Figure 5.6.16. Loop A Cold Leg (Venturi) Flow Rate (CnVN20s)

Wed Mar 1 15:29:49 1989

PRFLS

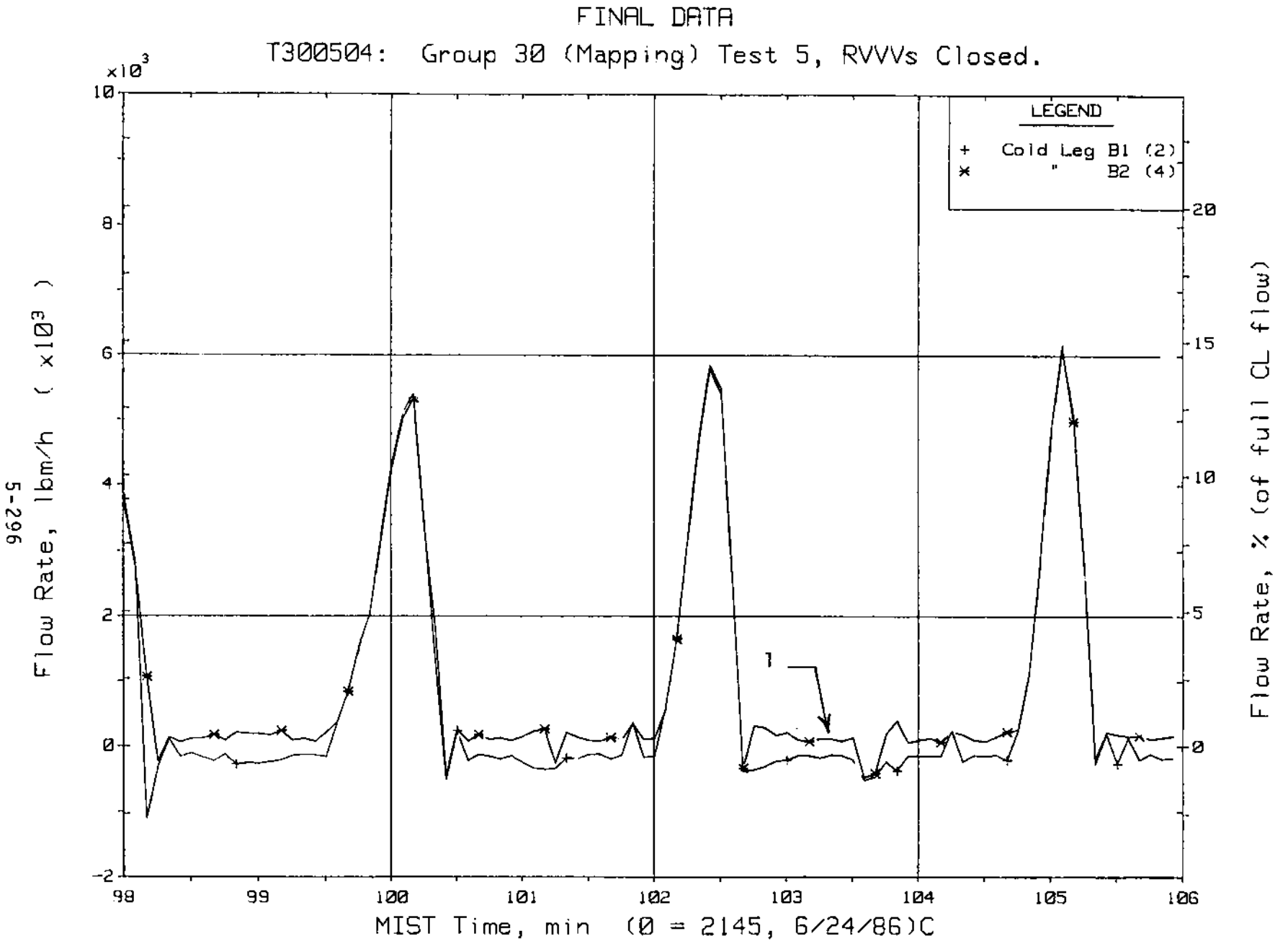

Figure 5.6.17. Loop B Cold Leg (Venturi) Flow Rates (CnVN20s)

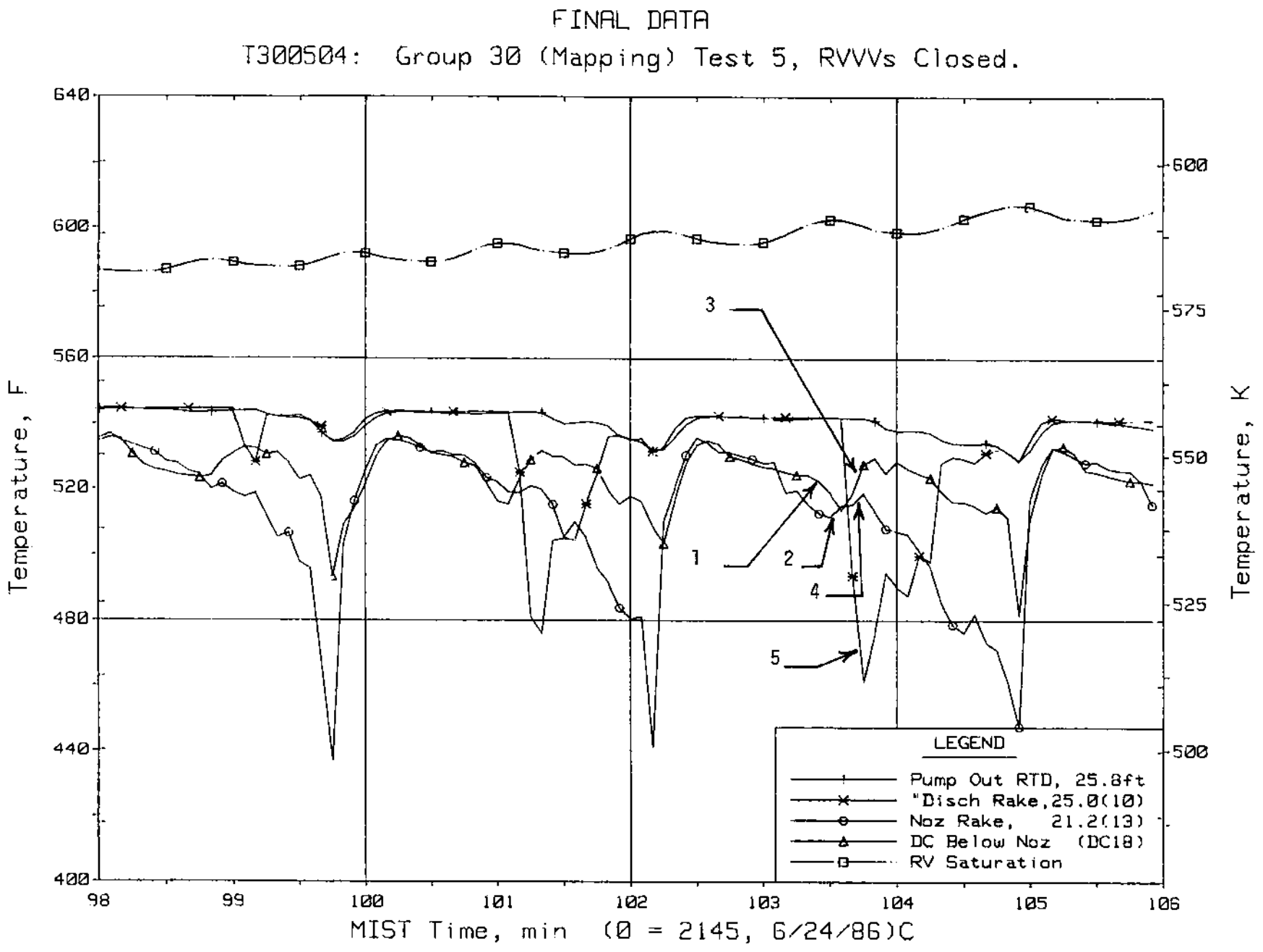

Figure 5.6.18. Cold Leg B1 Discharge Fluid Temperatures (C2TCs)

Wed Mar 1 15:22:40 1989

C2TC2

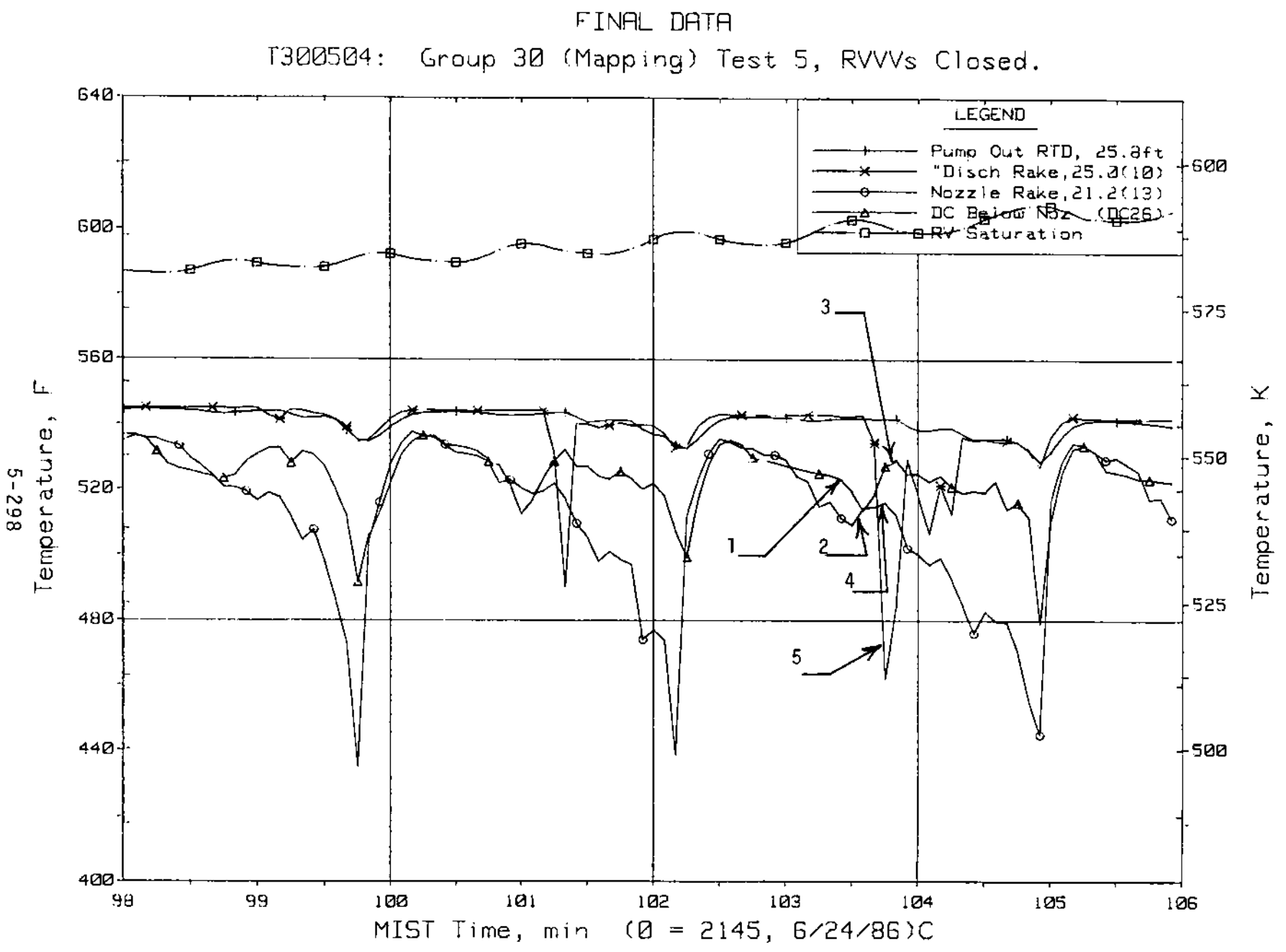

Figure 5.6.19. Cold Leg B2 Discharge Fluid Temperatures (C4TCs)

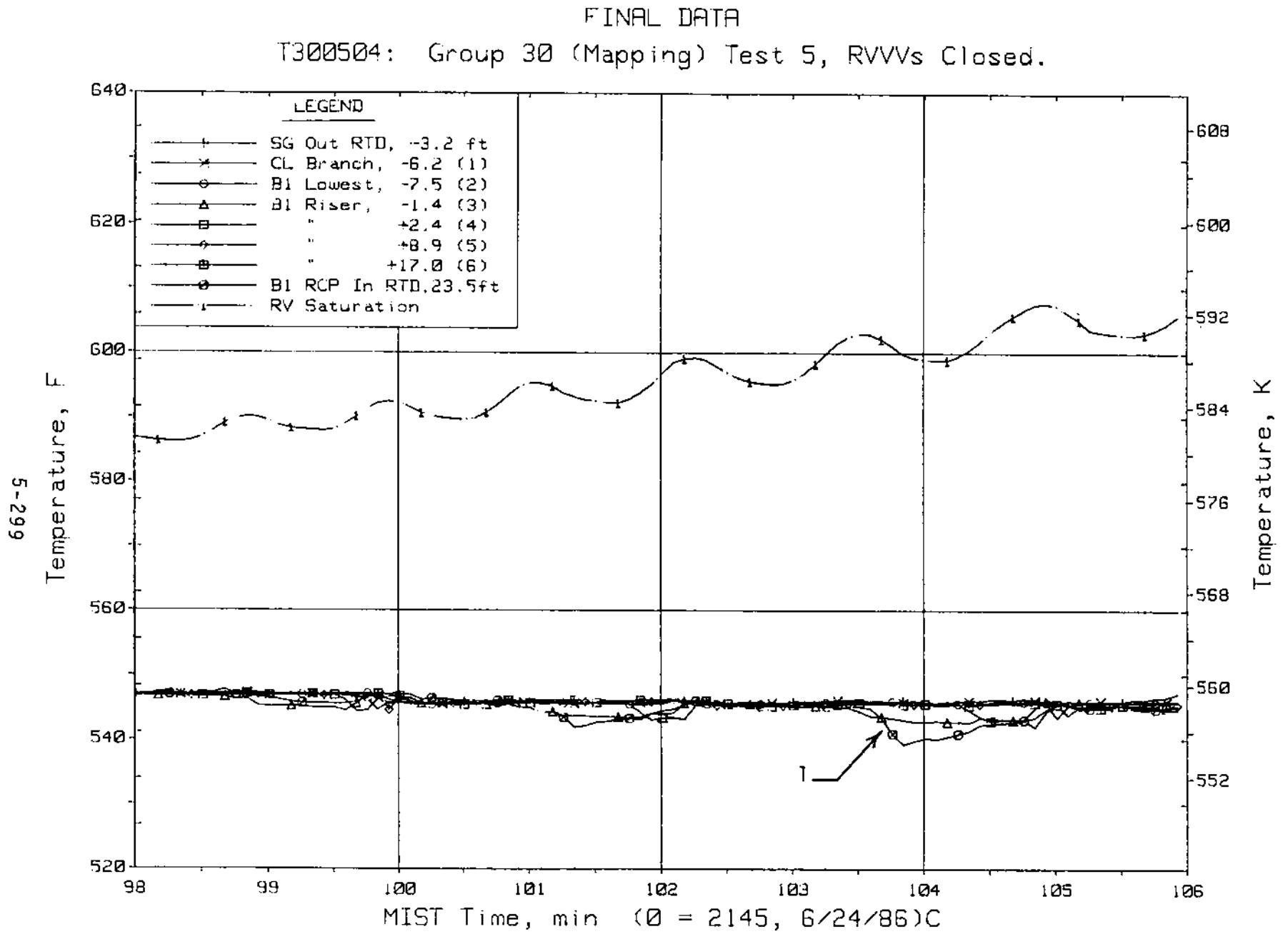

Figure 5.6.20. Cold Leg B1 Suction Fluid Temperatures (C2TCs)

Wed Mar 1 15:10:11 1989

C2TC1

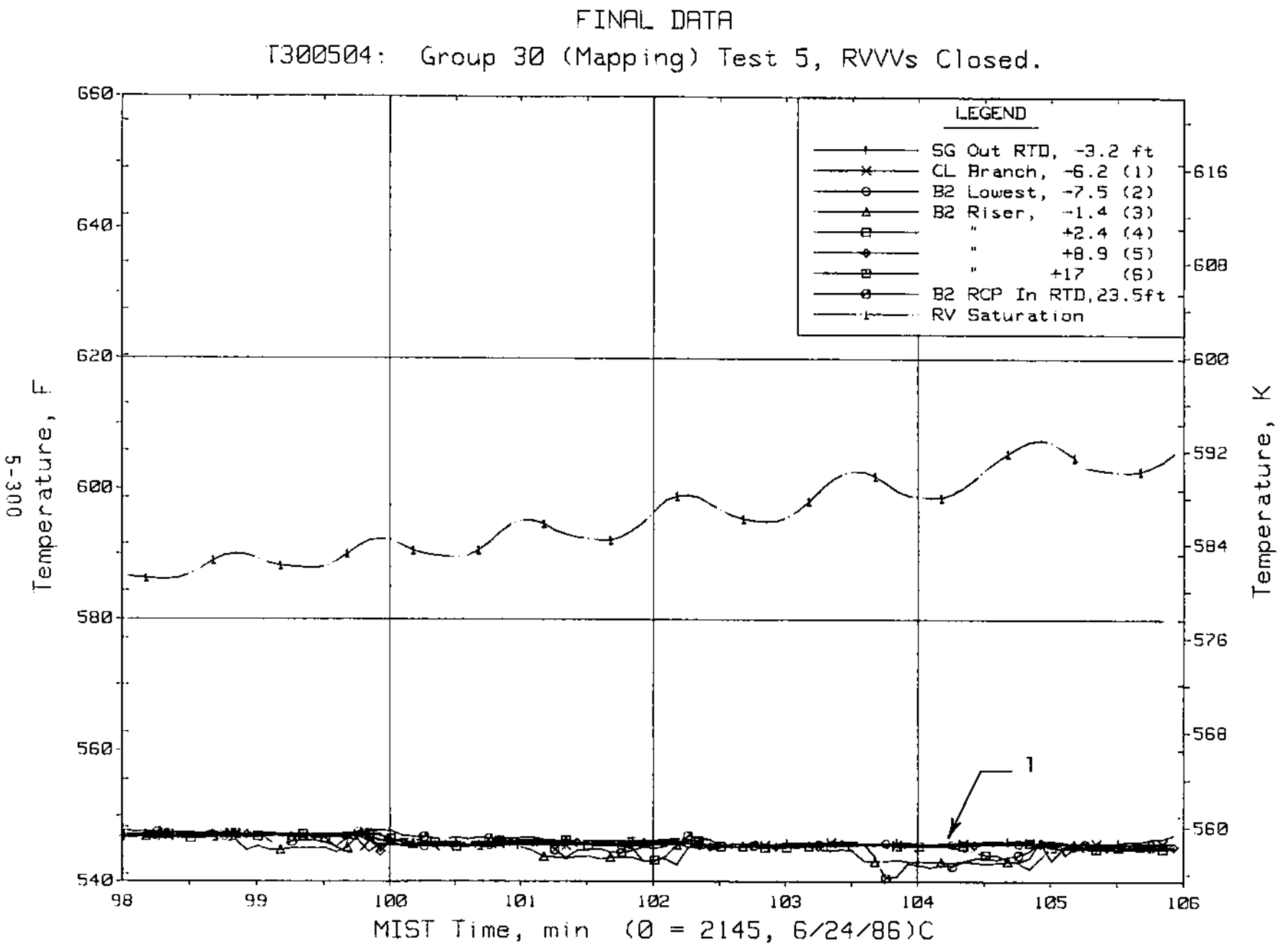

Figure 5.6.21. Cold Leg B2 Suction Fluid Temperatures (C4TCs)

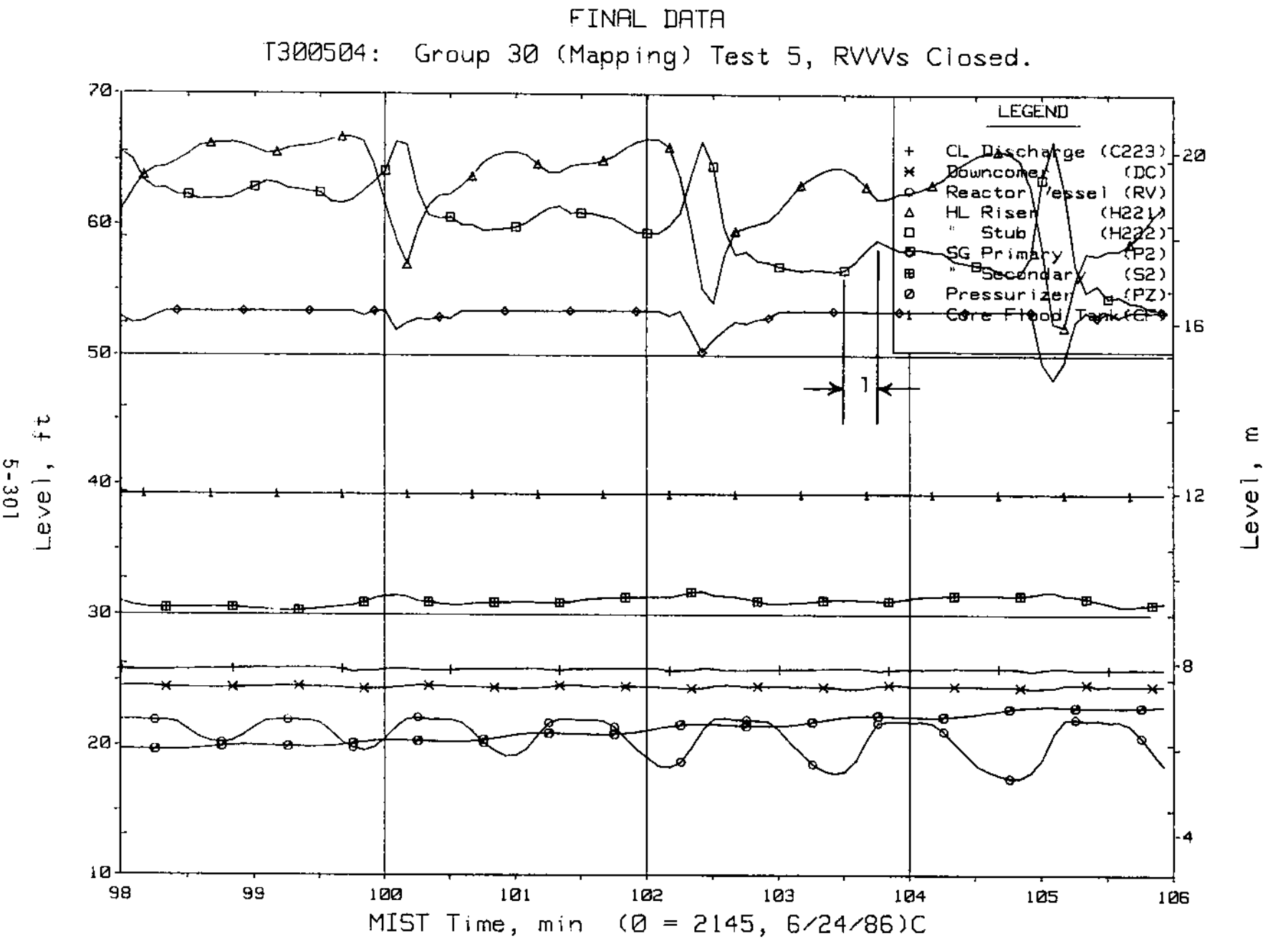

Figure 5.6.22. Loop B Collapsed Liquid Levels (LV20s)

Wed Mar 1 15:12:59 1989

PRLV2

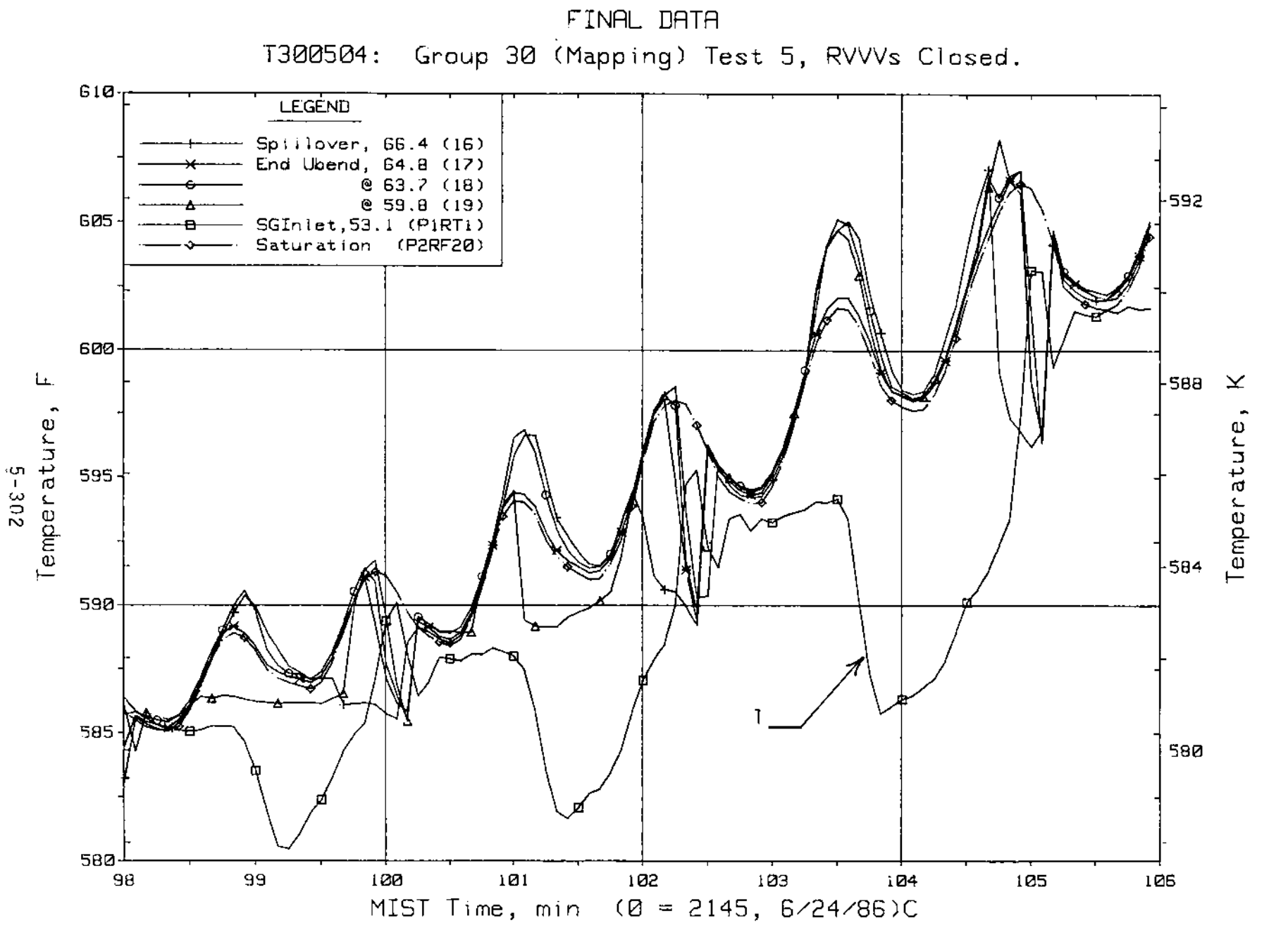

Figure 5.6.23. Hot Leg B Fluid Temperatures Beyond U-Bend (H2TCs)

Wed Mar 1 15:01:27 1989

H2TC3

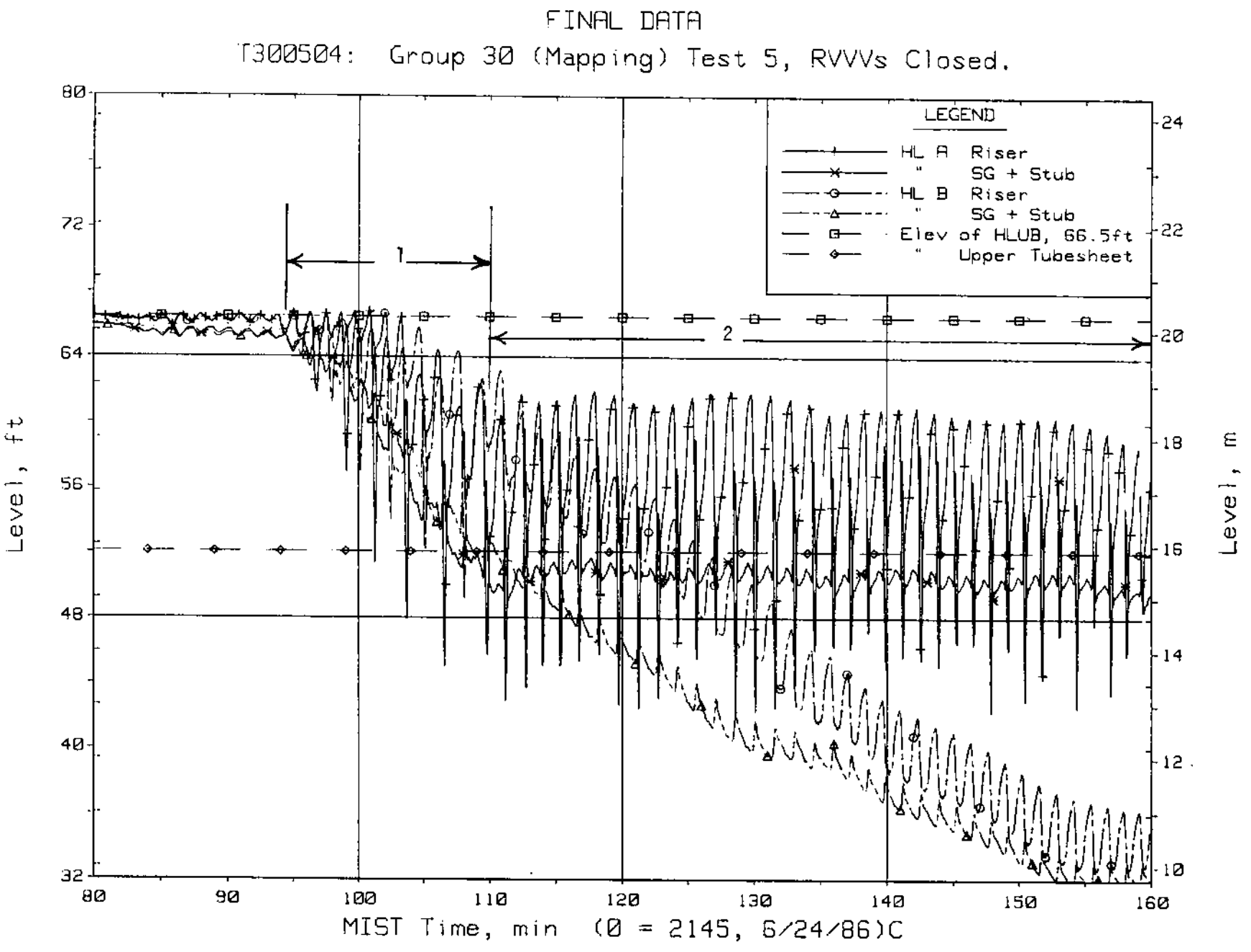

Figure 5.6.24. Hot Leg Riser and Stub Collapsed Liquid Levels

Wed Mar 8 13:34:01 1989

HLLV1

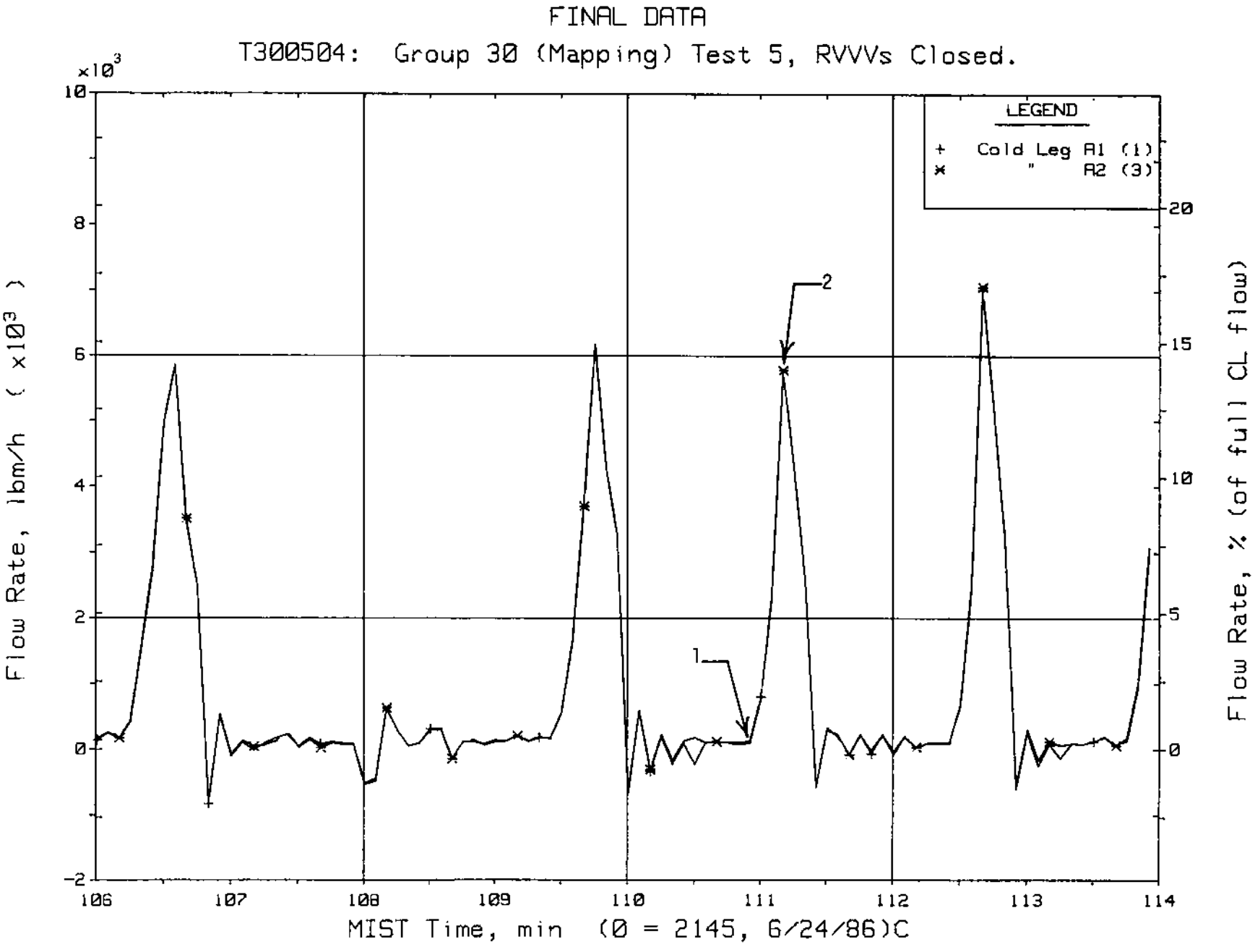

Figure 5.6.25. Loop A Cold Leg (Venturi) Flow Rates (CnVN2Os)

Wed Mar 1 14:54:35 1989

PRFL5

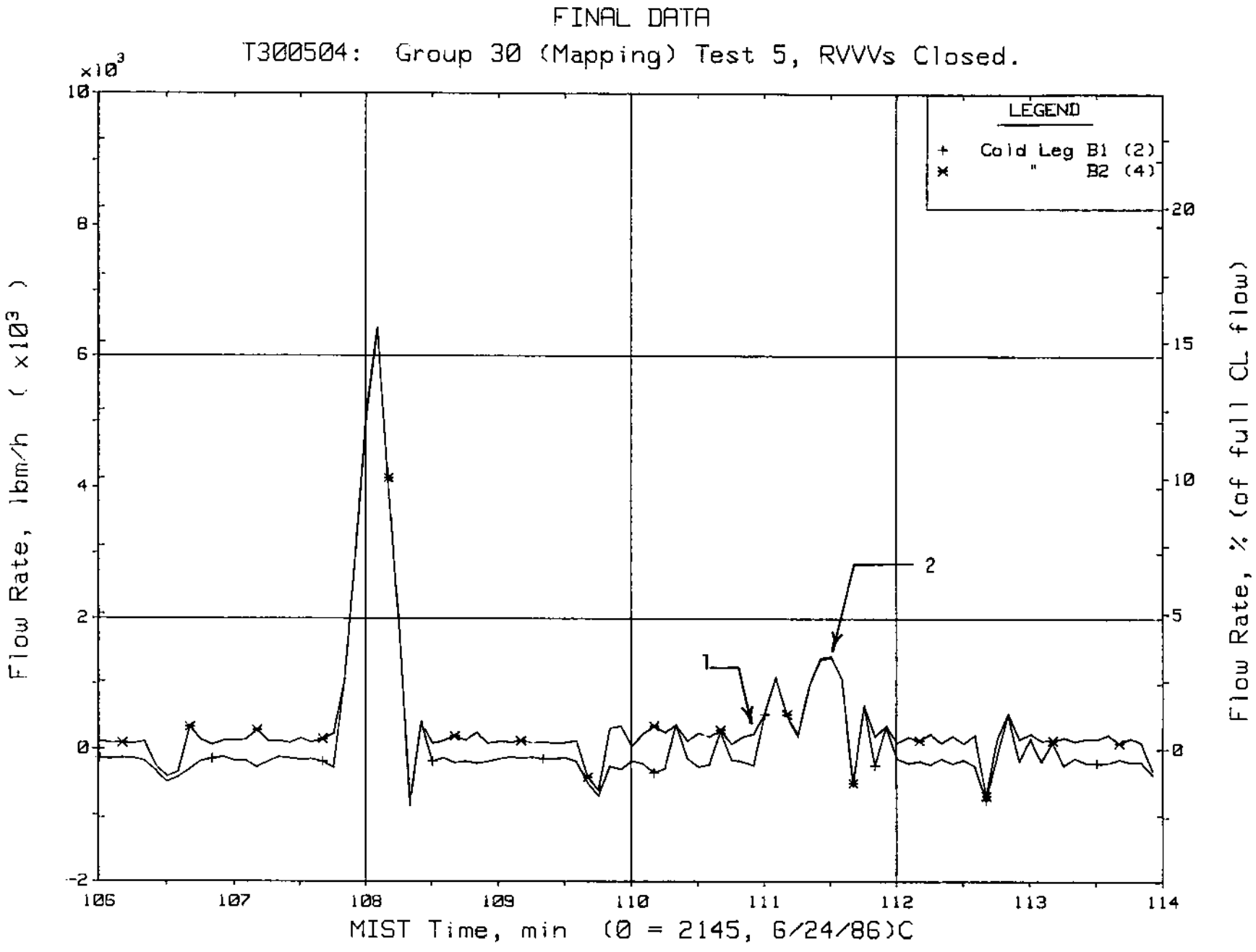

Figure 5.6.26. Loop B Cold Leg (Venturi) Flow Rates (CnVN20s)

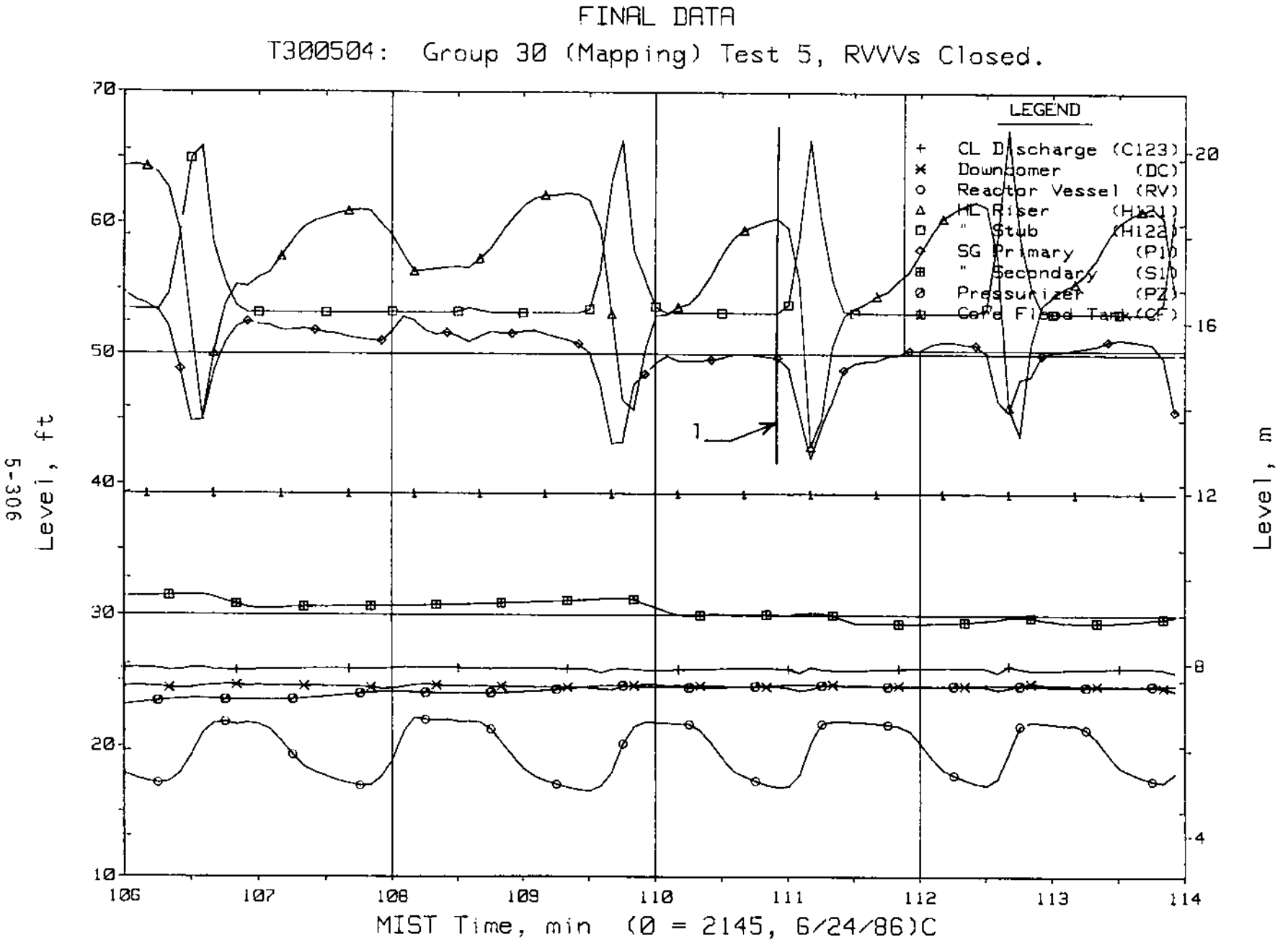

Figure 5.6.27. Loop A Collapsed Liquid Levels (LV20s)

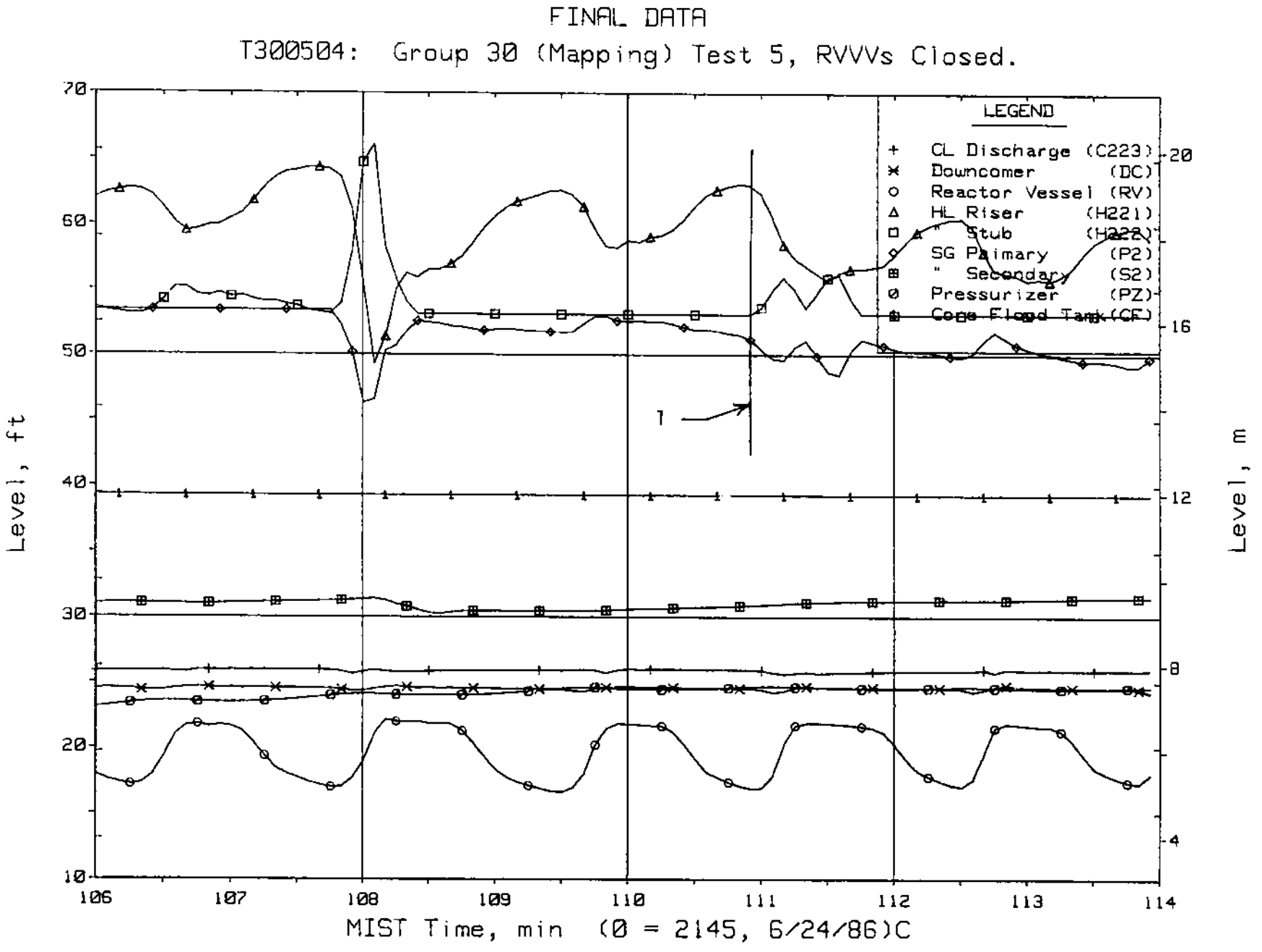

Figure 5.6.28. Loop B Collapsed Liquid Levels (LV20s)

Wed Mar 1 14:44:55 1989

PRLV2

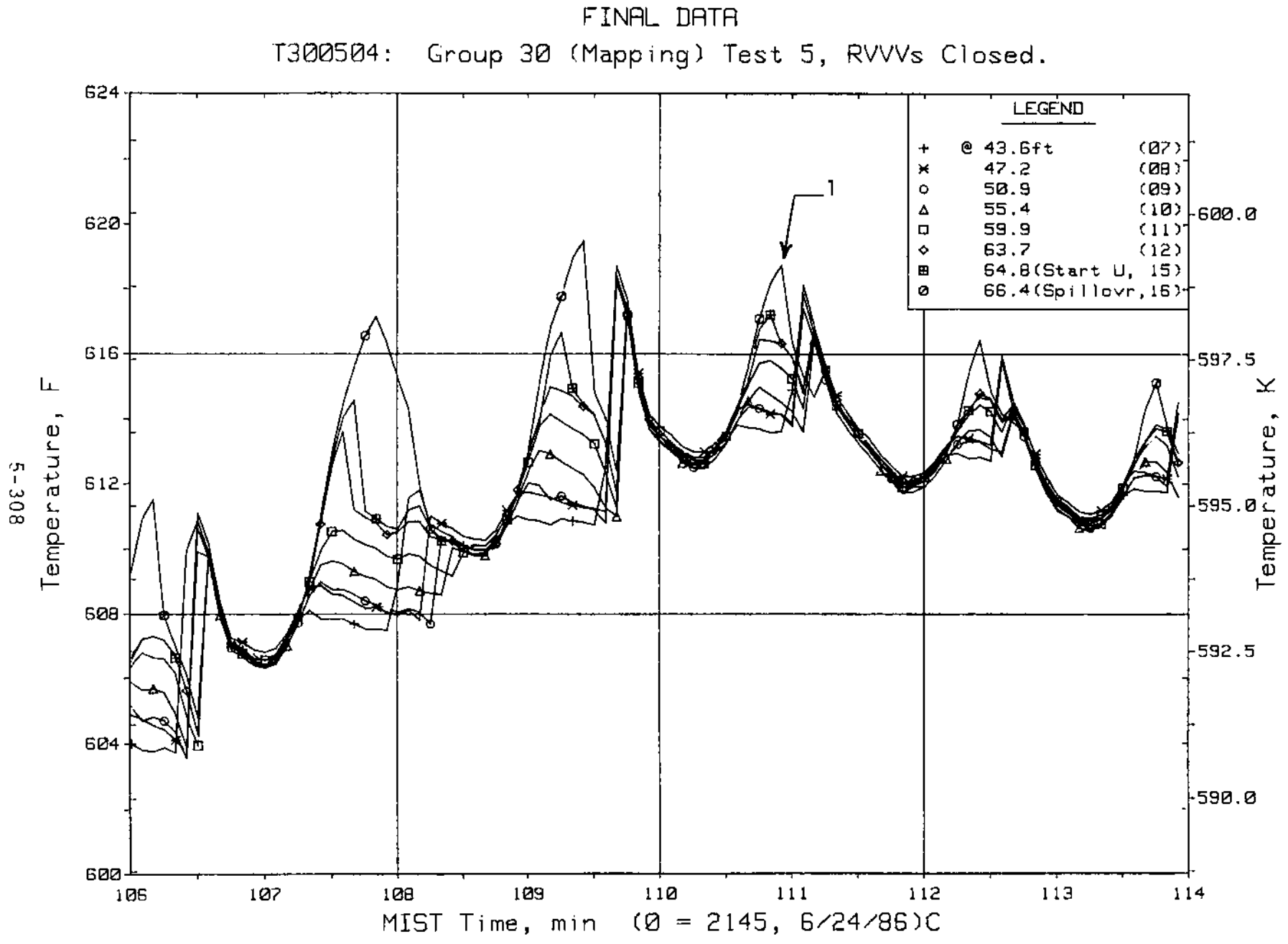

Figure 5.6.29. Hot Leg A Upper-Elevation Riser Fluid Temperatures (H1TCs)

Wed Mar 1 14:42:21 1989

H1TC2

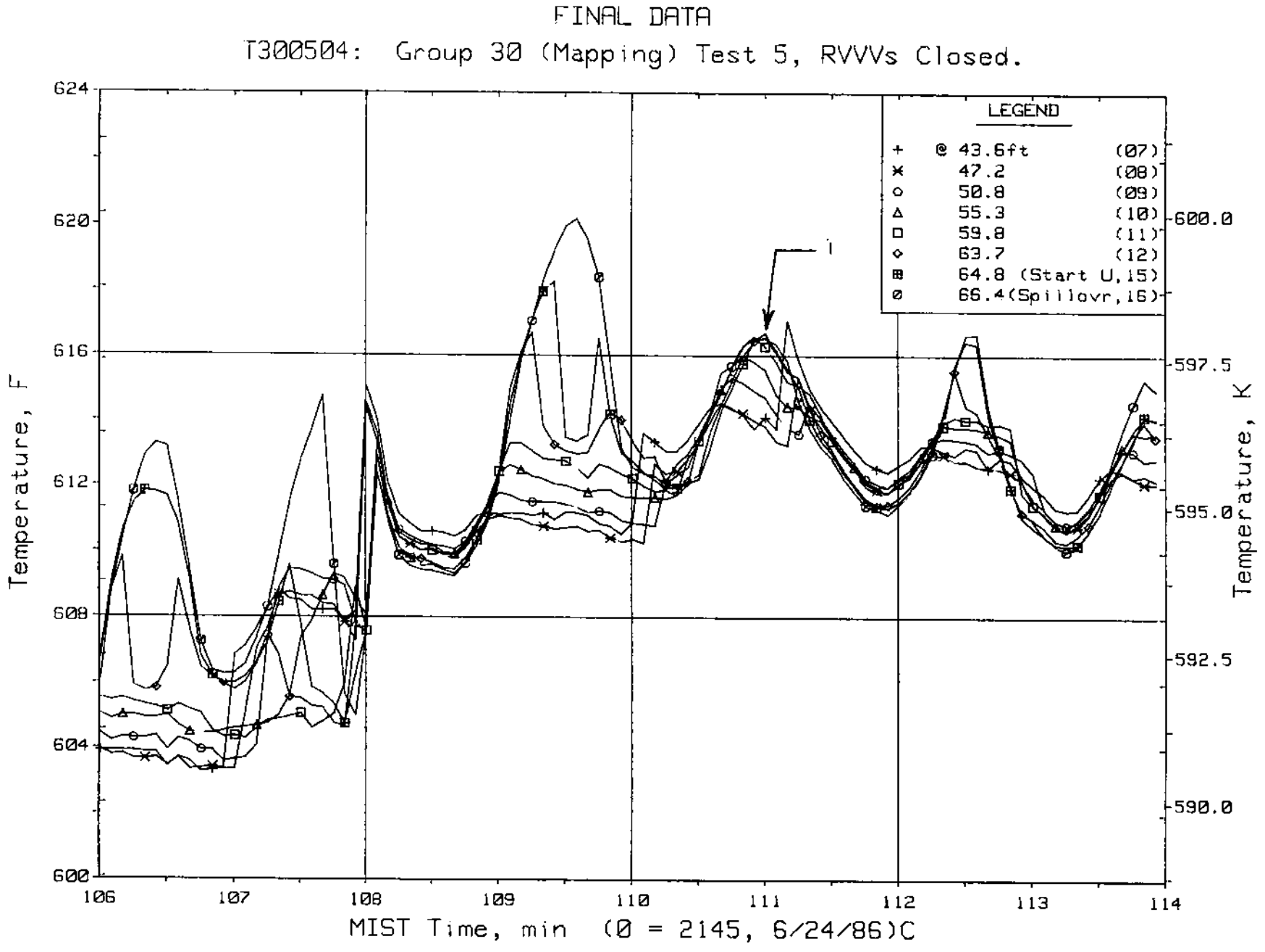

Figure 5.6.30. Hot Leg B Upper-Elevation Riser Fluid Temperatures (H2TCs)

Wed Mar 1 14:39:50 1989

H2TC2

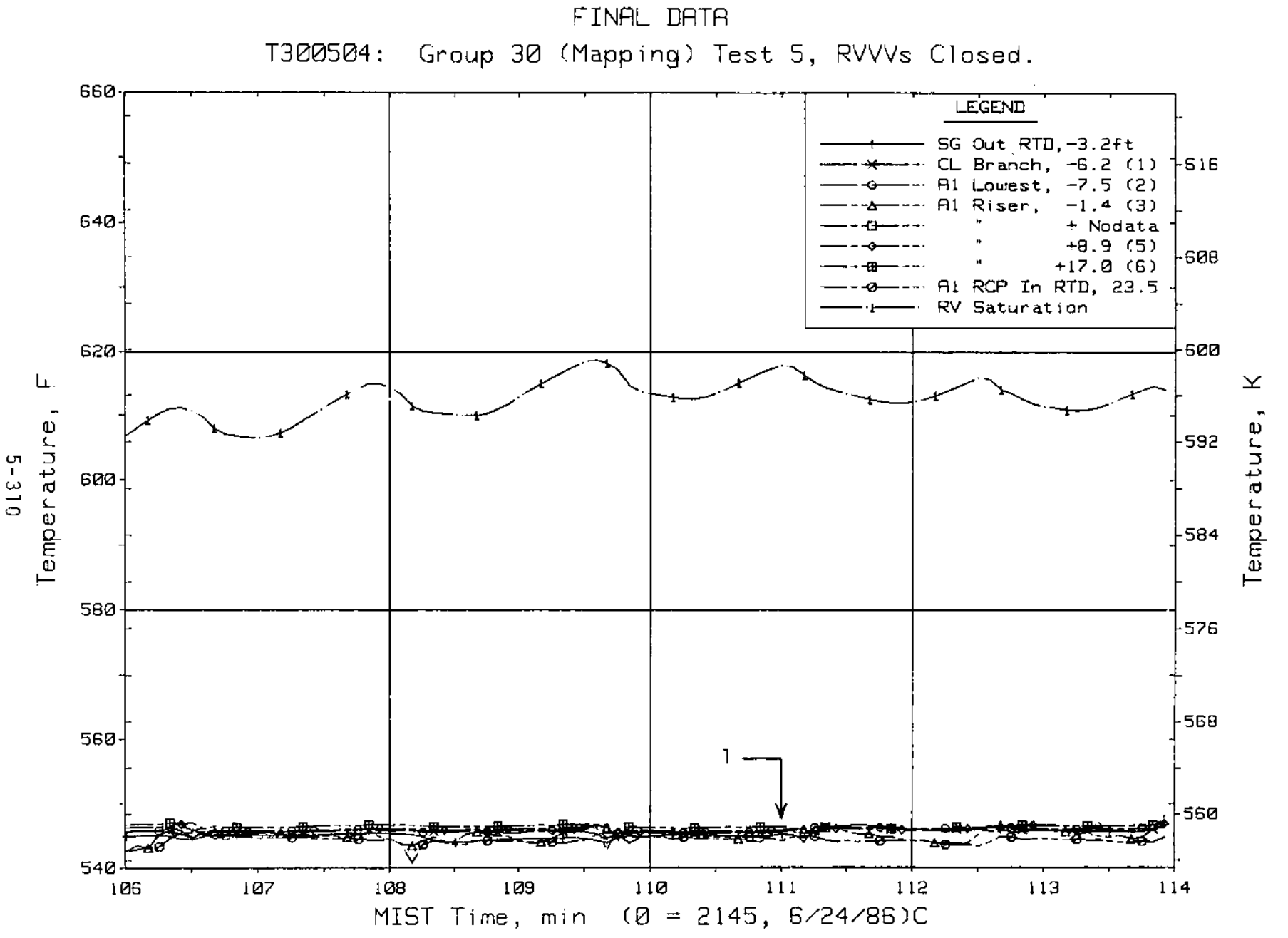

Figure 5.6.31. Cold Leg A1 Suction Fluid Temperatures (C1TCs)

Wed Mar 1 14:37:08 1989

C1TC1

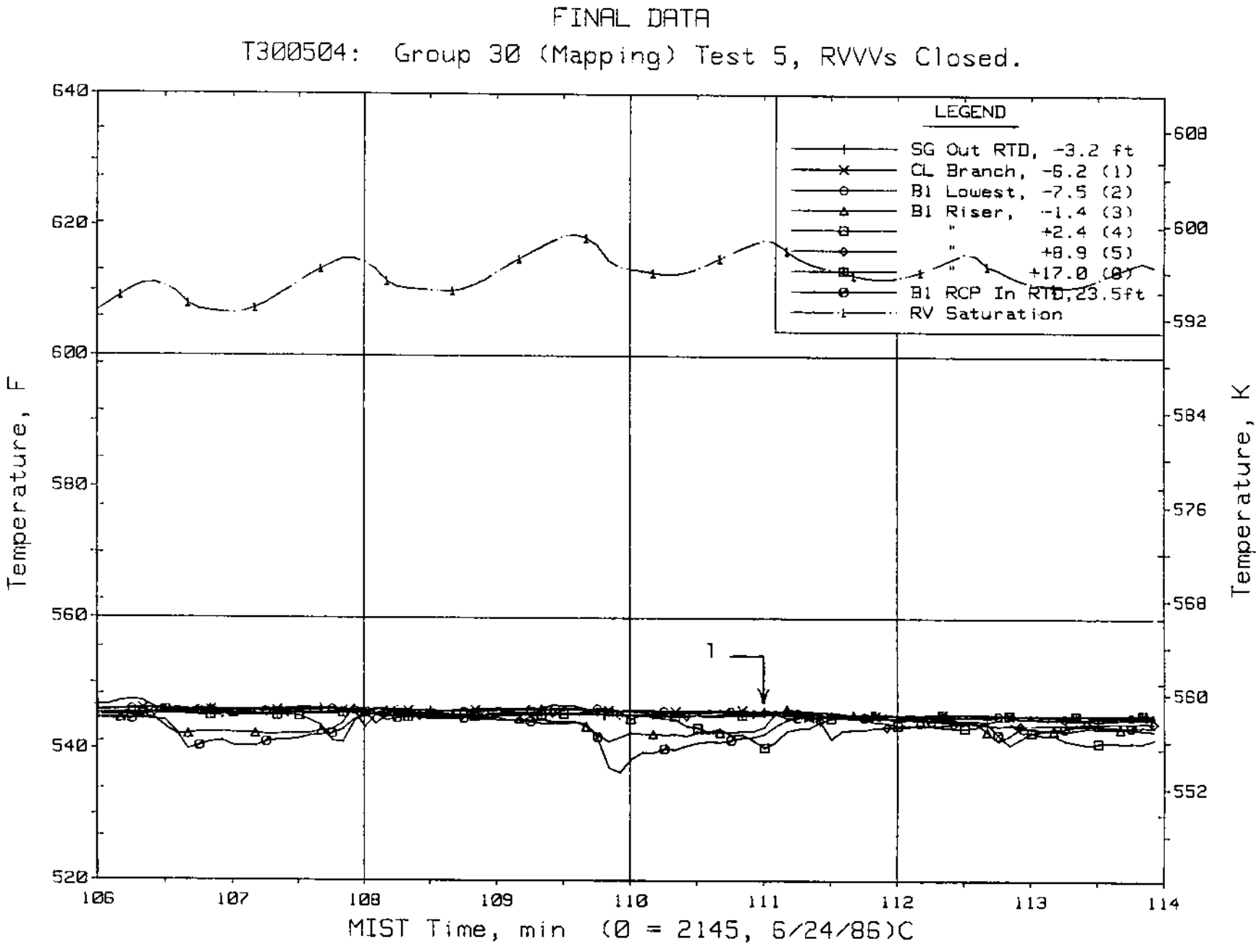

Figure 5.6.32. Cold Leg B1 Suction Fluid Temperatures (C2TCs)

Wed Mar 1 14:34:15 1989

C2TC1

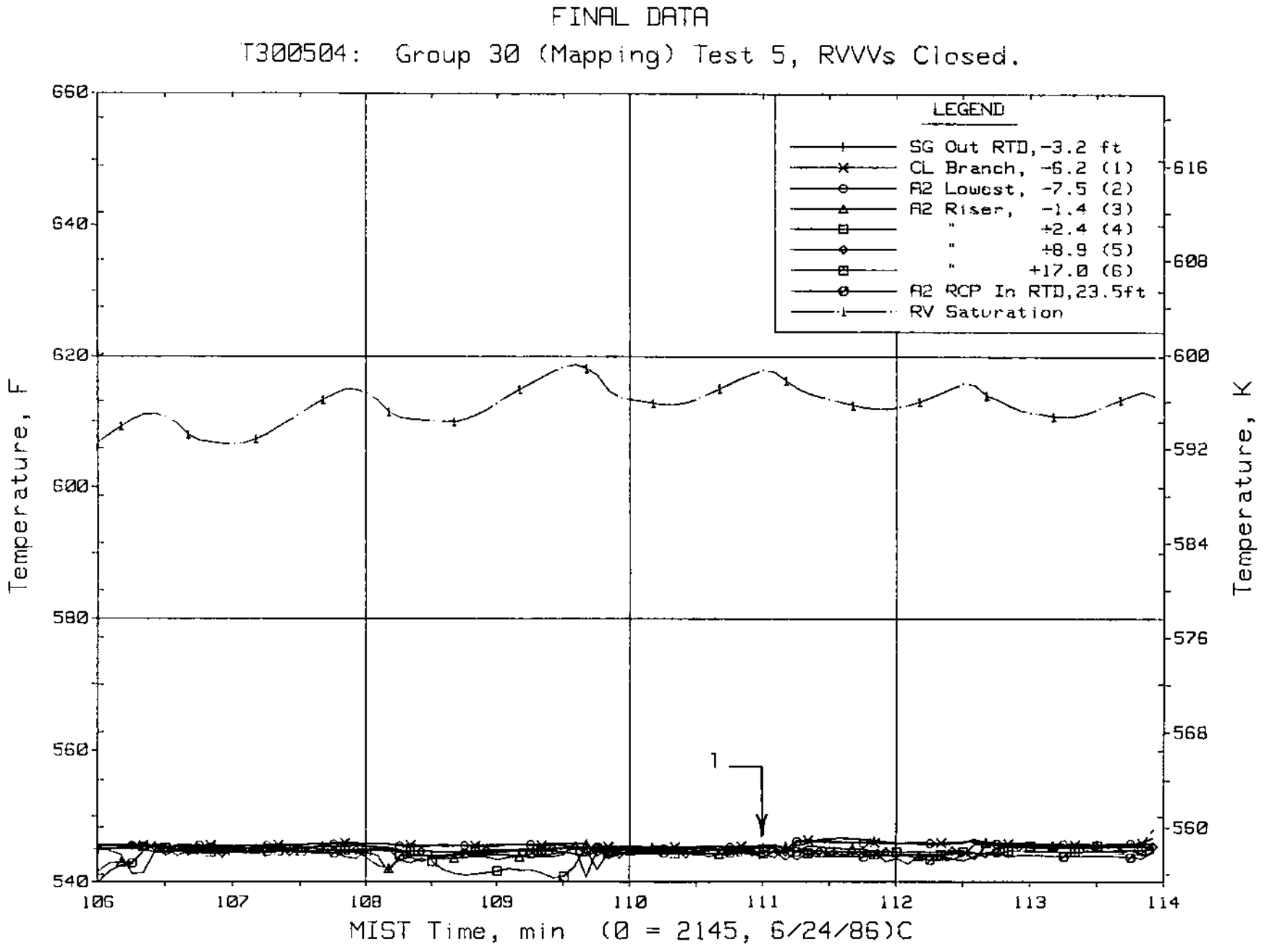

Figure 5.6.33. Cold Leg A2 Suction Fluid Temperatures (C3TCs)

Wed Mar 1 14:31:34 1989

C3TC1

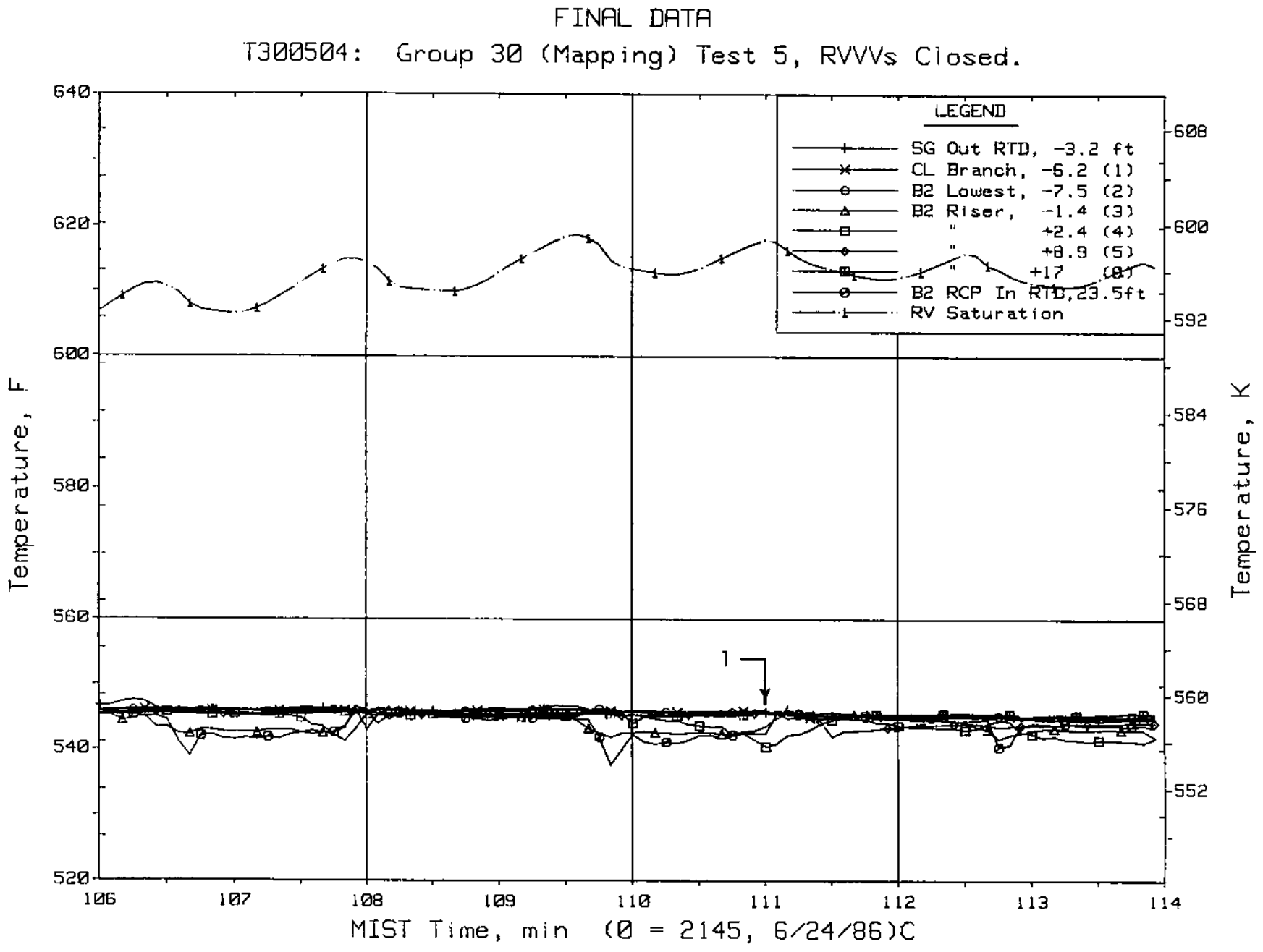

Figure 5.6.34. Cold Leg B2 Suction Fluid Temperatures (C4TCs)

Wed Mar 1 14:28:53 1989

C4TC1

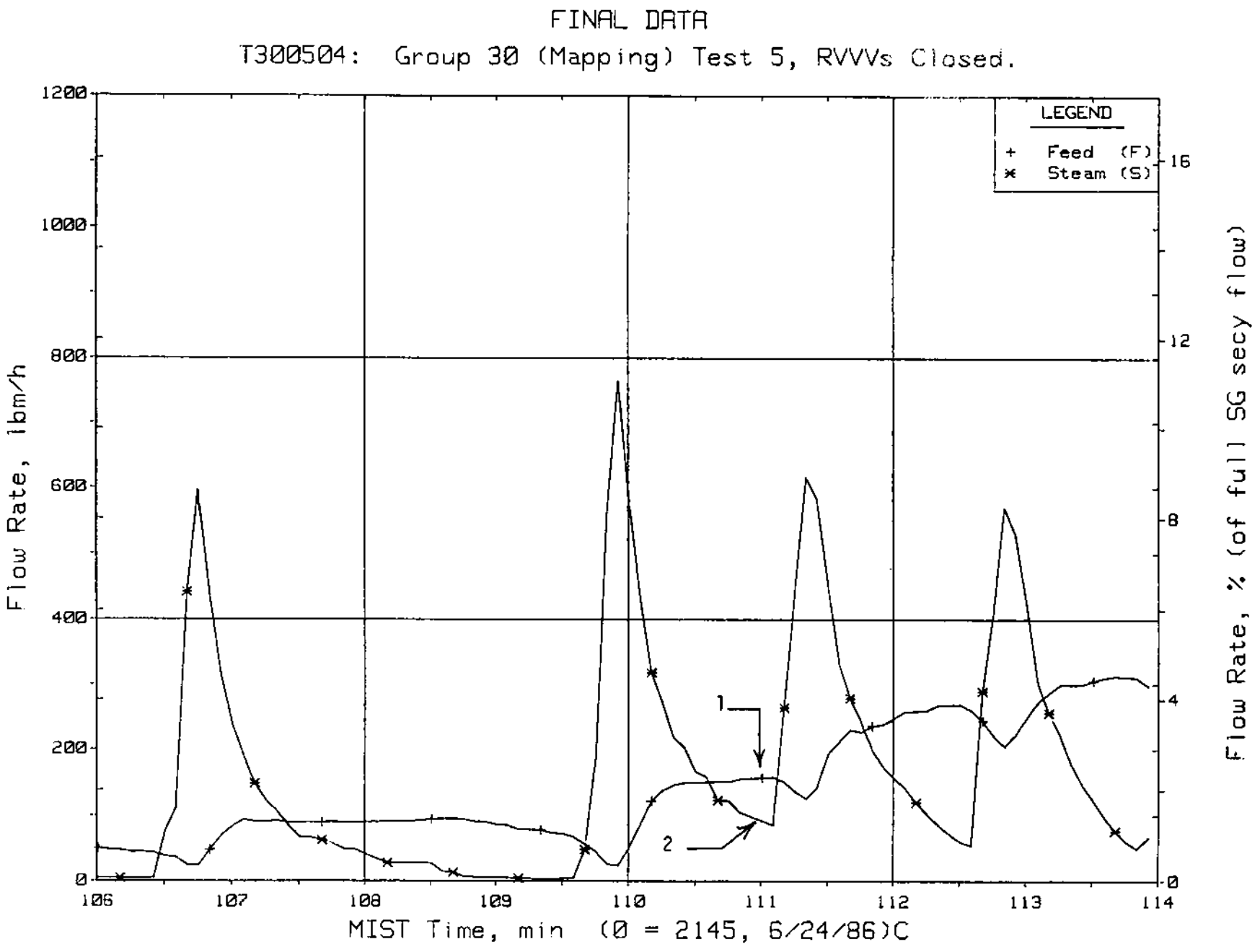

Figure 5.6.35. Steam Generator A Flow Rates (SaOR20s)

Wed Mar 1 14:26:38 1989

SCFL1

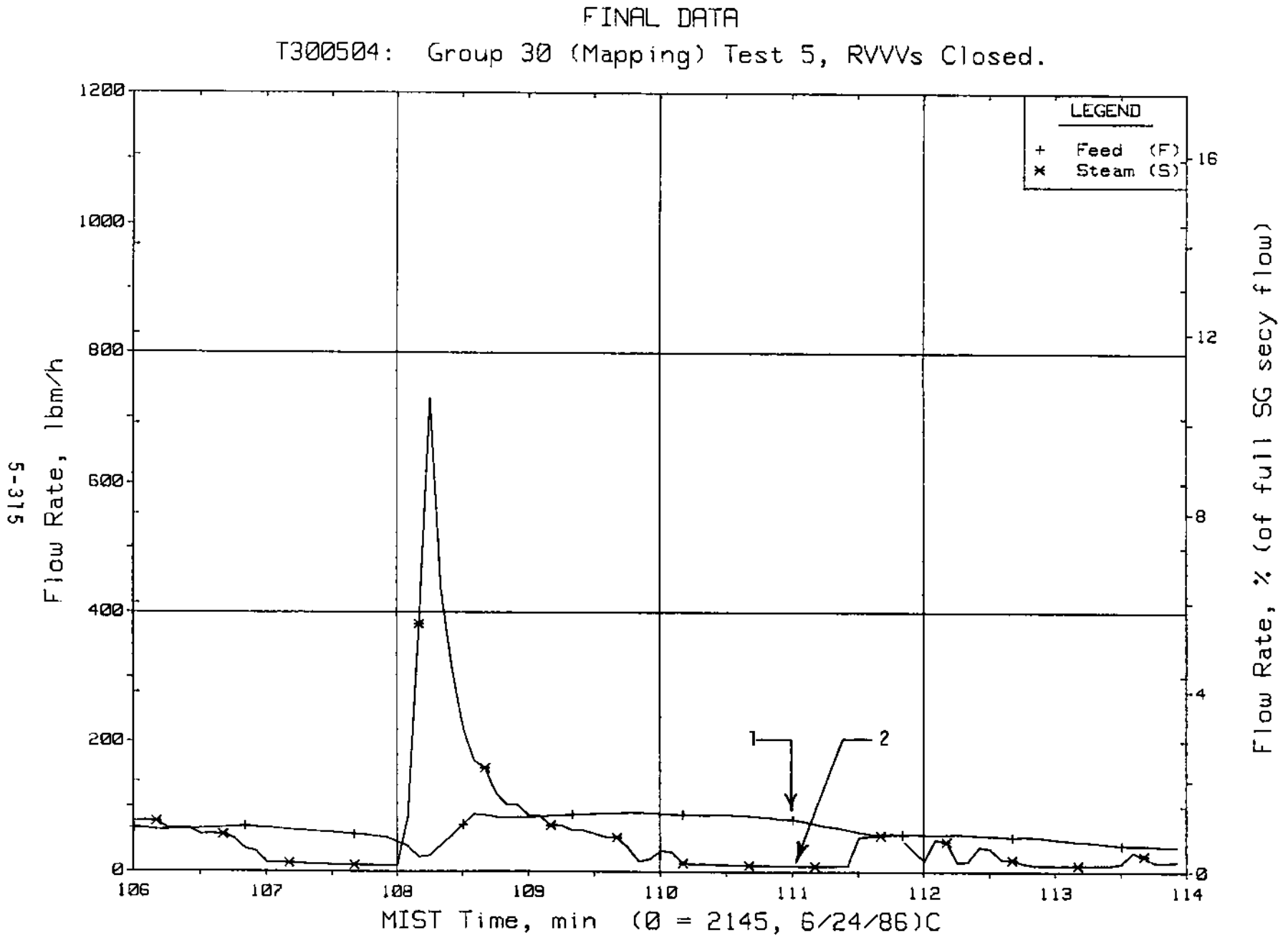

Figure 5.6.36. Steam Generator B Flow Rates (SaOR21s)

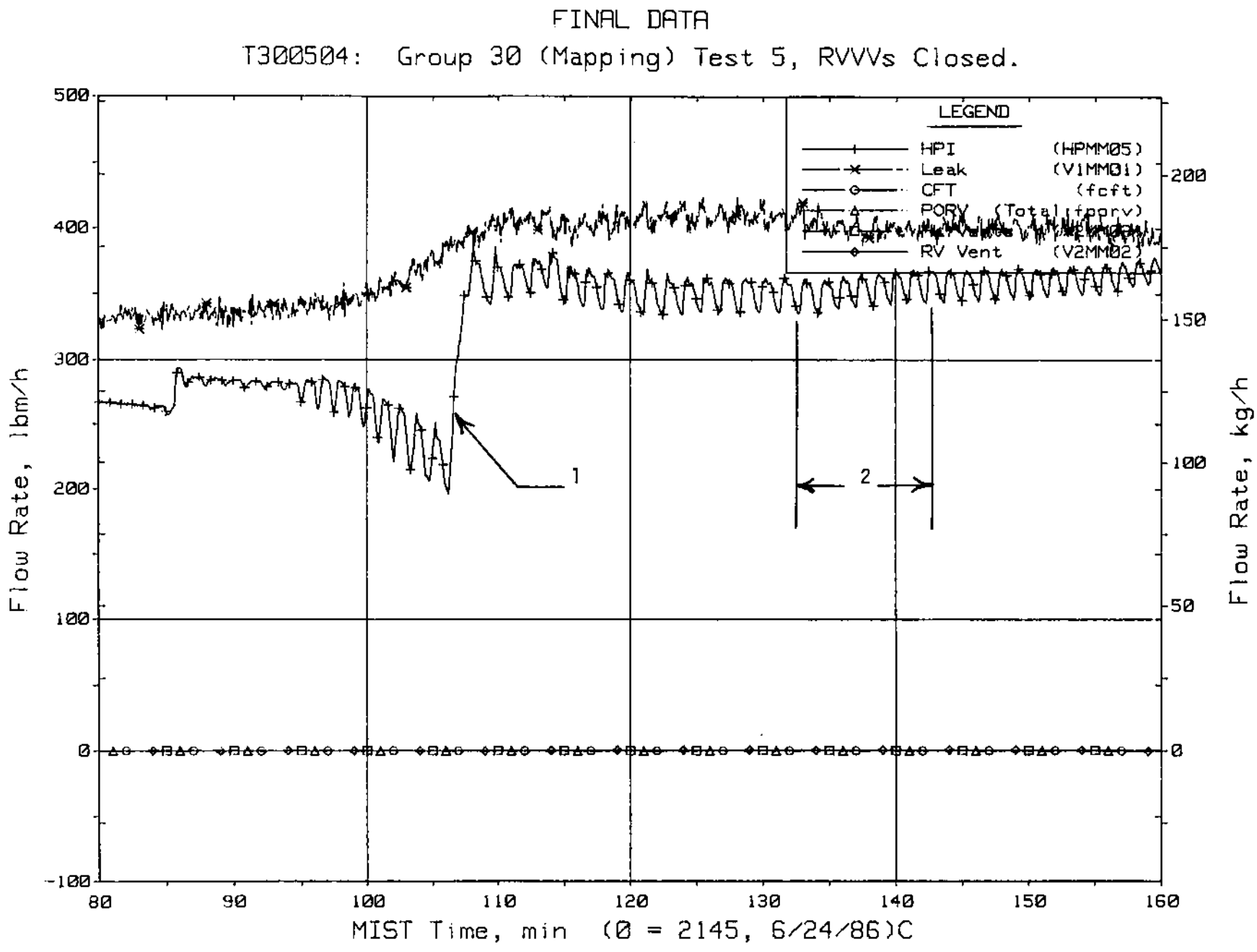

Figure 5.6.37. Primary System Boundary Flow Rates

Wed Mar 1 14:23:10 1989

PRFL3p

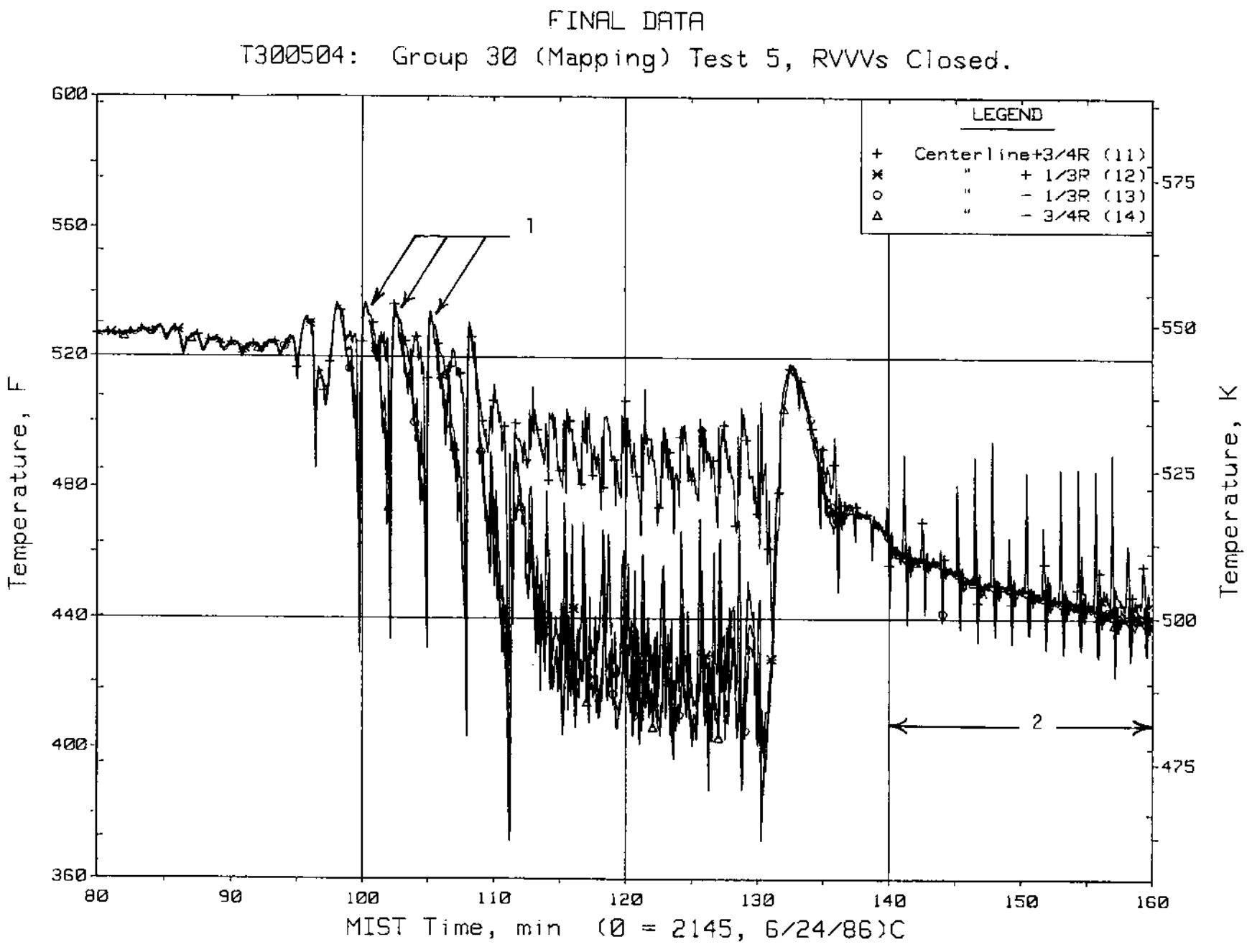

Figure 5.6.38. Cold Leg B2 Nozzle Rake Fluid Temperatures (21.2 ft, C4TCs)

Wed Mar 1 14:19:01 1989

C4TC4

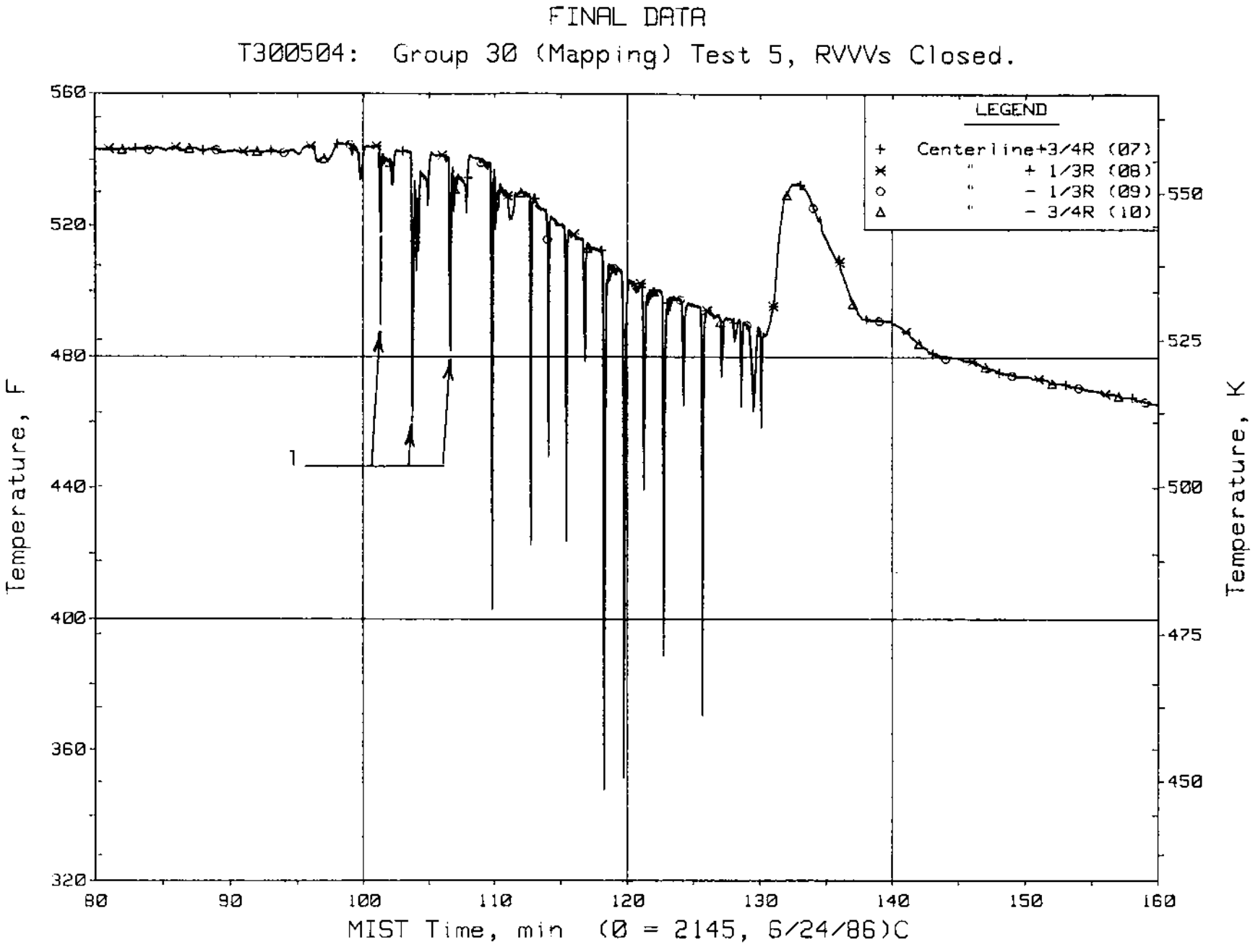

Figure 5.6.39. Cold Leg B2 Pump Discharge Rake Fluid Temperatures (25 ft, C4TCs)

Wed Mar 1 14:15:49 1989

C4TC3

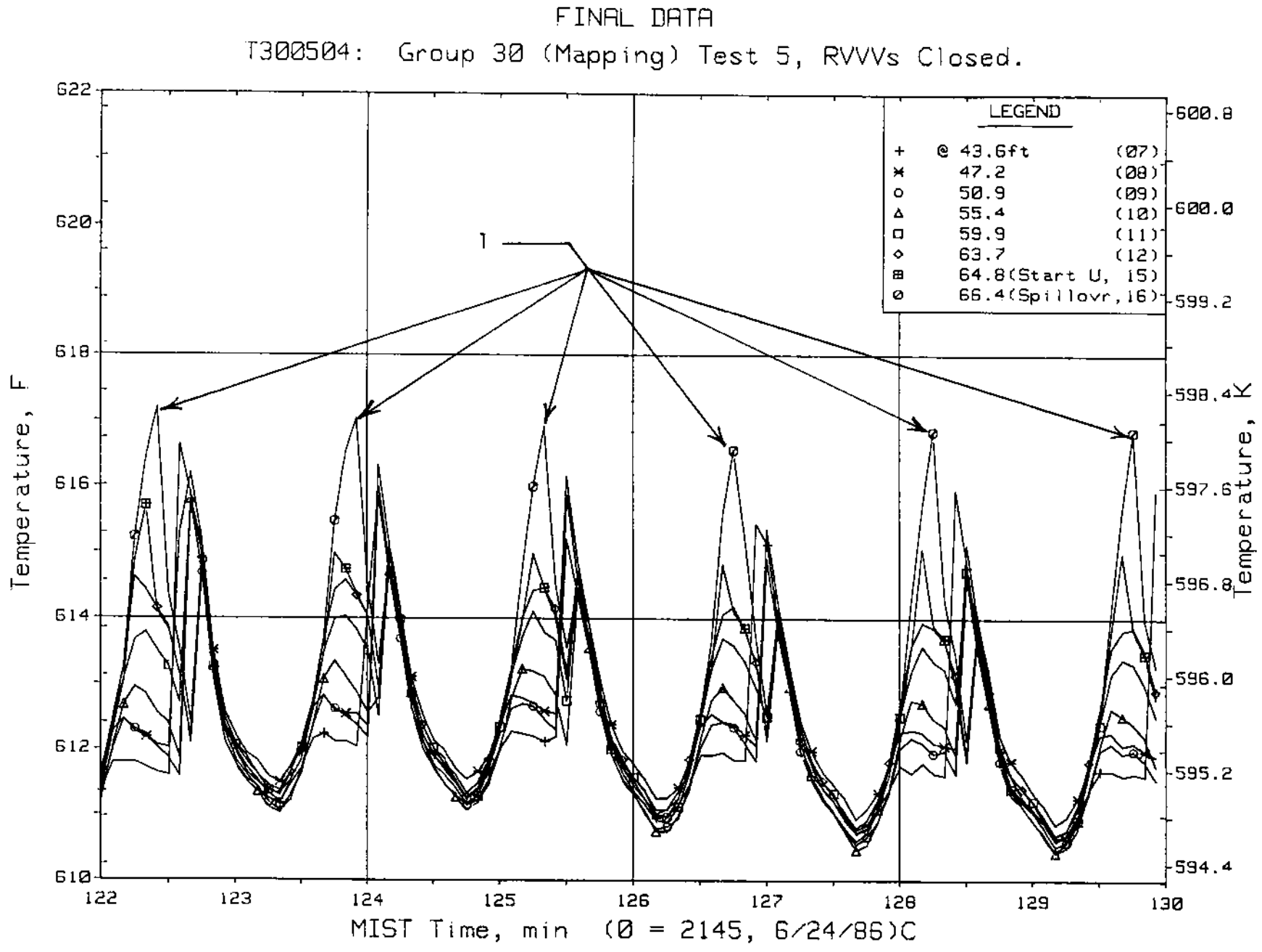

Figure 5.6.40. Hot Leg A Upper-Elevation Riser Fluid Temperatures (H1TCs)

Wed Mar 1 14:12:33 1989

H1TC2

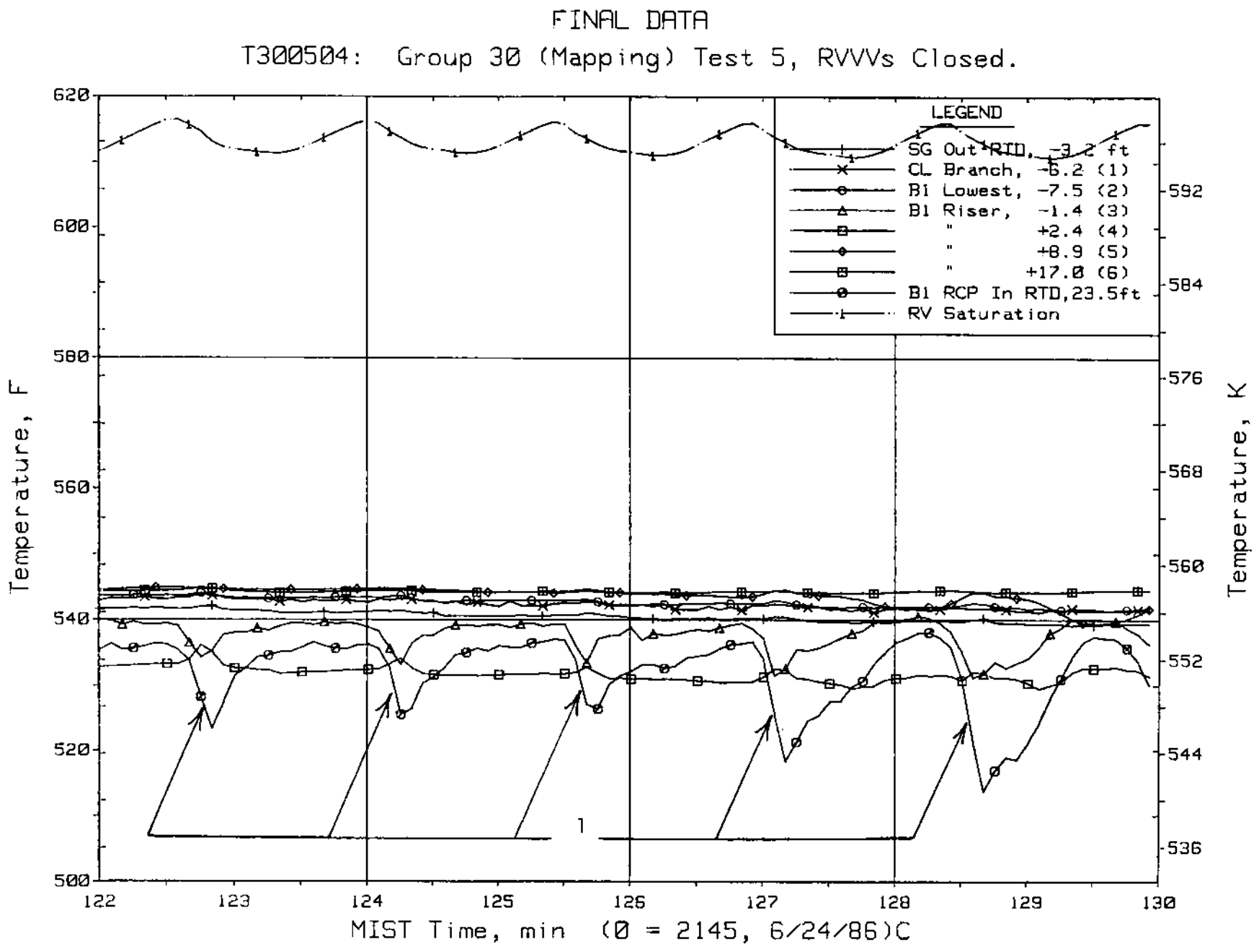

Figure 5.6.41. Cold Leg B1 Suction Fluid Temperatures (C2TCs)

Wed Mar 1 14:09:51 1989

C2TC1

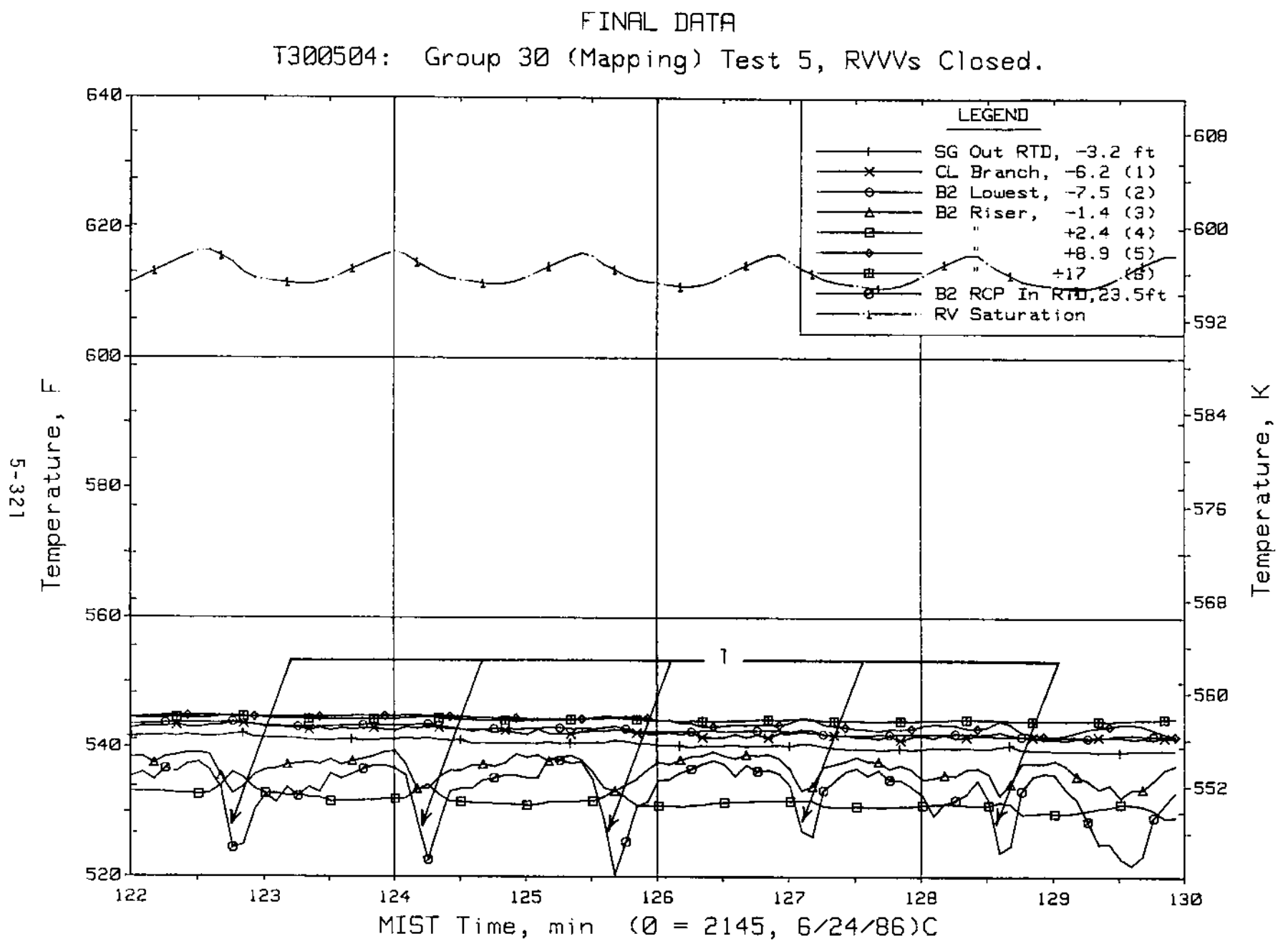

Figure 5.6.42. Cold Leg B2 Suction Fluid Temperatures (C4TCs)

Wed Mar 1 14:07:10 1989

C4TC1

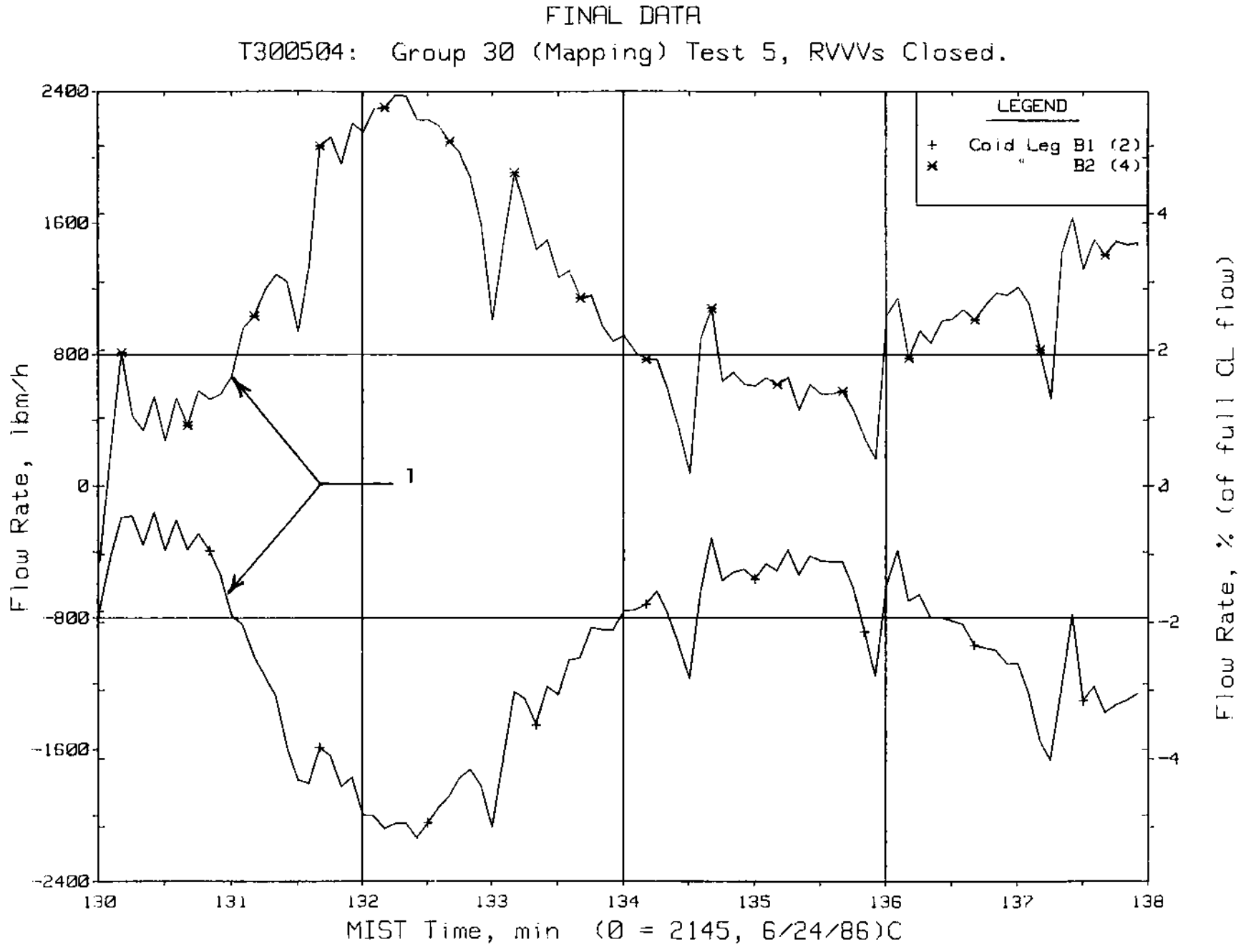

Figure 5.6.43. Loop B Cold Leg (Venturi) Flow Rates (CnVN20s)

Thu Mar 9 18:16:49 1989

FRFL6

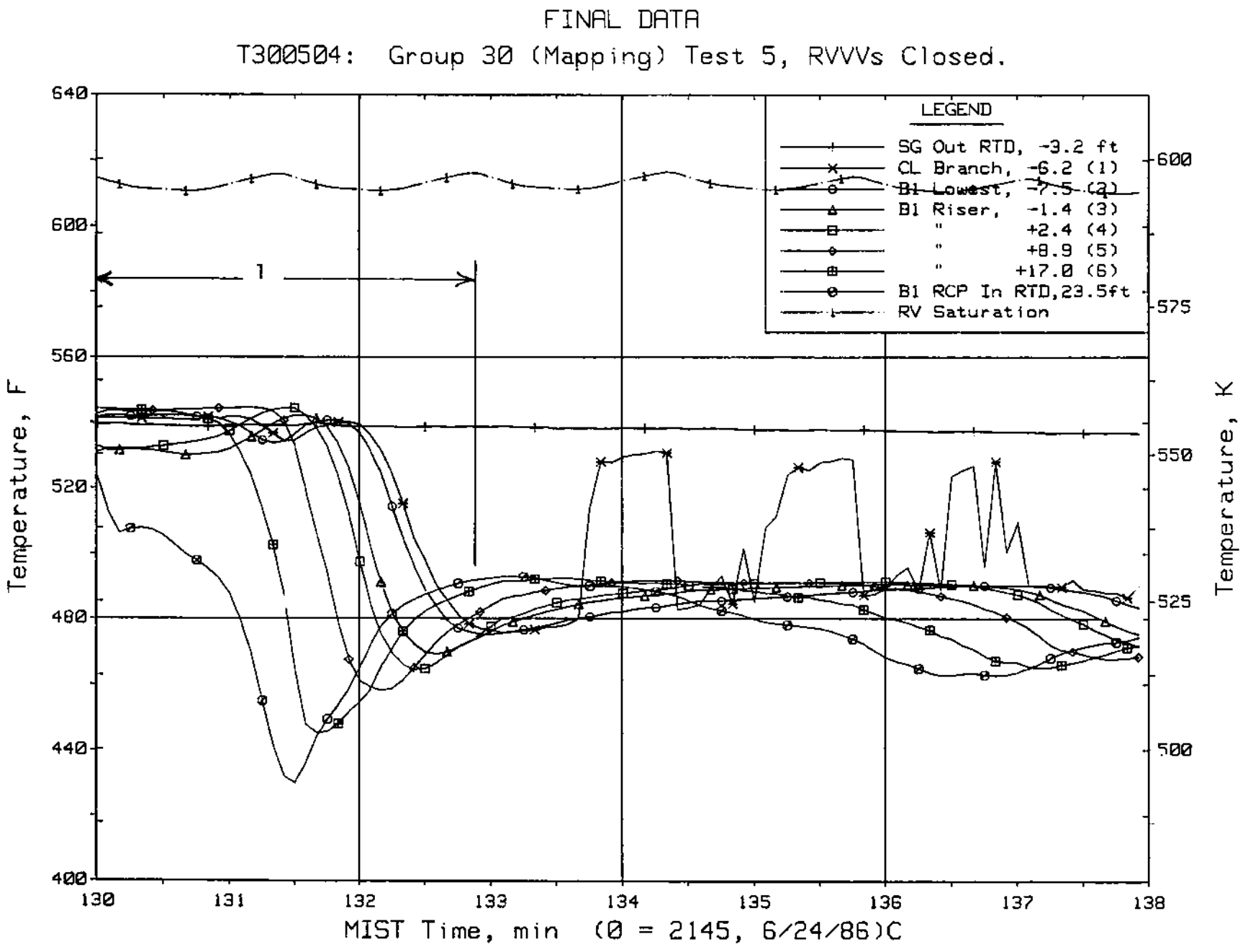

Figure 5.6.44. Cold Leg B1 Suction Fluid Temperatures (C2TCs)

Thu Mar 9 18:12:11 1989

C2TC1

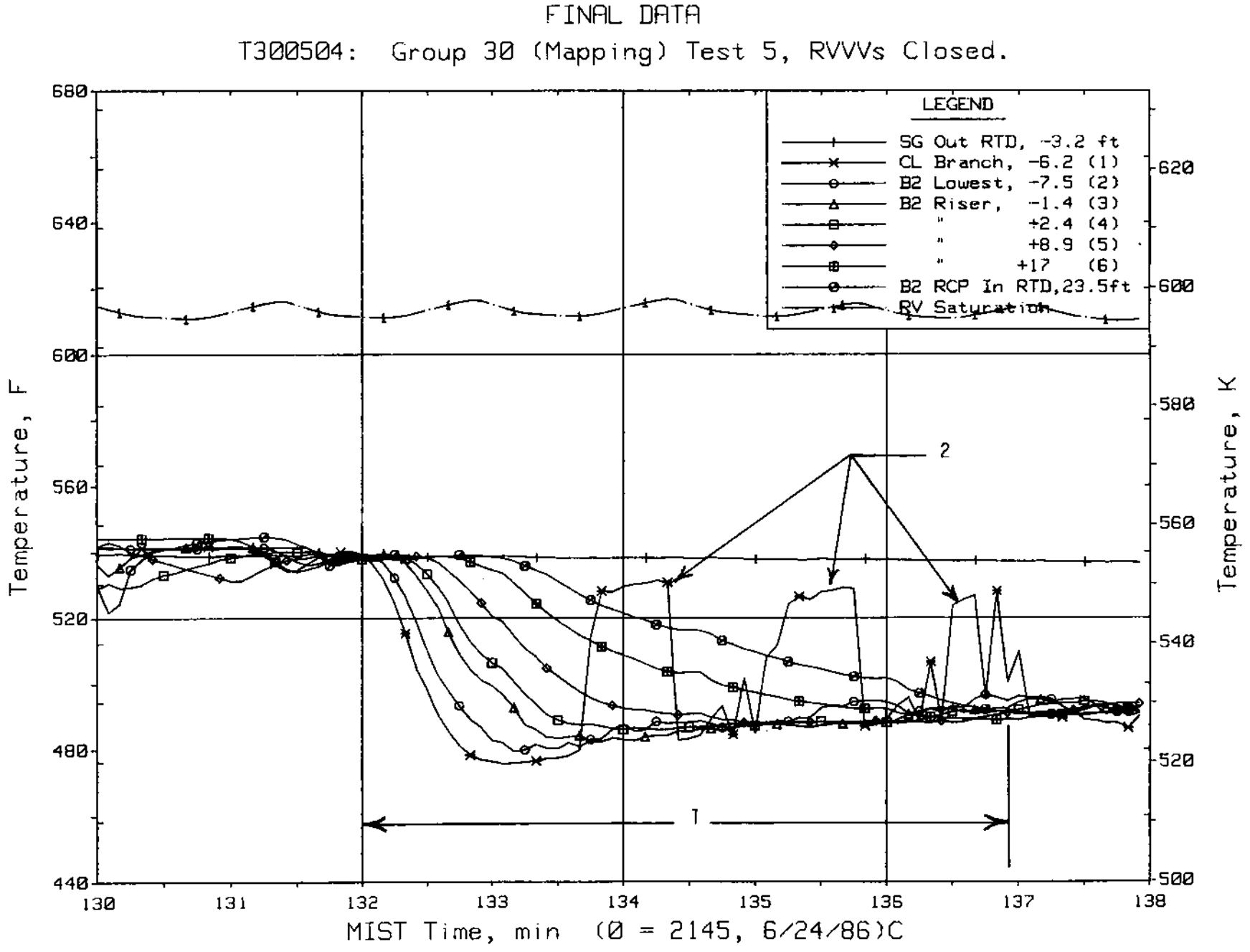

Figure 5.6.45. Cold Leg B2 Suction Fluid Temperatures (C4TCs)

Fri Mar 10 14:17:48 1989

C4TC1

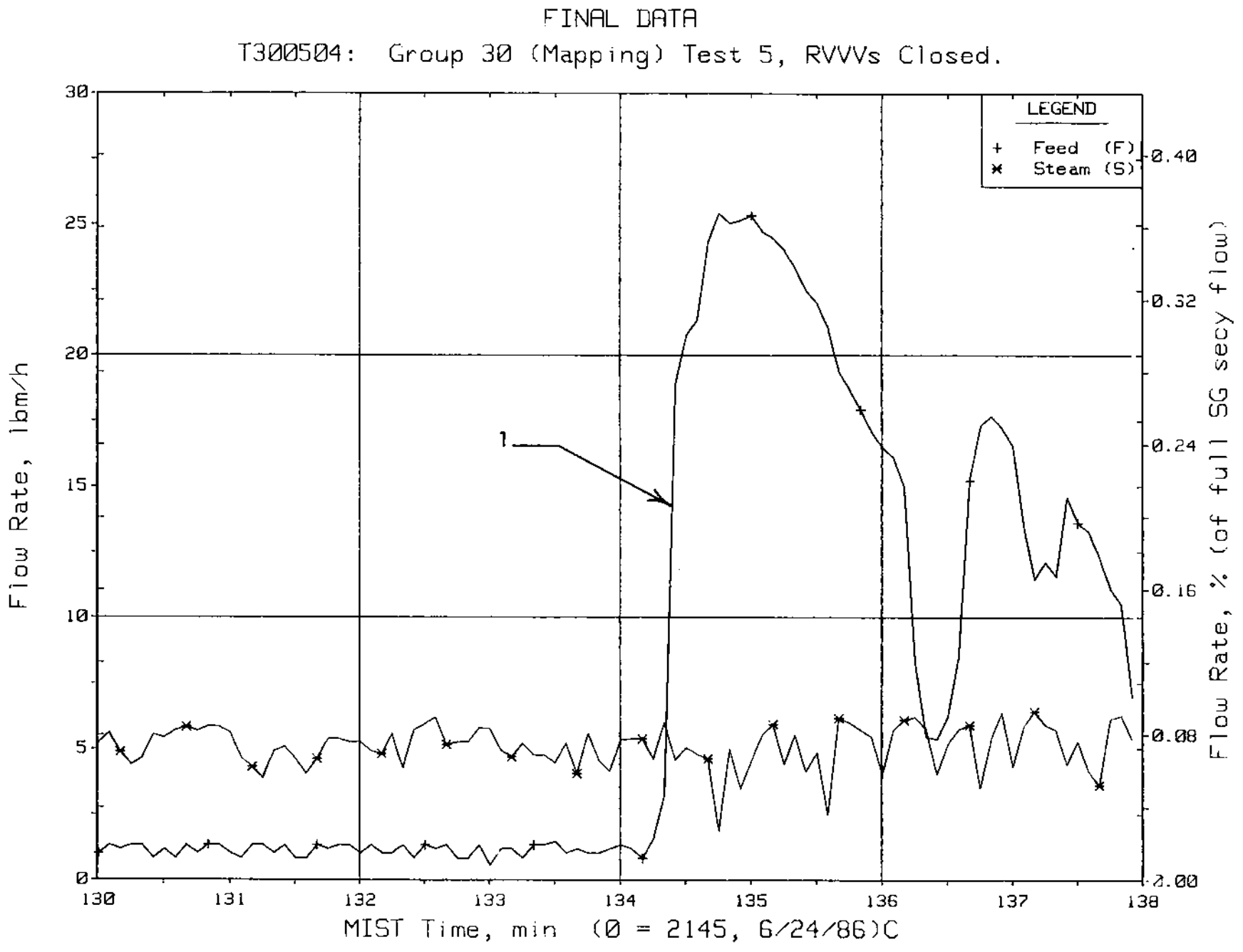

Figure 5.6.46. Steam Generator B Flow Rates (SaOR21s)

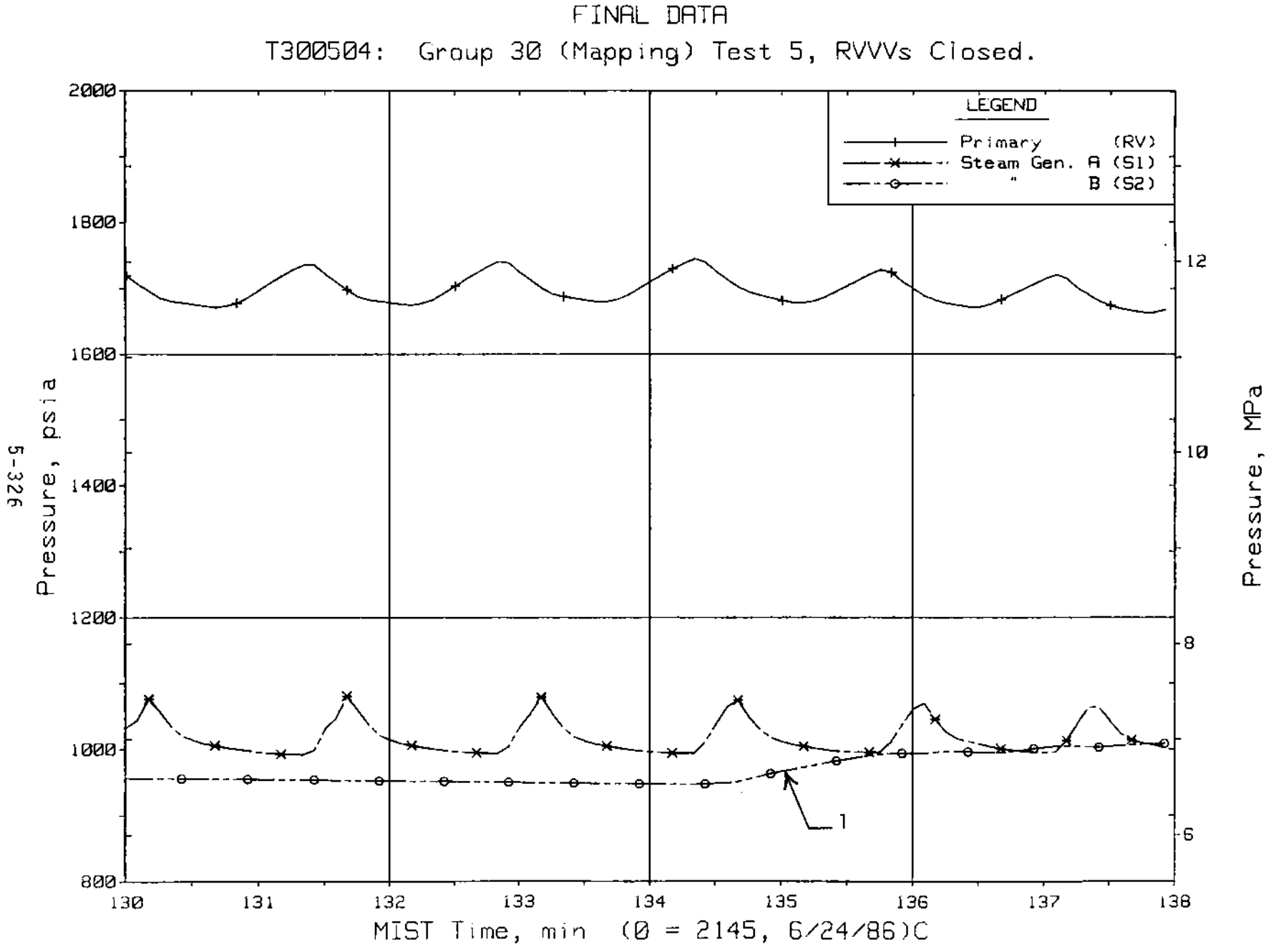

Figure 5.6.47. Primary and Secondary System Pressures (GPOIs)

Fri Mar 10 14:21:23 1989

PSGP1

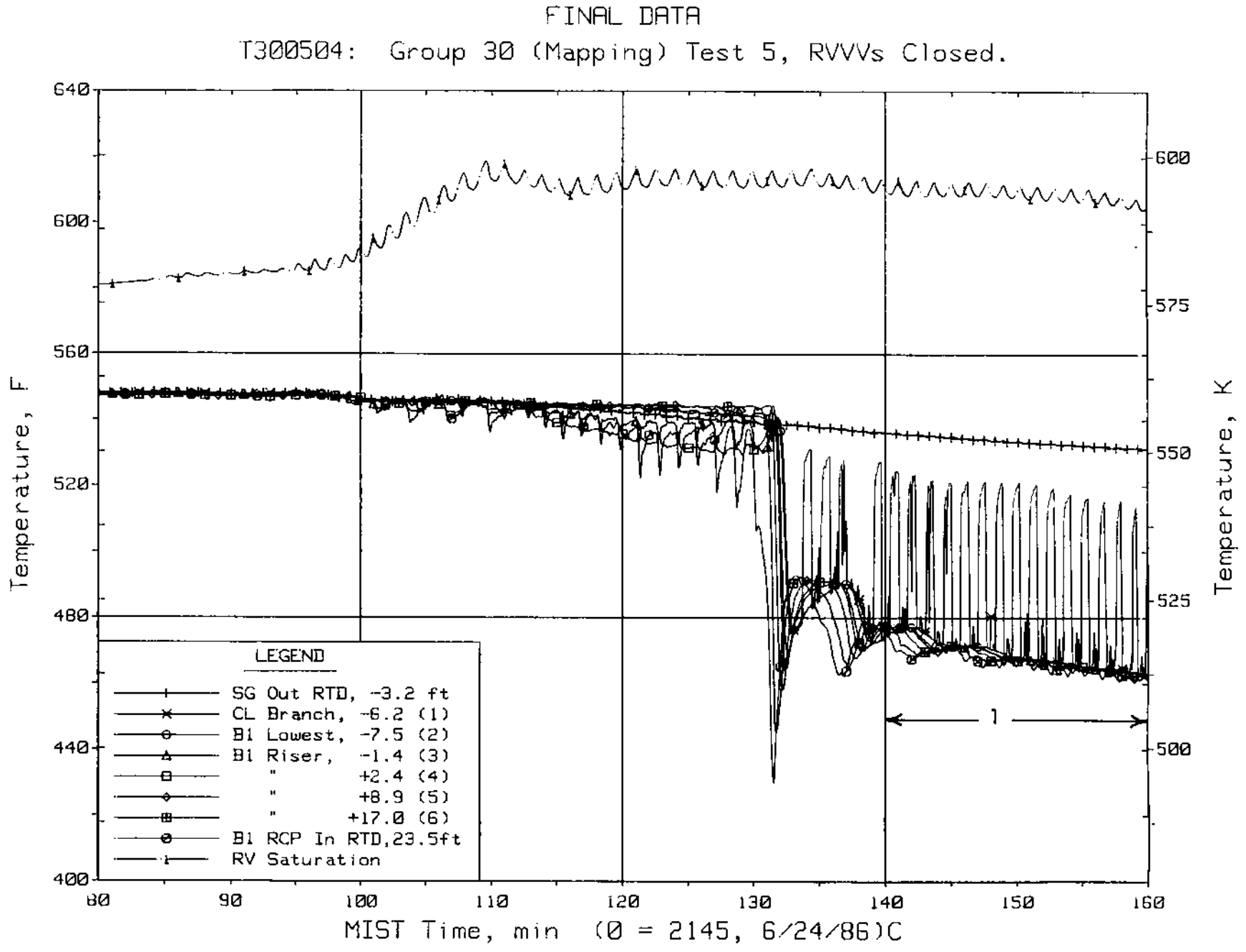

Figure 5.6.48. Cold Leg B1 Suction Fluid Temperatures (C2TCs)

Thu Mar 9 18:01:50 1989

C2TC1

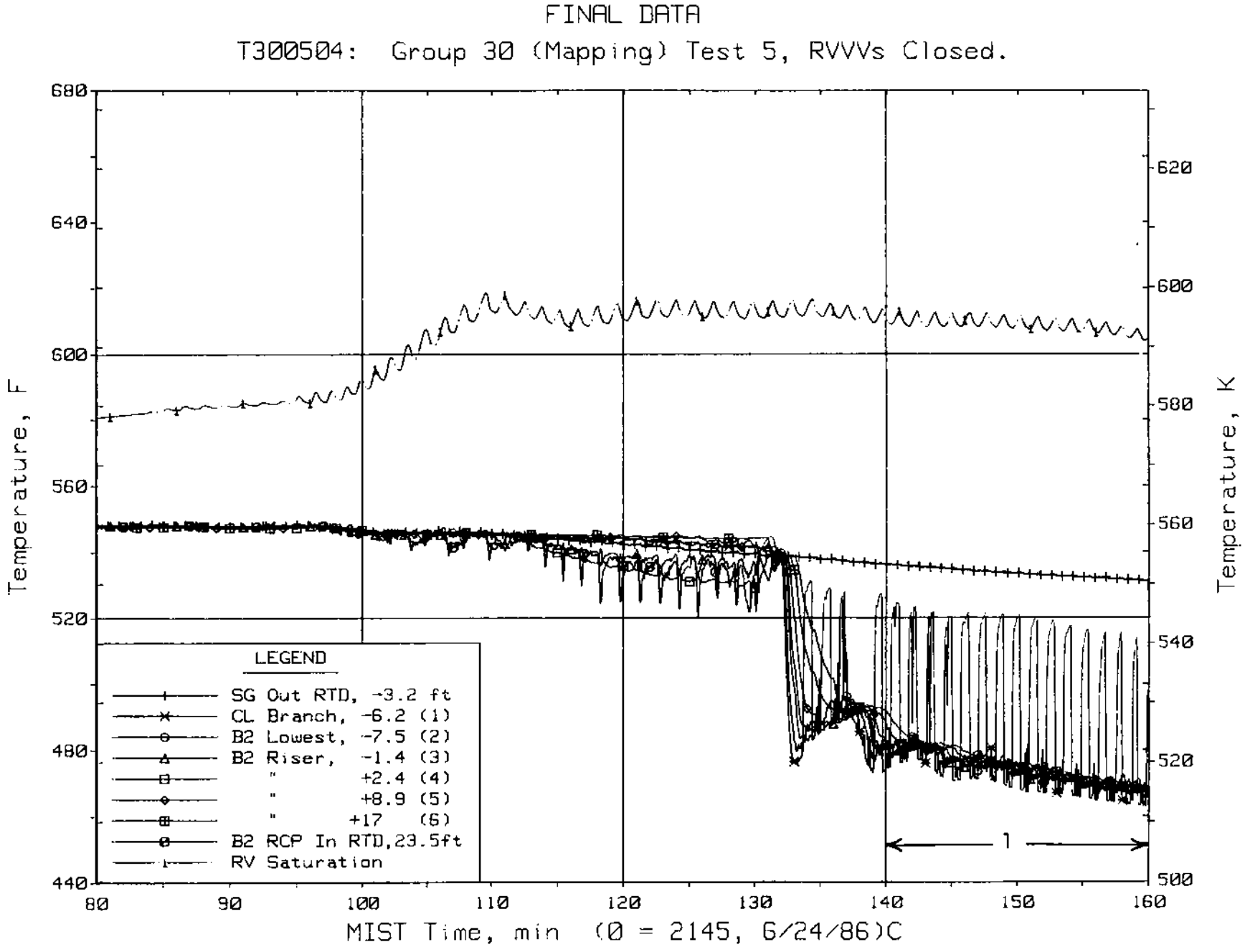

Figure 5.6.49. Cold Leg B2 Suction Fluid Temperatures (C4TCs)

Thu Mar 9 17:56:19 1989

C4TC1

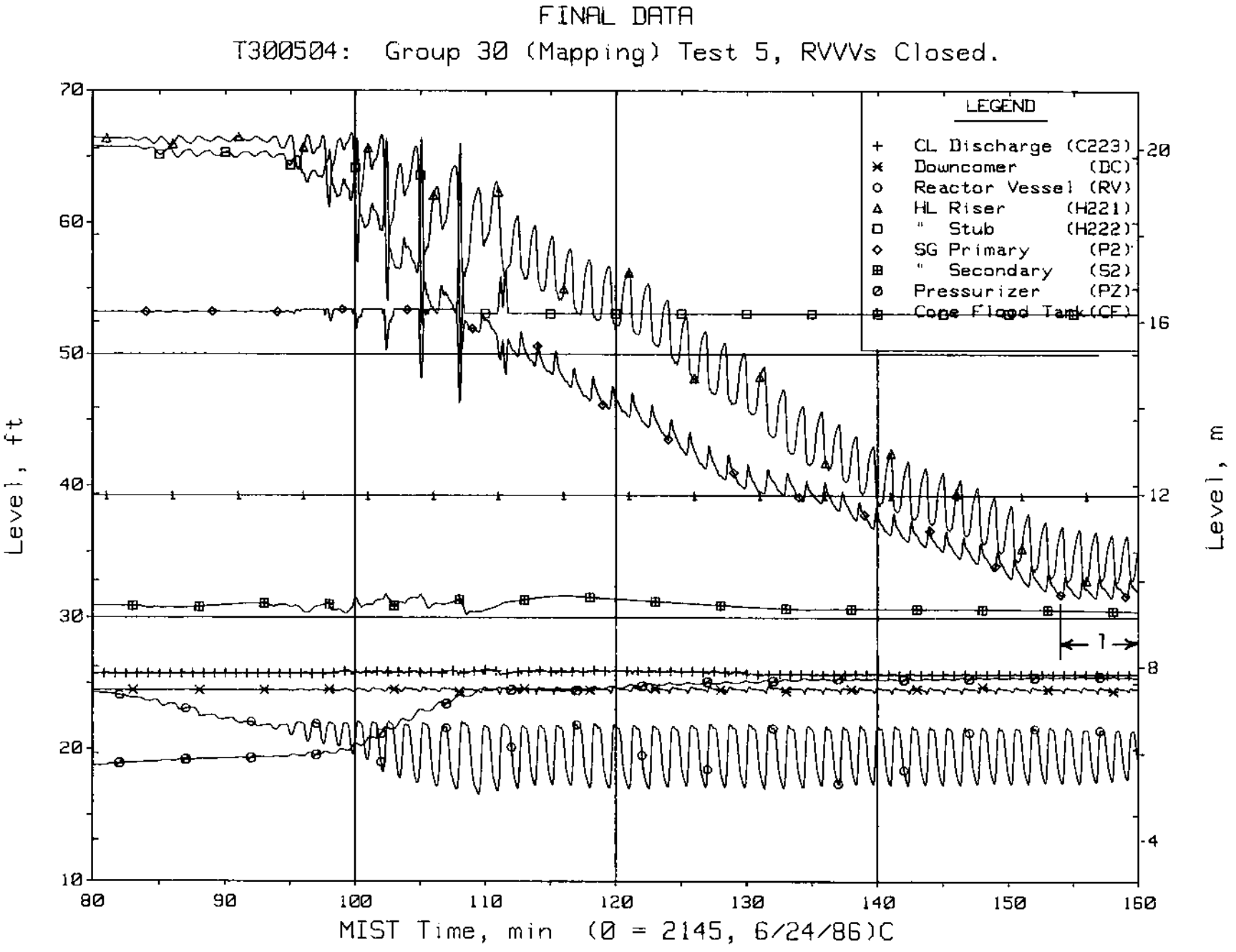

Figure 5.6.50. Loop B Collapsed Liquid Levels (LV20s)

Thu Mar 9 12:51:39 1989

PRLV2

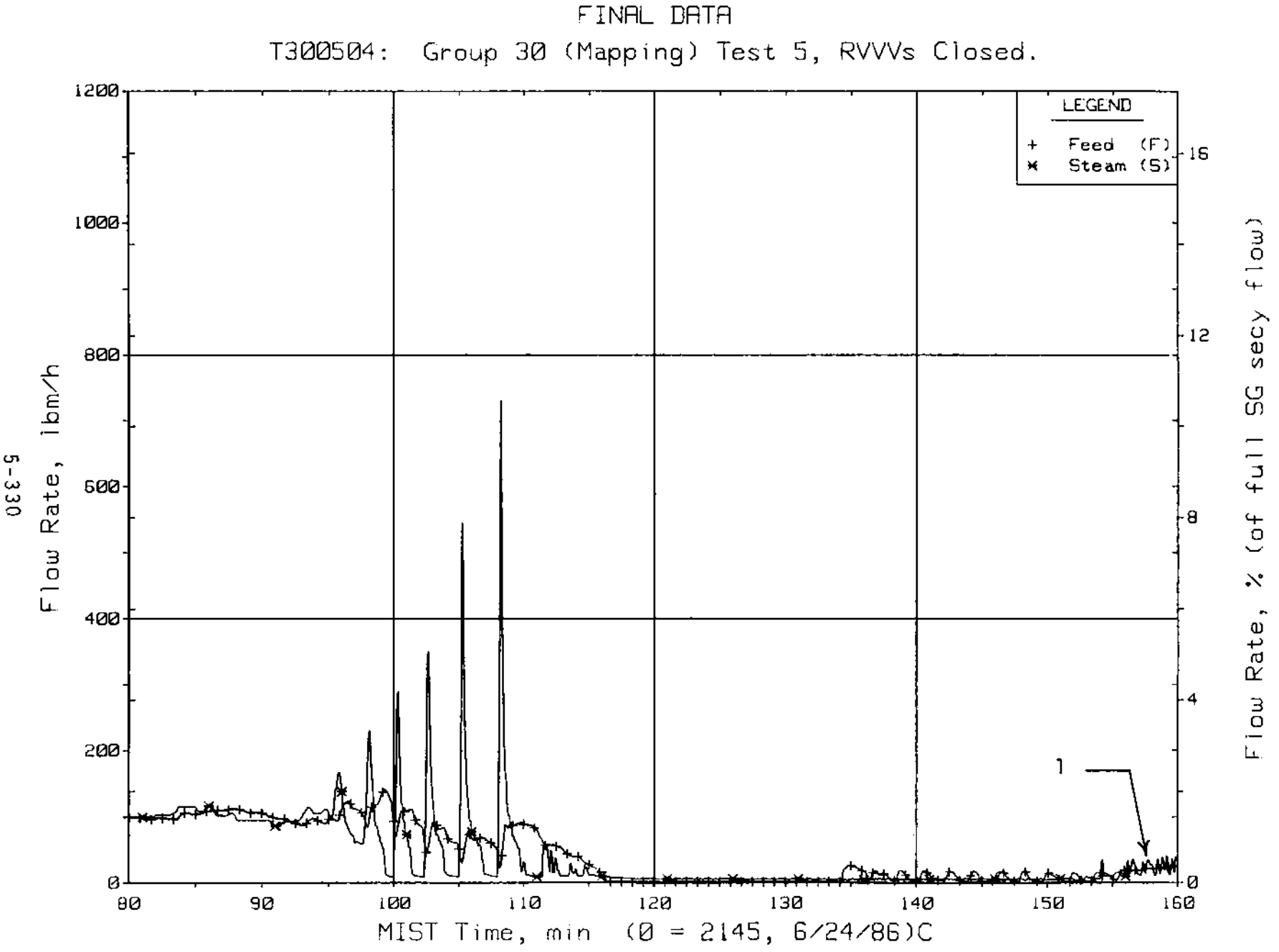

Figure 5.6.51. Steam Generator B Flow Rates (SaOR21s)

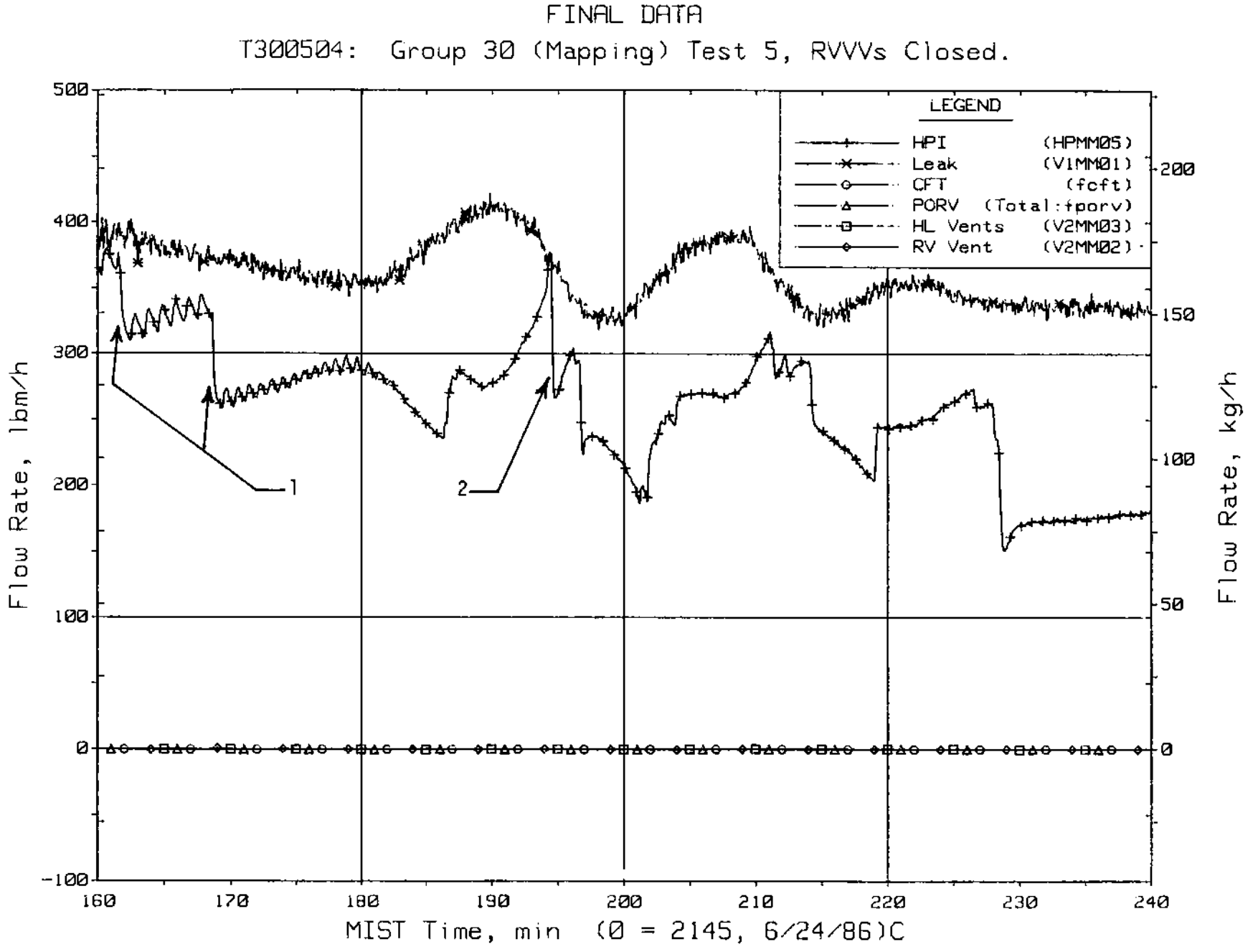

Figure 5.6.52. Primary System Boundary Flow Rates

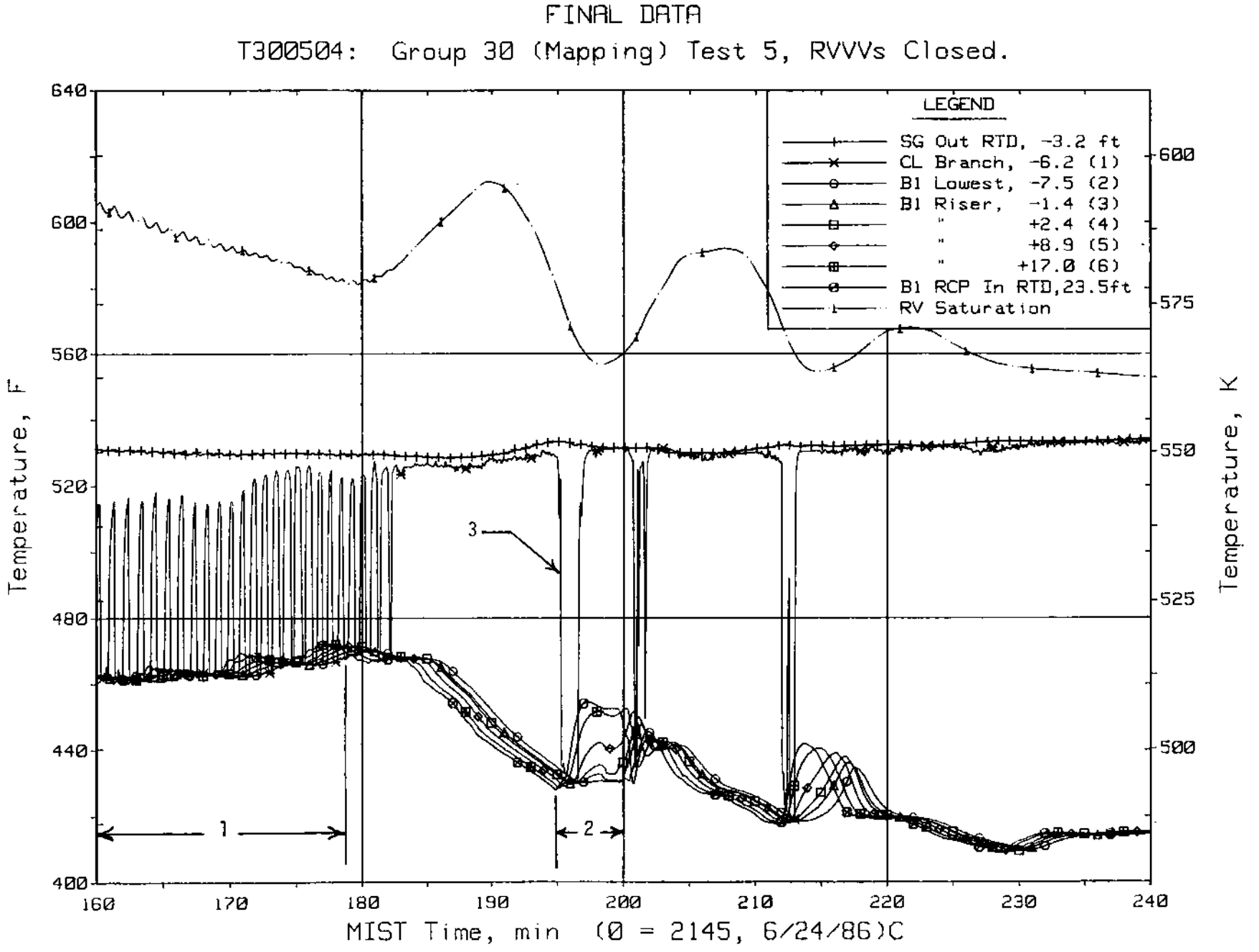

Figure 5.6.53. Cold Leg B1 Suction Fluid Temperatures (C2TCs)

Thu Mar 9 17:39:47 1989

C2TC1

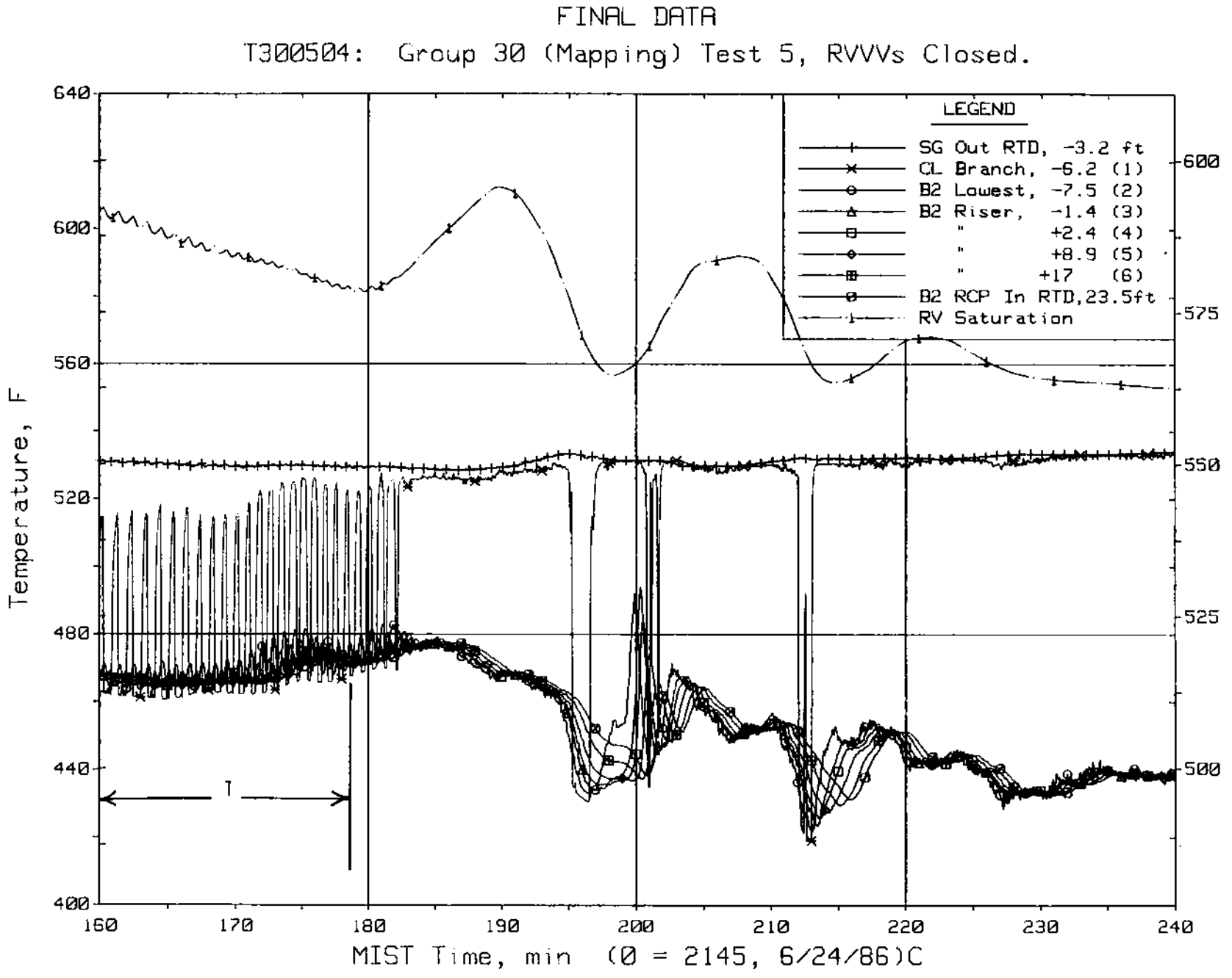

Figure 5.6.54. Cold Leg B2 Suction Fluid Temperatures (C4TCs)

Thu Mar 9 17:34:57 1989

C4TC1

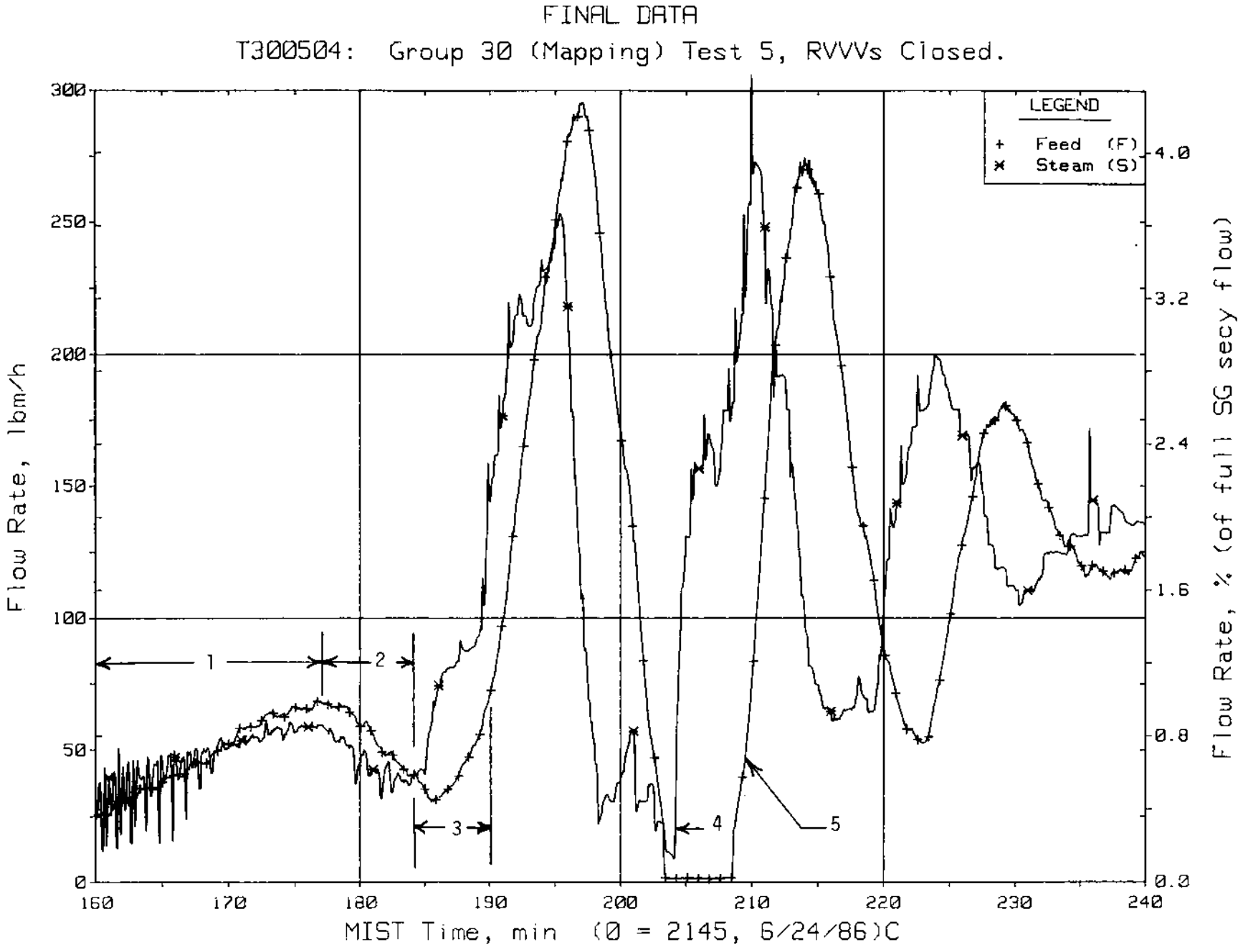

Figure 5.6.55. Steam Generator B Flow Rates (SaOR21s)

Fri Mar 10 14:44:05 1989

SCFL2

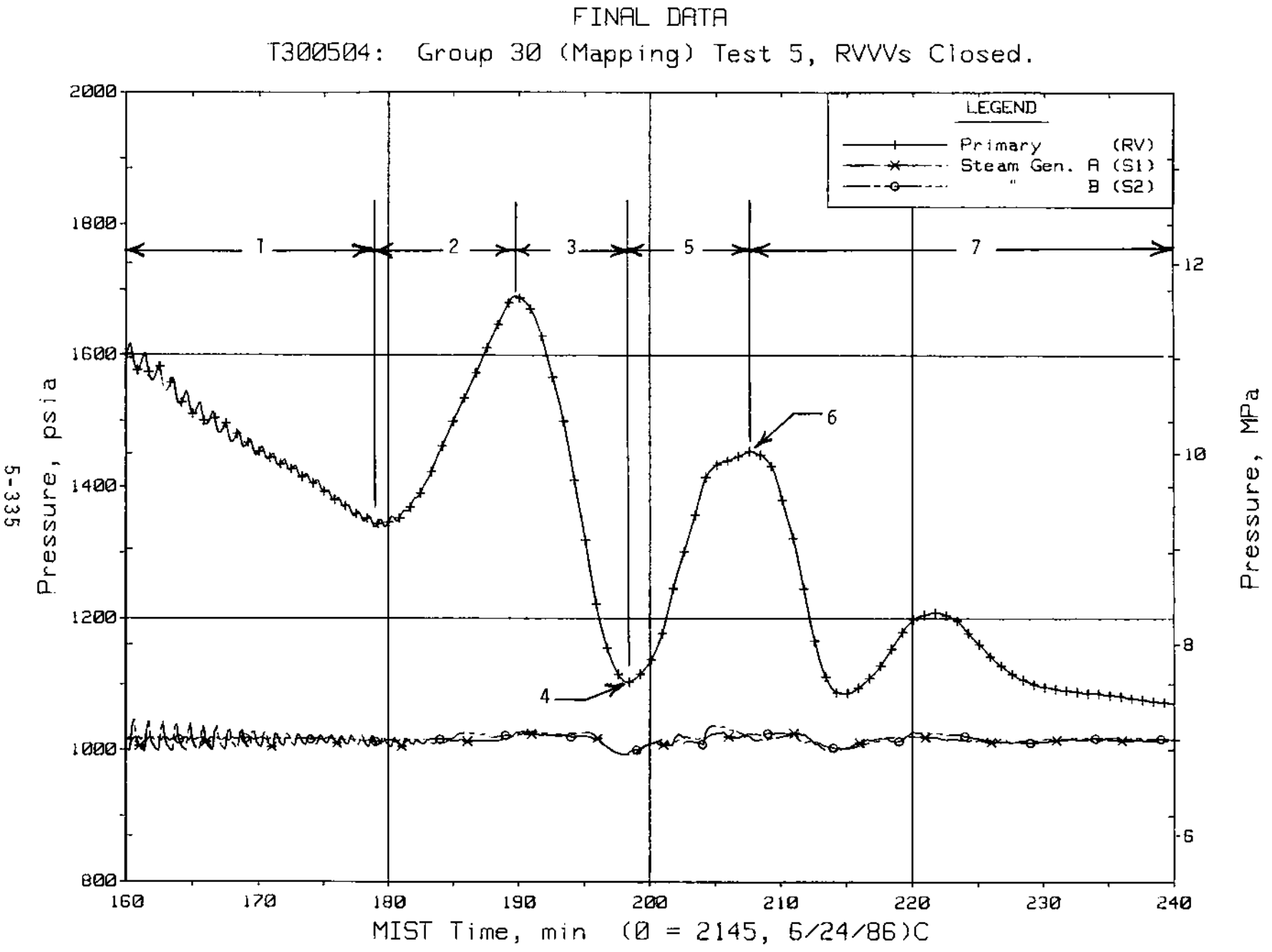

Figure 5.6.56. Primary and Secondary System Pressures (GPOIs)

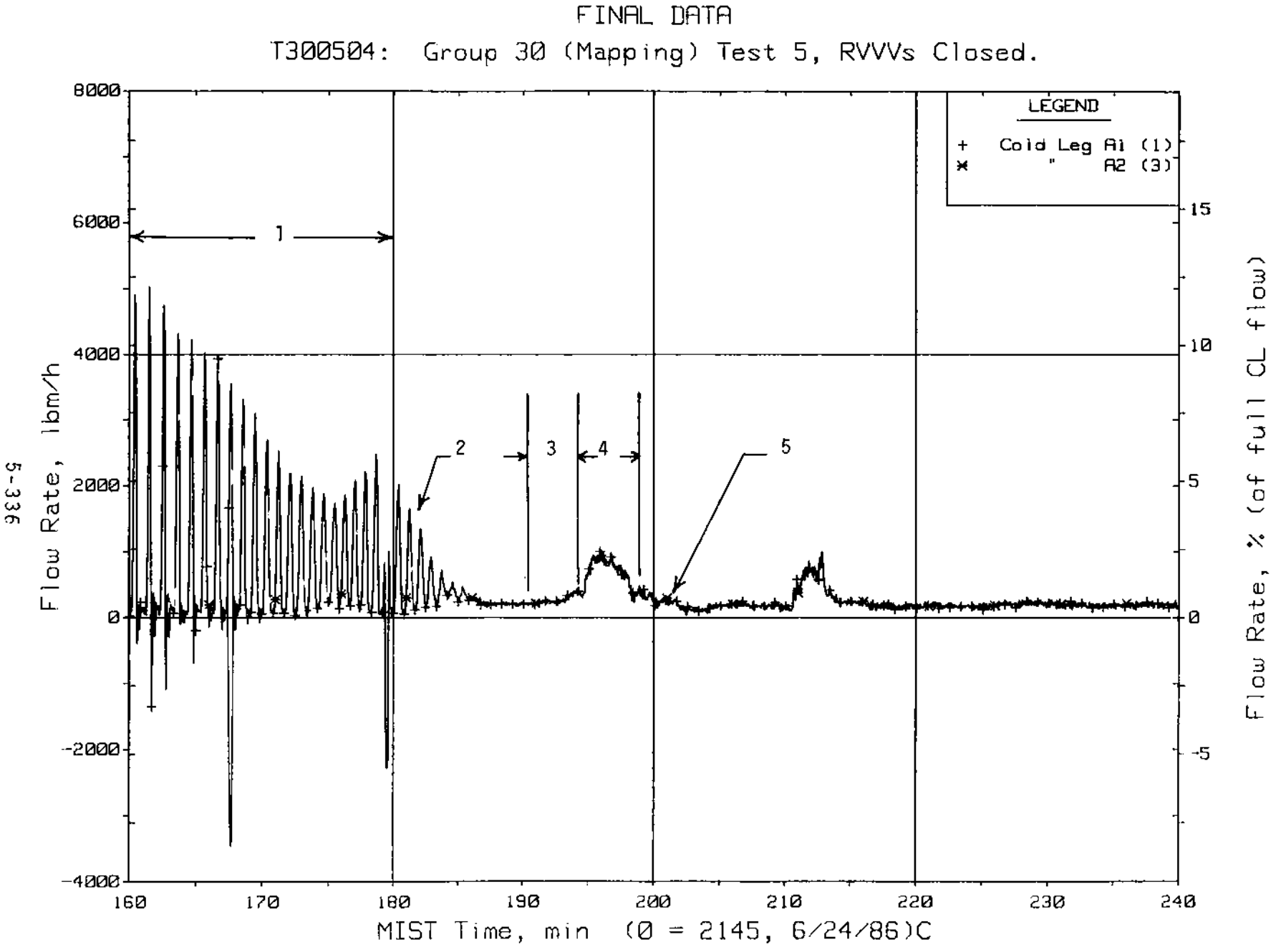

Figure 5.6.57. Loop A Cold Leg (Venturi) Flow Rates (CnVN20s)

Thu Mar 9 12:25:06 1989

FRFL5

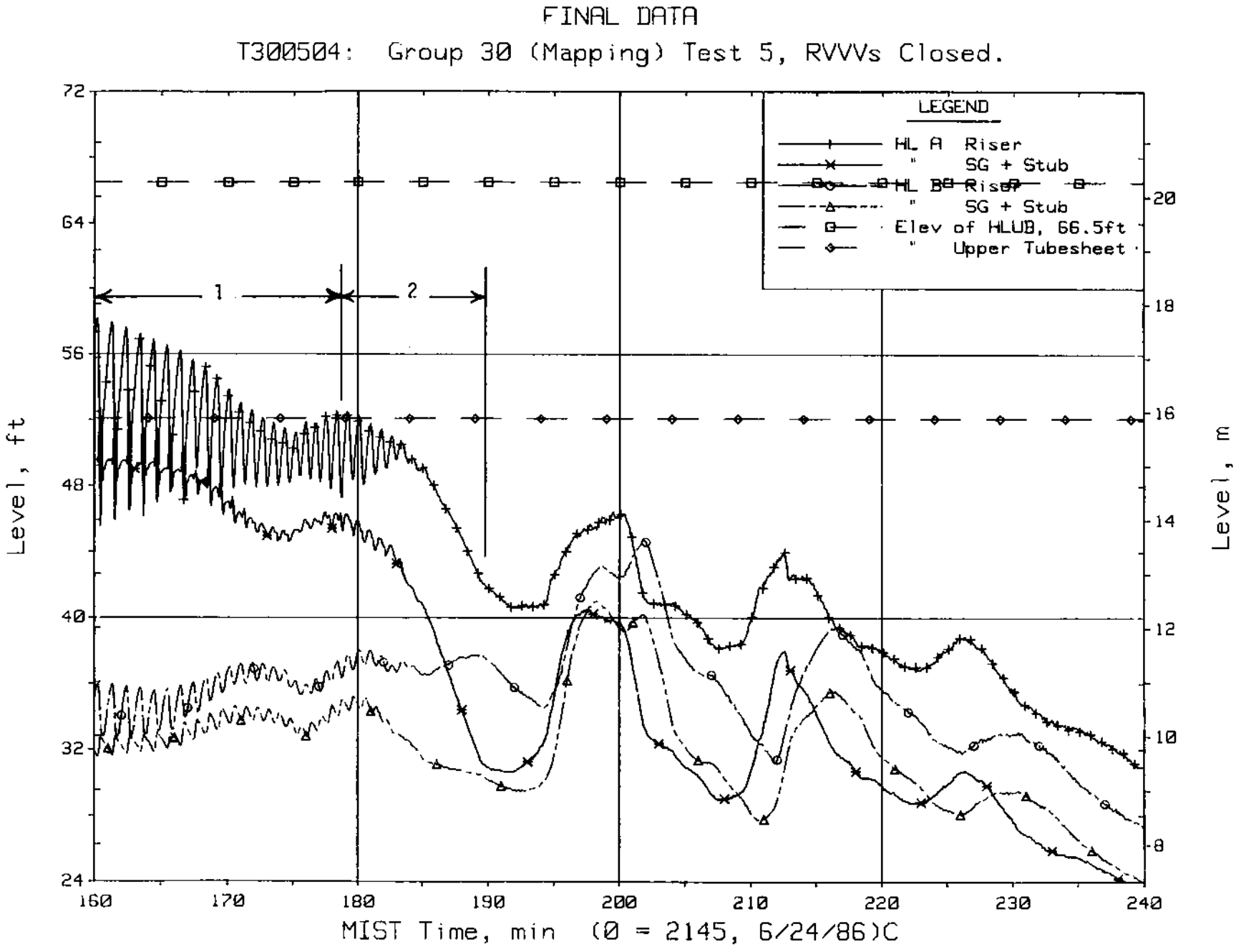

Figure 5.6.58. Hot Leg Riser and Stub Collapsed Liquid Levels

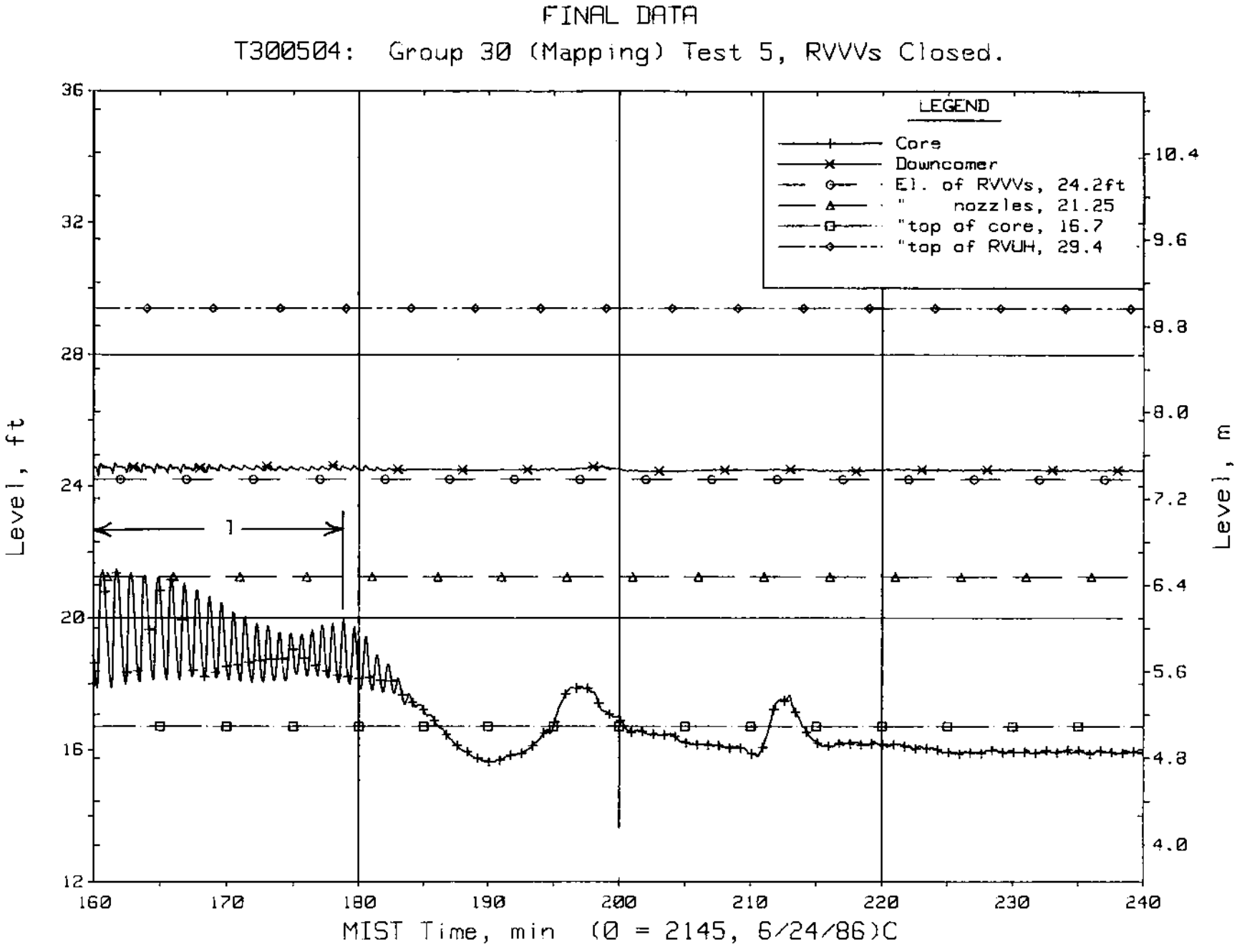

Figure 5.6.59. Core Region Collapsed Liquid Levels

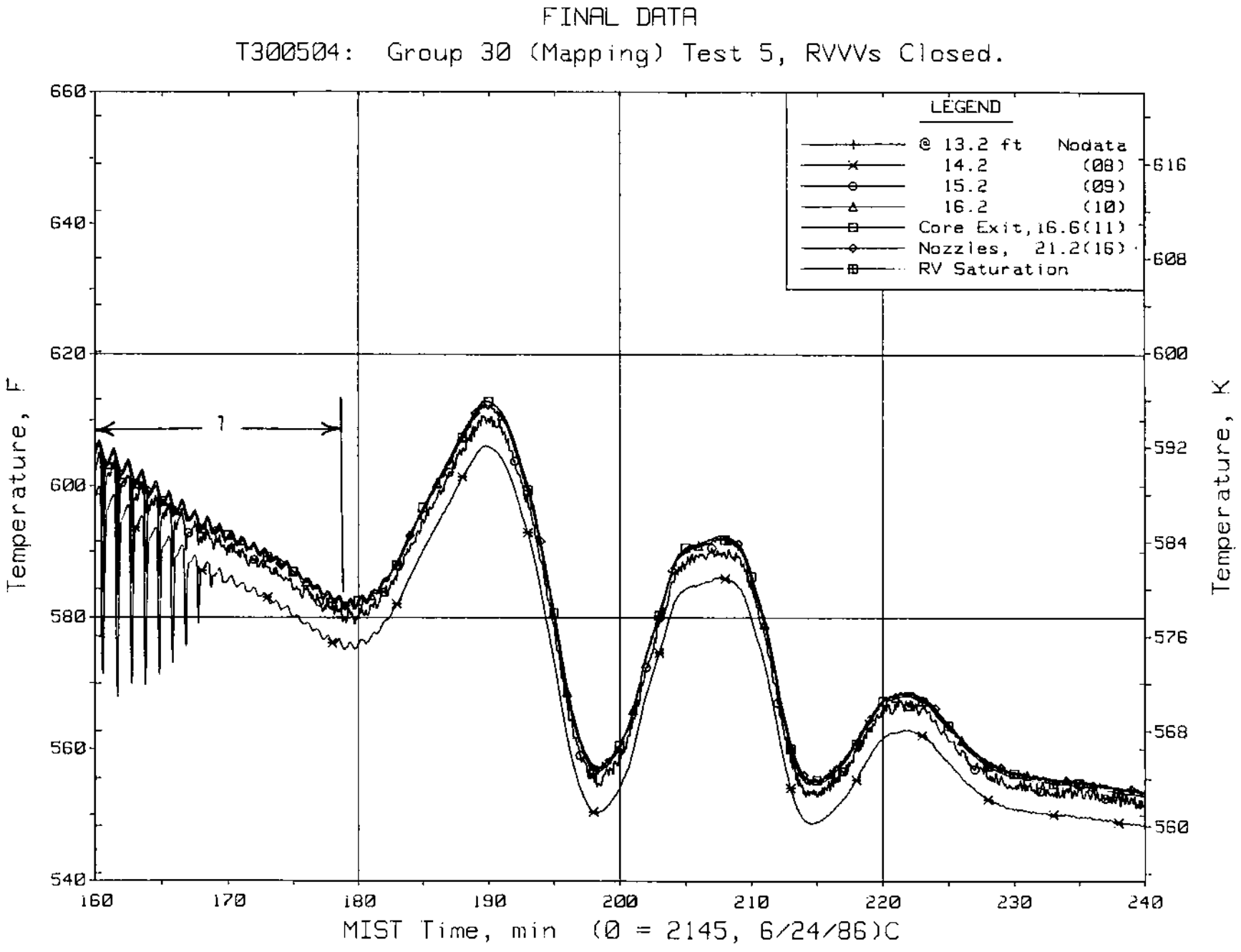

Figure 5.6.60. Reactor Vessel Mid-Elevation Fluid Temperatures (RVTCs)

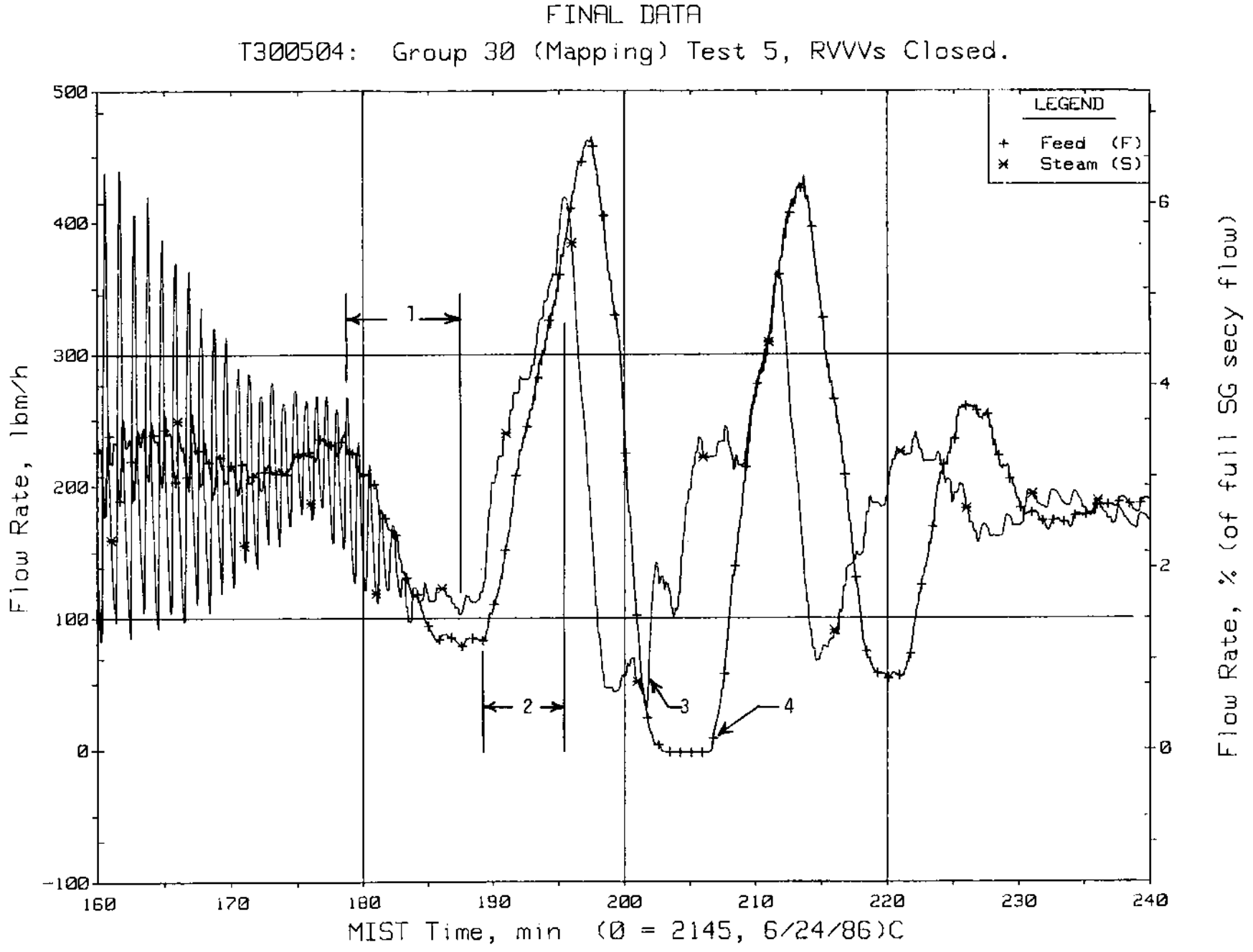

Figure 5.6.61. Steam Generator A Flow Rates (SaOR20s)

Thu Mar 9 17:08:09 1989

SCFL1

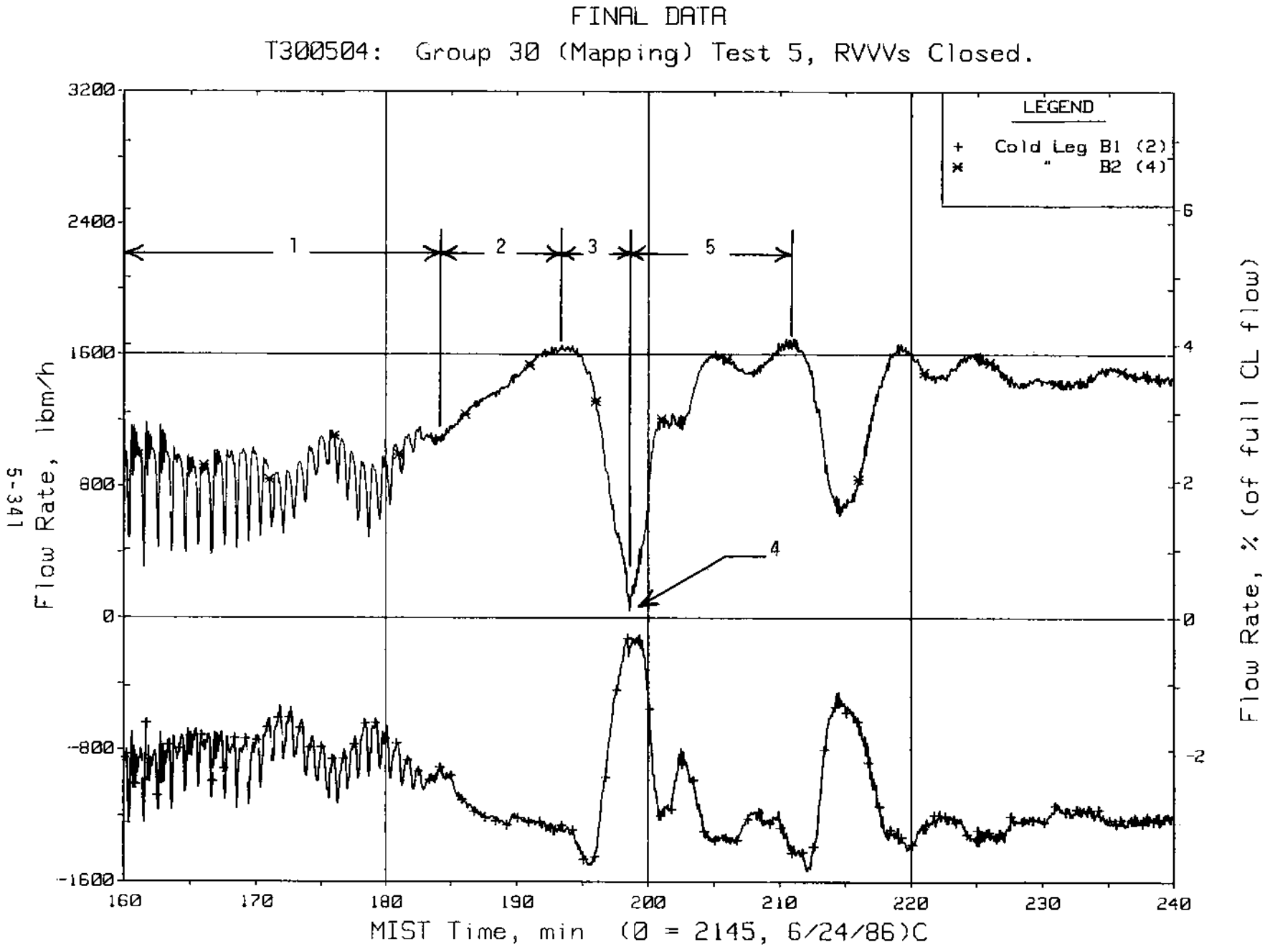

Figure 5.6.62. Loop B Cold Leg (Venturi) Flow Rates (CnVN20s)

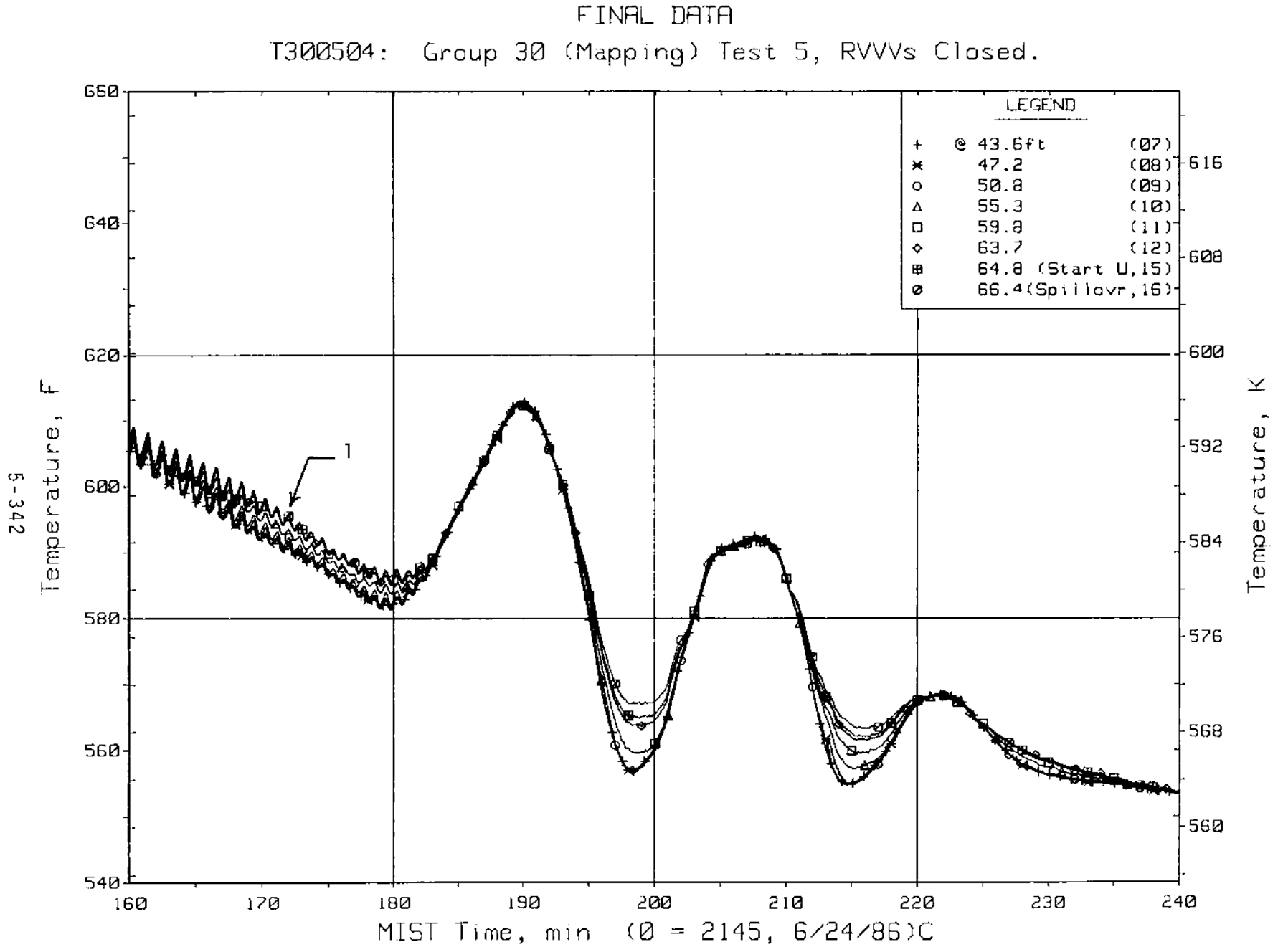

Figure 5.6.63. Hot Leg B Upper-Elevation Riser Fluid Temperatures (H2TCs)

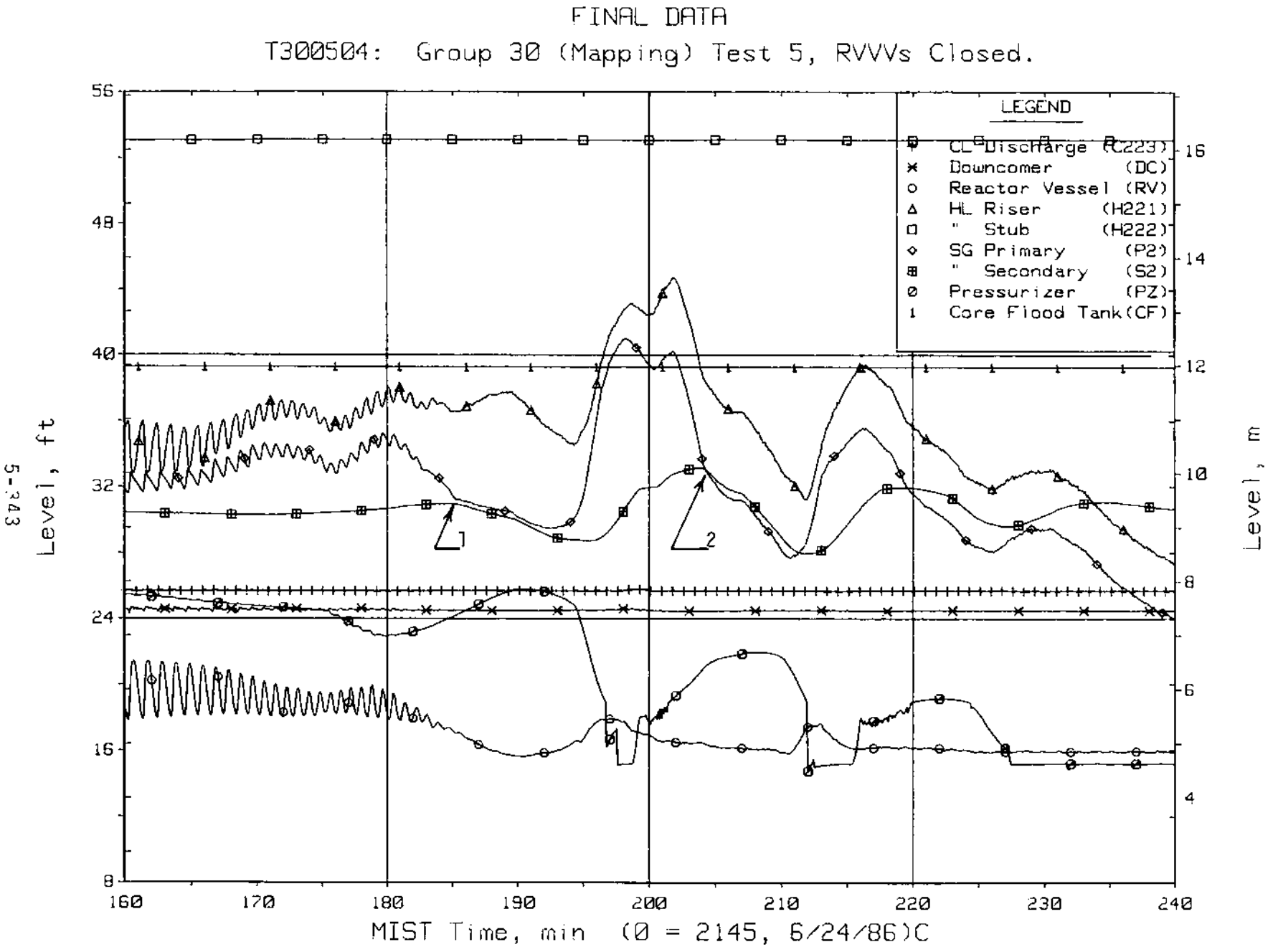

Figure 5.6.64. Loop B Collapsed Liquid Levels (LV20s)

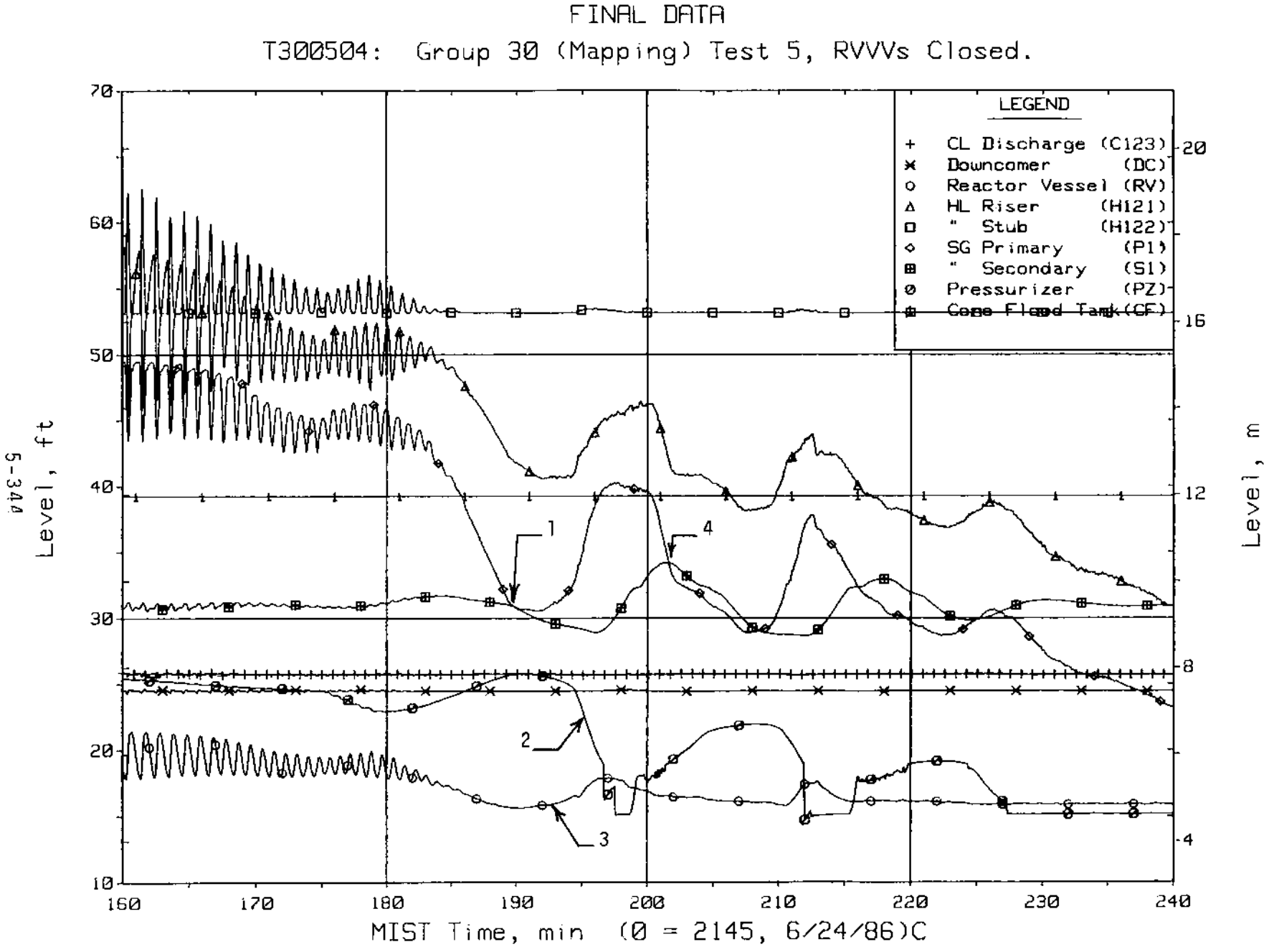

Figure 5.6.65. Loop A Collapsed Liquid Levels (LV20s)

Thu Mar 9 16:53:13 1989

PRLV1

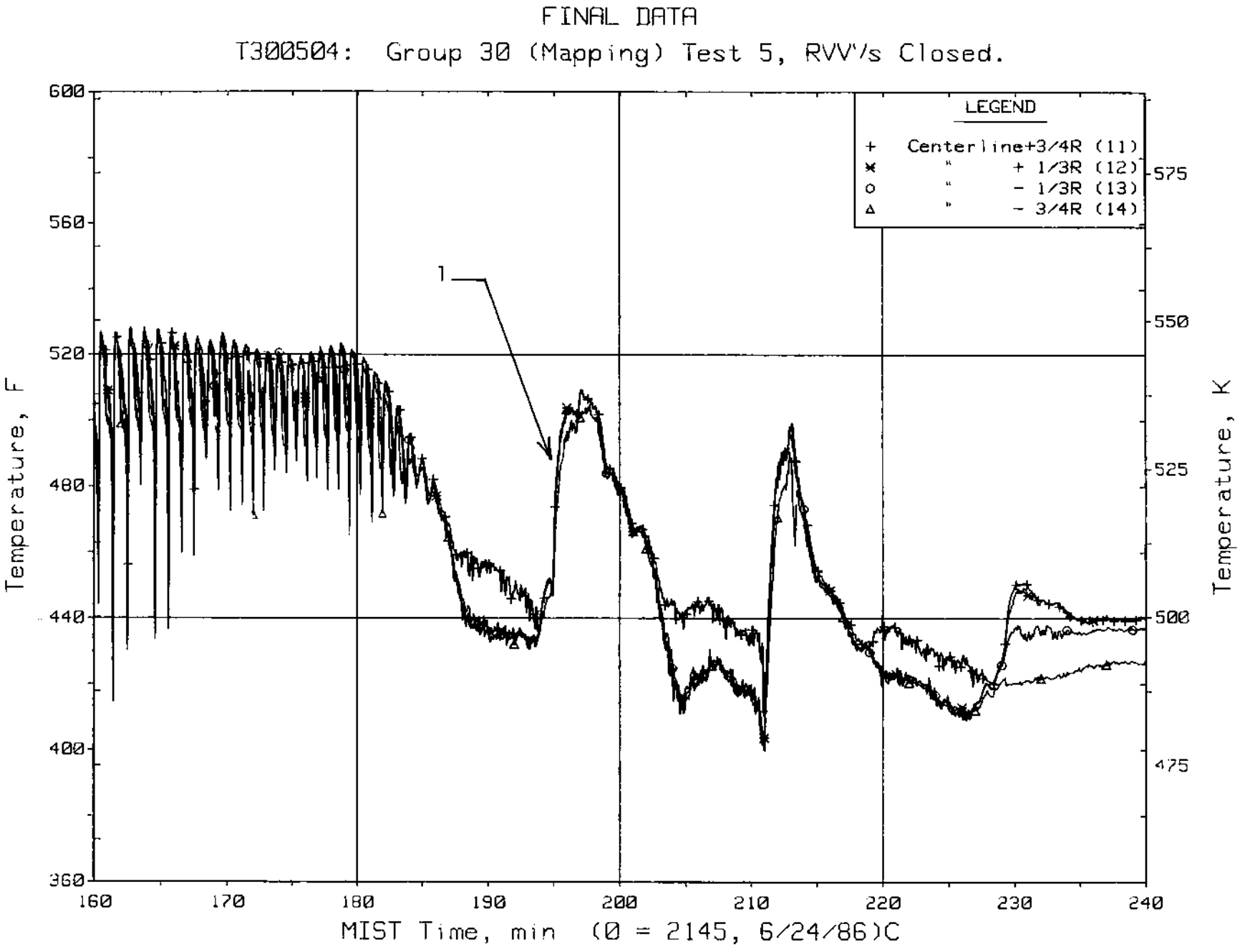

Figure 5.6.66. Cold Leg A1 Nozzle Rake Fluid Temperatures (21.2 ft, C1TCs)

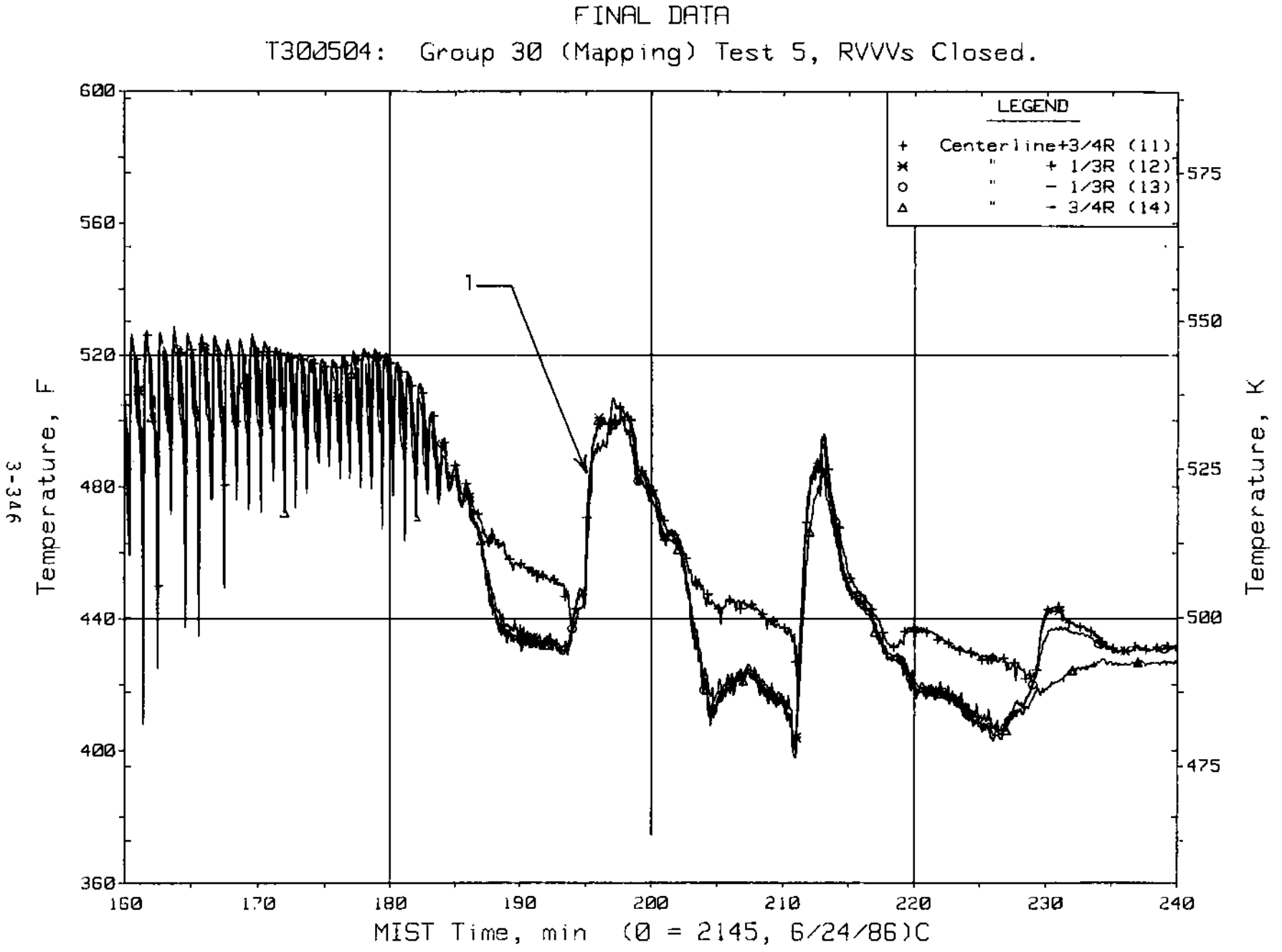

Figure 5.6.67. Cold Leg A2 Nozzle Rake Fluid Temperatures (21.2 ft, C3TCs)

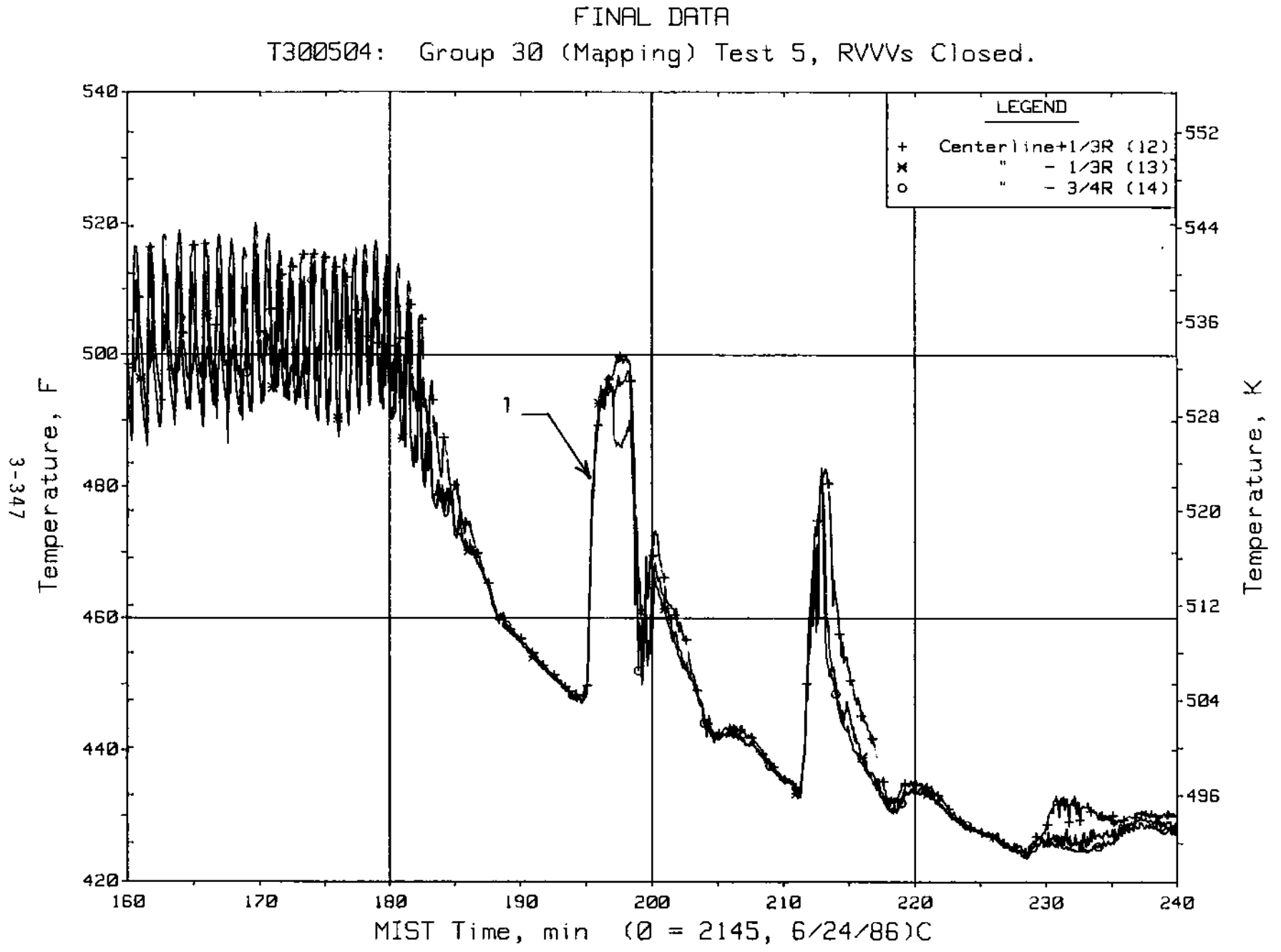

Figure 5.6.68. Cold Leg B1 Nozzle Rake Fluid Temperatures (21.2 ft, C2TCs)

Thu Mar 9 16:42:19 1989

C2TC4

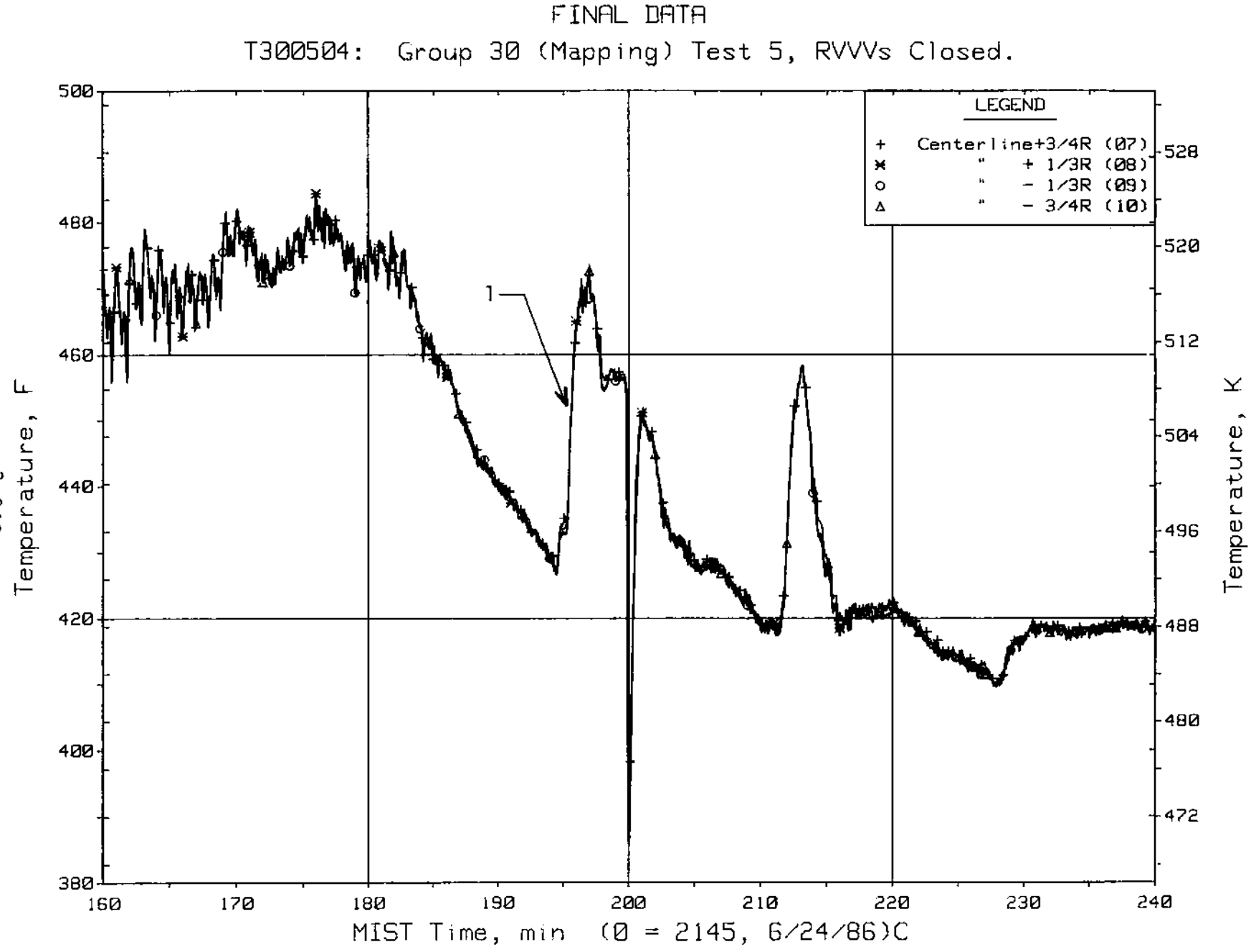

Figure 5.6.69. Cold Leg B1 Pump Discharge Rake Fluid Temperatures (25 ft, C2TCs)

Thu Mar 9 16:39:22 1989

C2TC3

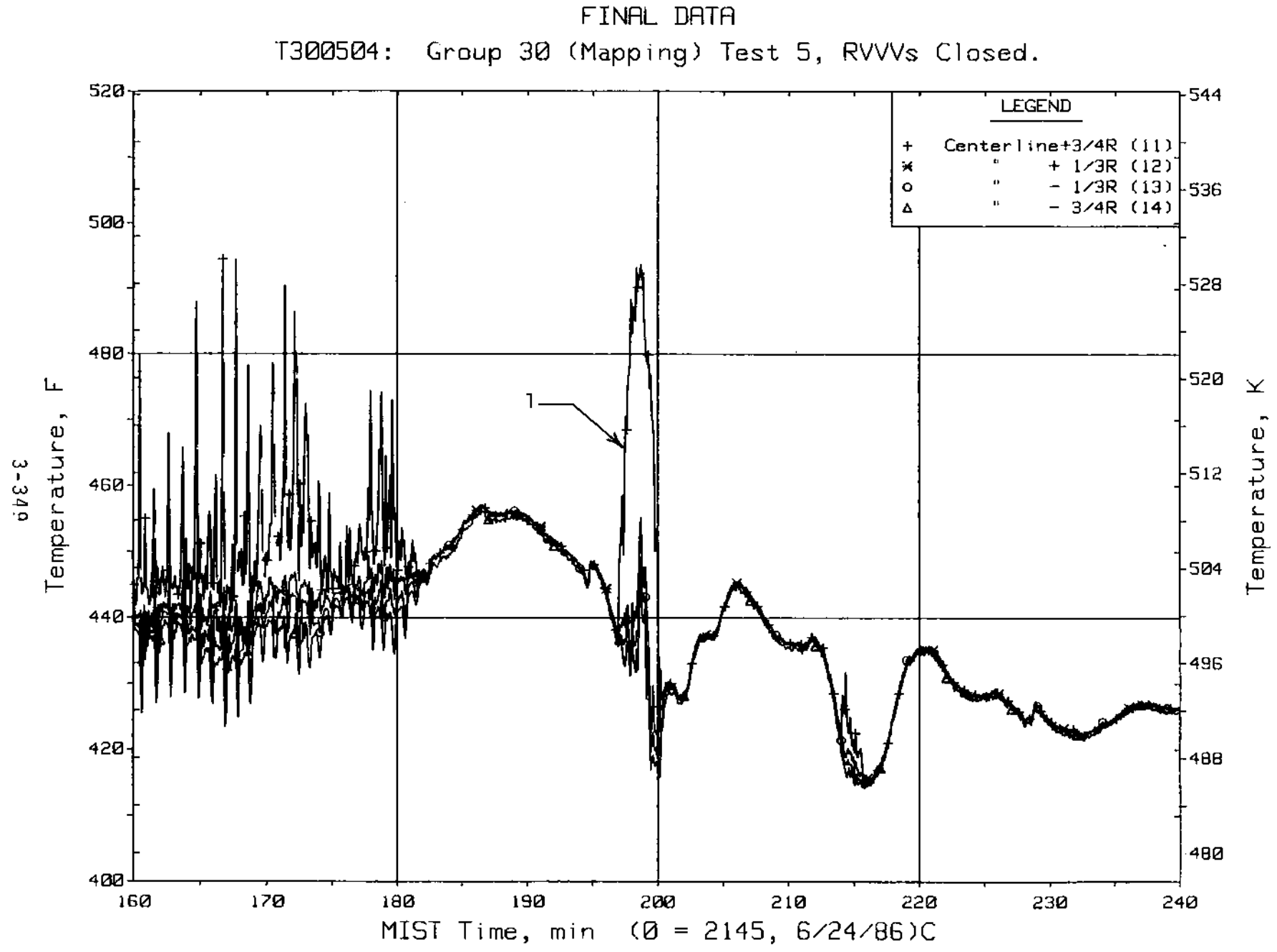

Figure 5.6.70. Cold Leg B2 Nozzle Rake Fluid Temperatures (21.2 ft, C4TCs)

Thu Mar 9 16:36:12 1989

C4TC4

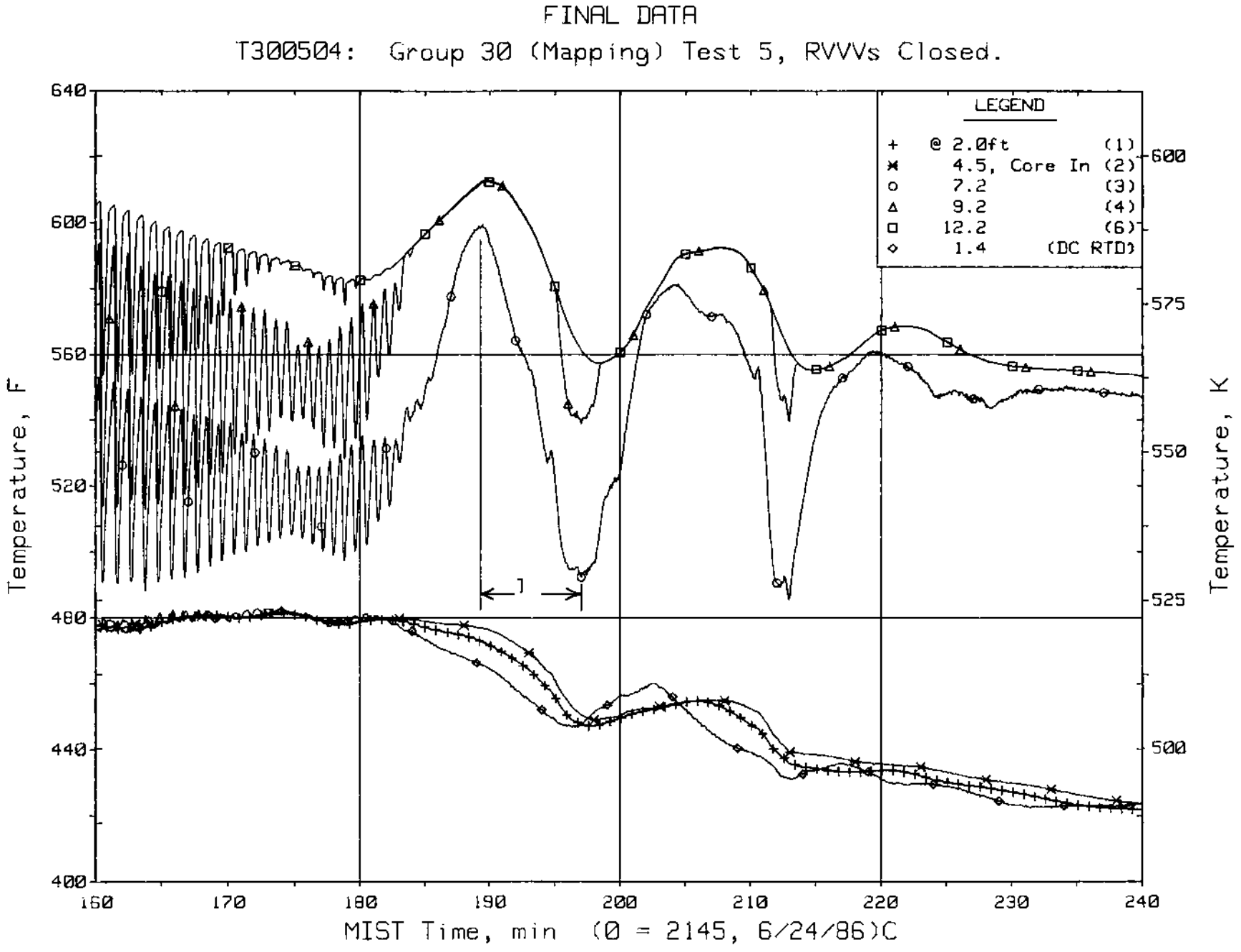

Figure 5.6.71. Reactor Vessel Lower-Elevation Fluid Temperatures (RVTCs)

Thu Mar 9 16:33:04 1989

RVTC1

5.7. No HPI-Leak Cooling Test (3004CC)

Test 3004CC was performed at a reduced core power (1% plus losses to ambient) and HPI was not activated. The reduction of primary system inventory was accomplished using a scaled 1-cm^2 leak at the lower downcomer-to-reactor vessel line for 3.5 hours of testing and a scaled 2-cm^2 leak at the same location for the remainder of the test.

After steady-state conditions were established, the scaled 1-cm^2 leak was opened and the primary system inventory reduction was initiated. The primary system pressure decreased to approximately 1180 psia (Figure 5.7.1, See 1), which corresponds to the saturation pressure at the core exit temperature (564F). The lower core exit temperature and, therefore, the lower pressure attained, when compared to the Nominal Test (3003AA), were a direct result of the reduced core power.

The primary system depressurization for this test appeared to progress more rapidly than that observed for the Nominal Test (3003AA). The depletion of primary system inventory for this test (Figure 5.7.2) progressed at a rate (84 lb/h) that was greater than the specified leak-HPI deficit of 50 lb/h for the Nominal Test (3003AA). Thus, a more rapid depressurization resulted.

The rapid depressurization resulted in a loop flow response that had not been observed in the Nominal Test (3003AA) or the other previously discussed Mapping Tests. The increased depressurization rate resulted in an increased rate of pressurizer inventory depletion. As the pressurizer inventory was discharged into hot leg A, the fluid temperatures above the surge line elevation increased (Figure 5.7.3, See 1). This temperature increase was a result of the discharge of hotter fluid from the pressurizer into the hot leg. The increased hot leg A fluid temperature resulted in a decrease in the fluid density, thus resulting in an increase in the loop A driving head. The increased driving head in turn resulted in an increase in the loop A flow rate (Figure 5.7.4, See 1). This response was not observed in the Nominal Test since the pressurizer inventory was discharged into hot leg A at a much lower rate and therefore did not significantly affect the fluid temperatures.

When the pressurizer emptied, the fluid temperatures above the surge line elevation began decreasing (See 1 on Figures 5.7.5 and 5.7.6). The decreasing

fluid temperature trend propagated upward in hot leg A; thus, a decrease in the A loop driving head and flow occurred (Figure 5.7.7, See 1). The decreased flow in loop A caused an increase in the core region fluid temperatures (Figure 5.7.8, See 1). This action resulted in an increase in the driving head for loop B, the loop B flow rate increased (Figure 5.7.9, See 1), and a heatup to saturated conditions propagated up hot leg B (See 1 on Figures 5.7.10 and 5.7.11).

Hot leg A, however, began a gradual heatup of the fluid below the surge line elevation (Figure 5.7.5, See 2), loop A flow continued to decrease (Figure 5.7.7, See 2), the hot leg A level indicated a collapsed liquid level that was above the U-bend spillover (Figure 5.7.12, See 1), and the hot leg A stub collapsed liquid level decreased slightly (Figure 5.7.12, See 2). When the fluid below the surge line elevation in hot leg A heated up to the temperature of the fluid above the surge line, a heatup of hot leg A again commenced and propagated up the hot leg (Figure 5.7.5, See 3). This heatup resulted in an increased driving head and the loop A flow increased (Figure 5.7.7, See 3).

The fluid temperature response in the A cold legs during the initial depressurization and loop A flow reduction resulted in two observations that provided additional insight to the phenomena occurring in the cold legs. For this test, HPI was not actuated, and therefore the effects of injecting cold liquid into the cold legs on the system response and/or phenomena were eliminated. The first observation concerns heat losses in the cold legs. Prior to the previously discussed loop A flow reduction, an examination of the cold leg suction and cold leg discharge temperatures revealed that heat losses existed between the uppermost thermocouple in the cold leg suction pipe and the reactor coolant pump discharge thermocouple rake. The heat losses resulted in an approximately 6 to 8F reduction in the fluid temperature between these locations for each cold leg, e.g., for cold leg A1 see 1 on Figures 5.7.13 and 5.7.14. As the loop A flow decreased, the fluid temperatures at the reactor coolant pump discharge thermocouple rake decreased (Figure 5.7.14, See 2) while the fluid temperatures in the cold leg suction pipe remained essentially constant (Figure 5.7.13, See 2). The maximum fluid temperature difference between these two locations was approximately

16 to 17F and was attained when the loop A flow was at a minimum (Figure 5.7.14, See 3). Similarly as the loop A flow increased, the fluid temperatures at the reactor coolant pump discharge thermocouple rake increased (Figure 5.7.14, See 4). This response indicated the presence of heat losses that appear to be associated with the reactor coolant pumps. The reactor coolant pump metal temperatures were approximately 500F (48F colder than the fluid in the cold leg suction pipe) during this time (Figure 5.7.15), thus indicating the presence of a heat sink. The response of cold leg A2 was similar to that of cold leg A1 (Figures 5.7.16 and 5.7.17).

The second observation concerns the backflow of fluid from the downcomer into the cold leg discharge pipes. As loop A flow decreased, the flow through the open RVVV (A2) increased (Figure 5.7.18, See 1). This action was followed by the opening of the A1 and B2 RVVVs, thus further increasing the flow through the reactor vessel vent valves (Figure 5.7.18, See 2). When these RVVVs opened, counter-current liquid flow was observed at both the cold leg A1 and A2 nozzles. Warmer fluid entered the cold leg discharge pipes (flowed backward) at the top of the pipe, mixed with the colder fluid that was flowing in the forward direction in the cold leg, and was discharged at the bottom of the pipe into the downcomer (See 1 on Figures 5.7.19 and 5.7.20). The effect of the backflow in the cold leg discharge pipes appeared to propagate to the reactor coolant pump discharge elevation since temperature fluctuations were observed at the thermocouple rakes (Figure 5.7.14, See 5 and Figures 5.7.17, See 1). The loop A flow rate continued decreasing (Figure 5.7.7, See 2) and appeared to be on the verge of flow interruption or the establishment of intra-cold leg flow when the heatup of hot leg A resulted in an increased flow rate and the subsequent termination of counter-current flow in the cold leg discharge pipes (See 2 on Figures 5.7.19 and 5.7.20). The response of the loop A flow for this test was not observed in any of the other Mapping Tests and appears to be related to the lack of HPI during the depressurization phase.

These two observations (reactor coolant pump heat losses and backflow, without HPI, in the cold leg discharge pipe) will be investigated during the initial flow interruption and/or intra-cold leg flow phase in an attempt to

establish the mechanism(s) that initiate the observed flow response of this test.

When the core exit saturated, the reactor vessel upper head region began voiding (Figure 5.7.21, See 1) and a gradual primary system repressurization began (Figure 5.7.1, See 2). As the reactor vessel upper head region voided, the reactor vessel level descended and approached the reactor vessel vent valve elevation. Steam began to be discharged through the reactor vessel vent valves as indicated by the increased pressure drop across the valves (Figure 5.7.22, See 1), and the downcomer began voiding (Figure 5.7.21, See 2). The pressure equalization between the reactor vessel and the downcomer resulted in the characteristic cyclical operation of the reactor vessel vent valves (Figure 5.7.22, See 2 and Figure 5.7.23, See 1).

As the reactor vessel and downcomer voided, a gradual decreasing trend was observed in the flow rate of both loops A and B (See 1 on Figures 5.7.24 and 5.7.25). The decreasing trend in the loop flow rates resulted from the pressure equalization between the reactor vessel and the downcomer, which occurred while a liquid level (above the cold leg nozzle elevation) existed in the downcomer. As the reactor vessel vent valves opened, the pressure in the downcomer essentially equaled the pressure in the reactor vessel. This equal pressure resulted in an increase in the back pressure at the cold leg nozzle elevation, thus retarding primary loop flow.

As the downcomer level descended and approached the cold leg nozzle elevation (Figure 5.7.21, See 3), backflow was observed at the cold leg nozzle thermocouple rake in each cold leg (See 1 on Figures 5.7.26, 5.7.27, 5.7.28, and 5.7.29). The diversion of more steam from the core region to the downcomer, the increased frequency of the cyclical RVVV operation and, therefore, the increased back pressure effect at the cold leg nozzle resulted in a more rapidly decreasing primary loop flow (See 2 on Figures 5.7.24 and 5.7.25).

The previously discussed events and phenomena were similar to those observed in the Nominal Test (3003AA). This similarity implies that HPI has little or no effect on the observed phenomena, which led to flow interruption during the depressurization and gradual repressurization phase of the test.

The gradual repressurization continued and attained a pressure of approximately 1230 psia (Figure 5.7.1, See 3). At this time, the downcomer level had descended to the cold leg nozzle elevation (Figure 5.7.21, See 4), and the three reactor vessel vent valves that had been cycling cycled at a higher frequency and then remained open (Figure 5.7.23, See 2). This action resulted in the discharge of steam from the downcomer into the four cold leg discharge pipes, and backflow was observed in cold legs A1 and B1 (See 3 on Figures 5.7.24 and 5.7.25). This event was also confirmed by the temperature response of the reactor coolant pump discharge thermocouple rakes, because only the A1 and B1 temperatures saturated (Figures 5.7.30 through 5.7.33), and the cold leg suction temperatures, because colder fluid spilled over and then the fluid temperatures increased in only cold legs A1 and B1 (Figures 5.7.34 through 5.7.37). The decrease in the cold leg A1 and B1 suction temperatures (See 1 on Figures 3.7.34 and 3.7.35) also confirmed the existence of colder fluid due to heat losses in the region of the reactor coolant pumps.

The spillover of fluid from the cold leg discharge pipe into the suction pipe again occurred in the same cold leg (A1 and B1) as observed in the other Mapping Tests and initiated intra-cold leg flow in both loops. Since HPI was not actuated in this test, the significant decrease in the reactor coolant pump discharge thermocouple rake temperature (observed in the other Mapping Tests when backflow occurred) did not occur for this test. Thus, the conclusion drawn is that slight variations in the individual HPI flow rate to each cold leg was not the primary cause that established which cold legs flowed backward and which flowed forward.

The cause for establishing the flow direction in the cold legs of one loop appears to be related to the elevation head of the individual cold legs in one loop. The cold leg that has the highest elevation head contained between the cold leg branch and the cold leg discharge nozzle elevations will be more prone to establishing reverse flow. The net driving head between the two cold legs of one loop is dependent on physical elevations of the pipes and the fluid density in the cold legs. The fluid density in each cold leg is affected by the fluid temperature distribution in the cold legs. The fluid temperatures in turn are affected by the flow rates (both primary loop flow

and counter-current flow) and heat losses (from the reactor coolant pumps and the piping) in each cold leg. The guard heaters that attempt to minimize heat losses from the piping can also affect the fluid temperature distribution in the cold legs.

Subsequent to the establishment of intra-cold leg flow in both loops, the flow response in loops A and B and the cold legs was again altered. In the A cold legs, the initially established intra-cold leg flow had the A1 flow backwards and the A2 flow forwards. Since HPI was not actuated, the fluid entering the cold leg A1 discharge pipe from the downcomer was not cooled prior to spilling over into the cold leg suction pipe. Also, since this fluid was hotter than the primary fluid at the steam generator outlet, the driving head relationship was altered between cold legs A1 and A2. This change resulted in an increasing fluid temperature in the cold leg A1 suction pipe (Figure 5.7.34, See 2), thus decreasing the intra-cold leg driving head and flow rates (Figure 5.7.38, See 1). The cold leg A2 suction temperatures remained lower than those of the cold leg A1 suction during this period (Figure 5.7.39, See 1 and Figure 5.7.40, See 1). The cold leg A2 suction fluid temperatures were lower and the density was greater than those of the cold leg A1 suction, thus the driving head relationship was such that when intra-cold leg flow was reestablished cold leg A2 flowed backward and cold leg A1 flowed forward (Figure 5.7.41, See 1). The phenomena occurred again (Figure 5.7.41, See 2) prior to flow interruption in cold leg A1.

The B cold legs also responded to the driving head relationship when intra-cold leg flow was established. However, the alternating cold leg backflow response was not observed (Figure 5.7.42). Cold leg B1 consistently exhibited backflow that appeared to be related to the heat losses (as discussed previously). The reason for this response appears to be a result of the higher loop B flow rate during periods when both cold legs exhibited forward flow. This action results in a more uniform temperature and, thus, density distribution in each B cold leg.

These observations indicated that intra-cold leg flow cannot be sustained in one particular direction without HPI fluid being injected into the cold leg discharge pipes. The injection of HPI altered the fluid density in the cold legs and aided in maintaining the driving head relationship between the cold

legs. These observations also highlighted the critical balances between the driving head of each loop and the driving head of the cold legs in the determination of the flow response of the MIST facility.

Subsequently, flow interruption occurred sequentially in cold legs B1, A1, B2, and lastly, in A2 (Figure 5.7.43 and 5.7.44). The primary system repressurized to a maximum value of approximately 1940 psia (Figure 5.7.45, See 1) and the system response through the remainder of the test (through 230 minutes) was similar to that observed in the Nominal and other previously discussed Mapping Tests. At test termination, the primary system had depressurized to approximately 1070 psia (Figure 5.7.46, See 1).

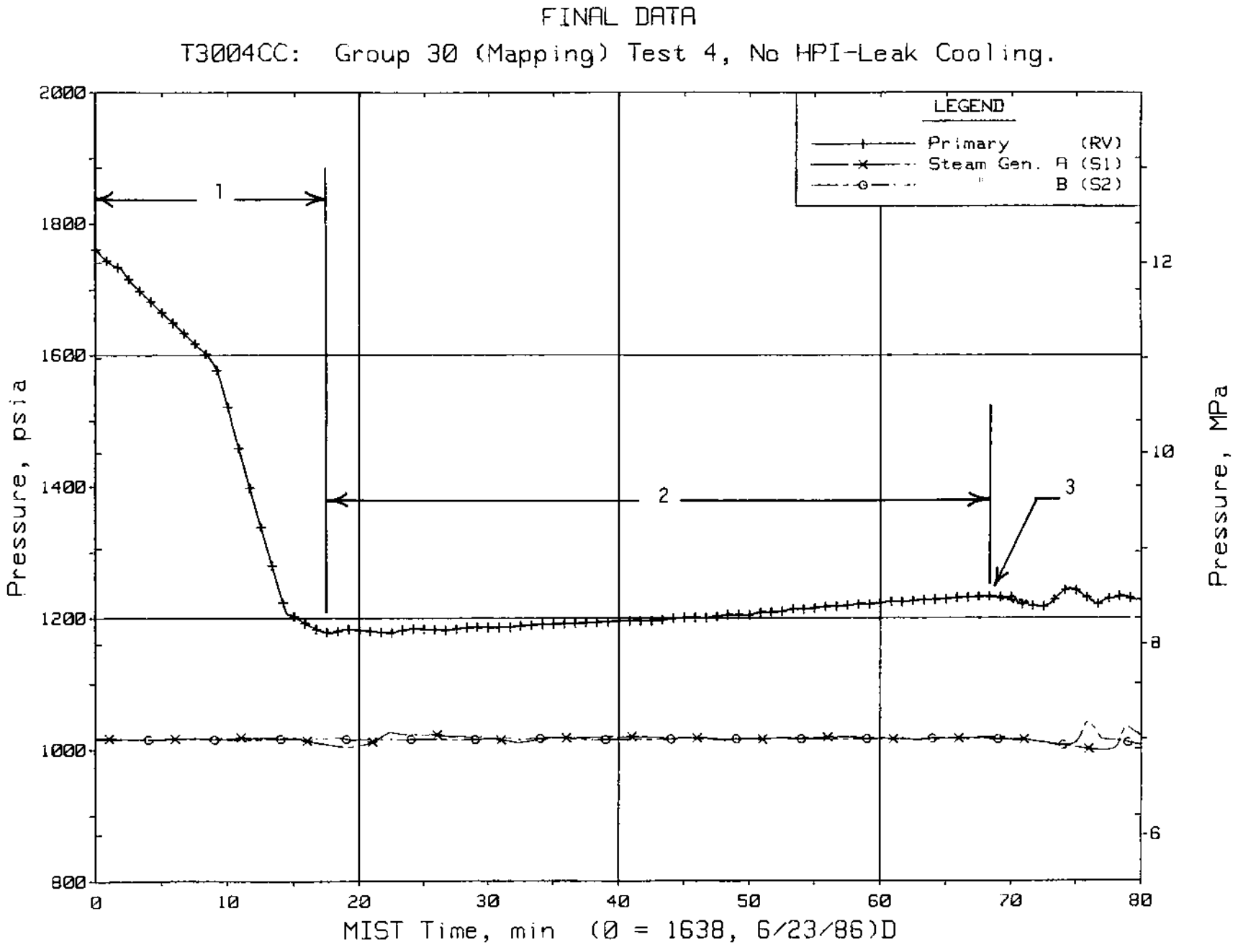

Figure 5.7.1. Primary and Secondary System Pressures (GP01s)

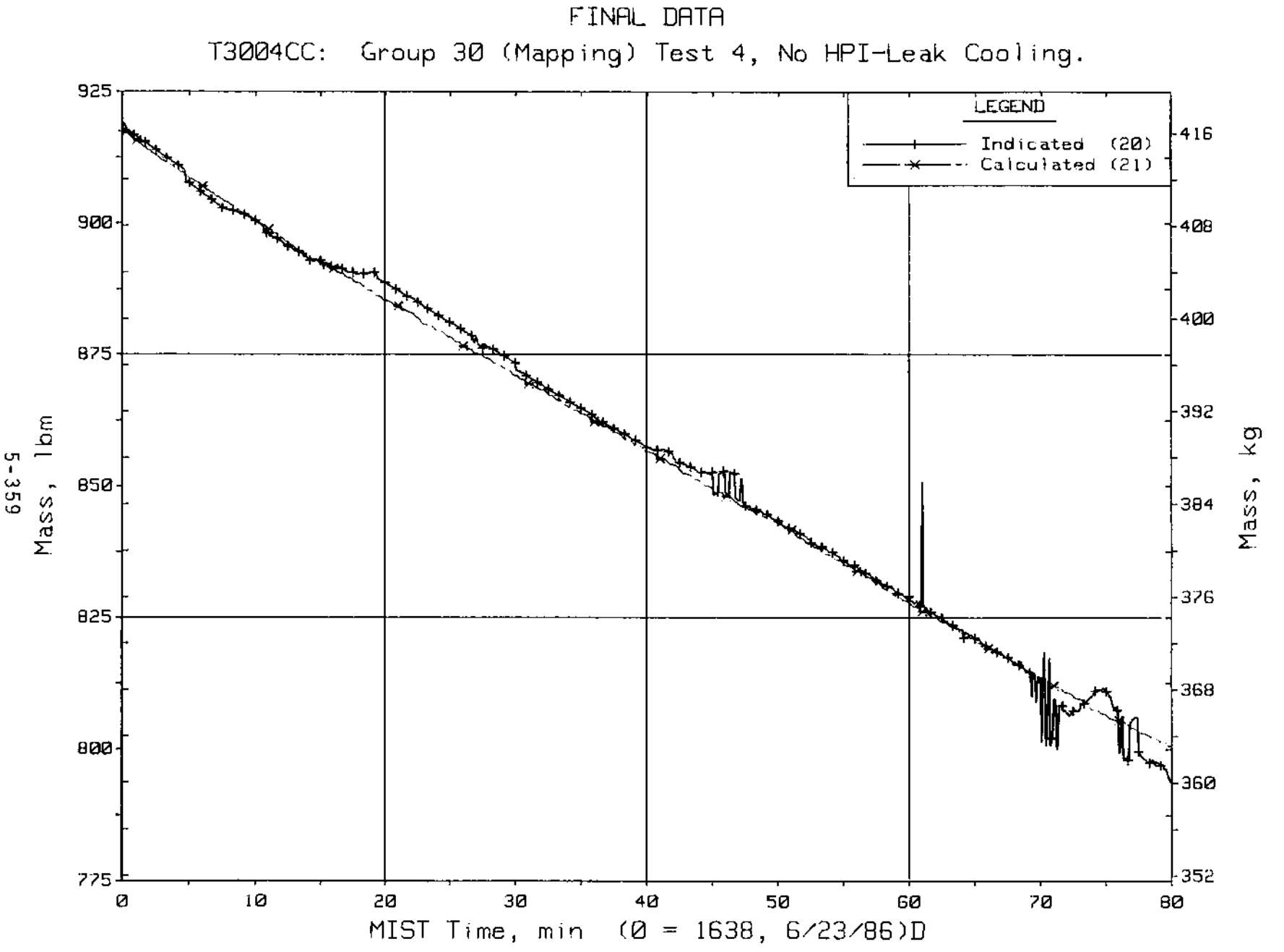

Figure 5.7.2. Primary System Total Fluid Mass (PLMLs)

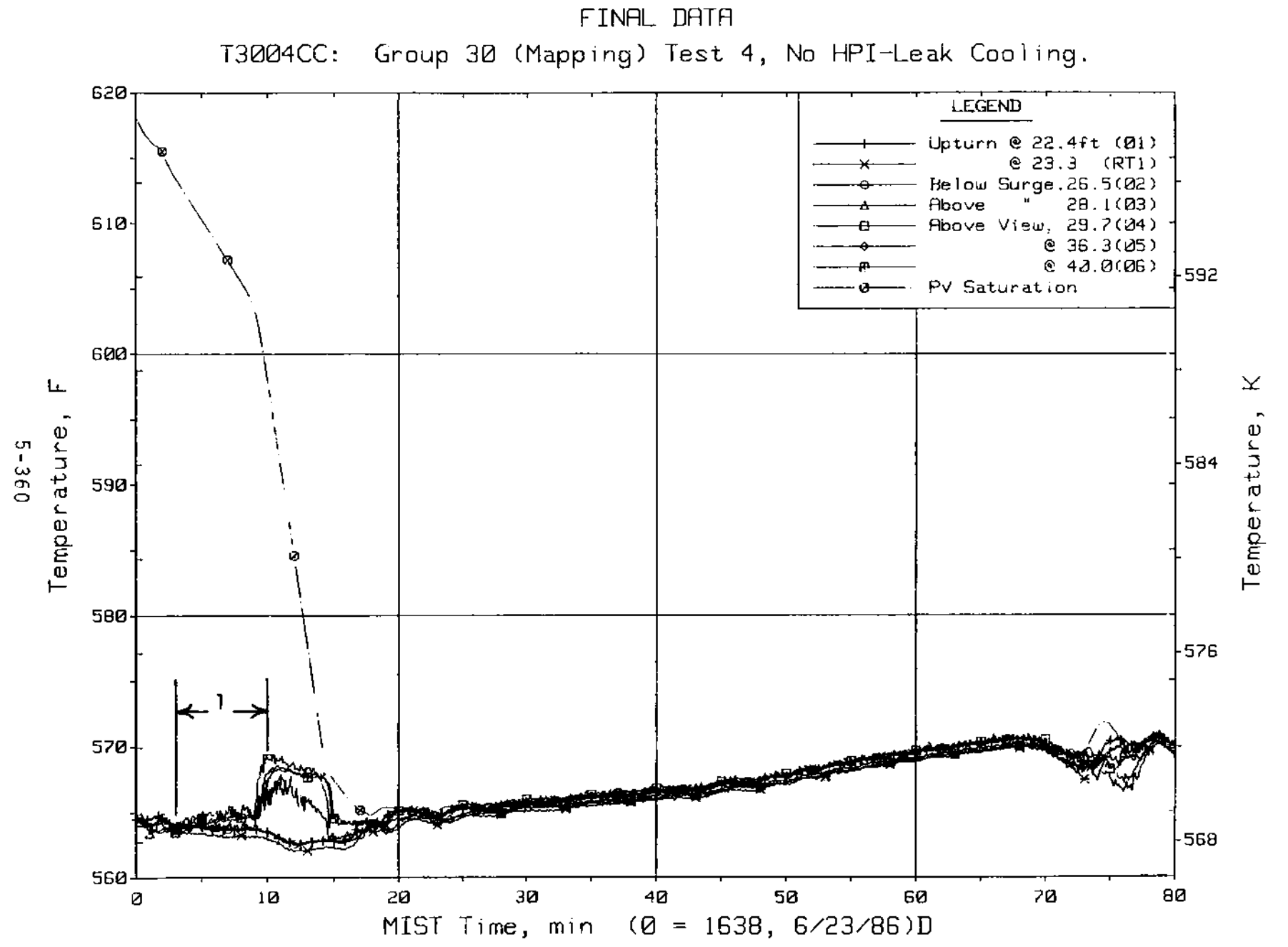

Figure 5.7.3. Hot Leg A Lower-Elevation Riser Fluid Temperatures (H1TCs)

Thu Mar 16 11:52:44 1989

H1TC1

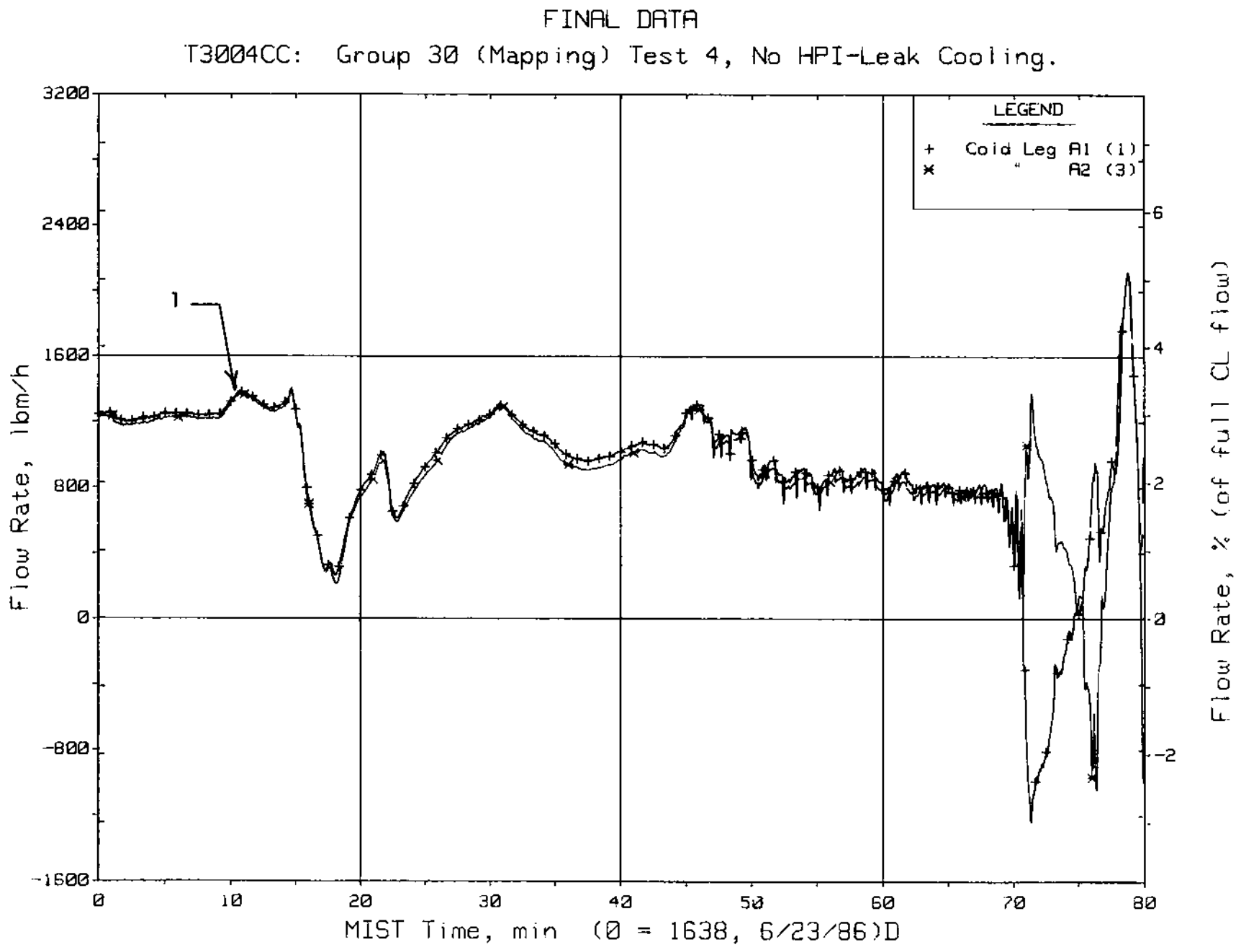

Figure 5.7.4. Loop A Cold Leg (Venturi) Flow Rates (CnVN20s)

Thu Mar 16 11:55:27 1989

PRFL5

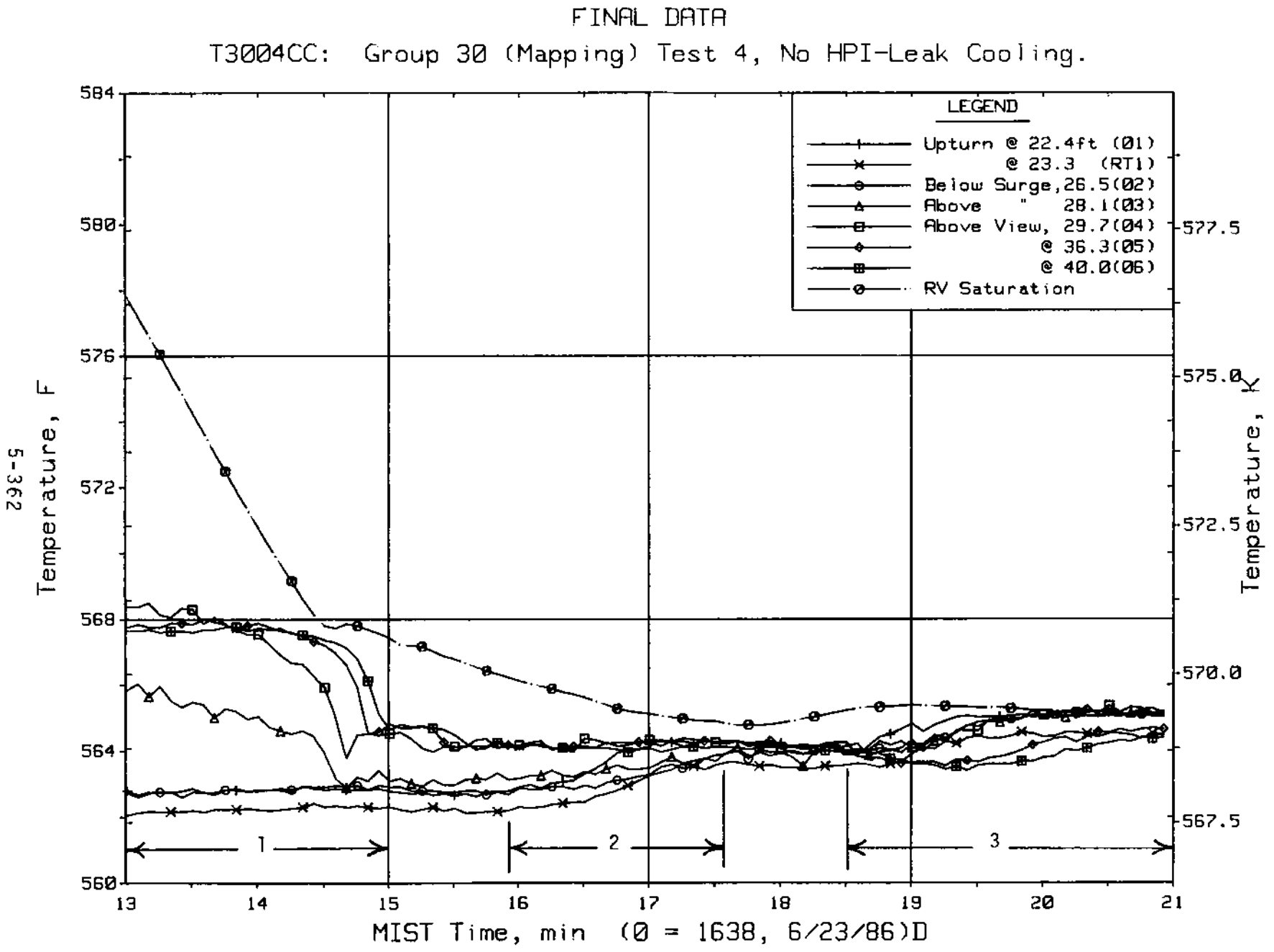

Figure 5.7.5. Hot Leg A Lower-Elevation Riser Fluid Temperatures (HITCs)

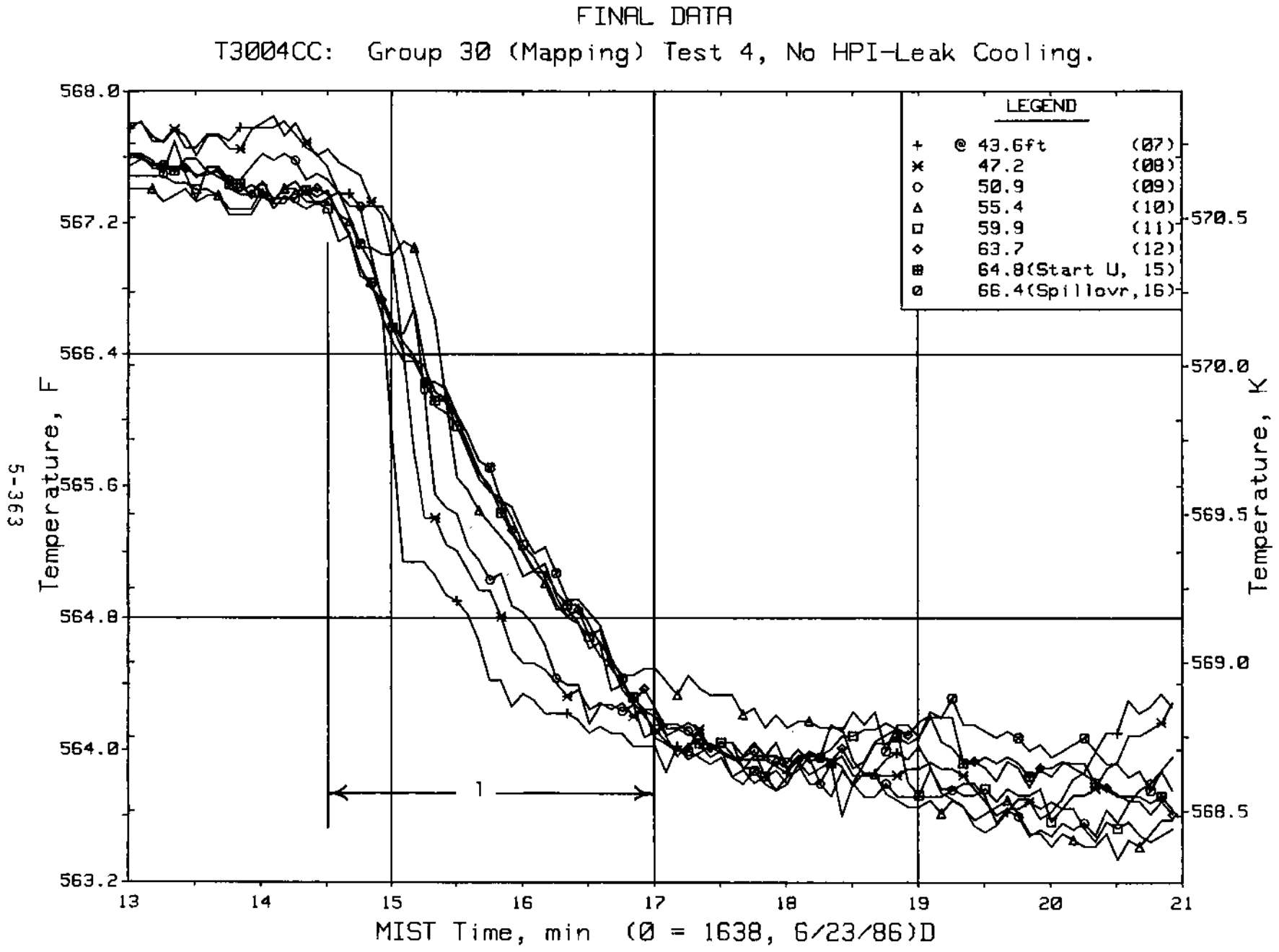

Figure 5.7.6. Hot Leg A Upper-Elevation Riser Fluid Temperatures (H1TCs)

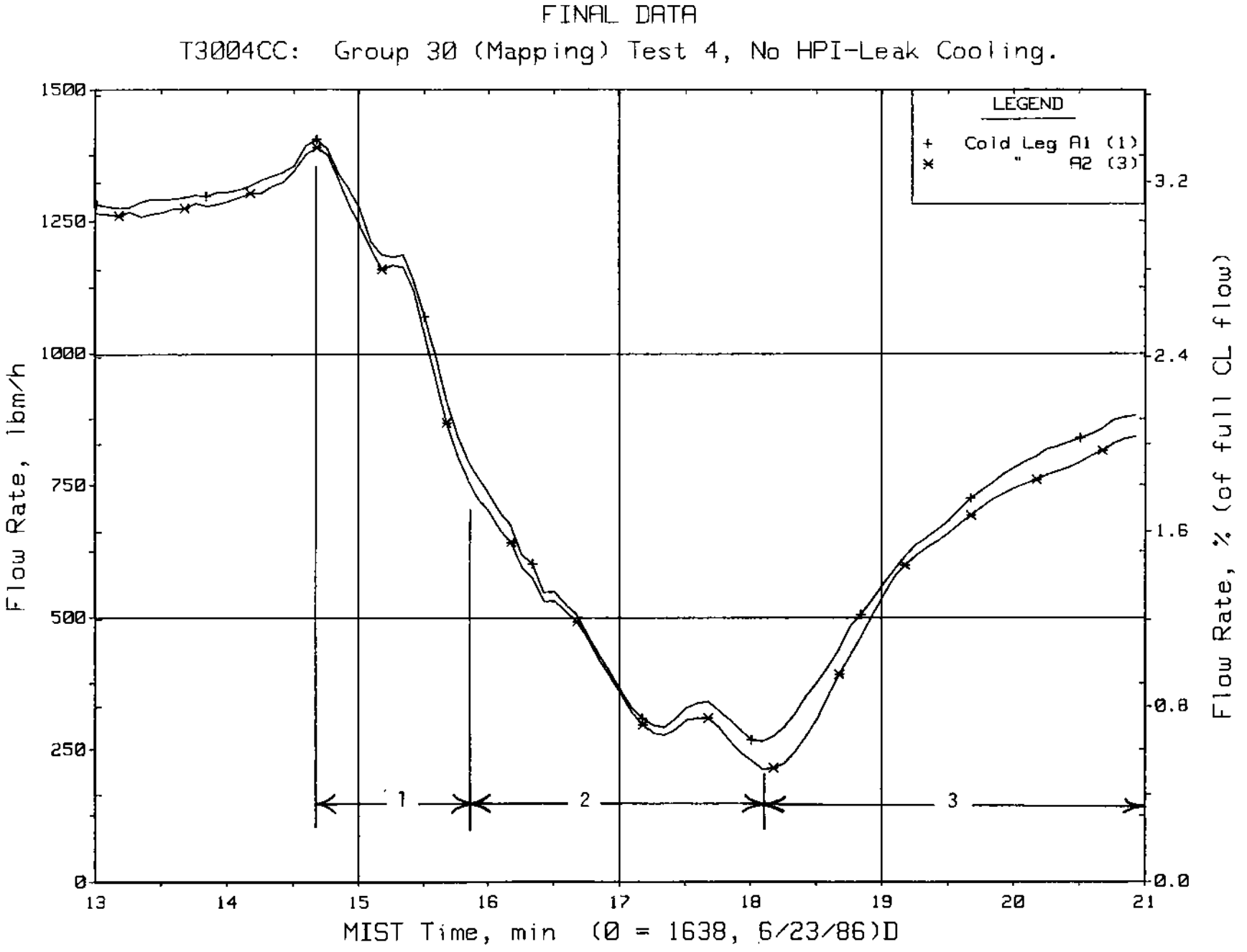

Figure 5.7.7. Loop A Cold Leg (Venturi) Flow Rates (CnVN20s)

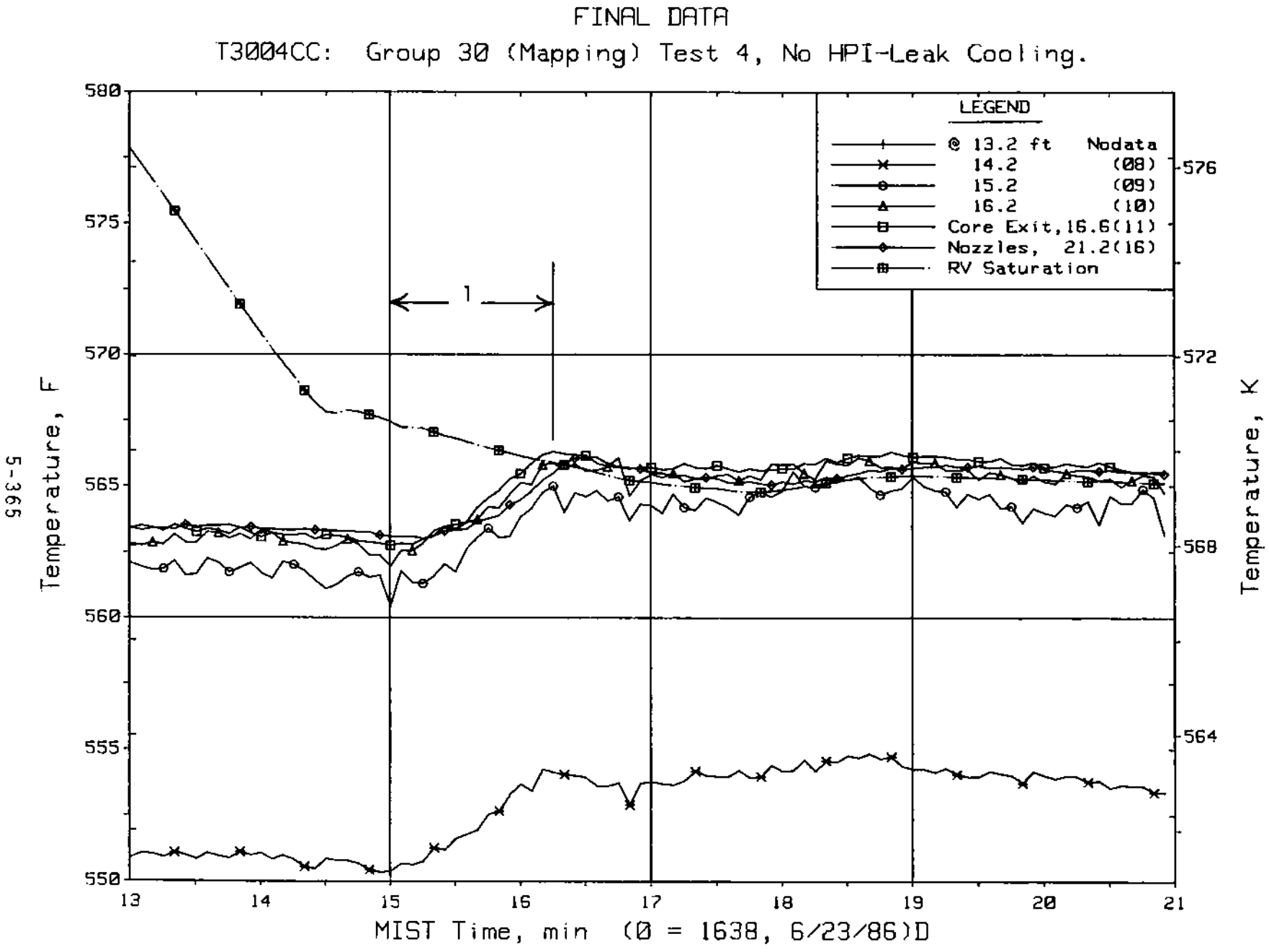

Figure 5.7.8. Reactor Vessel Mid-Elevation Fluid Temperatures (RVTCs)

Fri Mar 17 13:41:39 1989

RVTC2

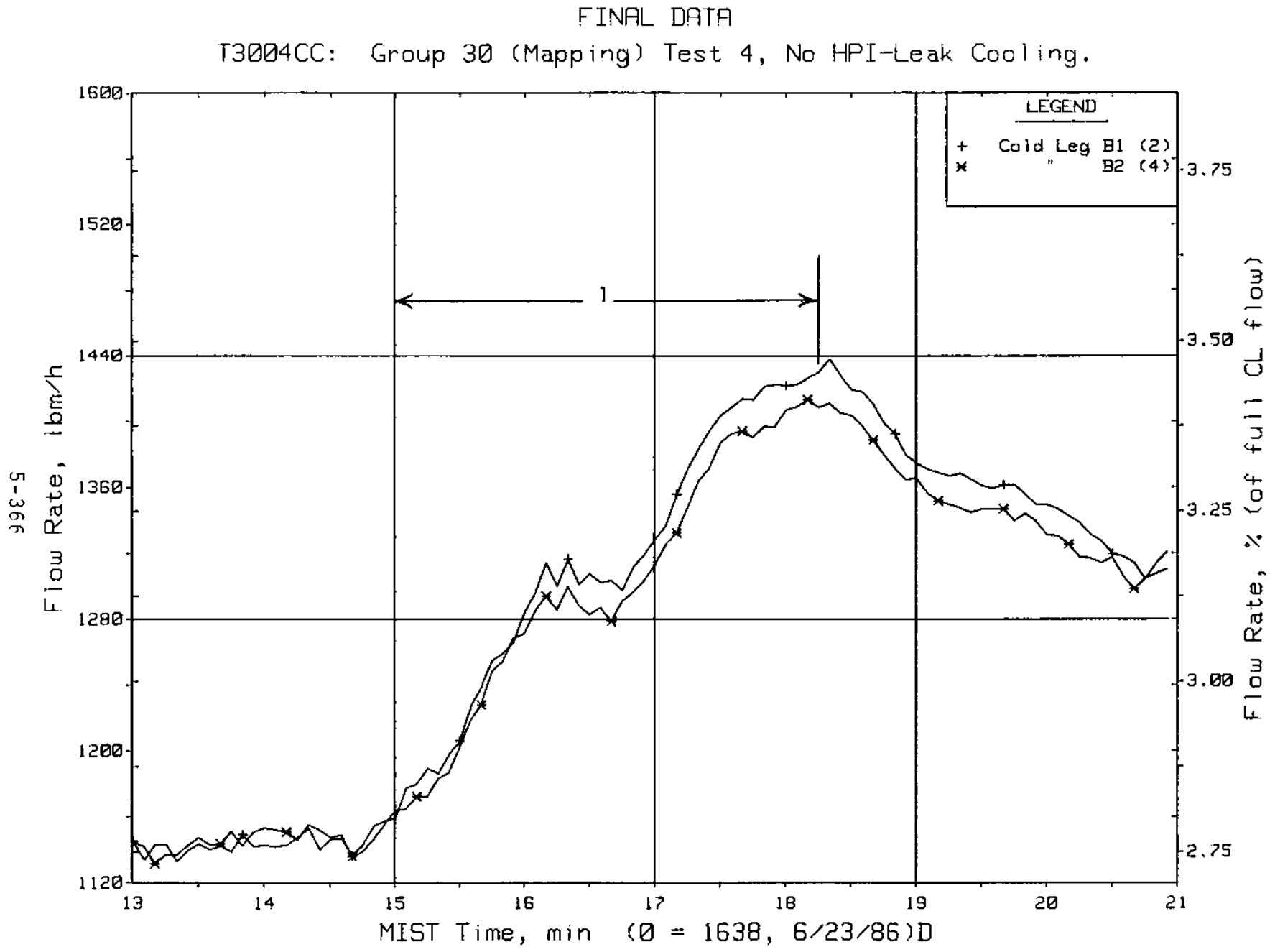

Figure 5.7.9. Loop B Cold Leg (Venturi) Flow Rates (CnVN20s)

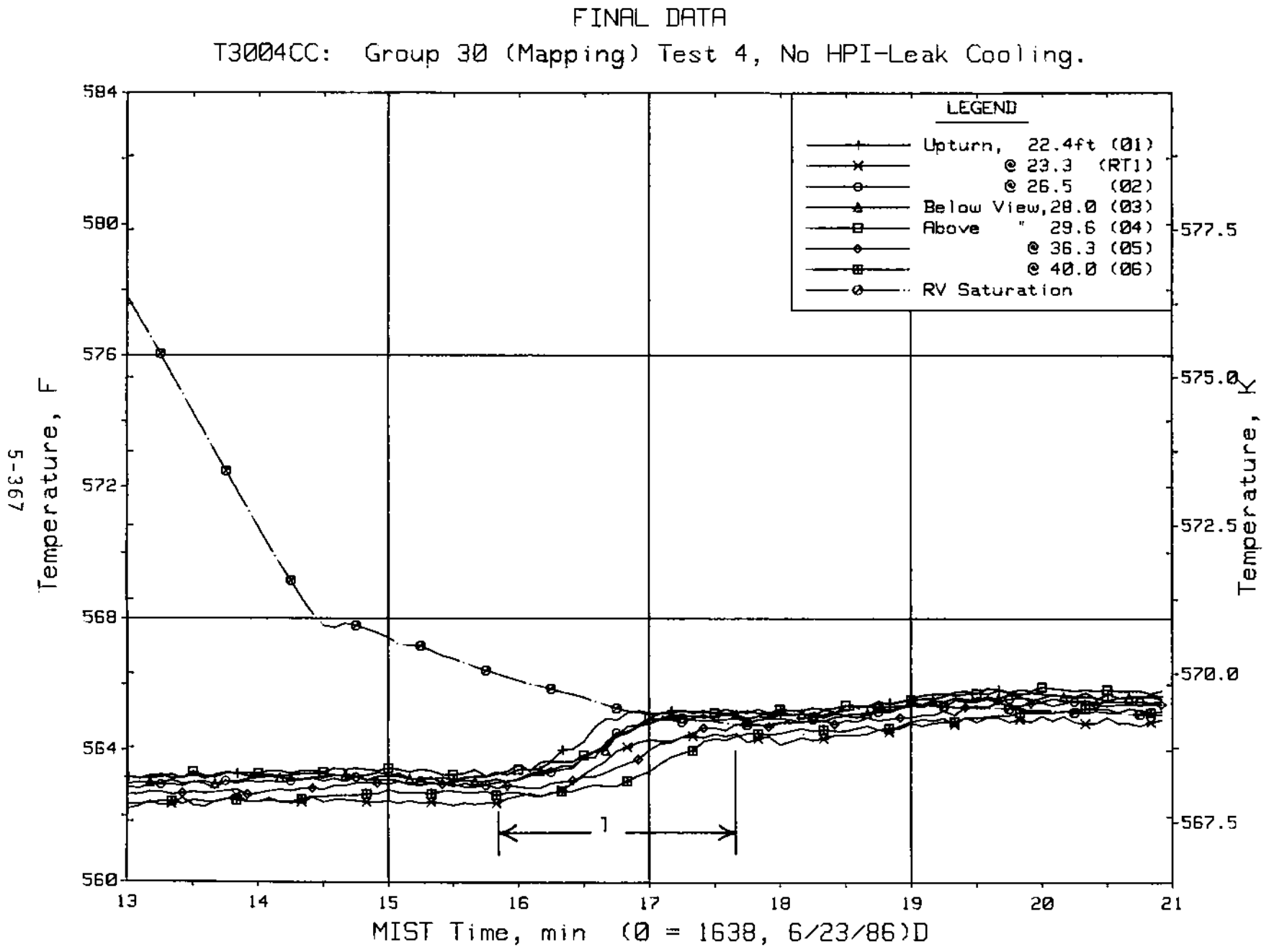

Figure 5.7.10. Hot Leg B Lower-Elevation Riser Fluid Temperatures (H2TCs)

Fri Mar 17 13:47:41 1989

H2TC1

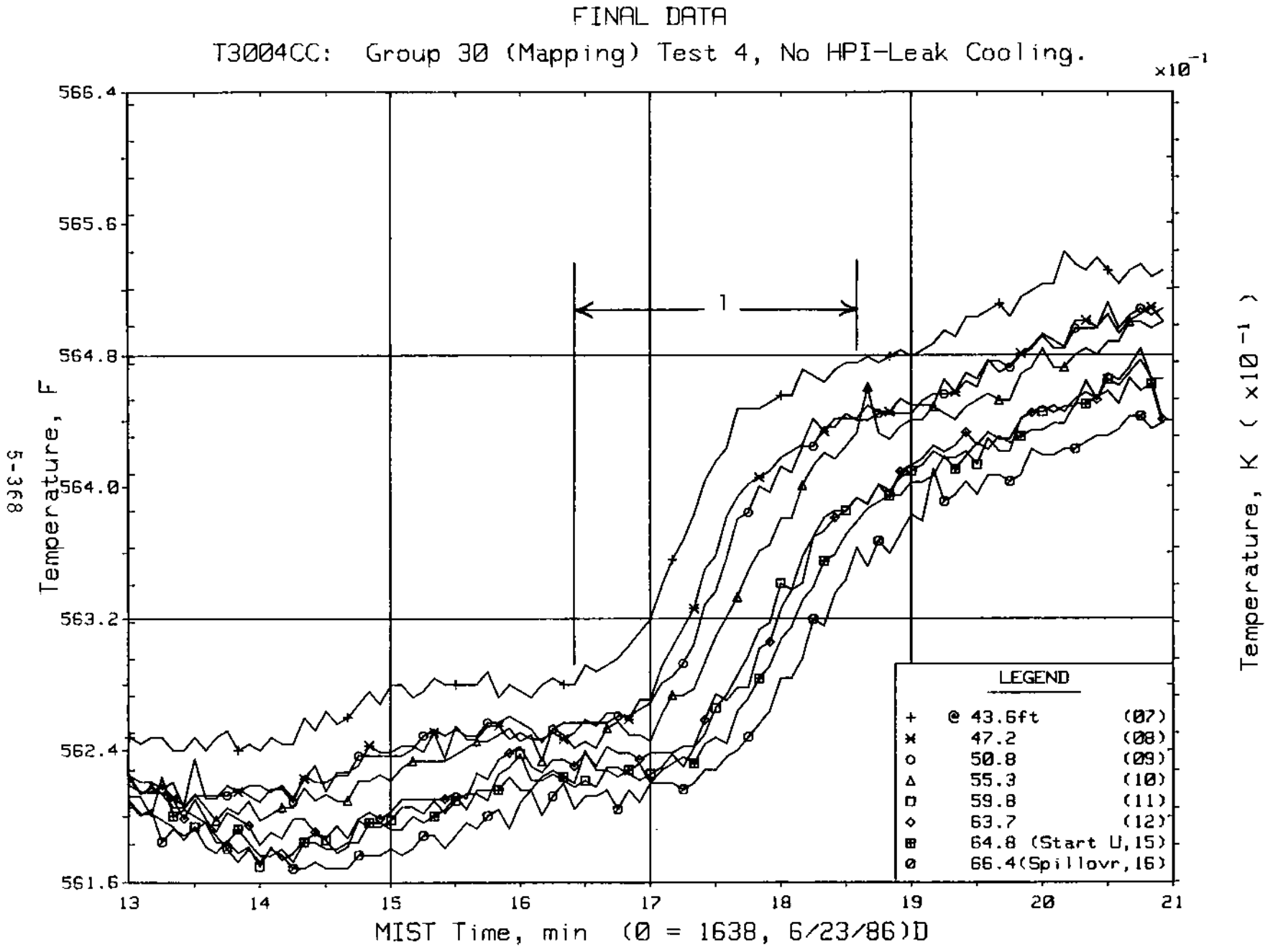

Figure 5.7.11. Hot Leg B Upper-Elevation Riser Fluid Temperatures (H2TCs)

Fri Mar 17 13:50:16 1989

H2TC2

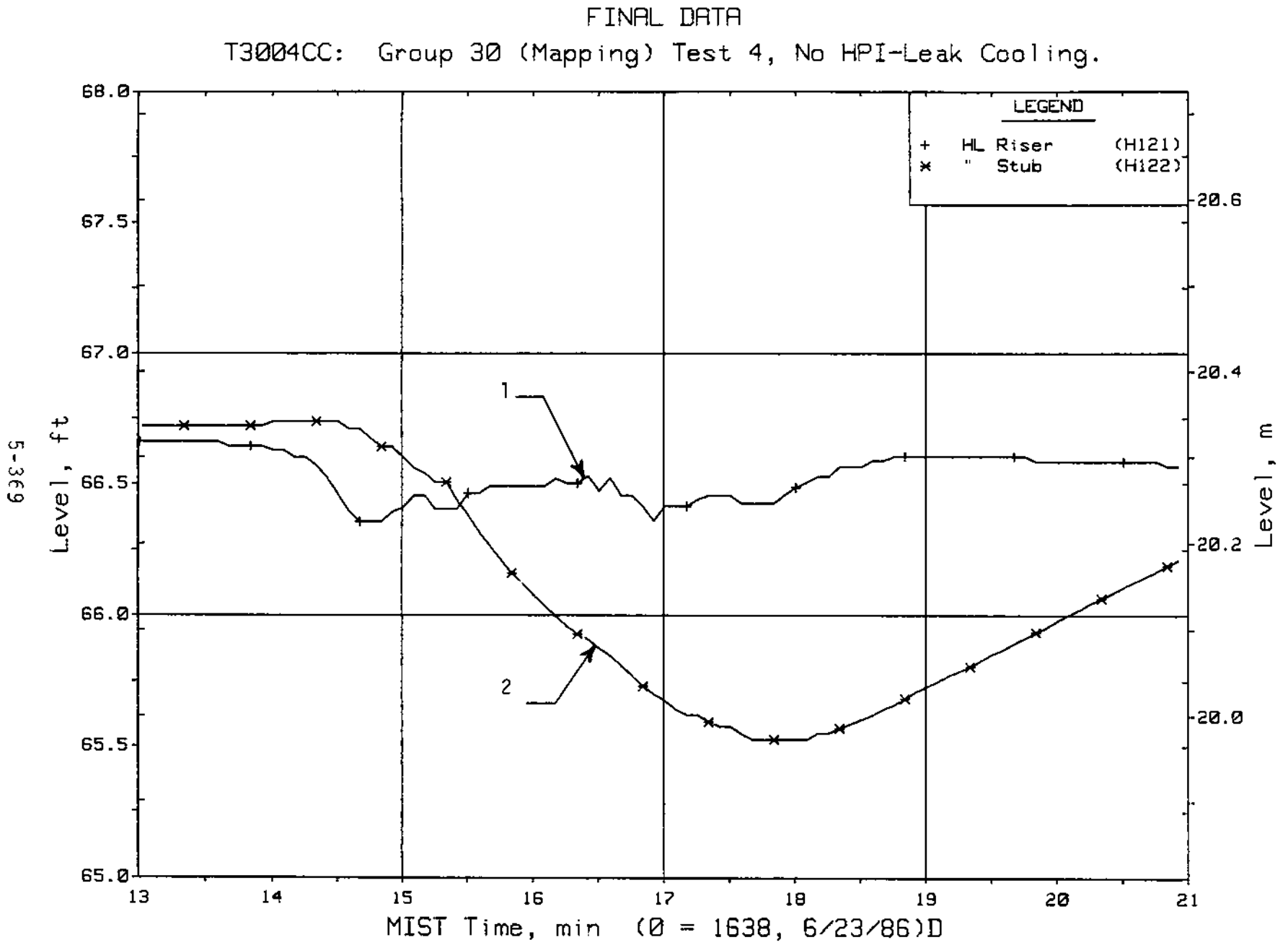

Figure 5.7.12. Loop A Collapsed Liquid Levels (LV20s)

Tue Mar 21 11:02:22 1989

PRLVi

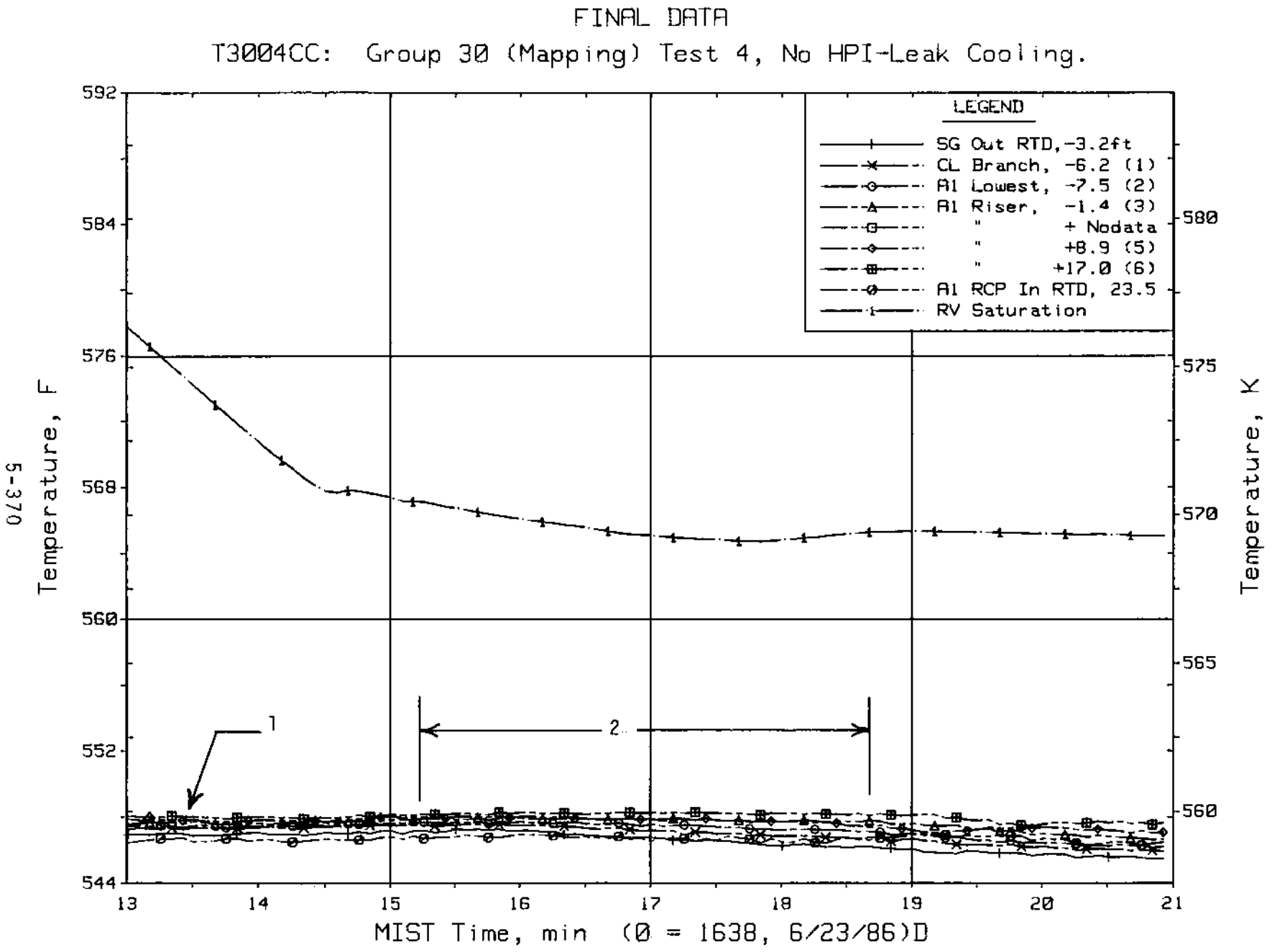

Figure 5.7.13. Cold Leg A1 Suction Fluid Temperatures (C1TCs)

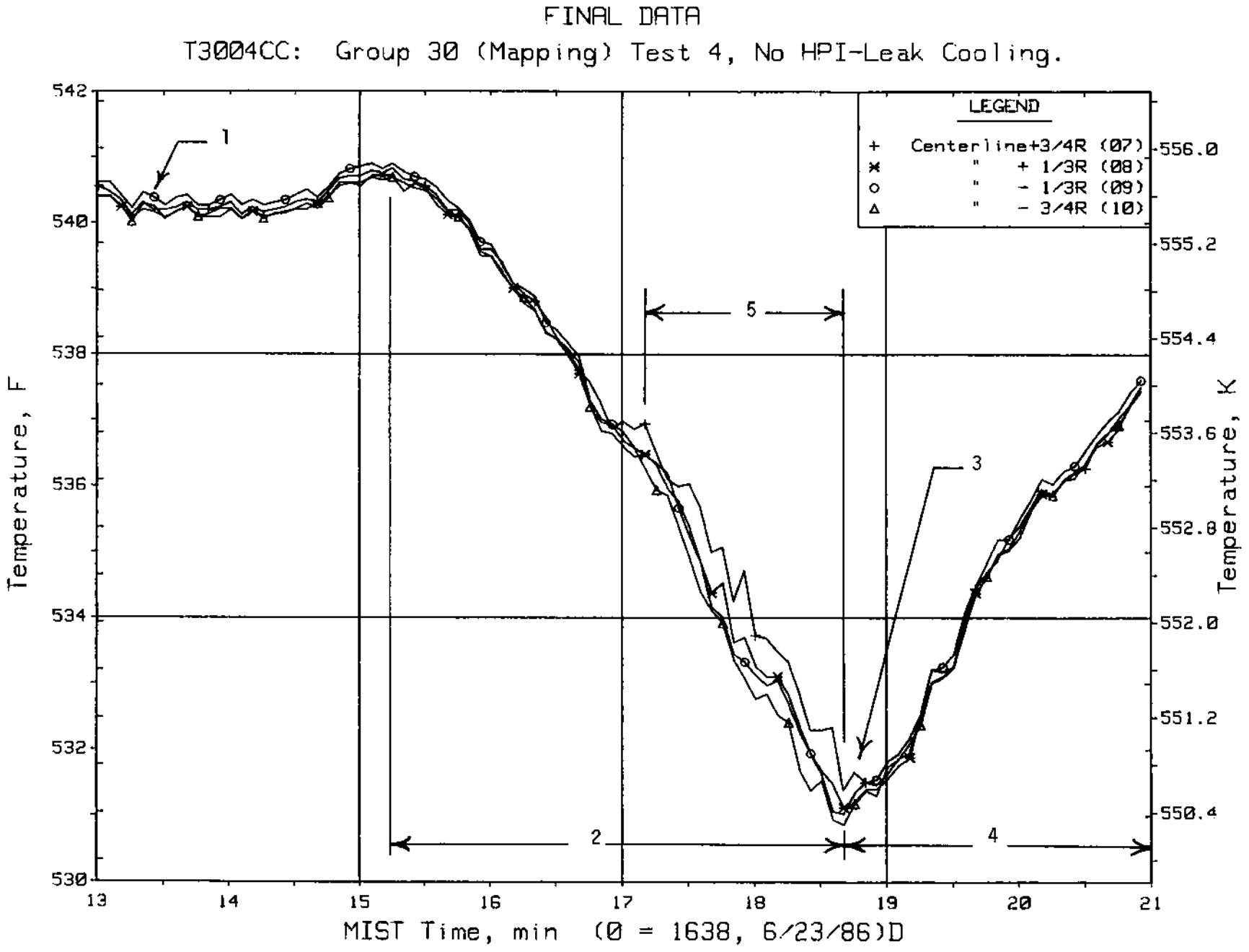

Figure 5.7.14. Cold Leg A1 Pump Discharge Rake Fluid Temperatures (25 ft, C1TCs)

Fri Mar 17 13:57:48 1989

C1TC3

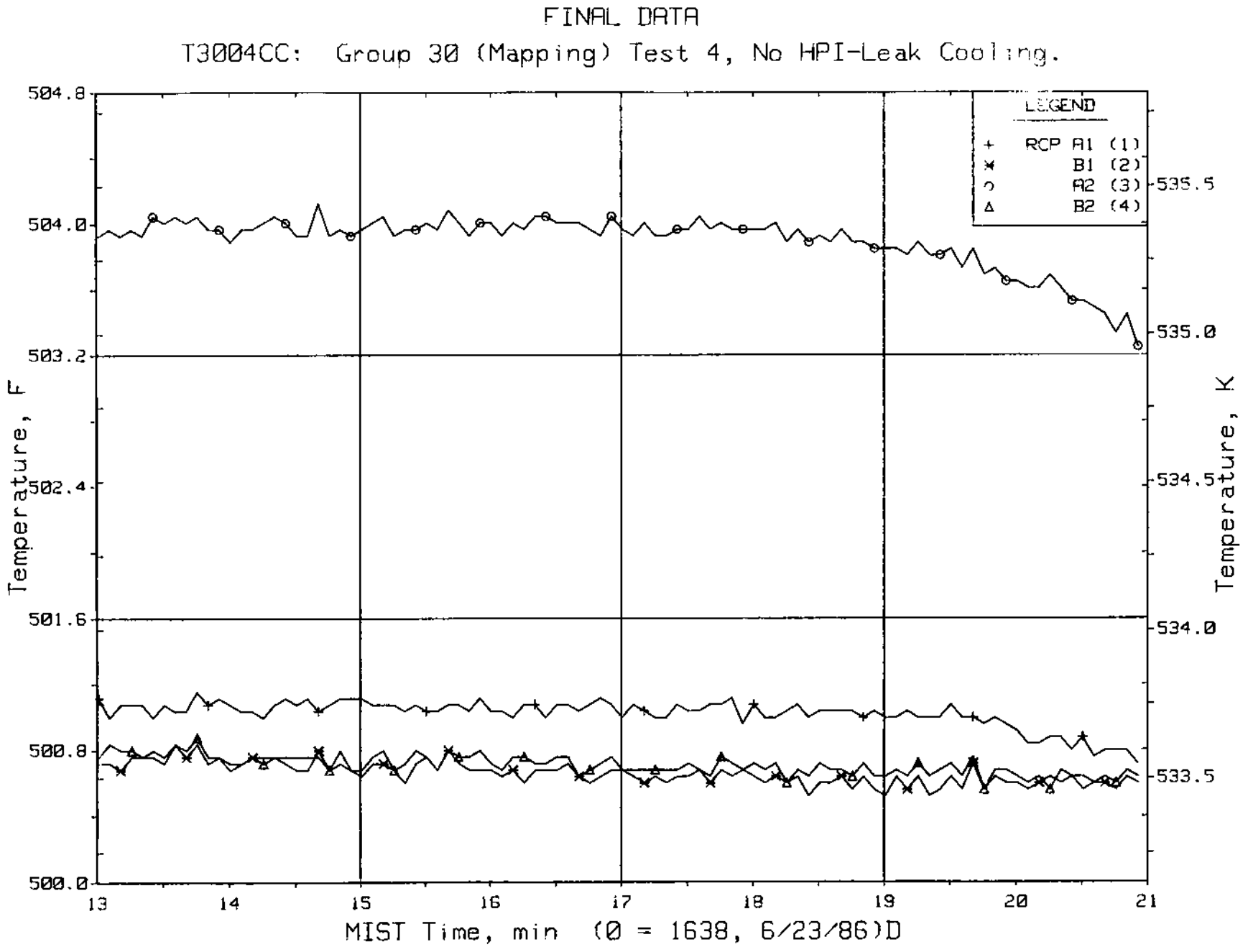

Figure 5.7.15. Reactor Coolant Pump Metal Temperatures (CnMT04s)

Fri Mar 17 15:19:54 1989

PUMT1

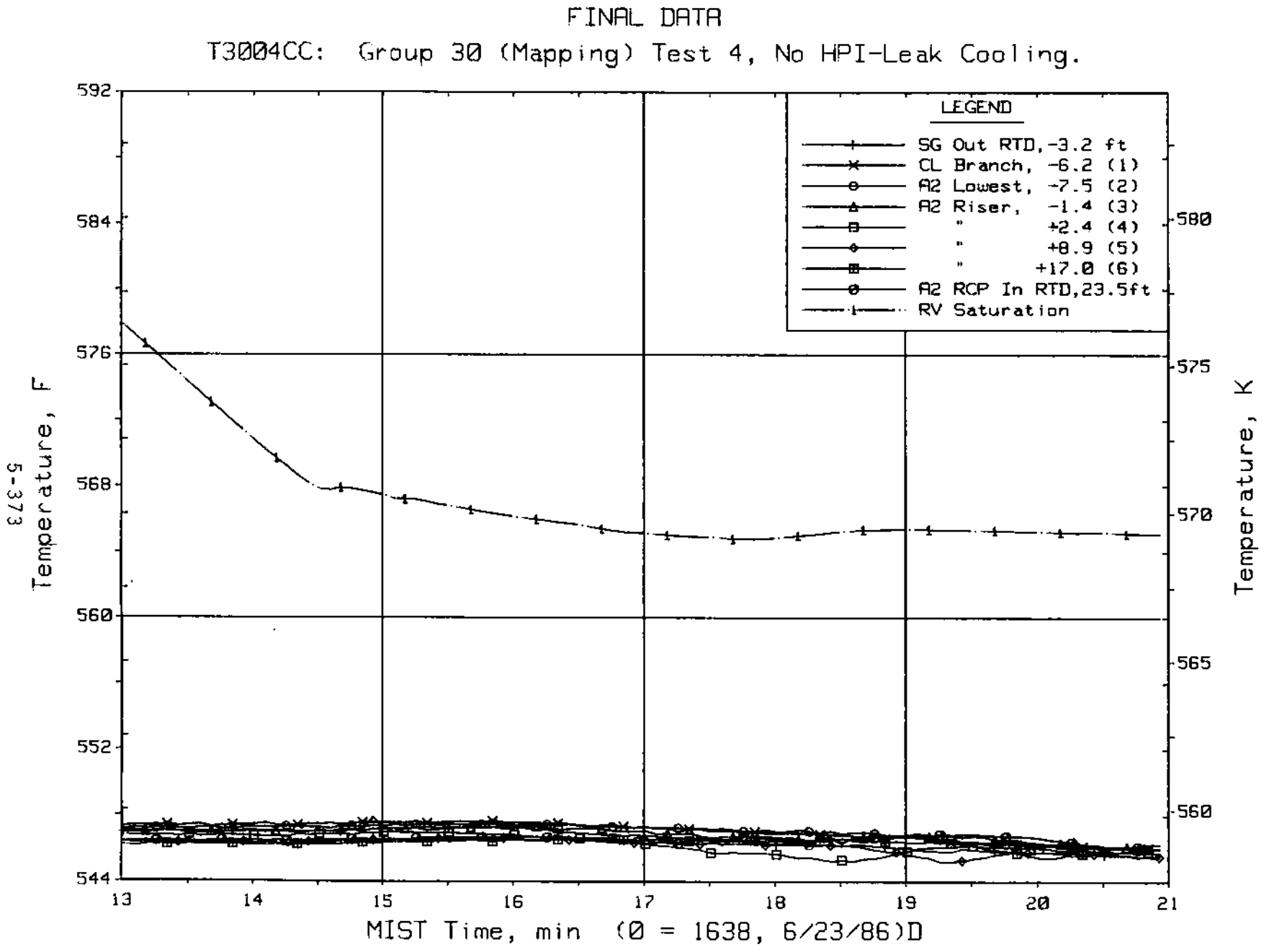

5-373

Figure 5.7.16. Cold Leg A2 Suction Fluid Temperatures (C3TCs)

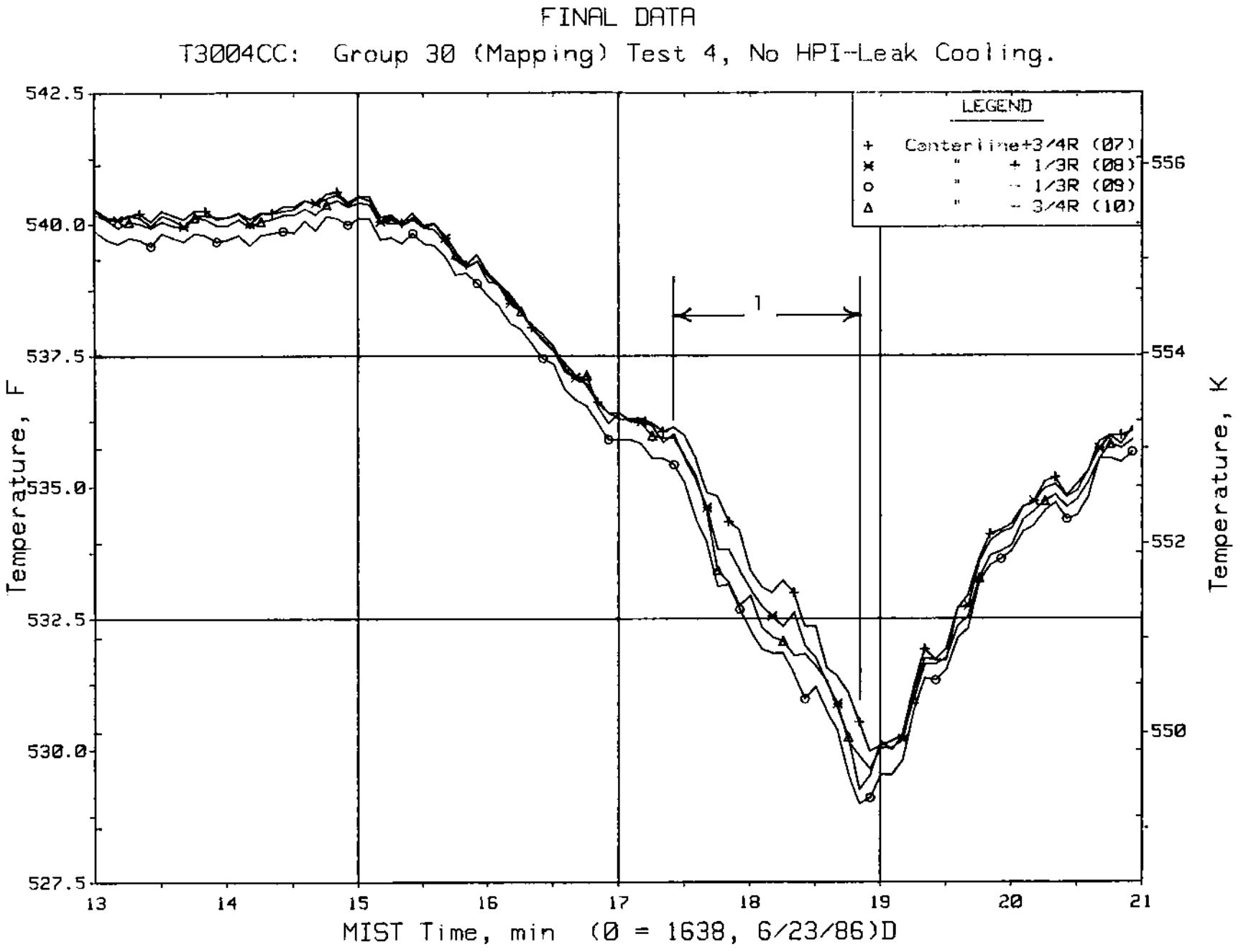

Figure 5.7.17. Cold Leg A2 Pump Discharge Rake Fluid Temperatures (25 ft, C3TCs)

Fri Mar 17 14:04:23 1989

C3TC3

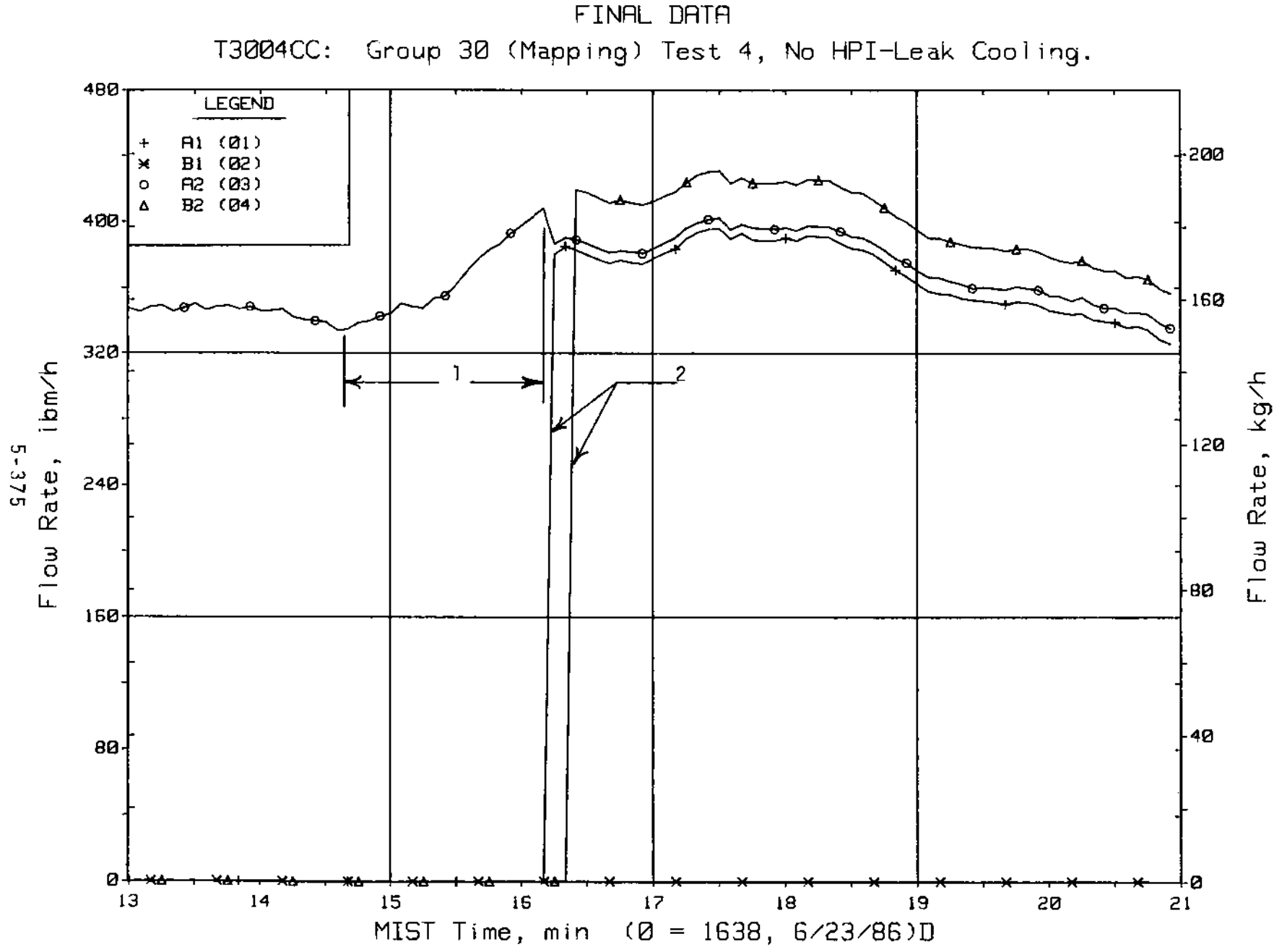

Figure 5.7.18. Reactor Vessel Vent Valve Flow Rates (RVORs)

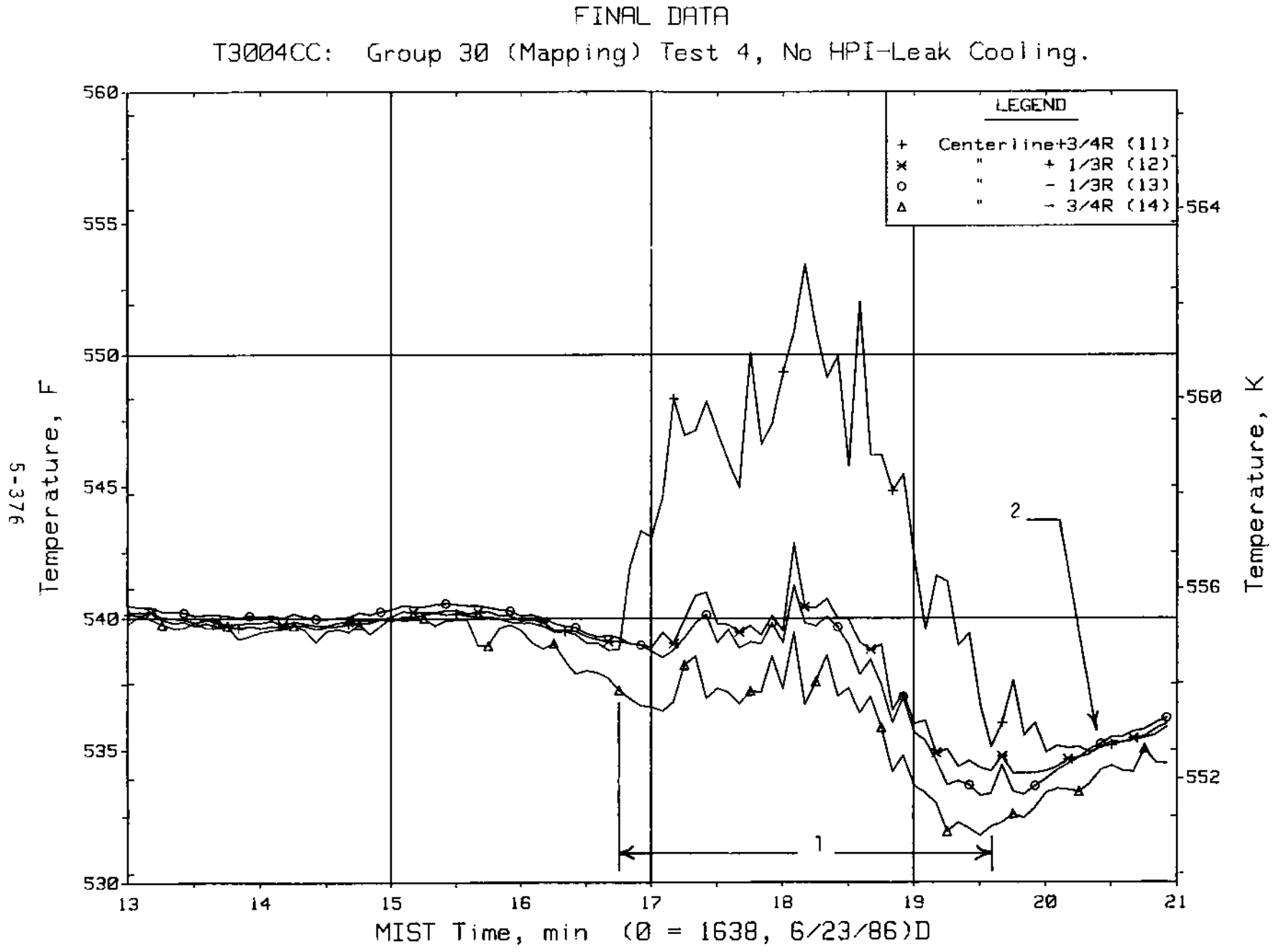

Figure 5.7.19. Cold Leg A1 Nozzle Rake Fluid Temperatures (21.2 ft, C1TCs)

Fri Mar 17 14:08:11 1989

C1TC4

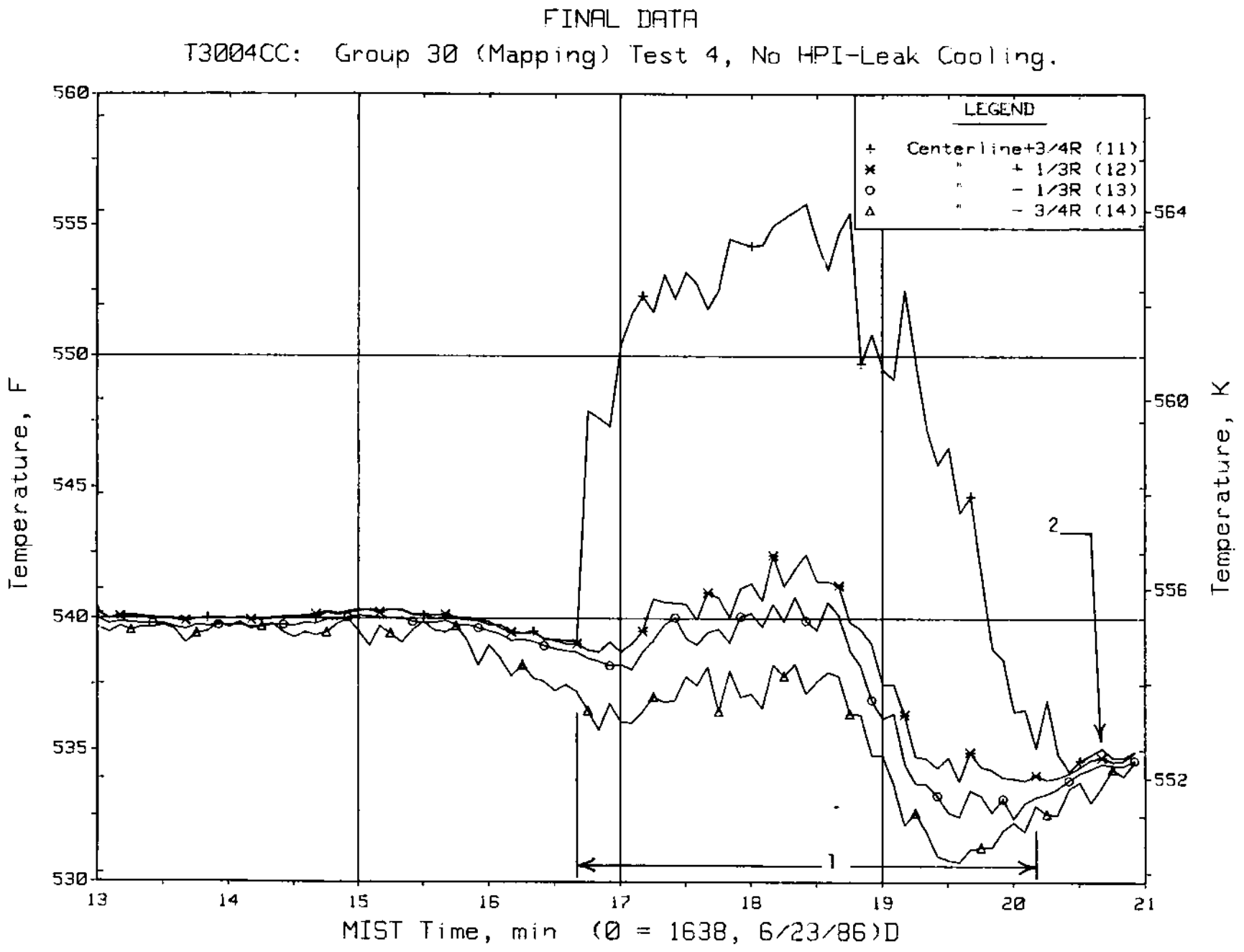

Figure 5.7.20. Cold Leg A2 Nozzle Rake Fluid Temperatures (21.2 ft, C3TCs)

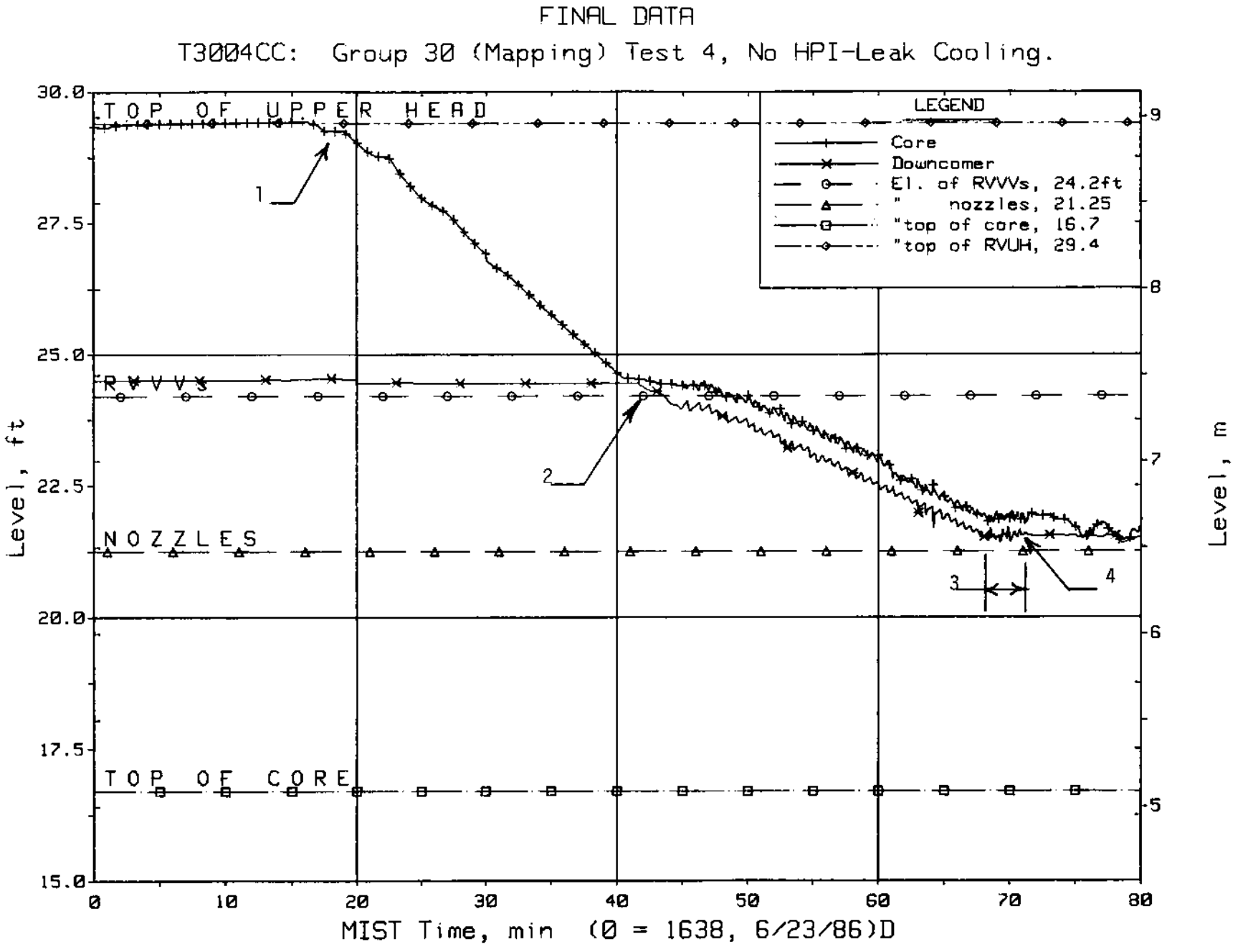

Figure 5.7.21. Core Region Collapsed Liquid Levels

Fri Mar 17 13:20:15 1989

COLV1

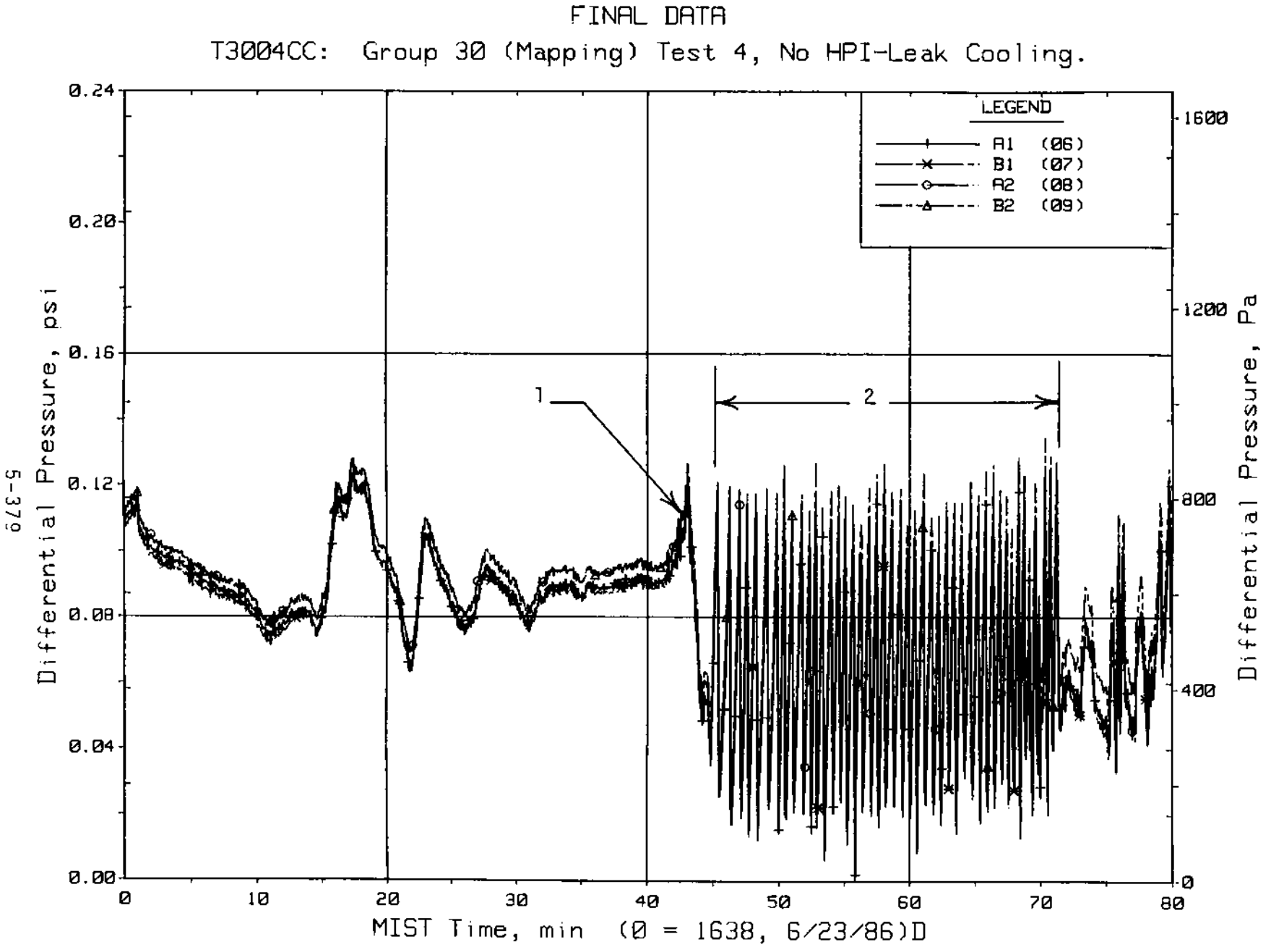

Figure 5.7.22. Reactor Vessel Vent Valve Differential Pressures (RVDPs)

Tue Mar 21 11:45:06 1989

VVDP1

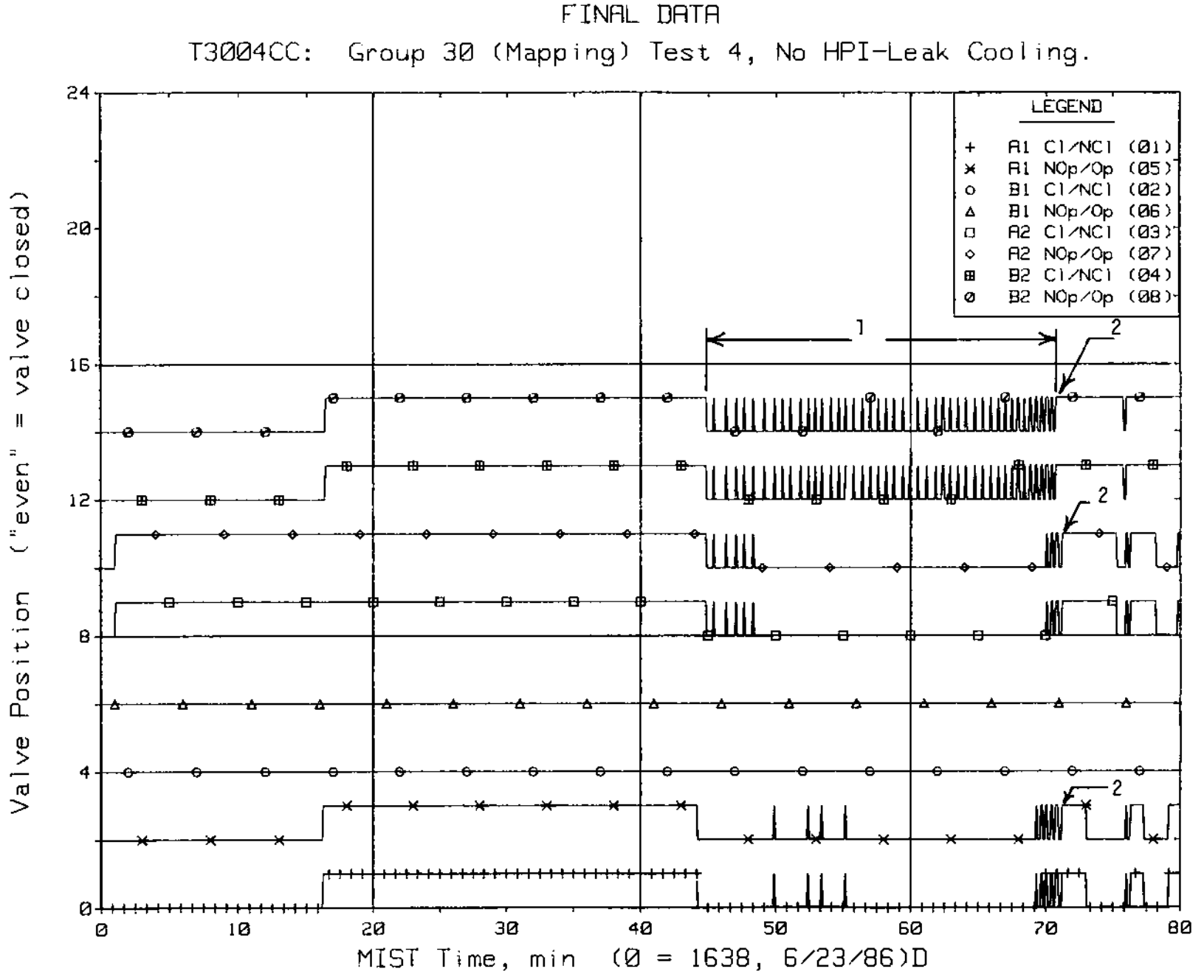

Figure 5.7.23. Reactor Vessel Vent Valve Limit Switch Indications (RVLSs)

Tue Mar 14 11:20:16 1989

VVLS2

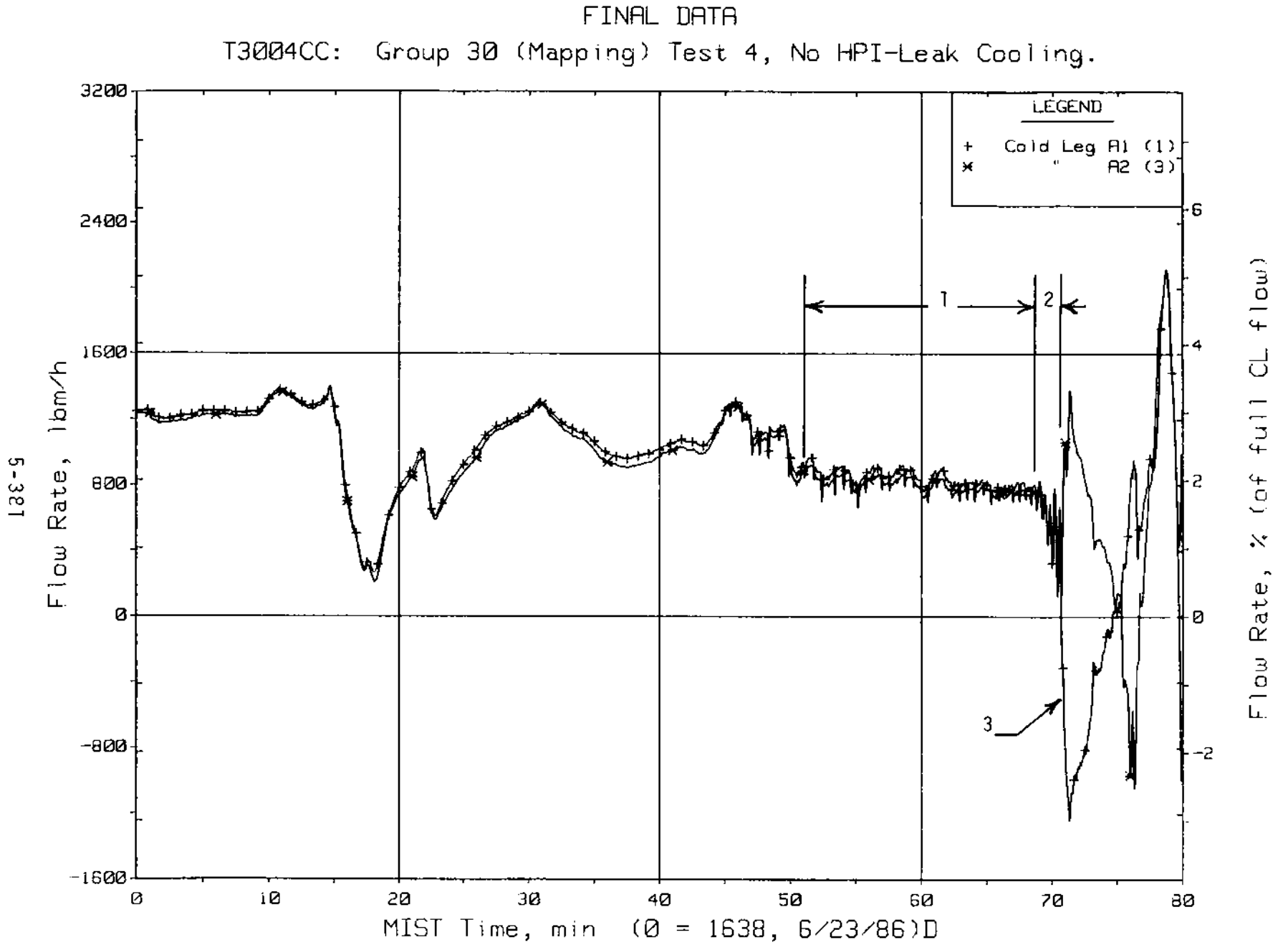

Figure 5.7.24. Loop A Cold Leg (Venturi) Flow Rates (CnVN20s)

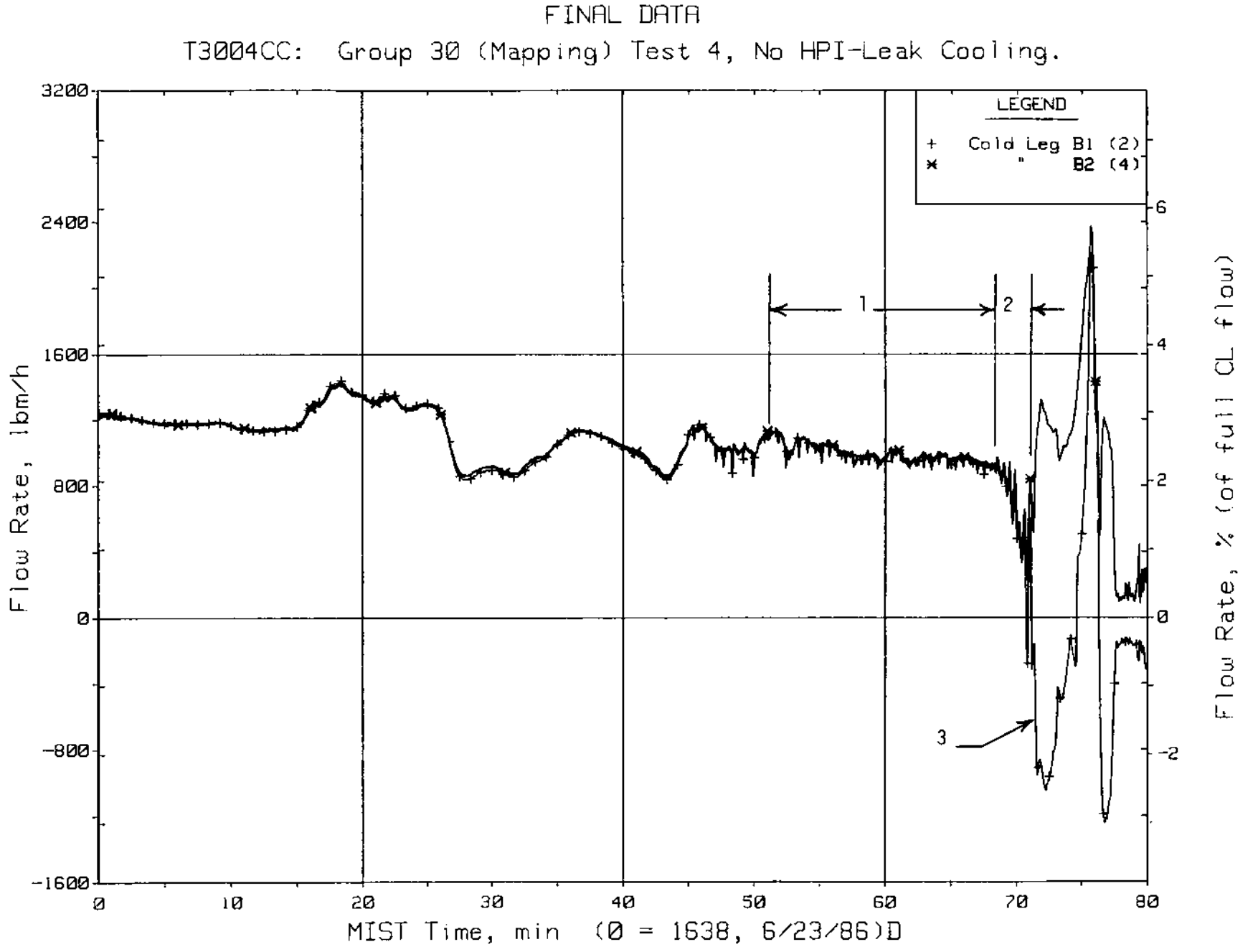

Figure 5.7.25. Loop B Cold Leg (Venturi) Flow Rates (CnVN20s)

Tue Mar 14 11:08:41 1989

PRFL6

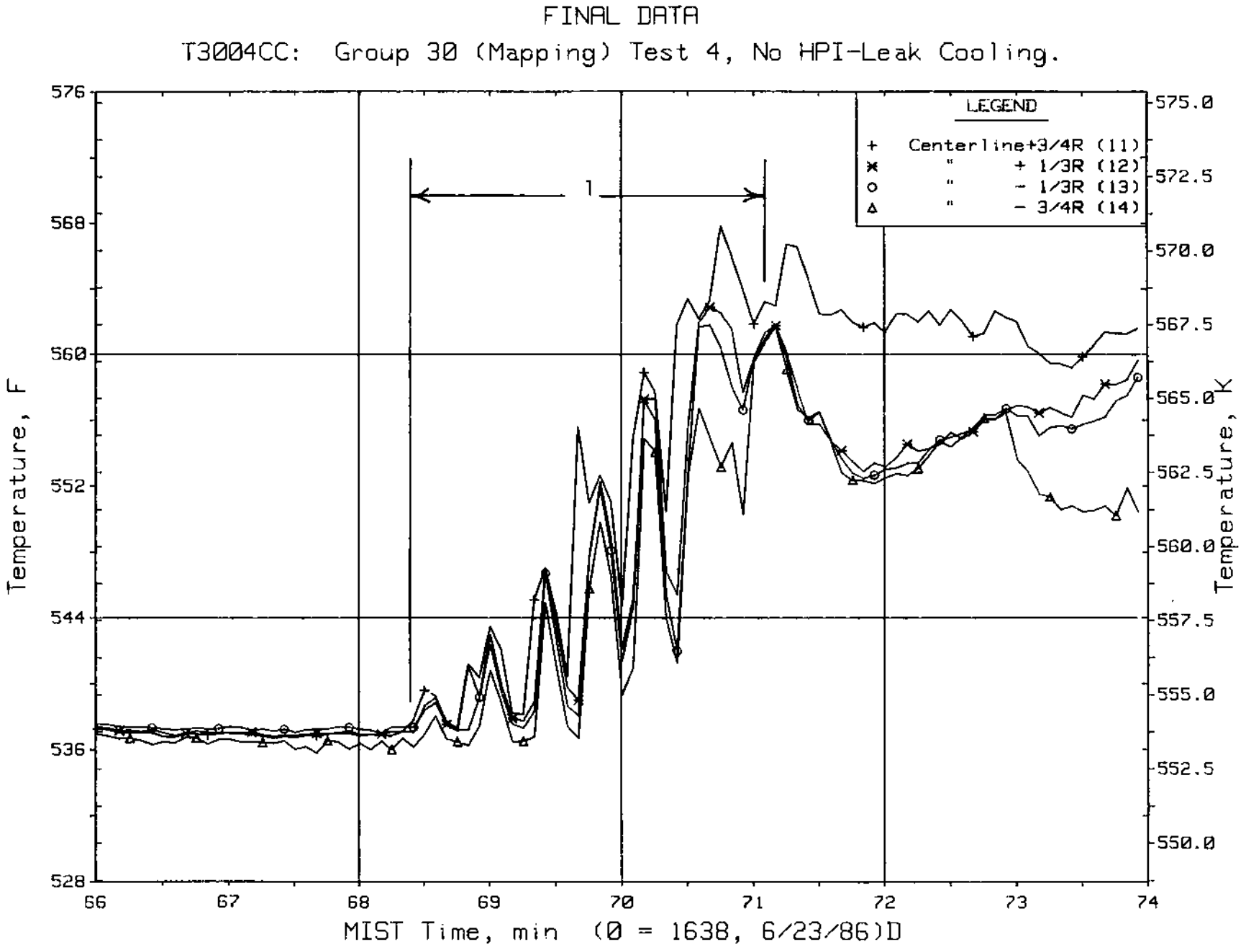

Figure 5.7.26. Cold Leg A1 Nozzle Rake Fluid Temperatures (21.2 ft, C1TCs)

Tue Mar 14 11:01:18 1989

C1TC4

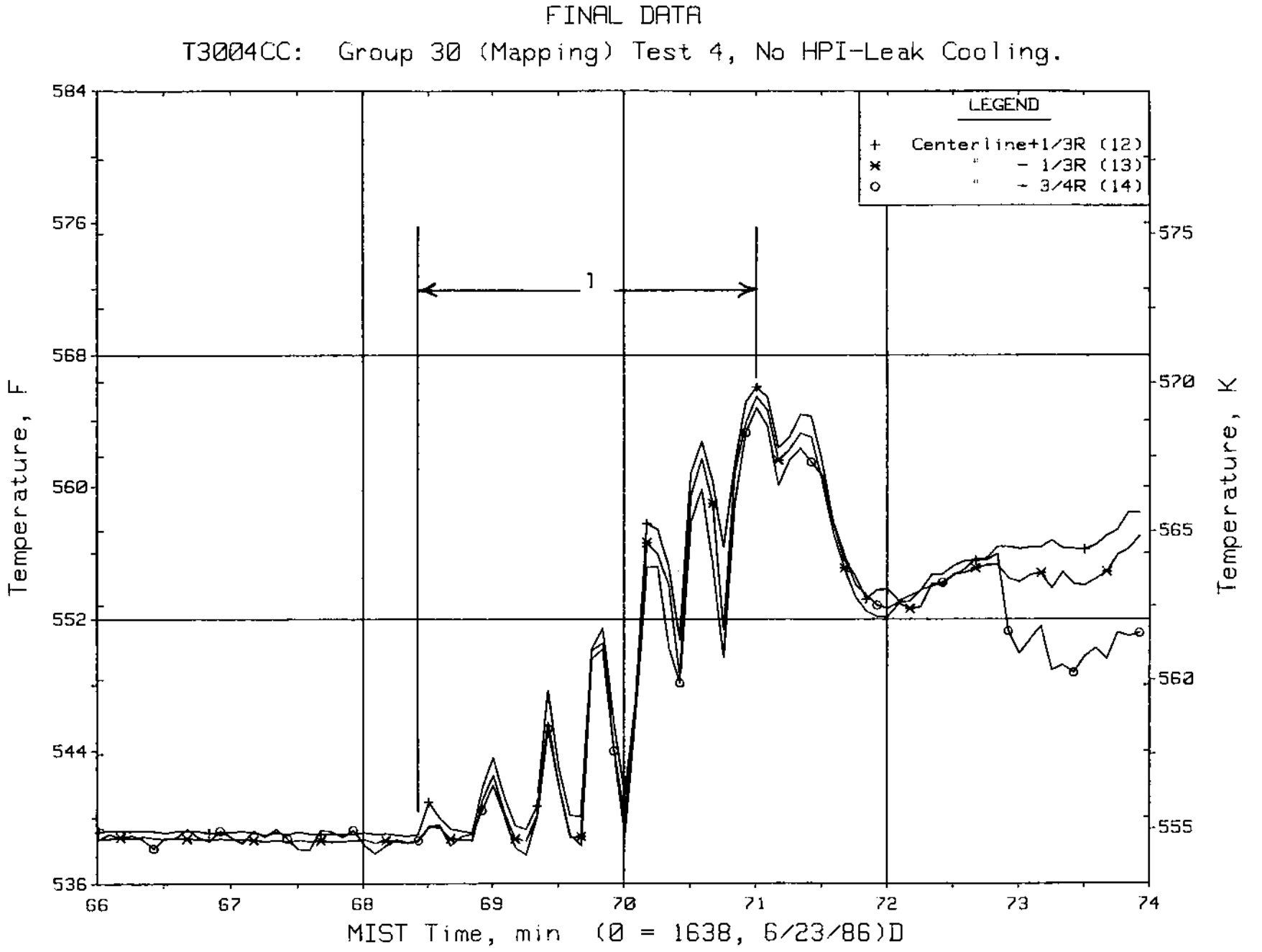

Figure 5.7.27. Cold Leg B1 Nozzle Rake Fluid Temperatures (21.2 ft, C2TCs)

Tue Mar 14 10:58:50 1989

C2TC4

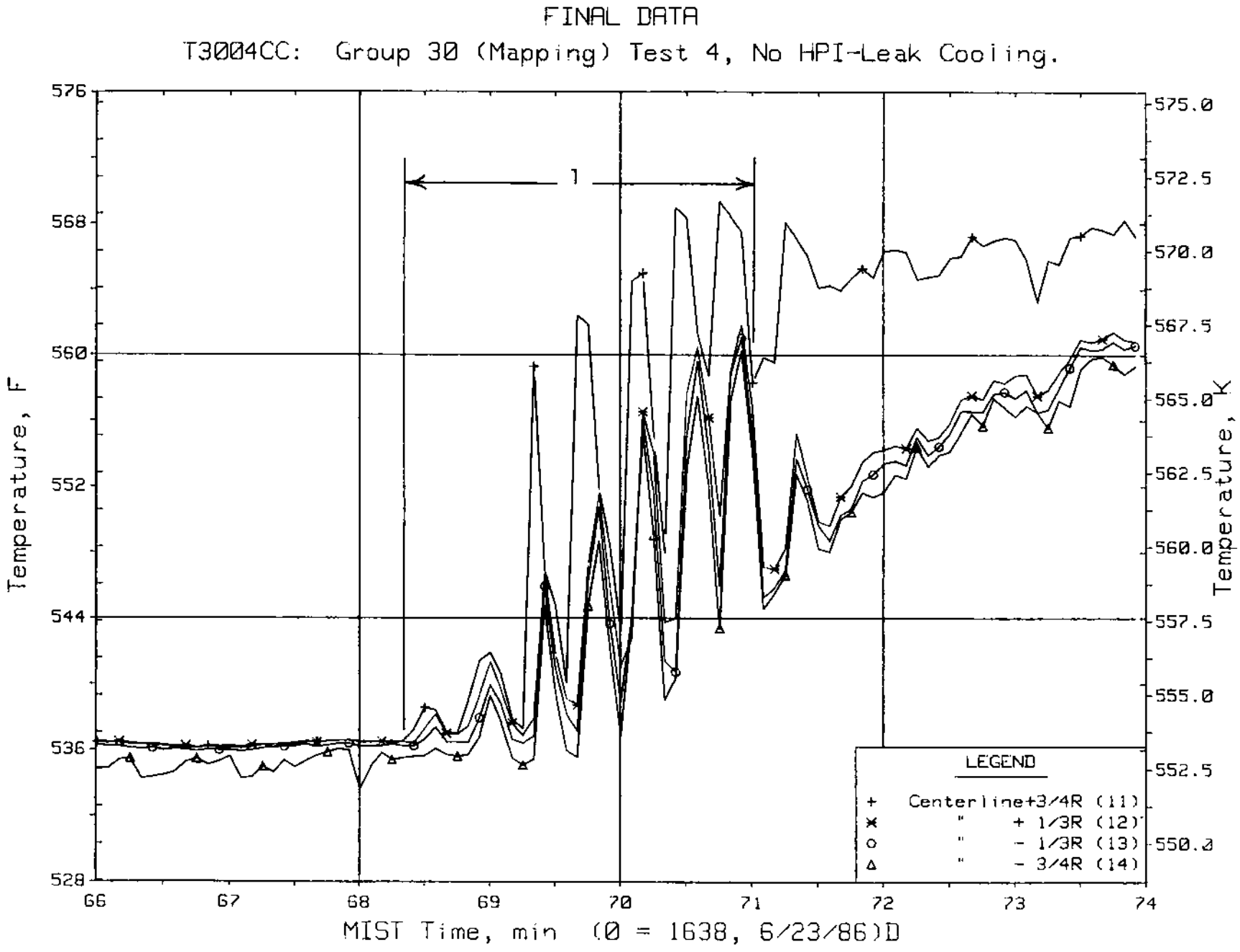

Figure 5.7.28. Cold Leg A2 Nozzle Rake Fluid Temperatures (21.2 ft, C3TCs)

Tue Mar 14 10:56:33 1989

C3TC4

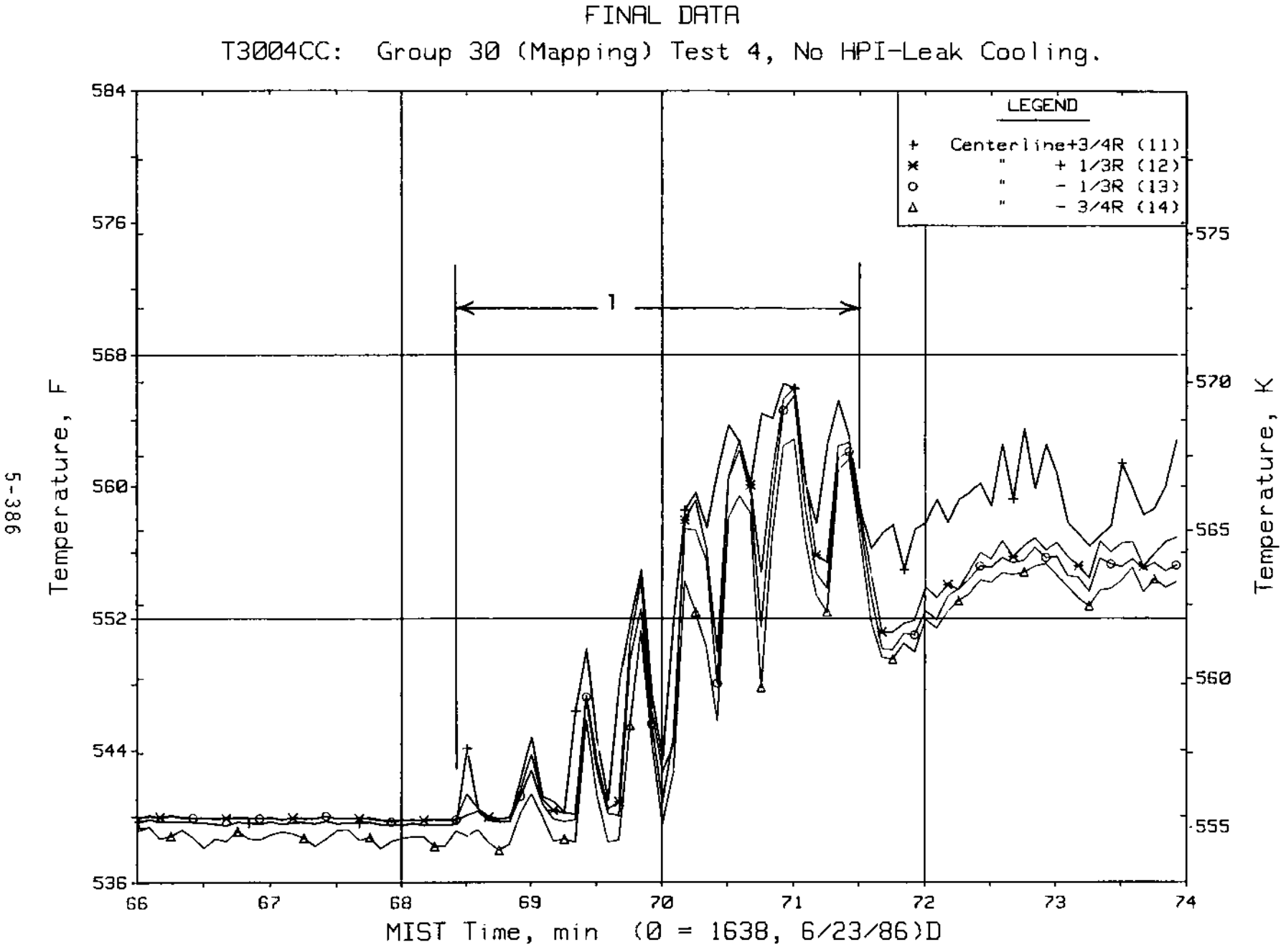

Figure 5.7.29. Cold Leg B2 Nozzle Rake Fluid Temperatures (21.2 ft, C4TCs)

Tue Mar 14 10:54:34 1989

C4TC4

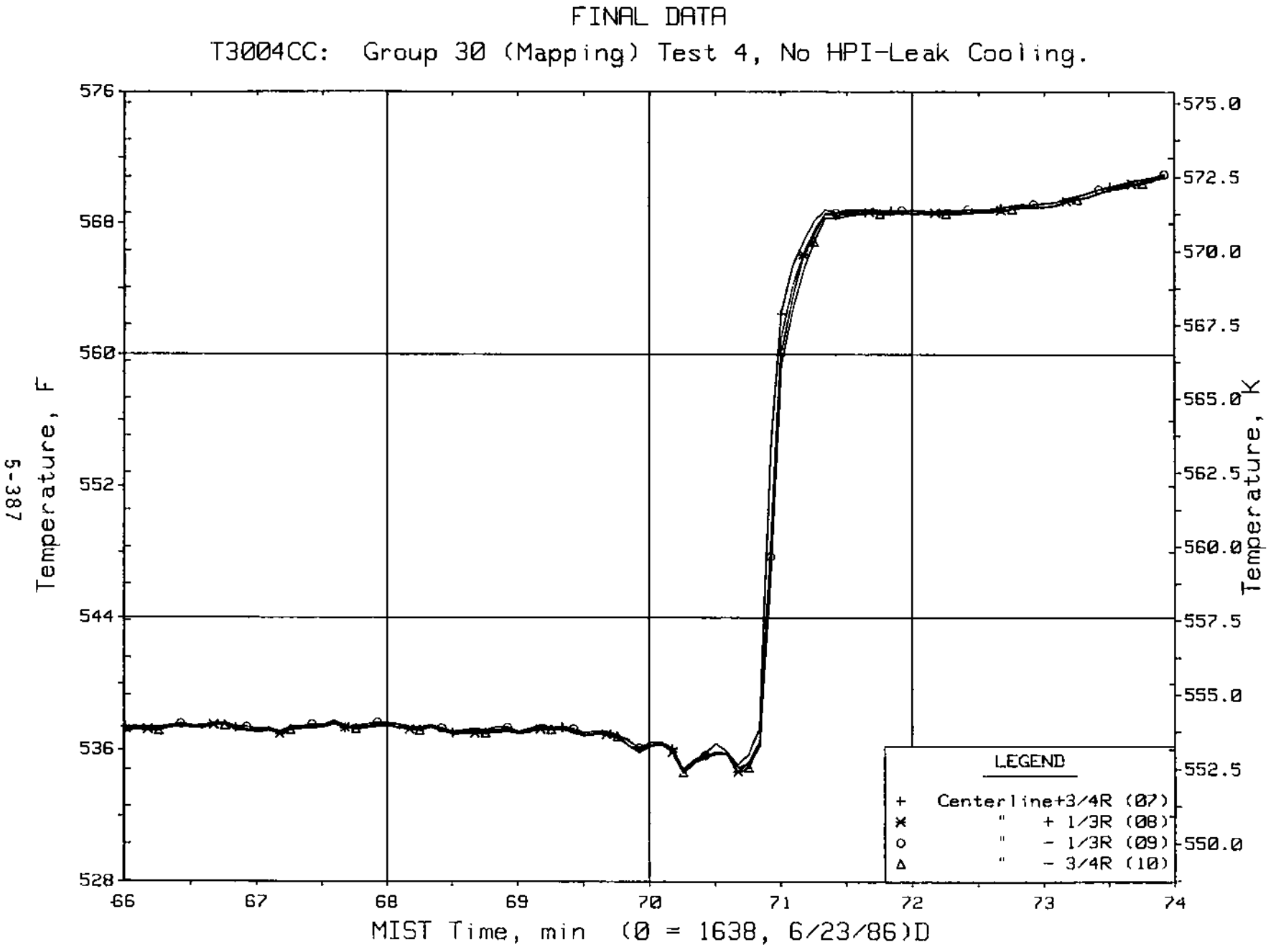

Figure 5.7.30. Cold Leg A1 Pump Discharge Rake Fluid Temperatures (25 ft, C1TCs)

Mon Mar 13 17:27:56 1989

C1TC3

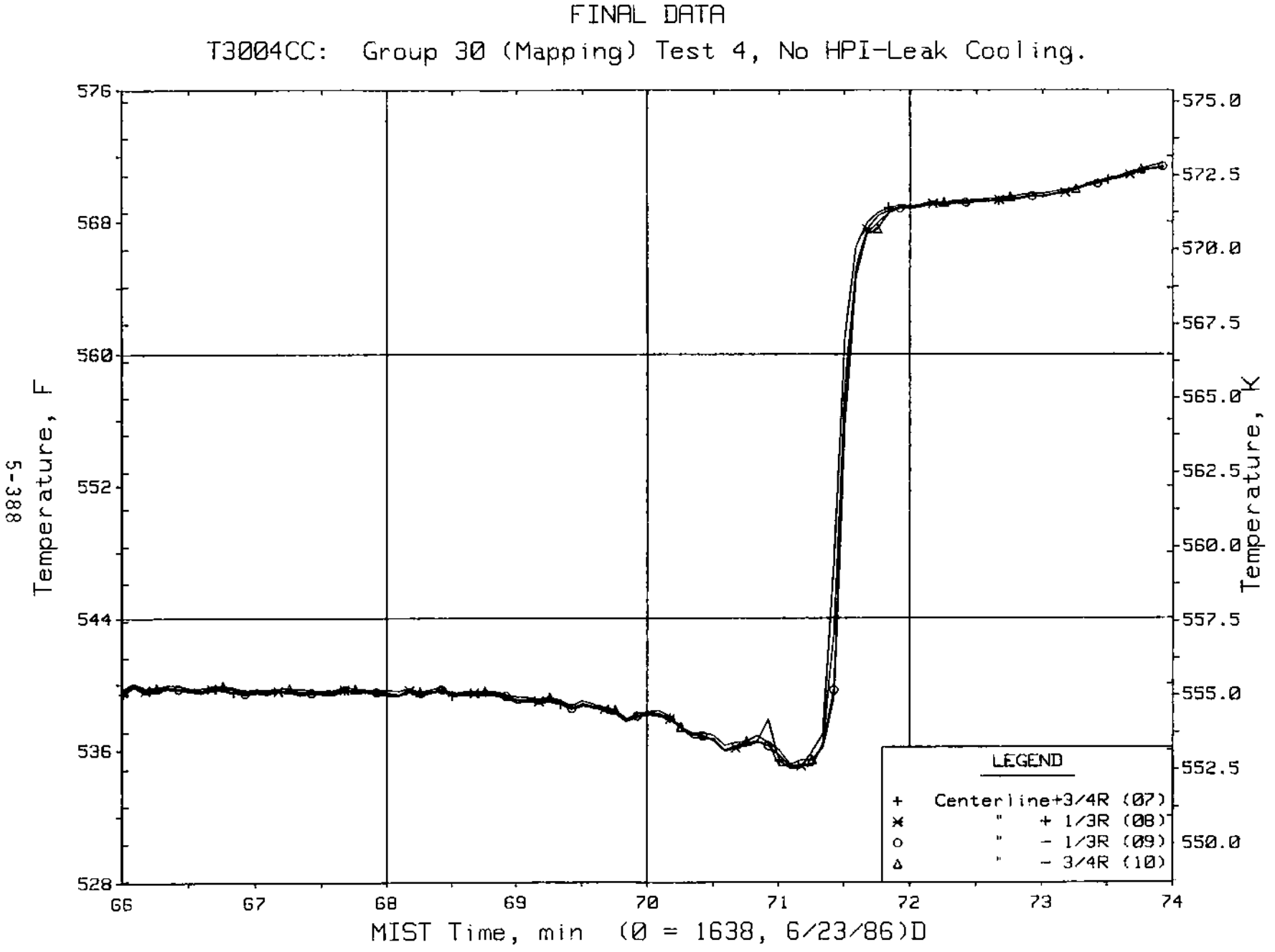

Figure 5.7.31. Cold Leg B1 Pump Discharge Rake Fluid Temperatures (25 ft, C2TCs)

Mon Mar 13 17:25:50 1989

C2TC3

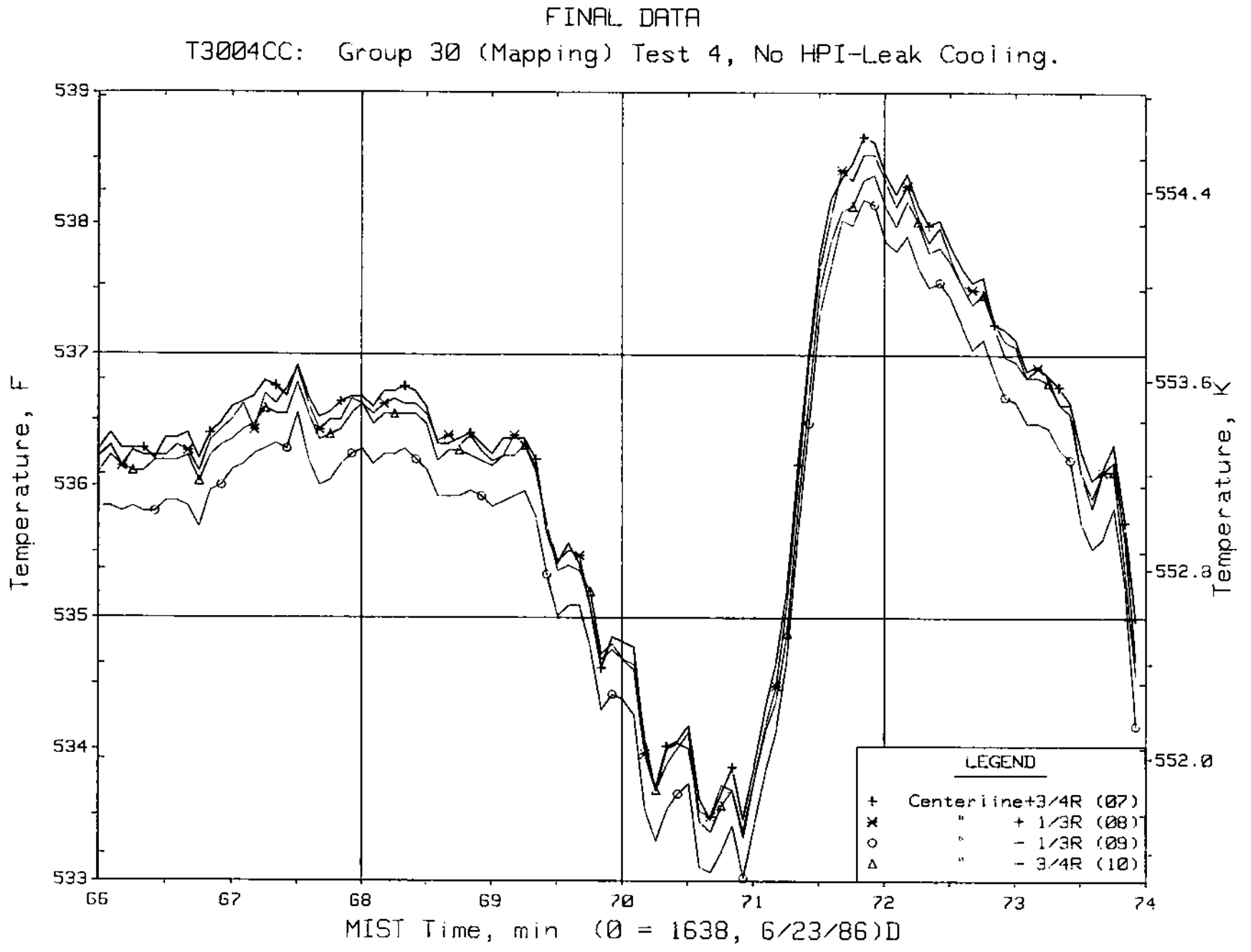

Figure 5.7.32. Cold Leg A2 Pump Discharge Rake Fluid Temperatures (25 ft, C3TCs)

Mon Mar 13 12:23:51 1989

C3TC3

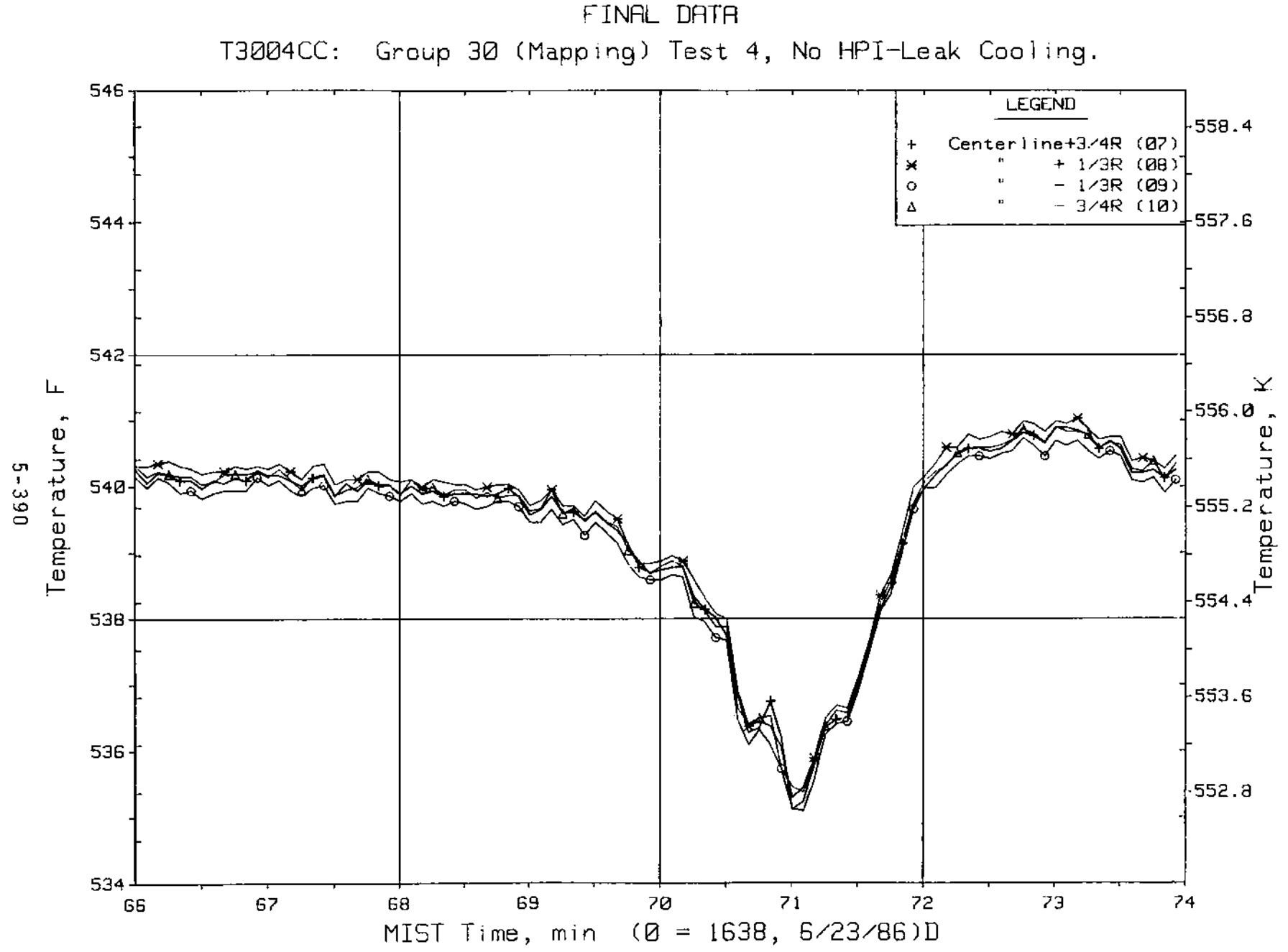

Figure 5.7.33. Cold Leg B2 Pump Discharge Rake Fluid Temperatures (25 ft, C4TCs)

Mon Mar 13 17:21:46 1989

C4TC3

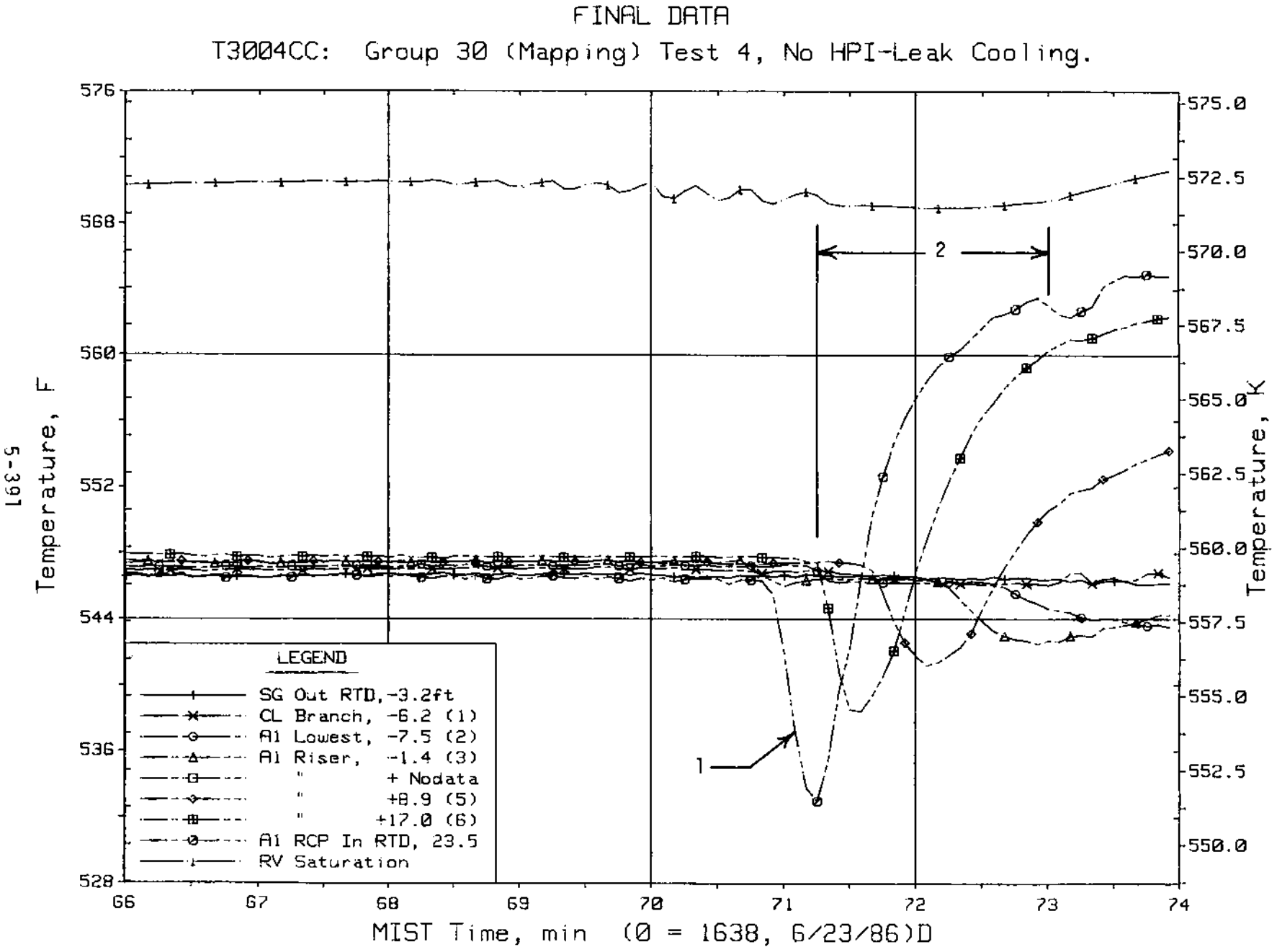

Figure 5.7.34. Cold Leg A1 Suction Fluid Temperatures (C1TCs)

Mon Mar 13 17:19:19 1989

C1TC1

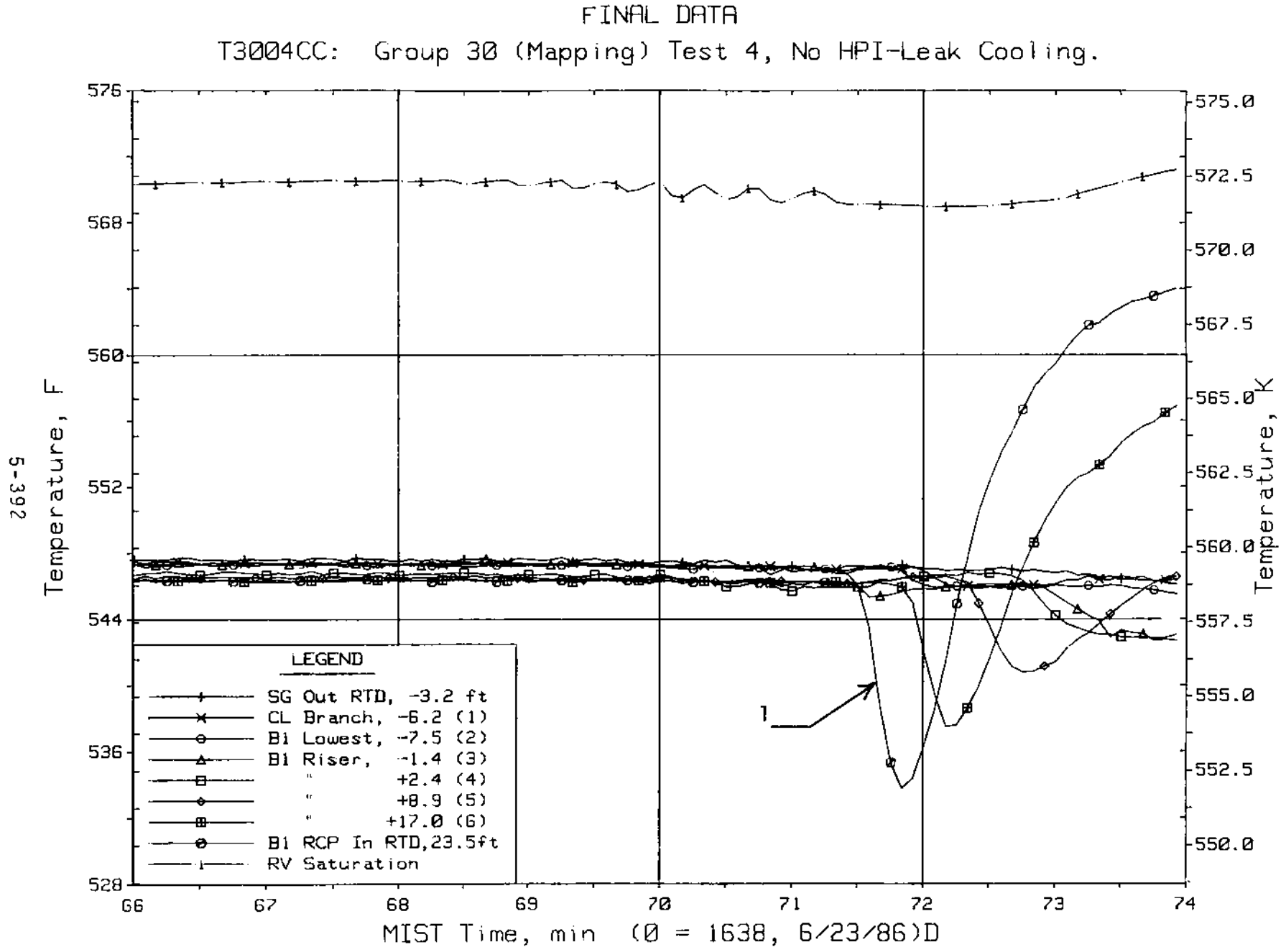

Figure 5.7.35. Cold Leg Bl Suction Fluid Temperatures (C2TCs)

Mon Mar 13 17:16:19 1989

C2TC1

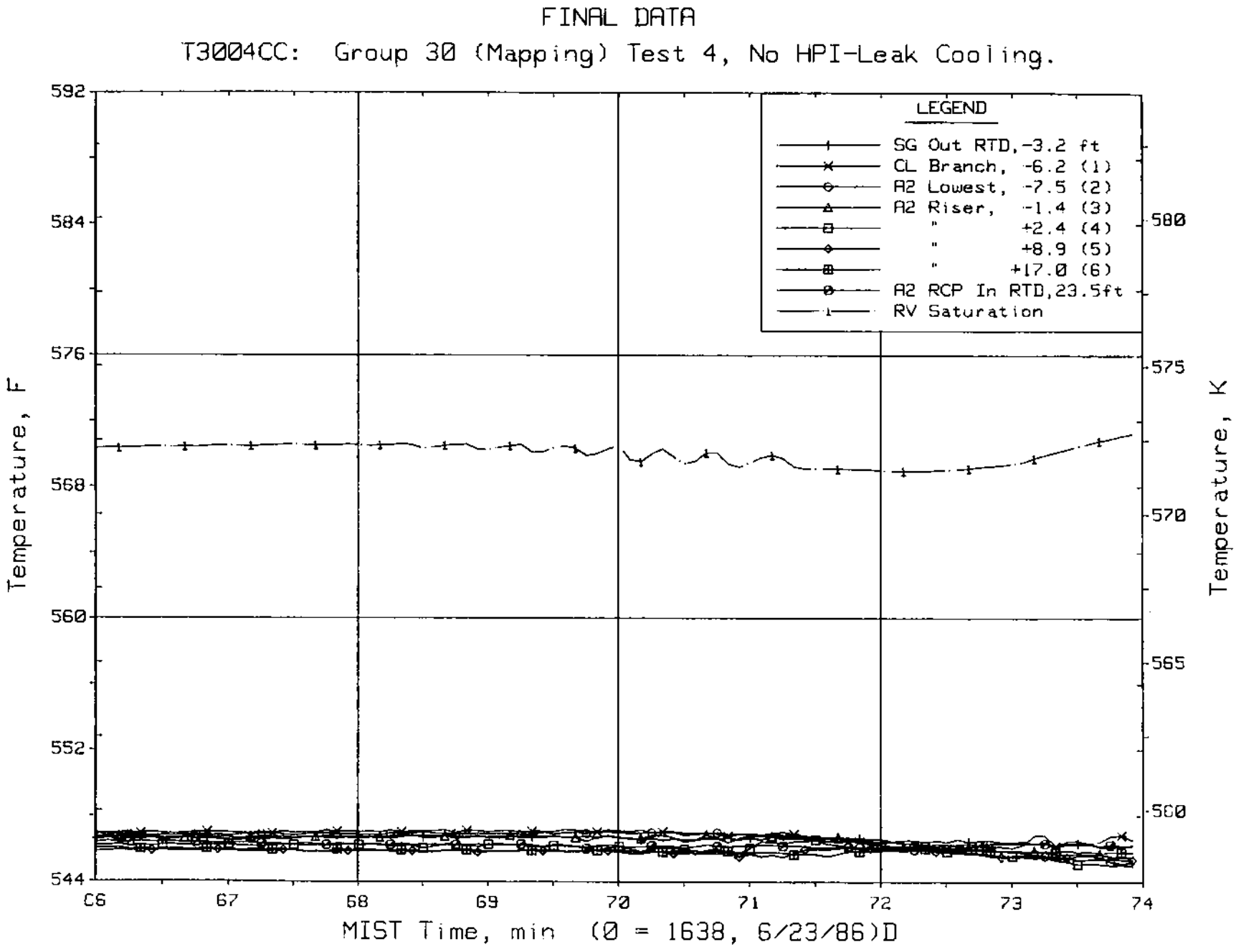

Figure 5.7.36. Cold Leg A2 Suction Fluid Temperatures (C3TCs)

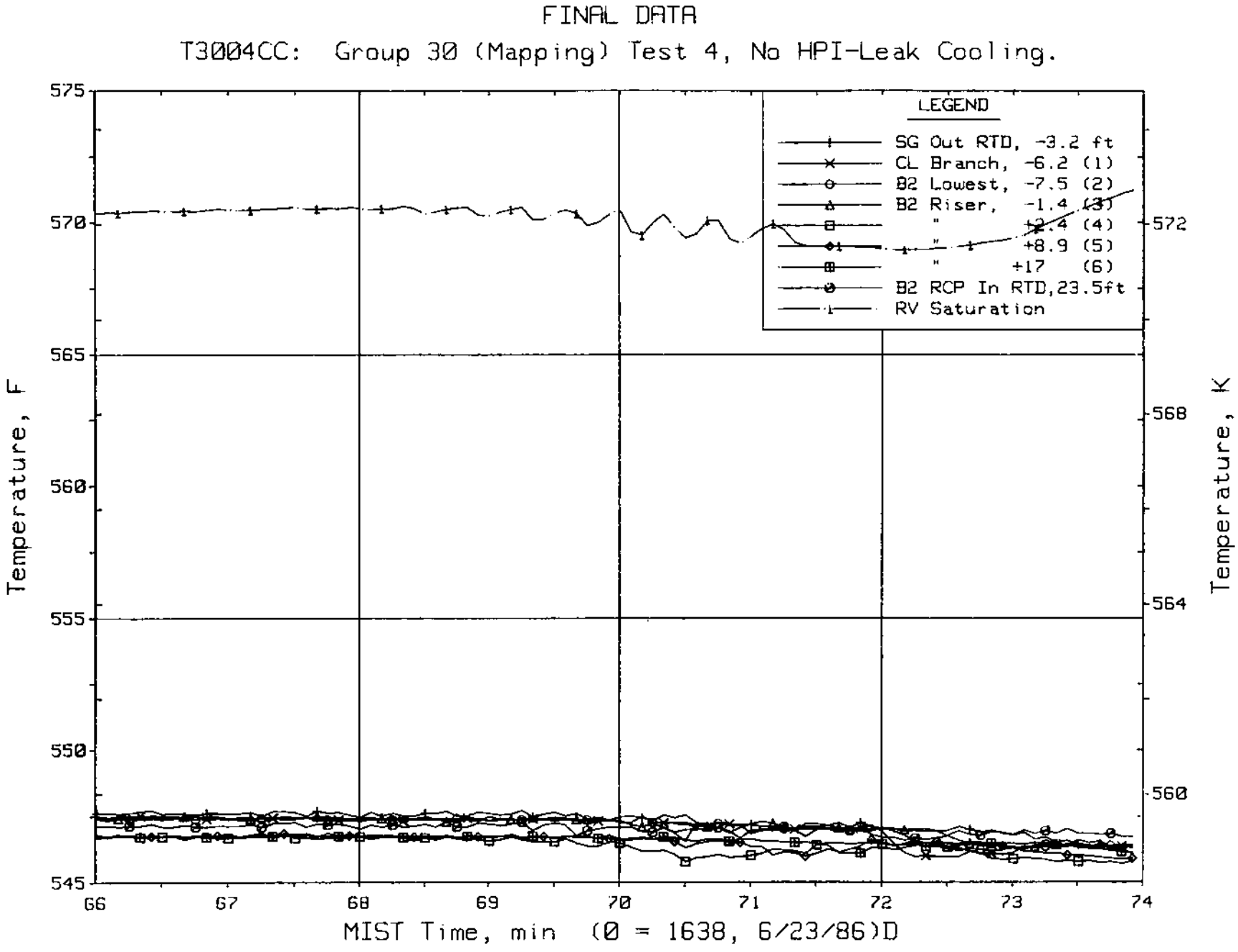

Figure 5.7.37. Cold Leg B2 Suction Fluid Temperatures (C4TCs)

Mon Mar 13 12:11:04 1989

C4TC1

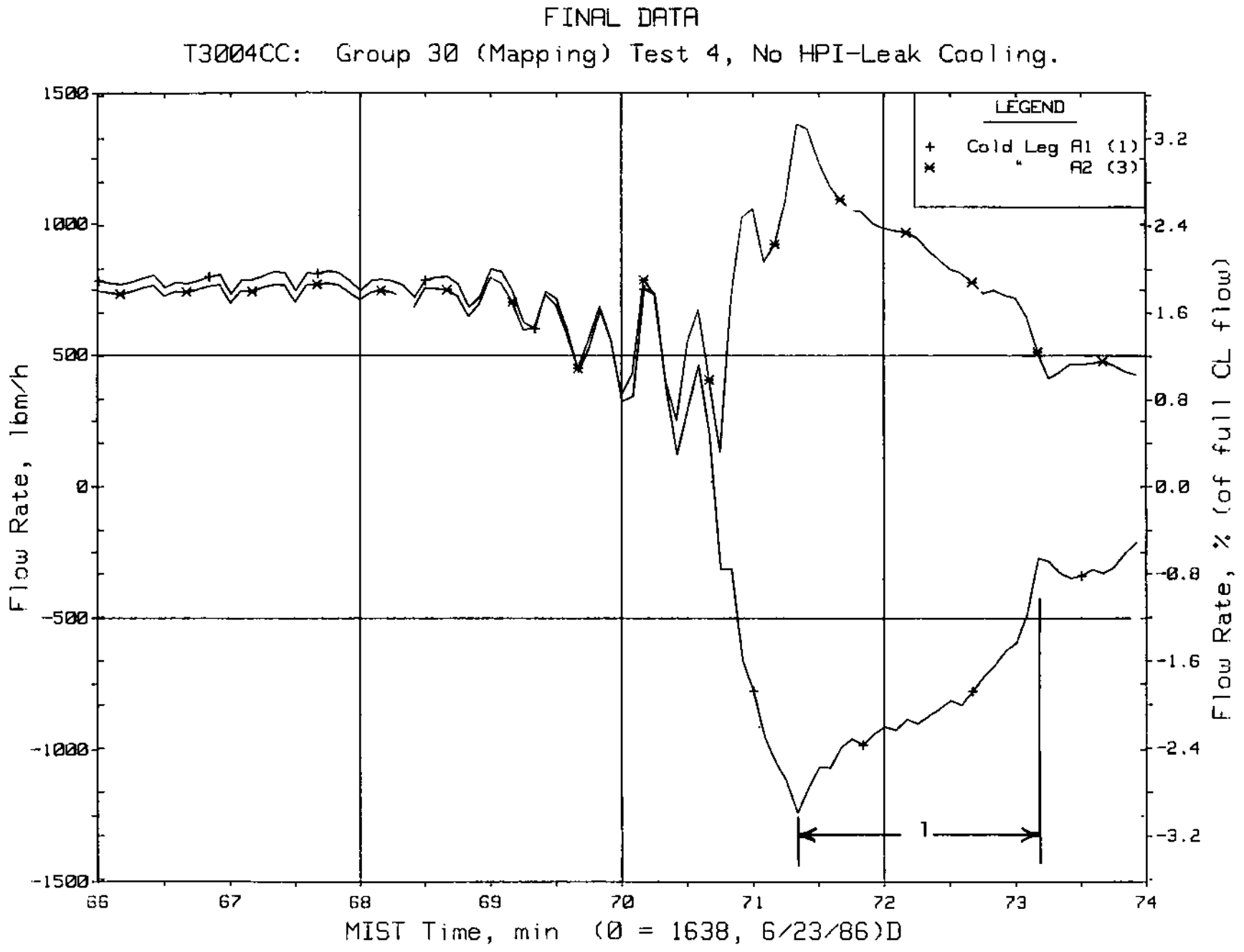

Figure 5.7.38. Loop A Cold Leg (Venturi) Flow Rates (CnVN20s)

Mon Mar 13 17:08:35 1989

PRFLS

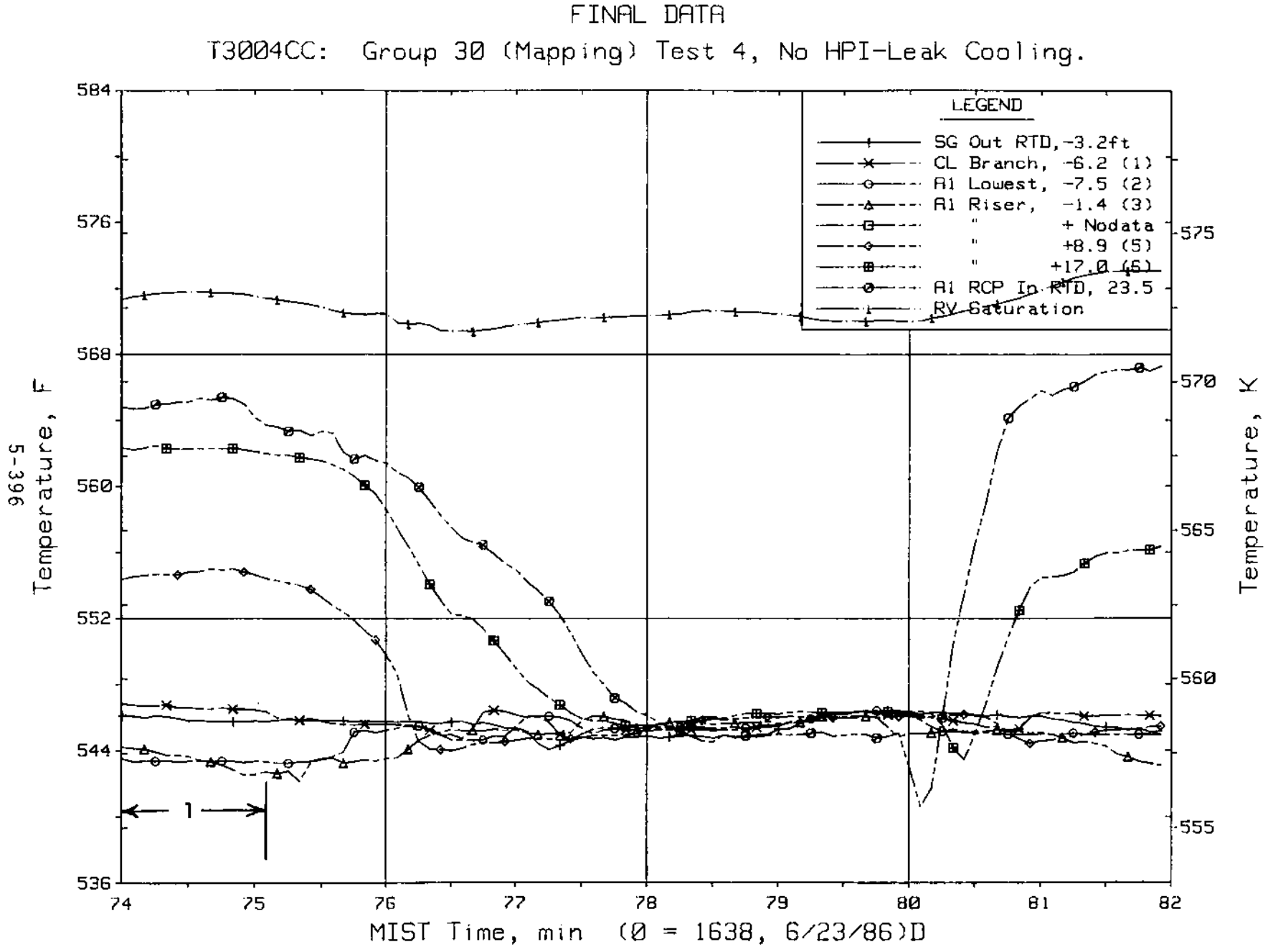

Figure 5.7.39. Cold Leg A1 Suction Fluid Temperatures (C1TCs)

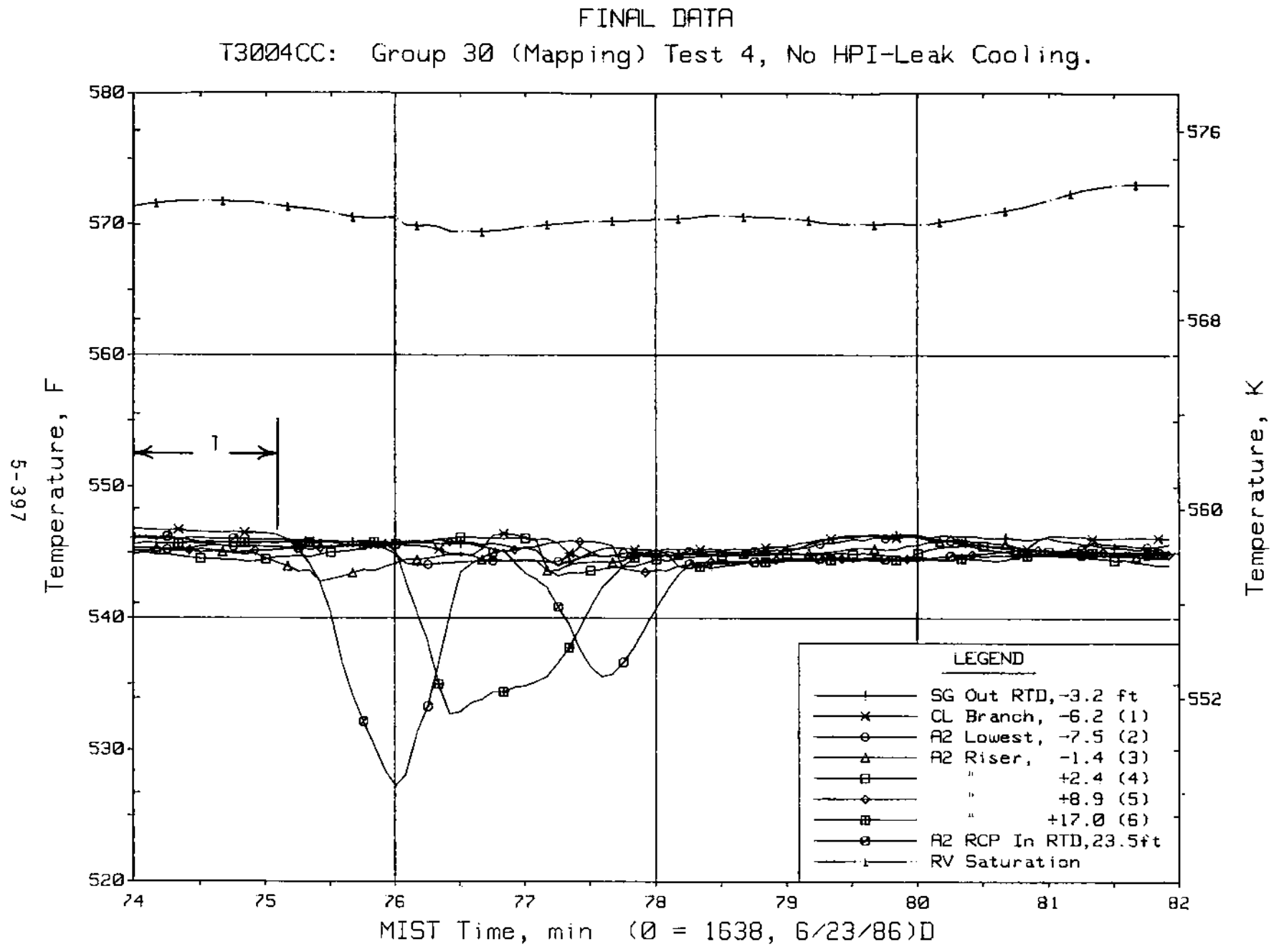

Figure 5.7.40. Cold Leg A2 Suction Fluid Temperatures (C3TCs)

Mon Mar 13 17:01:55 1989

C3TC1

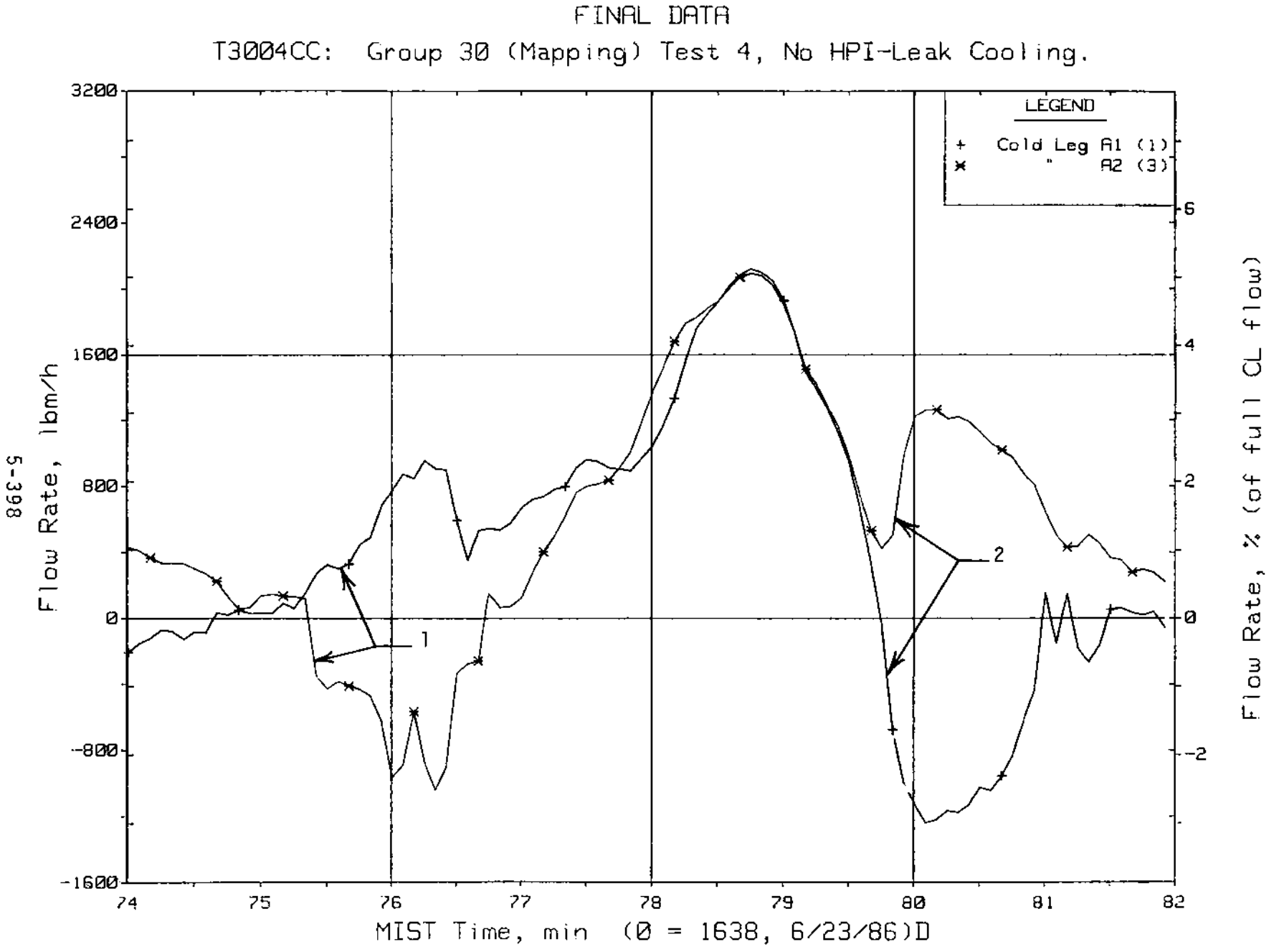

Figure 5.7.41. Loop A Cold Leg (Venturi) Flow Rates (CnVN20s)

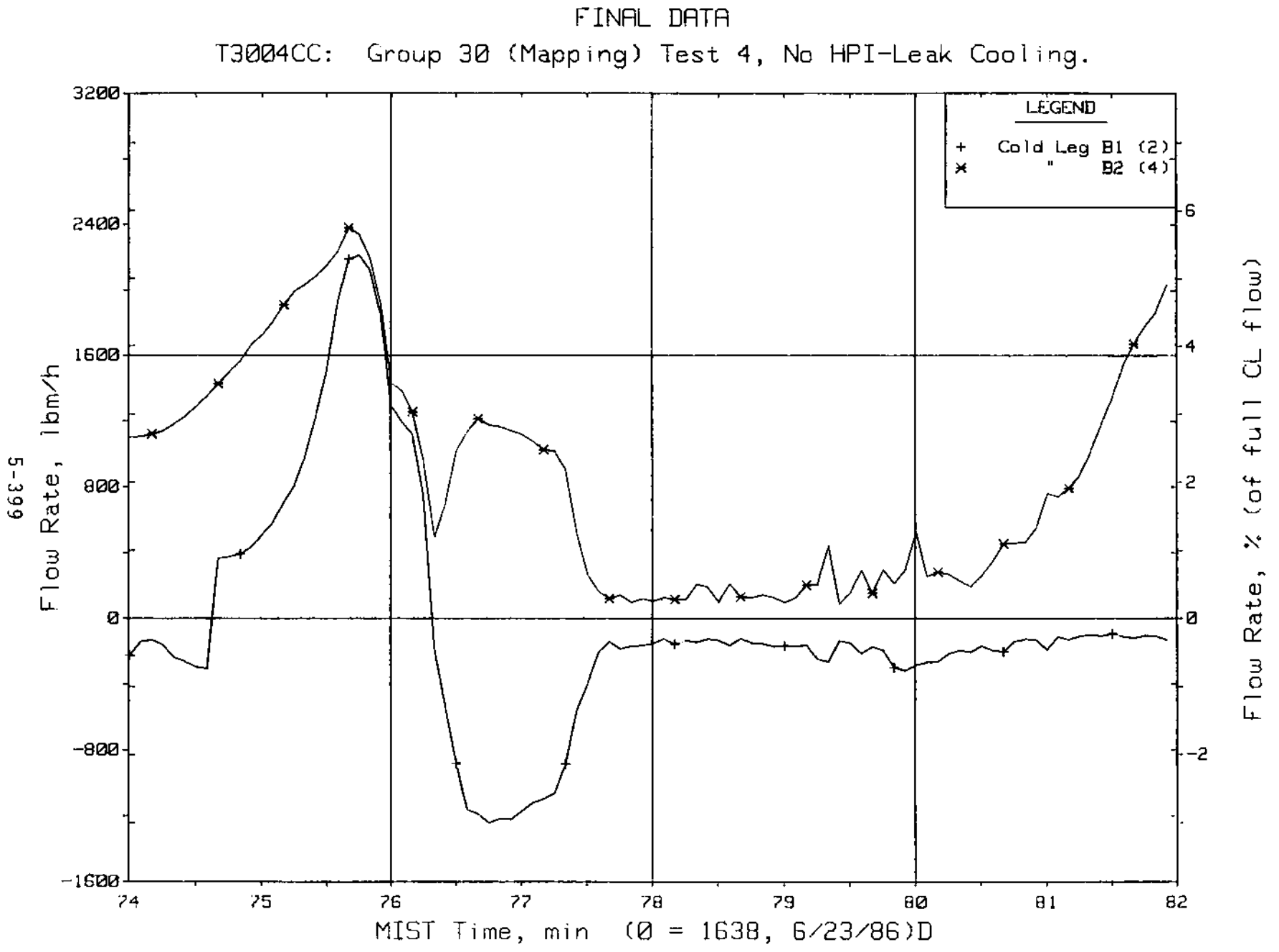

Figure 5.7.42. Loop B Cold Leg (Venturi) Flow Rates (CnVN20s)

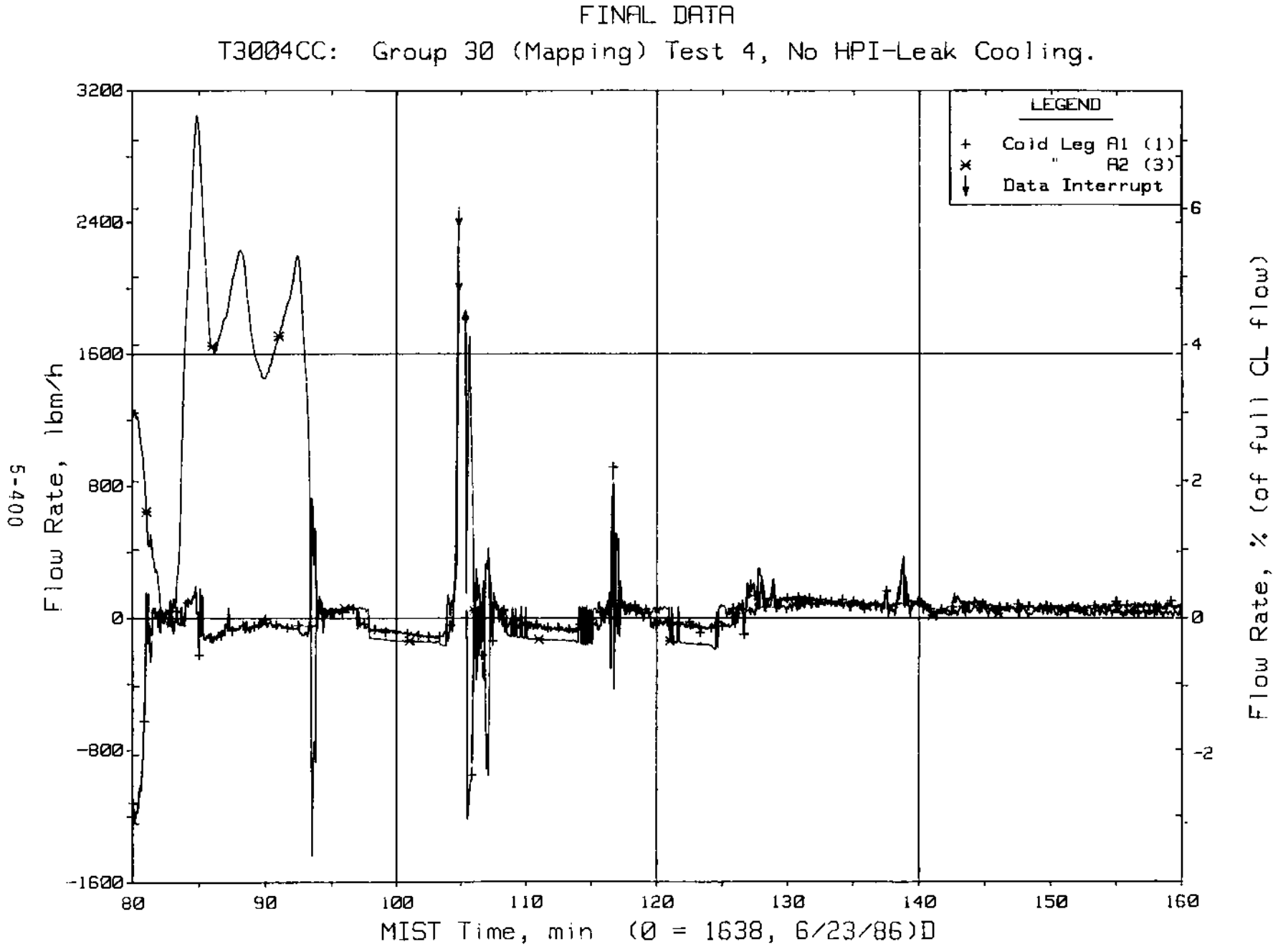

Figure 5.7.43. Loop A Cold Leg (Venturi) Flow Rates (CnVN20s)

Mon Mar 13 16:52:31 1989

PRFL5

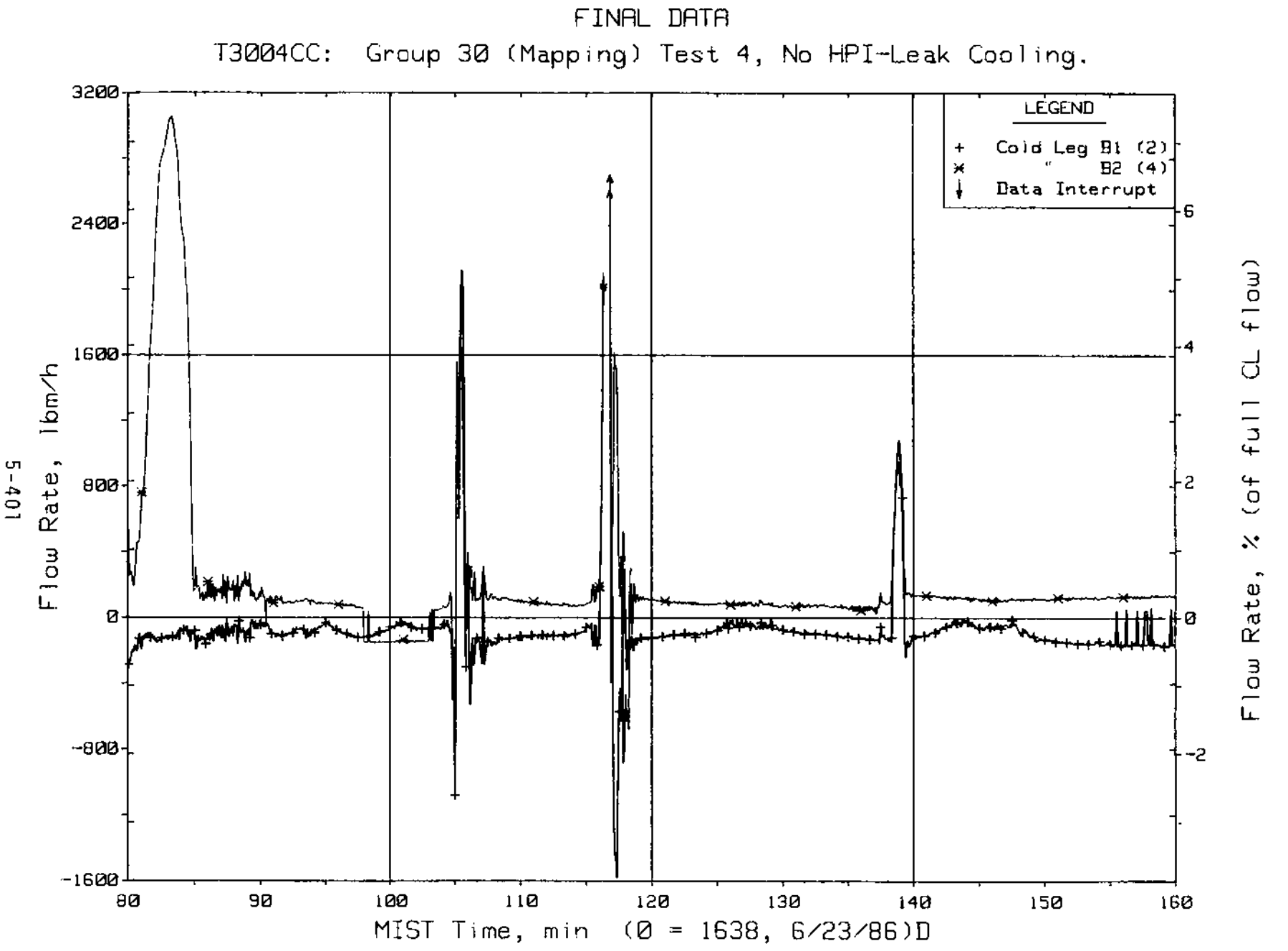

Figure 5.7.44. Loop B Cold Leg (Venturi) Flow Rates (CnVN20s)

Mon Mar 13 16:47:07 1989

PRFLG

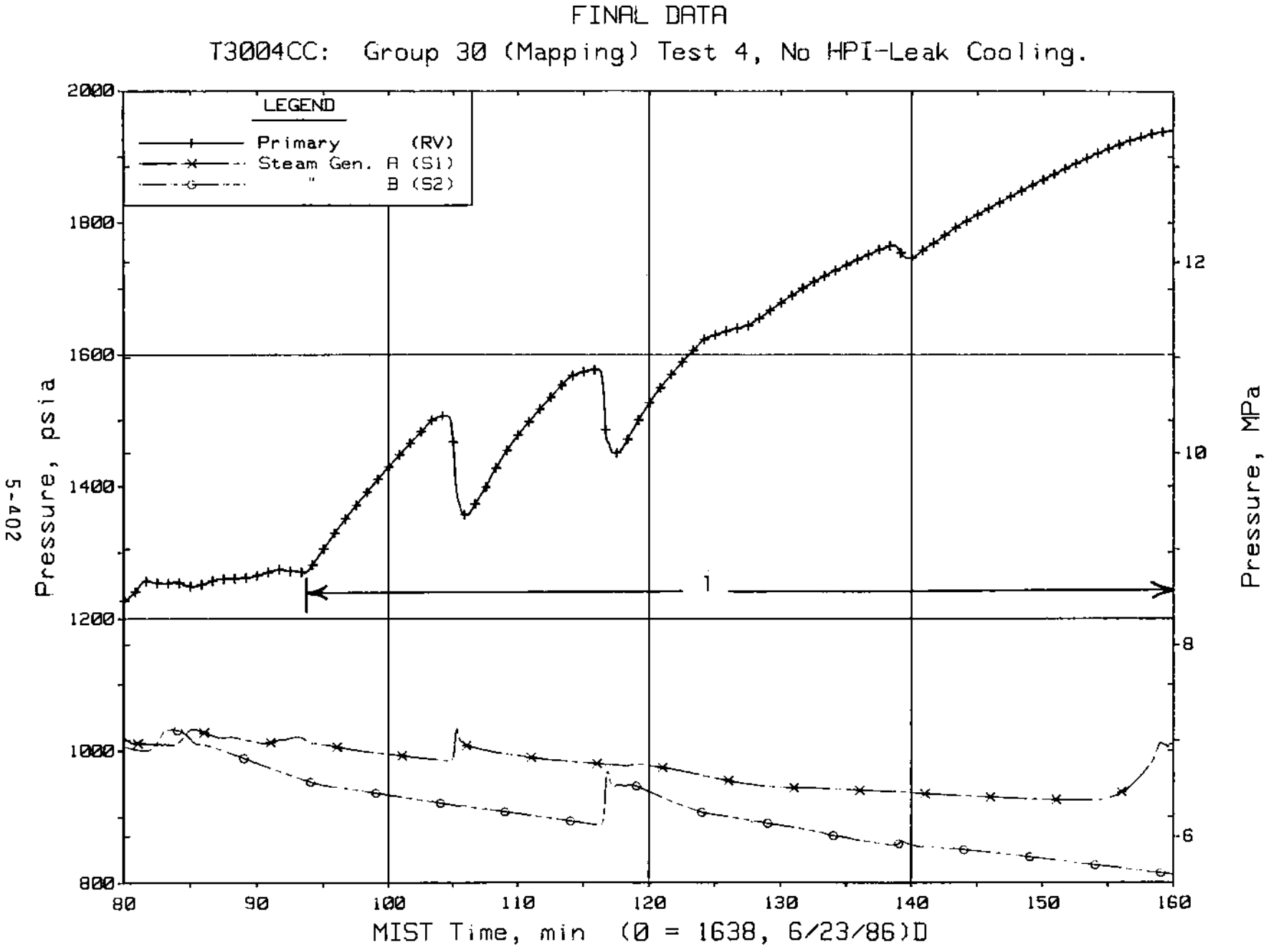

Figure 5.7.45. Primary and Secondary System Pressures (GPOIs)

Mon Mar 13 16:41:44 1989

PSGP1

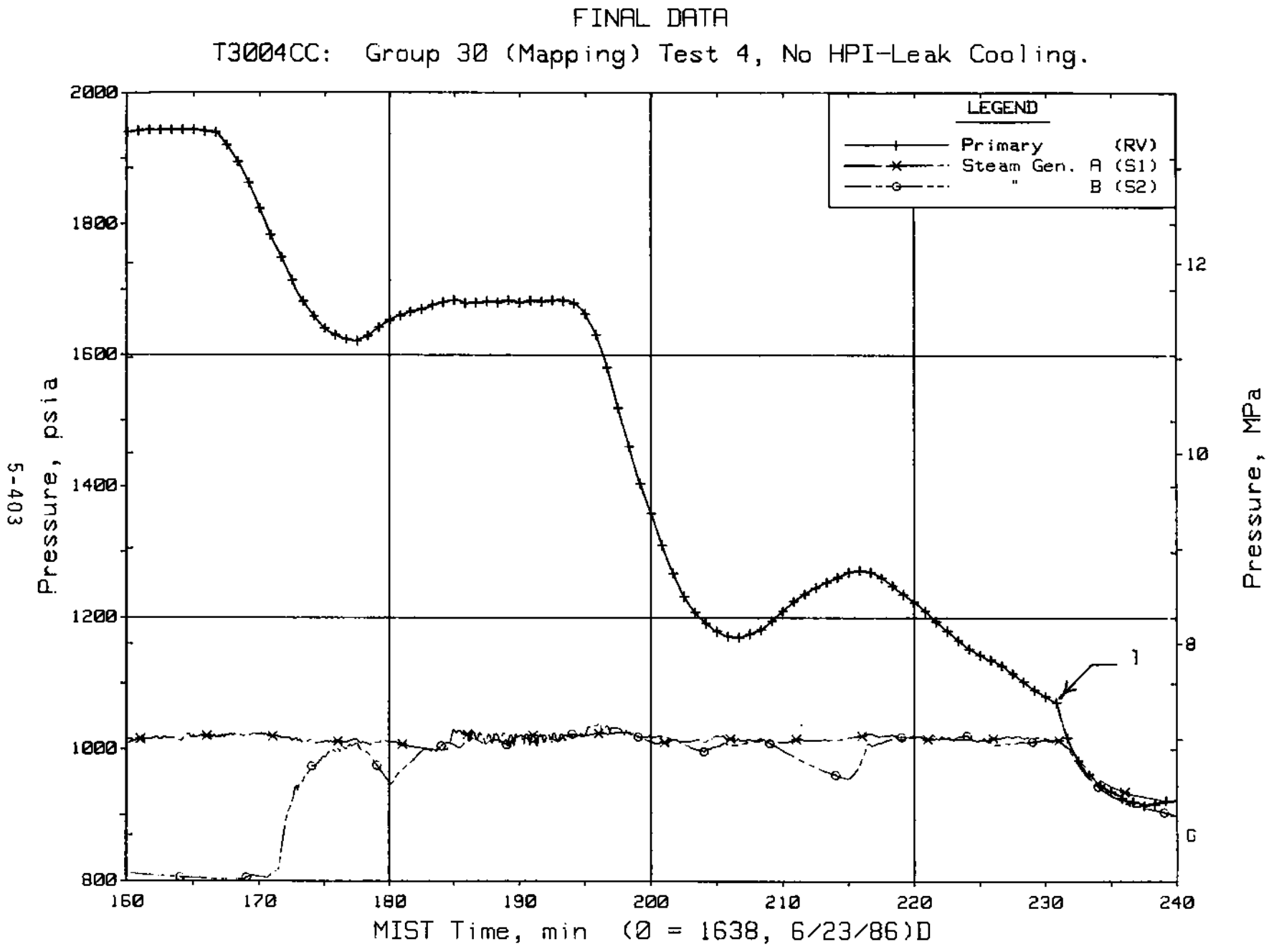

Figure 5.7.46. Primary and Secondary System Pressures (GP01s)

5.8. Increased Leak Size Test (30001)

This test differed from the Nominal Test (3003AA) in only the size of the leak. The leak size used was a scaled 10-cm^2 leak located at the downcomer-reactor vessel crossover pipe.

Test 300001 maintained approximately 10 minutes of steady-state conditions with the leak and HPI flow activated. The steam generator secondary pressure was not as specified for this test. As a result of the increased leak size, the leak-HPI cooling was in excess of that anticipated. The remaining energy to be transferred in the steam generators was therefore insufficient to maintain the steam generator secondary pressure at 1010 psia. As the HPI flow rate was reduced to establish the leak-HPI deficit, the primary system pressure decreased. The reduction in the primary system pressure resulted in a decreased leak flow rate and, therefore, less core energy was removed via leak-HPI cooling. This action resulted in a heatup of the primary system, which increased primary-to-secondary heat transfer, and the steam generator secondary pressure increased to 1010 psia. The response and the phenomena observed for this test did not appear to be affected by this difference in the specified initial condition.

The primary system pressure decreased as the leak-HPI deficit was established and attained a minimum pressure of approximately 1135 psia (Figure 5.8.1, See 1), at which time the core exit reached saturated conditions (Figure 5.8.2, See 1). The reactor vessel upper head then began voiding, the reactor vessel level decreased (Figure 5.8.3, See 1), and the primary system pressure began a gradual repressurization (Figure 5.8.4, See 1). All the reactor vessel vent valves were open from the time of test initiation until the time when the reactor vessel level descended to the reactor vessel vent valve elevation (Figure 5.8.3, See 2), at which time the reactor vessel vent valves began cycling (Figure 5.8.5, See 1). The characteristic reactor vessel vent valve cycling also occurred for this test as the pressure between the reactor vessel and the downcomer equalized as the downcomer level decreased.

This cyclical reactor vessel vent valve response also resulted in an oscillating and decreasing trend of the loop flow rates (See 1 on Figures 5.8.6 and 5.8.7), and counter-current flow began to be observed at the cold leg nozzle (See 1 on Figures 5.8.8 through 5.8.11). As the downcomer level

descended to the cold leg nozzle elevation, the reactor vessel vent valves cycled more frequently, then opened and remained open (Figure 5.8.12, See 1). The primary loop flow rates also decreased significantly during this period (See 2 on Figures 5.8.6 and 5.8.7).

The response and phenomena exhibited by this test were similar to that observed for the Nominal Test (3003AA) and other Mapping Tests through this phase of the test.

The primary system pressure had been increasing gradually, attaining a maximum of approximately 1245 psia (Figure 5.8.13, See 1). However, as the primary loop flows decreased significantly (See 2 on Figures 5.8.6 and 5.8.7), a gradual depressurization occurred (Figure 5.8.13, See 2). At this time, both hot leg risers indicated full to the spillover elevation (Figure 5.8.14, See 1), steam generator heat transfer decreased (Figure 5.8.13, See 3), AFW eventually terminated (See 1 on Figures 5.8.15 and 5.8.16), the reactor vessel vent valve flow rate increased (Figure 5.8.17, See 1), and core fluid temperatures increased (Figure 5.8.18, See 1). The initiating cause of this depressurization appears to be due to increased leak cooling as the downcomer and leak site temperatures increased because of the increased reactor vessel vent valve flow.

Subsequently, the flow rates in cold legs A1 and A2 increased (Figure 5.8.6, See 3). The cold leg B1 flow rate also increased, however, the cold leg B2 flow rate remained essentially constant and then reversed flow direction; thus, intra-cold leg flow was established in loop B (Figure 5.8.7, See 3). The loop B intra-cold leg flow rate then decreased (Figure 5.8.19, See 1) as the driving head of the two B cold legs equalized. Intra-cold leg flow was reestablished in loop B. However, cold leg B1 flowed in the reverse direction, while B2 flowed forward (Figure 5.8.19, See 2). Loop A also established intra-cold leg flow (occurred after loop B had established intra-cold leg flow) with cold leg A2 flowing in the reverse flow direction (Figure 5.8.20, See 1).

After a number of flow reversals occurred in each loop, forward flow remained established in the cold legs A1 and B2 while the flow in the cold legs A2 and B1 interrupted (See 1 on Figures 5.8.21 and 5.8.22). This action was followed later by flow interruption in cold legs A1 and B2. The order of the

occurrence of cold leg flow interruption was B1, A2, B2, and A1. This order differed from that observed in the Nominal Test (3003AA). During this depressurization phase, the minimum primary system pressure attained was approximately 1200 psia (Figure 5.8.23) and the cold leg flow interruptions occurred at this pressure.

The flow interruption that occurred in cold leg B2 indicated that the cause for the interruption was the voiding of the cold leg discharge pipe. Core-generated steam was discharged through the reactor vessel vent valves into the downcomer and backflowed into the cold leg discharge pipe, thus voiding the pipe and terminating flow.

Figures 5.8.22 and 5.8.24 through 5.8.27 provide an example of cold leg discharge pipe voiding and its effect on the flow. Counter-current flow existed at the cold leg B2 discharge nozzle as indicated by the nozzle rake fluid temperatures (Figure 5.8.24, See 1). As the backflow increased, an increase in the fluid temperatures of the lower thermocouples of the nozzle rake (Figure 5.8.24, See 2) followed by a decrease in the cold leg B2 flow rate (Figure 5.8.22, See 2) was observed. (The decreasing cold leg flow rate also aids the cold leg heatup as less colder fluid was available to mix with the fluid that was backflowing. Thus, an increase in the mixed-mean fluid temperature resulted.) As the cold leg heatup continued, a gradual reduction in the cold leg B2 discharge level occurred (Figure 5.8.25, See 1). This reduction signified the onset of void formation in the cold leg B2 discharge pipe. As the fluid temperatures of the lower thermocouples of the nozzle rake approached saturation (Figure 5.8.24, See 3), the cold leg B2 discharge level decreased more rapidly (Figure 5.8.25, See 2). When the fluid temperatures of the lower thermocouples of the nozzle rake saturated (Figure 5.8.24, See 4), a very rapid decrease in the cold leg B2 discharge level occurred (Figure 5.8.25, See 3). During this time, the hot leg B riser level indicated a collapsed liquid level above the U-bend spillover elevation and a stub level below the U-bend spillover elevation (Figure 5.8.26, See 1). Flow existed in loop B via cold leg B2 during the cold leg heatup. However, flow was on a continuously decreasing trend (Figure 5.8.22, See 3) and decreased rapidly as the cold leg fluid temperatures at the nozzle rake approached saturation (Figure 5.8.22, See 4). At this time, flow interruption occurred

in cold leg B2 and as the cold leg discharge pipe continued to void out completely (Figure 5.8.25, See 4), an increase in the hot leg stub level occurred followed by a decrease in the hot leg riser level (Figure 5.8.26, See 2). The increase in the hot leg stub level was confirmed by the fluid temperature response of the steam generator inlet RTD as colder fluid that had resided in the steam generator was displaced upwards into the stub (Figure 5.8.27, See 1). Thus, a pressure balance was established between the reactor coolant pump (the top of the cold leg suction pipe) and the hot leg stub region that supported a higher column of liquid (prior to the voiding of the cold leg discharge pipe, the pressure balance was between the cold leg nozzle and the hot leg stubs).

Upon complete flow interruption, the primary system repressurized, attaining a maximum pressure of approximately 1570 psia. The phenomena and the primary system response observed during this repressurization through test termination were similar to those observed for the Nominal Test (3003AA). The primary system depressurized to approximately 1090 psia at test termination (Figure 5.8.28, See 1).

Test 300001 experienced difficulty in maintaining the steam generator secondary side pressure at 1010 psia. The steam valves in both steam generators were believed to have had a slight amount of leakage during the conduct of this test. This leakage did not appear to significantly affect the primary system response or the phenomena observed during this test when compared to the other Mapping Tests.

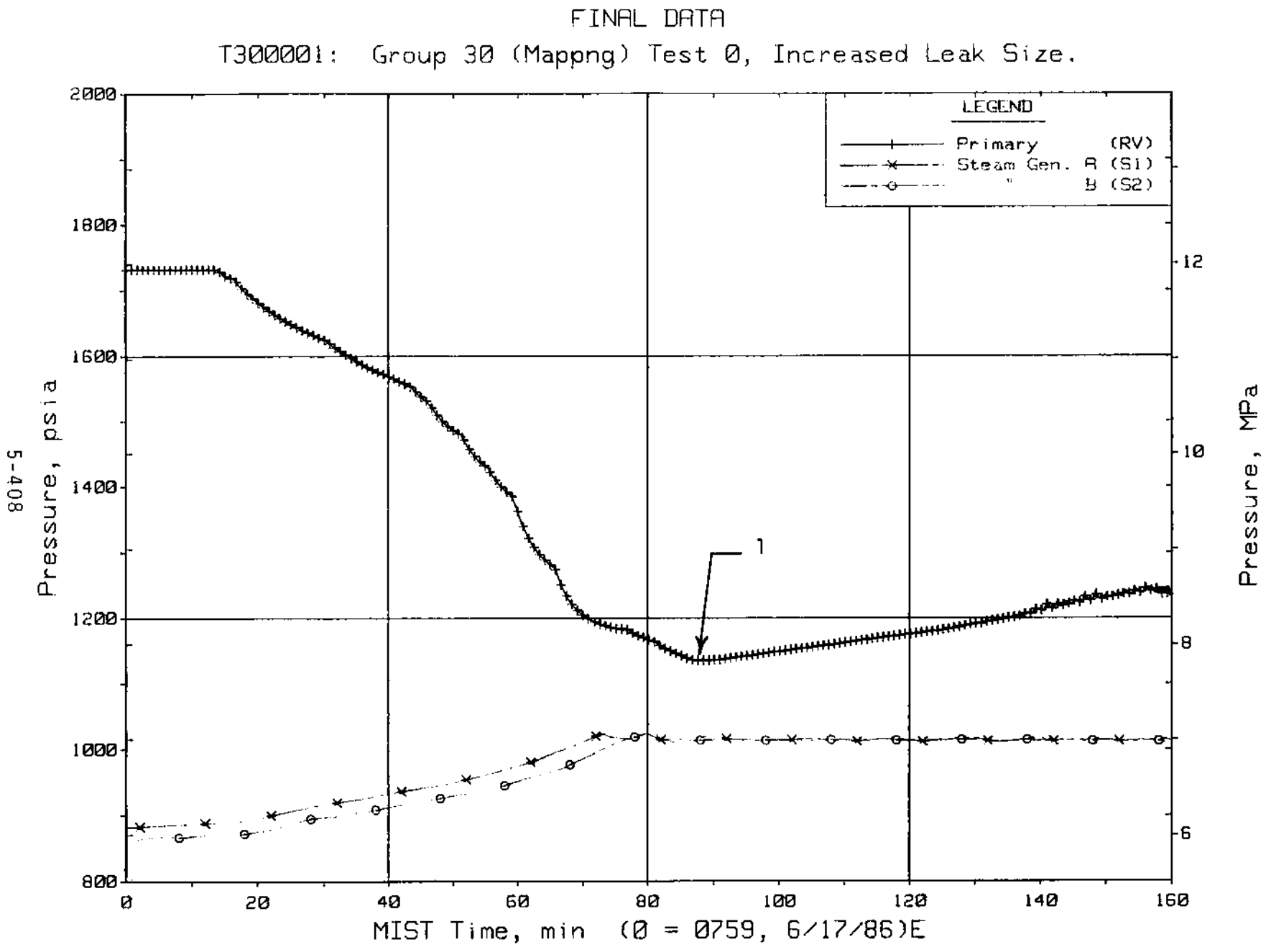

Figure 5.8.1. Primary and Secondary System Pressures (GP01s)

Wed Mar 15 16:27:01 1989

PSGP1

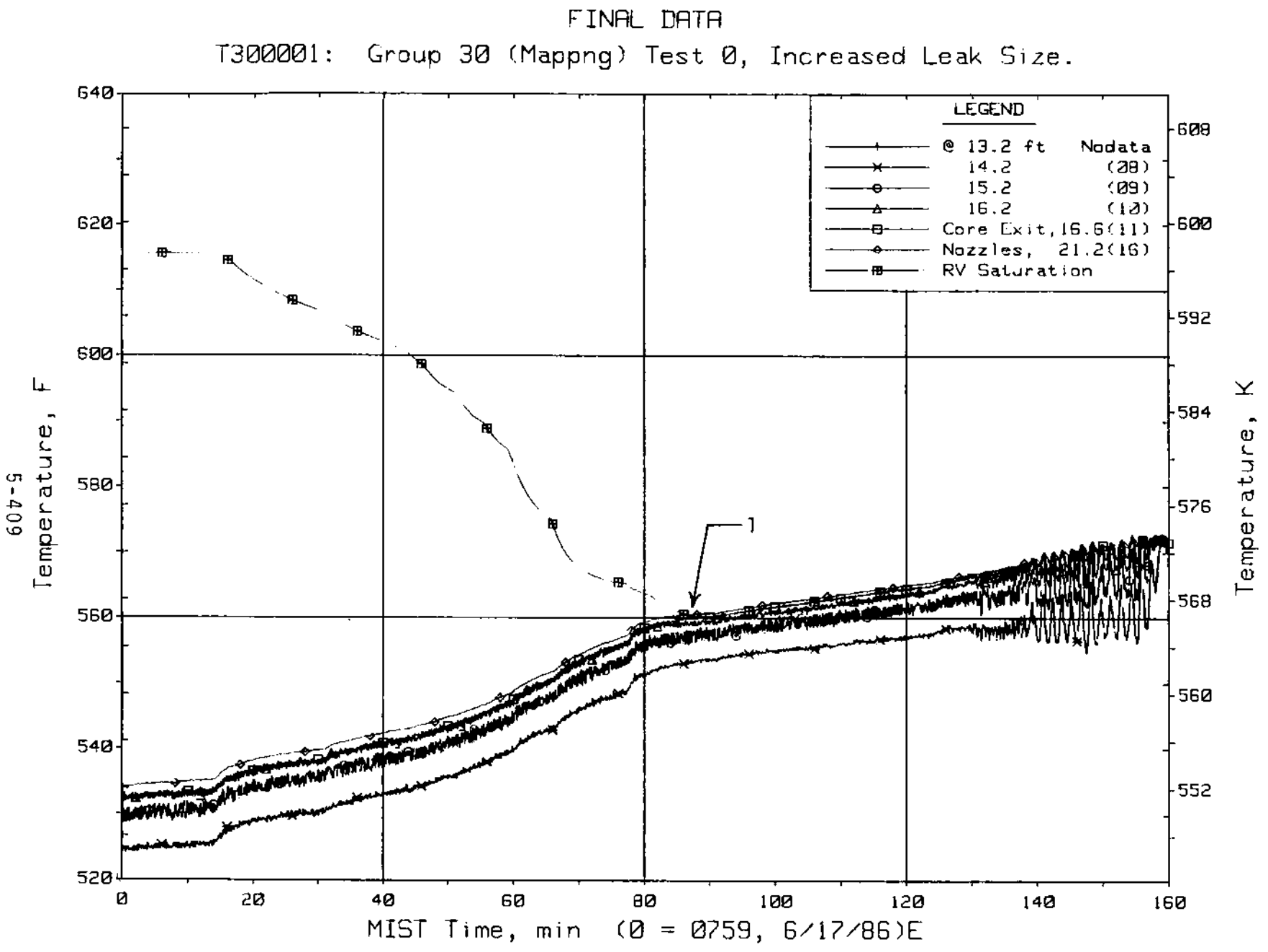

Figure 5.8.2. Reactor Vessel Mid-Elevation Fluid Temperatures (RVTCs)

Wed Mar 15 16:22:48 1989

RVTC2

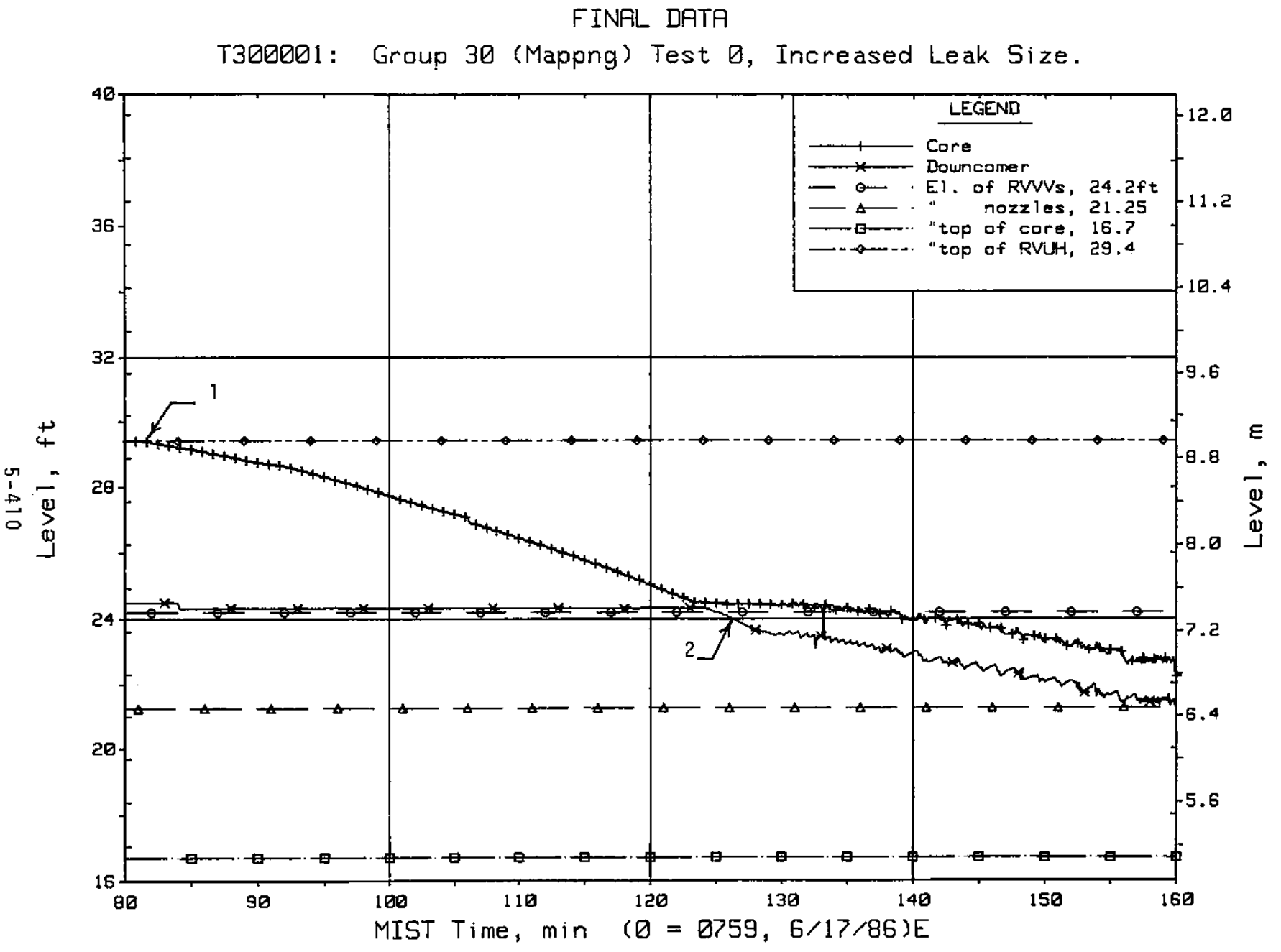

Figure 5.8.3. Core Region Collapsed Liquid Levels

Fri Mar 17 15:43:14 1989

COLV1

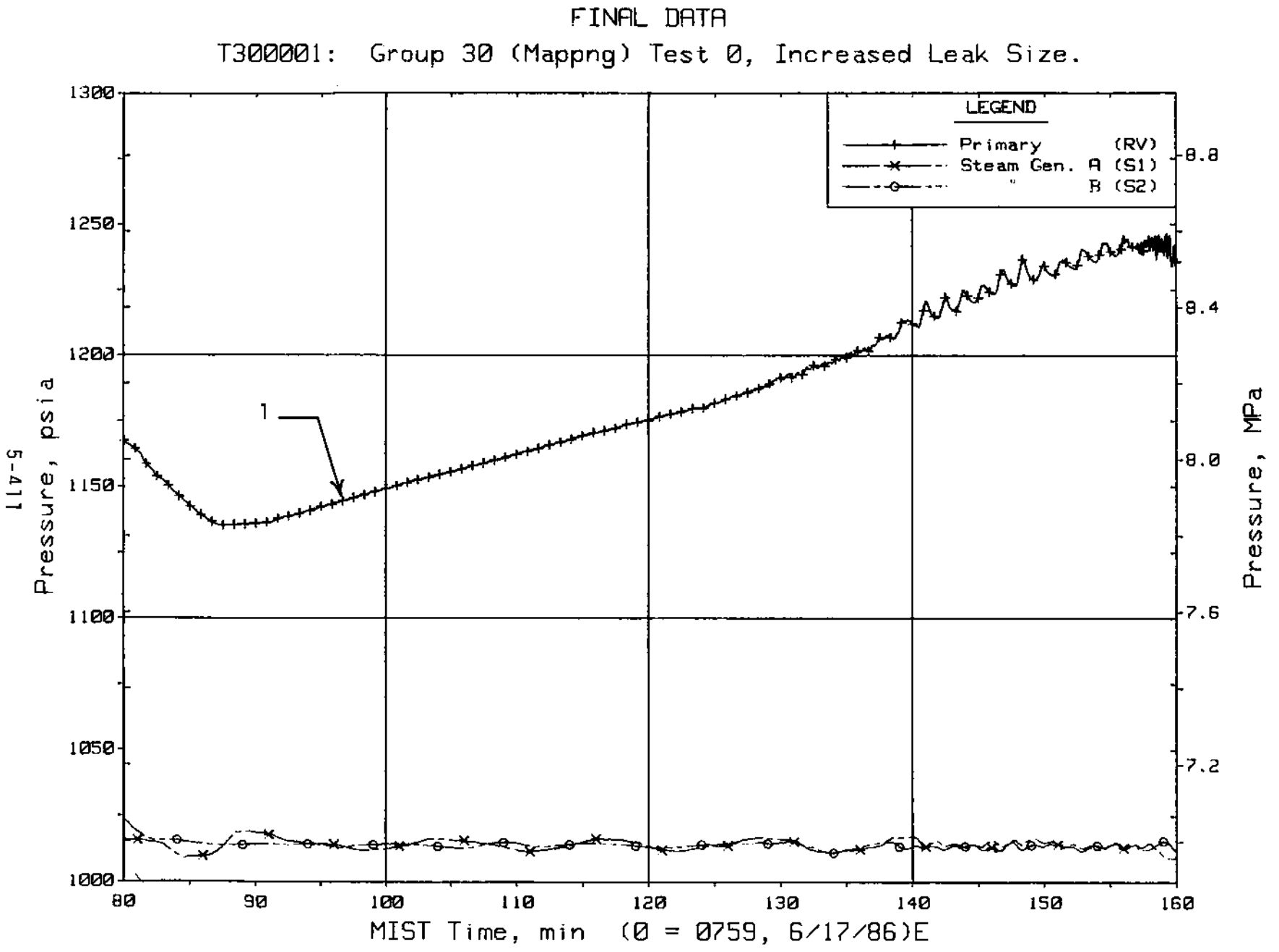

Figure 5.8.4. Primary and Secondary System Pressures (GP01s)

Wed Mar 15 16:14:08 1989

PSGP1

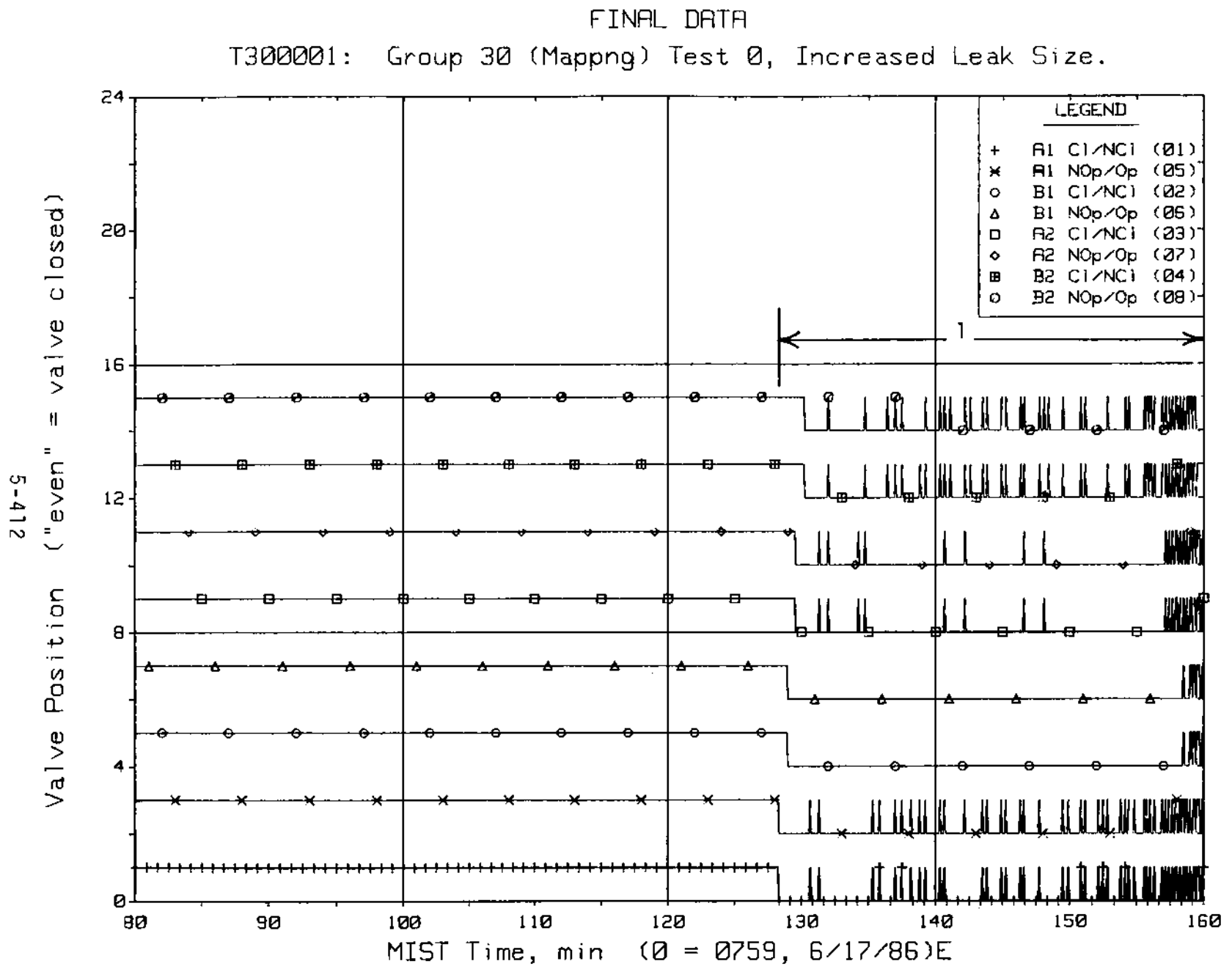

Figure 5.8.5. Reactor Vessel Vent Valve Limit Switch Indications (RVLSs)

Wed Mar 15 16:11:10 1989

VVLS2

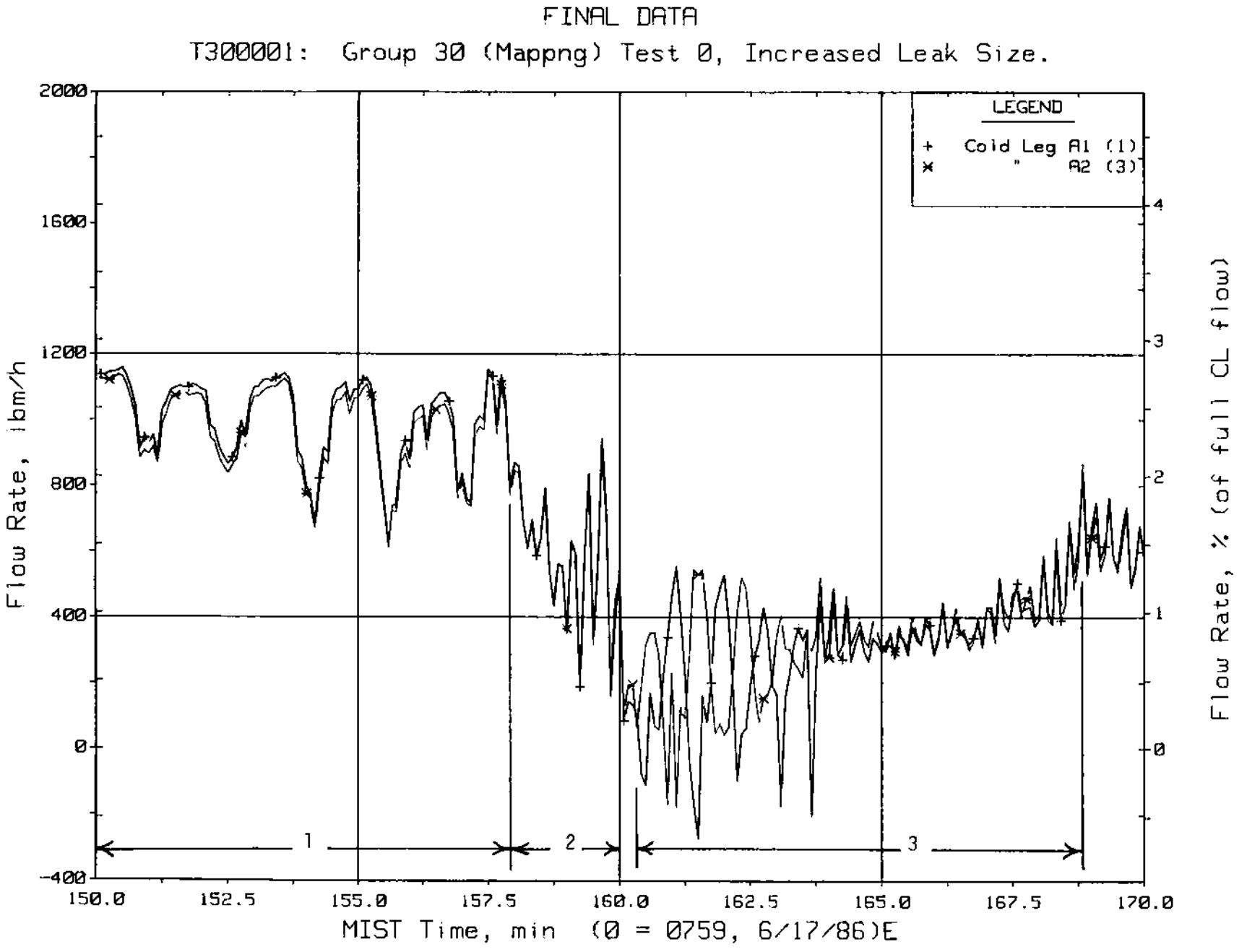

Figure 5.8.6. Loop A Cold Leg (Venturi) Flow Rates (CnVN20s)

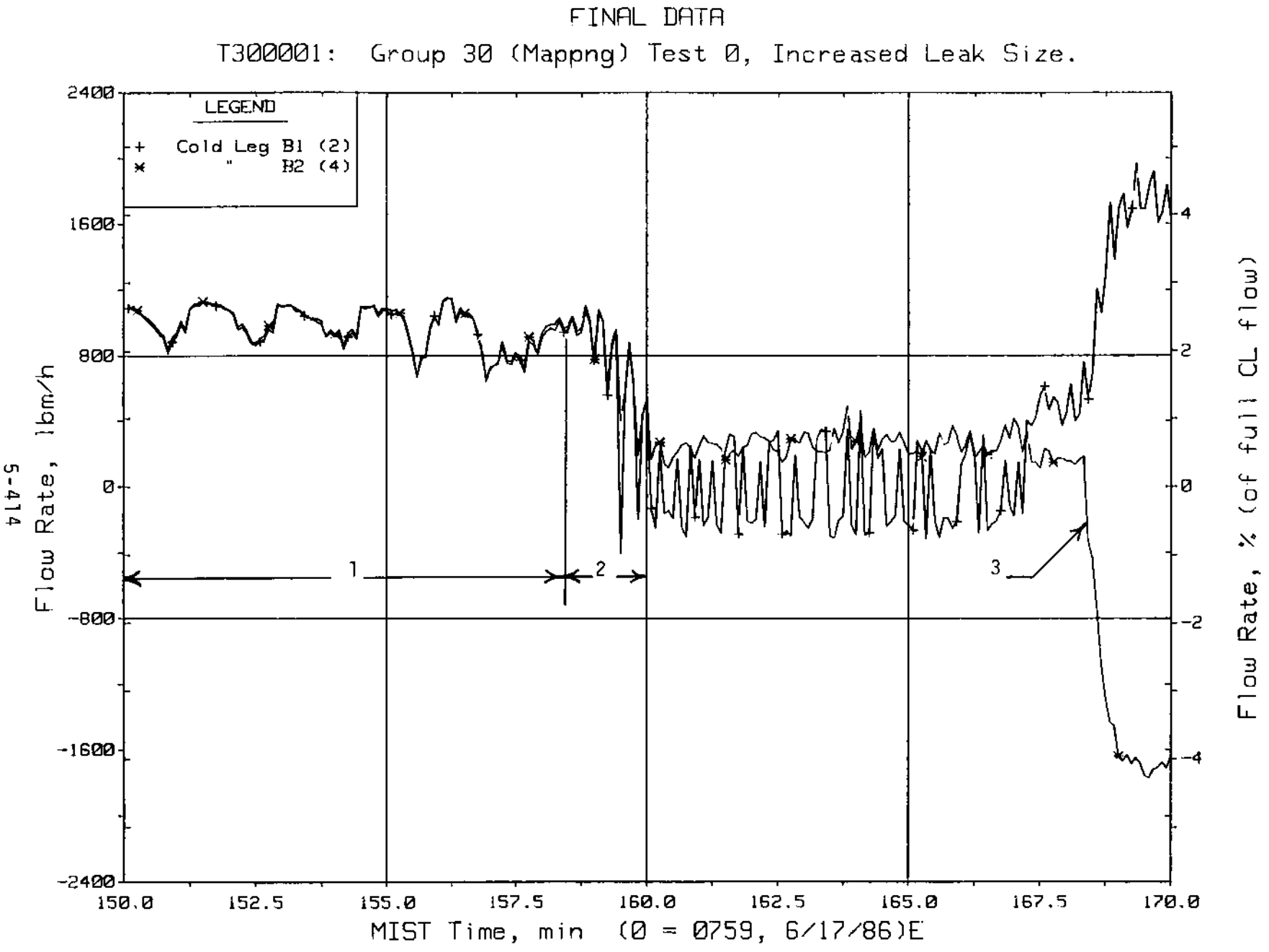

Figure 5.8.7. Loop B Cold Leg (Venturi) Flow Rates (CnVN20s)

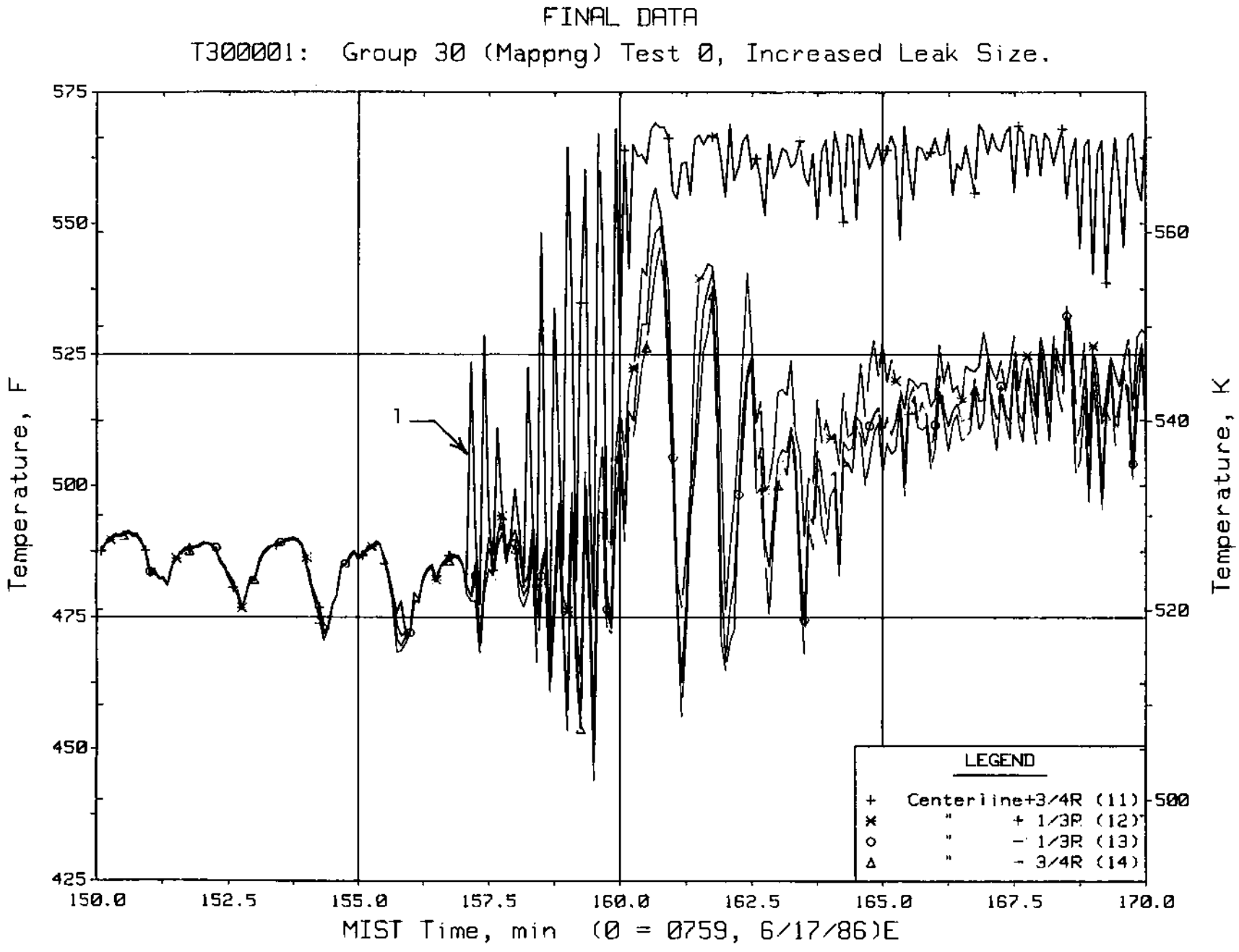

Figure 5.8.8. Cold Leg A1 Nozzle Rake Fluid Temperatures (21.2 ft, C1TCs)

Wed Mar 15 15:55:47 1989

C1TC4

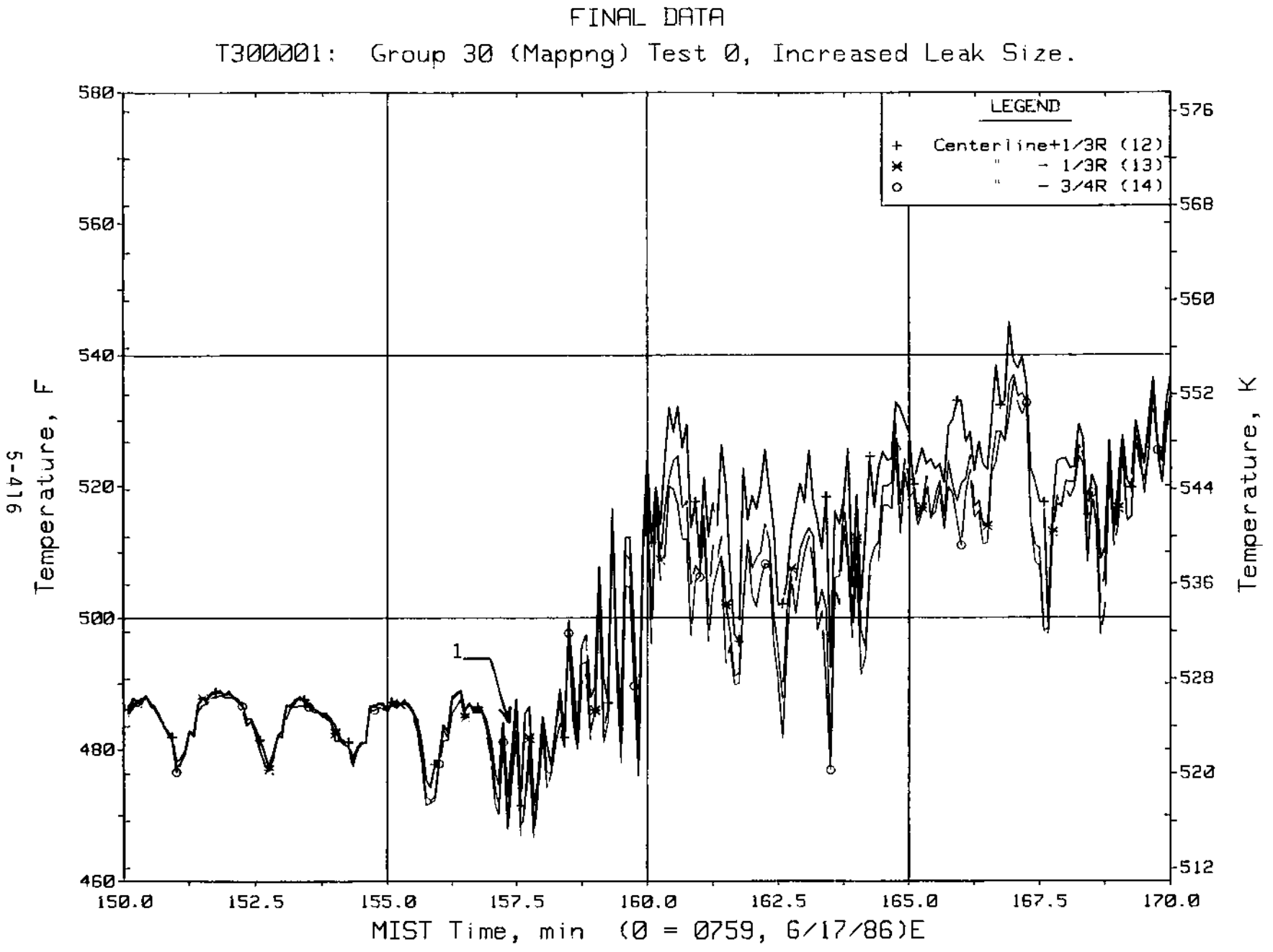

Figure 5.8.9. Cold Leg B1 Nozzle Rake Fluid Temperatures (21.2 ft, C2TCs)

Wed Mar 15 15:52:29 1989

C2TC4

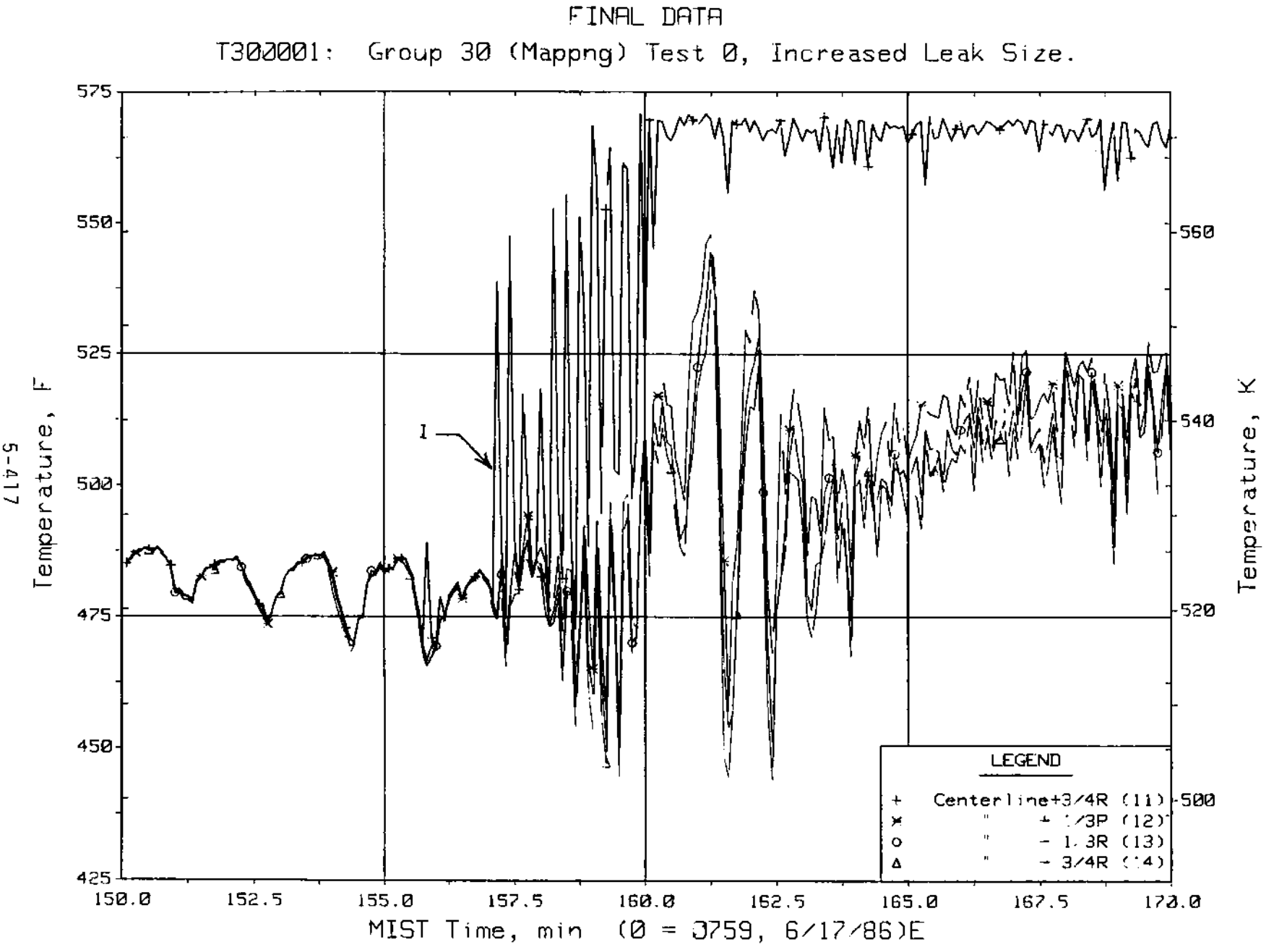

Figure 5.8.10. Cold Leg A2 Nozzle Rake Fluid Temperatures (21.2 ft, C3TCs)

Wed Mar 15 15:49:29 1989

C3TC4

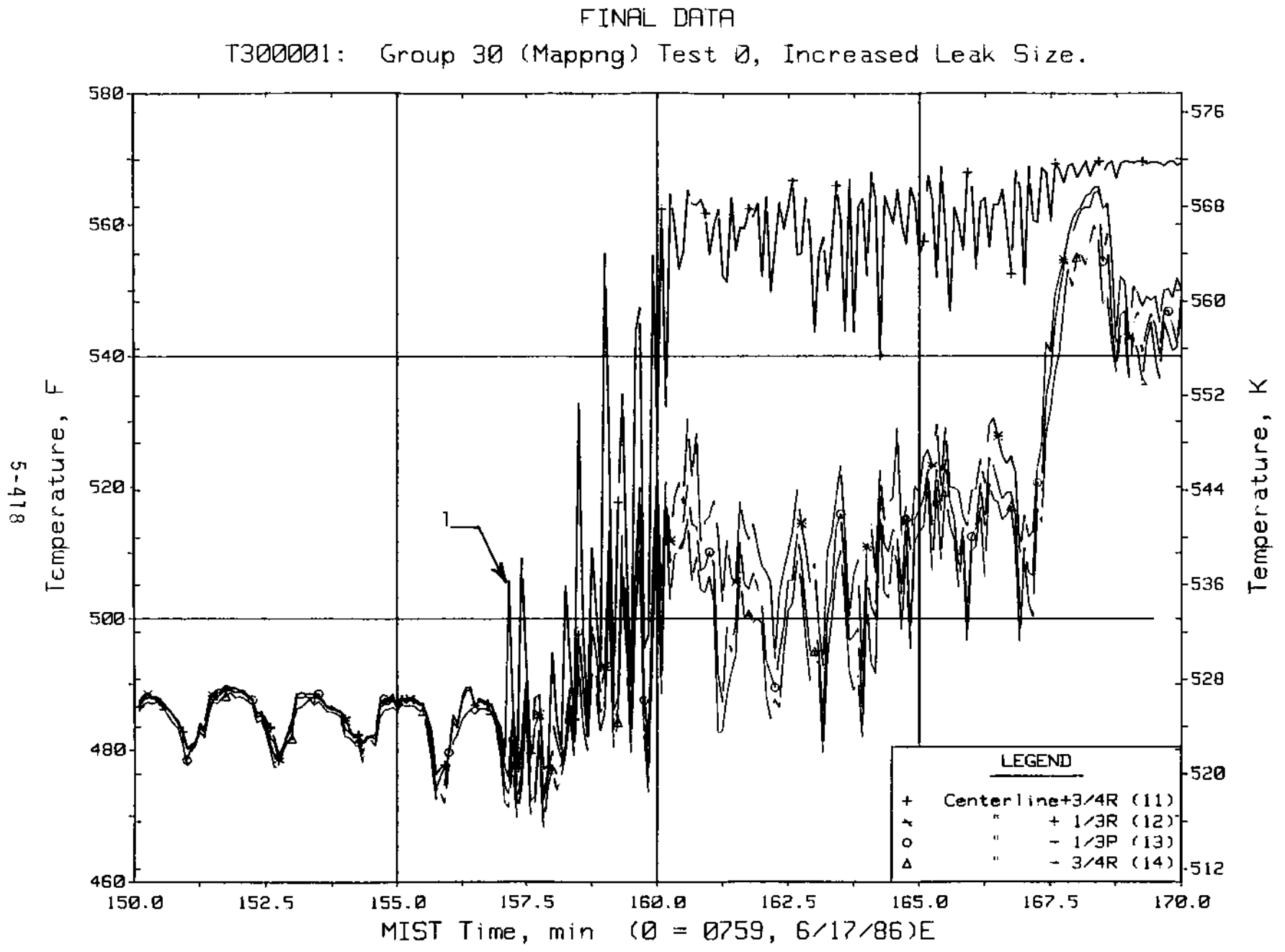

Figure 5.8.11. Cold Leg B2 Nozzle Rake Fluid Temperatures (21.2 ft, C4TCs)

Wed Mar 15 15:46:24 1989

C4TC4

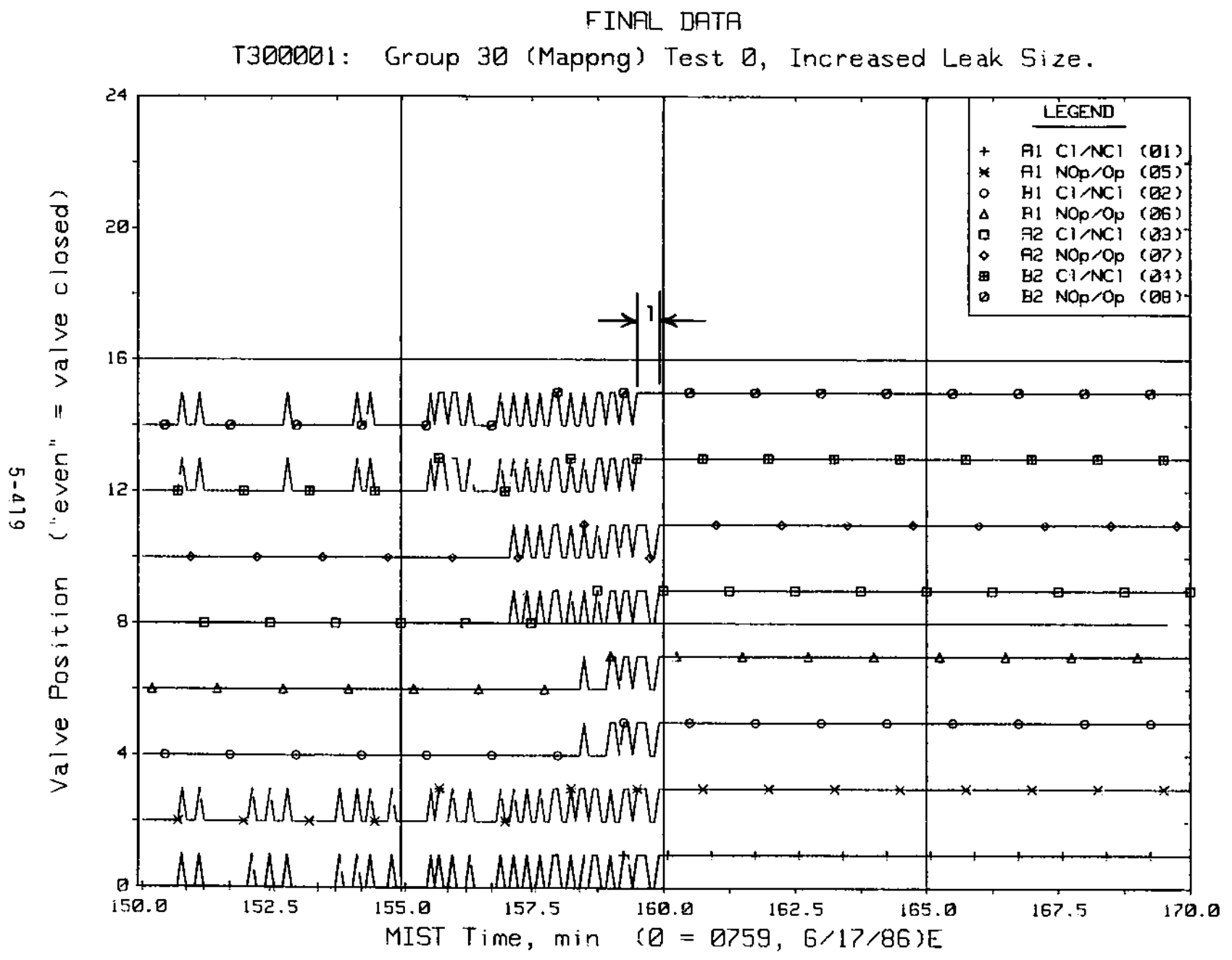

Figure 5.8.12. Reactor Vessel Vent Valve Limit Switch Indications (RVLSs)

Wed Mar 15 15:44:05 1989

VVLS2

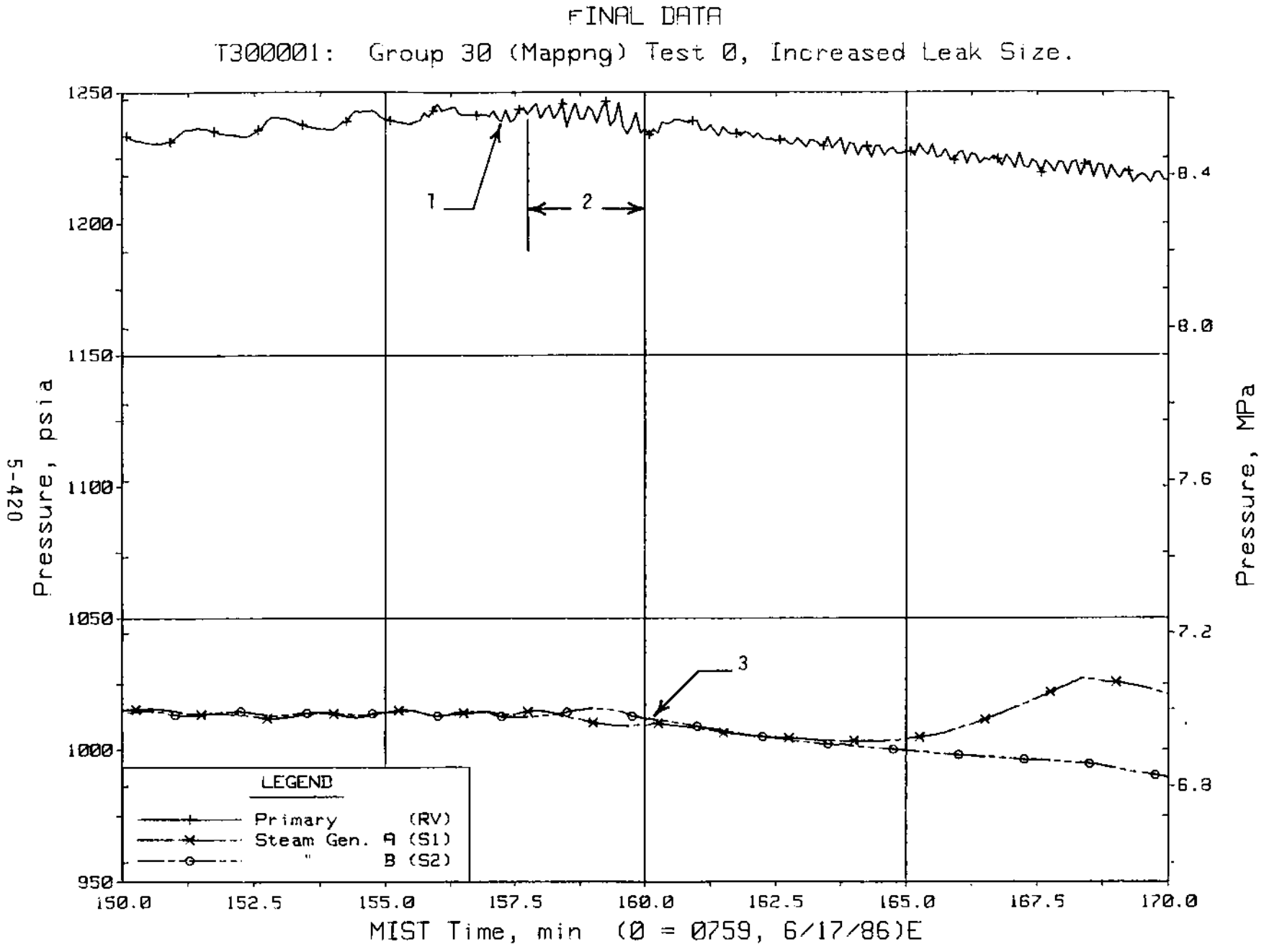

Figure 5.8.13. Primary and Secondary System Pressures (GP01s)

Thu Mar 16 11:16:26 1989

PSGP1

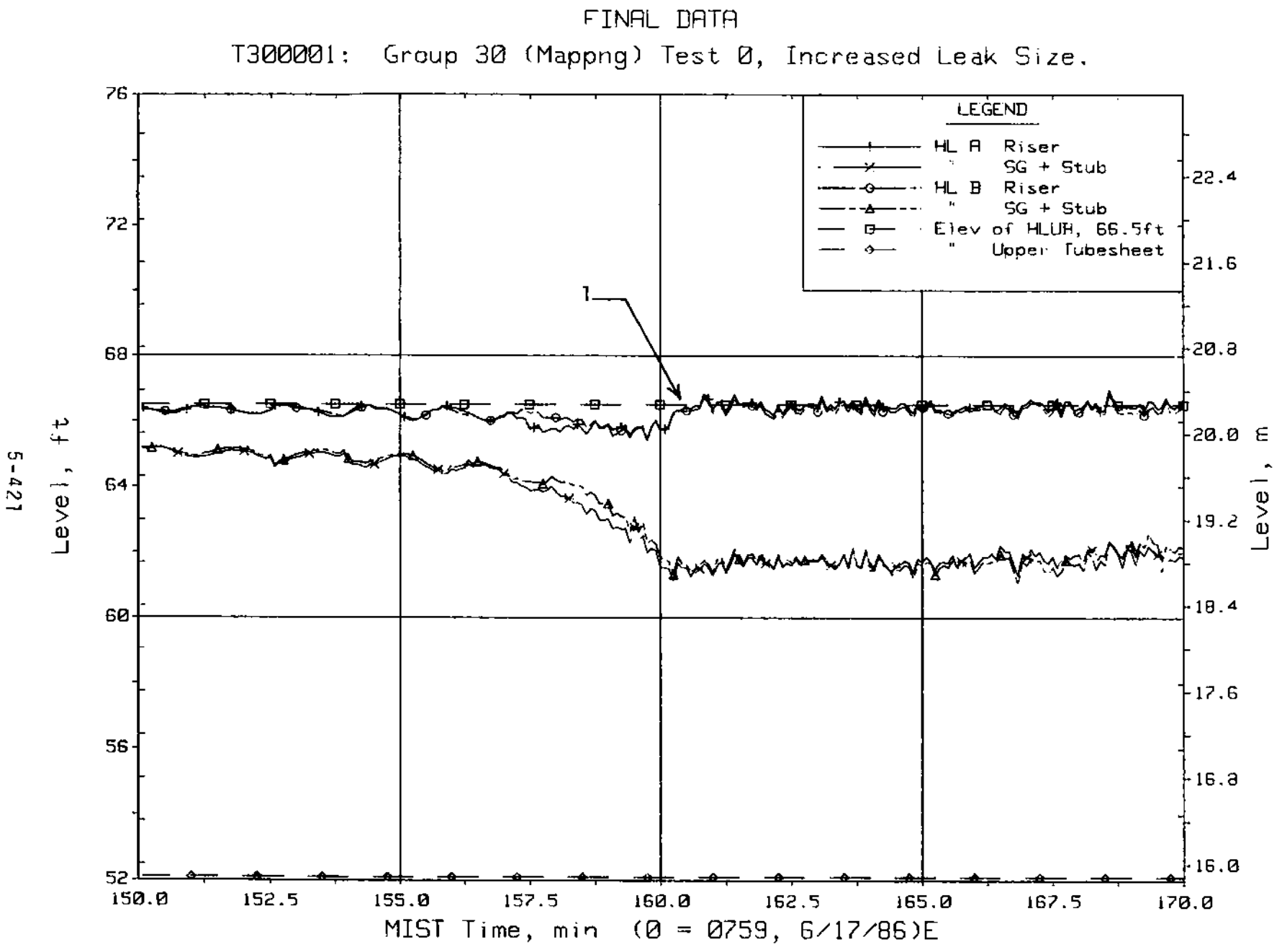

Figure 5.8.14. Hot Leg Riser and Stub Collapsed Liquid Levels

Wed Mar 15 15:29:08 1989

HLLV1

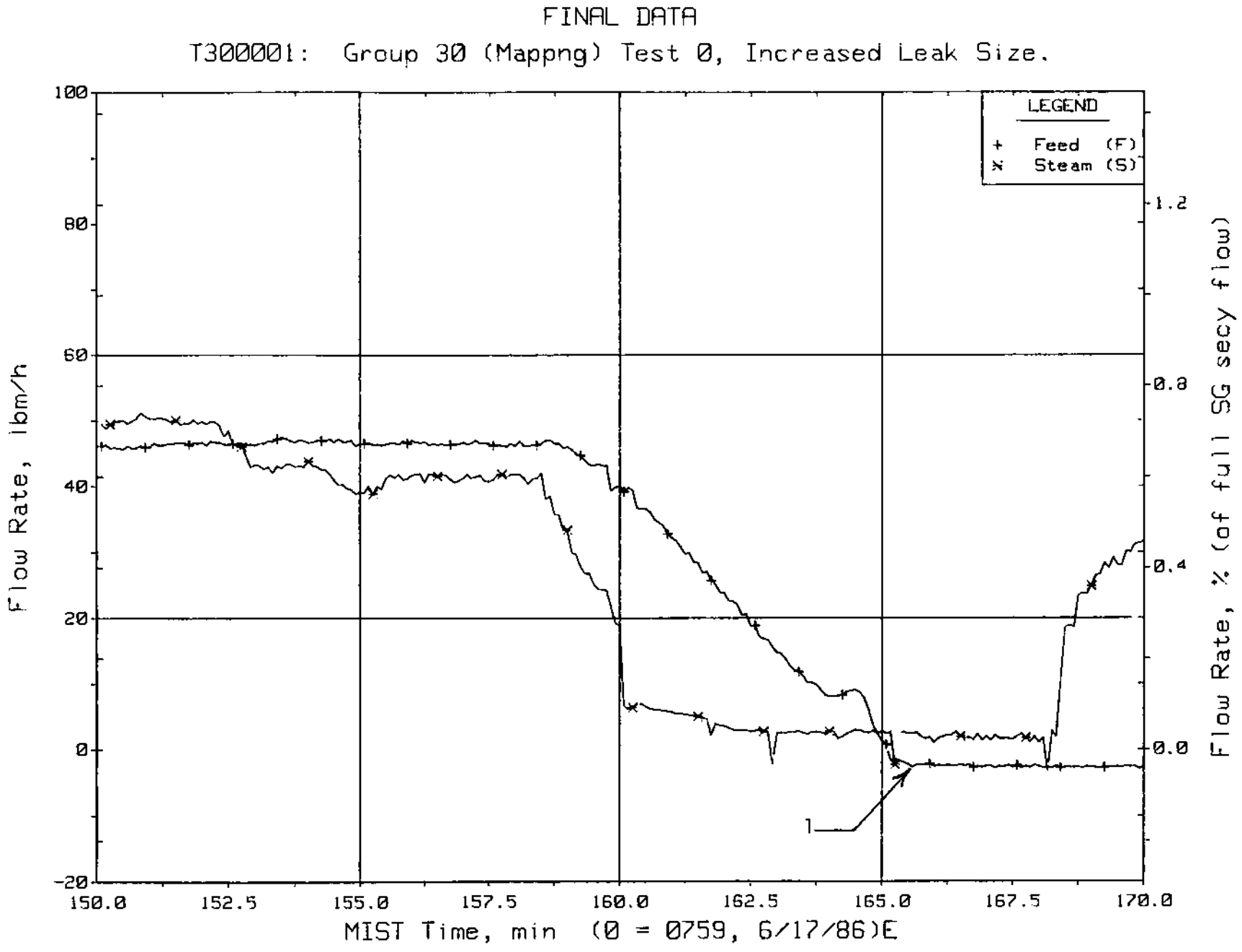

Figure 5.8.15. Steam Generator A Flow Rates (SaOR20s)

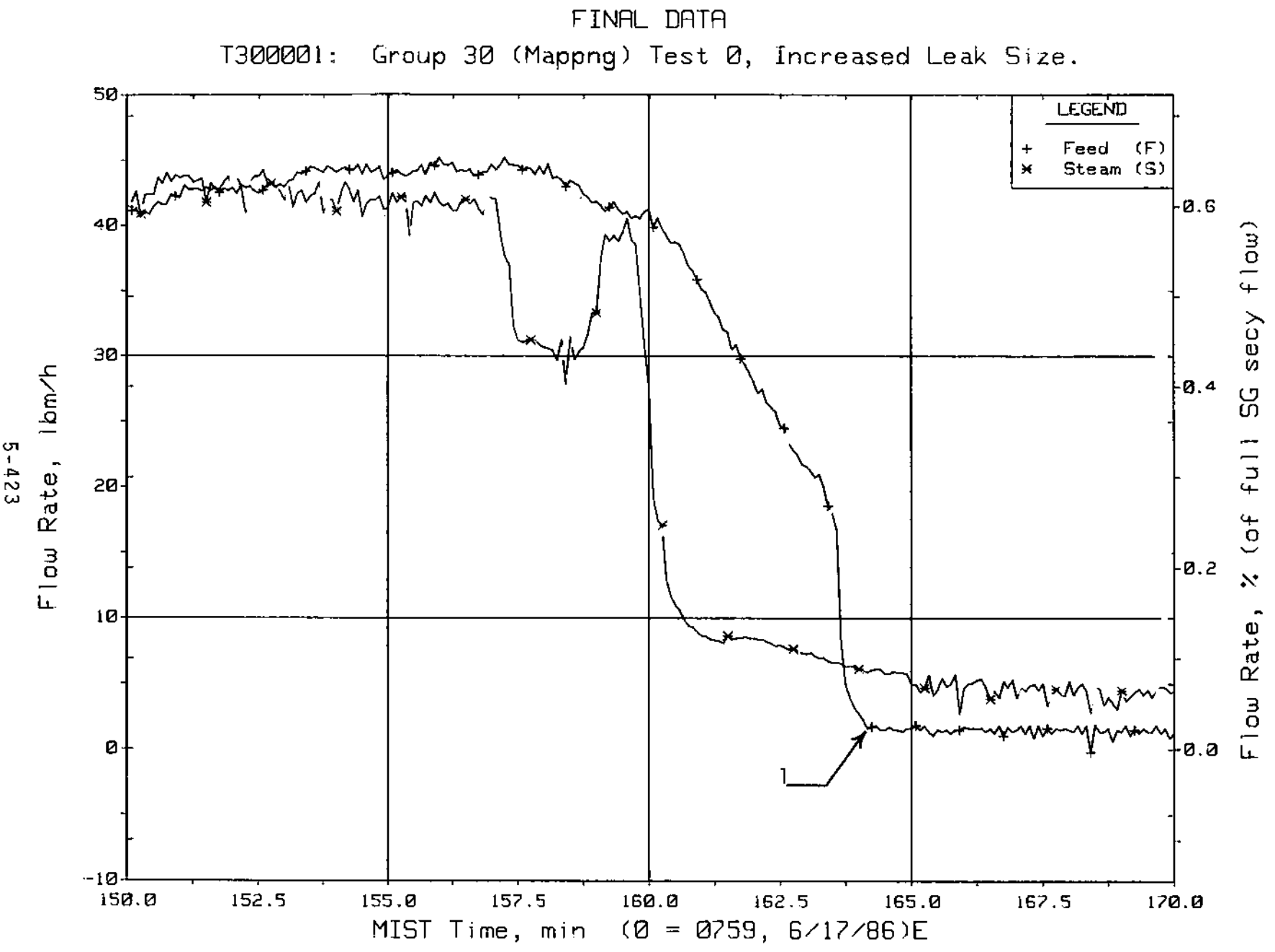

Figure 5.8.16. Steam Generator B Flow Rates (SaOR21s)

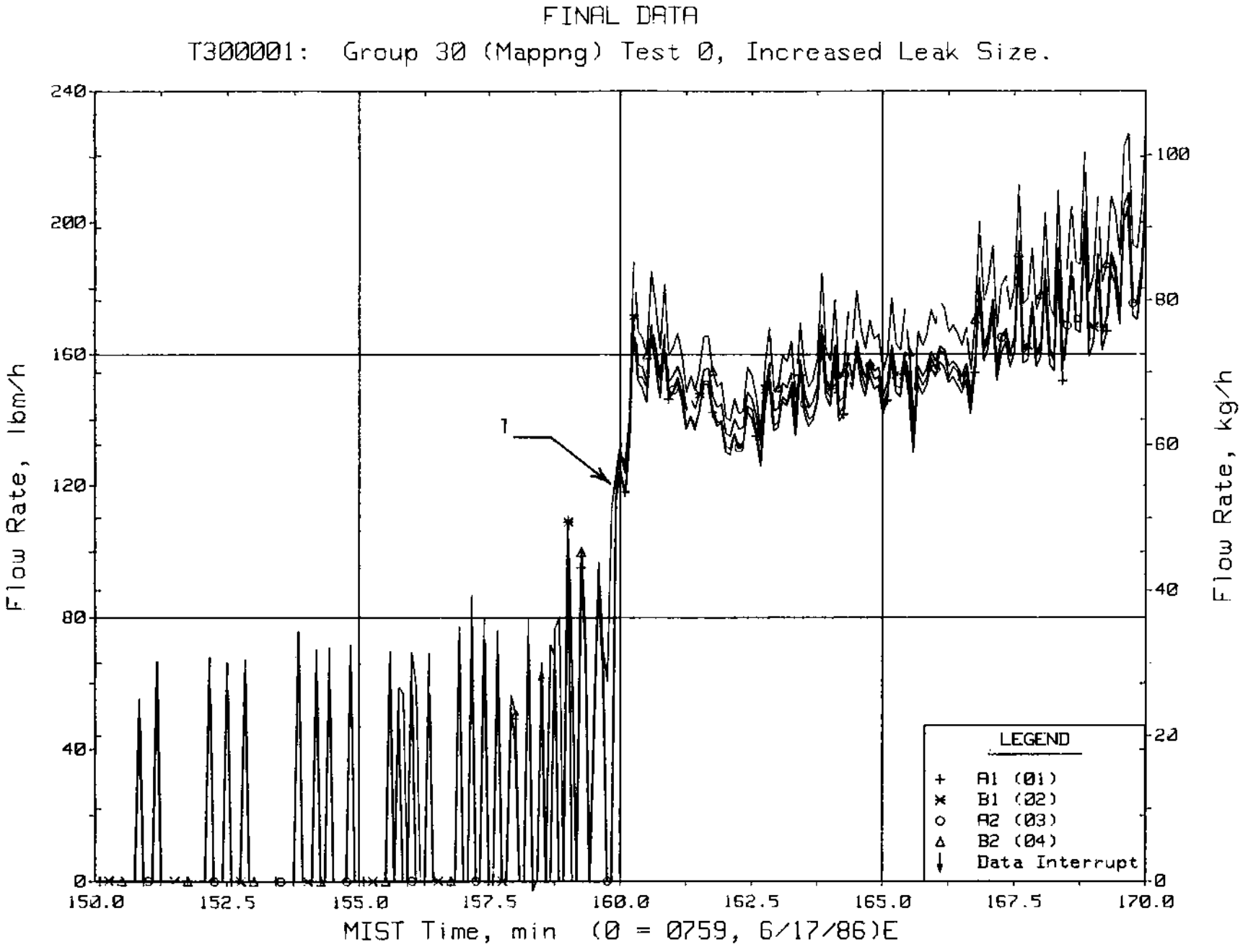

Figure 5.8.17. Reactor Vessel Vent Valve Flow Rates (RVORs)

Wed Mar 15 15:32:41 1989

VVFL1

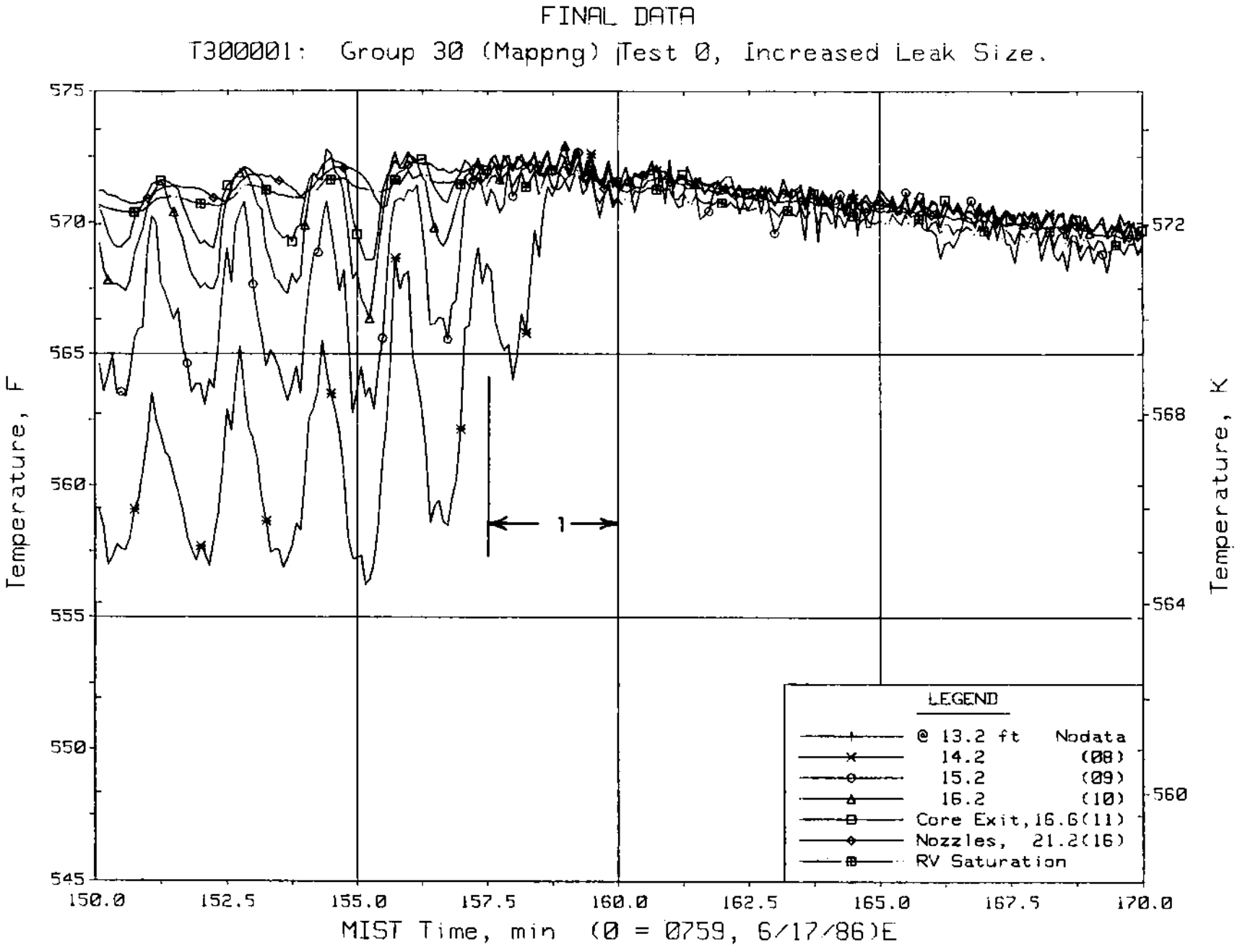

Figure 5.8.18. Reactor Vessel Mid-Elevation Fluid Temperatures (RVTCs)

Thu Mar 16 11:25:42 1989

RVTC2

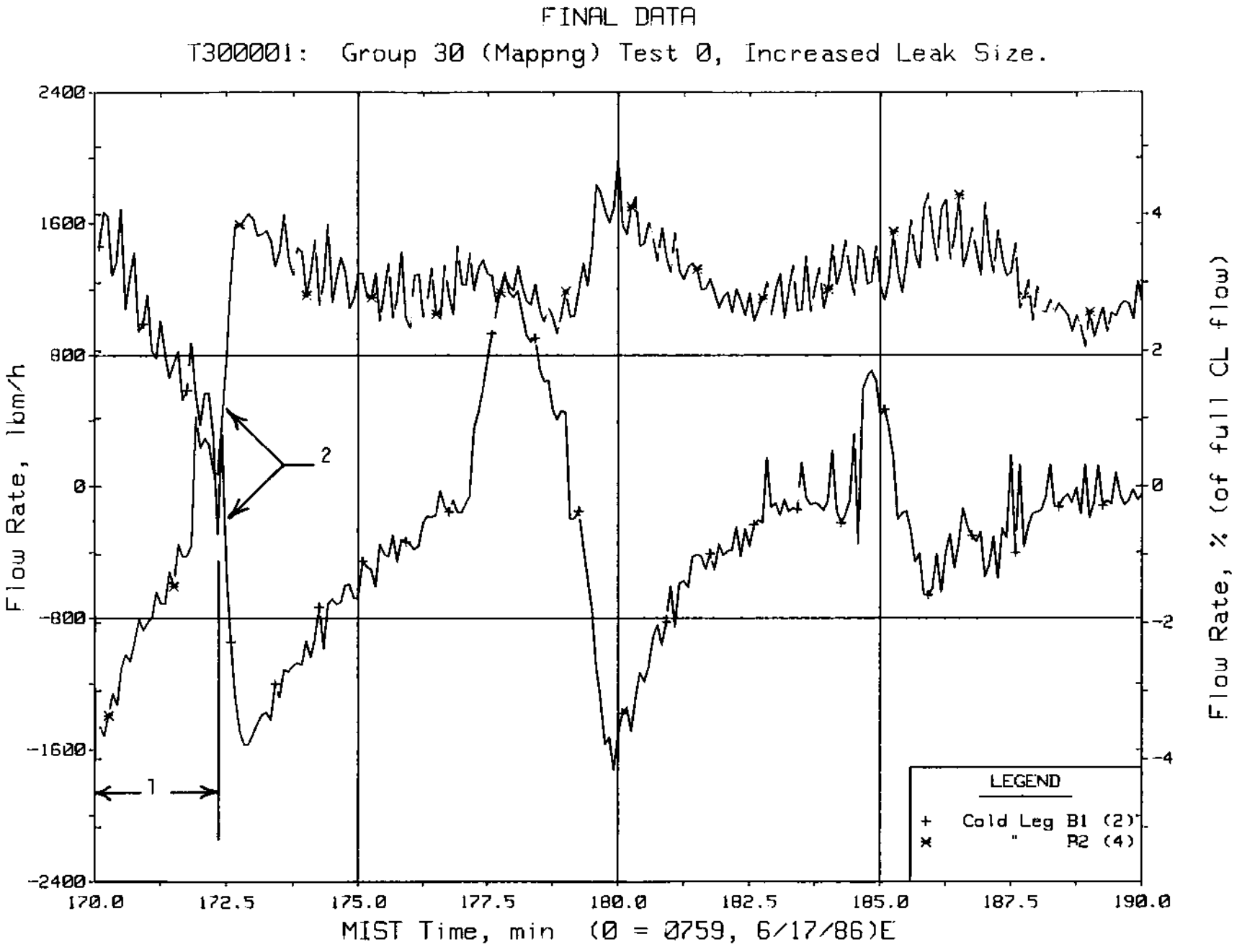

Figure 5.8.19. Loop B Cold Leg (Venturi) Flow Rates (CnVN20s)

Wed Mar 15 15:27:43 1989

PRFL6

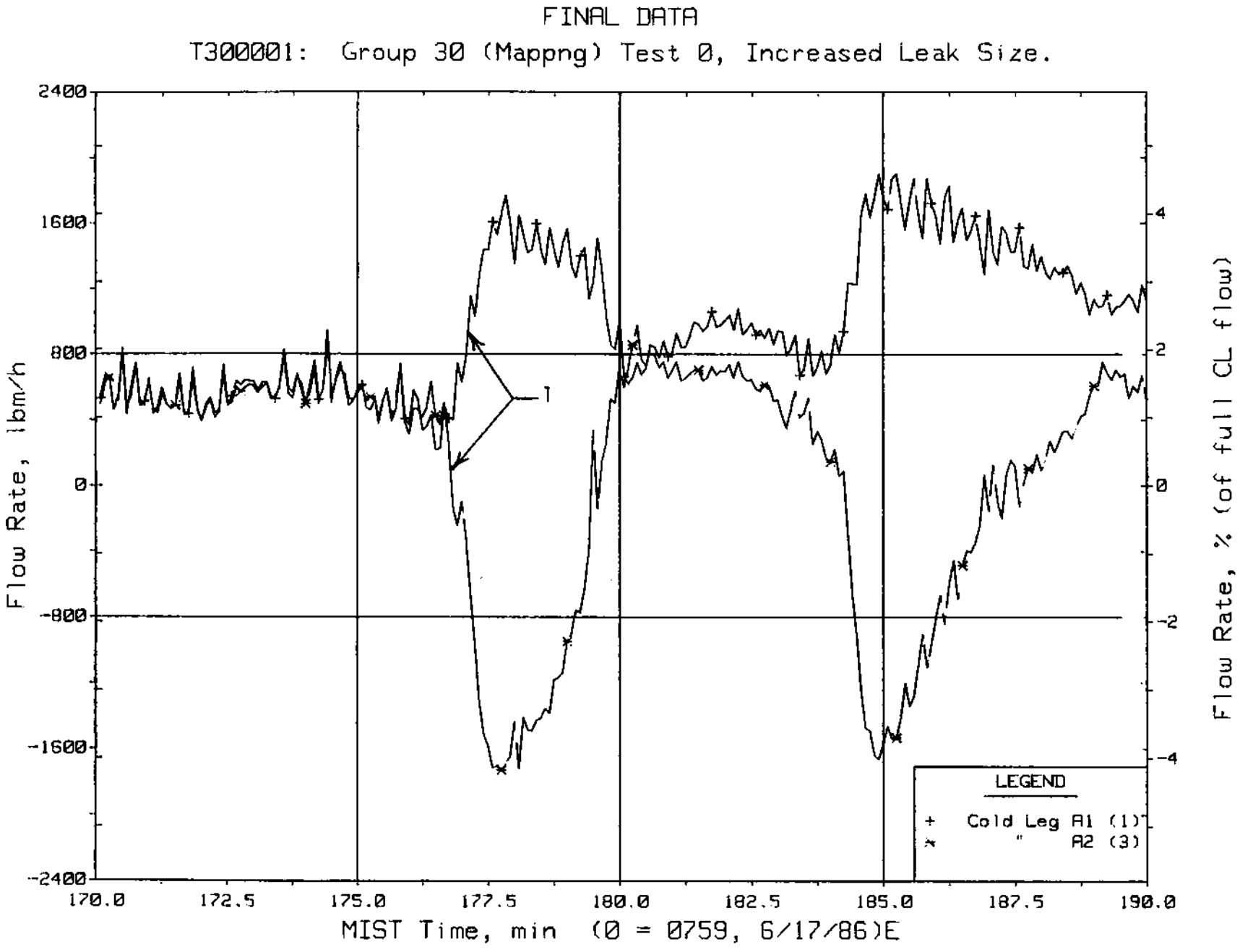

Figure 5.8.20. Loop A Cold Leg (Venturi) Flow Rates (CnVN20s)

Wed Mar 15 15:23:42 1989

PRFL5

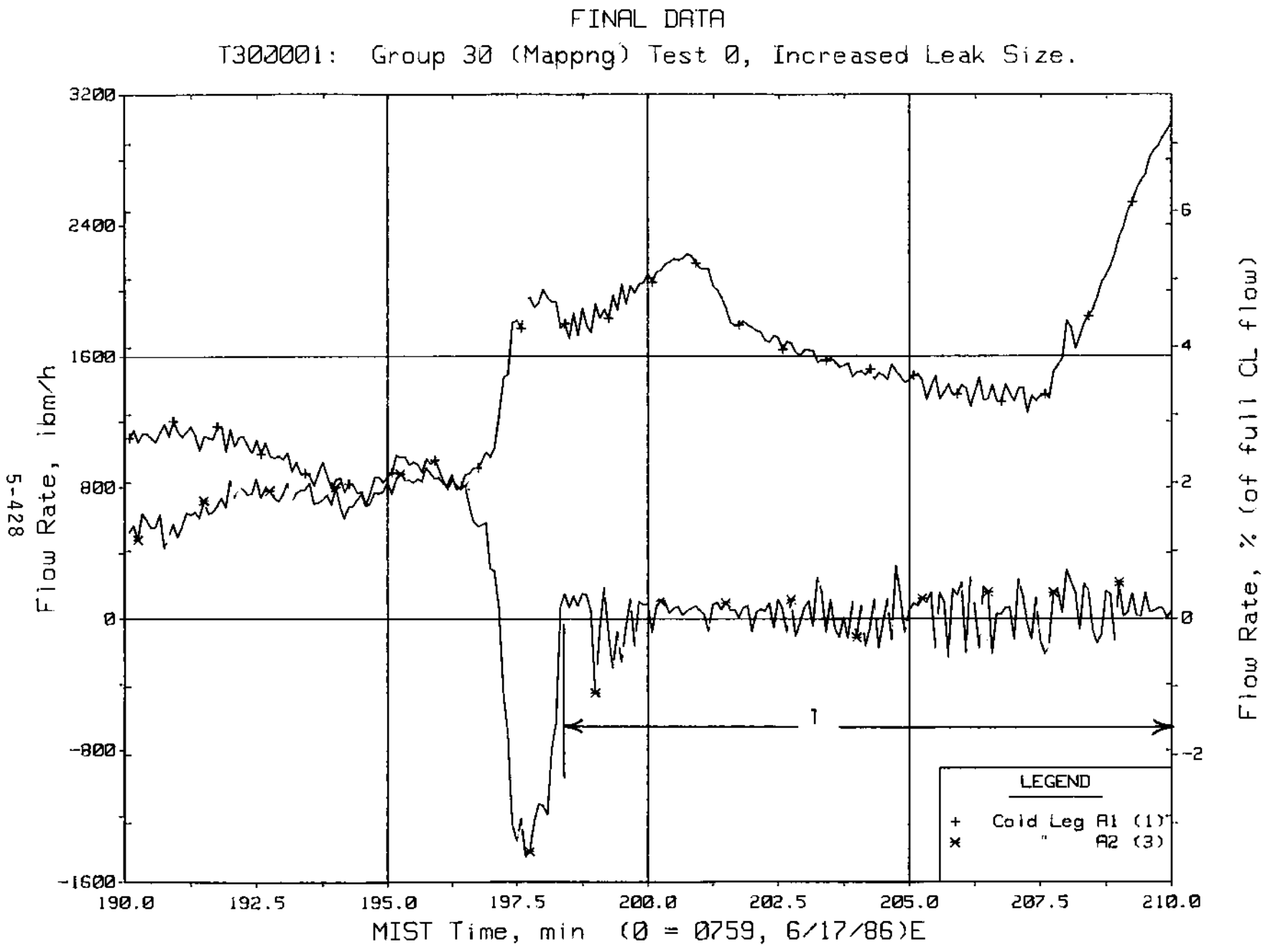

Figure 5.8.21. Loop A Cold Leg (Venturi) Flow Rates (CnVN20s)

Wed Mar 15 15:19:41 1989

PRFL5

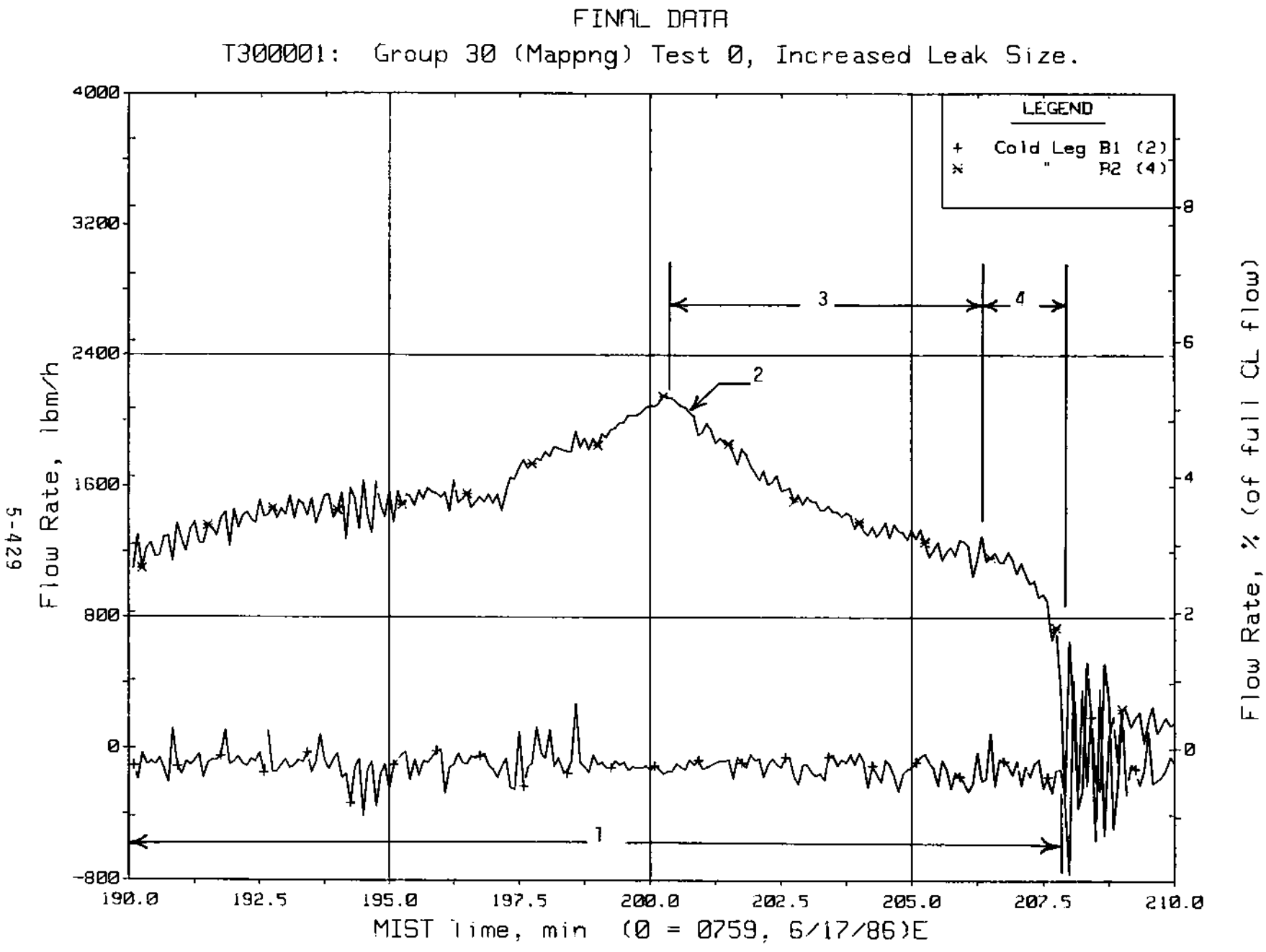

Figure 5.8.22. Loop B Cold Leg (Venturi) Flow Rates (CnVN20s)

Wed Mar 15 15:15:43 1989

PRFL6

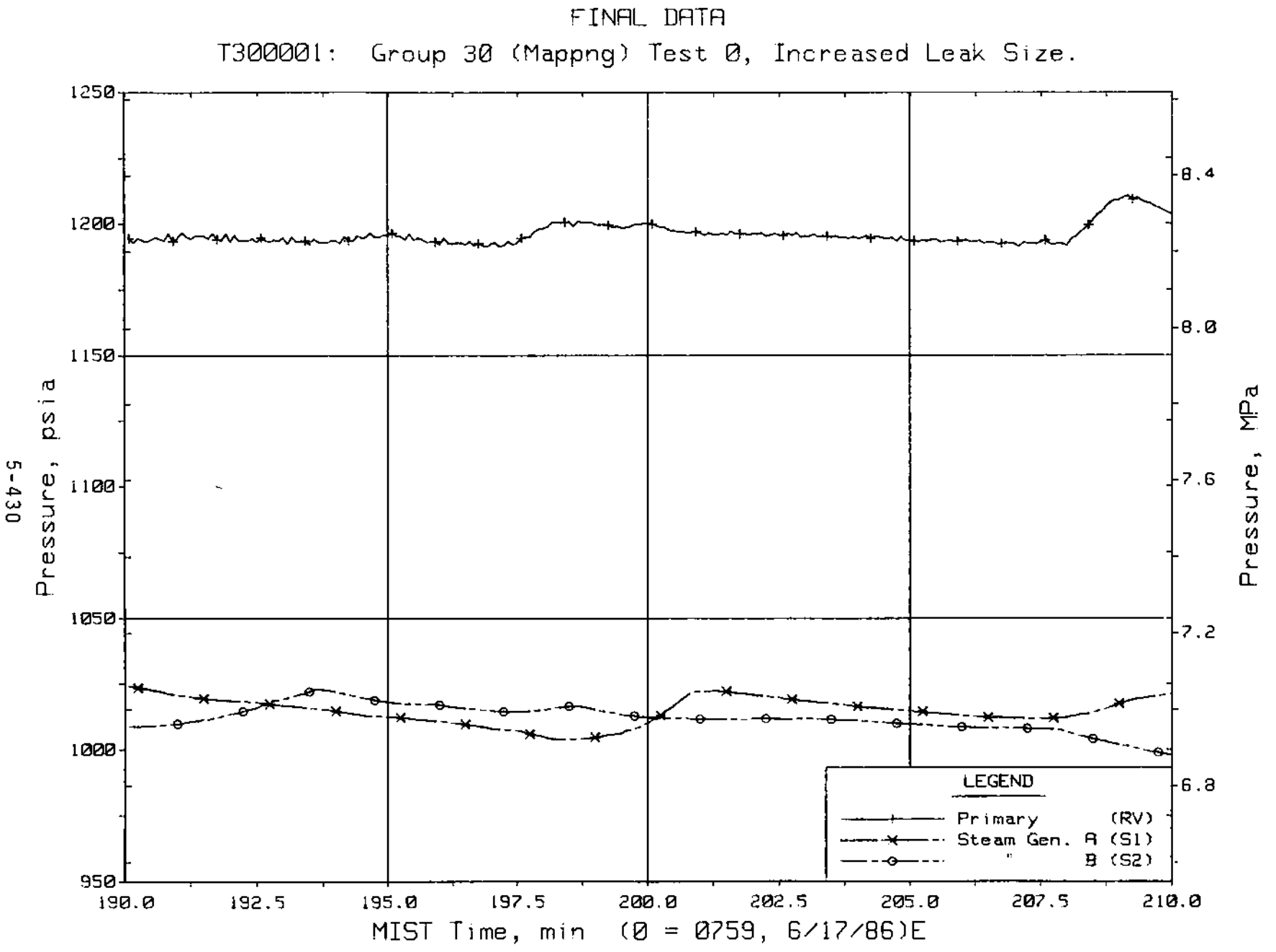

Figure 5.8.23. Primary and Secondary System Pressures (GP01s)

Thu Mar 16 11:32:55 1989

PSGP1

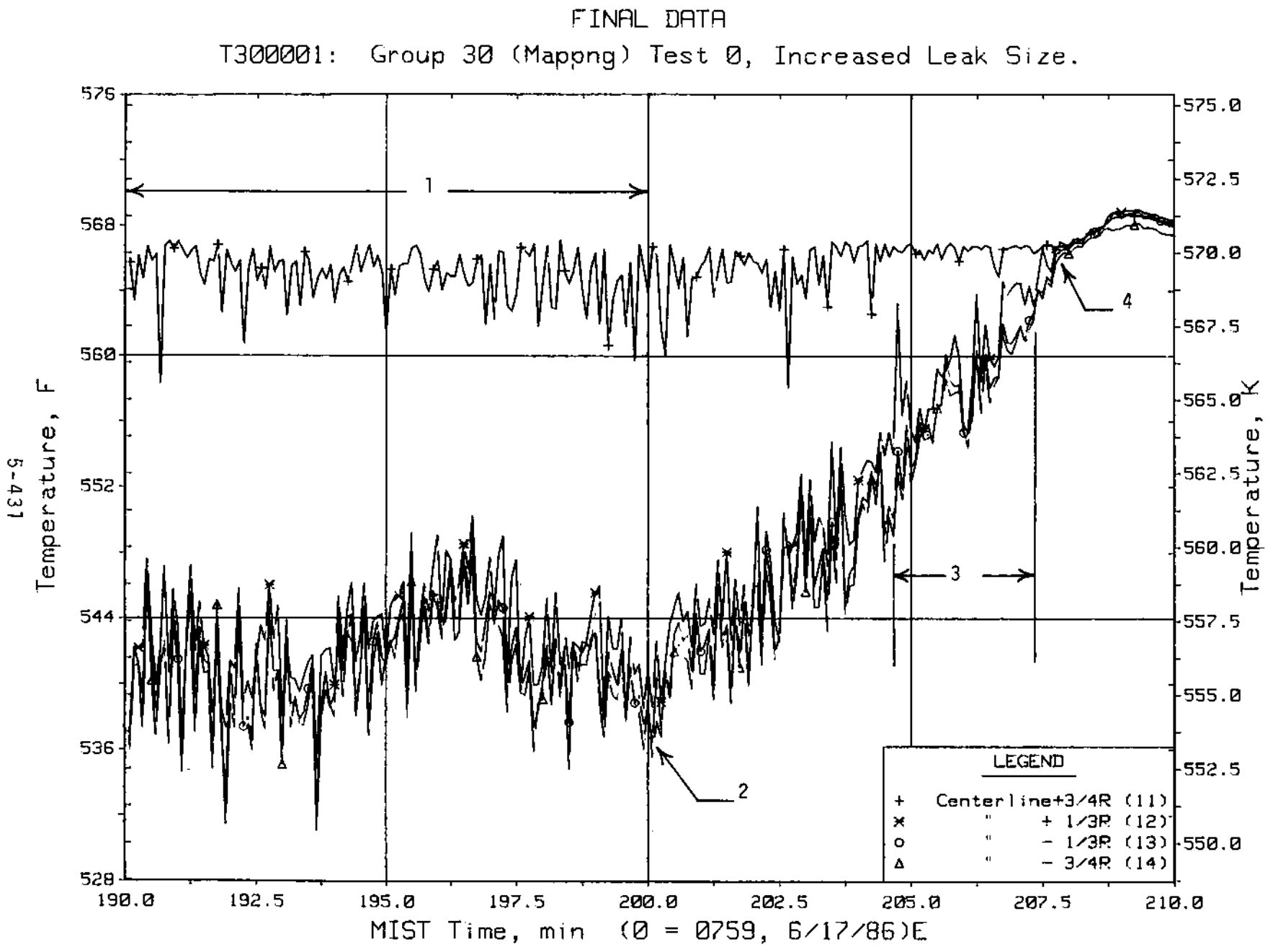

Figure 5.8.24. Cold Leg B2 Nozzle Rake Fluid Temperatures (21.2 ft, C4TCs)

Wed Mar 15 15:00:46 1989

C4TC4

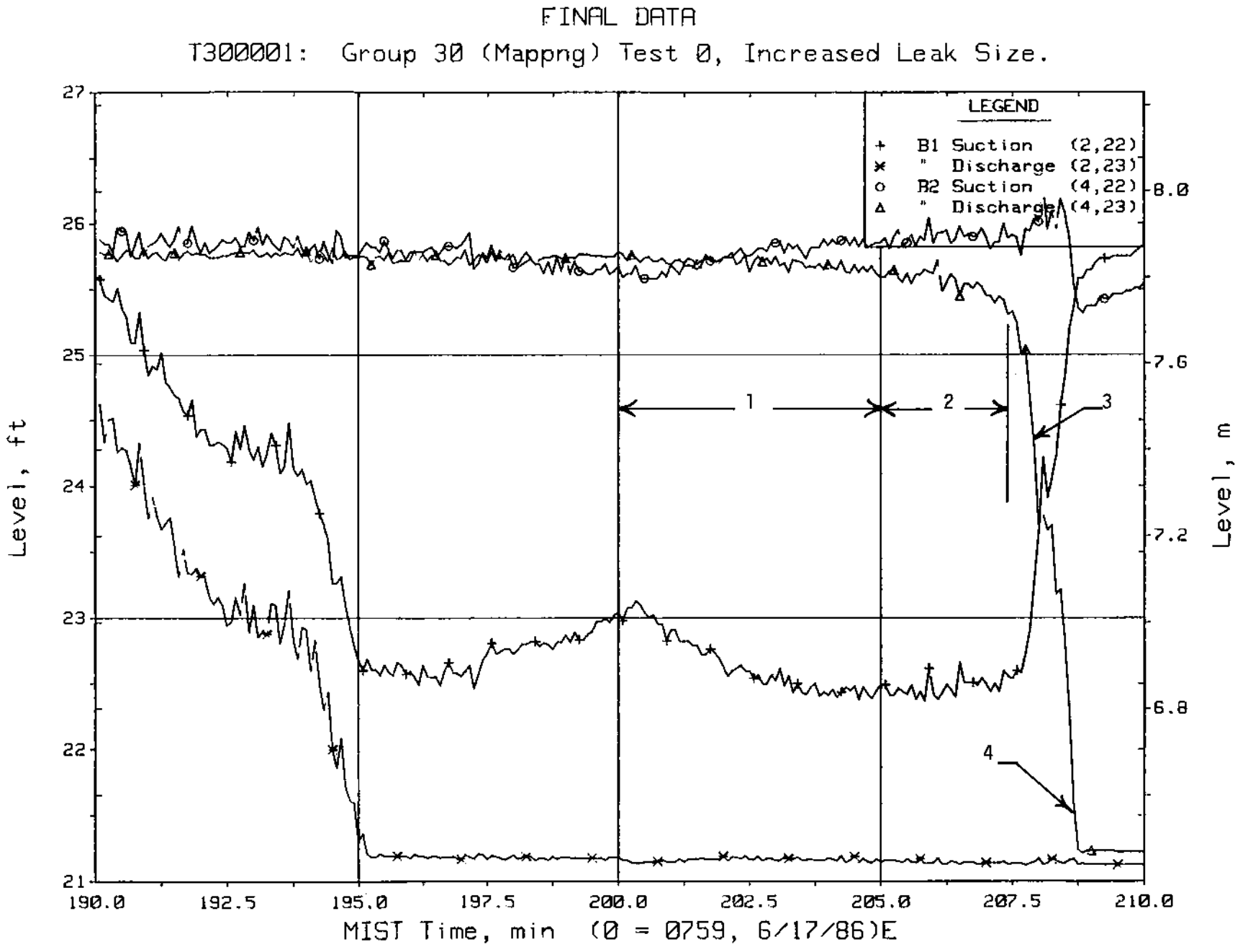

Figure 5.8.25. Loop B Cold Leg Collapsed Liquid Levels (LVs)

Wed Mar 15 15:06:32 1989

CLLV2

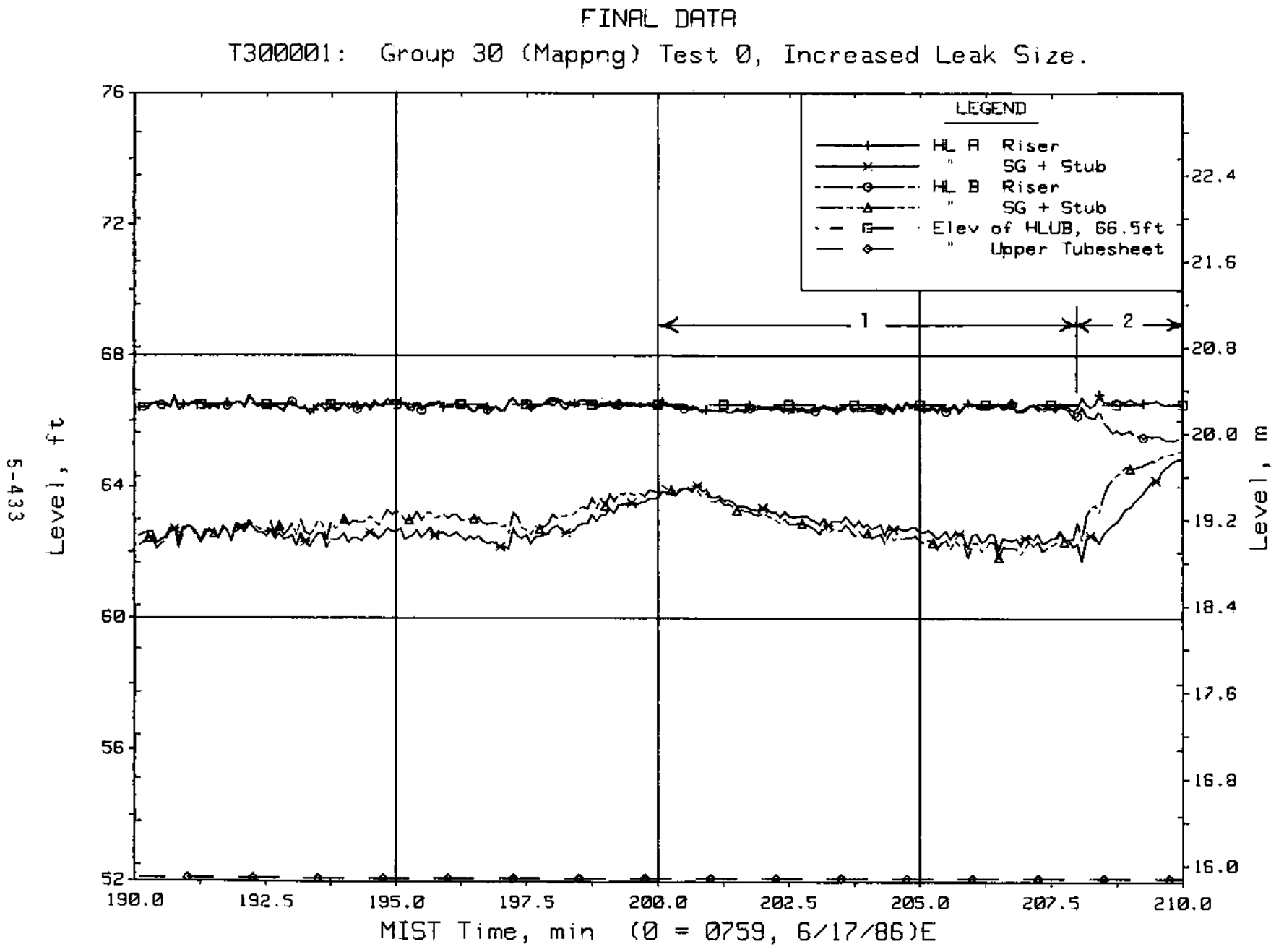

Figure 5.8.26. Hot Leg Riser and Stub Collapsed Liquid Levels

Wed Mar 15 15:04:05 1989

HLLV1

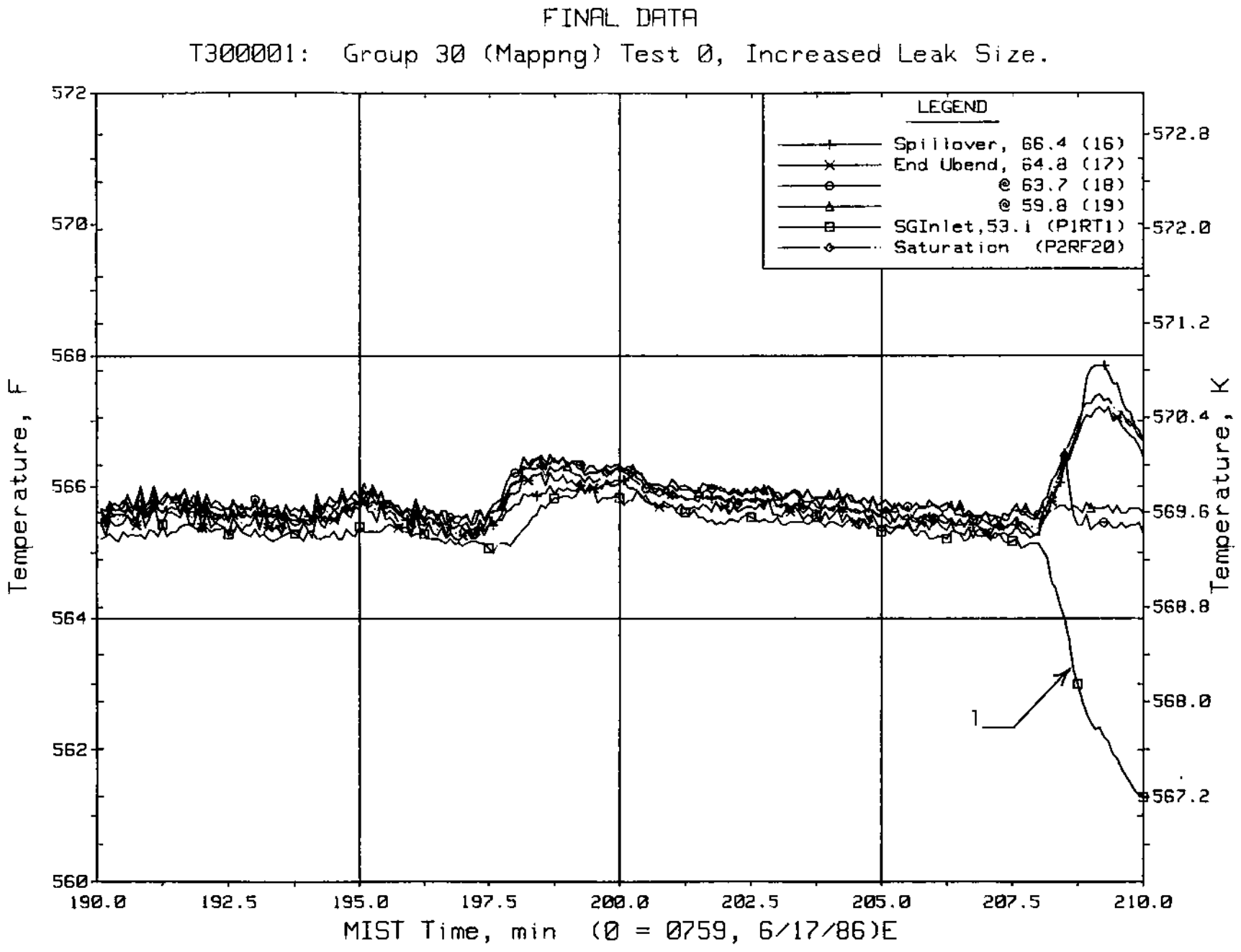

Figure 5.8.27. Hot Leg B Fluid Temperatures Beyond U-Bend (H2TCs)

Wed Mar 15 15:01:04 1989

H2TC3

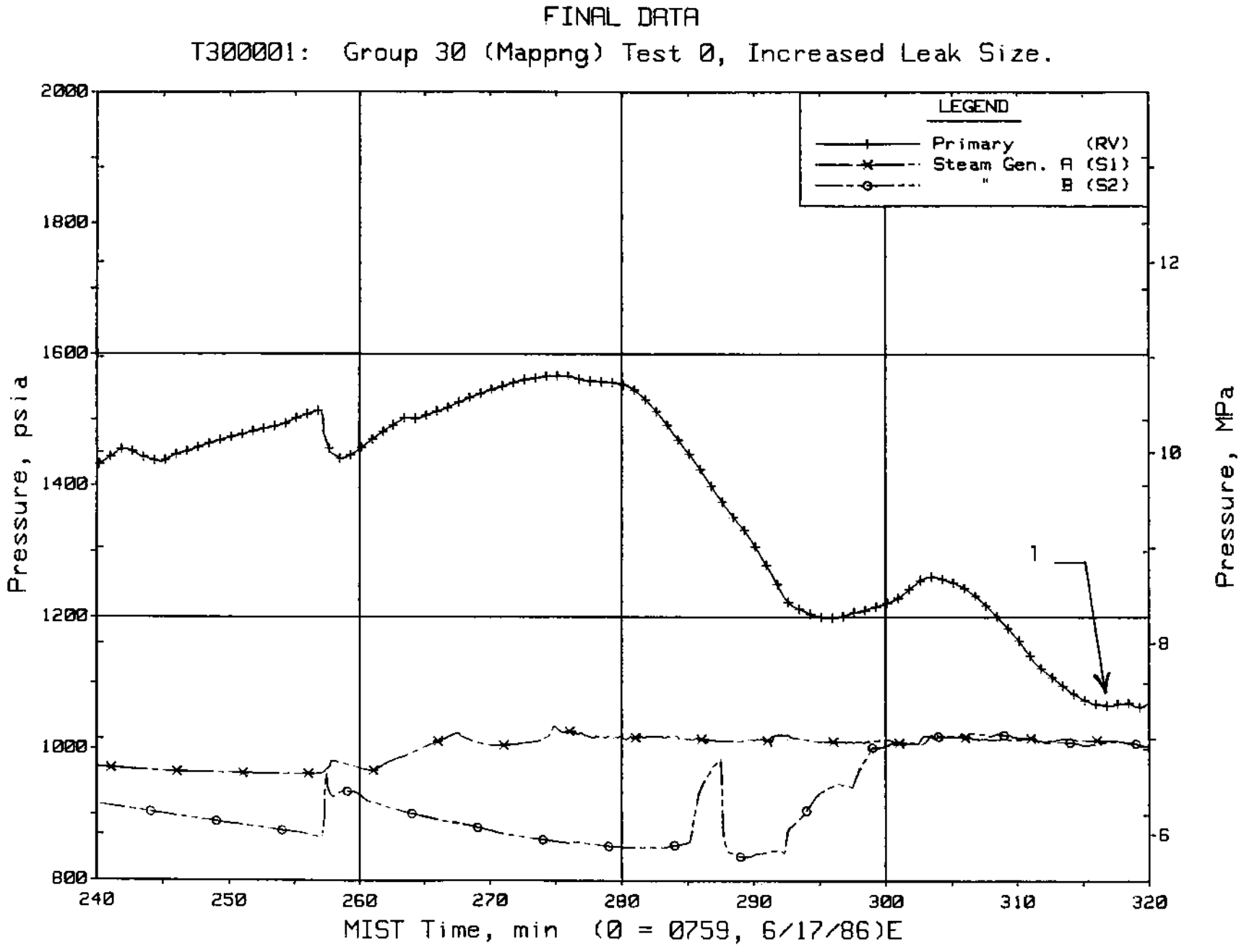

Figure 5.8.28. Primary and Secondary System Pressures (GP01s)

Wed Mar 15 14:58:42 1989

PSGP1

5.9. Pumps-On Mapping Test (300806)

Mapping Test 8 (300806) consisted of a gradual reduction of primary system total fluid inventory, followed by a post-termination refill, with all four pumps operating at rated speed throughout the test. This section addresses the system interactions, the pump characterization variables, and the pump performance observed during Mapping Test 30086.

System Interactions

Mapping Test 300806 was initialized with the leak and high-pressure injection (HPI) flow rates balanced, all pumps operating, and the loop full. The 0.0348-in. ID leak was located in the lower downcomer-to-reactor vessel piping. Core power was maintained near 125 kW, 3.8% of scaled full power, throughout the test. The steam generator secondary levels were maintained between 30.6 and 32.6 feet.

Pump two-phase characteristics were obtained by gradually reducing the primary system total fluid inventory (Figure 5.9.1) while continuing to operate all four pumps at rated speed. The reduction of primary system fluid inventory was accomplished by imposing a leak minus HPI flow rate imbalance (Figure 5.9.2) according to the following schedule:

Times, min	Approximate Imbalance, lbm/h	Estimated Primary System Total Fluid Mass (at start of period), lbm
-11 to 0	0	1040
0 to 51	30	1040
51 to 111	80	1015
111 to 172	200	935
172 to 202	280	735
202	(termination)	595

The flow rate imbalances were obtained by throttling HPI based on the current leak mass flow rate. In addition, the HPI flow rate was adjusted at approximately ten-minute intervals, when required, to accommodate variations in the leak mass flow rate as it responded to the changing fluid conditions at the leak site. The mass-reduction phase of the test was terminated at 202 minutes. The leak was closed, the hot leg vents were opened, and the HPI

flow rate was increased to 650 lbm/h (Figure 5.9.2). The pumps were kept in operation, thus the post-termination period continued to yield pump characterization information.

Pressurizer level and primary system pressure began to decline with the primary fluid mass reduction at time 0. The pressurizer drained at 20 minutes, causing the primary system to depressurize more rapidly from 1600 psia (Figure 5.9.3). The primary system pressure stabilized at 40 minutes as the leak mass flow rate declined to the current HPI mass flow rate, thus halting the primary system mass loss. The subsequent HPI adjustment to obtain a 100-lbm/h leak-minus-HPI imbalance at 51 minutes quickly depressurized the primary to saturation. The pump suction gamma densitometers began to register voiding (Figure 5.9.4) and the downcomer total primary mass flow rate began to decline from 120% of scaled full flow (Figure 5.9.5). (The MIST pumps were sized to provide more than scaled plant design full flow at rated speed, as in the plants.)

At 113 minutes, HPI was reduced further to obtain a 200-lbm/h difference between the leak and HPI mass flow rates (Figure 5.9.2). Immediately the pump A2 and B2 suction fluid temperatures increased approximately 3F, whereas the pump A1 and B1 temperatures remained approximately 7F below saturation at the reactor vessel pressure (Figure 5.9.6). The pump A2 and B2 inlet void fractions abruptly registered 100% (Figure 5.9.4) and the turbine meters associated with both pumps ceased to register flow (Figure 5.9.7). However, the pump A1 and B1 inlet void fractions dropped to zero. The cold leg nozzle fluid temperatures reflected a reduction or cessation of flow in loops A2 and B2 (Figure 5.9.8). Whereas the loop A1 and B1 fluid temperatures remained near saturation, the A2 and B2 cold leg nozzle fluid temperatures abruptly decreased due to HPI cooling with little loop flow. As pumps A2 and B2 voided, the downcomer mass flow rate dropped from 105 to 85% of scaled full flow (Figure 5.9.5).

The reactor coolant pump (RCP) A1 and B1 void fractions increased (Figure 5.9.4) as the primary system continued to lose inventory. These inlet void fractions became relatively variable at 140 minutes, and the downcomer mass flow rate registered another sharp decline from approximately 75 to 50% of scaled full flow (Figure 5.9.5). At this time, too, the feed and steam flow

rates of both generators began to decline (Figure 5.9.9) from 3% toward 2% of scaled full flow.

All pump inlet void fractions intermittently indicated complete voiding beyond 155 minutes, and the pump flow rates became similarly sporadic. The downcomer mass flow rate continued to decline, registering low off the scale (below approximately 10% of scaled full flow) beyond 170 minutes (Figure 5.9.5). HPI was terminated at 172 minutes (Figure 3.2) to obtain a 300-lbm/h primary fluid mass depletion rate. The primary system total fluid mass continued to decline from 735 lbm, achieving a maximum depletion of nearly 40% of its initial full value (Figure 5.9.1). The primary system pressure remained just above the secondary system pressures (Figure 5.9.3), apparently reflecting the boiler-condenser mode (BCM) in forced flow.

Description of Pump Characteristics

Pump performance was determined using the parameters defined by Tetratech (cf. PMG Correspondence 685, 20 May 1987). The basic variables were normalized pump speed, volumetric flow rate, and head. Each of these normalized variables involved its rated counterpart. Rather than using the MIST pump design values, the rated characteristics were extracted from the pre-test, steady-state data. These rated characteristics were as follows:

Rated Pump Characteristics

	Pump			
	A1	B1	A2	B2
Speed, rpm	3533	3485	3526	3498
Volumetric Flow Rate, gpm	134	133	132	132
Head, ft	345	337	338	336

The volumetric flow rates were obtained from the cold leg turbine meters. Heads were obtained by dividing the measured differential pressure (psf) by the corresponding pump suction fluid density (lbm/ft^3) obtained from the gamma densitometer measurements. Homologous flow was the ratio of normalized volumetric flow rate to normalized speed. Homologous head was the ratio of normalized head to the square of the homologous flow. These pump parameters defined by Tetratech were similar to but not the same as those in common

usage. To facilitate the comparison between the Tetratech parameters and those commonly encountered (such as those defined in EPRI NP-2578, "Two-Phase Performance of Scale Models of A Reactor Coolant Pump," September 1982), denote normalized speed, volumetric flow rate, and head as "sn, qn, and hn," respectively. Then, the Tetratech homologous flow is

$$hf = qn/sn$$

and the Tetratech homologous head is

$$hh = hn/hf^2 = hn\ (sn/qn)^2.$$

The generally encountered homologous flow and head are

$$hf' = sn/qn \text{ (and } qn/sn),$$

and $hh' = hn/sn^2$ (and hn/qn^2).

The Tetratech definitions are used herein. Because the MIST pumps were generally operated at full speed, the differences between the definitions of pump parameters had little net impact.

SEMISCALE/RELAP predictions of homologous head are also addressed. The SEMISCALE/RELAP predictions were obtained by linear interpolation among the values of head degradation versus void fraction given in RELAP. The fully degraded MIST head was assumed to be zero; then, for pump normalized speeds near unity, the normalized head predicted by SEMISCALE/RELAP was the head degradation factor. Using the homologous head definition

$$hh = hn/hf^2$$

and equating the normalized head (hn) to the SEMISCALE/RELAP head degradation factor (M), the homologous head predicted by SEMISCALE/RELAP and presented herein was

$$hh = M/hf^2.$$

Pump Performance

Pump performance is conveniently described in 5 phases keyed to the pump-suction void fractions. These 5 phases are as follows:

Phase	Times (min)	Description
1	0 to 51	No voiding.
2	51 to 113	Increasing void fractions.
3	113 to 115	RCPs A2 and B2 completely voided.
4	155 to 240	Complete voiding, intermittent pump activity.
5	240 to end of data acquisition	Refill period.

Phase 1, Subcooled

The pump suction void fractions remained zero from 0 to 51 minutes (Figure 5.9.4). The primary system total flow rate remained almost constant at 120% of scaled full flow (Figure 5.9.5) and the pump performance indicators remained at their rated values (Figure 5.9.10). The relatively low suction head requirements of the MIST pumps were thus confirmed -- the inlet pressure excess over saturation pressure dropped to less than 100 psi during this period (Figure 5.9.11).

Phase 2, Increasing Voiding

In response to the continuing depletion of primary system total fluid mass, the pump suction void fractions gradually increased from 51 to 111 minutes (Figure 5.9.12). The void fraction differences among loops was within the uncertainty associated with the preliminary nature of the gamma densitometer data. The pump speeds remained at their rated values, as they did throughout the test. The pump volumetric flow rates increased by nearly 5% as the void fractions increased from 0 to 10%, then behaved unequally among the pumps as the void fractions continued to increase to 15% (Figure 5.9.13). The pump B1 volumetric flow rate increased to 8% above rated, those of the other 3 pumps decreased to 2 to 4% above rated. The pump pressure rise exhibited similar performance, with the rise across pump B2 remaining near 103 psi after an initial decrease from 110 psi, while the rise across the other pumps decreased several more psi (Figure 5.9.14). The normalized heads behaved somewhat differently, reflecting the effects of both differential pressure and pump suction fluid density. Whereas the observed normalized heads generally rose to nearly 10% above rated (Figure 5.9.15), the normalized heads predicted by

the SEMISCALE/RELAP degradation decreased to about 4% below rated. The observed heads began to degrade toward the end of the phase near 110 minutes. The SEMISCALE/RELAP predicted degration simply reflects head degradation versus void fraction. However, the observed normalized head increased almost linearly with void fraction from unity at zero void fraction to 1.08 at 10% voids. The observed normalized head remained approximately constant until 13% void fraction, then began to degrade relatively rapidly.

The observed homologous head remained almost constant with void fraction (Figure 5.9.16). The SEMISCALE/RELAP prediction decreased to about 0.9 by 14% voids; lower values were predicted for pump B1 because of its increasing homologous flow, and vice versa for pump A2.

Pump electrical power diminished regularly with void fraction during Phase 2, decreasing by about 4% for a 15% increase in void fraction (Figure 5.9.17).

Phase 3, Two Pumps Voided

Pumps A2 and B2 voided completely at 111 minutes, coinciding with the reduction of the HPI flow rate from approximately 180 to 80 lbm/h. The pump suction fluid temperatures of the voided pumps then remained a few degrees higher than those of the non-voided pumps (Figure 5.9.18), their pressure rises dropped almost to 40 psi (versus 70 psi across the non-voided pumps, Figure 5.9.19), and their turbine meters ceased to indicate flow. Pumps A1 and B1 partially compensated for the voided pumps, however. Their inlet void fractions dropped almost to zero (Figure 5.9.20), and their normalized volumetric flow rates increased to 1.5 (Figure 5.9.21). The downcomer mass flow rate thus decreased only from 105 to 85% of scaled full flow (Figure 5.9.5). From 115 to 153 minutes, the suction void fractions of pumps A1 and B1 gradually increased while pumps A2 and B2 remained completely voided. Because the cold leg A2 and B2 turbine meters indicated no flow during this period, their homologous flows were likewise zero and their homologous heads were indeterminant. Therefore, only the characteristics of pumps A1 and B1 are pursued during this phase.

Although pumps A1 and B1 continued to operate throughout Phase 3, their behavior became noticeably erratic beyond 136 minutes. At this time, the downcomer fluid temperatures at the elevation of the reactor vessel vent

valves (RVVVs) abruptly increased from 30F subcooled to saturation, indicating the formation of a defined voided volume in the upper downcomer. Also at this time, the HPI flow rate became increasingly variable (Figure 5.9.22), although the time-averaged value remained approximately constant.

The pump A1 and B1 normalized heads increased gradually with void fraction (and with time) from 0.62 at 0 voids to about 0.7 at a void fraction of 16% (Figure 5.9.23). Over this range, the normalized head predicted by SEMISCALE/ RELAP remained constant and then decreased. System conditions became relatively variable beyond 138 minutes, as has been mentioned previously. This variability is reflected in the scatter of normalized head in the 11 to 25% void fraction range. Homologous heads versus void fractions indicated similar behavior (Figure 5.9.24), first remaining almost constant and then becoming scattered. The predicted homologous heads also scattered because of the involvement of homologous flow. Between 0 and 16% void fraction, the observed homologous head was approximately 0.7, versus 0.5 predicted by RELAP/SEMISCALE. Pump electrical power decreased gradually with void fractions up to 18%, then became scattered at much lower powers (Figure 5.9.25).

Phase 4, Intermittent Voiding

All pumps performed intermittently from 153 to approximately 240 minutes. The onset of this behavior occurred as the void fraction of the two non-voided pumps, A1 and B1, approached 20% (Figure 5.9.20). Throughout Phase 4, the pump characteristics were highly variable, and therefore not amenable to the usual point-by-point examination. Moreover, the cold leg turbine meters generally indicated zero volumetric flow throughout Phase 4; thus, the homologous flows were zero and the homologous heads were indeterminant. Some normalized head information was available. Although the data points are quite scattered, the observed normalized heads were apparently degraded even at low void fractions whereas the SEMISCALE/RELAP predictions did not degrade until void fractions exceeded 15% (Figure 5.9.26). Both the observed and predicted heads remained near zero from 25 to 80% void fraction. At the highest void fractions, the SEMISCALE/RELAP normalized head was predicted to recover, and recovery was observed. The observed normalized head sometimes approached 10 at unity void fraction. Apparently the liquid pulses through

the pump were of sufficiently short duration that the time lag between the ingredient measurements, pump suction fluid density from gamma densitometers, and pump differential pressures from transducers rendered inaccurate the instantaneous observed heads. The same sort of signal timing offset apparently affected pump power versus void fraction (Figure 5.9.27), suggesting that the timing of the gamma densitometer density determination caused the scatter observed at the highest void fractions. Pump power declined quite regularly through 40% void fraction, remained at a minimum value of approximately 8 kW through 80% void fraction, and then became scattered but with most data points still at the minimum power.

The system interactions between 153 and 240 minutes, although intermittent, were composed of repetitive and relatively high-frequency interactions. As a steam generator feed rate was increased to regain level, the primary fluid temperatures gradually cooled -- first near mid-height, then at the lower elevations. Although this occurred alternately in the two steam generators, it was more readily observed in steam generator B because of its larger set of primary fluid temperature measurements. For example, the generator B feed rate was increased beyond 181.3 minutes (Figure 5.9.28) to counteract the level decrease that began at 181.1 minutes (Figure 5.9.29). The generator B primary fluid at 26 ft began to cool at 181.7 minutes and the outlet fluid began to cool at 181.9 minutes (Figure 5.9.30). The densification of the steam generator primary fluid apparently raised the effective levels in the loop B cold leg risers, presenting lower void fraction fluid to the B pumps (Figure 5.9.31). The loop B pump suction fluid density began to increase from just greater than that of saturated vapor at 181.9 minutes, approaching the saturated liquid density by 182.2 minutes. At 182.4 minutes, the electrical power, generated differential pressure, and associated volumetric flow rate of both the loop B pumps began to increase (Figure 5.9.32 through 5.9.34), with pump B1 exceeding pump B2. (The volumetric flow rate indications are delayed approximately 15 seconds in this presentation of preliminary data due to the turbine meter signal processing.) The loop B flow pulse was short-lived. The relatively dense loop B steam generator outlet fluid was quickly drawn through the pumps and replaced with warmer primary fluid (Figures 5.9.35 and 5.9.36), the pump suction fluid density subsided (Figure 5.9.37), and the loop B pumps lost suction. But the steam generator B

activity elevated the generator B secondary pressure (Figure 5.9.38) and caused increased steaming (Figure 5.9.28), thus returning conditions towards those that preceded the cycle. Although these cyclic events occurred separately in the two loops, they did not occur alternately or at a constant inter-loop frequency. This inter-loop independence is apparent, for example, in the behavior of pump power (Figure 5.9.32) and pump differential head (Figure 5.9.33). The interaction frequency appears to have been dependent not only on the pump characteristics and suction geometry, but also on the characteristics of the steam generator secondary feed and steam controls.

Phase 5, Pump Recovery

Loop refill was begun at 202 minutes, but the pumps continued to perform intermittently through 240 minutes. Between 251 and 256 minutes, the void fraction of the last two voided pumps, A1 and B2, abruptly dropped from 1 to 0 (Figure 5.9.39). However, the pump A1 inlet fluid temperature continued to follow saturation (Figure 5.9.40), the cold leg A1 turbine meter continued to register zero flow (Figure 5.9.41), and the power to pump A1 remained at its degraded value (Figure 5.9.42) although it did rise briefly. In loop B, however, as pump B2 regained suction, the flow and power requirements of pump B1 decreased (Figures 5.9.41 and 5.9.42), and pumps B1 and B2 began to operate symmetrically.

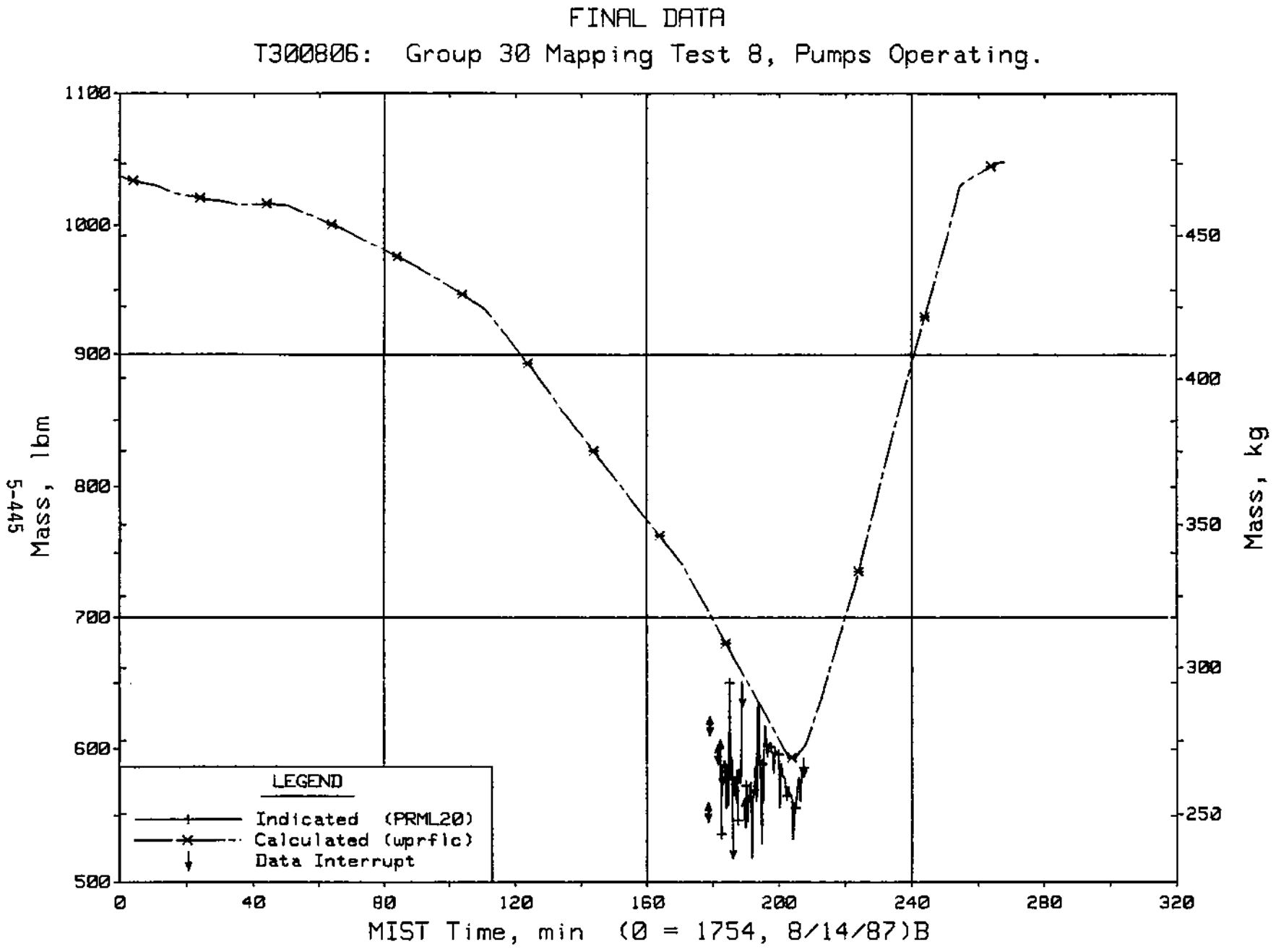

Figure 5.9.1 Primary System Total Fluid Mass

Tue Mar 21 13:19:29 1989

PRML5

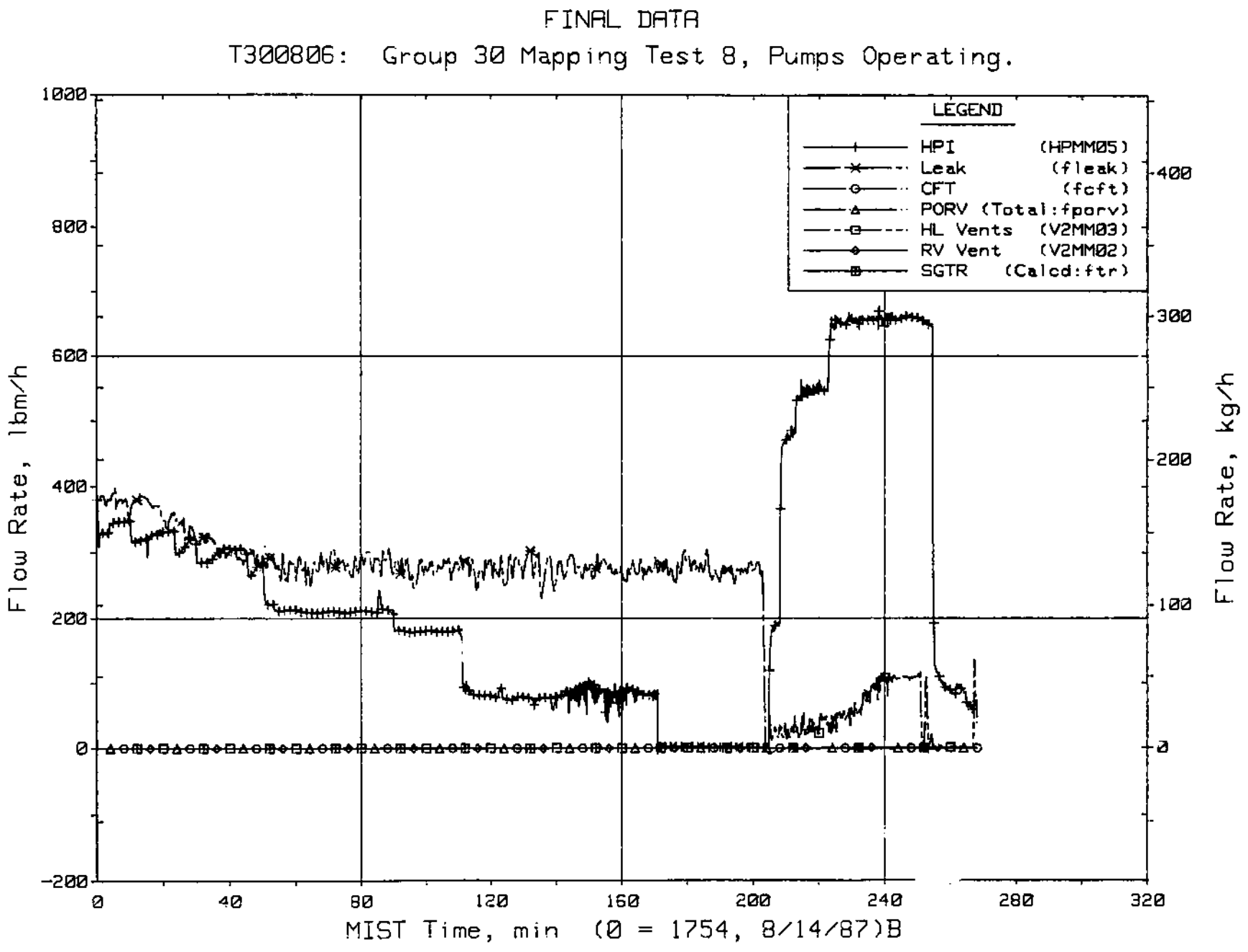

Figure 5.9.2 Primary System Boundary Flow Rates

Wed Mar 22 15:05:27 1989

PRFL3

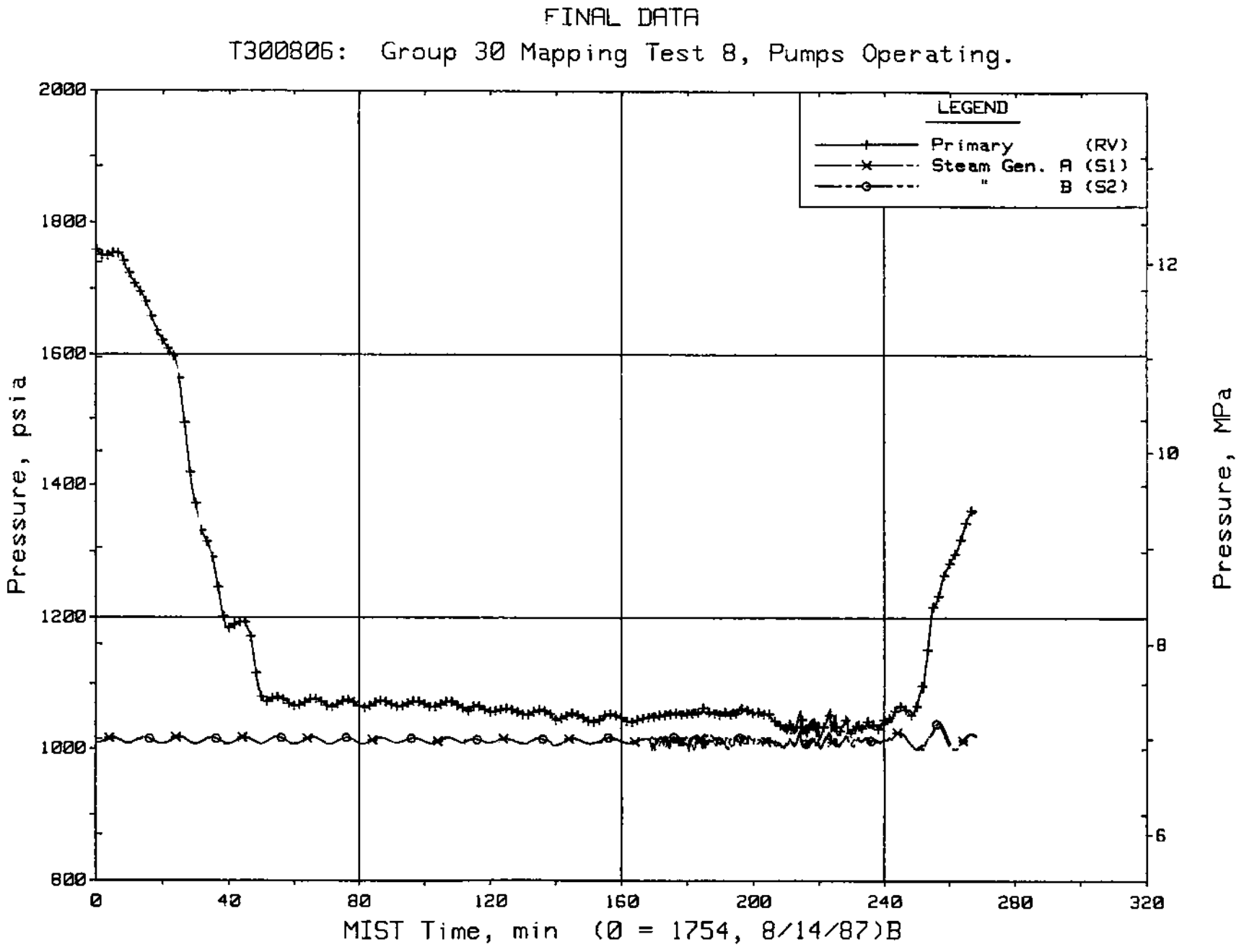

Figure 5.9.3 Primary and Secondary System Pressures (GPOIs)

Wed Mar 22 14:51:39 1989

PSGP1

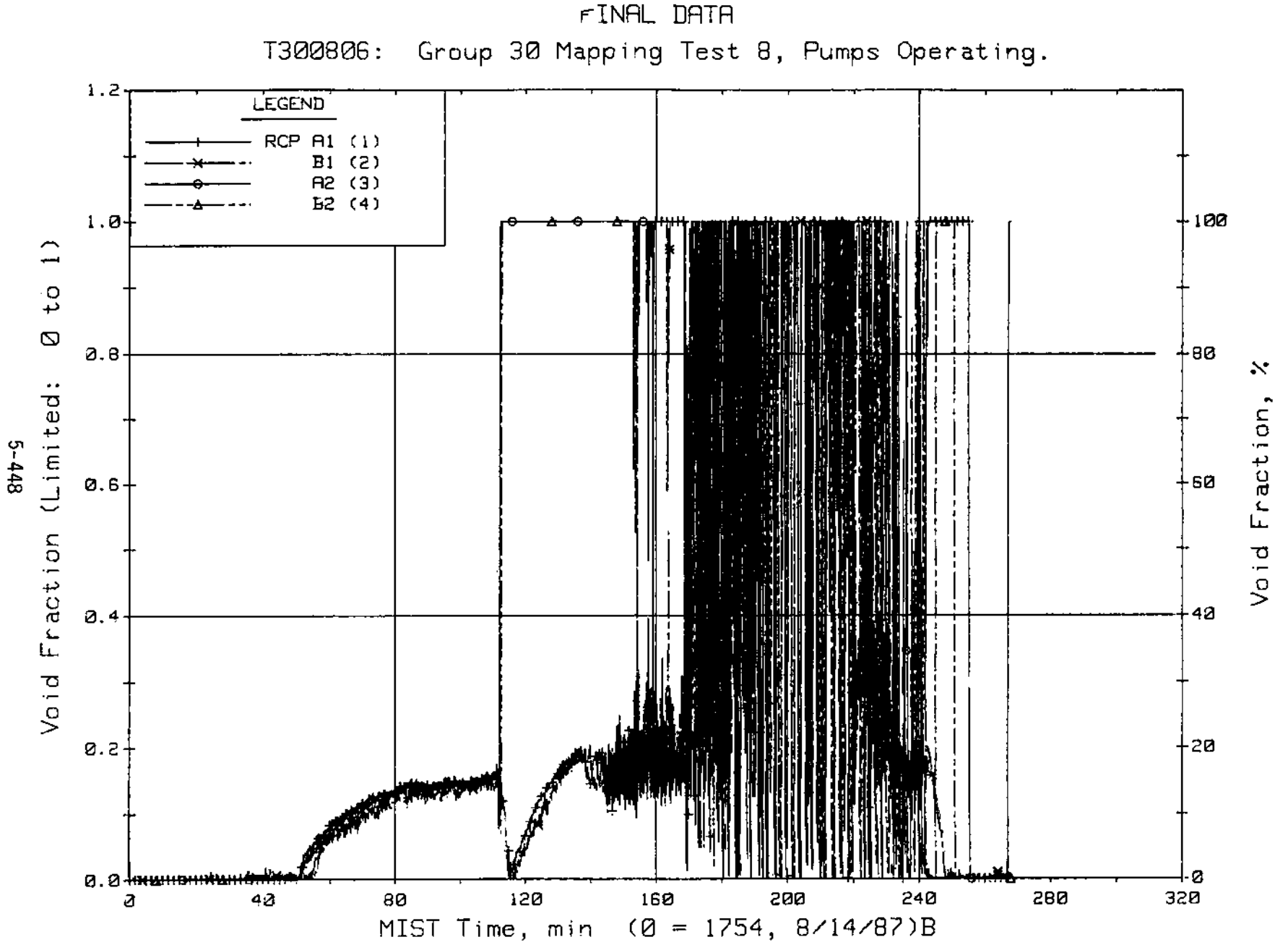

Figure 5.9.4 Pump Suction Void Fraction From Gamma Densitometers (puNfv)

Wed Mar 22 14:42:54 1989

PUVF1

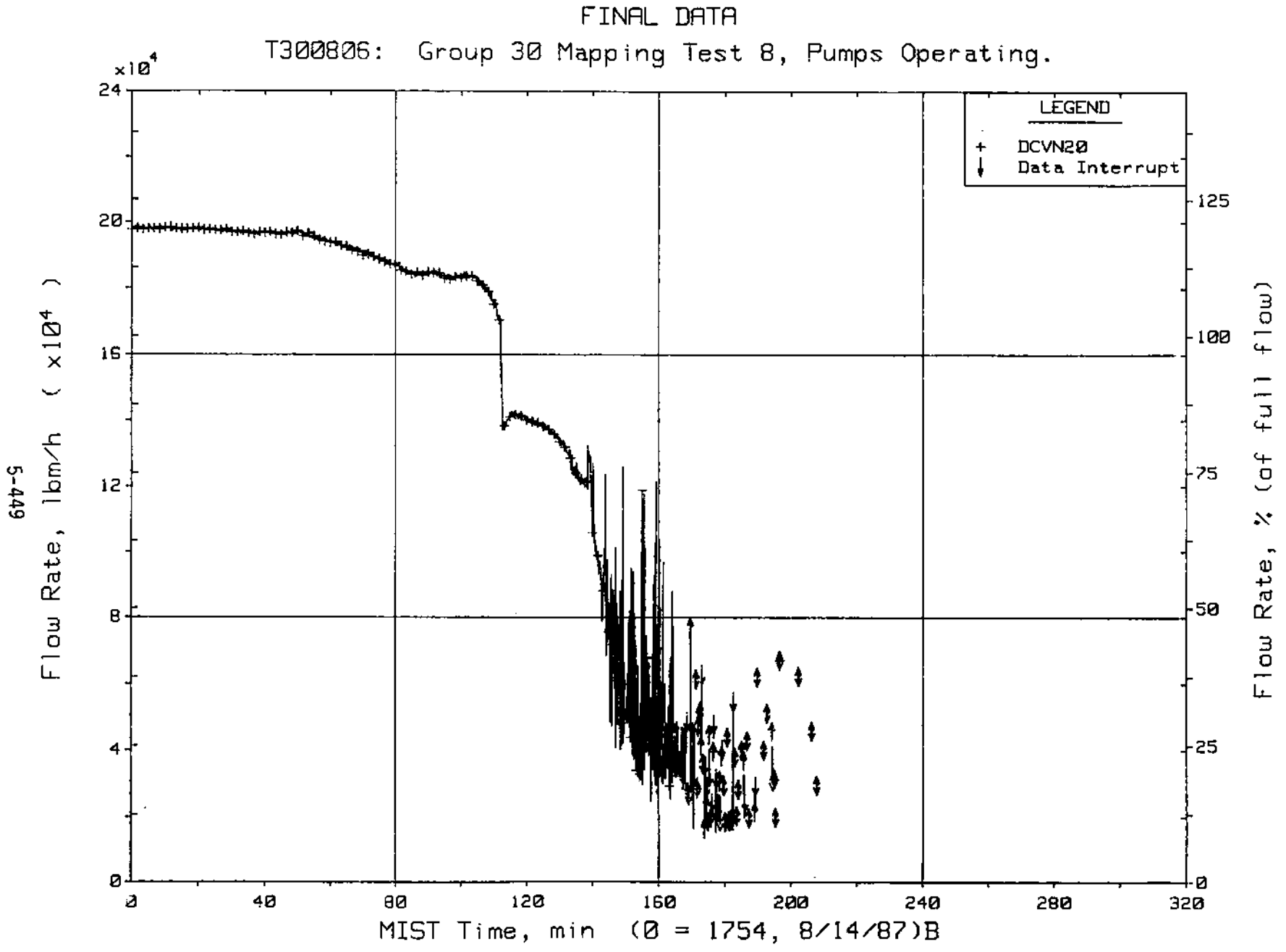

Figure 5.9.5 Downcomer (Venturi) Flow Rate

Wed Mar 22 14:31:46 1989

DCFL1

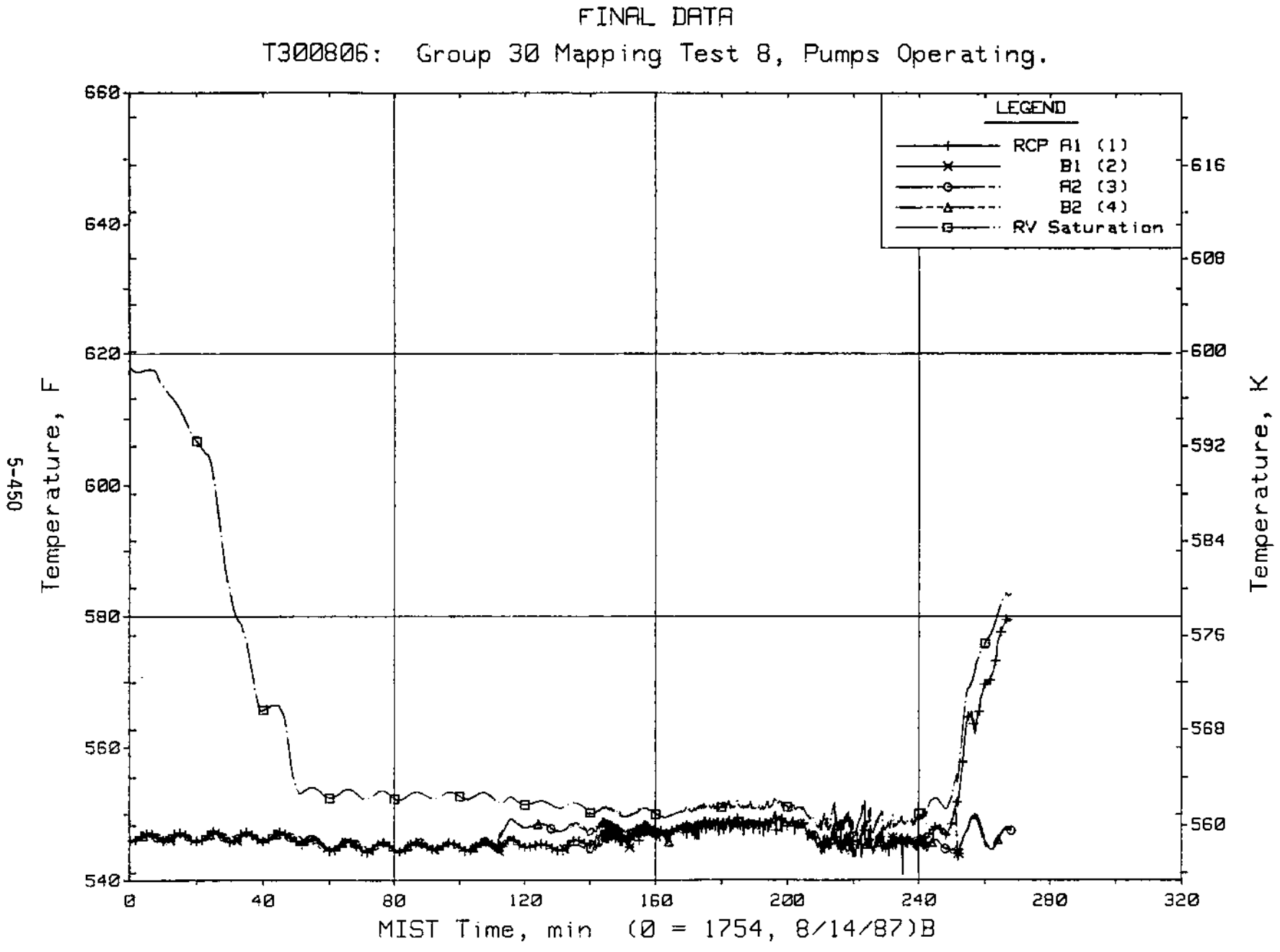

Figure 5.9.6 Pump Suction Fluid Temperature (CnRTDIs)

Wed Mar 22 14:26:55 1989

PLRT0

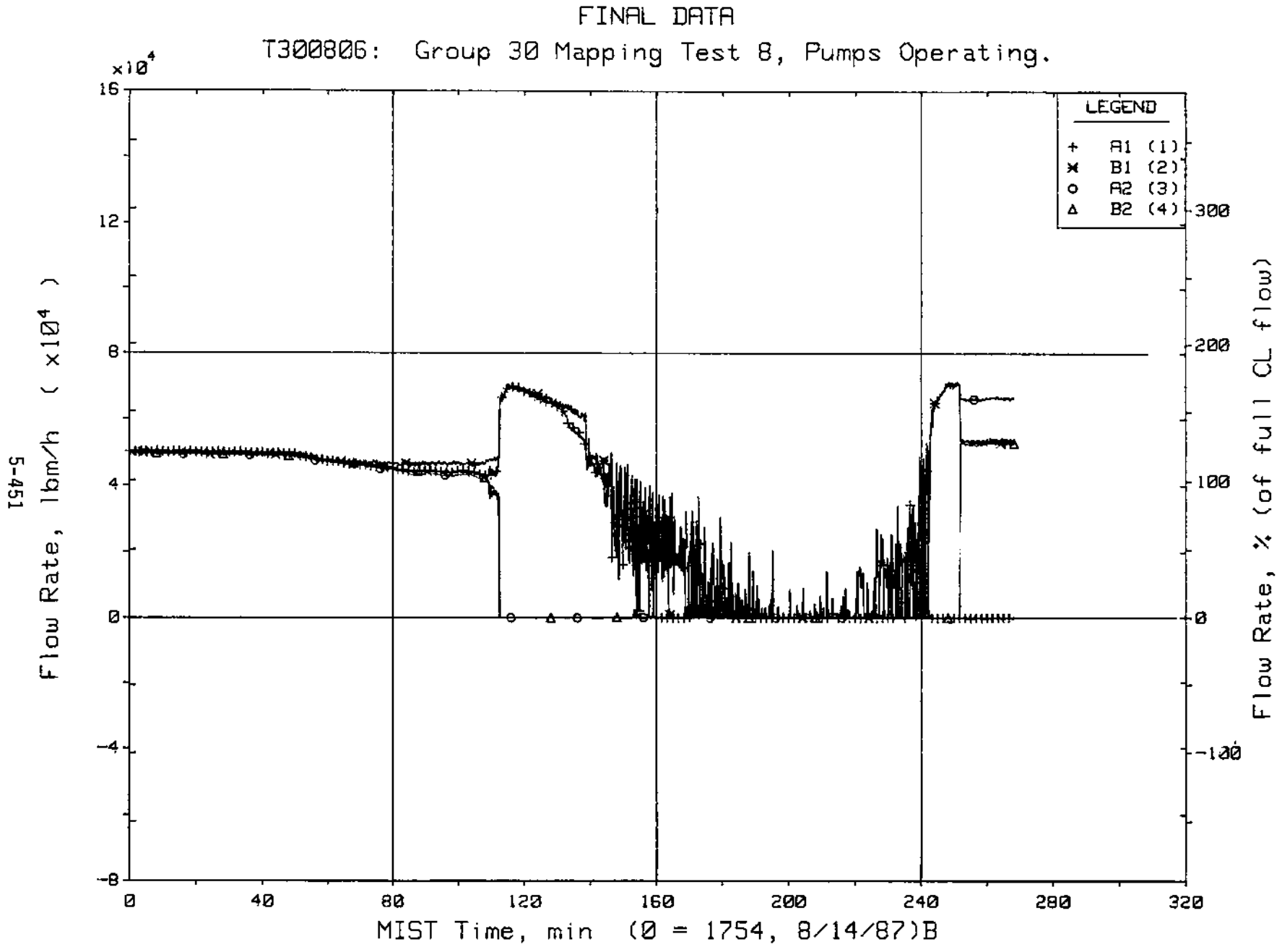

Figure 5.9.7 Cold Leg (Turbine Meter) Mass Flow Rates (CnTM01s)

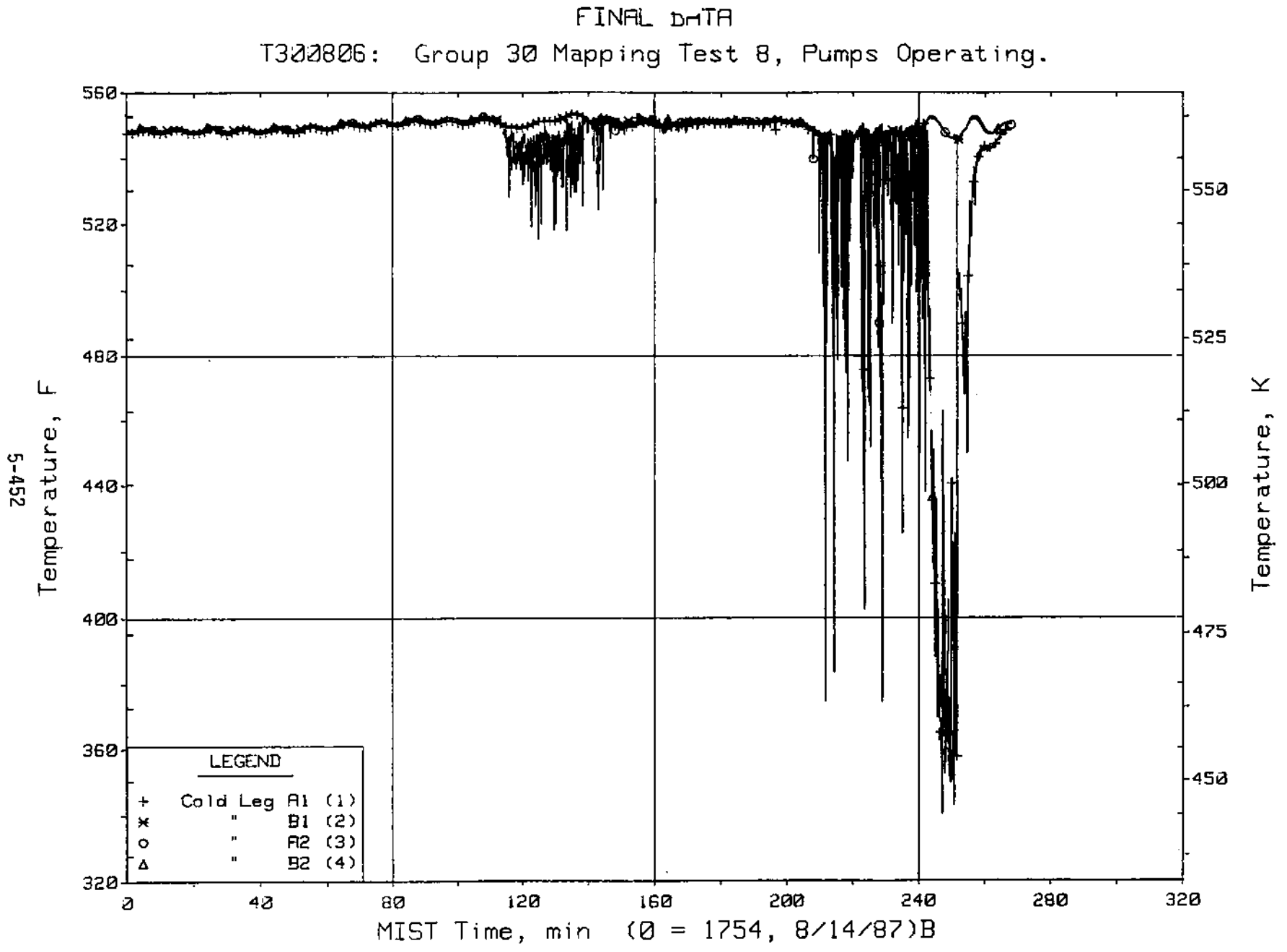

Figure 5.9.8 Cold Leg Nozzle Fluid Temperatures, Bottom of Rake (21.2 ft, CnTC14s)

Wed Mar 22 14:09:34 1989

CLTC2

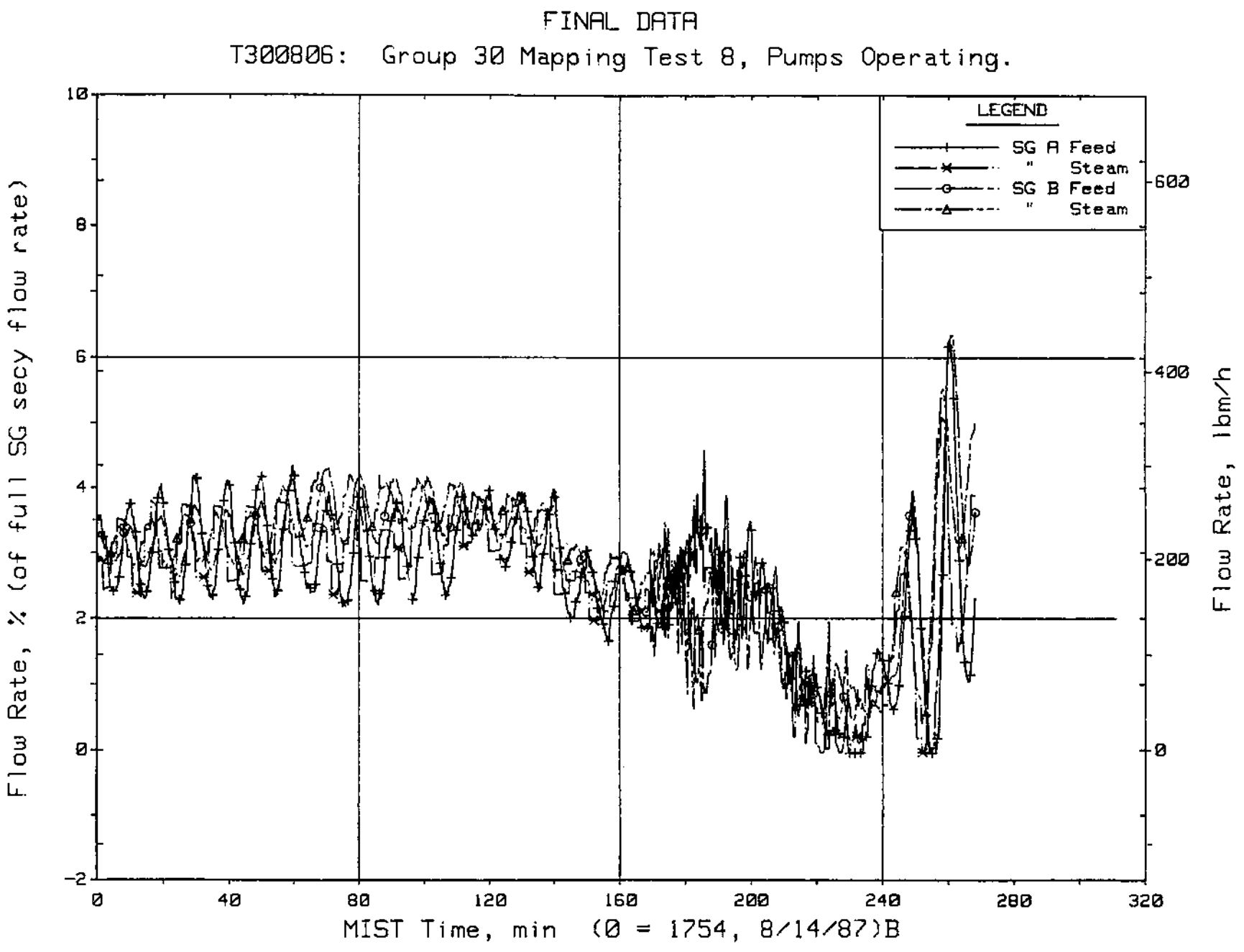

Figure 5.9.9 Secondary System Flow Rates

Wed Mar 22 14:02:36 1989

SGFL2

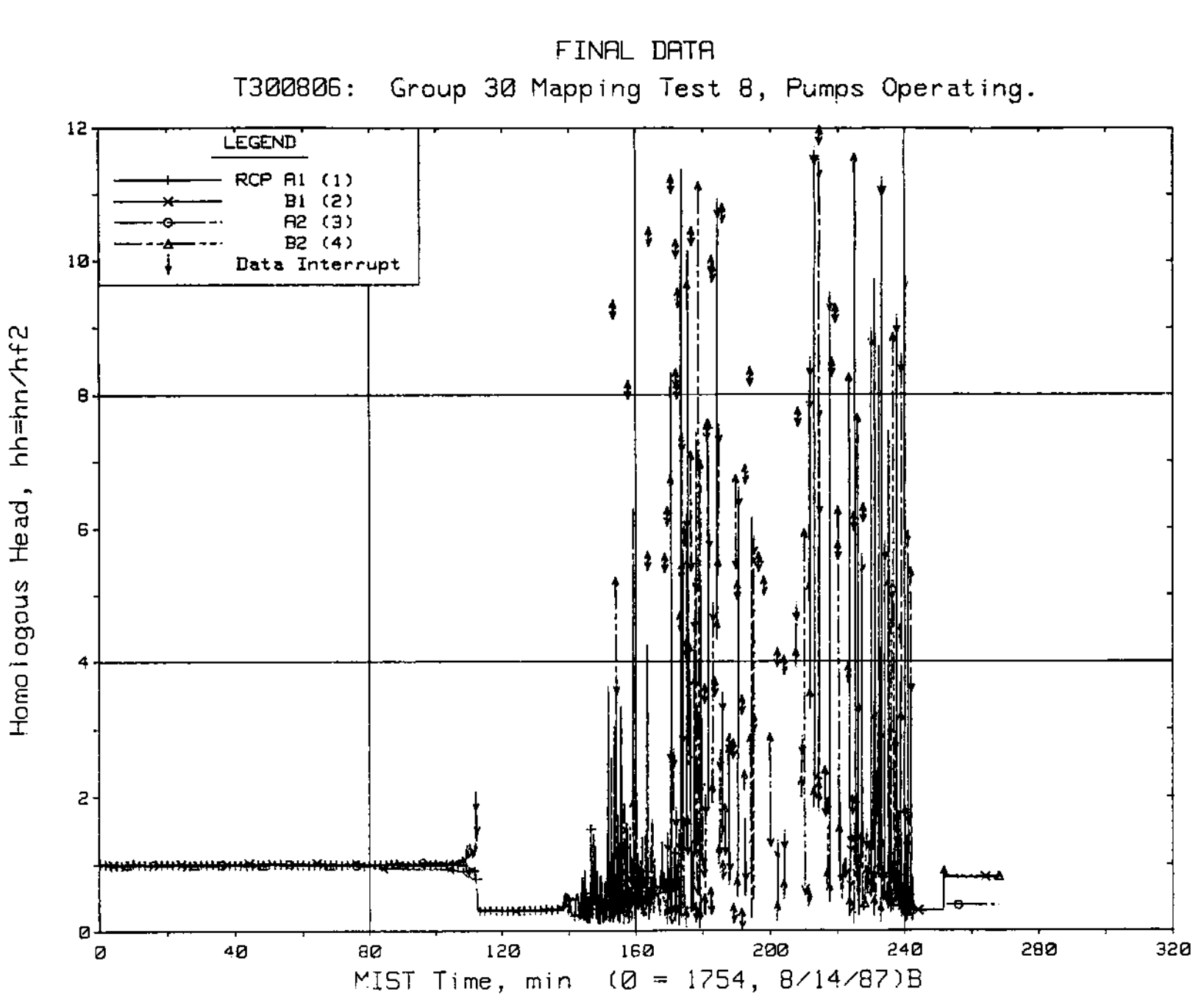

Figure 5.9.10 Observed Pump Homologous Head Parameter (puNhh)

Wed Mar 22 13:49:30 1989

PUHH1

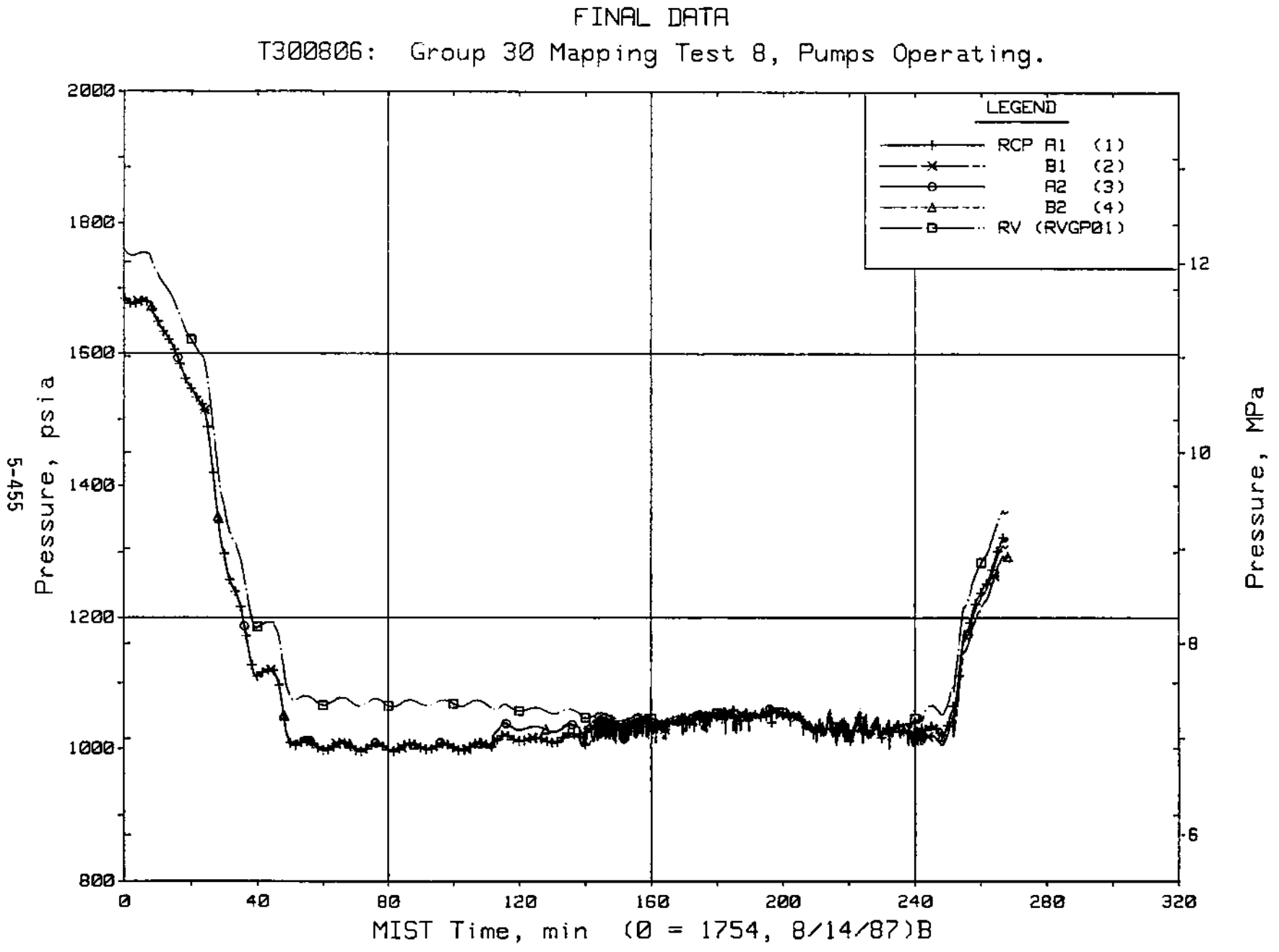

Figure 5.9.11 Pump Suction Pressure (puNpr)

Wed Mar 22 13:43:28 1989

PUGP1

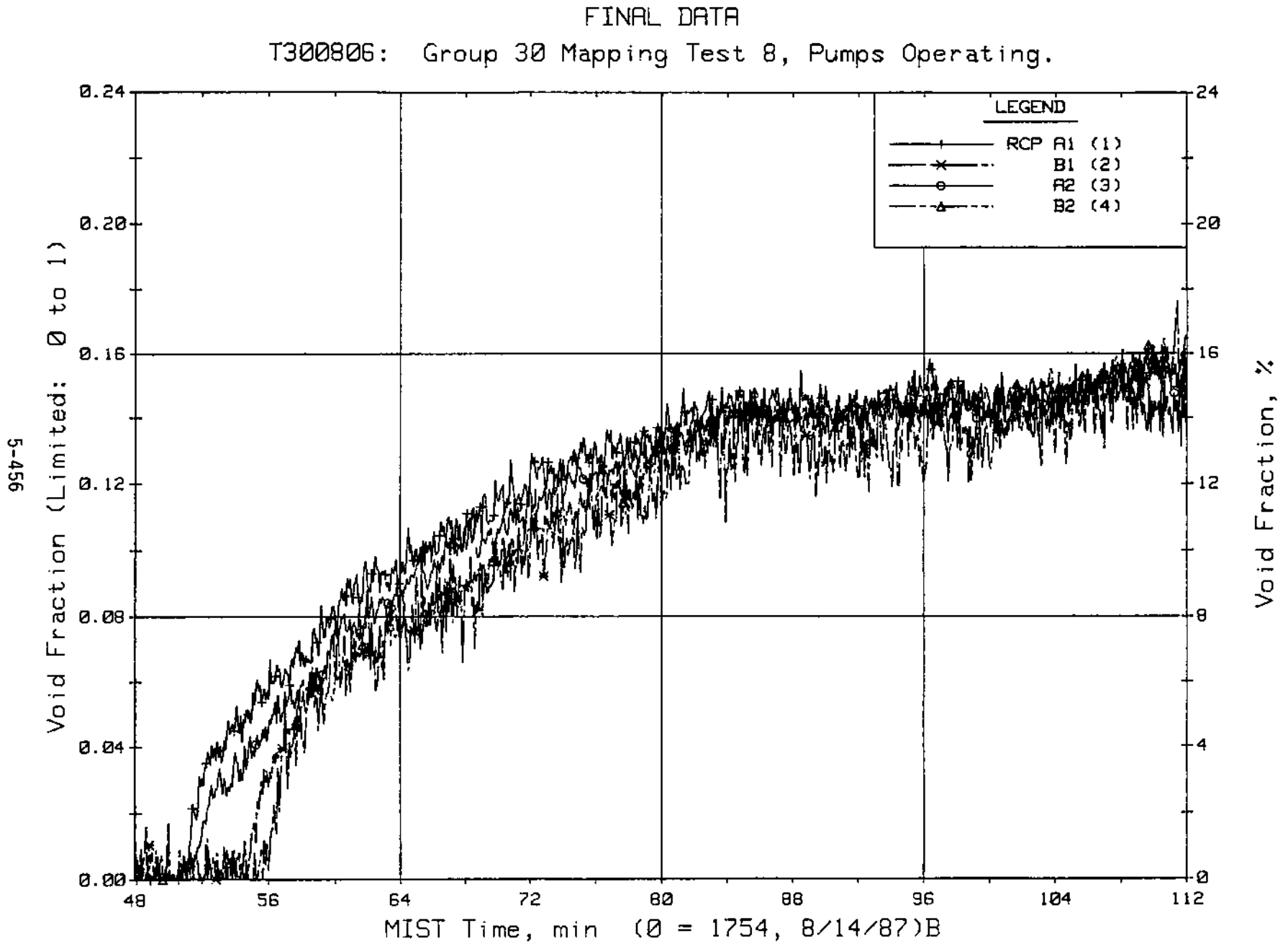

Figure 5.9.12 Pump Suction Void Fraction From Gamma Densitometers (puNfv)

Wed Mar 22 13:35:13 1989

PUVF1

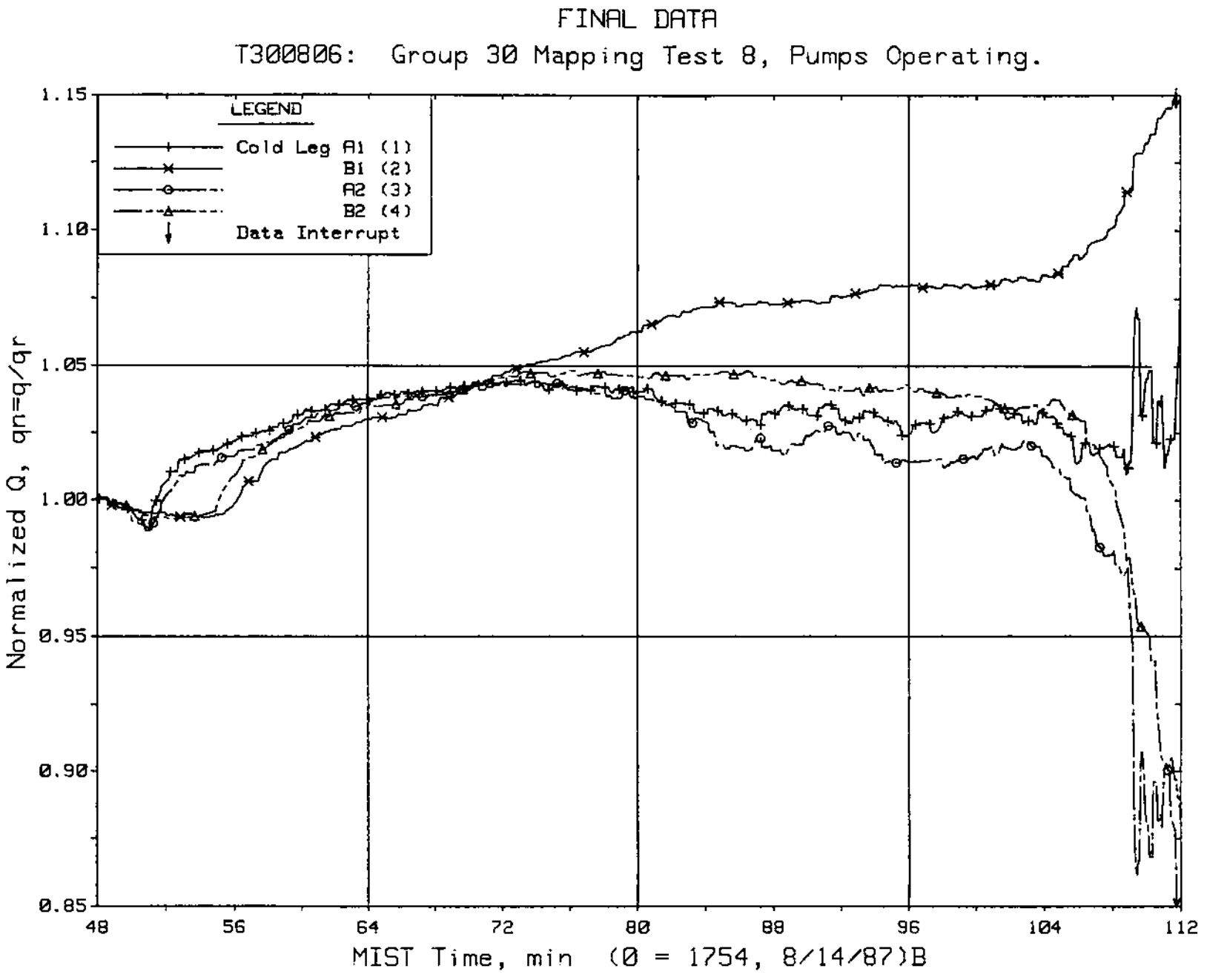

Figure 5.9.13 Pump Normalized Volumetric Flow Rate

Wed Mar 22 13:26:46 1989

PUQN1

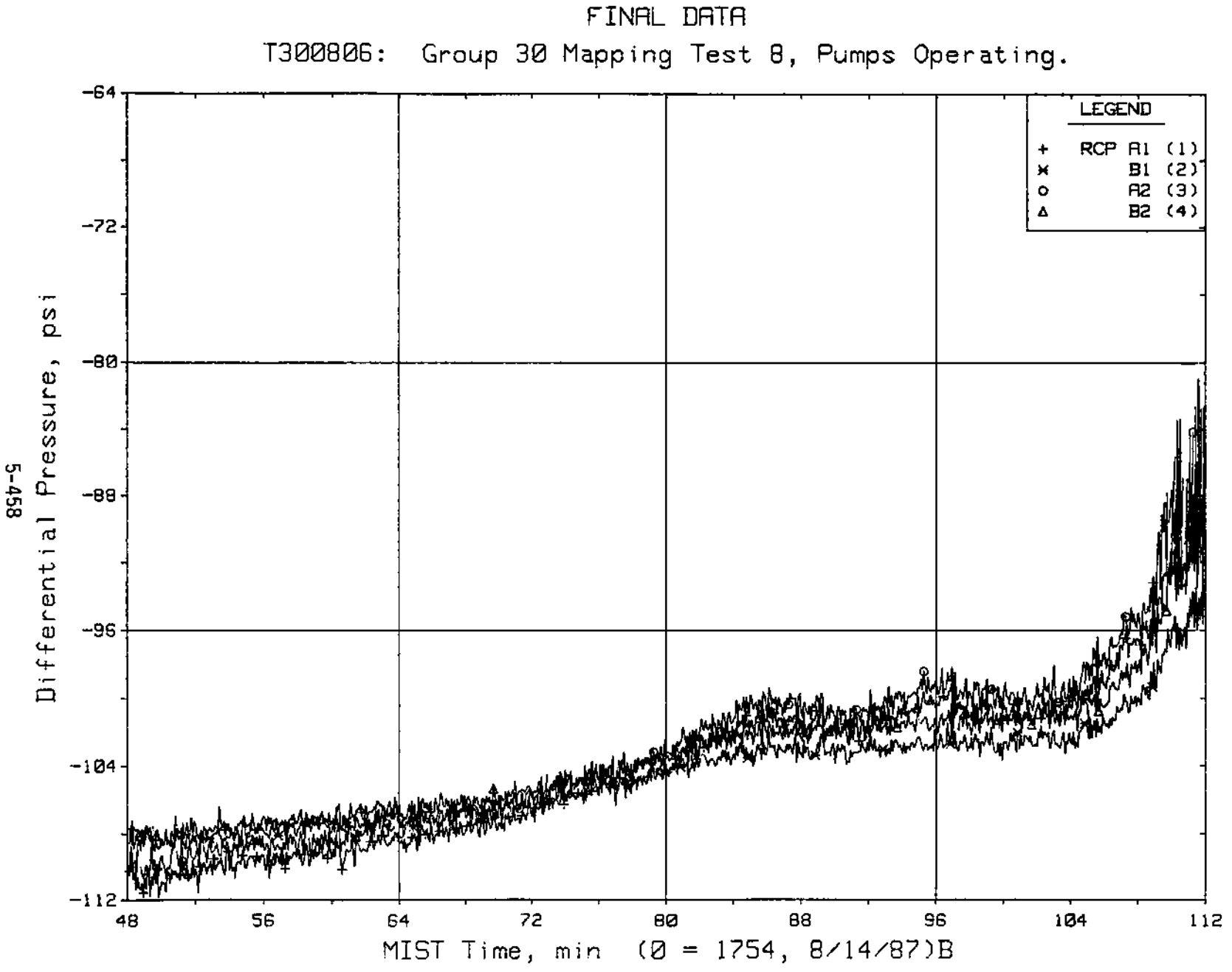

Figure 5.9.14 Pump Pressure Drop (CnDP07s)

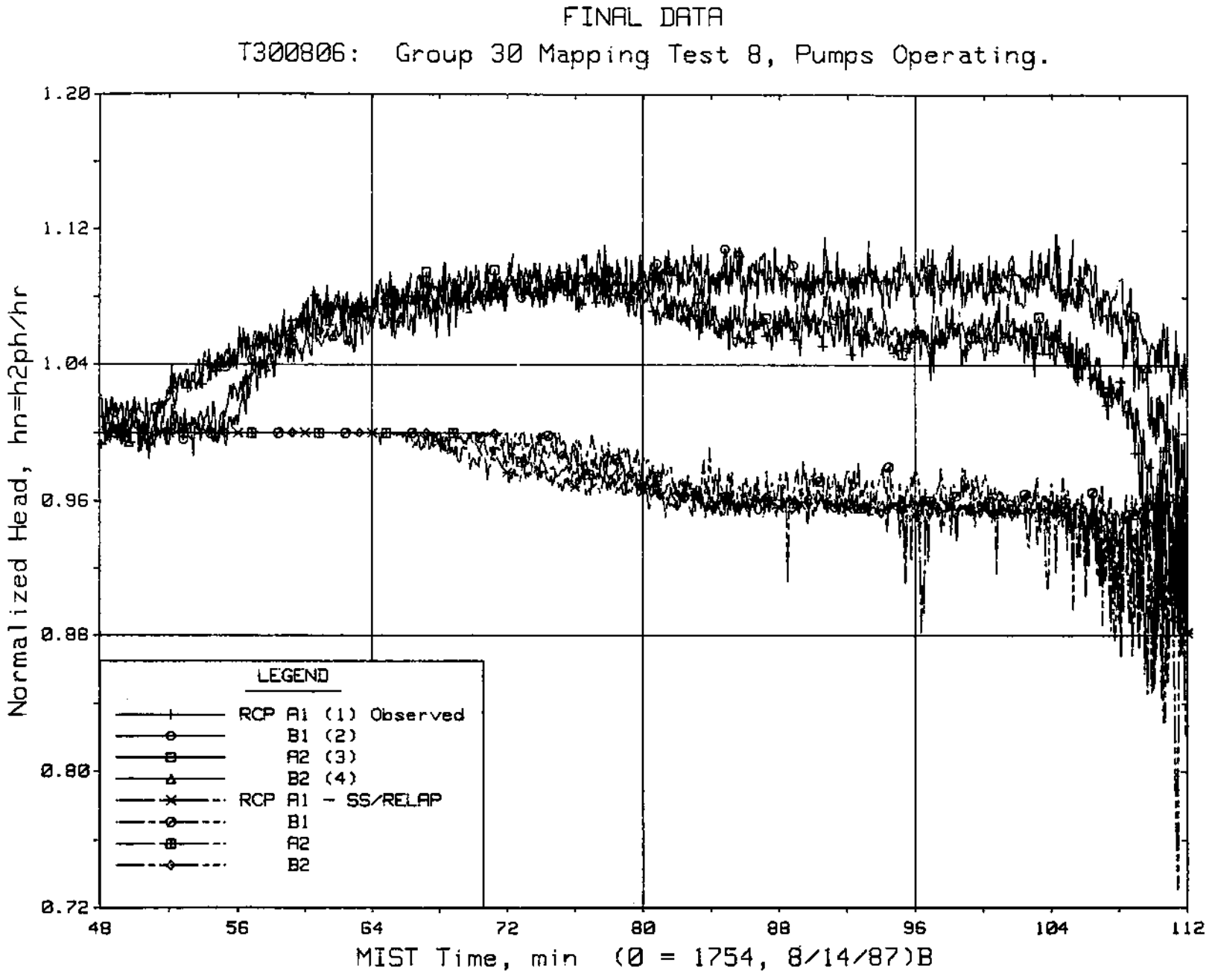

Figure 5.9.15 Pump Normalized Head

Wed Mar 22 13:17:35 1989

PUHN1

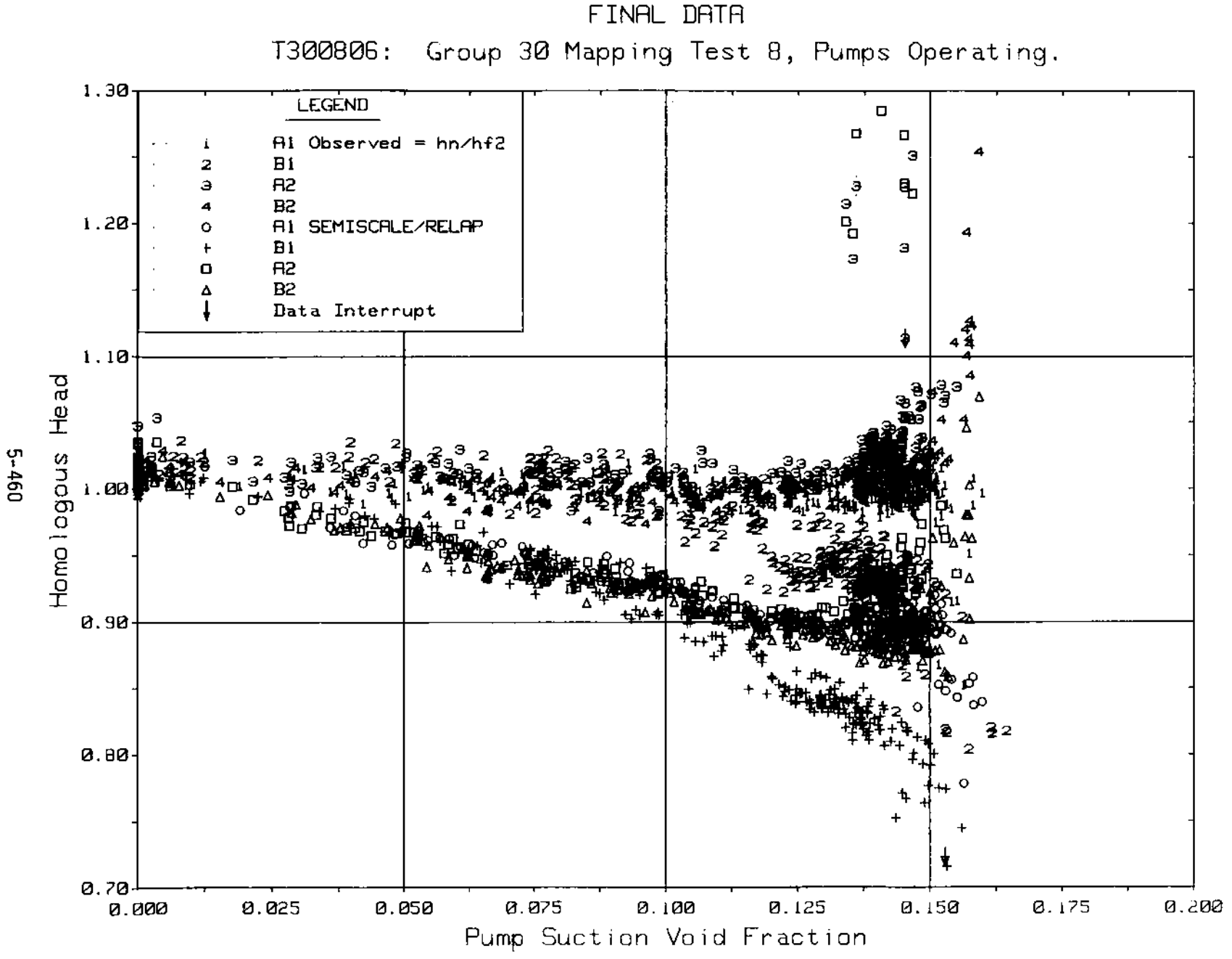

Figure 5.9.16 Pump Homologous Head Vs Void Fraction, 50 to 111 Minutes

PUHvA

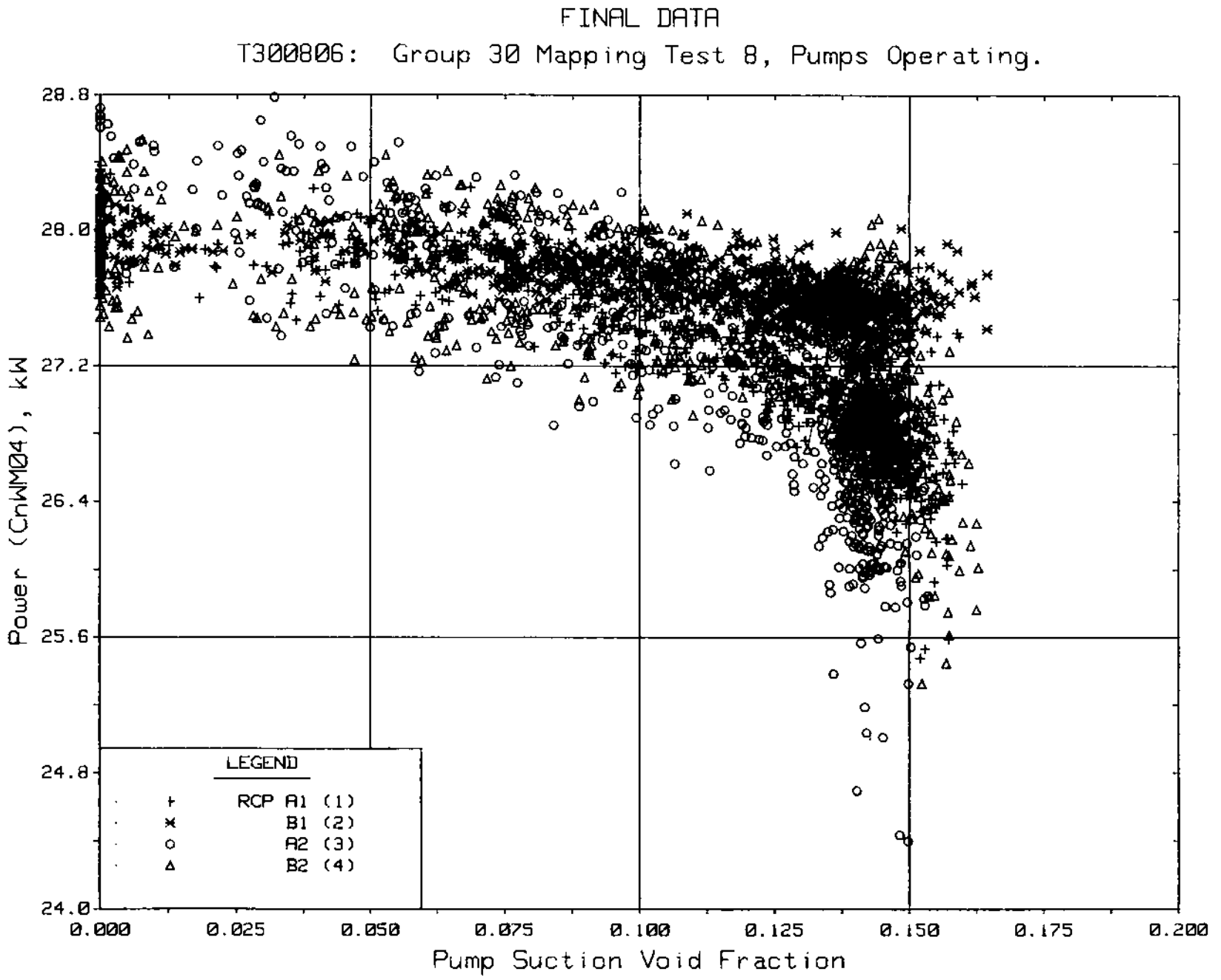

Figure 5.9.17 Pump Electrical Power Vs Void Fraction, 50 to 111 Minutes

Mon Mar 27 13:44:35 1989

PUWvA

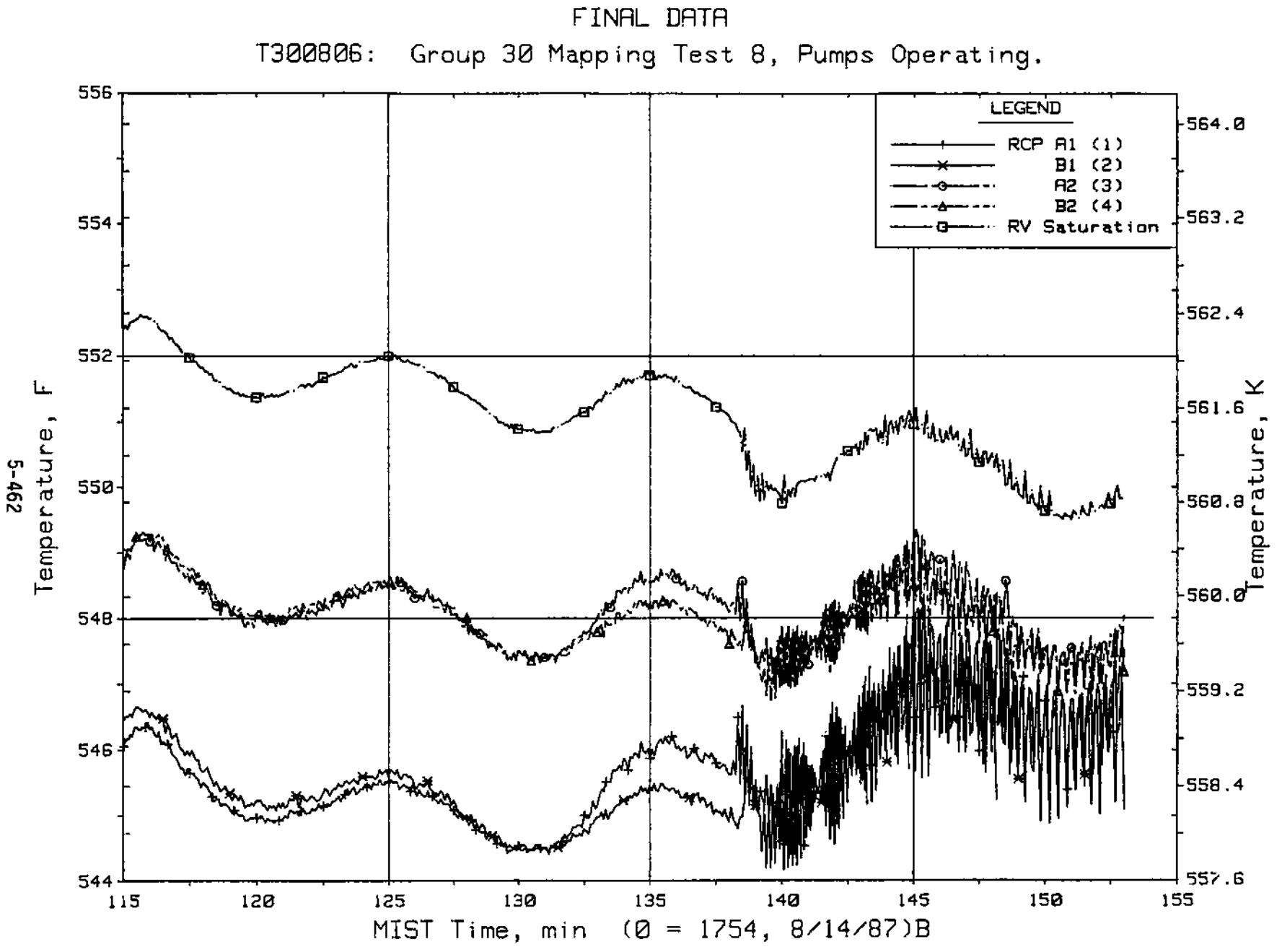

Figure 5.9.18 Pump Suction Fluid Temperature (CnRTOIs)

Wed Mar 22 11:23:13 1989

PURT0

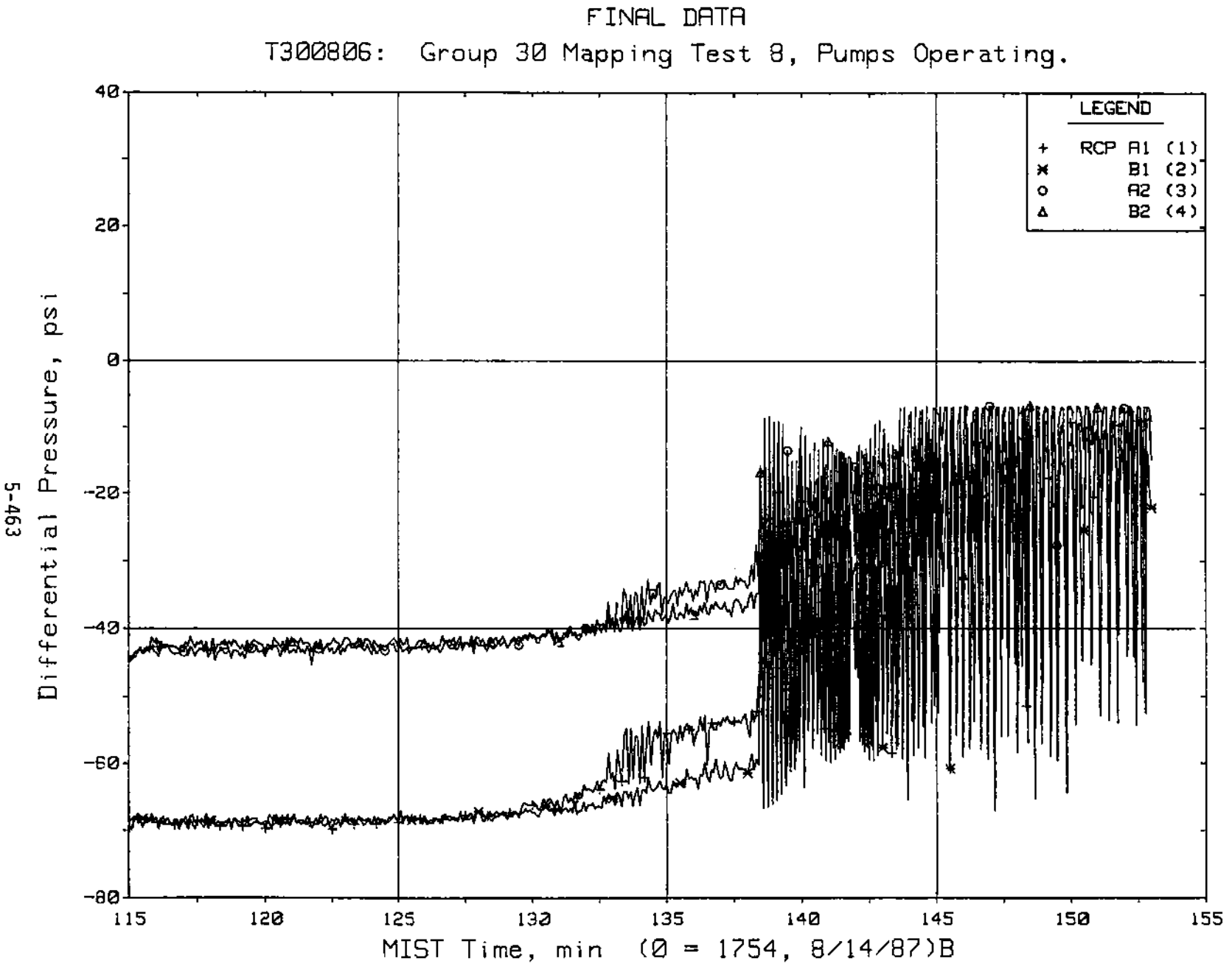

Figure 5.9.19 Pump Pressure Drop (CnDP07s)

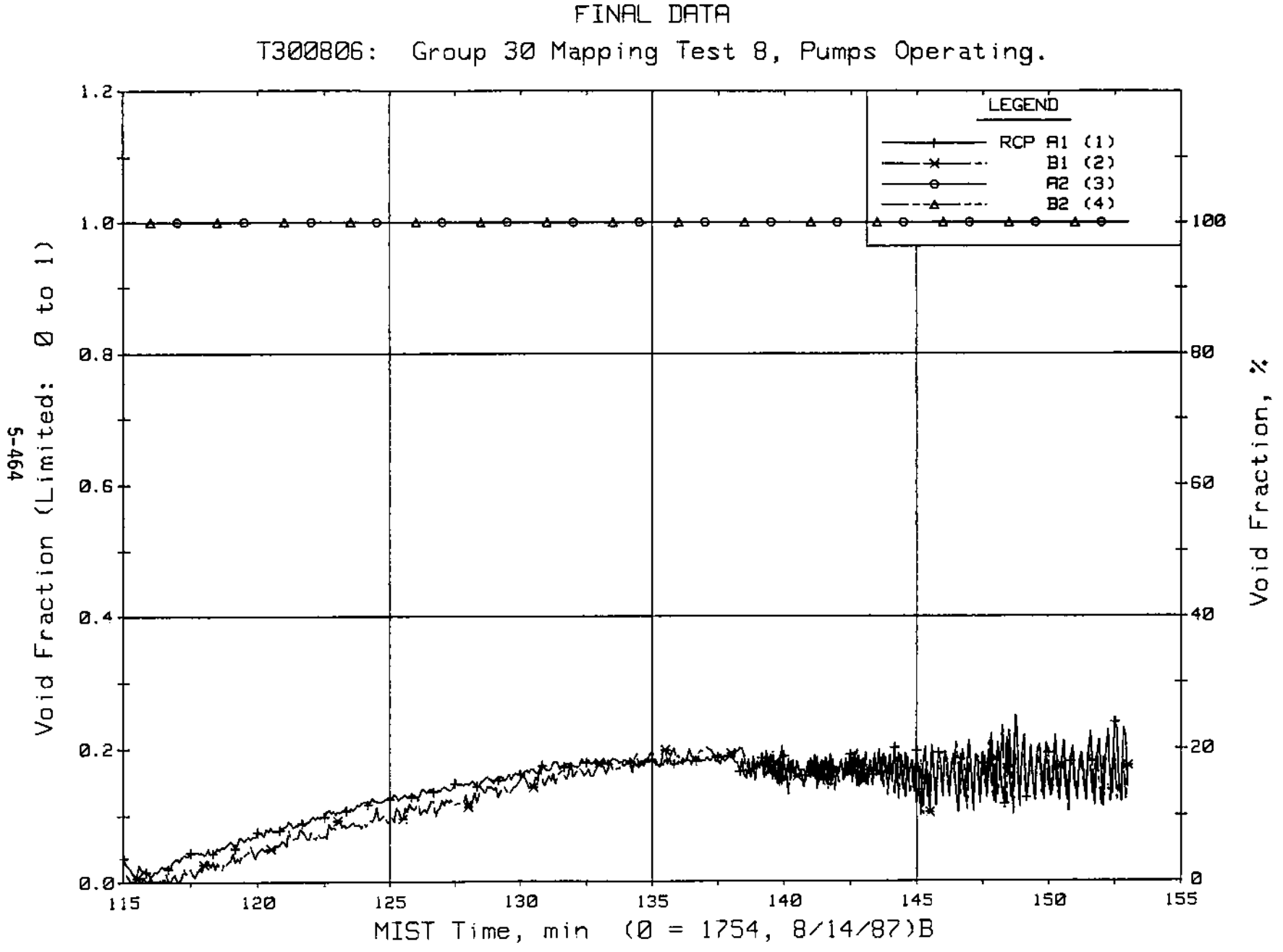

Figure 5.9.20 Pump Suction Void Fraction From Gamma Densitometers (puNfv)

Wed Mar 22 11:06:15 1989

PUVF1

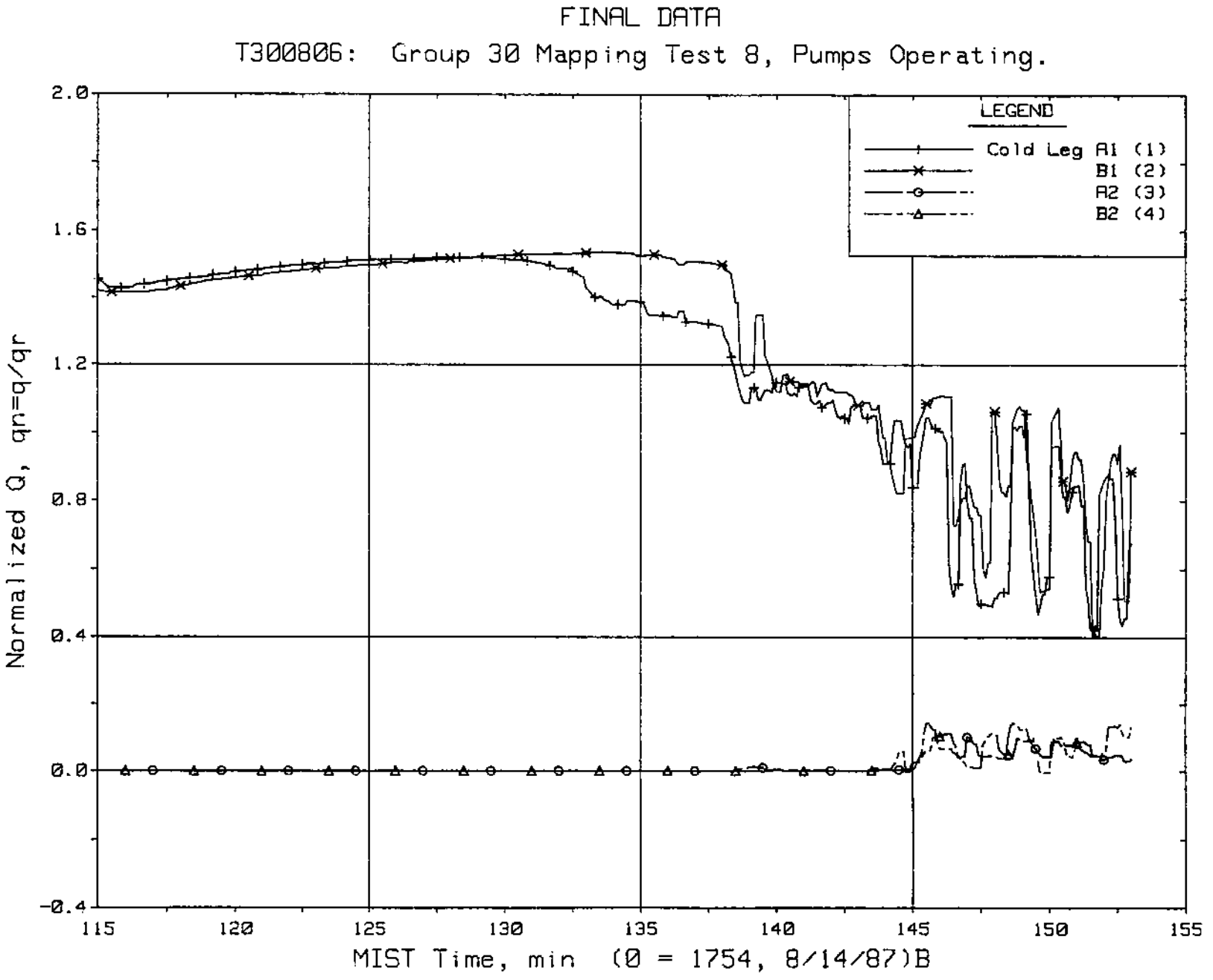

Figure 5.9.21 Normalized Cold Leg Volumetric Flow Rate

Wed Mar 22 11:10:01 1989

PUQN1

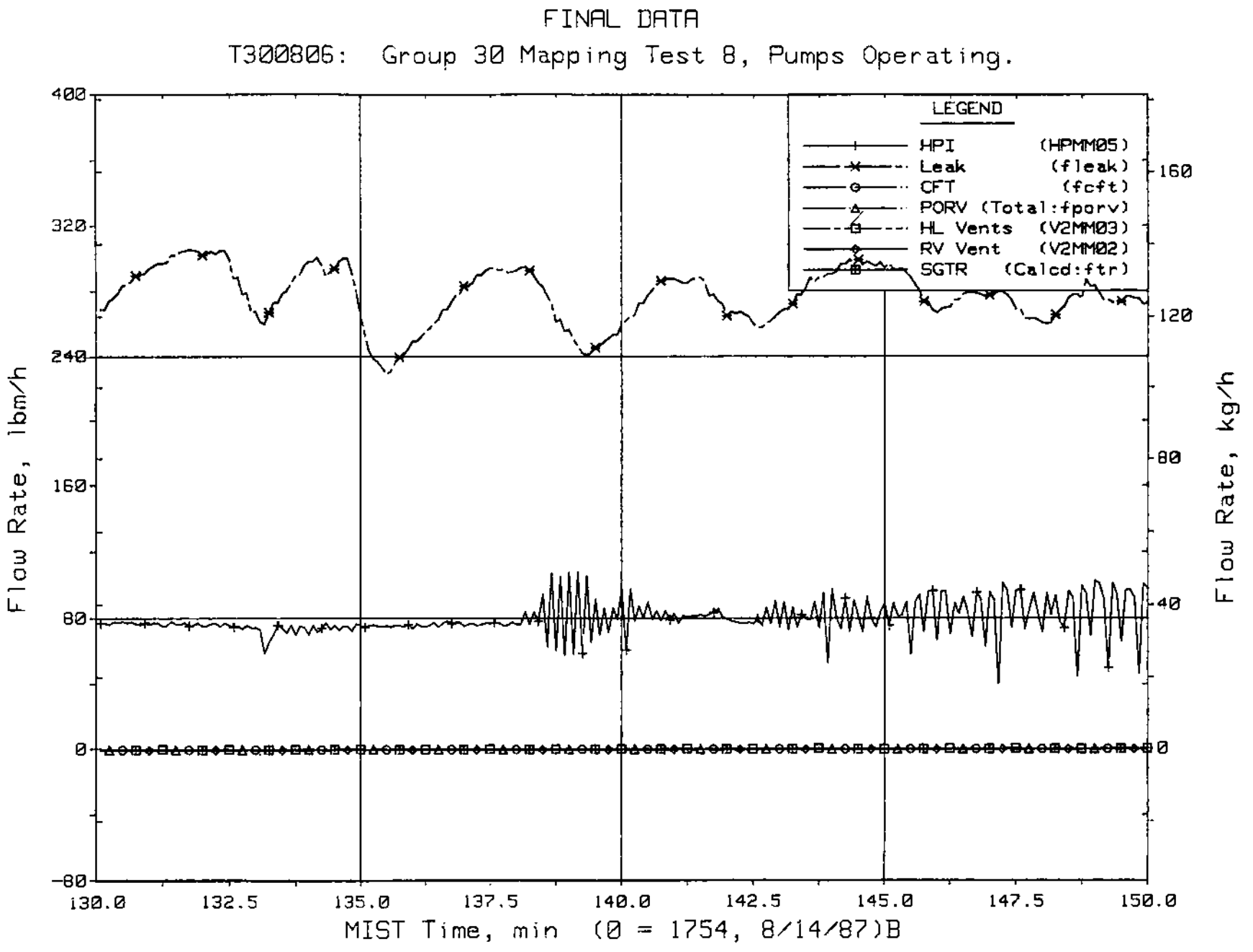

Figure 5.9.22 Primary System Boundary Flow Rates

Wed Mar 22 10:43:54 1989

PRFL3

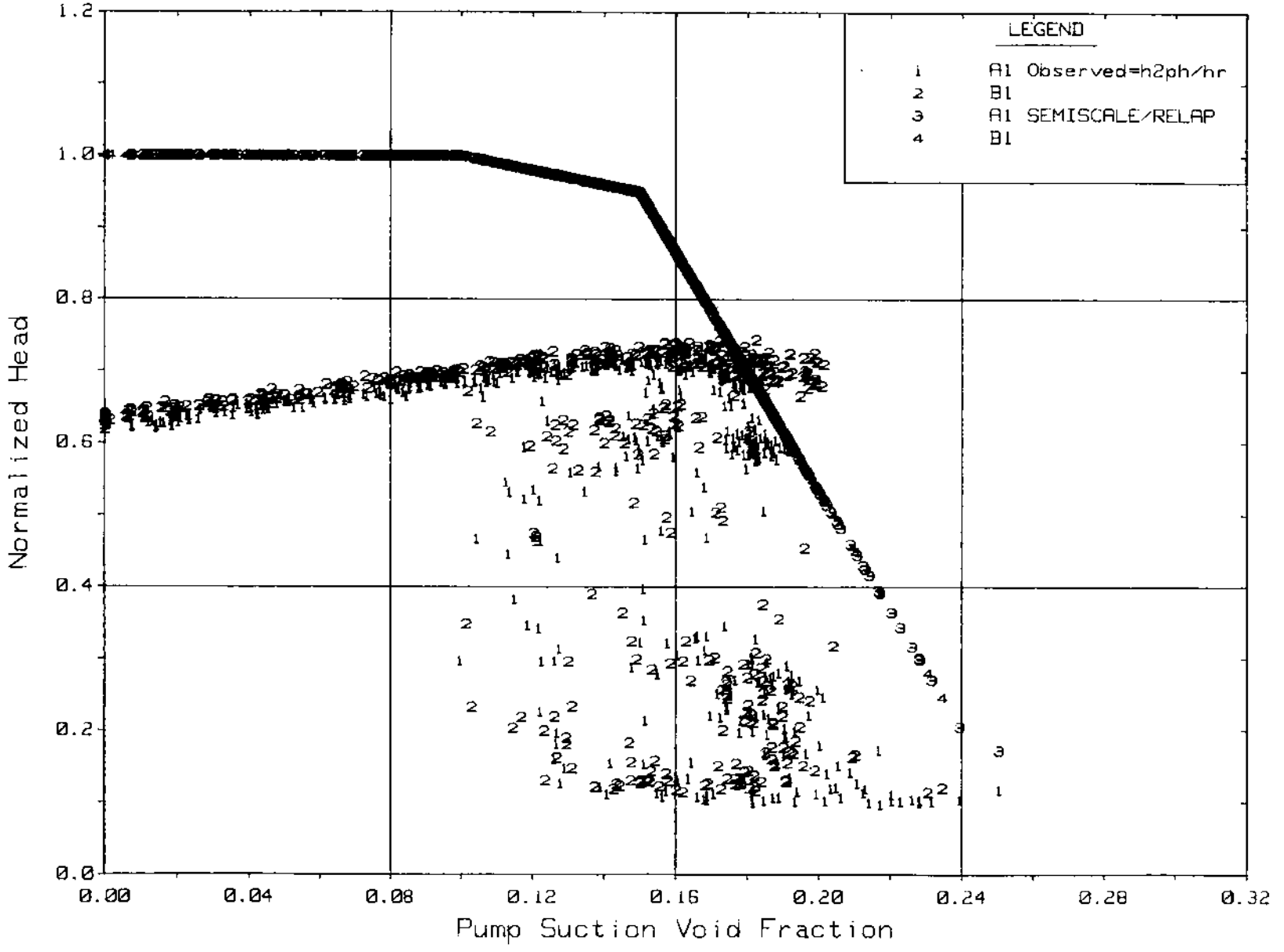

Figure 5.9.23 Pump Normalized Head Vs Void Fraction, 115 to 153 Minutes

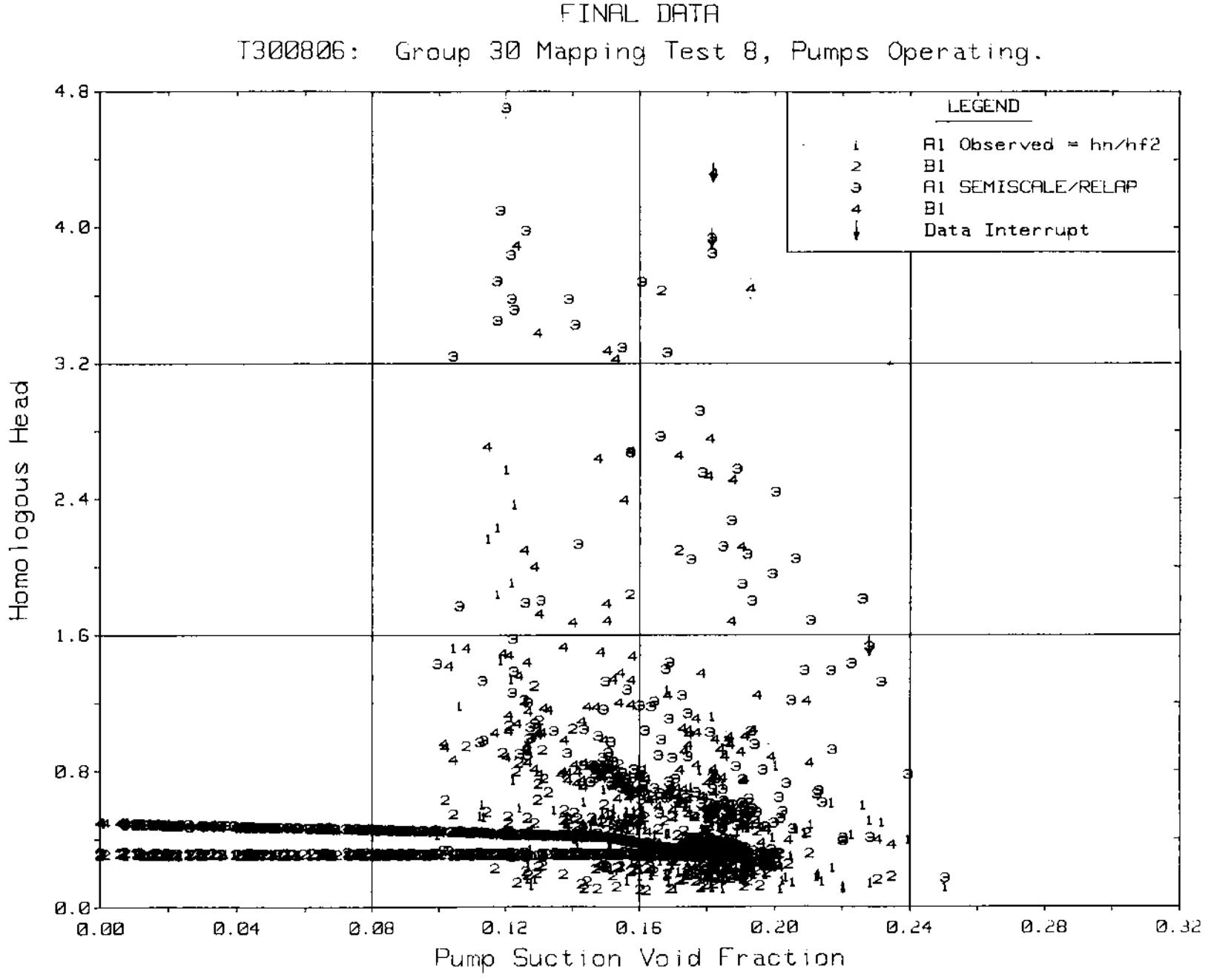

Figure 5.9.24 Pump Homologous Head Vs Void Fraction, 115 to 153 Minutes

Thu Mar 21 11:16:25 1989

PUHVA

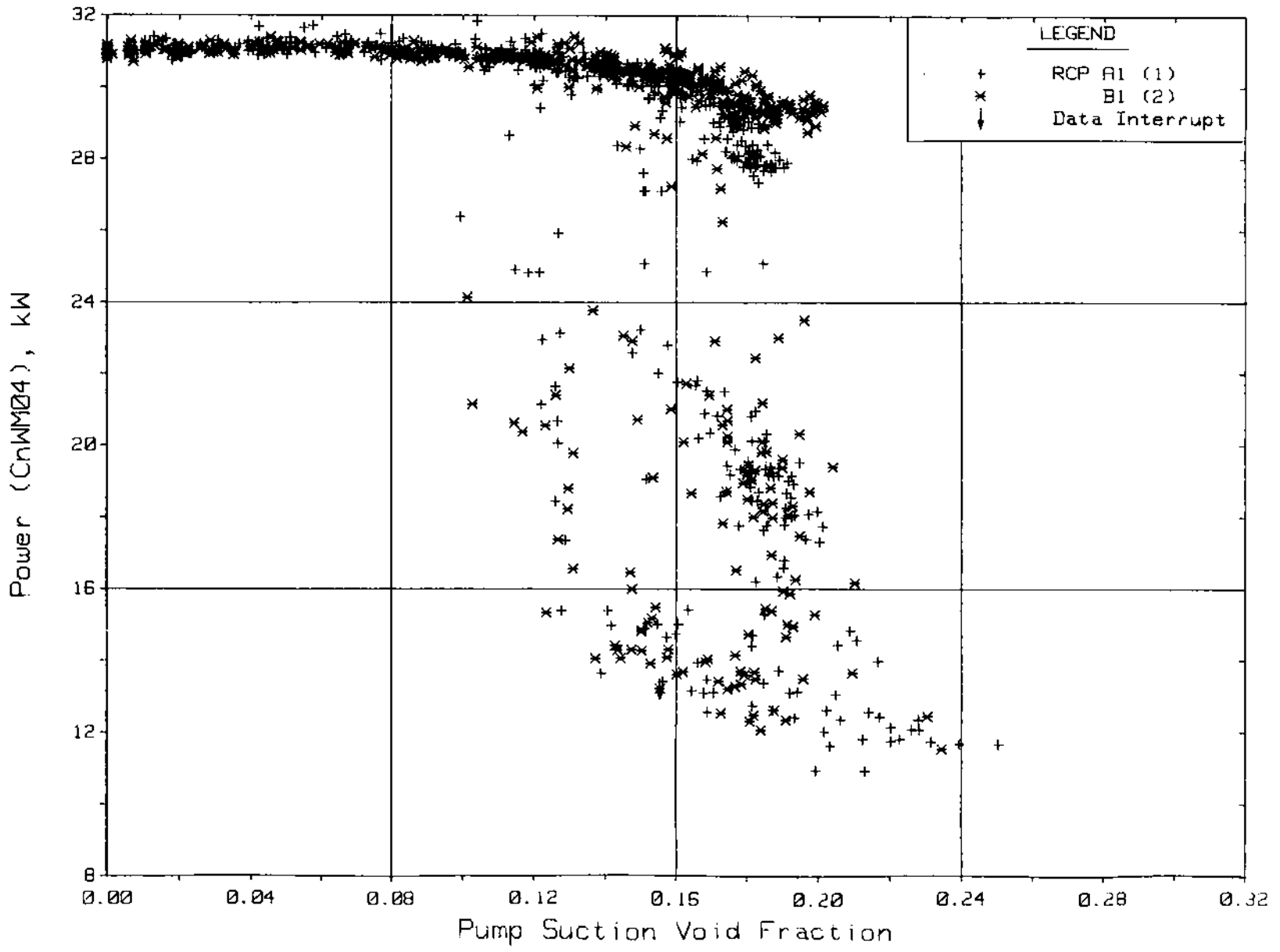

Figure 5.9.25 Pump Electrical Power Vs Void Fraction, 115 to 153 Minutes

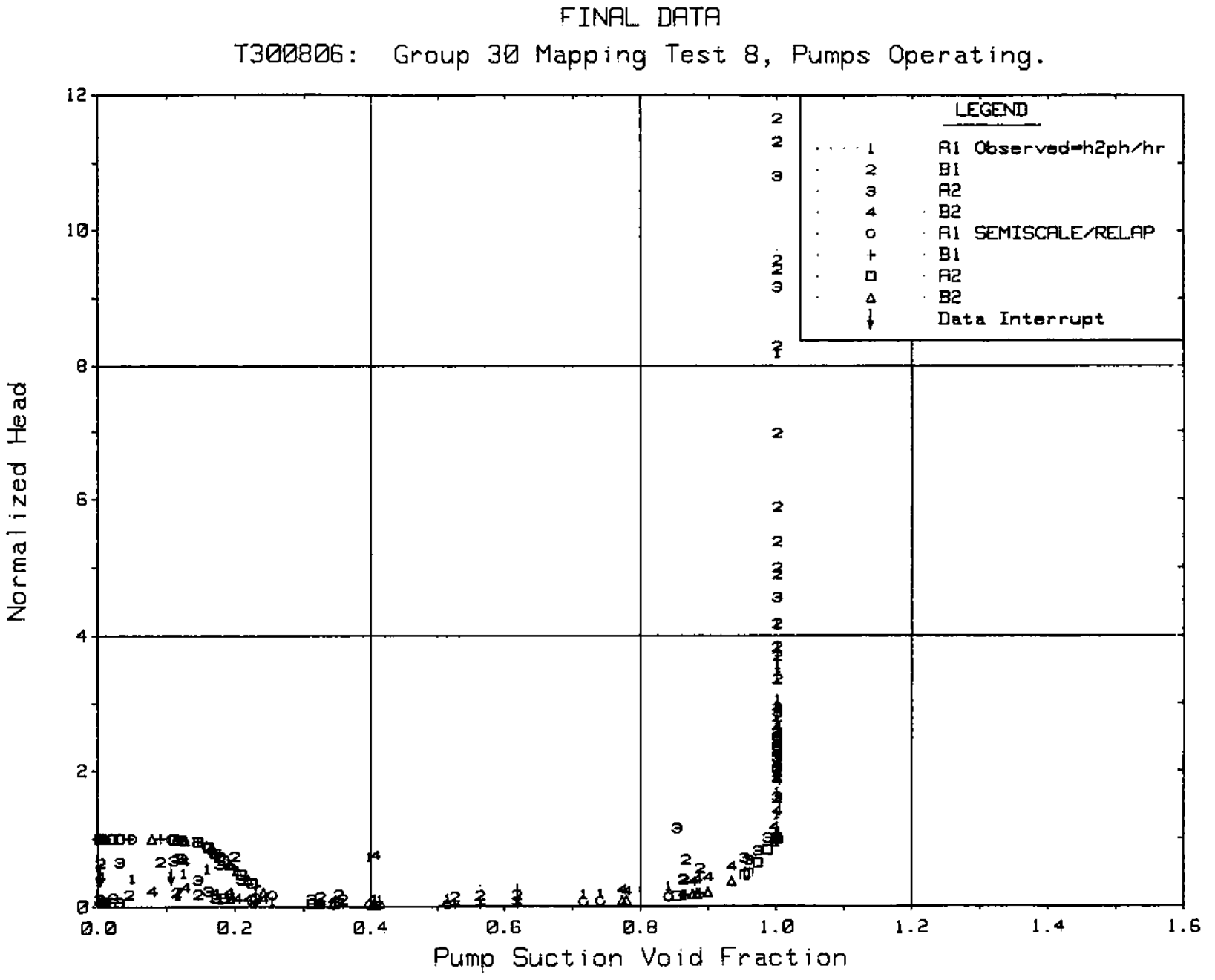

Figure 5.9.26 Pump Normalized Head Vs Void Fraction, 153 to 250 Minutes

Tue Mar 21 16:06:47 1989

PUPvA

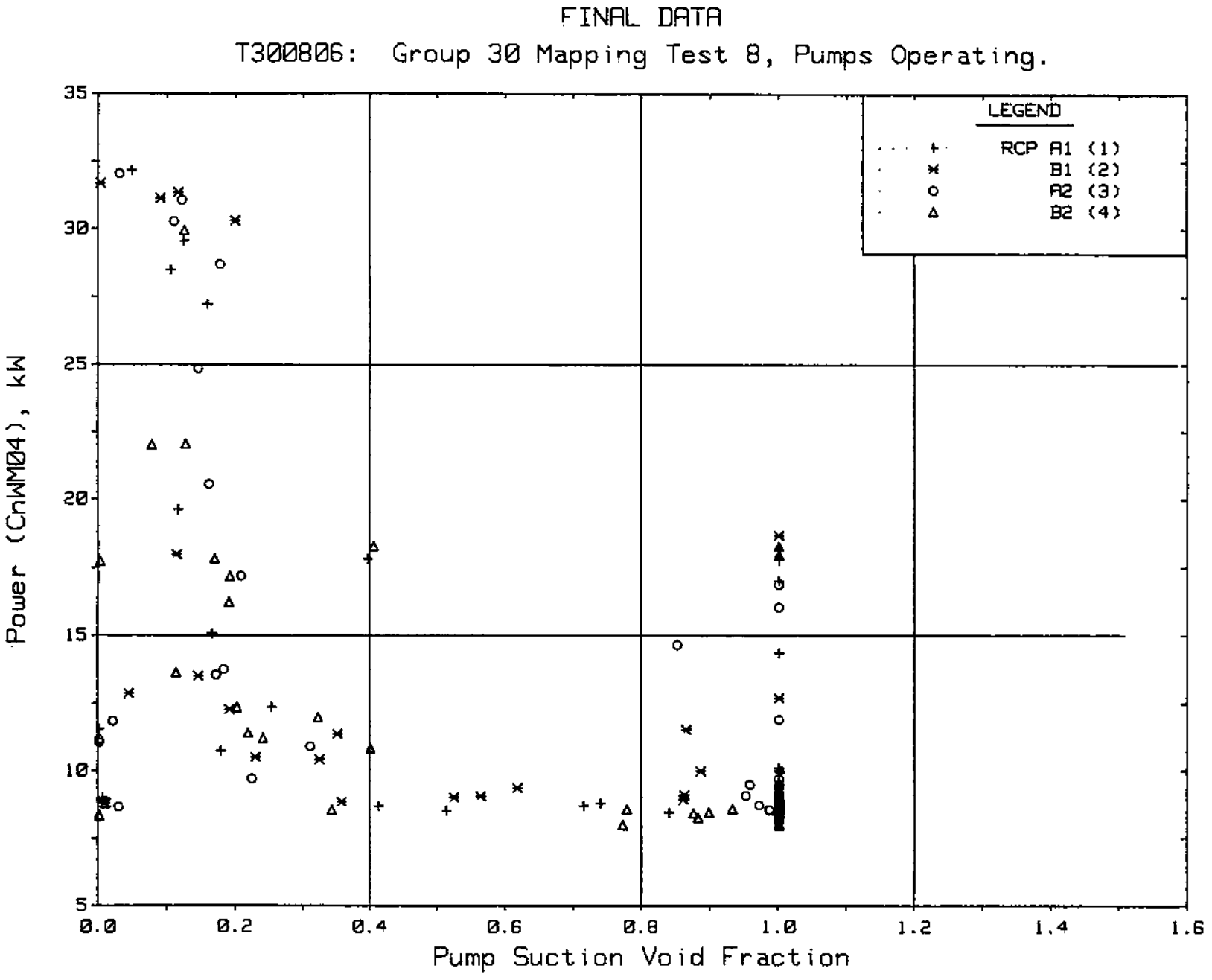

Figure 5.9.27 Pump Electrical Power Vs Void Fraction, 153 to 250 Minutes

Tue Mar 21 16:01:58 1989

PUWVA

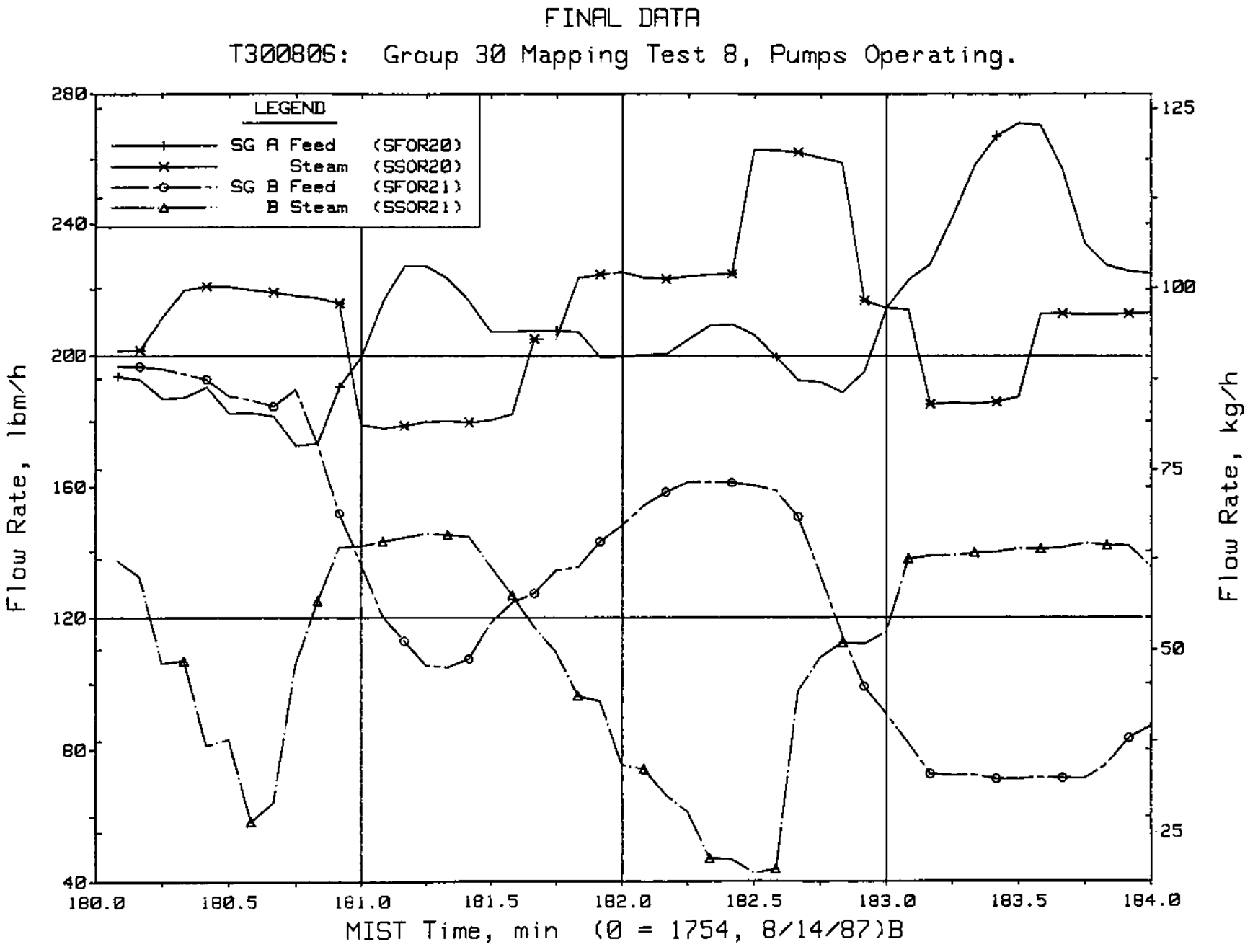

Figure 5.9.28 Steam Generator Secondary Flow Rates

Tue Mar 21 15:27:21 1989

SGFL0

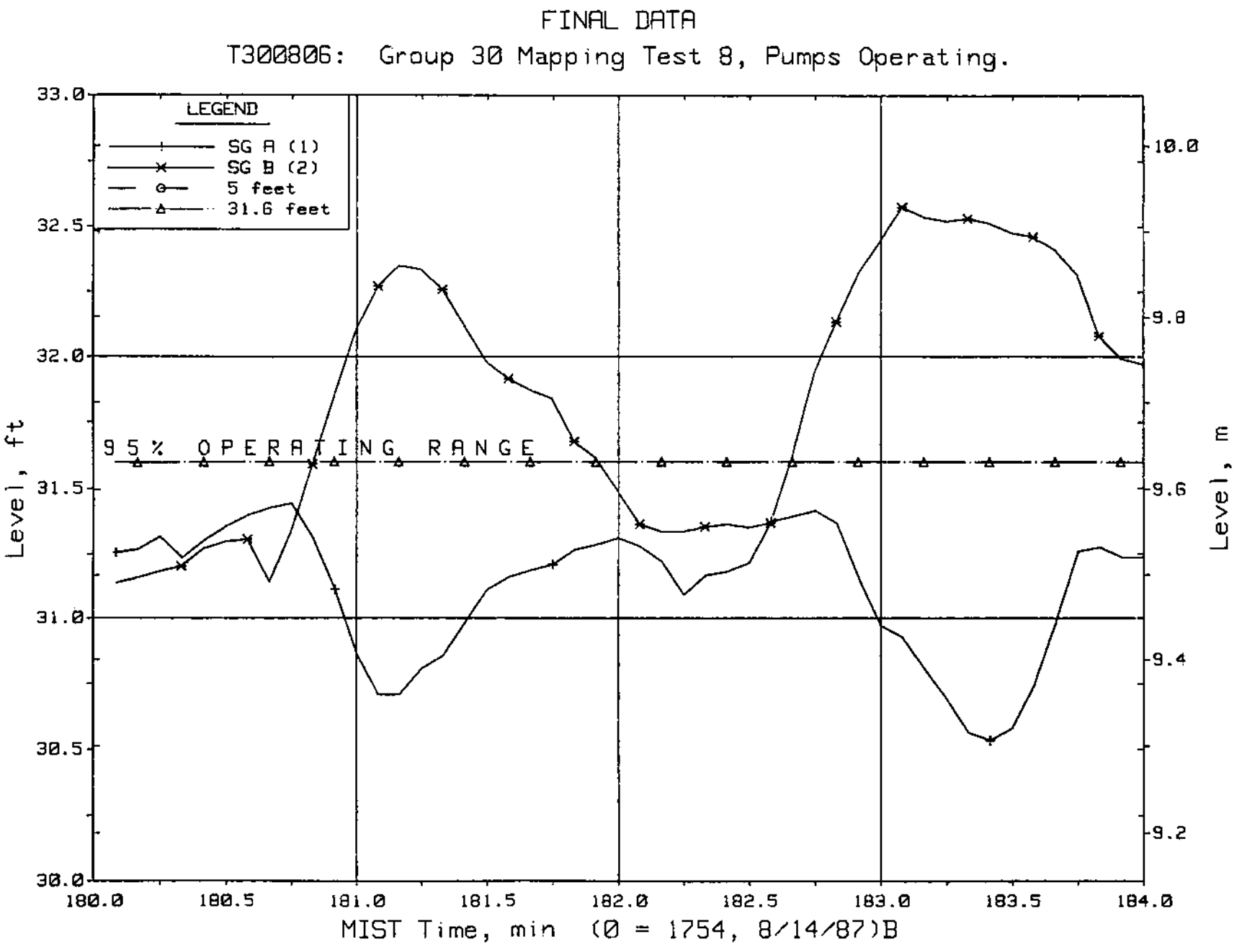

Figure 5.9.29 Steam Generator Secondary Collapsed Liquid Levels (SnLV20s)

Tue Mar 21 15:23:43 1989

SCLV1

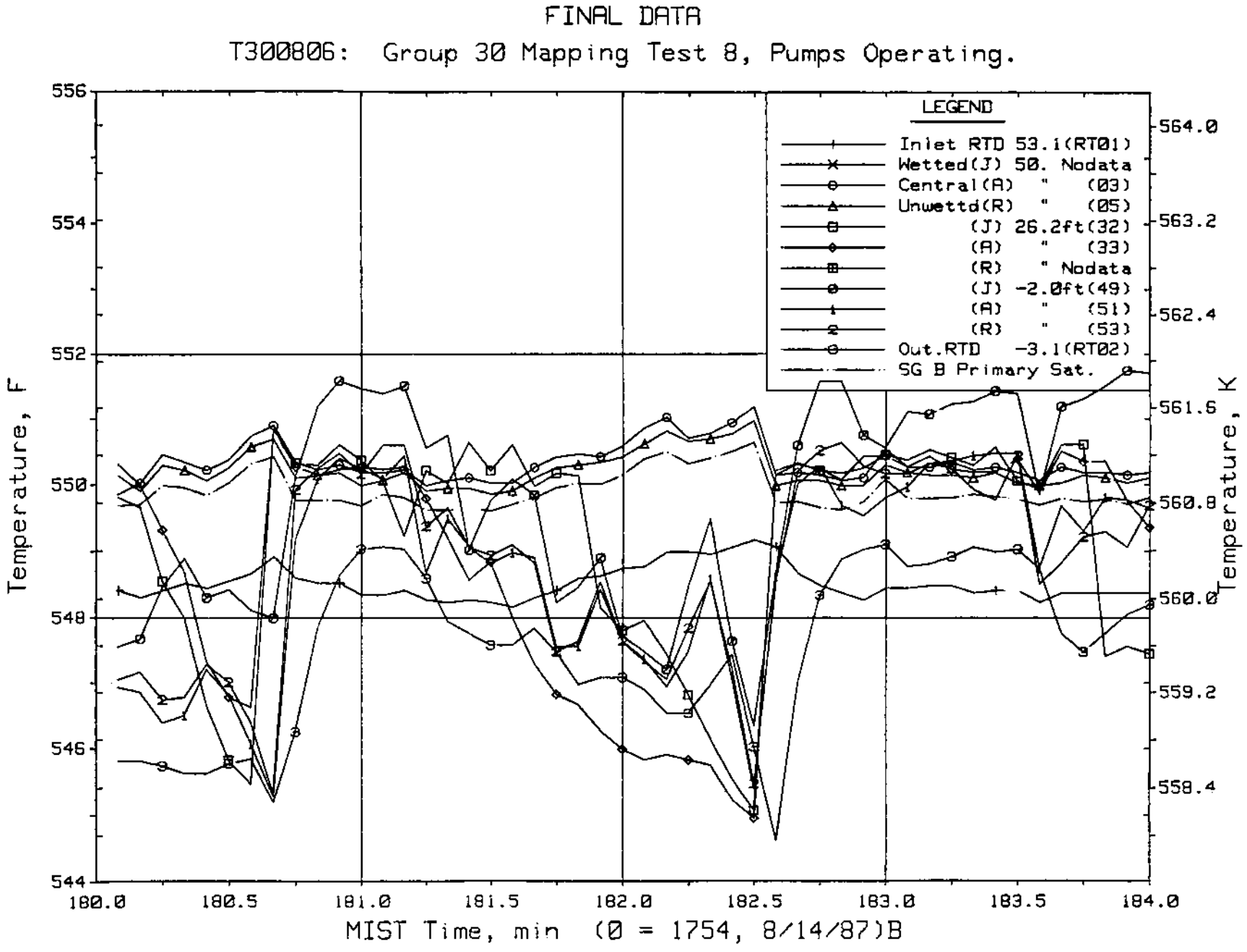

Figure 5.9.30 Steam Generator B Primary Fluid Temperatures, Tubes J, A, and R (P2TCs)

Tue Mar 21 15:18:05 1989

P2TC0

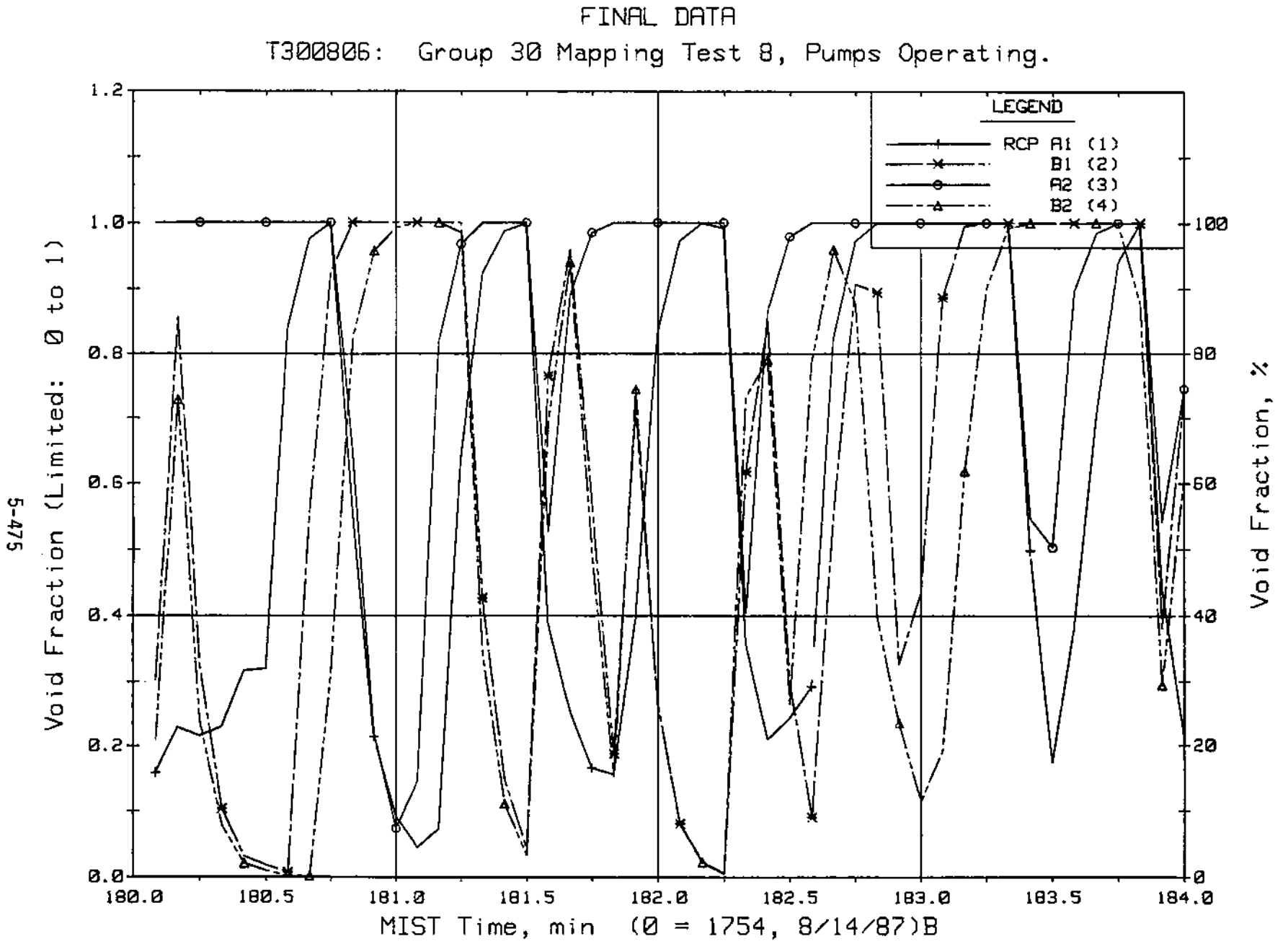

Figure 5.9.31 Pump Suction Void Fraction from Gamma Densitometers (puNvf)

Tue Mar 21 15:13:57 1989

PUVF1

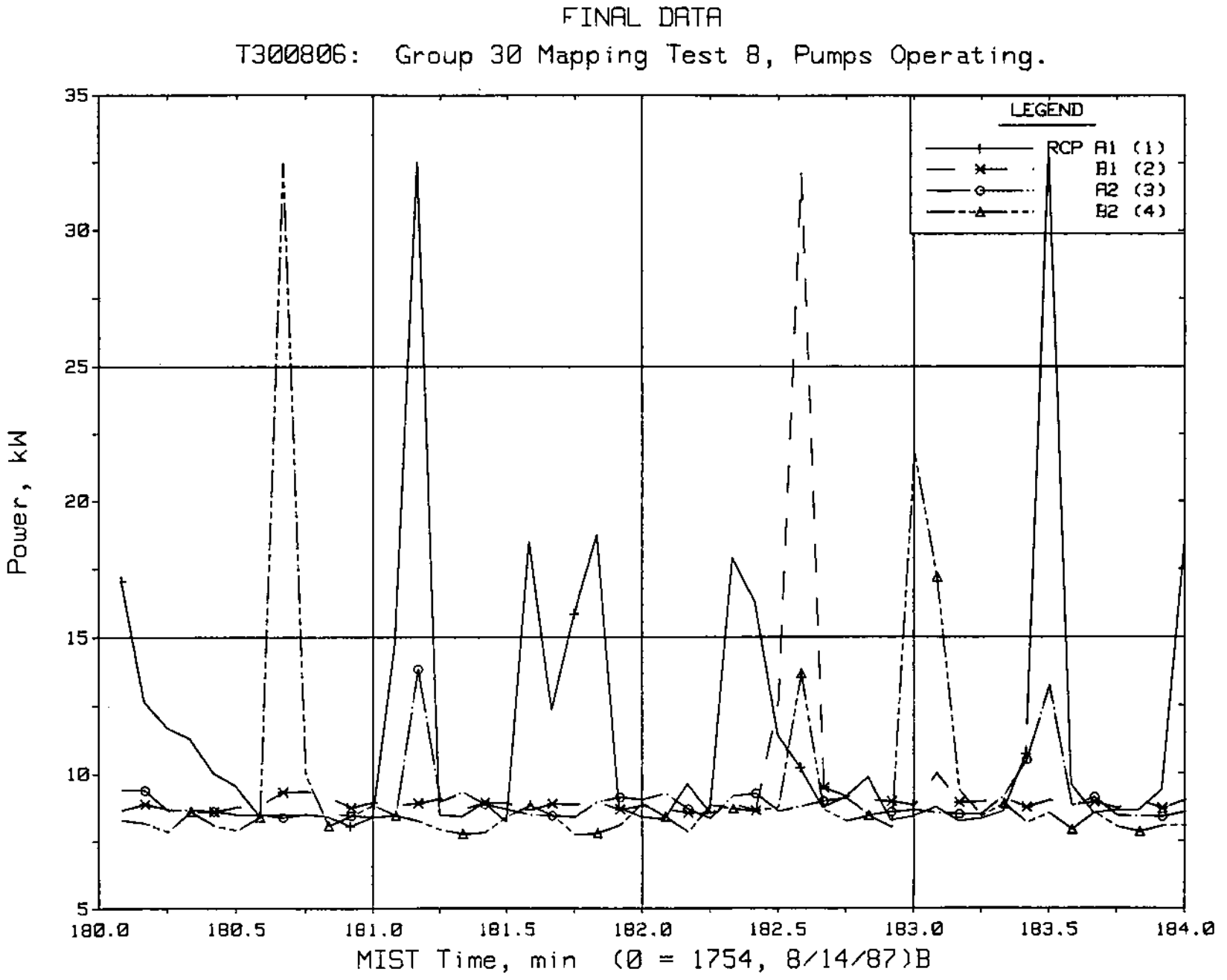

Figure 5.9.32 Pump Electrical Power (CnWM04s)

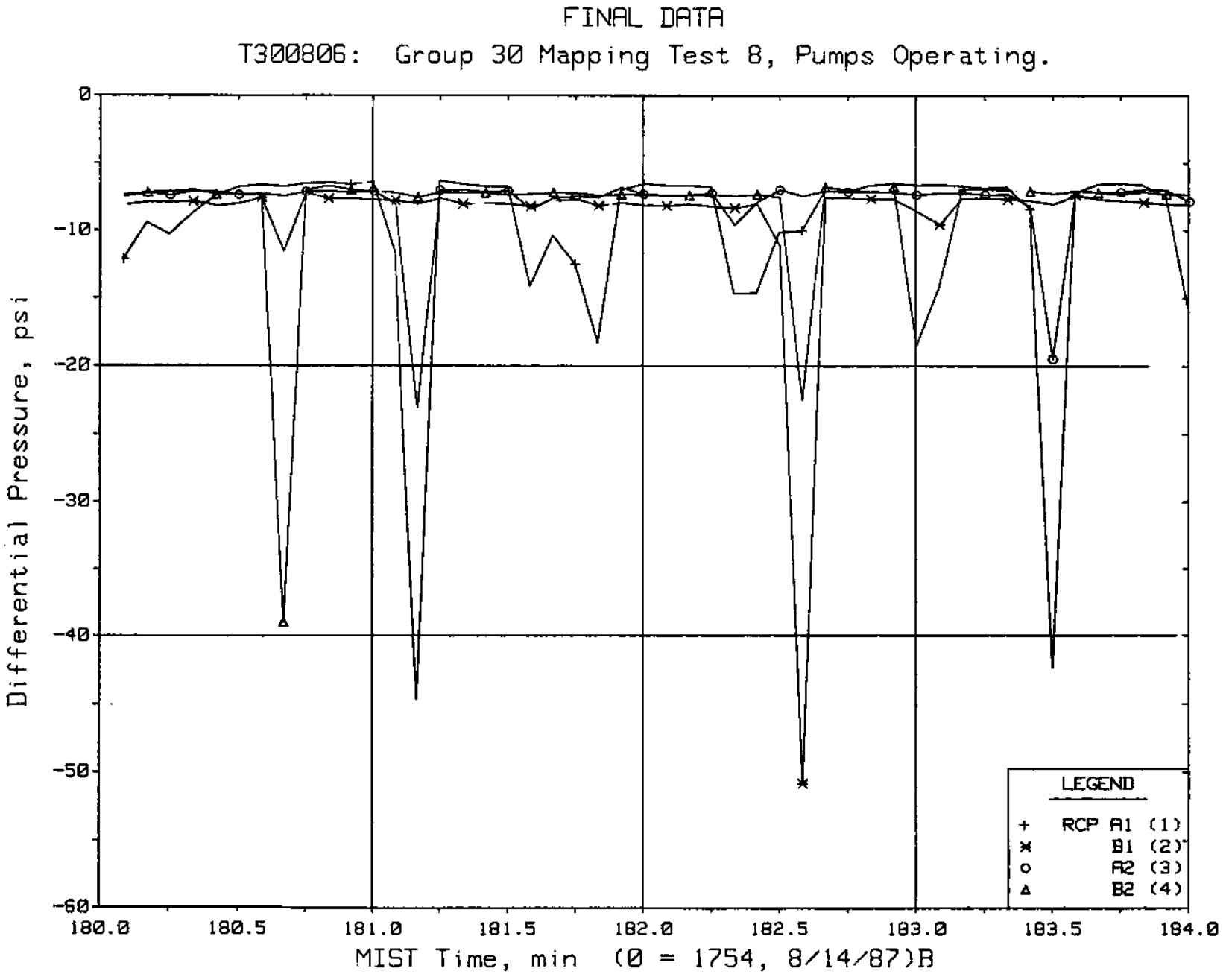

Figure 5.9.33 Pump Pressure Drop (CnDP07s)

Tue Mar 21 15:06:35 1989

PUDP1

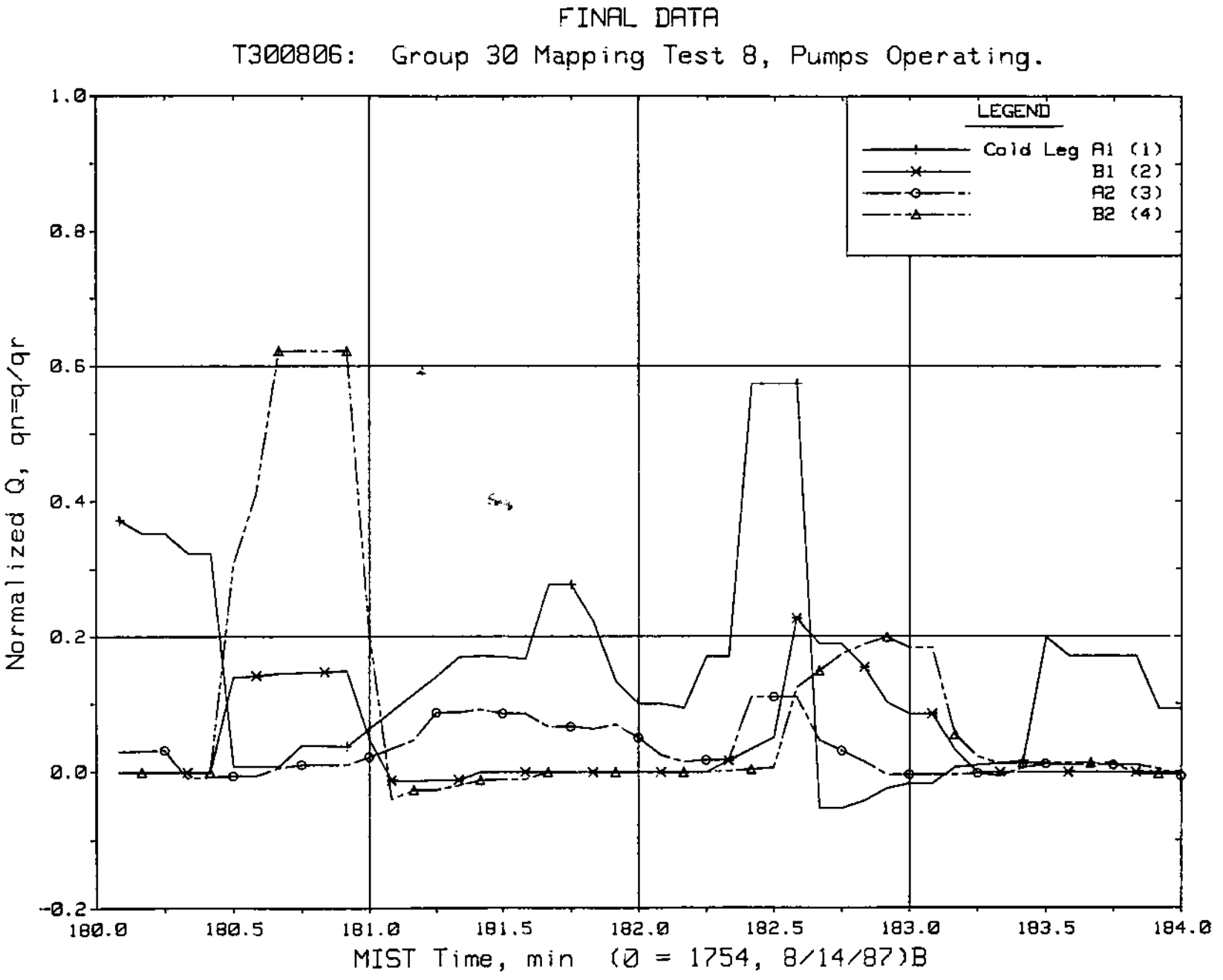

Figure 5.9.34 Pump Normalized Volumetric Flow Rate

Tue Mar 21 14:58:48 1989

PUQN1

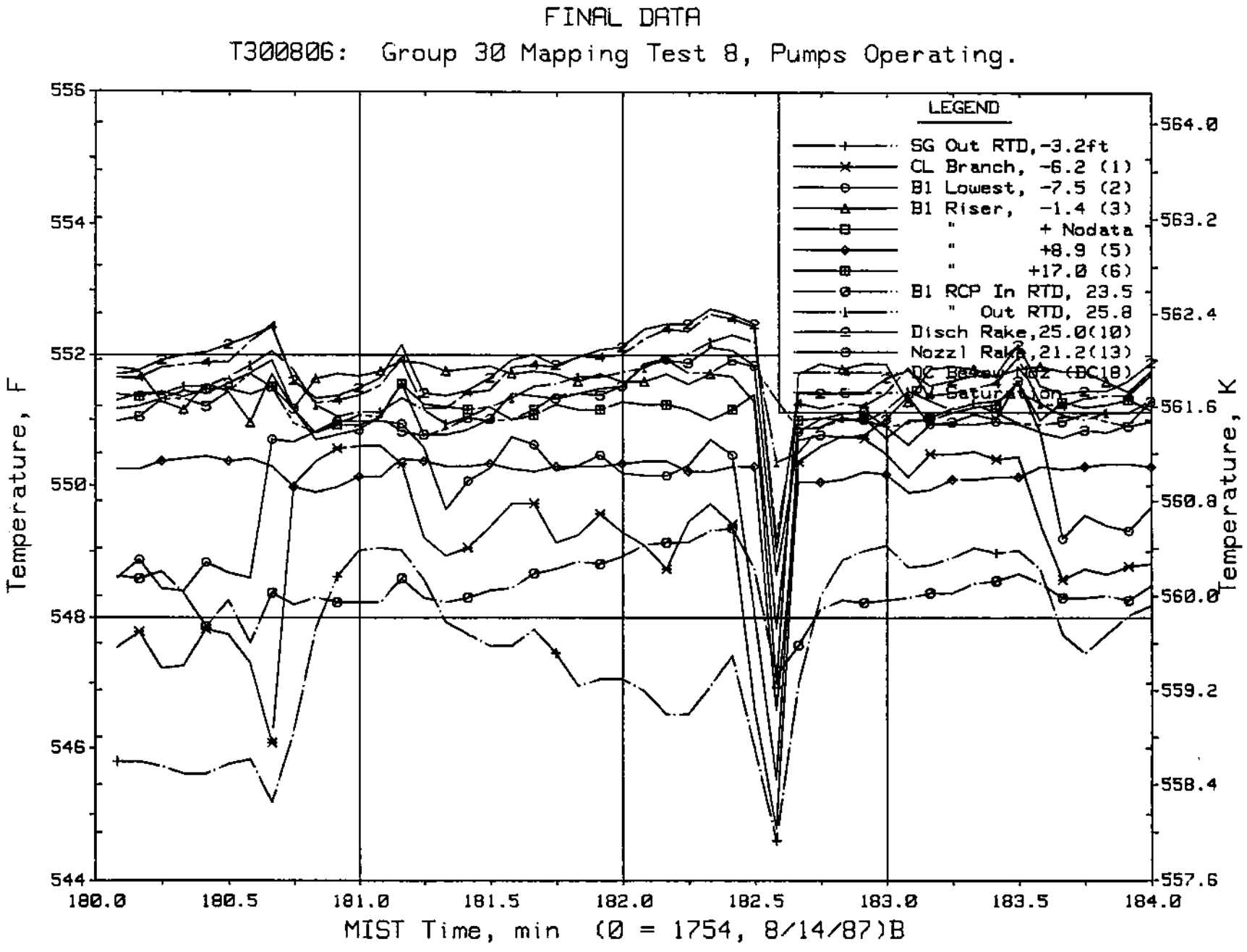

Figure 5.9.35 Cold Leg B1 Fluid Temperatures (C2TCs)

Tue Mar 21 14:53:45 1989

C2TC0

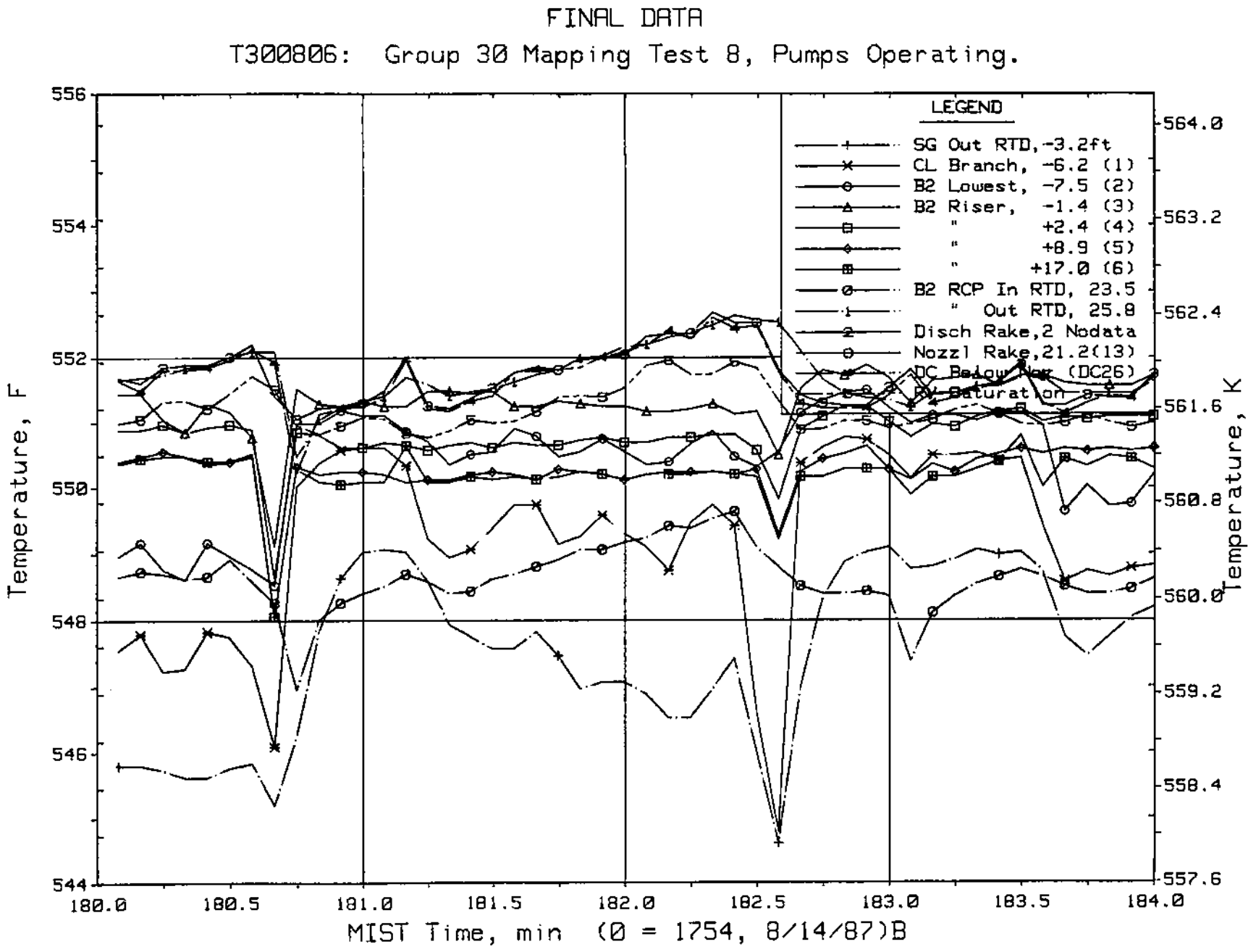

Figure 5.9.36 Cold Leg B2 Fluid Temperatures (C4TCs)

Tue Mar 21 14:47:27 1989

C4TC0

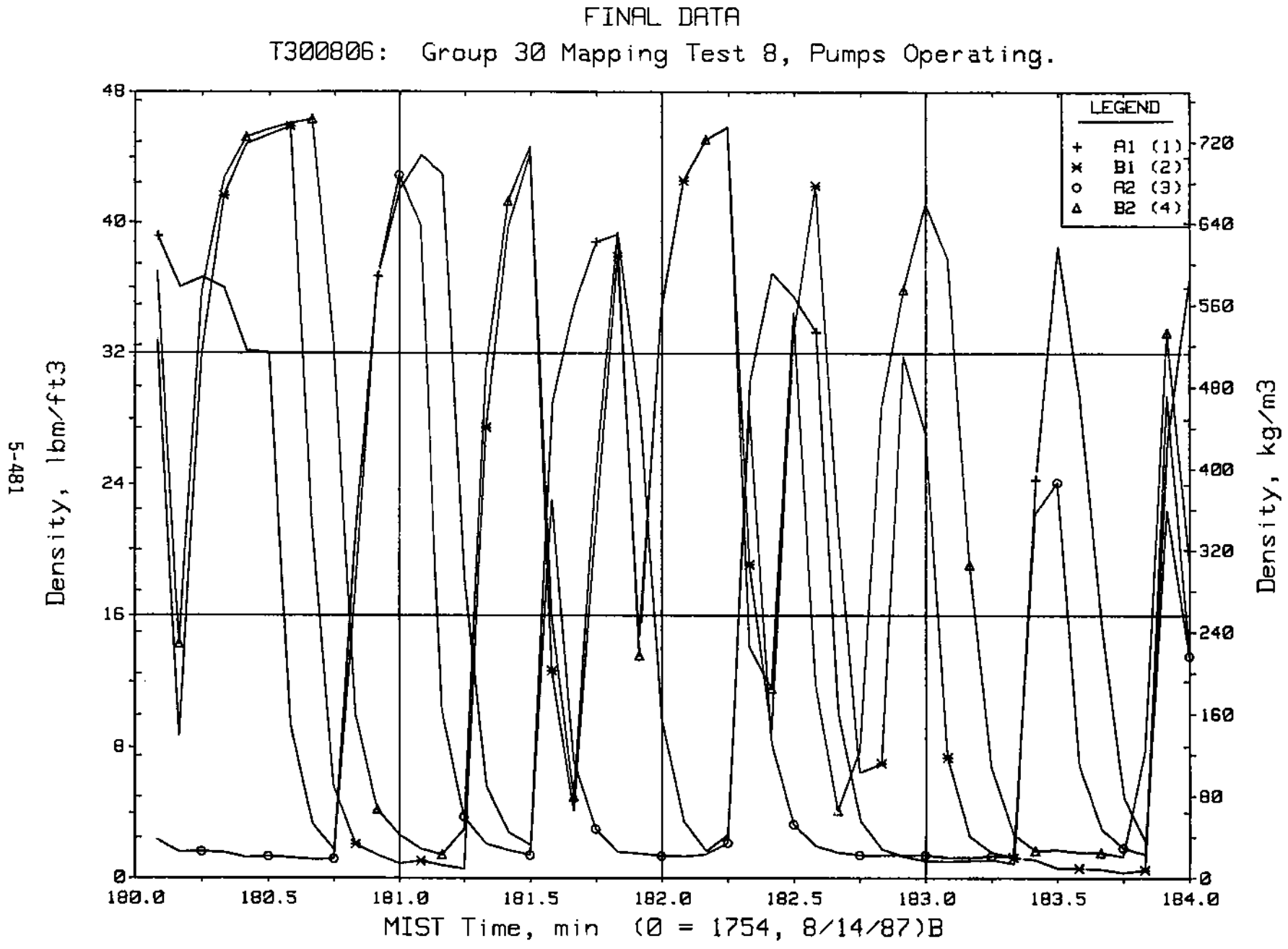

Figure 5.9.37 Cold Leg Fluid Density from Gamma Densitometers (CnGD20s)

Tue Mar 21 14:37:54 1989

CLGD1

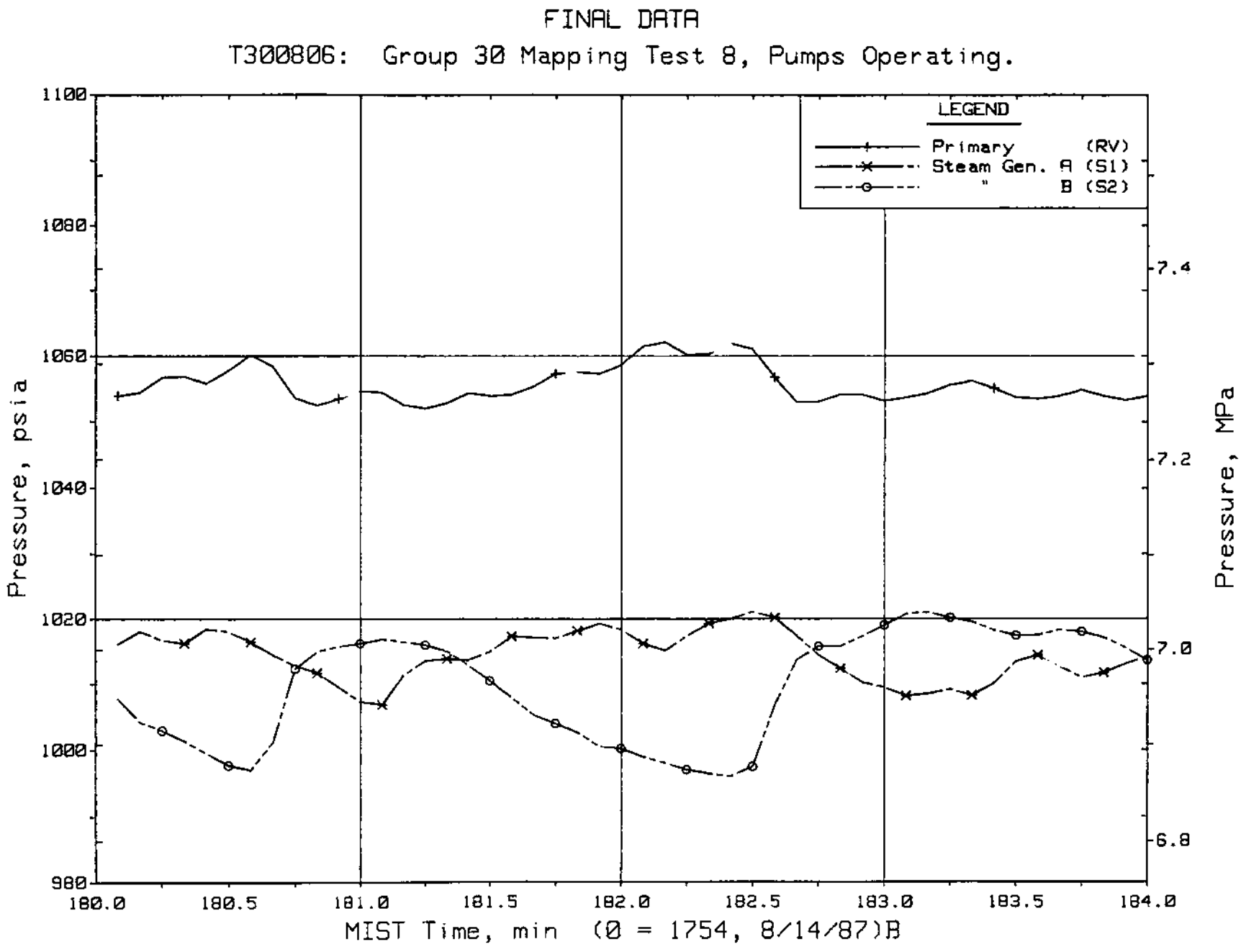

Figure 5.9.38 Primary and Secondary System Pressures (GPOIs)

Tue Mar 21 13:42:14 1989

PSGP1

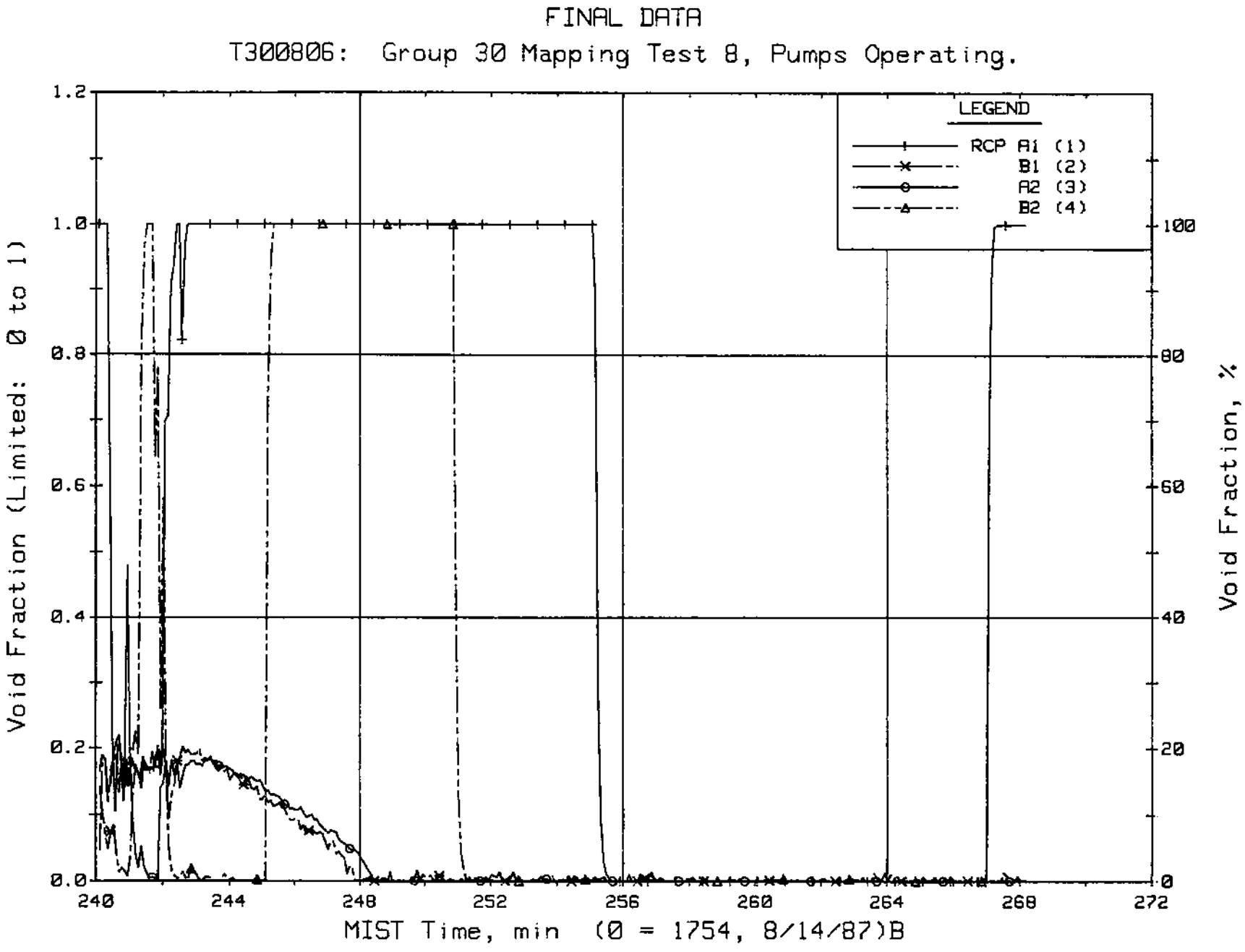

Figure 5.9.39 Pump Suction Void Fraction from Gamma Densitometers (puNfV)

Tue Mar 21 13:38:26 1989

PUVF1

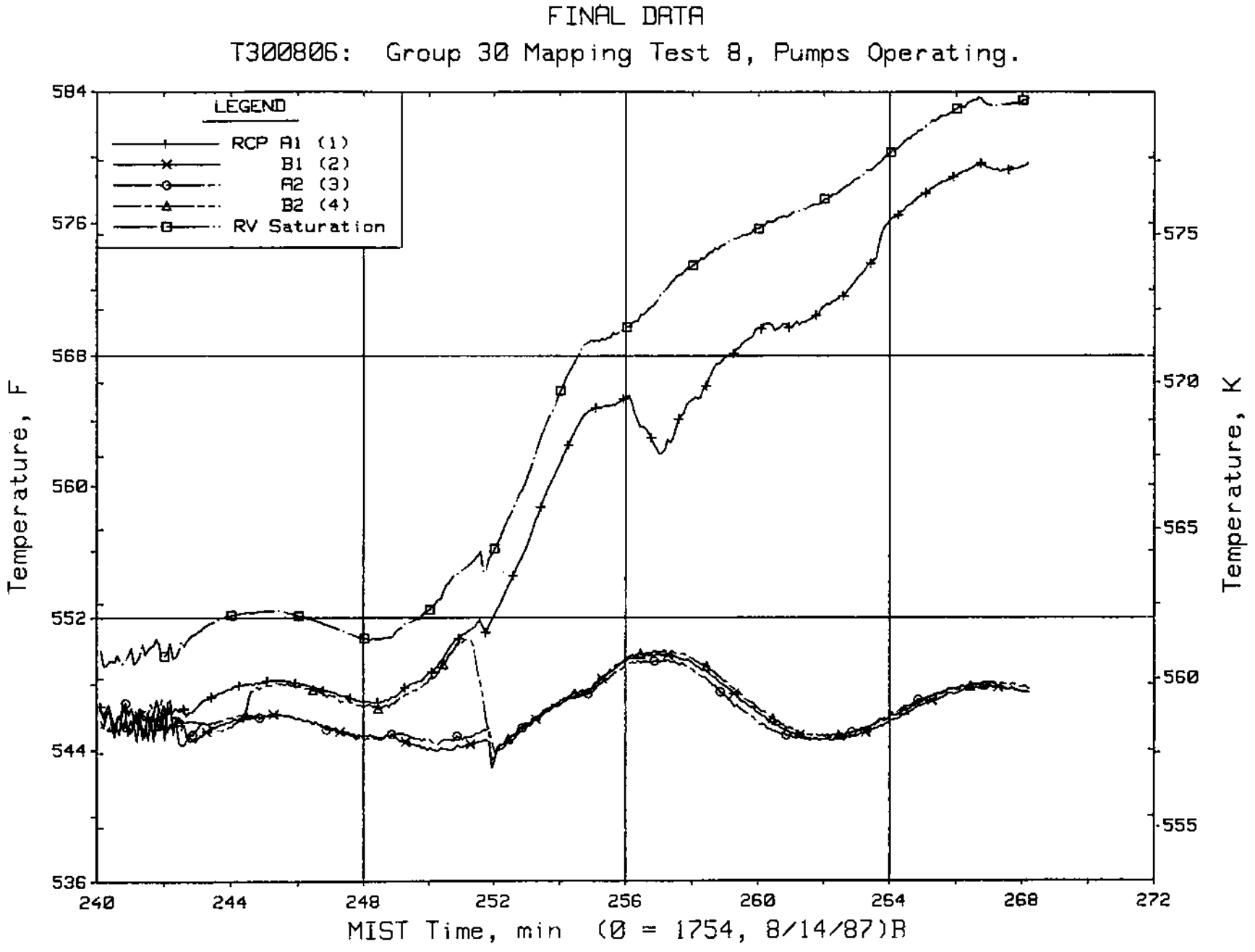

Figure 5.9.40 Pump Suction Fluid Temperatures (CnRTOls)

Tue Mar 21 13:35:22 1989

PURT0

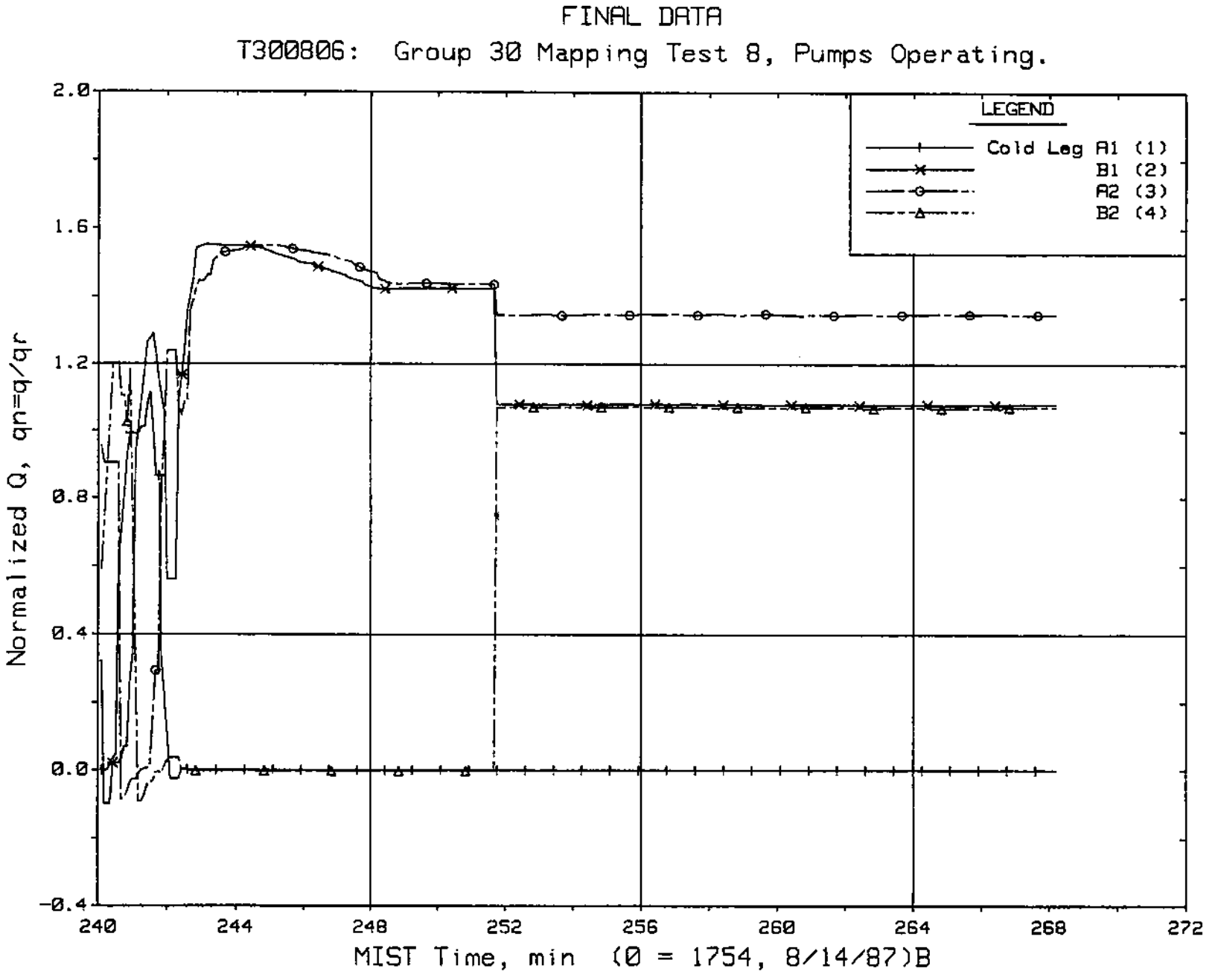

Figure 5.9.41 Normalized Cold Leg Volumetric Flow Rate

Tue Mar 21 13:31:06 1989

PUQN1

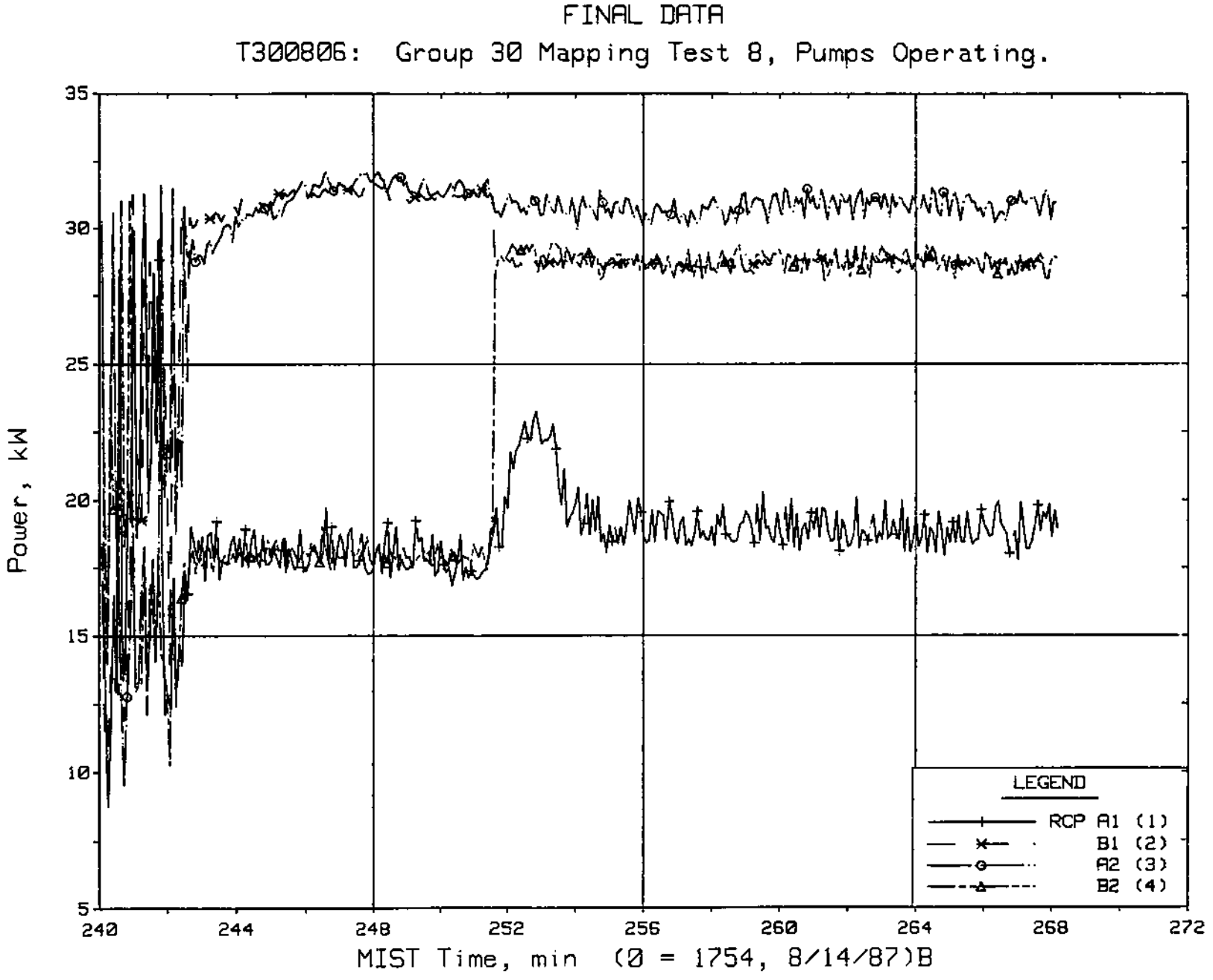

Figure 5.9.42 Pump Electrical Power (CnWM04s)

Tue Mar 21 13:26:55 1989

PUWM1

6. SUMMARY AND CONCLUSIONS

The objective of the natural circulation Mapping Tests was to aid in the identification of the system conditions at the transitions among the early SBLOCA events. These events included saturated and two-phase natural circulation, intermittent circulation, flow interruption, and the BCM. The natural circulation mapping tests of Group 30 met the proposed objective and provided additional insight into the post-SBLOCA phenomena.

Each of these natural circulation tests traversed the major SBLOCA events through flow interruption and repressurization. Only two tests (3009AA and 3007CC) did not achieve BCM and the subsequent depressurization of the primary system. The MIST Test Facility design limits were challenged for these two tests and resulted in the termination of the tests.

In general, with the exception of the closed reactor vessel vent valve test (300504), each of the natural circulation Mapping Tests exhibited very similar responses. These responses in order of their occurrence were as follows:

1. A depressurization to saturated conditions.

2. A slight repressurization trend as reactor vessel upper head voiding occurred.

3. The characteristic reactor vessel vent valve cycling as steam was discharged into the downcomer and the pressure in the downcomer and the reactor vessel equalized.

4. The decreasing trend in the primary loop flow in response to the cyclical steam flow through the reactor vessel vent valves.

5. The occurrence of backflow in the cold leg discharge pipe (observed as counter-current flow at the cold leg nozzles) when steam was discharged through the reactor vessel vent valves into the downcomer as the downcomer level descended toward the cold leg nozzle elevation.

6. The increase in the back pressure and counter-current flow at the cold leg discharge nozzles in response to the cyclical steam flow through the reactor vessel vent valves.

7. The backflow of steam into the cold legs as the upper downcomer voided.

8. The momentary flow interruption in all four cold legs and the subsequent establishment of intra-cold leg flow.

9. The voiding of the cold leg discharge pipes.

10. The sequential occurrence of complete flow interruption in the cold legs at essentially a constant pressure.

11. The heatup of the core region after complete flow interruption that resulted in a primary system repressurization.

12. The heatup of the hot legs that resulted in the U-bend spillover of fluid and the establishment of a sufficient driving head that resulted in forward loop flow (initiation of intermittent flow).

13. The collapse of the voids in the cold legs as forward loop flow occurred.

14. The reduced driving head that occurred as a result of the forward loop flow, i.e., the increase in flow increased the fluid density in the core and hot legs, which then resulted in flow interruption.

15. Continued intermittent flow as the primary system pressure continued increasing.

16. The termination of intermittent flow in one loop while intermittent flow continued in the other loop and the resulting stabilization of the primary system pressure.

17. The reduction of the primary system pressure as AFW and/or pool BCM was established.

18. The termination of BCM as a result of the flow interruption that was caused by the backflow of superheated steam (a result of the depressurization and the downcomer metal heat) into the cold legs.

19. The repressurization of the primary system as BCM was terminated.

20. The reestablishment of pool BCM and the depressurization of the primary system to a value that approached the steam generator secondary pressure.

The closed reactor vessel vent valve test (300504) did not experience cold leg voiding (the cold legs remained liquid full and subcooled) or complete

flow interruption as observed in the other natural circulation Mapping Tests. This test exhibited a flow response that resulted in a pulsating forward loop flow (similar to spillover-induced flow) that initially alternated between the loops and then established a predominant flow path via loop A. Each forward flow pulse that occurred resulted in the backflow of fluid into the cold legs of the other loop. As the pulsating loop flow was established, the primary system pressure increased. The maximum pressure attained for this test, during the repressurization phase, was considerably lower than that attained in the other natural circulation Mapping Tests, which had similar leak sizes but wherein the reactor vessel vent valves were operable.

The response of the primary system, although similar for all of the natural circulation Mapping Tests, was affected by variations in the local phenomena that occurred as a result of the specified differences in the boundary conditions and the inherent loop asymmetries. The relationship among the driving heads of the various subcomponents of each loop and between loops is critical in determining the expected flow path(s). The relationship between the loop driving heads (consisting of the reactor vessel, hot leg, steam generator primary, cold leg suction, cold leg discharge, and the downcomer for loops A and B) determines which loop has the highest potential for establishing forward loop flow. The relationship between the cold leg driving heads (consisting of the cold leg suction and the cold leg discharge of each cold leg in one loop) determines the potential for establishing backflow and intra-cold leg flow direction.

Therefore, all parameters that can affect these driving heads are concluded to be critical for the determination of the flow response of the MIST Test Facility. The parameters that are significant can be either physical (such as loop component elevations) or boundary control systems (those that establish the fluid temperature distribution throughout the test facility). Thus, loop-to-loop and cold leg-to-cold leg variations in these parameters establish the flow response of the MIST Test Facility.

A thorough understanding of the parameters that can produce asymmetric driving heads and the incorporation of those deemed significant into the computer code analysis is essential for determining computer code benchmarking acceptability.

Mapping Test 300806 involved the operation of all four model pumps throughout the entire test. A wealth of pump characterization information was generated and five types of pump operation were observed:

- Subcooled
- Increased voiding, all pumps operating
- Increased voiding, two pumps completely degraded
- Intermittent voiding and performance
- Recovery during loop refill

The observed pump characteristics were compared to the SEMISCALE/RELAP predictions. This test also appears to have been affected by loop asymmetries and/or model reactor coolant pump asymmetries.

7. REFERENCES

1. H. R. Carter and J. R. Gloudemans, "An Experimental Study of the Post-Small Break Loss-of-Coolant Accident Phenomena in a Scaled Babcock & Wilcox System," NUREG/CP-0058, Vol. 1, pp. 113-135. Proceedings of the U.S. Nuclear Regulatory Commission, Twelfth Water Reactor Safety Research Information Meeting, October 1984.

2. J. R. Gloudemans, "Simulation of Reactor Vessel Vent Valves," Paper presented at the 106th ASME Winter Annual Meeting, November 1985.

3. "Multi-Loop Integral System Test (MIST) Facility Specification," RDD:84:4091-01-01:01 (distributed November 1984, revision pending).

4. "Multi-Loop Integral System (MIST) Instrumentation -- Revision 3," RDD:84:4127-30-01:03, March 1987.

5. "MIST Test Specifications," BAW-1894, Rev. 1, March 1986.

NRC FORM 335 (2-89) NRCM 1102, 3201, 3202

U.S. NUCLEAR REGULATORY COMMISSION

BIBLIOGRAPHIC DATA SHEET

(See instructions on the reverse)

1. REPORT NUMBER (Assigned by NRC. Add Vol., Supp., Rev., and Addendum Numbers, If any.)

NUREG/CR-5395, Vol. 2
EPRI/NP-6480
BAW-2080

2. TITLE AND SUBTITLE

Multiloop Integral System Test (MIST): Final Report
Test Group 30, Mapping Tests

3. DATE REPORT PUBLISHED

MONTH: December
YEAR: 1989

4. FIN OR GRANT NUMBER

B8909 & D1734

5. AUTHOR(S)

G. O. Geissler

6. TYPE OF REPORT

Technical

7. PERIOD COVERED *(Inclusive Dates)*

June 1986-March 1988

8. PERFORMING ORGANIZATION – NAME AND ADDRESS *(If NRC, provide Division, Office or Region, U.S. Nuclear Regulatory Commission, and mailing address; if contractor, provide name and mailing address.)*

Babcock & Wilcox
Nuclear Power Division
3315 Old Forest Road
Lynchburg, VA 24506-0935

Babcock & Wilcox
Research & Development Division
Alliance Research Center
1562 Beeson Street
Alliance, OH 44601

9. SPONSORING ORGANIZATION – NAME AND ADDRESS *(If NRC, type "Same as above"; if contractor, provide NRC Division, Office or Region, U.S. Nuclear Regulatory Commission, and mailing address.)*

Division of Systems Research
Office of Nuclear Regulatory Research
U. S. Nuclear Regulatory Commission
Washington, DC 20555

Electric Power Research Institute
P. O. Box 10412
Palo Alto, CA 94303

Babcock & Wilcox
Owners Group
P. O. Box 10935
Lynchburg, VA 24506-0935

10. SUPPLEMENTARY NOTES

11. ABSTRACT *(200 words or less)*

The Multiloop Integral System Test (MIST) is part of a multiphase program started in 1983 to address small-break loss-of-coolant accidents (SBLOCAs) specific to Babcock and Wilcox designed plants. MIST is sponsored by the U. S. Nuclear Regulatory Commission, the Babcock & Wilcox Owners Group, the Electric Power Research Institute, and Babcock and Wilcox. The unique features of the Babcock and Wilcox design, specifically the hot leg U-bends and steam generators, prevented the use of existing integral system data or existing integral facilities to address the thermal-hydraulic SBLOCA questions. MIST and two other supporting facilities were specifically designed and constructed for this program, and an existing facility--the Once Through Integral System (OTIS)--was also used. Data from MIST and the other facilities will be used to benchmark the adequacy of system codes, such as RELAP5 and TRAC, for predicting abnormal plant transients.

The MIST program is reported in 11 volumes. The program is summarized in Volume 1; Volumes 2 through 8 describes groups of tests by test type; Volume 9 presents inter-group comparisons; Volume 10 provides comparisons between the calculations of RELAP5/MOD2 and MIST observations, and Volume 11 presents the later Phase 4 tests. This Volume 2 pertains to MIST mapping tests performed to traverse the early post-SBLOCA events slowly. The tests investigated the effect of test-to-test variations in boundary system controls, and only the primary fluid mass varied during a specific test in this test group.

12. KEY WORDS/DESCRIPTORS *(List words or phrases that will assist researchers in locating the report.)*

Multiloop Integral System Test (MIST), Babcock and Wilcox
Small break loss-of-coolant accident, transient testing, reactor safety
steam generator (once through), feed and bleed
steam generator tube rupture, station black out
Two-phase flow, SBLOCA without HPI injection, RELAP5/MOD2 calculations

13. AVAILABILITY STATEMENT

Unlimited

14. SECURITY CLASSIFICATION

(This Page) Unclassified

(This Report) Unclassified

15. NUMBER OF PAGES

16. PRICE

UNITED STATES
NUCLEAR REGULATORY COMMISSION
WASHINGTON, D.C. 20555